Osvaldo Gervasi · Beniamino Murgante ·
Chiara Garau · Ana Maria A. C. Rocha ·
M. Noelia Faginas Lago · Ana C. Braga ·
Yeliz Karaca (Eds.)

LNCS 16761

Computational Science and Its Applications – ICCSA 2026 Workshops

Braga, Portugal, June 30 – July 3, 2026
Proceedings, Part IV

Springer

Lecture Notes in Computer Science **16761**

Founding Editors

Gerhard Goos
Juris Hartmanis

Editorial Board Members

Elisa Bertino, *Purdue University, West Lafayette, IN, USA*
Wen Gao, *Peking University, Beijing, China*
Bernhard Steffen, *TU Dortmund University, Dortmund, Germany*
Moti Yung, *Columbia University, New York, NY, USA*

The series Lecture Notes in Computer Science (LNCS), including its subseries Lecture Notes in Artificial Intelligence (LNAI) and Lecture Notes in Bioinformatics (LNBI), has established itself as a medium for the publication of new developments in computer science and information technology research, teaching, and education.

LNCS enjoys close cooperation with the computer science R & D community, the series counts many renowned academics among its volume editors and paper authors, and collaborates with prestigious societies. Its mission is to serve this international community by providing an invaluable service, mainly focused on the publication of conference and workshop proceedings and postproceedings. LNCS commenced publication in 1973.

Osvaldo Gervasi · Beniamino Murgante ·
Chiara Garau · Ana Maria A. C. Rocha ·
M. Noelia Faginas Lago · Ana C. Braga ·
Yeliz Karaca
Editors

Computational Science and Its Applications – ICCSA 2026 Workshops

Braga, Portugal, June 30 – July 3, 2026
Proceedings, Part IV

Springer

Editors
Osvaldo Gervasi
University of Perugia
Perugia, Perugia, Italy

Chiara Garau
University of Cagliari
Cagliari, Italy

M. Noelia Faginas Lago
University of Perugia
Perugia, Italy

Yeliz Karaca
University of Massachusetts
Worcester, MA, USA

Beniamino Murgante
University of Basilicata
Potenza, Italy

Ana Maria A. C. Rocha
University of Minho
Braga, Portugal

Ana C. Braga
University of Minho
Braga, Portugal

ISSN 0302-9743 ISSN 1611-3349 (electronic)
Lecture Notes in Computer Science
ISBN 978-3-032-30526-8 ISBN 978-3-032-30527-5 (eBook)
https://doi.org/10.1007/978-3-032-30527-5

© The Editor(s) (if applicable) and The Author(s), under exclusive license
to Springer Nature Switzerland AG 2027

This work is subject to copyright. All rights are solely and exclusively licensed by the Publisher, whether the whole or part of the material is concerned, specifically the rights of translation, reprinting, reuse of illustrations, recitation, broadcasting, reproduction on microfilms or in any other physical way, and transmission or information storage and retrieval, electronic adaptation, computer software, or by similar or dissimilar methodology now known or hereafter developed.
The use of general descriptive names, registered names, trademarks, service marks, etc. in this publication does not imply, even in the absence of a specific statement, that such names are exempt from the relevant protective laws and regulations and therefore free for general use.
The publisher, the authors and the editors are safe to assume that the advice and information in this book are believed to be true and accurate at the date of publication. Neither the publisher nor the authors or the editors give a warranty, expressed or implied, with respect to the material contained herein or for any errors or omissions that may have been made. The publisher remains neutral with regard to jurisdictional claims in published maps and institutional affiliations.

This Springer imprint is published by the registered company Springer Nature Switzerland AG
The registered company address is: Gewerbestrasse 11, 6330 Cham, Switzerland

If disposing of this product, please recycle the paper.

Preface

These 9 volumes (LNCS volumes 16758–16766) comprise the peer-reviewed papers from the 57 Workshops of the 2026 International Conference on Computational Science and Its Applications (ICCSA 2026), held between June 30 and July 3, 2026, in Braga, Portugal. The peer-reviewed papers from the six main conference tracks are published in a separate set of 3 volumes (LNCS volumes 16767–16769).

The conference was held in a hybrid format, with the vast majority of participants attending in person, hosted by the University of Minho in Braga, Portugal.

We enabled virtual participation for those who did not attend the event in person due to logistical, political, or economic constraints by adopting a technological infrastructure based on open-source software (Jitsi + Riot) and a commercial Cloud infrastructure. ICCSA 2026 was organized by the University of Minho (Portugal), the University of Perugia (Italy), the University of Basilicata (Italy), the University of Cagliari (Italy), Monash University (Australia), and Kyushu Sangyo University (Japan).

With the 2026 edition, ICCSA celebrated its 26th anniversary, marking a new chapter in its longstanding history after its memorable 25th anniversary celebrated in Istanbul, Türkiye. Hosted in Braga, Portugal, the conference found a particularly meaningful setting in one of Europe's oldest and most vibrant academic cities, a place where historical depth, cultural continuity, and contemporary scientific exchange meet. Braga offers an inspiring European context for renewing the international and intercultural dialogue that has always characterized ICCSA, while giving new visibility to the role of computational science in addressing the complex challenges of cities, territories, technologies, and societies.

ICCSA 2026 marked another fruitful and thought-provoking academic event in the International Conference on Computational Science and Its Applications (ICCSA) conference series, previously held in Istanbul, Türkiye (2025), Hanoi, Vietnam (2024), Athens, Greece (2023), Málaga, Spain (2022), Cagliari, Italy (hybrid with few participants in presence in 2021 and completely online in 2020), Saint Petersburg, Russia (2019), Melbourne, Australia (2018), Trieste, Italy (2017), Beijing, China (2016), Banff, Canada (2015), Guimarães, Portugal (2014), Ho Chi Minh City, Vietnam (2013), Salvador, Brazil (2012), Santander, Spain (2011), Fukuoka, Japan (2010), Suwon, South Korea (2009), Perugia, Italy (2008), Kuala Lumpur, Malaysia (2007), Glasgow, UK (2006), Singapore (2005), Assisi, Italy (2004), Montreal, Canada (2003), and (as ICCS) Amsterdam, the Netherlands (2002) and San Francisco, USA (2001).

Computational Science constitutes the main pillar of most present research, industrial, and commercial applications, and plays a unique role in exploiting innovative ICT technologies, and the ICCSA conference series has, accordingly, provided ample opportunities to researchers and industry practitioners to discuss new ideas, to share complex problems and their solutions, and to shape new trends in Computational Science. As the conference mirrors society from a scientific point of view, this year's undoubtedly dominant theme was large language models, machine learning, and Artificial Intelligence,

and their applications across the most diverse technological, economic, and industrial fields, amongst others.

The ICCSA 2026 conference included 57 workshops, focusing on topical issues of utmost importance to science, technology, and society: from new computational approaches for earth science, to mathematical methods for image processing, new statistical and optimisation methods, several Artificial Intelligence approaches, sustainability issues, smart cities and related technologies, to name a few. In addition, ICCSA 2026 included six general tracks covering computational science and its applications: Computational Methods, Algorithms and Scientific Applications; High-Performance Computing and Networks; Geometric Modelling, Graphics and Visualisation; Advanced and Emerging Applications; Information Systems and Technologies; and Urban and Regional Planning.

For these Workshops Proceedings, we accepted 328 full papers, 23 short papers, and 3 Ph.D. Showcase papers from a total of 1184 submissions (acceptance rate 29.9%). Reviews were single blind, and submissions received 2.6 reviews each, on average. In the Main Conference Proceedings, we accepted 119 full papers, 3 short papers, and 2 Ph.D. Showcase papers from 431 submissions to the General Tracks of the Conference (acceptance rate of 29.9%). We would like to convey our sincere appreciation to the workshop chairs and co-chairs and program committee members, for their diligent work, commitment, and dedication.

The success and consistent maintenance of the ICCSA conference series in general, and of ICCSA 2026 in particular, rely upon the support of many people: authors, presenters, participants, keynote speakers, workshop chairs, session chairs, Organizing Committee members, student volunteers, Program Committee members, Advisory Committee members, International Liaison chairs, reviewers, and other individuals in various roles. Thus, we take this opportunity to wholeheartedly thank each and every one.

We also wish to thank the publisher, Springer, for accepting the proceedings, and for their kind assistance and cooperation during the editing process. We would cordially like to invite you to refer to the ICCSA website https://iccsa.org, where you can find the relevant details regarding this academic endeavour and our event.

June 2026

Chiara Garau
Ana Maria A. C. Rocha
Osvaldo Gervasi
Beniamino Murgante

Welcome Message from the Organizers

On behalf of the Local Organizing Committee of ICCSA 2026, it is our great pleasure to welcome you to the 26th International Conference on Computational Science and Its Applications, held from June 30 to July 3, 2026, at the University of Minho in Braga, Portugal.

We are deeply honoured by the trust placed in us by the ICCSA General Chairs in organizing another edition of this successful conference series. We hope that ICCSA 2026 provided an inspiring environment for scientific exchange, collaboration, and discussion among researchers from all over the world.

The conference took place at the University of Minho, one of the most prestigious higher education institutions in Portugal. Founded in 1973, the University of Minho has campuses in Braga and Guimaraes and is widely recognized for its academic excellence, research activity, and strong international outlook.

Braga, one of the oldest cities in Portugal, is renowned for its historical heritage, cultural vitality, and welcoming atmosphere.

Located in the heart of the Minho region, the city combines tradition with modernity, offering visitors renowned gastronomy, beautiful landscapes, and the unique character of *Vinho Verde* wine.

The scientific program of ICCSA 2026 included plenary lectures delivered by distinguished scientists, together with a broad range of workshops covering several areas of Computational Science and its Applications. We believe that the conference provided excellent opportunities to share ideas, discuss emerging challenges, and foster new collaborations.

In addition to the scientific sessions, participants had the opportunity to enjoy a rich social program.

Planned activities included a Welcome Reception at Largo do Paço, the Rectorate of the University of Minho, located in the former Archbishop's Palace - one of the most emblematic historical buildings in the city center; a *Vinho Verde* wine-tasting experience at Quinta d'Amares, where particiapnts could discover the art of winemaking; and a guided visit to the coastal city of Viana do Castelo, renowned for its maritime heritage, traditional architecture, and beautiful Atlantic scenery. The conference gala dinner took place at Colunata Eventos, located within the Bom Jesus do Monte sanctuary, a UNESCO World Heritage Site, where ICCSA participants enjoyed delicious recipes and a wonderful view over the city of Braga.

The success of ICCSA 2026 would not have been possible without the dedication and enthusiasm of many collaborators and volunteers, whose hard work and commitment greatly contributed to the organization of the conference.

On behalf of the Local Organizing Committee, it was our honour to warmly welcome you to the beautiful city of Braga and we hope you had an enjoyable and productive conference.

We enjoyed meeting you in Braga.

Sincerely yours,

On behalf of the Local Organizing Committee.

June 2026 Ana Maria A. C. Rocha

Organization

Honorary General Chairs

Bernady O. Apduhan	Kyushu Sangyo University, Japan
Kenneth C. J. Tan	Sardina Systems, UK

General Chairs

Ana Maria A. C. Rocha	University of Minho, Portugal
David Taniar	Monash University, Australia
Osvaldo Gervasi	University of Perugia, Italy

Program Committee Chairs

Beniamino Murgante	University of Basilicata, Italy
Chiara Garau	University of Cagliari, Italy

International Advisory Committee

Jemal Abawajy	Deakin University, Australia
Dharma P. Agarwal	University of Cincinnati, USA
Jagannath Aryal	University of Melbourne, Australia
Rajkumar Buyya	University of Melbourne, Australia
Claudia Bauzer Medeiros	University of Campinas, Brazil
Carl K. Chang	Iowa State University, USA
Elizabeth Chang	University of the Sunshine Coast, Australia
Manfred M. Fisher	Vienna University of Economics and Business, Austria
Pierre Frankhauser	University of Franche-Comté/CNRS, France
Marina L. Gavrilova	University of Calgary, Canada
Sumi Helal	University of Florida, USA & Lancaster University, UK
Bin Jiang	University of Gävle, Sweden
Yee Leung	Chinese University of Hong Kong, China
Biswajeet Pradhan	University of Technology Sydney, Australia
My Thai	University of Florida, USA

International Liaison Chairs

Giuseppe Borruso	University of Trieste, Italy
Elise De Donker	Western Michigan University, USA
Maria Noelia Faginas Lago	University of Perugia, Italy
Maria Irene Falcão	University of Minho, Portugal
Robert C. H. Hsu	Chung Hua University, Taiwan
Yeliz Karaca	UMass Chan Medical School, USA
Tae-Hoon Kim	Zhejiang University of Science and Technology, China
Vladimir Korkhov	Saint Petersburg University, Russia
Takashi Naka	Kyushu Sangyo University, Japan
Rafael D. C. Santos	National Institute for Space Research, Brazil
Maribel Yasmina Santos	University of Minho, Portugal
Anastasia Stratigea	National Technical University of Athens, Greece
Nguyen Canh Thai	Thuyloi University, Vietnam
Kh Md Nahiduzzaman	Mohammed VI Polytechnic University, Rabat, Morocco

Workshop and Session Organizing Chairs

Beniamino Murgante	University of Basilicata, Italy
Chiara Garau	University of Cagliari, Italy

Award Chair

Wenny Rahayu	La Trobe University, Australia

Publicity Committee Chairs

Elmer Dadios	De La Salle University, Philippines
Nataliia Kulabukhova	Saint Petersburg University, Russia
Daisuke Takahashi	Tsukuba University, Japan
Doan Quang Tu	Academy of Military Science and Technology, Vietnam
Shangwang Wang	Beijing University of Posts and Telecommunications, China

Local Organizing Committee Chairs

Maria Irene Falcão	University of Minho, Portugal
Ana Cristina Braga	University of Minho, Portugal
Rui José	University of Minho, Portugal
José Manuel Machado	University of Minho, Portugal
Jorge G. Rocha	University of Minho, Portugal

Technology Chair

Damiano Perri	University of Perugia, Italy

Workshops

Workshop on Advancements in Applied Machine-learning and Data Analytics (AAMDA 2026)

Workshop Organizers

Alessandro Costantini	INFN, Italy
Elisabetta Ronchieri	INFN CNAF, Italy

Workshop Program Committee Members

Luca Dell'Agnello	INFN, Italy
Barbara Martelli	INFN, Italy
Daniele Cesini	INFN CNAF, Italy
Giovanni Zurlo	INFN CNAF, Italy
Luca Giommi	INFN CNAF, Italy
Valentino Santucci	Università per Stranieri di Perugia, Italy
Francesco Santini	University of Perugia, Italy
Paolo Mengoni	Hong Kong Baptist University, China
Alessandro Bombini	Istituto Nazionale di Fisica Nucleare, Italy

Artificial Intelligence Tools In Managing Future Communities (AiMFutCOM 2026)

Workshop Organizers

Marco Vona	University of Basilicata, Italy
Francesco Scorza	University of Basilicata, Italy
Donatello Cardone	University of Basilicata, Italy
Maurizio Pollino	ENEA, Italy
Gregorio DAgostino	ENEA, Italy

Workshop Program Committee Members

Maria Danese	CNRISPC, Italy
Rachele Vanessa Gatto	Università della Basilicata, Italy
Simone Corrado	University of Basilicata, Italy
Alessandro Plaisant	University of Sassari, Italy
Sabrina Lai	University of Cagliari, Italy
Alfonso Annunziata	University of Basilicata, Italy
Jolanta Dvarioniene	Kaunas University of Technology, Lithuania

Advanced and Innovative Web Apps 2026 (AIWA 2026)

Workshop Organizers

Damiano Perri	University of Perugia, Italy
Osvaldo Gervasi	University of Perugia, Italy
Luciano Alessandro Ipsaro Palesi	University of Florence, Italy

Workshop Program Committee Members

David Berti	ART SpA, Italy
JungYoon Kim	Gachon University, South Korea
Taihoon Kim	Chonnam National University, South Korea

Advanced Mathematics and Computing Models in Complex Data-Intensive Computational Systems (AMCM 2026)

Workshop Organizers

Yeliz Karaca	UMass Chan Medical School and Massachusetts Institute of Technology, USA
Dumitru Baleanu	Lebanese American University, Lebanon
Osvaldo Gervasi	University of Perugia, Italy
Yudong Zhang	University of Leicester, UK
Majaz Moonis	UMass Chan Medical School, USA

Workshop Program Committee Members

Aziz Dursun	Virginia Tech University, USA
Akif Akgul	Hitit University, Turkey
Nizamettin Aydin	Istanbul Technical University, Turkey
Martin Bohner	Missouri University of Science and Technology, USA
Khan Muhammad	Sungkyunkwan University, South Korea

Advanced Numerical Approaches for assessment and design of no-tension Masonry Structures (ANAMS 2026)

Workshop Organizers

Antonino Iannuzzo	Universitá degli studi del Sannio, Italy
Natalia Pingaro	Politecnico di Milano, Italy
Andrea Montanino	International Centre for Numerical Methods in Engineering, Spain
Elham Mousavian	University of Edinburgh, UK
Stefano Galassi	University of Florence, Italy

Workshop Program Committee Members

Amal Gerges	University of Cagliari, Italy
Vittorio Paris	University of Bergamo, Italy
Alessandra Capolupo	Polytechnic University of Bari, Italy
Carlo Olivieri	Pegaso University, Italy
Generoso Vaiano	Pegaso University, Italy

Luigi Sibille	Norwegian University of Science and Technology, Norway
Francesco Picariello	Universitas Mercatorum, Italy
Ilaria Scarcelli	Politecnico di Bari, Italy
Fabian Bernal Orozco Barrera	National Autonomous University of Mexico, Mexico
Gabriel Barbat	Universitat Politècnica de Catalunya, Spain
Alejandro Cornejo	Universitat Politècnica de Catalunya, Spain
Mohammad Pourfouladi	Politecnico di Milano, Italy

Artificialization of land, Urban Transformation, and Territorial Resilience in a changing Climate (AUTTREC 2026)

Workshop Organizers

Celestina Fazia	Università di Enna Kore, Italy
Kh Md Nahiduzzaman	Mohammed VI Polytechnic University, Morocco
Hassan Radoine	Mohammed VI Polytechnic University, Morocco
Cezar Morar	University of Oradea, Romania
Antonio García Martínez	Universidad de Sevilla, Spain
Clara Stella Vicari Aversa	Università degli Studi Mediterranea di Reggio Calabria, Italy

Workshop Program Committee Members

Federica Sortino	Universitià degli studi di Enna Kore, Italy
Giulia Fernanda Grazia Catania	Universit di Enna Kore, Italy
Maria Francesca Faro	Ministry of Education and Merit (MIM), Italy
Aleksandar Valjarević	University of Belgrade, Serbia
Laila El Ghazouani	Mohammed VI Polytechnic University, Morocco
Adnane Labbaci	Ibn Tofail University, Morocco

Blockchain and Distributed Ledgers: Technologies and Applications (BDLTA 2026)

Workshop Organizers

Vladimir Korkhov	Saint Petersburg State University, Russia
Elena Stankova	Saint Petersburg State University, Russia
Nataliia Kulabukhova	AutoTech, Russia

Workshop Program Committee Members

Vasily Solodkov	National Research University Higher School of Economics, Moscow, Russia
Alexander Bogdanov	St. Petersburg State University, Russia
Alexander Degtyarev	Saint Petersburg State University, Russia
Dmitrii Vasiunin	Deutsche Telekom Cloud Services E.P.E., Greece
Serob Balyan	Institute for Informatics and Automation Problems, National Academy of Sciences of Armenia, Armenia
Suren Abrahamyan	Institute for Informatics and Automation Problems of NAS RA, Armenia
Ashot Gevorkyan	Institute for Informatics and Automation Problems NAS of Armenia, Armenia
Martin Vala	Pavol Jozef Šafárik University, Slovak Republic
Nodir Zaynalov	Samarkand Branch of Tashkent University of Information Technologies Named After Muhammad al Khwarizmi, Uzbekistan
Michail Panteleyev	Saint Petersburg Electrotechnical University, Russia
Alexander Degtyarev	St. Petersburg State University, Russia
Alexander Bogdanov	St. Petersburg State University, Russia

Bio and Neuro inspired Computing and Applications (BIONCA 2026)

Workshop Organizers

Nadia Nedjah	State University of Rio de Janeiro, Brazil
Luiza de Macedo Mourelle	State University de Rio de Janeiro, Brazil

Workshop Program Committee Members

Alan Oliveira	Universidade de Lisboa, Portugal
Rogerio Calazan	Instituto de Estudos do Mar Almirante Paulo Moreira - Brazilian Navy, Brazil
Marcos Farias	Instituto de Engenharia Nuclear, Brazil
Joelmir Ramos	State University de Rio de Janeiro, Brazil
Luigi Maciel Ribeiro	State University of Rio de Janeiro, Brazil

Computational and Applied Mathematics (CAM 2026)

Workshop Organizers

Maria Irene Falcao	University of Minho, Portugal
Fernando Miranda	Universidade do Minho, Portugal

Workshop Program Committee Members

Graca Tomaz	Instituto Politécnico da Guarda, Portugal
Helmuth Malonek	University of Aveiro, Portugal
Isabel Cacao	University of Aveiro, Portugal
Joao Morais	Autonomous Technological Institute of Mexico (ITAM), Mexico
Lidia Aceto	Università del Piemonte Orientale, Italy
Luís Ferrás	University of Minho, Portugal
Patricia Beites	University of Beira Interior, Portugal
Paulo Amorim	Escola de Matemática Aplicada da Fundação Getulio Vargas, Brazil
Regina de Almeida	University of Trás-os-Montes and Alto Douro, Portugal
Ricardo Severino	University of Minho, Portugal

Computational and Applied Statistics for Data & AI (CAS 2026)

Workshop Organizers

Ana Cristina Braga	University of Minho, Portugal
Ines Sena	University of Minho, Portugal
Joao Mendes	Polytechnic Institute of Bragança, Portugal

Workshop Program Committee Members

A. Manuela Goncalves	University of Minho, Portugal
Vera Afreixo	University of Aveiro, Portugal
Ivan Rodriguez Conde	University of Arkansas at Little Rock, USA
Isabel Natário	Universidade Nova de Lisboa, Portugal
Luca Parodi	University of Genoa, Italy
Flávia Pires	Instituto Politecnico de Bragança, Portugal
Beatriz Flamia Azevedo	Instituto Politecnico de Bragança, Portugal
Adriano Silva	Instituto Politecnico de Bragança VAT 600013758, Portugal

Ana Paula Amorim	Universidade do Minho, Portugal
Angela Silva	Universidade do Minho, Portugal
Arunasalam Rahunanthan	Central State University, USA
Bruna Ramos	University of Minho, Portugal
Cecília Maria Vasconcelos Costa e Castro	Universidade do Minho, Portugal
Florbela Correia	Polytechnic Institute of Viana do Castelo, Portugal
Joaquim Goncalves	Polytechnic Institute of Cávado and Ave, Portugal
Lino Costa	University of Minho, Portugal
Luís Miguel Matos	Universidade do Minho, Portugal
Marco Reis	University of Coimbra, Portugal
Maria Mourao	Polytechnic Institute of Viana do Castelo, Portugal
Martin Perez Perez	University of Vigo, Spain
Sandra Aleixo	FCiências.ID, Portugal
Paula Odete Fernandes	Instituto Politecnico de Bragança, Portugal
Iván Rodríguez Conde	Universidade de Vigo, Spain
Telmo Miguel Pires Pinto	University of Minho, Portugal

Circular Economy and Territorial Competitiveness (CETC 2026)

Workshop Organizers

Gerardo Carpentieri	University of Naples Federico II, Italy
Carmen Guida	Università degli Studi di Napoli Federico II, Italy
Floriana Zucaro	University of Naples Federico II, Italy
Zhadyra Konurbaeva	D. Serikbayev East Kazakhstan Technical University, Kazakhstan
Saule Kumargazhanova	D. Serikbayev East Kazakhstan Technical University, Kazakhstan

Workshop Program Committee Members

Rosaria Battarra	ISMed-CNR, Italy
Laura Ascione	Università degli studi di Napoli Federico II, Italy
Valerio Martinelli	Università di Napoli Federico II, Italy
Madina Yussubaliyeva	D. Serikbayeva East Kazakhstan Technical University, Kazakhstan
Samat Baigereyev	D. Serikbayev East Kazakhstan Technical University, Kazakhstan

Circular Ecological Heritage Communities: Regeneration and Evaluation Strategies for Historic Villages, Landscapes and Rural Territories (CHEC 2026)

Workshop Organizers

Mariarosaria Angrisano	Pegaso University, Italy
Antonia Gravagnuolo	CNR Institute of Heritage Science, Italy
Francesca Buglione	CNR ISPC, Italy
Piera Della Morte	Pegaso Telematic University, Italy

Workshop Program Committee Members

Giulia Datola	Politecnico di Milano, Italy
Marco Rossitti	Politecnico di Milano, Italy
Federico DellAnna	Politecnico di Torino, Italy
Grazia Neglia	Pegaso Telematic University, Italy
Vanessa Assumma	University of Bologna, Italy
Ippolita Mecca	Pegaso Telematic University, Italy
Ferdinando Verardi	Pegaso Telematic University, Italy
Eleonora Sottile	University of Cagliari, Italy
Dina Jovanovic	Politecnico di Milano, Italy
Martina Mulinacci	Politecnico di Milano, Italy
Davide Cerati	Politecnico di Milano, Italy
Daniela Oreni	Politecnico di Milano, Italy
Patrizia Riganti	University of Glasgow, UK
Carlo Olivieri	Pegaso University, Italy
Giulio Cavana	Politecnico di Torino, Italy
Maria Tartari	CNR, Italy
Luigi Fusco Girard	Pegaso Telematic University, Italy
Albina Scioti	Università Telematica Pegaso, Italy
Eleonora Righetto	Università degli Studi di Padova, Italy
Chiara D'Alpaos	University of Padua, Italy
Anthony Suppa	Politecnico di Torino, Italy
Giorgia Malavasi	Politecnico di Torino, Italy
Kaoutare Amini Alaoui	Mohamed VI Polytechnic University, Morocco
Elena Todella	University of Parma, Italy
Leonhard Seyboth	Federal University of Santa Catarina, Brazil
Jianzhuo Xu	Politecnico di Milano, Italy
Ludovica Nasca	University of Catania, Italy
Alessandro Plaisant	University of Sassari, Italy

Maria Carla Saliu	University of Cagliari, Italy
Ons Zoghlami	Sapienza University of Rome, Italy
Irena Ištoka Otković	Josip Juraj Strossmayer University of Osijek, Croatia
Daniele Cannatella	TU Delft, Italy
Tanja Congiu	University of Sassari, Italy
Juan Camilo Giraldo	Institute for Advanced Architecture of Catalonia, Spain
YiChang Liu	Bio-Architecture Formosana, Taiwan
Yasmine Selim	Ain Shams University, Egypt
Simona Tondelli	Alma Mater Studiorum University of Bologna, Italy
Efrossyni Tsakiri	National Technical University of Athens, Greece

Cyber Intelligence and Applications (CIA 2026)

Workshop Organizers

Gianni D'Angelo	University of Salerno, Italy
Francesco Palmieri	University of Salerno, Italy
Massimo Ficco	University of Salerno, Italy

Workshop Program Committee Members

Arcangelo Castiglione	University of Salerno, Italy
Ugo Fiore	University of Salerno, Italy
Michele Mastroianni	University of Foggia, Italy
Marcello Trovati	Edge Hill University, UK
Raffaele Esposito	University of Salerno, Italy
Marek Ogiela	AGH University of Science and Technology, Poland
Chang Choi	Gachon University, South, South Korea
Mauro Migliardi	University of Padua, Italy

Computational Methods, Statistics and Industrial Mathematics (CMSIM 2026)

Workshop Organizers

Maria Filomena Teodoro	CINAV, Escola Naval, Instituto Universitário Militar, Portugal

Paula Simões	Academia Militar, Portugal
Teresa A. Oliveira	University of Lisbon and Universidade Aberta, Portugal

Workshop Program Committee Members

Luis Teodoro	University of Oslo, Norway
Eliana Costa e Silva	Polytechnic of Porto, Portugal
Ana Borges	Instituto Politécnico do Porto, Portugal
Cristina Lopes	Polytechnic Institute of Porto, Portugal
Fernando Lucas Carapau	University of Évora, Portugal
Antonio S. Macias	University of A Coruña, Spain
Matteo Sacchet	University of Turin, Italy
Marina Marchisio Conte	University of Turin, Italy
Christos Kitsos	University of West Attica, Greece
M. Rosário Ramos	Universidade Aberta, University of Lisbon, Portugal
António Pacheco	Instituto Superior Técnico, Portugal
Ana Sofia Rézio	Polytechnic Institute of Lisbon, Portugal
Paula Simões	Military Academy Portuguese Army, Portugal
Ricardo Moura	NOVA University of Lisbon, Portugal
Ana Oliveira	Academia Militar, Portugal
Sílvia Chá	Military Academy, Portugal
Carlos Rodrigues	Instituto Politecnico de Bragança, Portugal

Computational Optimization and Applications (COA 2026)

Workshop Organizers

Ana Maria A. C. Rocha	University of Minho, Portugal
Humberto Rocha	University of Coimbra, Portugal

Workshop Program Committee Members

Eligius Hendrix	Universidad de Málaga, Spain
Joana Dias	University of Coimbra, Portugal
Ana Pereira	Polytechnic Institute of Bragança, Portugal
Lino Costa	University of Minho, Portugal, Portugal
Filipe Alvelos	Universidade do Minho, Portugal
Ana Paula Teixeira	Universidade do Minho, Portugal

Florbela P. Fernandes	Politecnico de Bragança, Portugal
Ana Monteiro	University of Coimbra, Portugal
Rui Pascoal	University of Coimbra, Portugal
Rommel Regis	Saint Joseph's University, USA
Telmo Miguel Pires Pinto	University of Minho, Portugal
Emerson Paiva	Minho University, Portugal

Computational Methods in Advanced Networking Technologies (CoMANT 2026)

Workshop Organizers

Eslam Farsimadan	University of Salerno, Italy
Leila Moradi	University of Salerno, Italy
Francesco Palmieri	University of Salerno, Italy

Workshop Program Committee Members

Massimo Ficco	University of Salerno, Italy
Ugo Fiore	University of Salerno, Italy
Michele Mastroianni	University of Foggia, Italy
Arcangelo Castiglione	University of Salerno, Italy
Francesco Giuseppe Zammarrelli	University of Salerno, Italy
Annalaura Miglino	University of Salerno, Italy
Mojtaba Sharifzadeh	Università di Trento, Italy
Zahra Ebadi Ansaroudi	Fondazione Bruno Kessler, Italy
Mohammad Vazir Panah	University of Salerno, Italy
Gennaro Pio Rimoli	Università degli Studi di Salerno, Italy

Computational Astrochemistry 2026 (CompAstro 2026)

Workshop Organizers

Marzio Rosi	University of Perugia, Italy
Daniela Ascenzi	Università degli Studi di Trento, Italy
Nadia Balucani	University of Perugia, Italy
Stefano Falcinelli	University of Perugia, Italy

Workshop Program Committee Members

Luca Mancini	University of Perugia, Italy
Andrea Giustini	University of Perugia, Italy
Albert Rimola	Universitat Autònoma de Barcelona, Spain
Piero Ugliengo	Università degli Studi di Torino, Italy
Dario Campisi	University of Perugia, Italy
Gianmarco Valuzzo	University of Perugia, Italy
Giacomo Pannacci	Università degli Studi di Perugia, Italy
Giacomo Giorgi	Università degli Studi di Perugia, Italy
Gabriella Di Genova	Università degli Studi di Perugia, Italy
Lisa Giani	Université Grenoble Alpes, IPAG, France
Emilia Valenca Ferreira de Aragao	University of Montpellier, CEA, CNRS, ENSCM, France
Marco Parriani	Università degli studi di Perugia, Italy
Costanza Borghesi	CNR Istituto Nanoscienze, Italy

Computational methods for Porous materials (CompPor 2026)

Workshop Organizers

Vadim Lisitsa	Institute of Petroleum Geology and Geophysics SB RAS, Russia
Evgeniy Romenski	Sobolev Institute of Mathematics, Russia

Workshop Program Committee Members

Tatyana Khachkova	Institute of Petroleum Geology and Geophysics SB RAS, Russia
Dmitry Prokhorov	Institute of Petroleum Geology and Geophysics SB RAS, Russia
Mikhail Novikov	Sobolev Institute of Mathematics SB RAS, Russia
Galina Reshetova	Institute of Computational Mathematics and Mathematical Geophysics SB RAS, Russia
Sergey Solovyev	Sobolev Institute of Mathematics SB RAS, Russia
Vladimir Cheverda	Sobolev Institute of Mathematics SB RAS, Russia

Workshop on Computational Science and HPC (CSHPC 2026)

Workshop Organizers

Elise de Doncker	Western Michigan University, USA
Hideo Matsufuru	High Energy Accelerator Research Organization, Japan
Robert Makin	Western Michigan University, USA

Workshop Program Committee Members

Hiroshi Daisaka	Hitotsubashi University, Japan
James Rhodes	Western Michigan University, USA
Naohito Nakasato	University of Aizu, Japan
Issaku Kanamori	RIKEN, Japan
Takahiro Ueda	Juntendo University, Japan
Keigo Nitadori	RIKEN, Japan
Fukuko Yuasa	KEK, Japan
Shigeyoshi Aoyama	KEK, Japan
Tatsumi Aoyama	University of Tokyo, Japan
Tasnim Gharaibeh	Kalamazoo College, USA

Cities, Technologies and Planning (CTP 2026)

Workshop Organizers

Giuseppe Borruso	University of Trieste, Italy
Beniamino Murgante	University of Basilicata, Italy
Malgorzata Hanzl	Lodz University of Technology, Poland
Anastasia Stratigea	National Technical University of Athens, Greece
Ljiljana Zivkovic	Republic Geodetic Authority, Serbia
Ginevra Balletto	University of Cagliari, Italy

Workshop Program Committee Members

Silvia Battino	University of Sassari, Italy
Mara Ladu	University of Cagliari, Italy
Maria del Mar Munoz	University of Cádiz, Spain
Ainhoa Amaro	EVOCONS, Spain
Enrico Dagostini	University of Malta, Malta

Francesca Krasna	Università degli Studi di Trieste, Italy
Brisol García García	Universidad Politécnica de Quintana Roo, Mexico
Giovanni Mauro	University of Campania Luigi Vanvitelli, Italy
Maria Ronza	University of Naples Federico II, Italy
Clara Di Fazio	University of Trieste, Italy
Andrea Gallo	Università degli Studi di Trieste, Italy
Francesca Sinatra	University of Trieste, Italy

Evaluating Inner Areas Potentials (EIAP 2026)

Workshop Organizers

Diana Rolando	Politecnico di Torino, Italy
Manuela Rebaudengo	Politecnico di Torino, Italy
Alice Barreca	Politecnico di Torino, Italy
Giorgia Malavasi	Politecnico di Torino, Italy

Workshop Program Committee Members

John Accordino	Virginia Commonwealth University, USA
Sara Favargiotti	University of Trento, Italy
Barbara Lino	Università degli Studi di Palermo, Italy
Maddalena Ferretti	Università Politecnica delle Marche, Italy
Eugenio Muccio	University of Naples Federico II, Italy
Giuliano Poli	University of Naples Federico II, Italy
Giulia Datola	Politecnico di Milano, Italy
Elena Todella	University of Parma, Italy
Asja Aulisio	Politecnico di Torino, Italy
Marco Rossitti	Politecnico di Milano, Italy
Martina Spinelli	Politecnico Torino, Italy
Amina Pereno	Politecnico di Torino, Italy
Francesco Bruzzone	Università Iuav di Venezia, Italy
Alexandra Stankulova	Politecnico di Torino, Italy
Benedetta Di Leo	Università Politecnica delle Marche, Italy
Edda Donati	University of Rome Tor Vergata, Italy
Vanessa Assumma	University of Bologna, Italy
Beatrice Mecca	Politecnico di Torino, Italy

sustainablE mobiLity and Last mIle lOgisTic in urban context (ELLIOT 2026)

Workshop Organizers

Tiziana Campisi	University of Enna Kore, Italy
Socrates Basbas	Aristotle University of Thessaloniki, Greece
Florin Rusca	National University of Science and Technology Politehnica Bucharest, Romania
Grigorios Fountas	Aristotle University of Thessaloniki, Greece
Aleksandra Deluka-Tibljas	University of Rijeka, Croatia

Workshop Program Committee Members

Francesco Russo	University of Reggio Calabria, Italy
Oana Dinu	National University of Science and Technology Politehnica Bucharest, Romania
Antonio Polimeni	Università di Messina, Italy
Antonio Russo	University of Enna Kore, Italy
Elena Cocuzza	Univesity of Catania, Italy
Corrado Rindone	Università degli studi Mediterranea di Reggio Calabria, Italy

Econometrics and Multidimensional Evaluation in Urban Environment (EMEUE 2026)

Workshop Organizers

Maria Cerreta	University of Naples Federico II, Italy
Giuseppe Ciciriello	University of Naples Federico II, Italy
Simona Panaro	University of Sussex Business School, UK
Piero Zizzania	Università of Naples Federico II, Italy
Pierluigi Morano	Polytechnic University of Bari, Italy
Francesco Tajani	Sapienza University of Rome, Italy

Workshop Program Committee Members

Giuliano Poli	Università Federico II di Napoli, Italy
Ludovica La Rocca	University of Naples Federico II, Italy
Sabrina Sacco	University of Naples Federico II, Italy

Ecosystem Services in Spacial Planning for climate neutral urban and rural areas (ESSP 2026)

Workshop Organizers

Sabrina Lai	University of Cagliari, Italy
Carmela Gargiulo	Università Federico II di Napoli, Italy
Beniamino Murgante	University of Basilicata, Italy
Francesco Scorza	University of Basilicata, Italy
Corrado Zoppi	University of Cagliari, Italy
Floriana Zucaro	University of Naples Federico II, Italy

Workshop Program Committee Members

Alfonso Annunziata	University of Basilicata, Italy
Ginevra Balletto	University of Cagliari, Italy
Ivan Blečić	University of Cagliari, Italy
Giuseppe Borruso	University of Trieste, Italy
Barbara Caselli	Università degli Studi di Parma, Italy
Maria Cerreta	University of Naples Federico II, Italy
Carmen Guida	Università degli Studi di Napoli Federico II, Italy
Federica Isola	University of Cagliari, Italy
Francesca Leccis	University of Cagliari, Italy
Federica Leone	University of Cagliari, Italy
Silvia Rossetti	Università degli Studi di Parma, Italy
Luigi Santopietro	Institute of Methodologies for Environmental Analysis CNR IMAA, Italy
Simone Corrado	University of Basilicata, Italy
Rachele Vanessa Gatto	Università della Basilicata, Italy

The 16th International Workshop on Future Information System Technologies and Applications (FiSTA 2026)

Workshop Organizers

Bernady O. Apduhan	Kyushu Sangyo University, Japan
Rafael Santos	National Institute for Space Research (INPE), Brazil

Workshop Program Committee Members

Agustinus Waluyo	La Trobe University, Australia
Earl Ryan Aleluya	Mindanao State University Iligan Institute of Technology, Philippines
Eric Pardede	La Trobe University, Australia
Kai Cheng	Kyushu Sangyo University, Japan
Fenghui Yao	Tennessee State University, USA
Yusuke Gotoh	Okayama University, Japan
Kazuaki Tanaka	Kyushu Institute of Technology, Japan
Toshihiro Yamauchi	Okayama University, Japan
Toshihiro Uchibayashi	Kyushu University, Japan
Krishnamoorthy Ranganathan	Chennai Institute of Technology, India
Orven Llantos	MSU-Iligan Institute of Technology, Philippines
Anton Louise De Ocampo	Batangas State University, Philippines

Geographical Analysis, Urban Modeling, Spatial Statistics (Geog-And-Mod 2026)

Workshop Organizers

Giuseppe Borruso	University of Trieste, Italy
Beniamino Murgante	University of Basilicata, Italy
Hartmut Asche	Hasso Plattner Institute for Digital Engineering, Germany
Rodrigo Tapia-McClung	Centro de Investigación en Ciencias de Información Geoespacial, Mexico
Andreas Fricke	Hasso Plattner Institute for Digital Engineering, University of Potsdam, Germany

Workshop Program Committee Members

Ginevra Balletto	University of Cagliari, Italy
Mara Ladu	University of Cagliari, Italy
Gabriella Schoier	Università di Trieste, Italy
Marco Mazzarino	Iuav University of Venice, Italy
Malgorzata Hanzl	Lodz University of Technology, Poland
Anastasia Stratigea	National Technical University of Athens, Greece
Maria del Mar Munoz	University of Cádiz, Spain
Veronica Camerada	Università degli Studi di Sassari, Italy

Generative and Neuro-Symbolic Artificial Intelligence for Real-World Systems (GNS-AI 2026)

Workshop Organizers

Hugo Peixoto	University of Minho, Portugal
Manuel Rodrigues	University of Minho, Portugal
Regina Sousa	University of Minho, Portugal

Workshop Program Committee Members

Dalila Duraes	Universidade do Minho, Portugal
Paulo Novais	Universidade do Minho, Portugal
Laura Cavalcante	Instituto Superior de Engenharia do Porto, Portugal
Diogo Martinho	Instituto Superior de Engenharia de Porto, Portugal
Hélia Guerra	University of the Azores, Portugal
Rohit Raja	Guru Ghasidas Vishwavidyalaya, India
Hien Nguyen	University of Information Technology, Vietnam
Antonio Carlos Da Silva Abelha	Universidade do Minho, Portugal
Cristiana Neto	University of Minho, Portugal
José Machado	University of Minho, Portugal
Luís Conceicao	Instituto Superior de Engenharia do Porto, Portugal
Omar Gomez	Universidad Nacional de Colombia, Colombia
Luis Mendes Gomes	University of the Azores, Portugal
Nicolas Lori	University of the Azores, Portugal
Sara Balderas Díaz	University of Cádiz, Spain
Gabriel Guerrero Contreras	University of Cádiz, Spain
Francisco Zayas Gato	Universidade da Coruña, Spain
Diana Ferreira	University of Minho, Portugal
Jolanta Miliauskaite	Vilnius University, Lithuania

Geomatics for Resource Monitoring and Management (GRMM 2026)

Workshop Organizers

Alberico Sonnessa	Politecnico di Bari, Italy
Eufemia Tarantino	Politecnico di Bari, Italy
Marco Locurcio	Polytechnic University of Bari, Italy

Workshop Program Committee Members

Valeria Belloni	Sapienza University of Rome, Italy
Roberta Ravanelli	University of Liège, Belgium
Michela Ravanelli	Sapienza Università di Roma, Italy
Alessandra Mascitelli	University of Chieti Pescara, Italy
Francesco Bimbo	University of Foggia, Italy
Francesco Di Capua	University of Basilicata, Italy
Gaetano Falcone	Università degli Studi di Napoli Federico II, Italy
Francesco Tajani	Sapienza University of Rome, Italy
Paola Amoruso	LUM Giuseppe Degennaro University, Italy
Pierfrancesco De Paola	University of Naples Federico II, Italy
Isidora Đurić	University of Novi Sad, Serbia
Rossella Petti	Politecnico di Bari, Italy
Valeria Cera	University of Naples Federico II, Italy
Antonino Iannuzzo	Universitá degli studi del Sannio, Italy
Pier Francesco Recchi	Università di Napoli Federico II, Italy
Giuseppe Francesco Cesare Lama	University of Naples Federico II, Italy
Ester Scotto di Perta	University of Naples Federico II, Italy
Antonino Maltese	University of Palermo, Italy
Andrea Montanino	University of Naples, Italy
Carla Cavallo	University of Salerno, Italy
Dario Esposito	Polytechnic University of Bari, Italy
Rosaria Parente	Universitas Mercatorum, Italy
Claudia Panciera	Water Research Institute (IRSA) CNR, Italy
Pasquale Perrini	Consorzio Interuniversitario per l'Idrologia, Italy
Beniamino Onorati	Università degli Studi della Basilicata, Italy
Francesco Sica	Sapienza University of Rome, Italy

International Workshop on Information and Knowledge in the Internet of Things (IKIT 2026)

Workshop Organizer

Teresa Guarda	Universidad Estatal Península de Santa Elena, Ecuador

Workshop Program Committee Members

Isabel Lopes	Instituto Politécnico de Bragança, Portugal
Luis Mazon	Bitrum Research Group, Spain

Arnulfo Alanis	Tecnológico Nacional de México, Campus Tijuana, Mexico
Filipe Mota Pinto	Instituto Politécnico de Leiria, Portugal
Luis Enrique Chuquimarca Jiménez	Universidad Estatal Penìnsula de Santa Elena, Ecuador
Gustavo Gatica	Universidad Andres Bello, Chile
Jairo Coronado Hernandez	Universidad de la Costa, Colombia
Maria Fernanda Augusto	BITrum Research Center, Spain
José María Díaz Nafría	Universidad a Distancia de Madrid, Spain
Modestos Stavrakis	University of the Aegean, Greece
Isabel Ribeiro	Instituto Politécnico Bragança, Portugal
Bruno Sousa	University of Coimbra, Portugal
Datzania Villao	Universidad Estatal Península de Santa Elena, Ecuador

Intelligent Sustainable Development: from Models to Real-World Impact (ISD 2026)

Workshop Organizers

Diego Brandão	Federal Center for Technological Education of Rio de Janeiro, Brazil
Angela Ferreira	Polytechnic University of Bragança, Portugal
Eduardo Bezerra	Federal Center for Technological Education of Rio de Janeiro, Brazil
Raphael Guerra	Universidade Federal Fluminense, Brazil
Douglas Cardoso	University of Coimbra, Portugal
Rui Pedro Lopes	Instituto Politecnico de Bragança, Portugal

Workshop Program Committee Members

Wagner Telles	Universidade Federal Fluminense, Brazil
Jader Lugon Junior	Instituto Federal Fluminense, Brazil
Edcarllos Santos	Universidade Federal do Sul da Bahia, Brazil
Kennedy Fernandes	Universidade Federal de Juiz de Fora, Brazil
Israel Mendonca	Kumamoto University, Japan
Pedro Henrique Gonzalez	Federal University of Rio de Janeiro, Brazil
Pablo Luiz Araujo Munhoz	Federal University of Ouro Preto, Brazil
Elloa Guedes	Amazonas State University, Brazil
Danielli Araújo Lima	Instituto Federal do Triângulo Mineiro, Brazil
Ary Henrique Oliveira	Universidade Federal de Tocantins, Brazil

Paula Odete Fernandes	Instituto Politecnico de Bragança, Portugal
Hiago Rocha	National Laboratory for Scientific Computing, Brazil
Andre Luiz Coutinho Merlo	Centro Federal de Educacao Tecnologica Celso Suckow da Fonseca CEFET RJ, Brazil
Kennedy Fernandes	Universidade Federal de Juiz de Fora, Brazil
Ary Henrique Oliveira	Universidade Federal de Tocantins, Brazil
Mayara Omai	Centro Federal de Educacao Tecnologica Celso Suckow da Fonseca CEFET RJ, Brazil

Multidimensional Evolutionary Evaluations for Transformative Approaches (MEETA 2026)

Workshop Organizers

Maria Cerreta	University of Naples Federico II, Italy
Giuliano Poli	Università Federico II di Napoli, Italy
Gaia Daldanise	CNR Institute for Research on Innovation and Services for Development, Italy
Ludovica La Rocca	University of Federico II of Naples, Italy
Maria Somma	University of Naples Federico II, Italy
Sabrina Sacco	University of Naples Federico II, Italy

Workshop Program Committee Members

Chiara Mazzarella	TUDelft, The Netherlands
Simona Panaro	University of Sussex Business School, UK
Eugenio Muccio	University of Naples Federico II, Italy

Building multi-dimensional Models for assessing complex Environmental Systems (MES 2026)

Workshop Organizers

Vanessa Assumma	University of Bologna, Italy
Caterina Caprioli	Politecnico di Torino, Italy
Giulia Datola	Politecnico di Milano, Italy
Federico DellAnna	Politecnico di Torino, Italy
Marta Dell'Ovo	Politecnico di Milano, Italy
Marco Rossitti	Politecnico di Milano, Italy

Workshop Program Committee Members

Mariarosaria Angrisano	Pegaso University, Italy
Giuliano Poli	University of Naples Federico II, Italy
Francesco Sica	Sapienza University of Rome, Italy
Eugenio Muccio	University of Naples Federico II, Italy
Sebastiano Barbieri	Politecnico di Torino, Italy
Giulio Cavana	Politecnico di Torino, Italy
Marta Bottero	Politecnico di Torino, Italy
Francesca Torrieri	Politecnico di Milano, Italy
Maksims Feofilovs	Riga Technical University, Latvia
Daniela Maiullari	Delft University of Technology, The Netherlands
Elena Todella	University of Parma, Italy
Yvonne Russo	University of Campania L. Vanvitelli, Italy
Tommaso Lazzarin	University of Padua, Italy
Francesco Tajani	Sapienza University of Rome, Italy
Claudia Amadei	University of Padua, Italy
Isabella Maria Lami	Politecnico di Torino, Italy
Federico Vagnon	Politecnico di Torino, Italy
Francesca Torrieri	Politecnico di Milano, Italy
Elena De Angelis	Politecnico di Torino, Italy
Piergiorgio Farfariello	Politecnico di Torino, Italy
Francesca Biondi	Politecnico di Torino, Italy
Giulio Cavana	Politecnico di Torino, Italy
Fabiana Forte	Università della Campania Luigi Vanvitelli, Italy
Siyu Qiu	University of Bologna, Italy
Eugenio Muccio	University of Naples Federico II, Italy
Iuliia Kozlova	University of Bologna, Italy
Danny Casprini	Politecnico di Milano, Italy
Franco Corti	University of Padua, Italy
Elisa Sbardella	Politecnico di Torino, Italy
Andrea Sarcina	Università di Padova, Italy
Daniela Menna	Università degli studi della Campania Luigi Vanvitelli, Italy
Sebastiano Barbieri	Politecnico di Torino, Italy
Ana Soares	University of Minho, Portugal
Francesco Sica	Sapienza University of Rome, Italy
Chiara D'Alpaos	University of Padua, Italy
Alessandra Oppio	Politecnico di Milano, Italy
Maria Rosaria Guarini	Sapienza University of Rome, Italy
Alessia Crisopulli	Politecnico di Milano, Italy
Elisabetta Colucci	Politecnico di Torino, Italy

Giorgia Sugoni	Links Foundation, Italy
Lucia Petronio	University of Bologna, Italy
Marco Alvise Bragadin	University of Bologna, Italy

Computational Mechanics, Intelligence, and Data (MIND 2026)

Workshop Organizers

Lelio Campanile	Università degli Studi della Campania Luigi Vanvitelli, Italy
Renato Zona	Università della Campania Vanvitelli, Italy

Workshop Program Committee Members

Vincenzo Minutolo	Università degli Studi della Campania Luigi Vanvitelli, Italy
Fiammetta Marulli	University of Campania Luigi Vanvitelli, Italy
Simone Palladino	Università degli Studi della Campania Luigi Vanvitelli, Italy
Ali Forooghi	University of Campania Luigi Vanvitelli, Italy
Mario Argenziano	University of Palermo, Italy
Donato Perfetto	University of Campania Luigi Vanvitelli, Italy

Modelling Liveable Cities: Techniques, Methods, Challenges, and Perspectives Behind the X-Minute City (MLC 2026)

Workshop Organizers

Federico Mara	University of Pisa, Italy
Valerio Cutini	University of Pisa, Italy

Workshop Program Committee Members

Beniamino Murgante	University of Basilicata, Italy
Chiara Garau	University of Cagliari, Italy
Francesco Zullo	University of LAquila, Italy
Alessandro Marucci	University of L Aquila, Italy
Chiara Di Dato	University of L Aquila, Italy
Giampiero Lombardini	University of Genoa, Italy

Alfonso Annunziata	University of Basilicata, Italy
Simone Corrado	University of Basilicata, Italy
Müslüm Hacar	Yildiz Technical University, Turkey
Federica Deri	University of Pisa, Italy
Chiara Anselmi	University of Pisa, Italy

Mathematical Methods for Image Processing and Understanding 2026 (MMIPU 2026)

Workshop Organizers

Ivan Gerace	Università degli Studi di Perugia, Italy
Gianluca Vinti	Università degli Studi di Perugia, Italy
Arianna Travaglini	Lucian Blaga University of Sibiu, Romania

Workshop Program Committee Members

Marco Baioletti	University of Perugia, Italy
Marco Donatelli	University of Insubria, Italy
Muhammad Hanif	Ghulam Ishaq Khan Institute of Engineering Sciences and Technology, Pakistan
Francesco Marchetti	University of Padua, Italy
Wolfgang Erb	Università degli Studi di Padua, Italy
Ana Maria Acu	Lucian Blaga University of Sibiu, Romania
Simone Rebegoldi	University of Modena and Reggio Emilia, Italy
Valentina Giorgetti	Università degli Studi di Perugia, Italy
Vita Leonessa	University of Basilicata, Italy

MOdels and indicators for assessing and measuring the urban settlement deVElopment in the view of NET ZERO by 2050 (MOVEto0 2026)

Workshop Organizers

Lorena Fiorini	University of L'Aquila, Italy
Lucia Saganeiti	Institute of Methodologies for Environmental Analysis (IMAA) CNR, Italy
Angela Pilogallo	Institute of Methodologies for Environmental Analysis (IMAA) CNR, Italy

Francesco Zullo	University of L'Aquila, Italy
Alessandro Marucci	University of L'Aquila, Italy

Workshop Program Committee Members

Ginevra Balletto	University of Cagliari, Italy
Giuseppe Borruso	University of Trieste, Italy
Chiara Garau	University of Cagliari, Italy
Beniamino Murgante	University of Basilicata, Italy
Ljiljana Zivkovic	Republic Geodetic Authority, Serbia
Luigi Santopietro	Institute of Methodologies for Environmental Analysis National Research Council of Italy CNR IMAA, Italy
Ilaria Delponte	University of Genoa, Italy
Carmen Guida	Università degli Studi di Napoli Federico II, Italy
Chiara Di Dato	University of L'Aquila, Italy

Numerical Aspects in Machine Learning For Dynamical Systems (NAMLYS 2026)

Workshop Organizers

Pasquale De Luca	Parthenope University of Naples, Italy
Livia Marcellino	University of Naples Parthenope, Italy
Valeria Mele	University of Naples Federico II, Italy

Workshop Program Committee Members

Dario Caramiello	University of Naples Parthenope, Italy
Giuseppe Fiorillo	Parthenope University of Naples, Italy
Marco Lettiero	University of Naples Parthenope, Italy
Francesco Peluso	University of Naples Parthenope, Italy

Numerical Methods and Machine Learning in Science & Engineering (NMLSE 2026)

Workshop Organizers

Cecília Coelho	Helmut Schmidt University, Germany
M. Fernanda P. Costa	University of Minho, Portugal

Luís Ferrás	University of Minho, Portugal
Eliana Costa e Silva	Polytechnic of Porto, Portugal

Workshop Program Committee Members

Osvaldo Gramaxo de Freitas	Universitat de València, Spain
Estela Bicho	University of Minho, Portugal
Flora Ferreira	University of Porto, Portugal
Bruno Veloso	Universidade do Porto, Portugal
Luís Louro	University of Minho, Portugal
Weronika Wojtak	CCG/ZGDV Institute, Portugal
Wolfram Erlhagen	University of Minho, Portugal

6th Workshop on Privacy in the Cloud/Edge/IoT World 2026 (PCEIoT 2026)

Workshop Organizers

Lelio Campanile	Università degli Studi della Campania Luigi Vanvitelli, Italy
Mauro Iacono	Università degli Studi della Campania Luigi Vanvitelli, Italy
Michele Mastroianni	University of Foggia, Italy

Workshop Program Committee Members

Fiammetta Marulli	University of Campania Luigi Vanvitelli, Italy
Christian Riccio	Università degli Studi della Campania Luigi Vanvitelli, Italy
Arcangelo Castiglione	University of Salerno, Italy
Gianni D'Angelo	University of Salerno, Italy
Biagio Boi	University of Salerno, Italy
Luigi Piero Di Bonito	Università degli Studi della Campania, Italy

Preserving Our Past: Spatial and Remote Sensing Technologies for Cultural Heritage in a Changing Climate (POP 2026)

Workshop Organizers

Maria Danese	Institute of Heritage Science of the National Research Council of Italy (CNR ISPC), Italy
Rosa Lasaponara	Institute of Methodologies for Environmental Analysis (CNR IMAA), Italy
Nicola Masini	Institute of Heritage Science of the National Research Council of Italy (CNR ISPC), Italy

Workshop Program Committee Members

Dario Gioia	Institute of Heritage Science of the National Research Council of Italy (CNR ISPC), Italy
Marilisa Biscione	Institute of Heritage Science of the National Research Council of Italy (CNR ISPC), Italy
Valentina Florio	CNR, Italy
Antonio Minervino Amodio	Institute of Heritage Science of the National Research Council of Italy (CNR ISPC), Italy

Scientific Computing Infrastructure (SCI 2026)

Workshop Organizers

Vladimir Korkhov	Saint Petersburg State University, Russia
Elena Stankova	Saint Petersburg State University, Russia

Workshop Program Committee Members

Adam Belloum	University of Amsterdam, The Netherlands
Dmitrii Vasiunin	Deutsche Telekom Cloud Services E.P.E., Greece
Serob Balyan	Institute for Informatics and Automation Problems, National Academy of Sciences of Armenia, Armenia
Suren Abrahamyan	Institute for Informatics and Automation Problems of NAS RA, Armenia
Ashot Gevorkyan	Institute for Informatics and Automation Problems NAS of Armenia, Armenia

Michal Hnatič	P.J. Šafárik University in Košice, Slovak Republic
Martin Vala	Pavol Jozef Šafárik University, Slovak Republic
Nodir Zaynalov	Samarkand Branch of Tashkent University of Information Technologies Named After Muhammad al Khwarizmi, Uzbekistan
Michail Panteleyev	Saint Petersburg Electrotechnical University, Russia
Alexander Degtyarev	Saint Petersburg State University, Russia
Alexander Bogdanov	St. Petersburg State University, Russia
Nataliia Kulabukhova	AutoTech, Russia
Alexander Degtyarev	St.Petersburg State University, Russia
Alexander Bogdanov	St. Petersburg State University, Russia

Socio-Economic and Environmental Models for Land Use Management (SEMLUM 2026)

Workshop Organizers

Debora Anelli	Sapienza University of Rome, Italy
Pierluigi Morano	Polytechnic University of Bari, Italy
Francesco Tajani	Sapienza University of Rome, Italy
Felicia Di Liddo	Polytechnic University of Bari, Italy

Workshop Program Committee Members

Benedetto Manganelli	Università degli Studi della Basilicata, Italy
Emma Sabatelli	Sapienza Università di Roma, Italy
María Paz Sáez-Pérez	University of Granada, Spain
Yasmine Selim	Ain Shams University, Egypt
Daniela Tavano	University of Calabria, Italy
Francesco Calabrò	Mediterranea University of Reggio Calabria, Italy
Pierfrancesco De Paola	University of Naples Federico II, Italy
Francesco Paolo Del Giudice	University of Rome La Sapienza, Italy
Paola Amoruso	LUM Giuseppe Degennaro University, Italy
Rubina Canesi	Università degli Studi di Padova, Italy
Daniele La Rosa	University of Catania, Italy
Giuseppe Cerullo	Sapienza University of Rome, Italy
Antonella Roma	Sapienza University of Rome, Italy
Francesca Fariello	Sapienza University of Rome, Italy

Ports and logistics of the future - Smartness and Sustainability (SmartPorts 2026)

Workshop Organizers

Andrea Gallo	Università degli Studi di Trieste, Italy
Giuseppe Borruso	University of Trieste, Italy
Gianfranco Fancello	University of Cagliari, Italy
Veronica Camerada	Università degli studi di Sassari, Italy
Clara Di Fazio	University of Trieste, Italy

Workshop Program Committee Members

Patrizia Serra	University of Cagliari, Italy
Francesco Bruzzone	Università Iuav di Venezia, Italy
Marco Mazzarino	University Iuav of Venice, Italy
Maria del Mar Munoz	University of Cádiz, Spain
Ainhoa Amaro	EVOCONS, Spain
Brunella Brundu	University of Sassari, Italy
Giovanni Mauro	University of Campania Luigi Vanvitelli, Italy
Maria Ronza	University of Naples Federico II, Italy
Marcello Tadini	Università del Piemonte Orientale, Italy
Luca Toneatti	University of Trieste, Italy
Mara Ladu	University of Cagliari, Italy
Ginevra Balletto	University of Cagliari, Italy
Francesca Sinatra	University of Trieste, Italy

Sustainable evolution of long-Distance frEight and paSsenger Transport (SOLIDEST 2026)

Workshop Organizers

Antonio Russo	University of Enna Kore, Italy
Giuseppe Musolino	Università Mediterranea di Reggio Calabria, Italy
Socrates Basbas	Aristotle University of Thessaloniki, Greece
Oana Dinu	National University of Science and Technology Politehnica Bucharest, Romania
Sanja Šurdonja	University of Rijeka, Croatia
Elen Twrdy	University of Ljubljana, Slovenia

Workshop Program Committee Members

Tiziana Campisi	University of Enna Kore, Italy
Massimo Di Gangi	Università di Messina, Italy
Antonio Polimeni	Università di Messina, Italy
Efstathios Bouhouras	Aristotle University of Thessaloniki, Greece
Florin Rusca	National University of Science and Technology Politehnica Bucharest, Romania
Vittorio Astarita	University of Calabria, Italy
Giuseppe Guido	Università della Calabria, Italy
Stefanos Tsigdinos	National Technical University of Athens, Greece
Chiara Garau	University of Cagliari, Italy

Sustainability Performance Assessment: Models, Approaches, and Applications Toward Interdisciplinary and Integrated Solutions (SPA 2026)

Workshop Organizers

Francesco Scorza	University of Basilicata, Italy
Sabrina Lai	University of Cagliari, Italy
Jolanta Dvarioniene	Kaunas University of Technology, Lithuania
Michele Campagna	University of Cagliari, Italy

Workshop Program Committee Members

Corrado Zoppi	University of Cagliari, Italy
Maria Cerreta	University of Naples Federico II, Italy
Giuseppe Borruso	University of Trieste, Italy
Chiara Garau	University of Cagliari, Italy
Ginevra Balletto	University of Cagliari, Italy
Alenka Poplin	Iowa State University, USA
Francesco Zullo	University of L'Aquila, Italy
Alessandro Marucci	University of L'Aquila, Italy
Federica Leone	University of Cagliari, Italy
Simone Corrado	University of Basilicata, Italy
Alfonso Annunziata	University of Basilicata, Italy
Rachele Vanessa Gatto	Università della Basilicata, Italy
Francesco Paolo Del Giudice	University of Basilicata, Italy

Specifics of smart cities development in Europe (SPEED 2026)

Workshop Organizers

Chiara Garau	University of Cagliari, Italy
Katarína Vitálišová	Matej Bel University, Slovak Republic
Marco Fanfani	University of Florence, Italy
Anna Vaňová	Matej Bel University, Slovak Republic
Kamila Borsekova	Matej Bel University, Slovak Republic
Paola Zamperlin	University of Pisa, Italy

Workshop Program Committee Members

Francesca Maltinti	University of Cagliari, Italy
Silvia Rossetti	Università degli Studi di Parma, Italy
Carmen Guida	Università degli Studi di Napoli Federico II, Italy
Floriana Zucaro	University of Naples Federico II, Italy
Giovanna Concu	University of Cagliari, Italy
Paolo Nesi	University of Florence, Italy
Pierfrancesco Bellini	University of Florence, Italy
Gerardo Carpentieri	University of Naples Federico II, Italy
Radoslav Kožiak	Matej Bel University, Slovak Republic
Lucia Dobrotová	Matej Bel University in Banská Bystrica, Slovak Republic
Veronika Piscová	Institute of Landscape Ecology Slovak Academy of Sciences, Slovak Republic
Darina Rojíková	Matej Bel University, Slovak Republic
Katarína Sýkorová	Matej Bel University, Slovak Republic
Silvia Ondrejičková	Comenius University Bratislava, Slovak Republic
Vladimír Ondrejička	Comenius University Bratislava, Slovak Republic
Maros Finka	Comenius University Bratislava, Slovak Republic
Jan Nevima	Masaryk University, Czech Republic
Christian Corral Burau	Leibniz University Hannover, Germany
Kamila Turečková	Silesian University in Opava, Czech Republic
Luciano Alessandro Ipsaro Palesi	University of Florence, Italy
Enrico Collini	University of Florence, Italy
Gianni Pantaleo	University of Florence, Italy
Krishnamoorthy Ranganathan	Chennai Institute of Technology, India

Smart, Safe, and Health Cities (SSHC 2026)

Workshop Organizers

Chiara Garau	University of Cagliari, Italy
Gerardo Carpentieri	University of Naples Federico II, Italy
Carmen Guida	Università degli Studi di Napoli Federico II, Italy
Martina Carra	University of Brescia, Italy
Vincenza Torrisi	University of Catania, Italy
Silvia Rossetti	Università degli Studi di Parma, Italy

Workshop Program Committee Members

Romano Fistola	University of Naples Federico II, Italy
Francesca Maltinti	University of Cagliari, Italy
Barbara Caselli	Università degli Studi di Parma, Italy
Tiziana Campisi	University of Enna Kore, Italy
Katarína Sýkorová	Matej Bel University, Slovak Republic
Tazyeen Alam	Università degli Studi di Cagliari, Italy
Francesco Zullo	University of L'Aquila, Italy
Giovanna Concu	University of Cagliari, Italy
Anastasia Stratigea	National Technical University of Athens, Greece
Ezio Riggi	National Research Council, Italy
Miriam Distefano	CNR, Italy

Smart and Sustainable Island Communities (SSIC 2026)

Workshop Organizers

Chiara Garau	University of Cagliari, Italy
Anastasia Stratigea	National Technical University of Athens, Greece
Yiota Theodora	National Technical University of Athens, Greece
Giovanna Concu	University of Cagliari, Italy
Tiziana Campisi	University of Enna Kore, Italy
Tanja Congiu	University of Sassari, Italy

Workshop Program Committee Members

Francesca Maltinti	University of Cagliari, Italy
Mauro Coni	University of Cagliari, Italy
Paola Zamperlin	University of Florence, Italy

Tarek Teba	University of Portsmouth, UK
Gerardo Carpentieri	University of Naples Federico II, Italy
Floriana Zucaro	University of Naples Federico II, Italy
Roberto Minunno	Curtin University, Australia
Apostolos Lagarias	University of Thessaly, Greece
Giuseppina Vacca	University of Cagliari, Italy
Carmen Guida	Università degli Studi di Napoli Federico II, Italy
Tazyeen Alam	Università degli Studi di Cagliari, Italy
Mauro D'Apuzzo	University of Cassino and Southern Lazio, Italy
Mana Dastoum	Polytechnic University of Madrid, Spain
Alfonso Annunziata	University of Basilicata, Italy
Barbara Caselli	Università degli Studi di Parma, Italy
Silvia Rossetti	Università degli Studi di Parma, Italy
Gian Felice Giaccu	University of Sassari, Italy
Anastasia Stratigea	National Technical University of Athens, Greece
Vincenza Torrisi	University of Catania, Italy

Sustainable Tourism Economy, Silk Road, Reuse and Enhancement of Cultural Heritage (STESilkRoad 2026)

Workshop Organizers

Celestina Fazia	Università di Enna Kore, Italy
Alexandru Ilies	University of Oradea, Romania
Dorina Camelia Ilies	University of Oradea, Romania
Cristina Natoli	Ministero dell'Ambiente e della Sicurezza Energetica, Italy
Bahodirhon Safarov	Samarkand Branch of Tashkent State University of Economics, Uzbekistan
Clara Stella Vicari Aversa	Università degli Studi Mediterranea di Reggio Calabria, Italy

Workshop Program Committee Members

Giulia Fernanda Grazia Catania	Università di Enna Kore, Italy
Federica Sortino	Università degli Studi di Enna Kore, Italy
Thowayeb Hassan	King Faisal University, Saudi Arabia
Tatar Corina	University of Oradea, Romania
Maria Francesca Faro	Ministry of Education and Merit (MIM), Italy

Theoretical and Computational Chemistry and its Applications (TCCM 2026)

Workshop Organizers

Noelia Faginas Lago	Università di Perugia, Italy
Andrea Lombardi	Università di Perugia, Italy
Marcos Mandado Alonso	University of Vigo, Spain

Workshop Program Committee Members

Jose Manuel Hermida Ramon	Universidade de Vigo, Spain
Luca Mancini	University of Perugia, Italy
Stefano Falcinelli	University of Perugia, Italy
Ángel Martín Pendás	Universidad de Oviedo, Spain
Enrique M. Cabaleiro Lago	Universidade de Santiago de Compostela, Spain
Giacomo Giorgi	Università degli Studi di Perugia, Italy
Stefano Evangelisti	Université de Toulouse, France
Nicolás Ramos Berdullas	University of Vigo, Spain
Juan José Nogueira	Universidad Autónoma de Madrid, Spain
Giacomo Pannacci	Università degli Studi di Perugia, Italy

Transport Infrastructures for Smart Cities (TISC 2026)

Workshop Organizers

Francesca Maltinti	University of Cagliari, Italy
Mauro Coni	University of Cagliari, Italy
Chiara Garau	University of Cagliari, Italy
Benedetto Barabino	University of Brescia, Italy
Nicoletta Rassu	Università di Cagliari, Italy
James Rombi	University of Cagliari, Italy

Workshop Program Committee Members

Tiziana Campisi	University of Enna Kore, Italy
Mauro D'Apuzzo	University of Cassino and Southern Lazio, Italy
Roberto Ventura	Università degli Studi di Brescia, Italy
Roberto Minunno	Curtin University, Australia

Giovanna Concu	University of Cagliari, Italy
Claudia Loggia	University of KwaZulu-Natal, South Africa

Transforming Urban Analytics: The Impact of Crowdsourced Mapping and Advanced AI Techniques on Future Cities (Tr-UrbAna 2026)

Workshop Organizers

Ayse Giz Gulnerman Gengec	Ankara Hacı Bayram Veli University, Turkey
Müslüm Hacar	Yildiz Technical University, Turkey

Workshop Program Committee Members

Beniamino Murgante	University of Basilicata, Italy
Abdulkadir Memduhoğlu	Harran University, Turkey
Zeynel Abidin Polat	Izmir Katip Celebi University, Turkey
Güzide Miray Perihanoglu	Van Yuzuncu Yil University, Turkey
Tugba Memisoglu Baykal	Hacı Bayram Veli University, Turkey
Federico Mara	University of Pisa, Italy
Himmet Karaman	Istanbul Technical University, Turkey
Özge Öztürk Hacar	Yildiz Technical University, Turkey

From structural to TRAnsformative-change of City Environment: challenges & solutions & perspectives (TRACE 2026)

Workshop Organizers

Maria Rosaria Guarini	Sapienza University of Rome, Italy
Pierluigi Morano	Polytechnic University of Bari, Italy
Francesco Sica	Sapienza University of Rome, Italy
Alejandro Segura	Universidad Politécnica de Madrid, Spain
Yilsy María Nuñez Guerrero	Universidad Politécnica de Madrid, Spain

Workshop Program Committee Members

Maria Cerreta	University of Naples Federico II, Italy
Francesco Scorza	University of Basilicata, Italy

Francesco Calabrò	Mediterranea University of Reggio Calabria, Italy
Felicia Di Liddo	Polytechnic University of Bari, Italy
Marco Locurcio	Polytechnic University of Bari, Italy
Valeria Saiu	University of Cagliari, Italy
Lucia Della Spina	University Mediterranea of Reggio Calabria, Italy
Fabrizio Battisti	University of Florence, Italy
Giuseppe Cerullo	Sapienza University of Rome, Italy
Fabiana Forte	Università della Campania Luigi Vanvitelli, Italy
Marta Dell'Ovo	Politecnico di Milano, Italy
Cristina Coscia	Politecnico di Torino, Italy
Debora Anelli	Sapienza University of Rome, Italy

Urban Artificial Intelligence for Modelling, Analysis & Planning (Urban plAnnIng 2026)

Workshop Organizers

Chiara Garau	University of Cagliari, Italy
Romano Fistola	University of Naples Federico II, Italy
Beniamino Murgante	University of Basilicata, Italy
Dessislava Petrova Antonova	Sofia University, GATE Institute, Bulgaria
Gianni Pantaleo	University of Florence, Italy
Rosa Anna La Rocca	University of Naples Federico II

Workshop Program Committee Members

Paola Zamperlin	University of Florence, Italy
Francesco Zullo	University of L'Aquila, Italy
Gerardo Carpentieri	University of Naples Federico II, Italy
Luciano Alessandro Ipsaro Palesi	University of Florence, Italy
Tazyeen Alam	Università degli Studi di Cagliari, Italy
Reza Askarizad	University of Cagliari, Italy
Mana Dastoum	Polytechnic University of Madrid, Spain
Alfonso Annunziata	University of Basilicata, Italy

Urban Space Accessibility and Mobilities (USAM 2026)

Workshop Organizers

Chiara Garau	University of Cagliari, Italy
Alessandro Plaisant	University of Sassari, Italy
Barbara Caselli	Università degli Studi di Parma, Italy
Mauro D'Apuzzo	University of Cassino and Southern Lazio, Italy
Francesco Pinna	University of Cagliari, Italy
Silvio Nocera	IUAV University of Venice, Italy

Workshop Program Committee Members

Mauro Coni	University of Cagliari, Italy
Martina Carra	University of Brescia, Italy
Tiziana Campisi	University of Enna Kore, Italy
Reza Askarizad	University of Cagliari, Italy
Giuseppe Cappelli	University of Cassino and Southern Lazio, Italy
Floriana Zucaro	University of Naples Federico II, Italy
Gerardo Carpentieri	University of Naples Federico II, Italy
Youssef El Ganadi	International University of Rabat, Morocco
Yiota Theodora	National Technical Univeristy of Athens, Greece
Silvia Rossetti	Università degli Studi di Parma, Italy
Aime Tsinda	University of Rwanda, Rwanda
Paola Zamperlin	University of Florence, Italy
Luciano Alessandro Ipsaro Palesi	University of Florence, Italy
Tazyeen Alam	Università degli Studi di Cagliari, Italy
Mariano Pernetti	Università della Campania Luigi Vanvitelli, Italy
Salvatore Leonardi	University of Catania, Italy
Francesco Galante	University of Naples Federico II, Italy

Virtual Reality, Augmented Reality and Applications (VRA 2026)

Workshop Organizers

Damiano Perri	University of Perugia, Italy
Osvaldo Gervasi	University of Perugia, Italy
Paolo Nesi	University of Florence, Italy

Workshop Program Committee Members

Taihoon Kim	Chonnam National University, South Korea
JungYoon Kim	Gachon University, South Korea
David Berti	ART SpA, Italy

Workshop on Advanced and Computational Methods for Earth Science applications (WACM4ES 2026)

Workshop Organizers

Luca Piroddi	University of Cagliari, Italy
Patrizia Caprizzi	University of Palermo, Italy
Marilena Cozzolino	Università del Molise, Italy
Giuseppina Vacca	University of Cagliari, Italy
Luigi Capozzoli	Hydrogeosite Laboratory of CNR-IMAA, Italy
Nikos Papadopoulos	Foundation for Research and Technology Hellas, Greece

Workshop Program Committee Members

Sebastiano D'Amico	University of Malta, Malta
Enrica Vecchi	University of Cagliari, Italy
Donatella Rita Fiorino	Università degli Studi di Cagliari, Italy
Chiara Garau	University of Cagliari, Italy
Emanuele Colica	University of Malta, Malta
Raffaele Martorana	Università di Palermo, Italy
Raffaele Persico	Università della Calabria, Italy
Andrea Angelini	Institute of Heritage Science of the National Research Council of Italy (CNR ISPC), Italy
Paolo Mauriello	Università del Molise, Italy
Dedalo Marchetti	Italian National Institute of Geophysics and Volcanology, Italy
Veronica Pazzi	University of Florence, Italy
Agnese Innocenti	University of Florence, Italy
Maurizio Ercoli	University of Perugia, Italy
Luciano Galone	University of Malta, Malta
Amr Abd El-Raouf	Zagazig University, Egypt
Peter Iregbeyen	University of Malta, Malta
Pietro Milillo	University of Houston, USA
Tommaso Beni	University of Florence, Italy

Cristiano Fidani	Central Italy Electromagnetic Network, Italy
Deodato Tapete	Italian Space Agency (ASI), Italy
Enzo Rizzo	University of Ferrara, Italy
Guido Luzi	Centre Tecnològic de Telecomunicacions de Catalunya, Spain
Sina Saneiyan	Binghamton University, USA
Alex Sendrós	Universitat de Barcelona, Spain
Mercedes Solla	Universidade de Vigo, Spain
Alessandra Carollo	University of Palermo, Italy
Andrea Vergnano	Università di Torino, Italy
Giorgio Alaia	Università di Perugia, Italy
Giorgio De Donno	Sapienza University of Rome, Italy
Samuel Bignardi	University of Chieti and Pescara, Italy
Athos Agapiou	Cyprus University of Technology, Cyprus
Gregory Tsokas	Aristotle University of Thessaloniki, Greece
Alexandru Hegyi	Oslo University, Norway
Ilaria Barone	Università degli Studi di Padova, Italy
Yuan Qi	University of Hong Kong, China
Carmen Cuenca García	Universitat de València, Spain
Ilaria Catapano	Institute for Electromagnetic Sensing of the Environment (IREA) CNR, Italy
Mariano Lisi	University of Basilicata, Italy
Adrien Dimech	École de Technologie Supérieure, Canada
Davide Campo	Independent Researcher, UK
Chiara Torre	University of Malta, Malta
Anna Forte	University of Bologna, Italy
Adam Gauci	University of Malta, Malta
Vittoria Borghese	TNO, The Netherlands
Andrea Scianna	Institute for High Performance Computing and Networking (ICAR) CNR, Italy
Maria Antonia Brovelli	Politecnico di Milano, Italy
Pietro Milillo	University of Houston, USA
Gregory Tsokas	Aristotle University of Thessaloniki, Greece

Sponsoring Organizations

ICCSA 2026 would not have been possible without tremendous support from many organizations and institutions, for which all organizers and participants of ICCSA 2026 express their sincere gratitude:

Universidade do Minho
Escola de Engenharia

University of Minho, Portugal (https://www.uminho.pt/)

University of Perugia, Italy (https://www.unipg.it)

University of Basilicata, Italy (http://www.unibas.it)

University of Cagliari, Italy (https://unica.it/)

Monash University, Australia (https://www.monash.edu/)

Kyushu Sangyo University, Japan (https://www.kyusan-u.ac.jp/)

Venue

ICCSA 2026 took place at: **the University of Minho campus:**
Campus de Gualtar
4710-057 Braga
Portugal

Additional Reviewers

Amr Abd Elraouf	Zagazig University, Egypt
Lidia Aceto	Università del Piemonte Orientale, Italy
Ana Maria Acu	Lucian Blaga University of Sibiu, Romania
Vera Afreixo	University of Aveiro, Portugal
Akif Akgul	Hitit University, Turkey
Sania Akhtar	Ghulam Ishaq Khan Institute of Engineering Sciences and Technology, Pakistan
Giorgio Alaia	Università di Perugia, Italy
Tazyeen Alam	Università degli Studi di Cagliari, Italy
Arnulfo Alanis	Tecnológico Nacional de México, Mexico
Sandra Aleixo	University of Lisbon, Portugal
Earl Ryan Aleluya	Mindanao State University Iligan Institute of Technology, Philippines
Muhammad Junaid Ali	Université de Haute Alsace, France
Filipe Alvelos	Universidade do Minho, Portugal
Claudia Amadei	University of Padua, Italy
Paulo Amorim	Escola de Matemática Aplicada da Fundação Getulio Vargas, Brazil
Ana Paula Amorim	Universidade do Minho, Portugal
Paola Amoruso	LUM Giuseppe Degennaro University, Italy
Debora Anelli	Sapienza University of Rome, Italy
Mariarosaria Angrisano	Pegaso University, Italy
Alfonso Annunziata	University of Basilicata, Italy
Chiara Anselmi	Università di Pisa, Italy
Shigeyoshi Aoyama	KEK, Japan
Tatsumi Aoyama	University of Tokyo, Japan
Bernady O. Apduhan	Kyushu Sangyo University, Japan
Pablo Luiz Araujo Munhoz	Federal University of Ouro Preto, Brazil
Muhammad Waqas Arshad	University of Bologna, Italy
Daniela Ascenzi	Università degli Studi di Trento, Italy
Laura Ascione	Università degli Studi di Napoli Federico II, Italy
Reza Askarizad	University of Cagliari, Italy
Vanessa Assumma	University of Bologna, Italy
Vittorio Astarita	University of Calabria, Italy
Maria Fernanda Augusto	BITrum Research Center, Spain
Asja Aulisio	Politecnico di Torino, Italy
Samat Baigereyev	D. Serikbayev East Kazakhstan Technical University, Kazakhstan
Marco Baioletti	University of Perugia, Italy
Sara Balderas Díaz	University of Cádiz, Spain

Ginevra Balletto	University of Cagliari, Italy
Serob Balyan	Institute for Informatics and Automation Problems, National Academy of Sciences of Armenia, Armenia
Benedetto Barabino	University of Brescia, Italy
Sebastiano Barbieri	Politecnico di Torino, Italy
Ilaria Barone	Università degli Studi di Padova, Italy
Alice Barreca	Politecnico di Torino, Italy
Socrates Basbas	Aristotle University of Thessaloniki, Greece
Rosaria Battarra	Consiglio Nazionale delle Ricerche, Italy
Silvia Battino	University of Sassari, Italy
Fabrizio Battisti	University of Florence, Italy
Patricia Beites	University of Beira Interior, Portugal
David Berti	Art Spa, Italy
Samuel Bignardi	University of Chieti and Pescara, Italy
Francesco Bimbo	University of Foggia, Italy
Francesca Biondi	Politecnico di Torino, Italy
Marilisa Biscione	CNR, Italy
Alexander Bogdanov	St. Petersburg State University, Russia
Biagio Boi	University of Salerno, Italy
Alessandro Bombini	Istituto Nazionale di Fisica Nucleare, Italy
Ana Borges	Instituto Politécnico do Porto, Portugal
Vittoria Borghese	TNO, The Netherlands
Giuseppe Borruso	University of Trieste, Italy
Kamila Borsekova	Matej Bel University, Slovak Republic
Efstathios Bouhouras	Aristotle University of Thessaloniki, Greece
Ana Cristina Braga	University of Minho, Portugal
Diego Brandão	Federal Center for Technological Education of Rio de Janeiro, Brazil
Maria Antonia Brovelli	Politecnico di Milano, Italy
Francesco Bruzzone	Università Iuav di Venezia, Italy
Francesca Buglione	CNR ISPC, Italy
Enrique M. Cabaleiro Lago	Universidade de Santiago de Compostela, Spain
Francesco Calabrò	Mediterranea University of Reggio Calabria, Italy
Rogerio Calazan	Instituto de Estudos do Mar Almirante Paulo Moreira - Brazilian Navy, Brazil
Lelio Campanile	Università degli Studi della Campania Luigi Vanvitelli, Italy
Tiziana Campisi	University of Enna Kore, Italy
Dario Campisi	University of Perugia, Italy
Rubina Canesi	Università degli Studi di Padova, Italy
Alessandra Capolupo	Polytechnic University of Bari, Italy

Caterina Caprioli	Politecnico di Torino, Italy
Dario Caramiello	University of Naples Parthenope, Italy
Gerardo Carpentieri	University of Naples Federico II, Italy
Martina Carra	University of Brescia, Italy
Barbara Caselli	Università degli Studi di Parma, Italy
Danny Casprini	Politecnico di Milano, Italy
Arcangelo Castiglione	University of Salerno, Italy
Giulia Fernanda Grazia Catania	Università di Enna Kore, Italy
Ilaria Catapano	CNR IREA, Italy
Laura Cavalcante	Instituto Superior de Engenharia do Porto, Portugal
Giulio Cavana	Politecnico di Torino, Italy
Valeria Cera	University of Naples Federico II, Italy
Maria Cerreta	University of Naples Federico II, Italy
Giuseppe Cerullo	Sapienza University of Rome, Italy
Daniele Cesini	CNAF, INFN, Italy
Kai Cheng	Kyushu Sangyo University, Japan
Giuseppe Ciciriello	University Of Naples Federico II, Italy
Birol Ciloglugil	Ege University, Turkey
Cecília Coelho	Helmut Schmidt University, Germany
Enrico Collini	University of Florence, Italy
Luís Conceicao	Instituto Superior de Engenharia do Porto, Portugal
Giovanna Concu	University of Cagliari, Italy
Tatar Corina	University of Oradea, Romania
Alejandro Cornejo	Universitat Politècnica de Catalunya, Spain
Simone Corrado	University of Basilicata, Italy
Florbela Correia	Polytechnic Institute of Viana do Castelo, Portugal
Franco Corti	University of Padua, Italy
Cristina Coscia	Politecnico di Torino, Italy
Lino Costa	University of Minho, Portugal
Eliana da Costa e Silva	Polytechnic Institute of Porto, Portugal
Alessandro Costantini	INFN, Italy
Alessia Crisopulli	Politecnico di Milano, Italy
Valerio Cutini	University of Pisa, Italy
Mauro D'Apuzzo	University of Cassino and Southern Lazio, Italy
Hiroshi Daisaka	Hitotsubashi University, Japan
Sebastiano Damico	University of Malta, Malta
Maria Danese	CNR ISPC, Italy
Gianni Dangelo	University of Salerno, Italy
Mana Dastoum	Polytechnic University of Madrid, Spain

Giulia Datola	Politecnico di Milano, Italy
Regina De Almeida	University of Trás-os-Montes and Alto Douro, Portugal
Elena De Angelis	Politecnico di Torino, Italy
Elise de Doncker	Western Michigan University, USA
Pasquale De Luca	Parthenope University of Naples, Italy
Luiza De Macedo Mourelle	State University of Rio de Janeiro, Brazil
Pierfrancesco De Paola	University of Naples Federico II, Italy
Alexander Degtyarev	St.Petersburg State University, Russia
Francesco Paolo Del Giudice	University of Basilicata, Italy
Piera Della Morte	Pegaso Telematic University, Italy
Federico Dellanna	Politecnico di Torino, Italy
Marta Dellovo	Politecnico di Milano, Italy
Federica Deri	Università di Pisa, Italy
Francesco Di Capua	University of Basilicata, Italy
Clara Di Fazio	University of Trieste, Italy
Gabriella Di Genova	Università degli Studi di Perugia, Italy
Benedetta Di Leo	Università Politecnica delle Marche, Italy
Felicia Di Liddo	Polytechnic University of Bari, Italy
Joana Dias	University of Coimbra, Portugal
Oana Dinu	National University of Science and Technology Politehnica Bucharest, Romania
Lucia Dobrotová	Matej Bel University in Banská Bystrica, Slovak Republic
Edda Donati	University of Rome Tor Vergata, Italy
Aziz Dursun	Virginia Tech University, USA
Zahra Ebadi Ansaroudi	Fondazione Bruno Kessler, Italy
Maurizio Ercoli	University of Perugia, Italy
Dario Esposito	Polytechnic University of Bari, Italy
Noelia Faginas Lago	Università di Perugia, Italy
Maria Irene Falcao	University of Minho, Portugal
Stefano Falcinelli	University of Perugia, Italy
Marco Fanfani	University of Florence, Italy
Marcos Farias	Instituto de Engenharia Nuclear, Brazil
Francesca Fariello	Sapienza University of Rome, Italy
Maria Francesca Faro	Ministry of Education and Merit (MIM), Italy
Eslam Farsimadan	University of Salerno, Italy
Sara Favargiotti	University of Trento, Italy
Celestina Fazia	Università di Enna Kore, Italy
Maksims Feofilovs	Riga Technical University, Latvia
Florbela P. Fernandes Cedri	Instituto Politecnico de Bragança, Portugal
Paula Odete Fernandes	Instituto Politecnico de Bragança, Portugal

Flora Ferreira	University of Porto, Portugal
Maddalena Ferretti	Università Politecnica delle Marche, Italy
Luís Ferrás	University of Porto, Portugal
Massimo Ficco	University of Salerno, Italy
Maros Finka	Masaryk University, Slovak Republic
Ugo Fiore	University of Salerno, Italy
Lorena Fiorini	University of L'Aquila, Italy
Romano Fistola	University of Naples Federico II, Italy
Beatriz Flamia Azevedo	Instituto Politecnico de Bragança, Portugal
Valentina Florio	CNR, Italy
Ali Forooghi	University of Campania Luigi Vanvitelli, Italy
Anna Forte	University of Bologna, Italy
Grigorios Fountas	Aristotle University of Thessaloniki, Greece
Andreas Fricke	Hasso Plattner Institute for Digital Engineering, University of Potsdam, Germany
Luigi Fusco Girard	Pegaso Telematic University, Italy
Francesco Galante	University of Naples Federico II, Italy
Stefano Galassi	University of Florence, Italy
Andrea Gallo	Università degli Studi di Trieste, Italy
Chiara Garau	University of Cagliari, Italy
Gustavo Gatica	Universidad Andrés Bello, Chile
Rachele Vanessa Gatto	Università della Basilicata, Italy
Ivan Gerace	Università degli Studi di Perugia, Italy
Amal Gerges	University of Cagliari, Italy
Osvaldo Gervasi	University of Perugia, Italy
Tasnim Gharaibeh	Kalamazoo College, USA
Gian Felice Giaccu	University of Sassari, Italy
Dario Gioia	CNR ISPC, Italy
Luca Giommi	INFN CNAF, Italy
Valentina Giorgetti	Università degli Studi di Perugial, Italy
Giacomo Giorgi	Università degli Studi di Perugia, Italy
Hiago Mayk Gomes De Araújo Rocha	National Laboratory for Scientific Computing, Brazil
Omar Gomez	Universidad Nacional de Colombia, Colombia
A. Manuela Goncalves	University of Minho, Portugal
Joaquim Goncalves	Polytechnic Institute of Cávado and Ave, Portugal
Pedro Henrique Gonzalez	Federal University of Rio de Janeiro, Brazil
Yusuke Gotoh	Okayama University, Japan
Osvaldo Gramaxo De Freitas	Universitat de València, Spain
Antonia Gravagnuolo	National Research Council Italy (CNR) Institute of Heritage Science, Italy

Teresa Guarda	Universidad Estatal Península De Santa Elena, Ecuador
Maria Rosaria Guarini	Sapienza University of Rome, Italy
Raphael Guerra	Universidade Federal Fluminense, Brazil
Hélia Guerra	University of the Azores, Portugal
Gabriel Guerrero Contreras	University of Cádiz, Spain
Carmen Guida	Università degli Studi di Napoli Federico II, Italy
Eligius Hendrix	Universidad de Málaga, Spain
Jose Manuel Hermida Ramon	Universidade de Vigo, Spain
Antonino Iannuzzo	Universitá degli Studi del Sannio, Italy
Luciano Alessandro Ipsaro Palesi	University of Florence, Italy
Issaku Kanamori	Riken, Japan
Yeliz Karaca	UMass Chan Medical School and Massachusetts Institute of Technology, USA
Himmet Karaman	Istanbul Technical University, Turkey
Tatyana Khachkova	IPGG SB RAS, Russia
Jungyoon Kim	Gachon University, South Korea
Vladimir Korkhov	Saint Petersburg State University, Russia
Iuliia Kozlova	University of Bologna, Italy
Radoslav KožIak	Matej Bel University, Slovak Republic
Ludovica La Rocca	University of Naples Federico II, Italy
Rosa Anna La Rocca	University of Naples Federico II, Italy
Adnane Labbaci	Ibn Tofail University, Morocco
Sabrina Lai	University of Cagliari, Italy
Giuseppe Francesco Cesare Lama	University of Naples Federico Ii, Italy
Isabella Maria Lami	Politecnico di Torino, Italy
Salvatore Leonardi	University of Catania, Italy
Federica Leone	University of Cagliari, Italy
Vita Leonessa	University of Basilicata, Italy
Barbara Lino	Università degli Studi di Palermo, Italy
Vadim Lisitsa	Institute of Petroleum Geology and Geophysics SB RAS, Russia
Marco Locurcio	Polytechnic University of Bari, Italy
Andrea Lombardi	Università di Perugia, Italy
Cristina Lopes	Polytechnic Institute of Porto, Portugal
Isabel Lopes	Instituto Politécnico de Bragança, Portugal, Italy
Rui Pedro Lopes	Instituto Politécnico de Bragança, Portugal
Nicolas Lori	University of the Azores, Portugal
Luís Louro	University of Minho, Portugal
Jader Lugon Junior	Instituto Federal Fluminense, Brazil
Guido Luzi	Centre Tecnològic de Telecomunicacions de Catalunya, Spain

Antonio S. Macias	University of A Coruña, Spain
Daniela Maiullari	Delft University of Technology, The Netherlands
Robert Makin	Western Michigan University, USA
Giorgia Malavasi	Politecnico di Torino, Italy
Francesca Maltinti	University of Cagliari, Italy
Luca Mancini	University of Perugia, Italy
Marcos Mandado Alonso	University of Vigo, Spain
Benedetto Manganelli	Università degli Studi della Basilicata, Italy
Federico Mara	University of Pisa, Italy
Livia Marcellino	University of Naples Parthenope, Italy
Dedalo Marchetti	INGV, Italy
Francesco Marchetti	University of Padua, Italy
Alessandra Marra	University of Salerno, Italy
Barbara Martelli	INFN, Italy
Valerio Martinelli	Università degli Studi di Napoli Federico II, Italy
Ángel Martín Pendás	Universidad de Oviedo, Spain
Alessandra Mascitelli	University of Chieti Pescara, Italy
Michele Mastroianni	University of Foggia, Italy
Luís Miguel Matos	Universidade do Minho, Portugal
Hideo Matsufuru	High Energy Accelerator Research Organization, Japan
Luis Mazon	BITrum Research Group, Spain
Beatrice Mecca	Politecnico di Torino, Italy
Valeria Mele	University of Naples Federico II, Italy
Abdulkadir Memduhoğlu	Harran University, Turkey
Joao Mendes	Instituto Politecnico de Braganca, Portugal
Luis Mendes Gomes	University of the Azores, Portugal
Paolo Mengoni	Hong Kong Baptist University, China
Daniela Menna	Università degli Studi della Campania Luigi Vanvitelli, Italy
Antonio Minervino Amodio	CNR ISPC, Italy
Roberto Minunno	Curtin University, Australia
Fernando Miranda	Universidade do Minho, Portugal
Andrea Montanino	International Centre for Numerical Methods in Engineering, Spain
Andrea Montanino	University of Naples Parthenope, Italy
Ana Monteiro	University of Coimbra, Portugal
Leila Moradi	University of Salerno, Italy
Joao Morais	ITAM, Mexico
Filipe Mota Pinto	Instituto Politécnico de Leiria, Portugal
Ricardo Moura	NOVA University of Lisbon, Portugal

Maria Mourao	Polytechnic Institute of Viana do Castelo, Portugal
Eugenio Muccio	University of Naples Federico II, Italy
Beniamino Murgante	University of Basilicata, Italy
Giuseppe Musolino	Università Mediterranea di Reggio Calabria, Italy
Naohito Nakasato	University of Aizu, Japan
Isabel Natário	Nova University of Lisbon, Portugal
Nadia Nedjah	State University of Rio de Janeiro, Brazil
Grazia Neglia	Pegaso Telematic University, Italy
Paolo Nesi	University of Florence, Italy
Keigo Nitadori	Riken, Japan
Juan José Nogueira	Universidad Autónoma de Madrid, Spain
Mikhail Novikov	Sobolev Institute of Mathematics SB RAS, Russia
Yilsy María Nuñez Guerrero	Universidad Politécnica de Madrid, Spain
Ana Oliveira	Academia Militar, Portugal
Carlo Olivieri	Pegaso University, Italy
Vladimír Ondrejička	Comenius University in Bratislava, Slovak Republic
Beniamino Onorati	Università degli Studi della Basilicata, Italy
Fabian Bernal Orozco Barrera	UNAM, Mexico
M. Fernanda P. Costa	University of Minho, Portugal
António Pacheco	Instituto Superior Técnico, Portugal
Emerson Paiva	University of Minho, Portugal
Simone Palladino	Università degli Studi della Campania L. Vanvitelli, Italy
Francesco Palmieri	University of Salerno, Italy
Simona Panaro	University of Sussex Business School, UK
Claudia Panciera	IRSA CNR, Italy
Giacomo Pannacci	Università degli Studi di Perugia, Italy
Gianni Pantaleo	University of Florence, Italy
Eric Pardede	La Trobe University, Australia
Rosaria Parente	Universitas Mercatorum, Italy
Vittorio Paris	University of Bergamo, Italy
Luca Parodi	University of Genoa, Italy
Rui Pascoal	University of Coimbra, Portugal
Hugo Peixoto	University of Minho, Portugal
Francesco Peluso	University of Naples Parthenope, Italy
Ana Pereira	Polytechnic Institute of Bragança, Portugal
Amina Pereno	Politecnico di Torino, Italy
Martin Perez Perez	University of Vigo, Spain
Donato Perfetto	University of Campania Luigi Vanvitelli, Italy
Güzide Miray Perihanoglu	Van Yuzuncu Yil University, Turkey

Mariano Pernetti	Università della Campania Luigi Vanvitelli, Italy
Damiano Perri	University of Perugia, Italy
Pasquale Perrini	Consorzio Interuniversitario per l'Idrologia, Italy
Raffaele Persico	Università della Calabria, Italy
Lucia Petronio	University of Bologna, Italy
Rossella Petti	Politecnico di Bari, Italy
Francesco Picariello	Universitas Mercatorum, Italy
Angela Pilogallo	IMAA CNR, Italy
Natalia Pingaro	Politecnico di Milano, Italy
Telmo Miguel Pires Pinto	University of Minho, Portugal
Veronika Piscová	Institute of Landscape Ecology, Slovak Academy of Sciences, Slovak Republic
Zeynel Abidin Polat	Izmir Katip Celebi University, Turkey
Giuliano Poli	Università di Napoli Federico II, Italy
Antonio Polimeni	Università di Messina, Italy
Maurizio Pollino	ENEA, Italy
Mohammad Pourfouladi	Politecnico di Milano, Italy
Dmitry Prokhorov	IPGG SB RAS, Russia
Faiza Qamar	National University of Sciences and Technology, Pakistan
Yuan Qi	University of Hong Kong, China
Siyu Qiu	University of Bologna, Italy
Arunasalam Rahunanthan	Central State University, USA
Joelmir Ramos	Universidade do Estado do Rio de Janeiro, Brazil
Bruna Ramos	University of Minho, Portugal
Nicolás Ramos Berdullas	University of Vigo, Spain
Krishnamoorthy Ranganathan	Chennai Institute of Technology, India
Nicoletta Rassu	Università di Cagliari, Italy
Roberta Ravanelli	University of Liège, Belgium
Michela Ravanelli	Sapienza Università di Roma, Italy
Manuela Rebaudengo	Politecnico di Torino, Italy
Simone Rebegoldi	University of Modena and Reggio Emilia, Italy
Pier Francesco Recchi	Università di Napoli Federico II, Italy
Rommel Regis	Saint Joseph's University, USA
Marco Reis	University of Coimbra, Portugal
James Rhodes	Western Michigan University, USA
Luigi Maciel Ribeiro	State University of Rio de Janeiro, Brazil
Corrado Rindone	Università degli Studi Mediterranea di Reggio Calabria, Italy
Ana Maria A. C. Rocha	Universidade do Minho, Portugal
Humberto Rocha	University of Coimbra, Portugal
Carlos Rodrigues	Instituto Politécnico de Bragança, Portugal

Ivan Rodriguez Conde	University of Arkansas at Little Rock, USA
Darina Rojíková	Matej Bel University, Slovak Republic
Diana Rolando	Politecnico di Torino, Italy
Antonella Roma	Sapienza University of Rome, Italy
James Rombi	University of Cagliari, Italy
Elisabetta Ronchieri	INFN CNAF, Italy
Marzio Rosi	University of Perugia, Italy
Silvia Rossetti	Università degli Studi di Parma, Italy
Marco Rossitti	Politecnico di Milano, Italy
Florin Rusca	National University of Science and Technology Politehnica Bucharest, Romania
Yvonne Russo	University of Campania L. Vanvitelli, Italy
Antonio Russo	University of Enna Kore, Italy
Ana Sofia Rézio	Polytechnic Institute of Lisbon, Portugal
Emma Sabatelli	Sapienza Università di Roma, Italy
Matteo Sacchet	University of Turin, Italy
Sabrina Sacco	University of Naples Federico II, Italy
Lucia Saganeiti	Institute of Methodologies for Environmental Analysis, National Research Council, Italy
Valeria Saiu	University of Cagliari, Italy
Francesco Santini	University of Perugia, Italy
Rafael Santos	National Institute for Space Research (INPE), Brazil
Edcarllos Santos	Universidade Federal do Sul da Bahia, Brazil
Valentino Santucci	Università per Stranieri di Perugia, Italy
Andrea Sarcina	Università di Padova, Italy
Ilaria Scarcelli	Politecnico di Bari, Italy
Andrea Scianna	National Research Council of Italy, Italy
Francesco Scorza	University of Basilicata, Italy
Ester Scotto Di Perta	University of Naples Federico II, Italy
Alejandro Segura	Universidad Politécnica de Madrid, Spain
Yasmine Selim	Ain Shams University, Egypt
Ines Sena Cedri	Instituto Politécnico de Bragança and University of Minho, Portugal
Alex Sendrós	Universitat de Barcelona, Spain
Ricardo Severino	University of Minho, Portugal
Mojtaba Sharifzadeh	Università di Trento, Italy
Luigi Sibille	Norwegian University of Science and Technology, Norway
Francesco Sica	Sapienza University of Rome, Italy
Adriano Silva	Instituto Politecnico de Bragança, Portugal
Angela Silva	Universidade do Minho, Portugal

Paula Simões	Military Academy, Portuguese Army, Portugal
Francesca Sinatra	University of Trieste, Italy
Mercedes Solla	Universidade de Vigo, Spain
Sergey Solovyev	Sobolev Institute of Mathematics SB RAS, Russia
Maria Somma	University of Naples Federico II, Italy
Federica Sortino	Università degli Studi di Enna Kore, Italy
Eleonora Sottile	University of Cagliari, Italy
Martina Spinelli	Politecnico di Torino, Italy
Elena Stankova	Saint Petersburg State University, Russia
Alexandra Stankulova	Politecnico di Torino, Italy
Giorgia Sugoni	Links Foundation, Italy
Katarína Sýkorová	Matej Bel University, Slovak Republic
Francesco Tajani	Sapienza University of Rome, Italy
Deodato Tapete	Italian Space Agency (ASI), Italy
Rodrigo Tapia-McClung	Centro de Investigación en Ciencias de Información Geoespacial, Mexico
Maria Tartari	CNR, Italy
Daniela Tavano	University of Calabria, Italy
Tarek Teba	University of Portsmouth, UK
Ana Paula Teixeira	Universidade do Minho, Portugal
Wagner Telles	Universidade Federal Fluminense, Brazil
Luis Teodoro	University of Oslo, Norway
Maria Filomena Teodoro	Instituto Superior Técnico, Portugal
Yiota Theodora	National Technical University of Athens, Greece
Elena Todella	University of Parma, Italy
Graca Tomaz	Instituto Politécnico da Guarda, Portugal
Chiara Torre	University of Malta, Malta
Francesca Torrieri	Politecnico di Milano, Italy
Vincenza Torrisi	University of Catania, Italy
Arianna Travaglini	Lucian Blaga University of Sibiu, Romania
Stefanos Tsigdinos	National Technical University of Athens, Greece
Kamila Turečková	Silesian University in Opava, Czech Republic
Elen Twrdy	University of Ljubljana, Slovenia
Toshihiro Uchibayashi	Kyushu University, Japan
Takahiro Ueda	Juntendo University, Japan
Generoso Vaiano	Pegaso University, Italy
Aleksandar Valjarević	University of Belgrade, Serbia
Gianmarco Vanuzzo	University of Perugia, Italy
Dmitrii Vasiunin	Deutsche Telekom Cloud Services E.P.E., Greece
Mohammad Vazir Panah	University of Salerno, Italy
Anna Vaňová	Matej Bel University, Slovak Republic
Enrica Vecchi	University of Cagliari, Italy

Roberto Ventura	Università degli Studi di Brescia, Italy
Ferdinando Verardi	Pegaso Telematic University, Italy
Clara Stella Vicari Aversa	Università degli Studi Mediterranea di Reggio Calabria, Italy
Gianluca Vinti	Università degli Studi di Perugia, Italy
Katarína Vitálišová	Matej Bel University, Slovak Republic
Weronika Wojtak	CCG/ZGDV Institute, Portugal
Fukuko Yuasa	KEK, Japan
Madina Yussubaliyeva	D. Serikbayev East Kazakhstan Technical University, Kazakhstan
Paola Zamperlin	University of Florence, Italy
Francisco Zayas Gato	Universidade da Coruña, Spain
Nodir Zaynalov	Samarkand Branch of Tashkent University of Information Technologies Named After Muhammad Al Khwarizmi, Uzbekistan
Ljiljana Zivkovic	Republic Geodetic Authority, Serbia
Piero Zizzania	University of Naples Federico II, Italy
Renato Zona	Università della Campania L. Vanvitelli, Italy
Floriana Zucaro	University of Naples Federico II, Italy
Francesco Zullo	University of L'Aquila, Italy
Giovanni Zurlo	INFN CNAF, Italy
Özge Öztürk Hacar	Yildiz Technical University, Turkey
Isidora Đurić	University of Novi Sad, Serbia

Plenary Lectures

Digital Twins for Cities – The Rise of the Socio-Technical System

Claudia van der Laag

Department of Built Environment, Oslo Metropolitan University, Norway

Abstract. Cities are entering a new era in which digital twins are no longer simply technical replicas of urban systems, but evolving socio-technical infrastructures that shape how cities are planned, governed, and experienced. Across the world, urban digital twins are being adopted to address some of the most pressing challenges of our time — climate adaptation, urban resilience, mobility transitions, decarbonisation, infrastructure management, and inclusive governance. Yet as these technologies become increasingly sophisticated, a fundamental question emerges: can digital twins truly support more democratic and human-centred cities, or will they reinforce existing structures of power and expertise? In this keynote, Claudia van der Laag explores the transformation of urban digital twins from data-driven modelling tools into collaborative platforms for urban decision-making and societal change. It argues that the future of digital twins lies not only in advances in artificial intelligence, real-time data integration, simulation, and predictive analytics, but equally in the ability to connect technological innovation with governance, participation, and human agency. Drawing on emerging international research and practical case studies, the keynote examines the complex ecosystem surrounding urban digital twins, bringing together planners, policymakers, researchers, technologists, and communities. It highlights how digital twins increasingly function as meeting points between multiple forms of knowledge — technical, political, social, and experiential — and why interdisciplinary collaboration is essential for their success. The talk critically reflects on the tensions between technological ambition and civic inclusion, exploring themes such as transparency, interoperability, participation, and trust. It also discusses how digital twins can become powerful environments for scenario exploration, urban experimentation, and collective learning, enabling cities to better navigate uncertainty and complexity in an age of rapid urban transformation. Ultimately, this keynote presents a vision of digital twins not as neutral technological systems, but as living socio-technical infrastructures capable of reshaping urban governance itself. The challenge ahead is therefore not only how accurately cities can be modelled, but how inclusively they can be imagined, negotiated, and governed through these emerging digital environments.

Prescriptive AI in Practice: Bridging Optimisation, Generative AI and Agentic Decision-Making

Bernardo Almada-Lobo

Universidade do Porto, Faculdade de Engenharia, INESC TEC, Portugal

Abstract. Prescriptive AI, viewed through the lens of mathematical optimisation and operations research, addresses complex business decision-making problems involving limited resources, multiple decision options and competing objectives. This talk considers the full decision pipeline: problem framing, model formulation, computational solution, implementation, monitoring and organisational adoption. The practical success of prescriptive AI depends less on algorithmic sophistication alone than on the quality of the translation between real-world decision contexts and formal optimisation models. In practice, this translation remains a major bottleneck. Objectives are often ambiguous, constraints are incomplete or tacit, data may be fragmented, and the operational consequences of a recommendation may be poorly understood. As a result, optimisation projects can fail even when the underlying mathematical model is technically sound. The talk will address the persistent gap between optimisation theory and deployment practice. While optimisation has generated substantial value in domains such as supply chain planning, logistics, production, revenue management, workforce planning and inventory control, many initiatives still face a significant risk of under-delivery. Common failure modes include incorrect problem framing, weak data readiness, brittle assumptions, infeasible or non-actionable recommendations, limited explainability, insufficient ownership by business users and inadequate post-deployment monitoring. Closing this gap requires moving from one-off model building to an operational lifecycle in which models are stress-tested, embedded in workflows, monitored for drift and revised as the business environment changes. Recent developments in generative and agentic AI create new opportunities to reduce these barriers. Generative AI can support the elicitation of decision-maker preferences, the structuring of unstructured operational knowledge, the drafting of candidate formulations and the explanation of model outputs in business language. Agentic AI can extend this role by orchestrating multi-step workflows that involve model formulation, solver-code generation, execution, debugging, infeasibility diagnosis, sensitivity analysis and human review. However, these capabilities should not be interpreted as replacing optimisation expertise. Rather, they create a new interface between human judgement, analytical modelling and computational decision support. This talk will discuss a cross-fertilisation agenda between optimisation, generative AI and agentic AI, with a focus on how these technologies should be calibrated to the decision at hand.

Net-Zero Communities through Life Cycle Thinking: Canadian Lessons and Global Implications

Kasun Hewage

School of Engineering (Okanagan Campus), Clean Energy Research Centre (CERC), University of British Columbia (UBC), Canada

Abstract. This keynote presentation discusses how life cycle thinking supports the transformation of communities toward sustainable, resilient, and net-zero futures. Drawing on Canadian research, practice, and policy experience, the presentation highlights how integrated life cycle approaches can move beyond conventional carbon accounting to inform practical decision-making across buildings, infrastructure, energy systems, waste management, water systems, and industrial processes [1–8]. The keynote features research conducted at the Life Cycle Management Laboratory (LCML) at the University of British Columbia, Canada, an internationally recognized research hub led by Kasun Hewage. LCML brings together engineers, scientists, policy researchers, postdoctoral fellows, visiting scholars, and graduate researchers to translate data-intensive sustainability research into actionable climate solutions. The laboratory's work is organized around six interconnected research themes: energy systems, urban development, water systems, waste management, construction and asset management, and industrial processes and products. Together, these themes provide an integrated platform for advancing life cycle–based pathways to net-zero communities. Supported by strong partnerships with government, industry, and community stakeholders, LCML has contributed to a substantial body of applied sustainability research, including more than 400 journal articles, 100 conference papers, and numerous technical reports that have informed real-world planning and implementation. This keynote presentation highlights selected success stories that demonstrate how life cycle thinking can be translated into practical strategies for reducing environmental impacts while strengthening community resilience. These insights are especially relevant to the interdisciplinary focus of ICCSA 2026.

References

1. Weerasinghe, O., Hewage, K., Razi, F., Fatmi, M., Sadiq, R.: Applicability of land use models for sustainable urban planning: a review. J. Urban Plann. Dev. ASCE, **151**(3) (2025). https://doi:10.1061/JUPDDM.UPENG-5705

2. Sultana, S. R., et al.: Looking beyond energy efficiency targets: life cycle sustainability of mechanical and water heating equipment in Canadian homes. J. Clean. Prod. Elsevier, **473**, 143469 (2024). https://doi.org/10.1016/j.jclepro.2024.143469
3. Liyanage, D. R., Hewage, K., Hussain, S. H., Razi, F., Sadiq, R.: Climate adaptation of existing buildings: a critical review on planning energy retrofit strategies for future climate. Renew. Sustain. Energy Rev. Elsevier, **199**, 114476 (2024). https://doi.org/10.1016/j.rser.2024.114476
4. Liyanage, D. R., Hewage, K., Karunathilake, H., Sadiq, R.: Feasibility of carbon-capturing in building heating systems: a life cycle thinking-based approach. International J. Greenhouse Gas Control. Elsevier, **132** (2023). https://doi.org/10.1016/j.ijggc.2023.104056
5. Moudgil, V., Sadiq, R., Bakhtavar, E., Paudel, A., Hewage, K.: A cloud-oriented data-analysis framework to analyze peak demand dynamics in institutional building clusters. Sustain. Cities Soci. Elsevier, **111**, 105553 (2024). https://doi.org/10.1016/j.scs.2024.105553
6. Liyanage, D. R., Hewage, K., Ghobadi, M., Sadiq, R.: Thermal resiliency of single-family housing stock under extreme hot and cold conditions. Energy Build. Elsevier, **323**, 114809 (2024). https://doi.org/10.1016/j.enbuild.2024.114809
7. Wijayasekera, S. C., et al.: Sustainability of waste-to-hydrogen conversion pathways: a life cycle thinking-based assessment. Energy Convers. Manage. Elsevier, **270** (2022). https://doi.org/10.1016/j.enconman.2022.116218
8. Jayasena, A., Hewage, K., Siddiqui, O., Sadiq, R.: Socio-economic and environmental cost-benefit analysis of passive houses: a life cycle perspective. J. Clean. Prod. Elsevier, **373** (2022). https://doi.org/10.1016/j.jclepro.2022.133718

Machine Learning Based Methodologies for Grape and Wine Production

Pedro Melo-Pinto

University of Trás-os-Montes and Alto Douro, Engineering Department, Centre for the Research and Technology of Agro-Environmental and Biological Sciences, Portugal

Abstract. Wine production is a major area in the Portuguese economy. The sector accounts for approximately 2.6% of Portugal's GDP, and is crucial to the development of inland regions. Wine quality depends on grape quality, which is a result of different factors such as harvesting at the optimal point of maturity, or selecting the grapes according to quality features. The growing importance of precision agriculture demands novel methods to make the most out of the data generated. Machine learning approaches are particularly suitable for modelling complex processes, where too many arguments are involved. Many of the agricultural processes such as yield estimation or ripening fall into this category. However, several challenges may arise: even if models are available for particular cases, general models are difficult to come by, largely due to the high variability involved; with such models, there is a need for huge amounts of data, in a way which will not always be easy to obtain. This is particularly true in the case of grape production and the wine industry, where the number of grape varieties, climate, soil, etc., introduce a degree of variability that is uncommon in other sectors. One way of obtaining more information in such cases has been the use of images, whether RGB, multi-spectral, or hyperspectral. The use of images introduces additional challenges, such as data size and lighting conditions, which underscores the need for data-driven modelling methodologies. The use of machine learning (ML) techniques combined with images has been establishing itself as a viable alternative for predicting yields or quality parameters in grapes, and assisting with critical harvesting decisions. Several ML approaches have been proposed to handle such data characteristics, but selecting a suitable methodology that best addresses the problem under study and making sure it generalizes well is, most of the time, a cumbersome task. We will address three wine and grape production problems, yield estimation, grape quality assessment, and illness detection, presenting different difficulties. Yield estimation is a major aspect in the wine production industry. The number of berries is one of the most relevant yield aspects, and can be estimated using computer vision, namely image segmentation algorithms. Lighting is one of the key factors in computer vision approaches, and occlusions—which are common in this problem—can be minimized, but require estimation models to achieve reliable results. Early illness detection is, of course, of the utmost importance, with an impact on production and quality. Detecting early symptoms and distinguishing them from other conditions is a difficult task, which makes the use of machine learning algorithms advisable, using automatic visual inspection of the leaves, addressed as a pixel-based classification problem. However, the available datasets are limited and

complex to compile, as different diseases typically require very specific time-frames and locations. The use of generative models to overcome this obstacle, in conjunction with robust classification models, leads to models that are intended to be as general as possible. The evaluation of the grape's maturation profile based on the evolution of their oenological parameters over time is one of the most important aspects for ensuring wine quality, playing a decisive role in the definition of the optimal time for harvesting. The use of hyperspectral imaging combined with learning algorithms represents a faster and non-destructive grape ripeness assessment method. We focus in two fundamental aspects to address the resulting data variability: a possible wavelength bands selection (with the purpose of reducing the dimensionality of data without losing predictive power) and the generalization ability of the ML model under such demanding conditions.

Contents

Bio and Neuro Inspired Computing and Applications (BIONCA 2026)

Rescaling for Area Coverage in Swarm Robotics 3
Nadia Nedjah, Luiza de Macedo Mourelle, and Luneque Del Rio de Souza e Silva Junior

Breast Nodule Detection and Classification Using Convolutional Neural Network with Transfer Learning 22
Flávia Telles, Luiza de Macedo Mourelle, and Nadia Nedjah

Computational Methods for Porous Materials (CompPor 2026)

Stabilized Finite Element Framework for Transient Darcy–Brinkman–Forchheimer Flow Under Local Thermal Non-equilibrium 39
Rafael C. Moura, Isaac P. Santos, and Lucia Catabriga

Applicability of NDM-Net Simulated Data to Prestack Depth Migration 58
Elena Gondyul, Valeria Dubrovina, Vadim Lisitsa, and Dmitry Vishnevsky

3D NDM-Net Training Dataset Construction 70
Elena Gondyul, Vadim Lisitsa, and Dmitry Vishnevsky

Numerical Homogenization of 2D Heterogeneous Anisotropic Porous Medium Based on a Hyperbolic Thermodynamically Compatible Model 84
Galina Reshetova and Evgeniy Romenski

Influence of Wettability on Electrical Parameters Based on Numerical Simulation Results of Drainage and Imbibition in Digital Rock 98
Tatyana Khachkova and Vadim Lisitsa

Evaluating Inner Areas Potentials (EIAP 2026)

Undertourism and Physical, Social and Economic Sustainability. The *ECHE Lab Approach* to Evaluate the Cultural Tourism Sustainability in the Inner Areas 113
Rosa Maria Staropoli, Giovanna Emanuela Minniti, and Francesco Calabrò

Inner Areas and Territorial Marginality in Europe: Different Policy Responses to a Common Challenge 129
Ludovica Nasca and Maria Rosa Trovato

Short-Term Rentals in Rural Areas: Sustainable Tourism Perspectives Artificial within the SYSTOUR Project 148
Roberta Butticè, Asja Aulisio, Giorgia Malavasi, and Diana Rolando

Reinforcing Local Safety Ecosystems: Integrating the "Signal for Help" Detection in Urban and Inner Territories 162
Federico Buccellato, Sarah Azimi, Corrado De Sio, and Luca Sterpone

Co-Visioning Valsesia: Towards an Implementable Territorial Roadmap for Agri-food Short Supply Chains 177
Diana Rolando, Alice Barreca, Giorgia Malavasi, and Manuela Rebaudengo

Territorial Inequalities in Real Estate Markets' Flood Resilience: Evidence from the Forlì-Cesena Province (Italy) 194
Alessia Crisopulli, Marco Rossitti, and Francesca Torrieri

Designing Experiential Tourism Strategies in Rural Areas: A Systemic and Data-Driven Framework 206
Sara De Menech, Asja Aulisio, Silvia Barbero, and Alice Barreca

Sustainable Mobility and Last MIle LogisTic in Urban Context (ELLIOT 2026)

An Exploratory Analysis of Injury Severities in Crashes Involving Vulnerable Road Users: Evidence from Thessaloniki, Greece 227
Stavros Kontorinis, Athanasios Demiris, Grigorios Fountas, and Socrates Basbas

Who Owns the Space? A Near-Accident Perception of e-Scooters Riders in Interaction with Pedestrians 242
Argyrios Kalisperatos, Paraskevas Nikolaou, Andreas Nikiforiadis, Fountas Grigorios, Campisi Tiziana, and Basbas Socrates

From Anxious Rushers to Attentive Observers: A Cluster Analysis of University Student Pedestrian Profiles 256
Efstathios Bouhouras, Grigorios Fountas, Socrates Basbas, Panagiotis Giapitzoglou, Stefanos Tsouggaris, Georgios Zois, and Erlind Gishti

A Logical Framework Approach to the Monitoring of an Emergency Evacuation Exercise for an Urban Transport System 272
Corrado Rindone and Antonio Russo

Assessing the Potential of Demand Responsive Transit for Non-Emergency Healthcare Travel: An Accessibility-Based Approach 284
Antonio Russo, Tiziana Campisi, and Giovanni Tesoriere

Econometrics and Multidimensional Evaluation in Urban Environment (EMEUE 2026)

Pricing the Tide: The Effect of the Mo.S.E. System on the Venetian Residential Market 301
Pietro Bonifaci, Sergio Copiello, and Aurora Peloso

When Prices Exceed Expectations: An Empirical Analysis of Overbidding in the Swedish Housing Market 316
Benedetto Manganelli, Francesco Paolo Del Giudice, Pierfrancesco De Paola, Francesco Tajani, and Beatrice Manganelli

The Fair Exchange: Public-Private Agreements for Zoning Variances in Local Town Planning 334
Sergio Copiello, Alessandra Bacco, Ida Zelbi, and Pietro Bonifaci

Unveiling Human-Flood Governance Interlinkages from Forensic Investigations 351
Edda Donati and Fernando Nardi

Economic Feasibility of Vacant Public Housing Reuse: A Financial Valuation Model for Socially Sustainable Regeneration in Historic Urban Contexts 365
Ida Zelbi, Pietro Bonifaci, Carlo Grillenzoni, and Sergio Copiello

Assessing the Liveability in the European Metropolitan Cities by Interpreting the Property Markets 380
Federico Stara, Giuseppe Cerullo, Francesco Sica, and Francesco Tajani

Beyond Linear Impact: A Nonlinear Theory of Change and a Six-Level Indicator System for Evaluating Culture-Led Regeneration in Left-behind Territories 394
Giulia Candeloro, Alessandro Crociata, and PierLuigi Sacco

Ecosystem Services in Spatial Planning for Climate Neutral Urban and Rural Areas (ESSP 2026)

Urban Climate Adaptation in Naples: An Integrated Framework for Flood Risk, Urban Heat Island, and Nature-Based Intervention Planning 413
Carmela Gargiulo, Tonia Stiuso, Floriana Zucaro, Francesco Pugliese, Giuseppe Speranza, and Vincenzo Scarano

Mapping Gaps: Evidence-Based Analysis of Urban Emissions Trends and Climate Commitment in Major Italian Cities 429
Laura Ascione, Carmela Gargiulo, and Carmen Guida

Mapping Spatial Synergies and Trade-Offs: A Geographically Weighted Analysis of Ecosystem Services and Carbon Sequestration in Southern Italy ... 445
Federica Isola, Bilge Kobak, Sabrina Lai, Francesca Leccis, Federica Leone, and Corrado Zoppi

The 16th International Workshop on Future Information System Technologies and Applications (FiSTA 2026)

VM-Based Power Management for Embedded Multicore Systems 465
Kazuaki Tanaka, Hayato Tsuru, Ko-ichiro Sugiyama, and R. Krishnamoorthy

Two-Stage Pavement Distress Detection and Classification Using UAV Imagery in Unstructured Road Environments 479
Earl Ryan Aleluya, Melody Mae Maluya, Francis Jann Alagon, Edward Rowe Aleluya, and Carl John Salaan

Geographical Analysis, Urban Modeling, Spatial Statistics (Geog-And-Mod 2026)

Mitigating Weight Explosion in Rare-Feature Co-location Pattern Mining: A Cauchy Distribution-Based Approach 493
Vanhiep Duong, Vanthuc Nguyen, Xuankhang Pham, Thanhduy Pham, and Vanha Tran

Multi-model Data Warehouse for Multidimensional Analysis of Flavescence Dorée: Application to the Bordeaux Region 509
Sandro Bimonte, Fagniné Alassane Coulibaly, Frederic Fabre, Sylvie Malembic-Maher, and Stefano Rizzi

Spatial Assessment of PM10 Concentrations and Population Exposure in the Emilia-Romagna Region (Italy): A Geostatistical Approach 526
Beatrice Manganelli, Rachele Vanessa Gatto, Simone Corrado, and Benedetto Manganelli

Water Quality Predictors for Harmful Algal Blooms Occurrence in the Mississippi Sound, USA 542
Vladimir J. Alarcon, Paul F. Mickle, and Ruben A. Alvarado

Machine Learning Algorithms for Statistical Spatial Analysis of Waste Collection in an Italian Region 557
Gabriella Schoier and Giuseppe Borruso

Spatially Targeting the Expansion of Agricultural Land in a Mountainous Catchment for Maximal Sediment Export Avoidance: Heuristic Optimization Considering Spatial Interaction 568
Pablo Vanegas-Peralta, René Estrella, Geovanny García, Marcelo Peñafiel, Patricia Cazorla, Elina Ávila-Ordóñez, Grethell Castillo-Reyes, Gerdys Jiménez-Moya, Dirk Roose, and Jos Van Orshoven

Possible Relationships Between the Spread of Tourism and Urban Zoning 586
Francesco Rotondo, Paola Perchinunno, and Samuela L'Abbate

Generative and Neuro-Symbolic Artificial Intelligence for Real-World Systems (GNS-AI 2026)

Extracting Models of Dynamic Human Health Behaviour from Real-Life Personal Health Data 601
Afonso Sarmento and José Machado

Data-Driven Hospital Scheduling: A Multi-criteria Evaluation of Algorithmic Approaches 619
Rafael Amorim, Afonso Lobo, João Lopes, Tiago Guimarães, Júlio Duarte, and Manuel Filipe Santos

Supporting Hospital Operational Decision-Making Through Early Prediction of Length of Stay 631
Matilde Sousa, João Lopes, Tiago Guimarães, Agostinho Barbosa, and Manuel Filipe Santos

Lightweight Multi-sensor Modeling for Virtual Braking-Force Sensing 644
Mariana Fernandes, Mariana Almeida, Hugo Baptista, Suelma Pina, Ricardo Teixeira, Tiago Vale, Cristiana Neto, Diana Ferreira, Tiago Aston, Carlos Ferreira, Nuno M. C. da Costa, José Machado, Susana Bulas Cruz, and Hugo Peixoto

Author Index 663

Bio and Neuro Inspired Computing and Applications (BIONCA 2026)

Rescaling for Area Coverage in Swarm Robotics

Nadia Nedjah[1(✉)], Luiza de Macedo Mourelle[2], and Luneque Del Rio de Souza e Silva Junior[3]

[1] Department of Electronics Engineering and Telecommunications, State University of Rio de Janeiro, Rio de Janeiro, Brazil
nadia@eng.uerj.br

[2] Department of Systems Engineering and Computation, State University of Rio de Janeiro, Rio de Janeiro, Brazil
ldmm@eng.uerj.br

[3] Departamento de Information Engineering, Federal University of the ABC, São Paulo, Brazil
luneque.junior@ufabc.edu.br

Abstract. Swarm robotics studies collective behaviors in systems composed of multiple robots. In this work, a message wave strategy is used in which the swarm operates as a network of robots that interact through wireless communication. A distributed message wave algorithm is designed for use in robot swarms and serves as a foundation for controlling different collective tasks. This work introduces a general methodology that provides a systematic approach to task execution in robotic swarms. Using this methodology, control strategies for the well-known area coverage problem are proposed, implemented, and evaluated through simulation, focusing on rescaling behaviors such as aggregation and dispersion. Experimental results show that the time required to complete these tasks depends on the swarm size, message propagation, and the specific characteristics of each task. The design and execution of these tasks serve as a proof of concept for the proposed strategy, demonstrating its generality and potential applicability to a wide range of other collective swarm behaviors.

Keywords: Swarm robotics · area coverage · aggregation · dispersion

1 Introduction

Swarm robotics is a multidisciplinary research field concerned with the study and development of systems composed of multiple robots capable of performing tasks collectively.

Collective task execution is a central topic in swarm robotics research. A task is defined as an operation performed by a robot, such as moving a given distance or maintaining motion for a specified time. Tasks become collective when their execution depends not only on the actions of an individual robot

© The Author(s), under exclusive license to Springer Nature Switzerland AG 2027
O. Gervasi et al. (Eds.): ICCSA 2026 Workshops, LNCS 16761, pp. 3–21, 2027.
https://doi.org/10.1007/978-3-032-30527-5_1

but also on the actions of other robots in the swarm. In such cases, interaction among robots is required, which may occur through communication, via explicit information exchange or through sensing, whereby robots detect the presence of nearby swarm members.

Numerous collective tasks have been investigated in the literature [1,3,15]. However, many existing approaches focus on designing task-specific control software. As a result, each new behavior typically requires the development of a dedicated controller that accounts for both the task requirements and the robot hardware. While effective, this approach entails considerable design effort and limits the reuse and scalability of control strategies across different tasks.

The message wave strategy is task-independent and serves as a general foundation for implementing diverse collective behaviors [26,28]. It relies on two core processes: the propagation of messages from an initiating robot and the transmission of feedback messages in the reverse direction. Together, these processes enable coordinated task execution and synchronization, allowing subsequent tasks to begin only after the completion of previous ones.

The wave strategy is validated through the implementation of multiple tasks in a simulated swarm environment [10,27]. The simulation platform models physical phenomena such as gravity, friction, inertia, and collisions, while allowing customization of robot models. Experiments were conducted using a simulated version of the Kilobot [21], whose minimal communication capabilities are sufficient for message wave propagation. In particular, this work focuses on the design, implementation, and evaluation of rescaling collective behaviors for spatial area coverage, enabling aggregation and dispersion in robot swarms. These tasks serve as proof of concept for the proposed strategy, demonstrating its generality and applicability to a wide range of collective swarm behaviors.

Robot aggregation is required when a swarm that is initially dispersed needs to occupy a smaller region than its current spatial footprint. Similar to recruitment, aggregation can be employed as a subtask in several applications, including:

- Swarm collection: robots distributed throughout the environment during task execution must be gathered into a confined region so they can be retrieved by the user upon task completion.
- Object transportation: robots detect and grasp objects in the environment and collectively transport them to a designated location.
- Pursuit and capture: aggregation can be used to intercept a target by concentrating robots around it, thereby restricting its movement and preventing escape.
- Environmental transition: a moving group of robots may need to pass through a narrow passage or transition from a larger environment to a smaller one.

Dispersion exhibits the opposite behavior of aggregation: robots initially concentrated in a small area must spread out over the environment in which the swarm will operate. Dispersion-based subtasks can be applied in several scenarios:

- Initialization dispersion: the swarm is initially deployed near the user and subsequently disperses over a larger area. This behavior is particularly useful in search tasks, where robots must spread throughout the environment to locate regions with specific characteristics or to find objects.
- Coverage: in many applications, it is desirable for the swarm to occupy the largest possible area while maintaining communication connectivity, thereby avoiding fragmentation of the swarm topology.
- Localization support: once dispersed, some robots may remain stationary so that their positions can serve as reference points in a localization system.

This paper is organized into six sections. After the introduction, Sect. 2 presents the state of the art regarding the most widely studied and required collective tasks. Section 3 describes the general characteristics required of the swarm communication system to enable distributed algorithms, specifically information propagation using the wave strategy. Section 4 introduces rescaling tasks implemented using the message wave strategy, which enable aggregation and dispersion behaviors. Section 5, discusses the obtained performance results for several case-studies. Finally, Sect. 6 presents concluding remarks and outlines promising directions for future research.

2 Collective Tasks in Swarm Robotics

The analysis of survey and review works in swarm robotics provides valuable insight not only into how the field has evolved over the years, but also into how it has been interpreted by different researchers. Early studies highlighted the need to classify systems based on global characteristics, such as the architectural organization of the swarm, as proposed in [5]. Other authors have offered alternative perspectives, such as the work in [9], in which system characteristics are interdependent rather than treated in isolation.

In general, swarm tasks address three main aspects: (i) spatial organization among robots and/or between robots and the environment; (ii) robot motion within the environment, including search, object detection, and object transport; and (iii) collective decision-making processes, also known as consensus [3,15]. A wide range of problems and tasks has been investigated in swarm robotics.

One major class of swarm tasks concerns spatial organization, in which robots adjust their relative positions, either moving closer together or farther apart, leading to emergent global properties. Well-known examples include aggregation, dispersion, area coverage, pattern formation, and self-assembly. Aggregation, inspired by behaviors observed in insect societies [2], requires robots to converge toward a common region and has been widely studied due to its relevance to applications such as cooperative transport [13,14] and pattern formation [28]. Many aggregation strategies are biologically inspired, drawing from studies of bees [24] and cockroaches [8], where environmental cues combined with local interactions guide collective behavior. Dispersion represents the opposite behavior, in which robots spread over a larger area, often while maintaining connectivity. This behavior is closely related to the area coverage problem, which

is essential for applications such as environmental monitoring and distributed sensing [4]. More structured forms of spatial organization include pattern formation [7] and self-assembly, where robots physically connect to form composite structures, as explored in projects such as Symbrion [11].

Another important category of swarm tasks involves collective movement, in which the swarm as a whole moves from one region to another. This category includes exploration, foraging, collective navigation, and collective transport. Exploration of unknown environments is a fundamental robotics problem, often addressed using swarms to exploit parallelism and redundancy [6]. Foraging tasks, inspired by food-gathering behaviors in social insects, are widely regarded as benchmark problems in cooperative robotics [29], involving search, object identification, transport, and deposition [13,14]. Collective navigation, also known as flocking, refers to coordinated group motion and is inspired by biological systems [19,28]. Collective transport addresses the cooperative movement of objects that exceed the capabilities of individual robots and has been extensively studied using both communication-free and physics-based decentralized approaches, as well as methods relying on partial global information [14].

A third fundamental class of tasks involves collective decision-making, which is essential in decentralized swarm systems that lack global information. These tasks include consensus, task allocation, and localization. Consensus problems address how robots converge to a shared decision through local interactions [12]. Task allocation, also known as division of labor, concerns how robots distribute themselves among multiple tasks to achieve a desired global proportion, often using threshold-based or probabilistic methods [16,17]. Localization is another critical problem, where robots estimate their positions without external references such as GPS, typically relying on inter-robot measurements and distributed estimation techniques [22,23].

3 Distributed Algorithms for Swarm Robotics

Wave algorithms are a class of algorithms that manage message passing in distributed systems [26]. These algorithms are commonly used as a foundation for tasks that require an organized and reliable message transmission scheme. To be executed, wave algorithms require an architecture composed of devices capable of sending and receiving messages. The robotic system must exhibit the necessary characteristics for the execution of message waves:

- The swarm communication structure forms a network whose topology is defined by a graph $G = (V, A)$, where V is the set of robots and A is the set of communication channels between robots.
- The network topology does not change during the execution of the algorithm.
- The network is connected, meaning that every robot can transmit information, directly or indirectly, to any other robot in the swarm.
- Robots possess some initial knowledge, such as their own identifier or the identifiers of neighboring robots.

3.1 Information Propagation with Feedback

Wave algorithms can be employed to perform information propagation in distributed networks [25]. This operation is essential in systems that do not support broadcast communication, such as robot swarms that rely exclusively on local interactions.

During information propagation, each process completes its participation by forwarding messages to its neighbors. A process may confirm that its neighbors have received the information through acknowledgment messages; however, it has no direct confirmation regarding processes outside its local neighborhood. The Propagation of Information with Feedback (PIF) algorithm [25–27] extends basic propagation by providing an explicit event that indicates when the information has been received by all processes.

Synchronization can be achieved through successive executions of the PIF algorithm. In this case, propagation messages do not carry data, but instead signal that a local action a_0 may be executed. Once all processes have completed a_0, feedback messages are returned to the initiator, triggering the decision event. The initiator then starts a new wave, allowing each process to execute action a_1. Since the execution of a_1 occurs after the decision event, which is causally dependent on the completion of a_0 by all processes, global synchronization is guaranteed.

4 Proposed Model for Spatial Resizing Tasks

An important collective behavior that can be implemented using the message-wave strategy is swarm resizing or rescaling. This task requires a robot model equipped with sensing capabilities beyond those used in collective navigation. Specifically, each robot must be able to perceive the positions of all neighboring robots. Using this local spatial information, robots autonomously adjust their positions by increasing or decreasing their inter-robot distances. Depending on the selected control parameters, the swarm resizing process can lead to two emergent behaviors: aggregation or dispersion.

Generally, robot's model estimates inter-robot distances based on the intensity of the received communication signal. Accordingly, the simulated model associates distance measurements with inter-robot communication, thereby emulating the sensing mechanism available in the robot physical platform. Usually, this measurement provides information only about the distance between robots, without indicating their relative direction.

This task also requires neighborhood information to be collected. In this context, each robot uses the relative position of its parent to determine the speed and direction of its movement. To enable this behavior, the robot's model is modified so that each robot can observe the position of its corresponding parent robot during message reception. This modeling choice, however, ignores the positions of other neighboring robots, since such information is not required for the leader-follower control scheme. The modified model also incorporates a distance sensor that detects the position of the nearest obstacle. Moreover, the resizing

tasks reveal the need to detect the positions of all robots and obstacles within a defined neighborhood around each robot. This information is necessary to prevent collisions and to preserve connectivity within the swarm. This requirement differs from the coordinated motion task presented in [28], in which complete neighborhood information is not essential.

4.1 Agent's Flocking

The term flocking refers, in the context of artificial swarms, to the computational modeling of collective motion in groups of agents. This concept was originally introduced by Reynolds [18] for generating realistic animations of animal group movements.

Each individual in artificial flocking operates based on observations of its local neighborhood. An agent identifies nearby individuals and uses their positions and velocities to compute its own velocity. This process of (*i*) sensing, (*ii*) computation, and (*iii*) velocity update is continuously repeated during the flocking behavior.

The velocity of each individual (or agent) is defined by the contribution of different behavioral rules. Each rule corresponds to a specific group characteristic that should be reinforced or attenuated. The three fundamental rules are separation, alignment, and cohesion. The operation of these rules is illustrated in Fig. 1. In all cases, the dashed line represents the detection area surrounding the highlighted individual. As a result, this individual interacts with only three neighbors, while the positions of other agents do not influence its movement.

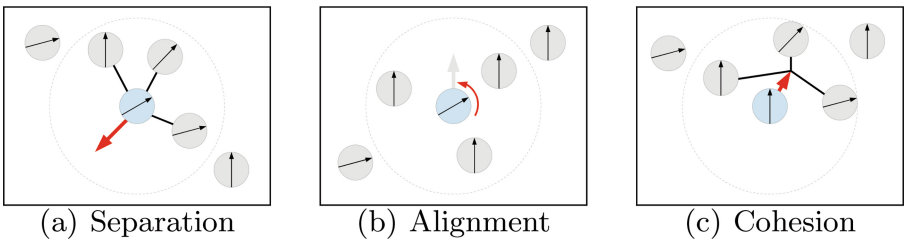

Fig. 1. Three basic flocking rules.

Separation is illustrated in Fig. 1(a). Under this rule, an individual moves away from its neighbors, preventing overcrowding and avoiding collisions. In the alignment rule shown in Fig. 1(b), the individual adjusts its direction in order to match the average heading of its neighbors. Finally, the cohesion rule depicted in Fig. 1(c) aims to prevent individuals from drifting away from the group. To achieve this, the computed movement is directed toward the average position of neighboring agents. In general, the flocking process is achieved through repeated cycles of neighborhood observation and position adjustment, as illustrated in

Algorithm 1. Each agent moves based on the observation of its own neighborhood. However, this movement alters the positions of all agents, meaning that at each sensing step, individuals perceive their neighbors at gradually changing locations. The contribution of each flocking rule is weighted by parameters w_1, w_2, and w_3 in Algorithm 1. The parameter w_0 represents the weight of the agent's current velocity relative to the newly computed velocity components. This factor models inertia; without it, abrupt velocity changes could occur due to fluctuations in the neighborhood configuration. TagImg

Algorithm 1. flocking of individuals.

1: Randomly initialize the individual's velocity;
2: **while** true **do**
3: Detect the neighborhood; Acquire neighborhood position information;
4: v_1 = separation velocity using neighborhood position information;
5: v_2 = alignment velocity using neighborhood position information;
6: v_3 = cohesion velocity using neighborhood position information;
7: velocity = $w_0 \times$ velocity + $(w_1 \times v_1)$ + $(w_2 \times v_2)$ + $(w_3 \times v_3)$;
8: position = position + velocity $\times \Delta t$;
9: **end while**

The tuning of the flocking parameters leads the group to exhibit different collective behaviors. For instance, varying w_0 can increase or decrease the overall speed of the group. Conversely, changing the balance between separation and cohesion, by varying w_1 and w_2, adjusts the spatial distribution of agents until an equilibrium condition is reached. The cohesion component causes agents to move closer together, while separation induces mutual repulsion. This balance between cohesion and separation forms the foundation of swarm resizing tasks in robot swarms.

4.2 Aggregation and Dispertion of Robots

Swarm resizing is a spatial organization behavior in which robots adjust their distances relative to their neighbors in order to achieve a desired collective property. Two resulting tasks are aggregation and dispersion. In aggregation, all robots move closer to one another, reducing the area of the environment occupied by the swarm. In dispersion, the opposite occurs: robots mutually repel each other, increasing the swarm's area of operation.

The flocking rules enable a swarm to exhibit different spatial behaviors. The aggregation and dispersion tasks presented in this chapter employ these rules to control the movement of the robots composing the swarm. In addition, swarm resizing based on flocking rules follows the message-wave strategy. Accordingly, the resizing process exhibits the following characteristics:

– A recruitment subtask is executed prior to the onset of movement. This establishes parent–child relationships among robots, which are required for message-based communication within the swarm [27].

- A message wave determines both the start and the termination of the resizing process.
- The movement strategy prevents parent robots and their respective children from moving beyond their communication range.
- During aggregation, a robot with two or more neighbors must avoid excessive distancing from one neighbor in order to approach another, as this could create robot-free regions within the swarm.
- Similarly, during dispersion, a robot must avoid approaching some neighbors while distancing itself from others. Instead, repulsion must occur in a balanced and mutual manner throughout the swarm.

During swarm resizing, robot motion is governed by flocking rules in conjunction with the detection system. Each robot observes its local neighborhood and computes its displacement accordingly. At the same time, the message-based communication system ensures that aggregation or dispersion is interrupted once a predefined stopping condition is reached.

The distributed algorithm governing swarm resizing consists of two components that operate in a coordinated manner. One component corresponds to robot motion based on the flocking rules, where each robot's displacement is determined by the relative positions of its neighboring robots. The second component is a message-wave algorithm that signals to swarm members the beginning and the termination of the resizing process. In general, the message-wave strategy employed for swarm resizing is identical to that used during alignment. An initial message wave is responsible for recruiting the robots and establishing the parent–child relationships. Subsequently, a new wave is initiated by the initializer robot. Upon receiving these messages, the remaining swarm members begin the motion that leads to either aggregation or dispersion.

The algorithm that regulates message transmission and reception during resizing can be represented by the state diagram shown in Fig. 2. As in the alignment task, each robot maintains two logical variables that guide the state transitions. The condition *res_p* indicates that the robot itself has reached a predefined resizing criterion, whereas the condition *res_f* indicates that its child robots have reached this criterion.

Three different types of messages are used during the resizing process, as summarized in Table 1. A message of type 7 is sent by a robot acting as a parent during the propagation wave that initiates the operation of its child robots. These children acknowledge reception by sending a message of the same type back to the parent. This exchange occurs in states $S_{AD}(01)$ and $S_{AD}(07)$ for a robot acting as a parent, and in states $S_{AD}(02)$ and $S_{AD}(08)$ when acting as a child. Message exchanges are repeated in states $S_{AD}(03)$, $S_{AD}(04)$, $S_{AD}(09)$, and $S_{AD}(10)$, but using messages of type 8. This procedure ensures that both parent and child robots confirm message reception. Messages of type 8 act as acknowledgments in a double-handshake scheme.

During the initial states, all robots execute the motion operation. This continues until a resizing condition is satisfied. This condition is defined by the parameter E, referred to as the *scaling factor*. Figure 3 illustrates the effect of E

on swarm resizing. Each robot is aware of the reference distance d_F relative to its child robots. This reference distance is measured during the initial recruitment subtask [27].

Table 1. Types of messages used during swarm resizing.

Message Type	msg_1	msg_2	msg_3	Message Type	msg_1	msg_2	msg_3
Propagation	id	–	7	Acknowledgment	id_{Parent}	id	8
Acknowledgment	id_{Parent}	id	7	Resizing confirmation	id	–	9
Propagation	id	–	8	Feedback	id_{Parent}	id	9

Robots evaluate their distance to their children in state $S_{AD}(04)$. Based on the measured values, they may transition to different states from $S_{AD}(05)$. If the resizing condition is satisfied for each child and the condition *res_p* is true, the robot stops moving and sends a type 9 message to its children. This message informs them that resizing has been achieved. Consequently, the robot's *res_f* condition becomes true, while the *res_p* condition of each child also becomes true. If resizing has not been achieved, two scenarios are possible. An intermediate robot for which both *res_p* and *res_f* are false returns to state $S_{AD}(07)$, operating again as a child in order to reposition itself at an appropriate distance from its parent. If *res_p* is true but *res_f* is false, the robot stops moving and returns to state $S_{AD}(01)$. Once the resizing conditions are satisfied, the initializer and intermediate robots transition from state $S_{AD}(05)$ to $S_{AD}(06)$, where they wait for a type 10 message. This message corresponds to a feedback signal sent by child robots, which are in state $S_{AD}(12)$. The algorithm terminates when all robots reach state $S_{AD}(13)$. At this point, the initializer can be certain that the swarm has successfully completed the resizing process.

4.3 Robot Movement

The confirmation that the swarm has reached the desired resizing condition depends on the distance between child robots and their respective parent, as illustrated in Fig. 3. However, if robots relied solely on this distance measurement, excessive proximity to other neighboring robots could occur. To address this issue, a motion rule was developed that takes into account the positions of all neighboring robots. In other words, each robot moves in response to the distances to all robots located within the sensing range of its detection system.

The proposed motion strategy is inspired by the flocking model introduced in Sect. 4.1. In this approach, the separation and cohesion rules are employed. The alignment rule was not required, as it is more suitable for situations in which the swarm as a whole must translate in space. Conversely, two additional rules were incorporated: one based on tracking the parent robot and another focused on obstacle avoidance.

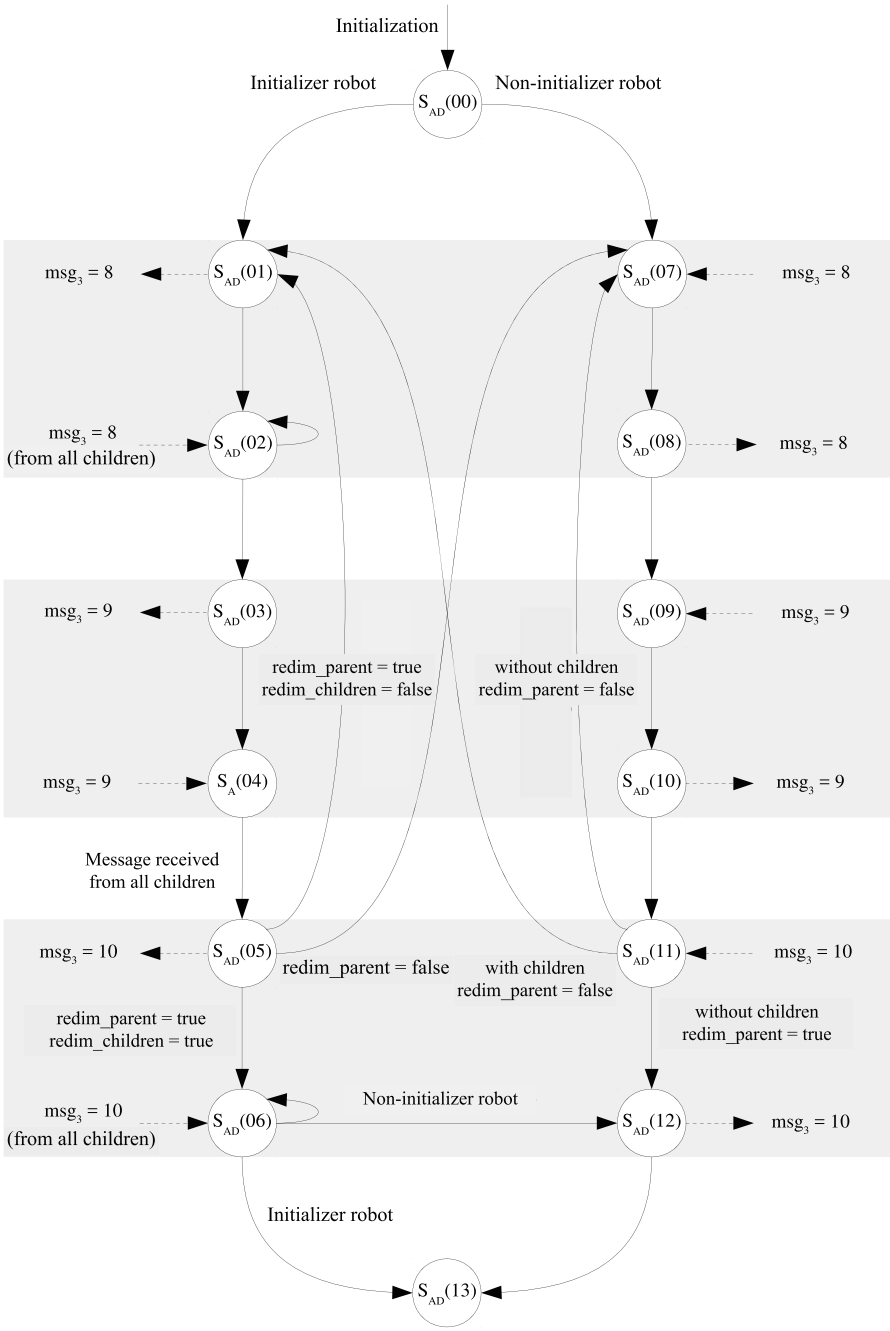

Fig. 2. State diagram describing the swarm resizing algorithm.

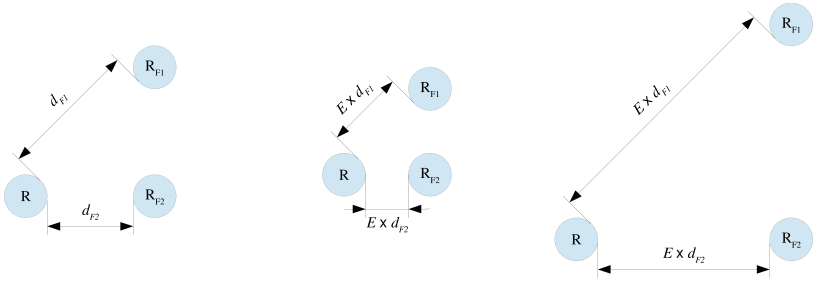

(a) Reference distances robot/children.

(b) Swarm aggregation behavior with $E < 1$.

(c) Swarm dispersion behavior with $E > 1$.

Fig. 3. Impact of the scaling factor E on swarm resizing.

For the cohesion behavior, each robot observes its neighborhood and computes the average position of the robots within its detection range, as described by Eq. 1. The cohesion distance $d_{x,y}(\text{coh})$ has (x, y) components defined in the coordinate frame of the robot performing the detection. The sum of the distances $d_{x,y}(\text{neighbor})$ is normalized by both the maximum sensing range (Sr) and the number of neighbors (Nn). As a result, each coordinate of the computed distance lies within the interval $[0, 1]$, where 0 corresponds to the minimum possible distance between robots and 1 represents the maximum detectable distance.

$$d_{x,y}(\text{coh}) = \frac{\sum_{i=1}^{Nn} d_{x,y}(\text{N}_i)}{Nn \times Sr}, \tag{1}$$

where Sr is the sensor radius and the N_i ith neighbor.

The distance $d_{x,y}(\text{coh})$ is used to compute the velocities of the robot's two motors. The expressions in Eq. 2 define four velocity components: two associated with the x-axis and two with the y-axis. It is important to note that the d_x component of the cohesion distance induces rotational motion, while the d_y component affects forward or backward motion. This behavior is analogous to that described the adjustment used for collective navigation [10].

$$\begin{aligned} velocity_{x1} &= v_{max} \times d_x & velocity_{y1} &= v_{max} \times d_y \\ velocity_{x2} &= -v_{max} \times d_x & velocity_{y2} &= v_{max} \times d_y \end{aligned} \tag{2}$$

The velocity of each motor is obtained by combining the velocity components associated with x and y, as expressed in Eq. 3. The velocity v_{cw} drives the motor responsible for clockwise rotation, whereas v_{ccw} controls the counterclockwise rotation, such that

$$\begin{aligned} v_{cw} &= 0.5 \times velocity_{x1} + 0.5 \times velocity_{y1} \\ v_{ccw} &= 0.5 \times velocity_{x2} + 0.5 \times velocity_{y2} \end{aligned} \tag{3}$$

In the separation rule, the value used for velocity computation is not the inter-robot distance itself, but rather the distance $d'x, y(\text{neighbor})$ between a neighbor

and the maximum detection radius in that direction. This value is summed over all neighbors, resulting in the separation distance $dx, y(sep)$ defined in Eq. 4:

$$d_{x,y}(sep) = -\frac{\sum_{i=1}^{N_n} d'_{x,y}(\mathrm{N}_i)}{Nn \times Sr}, \tag{4}$$

where as before Nn is the number of neighbors, Sr is the sensor radius and N_i represents the ith neighbor.

Robots that are farther apart exert less repulsive force on one another. Conversely, robots closer to the detecting robot *i.e.*, farther from the detection boundary, generate a stronger repulsion, and thus the separation velocity should be maximal. The negative sign in Eq. 4 indicates that the resulting motion occurs in the opposite direction of the summed vector, as expected for a separation behavior. So, the same velocity equations used for cohesion can also be applied to separation. Both $d_{x,y}(coh)$ and $d_{x,y}(sep)$ are illustrated in Fig. 4.

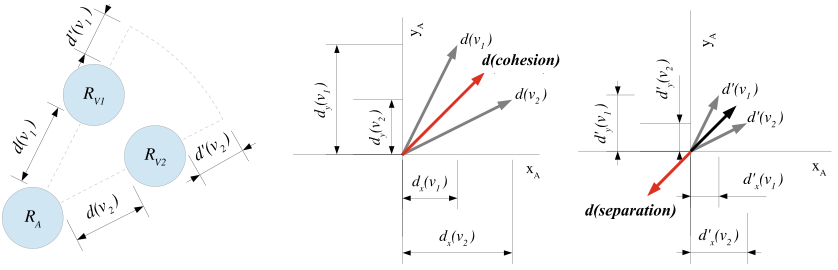

(a) Robots R_{V1}/R_{V2} as neighbors of R_A (b) Distances between R_{V1}/R_{V2}—R_A. (c) Distances between R_{V1}/R_{V2}—R_A's vicinity

Fig. 4. Distances used in the computation of $d_{x,y}(coh)$ and $d_{x,y}(sep)$ for a robot R_A with two neighbors, R_{V1} and R_{V2}.

Two additional rules are employed to define robot velocities during swarm resizing. The first is associated with tracking the parent robot, preventing child robots from drifting too far away and potentially causing a loss of connectivity within the swarm. The second rule is obstacle avoidance, whose purpose is to prevent collisions when the mutual distance between robots becomes smaller than a predefined threshold. Both rules are similar to those used in the navigation task described in [10]. In this context, each rule results from the detection of a single neighbor: either the parent robot or a robot posing a collision risk. These two distance measurements, $d_{x,y}(\text{parent})$ and $d_{x,y}(collision)$, are converted into velocity components using Eq. 2.

The final velocity of each robot is obtained by combining the velocities generated by the four rules. In Eq. 5, the parameters w_1, w_2, w_3, and w_4 represent the weights associated with rules 1 through 4. The maximum possible values of v_{cw} and v_{ccw} are limited by v_{max}, which corresponds to the maximum speed

supported by the robot.

$$\begin{aligned} velocity_{cw} &= w_1 \times v_{cw}(1) + w_2 \times v_{cw}(2) + w_3 \times v_{cw}(3) + w_4 \times v_{cw}(4) \\ velocity_{ccw} &= w_1 \times v_{ccw}(1) + w_2 \times v_{ccw}(2) + w_3 \times v_{ccw}(3) + w_4 \times v_{ccw}(4) \end{aligned} \tag{5}$$

From Eq. 2, it can be observed that v_{max} is scaled by the distance computed in each rule. Since these distances are normalized and lie within the interval $[0, 1]$, the velocities v_{cw} and v_{ccw} associated with each rule are not maximal in most situations. As robots move closer to one another, $d_{x,y}(coh)$ decreases, thereby reducing the velocity contribution of the cohesion rule. A similar effect occurs for $d_{x,y}(sep)$ and the separation velocity when robots move farther apart.

5 Performance Results

The proposed rescaling task based on message waves is evaluated via simulations. The simulation time required for the aggregation and dispersion tasks are assessed, considering the impact of different factors, such as the number of robots and the inter-robot spacing, on the total execution time.

The swarms are composed of Kilobot [21] robots simulated in the CopealiaSim, also known earlier as V-REP [20]. The simulated *Kilobot* extends the physical robot's capabilities by increasing communication range, adding directional proximity sensing, and enabling more flexible motion. These enhancements are necessary to support message-wave algorithms and complex collective behaviors such as navigation, alignment, aggregation, and dispersion. All simulations reported in this work are carried out on computers equipped with an Intel Core i7-950 processor, operating at 3.0 GHz, 8 GB of memory, and running the Microsoft Windows 7 Home Premium operating system. Videos of the experiments can be found at https://l1nq.com/2gy6A.

5.1 Simulation Settings

The simulations are divided into two groups, corresponding to aggregation and dispersion experiments. In each experiment, the time required to complete the swarm rescaling ia reported. Depending on the task, this time is referred to as the Aggregation Time (τ_A) or the Dispersion Time (τ_D). Simulations are conducted with different numbers of robots, in order to analyze the relationship between execution time and swarm size. Let ρ_C be the critical path defined as the longest path from the initializer to a leaf robot in the swarm. During the simulations, the robots were disposed so that the number of robots in the critical path varies from 2 to 5.

The same local control algorithm is used for both aggregation and dispersion. The behaviors differ only in the flocking weights and in the rescaling factor E. For the aggregation, $0.5 < E < 1$ with a step of -0.1, meaning that the final parent-child distance is a fraction of the initial one, with a minimum of half the original distance. For dispersion, $1 < E < 2$ with a step of 0.2, causing robots

to increase their separation, with the maximum distance being twice the initial value.

The flocking weights are tuned differently for aggregation and dispersion, as they directly influence the contribution of each motion rule and, consequently, the swarm behavior. Table 2 summarizes the values used in the simulations. These parameters were selected so that the same set of values could be applied consistently across all aggregation and dispersion experiments.

All dispersion experiments were successfully performed using only the separation rule, which is the primary mechanism responsible for mutual repulsion among robots. Aggregation, however, required the combined use of all four motion rules with carefully chosen weights. In this case, the cohesion weight was set higher than the separation weight to promote convergence, while maintaining a nonzero separation component to avoid uneven motion caused by differences in robot velocities. This balance resulted in a more uniform aggregation process.

Table 2. Weights setup during the simulations

Rule	Obstacles	Cohesion	Separation	Parent
weight	w_1	w_2	w_3	w_4
Aggregation	1	3	0.5	3
Dispertion	0	0	3	0

These simulations allow the evaluation of execution time as a function of both swarm size ρ and the critical path length ρ_C. During the initial recruitment subtask, which establishes the parent-child relationships among robots, neighborhood detection is limited to a maximum of four neighbors. During the aggregation experiments, this restriction is not required, since robots are initially positioned far enough apart such that each robot can detect at most four neighbors. As the swarm aggregates, however, the number of robots within each local neighborhood naturally increases. During the dispersion experiments, robots start in close proximity, allowing neighborhoods to initially include more than four robots. As mutual repulsion occurs and the swarm spreads out, the neighborhood size decreases. By the end of the dispersion process, each robot detects at most four neighbors, which correspond to the same robots identified in its neighborhood at the beginning of the task.

Figure 5 shows the simulation times obtained for swarm aggregation. For experiments with the same number of robots, the bars represent the aggregation times obtained for different values of the rescaling factor E. Overall, a clear trend of approximately linear growth in τ_A with respect to swarm size can be observed. This behavior differs from that observed in the alignment simulations, where execution time is strongly dependent on the communication density ρ_C.

The observed difference is primarily due to robot motion. During alignment, movement consists solely of in-place rotations, whereas in aggregation the robots physically translate relative to one another. As the number of robots increases,

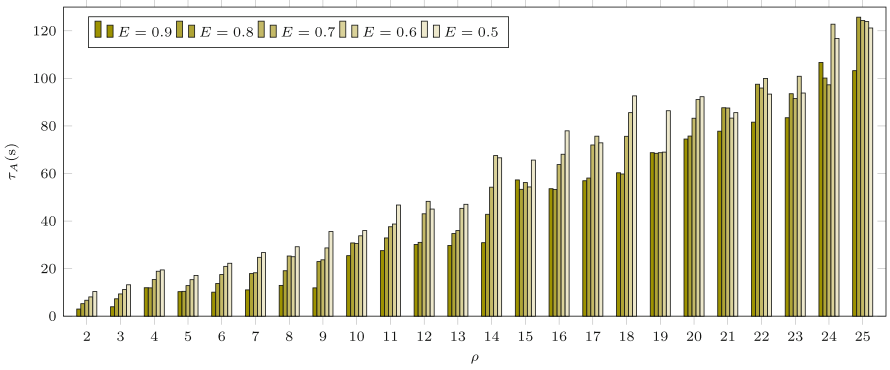

Fig. 5. Aggregation time for different swarm size and scaling factors.

more individuals participate in the flocking process, which directly affects each robot's velocity. Furthermore, as robots move closer together, the number of neighbors detected within each local neighborhood increases, further influencing motion dynamics. The results also highlight the variation of τ_A with respect to the rescaling factor E for experiments with the same swarm size. As expected, values of E closer to 1 generally lead to faster experiments, since smaller rescaling requires less robot movement. This trend is observed in most cases. However, for swarms with 12, 14, 15, 17, 21, 22, 23, 24, and 25 robots, some deviations from this behavior were observed. These exceptions can be attributed to non-uniform robot velocities during the aggregation process.

The results of the dispersion experiments are presented in Although the dispersion time τ_D increases with swarm size, this growth follows a pattern that differs from that observed in aggregation. In particular, τ_D consistently increases with the rescaling factor E for all swarm sizes considered. Moreover, this variation is more pronounced than the corresponding variation of τ_A observed in the aggregation experiments, as shown in Fig. 5.

The most notable behavior observed in the dispersion experiments is the oscillation of τ_D values. This effect is particularly evident in Fig. 6 for $E = 2$, especially in the cases with 10 and 21 robots. In the first case, τ_D increases more sharply when the swarm size changes from 9 to 10 robots than from 8 to 9. In the second case, τ_D decreases as the swarm size increases from 19 to 20 and from 20 to 21 robots. In both situations, this behavior can be attributed to the symmetry of the robot's disposition.

With 9 robots, the swarm configuration is symmetric, consisting of the initializer and 8 neighbors, where each of the four child robots has exactly one child of its own. With 10 robots, one of the initializer's children gains an additional child, breaking the symmetry. This asymmetry leads to an imbalance in the repulsive forces that govern dispersion, increasing the time required to reach the rescaling condition compared to the symmetric case. Conversely, when the swarm size increases from 20 to 21 robots, the added robot restores symme-

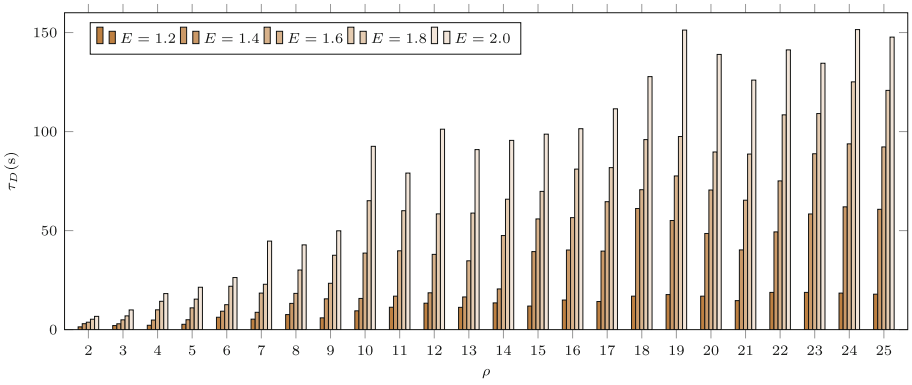

Fig. 6. Dispersion time for different swarm size and scaling factors.

try, which compensates for the increased swarm size and reduces the dispersion completion time.

Figure 7 shows Average aggregation and dispersion times, ($\overline{\tau_A}$) and ($\overline{\tau_D}$), respectively, considering the number of robots on the critical path, for different swarm size and scaling factors. These are computed as the mean simulation time for experiments with identical values of E and ρ_C.

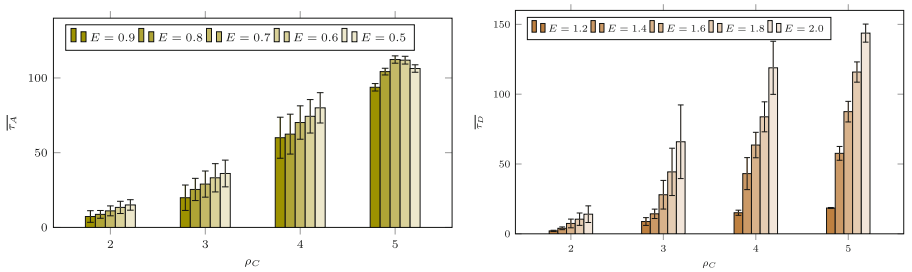

(a) Average aggregation time (s)

(b) Average dispersion time (s)

Fig. 7. Average aggregation and dispersion times considering the number of robots on the critical path, for different swarm size and scaling factors.

A significant variability in τ_A and τ_D alike is noticeable for $\rho_C = 3$ and $\rho_C = 4$, indicating a stronger sensitivity to swarm density under these conditions. The plot of $\overline{\tau_D}$ also highlights the influence of the rescaling factor E on dispersion time. For a given ρ_C, the values of $\overline{\tau_D}$ obtained with $E = 2$ are higher than those obtained with $E = 1.2$ for the immediately larger ρ_C. This behavior contrasts with the aggregation results, where $\overline{\tau_G}$ for a given ρ_C is always lower than all values corresponding to the next larger ρ_C, regardless of E.

6 Conclusions

This work employs a message-wave algorithm as the core mechanism for designing collective swarm behaviors. The main requirement for this approach is the presence of a message-based communication system, in which robots can exchange messages with neighbors within a defined communication range. Neighborhood relationships must be bidirectional: if a robot can send messages to a neighbor, it must also be able to receive messages from that same neighbor. These local communication links define the swarm's communication topology.

The focus of this study is swarm resizing, encompassing aggregation and dispersion behaviors. These tasks require an initial recruitment phase to establish parent-child relationships among robots. Robot motion is governed by flocking rules, which regulate attraction and repulsion relative to neighbors. While message waves coordinate task initiation and termination through the communication system, flocking-based motion relies on the detection system. The interaction between these two systems enables precise control over the degree of swarm resizing.

A natural extension of this work is a deeper investigation of the implemented resizing task. For instance, one may analyze the impact of additional factors on execution time, such as the number of neighboring robots. In the current experiments, robots were arranged in a grid topology with at most four neighbors per robot, although the task was shown to function under other spatial configurations. Exploring alternative regular topologies, such as those with three or six neighbors, is therefore of interest.

Acknowledgment. This work is supported by Fundação Carlos Chagas Filho de Amparo à Pesquisa do Estado do Rio de Janeiro (FAPERJ – Brazil) with grant numbers 201.013/2022 and 200.434/2026. This work is also supported by Conselho Nacional de Desenvolvimento Científico e Tecnológico (CNPq – Brazil). We are most grateful for their continuous financial support.

References

1. Bayındır, L.: A review of swarm robotics tasks. Neurocomputing **172**, 292–321 (2016). https://doi.org/10.1016/j.neucom.2015.05.116
2. Bonabeau, E., Theraulaz, G., Deneubourg, J.L., Aron, S., Camazine, S.: Self-organization in social insects. Trends Ecol. Evol. **12**(5), 188–193 (1997)
3. Brambilla, M., Ferrante, E., Birattari, M., Dorigo, M.: Swarm robotics: a review from the swarm engineering perspective. Swarm Intell. **7**(1), 1–41 (2013)
4. Broecker, B., Caliskanelli, I., Tuyls, K., Sklar, E., Hennes, D.: Social insect-inspired multi-robot coverage. In: Proceedings of the 2015 International Conference on Autonomous Agents and Multiagent Systems, pp. 1775–1776. International Foundation for Autonomous Agents and Multiagent Systems (2015)
5. Cao, Y.U., Fukunaga, A., Kahng, A.: Cooperative mobile robotics: antecedents and directions. Auton. Robot. **4**(1), 7–27 (1997)

6. Faigl, J., Kulich, M.: On benchmarking of frontier-based multi-robot exploration strategies. In: Proceedings of the 2015 European Conference on Mobile Robots, pp. 1–8. IEEE (2015)
7. Flocchini, P., Prencipe, G., Santoro, N., Widmayer, P.: Arbitrary pattern formation by asynchronous, anonymous, oblivious robots. Theoret. Comput. Sci. **407**(1), 412–447 (2008)
8. Garnier, S., Gautrais, J., Asadpour, M., Jost, C., Theraulaz, G.: Self-organized aggregation triggers collective decision making in a group of cockroach-like robots. Adapt. Behav. **17**(2), 109–133 (2009)
9. Iocchi, L., Nardi, D., Salerno, M.: Reactivity and deliberation: a survey on multi-robot systems, pp. 9–32. Springer (2001)
10. Junior, L.S., Nedjah, N.: Efficient strategy for collective navigation control in swarm robotics. Procedia Comput. Sci. **80**, 814–823 (2016). https://doi.org/10.1016/j.procs.2016.05.371
11. Liu, W., Winfield, A.: Self-assembly in heterogeneous modular robots, pp. 219–232. Springer (2014)
12. Mendonça, R., Nedjah, N., Mourelle, L.: Efficient distributed algorithm of dynamic task assignment for swarm robotics. Neurocomputing **172**, 345–355 (2016)
13. Nedjah, N., Cardoso, K.D.S., Mourelle, L.D.M.: Collaborative swarm robotics for object transport via caging. Sensors **25**(16) (2025). https://doi.org/10.3390/s25165063. https://www.mdpi.com/1424-8220/25/16/5063
14. Nedjah, N., Ferreira, G.B., de Macedo Mourelle, L.: Swarm robotics for collaborative object transport using a pushing strategy. Expert Syst. Appl. **271**, 126610 (2025). https://doi.org/10.1016/j.eswa.2025.126610
15. Nedjah, N., Junior, L.S.: Review of methodologies and tasks in swarm robotics towards standardization. Swarm Evol. Comput. **50**, 100565 (2019). https://doi.org/10.1016/j.swevo.2019.100565
16. Nedjah, N., Mendonça, R., Mourelle, L.: PSO-based distributed algorithm for dynamic task allocation in a robotic swarm. Procedia Comput. Sci. **51**, 326–335 (2015)
17. Nedjah, N., Ribeiro, L.M., de Macedo Mourelle, L.: Communication optimization for efficient dynamic task allocation in swarm robotics. Appl. Soft Comput. **105**, 107297 (2021). https://doi.org/10.1016/j.asoc.2021.107297
18. Reynolds, C.: Flocks, herds and schools: a distributed behavioral model. ACM SIGGRAPH Comput. Graph. **21**, 25–34 (1987)
19. Ribeiro, L.M., Nedjah, N., de Carvalho, P.V.R.: Optimized navigation for slam using marker-assisted region scanning, path finding, and mapping completion control. Appl. Sci. **15**(7) (2025). https://doi.org/10.3390/app15073433. https://www.mdpi.com/2076-3417/15/7/3433
20. Rohmer, E., Singh, S., Freese, M.: V-rep: a versatile and scalable robot simulation framework. In: Proceedings of the 2013 IEEE/RSJ International Conference on Intelligent Robots and Systems, pp. 1321–1326. IEEE (2013)
21. Rubenstein, M., Ahler, C., Hoff, N., Cabrera, A., Nagpal, R.: Kilobot: a low cost robot with scalable operations designed for collective behaviors. Robot. Auton. Syst. **62**(7), 966–975 (2014)
22. Sá, A., Nedjah, N., Mourelle, L.: Distributed efficient localization in swarm robotic systems using swarm intelligence algorithms. Neurocomputing **172**, 322–336 (2016)
23. Sá, A., Nedjah, N., Mourelle, L.: Distributed efficient localization in swarm robotics using min-max and particle swarm optimization. Expert Syst. Appl. **50**, 55–65 (2016)

24. Schmickl, T., Hamann, H.: Beeclust: a swarm algorithm derived from honeybees. Bio-inspired Comput. Commun. Netw. (2011)
25. Segall, A.: Distributed network protocols. IEEE Trans. Inf. Theory **29**(1), 23–35 (1983)
26. Silva, L., Nedjah, N.: Wave algorithm for recruitment in swarm robotics. In: Gervasi, O., et al. (eds.) Computational Science and Its Applications - ICCSA 2015, pp. 3–13. Springer, Cham (2015)
27. Silva Junior, L., Nedjah, N.: Distributed strategy for robots recruitment in swarm-based systems. Int. J. Bio-inspired Comput. **8**, 99–108 (2016). https://doi.org/10.1504/IJBIC.2016.076336
28. Silva Junior, L., Nedjah, N.: Wave algorithm applied to collective navigation of robotic swarms. Appl. Soft Comput. **57**, 698–707 (2017). https://doi.org/10.1016/j.asoc.2016.06.004
29. Winfield, A.: Foraging robots, pp. 3682–3700. Springer (2009)

Breast Nodule Detection and Classification Using Convolutional Neural Network with Transfer Learning

Flávia Telles[1], Luiza de Macedo Mourelle[2(✉)], and Nadia Nedjah[3]

[1] Postgraduate Program in Electronics Engineering, State University of Rio de Janeiro, Rio de Janeiro, Brazil
flaviaesanto@gmail.com

[2] Postgraduate Program in Electronics Engineering, Department of Systems Engineering and Computation, State University of Rio de Janeiro, Rio de Janeiro, Brazil
ldmm@eng.uerj.br

[3] Postgraduate Program in Electronics Engineering, Department of Electronics Engineering, State University of Rio de Janeiro, Rio de Janeiro, Brazil
nadia@eng.uerj.br

Abstract. Diagnosing breast cancer using mammograms is not always easy, since it depends on human interpretation and the images can be complex. In this sense, early detection is still a challenge. In this paper, we propose and evaluate two methods based on Convolutional Neural Networks. We use U-Net and VGG16 architectures to analyze images from the CBIS-DDSM database. We compare semantic segmentation with direct classification using Transfer Learning. The goal is to check whether it is really necessary to identify the exact lesion area for diagnosis. The results show that the classification approach performed better than segmentation. The U-Net model had convergence problems with this dataset. The VGG16 model achieved the best results after applying regularization techniques, reaching an accuracy of 65.3% and a sensitivity of 66.0% in detecting malignant cases.

Keywords: Breast cancer · Deep learning · Transfer learning · Convolutional neural networks · Computer-aided diagnosis

1 Introduction

Cancer is a serious disease and a big health problem around the world. It causes many deaths and affects many families. Breast cancer is one of the most common types. It significantly affects the longevity and quality of life of women worldwide [1]. One problem is that it can grow without clear symptoms. Often, the diagnosis happens only when the disease has already reached advanced stages. This reduces treatment options and lowers survival rates. So, early detection is very important. We also need better ways to detect it earlier [2].

© The Author(s), under exclusive license to Springer Nature Switzerland AG 2027
O. Gervasi et al. (Eds.): ICCSA 2026 Workshops, LNCS 16761, pp. 22–35, 2027.
https://doi.org/10.1007/978-3-032-30527-5_2

Cancer is one of the most complex diseases today and a leading cause of early death worldwide [1]. In Brazil, as shown in Fig. 1, breast cancer has the highest mortality rates among women [5]. This highlights the need for more effective diagnosis methods [3]. The chance of survival is directly related to the detection stage, showing a 99% survival rate for early cases, compared to only 28% for advanced cases with distant metastasis [4].

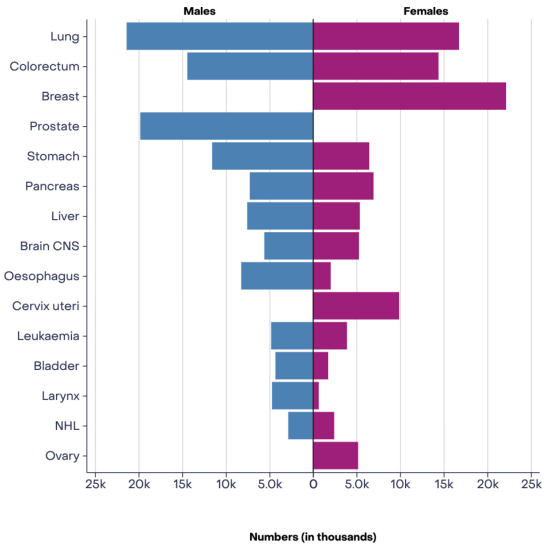

Fig. 1. Mortality according to primary tumor location and gender in Brazil in 2022 [5].

The first exams for cancer nodule detection are self-examination and physical exam by a doctor. Both are simple methods and non invasive, but their sensitivity and specificity are limited, which could not detect small tumors or confuse benign and malignant alterations. Mammogram is an x-ray exam, usually indicated as the first one, but it can be uncomfortable or has some limitations in dense breasts, where the glandular tissue can obscure lesions. Ultrasound is a complementary exam to mammogram, useful to differentiate solid nodules from cysts and evaluate lesions in dense breasts. Magnetic resonance (MR) is a more sensitive image exam, but less specific, of high cost, indicated for women with high risk of breast cancer, family history or genetic predisposition. Biopsy is the only exam that provides a definitive diagnosis for breast cancer, but it is very invasive.

Today, doctors usually analyze mammograms visually [15]. Although this is the standard method, it depends entirely on human visual accuracy. It is also subject to variables such as fatigue and professional experience, which can contribute to incorrect diagnosis [16]. Because of these problems, computer systems

can help doctors, acting as a second opinion. It can process large amounts of data and identify subtle patterns that the human eye cannot easily see [17].

To help clinical practice, computer-aided diagnosis systems use Artificial Neural Networks (ANNs), which are models inspired by the human brain [28]. The evolution of these architectures led to Convolutional Neural Networks (CNNs), which were designed to process grid-like data, such as mammogram images. They use convolution layers to detect patterns in images and pooling layers, reducing data dimensions and ensuring resistance to small movements [30]. In the context of breast diagnosis, this helps the model detect simple and complex patterns, finding everything from simple edges to complex morphological patterns of masses and calcifications.

In this work, we explore the potential of two CNN architectures to improve detection and diagnosis of breast cancer: U-Net and VGG16. The main objective is to investigate and compare the effectiveness of semantic segmentation versus direct image classification. This comparison helps us understand which method works best in practice.

This paper is organized as follows. Section 2 reviews related works and places this research in the current state of the art by analyzing similar approaches in the scientific literature. Section 3 introduces the theoretical background in artificial neural networks in the context of this work and the architectures applied. Section 4 shows the results obtained, the evaluation metrics, and the comparative performance analysis of the trained models. Finally, Sect. 5 summarizes the study findings, points out conclusions and directions for future work.

2 Related Works

Academic research on breast cancer diagnosis has evolved by integrating standardized databases and deep neural network architectures. Pinheiro [14] proposed a method using U-Net [33] and optimization algorithms. It approaches nodule detection through an innovative combination of the U-Net architecture and several swarm intelligence methodologies. By exploring a wide range of bio-inspired algorithms to optimize the segmentation process, the author tested different methods and compared the results. These consolidated results can be seen in detail in Table 1. Among the conducted experiments, particle swarm optimization achieved the best performance. It reached an average accuracy of 93.78% and a recall of 93.04%, showing that U-Net performs quite well for this task.

Regarding the classification of mammogram abnormalities, Falconi and his colleagues [13] conducted an extensive research. They specifically used the CBIS-DDSM database [32] to evaluate twenty pre-trained neural network models. The results showed that the VGG16 [34] architecture achieved an accuracy of 84.4% when subjected to fine-tuning. This consolidated this model as a robust feature extractor for diagnosing tumor masses. This evidence supports the choice of VGG16 in this research as a fundamental paradigm for the computer-aided diagnosis task.

In addition, Baffa *et al* [20] focused on ROI (Region of Interest) segmentation in mammary thermography, using the public database DMR-UFF [6] composed

Table 1. Best-performing comparison [14]

Algorithm	Accuracy (ReLU 2×2)	Recall (ReLU 2×2)
Particle Swarm Optimization (PSO)	93.78%	93.04%
Gravitational Search Algorithm (GSA)	93.52%	92.60%
Harmony Search (HS)	93.17%	92.39%
Artificial Bee Colony (ABC)	92.95%	91.95%
Gray Wolf Optimization (GWO)	92.80%	91.83%
Social Spider Algorithm (SSA)	92.62%	92.03%
Bacterial Foraging Optimization (BFO)	92.57%	90.49%

of 283 infrared images. The segmentation methodology used a variant of the U-Net aiming at segmenting the breast external region, defined from inflammatory pleats to the neck. The U-Net received input images in grey scale of 256×256 pixels and used 12 convolutional layers with ReLU activation function. The output layer was composed of a 1×1 convolution with Sigmoid as activation function. The proposed U-Net provided a better performance than other methods based on VGG, achieving a mean accuracy of 98.24% and precision of 98.86%. This last metric indicates the reliability in positive detections or how rarely it indicates a false tumor. Besides this, it obtained an Intersection over Union (IoU) of 94.38%, demonstrating high efficiency in precise segmentation of ROI. The research emphasized the importance of image pre-processing to improve accuracy. It demonstrated that deep models outperform traditional computer vision methods in distinguishing between benign and malignant cases.

Furthermore, the study by Mendez and Muñoz [23] explored the identification of the Region of Interest in malignant mammograms. They compared the U-Net and YOLO (You Only Look Once) [7] architectures. The research used two data sets from The Cancer Imaging Archive (TCIA) [8]. The first was CBIS-DDSM, with 1318 mammography images and the second was Brain MRI Segmentation, based on TCGA-LGG [9], with 2090 magnetic resonance images. The work implemented the YOLO architecture and the U-Net, specialized in semantic segmentation. The learning rate, that provided the best results, were 2×10^{-4} for YOLO and 0.0001 for U-Net, both trained with ADAM optimizer [10]. The authors concluded that U-Net showed superior performance in spatial localization accuracy, reaching an Intersection over Union (IoU) index of 0.67 for malignant mammograms.

Finally, the work by Silva [24] used the transfer learning technique for attribute extraction, based CNNs pre-trained in ImageNet [18], such as LeNet [19], ResNet50 [12], Inception V3 [28], SqueezeNet as feature extractors. Several traditional classifiers were tested, including Naive Bayes [21] Random Forest [22], Suppport Vector Machine (SVM) [25]. The best combination without attribute selection was from Inception V3 plus SVM polynomial (degree 3), achieving an accuracy of 79.92%.

The analysis of these five works supports the strategy adopted in this research. It validates the use of the CBIS-DDSM database and the focus on the potential of U-Net and VGG16 networks to overcome the limitations of conventional visual diagnosis.

3 Neural Network-Assisted Diagnosis for Cancer

Several architectures for CNNs were used with success in classification of cancer medical images, such as AlexNet [11], VGG Net [34], GoogleNet/Inception [28], ResNet. Among these, the VGG Net family, in particular VGG16, provides an efficient feature extractor for Transfer Learning technique. It stands out for using sequential convolution blocks with small filters of 3×3 pixels and a stride of one pixel. This setup allows us to increase the network depth while keeping a controlled number of parameters. It also makes learning discriminative features easier through the rectified linear activation function [31]. The implementation uses Transfer Learning with weights previously adjusted on the ImageNet dataset. This technique allows the model to reach convergence more efficiently when dealing with the mammogram images database [35]. Figure 2 displays the architecture of the VGG16 network used in this research.

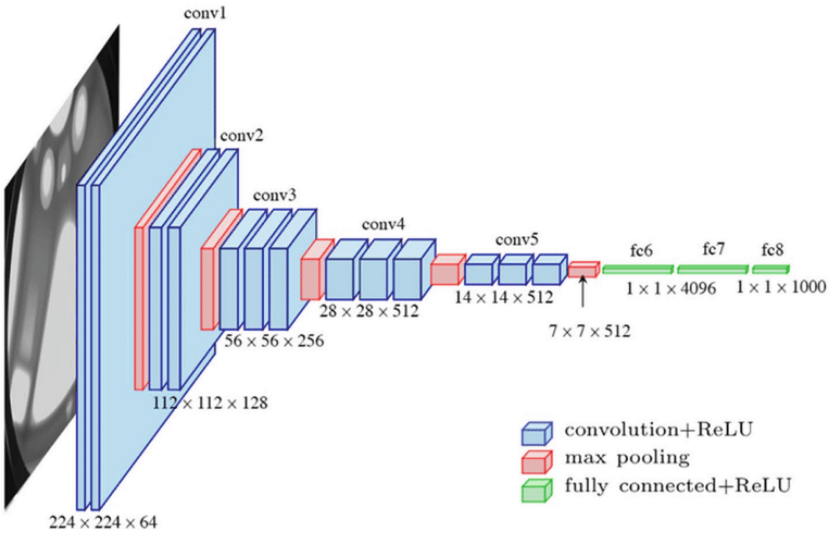

Fig. 2. Traditional VGG16 architecture.

Medical image segmentation is a challenging task that requires a class for each image pixel. CNN architectures were designed specifically for this aim, such as Fully Convolutional Networks (FCN) [26], SegNet [27], U-Net. In our work, we used U-Net for the segmentation process, featuring a contraction path

to capture context and a symmetric expansion path for precise localization [33]. The network uses skip connections to link feature maps from the contraction path with those from the expansion path. This preserves high-resolution information, which is essential to define the edges of a tumor. The complete structure of the U-Net architecture is presented in Fig. 3.

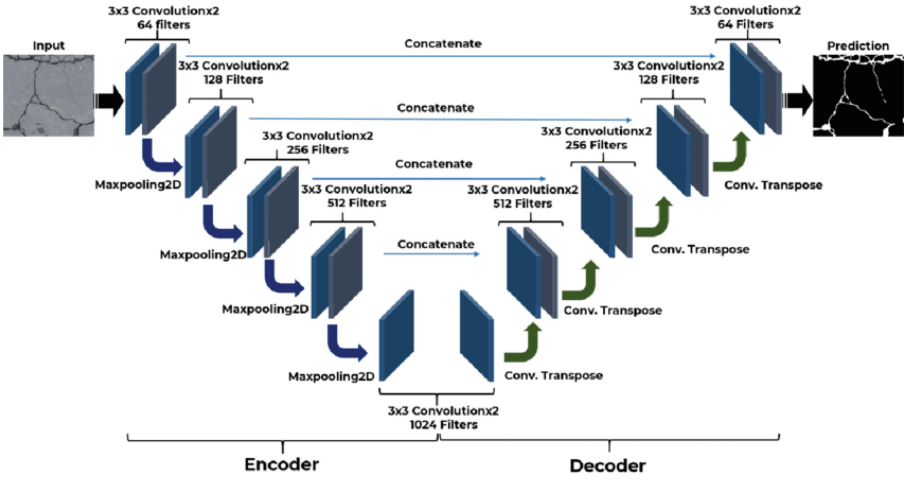

Fig. 3. Traditional U-Net architecture.

The database used for training and validation was the Curated Breast Imaging Subset of DDSM [32]. This repository provides digitized mammograms with precise annotations and segmentation masks. These masks serve as the gold standard for the supervised training of the proposed neural networks.

4 Results and Discussion

The experimental evaluation of this study is based on a structured methodology. It covers everything from data acquisition to the final performance analysis. The development environment was Google Colaboratory Platform [29], providing the necessary computational resources, like the NVIDIA T4 graphics processing unit [36], to train the deep learning models.

First, we prepared the dataset. The Curated Breast Imaging Subset of DDSM dataset contains mammogram images categorized into benign and malignant cases according to the breast imaging reporting and data system [32,38]. The experiment followed sequential pre-processing steps to ensure input data quality. First, we filtered the original database to select only images with mass annotations. We discarded calcification cases to keep the sample uniform. Then, we resized the images to a resolution of 224×224 pixels and converted them to the

RGB color space. Finally, we divided the images into training, validation, and test groups, in order to better evaluate the model.

For the U-Net segmentation architecture, we conducted four different experiments. These tests evaluated baseline settings, data augmentation, learning rate reduction and a hybrid loss function, consisting of Dice coefficient with binary cross entropy. For Experiment 1, we applied the standard learning rate of 1×10^{-4}, usually used as a starting point for computational vision tasks. For Experiment 2, data augmentation was introduced, while keeping the standard learning rate. For Experiment 3, the learning rate was reduced to 1×10^{-5}. For Experiment 4, a hybrid loss function was introduced, combining the Dice coefficient with binary cross entropy, while keeping data augmentation. Since this network did not perform well in identifying nodules, none of the optimization techniques outperformed the initial model.

The best result remained in the baseline, achieving an accuracy of 55%, a sensitivity of 60%, and a maximum regional similarity coefficient of about 64%. This shows that the model did not learn well (underfitting), highlighting its inability to capture the complex nature of the data for the tumor boundary detection task. Table 2 details the results of all attempts with the U-Net.

Table 2. U-Net results based on four models: baseline, data augmentation, learning rate and hybrid loss function

	Experiment 1	Experiment 2	Experiment 3	Experiment 4
Best Dice	0.6396	0.6349	0.6341	0.6290
Best IoU	0.4871	0.4819	0.4825	0.4749
Best Epoch	10	14	19	18
Accuracy	55%	55%	55%	55%
Precision	54%	54%	55%	55%
Recall	60%	49%	52%	45%
F1-Score	0.57	0.52	0.53	0.49

Due to the segmentation limits, the research moved to a second phase focused on direct classification using the VGG16 architecture. We subjected this model to four rigorous optimization experiments. The first experiment established the baseline through transfer learning with a fully frozen feature extractor, which means that the weights were fixed and only the final classification layers were trained with mammogram data. This approach allows the model to use the generalized knowledge achieved in ImageNet and adapt to the new specific task.

The graphic Accuracy per Epoch, in Fig. 4, shows that the training accuracy rises consistently, reaching values greater than 80%, indicating that the model

has the capacity to learn and memorize the training data. However, the Validation Accuracy stagnates prematurely, which is a symptom of overfitting. This diagnosis is confirmed by the graphic Loss per Epoch, in Fig. 4, in which we can see that, after Epoch 7, the model stopped learning patterns, losing performance with new data. The results on the test set showed an overall accuracy of 63.8% and a sensitivity of 65.3%.

Fig. 4. Accuracy and Loss per Epoch for the baseline experiment with VGG16.

However, the model produced a high volume of false positives, reducing precision to 52.7%. This indicates that, after 182 times, the model predicted malignant, while 47.3% of them were incorrect, which, in a real scenario, would generate a high volume of unnecessary biopsies. The clinical diagnosis pointed to severe overfitting. The network memorized the training data, but failed to generalize. This behavior can be seen in detail in Fig. 5 from the baseline confusion matrix.

The second experiment tried to increase the learning capacity by applying fine tuning. We changed the last convolutional block and introduced an automated scheduler to progressively reduce the learning rate. This intervention, without proper compensation, made the model unstable and uncontrollable. The graphic Accuracy and Loss per Epoch, seen in Fig. 6, shows that a Training Accuracy rising to more than 90%, while the Training Loss converges to values near zero. This demonstrates that the model, now more complex, learned the training data with extreme efficiency.

On the other hand, the Validation Loss is volatile, with a tendency to increase almost immediate, with high peaks. The Validation Accuracy stagnates and becomes erratic, confirming that the model was overfitting more aggressively and unstable than the baseline. The sensitivity dropped drastically to 54% because the network failed to identify almost half of the malignant cases. Although with 53% of precision, F1-score dropped to 54%, confirming loss in general performance. As illustrated by the confusion matrix in Fig. 7, this generated the worst

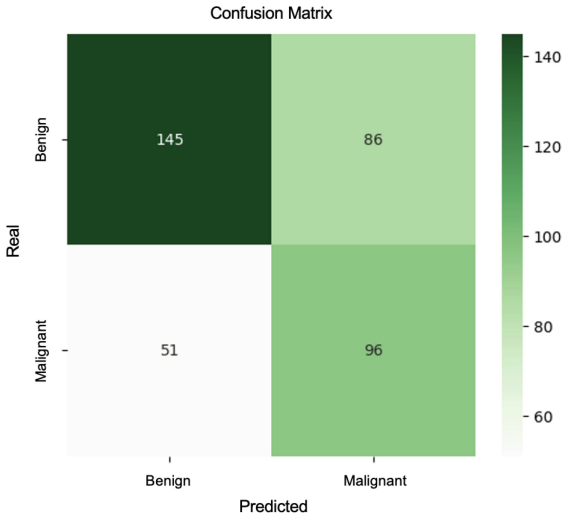

Fig. 5. Confusion Matrix for VGG16 baseline experiment.

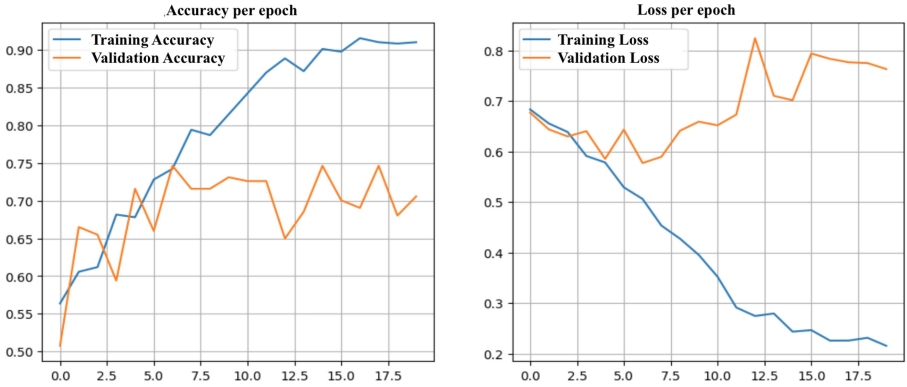

Fig. 6. Accuracy and Loss per Epoch for VGG16 with fine tuning.

clinical result of the phase. The application of fine tuning, without a strong and increase in regularization, was prejudicial. The model became more powerful, but also unstable, compromising sensibility.

To control the instability of the second experiment, the third one implemented a strong regularization strategy. We kept the fine tuning, but added data augmentation, to increase training data variability, and raised the neuron dropout rate to the extreme value of 0.7, forcing the network to be less dependent on specific neurons. The validation curves stopped diverging, proving that the aggressive regularization was successful in stabilizing the training and preventing learning collapse. This evolution is demonstrated in Fig. 8 through the accuracy and loss curves per epoch. The Validation curves are extremely volatile,

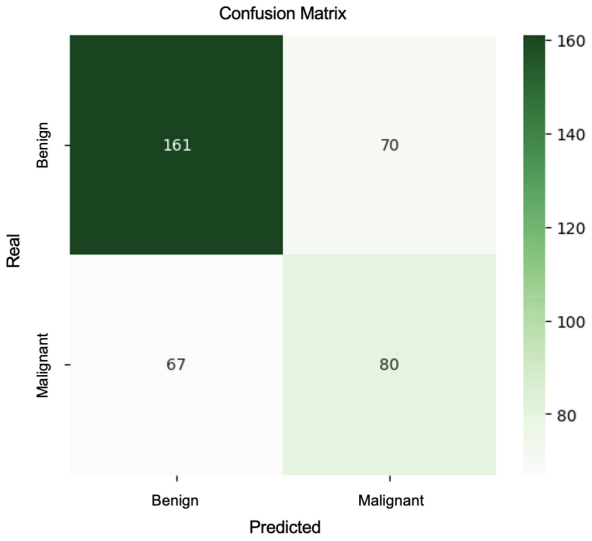

Fig. 7. Confusion Matrix for VGG16 fine tuning experiment.

but they stopped diverging, indicating that the regularization was successful in controlling the model and avoiding the learning collapse.

The fourth and final experiment evaluated whether introducing class balancing through weighted sampling would optimize the system even more [39]. This technique forced the data loader to select samples from the minority class more frequently in order to ensure balanced training batches. The training and validation curves, in Fig. 9, are quite similar to those of experiment three. Both experiments three and four converged to the same performance, establishing the

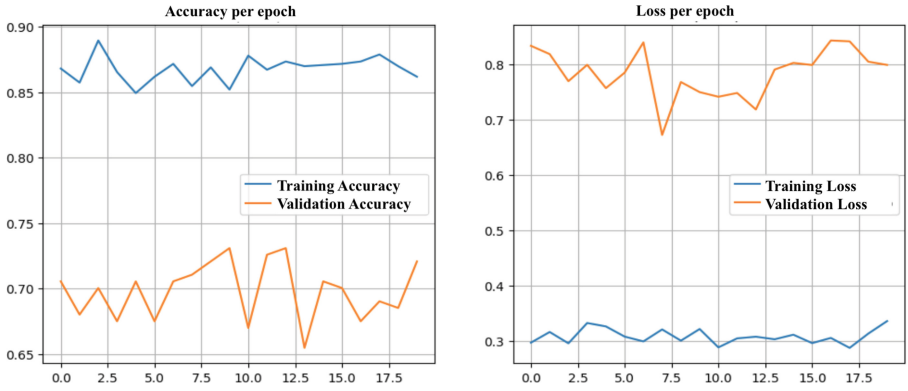

Fig. 8. Accuracy and Loss curves for training and validation per epoch for VGG16 with strong regularization.

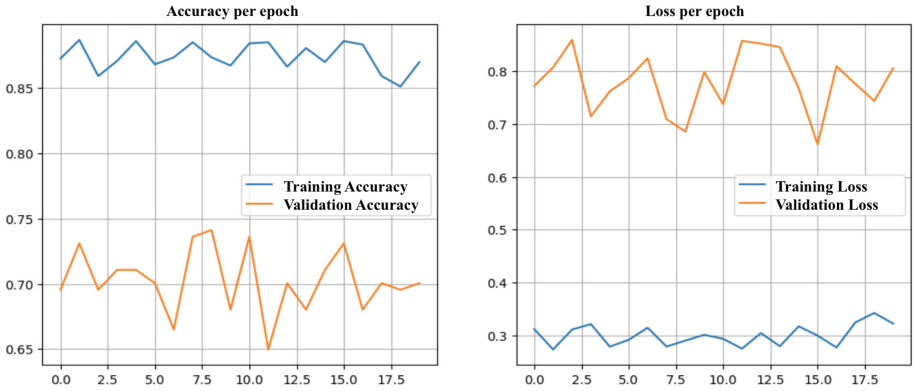

Fig. 9. Accuracy and Loss per Epoch for VGG16 with class balancing.

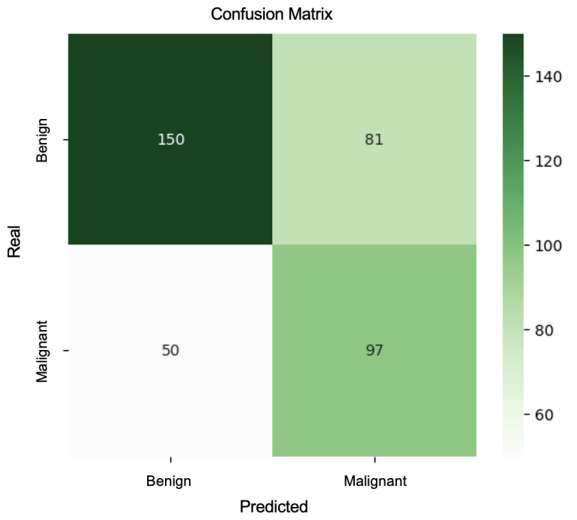

Fig. 10. Confusion Matrix for VGG16 with strong regularization and class balancing.

best results in this work. The significant finding of this experiment was that the methodological addition did not bring isolated improvements. The model converged to the exact same performance as experiment three on the test set. This combined result established the best performance of the work, with an overall accuracy of 65.3% and a sensitivity of 66.0% in detecting malignant cases. Figure 10 displays the resulting confusion matrix from this last step and conclusively illustrates the robustness of the model in correctly identifying pathologies.

5 Conclusion

This study compared semantic segmentation and direct classification strategies to help diagnose breast cancer. Experimental evidence showed that the U-Net architecture has theoretical potential for finding exact regions of interest. However, convergence was complex. The network also required massive amounts of data for pixel-by-pixel annotation. Under the evaluated conditions, this resulted in severe underfitting.

On the other hand, the VGG16 architecture worked better in our experiments. This model was based on the transfer learning paradigm. We implemented a strong regularization strategy using a neuron dropout rate of 0.7. This was the necessary methodological difference to reduce overfitting and ensure knowledge generalization. The system achieved a relevant diagnosis balance, with a 66.0% sensitivity in identifying malignant cases. This suggests that global features may be enough for this task.

In future work, it would be interesting to explore new architectural and methodological limits. Regarding classification, we suggest evaluating more modern and efficient networks, such as the EfficientNet family or Vision Transformers architectures. These models can capture long-range global connections in the image. For the segmentation task, research should move to more advanced U-Net versions, such as Attention U-Net or U-Net++ add attention mechanisms. These mechanisms focus selectively on the most relevant features of the lesion, which could potentially solve the observed underfitting problem.

Acknowledgments. This study was financed in part by the Coordenação de Aperfeiçoamento de Pessoal de Nível Superior, Brasil (CAPES) – Finance Code 001.

References

1. World Health Organization (WHO). https://www.who.int/news-room/fact-sheets/detail/noncommunicable-diseases. Accessed 03 Apr 2025
2. World Health Organization. https://gco.iarc.fr/tomorrow/en/dataviz. Accessed 03 Apr 2025
3. World Health Organization (WHO). https://www.who.int/news-room/fact-sheets/detail/cancer. Accessed 03 Apr 2025
4. National Cancer Institute. https://www.cancer.gov/types/breast/patient/breast_treatment-pdq_185. Accessed 03 Apr 2025
5. World Health Organization. https://gco.iarc.who.int. Accessed 03 Apr 2025
6. Silva, L.F.D., et al.: A new database for breast research with infrared image. J. Med. Imaging Health Inform. **4**(1), 92–100 (2014)
7. Redmon, J., Divvala, S., Girshick, R., Farhadi, A.: You only look once: unified, real-time object detection. In: Computer Vision Foundation, pp. 779–788 (2016)
8. The Cancer Imaging Archive. About - TCIA. https://www.cancerimagingarchive.net/about-the-cancer-imaging-archive-tcia/. Accessed 23 Nov 2025
9. BUDA, M. MRI brain segmentation. https://www.kaggle.com/mateuszbuda/lgg-mri-segmentation. Accessed 25 Nov 2025

10. Kingma, D.P., Ba, J.: Adam: a method for stochastic optimization. In: Proceedings of the 3rd International Conference on Learning Representations (ICLR), San Diego, CA, USA (2015). https://arxiv.org/abs/1412.6980. Accessed 25 Nov 2025
11. Krizhevsky, A., Sutskever, I., Hinton, G.E.: ImageNet classification with deep convolutional neural networks. In: Advances in Neural Information Processing Systems 25 (NIPS 2012), pp. 1097–1105 (2012)
12. He, K., et al.: Deep residual learning for image recognition. In: Proceedings of the IEEE Conference on Computer Vision and Pattern Recognition (CVPR), Las Vegas, NV, USA, pp. 770–778 (2016)
13. Falconi, L.G., et al.: Transfer learning and fine tuning in breast mammogram abnormalities classification on CBIS-DDSM database. Adv. Sci. Technol. Eng. Syst. J. **5**(2), 154–165 (2020)
14. Pinheiro, C.A.D.P.: Detecção e Classificação de Nódulos Pulmonares Utilizando Transferência de Aprendizagem Profunda e Inteligência de Enxame. Master's thesis. Universidade do Estado do Rio de Janeiro (UERJ), Rio de Janeiro, RJ (2019)
15. Conselho Nacional de Saúde. https://www.gov.br/conselho-nacional-de-saude/pt-br/atos-normativos/recomendacoes/2014/recomendacao-no-007.pdf/view. Accessed 03 Apr 2025
16. Rodríguez-Ruiz, A., et al.: Can we reduce the workload of mammographic screening by automatic identification of normal exams with artificial intelligence? A feasibility study. Eur. Radiol. **29**(9), 4825–4832 (2019)
17. Lundervold, A.S., Lundervold, A.: An overview of deep learning in medical imaging focusing on MRI. Z. Med. Phys. **29**(2), 102–127 (2019)
18. Russakovsky, O., et al.: ImageNet large scale visual recognition challenge. Int. J. Comput. Vision (IJCV) **115**, 211–252 (2015)
19. Lecun, Y., et al.: Gradient-based learning applied to document recognition. Proc. IEEE **86**(11), 1–46 (1998). ISSN 00189219
20. Baffa, M., Coelho, A.M., Conci, A.: Segmentação de imagens infravermelhas para detecção do câncer de mama utilizando U-net CNN. In: Proceedings of the XXXIV Conference on Graphics, Patterns and Images (SIBGRAPI), pp. 361–368 (2021)
21. John, G.H., Langley, P.: Estimating continuous distributions in Bayesian classifiers. In: Proceedings of the Eleventh Conference on Uncertainty in Artificial Intelligence (UAI), pp. 338–345. Morgan Kaufmann (1995)
22. Breiman, L.: Random forests. Mach. Learn. **45**(1), 5–32 (2001)
23. Méndez, M., Muñoz, J.P.: Identificación de la Región de Interés (ROI) en imágenes médicas, utilizando técnicas de Deep Learning. Master's thesis (2021)
24. Silva, A.F.D.: Sistema Inteligente para o Apoio ao Diagnóstico do Câncer de Mama através da análise de imagens termográficas e do uso de Redes Neurais Artificiais Profundas. Master's thesis. Universidade Federal de Pernambuco (UFPE), Recife, PE (2022)
25. Cortes, C., Vapnik, V.: Support-vector networks. Mach. Learn. **20**(3), 273–297 (1995)
26. Long, J., Shelhamer, E., Darrell, T.: Fully convolutional networks for semantic segmentation. In: Proceedings of the IEEE Conference on Computer Vision and Pattern Recognition (CVPR), Boston, MA, USA, pp. 3431–3440 (2015)
27. Badrinarayanan, V., Kendall, A., Cipolla, R.: SegNet: a deep convolutional encoder-decoder architecture for image segmentation. IEEE Trans. Pattern Anal. Mach. Intell. **39**(12), 2481–2495 (2017)
28. Szegedy, C., et al.: Going deeper with convolutions. In: Proceedings of the IEEE Conference on Computer Vision and Pattern Recognition (CVPR), Boston, MA, USA, pp. 1–9 (2015)

29. Bisong, E.: Building Machine Learning and Deep Learning Models on Google Cloud Platform: A Comprehensive Guide for Beginners. Apress (2019)
30. Nielsen, M.A.: Neural Networks and Deep Learning. Determination Press (2015). http://neuralnetworksanddeeplearning.com/
31. Goodfellow, I., Bengio, Y., Courville, A.: Deep Learning. MIT Press (2016). https://www.deeplearningbook.org/
32. Lee, R.S., et al.: A curated mammography data set for use in computer-aided detection and diagnosis research. Sci. Data **4**, 170177 (2017)
33. Ronneberger, O., Fischer, P., Brox, T.: U-Net: convolutional networks for biomedical image segmentation. In: Proceedings of the International Conference on Medical Image Computing and Computer-Assisted Intervention (MICCAI), Munich, Germany, pp. 234–241 (2015)
34. Simonyan, K., Zisserman, A.: Very Deep Convolutional Networks for Large-Scale Image Recognition. arXiv preprint, pp. 1097–1105 (2012)
35. Hosny, A., et al.: Artificial intelligence for precision oncology. Nat. Rev. Cancer **22**(10), 563–578 (2022)
36. Nvidia. A new level of acceleration has arrived. https://www.nvidia.com/pt-br/data-center/tesla-t4/. Accessed 25 Mar 2025
37. Bisong, E.: Google Colaboratory, pp. 59–64. Apress (2019). Cloud development environment
38. American College of Radiology: ACR BI-RADS Atlas: Breast Imaging Reporting and Data System, 5th edn. American College of Radiology, Reston, VA (2013)
39. Paszke, A., et al.: Pytorch: an imperative style, high-performance deep learning library. In: Advances in Neural Information Processing Systems (NeurIPS), vol. 32, pp. 8024–8035. Curran Associates, Inc. (2019)

Computational Methods for Porous Materials (CompPor 2026)

Stabilized Finite Element Framework for Transient Darcy–Brinkman–Forchheimer Flow Under Local Thermal Non-equilibrium

Rafael C. Moura(✉), Isaac P. Santos, and Lucia Catabriga

Federal University of Espírito Santo, Vitória, ES, Brazil
rafaelcabraldemoura@gmail.com, isaac.santos@ufes.br, luciac@inf.ufes.br

Abstract. Numerical simulation of fluid flow in porous media plays a central role in many scientific and engineering applications. Achieving a proper balance between model complexity and numerical discretization is crucial for computational efficiency. Classical Darcy-based models, however, lose accuracy in high-velocity regimes and in highly porous or permeable media, where viscous and inertial effects become significant. In this work, we consider the transient Darcy–Brinkman–Forchheimer (DBF) model, fully coupled with an energy formulation under Local Thermal Non-Equilibrium (LTNE), thereby providing a consistent extension beyond Darcy flow under mixed-convection conditions. The resulting nonlinear system presents significant challenges, particularly in advection-dominated and non-Darcy regimes. To address these challenges, we propose an efficient stabilized finite element framework based on equal-order linear interpolations for all primitive variables. The formulation combines the Streamline Upwind Petrov–Galerkin (SUPG) and Pressure-Stabilizing Petrov–Galerkin (PSPG) stabilization mechanisms, ensuring numerical stability and pressure–velocity compatibility in a strongly nonlinear transient simulation context. The method is evaluated using benchmark free-flow problems adapted to a porous-media setting and a synthetic fractured porous structure based on a Julia-set fractal geometry. The results demonstrate stable, accurate, and physically consistent solutions across different flow regimes, highlighting the robustness and applicability of the proposed framework to complex transient porous-media problems.

Keywords: Darcy-Brinkman-Forchheimer · Stabilized · SUPG · PSPG · SUPS · LSIC · BDF2 · Finite element · Local Thermal Non-Equilibrium

1 Introduction

Numerical simulation of fluid flow in porous media is central to several scientific and engineering applications, including oil reservoir engineering, geological carbon storage, groundwater hydrology, geothermal systems, and advanced

© The Author(s), under exclusive license to Springer Nature Switzerland AG 2027
O. Gervasi et al. (Eds.): ICCSA 2026 Workshops, LNCS 16761, pp. 39–57, 2027.
https://doi.org/10.1007/978-3-032-30527-5_3

materials processing. The classical mathematical framework relies on conservation of mass, Darcy's law [10], and, when required, the energy conservation equation. Although Darcy-based models are robust and widely implemented in both commercial and academic simulations, their validity is restricted to low-velocity regimes where inertial effects are negligible [29]. In highly porous or permeable formations, particularly in fractured systems or near wells, viscous shear and inertial contributions become significant, leading to deviations from Darcy's law. To address these limitations, several extensions have been proposed in the literature, as discussed in [23]. The Brinkman correction incorporates viscous diffusion effects [6], while the Forchheimer term introduces nonlinear inertial contributions relevant at higher Reynolds number regimes [13]. Together, these modifications yield the Darcy–Brinkman–Forchheimer (DBF) formulation, which can be derived from the volume-averaged Navier–Stokes equations [30] combined with generalized porous drag laws [23]. The DBF model provides a unified continuum framework that can represent creeping, viscous-dominated, and inertia-dominated regimes within a single formulation. This unified description is particularly relevant in fractured porous media and near injection or production wells, where flow transitions between regimes may occur.

Alternative strategies for modeling fractured porous media are extensively documented in the literature [4], including equivalent-porous-media models, dual-porosity, dual-permeability, and discrete-fracture-network (DFN) models. While these methods differ in their structural representation of fractures, the DBF framework is especially attractive in higher-velocity regimes where inertial effects must be explicitly accounted for within a continuum formulation.

When thermal effects are considered, additional modeling challenges arise. In high-velocity regimes or in media with significant solid–fluid heat exchange, the assumption of local thermal equilibrium may no longer hold. Under such conditions, separate energy equations must be introduced for the fluid and solid phases, leading to the Local Thermal Non-Equilibrium (LTNE) formulation. The resulting coupled DBF–LTNE system constitutes a strongly nonlinear, potentially advection-dominated problem. Quadratic nonlinearities arise from the Forchheimer term, whereas high Darcy or Reynolds numbers amplify convective transport, potentially leading to numerical instabilities. Furthermore, increasing physical model fidelity typically increases implementation complexity and computational cost, reinforcing the need for a balanced compromise between physical representativeness and numerical tractability.

Stabilized finite element methods offer an effective strategy for addressing these challenges while preserving implementation simplicity. In particular, the combination of Streamline Upwind Petrov–Galerkin (SUPG) [17], and Pressure Stabilized Petrov–Galerkin (PSPG) [25] techniques enables equal-order interpolation for the velocity and pressure fields, reducing implementation complexity while maintaining numerical robustness. Since the seminal developments in [7,27], SUPG and PSPG formulations have been widely employed in incompressible flow simulations. The combination of SUPG and PSPG is sometimes denoted as the SUPS formulation [9]. Variants of these stabilization approaches have also

been proposed in the literature, which incorporate modifications of stabilization parameters and additional shock-capturing mechanisms [2,18,26,28].

In this work, we investigate a stabilized finite element framework for the transient Darcy–Brinkman–Forchheimer model coupled with the Local Thermal Non-Equilibrium formulation. The present contribution extends our previous work [22] by incorporating a thermal LTNE model, adding a Least-Squares on the Incompressibility Constraint (LSIC) stabilized term, and adopting the second-order backward differentiation BDF2 for time discretization [12]. The proposed approach seeks a balanced compromise between physical model fidelity and numerical implementation complexity, enabling robust simulation of advection-dominated and non-Darcy flows in porous media. The formulation is assessed through a series of adapted benchmark problems, including classical flow configuration and fractured porous structures represented by Julia-set fractal geometry [3,8] which has been applied in the literature for other purposes [14,31].

The remainder of this paper is organized as follows. Section 2 presents the governing equations of the transient Darcy–Brinkman–Forchheimer model coupled with the Local Thermal Non-Equilibrium energy formulation. Section 3 describes the stabilized finite element framework, including the SUPS and LSIC formulations adopted for spatial discretization. Section 4 introduces the numerical applications and benchmark configurations, including verification analyses and representative porous-media flow scenarios. Finally, Sect. 5 summarizes the main conclusions of the present work.

2 Governing Equations

The transient Darcy-Brinkman-Forchheimer model is adopted to describe momentum conservation, while a Local Thermal Non-quilibrium model governs the energy balance in the fluid and porous solid phases. Buoyancy effects are incorporated through the Boussinesq approximation. We consider a viscous, incompressible, transient flow in a porous medium occupying a fixed spatial domain $\Omega \subset \mathbb{R}^2$, with boundary Γ. The space–time domain is denoted by $\Omega_T := \Omega \times (0,T]$ for $T > 0$, with the initial configuration prescribed on $\Omega_0 := \Omega \times \{0\}$, and boundary conditions are defined on $\Gamma_T := \Gamma \times (0,T]$.

In dimensional form, mass conservation for an incompressible fluid with no sources or sink terms is represented by:

$$\nabla \cdot \mathbf{u} = 0 \quad \text{in } \Omega_T, \tag{1}$$

where $\mathbf{u}$ is a bidimensional velocity field. Momentum conservation follows the Darcy–Brinkman–Forchheimer model [23], expressed in terms of the velocity $\mathbf{u}$ and pressure P in Ω_T as

$$\frac{\rho_f}{\phi}\left[\frac{\partial \mathbf{u}}{\partial t} + \nabla\left(\frac{\mathbf{u}\cdot\mathbf{u}}{\phi}\right)\right] + \nabla(P - \rho_f \mathbf{g} y) - \frac{\tilde{\mu}}{\phi}\nabla^2\mathbf{u} + \left(\frac{\mu}{\mathbf{K}} + \frac{c_F \rho_f ||\mathbf{u}||}{\mathbf{K}^{1/2}}\right)\mathbf{u} = \mathbf{0}, \tag{2}$$

where ρ_f and μ represent the fluid density and viscosity, respectively. The rock porosity ϕ is a scalar field, and $\mathbf{K}$ is an isotropic permeability tensor. The parameter $\tilde{\mu}$ accounts for the Brinkman viscous correction [6], and c_F denotes the Forchheimer quadratic drag correction. Finally, the gravitational acceleration vector is given by $\mathbf{g} = [0, -g]$. To account for natural and mixed convection effects, density variations are introduced via the Boussinesq approximation, assuming the linear equation of state $\rho_f = \rho_{f_{ref}}[1 - \beta_T(T_f - T_{f_{ref}})]$, where β_T is the thermal expansion coefficient. Substitution into the momentum equation leads to the modified formulation

$$\begin{aligned} &\rho_{f_{ref}} \left[\frac{1}{\phi} \frac{\partial \mathbf{u}}{\partial t} + \frac{1}{\phi} \nabla \left(\frac{\mathbf{u} \cdot \mathbf{u}}{\phi} \right) \right] + \nabla p - \frac{\tilde{\mu}}{\phi} \nabla^2 \mathbf{u} \\ &+ \frac{\mu}{\mathbf{K}} \mathbf{u} + \frac{c_F \rho_{f_{ref}}}{\mathbf{K}^{1/2}} \|\mathbf{u}\| \mathbf{u} + \rho_{f_{ref}} \beta_T \left(T_f - T_{f_{ref}} \right) \mathbf{e}_g = \mathbf{0} \ \text{ in } \Omega_T, \end{aligned} \tag{3}$$

where p is a modified pressure field incorporating the hydrostatic contribution $\rho_{f_{ref}} \mathbf{g}$. Following the validity discussion in [16], the Boussinesq approximation is used here as a controlled numerical modeling assumption to intentionally enhance buoyancy effects and assess the behavior of the numerical method, rather than as a strict small-temperature-difference approximation.

Heat transfer is modeled using a local thermal non-equilibrium approach, in which fluid and solid matrix temperatures are governed by separate energy equations [23]:

$$(\rho c_p)_f \left(\frac{\partial T_f}{\partial t} + \frac{\mathbf{u}}{\phi} \cdot \nabla T_f \right) = \nabla \cdot (\kappa_f \nabla T_f) + \frac{h}{\phi} (T_s - T_f) + \Phi_v \ \text{ in } \Omega_T, \tag{4}$$

$$(\rho c_p)_s \frac{\partial T_s}{\partial t} = \nabla \cdot (\kappa_s \nabla T_s) + \frac{h}{(1-\phi)} (T_f - T_s) \ \text{ in } \Omega_T. \tag{5}$$

Here, κ_f and κ_s denote the isotropic thermal conductivity tensors of the fluid and solid phases, respectively, and h is the convective heat transfer coefficient. Additionally, we assume that the viscous dissipation is neglected, i.e., $\Phi_v = \mathbf{0}$.

For numerical and physical interpretation purposes, the system is nondimensionalized using characteristic length, velocity, pressure, and temperature scales. The resulting formulation is expressed in terms of Reynolds (Re), Darcy (Da), Prandtl (Pr), Nusselt (Nu), and Richardson (Ri)numbers, appropriate for mixed convection regimes:

$$\mathbf{x}^* = \frac{\mathbf{x}}{L_{ref}}, \ \mathbf{t}^* = \frac{U_{ref}\, t}{L_{ref}}, \ \mathbf{u}^* = \frac{\mathbf{u}}{U_{ref}}, \ p^* = \frac{p}{\rho_{ref} U_{ref}^2}, \ T^* = \frac{T - T_{ref}}{\Delta T}, \tag{6}$$

where $\Delta T = T_{hot} - T_{cold}$ and $T_{ref} = (T_{hot} + T_{cold})/2$. For simplicity, the same notation is retained for the dimensionless primitive variables ($\mathbf{u}$, p, T_f, T_s). The resulting dimensionless primitive variable formulation is defined by

$$\nabla \cdot \mathbf{u} = \mathbf{0} \quad \text{in } \Omega_T, \tag{7}$$

$$\frac{\partial \mathbf{u}}{\partial t} + (\mathbf{u}\cdot\nabla)\left(\frac{\mathbf{u}}{\phi}\right) - \left(\frac{\Lambda_u}{Re}\right)\nabla^2\mathbf{u} + \phi\left(\frac{1}{Re\,Da} + \frac{c_F\,\|\mathbf{u}\|}{Da^{1/2}}\right)\mathbf{u} + \phi\,\nabla p + \phi\,Ri\,T_f\,\mathbf{e}_g = \mathbf{f}_u \quad \text{in } \Omega_T, \tag{8}$$

$$\frac{\partial T_f}{\partial t} + \frac{1}{\phi}\mathbf{u}\cdot\nabla T_f - \frac{1}{Re}\nabla\cdot\left(\frac{1}{Pr}\nabla T_f\right) - \frac{Nu}{Re\,Pr\,\phi}(T_s - T_f) = f_{T_f} \text{ in } \Omega_T, \tag{9}$$

$$\frac{\partial T_s}{\partial t} - \frac{1}{Re\,\Lambda_{\rho c_p}}\nabla\cdot\left(\frac{\Lambda_\kappa}{Pr}\nabla T_s\right) - \frac{Nu}{RePr\Lambda_{\rho c_p}(1-\phi)}(T_f - T_s) = f_{T_s} \text{ in } \Omega_T, \tag{10}$$

where $\Lambda_\mu = \tilde{\mu}/\mu$, $\Lambda_\kappa = \kappa_s/\kappa_f$, $\Lambda_{\rho c_p} = (\rho c_p)_s/(\rho c_p)_f$ and $\mathbf{e_g} = [0, -1]$. Source terms $\mathbf{f_u}$, f_{T_f}, and f_{T_s} are introduced when required for verification through manufactured analytical solutions. Initial conditions are prescribed for each primitive variable ψ in the form

$$\psi(\mathbf{x}, 0) = \psi_0(\mathbf{x}) \text{ in } \Omega_0, \tag{11}$$

and the boundary Γ is decomposed in Dirichlet and Neumann portions according to the field variable under consideration, such that $\Gamma = \Gamma_\psi^D \cup \Gamma_\psi^N$ with $\Gamma_\psi^D \cap \Gamma_\psi^N = \emptyset$. The corresponding space–time boundaries are defined over Γ_T, leading to

$$\psi(\mathbf{x}, t) = g_\psi(\mathbf{x}, t) \text{ in } \Gamma_\psi^D \text{ and } \nabla\psi(\mathbf{x}, t)\cdot\mathbf{n} = 0 \text{ in } \Gamma_\psi^N \quad \forall t \in (0, T]. \tag{12}$$

The Neumann boundary conditions are naturally incorporated into the weak formulation through the boundary terms arising from integration by parts. For the scalar pressure field p, no Neumann condition is prescribed.

3 Stabilized Finite Element Formulation

To ensure numerical stability and robustness in advection-dominated and non-Darcy flow regimes, we adopt a stabilized finite element formulation based on equal-order linear interpolations for all primitive variables. The proposed approach combines the SUPG and PSPG techniques with an LSIC stabilization. This unified strategy enables the use of continuous linear elements for both velocity and pressure fields while controlling spurious oscillations, enhancing pressure stability, and improving mass conservation in strongly nonlinear transient regimes. The domain Ω is approximated by a conforming triangulation Ω^h, composed of a finite set of non-overlapping triangular elements Ω_e, such that

$$\Omega^h = \bigcup_{e=1}^{n_e} \Omega_e, \qquad \Omega_i^\circ \cap \Omega_j^\circ = \emptyset \quad \text{for } i \neq j, \tag{13}$$

where Ω_e° denotes the interior of the element Ω_e, n_e is the number of elements in discretized domain Ω^h. Over this partition, finite-dimensional subspaces of

$H^1(\Omega)$ are constructed using continuous piecewise linear polynomials. The finite element approximation space for a generic primitive variable ψ is defined as:

$$\mathcal{H}^{1h} = \{\psi^h \,|\, \psi^h \in \mathcal{C}^0(\Omega), \psi^h|_{\Omega_e} \in \mathcal{P}^1(\Omega_e), \forall \Omega_e \in \Omega^h\}, \tag{14}$$

where $\mathcal{P}^1(\Omega_e)$ denotes the space of first-order polynomials defined on Ω_e. For a generic primitive variable ψ, the corresponding trial and test spaces are defined, respectively, as

$$\mathcal{S}_\psi^h = \{\psi^h \,|\, \psi^h \in [\mathcal{H}^{1h}(\Omega^h)]^d,\ \psi^h = \bar{\psi} \text{ on } \Gamma^D\}, \tag{15}$$

$$\mathcal{V}_\psi^h = \{w_\psi^h \,|\, w_\psi^h \in [\mathcal{H}^{1h}(\Omega^h)]^d,\ w_\psi^h = 0 \text{ on } \Gamma^D\}. \tag{16}$$

where $d = 2$ for the velocity field and $d = 1$ for scalar variables, and $\bar{\psi}$ denotes the prescribed Dirichlet boundary value of ψ on Γ^D.

Since equal-order interpolation is adopted for velocity and pressure fields, the resulting discrete formulation does not satisfy the classical inf-sup (Ladyzhenskaya–Babuška–Brezzi) stability condition [5]. This issue is addressed through the Pressure-Stabilizing Petrov–Galerkin (PSPG) stabilization, which ensures stability of the pressure approximation while allowing the use of continuous linear elements for all primitive variables.

The semidiscrete variational formulation consists of finding the discrete primitive variables $\psi^h \in \mathcal{S}_\psi^h$ for $t \in (0, T]$ such that $\forall\, w_\psi^h \in \mathcal{V}_\psi^h$, the weak form of each balance equation is satisfied. The resulting variational statements for mass, momentum, and energy conservation are described as follows. The Galerkin formulation of the conservation of mass equation onto the discrete space defined over Ω reads

$$\int_\Omega w_p^h \left(\nabla \cdot \mathbf{u}^h\right) d\Omega = 0. \tag{17}$$

The stabilized Petrov–Galerkin formulation adopted for the conservation of momentum combines SUPG, PSPG, and LSIC contributions and is written as

$$\begin{aligned} &\int_\Omega \mathbf{w}_u^h \cdot \mathcal{L}_m^h d\Omega + \sum_{e=1}^{n_e} \int_{\Omega_e} \tau_S (\mathbf{u}^h \cdot \nabla)\mathbf{w}_u^h \cdot \mathcal{L}_m^h d\Omega_e \\ &+ \sum_{e=1}^{n_e} \int_{\Omega_e} \tau_P \nabla w_p^h \cdot \mathcal{L}_m^h d\Omega_e + \sum_{e=1}^{n_e} \int_{\Omega_e} \tau_L (\nabla \cdot \mathbf{w}_u^h)(\nabla \cdot \mathbf{u}^h) d\Omega_e = \mathbf{0}, \end{aligned} \tag{18}$$

where

$$\begin{aligned} \mathcal{L}_m^h(\mathbf{u}^h, p^h, T_f^h) = \frac{\partial \mathbf{u}^h}{\partial t} + (\mathbf{u}^h \cdot \nabla)\left(\frac{\mathbf{u}^h}{\phi}\right) - \left(\frac{\Lambda_\mu}{Re}\right)\nabla^2 \mathbf{u}^h \\ + \phi\left(\tfrac{1}{ReDa} + \tfrac{c_F \|\mathbf{u}^h\|}{Da^{1/2}}\right)\mathbf{u}^h + \phi \nabla p^h + \phi\, Ri\, T_f^h\, \mathbf{e}_g - \mathbf{f}_u. \end{aligned} \tag{19}$$

The element-level stabilization parameters for SUPG, PSPG, and LSIC follow the adaptation proposed in [11] for the Darcy–Brinkman–Forchheimer formula-

tion and are computed as

$$\tau_S = \left\{ \left(\frac{1}{\Delta t}\right)^2 + \left(\frac{2\|\mathbf{u}_b\|}{h_e}\right)^2 + 9\left(\frac{4\Lambda_\mu}{Re\, h_e^2}\right)^2 + \left[\phi\left(\frac{1}{Re\, Da} + \frac{c_F\|\mathbf{u}_b\|}{Da^{1/2}}\right)\right]^2 \right\}^{-1/2}, \tag{20}$$

with $\tau_P = \tau_L = \tau_S$. Here, $\|\mathbf{u}_b\|$ denotes the Euclidean norm of the velocity evaluated at the element barycenter, and $h_e = 4A_e/\pi$ represents the equivalent element size computed from the element area A_e.

For the energy equations of the fluid and solid phases, a Petrov–Galerkin formulation with SUPG stabilization is employed for the fluid equation, while the solid equation retains the standard Galerkin form:

$$\int_\Omega w^h_{T_f} \mathcal{L}^h_{T_f} d\Omega + \sum_{e=1}^{n_e} \int_{\Omega_e} \tau_{S_{T_f}} (\mathbf{u}^h \cdot \nabla) w^h_T \mathcal{L}^h_{T_f} d\Omega_e = 0, \tag{21}$$

$$\int_\Omega w^h_{T_s} \left[\frac{\partial T^h_s}{\partial t} - \frac{1}{Re\, \Lambda_{\rho c_p}} \nabla \cdot \left(\frac{\Lambda_\kappa}{Pr} \nabla T^h_s \right) - \frac{Nu(T^h_f - T^h_s)}{RePr\, \Lambda_{\rho c_p}(1-\phi)} - f_{T_s} \right] = 0 \tag{22}$$

where

$$\begin{aligned} \mathcal{L}^h_{T_f}(\mathbf{u}^h, T^h_f, T^h_s) = \frac{\partial T^h_f}{\partial t} + \frac{\mathbf{u}^h_f}{\phi} \cdot \nabla T^h_f - \frac{1}{Re} \nabla \cdot \left(\frac{1}{Pr_f} \nabla T^h_f \right) \\ - \frac{Nu(T^h_s - T^h_f)}{RePr_f \phi} - f_{T_f}, \end{aligned} \tag{23}$$

and a similar SUPG stabilization parameter adapted from [11]:

$$\tau_{S_{T_f}} = \left[\left(\frac{1}{\Delta t}\right)^2 + \left(\frac{2\|\mathbf{u}_b\|}{h_e}\right)^2 + 9\left(\frac{4}{Re\, Pr\, h_e^2}\right)^2 + \left(\frac{Nu}{Re\, Pr\, \phi}\right)^2 \right]^{-1/2}. \tag{24}$$

The spatial discretization in terms of nodal unknows ($\mathbf{U}$, $\mathbf{P}$, $\mathbf{T}_f$ and $\mathbf{T}_s$) is obtained by restricting the weak forms, Eqs. (18), (21), and (22), to each element Ω_e, which leads to element-level matrices associated with the corresponding contributions of each term. The momentum Eq. (18) generates the standard Galerkin matrices (denoted by superscript G), which, combined with SUPG (S superscript) and LSIC (L superscript) stabilization terms, produce the first block of the discrete momentum equations. The resulting element matrices contributing to the nonlinear coupled system are indicated with overbraces in the expression below:

$$\begin{aligned} &\overbrace{(\mathbf{M}^{\mathbf{G}}_{\mathbf{u}} + \mathbf{M}^{\mathbf{S}}_{\mathbf{u}})}^{\mathbf{M_u}} \dot{\mathbf{U}} + \overbrace{(\mathbf{A}^{\mathbf{G}}_{\mathbf{u}}(\mathbf{u}) + \mathbf{A}^{\mathbf{S}}_{\mathbf{u}}(\mathbf{u}) + \mathbf{D}^{\mathbf{G}}_{\mathbf{u}} + \mathbf{R}^{\mathbf{G}}_{\mathbf{u}} + \mathbf{R}^{\mathbf{S}}_{\mathbf{u}} + \mathbf{K}^{\mathbf{L}}_{\mathbf{u}})}^{\mathbf{K_u}} \mathbf{U} \\ &+ \underbrace{(\mathbf{G}^{\mathbf{G}}_{\mathbf{u}} + \mathbf{G}^{\mathbf{S}}_{\mathbf{u}})}_{\mathbf{G_u}} \mathbf{P} + \underbrace{(\mathbf{R}^{\mathbf{G}}_{\mathbf{T_f}} + \mathbf{R}^{\mathbf{S}}_{\mathbf{T_f}})}_{\mathbf{R_{T_f}}} \mathbf{T}_f = \underbrace{\mathbf{F}^{\mathbf{G}}_{\mathbf{u}} + \mathbf{F}^{\mathbf{S}}_{\mathbf{u}}}_{\mathbf{F_u}}. \end{aligned} \tag{25}$$

The discretized continuity equation, combined with PSPG stabilization (superscript P), introduces additional pressure-coupling terms arising from the momentum residual, yielding the second block of equations:

$$\mathbf{M}_{\mathbf{u}}^{\mathbf{P}}\dot{\mathbf{U}} + \overbrace{(\mathbf{G}_{\rho}^{\mathbf{G}} + \mathbf{A}_{\mathbf{u}}^{\mathbf{P}}(\mathbf{u}) + \mathbf{R}_{\mathbf{u}}^{\mathbf{P}})}^{\mathbf{G}_{\rho}}\mathbf{U} + \mathbf{G}_{\mathbf{u}}^{\mathbf{P}}\mathbf{P} + \mathbf{R}_{\mathbf{T_f}}^{\mathbf{P}}\mathbf{T}_f = \mathbf{F}_{\mathbf{u}}^{\mathbf{P}}. \tag{26}$$

The third block corresponds to the discretization of the local thermal non-equilibrium model. It includes both Galerkin and SUPG contributions for the fluid temperature equation and standard Galerkin terms for the solid temperature equation. The resulting element-level thermal system is given by

$$\begin{aligned}\overbrace{(\mathbf{M}_{\mathbf{T}}^{\mathbf{G}} + \mathbf{M}_{\mathbf{T_f}}^{\mathbf{S}})}^{\mathbf{M}_{\mathbf{T_f}}}\dot{\mathbf{T}}_f + \overbrace{(\mathbf{A}_{\mathbf{T_f}}^{\mathbf{G}}(\mathbf{u}) + \mathbf{A}_{\mathbf{T_f}}^{\mathbf{S}}(\mathbf{u}) + \mathbf{D}_{\mathbf{T_f}}^{\mathbf{G}} + \mathbf{R}_{\mathbf{T_f}}^{\mathbf{G}} + \mathbf{R}_{\mathbf{T_{f,f}}}^{\mathbf{S}})}^{\mathbf{K}_{\mathbf{T_f}}}\mathbf{T}_f \\ + \underbrace{(\mathbf{R}_{\mathbf{T_{s,f}}}^{\mathbf{G}} + \mathbf{R}_{\mathbf{T_{s,f}}}^{\mathbf{S}})}_{\mathbf{R}_{\mathbf{T_{s,f}}}}\mathbf{T}_s = \underbrace{\mathbf{F}_{\mathbf{T_f}}^{\mathbf{G}} + \mathbf{F}_{\mathbf{T_f}}^{\mathbf{S}}}_{\mathbf{F}_{\mathbf{T_f}}},\end{aligned} \tag{27}$$

$$\mathbf{M}_{\mathbf{s}}^{\mathbf{G}}\dot{\mathbf{T}}_s + \overbrace{(\mathbf{D}_{\mathbf{T_s}}^{\mathbf{G}} + \mathbf{R}_{\mathbf{T_{s,s}}}^{\mathbf{G}})}^{\mathbf{K}_{\mathbf{T_s}}^{\mathbf{G}}}\mathbf{T}_s + \mathbf{R}_{\mathbf{T_{f,s}}}^{\mathbf{G}}\mathbf{T}_f = \mathbf{F}_{\mathbf{T_s}}^{\mathbf{G}}. \tag{28}$$

After stacking the corresponding element matrices, the fully coupled element-level system assumes the compact block structure, given by

$$\overbrace{\begin{bmatrix}\mathbf{M_u} & \mathbf{0} & \mathbf{0} & \mathbf{0}\\ \mathbf{M}_{\mathbf{u}}^{\mathbf{P}} & \mathbf{0} & \mathbf{0} & \mathbf{0}\\ \mathbf{0} & \mathbf{0} & \mathbf{M_{T_f}} & \mathbf{0}\\ \mathbf{0} & \mathbf{0} & \mathbf{0} & \mathbf{M}_{\mathbf{T_s}}^{\mathbf{G}}\end{bmatrix}}^{\mathcal{M}_e}\overbrace{\begin{bmatrix}\dot{\mathbf{U}}\\ \dot{\mathbf{P}}\\ \dot{\mathbf{T}}_{\mathbf{f}}\\ \dot{\mathbf{T}}_{\mathbf{s}}\end{bmatrix}}^{\dot{\mathcal{U}}_e} + \overbrace{\begin{bmatrix}\mathbf{K_u} & \mathbf{G_u} & \mathbf{R_{T_f}} & \mathbf{0}\\ \mathbf{G}_{\rho} & \mathbf{G}_{\mathbf{u}}^{\mathbf{P}} & \mathbf{R}_{\mathbf{T_f}}^{\mathbf{P}} & \mathbf{0}\\ \mathbf{0} & \mathbf{0} & \mathbf{K_{T_f}} & \mathbf{R_{T_{s,f}}}\\ \mathbf{0} & \mathbf{0} & \mathbf{R}_{\mathbf{T_{f,s}}}^{\mathbf{G}} & \mathbf{K}_{\mathbf{T_s}}^{\mathbf{G}}\end{bmatrix}}^{\mathcal{K}_e}\overbrace{\begin{bmatrix}\mathbf{U}\\ \mathbf{P}\\ \mathbf{T_f}\\ \mathbf{T_s}\end{bmatrix}}^{\mathcal{U}_e} = \overbrace{\begin{bmatrix}\mathbf{F_u}\\ \mathbf{F}_{\mathbf{u}}^{\mathbf{P}}\\ \mathbf{F_{T_f}}\\ \mathbf{F}_{\mathbf{T_s}}^{\mathbf{G}}\end{bmatrix}}^{\mathcal{F}_e}. \tag{29}$$

In this notation, the zero blocks in Eq. (29) represent submatrices with appropriate dimensions required for the assembly procedure. The element-level contributions provide the mass, stiffness, and source terms that are assembled into the global nonlinear system of Ordinary Differential Equations (ODEs):

$$\mathcal{M}\dot{\mathcal{U}} + \mathcal{K}(\mathcal{U})\mathcal{U} = \mathcal{F}, \tag{30}$$

with:

$$\mathcal{M} = \mathop{\mathbf{A}}_{e=1}^{n_e}\mathcal{M}_e, \quad \mathcal{K} = \mathop{\mathbf{A}}_{e=1}^{n_e}\mathcal{K}_e \quad \text{and} \quad \mathcal{F} = \mathop{\mathbf{A}}_{e=1}^{n_e}\mathcal{F}_e. \tag{31}$$

Time integration is performed using the second-order Backward differentiation method (BDF2), described in [12]. The semi-discrete system of ODEs (30) can be written as

$$\left(\frac{3}{2}\mathcal{M} + \Delta t\mathcal{K}^{n+1}\right)\mathcal{U}^{n+1} = \mathcal{M}\left(2\mathcal{U}^{n} - \frac{1}{2}\mathcal{U}^{n-1}\right) + \Delta t\mathcal{F}^{n+1}, \tag{32}$$

where Δt denotes the time step. Owing to the nonlinear dependence of the stiffness matrix $\mathcal{K}(\mathcal{U})$, a lagged linearization strategy based on the previous time level is employed, combined with a Picard iterative scheme. At each nonlinear iteration, a linearized system is solved using GMRES, preconditioned with an incomplete LU factorization. The iterative process continues until the norm of the nonlinear residual falls below a prescribed tolerance or the maximum number of nonlinear iterations is reached.

4 Numerical Applications

Numerical applications of the Darcy–Brinkman–Forchheimer model with local thermal non-equilibrium often explore idealized configurations and adopt nondimensional parameter ranges tailored to specific theoretical objectives. In the present work, however, the analysis is oriented toward scenarios arising in petroleum engineering. Nevertheless, because the formulation assumes incompressibility, the examples considered here represent simplified abstractions of realistic reservoir conditions. To ensure that the selected application remains within physically grounded magnitudes for the dimensionless groups, the primitive variables are scaled using representative thermophysical properties of the fluid and rock matrix evaluated at characteristic reference conditions. This approach allows the nondimensional groups governing the system to attain realistic magnitudes while preserving mathematical consistency. All results in the following sections are reported in dimensionless variables.

The working fluid is water at standard conditions (298 K and 1 atm) [20]. Its thermophysical properties are summarized in Table 1. The thermal expansion coefficient was obtained from isobaric density data using a second-order centered finite-difference approximation.

Table 1. Thermophysical properties of water at 298 K and 1 atm.

ρ_f	μ	c_p	κ_f	β_T	Pr
$\mathrm{kg/m^3}$	$\mathrm{Pa \cdot s}$	$\mathrm{kJ/(kg\,K)}$	$\mathrm{W/(m\,K)}$	$\mathrm{1/K}$	-
997.09	8.9307×10^{-4}	4.1814	0.60627	3.0×10^{-4}	6.16

Two synthetic porous media are considered in the applications to represent contrasting reservoir characteristics. Rock Type A corresponds to a lower-permeability sandstone-like formation, while Rock Type B represents a highly permeable fractured karst limestone-like structure. The adopted porosity, permeability, and thermal properties are given in Table 2, with values based on ranges reported in [24]. Permeability values are expressed in Darcy and converted to SI units using $1\mathrm{D} = 9.869 \times 10^{-13}, \mathrm{m}^2$ and $c_F(\phi) = 1.8/(\phi^{1.5}\sqrt{180})$ following modified Ergun [1,21].

The interphase heat transfer coefficient appearing in the energy Eqs. (9) and (10) is expressed through the Nusselt number, computed using the correlation

Table 2. Representative thermophysical properties of reference porous media.

Type	ϕ %	k D	c_F -	κ_s W/(m K)	ρ_s kg/m^3	c_p kJ/(kg K)	Λ_κ -	$\Lambda_{\rho c_p}$ -
A	50	0.1	0.38	4.1	2.35×10^3	1.64	6.76	0.92
B	80	1000	0.19	3.0	2.50×10^3	0.93	4.95	0.56

presented in [19]. In the present study, an adapted version is employed, replacing the original characteristic Reynolds number Re_D with the pore-scale Reynolds number $Re_k = \rho_f \mathbf{u}\sqrt{k}/\mu$ and $Pr = (\mu\, c_p)/\kappa_f$:

$$Nu = f(Re_k, Pr, \phi) = \left(1 + \frac{4(1-\phi)}{\phi}\right) + \frac{1}{2}(1-\phi)^{1/2} Re_k^{0.6} Pr^{1/3}. \tag{33}$$

Due to scale separation $L \gg \sqrt{k}$, the flow regimes are characterized in terms of Re_k, which governs inertial effects at the pore scale. For each application, a target Reynolds number is prescribed. The corresponding reference velocity is then computed from fluid properties, allowing evaluation of both Re_k and Ri. These parameters are verified to ensure consistency with the intended flow regime. The temperatures T_{hot}, T_{cold}, and length scale L_{ref} are selected according to the specific application scenario. In all numerical applications, the Brinkman factor in the momentum Eq. (8) is fixed as $\Lambda_\mu = 1$.

4.1 Numerical Solver Verification

To verify the numerical implementation, a manufactured analytical solution is considered. The primitive variables $\mathbf{u}$, p, T_f, and T_s are defined in the domain $\Omega = [0, 20] \times [0, 4]$ as

$$\mathbf{u} = \left[1 - \left(\frac{y-2}{2}\right)^2, 0\right], \quad p = 3 - \frac{x}{10} \quad \text{and} \quad T_f = T_s = 2 - \frac{x}{20}. \tag{34}$$

Substituting these expressions into Eqs. (7)–(10), the forcing terms $\mathbf{f_u}$, f_{T_f}, and f_{T_s} are obtained so that the analytical solution fields satisfy the governing equations. The forcing terms were computed by setting Re, Da, c_F, Pr, Nu, Ri, Λ_μ, Λ_κ, and $\Lambda_{\rho c_p}$ to unity, with porosity $\phi = 0.5$. In the numerical experiment, a porous-channel domain is considered in which the primitive variables are prescribed on the boundary, while the initial conditions are set to zero. The domain is discretized using a structured alternating triangular mesh with 1377 nodes and 2560 elements, generated using the Gmsh Julia API [15] and a dimensionless time step of $\Delta t = 1$. Figure 1 shows the recovered steady-state fields, and Table 3 reports the corresponding L_2 error.

The numerical solution accurately reproduces the expected analytical solution fields. The main deviation appears in the pressure solution, as expected given the use of equal-order linear interpolation for velocity and pressure.

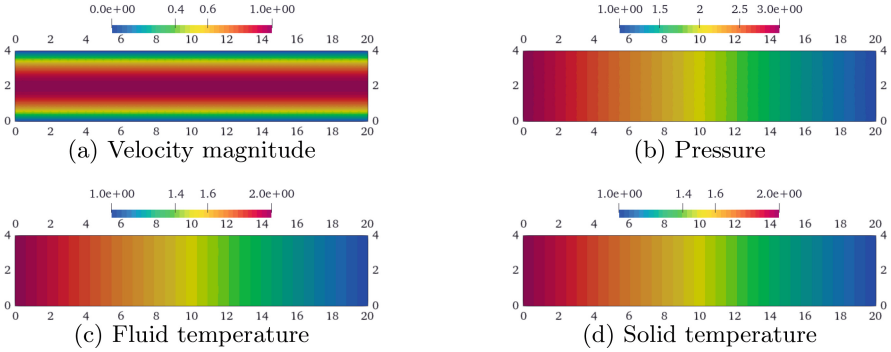

(a) Velocity magnitude (b) Pressure

(c) Fluid temperature (d) Solid temperature

Fig. 1. Numerical solutions of the solver verification problem at $t = 41$.

Table 3. L_2 norms of error $e^{\psi}_{L_2} = \|\psi^h - \psi\|_{L_2}$.

$\|u_x^h - u_x\|_{L_2}$	$\|u_y^h - u_y\|_{L_2}$	$\|p^h - p\|_{L_2}$	$\|T_f^h - T_f\|_{L_2}$	$\|T_s^h - T_s\|_{L_2}$
6.29×10^{-3}	1.97×10^{-4}	1.12×10^{-2}	6.40×10^{-5}	4.77×10^{-5}

4.2 Differentially Heated Porous Cavity

Figure 2 shows the porous media version of a classical benchmark for thermal flow applications. The problem consists of a heated cavity with two insulated walls: top and bottom. Different temperatures are fixed on the left and right walls, creating a thermal gradient that, driven by the thermal buoyancy, induces natural convection within the porous cavity.

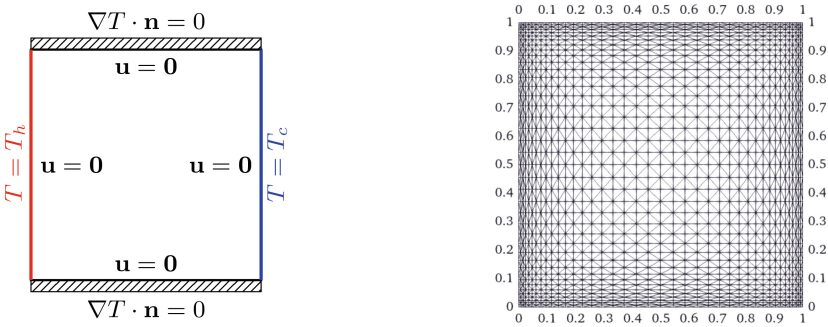

(a) Geometry and boundary conditions (b) Finite element mesh

Fig. 2. Heated porous cavity benchmark.

The solution to this problem is presented in Fig. 3 and was obtained using the finite element mesh shown in Fig. 2b, with 1115 nodes and 3200 elements.

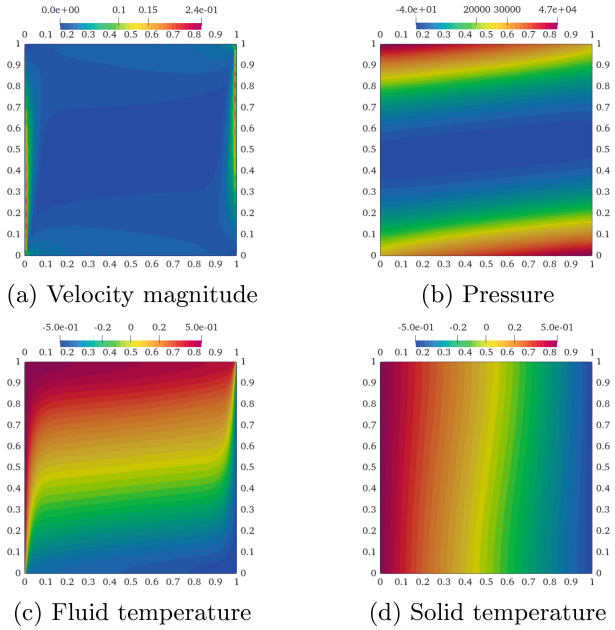

(a) Velocity magnitude (b) Pressure

(c) Fluid temperature (d) Solid temperature

Fig. 3. Solutions of the heated porous cavity application at $t = 250$.

A reference nondimensional pressure is set to $p_{ref} = 1$ at the central point of the cavity $C = (0.5, 0.5)$. The dimensionless time step is $\Delta t = 1$ and Table 4 shows the remain set of parameters used in the numerical solver.

Table 4. Parameters of the heated porous cavity with $L = 1\,\mathrm{m}$

		Re_L	Re_k	Da	ϕ	Nu	Ri
Type	**Regime**	$\rho \mathbf{u} L/\mu$	$\rho \mathbf{u}\sqrt{k}/\mu$	k/L^2	V_p/V	$f(Re_k, Pr, \phi)$	$\mathbf{g}\beta\Delta T L/{u_\infty}^2$
B	Darcy	1000	3.14×10^{-2}	9.87×10^{-10}	0.8	2.05	3.30×10^5

Despite the problem's porous nature, the thermal profiles are similar to those of classical solutions for free-flow problems. Due to buoyancy-driven fluid circulation, the temperature profile of the porous solid matrix deviates slightly from that of a quiescent (no-flow) scenario.

4.3 Thermal Fingers

A variation of the differentially heated cavity for a porous medium is shown in Fig. 4. The same set of parameters listed in Table 4 and reference pressure at the

central point is adopted in this case. The objective is to evaluate the stabilization performance in a more complex flow configuration with multiple thermal circulation cells. The domain is discretized using an alternating triangular mesh with 7803 nodes and 15000 elements. The dimensionless time step is set to $\Delta t = 1$, and the simulation is advanced up to $t = 25$, yielding a clear visualization of the convection cells.

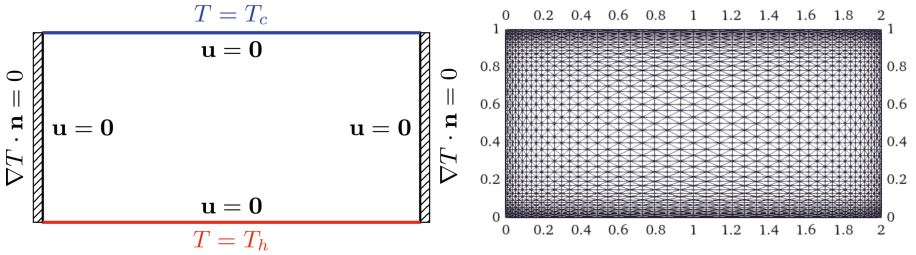

(a) Geometry and boundary conditions (b) Finite element mesh

Fig. 4. Porous thermal fingers application.

The results shown in Fig. 5 indicate that the method accurately captures the interaction between buoyancy-driven flow and thermal transport. In particular, the preservation of the thermal fingers (see Fig. 5c) and the symmetry of the

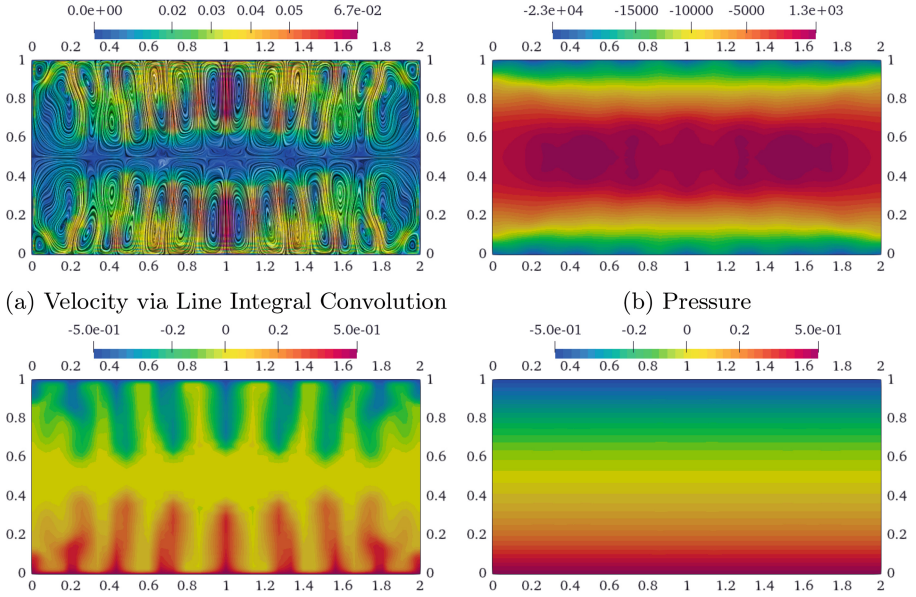

(a) Velocity via Line Integral Convolution (b) Pressure

(c) Fluid temperature (d) Solid temperature

Fig. 5. Solutions of the porous thermal fingers application at $t = 25$.

circulation patterns (see Fig. 5a) up to this time step highlight the method's capability to resolve complex flow structures. The transient evolution further demonstrates the robustness of the formulation under strongly convective conditions, where standard Galerkin methods can produce spurious oscillations. The solution remains stable throughout the simulation, with coherent flow patterns and no evidence of non-physical artifacts.

4.4 Flow in Heterogeneous Fractured Media

The last application considers a porous medium with spatially heterogeneous properties derived from a fractal-based field. The underlying scalar field is obtained from the escape-time of a Julia set fractal, mapped onto the physical domain Ω, and scaled to represent values ranging from type A to type B rocks presented in Table 2. This procedure introduces highly heterogeneous transport pathways that aim to mimic natural fractured or channelized structures.

The fractal field is generated using the standard quadratic iteration

$$z_{n+1} = z_n^2 + c \quad \text{for} \quad z \in \mathbb{C}, \tag{35}$$

with $c = -i$, corresponding to the Julia set $J(0, -i)$. The associated escape-time function is defined as

$$T(z) = \min \{n \in \mathbb{N} : |z_n| > R\}, \tag{36}$$

which assigns to each point $z \in \mathbb{C}$ the number of iterations required to exceed a prescribed escape radius R. To construct the fractal field over the physical domain, let $(x, y) \in \Omega = [0, 1]^2 \subset \mathbb{R}^2$ denote the spatial coordinates. We define the affine mapping

$$\zeta(x, y) = (4x - 2) + i(4y - 2), \tag{37}$$

which maps points from Ω to the complex plane region $[-2, 2] \times [-2, 2] \subset \mathbb{C}$ that contains the complete structure of the set $J(0, -i)$. The fractal field is then defined through the composition

$$F(x, y) = \mathcal{N}\big(T(\zeta(x, y))\big), \tag{38}$$

where $\mathcal{N}(\cdot)$ denotes a normalization operator mapping the escape-time values to the interval associated with type A and type B rocks. The resulting scalar field $F(x, y)$ is subsequently used to define the permeability, porosity, Forchheimer coefficient, and thermal conductivity distributions through appropriate scaling relations.

After $n = 15$ iterations using an escape radius $R = 10$, the resulting nondimensional permeability field is presented in Fig. 6b. Complex patterns characterized by branching structures and sharp transitions are clearly observed. These spatial features are directly reflected in the permeability, porosity, Forchheimer coefficient, and thermal conductivity fields, resulting in pronounced heterogeneity in both flow resistance and heat transfer.

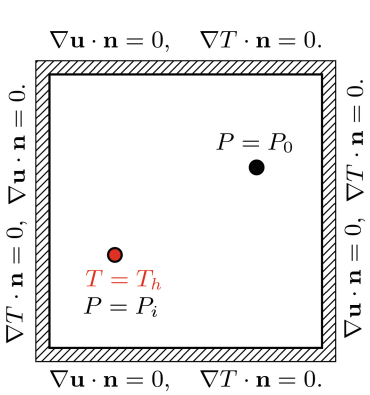

(a) Geometry and boundary conditions

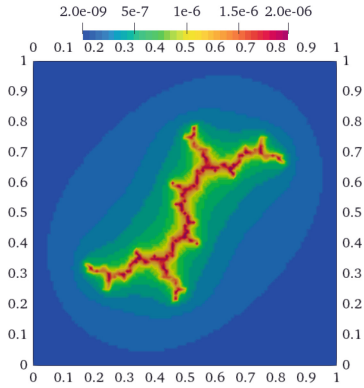

(b) Da field from $J(0, -i)$

Fig. 6. Julia fractal fracture application.

Figure 6a shows the geometry of the problem and the chosen boundary conditions. The internal points indicate a source (red) at $I = (0.24, 0.34)$ and a sink (black) at $P = (0.76, 0.66)$, with pressures set to $p = 1.2$ and $p = 0.8$, respectively, creating a pressure gradient that drives the flow. A thermal gradient is induced by fixing the nondimensional temperature at the injection point I at $T_I = 0.5$, and the rest of the domain set to a lower value of $T = -0.5$.

The Reynolds number is set to 1000, and the problem is solved using an alternating triangular mesh with 10201 nodes and 20000 elements. The velocity field, presented in Fig. 7a, shows that the flow is strongly guided by the high-permeability channels defined by the fractal structure. Preferential flow paths emerge, forming localized high-velocity regions where non-Darcy effects occur.

The pressure field, shown in Fig. 7b, exhibits a smooth global gradient ranging between the fixed source and sink values with local distortions due to heterogeneous resistance.

Thermally, both fluid and solid temperatures, Figs. 7c and 7d, present localized hot spots near the injection region, with LTNE effects appearing as slight deviations between the two fields, especially along dominant flow paths where convection is enhanced.

4.5 Discussion of Results

The proposed stabilized finite element framework demonstrated robust and consistent performance across all investigated flow regimes. The combination of SUPG, PSPG, and LSIC stabilization enabled stable solutions under advection-dominated and non-Darcy conditions, without spurious oscillations typically associated with standard Galerkin formulations.

The use of equal-order linear interpolation for all primitive variables represents a practical advantage of the formulation. While a slightly higher error

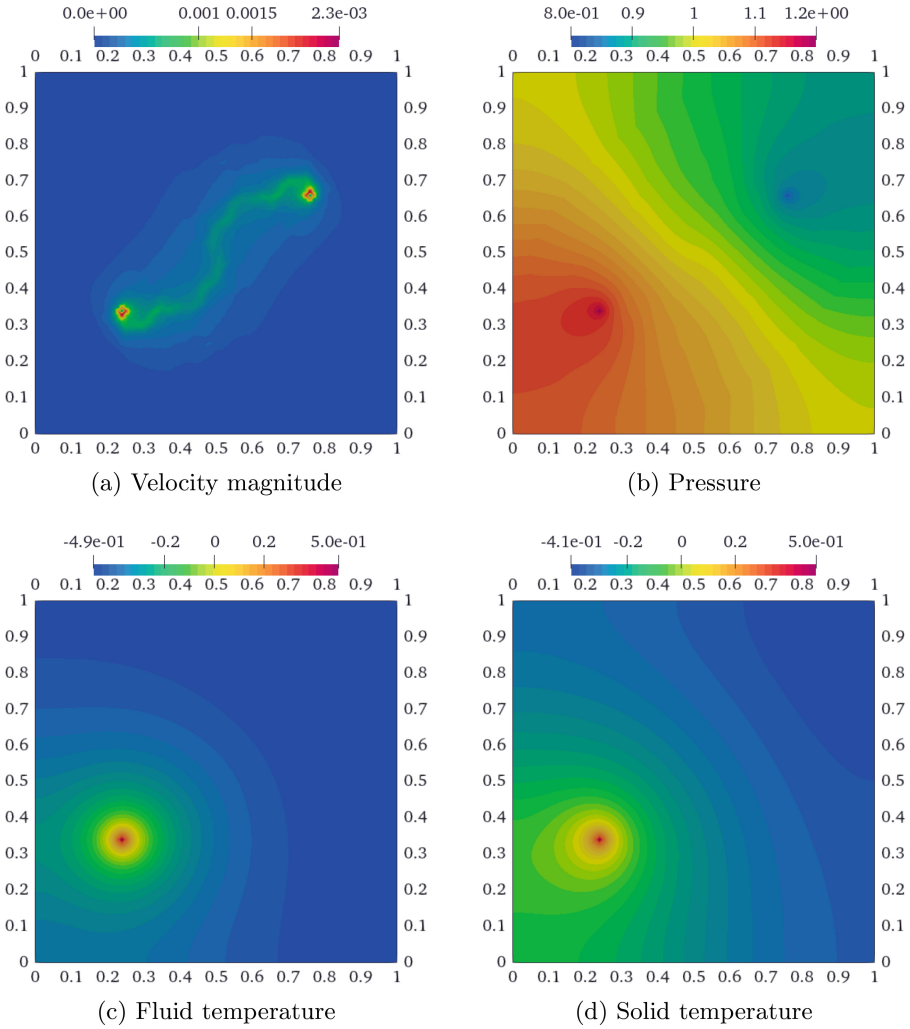

(a) Velocity magnitude (b) Pressure

(c) Fluid temperature (d) Solid temperature

Fig. 7. Solutions of the Julia fracture problem at $t = 200$.

is observed in the pressure field during the verification test, the PSPG stabilization ensures overall numerical stability and acceptable accuracy, providing a favorable balance between implementation simplicity and solution quality.

Although no direct comparison with alternative numerical methods is presented, the implementation's accuracy is supported by the manufactured solution test, which verifies the correct reproduction of the governing equations. Additionally, the benchmark applications exhibit physically consistent behavior, reinforcing the reliability of the proposed approach.

The results also highlight the formulation's ability to handle transitions between different flow regimes within a unified framework. The inclusion of

the Forchheimer term allows the capture of inertial effects at higher pore-scale Reynolds numbers, while the Brinkman term ensures a smooth transition toward viscous-dominated behavior.

Finally, the fractal-based permeability field naturally induces channelized flow patterns, demonstrating the method's ability to handle highly heterogeneous domains. The resulting flow and thermal fields exhibit strong spatial variability, consistent with expected behavior in fractured porous media.

5 Conclusions

In this work, a stabilized finite element framework for the transient DBF model coupled with a local thermal non-equilibrium formulation was presented. The approach combines SUPG, PSPG, and LSIC stabilization techniques within an equal-order interpolation setting, enabling a fully coupled and computationally efficient formulation.

The proposed method demonstrated stability and accuracy across different flow regimes, including advection-dominated and non-Darcy conditions. The verification study confirmed the correctness of the numerical implementation, while the benchmark applications showed physically consistent behavior in both thermal and flow fields.

The formulation successfully captures transitions between Darcy, Brinkman, and Forchheimer regimes without requiring model switching. In addition, the LTNE approach allows the resolution of thermal non-equilibrium effects between the fluid and solid phases, particularly in regions with strong convective transport.

The application to a fractal-based heterogeneous medium further demonstrated the method's ability to handle complex spatial variability, producing realistic channelized flow patterns and localized thermal effects.

Future work includes extending to three-dimensional configurations, investigating the tuning of stabilization parameters, applying other stabilization techniques, and evaluating GMRES and preconditioning options to improve performance.

Acknowledgments. This study was financed in part by the Coordenação de Aperfeiçoamento de Pessoal de Nível Superior - Brasil (CAPES) - Finance Code 001 - and by the Fundação de Amparo à Pesquisa e Inovação do Espírito Santo (FAPES), Grant Notice N° 02/2026.

Declaration of Generative AI and AI-Assisted Technologies in the Writing Process. During the preparation of this work the authors used ChatGPT (OpenAI) in order to assist with language revision and text improvement. After using this tool, the authors reviewed and edited the content as needed and take full responsibility for the content of the publication.

References

1. Akolkar, A., Petrasch, J.: Tomography-based characterization and optimization of fluid flow through porous media. Transp. Porous Media **95**(3), 535–550 (2012)
2. Baptista, R., dos Santos, I.P., Catabriga, L.: Solving incompressible Navier-stokes equations: a nonlinear multiscale approach. Comput. Math. Appl. **175**, 366–384 (2024)
3. Barnsley, M.F., et al.: The Science of Fractal Images, vol. 1. Springer, New York (1988). https://doi.org/10.1007/978-1-4612-3784-6
4. Berre, I., Doster, F., Keilegavlen, E.: Flow in fractured porous media: a review of conceptual models and discretization approaches. Transp. Porous Media **130**(1), 215–236 (2019)
5. Brezzi, F.: On the existence, uniqueness and approximation of saddle-point problems arising from Lagrangian multipliers. Publications des séminaires de mathématiques et informatique de Rennes **8**(R2), 129–151 (1974)
6. Brinkman, H.C.: A calculation of the viscous force exerted by a flowing fluid on a dense swarm of particles. Flow Turbul. Combust. **1**(1), 27–34 (1949)
7. Brooks, A.N., Hughes, T.J.: Streamline upwind/Petrov-Galerkin formulations for convection dominated flows with particular emphasis on the incompressible Navier-stokes equations. Comput. Methods Appl. Mech. Eng. **32**(1), 199–259 (1982)
8. Cannon, J.: The fractal geometry of nature. by benoit b. mandelbrot. Am. Math. Mon. **91**(9), 594–598 (1984)
9. Cengizci, S.: A sups formulation for simulating unsteady natural/mixed heat convection phenomena in square cavities under intense magnetic forces. Eur. Phys. J. Plus **139**(8), 713 (2024)
10. Darcy, H.: Les fontaines publiques de la ville de Dijon, vol. 2. V. Dalmont (1856)
11. Donea, J., Huerta, A.: Finite Element Methods for Flow Problems. Wiley, New York (2003)
12. Ern, A., Guermond, J.L.: Finite elements iii. first-order and time-dependent PDEs. Texts Appl. Math **74** (2021)
13. Forchheimer, P.: Wasserbewegung durch boden. Z. Ver. Deutsch, Ing. **45**, 1782–1788 (1901)
14. García-Garrido, V.J.: Unveiling the fractal structure of Julia sets with Lagrangian descriptors. Commun. Nonlinear Sci. Numer. Simul. **91**, 105417 (2020)
15. Geuzaine, C., Remacle, J.F.: GMSH: a 3-D finite element mesh generator with built-in pre-and post-processing facilities. Int. J. Numer. Meth. Eng. **79**(11), 1309–1331 (2009)
16. Gray, D.D., Giorgini, A.: The validity of the Boussinesq approximation for liquids and gases. Int. J. Heat Mass Transf. **19**(5), 545–551 (1976)
17. Hughes, T.J.: A multidimensional upwind scheme with no crosswind diffusion. Finite element methods for convection dominated flows. AMD **34** (1979)
18. Hughes, T.J., Mallet, M., Akira, M.: A new finite element formulation for computational fluid dynamics: Ii. beyond supg. Comput. Methods Appl. Mech. Eng. **54**(3), 341–355 (1986)
19. Kuwahara, F., Shirota, M., Nakayama, A.: A numerical study of interfacial convective heat transfer coefficient in two-energy equation model for convection in porous media. Int. J. Heat Mass Transf. **44**(6), 1153–1159 (2001)
20. Lemmon, E.W.: Thermophysical properties of fluid systems. NIST Chemistry WebBook (2010)

21. Macdonald, I., El-Sayed, M., Mow, K., Dullien, F.: Flow through porous media - the Ergun equation revisited. Ind. Eng. Chem. Fundam. **18**(3), 199–208 (1979)
22. de Moura, R.C., Catabriga, L.: Stabilized finite element approximation for the transient Darcy-Brinkman-Forchheimer model. In: 2023 IEEE 22nd International Conference on Trust, Security and Privacy in Computing and Communications (TrustCom), pp. 2357–2364. IEEE (2023)
23. Nield, D.A., Bejan, A.: Convection in Porous Media. Springer, Cham (2006). https://doi.org/10.1007/978-3-319-49562-0
24. Schön, J.H.: Physical Properties of Rocks: Fundamentals and Principles of Petrophysics, vol. 65. Elsevier, Amsterdam (2015)
25. Tezduyar, T.E.: Stabilized finite element formulations for incompressible flow computations. Adv. Appl. Mech. **28**, 1–44 (1991)
26. Tezduyar, T.E.: Calculation of the stabilization parameters in SUPG and PSPG formulations. Mecanica Computacional, 1–18 (2002)
27. Tezduyar, T.E., Mittal, S., Ray, S., Shih, R.: Incompressible flow computations with stabilized bilinear and linear equal-order-interpolation velocity-pressure elements. Comput. Methods Appl. Mech. Eng. **95**(2), 221–242 (1992)
28. Tezduyar, T.E., Osawa, Y.: Finite element stabilization parameters computed from element matrices and vectors. Comput. Methods Appl. Mech. Eng. **190**(3–4), 411–430 (2000)
29. Ward, J.: Turbulent flow in porous media. J. Hydraul. Div. **90**(5), 1–12 (1964)
30. Whitaker, S.: Diffusion and dispersion in porous media. AIChE J. **13**(3), 420–427 (1967)
31. Yu, T., Paradis, A.: On the simulation of artificial cracks in brittle materials using Julia set fractals. Multiscale Sci. Eng. **6**(4), 218–236 (2024)

Applicability of NDM-Net Simulated Data to Prestack Depth Migration

Elena Gondyul[1], Valeria Dubrovina[2], Vadim Lisitsa[1(✉)], and Dmitry Vishnevsky[1]

[1] Sobolev Institute of Mathematics SB RAS, Novosibirsk 630090, Russia
e.gondyul@yandex.ru, Valeria.Dubrovina@ptgeos.com
[2] LLC PetroTrace, Moscow 115114, Russia

Abstract. We present an analysis of the applicability of previously reported approach (NDM-net) to the construction of depth seismic images. The NDM-net allows us to simulate seismic data by combining finite differences with deep learning method. Coarse computational grids are used for the fast generation of inaccurate datasets. After that, the training dataset is simulated for a small number of shot points on fine grids. Then, the NDM-net is trained to map inaccurate data to accurate common shot gathers. Previously, we illustrated the high quality of the generated shot gathers. In this research, we applied the prestack depth migration to estimate the effect of the NDM-net numerical errors on the resulting seismic images.

Keywords: Seismic modeling · Machine learning · Prestack depth migration

1 Introduction

The development of mathematical apparatus and computational technologies has led to the spread of specialized data processing procedures, such as full waveform inversion or FWI [4,31]; depth migration based on the one-way wave equation [25,26]; reverse time migration or RTM [27,30]. However, the computational complexity and resource intensity of seismic modeling, as the main component of these procedures, are significant limiting factors in the development of these methods.

Seismic modeling can also be used to preliminarily assess the applicability of certain data processing procedures in specific complex geological settings [2,11,17]. This requires obtaining high-quality synthetic seismic data to enable testing of processing workflows with confidence that the processing result will not be affected by numerical errors associated with numerical modeling. Calculating high-quality common shot gathers requires the use of modern numerical meth-

© The Author(s), under exclusive license to Springer Nature Switzerland AG 2027
O. Gervasi et al. (Eds.): ICCSA 2026 Workshops, LNCS 16761, pp. 58–69, 2027.
https://doi.org/10.1007/978-3-032-30527-5_4

ods, such as the finite difference method [14,30], the spectral element method [12,29], the discontinuous Galerkin method [10,18] in combination with sufficiently detailed grids for discretizing the model and wavefield. Restricting the computational grid steps is the primary way to ensure acceptable computational accuracy: the smaller the grid step (the higher the number of degrees of freedom in the discretized problem), the higher the accuracy. Note that the numerical error, in general, decreases proportionally to the square of the grid step, while the problem size increases proportionally to the fourth power of the grid step. Therefore, attempts to suppress the numerical error solely by reducing the grid step quickly lead to excessive demands on computer memory and computation time, without significantly improving the quality of the solution.

Principally different results can be achieved by postprocessing the simulated data, aimed specifically at suppressing the specific numerical error expressed as numerical dispersion. There are approaches based on analytical estimates of dispersion followed by spectrum correction [20,24], and machine learning methods [5–9,33,34]. The quality measure of the resulting solution with such correction is the norm of the difference between common shot gathers, for example, the L_2 norm or NRMS [13]. However, these are integral measures applied to common shot gathers, which do not always allow for monitoring the impact of postprocessing on seismic events. In this work, prestack depth migration is performed on simulated, corrected, and uncorrected data, and the resulting seismic images are analyzed.

2 Seismic Modeling with NDM-Net

The classical formulation of a seismic modeling problem involves solving the elastic wave equation:

$$\begin{gathered} \rho \frac{\partial \boldsymbol{u}}{\partial t} = \nabla \cdot \sigma, \\ \frac{\partial \varepsilon}{\partial t} = \frac{1}{2}\left[\nabla u + \nabla u^T\right], \\ \sigma = C\varepsilon, \end{gathered}$$

where $\boldsymbol{u}$ is the velocity vector, σ and ε are the stress and strain tensors, respectively, ρ is the mass density, and C is the stiffness tensor. In this research we deal with the isotropic models, where tensor C has a simple form with only two independent parameters. The problem is stated in the half-space $x_3 > 0$ with free-surface boundary conditions at $x_3 = 0$. To avoid the reflections from the other boundaries the Perfectly matched layers are applied [1,3,19].

The calculation is performed for a set of sources located on the free surface at specified points $\boldsymbol{x}_j^s$. Wavefields (displacement velocities) are recorded on the free surface at receiver locations $\boldsymbol{x}_k^r$. In this case, the modeling can ensure a fixed geometry of the active array, identical for all source positions. As a result, all common shot gathers will have the same size, determined by the number of receivers in the active array and the number of time samples.

The numerical modeling is performed using the finite difference method. The accuracy of the calculations is determined by the grid step, which is selected based on the acceptable level of numerical dispersion. In this research we use the

second order accurate in time and the fourth order accurate in space staggered grid scheme [14]. This scheme possesses an acceptable level of numerical dispersion when approximately five points per dominant wavelength are used, which can range from 1 to 5 m, depending on the velocity model and the frequency of the probing signal [16,21]. As already noted, halving the grid step reduces the error by approximately a factor of four, since the numerical solution converges to the exact solution in the second order. In fact, the estimate is even coarser for heterogeneous models where the convergence rate may degenerate to the first order [15,22,23,28,32]. At the same time, the problem size increases by a factor of eight, and the computational time increases by 16 in the three-dimensional case (4 and 8 times, respectively, in the two-dimensional setting). Increasing the formal order of the approximation does not yield any significant improvement [23].

To reduce the amount of computation and running time, several studies [5–8] proposed an approach that combines the finite difference method and machine learning methods. This approach, called NDM-net, consists of the following steps:

- Calculation of a complete set of common shot gathers $V_c(t, \boldsymbol{x}_j^s, \boldsymbol{x}^o)$ on a coarse grid. In these notations, the subscript c denotes the solution computed on a coarse grid or coarse-grid solution, $\boldsymbol{x}_j^s$ is the coordinate of the $j-$th source, where $j = 1, ..., J$, and $\boldsymbol{x}^o$ is the offset of the receiver with respect to the considered source. This solution can be obtained in a short time; however, it has a high numerical error

$$\epsilon_c = \|V_c(t, \boldsymbol{x}_j^s, \boldsymbol{x}^o) - V(t, \boldsymbol{x}_j^s, \boldsymbol{x}^o)\|$$

  where $V(t, \boldsymbol{x}_j^s, \boldsymbol{x}^o)$ is the exact solution.
- Construction of a training sample that is the calculation of a set of shot gathers $V_f(t, \boldsymbol{x}_j^s, \boldsymbol{x}^o)$ on a fine grid for a small number of sources with $j \subset \{1, ..., J\}$. The calculation time for one common shot gather in this case is significantly higher than when using a coarse grid, and the total time for constructing the training sample is comparable to the time for calculating the full dataset on a coarse grid. However, the numerical error of the reference solution

$$\epsilon_f = \|V_f(t, \boldsymbol{x}_j^s, \boldsymbol{x}^o) - V(t, \boldsymbol{x}_j^s, \boldsymbol{x}^o)\|$$

  is significantly lower than ϵ_c. From now on we consider V_f as the exact solution.
- Training the NDM-net - the neural network based on the U-net architecture to map noisy data to fine grid solution, i.e.

$$\mathcal{N} : V_c(t, \boldsymbol{x}_j^s, \boldsymbol{x}^o) \rightarrow V_f(t, \boldsymbol{x}_j^s, \boldsymbol{x}^o).$$

  The aim of mapping is to minimize the error between common shot gathers:

$$\epsilon_{\mathcal{N}} = \|V_f(t, \boldsymbol{x}_j^s, \boldsymbol{x}^o) - V_c(t, \boldsymbol{x}_j^s, \boldsymbol{x}^o)\| \rightarrow \min$$

Note that there are two modifications of NDM-net. One is focused on working with source data in the time domain [7], the second is a modified network that works with data in the frequency domain [6]. A description of the advantages of each approach is presented in the above-mentioned works. This stage is also quite resource-intensive and comparable with time needed to the calculation of wavefields on a coarse grid.

– The final stage is the application of the trained neural network to correct the entire dataset. This part of the method is the least computationally intensive.

3 Prestack Depth Migration

In our previous studies, we showed that the use of the NDM-net can reduce the numerical error in synthetic data from 70–100% to 20–25%. However, these estimates were obtained by directly comparing common shot gathers, which still does not allow us to judge the suitability of these data for constructing seismic images. In this study, prestack depth migration was applied to three sets of synthetic data: those calculated on a coarse grid $V_c(t, \boldsymbol{x}_j^s, \boldsymbol{x}^o)$, those calculated on a fine grid (for all source positions) $V_f(t, \boldsymbol{x}_j^s, \boldsymbol{x}^o)$, and those obtained using NDM-net $\mathcal{N}\left[V_c(t, \boldsymbol{x}_j^s, \boldsymbol{x}^o)\right]$.

The Kirhgoff prestack depth migration was used to construct the seismic images. This algorithm involves summing the amplitude values along a diffraction hyperbola and placing the resulting value at the point corresponding to the hyperbola's apex. The aim of depth migration is to obtain seismic data at a depth scale that correctly accounts for spatial offset and, therefore, accurately determines the coordinates of the reflector, as well as provides the most complete representation of deep tectonics.

Prestack depth migration (PSDM) processes seismic data before stacking, working directly with common-shot or common-offset gathers to position reflections accurately. Unlike time migration, which assumes a flat earth and constant velocity, PSDM uses a depth-velocity model to trace ray paths from sources to receivers through laterally varying velocities. This corrects for complex structures like faults. In Kirchhoff PSDM, traveltime tables are first computed for every source-receiver pair to every image point in the subsurface grid, often via wavefront reconstruction or Eikonal solvers. For each trace, the algorithm then applies a weighted summation of amplitudes along the diffraction traveltime surface, imaging energy at the apex where specular reflection occurs.

The depth migration was performed with the following parameters: the depth-velocity model is the original BP velocity model. We used the wavefront reconstruction to calculate traveltimes. The aperture diameter was 6 km, the output offset ranged between 0–3200 m with a step of 25 m, the maximum frequency was 90 Hz, and the maximum depth was 12 km.

4 Numerical Experiment

The described seismic modeling and seismic imaging procedure was performed for the BP velocity model, the most complex and representative among the two-dimensional models available. The model is presented in Fig. 1. The model size is 67.4 km in the horizontal direction and 11.9 km in the vertical direction. The acquisition system includes 2696 sources with a step of 25 m between them. The active array is central, with 512 receivers with a step of 25 m and a maximum offset of 6.4 km. A Ricker wavelet with a central frequency of 30 Hz was used as the source. A coarse grid with a step of 6 m was used, while the step of the fine grid was equal to 3 m. The sample interval of the common shot gathers was 3 ms and the record length was 6 s. Ten percent of the total number of sources were used to construct the training dataset. As a result, the initial error between the data from the coarse and fine grids was 92%; after data correction using NDM-net, the error decreased to 31%, which confirms the results presented in [5].

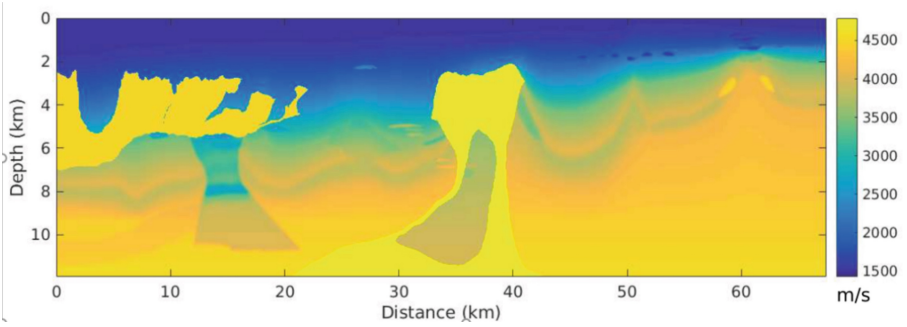

Fig. 1. BP velocity model (P-wave velocity).

The shot gather corresponding to the source located at $x_1 = 26.500$ m are shown in Fig. 2. We also provide the difference between the fine grid solution and the other two gathers to illustrate the numerical error before and after the application of the NDM-net (Fig. 3). The difference of the two shoth gathers consistently show an increase in numerical error with increasing recording time. This is because the main error is the numerical dispersion, which leads to deformation and decay of the wavepacket. Furthermore, a phase delay is evident, which increases with increasing time traveling. NDM-net effectively suppresses signal phase changes, but does not accurately correct its amplitude.

The depth seismic sections obtained for the three datasets are shown in Figs. 4, 5 and 6. The section constructed using the coarse grid data (Fig. 5)

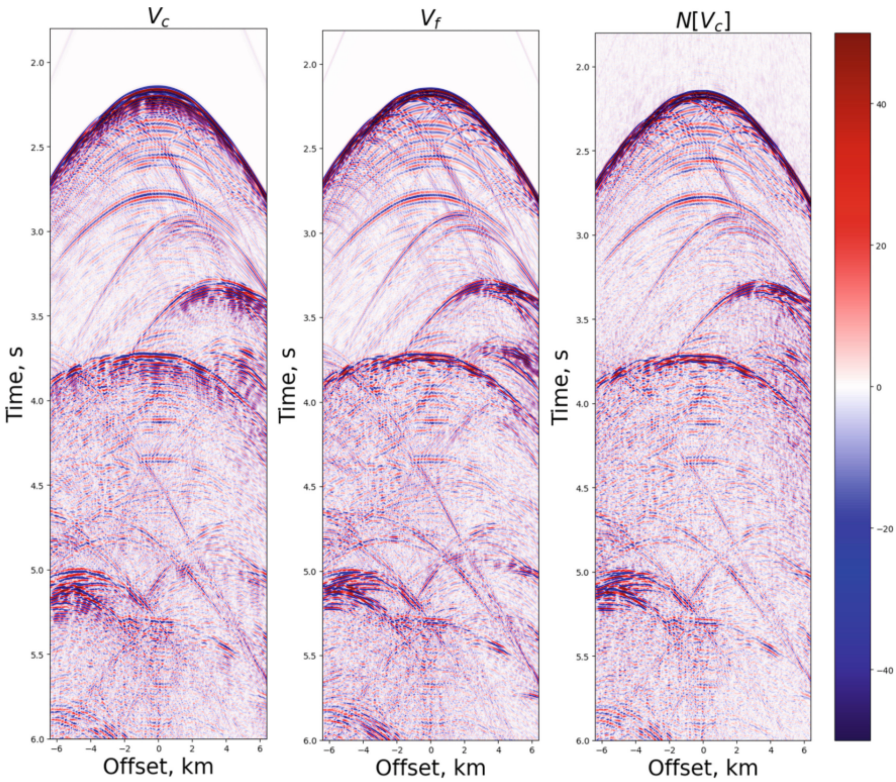

Fig. 2. Sample shot gather corresponding to the source position $x_1 = 26.500$. The coarse grid solution is at the left, the fine grid solution is at the center, and the solution corrected with the NDM-net is at the right.

reveals pronounced oscillations below the main seismic events. This effect is caused by numerical dispersion, which deforms the wavepacket. Some seismic events, clearly visible in the reference section (Fig. 4), are indistinguishable in Fig. 5 due to signal interference. This effect is observed in areas of thin layering (on the right side of the section and in the central part between the intrusive bodies). This effect is pronounced in the section constructed using the NDM-net-corrected data (Fig. 6).

For a more detailed analysis of the effect of the NDM-net correction, we considered the differences between the constructed sections as presented in Figs. 7 and 8. Note that all provided images are of the same gain to simplify visualization and comparison. The use of a coarse grid results in an extremely high error in the migrated data, which is evident in almost all seismic events, starting from the earliest ones. The use of NDM-net allows us to significantly suppress this error.

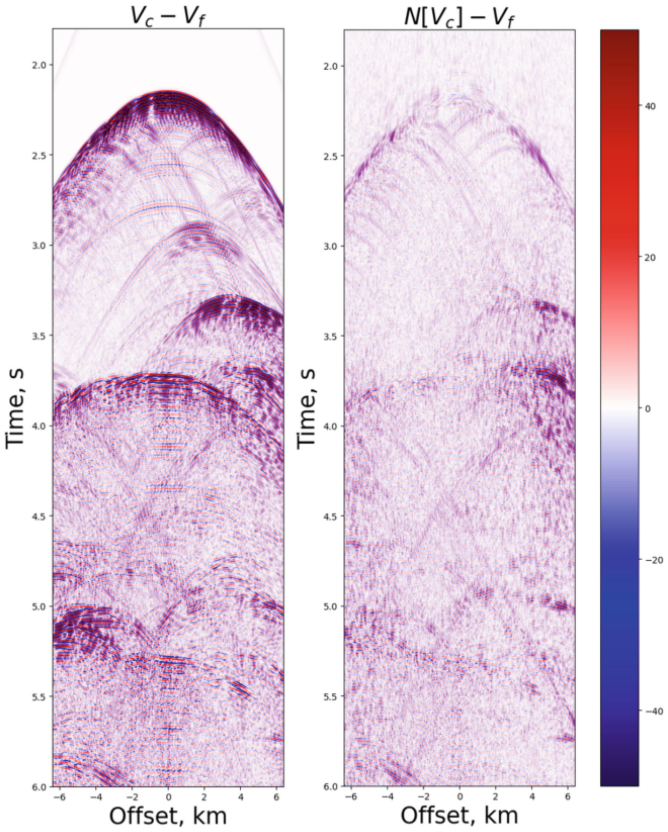

Fig. 3. The difference between the fine grid solution and the coarse grid solution is at the left. The difference between the fine grid solution and the NDM-net corrected solution is at the right.

The events at shallow depths contain mainly no numerical error after applying NDM-net. The magnitude of the residual error, on the one hand, increases with depth, and, on the other hand, it manifests itself at sharply contrasting boundaries (salt body boundaries). The first type of error is associated with the increase in error in the original data with depth due to the longer wave propagation path. The second type of error is related to the fact that NDM-net primarily corrects the most significant component of the error (the phase shift) while the amplitude error remains virtually uncorrected. However, NDM-net correction made a deep seismic event in the central part of the model out of phase. This

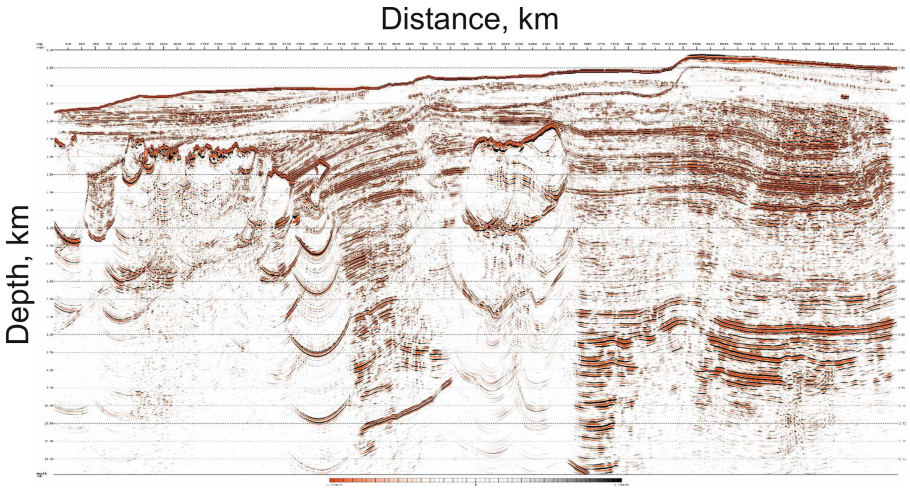

Fig. 4. The seismic depth section constructed from the fine grid data.

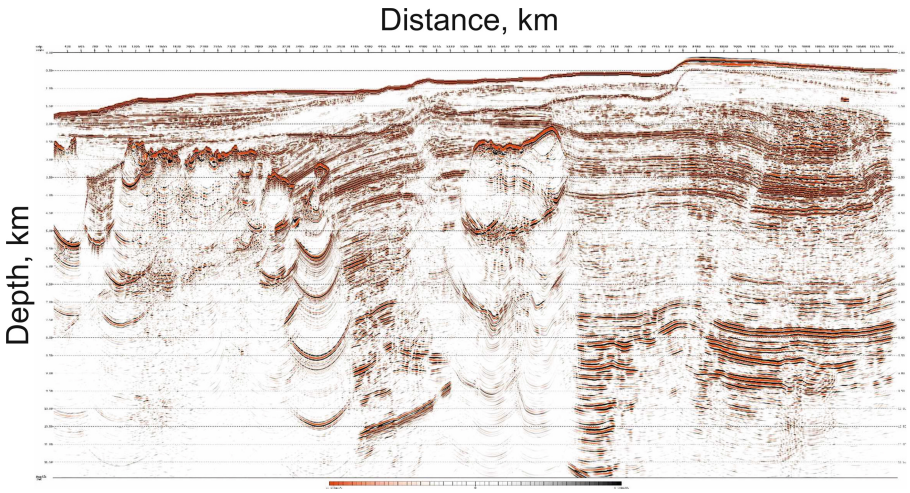

Fig. 5. The seismic depth section constructed from the coarse grid data.

is undoubtedly an error introduced by the neural network that requires further refinement.

The primary aim of the developed algorithm is to speed up seismic modelling. Therefore, we present a performance analysis of various scenarios. For the velocity model considered in this study, the computation time was 1 min per seis-

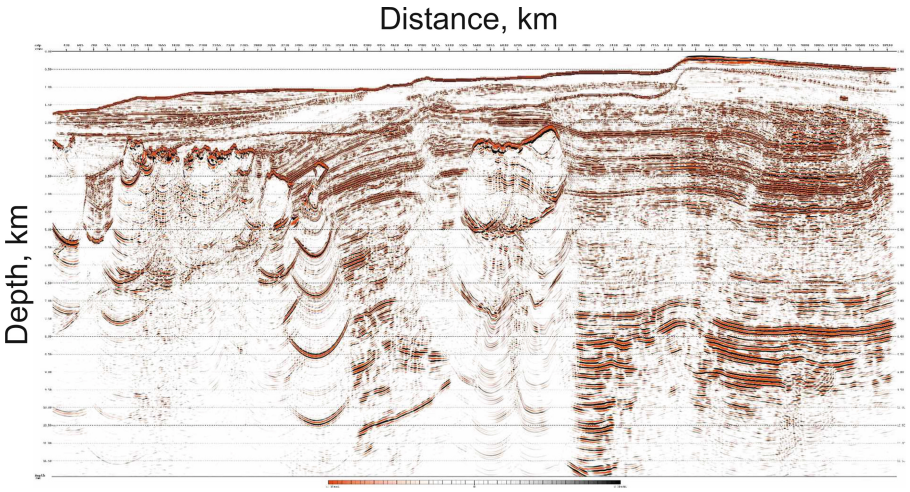

Fig. 6. The seismic depth section constructed from the NDM-net corrected data.

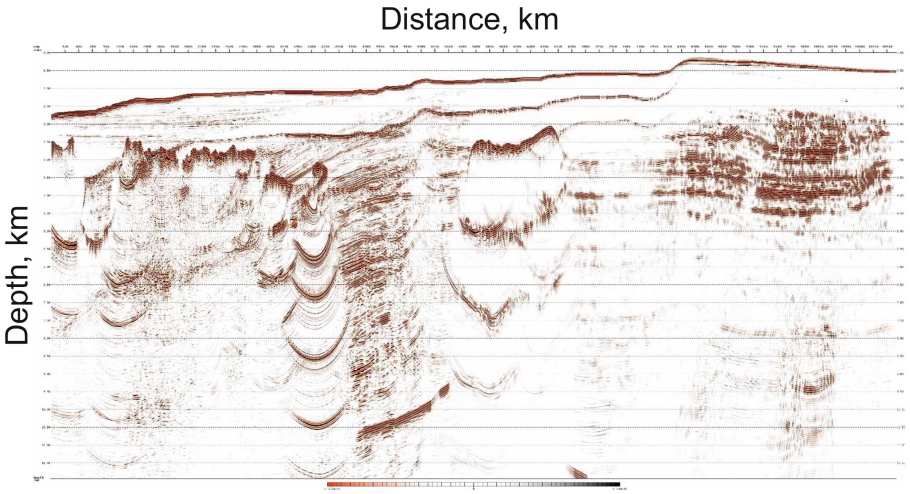

Fig. 7. The difference between seismic depth section constructed from the coarse grid data and fine grid data.

mogram (single souce) when using a coarse computational grid and 6 min when using a fine computational grid. The calculations and subsequent training of the neural network were carried out on a local server with 8 Nvidia A100 GPUs with 80 Gb of RAM. The training time for NDM-net is 60 min for a sample of 10% of the total number of sources, Thus, the speed-up factor is 3-4.

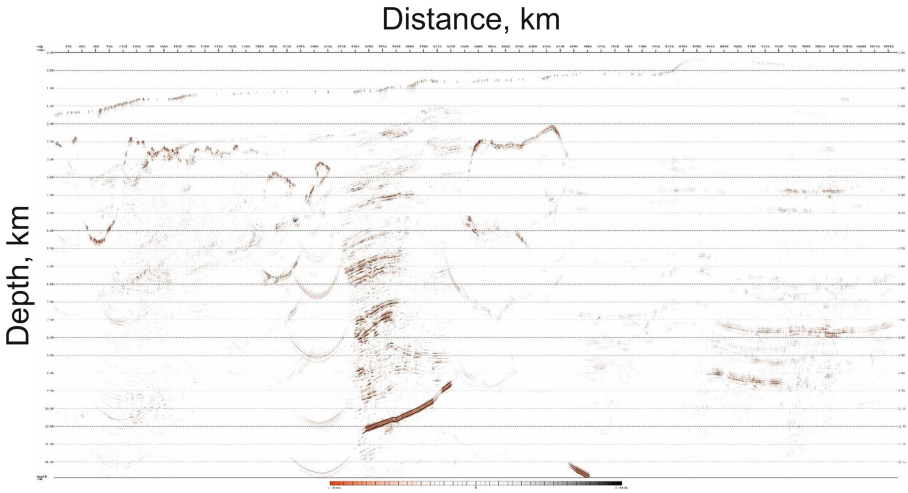

Fig. 8. The difference between seismic depth section constructed from the NDM-net corrected data and fine grid data.

5 Conclusions

This paper presented an analysis of the results of numerical modeling of seismic wavefields using a method based on a combined neural network approach and the finite difference method. Using the BP model as an example, numerical experiments were conducted using fine and coarse grids to compute the seismorgams, and NDM-net was also applied to correct noisy data. Prestack depth migration with a known velocity model was performed for all three datasets and depth sections were constructed. The images constructed from coarse grid data are shown to contain a significant error in seismic events. Data correction using NDM-net can significantly improve data quality. However, for events at high depths, the effectiveness of NDM-net may decrease. One possible way to improve the effectiveness of NDM-net in this case could be to modify the training set by increasing the number of sampling sources in the vicinity of target objects (increasing the illumination of objects within the training set).

Acknowledgments. Seismic modelling and NDM-net correction was done by the IM SB RAS group under the support of the Russian Science Foundation grant no. 22-11-00004-*П*.

Disclosure of Interests. The authors have no competing interests to declare that are relevant to the content of this article.

References

1. Berenger, J.P.: A perfectly matched layer for the absorption of electromagnetic waves. J. Comput. Phys. **114**, 185–200 (1994). https://doi.org/10.1006/jcph.1994.1159
2. Cheverda, V., et al.: Three-dimensional model of oil and gas reservoirs based on gaussian beam processing of scattered seismic waves. Russ. Geol. Geophys. **63**(1), 109–123 (2022). https://doi.org/10.2113/rgg20204231
3. Collino, F., Tsogka, C.: Application of the perfectly matched layer absorbing layer model to the linear elastodynamic problem in anisotropic heterogeneous media. Geophysics **66**, 294–307 (2001)
4. Egorov, A., et al.: Elastic full-waveform inversion of vertical seismic profile data acquired with distributed acoustic sensors. Geophysics **83**(3), R273–R281 (2018)
5. Gadylshin, K., Gondyul, E., Lisitsa, V., Gadylshina, K., Vishnevsky, D.: Mitigation of numerical dispersion in seismic data in spectral domain with neural networks. Soil Dyn. Earthq. Eng. **187**, 109028 (2024). https://doi.org/10.1016/j.soildyn.2024.109028
6. Gadylshin, K., Lisitsa, V., Vishnevsky, D., Gadylshina, K.: Hausdorff-distance-based training dataset construction for numerical dispersion mitigation neural network. Comput. Geosci. **180**, 105438 (2023). https://doi.org/10.1016/j.cageo.2023.105438
7. Gadylshin, K., Vishnevsky, D., Gadylshina, K., Lisitsa, V.: Numerical dispersion mitigation neural network for seismic modeling. Geophysics **87**(3), T237–T249 (2022). https://doi.org/10.1190/geo2021-0242.1
8. Gondyul, E., Lisitsa, V., Gadylshin, K., Vishnevsky, D.: Numerical dispersion mitigation neural network with velocity model correction. Comput. Geosci. **196**, 105806 (2025). https://doi.org/10.1016/j.cageo.2024.105806
9. Han, Y., Wu, B., Yao, G., Ma, X., Wu, D.: Eliminate time dispersion of seismic wavefield simulation with semi-supervised deep learning. Energies **15**(20), 7701 (2022)
10. Kaser, M., Dumbser, M.: An arbitrary high-order discontinuous galerkin method for elastic waves on unstructured meshes - i. the two-dimensional isotropic case with external source terms. Geophys. J. Int. **166**(2), 855–877 (2006)
11. Kolyukhin, D.R., et al.: Seismic imaging and statistical analysis of fault facies models. Interpretation **5**(4), SP71–SP82 (2017)
12. Komatitsch, D., Vilotte, J.P.: The spectral element method; an efficient tool to simulate the seismic response of 2D and 3D geological structures. Bull. Seismol. Soc. Am. **88**(2), 368–392 (1998). https://doi.org/10.1785/BSSA0880020368
13. Kragh, E., Christie, P.: Seismic repeatability, normalized RMS, and predictability. Lead. Edge **21**(7), 640–647 (2002)
14. Levander, A.R.: Fourth-order finite-difference P-SV seismograms. Geophysics **53**(11), 1425–1436 (1988). https://doi.org/10.1190/1.1442422
15. Lisitsa, V., Podgornova, O., Tcheverda, V.: On the interface error analysis for finite difference wave simulation. Comput. Geosci. **14**(4), 769–778 (2010). https://doi.org/10.1007/s10596-010-9187-1
16. Lisitsa, V.: Dispersion analysis of discontinuous galerkin method on triangular mesh for elastic wave equation. Appl. Math. Model. **40**, 5077–5095 (2016). https://doi.org/10.1016/j.apm.2015.12.039
17. Lisitsa, V., Kolyukhin, D., Tcheverda, V.: Statistical analysis of free-surface variability's impact on seismic wavefield. Soil Dyn. Earthq. Eng. **116**, 86–95 (2019)

18. Lisitsa, V., Tcheverda, V., Botter, C.: Combination of the discontinuous galerkin method with finite differences for simulation of seismic wave propagation. J. Comput. Phys. **311**, 142–157 (2016). https://doi.org/10.1016/j.jcp.2016.02.005
19. Lisitsa, V.V.: Optimal grids for numerical solution of wave equation with variable coefficients. Sib. Zh. Vychisl. Mat. **8**(3), 219–229 (2005). in Russian
20. Mittet, R.: Second-order time integration of the wave equation with dispersion correction procedures. Geophysics **84**(4), T221–T235 (2019)
21. Moczo, P., Kristek, J., Halada, L.: 3D fourth-order staggered-grid finite-difference schemes: stability and grid dispersion. Bull. Seismol. Soc. Am. **90**(3), 587–603 (2000)
22. Moczo, P., Kristek, J., Vavrycuk, V., Archuleta, R.J., Halada, L.: 3D heterogeneous staggered-grid finite-difference modeling of seismic motion with volume harmonic and arithmetic averaging of elastic moduli and densities. Bull. Seismol. Soc. Am. **92**(8), 3042–3066 (2002). https://doi.org/10.1785/0120010167
23. Moczo, P., Kristek, J., Galis, M.: The Finite-Difference Modelling of Earthquake Motion: Waves and Ruptures. Cambridge University Press (2014)
24. Mulder, W.A.: Temporal dispersion correction for wave-propagation modelling with a series approach. Geophys. Prospect. **72**(2), 301–314 (2024). https://doi.org/10.1111/1365-2478.13411
25. Pleshkevich, A., Lisitsa, V., Vishnevsky, D., Levchenko, V.: A multi-level parallel algorithm for seismic imaging based on one-way wave equation migration. Comput. Math. Appl. **97**, 344–354 (2021)
26. Pleshkevich, A., Vishnevskiy, D., Lisitsa, V.: Sixth-order accurate pseudo-spectral method for solving one-way wave equation. Appl. Math. Comput. **359**, 34–51 (2019)
27. Shragge, J., Girard, A.J., Oren, C., Krahenbuhl, R.: Elastic time-reverse imaging of backscattered surface-wave data. Geophysics **89**(4), KS119–KS128 (2024). https://doi.org/10.1190/geo2023-0569.1
28. Symes, W., Vdovina, T.: Interface error analysis for numerical wave propagation. Comput. Geosci. **13**(3), 363–371 (2009)
29. Tromp, J., Komatitsch, D., Liu, Q.: Spectral-element and adjoint methods in seismology. Commun. Comput. Phys. **3**(1), 1–32 (2008)
30. Virieux, J., Calandra, H., Plessix, R.E.: A review of the spectral, pseudo-spectral, finite-difference and finite-element modelling techniques for geophysical imaging. Geophys. Prospect. **59**(5), 794–813 (2011). https://doi.org/10.1111/j.1365-2478.2011.00967.x
31. Virieux, J., Operto, S.: An overview of full-waveform inversion in exploration geophysics. Geophysics **74**(6), WCC1–WCC26 (2009)
32. Vishnevsky, D., Lisitsa, V., Tcheverda, V., Reshetova, G.: Numerical study of the interface errors of finite-difference simulations of seismic waves. Geophysics **79**(4), T219–T232 (2014). https://doi.org/10.1190/geo2013-0299.1
33. Xiang, Y., Wang, Z., Song, Z., Huang, R., Song, G., Min, F.: Seismictransformer: an attention-based deep learning method for the simulation of seismic wavefields. Comput. Geosci. **190**, 105629 (2024). https://doi.org/10.1016/j.cageo.2024.105629
34. Yu, S., Ma, J.: Deep learning for geophysics: current and future trends. Rev. Geophys. **59**(3), e2021RG000742 (2021)

3D NDM-Net Training Dataset Construction

Elena Gondyul(✉), Vadim Lisitsa, and Dmitry Vishnevsky

Sobolev Institute of Mathematics SB RAS, 4 Koptug ave., Novosibirsk 630090, Russia
gondyulea@gmail.com

Abstract. One of the important stages in training neural networks is the construction of a training dataset, especially when it is necessary to minimise its size in order to achieve efficiency. Using the example of a neural network that approximates the fine-grid solution from a coarse-grid solution of a seismic modelling problem, we use a clustering algorithm to form a representative training dataset. In this case, the metric used is the distance between sources. This achieves a solution accuracy that is 10% higher than when using other training dataset construction scenarios.

1 Introduction

Seismic modelling is getting a common tool to study peculiarities of wave propagation in media with complex rheology, including anisotropic media [16,19,30], viscoelastic media [1,36], poroelastic media [2,3,21]. Also, seismic modelling results may be used to design acquisition system in seismic exploration and seismic monitoring, especially in the case of CO_2 sequestration where plum monitoring is crucial for preventing CO_2 leakage [28,32]. However, seismic modelling is computationally intense and time-consuming, especially if applied as a part of seismic processing algorithms [34,35].

A common tool to simulate seismic waves in the Earth's interior is the grid-based numerical methods such as finite differences [16,23,30,33], finite elements [39], spectral elements [31,40], discontinuous Galerkin [5,18,29], pseudo-spectral methods [6,27] and others. However, as it follows from the general theory of numerical methods, to compute an accurate enough solution, one needs to use fine enough grids, because the numerical error is supposed to vanish if the grid step tends to zero. However, the size of the discretized problem increased dramatically if the grid step was reduced. Indeed, if the grid step gets one-half of the original step, the number of grid points increases in 16 times.

The classical way to improve the accuracy of the numerical method is the increase the formal order of approximation (order of the local basis). This approach allows reducing the numerical error even for coarse discretizations [14,17,25]. However, it has two drawbacks. First, increase of the formal order of approximation reduces the Courant number making the stability condition stricter. Second, stencil length (for finite differences) or size of the local mass and

© The Author(s), under exclusive license to Springer Nature Switzerland AG 2027
O. Gervasi et al. (Eds.): ICCSA 2026 Workshops, LNCS 16761, pp. 70–83, 2027.
https://doi.org/10.1007/978-3-032-30527-5_5

stiffness matrices for the discontinuous Galerkin method also increases requiring a higher number of floating point operations per grid node. The other way to improve the accuracy of, at least, finite differences is the use of dispersion suppression schemes [4,11,20]. This approach over-performs the high-order schemes if coarse enough grids are used. However, it has just the same drawbacks as mentioned above; i.e., the high number of flops per grid node and strict stability condition.

The two described approaches allow to reduce the numerical dispersion (numerical error) due to spatial discretization. It is done by the increase of the degrees of freedom when the spatial operator is approximating. However, the approximation of the temporal derivative is typically restricted by the second-order accurate operator. A modern approach to reduce the temporal dispersion in pre- and post-processing of the input signal and output data, respectively. The approach was firstly proposed in [12], and then developed in [22,24]. In combination with the spatial dispersion suppression schemes, this approach may produce accurate enough results on relatively coarse grids with as few as three grid points per minimal grid points per wavelength [24]. However, if the number of flops is considered, the approach is still computationally intense.

A completely different and rapidly developing approach to mitigate numerical error is based on the data post-processing using Deep Learning methods. In particular, the Numerical Dispersion Mitigation Network (NDM-net) was recently suggested in [9]. The idea of the approach is to compute the entire seismic dataset (wavefileds corresponding to all source positions which is about 10^5) using conventional low-order finite difference schemes. After that, a small number of seismograms can be generated using high-order schemes or a fine enough grid to form a training dataset. Then a network is trained and applied to map low-accuracy solution to the accurate one. It was shown in [9] that the application of the NDM-net allows accelerating seismic modelling by a factor of five in 2D in comparison with conventional approaches. However, according to the previous study, the efficiency of the NDM-net strongly depends on the training dataset [8,10].

One of the essential points is to prepare training data and reduce its size without losing the quality of training. Various methods are used to optimize the training set. For example, [37] suggests a method for evaluating the quality of a training sample using the output of the loss function in the learning process, and [38] developed a modified method of RUS (Random Under Sampling) using a random forest classifier. The authors of the article [26] use t-distributed stochastic neighbor embedding (CAE t-SNE) before training a neural network to analyze the similarities between training and target data sets.

In this article, we look at a strategy for construction a dataset using a Voronoi diagram and cluster analysis. Thus, the representativeness of the training dataset increases, thereby increasing the quality of the neural network application.

2 Seismic Modelling

One of the important stages is seismic modelling and simulation of synthetic seismograms. In this section, we will present the system of equations and the numerical method used in the study. In this case, we simulate seismograms for all sources only when using a coarse computational grid for fast calculations. To construct the training dataset, we use a fine computational grid and only a small portion of the sources (up to 20% of the total number of sources).

The solvable system is a system of differential equations of elasticity theory in terms of velocity and components of the stress tensor:

$$\begin{gathered}
\rho\frac{\partial u_1}{\partial t} = \frac{\partial \sigma_{11}}{\partial x_1} + \frac{\partial \sigma_{12}}{\partial x_2} + \frac{\partial \sigma_{13}}{\partial x_3} + f_1(t)\delta(\boldsymbol{x} - \boldsymbol{x}_s), \\
\rho\frac{\partial u_2}{\partial t} = \frac{\partial \sigma_{12}}{\partial x_1} + \frac{\partial \sigma_{22}}{\partial x_2} + \frac{\partial \sigma_{23}}{\partial x_3} + f_2(t)\delta(\boldsymbol{x} - \boldsymbol{x}_s), \\
\rho\frac{\partial u_3}{\partial t} = \frac{\partial \sigma_{13}}{\partial x_1} + \frac{\partial \sigma_{23}}{\partial x_2} + \frac{\partial \sigma_{33}}{\partial x_3} + f_3(t)\delta(\boldsymbol{x} - \boldsymbol{x}_s), \\
\frac{\partial \sigma_{11}}{\partial t} = (\lambda + 2\mu)\frac{\partial u_1}{\partial x_1} + \lambda\frac{\partial u_2}{\partial x_2} + \lambda\frac{\partial u_3}{\partial x_3}, \\
\frac{\partial \sigma_{22}}{\partial t} = \lambda\frac{\partial u_1}{\partial x_1} + (\lambda + 2\mu)\frac{\partial u_2}{\partial x_2} + \lambda\frac{\partial u_3}{\partial x_3}, \\
\frac{\partial \sigma_{33}}{\partial t} = \lambda\frac{\partial u_1}{\partial x_1} + \lambda\frac{\partial u_2}{\partial x_2} + (\lambda + 2\mu)\frac{\partial u_3}{\partial x_3}, \\
\frac{\partial \sigma_{23}}{\partial t} = \mu\left(\frac{\partial u_2}{\partial x_3} + \frac{\partial u_3}{\partial x_2}\right), \\
\frac{\partial \sigma_{13}}{\partial t} = \mu\left(\frac{\partial u_3}{\partial x_1} + \frac{\partial u_1}{\partial x_3}\right), \\
\frac{\partial \sigma_{12}}{\partial t} = \mu\left(\frac{\partial u_1}{\partial x_2} + \frac{\partial u_2}{\partial x_1}\right),
\end{gathered} \tag{1}$$

where ρ is the mass density, λ and μ are the Lame parameters, $\boldsymbol{u} = (u_1, u_2, u_3)^T$, is the velocity vector, σ_{ij} are the components of the stress tensor, $\boldsymbol{f}(t)$ is the vector of the external forces, δ is the Dirac delta function, $\boldsymbol{x_s}$ are the coordinates of the source position.

The system is solved in half-space $D = [x_s - L_x, x_s + L_x] \times [0, Z]$, where L_x is the maximal offset. It should be noted that this system is solved for a set of right-hand sides, i.e. source positions. It is precisely because of this that the task is resource-intensive.

We used staggered-grid finite differences [13,15,33,34] to solve system (1), which is described in detail in [9]. We will denote $\boldsymbol{u_h}(t, x_0, x_s^k)$ as a numerical solution of system (1) using a grid step $h = h_x = h_z$.

For our study, we will use synthetic seismograms recorded at the surface at zero depth by receivers. The acquisition system will be described in the section Numerical Experiments. Let us denote the seismogram corresponding to the source position x_s as $S(t, x_s)$.

3 Neural Network

To solve system 1 with the lowest computational cost, we propose using a neural network to suppress numerical dispersion. A slightly modified U-net architecture is used as the neural network architecture. This architecture allows not only to solve the image-to-image problem, but also to train relatively quickly.

The network consists of four consecutive convolution operations and a nonlinear LeakyReLU activation function, and four reverse convolution operations and a nonlinear ReLU activation function (Fig. 1). The kernel of both types of convolutions has a dimension of 2 by 2. Concatenation are also used to preserve spatial information.

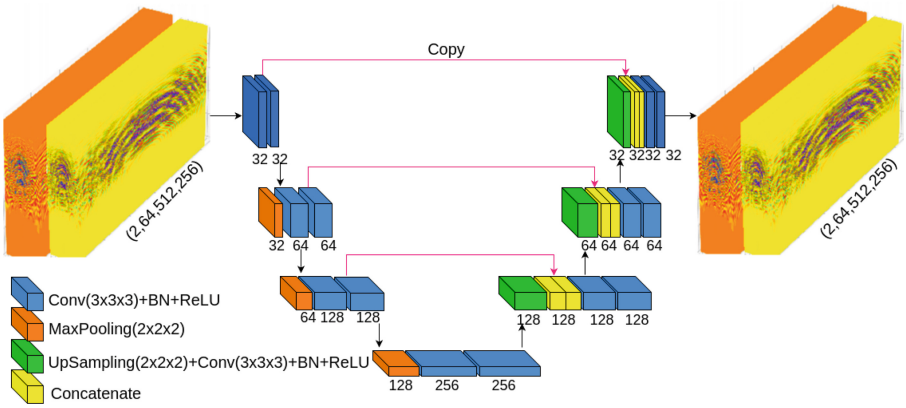

Fig. 1. 3D NDM-net architecture. Input and output data are two channels for the real and imaginary parts of the FFT. Red arrows represent copying skip connections, while black arrows represent operations specified by the colored boxes, such as Conv (convolution), BN (batch-normalization), ReLU (rectified linear unit) and MaxPooling (max pooling). (Color figure online)

As a result of using a neural network, seismograms are obtained, designated as $\mathcal{N}[S_c(t, x_s^j)]$, where $\mathcal{N} : S_c(t, x_s^j) \rightarrow S_f(t, x_s^j)$ is the map operator, $S_c(t, x_s^j)$ is the coarse-grid seismogram for $j - th$ source and $S_f(t, x_s^j)$ is the fine-grid seismogram.

4 Training Dataset Construction Algorithms

This section discusses three methods for construction a training dataset for a neural network that suppresses numerical dispersion in 3D synthetic seismograms.

4.1 Equidistantly Distributed Dataset

One obvious method is to use source positions located at equal distances from each other. This allows us to construct a dataset that is appropriately represented and covers the entire velocity model. Indeed, in 2D seismic modeling one may simply determine the distance between source positions as

$$d_d^{ij} = |\boldsymbol{x}_s^i - \boldsymbol{x}_s^j|,$$

where we assume all sources are placed at the same depth (typically $z = 0$).

In 3D surveys, acquisition typically employs a regular 2D grid of sources and receivers. Sources are positioned on a uniform rectangular lattice with inline spacing d_x and crossline spacing d_y, so $\boldsymbol{x}_s^{i,j} = (i \cdot d_x, j \cdot d_y, 0)$. The Euclidean distance between any two sources becomes

$$d_d^{i_1 j_1, i_2 j_2} = \sqrt{((i_1 - i_2)d_x)^2 + ((j_1 - j_2)d_y)^2},$$

which reduces to the 1D case when $d_x = d_y = d$ and $j_1 = j_2$. The resulting dataset D_d maintains regularity, facilitating efficient interpolation or decimation in processing workflows like NDM-net.

4.2 Randomly Distributed Dataset

The second method considered is to randomly select the source positions. This is the most popular construction method used in deep learning due to its simplicity of implementation. In addition, the construction of such training dataset does not depend on the properties of the data, which affects the representativeness. A uniform distribution is used to create a set of indexes. The seismograms included in this training dataset are denoted as $S(t, x_s^j) \in D_r$.

4.3 Dataset Based on Voronoi Diagram

The last method is to build using the Voronoi diagram and the clustering method. Since we have the distances between all the sources, we can construct a Voronoi diagram for the combined set of positions in terms of the k-mean. The first step of the algorithm is to randomly select the cluster centroids according to a uniform distribution.. Each segment of the Voronoi diagram corresponding to the selected centroids becomes a separate cluster. Next, the position of the centroids is updated in accordance with the minimization of the functional:

$$\sum_{i=1}^{K} \sum_{x \in S_i} (x - \mu_i)^2 \to min,$$

where K is the number of clusters, S_i is the obtained clusters in $i - th$ step, x is the vector of source positions and μ_i is the center of mass of all vectors from cluster S_i.

Finally, the algorithm stops when the relative decrease in the functional becomes less than the set value. To create the training dataset, the final centroids of the clustering algorithm are taken. The dataset constructed using the Voronoi diagram is denoted as D_{cl}.

5 Numerical Experiments

This section discusses the results of using three methods to construct training datasets to calibrate the NDM-net to suppress numerical dispersion in seismograms.

5.1 Training and Test Data

For experiments, we use the acoustic 3D SEG/EAGE Overthrust velocity model, which is shown in Fig. 2. The geological structure is a complex features with a fault. The size of the model is 20 km with a resolution of 25 m. The acquisition system uses an area system with lines of sources that are located 200 m apart, and the distance between the sources is 25 m. Perpendicular to the source lines are receiver lines, which are also located 200 m apart with a distance of 25 m between the receivers. For each source, a set of receivers is fixed with a maximum offsets of 6.4 km. Seismograms are recorded up to 3.2 s with a sampling rate of 2 ms.

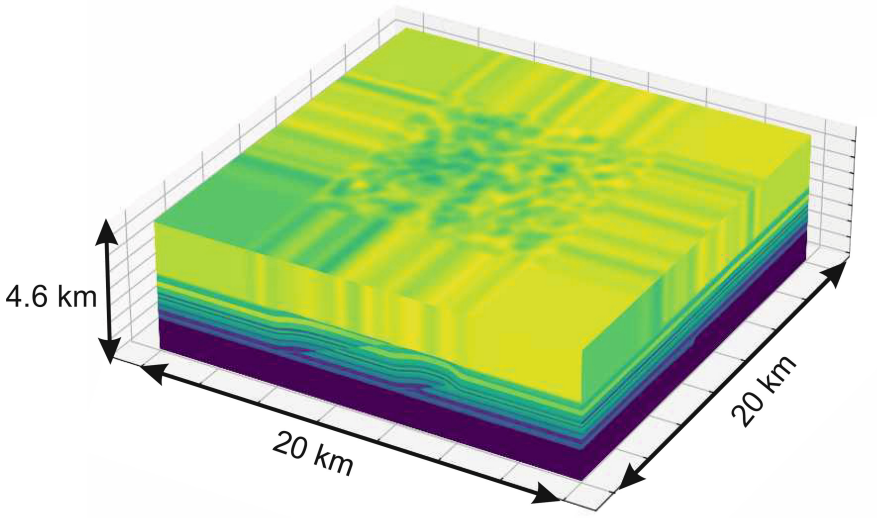

Fig. 2. The 3D SEG/EAGE Overthrust velocity model.

When calculating two sets of seismic data (a fine-resolution solution and a coarse-resolution solution), the Ricker pulse with centered frequency of 25 Hz is employed. To obtain a fine-resolution solution, a computational grid with a step of 2.5 m is used, for a coarse-resolution solution 5 m. The size of the training dataset is 2% of the total number of sources in the acquisition system.

For seismic modeling, as well as neural network training, a local server with 8 Nvidia A100 GPUs with 80 Gb of RAM was used. The duration of computation for each seismogram was 2 min when using a coarse computational grid, and 16 min when using a fine computational grid. The time required to train NDM-net was 20 h for a subset of 4% of the total number of sources. Therefore, the speed-up factor is between 5 and 6.

5.2 Training Scheme

The first step is data preprocessing, namely the mapping of seismograms from the time domain to the frequency domain using the Fast Fourier Transform (FFT). Due to the fact that seismograms are recorded with a fairly dense time grid, the high-frequency part of the signal is noise. Therefore, we are cutting off a significant unnecessary part of the signal. This procedure allows to significantly reduce the size of the data, and hence the RAM used during training. In addition, as shown in the [7], the use of FFT makes it possible to improve the quality of the neural network while suppressing numerical dispersion. Thus, one seismogram as a results of this procedure has a size of $32 \times 512 \times 256 \times 2$, where 32×512 is the number of traces of area receivers, 256 is the number of frequency samples, 2 is the real and imaginary part of the signal, instead of $32 \times 512 \times 1600$, where 1600 is the number of time samples.

The size of the training datasets, regardless of the method of its construction, is 2% of the total number of sources in the acquisition system. In the process of training the NDM-net, the mean-square error between the fine-resolution solution and the generated solution is minimized. Adam (Adaptive Moment Estimation) is used with increments of 10^{-4} to minimize the loss function. Training and validation losses are depicted in Fig. 3. Here, the early stopping and dropout techniques are used to prevent overfitting.

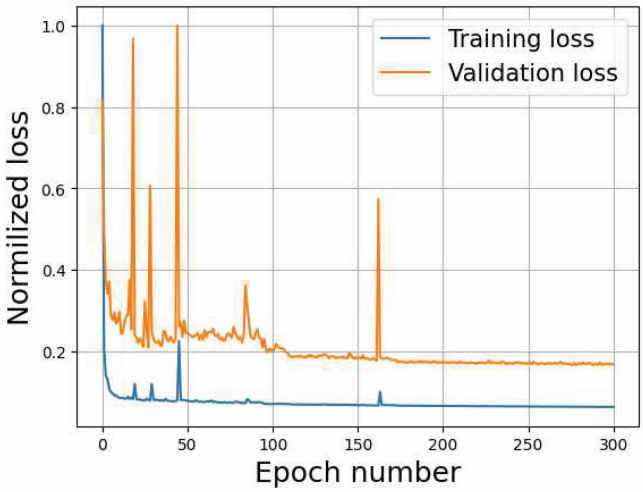

Fig. 3. Training and validation loss of NDM-net.

5.3 Results

This section presents the results of numerical experiments using three training datasets: equidistributed (D_d with source spacing $d = 25$ m), random (D_r), and Voronoi diagram-based (D_{cl} with $K = 200$ clusters initialized from D_d centroids). Figure 4 shows the seismograms obtained after applying three neural networks trained on three different training datasets. Thus, the seismogram on Fig. 4C was obtained using clustering in the formation of training data and has the lowest numerical dispersion compared to other seismograms (Fig. 4A, 4B, 4E). Figure 4 also shows the seismograms as the results of numerical modeling on a fine and coarse grid, as well as their difference. It is noticeable that numerical dispersion is more successfully suppressed when using a training dataset based on the Voronoi diagram.

A relative error is used to measure the accuracy of the results obtained from applying a neural network to seismograms:

$$\varepsilon^j = \varepsilon(S_f^j(t, x_s), \mathcal{N}[S_c^j(t, x_s)]) = \frac{\|S_f(t, x_s^j) - \mathcal{N}[S_c(t, x_s^j)]\|_2}{\|S_f(t, x_s^j)\|_2} \times 100\%,$$

$$\|S(t, x_s^j)\|_2^2 = \int_0^T \int_{-X}^{X} \int_{-Y}^{Y} u^2(x_s^j, t, x, y) dy dx dt,$$

where x and y are offsets along corresponding directions, X and Y are maximal offsets, and t is time.

The relative error for each source in the three source lines is shown in Fig. 5 when using different training datasets. It is noticeable that when using random sampling and equally distributed sampling, the error of using a neural network is almost the same. However, when using a Voronoi-based sample, we get the lowest relative error value for all sources.

We also calculate relative error maps for all the source positions in the acquisition system (Fig. 6). The NDM-net was observed to successfully reduce numerical dispersion by approximately 2-fold in all cases. However, it is recommended to use clustering when creating a training dataset based on information regarding the distance between sources, as this approach yielded the best results. The maps also indicate that numerical error fluctuates significantly in areas with complex structures, while it remains relatively stable in areas with homogeneous structures. Additionally, increasing the representativeness of the training dataset by using of a Voronoi diagram reduced this variation by 10%.

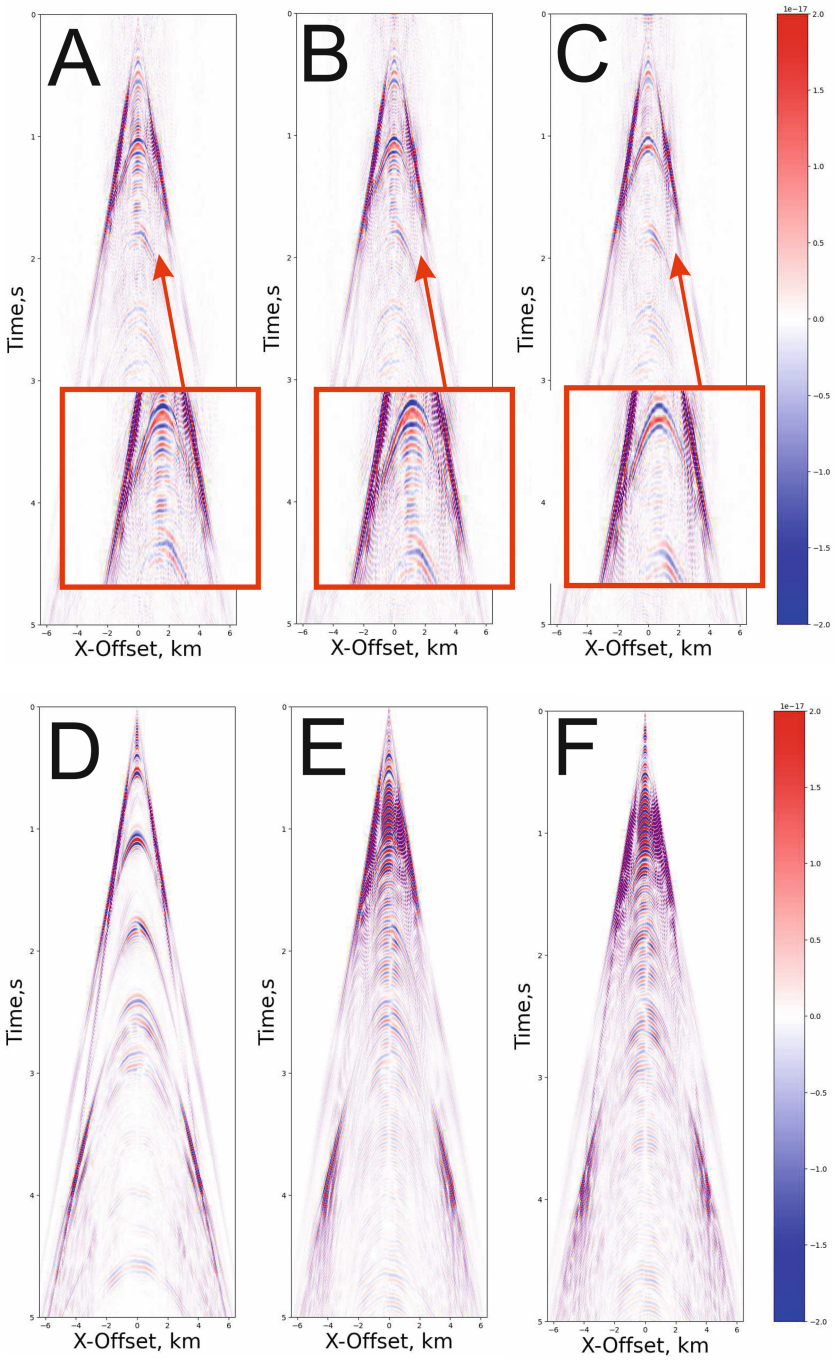

Fig. 4. Seismograms obtained using a neural network trained on a random dataset D_r (A), an equidistributed dataset D_d (B), a dataset using a Voronoi diagram D_{cl} (C) (the main differences are highlighted in red boxes), and obtained using seismic modeling on a fine grid (D), on a coarse grid (E), the difference between a fine-grid solution and a coarse solution (F). All seismograms were obtained for the same source with a position of $X = 2600$ m, $Y = 400$ m for Y-offset $= 0$ m. (Color figure online)

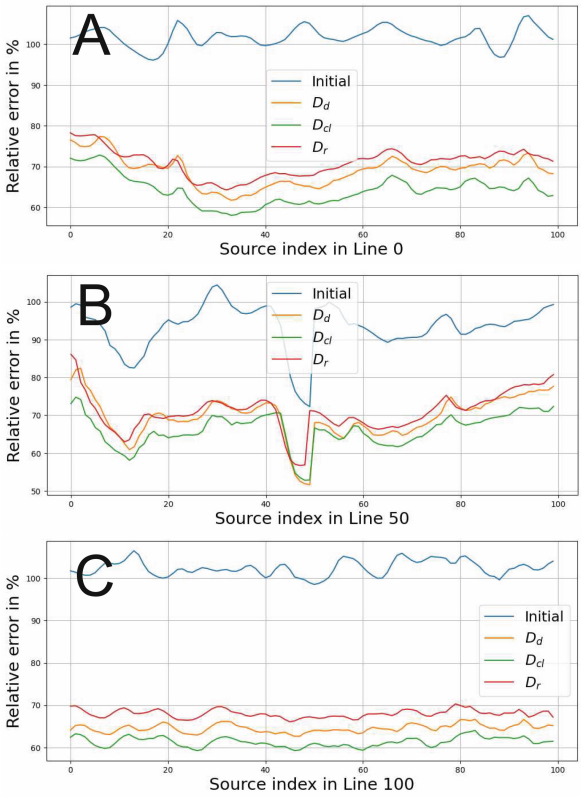

Fig. 5. The relative error between seismogram calculated on a coarse grid and fine grid solution (blue plot), and the relative errors between NDM-net post-processed seismogram and fine grid solution for different training datasets (D_d, D_{cl}, D_r) and lines of acquisition system with position Y-offset = 0 m (A), Y-offset = 10 km (B), Y-offset = 20 km (C). (Color figure online)

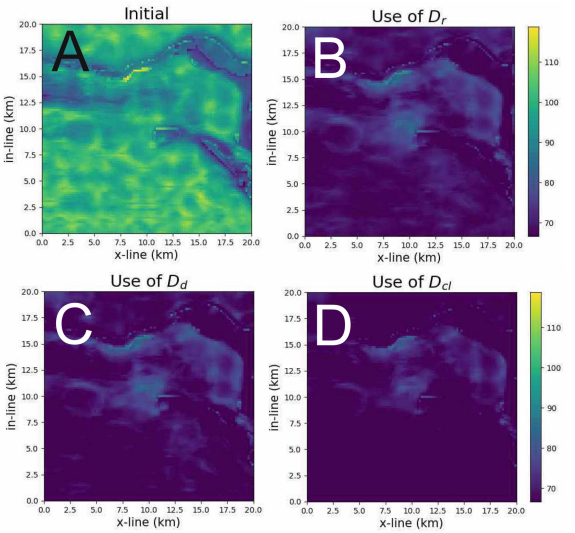

Fig. 6. Maps for the relative error (in %) between solutions on a coarse and a fine computational grid (A), between the fine grid solutions and 3D NDM-net postprocessing results for a training datasets D_r (B), D_d (C), D_{cl} (D).

6 Conclusion

We presented a detailed study of the effect of the training dataset construction on the accuracy of the NDM-net. The NDM-net was designed to reduce the numerical error in seismic modeling, where the elastic wave equation is solved for the multiple right-hand sides. Thus, the solution for all source positions can be computed using a low-order finite-difference scheme on a coarse grid. The training dataset is generated using a fine enough mesh for a small number of source positions. After that, the NDM-net is trained to map the coarse grid solution to the fine grid solution. Generation of the training dataset is the most time-consuming part of the algorithm.

It has been demonstrated that the use of a more representative dataset obtained from the Voronoi diagram and clustering techniques reduces the relative error of applying the NDM-net by 10% compared to a conventional, equally distributed training sample. Additionally, numerical dispersion has been successfully reduced by a factor of two in areas with complex structures, which was not possible using other training sets.

Acknowledgments. Seismic modelling and NDM-net correction was done by the IM SB RAS group under the support of the Russian Science Foundation grant no. 22-11-00004-*П*.

Disclosure of Interests. The authors have no competing interests to declare that are relevant to the content of this article.

References

1. Carcione, J.M., Cavallini, F.: A rheological model for anelastic anisotropic media with applications to seismic wave propagation. Geophys. J. Int. **119**, 338–348 (1994)
2. Carcione, J.M., Morency, C., Santos, J.E.: Computational poroelasticity – a review. Geophysics **75**(5), 75A229-75A243 (2010)
3. Caspari, E., et al.: Attenuation mechanisms in fractured fluid-saturated porous rocks: a numerical modelling study. Geophys. Prospect. **67**(4), 935–955 (2019)
4. Chen, J.B.: A 27-point scheme for a 3D frequency-domain scalar wave equation based on an average-derivative method. Geophys. Prospect. **62**(2), 258–277 (2014)
5. Dumbser, M., Kaser, M.: An arbitrary high-order discontinuous galerkin method for elastic waves on unstructured meshes - ii. the three-dimensional isotropic case. Geophys. J. Int. **167**(1), 319–336 (2006). https://doi.org/10.1111/j.1365-246X.2006.03120.x
6. Fornberg, B.: The pseudospectral method: accurate representation of interfaces in elastic wave calculations. Geophysics **53**(5), 625–637 (1988)
7. Gadylshin, K., Gondyul, E., Lisitsa, V., Gadylshina, K., Vishnevsky, D.: Mitigation of numerical dispersion in seismic data in spectral domain with neural networks. Soil Dyn. Earthq. Eng. **187**, 109028 (2024). https://doi.org/10.1016/j.soildyn.2024.109028
8. Gadylshin, K., Lisitsa, V., Vishnevsky, D., Gadylshina, K.: Hausdorff-distance-based training dataset construction for numerical dispersion mitigation neural network. Comput. Geosci. **180**, 105438 (2023). https://doi.org/10.1016/j.cageo.2023.105438
9. Gadylshin, K., Vishnevsky, D., Gadylshina, K., Lisitsa, V.: Numerical dispersion mitigation neural network for seismic modeling. Geophysics **87**(3), T237–T249 (2022)
10. Gondyul, E., Lisitsa, V., Gadylshin, K., Vishnevsky, D.: Numerical dispersion mitigation neural network with the model-based training dataset optimization. In: Gervasi, O., et al. (eds.) Computational Science and Its Applications – ICCSA 2023 Workshops, pp. 19–30. Springer (2023)
11. He, Z., Zhang, J., Yao, Z.: Determining the optimal coefficients of the explicit finite-difference scheme using the remez exchange algorithm. Geophysics **84**(3), S137–S147 (2019). https://doi.org/10.1190/geo2018-0446.1
12. Koene, E.F.M., Robertsson, J.O.A., Broggini, F., Andersson, F.: Eliminating time dispersion from seismic wave modeling. Geophys. J. Int. **213**(1), 169–180 (2017)
13. Kostin, V., Lisitsa, V., Reshetova, G., Tcheverda, V.: Local time-space mesh refinement for simulation of elastic wave propagation in multi-scale media. J. Comput. Phys. **281**, 669–689 (2015)
14. Levander, A.R.: Fourth-order finite-difference P-SV seismograms. Geophysics **53**(11), 1425–1436 (1988)
15. Levander, A.: Fourth-order finite-difference P-S. Geophysics **53**(11), 1425–1436 (1988). https://doi.org/10.1190/1.1442422
16. Lisitsa, V., Vishnevskiy, D.: Lebedev scheme for the numerical simulation of wave propagation in 3D anisotropic elasticity. Geophys. Prospect. **58**(4), 619–635 (2010). https://doi.org/10.1111/j.1365-2478.2009.00862.x
17. Lisitsa, V.: Dispersion analysis of discontinuous galerkin method on triangular mesh for elastic wave equation. Appl. Math. Model. **40**, 5077–5095 (2016). https://doi.org/10.1016/j.apm.2015.12.039

18. Lisitsa, V., Tcheverda, V., Botter, C.: Combination of the discontinuous galerkin method with finite differences for simulation of seismic wave propagation. J. Comput. Phys. **311**, 142–157 (2016)
19. Lisitsa, V., Tcheverda, V., Vishnevsky, D.: Numerical simulation of seismic waves in models with anisotropic formations: coupling virieux and lebedev finite-difference schemes. Comput. Geosci. **16**(4), 1135–1152 (2012)
20. Liu, Y., Sen, M.K.: Acoustic VTI modeling with a time-space domain dispersion-relation-based finite-difference scheme. Geophysics **75**(3), A11–A17 (2010)
21. Masson, Y.J., Pride, S.R.: Finite-difference modeling of biot's poroelastic equations across all frequencies. Geophysics **75**(2), N33–N41 (2010)
22. Mittet, R.: Second-order time integration of the wave equation with dispersion correction procedures. Geophysics **84**(4), T221–T235 (2019)
23. Moczo, P., Kristek, J., Galis, M.: The Finite-Difference Modelling of Earthquake Motion: Waves and Ruptures. Cambridge University Press (2014)
24. Mulder, W.A.: Temporal dispersion correction for wave-propagation modelling with a series approach. Geophys. Prospect. **72**(2), 301–314 (2024). https://doi.org/10.1111/1365-2478.13411
25. O'Reilly, O., Lundquist, T., Dunham, E.M., Nordstrom, J.: Energy stable and high-order-accurate finite difference methods on staggered grids. J. Comput. Phys. **346**, 572–589 (2017). https://doi.org/10.1016/j.jcp.2017.06.030
26. Park, J., Choi, J., Jee Seol, S., Byun, J., Kim, Y.: A method for adequate selection of training data sets to reconstruct seismic data using a convolutional u-net. Geophysics **86**, V375–V388 (2021)
27. Pleshkevich, A., Vishnevskiy, D., Lisitsa, V.: Sixth-order accurate pseudo-spectral method for solving one-way wave equation. Appl. Math. Comput. **359**, 34–51 (2019)
28. Prasad, M., Glubokovskikh, S., Daley, T., Oduwole, S., Harbert, W.: Co2 messes with rock physics. Lead. Edge **40**(6), 424–432 (2021)
29. Puente, J., Kaser, M., Dumbser, M., Igel, H.: An arbitrary high-order discontinuous galerkin method for elastic waves on unstructured meshes iv. anisotropy. Geophys. J. Int. **169**(3), 1210–1228 (2007). https://doi.org/10.1111/j.1365-246X.2007.03381.x
30. Saenger, E.H., Gold, N., Shapiro, S.A.: Modeling the propagation of the elastic waves using a modified finite-difference grid. Wave Motion **31**, 77–92 (2000)
31. Tromp, J., Komatitsch, D., Liu, Q.: Spectral-element and adjoint methods in seismology. Commun. Comput. Phys. **3**(1), 1–32 (2008)
32. Verliac, M., Calvez, J.L.: Microseismic monitoring for reliable co2 injection and storage – geophysical modeling challenges and opportunities. Lead. Edge **40**(6), 418–423 (2021)
33. Virieux, J.: P-SV wave propagation in heterogeneous media: velocity-stress finite-difference method. Geophysics **51**(4), 889–901 (1986)
34. Virieux, J., Calandra, H., Plessix, R.E.: A review of the spectral, pseudo-spectral, finite-difference and finite-element modelling techniques for geophysical imaging. Geophys. Prospect. **59**(5), 794–813 (2011). https://doi.org/10.1111/j.1365-2478.2011.00967.x
35. Virieux, J., et al.: Seismic wave modeling for seismic imaging. Lead. Edge **28**(5), 538–544 (2009)
36. Vishnevsky, D.M., Solovyev, S.A., Lisitsa, V.V.: Numerical simulation of wave propagation in 3d elastic media with viscoelastic formations. Lobachevskii J. Math. **41**(8), 1603–1614 (2020)

37. Wang, R., Meng, Y., Zhang, W., Li, Z., Hu, F., Meng, L.: Remote sensing semantic segregation for water information extraction: optimization of samples via training error performance. IEEE Access (2019). https://doi.org/10.1109/ACCESS.2019.2894099
38. Yan, S., Zhang, L., Liu, D.: An empirical study on optimization of training dataset in harmfulness prediction of code clone using ensemble feature selection model. In: 018 5th International Conference on Information and Communication Technologies for Disaster Management, pp. 1–4 (2018). https://doi.org/10.1109/ICT-DM.2018.8636375
39. Zhang, J., Verschuur, D.J.: Elastic wave propagation in heterogeneous anisotropic media using the lumped finite-element method. Geophysics **67**(2), 625–638 (2002)
40. Zhang, Y., Fisser, J., Gerritsma, M.: A hybrid mimetic spectral element method for three-dimensional linear elasticity problems. J. Comput. Phys. **433**, 110179 (2021). https://doi.org/10.1016/j.jcp.2021.110179

Numerical Homogenization of 2D Heterogeneous Anisotropic Porous Medium Based on a Hyperbolic Thermodynamically Compatible Model

Galina Reshetova[1] and Evgeniy Romenski[2(✉)]

[1] Trofimuk Institute of Petroleum Geology and Geophysics SB RAS, Novosibirsk 630090, Russia
kgv@nmsf.sscc.ru

[2] Sobolev Institute of Mathematics SB RAS, Novosibirsk 630090, Russia
evrom@math.nsc.ru

Abstract. For the numerical homogenization of a heterogeneous porous medium, a method based on strain energy is proposed in combination with a hyperbolic thermodynamically compatible model of a saturated porous medium. The solution of stationary equilibrium problems, necessary for calculating the effective compliance moduli by comparing the energy of an inhomogeneous medium with the equivalent elastic energy, is obtained by the time-marching to a stationary solution method. A number of numerical examples for calculating the effective moduli of macroscopically anisotropic heterogeneous porous samples are presented and discussed.

Keywords: Numerical homogenization · Fluid saturated porous medium · Effective elastic moduli · Hyperbolic thermodynamically compatible model · Staggered grid finite difference scheme

1 Introduction

The evaluation of effective elastic moduli of heterogeneous media is of interest in many applied engineering sciences, for example, in seismic exploration, the development of new materials with specified properties, biomechanics, 3D printing and so on.

There are a number of methods for evaluating the effective moduli of heterogeneous media, a far from complete list of which includes: asymptotic homogenization for periodic structures based on the analytical method of decomposition of fields in terms of a small parameter (the ratio of the microstructure scale to the macroscale), see [16] and references therein; the classical method of representative volume element, in which for a minimum volume of material containing all statistical features of the microstructure, the stiffness tensor is calculated by averaging the stress and strain fields over the volume [1,4,6,17]; the FFT-based

© The Author(s), under exclusive license to Springer Nature Switzerland AG 2027
O. Gervasi et al. (Eds.): ICCSA 2026 Workshops, LNCS 16761, pp. 84–97, 2027.
https://doi.org/10.1007/978-3-032-30527-5_6

homogenization method, in which the solution of the equilibrium equations is sought in the frequency domain using the fast Fourier transform [2,15]; variational homogenization methods which uses variational principles to obtain strict upper and lower bounds on the effective properties of materials (see [5,7,20] and references therein.

We propose a novel numerical homogenization method using a strain energy-based approach [3,14,18,19], which essentially calculates the strain energy of an inhomogeneous medium and compares it with the energy of an equivalent elastic medium. This allows us to calculate all components of the compliance tensor by solving a series of simple equilibrium problems for stressed samples. We apply a strain energy-based method to a linear Hyperbolic Thermodynamically Compatible (HTC) model of porous media, which allows simulating wave processes in porous media with inclusions of pure solid and fluid phases using a single system of partial differential equations by a diffuse interphase approach. The linear HTC equations we use is derived from the general model [13] of a saturated porous medium for the case of finite deformations. It can be generalized to the case where the saturating fluid is a mixture of several fluids [12], and some applications of it can be found in the papers [8–10]. The governing equations of the model belong to the class of hyperbolic thermodynamically compatible systems, which ensures their solvability and allows the use of effective numerical methods. To solve a series of stationary problems required for the application of the strain energy-based method, we apply the time-marching method in conjunction with a finite difference scheme on staggered grids to obtain the equilibrium solution.

The rest of the paper is organized as follows. In Sect. 2 the governing equations of HTC linear poroelasticity are formulated. In Sect. 3 the strain energy-based method and test problems required for calculation of compliance moduli are presented. Section 4 briefly describes the time marching method applied for solving test problems studied in the next Sect. 5. This section presents the simulation results for various samples of porous media with differently oriented inclusions having other properties. In this section, the obtained anisotropy properties of the samples under consideration are also discussed.

2 Governing Equations of the Fluid Saturated Porous Medium in Case of Small Deformations

The numerical homogenization method presented in the paper is based on the use of a Hyperbolic Thermodynamically Compatible (HTC) model of fluid saturated porous media to calculate the strain energy of a heterogeneous porous sample in a stressed equilibrium state and its subsequent comparison with the strain energy of an equivalent elastic sample. Such a comparison allows us to compute the effective compliance moduli and then the stiffness moduli and sound velocities.

To calculate the deformation energy of a saturated porous medium, a linear system of equations is used, obtained by linearization the equations of the full HTC model of a two-phase solid-fluid medium [13]. Linearization is carried out for the solution of the complete system in a steady, stress-free state with a given

phase volume fractions of saturating fluid and skeleton α_1, α_2 ($\alpha_1 + \alpha_2 = 1$) and mass densities ρ_1, ρ_2.

It is assumed that in the three-dimensional space x_1, x_2, x_3, the porous medium, considered as a two-phase mixture, is characterized by the following state variables.:

- u_i, $(i = 1, 2, 3)$ - the velocity of the mixture along the axes x_i.
- w_i, $(i = 1, 2, 3)$ - the relative velocity of movement of the first phase relative to the second phase.
- p - the pressure in the medium.
- $\Sigma_{ij} = \Sigma_{ji}$ $(i, j = 1, 2, 3)$ - the stress deviator ($\Sigma_{11} + \Sigma_{22} + \Sigma_{33} = 0$).

It should be noted that the linear system is derived under the assumption of pressure equilibrium, that is, it is assumed that the pressures of the fluid and the solid skeleton are equal.

The complete system of governing equations reads as

$$\rho \frac{\partial u_i}{\partial t} + \frac{\partial p}{\partial x_i} - \frac{\partial \Sigma_{ik}}{\partial x_k} = 0, \tag{1a}$$

$$\frac{\partial w_i}{\partial t} + \left(\frac{1}{\rho_1} - \frac{1}{\rho_2}\right) \frac{\partial p}{\partial x_i} = -\lambda w_i, \tag{1b}$$

$$\frac{\partial p}{\partial t} + K \frac{\partial u_k}{\partial x_k} + \frac{\alpha_1 \alpha_2}{\rho} (\rho_2 - \rho_1) K \frac{\partial w_k}{\partial x_k} = 0, \tag{1c}$$

$$\frac{\partial \Sigma_{ik}}{\partial t} - \mu \left(\left(\frac{\partial u_i}{\partial x_k} + \frac{\partial u_k}{\partial x_i} \right) - \frac{2}{3} \delta_{ik} \left(\frac{\partial u_1}{\partial x_1} + \frac{\partial u_2}{\partial x_2} + \frac{\partial u_3}{\partial x_3} \right) \right) = -\frac{\Sigma_{ik}}{\tau}, \tag{1d}$$

and consists of the total momentum Eq. (1a), equation for the relative velocity (1b), equation for the pressure (1c) and equation for the stress deviator (1d).

Here $i, k = 1, 2, 3$ are the spacial indices, $\rho = \alpha_1 \rho_1 + \alpha_2 \rho_2$ is the mixture density. $K = \left(\frac{\alpha_1}{K_1} + \frac{\alpha_2}{K_2} \right)^{-1}$ is the bulk modulus of the two-phase mixture, where K_1, K_2 are the bulk moduli of the phases. $\mu = \rho V_s^2 = \rho(c_1 V_{s1}^2 + c_2 V_{s2}^2) = \alpha_1 \mu_1 + \alpha_2 \mu_2$ is the shear modulus of the mixture, $V_{sa} (a = 1, 2)$ are the phase shear velocities, $\mu_a = \rho_a V_{sa}^2 (a = 1, 2)$ are the phase shear moduli. If one of the phases, for example the first, is a liquid, we assume that its shear modulus is zero, and hence $\mu = \alpha_2 \mu_2$. Throughout the paper the repeating indices denote the summation over the corresponding index.

There are two dissipative sources in the system (1): $-\lambda w_i$ describes interfacial friction with the relaxation rate of the relative velocity λ, and $-\frac{\Sigma_{ik}}{\tau}$ describes the relaxation of the shear stress. In our studies, we neglect these terms, since our goal is to derive effective elastic moduli for reversible processes.

The stress deviator Σ_{ik} and pressure P are connected with the Almansi strain tensor ε_{ij} via linear relationships

$$\Sigma_{ik} = 2\mu \left(\varepsilon_{ik} - \delta_{ik} \frac{(\varepsilon_{11} + \varepsilon_{22} + \varepsilon_{33})}{3} \right), \quad P = -K(\varepsilon_{11} + \varepsilon_{22} + \varepsilon_{33}). \tag{2}$$

with defined above bulk and shear moduli $K = \left(\frac{\alpha_1}{K_1} + \frac{\alpha_2}{K_2}\right)^{-1}$, $\mu = \alpha_1\mu_1 + \alpha_2\mu_2$. These relations are used to derive the (1) system from the general HTC system of a saturated porous medium [13]. It should be noted that, if necessary, the Lamé constant λ can be calculated from the definition of the bulk modulus $K = \lambda + \frac{2}{3}\mu$ if the Lamé constant μ (shear modulus) is known. The total stress tensor of the saturated porous medium can be computed as $\sigma_{ik} = \Sigma_{ik} - P\delta_{ij}$ and is connected to the Almansi strain tensor ε_{ik} via Hooke's law for isotropic linear elasticity:

$$\sigma_{ik} = \lambda(\varepsilon_{11} + \varepsilon_{22} + \varepsilon_{33})\delta_{ik} + 2\mu\varepsilon_{ik}. \tag{3}$$

A very important property of the presented model of a porous medium, which we will need later to calculate the effective moduli, is the presence of an additional law of conservation of energy. The total energy for the solution to system (1) can be defined as $\mathcal{E} = \mathcal{E}_1 + \mathcal{E}_2$, where

$$\mathcal{E}_1 = \rho\frac{u_k u_k}{2} + \rho c_1 c_2 \frac{w_k w_k}{2},\ \mathcal{E}_2 = \frac{p^2}{2K} + \frac{\Sigma_{ij}\Sigma_{ji}}{4\mu}. \tag{4}$$

Assuming no dissipation and using the definition of (4), the law of conservation of energy follows from Eq. (1) and reads as

$$\frac{\partial \mathcal{E}}{\partial t} + \frac{\partial \Pi_k}{\partial x_k} = -\mathcal{Q}, \tag{5}$$

where $\Pi_k = u_k P + \frac{\alpha_1\alpha_2}{\rho}(\rho_2 - \rho_1)w_k P - u_i\Sigma_{ik}$ is the energy flux.

We emphasize that the two-phase model formulated in this section for a non-zero shear modulus of the first phase ($\mu_1 \neq 0$) can describe wave processes in a solid-solid mixture.

As described below, the strain energy-based numerical homogenization method involves calculating the energy $\mathcal{E}_2$ for a number of simple equilibrium problems and comparing it with the energy of an equivalent elastic medium.

3 Strain Energy of Homogeneous Elastic Medium. Calculation of Compliance Moduli by Solving Simple Equilibrium Problems

The stress-strain relations for an arbitrary linear-elastic medium can be written in two equivalent forms of Hooke's law:

$$\sigma_{ij} = c_{ijkl}\varepsilon_{kl}, \tag{6}$$

$$\varepsilon_{ij} = s_{ijkl}\sigma_{kl}, \tag{7}$$

where c_{ijkl} is the stiffness tensor and s_{ijkl} is the compliance tensor, which is inverse to the stiffness tensor.

The elastic energy expressed through the strain tensor has the following form

$$\mathcal{U} = \frac{1}{2}\sigma_{ij}\varepsilon_{ij} = \frac{1}{2}c_{ijkl}\varepsilon_{kl}\varepsilon_{ij}, \tag{8}$$

and can be written in equivalent form in terms of stress tensor

$$\mathcal{U} = \frac{1}{2}\sigma_{ij}\varepsilon_{ij} = \frac{1}{2}s_{ijkl}\sigma_{kl}\sigma_{ij}. \tag{9}$$

The latter formula (9) gives a direct way to calculate the components of the compliance tensor by solving a set of simple equilibrium problems.

Below we study the two-dimensional case of plane strain, for which $\varepsilon_{33} = \varepsilon_{13} = \varepsilon_{23} = \varepsilon_{31} = \varepsilon_{32} = 0$ and elastic energy (9) is equal to

$$\begin{aligned}\mathcal{U} = &\frac{1}{2}\left(\sigma_{11}\varepsilon_{11} + 2\sigma_{12}\varepsilon_{12} + \sigma_{22}\varepsilon_{22}\right) = \\ &s_{1111}(\sigma_{11})^2 + 2s_{1122}\sigma_{11}\sigma_{22} + s_{2222}(\sigma_{22})^2 + \\ &2s_{1212}\sigma_{12}\sigma_{12} + 2s_{1112}\sigma_{11}\sigma_{12} + 2s_{2212}\sigma_{22}\sigma_{12}.\end{aligned} \tag{10}$$

Let us consider two-dimensional elasticity equilibrium equations

$$\frac{\partial \sigma_{ij}}{\partial x_j} = 0, \quad i,j = 1,2. \tag{11}$$

in a rectangle $[-L_x, L_x] \times [-L_y, L_y]$ of volume $V = 2L_x \times 2L_y$.

To determine the six components of the compliance tensor s_{1111}, s_{1122}, s_{2222}, s_{1212}, s_{1112}, s_{2212} we need to solve six equilibrium boundary problems for Eq. (11) in the two-dimensional domain $[-L_x, L_x] \times [-L_y, L_y]$:

- Test 1
  $\sigma_{11}|_{x=\pm L_x} = 1, \quad \sigma_{22}|_{y=\pm L_y} = 0, \quad \sigma_{12}|_{x=\pm L_x} = 0, \quad \sigma_{12}|_{y=\pm L_y} = 0.$
  In this test problem, the deformation energy $\mathcal{U}^0$ is calculated, and at equilibrium it is equal to $\mathcal{U}^{01} = \frac{V}{2}s_{1111}(\sigma_{11})^2 = \frac{V}{2}s_{1111}$. Using this energy value, we find the compliance modulus s_{1111}.
- Test 2
  $\sigma_{11}|_{x=\pm L_x} = 0, \quad \sigma_{22}|_{y=\pm L_y} = 1, \quad \sigma_{12}|_{x=\pm L_x} = 0, \quad \sigma_{12}|_{y=\pm L_y} = 0.$
  And in this test problem we find the energy $\mathcal{U}^0$. For the equilibrium solution it is equal to $\mathcal{U}^{02} = \frac{V}{2}s_{2222}(\sigma_{22})^2 = \frac{V}{2}s_{2222}$, and therefore we find s_{2222}.
- Test 3
  $\sigma_{11}|_{x=\pm L_x} = 1, \quad \sigma_{22}|_{y=\pm L_y} = 1, \quad \sigma_{12}|_{x=\pm L_x} = 0, \quad \sigma_{12}|_{y=\pm L_y} = 0.$
  It turns out that the solution to this test problem can be found as the sum of the solutions to Test 1 and Test 2: $\sigma_{ij} = \sigma^1_{ij} + \sigma^2_{ij}$. Therefore, it is possible to use the results already obtained for previous test problems and there is no need to carry out additional numerical calculations. Indeed, the elastic energy for this test problem is calculated using the formula (10). Denoting the solution of the Test 1 as σ^1_{ij} where $\sigma^1_{11} = 1, \sigma^1_{ij} = 0$ if $(ij) \neq (11)$ and solution of the Test 2 as σ^2_{ij} where $\sigma^2_{22} = 1, \sigma^2_{ij} = 0$ if $(ij) \neq (22)$, we calculate strain energies $\mathcal{U}^{01} = \frac{V}{2}s_{1111}$, $\mathcal{U}^{02} = \frac{V}{2}s_{2222}$. This means that compliance moduli s_{1111}, s_{2222} are found and we can compute deformations ε^1_{11}, ε^1_{22}, ε^2_{11},

ε^2_{22}:

$$\begin{aligned}
\varepsilon^1_{11} &= s_{1111}\sigma^1_{11} + s_{1122}\sigma^1_{22} = s_{1111}\sigma^1_{11} = s_{1111},\\
\varepsilon^1_{22} &= s_{2211}\sigma^1_{11} + s_{2222}\sigma^1_{22} = s_{2211}\sigma^1_{11} = s_{2211}\\
\varepsilon^2_{11} &= s_{1122}\sigma^2_{11} + s_{2222}\sigma^2_{22} = s_{2222}\sigma^2_{22} = s_{2222},\\
\varepsilon^2_{22} &= s_{2211}\sigma^{02}_{11} + s_{2222}\sigma^2_{22} = s_{2222}\sigma^2_{22} = s_{2222}.
\end{aligned} \tag{12}$$

Finally, since the solution to this test problem is the sum of the solutions for Test 1 and Test 2, we numerically calculate the energy $\mathcal{U}^0$, which should be equal to

$$\mathcal{U}^0 = \frac{1}{2}\int\limits_V \sigma_{ij}\varepsilon_{ij}dV = \frac{1}{2}\int\limits_V \left(\sigma^1_{ij} + \sigma^2_{ij}\right)\left(\varepsilon^1_{ij} + \varepsilon^2_{ij}\right)dV = \tag{13}$$

$$\mathcal{U}^{01} + \mathcal{U}^{02} + \frac{1}{2}\int\limits_V \left(\sigma^1_{ij}\varepsilon^2_{ij} + \sigma^2_{ij}\varepsilon^1_{ij}\right)dV.$$

Thus, from the above equality we conclude that
$s_{1122} = \frac{1}{2V}\int\limits_V \left(\sigma^1_{ij}\varepsilon^2_{ij} + \sigma^2_{ij}\varepsilon^1_{ij}\right)dV$, where $\sigma^1_{ij}, \varepsilon^1_{ij}, \sigma^2_{ij}, \varepsilon^2_{ij}$ are solutions of Test 1 and Test 2 already obtained numerically. Thus, it is possible to solve the equilibrium problem in the case of a complex stress state without its direct numerical solution and, therefore, reduce the computation time. However, this requires the use of additional memory to store all stress and strain components for simple stress states.

- Test 4
  $\sigma_{11}|_{x=\pm L_x} = 0, \quad \sigma_{22}|_{y=\pm L_y} = 0, \quad \sigma_{12}|_{x=\pm L_x} = 1, \quad \sigma_{12}|_{y=\pm L_y} = 1.$
  In this test problem, the calculated numerically energy for the equilibrium solution is equal to $\mathcal{U}^0 = \frac{V}{2}\left(2s_{1212}(\sigma_{12})^2\right) = Vs_{1212}$. Thus, s_{1212} is found.
- Test 5
  $\sigma_{11}|_{x=\pm L_x} = 0, \quad \sigma_{22}|_{y=\pm L_y} = 1, \quad \sigma_{12}|_{x=\pm L_x} = 1, \quad \sigma_{12}|_{y=\pm L_y} = 1.$
  Similar to how the solution is found in Test 3, the solution to this problem can be obtained as the sum of the solutions from Tests 2 and 4, and we can find $s_{2212} = \frac{1}{2V}\int \left(\sigma^1_{ij}\varepsilon^2_{ij} + \sigma^2_{ij}\varepsilon^1_{ij}\right)dV$, where $\sigma^1_{ij}, \varepsilon^1_{ij}, \sigma^2_{ij}, \varepsilon^2_{ij}$ are solutions of the problems Test 2 and Test 4 obtained numerically.
- Test 6
  $\sigma_{11}|_{x=\pm L_x} = 1, \quad \sigma_{22}|_{y=\pm L_y} = 0, \quad \sigma_{12}|_{x=\pm L_x} = 1, \quad \sigma_{12}|_{y=\pm L_y} = 1.$
  Just like in the previous test problem, we can find
  $s_{1112} = \frac{1}{2V}\int\limits_V \left(\sigma^1_{ij}\varepsilon^2_{ij} + \sigma^2_{ij}\varepsilon^1_{ij}\right)dV$, where $\sigma^1_{ij}, \varepsilon^1_{ij}, \sigma^2_{ij}, \varepsilon^2_{ij}$ are solutions of the problems Test 1 and Test 4 respectively.

4 Numerical Homogenization of Heterogeneous Anisotropic Mixture of Solid/Fluid/Porous Media

Wave processes in a heterogeneous mixture consisting of regions of elastic solid, liquid and porous media can be described by a single HTC system of differential

equations formulated in Sect. 2. In this case, the interfaces between regions of different media are described by jumps in the phase volume concentrations.

The essence of the method is as follows: we select a sample of a heterogeneous material with a given structure and solve a series of six stationary equilibrium problems for this sample with the boundary conditions listed in Sect. 3 and calculate the energy for each problem. Next, assuming heterogeneous sample equivalent to a homogeneous elastic one, we can calculate the corresponding effective compliance modulus of based on the known energy of the heterogeneous sample.

The main issue is how to solve the stationary equilibrium problem for a heterogeneous medium. For the HTC model from Sect. 2, direct solution of the equilibrium equations appears to be a difficult task. We propose to apply the time-marching method for solving the boundary value problem, and as a result of integration for a large value of time we will obtain an approximation to the stationary solution of the HTC equilibrium equations. To speed up the calculations, we introduce artificial velocity relaxation, which ensures zero velocity in a finite time. The resulting PDE's system reads as

$$\rho\frac{\partial u_i}{\partial t}+\frac{\partial p}{\partial x_i}-\frac{\partial \Sigma_{ik}}{\partial x_k}+\theta u_i=0, \tag{14a}$$

$$\frac{\partial w_i}{\partial t}+\left(\frac{1}{\rho_1}-\frac{1}{\rho_2}\right)\frac{\partial p}{\partial x_i}+\theta w_i=0, \tag{14b}$$

$$\frac{\partial p}{\partial t}+K\frac{\partial u_k}{\partial x_k}+\frac{\alpha_1\alpha_2}{\rho}(\rho_2-\rho_1)K\frac{\partial w_k}{\partial x_k}=0, \tag{14c}$$

$$\frac{\partial \Sigma_{ik}}{\partial t}-\mu\left(\left(\frac{\partial u_i}{\partial x_k}+\frac{\partial u_k}{\partial x_i}\right)-\frac{2}{3}\delta_{ik}\left(\frac{\partial u_1}{\partial x_1}+\frac{\partial u_2}{\partial x_2}+\frac{\partial u_3}{\partial x_3}\right)\right)=0, \tag{14d}$$

Obviously, as soon as the velocities u_i and w_i become equal to zero, we obtain a solution to the stationary equilibrium problem. In our calculations we take $\theta = 0.005$, which provides a reasonable rate of velocity relaxation. For the resulting steady-state solution, the energy of the inhomogeneous sample can be calculated and compared with the energy of the equivalent elastic sample. This allows one to find all the effective compliance moduli by solving the problems listed in Sect. 3.

5 Numerical Modeling of Effective Anisotropy of Porous Samples with Different Fracture Geometries

In this section, we present the results of applying a numerical homogenisation technique to study the effective anisotropic properties of fluid-saturated porous samples with various inclusion geometries. The simulations are based on the time-marching method for solving system (14) using the finite-difference method on a staggered grid, as described in [11]. The aim of our analysis is to determine the effect of fracture or inclusion geometry on the effective stiffness tensor and the resulting anisotropy of the medium.

5.1 Generation of Heterogeneous Samples with Controlled Geometry

In order to investigate the influence of fracture geometry on effective elastic properties, we generated a set of two-dimensional samples measuring 500×500 pixels, featuring various crack orientations and spatial distributions. The samples consist of two porous phases:

- **Skeleton**: a porous matrix with parameters $V_p = 3800$ m/s, $V_s = 2200$ m/s, $\rho = 2600$ kg/m^3, and porosity $\phi = 0.05$ (water-saturated);
- **Inclusions**: a softer material with parameters $V_p = 1500$ m/s, $V_s = 600$ m/s, $\rho = 1800$ kg/m^3, and porosity $\phi = 0.20$ (water-saturated).

The pore fluid is water with parameters of $V_p^f = 1500$ m/s, $V_s^f = 0$ m/s and density of $\rho_f = 1040$ kg/m^3.

These parameters were chosen to demonstrate a simplified geological model of a sequence of low-permeability sandstones and clays. The matrix corresponds to cemented sandstone with low porosity, while the inclusions represent softer, clay-rich layers with high porosity. Such combinations are typical of thin-bedded sedimentary formations, where the contrast between the constituent phases determines the effective anisotropic response.

The synthetic samples were generated using a stochastic algorithm. Each sample contains a specified number of inclusions, typically 60–100, with a chosen orientation (0°, 45°, 90°, or random) and a fixed thickness of three pixels. Several geometric characteristics were included in the generation procedure. Roughness controls tortuosity by introducing random deviations from a straight line and was set at 50%. Fracture probability determines the probability of crack segmentation along the inclusion length and was set at 40%. Displacement probability determines the probability of lateral displacements and was also set at 40%. Gap size, which controls the length of discontinuities, was set at 2 pixels. This approach allows for the creation of realistic models of layered and fractured media while maintaining control over the dominant fracture geometry.

Using this algorithm, four geometric configurations were considered, as shown in Fig. 1: vertical bands, diagonal bands at 45° to the horizontal axis, a network of intersecting fractures, and a random fracture system. These configurations represent typical fracturing patterns observed in natural geological formations.

After generation, the actual volume fraction of inclusions was calculated for each model and used in the homogenization procedure. The model with vertical stripes contains 48% inclusions and 52% skeleton, while the other three configurations contain 42% inclusions and 58% skeleton. Using these volume fractions together with the saturated phase densities, the average density of the vertical bands model is 2103 kg/m^3, while the average density of the other three samples is 2155 kg/m^3.

5.2 Calculation of Effective Stiffness Tensor

Using the time-marching method described in Sect. 4, we calculated the effective stiffness tensor for each sample with the geometry shown in Fig. 1. The results are

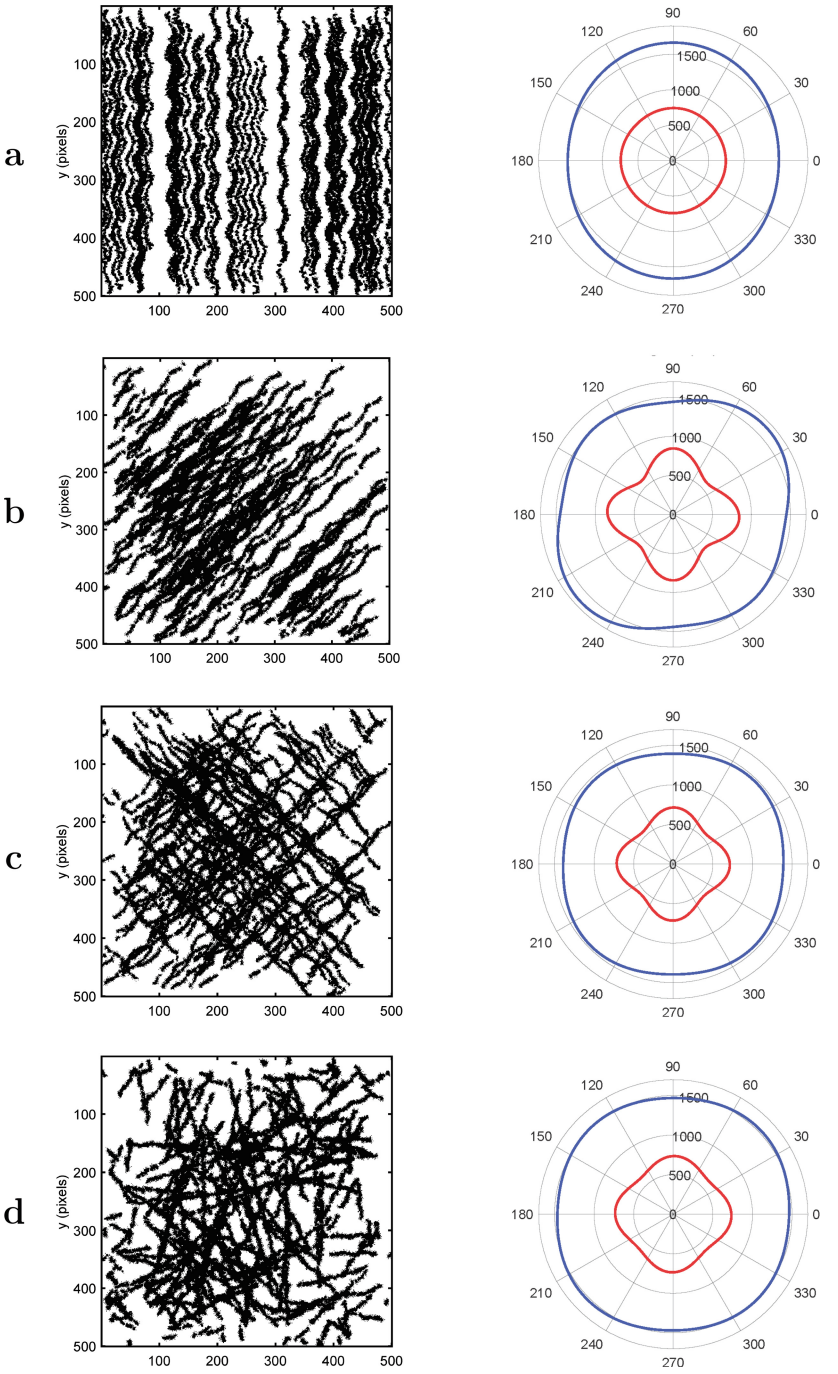

Fig. 1. Synthetic fracture geometries and the corresponding wave-velocity indicatrices: vertical bands (a), diagonal bands at 45° (b), crossed network (c), and random network (d). Blue curves denote V_p, and red curves denote V_s. (Color figure online)

summarized in Table 1, where the stiffness matrix components C_{ij} are given in GPa. In the two-dimensional case, the two-index stiffness matrix C_{ij} is related to the four-index stiffness tensor c_{ijmn} in Hooke's law (6) through the stress–strain relation

$$\begin{pmatrix}\sigma_{11}\\ \sigma_{22}\\ \sigma_{12}\end{pmatrix} = \begin{pmatrix}C_{11} & C_{12} & C_{13}\\ C_{12} & C_{22} & C_{23}\\ C_{13} & C_{23} & C_{33}\end{pmatrix}\begin{pmatrix}\varepsilon_{11}\\ \varepsilon_{22}\\ 2\varepsilon_{12}\end{pmatrix} = \begin{pmatrix}c_{1111} & c_{1122} & c_{1112}\\ c_{1122} & c_{2222} & c_{2212}\\ c_{1112} & c_{2212} & 1212\end{pmatrix}\begin{pmatrix}\varepsilon_{11}\\ \varepsilon_{22}\\ 2\varepsilon_{12}\end{pmatrix}. \tag{15}$$

Table 1. Comparison of effective stiffness tensor components for different fracture geometries (in GPa).

Component	Vertical	Single	Crossed	Random
C_{11}	4.775	4.488	4.156	4.607
C_{22}	5.958	4.467	4.183	4.637
C_{33}	1.181	1.547	1.097	1.159
C_{12}	3.042	2.972	2.822	2.999
C_{13}	0.023	0.274	0.034	0.057
C_{23}	0.014	0.173	0.013	0.010

6 Analysis of Anisotropy

The anisotropy of the effective medium can be characterised using several parameters derived from the stiffness tensor components. These include the ratios and differences between the in-plane moduli, the coupling coefficients and the directional wave speeds.

6.1 Velocity Indicatrices from the Christoffel Equation

The wave velocities in the fractured samples were obtained by solving the two-dimensional Christoffel equation. The effective wave velocities V^{eff} in an anisotropic medium are determined from

$$\det\left(\Gamma_{ik} - \rho(V^{\text{eff}})^2\delta_{ik}\right) = 0, \tag{16}$$

where $\Gamma_{ik} = c_{ijkl}n_j n_l$ and $\mathbf{n}$ is the propagation direction. This formulation enables the velocities of compressional and shear waves to be computed in each direction and represented as two-dimensional indicatrices. These provide a convenient visualisation of the angular dependence of the wave field. Figure 1 shows the indicatrices for the samples considered. The density ρ in Eq. (16) is the average mixture density of the sample and is calculated as

$$\rho_{avg} = f_{sk}\rho_{sat}^{sk} + f_{inc}\rho_{sat}^{inc}, \tag{17}$$

where f_{sk} and f_{inc} are the volume fractions of skeleton and inclusions, respectively. The saturated phase densities are given by

$$\rho_{sat} = (1 - \phi)\rho_{matrix} + \phi\rho_{fluid}, \tag{18}$$

where ρ_{matrix} is the density of the solid matrix or inclusions, ρ_{fluid} is the pore-fluid density, and ϕ is the porosity. For the considered geometries, the vertical bands model contains 48% inclusions and 52% skeleton, whereas the other three models contain 42% inclusions and 58% skeleton. Using these volume fractions, the average density is found to be $2103\,\mathrm{kg/m^3}$ for the vertical bands model and $2155\,\mathrm{kg/m^3}$ for the remaining configurations.

6.2 Stiffness Anisotropy Parameters

Table 2 summarizes the main anisotropy indicators for the four fracture geometries considered. These quantities are derived from the effective stiffness tensor in Table 1 and provide a compact description of the directionality of the elastic response.

Table 2. Anisotropy parameters for different fracture geometries.

Parameter	Vertical bands	Diagonal (45°)	Crossed network	Random network
C_{11}/C_{22} ratio	0.802	1.005	0.994	0.994
$C_{33}/((C_{11} + C_{22})/2)$	0.219	0.345	0.263	0.252
C_{13} (GPa)	0.023	0.274	0.034	0.057
C_{23} (GPa)	0.014	0.173	0.013	0.010

The C_{11}/C_{22} ratio reflects the degree of in-plane anisotropy. The vertical band configuration exhibits the strongest directional contrast, while the diagonal, cross, and random geometries are much closer to in-plane isotropy. The normalized shear stiffness follows a different trend: it is lowest for vertical bands and highest for diagonal geometries, indicating that oblique cracks redistribute stiffness more strongly toward the shear response.

The off-diagonal coefficients C_{13} and C_{23} quantitatively describe the coupling between normal and shear strains. These terms are small for vertical stripes but increase significantly for a 45° diagonal, confirming strong mode coupling in obliquely cracked media. In cross-fractured and random networks, the coupling remains relatively weak, suggesting that symmetry and statistical averaging reduce the interaction between strain modes.

The effective densities of the samples differ only slightly, so the observed patterns of wave velocity changes are determined primarily by stiffness anisotropy rather than density changes. This means that the angular dependence of velocity indicators primarily reflects the geometry and orientation of the fracture system.

Interpretation of Results. Numerical homogenization shows that the effective elastic response is strongly dependent on the fracture geometry. Vertical bands and bands inclined at 45° are the most anisotropic configurations, while the cross-section and random geometries exhibit a more balanced in-plane response.

The vertical band geometry provides the clearest directionality dependence of the P-wave field. The stiffness tensor exhibits a strong contrast between the principal moduli in the plane, consistent with the vertical orientation of the failure bands. The low normalized shear stiffness and weak coupling coefficients further indicate that the directional contrast in normal stiffness predominates in this configuration.

The single diagonal geometry doesn't simply reduce anisotropy; instead, it rotates and redistributes it. The P-wave indicatrix retains a shape similar to that of vertical stripes, but is rotated by approximately 45°, indicating that the principal axes of anisotropy follow the crack orientation. At the same time, the S-wave indicatrix becomes more dependent on azimuth, reflecting a stronger coupling between normal and shear strain. Thus, diagonal geometry leads to a rotation of P-wave anisotropy and a more pronounced S-wave anisotropy.

The crossing and randomly distributed network structures maintain near-planar isotropy. Stiffness contrasts in them are weak, coupling coefficients are small, and wave velocity indicatrices are more symmetrical than in vertical or diagonally band structures. These results indicate that the crossed and randomly distributed fracture systems redistribute deformation more uniformly and, therefore, suppress strong directional effects.

The differences in density between the samples are small, so the wave velocity behavior is determined primarily by the effective stiffness tensor. In this sense, crack orientation is the dominant factor determining anisotropy, but the P- and S-wave fields respond differently: V_p is more sensitive to the layered structure, while V_s is more sensitive to inclined cracks and mode coupling.

7 Conclusion

This paper presents a numerical approach to estimating the effective elastic properties of heterogeneous porous media saturated with fluid. The method is based on comparing the strain energy of a heterogeneous sample with the strain energy of an equivalent homogeneous elastic medium. Using a thermodynamically consistent hyperbolic model of a two-phase porous medium and additional relaxation terms in the momentum equations, we obtain the effective compliance tensor. The steady-state solutions are computed using a time-marching procedure, providing a stable and convergent numerical algorithm.

The numerical experiments show that the effective elastic response is strongly dependent on crack geometry. The vertical bands and the 45° inclined bands are the most anisotropic configurations, while crossed and random network exhibit a much more balanced in-plane response. The vertical bands exhibit the greatest stiffness contrast between the principal directions, consistent with the vertical orientation of the cracks. Diagonal geometry does not simply reduce anisotropy;

instead, it redistributes it by rotating the principal axes of the P-wave indicatrix and creating more pronounced S-wave anisotropy due to a stronger coupling between normal and shear deformation modes. In contrast, the crossed and random fracture networks remain close to in-plane isotropy, indicating a more uniform strain redistribution.

The density of the samples changes only slightly, so the differences in the wave velocity patterns are mainly influenced by the effective stiffness tensor. Therefore, crack orientation is the primary factor governing anisotropy. However, the sensitivities of P-wave and S-wave propagation differ: P-waves are more affected by layered structures, while S-waves are more sensitive to inclined cracks and the resulting mode interactions.

The proposed approach provides an effective framework for estimating the effective elastic properties of complex heterogeneous materials, explicitly accounting for pore space geometry and the saturating fluid. It is applicable to sedimentary rocks, fractured reservoirs, and composite materials with specified anisotropic properties, and is also relevant for geophysical applications such as seismic interpretation and acoustic logging. Future work will focus on frequency-dependent behaviour, viscoelastic effects, and 3D models with more complex inclusion topologies.

Future work will focus on extending the model to include frequency-dependent behavior and viscoelastic effects, as well as on developing three-dimensional simulations for media with more complex inclusion topology and fracture connectivity.

Acknowledgments. This work was financially supported by the Russian Science Foundation (Project No. 26-11-00165).

Disclosure of Interests. The authors declare that they have no known competing financial interests or personal relationships that could have appeared to influence the work reported in this article.

References

1. Allaire, G., Brizzi, R.: A multiscale finite element method for numerical homogenization. Multiscale Model. Simul. **4**(3), 790–812 (2005)
2. Chen, Z., Xie, Y.M., Wang, Z., Li, Q., Wu, X., Zhou, S.: A comparison of fast fourier transform-based homogenization method to asymptotic homogenization method. Compos. Struct. **238**, 111979 (2020)
3. Gad, A.I., Gao, X.L.: A generalized strain energy-based homogenization method for 2-D and 3-D cellular materials with and without periodicity constraints. Symmetry **13**(10) (2021)
4. Khoei, A.R., Saeedmonir, S., Misaghi Bonabi, A.: Computational homogenization of fully coupled hydro-mechanical analysis of micro-fractured porous media. Comput. Geotech. **154**, 105121 (2023)
5. Otero, F., Oller, S., Martinez, X.: Multiscale computational homogenization: review and proposal of a new enhanced-first-order method. Arch. Comput. Methods Eng. **25**, 479–505 (2018)

6. Otero, F., Oller, S., Martinez, X., Salomon, O.: Numerical homogenization for composite materials analysis. comparison with other micro mechanical formulations. Compos. Struct. **122**, 405–416 (2015)
7. Ponte Castañeda, P.: Variational linear comparison homogenization estimates for the flow of yield stress fluids through porous media. J. Nonnewton. Fluid Mech. **321**, 105104 (2023)
8. Reshetova, G., Romenski, E.: Diffuse interface approach to modeling wavefields in a saturated porous medium. Appl. Math. Comput. **398**, 125978 (2021)
9. Reshetova, G., Romenski, E.: Modeling of temperature-dependent wave fields in deformable porous media saturated with fluid. Numer. Anal. Appl. **17**(4), 358–371 (2024)
10. Reshetova, G., Romenski, E.: Modeling the variability of seismic properties of frozen multiphase media depending on temperature. Sib. Electron. Math. Rep. **21**, B203–B231 (2024)
11. Reshetova, G., Romenski, E.: Numerical implementation of boundary conditions for finite difference method on staggered grid for wave propagation in saturated porous medium. In: Gervasi, O., et al. (eds.) Computational Science and Its Applications - ICCSA 2025 Workshops, pp. 359–375. Springer, Cham (2026)
12. Romenski, E., Reshetova, G., Peshkov, I.: Thermodynamically compatible hyperbolic model of a compressible multiphase flow in a deformable porous medium and its application to wavefields modeling. AIP Conf. Proc. **2448**(1), 020019 (2021)
13. Romenski, E., Reshetova, G., Peshkov, I., Dumbser, M.: Modeling wavefields in saturated elastic porous media based on thermodynamically compatible system theory for two-phase solid-fluid mixtures. Comput. Fluids **206**, 104587 (2020)
14. Saxena, N., Mavko, G.: Estimating elastic moduli of rocks from thin sections: digital rock study of 3D properties from 2D images. Comput. Geosci. **88**, 9–21 (2016)
15. Schneider, M.: A review of nonlinear FFT-based computational homogenization methods. Acta Mech. **232**, 2051–2100 (2021)
16. Tartar, L.: The General Theory of Homogenization: A Personalized Introduction. Lecture Notes of the Unione Matematica Italiana, vol. 7. Springer, Heidelberg (2009)
17. Wei, X., Li, Z., Zhao, G.: A review of multiscale numerical modeling of rock mechanics and rock engineering. Deep Undergr. Sci. Eng. **4**(3), 382–405 (2025)
18. Yesiloglu-Gultekin, N., Dogan, A.: Estimation of the elastic modulus of basaltic rocks using machine learning methods. Earth Sci. Inf. **17**, 5941–5966 (2024)
19. Zhang, W., Dai, G., Wang, F., Sun, S., Bassir, H.: Using strain energy-based prediction of effective elastic properties in topology optimization of material microstructures. Acta. Mech. Sin. **23**, 77–89 (2007)
20. Zochowski, A.: A variational interpretation of homogenization and its extensions. Comput. Struct. **23**(5), 665–669 (1986)

Influence of Wettability on Electrical Parameters Based on Numerical Simulation Results of Drainage and Imbibition in Digital Rock

Tatyana Khachkova[1(✉)] and Vadim Lisitsa[2]

[1] Institute of Petroleum Geology and Geophysics SB RAS, Koptug ave. 3, Novosibirsk 630090, Russia
KhachkovaTS@ipgg.sbras.ru

[2] Institute of Mathematics SB RAS, Koptug ave. 4, Novosibirsk 630090, Russia

Abstract. The present study investigates the influence of wettability on the hysteresis of electrical parameters through numerical simulation of drainage and imbibition processes. Using a three-dimensional digital sandstone sample and numerical algorithms for simulating two-phase filtration and electric current flow, a series of numerical experiments are conducted over a full range of contact angles. The dependence of the resistivity index on the water saturation is then established for each value of angle, and the parameters of Archie's law – namely, the saturation exponent and the saturation distribution factor – are estimated. The principle objective is to derive functional relationships between these parameters and the contact angle. The resulting dependencies are constructed as piecewise linear functions, exhibiting different trends for drainage and imbibition. Validation at intermediate contact angles revealed that the relative errors of the estimates remain below 3%.

Keywords: Wettability · Electrical parameters · Resistivity index · Saturation exponent · Water saturation · Digital models · Numerical simulation · Drainage · Imbibition · CT-images

1 Introduction

Numerical simulation of physical processes has become an indispensable tool across various scientific disciplines, including exploration geophysics. It enables the computation of physical fields necessary for estimating petrophysical properties of porous media. Traditionally, such estimates have relied on laboratory core analysis; however, this approach is labor-intensive, time-consuming, and often results in irreversible damage or complete failure of rock samples.

Recent advances in X-ray microtomography have enabled the construction of three-dimensional digital rock models that accurately replicate the microstructure of natural samples. These digital twins serve as a realistic basis for numerical

© The Author(s), under exclusive license to Springer Nature Switzerland AG 2027
O. Gervasi et al. (Eds.): ICCSA 2026 Workshops, LNCS 16761, pp. 98–110, 2027.
https://doi.org/10.1007/978-3-032-30527-5_7

simulations. To date, a wide range of algorithms have been developed for estimating key petrophysical parameters, including porosity, absolute permeability [2,6,12,16], relative permeability [1,3,10], elastic moduli [2,7,18,20], electrical resistivity [2,8,22], pore space geometry and topology [5], and etc. These tools enable researchers to investigate the inter-parameter relationships, the influence of various factors on petrophysical estimates, and to predict of reservoir behavior under changing conditions.

The present study employs digital rock physics to investigate the effect of wettability on the electrical parameters during two-phase flow. In hydrocarbon exploration, reserves are typically estimated from electrical logging data interpreted using Archie's empirical laws. Consequently, accurate determination of Archie's parameters – namely, the saturation exponent and the saturation distribution factor – is of critical importance for reservoir development planning. The saturation exponent is known to depend on several factors: microstructure (heterogeneity, pore connectivity, pore size distribution), wettability, the presence of cement, and pore water salinity. In laboratory experiments, isolating the individual effects of microstructure and wettability is extremely challenging. Moreover, systematically studying the influence of the entire spectrum of contact angles – beyond the conventional classification of rocks as hydrophilic, hydrophobic, neutrally wet, or mixed-wet – is practically infeasible. However, such a detailed investigation is essential, as wettability governs fluid distribution and flow patterns, particularly under conditions of enhanced oil recovery by imbibition.

It should also be noted that prolonged field development leads to reservoir hydrophobization. Consequently, accounting for wettability alterations – particularly their spatial heterogeneity – is essential for reservoir monitoring and the timely adjustment of production strategies. This, in turn, necessitates the development of novel numerical methodologies that enable rapid and reliable determination of the saturation exponent and saturation distribution factor as functions of varying wettability.

The present paper proposes a new approach for refining these parameters, based on numerical modeling of steady-state two-phase flow and subsequent simulation of electrical current flow. A series of numerical experiments is conducted to construct the dependence of the resistivity index on water saturation for a range of contact angles. This enables a systematic investigation of the effect of wettability on the hysteresis observed during displacement of the wetting phase (drainage) and the non-wetting phase (imbibition). The primary objective of this study is to derive new functional relationships that enhance the reliability of saturation exponent estimates. The obtained dependencies will contribute to more accurate assessments of recoverable hydrocarbon reserves, improve the construction of hydrodynamic reservoir models, and support the selection of optimal reservoir stimulation techniques for enhanced hydrocarbon recovery.

2 Methodology

The methodology for establishing the dependence of electrical parameters on rock wettability is based on numerical simulations of primary drainage and imbibition processes within a digital rock sample. The results of these simulations are utilized to generate models of partially saturated rock and to calculate the corresponding electrical parameters, namely the resistivity index and the saturation exponent. This section provides a brief description of the basic algorithms employed in this workflow.

2.1 Algorithm for Numerical Simulation of Two-Phase Flows

To simulate primary drainage and subsequent imbibition, a three-dimensional numerical algorithm for pore-scale simulation of two-phase flows is employed [9,10]. The algorithm is based on the phase field method, in which concentration functions are used to identify the phases, and a thin transition region (smoothed over several grid cells) defines the boundary between them.

To simulate the fluid flow in the pore space, the Stokes equation is considered, with the nonlinear term neglected due to the low flow velocity:

$$\begin{aligned} &\frac{\partial \rho(\psi)\boldsymbol{u}}{\partial t} = -\nabla p + 2\nabla \cdot (\nu\epsilon(\boldsymbol{u})) + \boldsymbol{G}(\psi), \\ &\nabla \cdot (\boldsymbol{u}) = 0. \end{aligned} \tag{1}$$

In these equations, $\psi \in [0,1]$ is the phase-determining concentration function, $\rho(\psi)$ is the fluid density, $\nu(\psi)$ is the fluid viscosity, $\boldsymbol{u}$ is the vector of velocity, p is the pressure, $2\epsilon(u) = \nabla \boldsymbol{u} + \nabla \boldsymbol{u}^T$ is doubled strain tensor, $\boldsymbol{G}(\psi)$ are external forces. It was assumed that gravitational forces could be neglected; so that external forces were caused only by surface tension at the phase boundary.

To simulate the phase field, the Cahn-Hilliard equation is considered:

$$\begin{aligned} &\frac{\partial \psi}{\partial t} + \boldsymbol{u} \cdot \nabla \psi = \nabla \cdot (M(\psi)\nabla \mu), \\ &\mu = F'(\psi) - \varepsilon^2 \Delta \psi, \end{aligned} \tag{2}$$

where μ denotes the variable for determining the chemical potential, M is the mobility, ε is the width of the diffuse boundary between phases. For the potential $F(\psi)$ it is employed the expression $F'(\psi) = 2\psi(\psi-1)(2\psi-1)$, and for the external forces related to the interfacial surface tension: $\boldsymbol{G}(\psi) = -\frac{6\sqrt{2}}{\varepsilon}\psi\nabla\mu$.

Since the present study is aimed at investigating the influence of wettability on electrical parameters, the algorithm for simulating two-phase flows was modified by incorporating a new boundary condition at the liquid-solid interface (rock matrix). This condition accounts for the phase contact angle, thereby enabling a more accurate representation of phase dynamics at low wetting angles [19,21]:

$$\nabla \psi \cdot \boldsymbol{n} = -\frac{\sqrt{2}\pi \cos((\psi-0.5)\pi)}{12\varepsilon} \cos(\theta), \tag{3}$$

where θ is the contact angle for the first phase.

The finite-difference approximation was described in detail in earlier works [9,10]. It was also noted that the proposed finite-difference scheme provides first-order approximation in both time and space, employing a simplest upwind scheme for the spatial approximation of the phase transfer. For the purposes of the present study, the order of spatial approximation was improved by implementing a more accurate third-order WENO scheme [14,17].

The implementation of the described algorithm was designed for use on graphics processing units (GPUs) and was carried out in CUDA. Recently, the algorithm has been further improved with respect to solving the Poisson equation; this enhancement is described in more detail in the following subsection.

2.2 Algorithm for Numerical Simulation of Electric Current and Evaluation of Electrical Resistivity

The fundamentals of the algorithm for the numerical evaluation of electrical resistivity in digital rock samples were presented in [8]. This algorithm was developed specifically for application to strongly heterogeneous models, such as digital rock samples. To numerically estimate the resistivity of core samples, the electric potential distribution is first calculated under an applied voltage difference imposed on opposite faces of the sample. Then, the conductivity is estimated as the ratio of the resulting electric current to the applied voltage difference. The most computationally demanding and complex component of this algorithm is the calculation of the electric potential, which requires solving the Poisson equation in a domain characterized by a highly heterogeneous medium. Such a medium is defined as one in which the characteristic size of heterogeneities spans only a few grid cells, namely, where the correlation length of the model ranges from five to ten grid points [4]. Moreover, the amplitude of these inhomogeneities may vary by several orders of magnitude.

The approach proposed in [8] is based on a Krylov-type iterative solver, which employs the inverse of the discrete Laplace operator for a homogeneous medium as a preconditioner. To invert the Laplace operator, spectral decomposition along the directions normal to the current flow is applied, followed by the Thomas algorithm to solve a series of one-dimensional problems. A development of this approach with respect to the numerical solution of the Poisson equation was presented in [13]. In new improved version, the Conjugate Gradient method was employed in place of BiCGStab, spectral decomposition of the discretized operator was used instead of its continuous one, and cuBLAS functionality was also utilized. As a result, the proposed approach significantly increases the size of digital samples that can be processed on a single GPU while simultaneously reducing computation time.

The next improvement to this algorithm concerns the construction of a preconditioner for the numerical solution of the Poisson equation [15]. Employing the inverted Laplace operator for a layered medium (instead of homogeneous one) as a preconditioner reduces the number of iterations required by the Conjugate Gradient method by 10–40%. Moreover, the efficiency of this approach improves with increasing contrast in the coefficients of the digital model. Given

that in models partially saturated with water and oil, the electrical conductivities of water, oil and the rock matrix differ by several orders of magnitude, the convergence rate was substantially enhanced through the use of this method.

It should also be noted that this approach was adopted to improve the algorithm for simulation of two-phase flows, as it likewise requires the efficient solution of Poisson equations.

2.3 Numerical Simulation of Primary Drainage and Imbibition

Primary drainage is a process in which a non-wetting phase displaces a wetting one. Conversely, during imbibition, the wetting phase displaces the non-wetting one. In an oil-water system considered for numerical simulation, water represents the wetting phase, while oil represents the non-wetting one.

Thus, during drainage, oil displaces water. The numerical simulation of primary drainage begins with a model fully saturated with water, and only oil is injected into the digital sample. This simulation replicates processes occurring in nature, when a water-saturated reservoir gradually becomes charged with oil migrating from a source rock. As a result of drainage, oil displaces the mobile water, leaving the irreducible water saturation S_{irr}.

Starting from this state, imbibition is then simulated, during which water begins to displace oil. In this part of study, a laboratory experiment on steady-state two-phase filtration is numerically reproduced, with water being gradually introduced into the mixture. Under this approach, imbibition is represented not as a single numerical (or laboratory) experiment, but as a series of experiments. At each stage, the proportion of water in the injected mixture is increased; for instance, in a series of ten experiments, the water fractions are 0.1, 0.2, ... 1. At the final stage, only water is injected into the sample. As a result of imbibition, water displaces all mobile oil, reaching the residual oil saturation S_{res}.

All experiments are conducted until steady-state flow is achieved. For the numerical simulations performed using the two-phase flow algorithm, steady-state conditions are assumed to be reached after five pore volumes of fluid have been pumped through the sample.

2.4 Numerical Evaluation of the Resistivity Index and the Saturation Exponent

During the numerical experiments, phase distributions across the sample volume are recorded. For the drainage process, 15 snapshots are taken, including the final state, as the evolution of the process itself is of interest. For the imbibition, only the final state following each injection mode is recorded, resulting in 10 snapshots in this case.

From the obtained phase distributions, the current water saturations S_w, as well as the irreducible water saturation S_{irr} and the residual oil saturation S_{res}, are determined. These distributions are subsequently used to construct partially saturated water-oil models for the purpose of calculating electrical parameters.

Using the algorithm for numerical simulation of electric current, the electrical resistivity is then computed for all partially saturated models. In addition, the same calculation is performed for a fully water-saturated model, i.e., a model in which all pores are numerically filled with water. Based on these results, the resistivity index is estimated according to the following formula:

$$RI = \frac{\rho_t}{\rho_0}, \tag{4}$$

where ρ_t is the electrical resistivity at a given water saturation S_w, and ρ_0 is the resistivity of the fully water-saturated rock.

Thus, two sets of values, $S_w - RI(S_w)$, are obtained: one for drainage and one for imbibition. To estimate the saturation exponent, the classical form of Archie's law for the resistivity index is employed:

$$RI(S_w) = S_w^{-n}, \tag{5}$$

where n is the saturation exponent, along with the generalized form of Archie's law:

$$RI(S_w) = \alpha S_w^{-n}, \tag{6}$$

where α is the saturation distribution factor. The methodology for estimating the saturation exponent has been described in detail in [11]. It is based on constructing a linear regression on a logarithmic scale using the obtained datasets and solving two optimization problems corresponding to the classical and generalized formulations of Archie's law.

Given that the objective of this study is to investigate the influence of wettability on electrical parameters, the described methodology is applied to estimate the parameters of Archie's law for both drainage and imbibition across different wetting angles.

3 Numerical Experiments

For all numerical experiments conducted in this study, a digital model of Bentheimer sandstone was employed. The model dimensions are $200 \times 750 \times 750$ voxels, with a microtomographic images resolution of 2 μm per voxel. As previously noted, water (wetting phase) and oil (non-wetting one) were considered as the two phases in the flow simulation. The following physical parameters were assigned to water and oil, respectively: densities of 1000 kg/m^3 and 880 kg/m^3, dynamic viscosities of $3.8 \cdot 10^{-4}$ $Pa \cdot s$ and $4.027 \cdot 10^{-3}$ $Pa \cdot s$, and an interfacial tension of $2.571 \cdot 10^{-2}$ N/m. The contact angles for the water phase were selected from the set $[20, 30, 40, 50, 60, 70, 80, 90]$ degrees. For each contact angle, a separate series of simulations was performed. Two-phase flow was simulated in the X direction, with a constant flow rate of $1.225 \cdot 10^{-8}$ m^3/s specified at the inlet face.

Subsequently, for all obtained partially saturated models, the electrical resistivity was computed using formula 4. In the numerical algorithm for simulating

electric current, the following electrical conductivity values were assigned to water, oil and the rock matrix, respectively: 1 S, $1 \cdot 10^{-3}$ S and $1 \cdot 10^{-5}$ S.

As a result of the numerical experiments, sets of $S_w - RI(S_w)$ values for both drainage and imbibition were obtained for each contact angle within the set $[20, 30, 40, 50, 60, 70, 80, 90]$.

The following section presents the processing and analysis of the results from these numerical experiments.

3.1 Construction of Dependencies: Resistivity Index Versus Water Saturation and Saturation Exponent Versus Contact Angle

First, the dependencies of the resistivity index on water saturation were established for all specified contact angles. That is, linear regressions were constructed on a logarithmic scale by solving two optimization problems corresponding to the classical (Eq. 5) and generalized forms of Archie's law (Eq. 6).

The results for contact angles of 20 and 60 are presented in the Figs. 1 and 2, respectively. The blue lines correspond to the drainage simulation results, while the violet lines represent the imbibition results. Solid lines denote the generalized Archie's law, whereas dashed lines indicate the classical formulation of Archie's law.

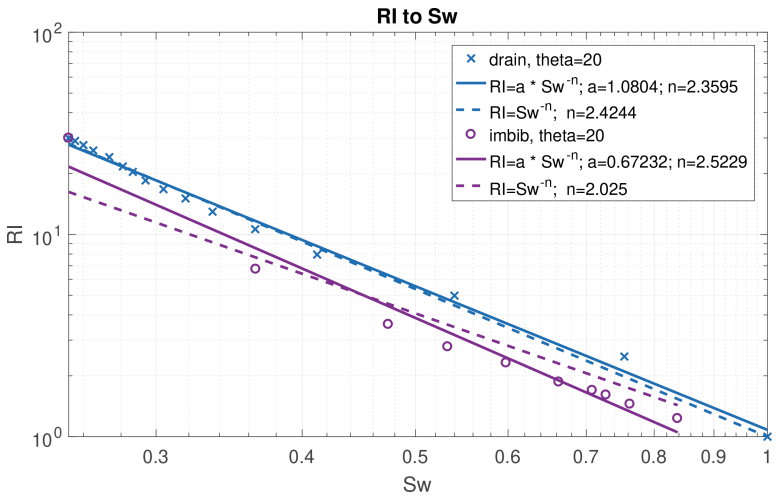

Fig. 1. Dependence of the resistivity index on water saturation for Bentheimer sandstone during drainage and imbibition simulation at a water contact angle of $\theta = 20°$ (logarithmic scales).

Thus, for each contact angle, the following parameters were estimated: the saturation exponent n_{cl} corresponding to the classical form of Archie's law (Eq. 5), as well as the saturation exponent n and the saturation distribution

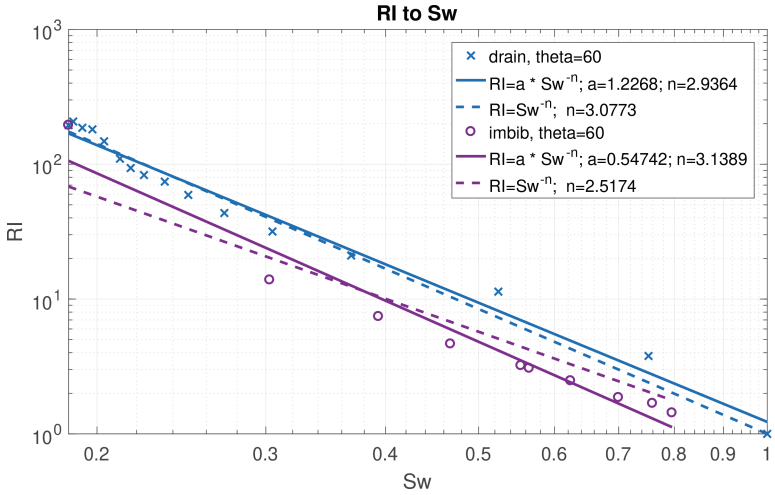

Fig. 2. Dependence of the resistivity index on water saturation for Bentheimer sandstone during drainage and imbibition simulation at a water contact angle of $\theta = 60°$ (logarithmic scales).

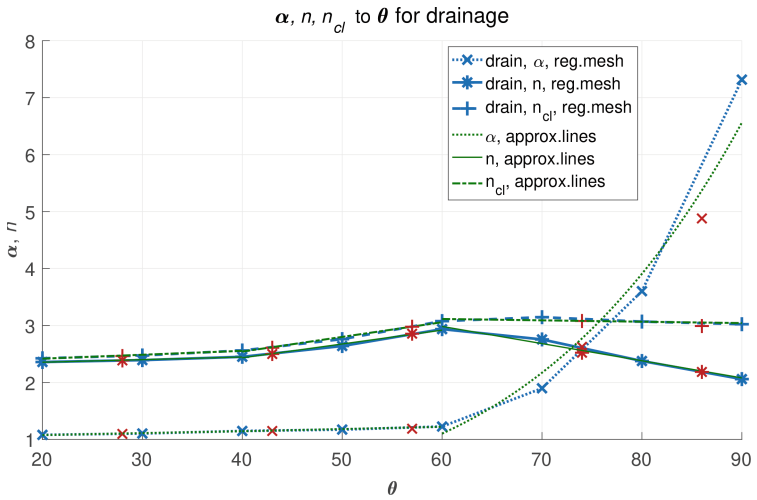

Fig. 3. Dependence of Archie's parameters on contact angle for Bentheimer sandstone based on drainage simulation results.

factor α corresponding to the generalized form (Eq. 6). The obtained values are presented in Figs. 3 and 4, with blue and violet markers, respectively.

In Figs. 3 and 4, it can be observed that the dependencies of Archie's parameters on the contact angle are piecewise linear, with the solo exception being the parameter α for drainage within the range of 60 to 90°. Therefore, this particular dependence was approximated by constructing a linear regression on a

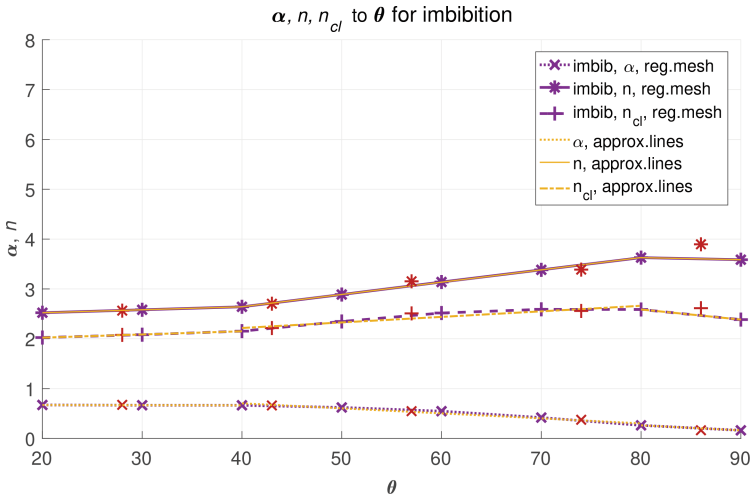

Fig. 4. Dependence of Archie's parameters on contact angle for Bentheimer sandstone based on imbibition simulation results.

logarithmic scale, whereas all other dependencies were approximated using linear functions. The resulting approximation lines are shown in green (for drainage) in Fig. 3, and in yellow (for imbibition) in Fig. 4. The corresponding approximation formulas are presented in Table 1.

To validate the obtained dependencies, a series of additional numerical experiments was conducted, following the same methodology as before but employing contact angles between the previously selected grid points, specifically, $\theta = 28$, 43, 57, 74 and 86°. As in the primary simulations, the electrical parameters were calculated and the values of Archie's parameters were estimated then. These results are shown in Figs. 3 and 4 using red markers. Subsequently, the relative errors in the estimation of these parameters using the derived approximation formulas were computed. The obtained values for all specified angles and parameters are presented in Table 1. The angle values used for validation are indicated in red.

Analysis of the 30 relative error values reveals that the majority are below 3%: 14 values are less than 1%, and 10 values lie between 2% and 3%. Only 5 values fall within the 5–10% range. Notably, these elevated errors correspond to all parameters at $\theta = 86$ (in the case of imbibition), and solely to the parameter α at $\theta = 74$ and $\theta = 86$ (for drainage).

In the imbibition case, the red markers corresponding to $\theta = 86$ in Fig. 4 extend the straight lines fitted for the 40–80 range. This observation suggests that the linear dependencies may be applicable up to 90°, despite possible changes in fluid behavior near $\theta = 90$. A correction was implemented, and the revised formulas for the angle of $\theta = 86$ produced relative errors of 2–3% (see the lower rows of Table 1).

Table 1. Dependence of Archie's parameters on contact angle for Bentheimer sandstone: approximation formulas and validation relative errors.

θ	α	Rel.err.	n	Rel.err.	n_{cl}	Rel.err.
Drainage						
20–40	$0.0034 \cdot \theta + 1$		$0.0046 \cdot \theta + 2.26$		$0.0069 \cdot \theta + 2.28$	
28		0.0066		0.002		0.0038
40–60	$0.0039 \cdot \theta + 0.99$		$0.024 \cdot \theta + 1.46$		$0.026 \cdot \theta + 1.51$	
43		0.0061		0.0024		0.0041
57		0.0185		0.0036		0.00058
60–90	$e^{4.4 \cdot ln(\theta) - 17.91}$		$-0.03 \cdot \theta + 4.79$		$-0.0024 \cdot \theta + 3.26$	
74		0.0563		0.0158		0.00067
86		0.101		0.0074		0.0206
Correction						
60–70	$0.0671 \cdot \theta - 2.8$					
70–89	$0.186 \cdot \theta - 11.143$					
74		0.0069				
80		0.04				
Imbibition						
20–40	$0.0003 \cdot \theta + 0.68$		$0.0059 \cdot \theta + 2.4$		$0.0064 \cdot \theta + 1.895$	
28		0.0086		0.0022		0.0022
40–80	$-0.01 \cdot \theta + 1.108$		$0.025 \cdot \theta + 1.655$		$0.011 \cdot \theta + 1.77$	
43		0.0189		0.0047		0.0157
57		0.0249		0.0289		0.0412
74		0.0336		0.0277		0.0144
80–90	$-0.01 \cdot \theta + 1.07$		$-0.0042 \cdot \theta + 3.96$		$-0.02 \cdot \theta + 4.2$	
86		0.053		0.0750		0.0565
Correction						
80–89	$-0.01 \cdot \theta + 1.108$		$0.025 \cdot \theta + 1.655$		$0.011 \cdot \theta + 1.77$	
86		0.034		0.0233		0.0326

For drainage, a logarithmic scale was initially employed for the approximation. However, a linear approximation may also be considered, as the point for α at $\theta = 86$ (marked in red in Fig. 3) approximately extends the line trend for 70–80 range. A correction was introduced by constructing piecewise linear functions for the intervals of 60–70 and 70–86°. The values at $\theta = 74$ and $\theta = 80$ were used as validation points (the correction is highlighted in green in Table 1). Such approximation resulted in relative errors of 0.6% and 4%, respectively.

The resulting piecewise linear approximations are summarized in Table 2.

Table 2. Summary of approximations for Archie's parameters as functions of contact angle for Bentheimer sandstone.

θ	α	n	n_{cl}
Drainage			
20–40	$0.0034 \cdot \theta + 1$	$0.0046 \cdot \theta + 2.26$	$0.0069 \cdot \theta + 2.28$
40–60	$0.0039 \cdot \theta + 0.99$	$0.024 \cdot \theta + 1.46$	$0.026 \cdot \theta + 1.51$
60–70	$0.0671 \cdot \theta - 2.8$	$-0.03 \cdot \theta + 4.79$	$-0.0024 \cdot \theta + 3.26$
70–89	$0.186 \cdot \theta - 11.143$		
Imbibition			
20–40	$0.0003 \cdot \theta + 0.68$	$0.0059 \cdot \theta + 2.4$	$0.0064 \cdot \theta + 1.895$
40–89	$-0.01 \cdot \theta + 1.108$	$0.025 \cdot \theta + 1.655$	$0.011 \cdot \theta + 1.77$

4 Conclusions

The present study investigates the influence of wettability on the hysteresis of electrical parameters, specifically the resistivity index and the saturation exponent. Accurate estimation of these parameters is crucial, as they are employed both in the assessment of hydrocarbon reserves at the field and in reservoir development planning.

A digital model of Bentheimer sandstone (a high-permeability rock sample) is utilized in conjunction with two numerical algorithms: one for simulating two-phase flow and another for modeling electric current flow and estimating the corresponding electrical parameters. Initially, drainage and imbibition processes are numerically simulated, with the contact angle varying between 20 and 90°. The obtained numerical results are subsequently employed to construct digital models of partially water- and oil-saturated samples, for which electric current flow is simulated and electrical parameters are evaluated.

For each obtained model, the current water saturations, as well as the irreducible water saturations and the residual oil saturations are calculated, together with the corresponding values of the resistivity index. Based on these data, the dependencies of the resistivity index on the water saturation are established across the entire range of contact angles. Consequently, for each contact angle, the saturation exponent corresponding to the classical formulation of Archie's law is derived, as well as the saturation exponent and the saturation distribution factor for its generalized form.

The principal objective of this work is to establish the dependence of Archie's law parameters on the contact angle. These dependencies are constructed as piecewise linear functions for specific intervals of angles, with different trends observed for drainage and imbibition process.

To validate the derived dependencies, numerical experiments are conducted for intermediate contact angle values, with the calculation of the Archie's parameters and the associated relative errors. Based on an analysis of the obtained

errors, several formulas are corrected, thereby reducing the errors to an acceptable level of 3%.

In summary, this study demonstrates that Archie's law parameters – namely, the saturation exponent and the saturation distribution factor – are significantly dependent on the wettability of the rock. Moreover, hysteresis is observed in both parameters, as well as in the resistivity index, during drainage and imbibition process. The established functional dependencies enable the rapid and reliable determination of the key electrical parameters based on varying wettability, which is essential for reservoir monitoring and for timely adjustment of technological solutions.

Acknowledgments. T. Khachkova performed numerical simulations under the support of Russian Science Foundation grant no. 25-21-00352.

Disclosure of Interests. The authors have no competing interests to declare that are relevant to the content of this article.

References

1. Alpak, F.O., Riviere, B., Frank, F.: A phase-field method for the direct simulation of two-phase flows in pore-scale media using a non-equilibrium wetting boundary condition. Comput. Geosci. **20**(5), 881–908 (2016)
2. Andra, H., et al.: Digital rock physics benchmarks - Part II: computing effective properties. Comput. Geosci. **50**, 33–43 (2013)
3. Apourvari, S.N., Arns, C.H.: Image-based relative permeability upscaling from the pore scale. Adv. Water Resour. (2015)
4. Bazaikin, Y., et al.: Effect of CT image size and resolution on the accuracy of rock property estimates. J. Geophys. Res. Solid Earth **122**(5), 3635–3647 (2017)
5. Bazaikin, Y.V., Malkovich, E.G., Derevschikov, V.S., Lysikov, A.I., Okunev, A.G.: Evolution of sorptive and textural properties of CAO-based sorbents during repetitive sorption/regeneration cycles. Chem. Eng. Sci. **152**, 709–716 (2016)
6. Gerke, K.M., Karsanina, M.V., Katsman, R.: Calculation of tensorial flow properties on pore level: exploring the influence of boundary conditions on the permeability of three-dimensional stochastic reconstructions. Phys. Rev. E **100**(5), 053312 (2019)
7. Khachkova, T., Lisitsa, V., Reshetova, G.: Effect of interface roughness on the elastic properties of 3D layered media. Probab. Eng. Mech. **75**, 103571 (2024)
8. Khachkova, T., Lisitsa, V., Reshetova, G., Tcheverda, V.: GPU-based algorithm for evaluating the electrical resistivity of digital rocks. Comput. Math. Appl. **82**, 200–211 (2021)
9. Khachkova, T.S., Lisitsa, V.V.: Construction of relative permeability curves by numerical simulation of two-phase flow in 3D CT-models. Lecture Notes in Computer Science, vol. 14817, pp. 250–262 (2024). https://doi.org/10.1007/978-3-031-65238-7_17
10. Khachkova, T.S., Lisitsa, V.V., Gondul, E.A., Prokhorov, D.I., Kostin, V.I.: Two-phase flow simulation algorithm for numerical estimation of relative phase permeability curves of porous materials. Russ. J. Numer. Anal. Math. Model. **39**(4), 209–221 (2024). https://doi.org/10.1515/rnam-2024-0020

11. Khachkova, T.S., Lisitsa, V.V., Krutko, V.V., Avdonin, A.S.: Constructing dependence of electrical parameters on porosity and water saturation for digital models of high-permeability rock samples. Lecture Notes in Computer Science, vol. 15888, pp. 419–432 (2025). https://doi.org/10.1007/978-3-031-97596-7_28
12. Lisitsa, V., Khachkova, T., Sotnikov, O., Islamov, I., Ganiev, D.: Numerical evaluating the permeability of rocks based on correlation dependence on geometry. Lecture Notes in Computer Science, vol. 14106, pp. 91–102 (2023). https://doi.org/10.1007/978-3-031-37111-0_7
13. Lisitsa, V., Manaev, A., Solovyev, S.: Implementation of the spectral preconditioner to solve poisson equation. In: Gervasi, O., et al. (eds.) Computational Science and Its Applications – ICCSA 2025 Workshops, pp. 388–401. Springer (2025). https://doi.org/10.1007/978-3-031-97596-7_26
14. Luo, K., Zhuang, Z., Fan, J., Haugen, N.E.L.: A ghost-cell immersed boundary method for simulations of heat transfer in compressible flows under different boundary conditions. Int. J. Heat Mass Transf. **92**, 708–717 (2016)
15. Manaev, A.A., Lisitsa, V.V.: Spectral preconditioner for solving poisson equation. Comput. Methods Program. **26**(2), 111–128 (2025). https://doi.org/10.26089/NumMet.v26r208. (in Russian)
16. Mostaghimi, P., Blunt, M., Bijeljic, B.: Computations of absolute permeability on micro-CT images. Math. Geosci. **45**(1), 103–125 (2013)
17. Prokhorov, D., Lisitsa, V., Khachkova, T., Bazaikin, Y., Yang, Y.: Topology-based characterization of chemically-induced pore space changes using reduction of 3D digital images. J. Comput. Sci. **58**, 101550 (2022)
18. Saenger, E.H., et al.: Analysis of high-resolution X-ray computed tomography images of bentheim sandstone under elevated confining pressures. Geophys. Prospect. **64**(4), 848–859 (2016)
19. Shen, J., Yang, X., Yu, H.: Efficient energy stable numerical schemes for a phase field moving contact line model. J. Comput. Phys. **284**, 617–630 (2015)
20. Shulakova, V., et al.: Computational elastic up-scaling of sandstone on the basis of X-ray micro-tomographic images. Geophys. Prospect. **61**(2), 287–301 (2013)
21. Yu, H., Yang, X.: Numerical approximations for a phase-field moving contact line model with variable densities and viscosities. J. Comput. Phys. **334**, 665–686 (2017)
22. Zhan, X., Schwartz, L.M., Toksöz, M.N., Smith, W.C., Morgan, F.D.: Pore-scale modeling of electrical and fluid transport in berea sandstone. Geophysics **75**(5), F135–F142 (2010)

Evaluating Inner Areas Potentials (EIAP 2026)

Undertourism and Physical, Social and Economic Sustainability. The *ECHE Lab Approach* to Evaluate the Cultural Tourism Sustainability in the Inner Areas

Rosa Maria Staropoli, Giovanna Emanuela Minniti, and Francesco Calabrò(✉)

Mediterranea University, Via dell'Università, 25, 89124 Reggio Calabria, Italy
francesco.calabro@unirc.it

Abstract. This article addresses the sustainability of tourism development projects in contexts characterized by weak demand, such as Inner Areas. The primary purpose of this paper is to outline the key aspects to consider in project sustainability assessment procedures within strategic planning tools for cultural tourism destinations currently experiencing undertourism. Specifically, the article focuses on the maximum and minimum tourist attendance limits that can simultaneously guarantee the physical integrity of cultural heritage, the socio-cultural integrity of communities, and the economic sustainability of services. To this end, two fundamental tools are identified: carrying capacity assessment, in its various forms—of sites, territories, and communities—and break-even analysis, for identifying the break-even point of project budgets. The conceptual framework is the 2022 ICOMOS International Charter for Cultural Tourism.

Keywords: Undertourism · Economic Sustainability · Carrying Capacity · Inner Areas

1 Introduction

1.1 The Reference Context

In the field of Tourism, the scientific, cultural and political debate of recent years has mainly focused on the effects produced by the phenomenon of so-called overtourism. The 2022 ICOMOS Charter for Cultural Tourism itself, as we will see better later, essentially has the aim of providing useful information to counteract the effects produced by overtourism on Cultural Heritage and Local Communities [1].

For these reasons, the sustainability of policies, programs and projects in the field of Tourism, since the first studies (among others Cifuentes 1992, for example) has been treated mainly by looking at the excess pressure produced by *Overtourism* [2].

Only recently did the Italian Ministry of Tourism, on the occasion of the International Tourism Forum organized in Milan in January 2026, also begin to place emphasis on the risks and opportunities connected with the opposite phenomenon, that of *Undertourism*,

© The Author(s), under exclusive license to Springer Nature Switzerland AG 2027
O. Gervasi et al. (Eds.): ICCSA 2026 Workshops, LNCS 16761, pp. 113–128, 2027.
https://doi.org/10.1007/978-3-032-30527-5_8

essentially unexplored until now, a phenomenon which particularly characterizes the Inner Areas.

However, *Undertourism* must also be considered from a sustainability perspective: if in the first case the conservation of the heritage is jeopardized by excessive pressure, in the second one the risks instead derive precisely from the scarcity of presences, which often does not allow to intercept the minimum quantity of economic resources, public and private, necessary for the management of the sites.

On the other hand, a greater enhancement of currently less visited sites, some extent, could to also help to counteract the phenomena of overtourism.

It is evident, therefore, that to speak correctly about the sustainability of Tourism, it is necessary to treat the topic in its entirety and multidimensionality, looking simultaneously at the upper limit of pressures but also at the lower limit, as well as at the aspects of physical sustainability but also of social and economic sustainability.

This contribution fits precisely into this context, illustrating an approach, developed by the ECHE Lab laboratory of the Mediterranean University of Reggio Calabria, which tries to integrate into the same procedure a sustainability assessment of policies, programs and projects that allows all these dimensions to be verified simultaneously.

The contribution is configured as a conceptual/methodological framework paper, the first experimental applications have just been started in some areas of Calabria..

1.2 Structure of the Paper

This article aims to present the ECHE Lab's approach to assessing the physical, social, and economic sustainability of Cultural Tourism in Inner Areas, especially where undertourism exists.

The article is essentially divided into two parts:

- The first part provides the framework within which the approach is developed, which stems from an examination of the 2022 ICOMOS International Charter for Cultural Tourism. It then briefly reviews the concepts of cultural tourism destinations and the trend in demand for services in Inner Areas; the article then proceeds to outline the strategic planning of cultural tourism in Inner Areas.
- The second part of the article is specifically dedicated to the evaluation aspects of the ECHE Lab Approach, aimed at evaluating projects for the enhancement of Cultural Heritage for tourism purposes. The procedure developed is based on well-known concepts and tools, such as the assessment of carrying capacity, for the physical and social dimensions of sustainability, and the concept of budget equilibrium, verified through Break-Even Analysis, for the economic dimension: the specific aspect of the approach consists in their combined use, which allows for verifying the simultaneous existence of both equilibrium conditions mentioned above.

2 Undertourism and the ICOMOS International Charter for Cultural Heritage Tourism

2.1 A Charter for the Protection of Cultural Heritage

The ICOMOS International Charter for Cultural Heritage Tourism has been adopted by the ICOMOS Annual General Assembly (Bangkok, Thailand) in November 2022. The title of the Charter is: *"Reinforcing cultural heritage protection and community resilience through responsible and sustainable tourism management"*.

The title itself makes it clear that the Charter, similarly to those of the previous year (1976, 1999) [3, 4], was created with the aim of protecting heritage and communities from the risks associated with the phenomenon of so-called *Overtourism.*

The first two declared objectives of the Charter, in fact, are:

- *Objective 1 - To place the protection of cultural heritage and community rights at the heart of cultural heritage tourism policy and projects, by providing principles that will inform responsible tourism planning and management for cultural heritage protection, community resilience and adaptation;*
- *Objective 2 - To promote stakeholder collaboration and participatory governance in the stewardship of cultural heritage and management of tourism, applying a people-centered and rights-based approach, emphasizing access, education and enjoyment*.

The almost exclusive focus on the effects of overtourism, however, inevitably leads to ignoring the risks associated with the opposite phenomenon, so-called undertourism, which actually affects the vast majority of the territory.

The risks to the survival of cultural heritage in undertouristed areas are linked to its progressive abandonment and the insufficiency of public resources available for its conservation.

Therefore, a strategy for this heritage is urgently needed that balances the needs of conservation with those of enhancement. It is a difficult but essential balance.

3 Cultural Tourism Destinations

3.1 Some Definitions

The Department of Economic and Social Affairs of United Nations, Statistics Division, in the *International Recommendations for Tourism Statistics* (2008) defines the concept of **Destination** as *"…the place visited that is central to the decision to take the trip. See also purpose of a tourism trip."* (IRTS 2008, 2.31) [5].

The same Recommendations defines the concept of **Tourism Destination** as *"…a physical space with or without administrative and/or analytical boundaries in which a visitor can spend an overnight. It is the cluster (co-location) of products and services, and of activities and experiences along the tourism value chain and a basic unit of analysis of tourism. A destination incorporates various stakeholders and can network to form larger destinations. It is also intangible with its image and identity which may influence its market competitiveness.*"

United Nations World Tourism Organization - UNWTO has defined **Destination management** as: "*the coordinated management of all the elements that make up a destination (attractions, amenities, accessibility, human resources, image and price).* [...] *Its role is to lead and coordinate activities under a coherent strategy or plan, serving the interests of all stakeholders*" [6].

The organization of tourist destination services can take various forms, among which are particularly noteworthy:

- Local Tourism Systems;
- Tourism Districts;
- Destination Management Organizations (DMOs).

Let us focus in particular on this last form, which the Department of Economic and Social Affairs of the United Nations, Statistics Division, and the UNWTO define as "*…the leading organizational entity which may encompass the various authorities, stakeholders and professionals and facilitates tourism sector partnerships towards a collective destination vision. The governance structures of DMOs vary from a single public authority to a public/ private partnership model with the key role of initiating, coordinating and managing certain activities such as implementation of tourism policies, strategic planning, product development, promotion and marketing and convention bureau activities. The functions of the DMOs may vary from national to regional and local levels depending on the current and potential needs as well as on the decentralization level of public administration. Not every tourism destination has a DMO.*

Destination Management has two main purposes:

- To maximize the benefits of tourism to the destination, making tourism 'work for everyone';
- To ensure that tourism is genuinely sustainable for the long term.

Sustainability, therefore, is and must be one of the guiding principles of any form of tourism organization.

The same UNWTO Glossary provides a definition of Cultural Tourism: "*Cultural tourism: Cultural tourism is a type of tourism activity in which the visitor's essential motivation is to learn, discover, experience and consume the tangible and intangible cultural attractions/products in a tourism destination. These attractions/products relate to a set of distinctive material, intellectual, spiritual and emotional features of a society that encompasses arts and architecture, historical and cultural heritage, culinary heritage, literature, music, creative industries and the living cultures with their lifestyles, value systems, beliefs and traditions.*"

This definition highlights the relevance of preserving Cultural Heritage, both in its tangible and intangible manifestations: the disappearance of such Heritage automatically entails the disappearance of the reasons why visitors travel to a destination, thus marking the end of related activities [7].

4 Supply and Demand of Cultural Services in Inner Areas

4.1 The Place-Based Approach to Enhance Inner Areas: the Italian SNAI

"*…These 'Inner Areas' are defined as areas being at some considerable distance from centres offering such services, and where there has been a fall in population and a rise in degradation.*": thus the UVAL – the Public Investment Evaluation Unit, active at the Presidency of the Council of Ministers, defines the Inner Areas [8].

While this definition emphasizes the lack of services (essential and otherwise), it is clear that the low population density that characterizes these territories leads to a demand for services that is insufficient to ensure their economic sustainability, especially when it comes to services provided by the free market.

Weak demand, in fact, often prevents companies from achieving a balanced budget, much less generating sufficient profits, as will be discussed in more detail later.

To make unused territorial capital productive and to limit or eliminate the social costs of hydrogeological instability, landscape deterioration and biological diversity lost the Italian National Agency for Territorial Cohesion has developed a place-based approach, the so-called "National Strategy for Inner Areas" (SNAI).

Among the various resources present in the Inner Areas, considered useful for promoting their relaunch, SNAI attributes a leading role to Culture, in its broadest sense: "*…not only as artistic and landscape heritage, but also in terms of traditions and creativity, material and immaterial factors that contribute to building the image of places and strengthening their identity. Culture - museums, archaeological areas and sites, historical settlements, accompanied by the presence of libraries that contribute to the dissemination of local identities and traditions - can make places more attractive, stimulate tourism and, in this way, counteract depopulation and the closing of territorial gaps.*" [9]

4.2 Cultural Heritage of Inner Areas and Public-Private Partnership

It is also in contexts characterized by weak demand, such as the Inner Areas, that it is necessary to verify the sustainability of tourist-cultural development projects.

The previous considerations regarding the weakness of demand for services also apply to the conservation and accessibility of cultural heritage: the extremely low influx of visitors does not justify the use of public resources to ensure the opening to the public of a significant number of sites, which, therefore, cannot fulfill their potential and contribute, more generally, to increasing the attractiveness of the territories.

This process, in turn, also affects the allocation of resources intended for heritage conservation, which, in the long term, can hardly be consistently allocated to sites for which there is no adequate demand.

A possible solution is sometimes represented by the involvement of non-profit organizations in the management [10]: this solution certainly allows for a drastic reduction in management costs, but, beyond the considerations of expediency associated with forms of job insecurity, it is essential that at least two conditions are met simultaneously:

– The presence in the territory of non-profit organizations interested and equipped with the necessary expertise;

– Demand that is still sufficient to cover fixed costs in the long run.

A site of cultural and tourist interest, however, unless it is a highly renowned site such as a UNESCO World Heritage site, is unlikely to be able to generate significant tourist flows on its own. Therefore, it is necessary to develop a supra-municipal supply system that encompasses and integrates not only the attractions but also the other services necessary for hosting visitors.

5 Strategic Planning of Cultural Tourism in the Inner Areas

We have seen so far that DMOs can be a particularly effective tool for organizing a territory's tourism offerings and that Inner Areas have a wealth of cultural heritage that can help trigger development processes through the use of a place-based approach.

The question at this point is: how should we proceed methodologically to structure DMOs so that they enhance the cultural heritage of Inner Areas in terms of tourism?

"*DMOs today should not only lead on marketing, but must also be strategic leaders in destination development. This role requires them to drive and coordinate destination management activities within the framework of a coherent strategy.*" (UNWTO, 2007)

What are the elements that make up a development strategy for a tourist destination? In this case too, we can refer to the UNWTO's outline:

1. **Situation assessment (Where are we now?)** regarding the tourism competitiveness of the destination;
2. **A strategic framework (Where would we like to be?)** for future tourism growth based on the findings of the situation analysis;
3. **An integrated, multi-year Implementation Plan (How do we get there?)** with specific programmes and projects, budget indicators and monitoring mechanisms to implement the strategic framework;
4. Institutional and performance management arrangements (How do we organise ourselves to get there and measure success?).

During this stage the impact of the strategy would have to be evaluated. This would be likely to cover a number of differing factors (e.g. growing the economic benefits, spreading seasonality or levelling demand, securing investment, raising quality, etc.) depending on the priorities of the strategy. Different research methods will be required to assess different types of impact but they can be broadly divided into two categories:

– Assessment of macro impacts through destination wide research such as national surveys, occupancy surveys etc.
– Assessments of the impacts of individual programme – e.g. campaign evaluations.

6 Outlines for Assessing the Sustainability of Cultural Tourism in the Inner Areas: The ECHE Lab Approach

6.1 Evaluating the Cultural Tourism Sustainability in the Inner Areas

A model that allows you to easily understand the interactions to be considered in sustainability assessments is the so-called "*Visitors, Industry, Community, Environment - VICE model*", developed by the English Tourist Board, which considers a tourist destination "*…as the interactions between the **Visitors,** the **Industry** that serves them, the*

Community *that hosts them and the* ***Environment*** *where this interaction takes place*." [11].

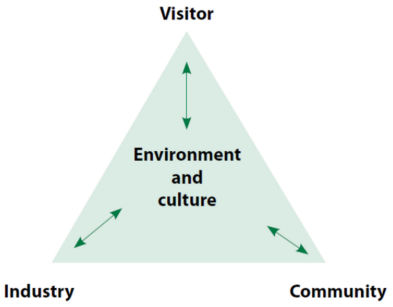

Fig. 1. The VICE Model

Culture's potential contribution to economic development has long been recognized: *"… culture has also been recognized as a driver of economic development, with community-wide social and environmental impacts."* [12], but to avoid the risks associated with the implementation of inappropriate actions, it is necessary to promote a sustainable approach to tourism, particularly in relation to cultural tourism destinations: *"… sustainable tourism approaches to generate positive economic and social benefits in cultural destinations are recommended by both European and international stakeholders."* [13]

The scientific debate on the different approaches to assessing tourism sustainability is extremely broad, but universally accepted methods have not yet been reached: *"Existing indicators cover the most important aspects of the sustainability of tourism at cultural destinations, including both tangible and intangible heritage. Nevertheless, there is not a universally accepted approach to measuring cultural tourism's impacts, and the available indicator systems lean toward the broader concept of sustainable tourism.*" [14, 15], although there is a significant amount of research and publications that have addressed the topic, including Bosone and Rolando [16, 17], among others.

6.2 Physical and Social Sustainability: The Dimensions of Carrying Capacity

The concept of carrying capacity has been defined in various ways by different scholars, (Bencardino, among many others, for example) [18]; many of these definitions deal with the topic by looking exclusively at the physical capacity of the containers, without paying attention to the consequences of the presence: "*the maximum number of visitors that could physically fit into a defined space over a particular time* [19].

Other definitions also look in the direction of the impacts determined by the presence of visitors, defining the carrying capacity as:

– "*the level of use of an area offering a high level of satisfaction with a small impact on resources*" [20];

– "*the maximum number of people that could visit a tourist destination at the same time, without causing destruction of the physical, economic or socio-cultural environment and an unacceptable decrease in the quality of visitors' satisfaction*" [21].

Carrying capacity assessment can be performed at different scales: at the scale of individual sites or at the scale of the territories in which they are located [22]; different limits correspond to each scale. Similarly, even for the same scale and the same type of site, there is no universally valid carrying capacity but it must be calculated from time to time for each specific situation [23].

The two main dimensions of carrying capacity that, according to some authors, must be taken into consideration are: [24]:

– the physical carrying capacity;
– the real carrying capacity.

They describe the physical carrying capacity "*as the maximum number of people who can use a site without an unacceptable alteration in the physical environment and without an unacceptable decline inexperience quality*." and the real carrying capacity "*as the maximum permissible number of visits of a given site, which is calculated by taking into account the limiting factors (translated into quantitative values) resulting from specific conditions of a given place*.".

Keeping the VICE model in mind, however, this definition only considers the binary relationships between environment and visitors, but does not explore the three-dimensional relationships between environment, visitors, and the community.

This dimension, however, is extremely relevant for preserving the authenticity of sites, which often consists not only of their material component but also of their immaterial one [25–28]. Indeed, the relationship between the material and immaterial dimensions is becoming increasingly important, as emphasized by the ICOMOS Charter for Cultural Tourism.

6.3 Economic Sustainability: the Break-Even Point in Budgets

The difficulties of reconciling the three dimensions of sustainability, even from a methodological perspective, are well-known. In particular, when discussing the economic dimension of sustainability, solutions are often confined to public policies, with no regard for balanced budgets.

There is no doubt that the preservation of Cultural Heritage has a strong public dimension, arising as a collective issue; on the other hand, however, it must also be taken into account that budgetary constraints for public policies are increasingly increasing, despite the brief interlude immediately following the COVID-19 pandemic.

If we truly want to work effectively to pass on Cultural Heritage to future generations, due attention must be paid to the economic dimension of sustainability, otherwise the risk of the permanent disappearance of a significant portion of this Heritage is absolutely real.

Fortunately, in recent years, a growing number of scholars have been paying attention to this dimension, lifting the taboo on private intervention even in policies promoting Cultural Heritage, as is now the case in many other sectors [29–32].

It is clear that this is a highly sensitive area, requiring careful attention to ensure the absolute protection of the public interest, which must nevertheless remain paramount. However, overcoming clearly ideological resistance in this field, synergies between public and private entities must be encouraged wherever possible, in order to significantly increase the amount of resources available for the conservation and enhancement of Heritage.

It should also be considered that in the various forms of public-private partnerships, it is advisable to use private social entities, which, being non-profit, allow two objectives to be effectively pursued:

- ensuring that the actions undertaken truly respond to public interests;
- asset management costs can be reduced by eliminating the profit component, which, however, must legitimately be considered when the entities involved are profit-making.

A point of reference in this regard is Throsby, who, regarding economic sustainability, states: "***Economic sustainability*** *The project should produce a stable and predictable flow of net economic benefits into the future, where both market and nonmarket effects are included in the assessment. Market effects include revenues from tourist admission charges and, in certain types of analysis and under certain assumptions, the net incremental value ('impact') of tourist expenditures (see further under Rule 3 below). If externality or public-good benefits or costs are significant relative to direct market revenues, the project may need to incorporate some means for revenue capture in order to ensure continued financial viability of the project, for example, via taxes levied on those enjoying the external benefits or imposing the external costs. For tourists, such revenue capture is typically achieved through arrival/departure levies at airports, hotel occupancy taxes, and so on. Application of the third sustainability principle above (intragenerational equity) would also ensure that, for example, local residents in an area affected by the tourist project would have equitable access to the project's economic benefits.*" [33]

6.4 Economic Sustainability: The Public-Private Partnership to Enhance the Cultural Heritage

Private entities that may be involved in initiatives aimed at enhancing cultural heritage can be of a different nature, profit-making or not-for-profit, depending on their social goals [34].

In the case of profit-making entities (businesses), their survival is only possible through the generation of revenues from entrepreneurial activity; these revenues must cover all costs and generate a profit share that is greater than the sum of the return on invested capital and the risk associated with the entrepreneurial activity [35].

In the case of not-for-profit entities (associations, foundations, etc.), revenues may come from the activities carried out or from donations and contributions from members and other public and/or private entities. In this case, for the purposes of budget balance, revenues may be lower than those of businesses, as these entities do not aim to generate profits, so a return on invested capital is not essential. The management costs of these entities are also usually lower, especially when it comes to limited-scale activities that do not require a full-time commitment. In such cases, in fact, due to the nature and purposes

of the entity, part or all of the human resource costs are replaced by the voluntary work of the members, particularly with regard to the fixed costs of any employees [36]. For the purposes of the economic sustainability of the activities of these entities, therefore, revenues can be limited to covering management costs and replenishing the initial capital, without any remuneration.

In reality, the cost structure for both entities is not constant as the quantities produced vary: as the quantities increase, the costs, especially management costs, of not-for-profit entities increase more quickly than those of for-profit entities, due to the inevitable inefficiencies of entities that do not have the carrying out of entrepreneurial activities among their founding reasons.

One of the purposes of the economic and financial checks prior to awarding the management of services is therefore to verify the nature of the private entity to be involved in the partnership in relation to the expected revenues.

In the case of public-private partnerships, therefore, the role of the public entity must first and foremost be to ensure the pursuit of collective interests in the provision of services.

In some cases, when the necessary preliminary economic and financial checks indicate this need, the public entity may be required to contribute to the investment and/or management costs through appropriate forms of co-financing [37].

6.5 Economic Sustainability: The Break-Even Analysis

There are several tools for assessing a project's financial balance, the most well-known of which is Cash Flow Analysis (CFA), which allows you to verify in a summary table whether the revenue generated by a given activity exceeds its operating costs. When you want to verify whether the revenue generated over a certain number of years is capable of remunerating the initial invested capital, the time horizon considered changes and the need arises to discount costs and revenues at the time of evaluation: in this case, the CFA takes the form of Discounted Cash Flow Analysis (DCFA) [38].

A technique that also uses the revenue and expenditure data generated by a given project, but with a different logic, is Break-Even Analysis (BEA): this technique allows you to identify the break-even point of project budgets [39].

In other words, the BEA allows you to identify the minimum amount of revenue capable of achieving the managing entity's objectives. Depending on the managing entity and the form taken by the PPP, four different situations may arise [40]:

- Revenues must fully cover management costs and adequately remunerate the invested capital: the managing entity should be of the "profit" type and must also fully cover the investment costs, assuming the related risks;
- Revenues must fully cover management costs and adequately remunerate a portion of the invested capital (a profit-making managing entity also covers a portion of the investment costs; the remainder is covered by public co-financing);
- Revenues must fully cover only management costs; the managing entity can be for-profit or not-for-profit depending on the size of the cash flows generated by the project; in this case, the investment costs are borne entirely by the public entity, which merely entrusts the management of the services. In this form of partnership, to assess the

long-term sustainability of the services provided, it is essential to determine whether revenues are sufficient to cover extraordinary maintenance costs. This is especially crucial when managing historic buildings, which typically have high maintenance costs.
– Revenues partially cover management costs: in this case, the managing entity should be a non-profit organization that receives public co-financing for management. This co-financing can also be in kind, with the public entity responsible for certain types of costs, such as utilities or ordinary maintenance.

6.6 The *ECHE Lab Approach*

The specific purpose of sustainability assessments must be to identify the limits of tourist flows.

The plural is mandatory because, as already introduced in the first paragraph, based on the pressures triggered by overtourism, evaluators usually focus on the upper limit: in other words, assessments are often aimed at identifying the maximum limit of tourist flow, beyond which the very survival of the Heritage Site and/or its community is jeopardized, more or less quickly.

In reality, there is also a lower limit of sustainability, represented by the minimum threshold of tourist flow capable of generating sufficient revenue to guarantee the survival of the management entities.

The relevance of calculating the lower limit is obviously less, indeed almost always nonexistent, in sites characterized by *Overtourism*, while it becomes absolutely crucial in situations of *Undertourism*. This is why the ECHE Lab approach is particularly suitable for assessing the sustainability of Cultural Tourism in Inner Areas.

The ECHE Lab approach uses existing evaluation techniques and approaches, combining them in an innovative way, calibrated for the specific evaluation purposes.

In other words, the ECHE Lab approach aims to identify, within the same evaluation procedure, both a maximum and a minimum limit for tourist presence, in order to simultaneously guarantee the physical integrity of the Cultural Heritage, the socio-cultural integrity of the Communities, and the economic sustainability of the services.

The ECHE Lab approach is particularly suitable for use within strategic planning tools to select effective and sustainable actions.

6.7 Strategic Planning and ECHE Lab Approach: Stages and Methodological Aspects

The ECHE Lab approach is particularly suitable for evaluating the sustainability of Strategic Plans for the development of Cultural Tourism at the DMO scale.

In fact, it introduces the evaluation process in a structured way as an integral part of the strategic planning process, with particular attention to aspects of its sustainability and does so differently in the various phases of the process, as can be seen from Fig. 2.

In summary, the ECHE Lab approach combines monetary and non-monetary techniques to calculate two key factors for the sustainability of Cultural Tourism:

– Carrying capacity (of sites; territories; Communities), to calculate the upper limit;
– Balanced budget, to calculate the lower limit.

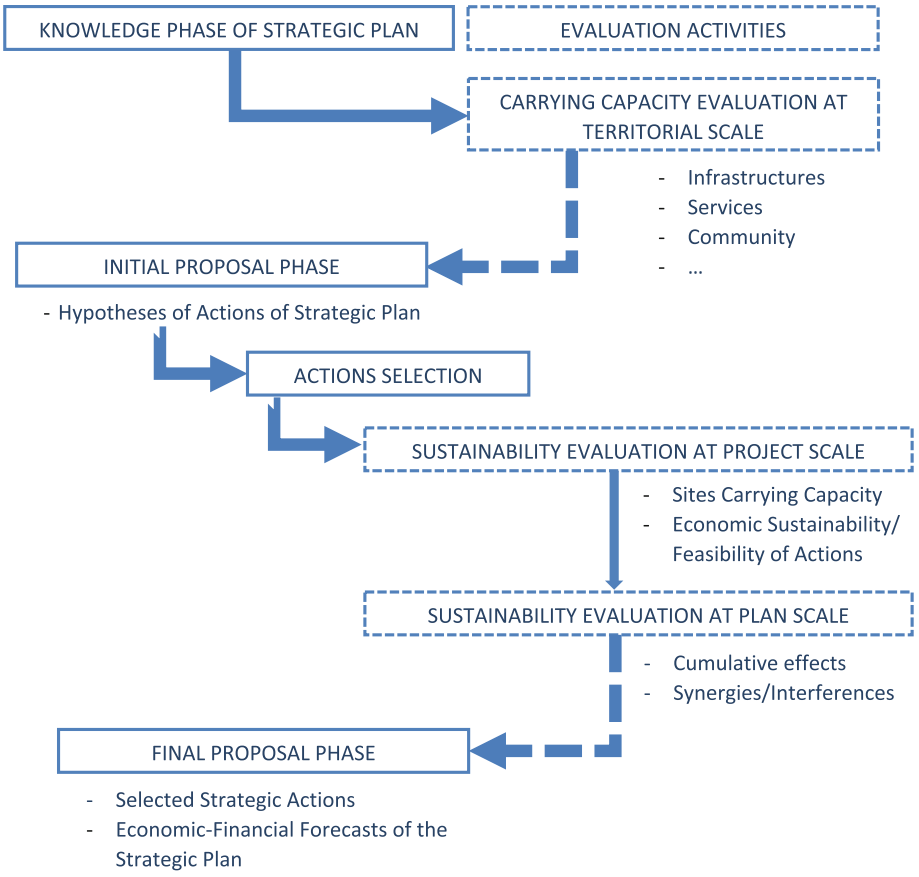

7 Conclusions and Perspectives

In light of the above, it can be stated that assessing the sustainability of Cultural Heritage enhancement projects must follow different procedures and use different techniques depending on the contexts for which they are developed.

The approach developed by the ECHE Lab involves different procedures and techniques depending on whether the contexts are characterized by overtourism or undertourism, especially in Inner Areas, but also depending on whether the focus is on physical and social sustainability or whether the objective is to assess economic sustainability [41].

In the latter case, Break-Even Analysis allows for a relatively simple, quick, and effective assessment of whether balanced budget conditions exist.

Research activities continue, particularly in the direction of testing the ECHE Lab approach, currently being applied in several case studies in Calabria.

In particular, there are two areas in the Metropolitan City of Reggio Calabria, characterized by very different dynamics, in which ECHE Lab is developing some experiments: the Costa Viola and the Valle degli Armeni.

The Costa Viola, on the Tyrrhenian coast, includes the municipalities of Villa S. Giovanni, Scilla, Bagnara, Palmi, and Seminara. Scilla, in particular, is the area's most popular destination, especially for beach tourism, and during the summer months experiences typical overtourism trends. The neighboring municipalities, while experiencing a clear increase in summer visitors, do not experience the same situation.

The Valle degli Armeni, on the other hand, is located on the Ionian coast and includes the municipalities of Brancaleone, Staiti, and Bruzzano Zeffirio. The area studied for the pilot project is slightly larger, as it also includes the municipalities of Palizzi, Ferruzzano, and Bianco. This area also experiences a significant increase in summer visitors, although this has not yet resulted in significant negative impacts.

Both areas are characterized by highly valuable environmental resources and, at the same time, aim to increase tourist numbers, especially to create new job opportunities for young people, thus countering the depopulation of these areas [42].

Despite their diversity, the challenge in both areas is to build a comprehensive tourism development strategy that can prevent overtourism or effectively combat it where it already exists [43].

These first two applications, which constitute the immediate future developments of the research, have just been started and constitute the experimentation necessary to confirm the theoretical hypotheses formulated through the model illustrated previously or to provide indications for any necessary corrective measures.

References

1. ICOMOS: International Charter for Cultural Heritage Tourism. Reinforcing Cultural Heritage Protection and Community Resilience through Responsible and Sustainable Tourism Management, Bangkok, Thailand (2022)
2. Cifuentes, M.: Determinación de Capacidad de Carga Turística en Áreas Protegidas; Centro Agronómico tropical de Investigación y Enseñanza (CATIE), Turrialba, Costa Rica, p. 23 (1992)
3. ICOMOS: Tourism Committee: Charter for Cultural Tourism, Brussels, Belgium (1976)
4. ICOMOS: International Cultural Tourism Charter. Managing Tourism at Places of Heritage Significance, Mexico City (1999)
5. United Nations - Department of Economic and Social Affairs, Statistics Division International Recommendations for Tourism Statistics 2008. Sales No. E.08.XVII.28. United Nations Publication, New York (USA) (2010)
6. UNWTO: A Practical Guide to Tourism Destination Management. World Tourism Organization, Madrid, Spain (2007)
7. Viglianisi, A., Calabrò, F.: The Management Models of a Tourist Destination in Italy. In: Lecture Notes in Networks and Systems, LNNS, vol. 482, pp. 2325–2334 (2022). https://doi.org/10.1007/978-3-031-06825-6_223
8. UVAL: Strategia Nazionale per le Aree Interne: definizione, obiettivi, strumenti e governance. Collana Materiali UVAL - Documenti, Numero 31 - Anno 2014. UVAL, Roma (2014)
9. ISTAT: The Geography of Inner Areas in 2020. Territories between Potential and Weaknesses. ISTAT Press Office (2022) https://www.istat.it/wp-content/uploads/2024/11/20220720_FOCUS_Inner_Areas_en.pdf

10. Calabrò, F.: Promoting peace through identity. evaluation and participation in an enhancement experience of calabria's endogenous resources | Promuovere la pace attraverso le identità. Valutazione e partecipazione in un'esperienza di valorizzazione delle risorse endogene della Calabria. In: Archistor, 12(6), pp. 84–93. (2019). https://doi.org/10.14633/AHR146
11. Carver, R., Nevill, H.: Destination Management Handbook. World Bank Group, Washington DC, USA (2022)
12. UNESCO: Culture: A Driver and an Enabler of Sustainable Development. Thematic Think Piece: 2012; 10p (2012). Available online: https://www.un.org/millenniumgoals/pdf/Think%20Pieces/2_culture.pdf.
13. Potts, A.: European Cultural Heritage Green Paper "Putting Europe's Shared Heritage at the Heart of the European Green Deal". Europa Nostra, Brussels, Belgium (2022)
14. Calabrò, F., Lorè, I., Minniti, G.E., Staropoli, R.M.: Undertourism and destination Management in the Inner Areas. The case of Locride, Reggio Calabria. In: Lecture Notes in Computer Science, LNCS, vol. 15889, pp. 283–300 (2026). https://doi.org/10.1007/978-3-031-97603-2_18
15. Zubiaga, M., Sopelana, A., Gandini, A., Aliaga, H.M., Kalvet, T.: Sustainable cultural tourism: proposal for a comparative indicator-based framework in European destinations. Sustainability 2024. **16**, 2062 (2024). https://doi.org/10.3390/su16052062
16. Nocca, F., Bosone, M., De Toro, P., Fusco Girard, L.: Towards the human circular tourism: recommendations, actions, and multidimensional indicators for the tourist category. Sustainability 2023. **15**, 1845 (2023)
17. Stankulova, A., Barreca, A., Rebaudengo, M., Rolando, D.: The quantitative indicator-based evaluation for rural development. Int. Reg. Sci. Rev. **48**, 01600176241268028 (2024)
18. Bencardino, M., Cresta, A., Esposito, V., Senatore, A., Valanzano, L.: A model for estimating the tourism carrying capacity (TCC) of a serial cultural heritage: the case of the via Appia. Regina Viarum. Sustain. **17**(18), 8213 (2025)
19. Lagarense, B.E.S.: Stakeholder Involvement in Waterfront Planning and Development in Manado, Indonesia. University of Waterloo, Ontario, Canada (2011)
20. Aminian, N., Khodayar, S.: Tourism carrying capacity assessment for historical sites – Isfahan Emam mosque. In: Savanna, A., Smith, M. (eds.) Advancing Tourism Research Globally, the 12. International Conference, pp. 53–63. Travel and Tourism Research Association, Massachusetts (2016)
21. UNWTO: Overtourism, Understanding and Managing Urban Tourism Growth beyond Perceptions. Executive Summary, UNWTO, Madrid, Spain (2020)
22. Pasko, G.: Carrying capacity Assesment as an essential tool for sustainable tourism development. Eur. J. Econ. Bus. Stud. **2**(1), 164–171 (2016)
23. Petronijevic, A.: Practical application of the tourism carrying capacity concept in cultural tourism. Turizam. **26**(2) (2022)
24. Attallah, N.F.: The estimation of physical and real carrying capacity with application on Egypt's tourist sites. J. Tourism Res. **12**, 1–6 (2015)
25. Seidl, I., Tisdell, C.A.: Carrying capacity reconsidered: from Malthus' population theory to cultural carrying capacity. Ecol. Econ. **31**(3), 395–408 (1999)
26. Cimnaghi, E., Mussini, P.: An application of tourism carrying capacity assessment at two Italian cultural heritage sites. J. Herit. Tour. **10**(3), 302–313 (2015)
27. Calabrò, F., Cassalia, G., Lorè, I.: A project of enhancement and integrated management: the cultural heritage agency of Locride. In: Lecture Notes in Networks and Systems LNNS, vol. 482, pp. 278–288 (2022). https://doi.org/10.1007/978-3-031-06825-6_27
28. Cassalia, G., Calabrò, F.: The Valuation of Unused Public Buildings in Support of Culture-Led Inner Areas' Small Villages NRRP Strategies: An Application Model in Southern Italy. In: Lecture Notes in Networks and Systems, LNNS, vol. 482, pp. 3–15 (2022). https://doi.org/10.1007/978-3-031-06825-6_1

29. Foti, V.T., Scuderi, A., Stella, G., Sturiale, L., Timpanaro, G., Trovato, M.R.: The integration of agriculture in the politics of social regeneration of degraded urban areas. In: Green Energy and Technology, pp. 99–111 (2018). https://doi.org/10.1007/978-3-319-78271-3_8
30. Morano, P., Tajani, F., Di Liddo, F., Amoruso, P.: The public role for the effectiveness of the territorial enhancement initiatives: a case study on the redevelopment of a building in disuse in an Italian small town. Buildings. **11**(3), 87 (2021). https://doi.org/10.3390/buildings11030087
31. Musolino, M., Massimo, D.E., F., C.'., De Paola, P., Errigo, R., Malerba, A.: Appraisal of sustainable retrofitting of historic settlements: less 60% unexpected outcomes. Sustainability. **17**(13), 1–30 (2025). https://doi.org/10.3390/su17135695. ISSN: 2071-1050, doi:; WoS: 001527621100001; Scopus: 2-s2.0-105010340661
32. Scuderi, A., Sturiale, L.: Evaluations of social media strategy for green urban planning inmetropolitan cities. Smart Innov. Syst. Technol. **100**, 76–84 (2019). https://doi.org/10.1007/978-3-319-92099-3_10
33. Throsby, D.: Tourism, heritage and cultural sustainability: three 'Golden rules'. In: Fusco Girard, L., Nijkamp, P. (eds.) Cultural Tourism and Sustainable Local Development, p. 22. Routledge, Taylor & Francis Group, London and New York (2009) ISBN 978-1-138-25368-1
34. Musolino, M., Massimo, D.E., F., C.'., Errigo, R.: Green building renovation of a chalet through the benefits of the 110% Superbonus. Procedural process, technical and economic-estimative aspects. Sustainability. **17**(21), 1–33. ISSN: 2071-1050 (2025). https://doi.org/10.3390/su17219566
35. Tajani, F., Cerullo, G., Stara, F., Sica, F.: Multidimensional Models for Building Decarbonization Pathways. Business Strategy and the Environment (2025). https://doi.org/10.1002/bse.70455
36. Nesticò, A., Maselli, G., Ghisellini, P., Ulgiati, S.: A dual probabilistic discounting approach to assess economic and environmental impacts. In: Environmental and Resource Economics, vol. 85, pp. 239–265. Springer Netherlands (2023). https://doi.org/10.1007/s10640-023-00766-6
37. Calabrò, F., Cassalia, G., Lorè, I.: The economic feasibility for valorization of cultural heritage. The restoration project of the reformed fathers' convent in francavilla angitola: the Zibìb territorial wine cellar. In: Smart Innovation Systems and Technologies SIST, vol. 178, pp. 1105–1115 (2021). https://doi.org/10.1007/978-3-030-48279-4_103
38. Calabrò, F., Mafrici, F., Meduri, T.: The valuation of unused public buildings in support of policies for the inner areas. The application of sostec model in a case study in condofuri (Reggio Calabria, Italy). In: Smart Innovation Systems and Technologies SIST, vol. 178, pp. 566–579 (2021). https://doi.org/10.1007/978-3-030-48279-4_54
39. Calabrò, F., Iannone, L., Pellicanò, R.: The historical and environmental heritage for the attractiveness of cities. The case of the umbertine forts of pentimele in Reggio Calabria, Italy. In: Smart Innovation Systems and Technologies SIST, vol. 178, pp. 1990–2004 (2021). https://doi.org/10.1007/978-3-030-48279-4_188
40. Calabrò, F., Lorè, I.: Evaluation aspects in the strategic planning of a reticular DMO for the promotion of inner areas of Calabria. In: Lecture Notes in Computer Science Including Subseries Lecture Notes in Artificial Intelligence and Lecture Notes in Bioinformatics LNCS, vol. 14107, pp. 54–72 (2023). https://doi.org/10.1007/978-3-031-37114-1_5
41. Calabrò, F., Lorè, I., Viglianisi, A.: The strategic planning for the promotion of cultural tourism in a wide area of Calabria: the Armeni Valley. In: Lecture Notes in Computer Science Including Subseries Lecture Notes in Artificial Intelligence and Lecture Notes in Bioinformatics LNCS, vol. 14106, pp. 485–504 (2023). https://doi.org/10.1007/978-3-031-37111-0_34
42. Spatari, G., Lorè, I., Viglianisi, A., Calabrò, F.: Economic feasibility of an integrated program for the enhancement of the byzantine heritage in the Aspromonte National Park. The case

of Staiti. In: Lecture Notes in Networks and Systems, LNNS, vol. 482, pp. 313–323 (2022). https://doi.org/10.1007/978-3-031-06825-6_30

43. Calabrò, F., Massimo, D.E., Musolinos, M.: Measures to Face Population Decline of Small Villages: Sustainable and Integrated Energy Strategies for the Internal Areas. Adv. Sci. Technol. Innov. **2022**, 43–45 (2022). https://doi.org/10.1007/978-3-031-00808-5_11

Inner Areas and Territorial Marginality in Europe: Different Policy Responses to a Common Challenge

Ludovica Nasca(✉) and Maria Rosa Trovato

Department of Civil Engineering and Architecture, University of Catania, 95124 Catania, Italy
ludovica.nasca@phd.unict.it, mariarosa.trovato@unict.it

Abstract. Territorial marginality, population decline and spatial inequalities are persistent challenges for rural and peripheral regions in Europe. This study compares the territorial policies implemented in Italy and France, which adopt proactive and reactive approaches to addressing these issues, respectively. The study adopts a qualitative comparative research design, combining document analysis with a theory-driven, case-oriented approach. A most-similar systems design (MSSD) allows for controlling structural similarities while highlighting differences in policy orientation, instruments, and territorial classification systems. The analysis was carried out at a national level, as well as through local case studies. The analysis focused particularly on the municipalities of Troina in Italy and Montargis in France. These municipalities are characterised by low population density and are experiencing depopulation. The findings reveal that, although Italy's proactive policies target high-risk areas, they are hampered by structural constraints, such as low population density, an ageing population and limited economic opportunities, which undermine their effectiveness. France's reactive policies effectively maintain demographic stability in structurally resilient municipalities but are less effective at reversing the decline in marginalised areas. The comparison highlights the importance of local context in determining policy outcomes, as well as the impact of territorial classification systems on the definition of objectives and the rationale behind interventions. It highlights the importance of a targeted, context-specific combination of proactive and reactive strategies to strengthen territorial cohesion, support demographic resilience and promote sustainable local development. It offers policymakers designing multi-level interventions in Europe's peripheral regions practical insights.

Keywords: Inner Areas · National and local territorial rebalancing policies · Italian and French experiences

1 Introduction

Among the effects of economic development that have affected Italy as a whole, particularly since the post-World War II period aspects of socio-economic and cultural imbalance have persisted and, in some cases, intensified. These are fueled by unequal

© The Author(s), under exclusive license to Springer Nature Switzerland AG 2027
O. Gervasi et al. (Eds.): ICCSA 2026 Workshops, LNCS 16761, pp. 129–147, 2027.
https://doi.org/10.1007/978-3-032-30527-5_9

regional competition between the North and the South, as well as by territorial disparities between urban/coastal areas and rural ones [1]. Official sources provide a highly informative breakdown of the extent of these imbalances, offering data on population, inclusion, education, employment, income, housing, buildings, real estate assets, the economy, the environment, infrastructure, and ser-vices. In particular, ISTAT's 8milaCensus platform represents material and social vulnerability through 99 indicators aggregated into 8 sections at the municipal and provincial scale. On this basis, it computes a composite index referring to the 1991, 2001, and 2011 censuses. The resulting maps clearly highlight the marginal condition of southern territories and less accessible areas. The transition from a predominantly agricultural and micro-manufacturing development model to a distinctly industrial one has reduced employment opportunities in southern and inland areas, triggering migratory movements. From the 1950s to the 1980s, this resulted in the large-scale transfer of labor both from the South to the North and from inland to urban areas. Similar phenomena have also occurred involving not only labor but also skills and, more recently, highly qualified human capital. From a macroeconomic perspective, the relocation of population leads to rising wages in depopulated areas and declining wages in destination areas. This is accompanied by a shift in demand for goods and services, rental housing, and real estate purchases. The sum of consumption and in-vestment increases in "receiving" areas to the same extent that it decreases in "sending" areas, thereby widening the socio-economic gap both between territories and across regions of the country. Territorial marginality, demographic decline, and spatial inequalities represent critical challenges for European regions, particularly in rural and peripheral areas. Both Italy and France have developed national strategies to address these challenges, yet the approaches differ significantly in orientation, scope, and implementation. These strategies exemplifies a targeted approach, aiming to preemptively support municipalities at risk of depopulation through enhanced service provision, local development initiatives, and multi-level governance. Both countries operate within similar institutional and European Union frameworks, providing an ideal context for comparative analysis. The primary research question guiding this study is, in what ways are the general European guidelines aimed at addressing the issue of territorial rebalancing implemented at the national and local levels? To answer this question, the study adopts a qualitative comparative research design, grounded in a case-oriented approach that combines document analysis with structured, theory-driven comparison. The analysis considers both national-level policy frameworks and classification systems and local-level case studies, exemplified by Troina (Italy) and Montargis (France), to explore how policy orientation translates into practice across different territorial contexts. The objective of the study is identify and compare the ways in which cohesion policies and these aimed at territorial rebalancing, as developed within the European context, are transposed and implemented at national level. By linking national policy frameworks with local outcomes, this study contributes to a deeper understanding of the mechanisms through which territorial policies operate and their potential to mitigate marginality.

2 Materials

The phenomenon of abandonment and the condition of depopulation [2] have constituted major drivers of territorial fragility in many inland and marginal areas, affecting both settlement systems and local socio-economic structures [3]. On the one hand, there is a lack of resources for maintaining the building, real estate, and infrastructural capital, which progressively deteriorates; on the other, the progressive reduction of population and services weakens the capacity of local communities to maintain existing territorial capital [4].

The growing interest in the phenomenon of abandonment in inland areas is also reflected in the specialized literature, with numerous contributions attempting to reinterpret small towns through strategies capable of transforming them "from a problem into a resource" [6]. The 2030 Agenda for Sustainable Development outlines general measures concerning less developed areas ("11.c: Support least developed countries, including through financial and technical assistance, in building sustainable and resilient buildings using local materials"), ensuring that culture and heritage are placed at the forefront across the broader debate on sustainable development [7].

In fragile territorial contexts, planning is called upon to identify and activate shared strategies for historic centers and settlement systems by introducing new models and opportunities for interaction and exchange into territories often affected by demographic decline and limited accessibility to services [8]. By identifying the specific characteristics, opportunities, and critical issues of these territories, it becomes possible to re-inhabit the built heritage and to reconstruct and revitalize the associated social fabric [9].

With regard to territorial disadvantage, the Italian policy framework for rebalancing known as the National Strategy for Inner Areas (NSIA) provides support measures for territories affected by structural processes of depopulation and abandonment [10]. In light of these considerations, the fragility of urban centers in inland areas can be assessed in terms of the gap between two primary economic-territorial categories: wealth and value. Small towns in inland areas constitute territorial units of high landscape, environmental, and cultural value which, being excluded from dominant development dynamics, are often unable to generate the flows of wealth necessary to sustain the underlying forms of territorial capital [11].

This condition has also contributed to the emergence of initiatives such as the "one-euro houses" phenomenon [1], frequently presented as tools for attracting new residents and investments into shrinking municipalities. However, these initiatives have produced heterogeneous and often limited results, while nevertheless highlighting broader conditions of demographic and economic fragility affecting local housing markets and existing building stock.

The policy guidelines for the revitalization of urban centers in inland areas outlined thus far identify the built and urban heritage as forms of capital capable of supporting broader processes of territorial regeneration and resilience.

2.1 Main Legal and Policy Instruments in Italy and France

Both countries face significant challenges in the field of territorial risk due to the presence of extensive rural and marginal areas, whose conditions of demographic, economic,

and environmental distress justify the development of policies aimed at rebalancing current disparities, as well as preventing higher levels of vulnerability affecting these fragile territories. Italy and France both adopt the guiding principles of European Union cohesion policies, yet they identify marginal territories through partially different criteria and strategic approaches.

In Italy, the transposition of EU policy frameworks culminates in the current National Recovery and Resilience Plan (NRRP) [12], which—although strongly shaped by the socio-economic impacts of the COVID-19 pandemic—also emphasizes prospects for territorial rebalancing. It integrates objectives related to ecological and digital transitions, as well as environmental risk reduction, particularly through Mission 2 (M2) Green Revolution and Ecological Transition, under component M2C4 Protection of Land and Water Resources, and Mission 5 (M5) Inclusion and Cohesion, under component M5C3 Special Interventions for Territorial Cohesion. Within the latter, Reform 1—aimed at strengthening Special Economic Zones (SEZs) [13]—provides investments supporting the National Strategy for Inner Areas.

In parallel with the measures adopted during the pandemic emergency, inner areas have also been supported through public funding via the Italian Fund for Marginal Municipalities [14].

For the Italian case, the primary reference framework is the National Strategy for Inner Areas (SNAI), developed within the national programming of European Structural and Investment Funds. According to this strategy, inner areas are defined as municipalities or clusters of municipalities significantly distant from essential service hubs, identified through accessibility indicators related to healthcare, education, and transport provision. The classification distinguishes between "poles" and peripheral areas according to travel time thresholds to essential services.

The territorial classification of municipalities generally combines accessibility indicators with indicators relating to demographic, socio-economic, environmental and institutional conditions. The network of municipalities that generate the NSIA is established by local authorities that apply to join it, based on a joint project for inter-municipal cooperation and the strengthening of local services and community infrastructure.

In France, the Revitalisation des centres-bourgs programme (Ministère de la Transition Écologique, 2014) [15] represents the first national initiative aimed at addressing the imbalances affecting small and medium-sized towns, which had previously been excluded from national urban policies primarily focused on grandes villes. Subsequently, in order to enhance the effectiveness of rebalancing policies in relation to the specific characteristics of the areas concerned, the French government introduced additional programmes, such as Action Cœur de Ville (Agence Nationale de la Cohésion des Territoires, 2018) [16], which aims to improve the living conditions of residents in medium-sized towns and to strengthen their leading role in territorial development.

In 2020, the programme Petites Villes de Demain (Agence Nationale de la Cohésion des Territoires, 2020) [17] was launched, targeting smaller towns and their surrounding areas, and supporting local communities in identifying dynamic pathways for their ecological transition. For the French case, the study relies on official programs and territorial classifications developed by national institutions, particularly the National Agency for Territorial Cohesion (ANCT) [18].

Rural and sparsely populated areas are often associated with the so-called Diagonal du vide, a macro-regional pattern characterized by low population density and structural socio-economic fragility, as documented by the National Institute of Statistics and Economic Studies (INSEE) [19]. Key policy materials include the national programme Petites Villes de Demain, which targets small and medium-sized towns facing demographic decline and economic contraction [17].

In Italy, territorial policies aimed at revitalising marginalised areas apply to territorial units within the group of municipalities that make up the NSIA. In France, however, they apply to individual small and medium-sized towns.

3 Method

This study adopts a qualitative comparative research design to investigate differences in territorial policy approaches between Italy and France. The study follows a most-similar systems design (MSSD), as both countries share comparable institutional frameworks as European Union member states, including access to cohesion policy funding and similar multi-level governance structures.

The analysis is conducted at two levels:

1. National level, focusing on policy frameworks, classification systems, and strategic orientations;
2. Local level, through illustrative case studies that reflect the implementation of national policies in specific territorial contexts.

The empirical material consists of a qualitative dataset of official and institutional sources, selected based on their relevance, authority, and comparability. These include:

- National policy frameworks, such as the National Strategy for Inner Areas and the French programme Petites Villes de Demain;
- Territorial classification methodologies produced by Istituto Nazionale Di Statistica (ISTAT) and Institut National De La Statistique Et Des Études Économiques (INSEE);
- Reports and policy documents from national institutions, including the Department for Cohesion Policies and the National Agency for Territorial Cohesion;
- International reports, such as those published by the United Nations Office for Disaster Risk Reduction, included as reference frameworks for interpreting territorial vulnerability and resilience within broader international risk reduction and territorial sustainability agendas;
- Local strategic plans and implementation documents, including area-based strategies for the selected case studies.

The selection of documents follows a purposive sampling strategy, aimed at capturing both the design and implementation dimensions of territorial policies.

A qualitative content analysis is developed on the selected documents, using a deductive coding scheme based on three main analytical dimensions:

1. Policy focus (service provision, spatial planning and regulation);
2. Policy instruments (financial incentives, regulatory tools, planning mechanisms);
3. Governance (multi-level coordination, role of local actors, degree of centralization).

**applied consistently to both national policy frameworks through three shared analytical dimensions:

1. Territorial targeting criteria (accessibility, demographic conditions, socio-economic fragility);
2. Policy instruments (financial incentives, planning mechanisms, service provision measures);
3. Governance and implementation scale (multi-level coordination, role of local actors, municipal or supra-municipal organisation).**

Each document was systematically coded to identify recurring policy patterns, priorities, and instruments. This approach allows for tracing how different policy logics are embedded within national strategies and local implementation practices.

To complement the national-level comparison, the study includes illustrative case studies (local level).

For Italy, the municipality of Troina was selected within the broader NSIA Strategic Area to illustrate the local implementation of a supra-municipal strategy in a peripheral rural context. For France, the municipality of Montargis was selected within the framework of the Petites Villes de Demain programme. The comparison does not aim to evaluate the overall effectiveness of the two national policies, nor to establish generalisable conclusions at the national scale. Instead, the selected municipalities are used as illustrative and context-specific examples intended to explore how different policy frameworks and territorial scales of intervention are translated into local implementation practices.

The cases are selected based on three criteria:

(i) inclusion in national programmes;
(ii) exposure to demographic decline or territorial marginality;
(iii) availability of official planning documents.

4 Results

In relation to policies supporting the development of inner and rural areas in Italy and France, and within the identified methodological framework, the following differences can be identified (Table 1).

In Italy, the implementation area corresponds to the NSIA Strategic Areas, which comprise several municipalities. In the French case, however, it corresponds to a single municipality.

Given that policies are adopted differently in terms of implementation areas in the two countries, in order to compare the modalities of policy implementation at the local level, one municipality within the NSIA Troina Strategic Area – namely the municipality of Troina – was selected as the Italian case, while the municipality of Montargis was chosen as the French case.

The comparison between these two cases is not intended to provide general conclusions regarding the overall effectiveness of the Italian and French policy frameworks at the national scale. Rather, the selected municipalities are used as exploratory case studies aimed at illustrating how different policy approaches and implementation scales

Table 1. Highlights the structural differences between the Italian and French approaches, particularly in terms of classification criteria and policy orientation, revealing a predominantly service-oriented and compensatory model in Italy, compared to a more anticipatory and spatially integrated approach in France.

Dimension	Italy	France
Definition of target areas	"Inner areas" (aree interne) defined within the National Strategy for Inner Areas as municipalities distant from essential service hubs	Rural and low-density territories often associated with the Diagonal du vide and small declining towns targeted by national programmes
Classification criteria	Accessibility-based: distance (travel time) from key services (healthcare, education, transport); classification into poles, intermediate, peripheral, and ultra-peripheral areas (based on Italian National Institute of Statistics methodology)	Multi-criteria: demographic density, socio-economic indicators, and functional roles (urban/rural typologies) defined by National Institute of Statistics and Economic Studies
Main policy framework	Place-based strategy under EU cohesion policy (NSIA), coordinated by Department for Cohesion Policies	National territorial cohesion policies coordinated by National Agency for Territorial Cohesion
Key programmes	NSIA + local "area strategies" (e.g., Troina)	Petites Villes de Demain and other rural revitalization programmes
Policy focus	Improving access to essential services; strengthening local development (healthcare, mobility, education)	Revitalization of small towns; territorial attractiveness; economic diversification; urban regeneration
Economic instruments	EU structural funds; national co-financing; support for SMEs, local production systems	Fiscal incentives; subsidies for housing and relocation; funding for local projects and infrastructure
Social/demographic measures	Counteracting depopulation through service provision and local employment strategies	Incentives for in-migration; support for remote workers; housing policies in rural areas
Innovation and digitalization	Promotion of "smart villages", digital services, and innovation in marginal areas	Strong emphasis on telework, digital infrastructure, and rural coworking spaces

(*continued*)

Table 1. (*continued*)

Dimension	Italy	France
Risk management approach	Slightly reactive/compensatory, focused on addressing service gaps and socio-economic decline	More proactive/preventive, integrating spatial planning, land-use regulation, and risk prevention
Governance model	Multi-level (national–regional–local), with strong role of local partnerships and municipalities	Central coordination with strong technical support to municipalities (ANCT), combined with local implementation
Scale of intervention	Selected pilot areas (project-based approach)	Broad national coverage (thousands of municipalities involved in programmes)

may influence local strategies for addressing marginality, demographic decline, and spatial inequalities. The analysis therefore represents a preliminary and context-specific observation of policy implementation dynamics within two distinct territorial settings.

4.1 Montargis

The case of Montargis illustrates a comprehensive and multi-level approach to urban regeneration, primarily driven by the Action Cœur de Ville (ACV) programme [16] and complemented by additional national and local policy instruments.

Beyond initial interventions in housing rehabilitation and public space renewal, the municipality has implemented a broad set of measures targeting the urban fabric, local economy, and governance structures. In terms of real estate strategies, Montargis has launched competitive calls for projects (appels à projets) aimed at the redevelopment of entire urban blocks (îlots), encouraging mixed-use development and private sector involvement [20]. These actions are supported by tools such as local commercial property vehicles (foncières commerciales), designed to acquire vacant retail units and reintroduce them into the market, thereby addressing commercial vacancy [21]. Spatial interventions extend beyond single streets to include major public space projects such as the redevelopment of Place de la République, which involved pedestrianisation, urban design improvements, and enhanced accessibility [22]. In parallel, mobility and accessibility have been addressed through the reorganisation of pedestrian and cycling networks and the exploration of sustainable urban logistics solutions, including last-mile delivery systems and local digital marketplaces [21]. The ACV programme has also been leveraged to finance public facilities, including a large educational and childcare complex (approx. €9.5 million), sports infrastructure, and the extension of district heating networks, demonstrating a broader strategy aimed at increasing residential attractiveness [23]. Importantly, Montargis integrates these physical interventions with social and cultural policies. Initiatives such as the “Jumelage Quartiers de Culture”

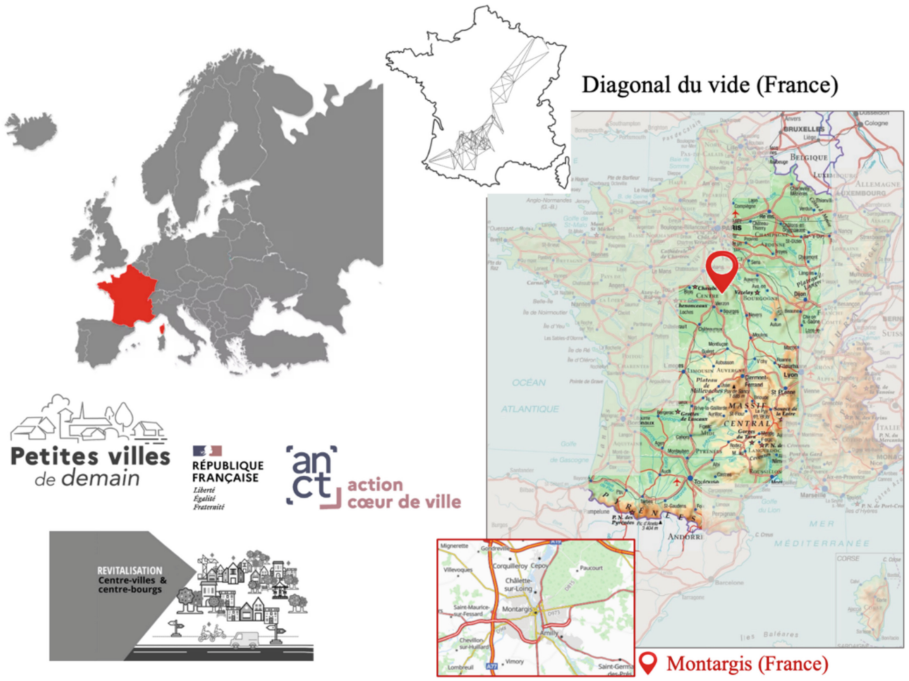

Fig. 1. Case study. French policies. Montargis, France

programme (2025–2027) promote cultural inclusion in priority neighbourhoods, while broader frameworks such as the Contrat de ville and the "Attracti'Cités" plan address social cohesion and urban inequalities [24, 25]. These actions are coordinated through the Opération de Revitalisation du Territoire (ORT), which provides a governance framework aligning multiple funding streams and policy objectives across five strategic axes: housing, commerce, mobility, public space, and services [26].

Table 2. Montargis french policies

Intervention Type	Actions Implemented	Policy Instrument	Scale	Objective	Sources
Housing & Real Estate	Rehabilitation of housing, redevelopment of urban blocks (*îlots*), calls for projects	ACV, ORT	Building / Block	Reduce vacancy, attract residents	Marchés Online; Montar
Commercial Revitalisation	Creation of commercial foncière, reuse of vacant shops	ACV	City centre	Reactivate local economy	Montar

(*continued*)

Table 2. (*continued*)

Intervention Type	Actions Implemented	Policy Instrument	Scale	Objective	Sources
Public Space	Redevelopment of Place de la République, street improvements	ACV	Urban core	Improve attractiveness, walkability	Urbicus
Mobility & Logistics	Pedestrian/cycling improvements, last-mile logistics strategies	ACV	City-wide	Accessibility, sustainable mobility	Montar
Public Facilities	School & childcare centre (€9.5 M), sports infrastructure, district heating	ACV + other funding	Neighbourhood / City	Increase residential attractiveness	Le Moniteur
Social & Cultural Policies	Cultural programmes in priority neighbourhoods	Contrat de ville, national programmes	Neighbourhood	Social inclusion	Agglomération Montargoise
Integrated Governance	Multi-sector coordination (housing, commerce, mobility, services)	ORT	Territorial	Policy integration	Ville de Montargis
Territorial Role	Coordination with surrounding small towns	ACV + indirect PVD context	Regional	Strengthen urban network	Analytical synthesis

4.2 Troina

The Inner Area of Troina represents a paradigmatic example of a place-based and multi-municipal governance model within the Italian National Strategy for Inner Areas (NSIA) [10].

Fig. 2. Case study. Italian policies. Troina, Italy

Importantly, the case does not correspond to the municipality of Troina alone, but to a wider territorial system including fourteen municipalities across the provinces of Enna and Caltanissetta, reflecting the functional rather than administrative nature of NSIA intervention areas [27, 28]. Within this framework, the strategy is structured around a dual objective: improving access to essential services – such as education, healthcare, and mobility – and fostering local development through integrated investments [10, 29]. In governance terms, the area has established forms of inter-municipal cooperation, including the creation of an Unione dei Comuni and shared administrative structures (e.g. joint planning offices, procurement units, and one-stop shops for productive activities), aimed at strengthening institutional capacity and overcoming fragmentation [30]. The strategic framework identifies five key development domains: renewable energy, natural and cultural heritage, tourism, local crafts, agro-food systems, and environmental protection [30]. Concrete interventions include investments in essential services, such as the reorganisation of school systems, enhancement of healthcare provision through innovative solutions (e.g. telemedicine and mobile diagnostics), and the development of flexible and demand-responsive transport services to improve accessibility in low-density areas [29]. Alongside these, the strategy promotes local economic development through support for agri-food supply chains, including the valorisation of traditional products, sustainable livestock systems, and innovation in production processes, as well as initiatives linked to renewable energy and circular economy practices [30]. Furthermore, the NSIA framework enables the mobilisation of multiple funding streams –national resources combined with European Structural and Investment Funds (ERDF, ESF, EAFRD)– to support integrated territorial projects [29]. Recent developments confirm the strengthening of the Troina inner area within the 2021–2027 programming cycle, with dedicated funding

aimed at infrastructure, environmental management, and service provision to counteract demographic decline and socio-economic marginalisation [31] (Table 3).

Table 3. Troina Inner Area policies

Dimension	Interventions / Actions	Policy Instrument	Scale	Objective	Sources
Territorial Structure	14 municipalities (Troina + surrounding areas)	NSIA	Inter-municipal	Functional territorial governance	Regione Siciliana; Enna Live
Governance	Union of municipalities, shared offices (planning, procurement, SUAP)	NSIA	Area-wide	Administrative capacity building	Comune di Troina
Essential Services	Schools reorganisation, healthcare (telemedicine), transport services	NSIA (national funds)	Territorial	Accessibility and quality of life	Agenzia Coesione
Mobility	Demand-responsive transport, connections to service hubs	NSIA	Area-wide	Reduce isolation	Agenzia Coesione
Local Development	Agro-food chains, local production, crafts	NSIA + EU funds	Local/regional	Economic diversification	Comune di Troina
Environment & Energy	Renewable energy, environmental protection	NSIA + EU funds	Area-wide	Sustainability	Comune di Troina
Tourism & Culture	Valorisation of natural and cultural heritage	NSIA	Territorial	Attractiveness	Comune di Troina
Funding Model	Integration of national + EU funds (FESR, FSE, FEASR)	Cohesion Policy + NSIA	Multi-level	Integrated development	OpenCoesione

While the Inner Area of Troina operates as a multi-municipal system, a focused analysis on the municipality of Troina itself is both relevant and analytically useful, as it functions as a key service and governance hub within the area. Troina plays a central role in the implementation of the National Strategy for Inner Areas (NSIA), particularly in relation to the provision and reorganisation of essential services. For instance, the municipality hosts important healthcare facilities, including specialised medical centres, which have been strengthened through NSIA-related investments and innovations such as telemedicine and integrated care models. In the field of education,

Troina acts as a central node for the reorganisation of school services across the area, helping to rationalise provision in a context of demographic decline.

At the local development level, Troina has promoted initiatives linked to agro-food production, environmental sustainability, and renewable energy, often serving as a pilot location for projects later extended to the wider area. Moreover, the municipality has been actively involved in strengthening administrative capacity through inter-municipal cooperation mechanisms, contributing to the establishment of shared governance structures and planning tools.

However, these interventions should not be interpreted as isolated municipal policies; rather, they are embedded within a broader territorial strategy, where Troina operates as a functional centre within a network of smaller municipalities. This highlights a key characteristic of NSIA: the shift from a municipality-based approach to a place-based and network-oriented model of local development (Table 4).

Table 4. Troina policies

Intervention Type	Specific Actions (Troina-focused)	Policy Instrument / Funding Source	Estimated Funding	Scale	Role of Troina	Objective
Healthcare	Strengthening local healthcare facilities; telemedicine; mobile diagnostics	NSIA + National Health Funds + ESF	~€1–3 M (service innovation projects)	Territorial	Service hub	Improve access to healthcare
Education	School network reorganisation; centralisation in key nodes	NSIA + National Education Funds	~€1–2 M	Territorial	Educational hub	Maintain services despite depopulation
Mobility	Demand-responsive transport; connections to service centres	NSIA + ERDF	~€2–4 M	Area-wide	Accessibility node	Reduce spatial isolation
Governance	Union of Municipalities; shared offices (SUAP, planning, procurement)	NSIA (capacity building)	~€0.5–1 M	Inter-municipal	Administrative centre	Strengthen institutional capacity
Agro-food	Support to local supply chains; product valorisation	EAFRD + NSIA	~€2–5 M	Local / Territorial	Pilot role	Economic diversification
Environment & Energy	Renewable energy projects; land/environmental management	ERDF + NSIA	~€3–6 M	Area-wide	Pilot territory	Sustainability transition
Cultural Heritage & Tourism	Valorisation of natural/cultural assets; slow tourism	NSIA + ERDF	~€1–3 M	Territorial	Central node	Increase attractiveness
Public Services	Strengthening administrative and social services	NSIA + national funds	~€1–2 M	Territorial	Service centre	Guarantee essential services

(*continued*)

Table 4. (*continued*)

Intervention Type	Specific Actions (Troina-focused)	Policy Instrument / Funding Source	Estimated Funding	Scale	Role of Troina	Objective
Local Development & Innovation	Circular economy, rural innovation pilots	NSIA + Cohesion Policy	~€1–3 M	Local / Area-wide	Experimental hub	Stimulate local economy

4.3 Policies Impact of Demographic's Trend

Based on the interventions identified above, the current demographic situation highlights positive impacts in some cases and unresolved issues in others.

Figure 1 shows a persistent demographic decline in Troina, from approximately 10,061 inhabitants in 2001 to 8,405 in 2023, with an average annual decrease of 1.45%. This trend reflects the town's vulnerability to outmigration and population ageing, suggesting that previous interventions under the 2014–2020 programming cycle were insufficient to halt depopulation.

The scale and pace of demographic decline indicate that policy implementation is constrained by structural and local factors, including limited economic opportunities and accessibility challenges. By contrast, Montargis maintains a relatively stable population, with minor fluctuations and a slight recovery to 14,825 inhabitants in 2023 (Table 2, Fig. 1).

Montargis' higher population density (3,392.7 vs. 49.9 inhabitants/km^2) and smaller territorial area contrast sharply with Troina's dispersed settlement pattern (Table 2). Troina's low density exacerbates challenges for delivering public services and sustaining local economies, highlighting a structural limitation that policies struggle to overcome. Italian policies are explicitly designed to target such "inner areas," yet the slow demographic recovery indicates that strategies require complementary measures in employment, mobility, and digital connectivity to be fully effective.

In Montargis, dense urban settlement facilitates access to infrastructure and public services, reducing the immediate pressure on policy interventions. Here, the French approach appears effective in maintaining baseline territorial equity, but less oriented toward actively fostering growth in lagging areas (Fig. 3), (Table 5).

Table 5. Population, age, foreigners' data

Indicator	**Troina (Italy)**	**Montargis (France)**
Area (km^2)	168.28	4.41
Resident population	8,405 (2023) (ISTAT)	14,976 (2023) (INSEE)
Population density (inhabitants/km^2)	49.9	3,392.7
Average age (years)	47.6	41.5
Average annual population change	−1.45%	+1.36%

(*continued*)

Table 5. (*continued*)

Indicator	Troina (Italy)	Montargis (France)
Percentage of foreigners	1.8%	16.5%
Population trend	**Decreasing**	**Stable / slight increase**

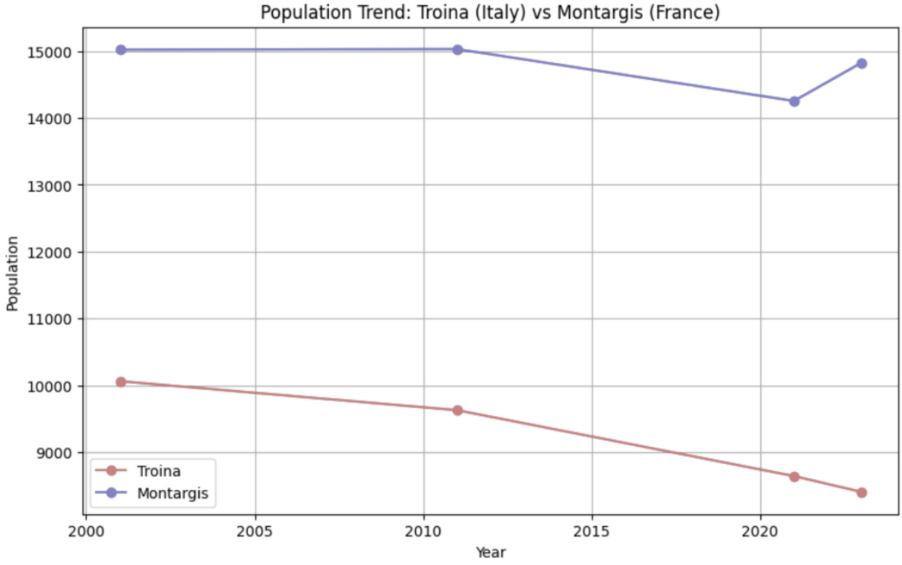

Fig. 3. Population trend

The relative demographic stability in Montargis comes from broader French territorial cohesion policies and regional development investments, which, while not highly targeted to marginal municipalities, provide infrastructural and economic support that can absorb demographic shocks. This suggests that these approaches, if properly applied, can maintain stability, though they may not actively reverse local decline in less favored areas.

Troina's population is heavily aged, with 28% over 65 and only 12% aged 0–14 (Table 2, Fig. 2). This demographic profile highlights the urgent need for structural policies to improve education, healthcare and transport links in inland areas, in order to encourage younger residents to stay. These are objectives that the NSIA has been trying to achieve, but has not yet succeeded in doing so.

Montargis exhibits a more balanced age structure, with 20% over 65 and 18% under 14. While this reflects less immediate demographic vulnerability, it also suggests that French policies benefit from pre-existing territorial advantages and are less pressured to intervene at the local scale (Fig. 4).

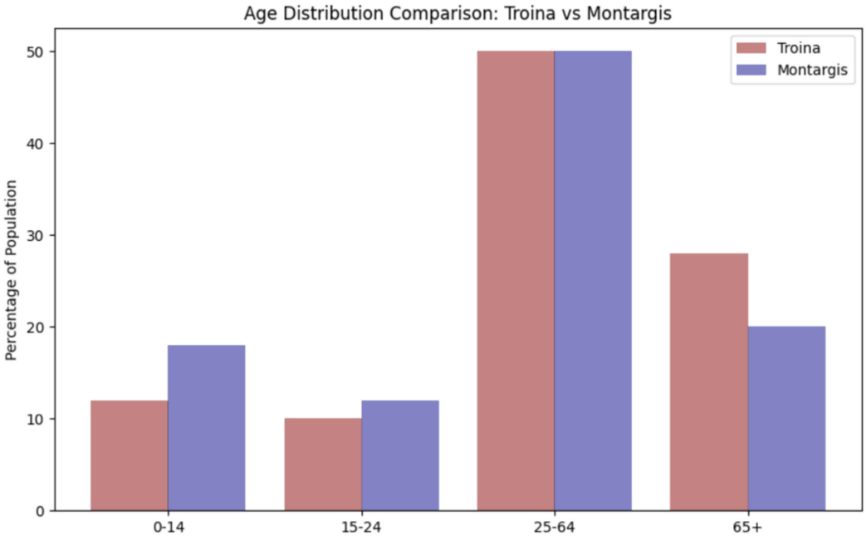

Fig. 4. Ages distribution comparison

These findings emphasise that the Italian approach is effective in areas at risk of severe depopulation. However, its success hinges on overcoming structural barriers and ensuring integrated local implementation. While the French approach maintains stability in relatively resilient municipalities, it could leave severely marginalised areas unaddressed if broader redistributive mechanisms prove insufficient.

5 Discussion and Conclusion

This study has examined differences in territorial policy orientation between Italy and France, focusing on different approaches, and has illustrated these differences through the comparative cases of Troina and Montargis.

The comparative analysis of Troina (Italy) and Montargis (France) provides significant insights into the operationalization of territorial policies and their effectiveness in addressing marginality, demographic decline, and spatial inequalities. The contrasting demographic and territorial characteristics of the two municipalities illustrate how national policy orientations interact with local conditions to shape outcomes.

Troina exemplifies a sparsely populated and aging municipality, with a population density of only 49.9 inhabitants/km^2 and an average annual population decline of -1.45%. These structural conditions highlight the inherent vulnerability of inner areas in Italy. While the Italian National Strategy for Inner Areas (NSIA) embodies an approach aimed at preemptively supporting municipalities at risk of depopulation through improved service provision, multi-level governance, and local development initiatives.

Montargis has a higher population density (3,392.7 inhabitants/km^2) and a relatively stable population, with slight growth of $+1.36\%$ annually. The municipality's demographic stability reflects the operation of France's territorial policies, which aim to maintain regional cohesion and population stability. These interventions –while not

highly targeted– provide sufficient infrastructural and economic support to buffer against demographic shocks. However, the approach does not appear designed to actively reverse decline in structurally disadvantaged or depopulating areas.

The stark contrast in population density between Troina and Montargis underscores the importance of settlement patterns in shaping policy effectiveness. Troina's low-density and dispersed population exacerbate challenges in delivering public services and sustaining local economic activity, highlighting a structural constraint that proactive policies alone may struggle to overcome. This observation suggests that successful interventions in Italian inner areas may require complementary strategies addressing employment generation, mobility infrastructure, and digital connectivity to achieve tangible demographic stabilization.

In Montargis, higher population density allows for more efficient access to public services and local infrastructure, reducing the urgency of intensive policy intervention.

The case comparison:

Italy, Troina:

- Strengths: targeted support to at-risk municipalities, anticipatory planning, emphasis on multi-level governance and local development.
- Limitations: structural constraints (low population, economic stagnation, geographic remoteness) may slow impact; implementation is resource-intensive and requires complementary measures beyond service provision.

France, Montargis:

- Strengths: effective in maintaining demographic stability and territorial cohesion where structural conditions are favorable; cost-efficient and scalable across many municipalities.
- Limitations: limited capacity to address deep-seated demographic decline or socio-economic fragility in structurally disadvantaged areas; less oriented toward transformational growth.

The analysis highlights how national regulatory frameworks interact with local structural conditions to determine both the scope and effectiveness of measures aimed at combating territorial marginalisation, demographic decline and spatial inequalities.

Political direction is important, but the local context is decisive.

Whilst Italian strategies focus on the depopulation of inland areas (NSIA), aiming to strengthen service provision, governance and local development, French strategies (Petites Villes de Demain) stabilise municipalities with relatively favourable structural conditions, but do not actively reverse the decline in heavily marginalised territories. The latter, in fact, stabilise municipalities with relatively favourable structural conditions, but do not actively reverse the decline in heavily marginalised areas.

This highlights the need to identify complementary measures regarding employment, mobility and digital connectivity to achieve tangible demographic stabilisation.

Territorial classification systems influence the definition of policy objectives.

In Italy, classifications based on accessibility focus interventions on areas distant from essential services. In France, multi-criteria classifications allow for broader coverage and stabilisation, but may overlook highly vulnerable micro-territories.

Refining territorial classification frameworks is key to ensuring that measures aimed at supporting both vulnerable and structurally stronger municipalities receive adequate attention [32].

Effective implementation requires adequate institutional capacity, including technical assistance, planning skills, and monitoring mechanisms, in order to improve policy coherence and impact. This highlights the importance of strengthening local governance and multi-level coordination in both national contexts.

Italian and French policymakers could benefit from sharing best practices: Italy can learn from France's scalable governance structures, whilst France can explore proactive, targeted measures for municipalities at risk of decline.

In this perspective, promoting the exchange of knowledge between national contexts becomes a relevant strategy to enhance policy learning and improve the adaptability of territorial interventions.

While the qualitative comparative approach enables an in-depth understanding of policy design and implementation, it presents some limitations. First, the analysis relies primarily on official documents, which may emphasize formal objectives rather than actual outcomes. Second, the case selection is illustrative rather than statistically representative. Finally, differences in administrative structures and data availability between Italy and France may affect the degree of comparability.

Despite these limitations, the study provides a structured and theory-informed comparison of territorial policies, linking classification systems, policy instruments, and governance models to broader distinctions between proactive and reactive approaches. This methodological framework enables a nuanced interpretation of how different national contexts shape responses to territorial marginality and spatial inequalities.

Disclosure of Interests. The authors have no competing interests to declare that are relevant to the content of this article.

References

1. Giuffrida, S., Trovato, M.R., Strigari, A., Napoli, G.: "Houses for one euro" and the territory. Some estimation issues for the "geographic debt" reduction. In: Bevilacqua, C., Calabrò, F., Della, S.L. (eds.) New Metropolitan Perspectives. NMP 2020. Smart Innovation, Systems and Technologies, vol. 178, pp. 1043–1052. Springer, Cham (2021). https://doi.org/10.1007/978-3-030-48279-4_98
2. Teti V.: Quel che resta. L'Italia dei paesi, tra abbandoni e ritorni. Collana: Saggi. Storia e scienze sociali, pp. XII-308, ISBN: 9788868436230 (2017)
3. Barbieri C., et al.: Architettura e progetto per la ricostruzione delle aree interne delle piccole regioni. Una strategia di sviluppo, FrancoAngeli, Milano (2019)
4. Teti V.: Il senso dei luoghi. Memoria e vita dei paesi abbandonati, Donzelli, Roma (2004)
5. Associazione Nazionale Centri Storico Artistici (ANCSA), Centro Ricerche Economiche e Sociali del Mercato dell'Edilizia (Cresme) Centri storici e futuro del paese. Indagine nazionale sulla situazione dei Centri Storici, Ancsa-Cresme (2017)
6. Trovato, M.R., Nasca, L.: Territorial rebalancing from an axiological perspective: a reaction capacity index of Sicily's inner areas. Land. **14**(9), 1916 (2025). https://doi.org/10.3390/land14091916
7. Baratta, A., et al.: Heritage Preservation: Challenges and Perspective. FrancoAngeli, Milano (2019)

8. Carluccio, M., Del Regno, R., Roselli, A.: I borghi abbandonati dell'Irpinia: un'eredità dimenticata. FrancoAngeli, Milano (2019)
9. Chimirri, R., Meijer, M.: Le culture dell'abitare tradizionale per un riuso dei paesi della Calabria. FrancoAngeli, Milano (2019)
10. Agenzia per la Coesione Territoriale, Strategia Nazionale Aree Interne (SNAI.) (2021)
11. Nasca, L., Giuffrida, S., Trovato, M.R.: Value and quality in the dialectics between human and Urban Capital of the City networks on the Land District scale. Land. **11**(1), 34 (2021). https://doi.org/10.3390/land11010034
12. Piano Nazionale di Ripresa e Resilienza (PNRR), Governo Italiano (2021). https://www.governo.it/it/pnrr.
13. Ministero dello Sviluppo Economico (MISE), Riforma delle Zone Economiche Speciali (SEZ) (2021). https://www.mise.gov.it.
14. Fondo per i Comuni Marginali, Agenzia per la Coesione Territoriale (2021). https://www.agenziacoesione.gov.it.
15. Ministère de la Transition Écologique, Revitalisation des centres-bourgs (2014). https://www.centres-bourgs.logement.gouv.fr.
16. Agence Nationale de la Cohésion des Territoiresx, Action Cœur de Ville (2014). https://agence-cohesion-territoires.gouv.fr/action-coeur-de-ville-42.
17. Agence Nationale de la Cohésion des Territoires, Petites Villes de Demain (2020). https://www.agence-cohesion-territoires.gouv.fr/petites-villes-de-demain-45.
18. Agence Nationale de la Cohésion des Territoires (ANCT), Guidelines and Territorial Classifications (2021). https://www.anct.gouv.fr.
19. INSEE (Institut National de la Statistique et des Études Économiques), Population and Socio-Economic Indicators, https://www.insee.fr.
20. Marchés Online, Appels à projets Montargis (n.d.). https://www.marchesonline.com.
21. Montar, Outils fonciers et urbanisme à Montargis (n.d.). https://www.montar.fr.
22. Urbicus, Place de la République, Montargis: Projet de réaménagement, (n.d.). https://www.urbicus.fr.
23. Le Moniteur, Montargis: Financement infrastructures publiques, (n.d.). https://www.lemoniteur.fr.
24. Agglomération Montargoise, Jumelage Quartiers de Culture 2025–2027 (n.d.). https://www.agglo-montargoise.fr.
25. Préfecture du Loiret, Contrat de ville et Attracti'Cités (n.d.). https://www.loiret.gouv.fr.
26. Ville de Montargis, Opération de Revitalisation du Territoire (ORT) – Gouvernance et axes stratégiques (2023). https://www.ville-montargis.fr.
27. Regione Siciliana, Strategia Nazionale Aree Interne – Aree interne della Sicilia (2022). https://pti.regione.sicilia.it.
28. Enna Live, Troina e i comuni SNAI, (n.d.). https://www.ennalive.it.
29. OpenCoesione, Progetti e interventi SNAI – Area di Troina, (n.d.). https://www.opencoesione.gov.it.
30. Comune di Troina, Piano strategico intercomunale per le Aree Interne (2023). https://www.comune.troina.en.it.
31. Regione Siciliana, Programmazione 2021–2027: Rafforzamento delle Aree Interne di Troina (2025). https://pti.regione.sicilia.it.
32. Trovato, M.R., Nasca, L.: An axiology of weak areas: the estimation of an index of abandonment for the definition of a cognitive tool to support the enhancement of inland areas in Sicily. Land. **11**(12), 2268 (2022). https://doi.org/10.3390/land11122268

Short-Term Rentals in Rural Areas: Sustainable Tourism Perspectives Artificial within the SYSTOUR Project

Roberta Butticè[1], Asja Aulisio[2], Giorgia Malavasi[2(✉)], and Diana Rolando[2]

[1] OWAC Engineering Company, Via Resuttana, 360, 90146 Palermo PA, Italy
r.buttice@owac.it

[2] Department of Architecture and Design, Politecnico di Torino, Viale P.A. Mattioli 39, 10125 Torino, Italy
{asja.aulisio,giorgia.malavasi,diana.rolando}@polito.it

Abstract. The rise of short-term rentals, fueled by digital platforms, is changing tourism trends in rural areas. These changes have implications for rural development in the transition towards more sustainable and place-based tourism models. This study aims to explore how short-term rentals contribute to sustainable tourism in six rural areas across Europe, as part of the SYSTOUR project. The research uses a mixed-method approach that combines both quantitative and qualitative analyses. A structured database of short-term rental listings was developed using Airbnb data, including spatial, economic, and service-related factors. Descriptive statistics and spatial analysis were supplemented by participatory workshops with local stakeholders. These workshops were guided by the Systemic Policies Model Canvas to examine governance dynamics and future scenarios. The results revealed a polycentric distribution of short-term rentals, with clusters located around important cultural and natural sites. A dual market structure emerged: Southern and Western regions experience significant seasonal price changes, while Central and Northern regions have more stable pricing patterns. The analysis also highlighted how accessibility and local appeal impact pricing and distribution, along with common governance issues. Short-term rentals can aid in rural regeneration by redistributing tourism flows and increasing local value creation. However, their success relies on coordinated, place-based governance strategies that combine data-driven insights with stakeholder involvement.

Keywords: Short-term rental · Sustainable Tourism · Rural Areas

1 Introduction

In recent decades, tourism has experienced persistent growth and diversification, becoming a key driver of economic development while simultaneously generating significant socio-territorial pressures [1]. In response to the negative externalities associated with mass tourism, such as spatial concentration, environmental degradation, and social conflict, academic research and policy agendas have increasingly called for more sustainable,

© The Author(s), under exclusive license to Springer Nature Switzerland AG 2027
O. Gervasi et al. (Eds.): ICCSA 2026 Workshops, LNCS 16761, pp. 148–161, 2027.
https://doi.org/10.1007/978-3-032-30527-5_10

inclusive, and territorially balanced tourism models. Within this transition, rural areas have gained attention as potential spaces for redistributing tourist flows and fostering place-based development. Rural areas can be defined as non-urbanised geographical areas, such as inland regions, the countryside, coastal landscapes, or mountainous areas, characterised by small- and medium-sized settlements and low population density [2]. In this context, the concept of rural tourism emerges, which the World Tourism Organisation (UNWTO) defines as a type of tourism activity in which the visitor's experience is connected to a wide range of experiences, generally related to nature, agriculture, and a simple and traditional lifestyle [1–3]. The characteristic elements of this type of tourism are closely linked to the territory [4, 5], the local economy [6], and the community [7].

At the same time, the rapid diffusion of digital platforms has profoundly reshaped the hospitality sector in rural areas [8]. Short-term rentals, mediated by online platforms, have expanded well beyond urban contexts, increasingly affecting rural and peripheral areas [9]. Despite their growing relevance, the role of short-term rentals in rural tourism systems remains insufficiently explored, particularly in terms of their interaction with local socio-economic structures [10], governance capacity [11, 12], and sustainability objectives [13].

Against this background, this paper aims to analyse the short-term rental market in six European rural areas [14, 15], with particular attention to the impact of digital platforms on the transformation of local hospitality systems and to the related pricing dynamics. Adopting a systemic approach, the research combines past experiences [16, 17], recent theoretical contributions, co-design experiences and short-term rental market data analysis to examine how emerging platform-mediated accommodation influences social, economic, and territorial tourism dynamics in rural contexts. The study is characterised by a multiscalar perspective and integrates quantitative and qualitative analysis tools, including descriptive and spatial statistical analysis, and visual design methods, in order to address the complexity of contemporary rural tourism systems [18].

The study is developed within the framework of the European project SYSTOUR (Systemic approach for sustainable tourism strategies in rural areas) [19] and focuses on six rural regions across Europe.

The research addresses the following questions:

- What are the main structural and spatial characteristics of short-term rental markets in European rural areas?
- How do short-term rentals interact with local socio-economic and territorial dynamics in rural contexts?
- How can systemic design tools support governance strategies for sustainable rural tourism development?
- How do pricing variability, seasonal demand, and territorial accessibility influence the spatial distribution and market behaviour of short-term rentals across different European rural regions?

The paper is structured as follows: Sect. 2 presents the Methodological framework and the Case Study of the present research; results are discussed in Sect. 3, which illustrates the empirical findings; and Sect. 4 reflects on the conclusion, policy implications and future research directions.

2 Materials and Methods

The following sections present the methodological framework of the research (Sect. 3.1) and the territorial context in which it is applied (Sect. 3.2). The study is grounded in a systemic perspective that integrates data-driven analysis with participatory processes, allowing for a comprehensive understanding of short-term rental dynamics in rural areas.

2.1 Methodological Framework

The methodological framework is structured as a sequence of interconnected analytical phases aimed at investigating the phenomenon of short-term rentals in rural areas.

The research combines qualitative and quantitative approaches, enabling the integration of empirical data, spatial investigation and participatory insights from local stakeholders in order to capture the multidimensional nature of tourism dynamics in rural territories. This mixed-method approach allows the study to address both the structural characteristics of the short-term rentals market and the experiential dimension of tourism practices.

The methodological path begins with the research objectives definition (Phase 1) and a focused literature review (Phase 2 – Background) aimed at identifying the main theoretical frameworks related to the topics of sustainable tourism, rural development and the diffusion of short-term rentals. Within this context, the study examines how these forms of accommodation influence tourism development in rural areas in targeted regions.

Subsequently, data collection is conducted in Phase 3: a qualitative approach based on participatory World Café workshops, is integrated by quantitative analyses involving the collection of short-term rental data from short-term platforms. In particular, a database is developed through the collection, harmonisation, and coding of real estate data related to short-term rental listings available on the selected platform in a defined time period. In the following Phase 4 (Implementation of Database and systemic policies canvas), it is necessary to define metadata and variables describing accommodation characteristics, services offered in the study area, pricing dynamics, user ratings and geographic coordinates of records. This database enables the definition of the objective and structure of the systemic policies canvas, the integration of statistical and spatial analyses in the following Phase 5 (Data processing) and supports a comparative analysis across the selected case studies in different rural contexts.

Data analysis combines qualitative and quantitative approaches. Participatory outputs are interpreted to develop future-oriented scenarios. The short-term sample from platforms is analysed using descriptive statistics, mapping, and exploratory spatial data analysis (ESDA). In parallel, the research incorporates participatory activities [20], involving local stakeholders through workshops supported by the formalisation of visual canvas models [21] (Phase 4), which facilitates collaborative reflection [22] on local tourism dynamics and contribute to the identification of innovative directions [23] for sustainable rural tourism strategies development (Fig. 1).

Fig. 1. Methodological framework of the present research (Elaboration of the authors on Butticè, 2025)

2.2 Case Study: The Empirical Analysis within the SYSTOUR Project and the Co-design Session with Partners and Stakeholders

This study examines six rural regions selected for the SYSTOUR project (Fig. 2). These areas provide a balanced geographical representation across Europe: Molise in Italy, Nouvelle-Aquitaine in France, Lea-Artibai in Spain, Central Ostrobothnia in Finland, Świętokrzyskie in Poland, and Hajdú-Bihar in Hungary. The regions involved in the SYSTOUR project are characterised by the presence of inland rural areas undergoing sustainable tourism transformation. These regions share common challenges, including depopulation, seasonal tourism demand, and limited accessibility, while also displaying diverse territorial identities and governance structures [24, 25]. SYSTOUR expects to support territorial policies and strategies in close dialogue with stakeholders located within the selected regions. The approach used for this research recognises the effectiveness of a deep understanding of the interconnected and interdependent elements in change and transformation processes, often grounded in data, information, and knowledge systems.

Fig. 2. Geographic location of the six rural regions (Authors' elaboration)

The phenomenon of short-term rentals in European rural areas [8–10, 18] presents itself as a complex system, shaped by a multiplicity of interrelated factors (such as regulatory, economic, infrastructural and social). To analyse its dynamics in depth, it is necessary to adopt an approach that captures these interconnections and provides

an integrated view of the territorial system. To implement this systemic perspective, the adoption of specially designed canvas models (examined in greater depth in the following sections) facilitates interaction, communication, and strategies co-creation with local stakeholders in contexts characterised by high levels of complexity.

3 Results

The following two sections present the research results. They combine insights from participants in Sect. 3.1 with a data-based analysis of short-term rental listings in Sect. 3.2. This approach explores the dynamics of short-term rentals in rural areas. This part of the study builds on the methods outlined in Sect. 2 and the research conducted in the SYSTOUR project. It shows how a systematic interpretation, based on real evidence, can help create more sustainable and context-sensitive tourism strategies. The two analytical components are closely linked. Insights from the participatory workshops helped shape the research focus. They also guided the choice of variables and the geographic area for the following data-driven analysis on short-term rental listings.

3.1 Systemic Policies Canvas

The organisation and setup of participatory workshops represented a key phase in activating co-design processes with local stakeholders and in collectively validating the analytical and design hypotheses developed. The workshop sessions followed the World Café methodology [26], a widely recognised collaborative facilitation method known to fostering mutual listening and convergence towards shared visions. The World Café can be understood as a simple yet effective dialogic tool for stimulating collective reflection, knowledge sharing, and the generation of design ideas through meaningful conversations among small groups of participants [27].

To manage the participatory session, a set of systemic policies canvas was designed to represent interactions concisely and coherently, articulated into two complementary visual formats presented as separate posters. The first canvas adopts an operational and design-oriented perspective, supporting a systematic reflection on enabling factors and barriers to the development of short-term rentals in rural areas, including infrastructural needs, regulatory constraints, and policy priorities. The second component takes a forward-looking perspective and focuses on long-term dynamics, fostering strategic visioning on future scenarios, emerging trends, and systemic transformation processes.

The workshops included project partners and local stakeholders from the six SYSTOUR regions, representing various institutional, professional, and territorial viewpoints. The application of the canvas followed a sequence of phases which allowed participants to identify critical elements, interdependencies, and emerging patterns depending on their knowledge of the study area and their backgrounds. Through facilitated discussion, the canvas fosters shared understanding and collective reflection among stakeholders [21]. The resulting outputs are then analysed to interpret systemic dynamics and to identify strategic directions for the case study. In this way, the canvas functions not only as an analytical device, but also as a tool for co-design and alternative scenario-building [22], supporting the development of sustainable [28] and context-sensitive strategies.

The collected information was then reorganised to hypothesise evolutionary scenarios. The components related to innovation, pricing, accessibility, relationships, and storytelling are positioned along a dual interpretative axis that distinguishes between what is visible and measurable (such as data, prices, services) and what is latent or emerging (like emotions, perceptions, expectations). In this way, scenario-building is not reduced to a predictive exercise, but becomes an exploratory and strategic tool, useful for examining the future conditions for rural tourism in terms of sustainability, territorial cohesion, quality of living, and new forms of hospitality.

The results emerging from the workshop session were oriented towards the construction of future scenarios and the identification of evolutionary trajectories for the short-term rental sector in European rural areas. The starting point for building the models was the analytical results from the previous phases: quantitative data, spatial analyses, and workshop outputs. These elements were then reinterpreted holistically, with the aim of constructing matrices of relationships among key variables, including local regulations, accessibility infrastructure, pricing strategies, the quality of host–guest relationships, the presence of welcoming communities, and the use of technologies and the degree of experiential innovation.

At the end of the sessions, the workshop concluded with a plenary feedback session, in which each moderator presented the main findings from their table, highlighting both shared perspectives and differences in viewpoints (Fig. 3).

The material produced during the participatory workshops was analysed to systematise the content that emerged from completing the canvas models. The qualitative analysis of the results enables the identification of shared perspectives, local challenges, and operational proposals, thereby contributing to the development of intervention strategies grounded in needs directly expressed by local stakeholders.

As a further creative output of the workshop, a ‘postcard from the future’ (Fig. 4) was produced through a generative prompt developed with artificial intelligence, offering an evocative and synthetic vision of rural hospitality in 2050.This narrative imagines a Europe where tourism serves as a regenerative tool. It focuses on genuine relationships, slow and personalized experiences, and lightweight technologies. However, the AI-generated image shows some limitations in capturing the identity of places. It lacks recognizable, place-based elements, making it hard to link the scene to a specific region, such as Molise or Poland. This points to a larger problem with generative AI; its visual outputs often create uniform and detached representations. This raises important questions about how well they convey local identity and regional uniqueness.

3.2 Data-Driven Analysis on Short-Term Listings

The analysis of short-term market trends across the six rural regions examined in the SYSTOUR project showed a varied short-term rental market influenced by local conditions and seasonal demand. Using the organised database and the spatial analyses created in the first phase of the SYSTOUR project, this research brought together descriptive summary statistics, thematic maps, and visual comparisons to show how pricing differs across the six European regions.

Data were collected from the Airbnb platform [29] between November 2024 and January 2025 using a specific sampling method. This was aimed at ensuring a balanced

Fig. 3. Workshop session and template of "Systemic Policies Model Canvas" completed by participants during the workshop, Turin, March 2025. (Source: Butticè, 2025)

representation of listings across the territories being studied. For each country, around 30 listings were chosen from a group of eight to twelve municipalities. These were identified based on their relevance to the study areas of the SYSTOUR project. Given the relatively small sample size, the findings should be interpreted as exploratory; they are not intended to be statistically representative of the broader short-term rental market, nor generalisable beyond the analysed cases. The choice of listings was not made randomly. It depended on verifying their geographical location and ensuring they fell within municipal or sub-municipal boundaries that matched the Good Governance and Practices (GGPPs) areas, identified and confirmed by regional project partners during the SYSTOUR project. For the short-term rental analysis, priority was given to municipalities that were either hosting or close to the GGPPs areas.

As these GGPPs represented key points for the analysis, short-term rental records were included only if their geographical location matched the defined reference areas. The database was designed to include listing-level features such as accommodation type, location, accessibility, rating, and average price per guest in both low and high seasons. This allows for both regional comparisons and localised interpretations of market trends.

An initial comparative result highlighted a clear divide between Mediterranean/Atlantic and Central-Northern European contexts. France, Spain, and Italy show

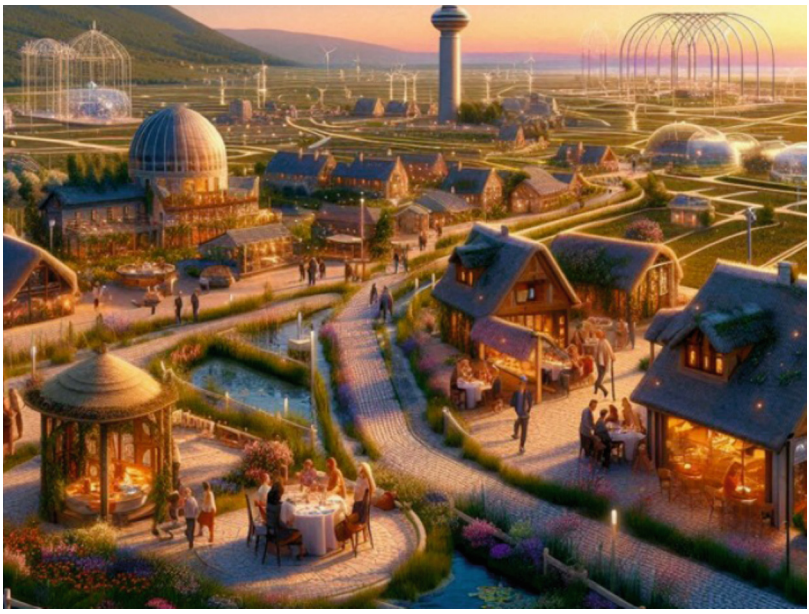

Fig. 4. AI-generated creative vision representing the desired future of rural tourism. (Source: Butticè, 2025)

a stronger seasonal pricing structure, with significant increases during the peak tourist season. Meanwhile, Poland, Finland, and Hungary have more stable price patterns throughout the year (Fig. 5).

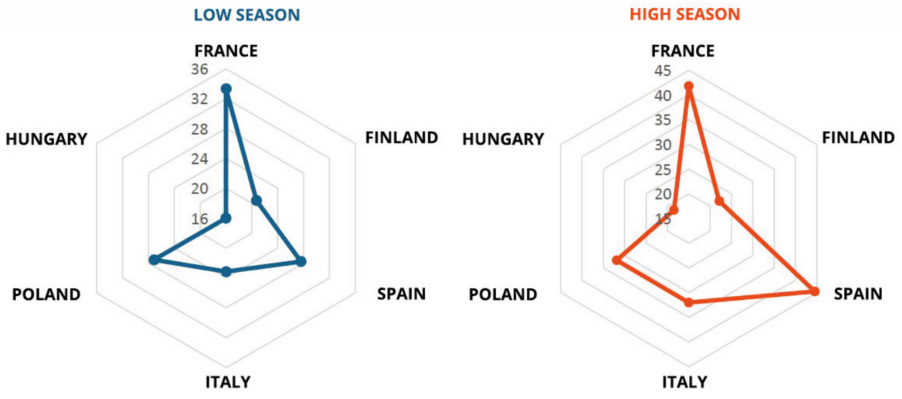

Fig. 5. Spider chart showing the average price per guest per night in the high season (orange) and low season (blue) across the six countries analysed. (Source: Butticè, 2025)

This pattern suggests that in the southern and western case studies, hosts tend to adopt a more demand-responsive pricing strategy, calibrating rates to summer high-season

peaks and the concentration of tourist flows. By contrast, in the northern and eastern regions, the lower seasonal gap indicates a more balanced and temporally distributed demand, which corresponds to less volatile pricing behaviour. The highest high-season averages (price per person per night) are in Spain (44.53 €) and France (41.83 €), followed by Italy (32.01 €), Poland (31.87 €), Finland (22.14 €), and Hungary (18.47 €).

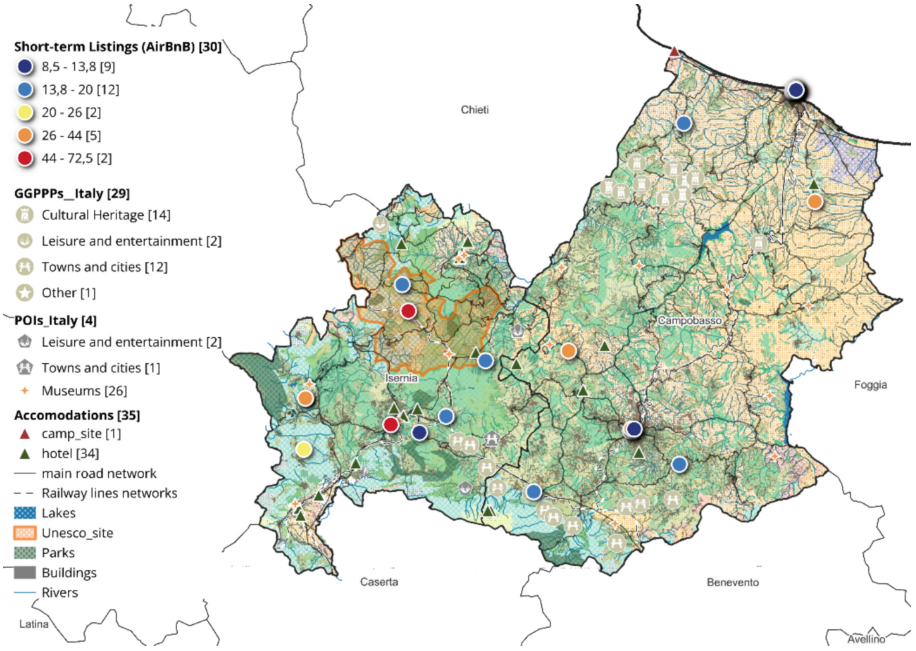

Fig. 6 The Molise Region in Italy, example of a territorial map (Elaboration of the authors)

The territorial map (Fig. 6) further refined this analysis by showing that pricing is not only shaped by macro-regional seasonality, but also by micro-spatial factors such as proximity to coasts, urban centres, railway stations, and tourism services. In the Molise case, for instance, the spatial distribution of prices highlights higher values in coastal and more central areas of Termoli, while more peripheral zones remain associated with lower rates. The map integrates price classes (ranging approximately from €34 to over €100) with the distribution of points of interest (particularly cultural heritage sites, leisure facilities, and accommodation types), revealing a partial spatial correspondence between higher prices and areas with greater tourism infrastructure and attraction density.

The statistical descriptive analyses results confirmed this tendency (Table 1): the average price per guest per night rises from 23.15 € in low season to 32.01 € in high season, corresponding to an absolute increase of 9.35 € and a relative increase of + 56.85%. This substantial gap indicates that market trends in emerging rural destinations are strongly influenced by seasonal demand pressure and by the uneven spatial distribution of local attractiveness.

Table 1. Statistical distribution of short-term accommodation prices per guest per night in Molise (Italy), comparing low and high seasons. (Elaboration of the authors on Butticè, 2025)

Season	Min (€)	Max (€)	Mean (€)	Median (€)	Weighted Mean (€)	Std. Dev.	Absolute Delta (€)	Relative Delta
Low season	8.5	72.5	23.15	17.5	20.07	15.3	9.35	56.85%
High season	12.5	68.5	32.01	31.76	30.37	13.01		

Overall, the combined reading of database outputs, thematic maps, and descriptive statistics showed that rural short-term rental markets cannot be interpreted as purely economic adjustments. Rather, they reflect the interaction between seasonal tourism intensity, territorial accessibility, and the degree of market consolidation in each region. From this perspective, price variability serves as a useful proxy for understanding not only market performance but also the different levels of maturity, resilience, and temporal diversification that characterise rural tourism systems across Europe.

4 Conclusion

This research confirms that short-term rentals, particularly those mediated by platforms such as Airbnb, represent an increasingly relevant component of rural tourism systems in Europe, contributing to their diversification and potential sustainable development. Moving beyond the initial hypothesis, the results demonstrate that rural areas are not marginal within the contemporary tourism landscape [30]; rather, they are integrated into new paradigm and differentiated real estate market structures.

The analysis of the short-term rental market across the six regions shows a clear pattern that goes beyond just the Molise case. A key finding is the rise of a dual market setup at the European level. Southern and Western regions, like Italy, Spain, and France, experience strong seasonal price swings. Prices can jump significantly during peak times, such as an increase of up to 56.85% in the Molise case. This reflects a pricing strategy driven by demand, which is closely connected to high tourist traffic. In contrast, Central and Northern regions, including Poland, Finland, and Hungary, have more stable pricing. This stability suggests a more even demand throughout the year and less noticeable seasonality. This difference shows how geography and tourism demand shape market dynamics. At the territorial level, the findings show that pricing is affected not only by seasonal changes but also by local factors. The distribution of listings shows a polycentric pattern, with clusters of short-term rentals focused around important cultural, natural, and infrastructure resources. Being close to coasts, urban centres, transport hubs, and tourism services plays a key role in determining prices and the density of accommodations. The Molise case illustrates a wider trend seen in the study areas: higher prices tend to be linked to areas with better accessibility and a greater number of attractions, while more remote areas stay in lower price ranges. The combination of statistical analysis, spatial mapping, and database structuring shows that pricing strategies in rural short-term

rental markets cannot be viewed just as economic changes. Instead, they represent the interaction between seasonal tourism intensity, territorial accessibility, and the level of market consolidation. In this context, price variability serves as a way to understand larger structural conditions, including the maturity, competitiveness, and seasonal diversity of rural tourism systems.

The participatory dimension of the research, developed through the Systemic Policies Model Canvas, supports these findings by pointing out shared systemic challenges in different regions. These challenges include fragmented governance, limited infrastructure, and the need for coordinated policy frameworks. Using AI-supported tools in workshops has improved the ability to gather stakeholder perspectives in real time. This change helps create better co-design processes and supports decision-making based on evidence.

Overall, the study suggests that short-term rentals can drive territorial regeneration when included in clear policy strategies and inclusive governance models. They can shift tourism flows, highlight local assets, and offer flexible accommodation options. This makes them an important tool for rural development. Lastly, these findings highlight the need to view short-term rentals not as separate market issues, but as important parts of place-based development strategies. They can help create more balanced, strong, and sustainable rural tourism systems across Europe.However, some limitations still exist, especially regarding the sample size and its representativeness. Expanding the dataset and adding long-term analyses would provide a clearer view of changing market dynamics and improve the strength of future research.

Acknowledgments. The SYSTOUR project is funded by Interreg Europe (2021–2027), with project ID 01C0279. It is relevant to give a special acknowledgement to all SYSTOUR partners: Politecnico di Torino (IT), Molise Region (IT), Hajdú-Bihar County Government (HU), Leartibai Foundation (ES), APESA and Nouvelle-Aquitaine Regional Council (FR), Marshal Office of ´Swi¸etokrzyskie Region (PL), Central Ostrobothnia Regional Council (FI), who are supporting the process of the research project. This contribution builds upon the Master's thesis "Analysis of the Short-Term Rental Market in Six Rural Areas in Europe: A Systemic Approach to Sustainable Tourism Development" by Roberta Buttice' (Politecnico di Torino, Master's Degree Programme in Systemic Design, 2025), supervised by Diana Rolando, Asja Aulisio, and Giorgia Malavasi, developed within the framework of the SYSTOUR project.

Author Contributions. This paper is to be attributed in equal parts to the authors. Conceptualisation, D.R. A.A. G.M.; data curation, R.B.; formal analysis, R.B.; investigation, D.R. A.A. G.M. R.B.; methodology, D.R. A.A. G.M.; supervision, D.R.; writing—original draft, A.A. G.M. R.B.; writing—review and editing, D.R. A.A. G.M. All authors have read and agreed to the published version of the manuscript.

Disclosure of Interests.. The authors have no competing interests to declare that are relevant to the content of this article.

References

1. Ladu, M., Battino, S., Balletto, G., Amaro García, A.: Green infrastructure and slow tourism: a methodological approach for mining heritage accessibility in the Sulcis-Iglesiente bioregion (Sardinia, Italy). Sustainability 2023. **15**, 4665 (2023). https://doi.org/10.3390/su15054665

2. Olimovich, S.O.: Agrotourism as one of the prospective directions of the tourist industry. Am. J. Soc. Sci. Educ. Innov. **2**, 254–259 (2020). https://doi.org/10.37547/tajssei/volume02issue09-39
3. Lumsdon, L.M., McGrath, P.: Developing a conceptual framework for slow travel: a grounded theory approach. J. Sustain. Tour. **19**, 265–279 (2011). https://doi.org/10.1080/09669582.2010.519438
4. Dezio, C.: A bioregional reading of the rural landscapes of the Italian inner areas and the regenerative potential of rural tourism. The case study of the VENTO project. Ciudades. 49–69 (2020). https://doi.org/10.24197/CIUDADES.23.2020.49-69.
5. Liu, S., Ge, J., Bai, M., Yao, M., He, L., Chen, M.: Toward classification-based sustainable revitalization: assessing the vitality of traditional villages. Land Use Policy. **116**, 106060 (2022). https://doi.org/10.1016/j.landusepol.2022.106060
6. Balletto, G., Milesi, A., Ladu, M., Borruso, G.: A dashboard for supporting slow tourism in green infrastructures. A methodological proposal in Sardinia (Italy). Sustainability (Switzerland). **12**, 3579 (2020). https://doi.org/10.3390/SU12093579
7. Sharma, G.D., Thomas, A., Paul, J.: Reviving tourism industry post-COVID-19: a resilience-based framework. Tour. Manag. Perspect. **37**, 100786 (2021). https://doi.org/10.1016/j.tmp.2020.100786
8. Almeida-García, F., Monserrat-Febrer, A., Cortés-Macías, R., Coll-Ramis, M.À.: Touristification and expansion of short-term rentals in Mediterranean destinations: the case of rural areas. Land (Basel). **14**, 881 (2025). https://doi.org/10.3390/land14040881
9. Adenegan, M.A., Yusuf, J.A.: Airbnb's role in rural housing shortages: a case study of Sussex. Manage. Analytics Soc. Insights. **2**, 265–274 (2025). https://doi.org/10.22105/masi.v2i4.80
10. DiNatale, S., Lewis, R., Parker, R.: Short-term rentals in small cities in Oregon: impacts and regulations. Land Use Policy. **79**, 407–423 (2018). https://doi.org/10.1016/j.landusepol.2018.08.023
11. Guttentag, D.: Airbnb: disruptive innovation and the rise of an informal tourism accommodation sector. Curr. Issue Tour. **18**, 1192–1217 (2015). https://doi.org/10.1080/13683500.2013.827159
12. Martin, C.J.: The sharing economy: a pathway to sustainability or a nightmarish form of neoliberal capitalism? Ecol. Econ. **121**, 149–159 (2016). https://doi.org/10.1016/j.ecolecon.2015.11.027
13. Zemła, M.: Reasons and consequences of overtourism in contemporary cities-knowledge gaps and future research. Sustainability (Switzerland). **12**, 1729 (2020). https://doi.org/10.3390/su12051729
14. Barca, F., Casavola, P., Lucatelli, S.: A strategy for Inner Areas in Italy: definition, objectives, tools and governance. Materiali Uval Series (2014)
15. Rossitti, M., Dell'ovo, M., Oppio, A., Torrieri, F.: The Italian national strategy for inner areas (SNAI): a critical analysis of the indicator grid. Sustainability (Switzerland). **13**, 6927 (2021). https://doi.org/10.3390/su13126927
16. Ferretti, M., Favargiotti, S., Lino, B., Rolando, D.: (a cura di): Atlante – BRANDING4RESILIENCE. Ritratto di quattro territori interni italiani. LetteraVentidue Edizioni S.r.l., "in press," Siracusa (2024)
17. Rolando, D., Rebaudengo, M., Barreca, A.: From vulnerability to vibrancy: Cross-dimensional indexes for the evaluation of inner areas. Paper submitted to International Journal of Urban and Regional Research (2024)
18. Buttice', R.: Analisi del mercato degli affitti brevi in sei aree rurali d'Europa: un approccio sistemico per lo sviluppo del turismo sostenibile = Analysis of the short-term rental market in six rural areas in Europe: a systemic approach to sustainable tourism de (2025). https://webthesis. biblio.polito.it/36014/?template=default

19. SYSTOUR - Systemic approach for sustainable tourism strategies in rural areas | Interreg Europe, https://www.interregeurope.eu/systour, last Accessed 27 Mar 2026
20. Sanders, E., Stappers, P.: Co-creation and the new landscapes of design. CoDesign. **4**, 5–18 (2008)
21. Osterwalder, A., Pigneur, Y.: Business Model Generation: a Handbook for Visionaries, Game Changers, and Challengers. A Handbook for Visionaries, Game Changers, and Challengers, vol. 288, (2010). https://doi.org/10.1523/JNEUROSCI.0307-10.2010
22. Moscardo, G.: Building community capacity for tourism development. 184 (2008)
23. Manzini, E.: Design, when everybody designs: an introduction to design for social innovation. 241 (2015).
24. Apostolopoulos, N., et al.: Sustaining rural areas, rural tourism enterprises and EU development policies: a multi-layer conceptualisation of the obstacles in Greece. Sustainability (Switzerland). **12**, 7687 (2020). https://doi.org/10.3390/su12187687
25. Johansen, P.H., Nielsen, N.C.: Bridging between the regional degree and the community approaches to rurality—a suggestion for a definition of rurality for everyday use. Land Use Policy. **29**, 781–788 (2012). https://doi.org/10.1016/j.landusepol.2011.12.003
26. Löhr, K., Weinhardt, M., Sieber, S.: The "World Café" as a Participatory Method for Collecting Qualitative Data. Int. J. Qual. Methods. **19** (2020). https://doi.org/10.1177/1609406920916976
27. Brown, J., Isaacs, D.: The World Café – Shaping Our Futures through Conversations that Matter. J. Organ. Change Manage. **19**, 266–268 (2006). https://doi.org/10.1108/09534810610648951
28. Joyce, A., Paquin, R.L.: The triple layered business model canvas: a tool to design more sustainable business models. J. Clean. Prod. **135**, 1474–1486 (2016). https://doi.org/10.1016/j.jclepro.2016.06.067
29. Airbnb | Case vacanze, baite, case sulla spiaggia e molto altro ancora, https://www.airbnb.it/, last Accessed 27 Mar 2026
30. Musacchio, L.R.: The scientific basis for the design of landscape sustainability: a conceptual framework for translational landscape research and practice of designed landscapes and the six Es of landscape sustainability. Landsc. Ecol. **24** (2009). https://doi.org/10.1007/s10980-009-9396-y

Reinforcing Local Safety Ecosystems: Integrating the "Signal for Help" Detection in Urban and Inner Territories

Federico Buccellato(✉), Sarah Azimi, Corrado De Sio, and Luca Sterpone

Dipartimento di Automatica e Informatica, Politecnico di Torino, Turin, Italy
{federico.buccellato,sarah.azimi,corrado.desio,luca.sterpone}@polito.it

Abstract. The *Signal for Help* is a discrete hand gesture that allows a person in a situation of risk to ask for help without speaking and without attracting the attention of a potential aggressor. Although the gesture is widely recognized, it produces a concrete effect only if it is detected promptly and if the alert reaches someone able to intervene. This paper addresses the gap between recognition and intervention by examining how a gesture detection system can be integrated into existing territorial security infrastructures.

Building on a previously validated recognition model, the work focuses on its effective integration into existing video surveillance networks, operational workflows, and local security services. The analysis highlights the architectural, organizational, and governance conditions that enable a sustainable and responsible implementation, both in urban contexts with higher institutional density and in inner areas characterized by more limited resources.

From this perspective, the contribution shows how a silent signal can be incorporated into a structured and traceable decision-making chain, strengthening local security ecosystems while maintaining human oversight and compliance with data protection principles.

Keywords: Signal for Help · Territorial Security · AI for Social Good · Privacy-by-Design · Territorial Deployment

1 Introduction

One in three women worldwide experiences physical or sexual violence during her lifetime [1]. This figure is not merely a statistic; it reflects a structural condition of vulnerability that spans different social, geographic, and cultural contexts. In many cases, a person at risk is not able to ask for help explicitly. She may be under the direct control of the aggressor, in a situation where a verbal request would immediately attract his attention.

During the COVID-19 pandemic, forced isolation and reduced social interaction made this vulnerability even more visible. In this context, the *Signal for Help* was introduced, a simple and silent hand gesture designed to allow a person

© The Author(s), under exclusive license to Springer Nature Switzerland AG 2027
O. Gervasi et al. (Eds.): ICCSA 2026 Workshops, LNCS 16761, pp. 162–176, 2027.
https://doi.org/10.1007/978-3-032-30527-5_11

to indicate that she is in danger without speaking. The gesture is performed by raising one hand with the palm facing outward, folding the thumb into the center of the palm, and then closing the remaining fingers over it, as shown in Fig. 1. The sequence is discreet but intentional and can be recognized by those who are familiar with its meaning. In several documented cases, its correct interpretation enabled timely interventions [2].

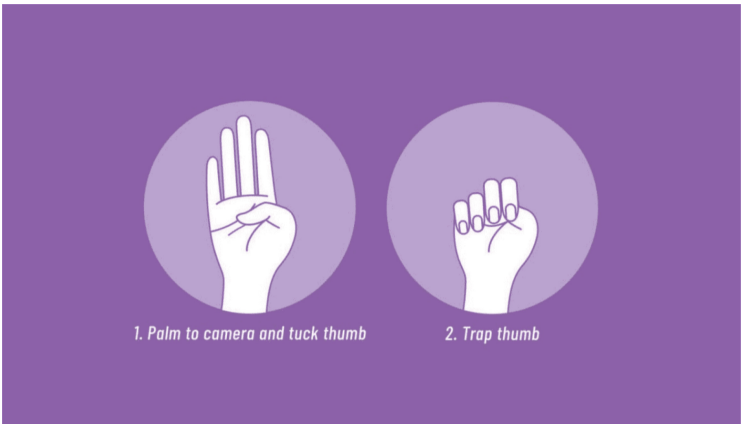

Fig. 1. The "Signal for Help" hand gesture.

However, its effective use is contingent on certain circumstances which cannot always be ensured. In situations when the environment features an increased level of visual complexity, overcrowding, or other factors which distract a person's attention, a gesture may either go unnoticed or get misinterpreted [4]. It indicates that there is a structural problem in question. The mere presence of means of communication does not suffice if there is no way to detect it and implement an appropriate operational reaction.

In recent years, advances in computer vision and gesture recognition have made it possible to automatically identify hand movements in real time, even within video streams from large-scale surveillance networks. Methods based on hand landmark detection, spatiotemporal modeling of the sequences, and training a neural network classifier specifically to perform tasks at the edge have shown their ability to recognize complex configurations of gestures in realistic conditions. In this context, a system capable of detecting the *Signal for Help* within video streams and generating structured events for security operators has been developed and validated. The model described in [3] provides the technological foundation for the present work.

Automatic recognition, however, constitutes only one side of the coin. Gesture detection attains practical significance when it is placed within a broader operational framework that encompasses alert triggering, operator confirmation, and possibly the initiation of action plans.

The purpose of this paper is to explore how the technology can be integrated into different territorial contexts, with specific emphasis on the contrast between urban settings and rural regions. Variations in connectivity, access to computing facilities, institutional presence, and arrangement of security forces have an immediate impact on the selection of deployment strategies. The research highlights the architectural, organizational, and administrative factors that allow for the sustainable application of the innovation amid diverse circumstances.

The objective is to demonstrate how a silent signal can be incorporated into a traceable decision-making structure that is proportionate to the resources available, thereby strengthening local security ecosystems while maintaining human oversight and compliance with data protection requirements.

2 Related Works

In the last few years, there have been several developments regarding the utilization of technological systems for providing assistance in ensuring safety, especially when it comes to automatic detection of situations involving violence or danger. The currently available systems try to identify aggression by recognizing various signs like physical fights, abrupt body movement, facial expression of fear or sound of distress.

In this regard, various video-based techniques have been devised. Some of these techniques depend upon identifying the visual cues of physical attacks that may include the variation in colors indicating the presence of blood or specific body postures for attacks [5,6]. Some other techniques make use of combining visual and audio clues like screaming and unusual sounds to make detection more effective [7]. Such techniques prove effective when there are some distinct signs of violence that can be easily observed. However, they show limitations in situations where a person at risk cannot openly express her condition and must rely on more discreet forms of communication.

Signal for Help constitutes such form of communication. Signal for Help is an intended and silent signal that one sends out requesting help without alarming any potential aggressor. Since it does not involve abrupt movements, audible signals, or visible physical evidence, it cannot be effectively detected by traditional violence detection systems, which are designed to identify explicit and visually marked events.

This specificity requires a shift in perspective. Instead of focusing on the recognition of violent actions, attention moves toward gesture recognition, that is, the identification of intentional hand movements within video sequences. Automatic gesture recognition is widely used in several application domains, including humanâĂŞcomputer interaction, device control, and automatic sign language translation. Techniques developed in these contexts, based on convolutional neural networks, temporal modeling, and hand landmark analysis [8–11], have demonstrated the ability to describe and distinguish complex movements in video sequences by capturing both their spatial structure and temporal evolution.

On this basis, such methodologies have progressively been applied to the recognition of the *Signal for Help*. Some contributions have focused on training models capable of distinguishing the gesture from similar hand movements [12, 13], achieving relevant technical results. However, in many cases the analysis has remained limited to the classification phase, with primary attention given to model performance and limited consideration of integration into real operational contexts.

One element that has not yet been extensively examined within the academic literature is the systematic element of gesture recognition in a critical context. While most studies concentrate on detection reliability and performance assessment, research on how such systems may be incorporated into the present security framework and linked to formalized warning handling protocols is still limited. In the absence of incorporation within the decision-making process, gesture detection technology runs the risk of being merely a technical achievement without an impact on intervention procedures.

Our research group has actively worked to overcome these technical barriers through a consolidated line of work initiated in 2023 [14]. By developing an extensive dataset of 4,500 video sequences featuring hundreds of participants, we validated a system based on a Random Forest classifier capable of 94% accuracy [1], specifically designed to recognize the gesture in realistic and difficult positions, such as when the hand is held low or behind the back. However, having established this robust technological foundation, the challenge now shifts from the reliability of the detection to its actual territorial deployment.

The present work addresses this research gap. Moving beyond the algorithmic validation achieved in our previous studies, the focus is now on analyzing the conditions that enable the adoption of this technology in real contexts. In particular, the research is aimed at analyzing the ways of configuring and incorporating the technology in urban contexts and inner territories in view of infrastructure, organizational, and institutional peculiarities of different territories. The goal is to conceptualize the introduction of the signal as part of a security system of territories, not just a technical innovation.

3 System Architecture

This section includes all information needed about the operation of the system to understand its performance, architecture, and integration into the existing surveillance system. Such a description builds a bridge between the technological side of the system and its further evaluation from the architecture and territorial perspectives.

The system is a technological component of a security system that will detect silent alarms in existing video surveillance systems. As mentioned above, the technology used in the proposed solution is based on the technology presented in [3]. The technology allows detecting a *Signal for Help* in a video stream and notifying security officers about it.

The system consists of several layers, including gesture detection and alarm notification. The system was created in such a way to ensure its compatibility with existing surveillance systems.

Video Analysis and Gesture Recognition Layer

The first level of the architecture concerns the analysis of videos and the recognition of gestures. As shown in Fig. 2, the procedure starts by capturing video sequences using the surveillance cameras. For each frame that is captured in real time, a determination is made whether a hand appears and triggers the tracking procedure.

In case a hand is detected, keypoints are extracted in order to characterize the structure of the hand. Keypoints are then assembled in temporal sequences such that the shape of the hand in a given instant, as well as the evolution of the gesture in time, are taken into account. The spatiotemporal sequence is then fed into the classification module to assess the probability that the observed gesture is the *Signal for Help*.

In order to avoid generating events that have low probabilities, temporal consistency must be ensured. An event is generated if the detected movement is consistent throughout time. It signals the end of the recognition step and the start of the alarms handling step.

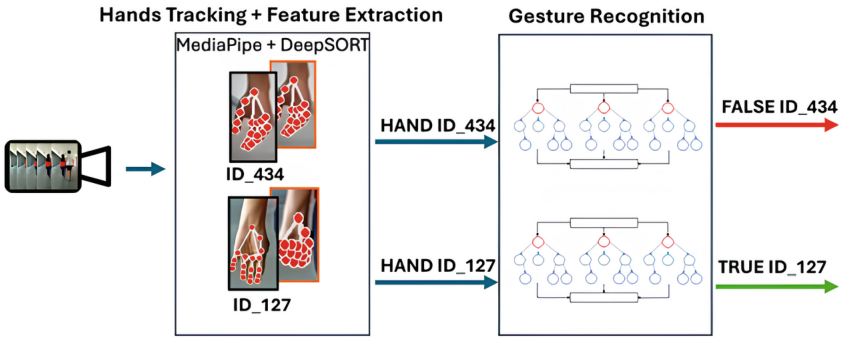

Fig. 2. Overall processing pipeline of the proposed system, from video acquisition to operator notification.

Event Management and Alarm Processing Layer

The second layer processes the event produced by the recognition module and structures it into an operational alert. This means that at this stage, the event is assigned appropriate metadata such as the camera ID, the location of the detection, and the time. Additionally, a video segment from the detection moment is included in order to allow the verification of the event context.

At this level, the technical result produced by the classifier algorithm is translated into an alert suitable for inclusion into the existing workflow of the organization. Structured in such way, the alert is transferred via the system backend to appropriate operators.

Interaction with the Operator Layer

The last layer involves interaction with the operator. The alert, together with the video segment, is transferred to the operator via the mobile app interface, which is presented on Fig. 3.

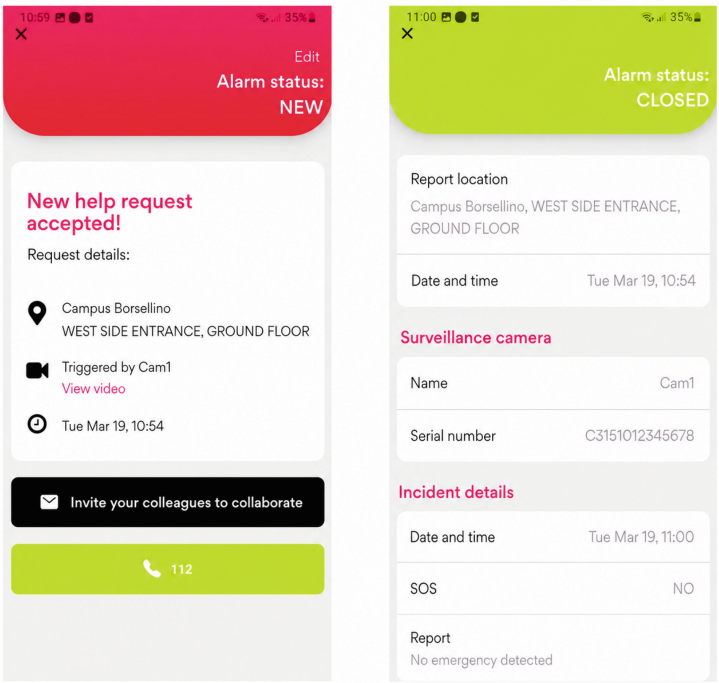

Fig. 3. Mobile application interface displaying alert information and related video preview.

The interface is meant to allow for rapid and informed analysis of the situation. The operator analyses the notification and determines if it is necessary to confirm the warning or not. Upon confirmation, the event will be handled based on the organization's procedures, including contacting personnel at the scene. All processes will be logged for transparency purposes.

The distinction between automatic recognition and human verification enables the system to augment current security systems without compromising the importance of the operator.

4 Deployment in Urban and Inner Areas

After having specified the architecture of the system and its components, it is necessary to proceed with its analysis for implementation within real territorial settings. The purpose of this section is to show how the model can be configured under the given infrastructure and organizational setting within a territory and identify key aspects of its design that determine its efficiency.

In the following, the two simplified types of areas âĂŞ *urban area* and *inner area* âĂŞ will be mentioned. This classification does not imply any rigid definition in demographic or administrative terms but is purely typological and operational. While these areas are traditionally defined by their proximity to essential service hubs like hospitals or schools, from the perspective of the proposed system, the distinction focuses primarily on technical and security-related dimensions, such as network stability and the density of the surveillance infrastructure. Both areas are defined in Table 1.

Table 1. Recurring territorial characteristics and possible implications for deployment

Analytical Dimension	Urban Area	Inner Area
Connectivity	Widespread broadband availability Greater stability of network infrastructures	Variability in connection quality Possible bandwidth or coverage limitations
Computational Infrastructure	Presence of or access to centralized infrastructures Use of data centers or dedicated cloud services	Lower availability of centralized nodes Greater reliance on distributed or edge solutions
Organizational Structure	Dedicated operational units Personnel with specialized roles	Light organizational structures Multifunctional roles and inter-municipal coordination
Access to Emergency Services	Geographical proximity to services Generally shorter intervention times	Greater geographical dispersion Potentially longer response times
Prevalent Technical Configuration	Tendency toward centralized processing models	Tendency toward distributed or hybrid models

The categorization does not mean generalized uniformity in any way, shape, or form. A small town can possess sophisticated networks, while a large city might struggle with its connectivity. The suggested differentiation should, thus, serve only as an analytical framework for making technical decisions.

This difference emphasizes the fact that decisions made in configuring systems should not be seen as detached from the environment in which they will be incorporated. The qualities of both infrastructure and organizations influence how computing work is distributed, events managed, and alerts integrated into the decision-making process.

Below in the text we will consider these aspects separately taking into account the typology suggested above.

Deployment in Urban Areas

In those environments that might be linked to the category *urban area*, more technological infrastructure is available, as well as a better-organized approach to the management of the security process. Such aspects affect the integration and architecture design of the system.

Thanks to the relative stability of the connection and computing capacity of the system, the use of a centralized architecture will be quite possible. Under such architecture, the system will be embedded into the application that is run on the central node of the network, which receives video streams from the cameras deployed in the territory. All sources are collected in one place, analyzed through the recognition algorithm with a unified output of the results depending on parameters.

With centralized processing, there will be possibilities for managing configuration changes, updating algorithms, and maintaining models all at one place. Parameters, detections levels, and algorithms can be changed at the central infrastructure level and will have an immediate impact throughout the whole set of cameras. There will be no need to carry out any intervention in a distributed manner.

For urban settings where the visual density and complexity is high, such as stations, public places, shopping centers, or city centers having high pedestrian density, the amount of live video streams may be considerable, and manually watching all of them would require substantial efforts. Here, the system provides a function of automatic selection of events where there are requests for help that are unlikely to attract attention in situations when many visual stimuli exist at once.

Configuration of the system can also be made to match the resources on which it operates. Adjusting the threshold value and parameters of the model can be achieved through the sensitivity parameter of the algorithm. Sensitivity in the configuration makes detection of faint signals probable; however, it also makes false alerts more likely, increasing the number of notifications generated.

On the other hand, restricting the sensitivity decreases alert generation but may also increase the chance of overlooking an incident. Selection of the sensitivity value depends on the number of operatives available, their monitoring capability, and the feasibility of alert generation. In this way, the model can accommodate real-world circumstances without the risk of overwhelming the operatives or limiting detection capability excessively.

In general, for deployments that fit into the *urban area* category, emphasis is placed on centralized processing of the data and gesture recognition through current infrastructure. The model serves as an improvement to current capabilities, seeking to enhance the detection of silent cries for assistance without modifying the technological configuration.

Deployment in Inner Areas

Where the *inner area* concept applies, the availability of infrastructure will be poorer, connectivity will not always be reliable, and real-time transmission of video streams to the central servers might not be always possible. This directly influences architectural design and makes a solution that would be built around real-time transmission of all video streams to a processing center at a distance suboptimal.

Here a different design approach would be required. Gesture recognition of the *Signal for Help* will take place using edge computing solutions located next to the camera or on territorial nodes that several cameras share. Processing takes place right on-site and transmission is done only in response to detected events; continuous transmission of video streams is unnecessary.

Short clips related to an attempt to make a signal will be transmitted along with relevant metadata that is required for context analysis. By doing things this way, we minimize data traffic while simultaneously providing functionality under the condition of insufficient or unreliable Internet connectivity. Locally processed signals give us robustness. Should connectivity fail, video streams will still be monitored and events recorded.

From an operational perspective, inner areas may be characterized by a lower density of active video streams and fewer simultaneous events. Under these conditions, the model can be configured with higher sensitivity, increasing the probability of detecting even weak or ambiguous signals. Although this may lead to a higher number of generated alerts, the overall information load generally remains manageable due to the lower number of active sources.

The goal here is to avoid overlooking anything, regardless of the cost of getting more false alarms, as long as information overload does not become a problem.

It becomes clear that, when fewer resources are available in terms of infrastructure and organization, the conditions of operation might not necessarily be able to be replicated in the same way as seen in more controlled urban environments. Yet, by virtue of its distributed architecture and adaptability, the system will be able to provide services at a level in line with the environment's characteristics. The goal is not to reproduce an urban model on a smaller scale, but to ensure a balance between detection reliability, technical sustainability, and compatibility with local resources.

5 Privacy and Obfuscation Configuration

The introduction of an automatic recognition system in the security infrastructure of territories implies a certain responsibility concerning data protection. Indeed, the identification of the *Signal for Help* results in the creation of video clips with potential identifiable data, in an operational environment. Therefore, data protection must be a structural part of the deployment strategy rather than a secondary one.

That is why the system was built following the *Privacy by Design* principle, which means that all necessary data protection measures have been incorporated in the architectural design. Inter-module communications are ensured by encrypted channels, video clips are stored in secure environments that require authentication, while the interface for consultations is available only to authenticated operators. All accesses, displays, and modifications of any status of the events will be logged in order to establish the limits of decision-making when it comes to visual data processing.

In the frame of such architecture, the system offers some settings for the adjustment of the visual data processing process in accordance with the deployed territory. It is possible, for example, to set the level of data obfuscation of video content differently.

5.1 Obfuscation Levels

Depending on the operational necessities and specific territories' features, the system offers three types of control over visual data, distinguished based on the level of content obfuscation.

No Obfuscation Mode: The video is transmitted and stored without any alterations. No method of anonymization is used. Such an approach is generally utilized in circumstances where the process of identifying individuals is a part of official procedures.

Dynamic Obfuscation Mode: The file is kept in its pristine format; however, obfuscation occurs dynamically when visualizing. This manipulation will be imposed on the images during playback, and only authorized individuals are allowed access to the unobfuscated version of the same. With this approach, there is decreased systematic exposure of identifiable information in the process, while still maintaining an option for verification.

Irreversible Obfuscation Mode: The obfuscation technique is directly implemented into the processing pipeline and is carried out prior to storing and transmitting the video clip. The video clip is rendered permanently anonymous, and no copies of the original data are kept.

One such illustration of the visual impact of obfuscation can be seen in Fig. 4, wherein the important area has been obfuscated while ensuring that the rest of the scene remains comprehensible.

The selected configuration should be specified before system deployment, and it must be integrated into the territorial implementation plan. This configuration is not only a technical parameter, but it also represents a design choice with direct implications for data handling procedures and the balance between operational necessity and privacy safeguards.

Clearly stating the level of obfuscation prior to carrying out system tasks will allow for the setting up of certain boundaries with regard to visual data processing, avoid ambiguities during operations, and ensure compliance with existing laws concerning security and privacy in the territory. In doing so, the

Fig. 4. Example of obfuscation applied to the clip associated with a detected event.

obfuscation configurations are not decided on a case-by-case basis, but they become part of a controlled process.

The degree of anonymization therefore becomes a fundamental element of the local implementation process and of the operational architecture as a whole, forming part of the governance structure of the surveillance system and of the role definition in its use.

Beyond technical and regulatory considerations, the definition of obfuscation levels also contributes to the social feasibility of the system. In inner areas, where social norms, familial ties, and the risk of stigmatization may discourage individuals from seeking help explicitly, limiting the visibility of identifiable information becomes particularly relevant. In this context, the adoption of dynamic or irreversible obfuscation reduces the perceived intrusiveness of the system, as visual data is either conditionally accessible or permanently anonymized. This characteristic supports the deployment of the system in socially sensitive environments, where maintaining discretion and minimizing exposure are essential for ensuring acceptance, while still enabling the detection and analysis of critical events.

6 Operational Assessment and Territorial Resilience Metrics

To assess the effect of the system on its performance according to the various territorial environments, the quantitative assessment of the key indicators was made, taking into account the centralized and decentralized architecture. The measurements are carried out in controlled settings and form a numeric basis that reflects a real situation; thus, the effect of architectural design and privacy configuration on response time and sustainability is analyzed.

Performance Analysis and Operational Implications

The performance evaluation was done by separating the latency for detecting a single event from the entire end-to-end process. This approach ensures that the time taken by the algorithm on its own can be distinguished from the total time for the entire information cycle until it becomes an operationally actionable notification.

Regarding the detection stage, the mean delay recorded between the receipt of the frame and the construction of the event structure is 63 ms in the centralized setting and 340 ms in the distributed edge setting, as shown in Table 2. Such an evident disparity can be explained by the dissimilarities in the availability of computational resources. In a centralized system, there is more computation power and ability to parallelize. On the other hand, edge computing is constrained by power and memory limitations. Nonetheless, both systems are comparable in terms of low latencies.

Table 2. Average detection time by configuration

Configuration	Average Time (ms)	Std. Dev. (ms)
Centralized	63	8
Distributed	340	45

However latency in detection does not suffice in defining operationally effectiveness. When analyzing the entire duration from the emergence of the gesture until the notification appears on the interface, the average duration is 2.9 s for the urban centralized scenario, while in the distributed deployment in inner areas, the average duration reaches 5.2 s (Table 3). In this case, the difference is not attributable solely to inference time but reflects the impact of network connectivity and node placement. In urban contexts, network stability and bandwidth availability support faster transmission, whereas in inner areas greater connection variability and selective data transmission influence total notification time. From an operational perspective, both values remain within a time window compatible with coordinated response activation.

Table 3. Average end-to-end notification time

Configuration	Average Time (s)
Urban Centralized	2.9
Inner Areas Distributed	5.2

Another aspect analyzed was the influence of varying modes of anonymization upon the processing pipeline itself. As illustrated in Table 4, dynamic obfuscation

performed during visualization stage, which is run on the client side, has no impact whatsoever on event generation duration, and adds an average overhead of 52 ms in either case. Irreversible obfuscation, on the other hand, integrated within the processing pipeline and affecting detection stage, adds an average overhead of 80 ms to the centralized scenario, as well as 673 ms to the distributed one. In general, this overhead grows even further when we consider edge-based scenarios. This proves that the level of anonymization adopted has a clear impact on performances and needs to be tailored to the characteristics of the territory.

Table 4. Average overhead introduced by obfuscation

Mode	Centralized	Distributed
No obfuscation	0 ms (0%)	0 ms (0%)
Dynamic visualization obfuscation	52 ms (+82%)	52 ms (+15%)
Irreversible pipeline obfuscation	80 ms (+127%)	673 ms (+198%)

These metrics prove that the degree of anonymization impacts the performance characteristics of the system, especially in scenarios with limited computational capacity.

Finally, the system's impact on operational workload was estimated in a high-density urban environment. The false positive rate is approximately 2%, with an average verification time per event between 20 and 25 s (Table 5).

Table 5. Estimated operational workload

Parameter	Estimated Value
False positive rate	$\sim$ 2%
Average verification time per event	$\sim$ 20–25 s

A false positive rate of 2% implies that a portion of generated notifications requires manual verification even in the absence of a real emergency. In high-density environments with continuous video streams, this may translate into a non-negligible number of additional checks, requiring operator time and attention.

Therefore, an assessment of the organizational effect of the system should be conducted in the context of staff availability and the ability to accommodate verification tasks. The sustainability of the operation not only relies on the precision of the model but also on the connection between the number of notifications and the human capital invested in managing them.

Overall, the measurements suggest that architectural variations affect performance technologically without interfering with the main purpose of the whole

system. In both centrally structured and decentralized setups, measured times coincide well with instant triggering of the process of making decisions. This performance consistency across different infrastructures demonstrates the territorial resilience of the system, which we define as its ability to guarantee reliable safety standards even when operating under the technical and connectivity constraints typical of marginalized or isolated areas. This means that the model is adaptable to diverse infrastructure conditions and still achieves the proper balance of responsiveness, security, and sustainability.

7 Conclusions and Future Works

This research project has discussed the inclusion of Signal for Help identification in territorial security systems, looking at implementation methods in various settings.

It has been demonstrated that, different types of configuration of the proposed system may be utilized, depending on the territorial characteristics; thus, while centralized solutions work better in cities where infrastructure is well-developed, decentralized solutions correspond more to inner territories lacking resources. Through such adaptation to the specific circumstances, the technology becomes very effective in increasing safety within the territory. In the case of urban environments, the technology offers an automatic mechanism for filtering the silent calls for help from the high level of visual activity in the area, while in the case of internal territories, the technology serves as an important technological link where the presence of institutions is less dense.

The performance evaluation demonstrates that although there are some differences in technical aspects of operation, both configurations guarantee a response time sufficient to make a quick decision. Beyond technical efficiency, the social impact of this system lies in its ability to bridge the gap in emergency services, offering a discrete and safe communication channel for vulnerable groups who might otherwise remain invisible. By integrating this detection capability into existing infrastructures, territories can achieve a higher level of resilience, transforming standard surveillance into a proactive and socially responsible safety ecosystem.

As a next step, future studies should pay their attention to the verification of the system in the form of pilot projects implemented in different territorial settings. Such studies would help to test the efficiency of the model in practice, abandoning theoretical assumptions and examining practical restrictions, costs, and interactions between institutional agents. Experimenting would be of crucial importance for further improving response strategies and making sure that the system remains sustainable in local security governance in the long run.

References

1. World Health Organization. Devastatingly pervasive: 1 in 3 women globally experience violence (2021). https://www.who.int/news/item/09-03-2021-devastatingly-pervasive-1-in-3-women-globally-experience-violence, Retrieved 15 Mar 2025
2. MilanoToday. Violenza sessuale in centro a Milano: ragazza si salva col segnale anti-abuso (2025). https://www.milanotoday.it/cronaca/violenza-sessuale-piazza-scala.html
3. Buccellato, F., Vacca, E., Azimi, S., De Sio, C., Sterpone, L.: From detection to intervention: an end-to-end system for recognizing the signal for help. Gesture in real-time. Intell. Syst. Appl. **26**, 200536 (2025). https://doi.org/10.1016/j.iswa.2025.200536
4. Ossino, A.: Il mistero del segnale in codice non capito dal cameriere, la lite e l'assedio in bagno. Così è morta Martina Scialdone. La Repubblica (2023). https://roma.repubblica.it/cronaca/2023/01/15/news
5. Clarin, C., Dionisio, J., Echavez, M., Naval, P.: DOVE: Detection of movie violence using motion intensity analysis on skin and blood. Philippine Comput. Sci. Congress (PCSC) **6**, 150–156 (2005)
6. Zajdel, W., Krijnders, J.D., Andringa, T., Gavrila, D.M.: CASSANDRA: audio-video sensor fusion for aggression detection. In: IEEE Conference on Advanced Video and Signal Based Surveillance (AVSS), pp. 200–205 (2007)
7. Giannakopoulos, I., Pikrakis, A., Theodoridis, S., Manolopoulos, Y.: Aggression detection using audio and visual cues. In: IEEE International Conference on Image Processing (ICIP) (2009)
8. Tran, D.-S., Ho, N.-H., Yang, H.-J., Baek, E.-T., Kim, S.-H., Lee, G.: Real-time hand gesture spotting and recognition using RGB-D camera and 3D convolutional neural network. Appl. Sci. **10**(2), 722 (2020). https://doi.org/10.3390/app10020722
9. Junping, H., Siping, X.: Gesture recognition based on YCbCr color space and neural network. In: 6th International Conference on Intelligent Computing and Signal Processing (ICSP), Xi'an, China, pp. 738–741 (2021). https://doi.org/10.1109/ICSP51882.2021.9408765.
10. Peng, Y., Tao, H., Li, W., Yuan, H., Li, T.: Dynamic gesture recognition based on feature fusion network and variant ConvLSTM. IET Image Proc. **14**, 2480–2486 (2020). https://doi.org/10.1049/iet-ipr.2019.1248
11. Krishnan, G., Joshi, R., O'Connor, T., Pla, F., Javidi, B.: An overview of hand gesture recognition in degraded environments using three-dimensional integral imaging and deep neural networks. OSA Imaging and Applied Optics Congress (2021)
12. Elliott, G., Meehan, K., Hyndman, J.: Using CNN and tensorflow to recognize signal for help. IEEE Hand Gestures (2021)
13. Azimi, S., De Sio, C., Sterpone, L.: Enhanced video surveillance systems for signal for help. In: IEEE International Symposium on Technology and Society (ISTAS), Detection on Edge Devices(2023)
14. Azimi, S., De Sio, C., Carlucci, F., Sterpone, L.: Fighting for a future free from violence: a framework for real-time detection of signal for help. Intell. Syst. Appl. **17**, 200174 (2023). https://doi.org/10.1016/j.iswa.2022.200174

Co-Visioning Valsesia: Towards an Implementable Territorial Roadmap for Agri-food Short Supply Chains

Diana Rolando[1], Alice Barreca[1], Giorgia Malavasi[1], and Manuela Rebaudengo[2(✉)]

[1] Architecture and Design Department, Politecnico di Torino, Viale Mattioli 39, 10125 Turin, Italy
{diana.rolando,alice.barreca,giorgia.malavasi}@polito.it
[2] Interuniversity Department of Regiona and Urban Studies and Planning, Politecnico di Torino, Viale Mattioli 39, 10125 Turin, Italy
manuela.rebaudengo@polito.it

Abstract. Inner mountain areas are increasingly affected by socio-economic decline, requiring integrated and place-based strategies to enhance local development. Within this context, the paper investigates how collaborative processes and data-driven approaches can be combined to support the definition of an implementable territorial roadmap, focusing on the Valsesia Inner Area in Italy. The study adopts a co-visioning framework developed within the Branding4Resilience (B4R) project, integrating collaborative processes and AI-supported analytical tools. In particular, AI-based text and data mining techniques were applied to analyse past funded projects and structure qualitative inputs into strategic knowledge. The combined approach enabled the identification of key strategic axes, development areas, and suggested actions for the agri-food sector. It revealed recurring intervention patterns, funding gaps, and the central role of short supply chains in enhancing territorial resilience. The integration of collaborative insights and analytical evidence led to the formulation of a Shared Territorial Vision "*Valsesia: Land of Short Supply Chains*", positioning the agri-food system as a driver of repopulation and local revitalisation. This approach supports the development of preliminary place-based project concepts, strengthens collaboration between academia and local actors in more informed decision-making processes, and provides a replicable framework for the development of implementable Territorial Roadmaps in fragile inner areas.

Keywords: Inner Areas · AI-driven analyses · collaboration-based approach

1 Introduction

Inner mountain areas across Europe are increasingly recognised as complex socio-ecological systems, where structural fragilities coexist with significant territorial assets. These regions are typically affected by long-term processes of demographic decline,

© The Author(s), under exclusive license to Springer Nature Switzerland AG 2027
O. Gervasi et al. (Eds.): ICCSA 2026 Workshops, LNCS 16761, pp. 177–193, 2027.
https://doi.org/10.1007/978-3-032-30527-5_12

ageing populations, and the progressive withdrawal of essential services, which contribute to economic marginalisation and built environment abandonment and decay. At the same time, they retain high-value environmental resources, strong cultural identities, and locally embedded production systems, particularly in the agri-food sector, that play a crucial role in maintaining landscape quality, biodiversity, and reactivating social cohesion [1] and territorial vibrancy [2–7].

In Alpine contexts, agri-food chains represent a key component of local development, not only in economic terms but also as drivers of territorial resilience. Small-scale livestock farming, dairy production, and niche product cultivation are often closely intertwined with tourism, ecosystem management, and cultural heritage. However, these systems are typically characterised by fragmentation, limited economies of scale, and weak coordination among actors. As a result, while strategic visions for development are often articulated at the local level, their translation into coherent and implementable actions remains a critical challenge.

The Italian National Strategy for Inner Areas (SNAI) addresses these issues through a place-based policy approach that promotes integrated development strategies and multilevel governance [8, 9]. Central to this approach is the activation of participatory processes involving local institutions, economic actors, and civil society, organised by local coordinators through thematic working tables. These processes enable the emergence of shared priorities and foster local ownership of development trajectories. Nevertheless, participatory practices alone often produce heterogeneous and unstructured outputs, which can be difficult to synthesise into strategic frameworks capable of guiding implementation. This gap between collective visioning and actionable planning represents a key methodological issue in contemporary territorial governance.

In recent years, planning research has increasingly explored the potential of combining participatory approaches with data-driven methods to address this challenge. Within this evolving research field, Artificial Intelligence (AI) and computational tools are emerging as promising instruments to support the analysis of qualitative inputs, identify patterns and relationships, and enhance the consistency of strategic planning processes. Rather than replacing human decision-making, these tools can augment participatory practices by structuring knowledge, supporting scenario-building, and facilitating the translation of complex stakeholder inputs into operational strategies [10–12].

Taking up the challenge of developing a Territorial Roadmap within the Branding4Resilience (B4R) project (https://www.branding4resilience.it), the Research Unit from the Politecnico di Torino (Polito RU) experimented with a new methodological approach in Valsesia, a territory that in June 2022 was officially recognized as a new "Inner Area" under the second programming cycle of the Italian National Strategy for Inner Areas (SNAI), funded by the Minister for Territorial Cohesion and aligned with the European 2021–2027 programming framework.

Building on this perspective, this paper proposes a co-visioning framework to support the development of Territorial Roadmaps by integrating collaborative processes with AI-supported analysis [13–16]. The research framework adopted in this paper is grounded in the integration of two main approaches: (i) collaborative approach, as activated within the SNAI *Agri-food chains and rural development* Focus Group in Valsesia, and field-based co-design and knowledge exchange activities, developed also through

an applied educational experience (Summer School); and (ii) AI-supported analytical approach, used to systematize and interpret past projects and actions funded in the SNAI context. This combined approach is conceptualized as a strategy-oriented framework, in which different sources of knowledge (experiential, institutional, and data-driven) are brought together to construct a shared and operational territorial vision. The aim is to demonstrate how combining stakeholder engagement with data-driven insights can facilitate the construction of a shared territorial vision and inform the definition of strategic axes, development areas, and suggested actions for future development of preliminary place-based project concepts.

Within this framework, the case study of Valsesia SNAI inner area provides a relevant empirical ground to test the proposed approach, given that it represents a typical inner mountain context, where agri-food activities, tourism, and environmental management are deeply interconnected, and where the need for integrated and actionable development strategies is particularly evident.

This paper is structured as follows. Section 2 presents the Co-Visioning framework and the overall methodological approach. Section 3 introduces the case study. Section 4 reports the main results and discusses the findings and Sect. 5 concludes and identifies next steps for further research and implementation.

2 A Co-visioning Framework to Support Territorial Roadmap Definition

In the context of the B4R project, a methodological approach was developed, structured into three main phases, as outlined in previous authors' publications, which present intermediate research results [4–7, 17–23].

The first phase, "Exploration", supports the investigation of territorial contexts from multiple perspectives by combining quantitative and qualitative tools and methods integrated within a GIS-based knowledge system and validated through stakeholder engagement, enabling a comprehensive understanding of local dynamics, resources, and criticalities [4–6, 18].

The second phase, "Co-design", focuses on the definition of actionable transformations, including small-scale infrastructure interventions and operative branding actions, developed by means of collaborative workshops with local actors, using a pilot case to design strategic proposals to be further developed in the co-visioning phase [24].

The third phase, "Co-visioning", represents the last and most strategic component of the methodology. It aims to co-create a Shared Territorial Vision through structured interaction with local communities, stakeholders, and institutions [12, 20]. Building on the knowledge generated in the previous phases, co-visioning integrates collaborative processes with analytical insights to align local aspirations with strategic development trajectories. This phase is crucial for addressing uncertainties, framing long-term priorities, and supporting collective decision-making, ultimately guiding the definition of a Territorial Roadmap that includes coherent and adaptive development pathways.

Each Research Unit (RU) within the B4R project has tailored and refined these phases according to the specific characteristics of its selected Focus Area (FA). Figure 1 illustrates the methodological approach developed and applied by the Politecnico di Torino RU within the Alta Valsesia territorial context.

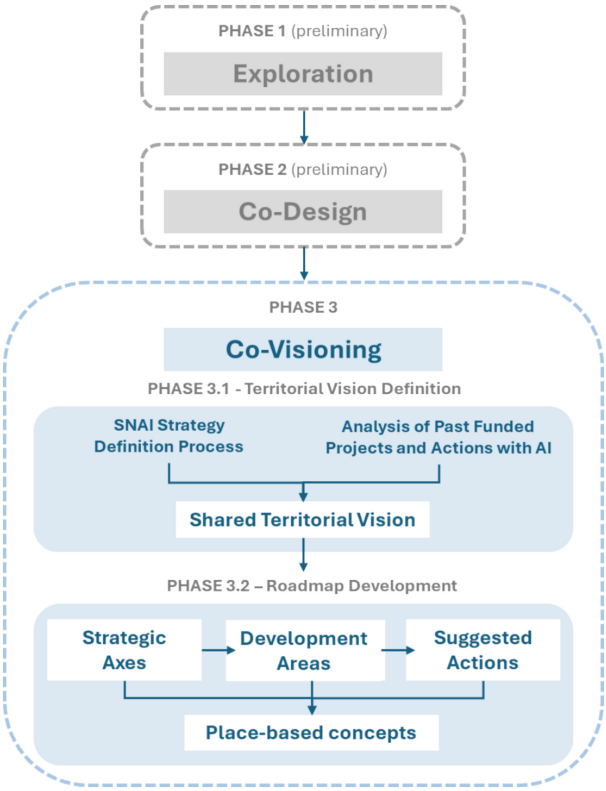

Fig. 1. The B4R Co-Visioning process to support Territorial Roadmap definition applied by the Polito RU for the Alta Valsesia, in the general framework of the B4R project (Source: Authors' elaboration)

Co-visioning - Shared Territorial Vision Definition.
This phase focuses on the co-creation of a Shared Territorial Vision to guide future decision-making within the Focus Area (FA). Two complementary and parallel processes are implemented:

- A collaborative process, embedded within the SNAI Strategy Definition Process, involving stakeholder meetings, focus groups, and co-visioning dialogues. This process enabled the emergence of collective priorities, local knowledge, and shared future trajectories.
- An analytical process, based on the AI-supported analysis of past funded projects and actions, aimed at structuring existing knowledge and identifying patterns, gaps, and performance dynamics.

The integration of these two processes allowed for a more robust interpretation of the territory, explicitly addressing uncertainties, risks, and opportunities. This combined approach supported the identification of strategic directions and led to the consolidation of a Shared Territorial Vision.

Co-visioning – Territorial Roadmap Development.
Building on the Shared Territorial Vision, this phase translates strategic orientations into an operational and adaptive Territorial Roadmap.

The Roadmap is structured across three sequential levels:

- Strategic Axes, which define the main thematic priorities for territorial development;
- Development Areas, which outline the approaches required to achieve these priorities;
- Suggested Actions, which identify concrete initiatives and pilot interventions.

Drawing on a Strategic Choice Approach (SCA) perspective [25–27], Suggested Actions are conceived not only as implementation measures, but also as exploratory options, designed to reduce the conditions of uncertainty. In particular, they allow for flexibility, learning, and progressive refinement over time, supporting decision-making in complex and evolving territorial contexts.

Overall, this process supports the development of place-based project concepts by grounding strategic orientations and actions in the specific territorial context, local resources, and community-driven visions.

3 Agri-food Entrepreneurship in Valsesia SNAI Inner Area

Valsesia is a mountain area located in the northern part of Piedmont (Italy), characterised by limited accessibility and facilities and by a progressive decline in population and ageing demographics, yet it retains significant development potential in the agri-food sector, rooted in traditional agro-silvo-pastoral systems, local supply chains, and the redevelopment of high-altitude pastures.

From an entrepreneurial perspective, the local agri-food system in Alta Valsesia is predominantly composed of micro and small family-run businesses, mainly active in livestock farming and dairy production, often integrating on-site processing and direct sales. These enterprises operate within structurally constrained conditions typical of inner mountain areas, including limited economies of scale, fragmented land ownership, and high production costs. The productive model is thus based on small herds and localised supply chains, where value creation increasingly depends on diversification strategies such as agritourism, direct marketing, and experiential services. A distinctive feature of the local entrepreneurial landscape is the strong interdependence between agriculture, tourism, and environmental management. Farmers and agri-food producers frequently combine production activities with hospitality functions (e.g., agritourism, mountain huts, educational farms), contributing to the maintenance of the landscape and the provision of ecosystem services. In this sense, agricultural enterprises are not only economic actors but also territorial stewards, playing a key role in preventing land abandonment and sustaining high-altitude settlements. However, this multifunctional role is challenged by structural weaknesses, including the progressive decline of active farms, the lack of generational renewal, and the increasing difficulty of managing dispersed and marginal agricultural land .

Within the SNAI *Agri-food chains and rural development* Focus Group, a shared vision emerged towards sector integration and improved coordination of policy instruments. In particular, stakeholders emphasised the importance of aligning agricultural,

Fig. 2. Farmers and agri-food producers in Alta Valsesia (Source: Authors' photos during the site visits, July 2024)

tourism, and forestry policies, as well as overcoming the fragmentation of funding mechanisms and governance tools. The role of intermediary actors, such as GALs (Local Action Group), proved to be crucial for enabling place-based development strategies, facilitating access to resources, and fostering collaboration among otherwise weakly connected local actors. At the same time, the discussion highlighted the need to support entrepreneurial capacity-building, especially in terms of business management, innovation, and market positioning, to enhance the long-term viability of local agri-food chains.

Building upon translating the issues and perspectives that emerged from this SNAI Focus Group into concrete project proposals, a Summer School was organized by the Polito RU, representing a follow-up phase aimed at investigating and deepening knowledge of small-scale actors within the agri-food sector. Through direct engagement with local stakeholders and entrepreneurs, the Summer School served as a knowledge co-production platform, linking academic research with local development practices and reinforcing the dialogue between institutions, researchers, and the local entrepreneurial fabric (Fig. 2).

Overall, the Alta Valsesia case portrays an agri-food system rooted in traditional practices but increasingly oriented towards hybrid and multifunctional models, where production, tourism, and territorial services converge. The effectiveness of future development trajectories will largely depend on the ability to reinforce coordination among institutional and economic actors while supporting the adaptive capacity of small-scale local entrepreneurship.

4 Results

The Co-visioning phase aimed to implement a process to construct a Shared Territorial Vision and formulate a Territorial Roadmap for political decision-makers and local communities of the FA. In the Alta Valsesia context, the B4R Polito RU conducted two parallel and complementary—analytical and collaborative (Fig. 3)—to support the development of a place-based Territorial Roadmap for the Valsesia Inner Area [28] (Fig. 3).

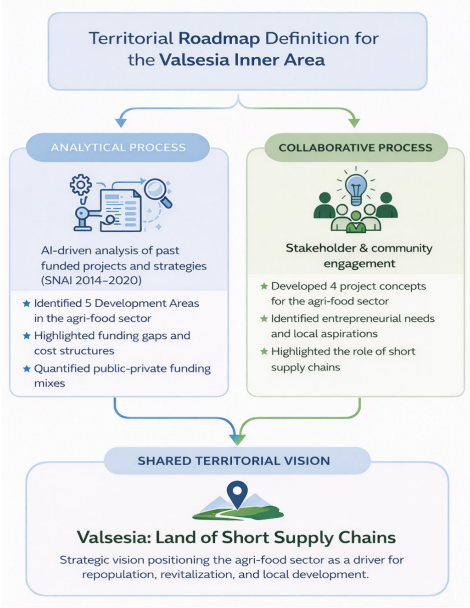

Fig. 3. The Shared Territorial Vision definition process for the Alta Valsesia area (Source: Authors' elaboration)

The analytical process consisted of structuring the acquired knowledge elements, identifying uncertainties and risks and suggesting Strategic Axes and actions for the SNAI strategy definition and implementation. In particular, AI-driven text and data mining techniques were applied to systematically analyse past funded projects and strategies from the first SNAI programming cycle (2014–2020), including APQs and the OpenCoesione database [29, 30]. This process enabled the identification of 5 Development

Areas in the agri-food sector (Productive Economy, Skills and Employment, Community Services, Infrastructures & Mobility, Environment & Landscape). It also highlighted funding gaps in previous programming—particularly the limited attention to research, innovation, and business competitiveness—and provided quantitative insights into cost structures and public-private funding mixes, supporting the definition of more effective and integrated future actions [31, 32].

The collaborative process was initiated following the recognition of Valsesia as an "Inner Area" in 2022 and the allocation of over 10 million euros in funds to counter negative socio-economic trends and foster local development. It was developed through a series of meetings and six focus groups with stakeholders:1) Mobility and transport; 2) Health and personal care; 3) Agri-food chains and rural development; 4) Tourism enhancement; 5) SMEs development; 6) Education and training, organised by the Valsesia Mountain Union in conjunction with the Biellese Orientale Mountain Union, and supported by contributions from professionals. In particular, the Focus Group on *Agri-food chains and rural development* played a pivotal role, as it brought together key local actors to identify both structural weaknesses and development opportunities within the sector, contributing significantly to the definition of 3 Strategic Axes [28].

This process was implemented through a Summer School organised by the Polito RU, which involved direct engagement with stakeholders, local actors, small entrepreneurs, and institutional bodies through interviews, site visits, and collaborative workshops (https://www.polito.it/en/polito/an-international-university/international-mobility-programmes/summer-schools/socio-economic-challenges-for-inner-areas-and-fragile). This process generated context-specific knowledge on local economic dynamics, entrepreneurial needs, and development opportunities, which were translated into four preliminary place-based project concepts focused on enhancing local agri-food value chains and fostering new business opportunities in the area. The interaction with local actors also revealed the central role of short supply chains, local production systems, and community-based economic models in strengthening territorial resilience [33–42].

The integration of the analytical and collaborative processes led to the definition of a Shared Territorial Vision "Valsesia: Land of Short Supply Chains", which positions the agri-food sector as a key driver for repopulation, economic revitalisation, and sustainable development in Valsesia [43]. This vision is grounded both in evidence derived from past funded actions and in locally expressed needs and aspirations, and it outlines a development trajectory based on the consolidation of local supply chains, the enhancement of territorial identity, and the activation of new entrepreneurial initiatives.

4.1 Strategic Axes

The identification of Strategic Axes was based on a systematic analysis of statements collected during two rounds of the *Agri-food chains and rural development* Focus Group. The main outputs were organized into a dataset and analyzed using AI-supported methods to identify patterns and relationships among the statements with the aim of highlighting the most strategic thematic priorities for territorial development within the Agri-food sector.

The following three Strategic Axes emerged from the issues and perspectives identified through the participatory process:

- *Governance, planning, and rural development.* This axis encompassed issues related to institutional coordination, the integration of funding instruments, and support for generational renewal in agriculture. The recurring nature of these statements suggested that governance mechanisms play a pivotal role in shaping the system's capacity to implement coherent and inclusive rural development strategies. In this sense, governance is not merely a contextual factor but a structural determinant influencing the effectiveness of policy interventions.
- *Forest infrastructure and energy supply systems.* This axis identified a critical nexus between infrastructural capacity and the development of the forest-based energy supply chain: statements related to the needs of biomass plant deployment, forest accessibility, and logistical systems indicated that technical and structural constraints directly affect sectoral performance. This configuration underscored the necessity of integrated investments combining infrastructure development, technological innovation, and financial support.
- *Depopulation mitigation through youth entrepreneurship.* This axis clearly pointed out that the enhancement of rural and mountain areas depends on a set of enabling factors: the presence of young entrepreneurs, the valorisation of local products, and the development of short supply chains emerged as outcomes contingent upon supportive policy frameworks, adequate infrastructure, and local economic activation. This perspective emphasized a systemic and interdependent approach to addressing demographic decline.

Overall, the analysis highlighted strong relationships between governance structures, infrastructure systems, and territorial dynamics: governance plays a central role in shaping effective local enhancement, while place-based development strategies are crucial for long-term sustainability and cohesion

4.2 Development Areas and Suggested Actions

Aiming at identifying recurring themes and intervention typologies, an AI-driven, data-oriented methodological approach was applied to analyse past territorial strategies and funded projects, with the aim of extracting transferable strategic knowledge [31, 32]. The AI-driven analysis highlighted several recurring patterns. From a thematic perspective, past strategies addressing the agri-food sector consistently focus on four main objectives: strengthening local supply chains, promoting territorial branding, developing agricultural business networks, and investing in processing and marketing infrastructure. These goals were implemented through a combination of soft and structural actions. Soft measures—such as territorial animation, training, and strategic planning—typically involve limited financial resources, while structural interventions—such as micro-processing facilities, logistics platforms, and cooperative infrastructures—require significantly higher investments. Integrated intervention packages supporting local supply chains generally combine multiple actions and fall within a medium investment range. From a financial perspective, the analysis showed that interventions rely predominantly on public funding sources, which cover most project costs, while private co-financing

is mainly associated with investments in physical assets and productive infrastructure. Different funding streams contribute to specific types of actions, with rural development funds and regional programs supporting structural investments, and national strategy resources more frequently allocated to preparatory and capacity-building activities. The results also revealed that interventions targeting agri-food development are consistently combined with complementary actions in training and education, mobility and accessibility, digital innovation, welfare services, and environmental protection. This integrated configuration emerged as a key condition for enhancing the effectiveness and sustainability of territorial development strategies.

Building on this evidence base,

This process enabled the identification of 5 Development Areas in the agri-food sector (Productive Economy, Skills and Employment, Community Services, Infrastructures & Mobility, Environment & Landscape) that were combined with the 3 Strategic Axes emerged from the Focus Group, enabling the identification of 18 Suggested Actions suitable for the Agri-food sector in the Valsesia area. These actions are intended to be translated into preliminary place-based project concepts and can be assembled in different combinations—according to local constraints, funding opportunities, and governance capacity—to form integrated implementation packages (Fig. 4).

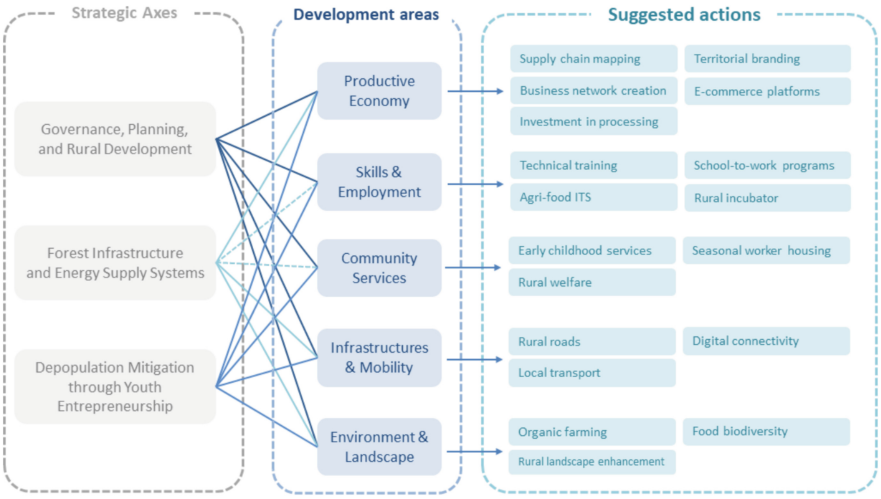

Fig. 4. Shaping a preliminary Territorial Roadmap for the Alta Valsesia area agri-food sector (Source: Authors' elaboration)

4.3 Preliminary Place-Based Project Concepts: Two Examples from the Polito Summer School

The Summer School was designed by the Polito RU as a prototyping device to translate the Shared Territorial Vision and the Territorial Roadmap developed for the Alta Valsesia area into discussable and actionable place-based project concepts, reducing

the gap between strategic orientation and implementation. In this sense, it functioned as a bridge between the strategic level (Strategic Axes, Development Areas and Suggested Actions) and the operational level, making explicit target groups, value propositions, enabling conditions, and feasible governance and management arrangements. The place-based project concepts were developed through the Business Model Canvas tool, complementing the SNAI project information sheets (i.e., the standardised project fiches used in the National Strategy for Inner Areas) —mainly programmatic and regulatory documents— with preliminary assumptions on implementation and medium–long term operating conditions (including management options and running costs). The resulting place-based project concepts can therefore be used as "negotiation objects" to align institutions, local communities, and potential investors around priorities and feasibility constraints. Among the four project concepts developed during the Summer School, two are presented here, because they clearly combine different Suggested Actions and highlight two distinct implementation logics, as summarised in Fig. 5: *Valpunt*, a Communication Hub and infrastructure for agri-food cooperation and market access; and *Alpine Hub*, a hub for nomadic workers and residence-based development program supported by enabling services.

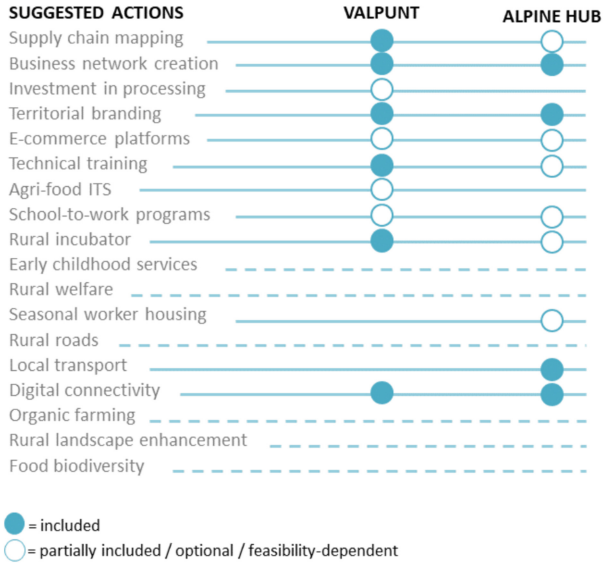

Fig. 5. Preliminary place-based project concept matrix linking Development Areas and Suggested Actions to the two Summer School project concepts (Valpunt and Alpine Hub). Filled circles indicate the actions explicitly activated by each concept (Authors' elaboration)

Valpunt Project Concept

Valpunt can be framed as an intermediary infrastructure for the agri-food ecosystem, rather than a simple digital platform. Its core complexity lies in its design to foster cooperation before generating sales: it must serve as a governance-and-capacity layer that

reduces informational fragmentation, builds trust, and creates a stable interface between micro-producers, institutions, and potential market channels. Operationally, this implies a two-legged architecture (digital platform + physical hub) that must be managed as a continuous service rather than as episodic events, with a strong "institutional" function (rules of engagement, producer onboarding, shared standards, and facilitation). In terms of suggested actions, *Valpunt* fully includes the backbone of Productive Economy and Skills & Employment strategic axes: it explicitly activates Supply chain mapping, Business network creation, and Territorial branding, and it embeds a structured pathway of Technical training and Rural incubator functions to strengthen non-core skills (marketing, ICT, management) and business viability. It also fully includes Digital connectivity as a non-negotiable enabling condition, because the platform, the training pipeline, and the future marketplace depend on stable connectivity. At the same time, some actions are only partially included because they are staged or feasibility-dependent: E-commerce platforms is partially included because it typically evolves from communication and coordination tools into a real marketplace (with governance, logistics, and quality assurance requirements); Investment in processing is partial because it may enter only as a later shared-service layer once bottlenecks are evidenced and partners are ready to manage CAPEX and compliance; Agri-food ITS and School-to-work programs are partial because they require institutional agreements (with schools/ITS, internships, accreditation) and a stable organizational capacity to host and coordinate placements. Conversely, *Valpunt* does not include Community Services actions (childcare, welfare, seasonal housing), Rural roads and Local transport, and most Environment & Landscape actions (organic farming, landscape enhancement, biodiversity) unless explicitly embedded as a strategic positioning choice—because *Valpunt* is primarily built as a supply chain/market and capability infrastructure.

***Alpine Hub* Project Concept**

Alpine Hub is not merely a "coworking in the Alps" concept: its complexity comes from being a residential development program that combines hospitality, infrastructure provision, and a structured knowledge-exchange mechanism between incomers (remote workers) and local actors. It has to operate simultaneously as (i) an accommodation-and-work service (eco-accommodation + coworking), (ii) a community-building device, and (iii) a skills-transfer program that converts temporary presence into local value creation (e.g., upgrading digital communication and market access for producers and micro-enterprises). This requires hard enabling conditions and non-trivial operational roles: beyond Digital connectivity (fully included), the model fully includes Local transport (e.g., shuttle/van logic) as a core enabler to compensate for limited public transport, ensure accessibility across valleys, and make long-stay mobility workable. From a roadmap perspective, *Alpine Hub* fully includes Territorial branding, as the proposition depends on positioning Valsesia as a distinctive, year-round destination for remote work and slow living; and it also fully includes Business network creation, as it requires stable partnerships among hospitality providers, local producers, artisans, and institutional actors. Several actions are partially included because *Alpine Hub* influences them indirectly or as optional extensions: Supply chain mapping is partial (it is not the hub's primary function, but it can emerge through structured linkages between guests and producers, and through the orchestration of experiences and local supply relationships);

E-commerce platforms is partial because the hub can support it through competence transfer and mentorship rather than directly operating the marketplace; Technical training, School-to-work programs, and Rural incubator are partial because the hub can host mentoring, micro-workshops, and internships, but these require formal agreements and dedicated management capacity to become a stable pipeline. Finally, Seasonal worker housing is partial: the hub's long-stay accommodation logic could be adapted to address housing shortages, but only if governance and allocation rules are re-designed for that target. Alpine Hub does not include processing investments, rural roads, and most environment/landscape actions unless they are deliberately added as a sustainability/heritage package.

5 Conclusion

Inner mountain areas face a persistent gap between participatory strategy-making and the production of implementable, evidence-grounded roadmaps, especially when local priorities must be aligned with fragmented policy instruments and limited administrative capacity. Against this background, the purpose of this research was to test how collaborative co-visioning (focus groups, control-room meetings, and Summer School prototyping) can be integrated with an AI-driven, data-oriented analysis of past territorial strategies and funded projects to support a more coherent and actionable agri-food development trajectory.

The study demonstrates the applicability of the proposed methodological approach in the real-world context of the Valsesia Inner Area, which is tasked within the SNAI framework with defining specific economic development strategies. In particular, three main results can be highlighted. First, the analysis of the first SNAI programming cycle makes recurring patterns and funding gaps explicit—most notably the limited attention to research/innovation and competitiveness—clarifying how soft and structural measures tend to cluster and how public and private resources combine across intervention types. Second, by combining evidence from past programming with priorities emerging from the SNAI Focus Groups, the process leads to a Shared Territorial Vision "*Valsesia: Land of Short Supply Chains*", which frames future development trajectories and guides the definition of coherent, place-based strategies.—. Third, the agri-food decision space is structured into 3 Strategic Axes, 5 Development Areas and 18 Suggested Actions that can guide the development of an implementable Territorial Roadmap. In particular, some Suggested Actions were further translated into preliminary place-based project concepts through the Polito Summer School, turning strategic intent into concrete, discussable implementation options.

The broader impact of these results is methodological and operational. Methodologically, the paper shows that AI-supported data mining of strategies and projects can augment collaborative processes by structuring heterogeneous qualitative inputs, reducing uncertainty, and enabling more transparent prioritisation. Operationally, it supports a reframing of the Valsesia agri-food system not as a purely tourism-oriented asset, but as an engine for revitalisation and repopulation, linking short supply chains to stable employment, youth entrepreneurship, service viability, and territorial stewardship.

More generally, the approach offers a replicable pathway for inner areas to treat strategies as adaptive roadmaps—capable of learning from past programming while remaining responsive to evolving constraints and opportunities.

This work also has limitations. The AI-driven analysis depends on the availability and quality of textual and project datasets and, in its current form, provides stronger support for identifying patterns and gaps than for establishing causal impact. In addition, co-visioning outcomes remains sensitive to stakeholder interpretation and to the institutional capacity that determines whether suggested actions can be packaged, financed, and delivered coherently. Future research will therefore focus on (i) strengthening the monitoring and decision-support layer (shared indicators, cross-programme dashboards, and feedback loops) to accompany implementation over the medium–long term; (ii) testing economic feasibility and sustainability through project-specific studies and business-model development, especially where SNAI project fiches need to be complemented with medium–long term management and operating cost assumptions; and (iii) refining coordination mechanisms across funding streams (SNAI, PNRR, foundations, GAL initiatives) to avoid fragmented delivery and improve strategic coherence over time.

Acknowledgments. The authors would like to thank Prof. John Accordino, who served as short-term visiting professor and co-organized the Polito Summer School, sharing his valuable experience in rural planning and economic development projects. The authors also wish to thank the students who participated in the Summer School for their active contribution and engagement, in particular Anano Simonia, Stefano Giletta, and Berhan Asan, who developed the *Valpunt* project concept, and Giorgia Cozzani, Wang Liying, and Anastasia Dremlyuga, who developed the *Nomad Hub* project concept. Finally, the authors would like to thank also Cecilia Torriani, Alexandra Stankulova and all other researchers for their work, contribution, and support in the B4R project.

Declaration of AI Usage. During the preparation of this manuscript, we used artificial intelligence-based tools to support analyses, language refinement, grammar and style improvement, and English editing. All outputs generated by these tools were critically reviewed, edited, and approved by the authors, who take full responsibility for the final content and language quality.

Disclosure of Interests. The authors have no competing interests to declare that are relevant to the content of this article.

Funding:. **"**B4R Branding4Resilience. Tourism infrastructure as a tool for the enhancement of small villages through resilient communities and new open habitats" (Project number: 201735N7HP) is a research project of relevant national interest (PRIN 2017—Youth Line) funded by the Ministry of University and Research (MUR) (Italy) for the three-year period 2020–2024.

References

1. Mantino, F., Vanni, F.: The Role of Localized Agri-Food Systems in the Provision of Environmental and Social Benefits in Peripheral Areas: Evidence from Two Case Studies in Italy - Cerca con Google (2018)
2. Barreca, A., Curto, R., Rolando, D.: Urban vibrancy: an emerging factor that spatially influences the real estate market. Sustainability (Switzerland). **12**, 346 (2020). https://doi.org/10.3390/su12010346

3. Stankulova, A., Barreca, A., Rebaudengo, M., Rolando, D.: Emerging trends in the territorial and rural vulnerability-vibrancy evaluation. A bibliometric analysis. In: International Conference on Computational Science and its Applications, pp. 277–288. Springer Nature Switzerland, Cham (2023). https://doi.org/10.1007/978-3-031-37111-0_20
4. Rolando, D., Rebaudengo, M., Barreca, A.: Exploring the resilience of inner areas: a cross-dimensional approach to bring out territorial potentials. In: Lecture Notes in Networks and Systems, New Metropolitan Perspectives 2022 International Symposium 5th Edition, 2022. Springer, Reggio Calabria (2022)
5. Rolando, D., Barreca, A., Rebaudengo, M.: The SAVV+P Method: Integrating Qualitative and Quantitative Analyses to Evaluate the Territorial Potential (2023). https://doi.org/10.1007/978-3-031-37111-0_18
6. Rolando, D., Rebaudengo, M., Barreca, A.: Managing knowledge to enhance fragile territories: resilient strategies for the Alta Valsesia area in Italy. In: IFKAD 2022 - Knowledge Drivers for Resilience and Transformation, Lugano, Switzerland (2022)
7. Rolando, D., Rebaudengo, M., Barreca, A.: From vulnerability to vibrancy: cross-dimensional indexes for the evaluation of inner areas. Paper Submitted to Int. J. Urban Reg. Res. (2024)
8. Barca, F., Carrosio, G.: Un modello di policy place-based: la Strategia Nazionale per le Aree Interne. In: Osti, G., Jachia, E. (eds.) Attivare Un Disegno Di Rinascita Delle Aree Interne. Il Mulino, Bologna (2020)
9. Barca, F., Casavola, P., Lucatelli, S.: A Strategy for Inner Areas in Italy: Definition, Objectives, Tools and Governance. Materiali Uval Series (2014)
10. Curto, R., Norese, M.F., Rolando, D.: A multicriteria decision aid perspective that guides an incremental development of knowledge and fosters relationships and decisions. EURO J. Decis. Process. **10**, 100023 (2022). https://doi.org/10.1016/j.ejdp.2022.100023
11. Norese, M.F., Galliano, R., Rolando, D.: A methodology to support a concerted approach when the context is non-collaborative. Int. J. Decis. Support Syst. **1**, 412 (2015). https://doi.org/10.1504/ijdss.2015.074545
12. Malavasi, G., Barreca, A., Rebaudengo, M., Rolando, D.: A Stakeholder Analysis to Support Resilient Strategies in the Alta Valsesia Inner Area (2023). https://doi.org/10.1007/978-3-031-37111-0_19
13. Mishra, M.K., Muthulakshmi, A., Mishra, B.R., Sasikala, J.E.M.: Optimizing decision-making process in supply chain management through intelligent systems. Migr. Lett., Dews publication. **21**, 1107–1113 (2024). https://doi.org/10.59670/ml.v21is6.8164
14. Valença, G., Moura, F., Morais de Sá, A.: How can we develop road space allocation solutions for smart cities using emerging information technologies? A review using text mining. Int. J. Inf. Manage. Data Insights, Elsevier. **3**, 100150 (2023). https://doi.org/10.1016/j.jjimei.2022.100150
15. Kavitha, P.N.: The concept of natural language processing and text Mining in Emerging Artificial Intelligence Techniques. Int. J. Eng. Dev. Res. **14**(1), 696–712 (2026)
16. Ghani, A., Alsaedi, N., Jalali Varnamkhasti, M., Mohammed, H.J., Aghajani, M.: Data mining classification techniques to improve decision-making processes. Oiccpress Com. **14**, 363–380 (2024). https://doi.org/10.71932/ijm.2024.1198139
17. Rolando, D., Rebaudengo, M., Barreca, A.: La valutazione delle potenzialità territoriali attraverso un approccio multidimensionale per le aree interne. LaborEst. **25**, 24–29 (2022)
18. Rolando, D., Rebaudengo, M., Barreca, A.: From vulnerability to vibrancy: a knowledge management approach to evaluate rural areas' potential. J. Knowl. Manag., 1–27 (2026)
19. Rolando, D., Rebaudengo, M., Barreca A.: Managing knowledge to enhance fragile territories: Resilient strategies for the Alta Valsesia area in Italy. Knowledge Drivers for Resilience and Transformation IFKAD (2022)

20. Ferretti, M., Favargiotti, S., Lino, B., Rolando, D.: Branding4Resilience: explorative and collaborative approaches for inner territories. Sustainability (Switzerland), MDPI. **14**, 11235 (2022). https://doi.org/10.3390/su141811235
21. Stankulova, A., Barreca, A., Rebaudengo, M., Rolando, D.: The quantitative indicator-based evaluation for rural development. A review. International Regional Science Review (2024)
22. Favargiotti, S., Ferretti, M., Rolando, D., Lino, B.: B4R Branding4Resilience: tourist infrastructure as a tool to enhance small villages by drawing resilient communities and new open habitats. In: Le politiche regionali, la coesione, le aree interne e marginali: atti della 23. conferenza nazionale SIU-Società Italiana degli Urbanisti: Downscaling, Rightsizing: Contrazione demografica e riorganizzazione spaziale, Torino, 17-18 giugno 2021, vol. 03: le politiche regionali, la coesione, le aree interne e marginali, pp. 346–354. Planum Publisher, Società Italiana degli Urbanisti (2021)
23. Rolando, D., Barreca, A., Malavasi, G., Rebaudengo, M., Savio, L.: Vibrè. Enhancement strategies to make resilient villages vibrant in Alta Valsesia. EURA 2022 Conference "Defrag-Europe: Fragility/Antifragility at Play in Contemporary Europe," Milan (2022)
24. Ferretti M., Favargiotti S., Lino B., Rolando D.: Branding4Resilience. ATLANTE. Ritratto di quattro territori interni italiani. 7th ed. Alleli | Research, editor. LetteraVentidue Edizioni S.r.l., Siracusa (2024)
25. Friend, J.: The strategic choice approach. In: Rosenhead, J. (ed.) Rational Analysis for a Problematic World: Problem Structuring Methods for Complexity, Uncertainty and Conflict. Wiley, Chichester (1989)
26. Friend, J.K., Jessop, W.N.: Local Government and Strategic Choice: an Operational Research Approach to the Processes of Public Planning. Local Government and Strategic Choice: an Operational Research Approach to the Processes of Public Planning, pp. 1–304. Taylor and Francis (2013). https://doi.org/10.4324/9780203075395
27. Rolando, D.: Multicriteria decision problem structuring: the strategic choice approach in the context of public projects in Italy. Int. J. Multicriteria Decis. Making, Inderscience Enterprises Ltd. **5**, 4–38 (2015)
28. Rolando, D., Barreca, A., Malavasi, G., Rebaudengo, M.: The Enhancement of the Alta Valsesia Territorial Potential: a Collaboration-Based Approach between Academia and Local Actors. Computational Science and its Applications – ICCSA 2024 Workshops, pp. 17–32. Springer Nature, Switzerland (2024). https://doi.org/10.1007/978-3-031-65282-0_2
29. Torriani, C., Barreca, A., Rebaudengo, M., Rolando, D.: Projects and funding in Italian inner areas: learning from the 2014–2020 programming of the SNAI National Strategy. In: International Conference on Computational Science and its Applications, pp. 233–248. Springer Nature Switzerland, Cham (2023). https://doi.org/10.1007/978-3-031-37111-0_17
30. Torriani, C., Barreca, A., Rebaudengo, M., Rolando, D.: Exploratory Data Analysis to Support the Second SNAI Programming Cycle. Firenze University Press, Aestimum (2025). https://doi.org/10.36253/aestim-17077
31. Rolando, D., Barreca, A., Malavasi, G., Rebaudengo, M.: Data-driven AI approach to address territorial strategies. In: Why Investing in Agri-Food Sector to Enhance the Valsesia Inner Area Lecture Notes in Computer Science LNCS, vol. 15889, pp. 177–198. Springer Science and Business Media Deutschland GmbH (2026). https://doi.org/10.1007/978-3-031-97603-2_12
32. Barreca, A., Malavasi, G., Rebaudengo, M., Rolando, D.: AI supports policies and territorial development: learning from SNAI 2014–2020. In: Navarro-Valverde, F.A., Martín-Rojas, R. (eds.) Landscape across the Mediterranean, pp. 1–11. ASTI, Granada, Spain (2025)
33. Hausmann, R., Hidalgo, C.A., Bustos, S., Coscia, M., Simoes, A., Yildirim, M.A.: The Atlas of Economic Complexity: Mapping Paths to Prosperity, vol. 51. Choice Reviews Online (2014). https://doi.org/10.5860/choice.51-5931

34. Hidalgo, D.M., Nunn, P.D., Beazley, H.: Uncovering multilayered vulnerability and resilience in rural villages in the pacific: a case study of Ono island, Fiji. Ecol. Soc. **26** (2021). https://doi.org/10.5751/ES-12197-260126
35. Galster, G., Tatian, P., Accordino, J.: Targeting investments for neighborhood revitalization. J. Am. Plan. Assoc.., Taylor & Francis. **72**, 457–474 (2006). https://doi.org/10.1080/01944360608976766
36. Accordino, J.: Introduction to Bridging the "Urban–Rural Divide." State and Local Government Review, **51** (2019). https://doi.org/10.1177/0160323X20932624
37. Accordino, J.J.: Rural Areas and Small Cities: Dependency, Adjustment, and Conversion. Captives of the Cold War Economy (2024). https://doi.org/10.5040/9798400623332.0009
38. Accordino, J., Fasulo, F.: Fusing technical and political rationality in community development: a prescriptive model of efficiency-based strategic geographic targeting. Taylor & Francis. **23**, 615–642 (2013). https://doi.org/10.1080/10511482.2013.814070
39. Galster, G., Tatian, P., Accordino, J.: Targeting investments for neighborhood revitalization. Taylor & Francis. **72**, 457–474 (2006). https://doi.org/10.1080/01944360608976766
40. Quarterly, J.A.-E.D.: Undefined. (1994) evaluating economic development strategies. J. SagepubCom. **8**, 218–229 (1994). https://doi.org/10.1177/089124249400800212
41. Accordino, J., Galster, G., Tatian, P.: The Impacts of Targeted Public and Nonprofit Investment on Neighborhood Development. Staging Community-WealthOrg, vol. 22, pp. 301–315. Blackwell Publishing Ltd (2005). https://doi.org/10.1111/0735-2166.00058
42. Accordino, J., Quarterly, C.M.-E.D. and 2026, Convergent development: integrating economic development and downtown revitalization in small cities and towns. J. SagepubCom., SAGE Publications Inc. 40, 72–87. https://doi.org/10.1177/08912424251365948
43. Scorrano, P., Borin, E., Thrassou, A., Cavallo, F., Mastroleo, G.: Knowledge sharing between businesses and stakeholders for systemic and sustainable regional development. Insights in the Agri-food sector. J. Knowl. Manag. **29**(4), 1278–1300 (2025). https://doi.org/10.1108/JKM-05-2024-0517

Territorial Inequalities in Real Estate Markets' Flood Resilience: Evidence from the Forlì-Cesena Province (Italy)

Alessia Crisopulli, Marco Rossitti, and Francesca Torrieri(✉)

Politecnico di Milano, Via Giuseppe Ponzio, 31, 20133 Milan, MI, Italy
francesca.torrieri@polimi.it

Abstract. Climate change is increasing the frequency and severity of extreme weather events, with significant implications for economic and territorial systems. Among these events, floods have emerged as a major threat due to their widespread geographical reach and their capacity to produce both severe damage and long-term socio-economic impacts. While a growing body of literature has examined the impact of flood risk on real estate prices, limited attention has been devoted to the resilience of real estate markets and spatial heterogeneity. This paper investigates the resilience of residential real estate markets to flood risk in Italy, a territory characterized by high hazard conditions and pronounced territorial disparities. We resort to a "stage-damage" methodology for the ex-ante evaluation of flood damages and derive a "critical stage" as a proxy for market resilience across municipalities. The results, based on the case study of Forlì-Cesena province (Italy), reveal a clear spatial pattern, with resilience systematically declining from central to peripheral municipalities, reflecting the climate resilience counterpart of existing socio-economic and demographic disparities. These findings highlight the need to integrate equity considerations into risk management and spatial planning policies.

Keywords: Inequalities · Flood risk · Resilience · Damage curves · Real estate market

1 Introduction

In recent years, climate change has emerged as one of the most pressing global challenges, with significant implications for economic systems, territorial structures, and human well-being [1, 2]. A growing body of studies shows that climate change is negatively impacting the frequency and severity of extreme events, including floods, storms, and heatwaves [3, 4].

Among these events, which generate severe disruptions for infrastructure, productive activities, and the safety of the population, floods are emerging as a severe threat due to their widespread geographical reach and their capacity to produce both severe damage and long-term socio-economic impacts [5].

© The Author(s), under exclusive license to Springer Nature Switzerland AG 2027
O. Gervasi et al. (Eds.): ICCSA 2026 Workshops, LNCS 16761, pp. 194–205, 2027.
https://doi.org/10.1007/978-3-032-30527-5_13

Given their strong spatial dependence and economic relevance, real estate markets provide a valuable lens to observe the impacts of flood risk. Many international studies have investigated how flood risk affects real estate prices, primarily focusing on the US context and housing markets [6, 7]. By contrast, a limited number of studies have focused on a central theme in national and international planning agendas: the resilience of real estate markets to this climate-related risk and its variation across locations. Italy offers a relevant setting for analyzing this theme, which reveals the tight connection between risk management and distributive equity in spatial planning. Indeed, about 20% of the Italian population lives in flood-prone areas [8]. According to the Bank of Italy, the value of housing exposed to flood risk amounts to approximately €1.000 trillion, and the expected annual losses in real estate wealth, related to flood events, can reach €3 billion [9]. However, this information, on its own, offers only a partial measure of the impact of flood risks on real estate markets.

Italy, indeed, exhibits significant spatial disparities between central areas and marginal areas - the so-called "inner areas" - which are likely to influence the resilience of real estate markets to flood risk. Italian inner areas[1] account for about 60% of the national territory (about 49% of Italian municipalities) and host about 23% of the national population [10]. Since 2014, these territories have been targeted by the National Strategy for Inner Areas (NSIA) - one of the most interesting laboratories of the EU's territorial cohesion policy - to tackle the ongoing marginalization and depopulation phenomena [11, 12].

While the NSIA proposes a differentiated, place-based approach to intervention for these territories, aimed at promoting local development and addressing deficits in essential services [13], the same level of "specific" attention is not devoted to managing climate-related risks. Given their lower population density and the lower value of other exposed assets, such risks may initially appear less relevant in absolute terms than those affecting urban areas. However, the vulnerability of their socio-economic systems - and, within them, of real estate markets - makes them less resilient to the impacts of climate events that, if not properly managed, can become a catalyst for the ongoing depopulation and marginalization dynamics. Understanding the extent of this phenomenon is crucial to not undermining NSIA's planning efforts.

Based on these premises and adopting the housing real estate market as the lens to observe the impacts of flood risk, the paper proposes a comparative analysis among different typologies of municipalities – in terms of NSIA's classification according to their accessibility conditions (centers, peri-urban areas, intermediate areas, peripheral areas, and ultra-peripheral areas) – to understand the differences in their markets' resilience to flood risk. To this aim, it resorts to an ex-ante evaluation of direct flood damages,

[1] Inner areas identification is based on a classification of Italian municipalities according to their accessibility conditions. Specifically, the national territory is divided into five zones (centers, peri-urban areas, intermediate areas, peripheral areas, and ultra-peripheral areas). The adopted accessibility indicator is measured in the number of minutes required to reach the closest center, i.e., a municipality or a cluster of neighboring municipalities, offering all secondary education provisions, hospitals with I-level DEA, and at least a silver railway station, according to RFI classification. Based on this indicator, the classification of "inner areas" applies to all municipalities, resulting in intermediate (20–40 min to reach the closest center), peripheral (40–75 min), and ultraperipheral (more than 75 min).

based on "stage-damage" curves, and compares the obtained damages with the average housing market value at the municipal level to identify the municipal "critical stage". Such a "critical stage", representing the most probable "water depth" causing economic damage equal to the property's market value, is adopted as a proxy of the real estate market resilience, thus allowing for comparison among different municipalities. After describing the adopted methodology in Sect. 2, Sect. 3 provides its application to a case study: the municipalities of Forlì-Cesena Province in the Emilia Romagna Region (Italy), which in 2023 was affected by a severe flood event. The comparison of results obtained for municipalities, characterized by different accessibility and marginality conditions, allows for reflecting on the methodology's contribution to detecting territorial inequalities in real estate markets' flood resilience and discussing its potential to better orient planning actions toward spatial equity.

2 Methodology

The willingness to understand the climate resilience conditions of different real estate markets (center vs. peripheral areas), as a basis to orient equity-based planning actions, calls for the definition of a robust methodological approach.

The methodology proposed for the ex-ante evaluation of direct damages is based on the "Stage-damage" curve as the most trusted and reliable forecasting tool to assess the Expected Annual Damage (EAD) from flood events. The "Stage-damage" curves are functions that relate the intensity of a hazardous event (hazard) to the resulting damage of a certain type of assets exposed [14–16]. These curves assume that the expected economic damage can be quantified based on both the vulnerability of the exposed elements and the level of water during flooding. Therefore, Total Damage (DT) is expressed as a function of the asset's economic value and its level of vulnerability. The economic value of an asset may be determined using different criteria: the market value, which reflects the conditions of the real estate market in which the asset is located, or the cost value, which may refer either to the depreciated replacement cost or to the restoration cost associated with repairing and eliminating the damage [17].

The methodology adopted for the case under analysis and shown in Fig. 1 is based on an analytical engineering approach that involves:

1. Identification of the reference building typology. Once the study area is selected, the choice of the building typology must be based on a combination of territorial, risk-related, and architectural criteria. Specifically, to allow comparability among different municipalities within the study area, the reference building typology must be representative of construction techniques in the area and widespread.
2. Breakdown of the identified building typology into its main components [18]. According to this approach, damage is assessed by types of standardized building elements, which can be considered "prototypes" of the exposed structural, mechanical, and finishing elements.
3. Estimation of a restoration/replacement cost for each at-risk element based on its conditions of intrinsic vulnerability to water.
4. Determination of a damage percentage for each component, exposed at different and significant water levels, based on the existing literature and expert opinions gathered through *ad hoc* interviews.

5. Estimation of the total damage to the property at different water levels, calculated as the sum of the estimated intervention costs for each component of the property and expressed in unit terms (€/sqm). These costs can be estimated through a synthetic or an analytic procedure [19].
6. Construction of the typology-specific stage-damage curve and comparison with the average unit market value for the building typology in different municipalities. Such a comparison allows to identify a "critical stage" for each municipality included in the analysis. Such a "critical stage", defined as the most probable water depth at which economic damage equals the market value of the reference property, can be used as a proxy for real estate market resilience, enabling comparisons across municipalities.

3 Investigating Territorial Inequalities in Real Estate Markets' Climate Resilience: The Case of Forlì-Cesena Province

3.1 Introduction to the Case Study

The opportunities and limitations of the proposed methodology toward detecting territorial inequalities in the climate resilience of different real estate markets in Italy are investigated through its implementation in a case study: the Province of Forlì-Cesena, located in the south-eastern part of the Emilia-Romagna Region (Italy). This province represents a relevant study area due to its recent and severe exposure to flood events, such as the 2023 Emilia-Romagna floods, which caused severe damage to the built environment, infrastructures, and population.

Furthermore, the Province of Forlì-Cesena is characterized by a heterogeneous territorial structure, including mountains and hills, plains and coastal zones. This morphological diversity is coupled with the presence of major rivers, channels, and proximity to the Adriatic coast. All these characteristics make the area prone to flooding at different scales. According to the flood hazard maps produced by ISPRA, the area presents different levels of flood hazard, from low to high probability scenarios, making it particularly

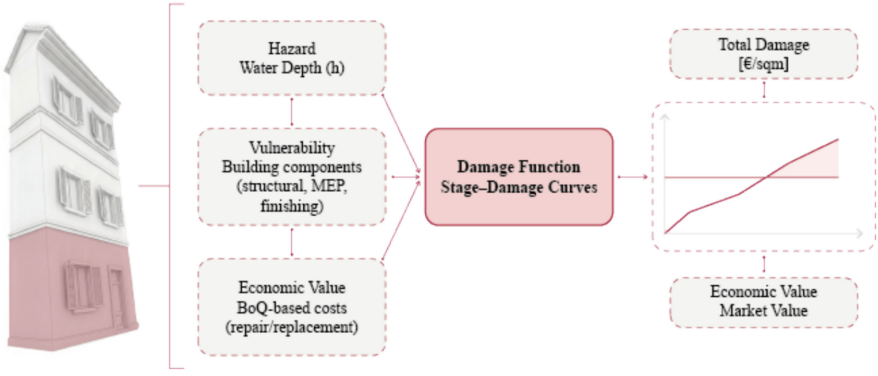

Fig. 1. Methodology adopted for the typology-specific assessment of ex-ante evaluation of flood damage and comparison with the market value (Authors' elaboration)

suitable for the application and testing of the proposed methodology in different risk conditions.

Within this context, municipalities in the Forlì-Cesena province are first analyzed in terms of the NSIA's classification according to their accessibility conditions (centers, peri-urban areas, intermediate areas, peripheral areas, and ultra-peripheral areas). Based on these classifications, the methodology is applied to eight municipalities, belonging to different classes:

- Forlì and Cesena are selected as municipalities classified as "centers", since they offer all secondary education provisions, hospitals with I-level DEA, and at least a silver railway station, according to RFI classification [20];
- Forlimpopoli and Montiano are selected as "peri-urban" municipalities, characterized by good accessibility conditions (less than 20 min to reach the closest center);
- Predappio and Mercato Saraceno are selected as "intermediate municipalities" (20–40 min to reach the closest center);
- Premilcuore and Santa Sofia are selected as "peripheral" municipalities (40–75 min to reach the closest center).

3.2 Methodology Implementation

Once the eight municipalities in the Forlì-Cesena Province were selected as representatives of the different marginality conditions affecting the Italian territory, the methodology implementation (Fig. 1) first required identifying a reference and comparable building typology. Based on the analysis of the main characteristics of the built environment in the study area, the reference building typology was identified in a residential masonry building with three above-ground floors, no basement, and a medium state of conservation. This typology, indeed, is commonly found in the historic centers of the selected municipalities (see Fig. 2).

Its choice, thus, allowed for controlling variations in architectural and structural characteristics, enabling the analysis to focus on territorial differences rather than on the building dimension. For this reason, the methodology implementation focused on an ordinary unit located on the ground floor of the reference building.

The reference property was, then, described in terms of its main building components: structural, mechanical, and finishing elements (see Table 1).

Coming to the estimation of a restoration/replacement cost for each at-risk element, it was based on a detailed Bill of Quantities (BoQ) by resorting to the 2025-edition of the Official Price List of the Emilia-Romagna Region [21]. The following step in the methodology implementation – the definition of a damage percentage of each element exposed to different and significant water depths – was based on integrating data provided by existing literature [22–24] with expert opinions gathered through ad hoc semi-structured interviews [25] (see Table 2). Specifically, interviews involved three experts with complementary backgrounds and expertise on the topic in two steps:

- First, they were asked to identify, among the selected building components, the ones more prone to being damaged in different flooding scenarios and express a qualitative judgement on the magnitude of the damage (low-medium-high);
- Later, they were involved in validating and refining the obtained preliminary "Stage-damage" curves.

Fig. 2. Selected municipalities in the Forlì-Cesena Province and examples of properties corresponding to the reference building type (Authors' elaboration)

Such a step was used as the basis for estimating the total damage to the property at different water stages, calculated as the sum of the estimated intervention costs for each component of the property and expressed in unit terms (€/sqm). Finally, a specific "stage-damage" curve was built for the reference building typology by relating the identified water levels to the corresponding expected economic damage. Such a curve was used as the basis for comparing the estimated total damage with the average unit market

Table 1. Breakdown of the reference building typology into its main structural, mechanical, and finishing components (Authors' elaboration)

Categories of components	Building components
Structural	Solid-brick masonry
	Timber floors
	Pitched roofs with a timber roof structure covered in clay tiles
Finishing	External smooth painted plaster finish
	Timber windows and wooden shutters
Mechanical	Electrical system
	Stormwater drainage system: gutters and downspouts in copper
	Water and gas system
	Heating system

Table 2. Damage assessment percentage of the identified building components according to different levels of water (Authors' elaboration)

Functional Elements	h30cm % damage	h 60 cm % damage	h 150 cm % damage	h 270 cm % damage	Source
Floors	30.0%	50.0%	80.0%	100.0%	[24]
Internal coverings – wall coverings	12.5%	25.0%	62.5%	100.0%	[23]
External finishing – Facades	12.5%	25.0%	62.5%	100.0%	[23]
Internal doors	15.0%	35.0%	60.0%	80.0%	[24]
Internal walls	12.5%	25.0%	62.5%	100.0%	[23]
External windows and doors	15.0%	35.0%	60.0%	80.0%	[24]
Elevation structures	20.0%	30.0%	35.0%	40.0%	[24]
Electrical system	30.0%	50.0%	80.0%	90.0%	[24]
Heating system	30.0%	50.0%	80.0%	90.0%	[24]

value (€/sqm) of the reference building typology in the case-study municipalities, thus identifying the "critical stage" for each municipality. Given the predominantly residential use of the reference typology, the unit market value for each municipality was placed equal to the average unit market value of civil housing in a normal conservation state, provided by the Italian Observatory for the Real Estate Market (OMI) for the 1st semester of 2025 [26].

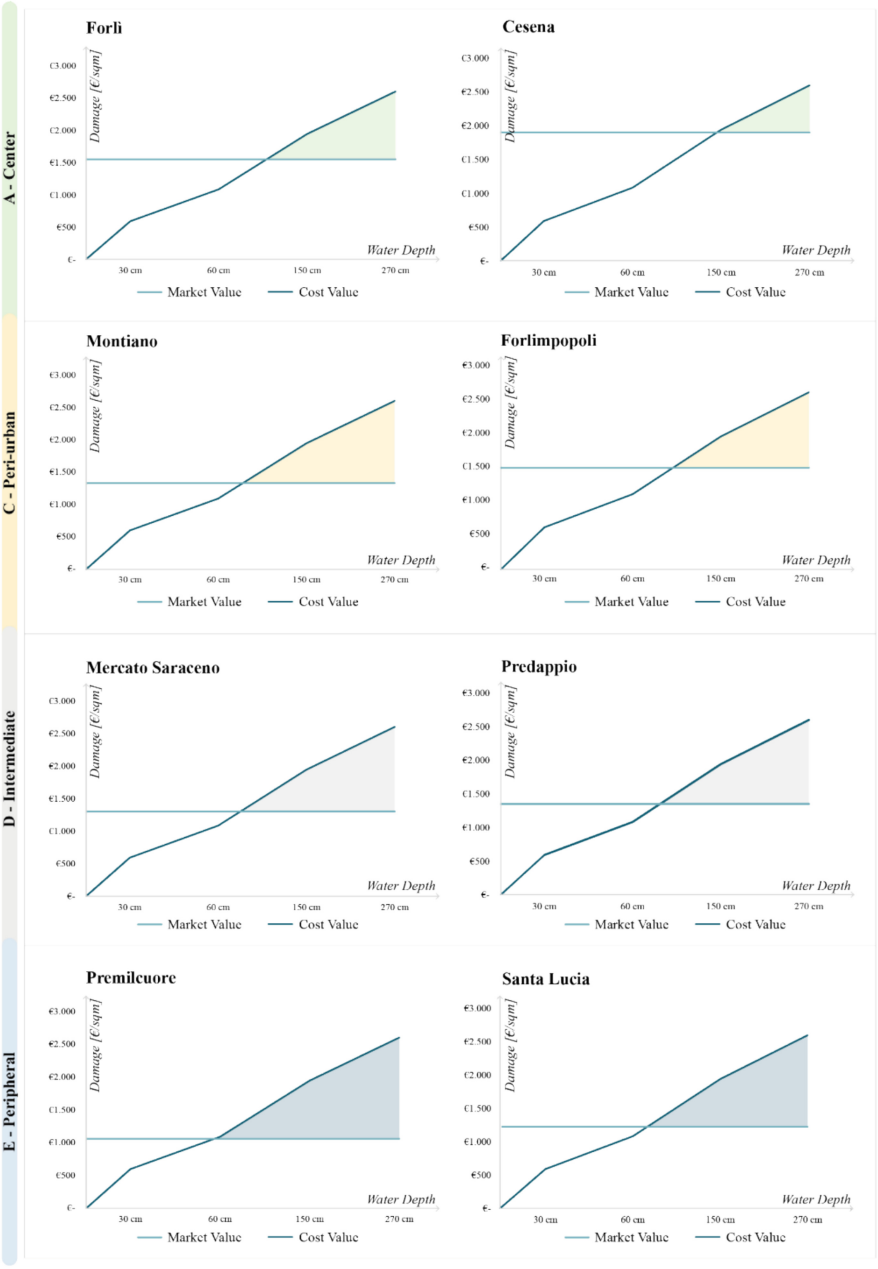

Fig. 3. Comparison between stage-damage curves and market values in the different municipalities and identification of each municipality's "critical stage" (Authors' elaboration)

3.3 Results

The analysis of the results obtained from the methodology implementation in the eight municipalities in the Forlì-Cesena Province allows for interesting reflections about their housing real estate markets' resilience to flood risk (see Fig. 3). The comparison among the different municipalities' "critical stages" – i.e., the most probable water depths at which economic damage equals the market value of the reference property – indeed, highlights that the existing disparities between central and peripheral areas are also mirrored in the resilience of real estate markets to flood risk. Specifically, moving from central to peripheral municipalities, a clear gradient of decreasing real estate market's resilience – proxied by the "critical stage" of water - can be observed.

Indeed, in the "center" municipality of Cesena, the "critical stage" is equal to about 1.5 m. Moving to the "intermediate" municipalities in the Province (Mercato Saraceno, Predappio), the "critical" threshold of water depth drops to about 0.70 m, coming respectively to about 0.65 and 0.6 m in the cases of the "peripheral" municipalities of Santa Lucia and Premilcuore. Given the inverse relationship between the magnitude of water depth/stage and the probability of a flood event with such a depth/stage, these results provide a relevant reading key to interpret the lower resilience to flood risk of real estate markets in peripheral municipalities. Indeed, such a lower resilience does not strictly depend on the magnitude of the hazardous event, but rather on the broader panels of possible flood events that can be "critical" compared to the central areas.

4 Discussion and Conclusions

The paper investigates the resilience of residential real estate markets to flood risk in Italy, a territory characterized by high hazard conditions and pronounced territorial disparities, well expressed by the dichotomy between central areas and "inner areas". By resorting to a multi-step methodology for the ex-ante evaluation of flood damages and their comparison with market values in different municipalities, it allows for reflecting on the existing territorial inequalities in real estate markets' resilience to flood risk, proxied by the "critical stage", defined as the most probable water depth at which economic damage equals the market value of a property.

The results from the methodology implementation, based on the case study of eight municipalities in Forlì-Cesena province (Italy), characterized by different conditions of accessibility to essential services, reveal a clear spatial pattern, with resilience systematically declining from central to peripheral municipalities. In this sense, these results reflect the climate resilience counterpart of the existing socio-economic and demographic disparities, clearly identified by the debate about the future of Italian "inner areas" and the related policy output: the National Strategy for Inner Areas". Furthermore, the lens of the real estate market clearly reveals the close link between climate resilience and other key issues of Italian inner areas, i.e., depopulation. Indeed, given their higher probability of experiencing a flood event with a "critical stage" of water, the obtained results reveal that in "peripheral" areas, climate events can be, more than in other territories, a catalyst for depopulation dynamics.

From this perspective, these findings can inform the spreading of a broader and climate risk-sensitive approach to the planning agenda for Italian peripheral areas, strongly

committed to reducing spatial inequalities. It highlights the need to transpose the differentiated and place-based approach, adopted to the design of intervention for marginal territories, also to the management of climate-related risks, which, till now, has not received the same level of "specific" attention. Specifically, the preliminary findings from this study point to the need to place climate-related risk mitigation and adaptation at the core of planning actions for these territories, which may appear to be less exposed to risk. Moreover, the results hint at the opportunity to adopt a place-based approach to risk planning in marginal territories, based on a more nuanced interpretation of risk beyond simplified application of the traditional hazard-exposure-vulnerability framework. Specifically, they clearly reveal that, in this context, exposure cannot be merely assessed in absolute terms based on the economic value of the assets at risk.

The proposed study, thus, offers insight that, if extended to other territories, may inform the rethinking of traditional planning approaches for risk mitigation and adaptation at the national scale by incorporating principles of spatial equity.

To this aim, future research perspectives will be devoted to extending the proposed analyses to other Italian territories, thus providing a more comprehensive picture of spatial inequalities in real estate markets' resilience, which can really contribute to strengthening the effectiveness and equity of the ongoing policy efforts. Furthermore, the informational value of the proposed approach could be further enhanced by extending the analysis to other building typologies, in terms of both function and structural characteristics, and by using more granular market data than the OMI one, to better capture the underlying mechanisms of spatial heterogeneity.

References

1. OECD: The Economic Consequences of Climate Change. OECD Publishing, Paris (2015). https://doi.org/10.1787/9789264235410-en
2. Weissbecker, I. (ed.): Climate Change and Human Well-being. Global Challenges and Opportunities. Springer, New York (2011). https://doi.org/10.1007/978-1-4419-9742-5
3. Goodess, C.M.: How is the frequency, location and severity of extreme events likely to change up to 2060? Environ. Sci. Pol. **27**(Supplement 1), S4–S14 (2013)
4. Behera, S.K.: Understanding the impact of climate change on extreme events. Front. Sci. **2**, 1433766 (2024). https://doi.org/10.3389/fsci.2024.1433766
5. Allaire, M.: Socio-economic impacts of flooding: a review of the empirical literature. Water Security. **3**, 18–26 (2018). https://doi.org/10.1016/j.wasec.2018.09.002
6. Beltrán, A., Maddison, D., Elliott, R.J.R.: Is it flood risk capitalized into property values? Ecol. Econ. **146**, 668–685 (2018). https://doi.org/10.1016/j.ecolecon.2017.12.015
7. Contat, J., Hopkins, C., Mejia, L., Suandi, M.: When climate meets real estate: a survey of the literature. Real Estate Econ. **52**(3), 618–659 (2024). https://doi.org/10.1111/1540-6229.12489
8. ISPRA. Rapporto sulle condizioni di pericolosità da alluvione in Italia e indicatori di rischio associati (2021). https://www.isprambiente.gov.it/files2021/pubblicazioni/rapporti/rapporto_alluvioni_ispra_353_16_11_2021_rev2.pdf, last Accessed 20 Mar 2026.
9. Loberto, M., Spuri, M.: L'impatto del rischio alluvione sulla ricchezza immobiliare in Italia. Questioni di Economia e Finanza. Banca d'Italia (Occasional Papers), 768 (2023). https://doi.org/10.32057/0.QEF.2023.0768.

10. Rossitti, M., Oteri, A.M., Torrieri, F.: Understanding geographies of architectural heritage abandonment in inner areas: a multi-dimensional investigation. In: Gervasi, O., et al. (eds.) Computational Science and its Applications – ICCSA 2024 Workshops. ICCSA 2024 Lecture Notes in Computer Science, vol. 14819, pp. 3–16. Springer, Cham (2024). https://doi.org/10.1007/978-3-031-65282-0_1
11. ISTAT: La Geografia delle aree interne nel 2020. Vasti territori tra potenzialità e debolezze (2022). https://www.istat.it/it/files/2022/07/FOCUS-AREE-INTERNE-2021.pdf, last Accessed 25 Mar 2026.
12. Cotella, G., Vitale Brovarone, E.: The Italian National Strategy for inner areas: a place-based approach to regional development. In: Banski, J. (ed.) Dilemmas of Regional and Local Development. Routledge, Abingdon-on-Thames (2020). https://doi.org/10.32057/10.4324/9780429433863-5
13. Rossitti, M., Torrieri, F.: The THEMA tool to support heritage-based development strategies for marginal areas: evidence from an Italian inner area in Campania region. Region 9(2), 109–129 (2022). https://doi.org/10.18335/region.v9i2.394
14. Merz, B., Kreibich, H., Thieken, A., Schmidtke, R.: Estimation uncertainty of direct monetary flood damage to buildings. Nat. Hazards Earth Syst. Sci. **4**(1), 153–163 (2004). https://doi.org/10.5194/nhess-4-153-2004
15. Thieken, A.H., et al.: Methods for the evaluation of direct and indirect flood losses. In: Simonovic, S.P., Bourget, P.G., Blanchard, F. (eds.) Proceedings 4th International Symposium on Flood Defence (ISDF), vol. 98,
16. Molinari, D., Ballio, F., Menoni, S., Handmer, J.: On the modeling of significance for flood damage assessment. Int. J. Disaster Risk Reduction. **10**, 381–391 (2014). https://doi.org/10.1016/j.ijdrr.2014.10.009
17. Torrieri F., Rossitti M. (2020). Spatial cost benefit analysis in flood risk management: evidence from a case study in Italy. Sustainable Mediterranean construction. Special Issue 4, 51–55 (2020). https://www.sustainablemediterraneanconstruction.eu/en/download/si-2020-04-051, last Accessed 30 Mar 2026.
18. Manganelli, B.: Il deprezzamento degli immobili urbani. FrancoAngeli Editore, Milano (2011)
19. Torrieri, F., Oppio, A., Rossitti, M.: Damage assessment for architectural heritage: the Cavallerizza Reale complex in Turin. Valori e Valutazioni. **30**, 71–84 (2022). https://doi.org/10.48264/vvsiev-20223005
20. DPS – Dipartimento per lo Sviluppo e la Coesione Economica: Le aree interne: Di quali territori parliamo? Nota esplicativa sul metodo di classificazione delle aree. (2014). http://www301.regione.toscana.it/bancadati/atti/Contenuto.xml?.id=5081285&-nomeFile=Delibera n.32 del 20-01-2014-Allegato-A, last Accessed 30 Mar 2026
21. Regione Emilia Romagna. Elenco Regionale dei prezzi delle opere pubbliche della Regione Emilia-Romagna (2025).
22. Giuliani, F., De Falco, A., Cutini, V., Di Sivo, M.: A simplified methodology for risk analysis of historic centers: the world heritage site of San Gimignano, Italy. Int. J. Disaster Resilience Built Environ. **12**(3), 336–354 (2021). https://doi.org/10.1108/IJDRBE-04-2020-0029
23. Davis, S.A., Skaggs, L.L.: Catalog of Residential Depth-Damage Functions Used by the Army Corps of Engineers in Flood Damage Estimations. U.S. Army Corps of Engineers, Fort Belvoir (1992)

24. FEMA: Hazus Flood Technical Manual. Hazus 5.1 (2022), https://www.fema.gov/sites/default/files/documents/fema_hazus-flood-model-technical-manual-5-1.pdf, last Accessed 15 Mar 2026.
25. Dell'Ovo, M., Torrieri, F., Oppio, A.: How to model stakeholder participation for flood management. In: Dargam, F., Delias, P., Linden, I., Mareschal, B. (eds.) Decision Support Systems VIII: Sustainable Data-Driven and Evidence-Based Decision Support. ICDSST 2018 Lecture Notes in Business Information Processing, vol. 313, pp. 67–75. Springer, Cham (2018). https://doi.org/10.1007/978-3-319-90315-6_6
26. Agenzia delle Entrate. Osservatorio del mercato immobiliare, https://www.agenziaentrate.gov.it/portale/aree-tematiche/osservatorio-del-mercato-immobiliare-omi, last Accessed 20 Mar 2026.

Designing Experiential Tourism Strategies in Rural Areas: A Systemic and Data-Driven Framework

Sara De Menech(✉), Asja Aulisio, Silvia Barbero, and Alice Barreca

Department of Architecture and Design, Politecnico Di Torino, Turin, Italy
sara.demenech@polito.it

Abstract. Rural areas across Europe are increasingly affected by long-term processes of demographic decline, economic marginalisation, and territorial fragmentation. In this context, tourism is often considered a potential driver of development; however, conventional tourism models have shown limited capacity to generate lasting benefits for fragile rural territories. In recent years, experience-based tourism models has emerged as an alternative paradigm, emphasising authenticity, local resources, and meaningful interactions between visitors and host communities. Despite growing academic interest, existing approaches to this field in rural areas remain fragmented and rarely translated into integrated, operational frameworks capable of supporting territorial decision-making. This paper addresses this gap by proposing a systemic design framework aimed at supporting the strategic development of tourism initiatives in rural contexts. The framework integrates territorial analysis, assessment of the local tourism offer, and systemic design tools within a coherent analytical process. Its objective is to move beyond isolated tourism products and toward the construction of territorial strategies grounded in local systems of resources, actors, and practices. The methodological approach adopted in this paper was originally developed in the framework of the SYSTOUR Interreg Europe project, and is here applied to the Lea-Artibai area (Basque Country, Spain). By constructing and analysing a knowledge base of tourism initiatives and integrating systemic design and evaluation tools, the approach supports the identification of leverage points and strategic directions for sustainable tourism development. The results show that a systemic and place-based perspective improves the understanding of these initiatives as a relational and co-designed process rather than an isolated product.

Keywords: experiential tourism · place-based strategies · economic development

1 Introduction and Research Background

Many rural and inner areas across Europe are currently facing long-term structural challenges, including demographic decline, limited economic opportunities, reduced accessibility and fragmented governance [1]. These dynamics have progressively weakened

© The Author(s), under exclusive license to Springer Nature Switzerland AG 2027
O. Gervasi et al. (Eds.): ICCSA 2026 Workshops, LNCS 16761, pp. 206–223, 2027.
https://doi.org/10.1007/978-3-032-30527-5_14

local communities and territorial systems, while at the same time intensifying the concentration of tourism flows in a limited number of highly pressured destinations, often associated with unsustainable development models [2]. In this context, the revitalisation of inner areas requires territorial-based strategies capable of redistributing tourism flows, strengthening local economies and preserving environmental and socio-cultural assets, but also of supporting processes of economic enhancement, territorial valuation, and value generation rooted in local specificities [3] [4] [5]. Over the last decades, tourism has undergone a significant transformation, shifting from mass-oriented models towards more sustainable, slow and experience-based forms [6]. The growing demand for authentic and locally grounded experiences has positioned experiential rural tourism as a potential lever for the revitalisation of inner areas, as it is strongly embedded in local landscapes, cultures and communities [7]. By focusing on meaningful interactions with places and local actors, experiential tourism can contribute to reinforcing territorial identity and supporting local economic systems, while responding to increasing concerns related to environmental sustainability and socio-cultural impacts [8]. In particular, walking paths and slow mobility infrastructures have emerged as strategic tools for structuring and connecting local experience offerings in rural contexts [9]. From the perspective of economic evaluation, these infrastructures and experiences can also be interpreted as territorial assets capable of activating local value chains, enhancing the value and attractiveness of places, and contributing to broader processes of sustainable territorial development [10] [11]. In this context, small and medium-sized enterprises play a key role as drivers of territorial development, often leveraging local knowledge, socio-cultural assets, and place-based traditions within local supply chains [12]. However, despite their strong territorial embeddedness, such enterprises frequently face limitations in terms of innovation capacity, skills, and access to resources, highlighting the need for integrated strategies capable of strengthening local economies through sustainable and experience-based tourism. In this sense, economic valuation becomes essential for understanding how experience-based tourism can contribute not only to visibility and attractiveness, but also to the consolidation of local entrepreneurial ecosystems, the enhancement of territorial capital, and the long-term sustainability of development processes [8]. At the same time, digital platforms play a central role in shaping how tourism experiences are communicated, accessed and perceived. They represent the primary interface between destinations and visitors, influencing visibility, narratives and decision-making processes, especially in less-known rural and inner areas. Beyond their promotional function, platform-generated data provide valuable insights into tourism practices, experiential patterns and information accessibility, offering new opportunities to analyse how experiences are communicated and discovered by potential visitors [13] [14]. Despite the growing relevance of experiential tourism for rural and inner area revitalisation, existing studies increasingly rely on platform-based data to analyse tourism dynamics [15] [16], yet their integration into holistic, data-driven frameworks capable of supporting territorially grounded strategies in inner areas remains limited. Current research tends to address either the promotional dimension of digital platforms or the qualitative dynamics of rural tourism separately, without bridging the two into a coherent analytical and strategic framework. As a result, the potential of platform-generated data to inform place-based policy design and territorial decision-making in

rural contexts remains largely unexplored [1] [2]. To address this gap, this paper proposes a systemic design framework aimed at supporting the strategic development of experiential tourism in rural contexts. The framework integrates territorial analysis, experiential tourism assessment, and design tools within a coherent analytical process. Its objective is to move beyond isolated tourism products and toward the construction of territorial strategies grounded in local systems of resources, actors, and practices. This desk-based investigation is complemented by field research, including on-site visits and interviews with institutions and professionals operating in the tourism sector, and is validated through a territorial case study focused on walking paths in the Lea-Artibai area, Basque Country, Spain. Overall, the framework is intended to support not only the interpretation of local tourism dynamics, but also the economic evaluation and strategic valorisation of territorial resources within a place-based development perspective. Against this backdrop, the main objective of the research is to develop an analytical framework capable of supporting the strategic design of this kind of tourism in rural areas through an integrated, data-driven, and evaluative approach. Specifically, the research aims to:

- structure and integrate heterogeneous territorial data within a coherent knowledge base;
- analyse experiential tourism initiatives in relation to territorial systems, local resources, and value-generation processes;
- apply systemic design tools to identify leverage points and strategic directions for sustainable tourism development;
- incorporate elements of economic evaluation and territorial valuation in order to interpret the development potential of experiential tourism initiatives;
- test the framework through an applied case study within a European policy context.

By addressing these objectives, the paper seeks to contribute to both academic debate and policy-oriented practice, offering a transferable framework for rural and mountain territories facing similar challenges. In particular, it contributes to advancing the dialogue between design, tourism studies, and economic evaluation, showing how experiential tourism can be analysed not only as a cultural and social phenomenon, but also as a driver of territorial enhancement, local value creation, and informed decision-making for inner-area development. The paper is structured as follows. Section 1 introduces the research background and problem. Section 2 presents the research framework and objectives. Sections 3 and 4 describe the methodology and case study. Section 5 discusses the results, which are interpreted in Section 6. Conclusions outline implications for policy and future research.

2 Methodological Approach

This research adopts a mixed-method approach aimed at analysing how experiential tourism can contribute to the revitalisation of rural territories [17]. The study is framed within a systemic perspective, which considers tourism as part of a broader territorial ecosystem composed of interconnected actors, resources and infrastructures [18]. Within this perspective, tourism dynamics are interpreted through the relationships between

local stakeholders, territorial resources and experiential offerings. The methodological design combines desk research, data analysis and field investigation in order to explore tourism dynamics in rural contexts. The research process follows a structured workflow articulated in several stages, including the definition of the theoretical framework, the analysis of digital tourism platforms, the implementation of qualitative field research and the interpretation of results through the integration of different sources of evidence (Fig. 1).

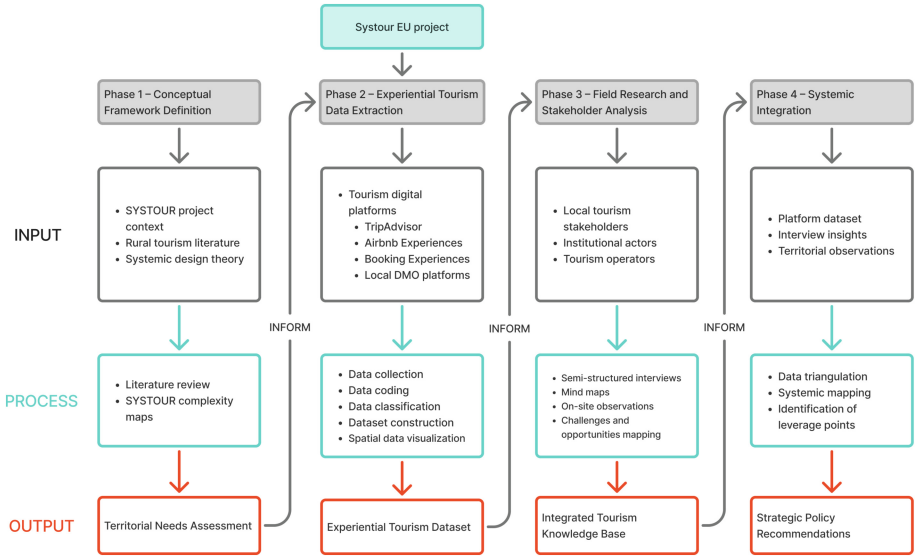

Fig. 1. Methodological workflow (Authors' elaboration)

The first phase consisted of defining the analytical framework and the main objective of the analysis through a targeted literature review in the framework of the Systour project [19, 20]. The second phase consisted of a desk-based analysis of digital tourism platforms presenting experiential tourism offers in rural contexts [20]. Digital platforms increasingly represent a key interface between destinations and visitors, particularly in rural areas where traditional marketing and distribution channels are often limited. Beyond their promotional function, these platforms constitute valuable sources of data for research, as they provide structured and comparable information on tourism experiences, including descriptions of activities, thematic categories, user feedback and spatial distribution [21]. For this reason, platform-based data were used as a primary analytical source to explore how the offers are structured, communicated and made accessible to potential visitors. To complement the desk research, the study was further developed through a qualitative field investigation conducted within the selected case study area (Third phase). The objective of this phase was to gain a deeper understanding of the local tourism ecosystem by collecting qualitative insights from actors directly involved in tourism development and territorial management. Additional qualitative data were collected through semi-structured interviews with stakeholders operating within

the local tourism system, including institutional actors, tourism operators and organisations involved in territorial development. To support the interview process, a structured questionnaire was developed in advance. The formulation of the questions followed the S.M.A.R.T. framework [22], ensuring that each question addressed at least one of the criteria related to specificity, measurability, achievability, relevance or time-bound objectives. This approach helped structure the interview process while allowing flexibility for respondents to provide qualitative insights based on their roles within the tourism ecosystem. The interviews were complemented by on-site observations and exploratory visits to relevant locations within the case study area. The qualitative information collected during this phase was subsequently synthesised through visual mapping tools, including mind maps, allowing the identification of key relationships, recurring themes and relational dynamics within the local tourism network. The final phase (4) of the research consisted of integrating the results obtained from the desk research and the field investigation. The triangulation between the theoretical framework derived from the literature review, the analysis of digital tourism platforms and the qualitative insights collected through stakeholder interviews enabled a comprehensive interpretation of experiential tourism dynamics in rural territories. This integration of different data sources supported the identification of opportunities and challenges related to tourism development and provided the basis for the formulation of strategic reflections aimed at strengthening sustainable experiential tourism in rural areas.

3 Case Study and Data Sampling: Lea-Artibai, Spain

Within the broader framework of the European SYSTOUR project, the Leartibai Fundazioa provided the institutional setting for testing and refining the proposed methodological framework within a real governance context. The foundation is a local development body operating through a multi-stakeholder governance model, positioned between public institutions and private actors. It acts as an intermediary organisation supporting rural development, innovation, entrepreneurship, and sustainable tourism strategies, translating strategic objectives into territorially adapted actions. This institutional context offered a relevant environment in which to apply the framework and assess its usefulness in relation to actual local development dynamics. The Lea-Artibai area was selected as the case study. It is a rural comarca located in northern Spain, characterised by a dispersed settlement structure and a population of approximately 26,000 inhabitants. Despite a relatively diversified economic base and a strong industrial legacy, the area faces structural challenges common to many European inner territories, including demographic ageing, limited international visibility, and seasonal tourism patterns [23, 24]. The unit of analysis adopted in this research is the experiential tourism initiative, defined as a tourism activity explicitly offered to visitors through digital platforms and organised by local actors. The platform analysis was initially conducted across six European rural regions involved in the broader research framework [2]. In order to ensure methodological consistency, TripAdvisor was selected as the common international platform for the comparative analysis across all regions. In addition, eleven national or regional tourism platforms were consulted in order to capture locally specific tourism offers that may not be fully represented on international platforms. For comparative purposes, the “Experiences” sections of Airbnb and Booking were also explored; however, in the analysed

rural contexts, these platforms presented a significantly smaller number of activities and largely reflected patterns already visible on TripAdvisor. Based on this platform selection, a structured dataset was created to systematically collect and organise information on tourism experiences available in the selected regions. A structured dataset composed of 90 experiences and 37 descriptive variables was constructed to analyse the characteristics of this specific sector across six European rural regions. Following a comparative cross-regional phase, this research focused more specifically on the Spanish case study to explore local dynamics in greater depth. For each of the six regions, the selection of the 15 experiences followed a two-stage process conducted within the geographical boundaries of the respective area. In the first stage, TripAdvisor was searched using the regional area as the reference and applying the eligibility criteria defined for the broader dataset. Where the number of results meeting the selection criteria on TripAdvisor was insufficient, a second stage was conducted on the corresponding national or regional DMO platform, which provided a more comprehensive and locally representative catalogue of experiences. Experiences were selected in the order in which they appeared on each platform until the target of 15 was reached, ensuring a sample that reflects the actual digital visibility of the local offer rather than a curated selection. This two-stage approach proved particularly relevant in the case of Lea-Artibai, where only two experiences met the eligibility criteria on TripAdvisor, and the Leartibai Turism platform — the official regional DMO — constituted the primary data source. The resulting dataset retains full analytical coverage of the dimensions central to this study: platform distribution, experience typology, operational characteristics, geographical reach, accessibility, cost-related aspects, management of the experiences, and the evaluation of sustainability and community embeddedness (Table 1).

Following the platform-based analysis, the methodology was further implemented through field research conducted during a two-month working period within the foundation. This phase was based on semi-structured interviews and direct on-site observation, with the aim of comparing digital representations of tourism experiences with on-the-ground dynamics. A total of five semi-structured interviews were conducted directly within the case study area with tourism operators, institutional representatives, and local professionals. In addition, the research was complemented by insights derived from a broader interview campaign conducted by an external consultancy across the 13 municipalities of the region, within which specific questions related to experiential tourism were integrated. This made it possible to access a wider range of qualitative perspectives on local tourism dynamics, stakeholder relationships, and place-based development opportunities. The interviews provided a deeper understanding of how experiential tourism is operationalised at the local level, how coordination among relevant actors takes place, and which structural barriers constrain territorial efficiency. At the same time, they helped identify latent opportunities that have not yet been fully leveraged within the local tourism ecosystem.

Table 1. Metadata description of tourism platform dataset (authors' elaboration based on [20])

DATASET METADATA			
Macrocategory	**Data content**	**Data value**	
Variable		**Type**	**Levels**
Experience Provider and Governance			
ATTRACTION/EXPERIENCE	The proposed activity is identified either as an experience or as a physical attraction to visit.	Text	ATTR, EXP
EXPERIENCE NAME	Title of the experience (EXP) as indicated on the platform	Text	–
PROPOSING SUBJECT	Organization or company proposing the experience	Text	–
PUBLIC/PRIVATE	Indicates whether the organization is public or private	Text	Public, private
PARTNERS	If applicable, external subjects involved in the experience and their respective roles	Text, close	YES/NO/NA
SCALE	specification of the geographical scale covered by the experience.	Text, close	Local, Regional, National, European, Global
AREA OF INTEREST	Specification of the geographical area of interest and the potential reach of the experience	Text, close	National, International
Experience Profile and Operational Characteristics			
TYPES OF EXPERIENCES OFFERED	Description of the main characteristics of the experience, indicating the type of proposed activity.	Text, open	Tour, Nature, Tastings, Architecture and Museums, ...
Municipality	Specification of the municipality where the experience takes place, and possibly the related province	Text, open	
Availability	Availability throughout the year, as recorded at the time of data collection	Text, close	Always available. Not available, Seasonal, NA
Duration	Duration of the experience indicated as hours.minutes	Number	

(*continued*)

Table 1. (*continued*)

DATASET METADATA			
Age range	Minimum and maximum age range requires to participate in the experience	Number	
Ticket	Whether a ticket is required to purchase or book.	Text	Yes/no/NA
Price	Ticket price per day	Number	
Languages	Language(s) in which the experience is delivered	Text, open	*Spanish, English,…*
Accessibility	Level of accessibility indicated on the platform	Text	Low…Total
Informative material	Availability of a written guide, brochure, or live guide	Text	live guide, written guide, NO, NA
Experience Evaluation and Territorial Value			
Valorisation	EXP makes possible to learn about, deepen and enhance local heritages and activities	Text	YES/NO/NA
Local reality	EXP is promoted by a local reality (at the most the region it belongs to)	Text	YES/NO/NA
Natural resource	EXP is based on a unique/rare natural feature of the territory	Text	YES/NO/NA
Testimony	EXP allows to get in touch with the local population (direct testimonies), narratives	Text	YES/NO/NA
Mobility	EXP allows to explore the territory through sustainable means of transport	Text	YES/NO/NA
Youth/women	EXP promotes/is promoted by/from the work of women/youth realities	Text	YES/NO/NA
Climate change	EXP raises awareness on climate change	Text	YES/NO/NA
Enogastronomy	EXP promotes traditional food and beverage-related experience	Text	YES/NO/NA
Inclusivity	EXP facilitates the accessibility to this area to more types of people/different types of abilities	Text	YES/NO/NA

4 Results

4.1 On-Desk Research: Digital Platforms Analysis

The platform-based analysis provides an initial overview of how experiential tourism is currently structured, communicated, and distributed across the Lea-Artibai area. The 87% of the tourist experiences were promoted through the Leartibai Turismo platform, while only two experiences, that satisfied the criteria, were founded on TripAdvisor. The DMO platform, managed by the Leartibai foundation, promotes all the touristic information of the comarca, including a section for the experiences, divided into Nature with offering for Active Tourism, Natural Heritage and Routes, Heritage that comprehend Cultural Heritage, Museums and Visits, and the last section for highlighting the peculiarity of Basque Identity. Each experience has a brief description, contact information and useful links. The organisations promoting the activities are almost entirely private, with one exception of a public entity, and the activities are available throughout the year (87%), although some outdoor activities may be more difficult at certain times of the year and are therefore part of the seasonal offer (13%). Despite the strong preservation and promotion of the Basque language (Euskera), the area of influence of the experiential offer extends to 60% of an international audience, with experiences extending locally in 67% of cases, regionally (Bizkaia) in 27% of cases and finally nationally in 6% of cases, with a single experience. The experiences offered are also quite affordable, with an average price of €6.30, and the need to book in advance or purchase an admission ticket was reported as positive for one-third of the experiences. Fig. 2 illustrates the distribution of the initiatives across the municipalities of the Lea-Artibai area, where each arc represents a different local context. The visualization highlights an uneven territorial distribution of experiences and reveals variations in thematic presence across municipalities, supporting a systemic interpretation of the tourism offer and the identification of spatial imbalances.

From a thematic point of view, the Lea-Artibai area is characterised by a relatively balanced distribution of experiences across different categories, with the exception of "Festivals & Events" and "Food & Wine tastings", which are less represented. In particular, the limited presence of food-related experiences appears inconsistent with the broader regional context, as the Basque Country is internationally recognised for its gastronomic excellence, hosting 24 Michelin-starred restaurants for a total of 34 stars [25]. This mismatch suggests a potential under-exploitation of gastronomy as a strategic asset within the local experiential tourism offer. Fig. 3 highlights the prevalence of nature- and outdoor-based activities within the local tourism offer, reflecting a strong connection between tourism practices and the natural landscape. This pattern confirms the role of environmental resources as a primary driver of the local tourism offer, while also indicating a potential lack of diversification toward other experiential domains.

A complementary perspective is provided by Fig. 4, which presents the aggregated scores across different fields of investigation. The results show a clear emphasis on local development and local business support, indicating that existing initiatives are strongly embedded within the local economic system. Natural resources, mobility, and diversification display moderate scores, suggesting partial integration of environmental and infrastructural dimensions. Conversely, aspects such as digitalisation, inclusivity, food

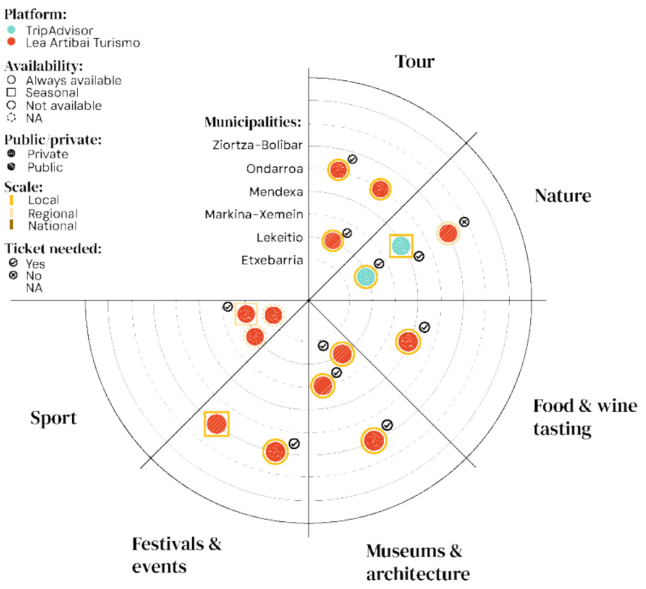

Fig. 2. Radial representation of experiential tourism initiatives across the municipalities of the Lea-Artibai area, showing the distribution of experience categories within the local territorial system (authors' elaboration based on [20])

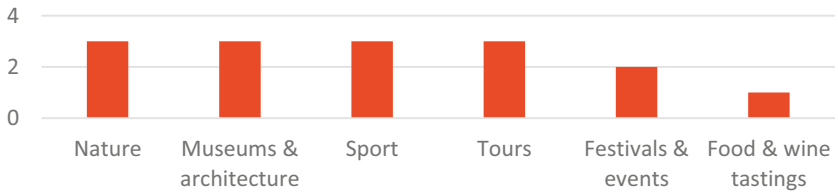

Fig. 3. Distribution of experiential tourism initiatives by type in the Lea-Artibai area, (authors' elaboration based on [20])

accessibility, and accessibility for diverse users remain underdeveloped. This distribution highlights animbalance, where strong local embeddedness is not yet matched by an equally developed set of enabling conditions, particularly in terms of accessibility and digital communication.

4.2 Results On-field Research: Stakeholders' Interviews

To complement and contextualise the findings of the digital platform analysis, a qualitative on-field research phase was conducted in the Lea-Artibai area, in collaboration with the local foundation. A total of five semi-structured interviews were conducted in person, in a one-to-one format, with stakeholders representing different roles within the local tourism ecosystem: tourism office representatives from the municipalities of Ondarroa

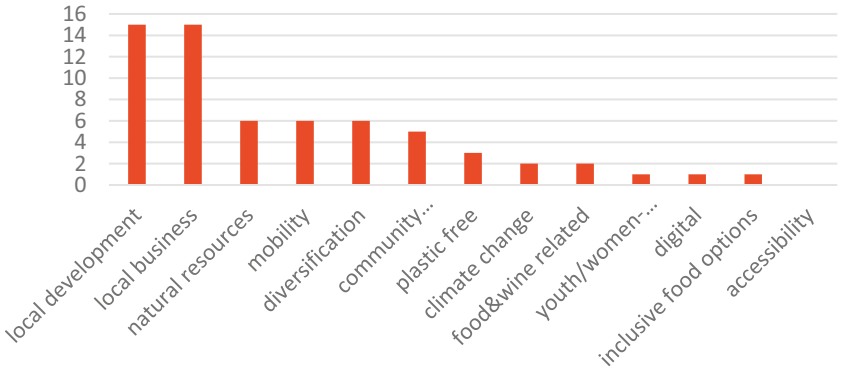

Fig. 4. Total scores of experiential tourism initiatives across the investigated dimensions in the Lea-Artibai area, showing the relative weight of local development, local business, natural resources, mobility, diversification, accessibility, and digital-related aspects (authors' elaboration based on [20]).

and Lekeitio, the tourism manager of Leartibai Fundazioa, and accommodation operators. Each interview was structured around a set of open-ended and semi-structured questions, organised thematically according to the four pillars of sustainability: environmental, social, economic and cultural. Given the diversity of profiles and the voluntary nature of participation, not all questions were addressed in every interview, and respondents were encouraged to prioritise the topics most relevant to their experience and role. Interview duration ranged approximately between 30 and 60 min. The qualitative data collected were subsequently analysed through thematic coding, identifying recurring patterns, emerging challenges and shared opportunities across the different stakeholder perspectives. The analysis highlights a shared orientation toward a territorially grounded and community-oriented model of tourism. Across stakeholders, experiential tourism is closely linked to local identity, with particular emphasis on Basque culture expressed through language, traditions and intangible heritage, alongside natural landscapes, gastronomy and maritime heritage as key attractors. Within this framework, different local strategies emerged through discussions with some key local actors. One of these is Ondarroa, which foregrounds the historical role of women in the port and canning industries as a distinctive experiential narrative, while Lekeitio focuses on maritime culture and gastronomy, with increasing attention to linguistic accessibility and inclusion. At the same time, inland actors such as Antsotegi Hotel illustrate how heritage conservation can be integrated with rural accommodation and active tourism, contributing to a partial redistribution of tourist flows toward less-visited areas.

To interpret the complexity of the local tourism system, the qualitative insights collected through interviews and field observations were organised through a thematic clustering process based on key sustainability dimensions (Fig. 5). Specifically, the identified elements were grouped into four main domains, social, economic, environmental, and cultural, allowing for a structured reading of challenges, opportunities, and ongoing initiatives within the Lea-Artibai area. This clustering approach supports the holistic

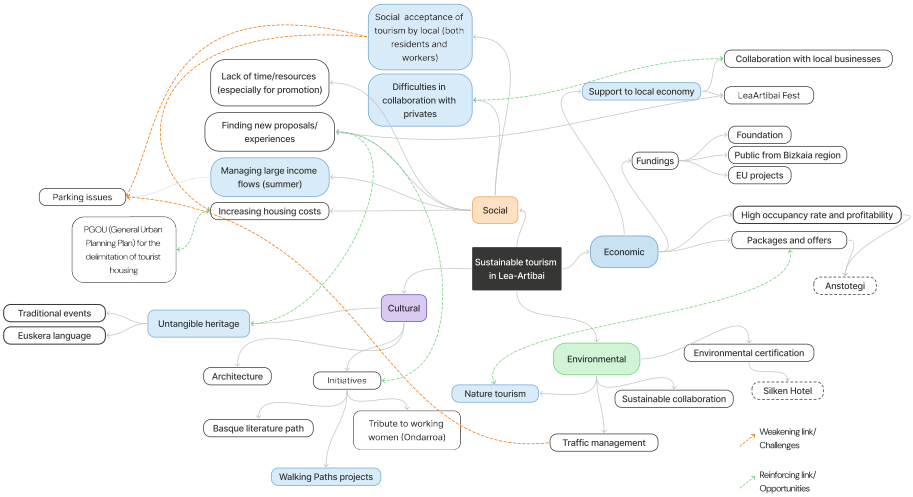

Fig. 5. Key insights mind map, categorised by the four sustainability pillars (authors' elaboration based on [20]).

interpretation of tourism development, highlighting the interconnections between different components of the territorial system and enabling the identification of critical issues and potential leverage points. These mappings reveal a diversified tourism offer, including outdoor activities such as hiking, cycling, canoeing and surfing, alongside cultural experiences and local gastronomy, which aligns with the predominantly domestic visitor profile. Secondary sources further support this alignment: according to the IBILTOUR Ocio 2023 study [26], tourism demand in the Basque Country shows a strong preference for nature-based and active experiences, typically associated with medium-length stays. At the same time, the analysis highlights a set of structural challenges affecting the development of the local tourism system. Governance fragmentation emerges as the most critical issue, as the multiplicity of actors involved, including public administrations, cultural organisations and private operators, generates a diversified but weakly coordinated offer. This condition limits the development of integrated strategies, reduces access to funding opportunities and weakens overall system coherence. Additional criticalities include the management of seasonal peaks, particularly in coastal areas such as Lekeitio and Ondarroa, where summer overcrowding and pressures on housing and mobility infrastructures generate increasing social tensions. Limited sustainable mobility options and an underdeveloped digital communication strategy further constrain the visibility and accessibility of tourism experiences. A central element emerging from the analysis is the strategic role of the walking path network within the territorial system. Across all stakeholder perspectives, these routes are recognised as key infrastructures capable of connecting landscapes, cultural heritage and local communities, enabling the development of distributed and experience-based tourism models. The area includes a network of six main trails crossing coastal and inland areas, among which the Lea Path (GR 38.3, where GR stands for Grande Randonnée, the European long-distance trail classification system [27]) represents a particularly significant case. Extending for

approximately 28 km from Munitibar to Lekeitio, the path follows the Lea River and connects multiple municipalities, integrating natural and cultural points of interest. It is important to acknowledge that participatory approaches carry an inherent risk of reproducing extractivist dynamics if they remain limited to consultation without ensuring tangible benefits for local communities. In the context of Lea-Artibai, this risk is partially mitigated by the institutional role of Leartibai Fundazioa as a locally embedded intermediary organisation with direct accountability to the municipalities it serves. Nevertheless, future implementations of the framework should explicitly consider mechanisms through which local stakeholders can derive concrete advantages from tourism development, whether through governance participation, revenue-sharing models, or community ownership of key assets. The analysis highlights both the potential and the current limitations of this infrastructure. While the Lea Path offers a strong basis for the development of slow and immersive tourism experiences, several infrastructural gaps persist, including irregular maintenance, insufficient signage, lack of service points and limited accessibility through public transport. These issues are not isolated but reflect broader governance challenges, particularly the separation between promotion and maintenance responsibilities, which affects planning capacity and funding allocation. The integration of insights from interviews, visual mappings, on-field observations and secondary sources provides a coherent picture of a territory characterised by high potential but limited systemic integration. The walking path network, and the Lea Path in particular, emerges as a strategic lever for the development of a low-impact tourism model based on slow mobility, local identity and distributed experiences. At the same time, fully activating this potential requires addressing the structural constraints identified, including improved coordination between stakeholders, investment in infrastructure and services, and the development of a coherent communication strategy.

4.3 Strategic Implications for Policy-Design

The findings from both the digital platform analysis and the on-field research converge on a set of structural challenges and opportunities that require targeted strategic intervention [20]. Building on the comprehensive understanding of the Lea-Artibai tourism ecosystem, its assets, challenges, stakeholder dynamics and infrastructural constraints, three interconnected recommendations are proposed. These are specifically oriented toward the sustainable development of the Lea Path as a model for slow, regenerative tourism, and are designed to be scalable to other rural areas facing similar challenges. The recommendations presented in Table 2 are grounded in the empirical findings of both the platform analysis and the stakeholder interviews, and are designed to support policymakers in translating territorial evidence into concrete strategic decisions. As demonstrated by the 2026 Tourism Action Plan recently developed by Leartibai Fundazioa [ref], this type of evidence-based approach can effectively inform local policy processes, contributing to the design of innovative and place-based tourism strategies for rural areas.

R1: Promoting Tourism Awareness through Strategic Communication and Community Engagement A prerequisite for the sustainable development of experiential tourism along the Lea Path is the construction of a shared territorial vision, built through

Table 2. Summary of policy recommendations with implementation parameters (authors' elaboration)

R	Empirical Evidence	Priority	Feasability
R1	Limited international digital visibility (87% DMO only); governance fragmentation; divergence between platform representation and on-field dynamics	Short-term	High — low cost, relies primarily on existing institutional structures and communication tools
R2	Underrepresentation of gastronomy and festivals; seasonal overcrowding in coastal areas; inland areas invisible despite rich territorial assets	Short/ Medium-term	Medium — requires coordination between actors and moderate investment in event design and digital promotion tools
R3	Low scores in accessibility and digital communication; infrastructural gaps along the Lea Path; separation between promotion and maintenance responsibilities	Medium/ Long-term	Low — requires significant investment in physical infrastructure, sensors and institutional coordination across multiple governance levels

the active involvement of local communities and the progressive activation of a coordinated stakeholder network. As emerged from the interviews, the current tourism offer suffers from fragmentation not only at the infrastructural level but also in terms of collective ownership: residents often perceive tourism as an external phenomenon rather than a community-driven process, and collaboration between public entities, private businesses and local associations remains inconsistent and difficult to sustain over time. Addressing this requires targeted communication initiatives, multilingual, place-based and rooted in local narrative, that frame the Lea Path as a resource generating tangible benefits for residents and visitors alike. Participatory processes such as co-design workshops and community mapping events can transform residents from passive recipients into active co-authors of the experience, while simultaneously serving as the entry point for building a structured stakeholder network connecting municipalities, cultural organisations, local businesses and activity providers around a shared development agenda.

R2: Balancing Tourism Flows through Sustainable Event and Territorial Promotion The coastal municipalities of the comarca absorb the vast majority of tourist flows, while inland areas along the Lea Path remain largely invisible to visitors despite their cultural and environmental richness. Addressing this imbalance requires the design of low-impact events and experiential itineraries that activate lesser-known territories and extend tourist stays beyond the summer peak. The existing Leartibai Fest (an annual event engaging over 149 participants that successfully combines local culture, community participation and environmental awareness) represents a proven model that could be expanded into a second annual edition or a series of thematic spin-off formats tied to seasonal rhythms and local traditions. Complementary digital tools, such as the integration of walking route tracks on platforms like Wikiloc or Strava through an official

DMO account, would increase route visibility and connect digital promotion directly to the territorial offer. The introduction of a traveller credential, whether printed or digital, that can be stamped at designated points along the path would further incentivise exploration of the full route, strengthen visitors' emotional connection to the territory and encourage repeat visits.

R3: Enhancing Paths Infrastructure and Services with a Data-Driven Approach One of the most critical barriers to the usability of the Lea Path is the lacking tourist services in its more rural segments, rest areas, water points, bike repair stations, adequate signage and sustainable transport connections to trail access points. Rather than pursuing a uniform infrastructural intervention across the entire route, a targeted, data-informed approach is recommended, focused on the identification of strategic nodes where concentrated investment would generate the highest impact on visitor experience and flow management. This approach involves two complementary tools: the installation of sensors at key points along the path to collect quantitative data on visitor flows, peak passage times and usage patterns; and the organisation of community-led mapping initiatives, to gather local knowledge and co-design the location and nature of service interventions. Wayfinding systems and multilingual signage at key intersections, light infrastructure such as rest stops and shuttle parking areas, and where appropriate, low-impact solar-powered lighting for evening use, would collectively enhance both the accessibility and the experiential quality of the route while minimising environmental disturbance.

5 Conclusions

This paper has investigated how experiential tourism can serve as a strategic lever for the revitalisation of rural inner areas, applying a systemic and data-driven framework to the case of Lea-Artibai in the Basque Country. By integrating digital platform analysis with qualitative field research, the study has produced a multi-layered reading of the local tourism ecosystem, revealing both its structural assets and its persistent gaps.

Three main findings emerge from the research. First, the experience-based tourism offer in Lea-Artibai is strongly locally embedded but weakly internationalised: despite a rich and diverse territorial base, the digital presence of local experiences remains largely confined to the regional DMO platform, with very limited visibility on international aggregators. This limits the region's capacity to attract broader visitor profiles and reduce its dependence on domestic, seasonally concentrated flows. Second, the offer is predominantly nature-based and low-cost, reflecting a genuine alignment between territorial identity and tourism strategy, but also pointing to underexplored dimensions, most notably gastronomy, cultural heritage interpretation and accessible tourism, that could significantly enrich and diversify the experiential proposition. Third, and perhaps most critically, a systematic divergence was identified between the image of Lea-Artibai as constructed through digital platforms and the actual dynamics of the local tourism ecosystem as revealed by stakeholder interviews. Platform-based data tend to foreground the most visible and easily bookable experiences, while the deeper relational, community-based and governance dimensions that shape the quality and sustainability

of the offer remain largely invisible to potential visitors and underrepresented in promotional narratives. Taken together, these findings point to a fundamental need for greater holistic integration, between digital communication and local identity, between governance structures and operational capacity, and between the experiences promoted online and the territorial resources that make them meaningful. The three policy recommendations proposed in this paper, community engagement and stakeholder network activation, flow redistribution through low-impact events and slow mobility, and data-driven infrastructure development, address precisely this integration gap, offering concrete and scalable directions for rural tourism strategy. From a methodological standpoint, the combination of quantitative platform analysis and qualitative field investigation proved particularly effective in capturing the complexity of experiential tourism dynamics in rural contexts. The use of visual mapping tools to synthesise interview findings enabled the identification of relationships and leverage points that would not have emerged from desk research alone. This mixed-method approach, grounded in systemic design principles, offers a transferable framework applicable to other European inner areas facing similar structural challenges.

The study presents some limitations that should be acknowledged. Although the platform analysis was conducted across the six rural areas involved in the SYSTOUR project, this paper focuses specifically on the Spanish case study of Lea-Artibai. As a result, the comparative cross-regional dimension of the broader research is not fully discussed here, which limits the extent to which the findings presented in this paper can be generalised. In addition, the accessibility evaluation focused mainly on physical dimensions, while cognitive, sensory, linguistic, and cultural aspects were not systematically addressed. Furthermore, the qualitative data collected through interviews, while providing rich contextual insights, reflect a specific moment in the ongoing evolution of the local tourism strategy and would therefore benefit from longitudinal validation. Future research could build on this foundation in two complementary directions. In the short term, the framework could be extended to the other five European regions involved in the broader research project, enabling a comparative cross-regional analysis that tests the consistency of the findings and the transferability of the methodological approach across different territorial, governance and cultural contexts. In the longer term, the framework holds potential for application to other rural and inner areas beyond the project's scope, particularly those sharing similar structural challenges such as demographic decline, seasonal tourism concentration and limited digital visibility. Further developments could also integrate economic valuation methods to assess the territorial impact of experiential tourism initiatives, and explore the intersection of walking tourism with adjacent sectors such as agriculture, cultural heritage management and health and wellness, as well as the progressive digitisation of rural walking routes through real-time flow monitoring and user-generated data collection, as promising tools for developing more adaptive and evidence-based governance models for inner-area development.

Acknowledgments. The authors would like to express their sincere gratitude to Leartibai Fundazioa, and in particular to Nekane Irusta Seara, Bakarne Larrinaga Arrasate, and Ainhoa Arrizubieta, for their support, collaboration, and valuable insights throughout the development of this research. Their contribution was fundamental in facilitating the fieldwork activities, deepening the understanding of the local territorial context, and supporting the finalisation of Sara De Menech's

Master's thesis, entitled *Toward a Systemic Design Framework for Experiential Tourism Strategies in Rural Areas*, supervised by Silvia Barbero, Alice Barreca, and Asja Aulisio at Politecnico di Torino - Department of Architecture and Design.

Disclosure of Interest: The authors have no competing interests to declare that are relevant to the content of this article.

Disclosure of Use of AI: The authors confirm that generative AI tools were used during the preparation of this manuscript solely to support text editing, language revision and qualitative data synthesis. All analytical processes, interpretations, findings and conclusions presented in this paper are the exclusive result of the authors' work. The authors take full responsibility for the integrity and accuracy of the content.

Funding. This research was conducted within the framework of the SYSTOUR project, co-funded by the Interreg Europe programme (Grant Agreement No. [ID 01C0279]). The funding body had no role in the design of the study, in the collection, analysis or interpretation of data, or in the writing of the manuscript.

References

1. Agapito, D., Valle, P., Mendes, J.: The sensory dimension of tourist experiences: capturing meaningful sensory-informed themes in Southwest Portugal. Tour. Manag. **42**, 224–237 (2014). https://doi.org/10.1016/J.TOURMAN.2013.11.011
2. Aulisio, A., Barbero, S., Barreca, A., Malavasi, G., Rolando, D.: From data collection to a cross-cutting analysis visualisation: territorial complexity overview to Foster responsible tourism in rural areas. In: Computational Science and its Applications – ICCSA 2024 Workshops. Springer Nature Switzerland, Hanoi, Vietnam (2024)
3. Rolando, D., Rebaudengo, M., Barreca, A.: Exploring the resilience of inner areas: a cross-dimensional approach to bring out territorial potentials. In: International Symposium: New Metropolitan Perspectives, pp. 182–190. Springer International Publishing (2022)
4. Ferretti, M., Favargiotti, S., Lino, B., Rolando, D.: Branding4Resilience: explorative and collaborative approaches for inner territories. Sustainability. **14**(18), 11235 (2022)
5. M. Ferretti, S. Favargiotti, B. Lino, D. Rolando: *Branding4Resilience\ ATLANTE. Ritratto di quattro territori interni italiani*. LetteraVentidue Edizioni (2024)
6. Bramwell, B., Higham, J., Lane, B., Miller, G.: Twenty-five years of sustainable tourism and the journal of sustainable tourism: looking back and moving forward. J. Sustain. Tour. **25**(1), 1–9 (2017). https://doi.org/10.1080/09669582.2017.1251689
7. E. Fiorenza: "L'influenza Del Turismo Esperienziale: Un'analisi Delle Nuove Tendenze Nel Settore Turistico," *Turismo e Psicologia* (2024)
8. Torriani, C., Barreca, A., Rebaudengo, M., Rolando, D.: Exploratory data analysis to support the second SNAI programming cycle. Aestimum. (2025)
9. D. Rolando, A. Barreca, A. Di Salvo, E. Fiore: Experiential tourism for undervalued territories: web platform objectives and quality features.
10. Stankulova, A., Barreca, A., Rebaudengo, M., Rolando, D.: The quantitative indicator-based evaluation for rural development. Int. Reg. Sci. Rev. **48**, 235–270 (2025)
11. Rolando, D., Barreca, A., Malavasi, G., Rebaudengo, M.: The enhancement of the Alta Valsesia territorial potential: a collaboration-based approach between academia and local actors. In: International Conference on Computational Science and its Applications, pp. 17–32. Springer Nature Switzerland (2024)

12. Maziliauske, E.: Innovation for sustainability through co-creation by small and medium-sized tourism enterprises (SMEs): socio-cultural sustainability benefits to rural destinations. Tour. Manag. Perspect. **50**, 101201 (2024). https://doi.org/10.1016/j.tmp.2023.101201
13. Deb, S.K., Mallik, N.: Effects of social Media in Tourism Marketing: outlook on user generated content. J. Digit. Mark. Commun. **3**(2), 49–65 (2023). https://doi.org/10.53623/jdmc.v3i2.316
14. van der Zee, E., Bertocchi, D., Vanneste, D.: Distribution of tourists within urban heritage destinations: a hot spot/cold spot analysis of TripAdvisor data as support for destination management. Curr. Issue Tour. **23**(2), 175–196 (2020). https://doi.org/10.1080/13683500.2018.1491955
15. I. O. Adekuajo, B. Oluwatosin Otokiti, F. Okpeke: Digital Platforms and Rural Tourism Transformation : A Case Study of E-Tourism Innovation in Underserved Regions, (2025) https://doi.org/10.32628/GISRRJ.
16. Yoo, K.H., Sigala, M., Gretzel, U.: Exploring TripAdvisor. In: *Tourism on the Verge*, Vol. Part sF1059, pp. 239–255 (2016). https://doi.org/10.1007/978-3-642-54089-9_17
17. P. Jones: Design methods for systemic design research Design Research Methods in Systemic Design, pp. 15–17 (2014). Accessed: 18 Jun. 2025
18. Pereno, A., Barbero, S.: Systemic design for territorial enhancement: an overview on design tools supporting socio-technical system innovation. Strateg. Des. Res. J. **13**(02), 113–136 (2020)
19. Aulisio, A.: Systemic Design & Sustainability Transitions. Co-Designing Policy Interventions within the Tourism Ecosystem.," Doctoral dissertation,. Politecnico di Torino, Torino (2025)
20. De Menech, S., Barbero, S., Barreca, A., Aulisio, A.: Toward a Systemic Design Framework for Experiential Tourism Strategies in Rural Areas, Master Degree. Politecnico di Torino, Torino (2025)
21. Luo, L., Zhou, J.: BlockTour: a blockchain-based smart tourism platform. Comput. Commun. **175**, 186–192 (2021). https://doi.org/10.1016/j.comcom.2021.05.011
22. S. O. Ahmad: Research Methodology : Interview Method, 2012, Accessed: 23 Jun. 2025
23. Atutxa, E., Calvo-Sotomayor, I., Laespada, T.: The employment ecosystem of Bizkaia as an emerging common in the face of the impact of COVID-19. Soc. Sci. **10**(11), 407 (2021). https://doi.org/10.3390/socsci10110407
24. Egberts, L.: Participatory heritage planning policy in coastal Europe: lessons from the HERICOAST project. In: Rodenberg, J., Wagenaar, P., Burgers, G.-J. (eds.) Calling on the Community: Understanding Participation in the Heritage Sector, an Interactive Governance Perspective, vol. 7, pp. 116–139. Berghahn Books (2023, ch. 6,)
25. Euskadi Basque Country: Gastronomia & Enoturismo, Spain (2022)
26. A. D. y A. Departamento de Gobernanza, "IBILTUR-OCIO Temporada 2023," (2024)
27. European Ramblers Association (ERA). Accessed: 30 Mar. 2026. Available: https://www.era-ewv-ferp.org/

Sustainable Mobility and Last MIle LogisTic in Urban Context (ELLIOT 2026)

An Exploratory Analysis of Injury Severities in Crashes Involving Vulnerable Road Users: Evidence from Thessaloniki, Greece

Stavros Kontorinis, Athanasios Demiris, Grigorios Fountas(✉), and Socrates Basbas

Department of Transportation and Hydraulic Engineering, School of Rural and Surveying Engineering, Aristotle University of Thessaloniki (AUTh), Thessaloniki 54124, Greece
gfountas@topo.auth.gr

Abstract. Despite the urgent need to improve urban mobility and ensure the safer co-existence of vehicles and road users, significant challenges remain. In Greece, the persistently high number of severe road traffic crashes highlights the urgent need to better understand the factors contributing to crash severity, particularly among the most affected groups—vulnerable road users (VRUs). This group typically includes pedestrians and cyclists who frequently face elevated crash and injury risks in the event of a collision. In this context, this study examines injury severity outcomes in road traffic crashes involving pedestrians and cyclists in Thessaloniki, Greece. Utilizing historical crash data (2019–2021) derived from the Hellenic Statistical Authority, a total of 906 injury crashes were analyzed, involving 764 pedestrians and 142 cyclists. The dataset contains detailed information on vehicles, individuals involved, road and environmental conditions at the time of each crash. To identify the factors associated with injury severity, binary logistic regression was applied, using the Backward Likelihood Ratio (LR) method for variable selection. Road characteristics, driver socio-demographic characteristics, and driving behavior were identified as significant determinants of injury severities. Our work provides a robust analytical framework for enhancing road safety analysis and supporting policymakers in their efforts to protect vulnerable road users.

Keywords: Road Safety · Vulnerable Road Users · Binary Logistic Models

1 Introduction – Literature Review

Vulnerable road users refer to individuals who are particularly exposed to the risk of road traffic crashes, due to either the lack of protective equipment or their physical inability to safeguard themselves in the event of a collision. In cases where a city or region lacks the necessary infrastructure to support the safe coexistence of road users, it is expected that a disproportionately high number of crashes is likely to involve either cyclists or pedestrians. Such infrastructure, including sidewalks, bike lanes, and pedestrian signals, provides safer conditions for vulnerable users and contributes to reducing the severity of injuries in the event of an accident [1].

© The Author(s), under exclusive license to Springer Nature Switzerland AG 2027
O. Gervasi et al. (Eds.): ICCSA 2026 Workshops, LNCS 16761, pp. 227–241, 2027.
https://doi.org/10.1007/978-3-032-30527-5_15

1.1 Road Traffic Crashes and Vulnerable Road Users (VRUs)

Road traffic injuries remain a major public health concern, ranking among the leading causes of death worldwide despite continuous advancements in vehicle safety and traffic management systems [2]. Previous research indicates a persistent burden of road traffic crashes, with reported frequencies increasing by approximately 12% between 1992 and 2018 [3]. In 2021, road traffic fatalities reached the number of 1.19 million globally, with 21% of them being pedestrians and 5% cyclists [4]. Vulnerable road users, particularly pedestrians and cyclists, are disproportionately affected, accounting for nearly 46% of road fatalities in Europe as indicated by previous research findings [5]. Additionally, the growing popularity of alternative mobility solutions, such as e-scooters, constantly proposes road safety challenge for VRUs [6]. This kind of evidence has led to a growing shift in road safety research from crash frequency analysis to the examination of injury severity, which provides a meaningful dimension of traffic safety evaluation and its impact on public health and society overall. Moreover, road safety is explicitly embedded within the United Nations Sustainable Development Goals (SDGs), which aim to reduce fatalities and serious injuries obtained from road traffic crashes and promote safe and sustainable transport systems, highlighting the critical role of traffic safety in achieving broader sustainability objectives [7].

In road safety analysis, risk is conceptualized as a function of three key components: exposure, crash occurrence, and vulnerability. Exposure reflects the extent to which road users are present in the transport system, while occurrence captures the probability of a crash taking place. Vulnerability refers to the likelihood that a crash results in severe or fatal injuries. The present study focuses specifically on the vulnerability component, by modelling injury severity outcomes in crashes involving VRUs. Our analysis provides targeted insights into the factors that increase the probability of severe injury conditional on crash occurrence, thereby complementing existing research that primarily emphasizes crash frequency or exposure patterns. This severity-oriented perspective is particularly relevant in congested urban environments such as Thessaloniki, where detailed exposure data are often unavailable, yet understanding injury outcomes remains critical for effective road safety interventions.

In crashes involving vulnerable road users, injury severity is mostly determined by the interaction of demographic characteristics, traffic conditions, roadway design, and behavioral nuances of the road users. VRUs are often road users with limited physical protection, and, as such, they are more exposed to high-speed traffic. This condition increases the likelihood of severe and fatal outcomes, particularly in the absence of dedicated infrastructure and effective speed management measures [1]. Recent studies tend to increasingly adopt severity-based analytical approaches to support targeted interventions aimed at reducing serious and fatal injuries rather than crash occurrence alone.

1.2 Pedestrian-Related Crashes and Injury Severity

Demographic Factors

Age is consistently identified as one of the strongest predictors of injury severity in pedestrian crashes. Elderly pedestrians are disproportionately affected, accounting for

42% of severe injuries and up to 71% of fatal pedestrian crashes on rural roads in Spain [8]. Several studies report that the average age of severely injured pedestrians exceeds 70 years [9], with individuals over 65 facing markedly increased fatality risk following both collisions and falls [10].

The continued ageing of the population contributes to the intensification of this trend. Head and neck injuries are particularly prevalent among elderly pedestrians and are significantly associated with fatal outcomes [11]. Moreover, delayed prioritization in emergency medical treatment often due to underestimation of injury severity has been shown to contribute to increased mortality among older pedestrians [12]. These findings highlight age as a critical determinant in injury severity modeling.

Gender-related disparities have also been observed as key determinants of crash injury severities. While male pedestrians are involved in a higher number of crashes overall, female pedestrians exhibit a higher propensity of sustaining severe injuries. Evidence from Sweden indicates that approximately 69% of injured pedestrians were women [10], suggesting that physiological vulnerability and higher exposure patterns may influence injury outcomes. In general, men tend to sustain a greater proportion of head and facial injuries, whereas women exhibit higher likelihood of lower-extremity fractures [9].

Speed, Temporal Factors and Visibility

Vehicle speed is a dominant factor affecting pedestrian injury severity. The risk of severe injury increases significantly at impact speeds exceeding 25 km/h, while fatal injury probability rises sharply beyond 40 km/h [13]. Notably, 63% of fatal pedestrian crashes occur on roads with speed limits above 30 km/h [13]. Crashes occurring during weekends are associated with increased injury severity, partly due to alcohol consumption, reduced lighting conditions, and altered traffic behavior [14]. Similarly, nighttime crashes present substantially higher severity levels, as reduced visibility impairs driver reaction times and pedestrian detection [15]. It is estimated that approximately 25% of pedestrian crashes result from drivers' failure to perceive pedestrians in time [16].

Vehicle Type and Roadway Characteristics

Heavy vehicles and freight trucks are particularly associated with severe and fatal pedestrian injuries due to their mass and longer stopping distances [17]. In this context, the type of intersection where the crash occurred also plays a critical role. Roundabouts have been associated with reductions in severe injuries and fatalities, whereas T-intersections exhibit increased probabilities of severe and fatal outcomes [18]. As for roadway geometry, signalized intersections demonstrate different risk profiles compared to unsignalized ones, with higher severity observed in environments with increased heavy vehicle presence and higher speed limits [19]. At unsignalized intersections, even small increases in speed limits markedly elevate the probability of severe pedestrian injury, while the presence of marked crosswalks has been shown to mitigate injury severity [19]. Additionally, wider roadways are consistently linked to more severe pedestrian injuries, primarily due to increased operating speeds [17]. However, drivers tend to overestimate their driving abilities and confidence and show less attention on familiar roads, a phenomenon

referred to as the JIMBY (Just in My Backyard) effect, which has been associated with an increased crash risk [20].

Pedestrian Behavior
Pedestrians often fail to comply with the traffic and road safety regulations. Signal violations, midblock crossings away from designated crosswalks, and walking along the carriageway are associated with increased crash severity [21, 22]. In Greece, risky pedestrian behaviors, particularly red-light violations and crossings more than 30 m away from crosswalks are commonly observed and strongly correlated with severe injury outcomes [23].

Contextual Factors
Factors such as inadequate lighting, obstructed visibility due to parked vehicles, and mobile phone use further exacerbate risk [24, 25]. These findings highlight the combined influence of behavioral and infrastructural deficiencies on pedestrian injury severity.

1.3 Cyclist-Related Crashes

Cycling is widely recognized as a sustainable and congestion reducing transport mode [26], actively promoted through European mobility policies [27]. Nevertheless, cyclists account for approximately 6% of fatal road traffic crashes in the EU [28], reflecting their high vulnerability in mixed-traffic environments. The global share of fatalities has risen up to 1% among cyclists since 2010 [6]. Unlike pedestrians, injured cyclists are typically younger, with most crash-involved cyclists aged between 34 and 54 years and an average age of approximately 44 years [29]. Most injured cyclists are male, a pattern consistent across multiple national datasets [29].

Protective Equipment and Visibility
As discussed previously, cyclists are particularly susceptible to injury in the event of a traffic crash due to their limited physical protection. In Italy, helmets were used in only 45.6% of recorded cycling crashes [30]. Helmet use is associated with a 32% reduction in severe facial and mandibular injuries [31]. Reduced nighttime visibility further increases injury severity, particularly when cyclists lack adequate lighting or reflective equipment [27].

Crash Type, Vehicle Interaction and Intersections
Single-bicycle crashes do not present consistent severity patterns. However, adverse weather and surface conditions increase the likelihood of severe injuries [32]. In multi-vehicle crashes, interaction with passenger cars significantly affects injury outcomes. Impact dynamics indicate that greater cyclist body mass may reduce post-impact velocity and injury severity, while larger collision angles are associated with less severe injuries [33].

The majority of cyclist–vehicle collisions occur during regular traffic flow, often involving turning vehicles and opposite-direction movements [29]. Collisions involving Sport Utility Vehicles (SUVs) are particularly severe. Due to their front-end design,

SUVs increase the likelihood of head injuries and fatal outcomes compared to conventional passenger cars [34]. Unsignalized intersections are linked to increased probabilities of both minor and severe cyclist injuries, as drivers frequently fail to decelerate adequately when approaching such locations [35]. This finding underscores the importance of traffic control and intersection design in mitigating injury severity among cyclists.

1.4 The Case of Thessaloniki

Urban environments with dense traffic, limited space allocation for active travel modes, and enforcement disparities present elevated risks for vulnerable road users. Thessaloniki exemplifies many of these challenges, including insufficient pedestrian infrastructure, fragmented cycling facilities, and high vehicle dominance. These conditions

Table 1. Summary of prior studies on VRUs safety.

Thematic Area	Peer-reviewed studies	Main Findings and Key Factors
Demographic related vulnerability	Casado-Sanz et al. (2019) [8] Gálvez-Pérez et al. (2023) [3] Etehad et al. (2015) [11] Ang et al. (2017) [12] Värnild et al. (2023) [9] Amin et al. (2022) [10]	Elderly pedestrians are disproportionately represented in severe/fatal crashes. Age-related physical frailty amplifies injury consequences even at low impact speeds. Gender and age interact with speed limit to determine serious injury risk.
Speed limit and road Infrastructure	Kröyer (2015) [13] Haleem et al. (2015) [19] Mokhtarimousavi et al. (2020) [14] Rifaat et al. (2011) [37] Zafri & Khan (2023) [39] Da Silva & Bezerra (2024) [1] Bassani et al. (2020) [2] Wennberg et al. (2024) [9] Tapp et al. (2015) [20]	Fatal pedestrian risk rises sharply above 30 km/h. Non-signalized locations carry significantly higher severe/fatal injury risk. Dedicated VRU infrastructure consistently reduces injury severity. Street pattern and spatial built environment impact crash severity. Public support for 20 mph limits is high but actual speed compliance remains inconsistent.
Behavioural factors and analytical methods	Alogaili & Mannering (2022) [15] Tamakloe et al. (2023) [25] Salehian et al. (2023) [18] Elalouf et al. (2023) [17] Nikolaou et al. (2023) [23] Raoniar & Maurya (2022) [22] Sheykhfard et al. (2023) [24]	Lighting conditions create distinct severity profiles. Random parameter & ML models outperform standard regression techniques. Safety attitudes and risk perception mediate self-declared pedestrian behaviour.

(*continued*)

Table 1. (*continued*)

Thematic Area	Peer-reviewed studies	Main Findings and Key Factors
Cyclist injury severity	Fountas et al. (2021) [32] Alnawmasi & Mannering (2023) [27] Bahrololoom et al. (2020) [33] Monfort & Mueller (2023) [34] Yang et al. (2021) [26] Wang et al. (2015) [35] Beck et al. (2016) [29] Levulytė et al. (2016) [28] Cittadini et al. (2024) [30] Stassen et al. (2024) [31] Kaya et al. (2021) [16] Marisamynathan & Vedagiri (2018) [21] Shinar (2012) [5] WHO (2023) [4] Fountas et al. (2026) [6]	Vehicle speed and mass jointly determine cyclist fatality risk; SUVs cause significantly worse injuries than cars. Nighttime crashes are consistently more severe. Junction type, road surface, and lighting are top risk contributors. Helmet use reduces injury severity in bicycle and e-scooter crashes. Driver scanning failures are a primary cause of VRUs crashes at intersections.

intensify exposure and amplify injury severity when crashes occur, reinforcing the need for severity-focused analyses rather than crash frequency alone.

In many developing countries, road traffic crashes are a major contributor to global deaths and injuries. Vulnerable road users are unable to protect themselves in the event of a collision, meaning not only drivers and passengers are at risk of sustaining an injury during a collision event [36]. It is emphasized that vulnerable road users are exposed to a higher level of risk on streets where vehicles travel at high speeds [37]. This highlights the importance of implementing speed limits as a traffic calming measure to, among others, mitigate the risk of hazardous incidents and associated injuries.

Although extensive research has studied injury severity in traffic crashes involving vulnerable road users and motorized vehicles, empirical evidence at the city level remains limited, particularly for Greek urban environments that exhibit unique challenges as far as the interactions between motorized and non-motorized users are concerned. In our study, we investigated the determinants of injury severity in Thessaloniki, using Binary Logistic Regression models, to estimate the probability of severe or fatal outcomes, based on crash-specific characteristics. A data-driven, severity-oriented assessment for Thessaloniki is provided, facilitating a better understanding of the factors associated with serious and fatal injuries among vulnerable road users. Table 1 summarizes the reviewed studies and their findings.

In this context, the findings of this study are relevant to a wide range of local stakeholders involved in urban mobility and road safety. Public authorities can utilize these results to design targeted interventions aimed at protecting VRUs and transport planners may benefit from the identification of high-risk infrastructural characteristics. In addition, enforcement authorities can use these insights to prioritize monitoring of traffic

violations, while private stakeholders, including mobility service providers and insurance companies, may leverage the results to better assess and mitigate risk associated with VRUs.

Our study is organized as follows: Sect. 2 presents the data collection process and the main characteristics of the study area, Sect. 3 describes the methodological framework and the statistical models used for the analysis of injury severity, Sect. 4 reports the empirical results and discusses the key findings for both pedestrian- and bicyclist-involved crashes and Sect. 5 summarizes the main conclusions, outlines policy implications, and highlights limitations and directions for future research.

2 Data

For the crash analysis, data obtained from the public database of the Hellenic Statistical Authority covering the period between 2019 to 2021. The dataset comprised traffic crashes recorded by police authorities within the regional unit of Thessaloniki, Greece including detailed information about the vehicles involved (type of vehicle, vehicle maneuvering during the crash, driver's license), the persons involved (age, gender, injury severity, travel purpose), roadway and environmental characteristics at the time of the crash. Crashes resulting in no injuries are not reported in the public crash dataset.

During the three-year span, 4,366 accidents occurred in our case study area, while 906 involved at least one vulnerable road user, pedestrian or cyclist. Specifically, out of the total crashes analyzed, 142 involved at least one cyclist, highlighting the significant presence of cycling-related incidents within the dataset. Meanwhile, 764 crashes involved at least one pedestrian, underscoring the vulnerability of pedestrians in traffic accidents. These figures reflect the considerable risks faced by vulnerable road users, which became a central focus of the analysis in order to better understand the dynamics and factors contributing to such incidents. Information relating to the exposure of vulnerable road users (e.g., traffic volumes for pedestrians and cyclists) was not available in the dataset. Regarding the severity of injuries observed, a composite indicator was created in Microsoft Excel that takes into consideration all the individuals injured by each accident provides the more severe injury outcome observed in the crash. Working through the environment of IBM SPSS Statistics, two separate datasets, and subsequently, statistical models were developed, one focusing on traffic crashes involving pedestrians and the other on crashes involving bicyclists.

The main reason for conducting two separate statistical analyses was that certain covariates may influence injury severity differently in bicycle-related crashes compared to pedestrian-related crashes, due to the distinct mobility and physical protection characteristics of each user group. In the pedestrian model, 93.5% of the crashes were slight injuries, 2.2% severe injuries and 4.3% fatal. Additionally, for cyclist-involved crashes, 95.1% were slight injuries, 2.1% severe injuries and 2.8% were fatal. In Tables 2 and 3, some key descriptive statistics are illustrated.

Table 2. Distribution of Injury Severity in crashes involving Vulnerable Road Users.

	Slight	Serious	Fatal
Accidents involving Pedestrians	(714) 93.5%	(17) 2.2%	(33) 4.3%
Accidents involving Bicyclists	135 (95.1%)	3 (2.1%)	4 (2.8%)

Table 3. Age Group of Vulnerable Road Users involved in accidents

	0–14	15–30	31–45	46–60	61+
Pedestrians	11.8%	19.7%	13.7%	16.5%	38.3%
Bicyclists	15.9%	30.4%	26.8%	17.4%	9.4%

3 Methodology

Prior to estimating the statistical models for crash injury severities, non-parametric inferential statistical analyses were conducted to explore the relationships between variables and identify pairs of variables that may exhibit statistically significant associations, thus warranting further statistical investigation.

To understand how multiple variables in the sample influence injury severity, we estimated a Binary Logistic Regression model. Binary Logistic Regression is a statistical modeling technique used when the dependent variable is binary (i.e., takes values of 0 or 1). It estimates the probability of a specific outcome, making it particularly suitable for analyzing relationships where the response variable represents two possible categories [38]. For the purposes of the analysis, serious and fatal injuries were combined into a single outcome category. The equation that best describes the model is as follows [39]:

$$\log\left(\frac{P}{1-P}\right) = \beta_0 + \beta_1 X_1 + \beta_2 X_2 + \cdots + \beta_n X_n \quad (1)$$

Where $\log\left(\frac{P}{1-P}\right)$ is the probability of the event occurring, meaning the higher value P gets, the likelihood of a serious or fatal injury increases [39]; β_0 is the constant; $\beta_1 + \beta_2 + \ldots + \beta_n$ are the regression coefficients; and $X_1 + X_2 + \ldots + X_n$ are the independent variables that affect the injury severity probability. This model is employed to evaluate the statistical significance of the independent variables in relation to injury severity and to quantify both the direction and magnitude of their effects. Specifically, the exponentiated coefficient (exp (β)) provides the multiplicative change in the odds of the injury outcome for a one-unit change of the independent variable. Furthermore, it enables the identification of the most influential predictors based on estimated coefficients. Models' performance was evaluated using goodness-of-fit measures: Hosmer and Lemeshow Test, Cox and Snell R Square, Nagelkerke R Square and log-likelihood values. Every variable included in the models was statistically significant at a confidence level of at least 90%.

4 Results and Analysis

4.1 Inferential Statistics

In the context of a preliminary investigation of possible statistical relationships among injury severity and various potential explanatory factors, a series of inferential analyses were conducted, with the findings summarized in Table 4. Inferential statistical analysis was conducted to investigate the presence of statistically significant relationships between injury severity and a wide range of variables describing the characteristics of vulnerable road users, roadway infrastructure, and accident conditions. Given that injury severity constitutes an ordinal variable and that normality assumptions were not satisfied, non-parametric statistical tests were used. Specifically, the Mann–Whitney U test, the Kruskal–Wallis H test, and the Friedman test were applied, depending on the nature and grouping of the examined variables. Statistical significance was assessed at the 5% level ($p < 0.05$), and all analyses were performed using IBM SPSS Statistics.

The results of the inferential analysis revealed that injury severity is significantly associated with several demographic, spatial, and roadway-related factors. In particular, the age group of involved pedestrians and vehicle drivers exhibited statistically significant differences in injury severity outcomes ($p < 0.05$), indicating an increased vulnerability among older groups. Furthermore, roadway characteristics such as road width and road type were found to be significantly related to injury severity, with wider road sections and arterial roads being associated with a higher likelihood of severe or fatal injuries. Variables capturing the overall crash context and user behavior, including pedestrian position and movement at the time of the accident, also demonstrated statistically significant relationships with injury severity.

Table 4. Inferential tests conducted among variables and crash injury severity

Independent Variables	Inf. Test
Age group of pedestrians involved	Friedman
Age group of drivers	Friedman
Residential area	Mann-Whitney U
Road type	Kruskal Wallis H
Lighting conditions	Friedman
Road width	Friedman
Age of driver when driver licence obtained	Friedman
Vehicle's time of first registration	Friedman
Breathalyzer test type	Friedman
Breathalyzer test result	Friedman
Position and movement of pedestrian	Friedman

4.2 Model Estimation Results for Pedestrian-Involved Crashes

The binary logistic regression model for injury severity in pedestrian-involved crashes was estimated following variable selection using the Backward Likelihood Ratio method. The dependent variable is binary: 1 = serious or fatal injury as the most severe outcome observed in the crash, 0 = slight injury. The model results, together with goodness-of-fit measures and key descriptive statistics of the independent variables, are presented in Table 5.

Table 5. Estimation results of the Binary Logistic model for pedestrian-involved crashes.

Variable Description	Coeff.	Std. Error	p-value	Exp.B
Constant	−5.505	0.824	0.000	0.004
Gender (1 if Female, 49.35%, 0 otherwise)	−1.091	0.358	0.002	0.336
Age group of pedestrian involved (1 if driver aged 61+, 38.30%, 0 otherwise)	0.359	0.131	0.006	1.432
Road width (if road width was 5 to 7 m, 22.30%, 0 otherwise)	0.404	0.123	0.001	1.498
Vehicle maneuver (if vehicle moved normally, 54.30%, 0 otherwise)	0.889	0.510	0.081	2.433
Traffic violation (1 if there was a violation of a traffic light or of a STOP sign, 5.10%, 0 otherwise)	2.908	0.606	0.000	18.315
Speed limit violation (1 if there was a speed limit violation, 6.30%, 0 otherwise)	2.669	0.895	0.003	14.429
Pedestrian position (1 if pedestrian moved regularly, 18.50%, 0 otherwise)	−1.923	0.748	0.010	0.146
Heavy vehicle involved (if heavy vehicle involved, 0 otherwise)	1.371	0.498	0.006	3.938
Goodness-of-fit measures				
Hosmer and Lemeshow test	Chi-square	Deg. Of freedom	Sig.	
	8.778	8	0.361	
−2 Log Likelihood	293.307			
Cox and Snell R Square	0.095			
Nagelkerke R Square	0.247			

Results of the pedestrian model indicate that several factors significantly influence the probability of serious or fatal injury outcomes in crashes involving pedestrians. Female pedestrians have substantially lower likelihood of sustaining serious or fatal injuries compared to males, a finding that has been also documented in previous studies [40]. Additionally, older pedestrians, aged more than 61 years old, are more likely to sustain severe pedestrian injury outcomes, potentially due to slower reaction times [41]. Road width is also found to be correlated with severe injuries, indicating that crashes

occurring on narrower road sects. (5–7 m), are linked to serious or fatal injuries for pedestrians. Narrower roads can sometimes be more hazardous, because of the limited space for pedestrians to comfortably move. Even though vehicles' speed is usually lower in these cases, the limited space makes it more difficult for road users to safely interact [42]. Moreover, the involvement of heavy vehicles in a road crash was found to increase the likelihood of serious pedestrian injuries, possibly capturing complex interaction mechanisms among road users [43].

Regarding road users' behavior, we found that even normal driving maneuvers can contribute to elevated injury severity, when combined with additional crash risk factors. This outcome may be attributable to pedestrians' non-compliant road behavior, a factor that has also been highlighted in existing literature [44]. It is also in line with the variable of pedestrian position, that was also found to be statistically significant in our first model, indicating that when pedestrians adhere to regular crossing or walking positions, the likelihood of serious or fatal injury related to a road crash is importantly reduced. Traffic violations, in particular violations of a traffic light or of a STOP sign, dramatically increase the possibility of severe injury. Similar effects are also observed for speed limits violations from the side of vehicle drivers; the latter result underscores the critical importance of driver compliance with traffic controls and speed limits in protecting vulnerable road users. This finding also suggests that policymakers should move beyond infrastructure interventions only and invest in targeted educational campaigns, which reinforce the legal and ethical responsibility of drivers toward pedestrian safety.

4.3 Model Estimation Results for Bicyclist-Involved Crashes

A separate binary logistic regression model was developed for bicyclist-involved crashes using the same Backward Likelihood Ratio approach for variable selection. The dependent variable again distinguishes serious or fatal injury from slight injury outcomes. Estimation results and goodness-of-fit statistics are presented in Table 6.

Table 6. Estimation results of Binary Logistic Model for bicyclist-involved accidents.

Variable Description	Coeff.	Std. Error	p-value	Exp.B
Constant	−3.976	0.701	0.000	0.019
Road width (if road width was 5 to 7 m, 22.3%, 0 otherwise)	1.863	0.840	0.027	6.441
Traffic violation (1 if there was a traffic violation of a traffic light or of a STOP sign, 5.10%, 0 otherwise)	1.639	0.959	0.087	5.150
Goodness-of-fit measures				
Hosmer and Lemeshow test	Chi-square	Deg. Of freedom		Sig.
	0.080	1		0.778
−2 Log Likelihood	49.138			
Cox and Snell R Square	0.046			
Nagelkerke R Square	0.141			

This model is more parsimonious in terms of the number of independent variables, which is expected given the smaller sample of bicyclist crashes. In line with our previous pedestrian-focused statistical model, road width emerges as the main influential predictor, as also suggested by the exponentiated coefficient. Crashes occurring on narrow road sections are associated with higher likelihood of serious or fatal injury for cyclists. This pronounced effect, likely stems from limited lateral space for evasive actions and, as such, higher conflict frequency and severity in mixed traffic environments [45]. Additionally, drivers' failure to comply with traffic signals or STOP signs increases the likelihood of severe cyclist injury [46]. This finding reinforces the importance of junction control and driver awareness, at locations where cyclists and motorized traffic frequently interact.

5 Discussion and Conclusion

This study examined injury severity outcomes among vulnerable road users, in particular pedestrians and cyclists, in Thessaloniki, Greece, by analyzing police-reported crash data, through separate binary logistic regression models. By focusing on the probability of serious or fatal injuries rather than crash frequency alone, the analysis contributes to evidence-based road safety research that supports the integration of road safety goals, in line with the Safe System approach [47], and the Greek National Road Safety Strategic Plan [48].

The results of the pedestrian-focused model show that several socio-demographic, infrastructural and behavioral factors significantly influence injury severity. Behavioral factors proved particularly influential; illegal driver's behavior was found to dramatically increase severe injury probability (increasing the odds of severe or fatal injury by more than 18 times in the case of signal or STOP violations and 14 times in the case of speed limit violation), while regular pedestrian positioning appears to reduce risk.

The bicyclist-focused model further reinforced the importance of infrastructural characteristics and of compliance with key traffic regulations. Narrow road widths play a key role in bicyclists' injury severity (increasing the odds of severe injury by more than six times), reflecting limited cycling space and higher conflict potential in mixed-traffic settings. The overlapping influence of road width and road users' behavior across both models underscores the existence of shared issues for vulnerable road users, while the more pronounced effect for cyclists emphasizes their greater sensitivity to limited road space in the absence of dedicated infrastructure.

Overall, our study provides a city-level, severity-oriented analysis of vulnerable road user crashes, in a Greek urban context, delivering empirical insights that can directly inform targeted interventions in similar geographical contexts. Study's findings highlight the urgent need for improved compliance with traffic controls, better management of urban streets, and complex interactions among road users and different type of vehicle, in order to protect vulnerable users. While our research provides valuable insights, several limitations should be acknowledged. The relatively small number of cyclist crashes in our sample maybe limits model's statistical robustness and police-reported data may under-represent minor injuries, due to subjective police's assessments. Moreover, another limitation is that the use of the 2019–2021 dataset may affect the robustness of the statistical inferences because of the unique traffic patterns and behavioral shifts induced by

the COVID-19 pandemic. Future research should use data from a longer, post-pandemic, period, to better understand the factors that influence bicyclist injury severity relevant to road crashes and integrate police-reported data with hospital records for more accurate severity assessment. Extending the analysis to a national scale would further strengthen the evidence base for safer mobility in Greece. In addition, the integration of emerging Information and Communication Technologies (ICT) could offer significant potential to enhance the understanding of VRUs safety. The availability of real-time traffic data, connected vehicle systems and sensor-based monitoring offers new opportunities to capture exposure and behavioral patterns. Such data sources could enable the joint modelling of crash occurrence and injury severity, providing a more comprehensive assessment of road safety risk. Furthermore, the use of machine learning techniques could support the development of proactive safety management systems, allowing for dynamic risk prediction and targeted interventions.

Acknowledgments. This research received no external funding.

Disclosure of Interests. The authors have no competing interests to declare that are relevant to the content of this article.

References

1. Da Silva, P.H.V., Bezerra, B.S.: A meta-analysis of safety countermeasures for vulnerable users on urban roads. Transp. Res. Procedia **78**, 452–459 (2024)
2. Bassani, M., Rossetti, L., Catani, L.: Spatial analysis of road crashes involving vulnerable road users in support of road safety management strategies. Transp. Res. Procedia **45**, 394–401 (2020)
3. Gálvez-Pérez, D., Guirao, B., Ortuño, A.: Analysis of the elderly pedestrian injury severity in urban traffic accidents in Spain using machine learning techniques. Transp. Res. Procedia **71**, 6–13 (2023)
4. WHO: Global Status Report on Road Safety 2023. 1st edn. World Health Organization, Geneva (2023)
5. Shinar, D.: Safety and mobility of vulnerable road users: pedestrians, bicyclists, and motorcyclists. Accid. Anal. Prev. **44**(1), 1–2 (2012)
6. Fountas, G., Fonzone, A., Demiris, A., Sheykhfard, A., Basbas, S.: Unveiling the determinants of crash injury severities in e-scooter crashes: a latent class binary logit analysis of single and multiple-vehicle crashes. J. Cycling Micromobility Res. **2**, 100116 (2026)
7. Wennberg, H., Dahlholm, O.: Traffic safety implementation at local level in line with 2030 agenda for sustainable development: synergies, challenges and enablers. Traffic Saf. Res. **5**, e000055 (2024)
8. Casado-Sanz, N., Guirao, B., Gálvez-Pérez, D.: Population ageing and rural road accidents: analysis of accident severity in traffic crashes with older pedestrians on Spanish crosstown roads. Res. Transp. Bus. Manag. **30**, 100377 (2019)
9. Värnild, A., Tillgren, P., Larm, P.: Road users seriously injured in single crashes – the impact of sex, age and speed limit on injuries for pedestrians, cyclists, car occupants and motorcyclists in Sweden, 2016–2019. J. Transp. Health **33**, 101717 (2023)
10. Amin, K., Skyving, M., Bonander, C., Krafft, M., Nilson, F.: Fall- and collision-related injuries among pedestrians in road traffic environment – a Swedish national register-based study. J. Saf. Res. **81**, 153–165 (2022)

11. Etehad, H., Yousefzadeh-Chabok, S., Davoudi-Kiakalaye, A., Moghadam, D.A., Hemati, H., Mohtasham-Amiri, Z.: Impact of road traffic accidents on the elderly. Arch. Gerontol. Geriatr. **61**(3), 489–493 (2015)
12. Ang, B.H., Chen, W.S., Lee, S.W.H.: Global burden of road traffic accidents in older adults: a systematic review and meta-regression analysis. Arch. Gerontol. Geriatr. **72**, 32–38 (2017)
13. Kröyer, H.R.G.: Is 30 km/h a 'safe' speed? Injury severity of pedestrians struck by a vehicle and the relation to travel speed and age. IATSS Res. **39**(1), 42–50 (2015)
14. Mokhtarimousavi, S., Anderson, J.C., Azizinamini, A., Hadi, M.: Factors affecting injury severity in vehicle-pedestrian crashes: a day-of-week analysis using random parameter ordered response models and artificial neural networks. Int. J. Transp. Sci. Technol. **9**(2), 100–115 (2020)
15. Alogaili, A., Mannering, F.: Differences between day and night pedestrian-injury severities: accounting for temporal and unobserved effects in prediction. Anal. Methods Accid. Res. **33**, 100201 (2022)
16. Kaya, N., Girgis, J., Hansma, B., Donmez, B.: Hey, watch where you're going! An on-road study of driver scanning failures towards pedestrians and cyclists. Accid. Anal. Prev. **162**, 106380 (2021)
17. Elalouf, A., Birfir, S., Rosenbloom, T.: Developing machine-learning-based models to diminish the severity of injuries sustained by pedestrians in road traffic incidents. Heliyon **9**(11), e21371 (2023)
18. Salehian, A., Aghabayk, M., Seyfi, M., Shiwakoti, N.: Comparative analysis of pedestrian crash severity at United Kingdom rural road intersections and non-intersections using latent class clustering and ordered probit model. Accid. Anal. Prev. **192**, 107231 (2023)
19. Haleem, K., Alluri, P., Gan, A.: Analyzing pedestrian crash injury severity at signalized and non-signalized locations. Accid. Anal. Prev. **81**, 14–23 (2015)
20. Tapp, A., Nancarrow, C., Davis, A.: Support and compliance with 20mph speed limits in Great Britain. Transport. Res. F: Traffic Psychol. Behav. **31**, 36–53 (2015)
21. Marisamynathan, S., Vedagiri, P.: Estimation of pedestrian safety index value at signalized intersections under mixed traffic conditions. Transp. Developing Econ. **4**(1), 5 (2018)
22. Raoniar, R., Maurya, A.K.: Pedestrian red-light violation at signalised intersection crosswalks: influence of social and non-social factors. Saf. Sci. **147**, 105583 (2022)
23. Nikolaou, D., Ntontis, A., Michelaraki, E., Ziakopoulos, A., Yannis, G.: Pedestrian safety attitudes and self-declared behaviour in Greece. IATSS Res. **47**(1), 14–24 (2023)
24. Sheykhfard, A., Haghighi, F., Kavianpour, S., Das, S., Farahani, P.S., Fountas, G.: Risk assessment of pedestrian red-light violation behavior using surrogate safety measures. IATSS Res. **47**(4), 514–525 (2023)
25. Tamakloe, R., Adanu, E.K., Atandzi, J., Das, S., Lord, D., Park, D.: Stability of factors influencing walking-along-the-road pedestrian injury severity outcomes under different lighting conditions. Accid. Anal. Prev. **193**, 107333 (2023)
26. Yang, Z., Yang, Z., Smith, J., Robert, B.A.P.: Risk analysis of bicycle accidents: a Bayesian approach. Reliab. Eng. Syst. Saf. **209**, 107460 (2021)
27. Alnawmasi, N., Mannering, F.: An analysis of day and night bicyclist injury severities in vehicle/bicycle crashes. Anal. Methods Accid. Res. **40**, 100301 (2023)
28. Levulytė, L., Baranyai, D., Török, Á., Sokolovskij, E.: Bicycles' role in road accidents a review of literature. Transport Telecommun. J. **17**(2), 122–127 (2016)
29. Beck, B., et al.: Bicycling crash characteristics: an in-depth crash investigation study. Accid. Anal. Prev. **96**, 219–227 (2016)
30. Cittadini, F., et al.: Bicycle-related accidents in Rome: investigating clinical patterns, demographics, injury contexts, and health outcomes. Injury **55**(4), 111464 (2024)
31. Stassen, H.S., et al.: Effect of helmet use on maxillofacial injuries due to bicycle and scooter accidents. Int. J. Oral Maxillofac. Surg. **53**(1), 28–35 (2024)

32. Fountas, G., Fonzone, A., Olowosegun, A., McTigue, C.: Addressing unobserved heterogeneity in the analysis of bicycle crash injuries in Scotland. Anal. Methods Accid. Res. **32**, 100181 (2021)
33. Bahrololoom, S., Young, W., Logan, D.: Modelling injury severity of bicyclists in bicycle-car crashes at intersections. Accid. Anal. Prev. **144**, 105597 (2020)
34. Monfort, S.S., Mueller, B.C.: Bicyclist crashes with cars and SUVs: injury severity and risk factors. Traffic Inj. Prev. **24**(7), 645–651 (2023)
35. Wang, C., Lu, L., Lu, J.: Statistical analysis of bicyclists' injury severity at Unsignalized intersections. Traffic Inj. Prev. **16**(5), 507–512 (2015)
36. Bouhouras, E., et al.: How signal phasing shapes university students' crossing decisions and confidence. Safety. **11**(4), 106 (2025)
37. Rifaat, S.M., Tay, R., De Barros, A.: Effect of street pattern on the severity of crashes involving vulnerable road users. Accid. Anal. Prev. **43**(1), 276–283 (2011)
38. Wilson, J.R., Lorenz, K.A.: Modeling binary correlated responses using SAS, SPSS and R. In: ICSA Book Series in Statistics, vol. 9. Springer, Cham (2015)
39. Washington, S., Karlaftis, M.G., Mannering, F., Anastasopoulos, P.: Statistical and econometric methods for transportation data analysis. 3rd edn. Chapman and Hall/CRC, Boca Raton (2020)
40. Semple, T., Fountas, G., Fonzone, A.: Trips for outdoor exercise at different stages of the COVID-19 pandemic in Scotland. J. Transp. Health **23**, 101280 (2021)
41. Lo, Y.-C., et al.: Space and time clustering of road traffic collisions among older adults in Taiwan. Injury **57**(2), 112935 (2026)
42. Wang, Y., Hespanhol, L., Worrall, S., Tomitsch, M.: Pedestrian-vehicle interaction in shared space: insights for autonomous vehicles. In: Proceedings of the 14th International Conference on Automotive User Interfaces and Interactive Vehicular Applications, pp. 330–339. ACM, New York (2022)
43. Muduli, K., Ghosh, I.: Predicting pedestrian-vehicle interaction severity at unsignalized intersections. Traffic Inj. Prev. **26**(2), 252–261 (2025)
44. Rampinelli, A., et al.: Investigating the risk factors associated with injury severity in pedestrian crashes in Santiago, Chile. Int. J. Environ. Res. Public Health **19**(17), 11126 (2022)
45. Macioszek, E., Granà, A.: The analysis of the factors influencing the severity of bicyclist injury in bicyclist-vehicle crashes. Sustainability **14**(1), 215 (2022)
46. Liu, S., Lin, Z., Fan, W.: Investigating contributing factors to injury severity levels in crashes involving pedestrians and cyclists using latent class clustering analysis and mixed logit models. J. Transp. Saf. Secur. **14**(10), 1674–1701 (2022)
47. U.S. Department of Transportation: What is a Safe System Approach? https://www.transportation.gov/safe-system-approach. Accessed 25 Oct 2025
48. National Technical University of Athens: National road safety strategic plan, Greece 2030. https://www.nrso.ntua.gr/nrss2030/wp-content/uploads/2022/10/NationalRoadSafetyStrategicPlan.pdf. Accessed 25 Oct 2025

Who Owns the Space? A Near-Accident Perception of e-Scooters Riders in Interaction with Pedestrians

Argyrios Kalisperatos[1], Paraskevas Nikolaou[2(✉)], Andreas Nikiforiadis[3], Grigorios Fountas[1], Tiziana Campisi[4], and Socrates Basbas[1]

[1] Aristotle University of Thessaloniki, 54124 Thessaloniki, Greece
[2] Cyprus University of Technology, 3603 Limassol, Cyprus
paraskevas.nikolaou@cut.ac.cy
[3] Democritus University of Thrace, 67100 Xanthi, Greece
[4] University of Enna "Kore", 94100 Enna, Italy

Abstract. The rapid growth of e-scooter usage in urban environments has introduced new safety challenges, particularly in shared spaces with pedestrians. This study investigates near-collision interactions between e-scooter riders and pedestrians in a pedestrianized area in Thessaloniki, Greece, based only on 100 observed near-miss incidents. A multidimensional approach is adopted to analyze behavioral responses and interaction dynamics. Ordinal Logistic Regression is employed to examine the factors influencing changes in e-scooter speed (acceleration, no reaction, and varying levels of deceleration) when riders encounter pedestrians. Subsequently, behavioral personas for both e-scooter riders and pedestrians are identified, and a Firth Logistic Regression model is applied to assess the likelihood of high-risk conflicts arising from different persona combinations. The results reveal that while most riders adopt defensive behaviors, a significant proportion of risky responses persists, particularly in the presence of inattentive or unresponsive pedestrians. The findings indicate that near-collision risk is primarily driven by behavioural interactions, while environmental conditions such as congestion further amplify these effects. The results are particularly relevant for urban planners, transport engineers, and policymakers, as they provide evidence to support the design of safer shared spaces and the development of targeted interventions addressing both rider and pedestrian behaviour.

Keywords: E-scooters · Micromobility safety · Pedestrian interactions · Risk perception · Collision avoidance behaviour

1 Introduction

While e-scooters are appearing to be used mainly in shorter distances and for the First- and Last-Mile commutes [1], they also appear to win ground in the "competition" between alternative modes. However, it raises concerns regarding rider and non-rider safety [2]. Since the widespread adoption of e-scooters there has been a significant

© The Author(s), under exclusive license to Springer Nature Switzerland AG 2027
O. Gervasi et al. (Eds.): ICCSA 2026 Workshops, LNCS 16761, pp. 242–255, 2027.
https://doi.org/10.1007/978-3-032-30527-5_16

increase in injuries and admissions [3]. To study the safety perspective of e-scooters is important to identify the socio-economic and behavioral background of the users. For example, low-income e-scooter users are increasing the use of this mode compared to other transportation modes [4]. Additionally, older riders with good physical condition and riders of private e-scooters and leisure travelers are more likely to use e-scooter for their commute [5].

Shared spaces give access to micromobility in urban environments, however the presence of various transport modes, such as cyclists, pedestrians and e-scooters, create concerns about safety since every commuter has a different perception of space. For instance, in Sweden female e-scooter riders feel less safe in shared spaces compared to their male counterparts. Additionally, young adults feel safer when overtaking other road users rather than encountering them head-on [6]. As it appears from [7] maneuvers and interaction with another road user consist two of the main accident causation. Main focus should be given on the relation between e-scooter riders and pedestrians where these users have the most different speed regimes in off-road facilities and these differences increase the chance of interactions, conflicts and potential collisions [8] and is considered as a weakness to the use of e-scooters [9].

Based on the EU regulation many countries have enforced their legislations on the use of e-scooters, focusing on some minimum age and maximum speed limitations but also on the space of allowing e-scooter riders to ride. For example, in Greece the minimum age of using e-scooter is 15 years with a maximum speed 25 km/h and a compulsory on wearing helmet. E-scooter riders are allowed to ride only on the cycle path and on the road, but only if the speed limit is 50 km/h and they are not allowed to ride on pavement, unless the e-scooters cannot go faster than 6 km/h [10]. Based on [11] 44,4% of the respondents in a survey from 22 European countries reported riding e-scooters on pedestrian pavement or sidewalk at least once, fact that indicates that e-scooter riders do not follow the current legislations.

Despite the growing body of literature on e-scooter safety, most existing studies rely on crash data, survey-based approaches, or general behavioural observations, which often fail to capture the detailed dynamics of interactions in shared spaces. In particular, limited attention has been given to near-collision events as indicators of potential risk, as well as to the role of behavioural typologies of both e-scooter riders and pedestrians in shaping these interactions. This study addresses these gaps by introducing a person-based analytical framework that combines near-collision observational data with the classification of users into distinct behavioural profiles. Furthermore, it proposes a risk classification approach based on observed behavioural responses and examines the combined effects of interaction context and congestion-related conditions on rider behaviour.

For analyzing the perception of e-scooter users and non-users, several studies used data from surveys [12, 13]. This study utilizes near-collision data between e-scooter riders and pedestrians collected on a pedestrian street in Thessaloniki, Greece. The research adopts a multidimensional approach. Initially, it examines the conditions under which e-scooter riders choose to accelerate, decelerate, or exhibit no reaction, considering contextual factors such as pedestrian density. Subsequently, the study explores the behavioral characteristics of both e-scooter riders and pedestrians and estimates the likelihood of

high-risk collisions arising from different combinations of risk-prone behaviors between the two groups. The findings provide valuable insights for local authorities and policy-makers, supporting the development of safer shared environments that accommodate both user groups while minimizing collision risks.

The remainder of this paper is structured as follows. Section 2 presents the data collection process and methodology adopted in this study. Section 3 provides the results of the statistical analysis, including the ordinal logistic regression model and the Firth logistic regression model, along with the proposed risk classification framework. Finally, last section, the paper concludes.

2 Methodological Framework

The methodological framework developed in this study provides a step-by-step approach for analyzing the factors that shape the behavioral characteristics of e-scooter riders. It further identifies distinct behavioral personas for both e-scooter riders and pedestrians sharing the same space, and determines which of these personas are more prone to collision risk.

To achieve this, the first step of the methodological framework involved the collection of near-collision incident data from a pedestrian street in the Kalamaria district of Thessaloniki, Greece. These data were subsequently used to identify the factors influencing the behavioral responses of e-scooter riders, namely acceleration, deceleration, or no reaction, upon encountering pedestrians in their path, using an Ordinal Logistic Regression model.

Furthermore, the study identified and examined distinct behavioral personas of both e-scooter riders and pedestrians within shared spaces, and assessed how different combinations of these personas contribute to collision risk. Specifically, the likelihood of high-risk collisions associated with various persona interactions was estimated using a Firth Logistic Regression model, alongside the effect of each individual persona type.

2.1 Data

For the purposes of this study, field observations were conducted in pedestrianized areas of the Kalamaria district in Thessaloniki, Greece. The observations focused on incidents involving interactions between e-scooter riders and both moving and stationary pedestrians, as well as hazardous situations with an evident potential to result in collisions. In total, 100 near-miss were recorded. An “incident” is defined as any interaction between an electric scooter (e-scooter) and one or more pedestrians within the study area that poses a potential threat to the physical safety of at least one of the involved parties. The identification and classification of incidents were based on the observer’s qualitative judgment in real time, considering factors such as proximity, abrupt maneuvers, and perceived collision risk. Therefore, the dataset used in this study exclusively includes interactions between e-scooter riders and pedestrians. No data regarding other mobility users, such as bicycles, motorcycles, or motor vehicles, were collected or analyzed.

The collected data provided all the necessary information for the analysis conducted in this study, as summarized in Table 1. The dataset captures multiple dimensions of

interactions between e-scooter riders and pedestrians. In most cases, e-scooter riders undertook avoidance actions (91%), whereas pedestrians exhibited significantly lower response rates (15%), indicating an imbalance in reactive behavior. Similarly, awareness levels were higher among e-scooter riders (83%) compared to pedestrians (33%), suggesting that pedestrians are more likely to remain unaware of approaching conflicts. The majority of incidents occurred outside designated cycling infrastructure (88%), and helmet usage among riders was notably low (12%).

Regarding behavioral responses, deceleration was the most common reaction, with moderate (26%) and strong (22%) deceleration accounting for nearly half of all cases, while acceleration and no reaction were observed in 19% of incidents each. Most interactions occurred under relatively low-to-moderate pedestrian densities (LoS A–B: 85%), indicating that conflicts are not limited to highly congested environments. Additionally, both riders (77%) and pedestrians (64%) generally had sufficient spatial margins to perform avoidance maneuvers, although conflicts still occurred. Overall, the descriptive statistics of the data highlight critical a range of potential behavioral and environmental factors influencing near-collision dynamics in shared pedestrian spaces.

The alluvial plot in Fig. 1 illustrates the relationships between e-scooter rider behavior, environmental conditions, and incident characteristics, highlighting clear patterns in reaction types. Overall, deceleration (particularly moderate and strong deceleration) dominates across most conditions, indicating that riders generally adopt defensive responses when encountering pedestrians. However, a notable presence of acceleration and no-reaction behaviors persists, especially in cases where no avoidance action is taken, suggesting higher-risk interactions. Importantly, even when sufficient margin of avoidance exists and pedestrian density is low (LoS A–B), conflicts still occur across all reaction types, implying that the availability of space alone does not ensure safe behavior. Additionally, most incidents take place outside designated cycle paths, which is a fact that should be considered by local authorities since this is against the EU and national legislation about e-scooters. These findings indicate that near-collision dynamics are primarily driven by behavioral factors rather than purely environmental conditions, emphasizing the importance of both rider and pedestrian behavior in shaping safety outcomes in shared spaces.

As for the second alluvial plot in Fig. 2 it further explores the role of pedestrian-related factors in shaping interaction dynamics and confirms the patterns observed in the previous Figure. Specifically, although a margin of avoidance is available for pedestrians in most cases, avoidance actions are rarely undertaken, as reflected by the dominance of "NO" responses. This lack of reaction is consistently associated with a broader spread of e-scooter responses, including riskier behaviors such as acceleration and no reaction. Additionally, even under low to moderate pedestrian densities (LoS A–B), a wide range of incident categories and reaction types is observed, reinforcing the notion that unsafe interactions are not confined to high-density conditions. Compared to the previous figure, which emphasized rider behavior, this visualization highlights the critical role of pedestrian passivity in the emergence of near-collision events. Overall, the findings suggest that both insufficient pedestrian response and rider behavior jointly contribute to conflict formation, further supporting the argument that safety in shared spaces is driven by the interaction of behaviors rather than infrastructure conditions alone.

Table 1. Variables Description from Near-Collision Measurements

Variable	Description	Levels
Avoidance_Action_escooter	Action from the e-scooter rider to avoid possible collision with pedestrian	Yes: 91% No: 9%
Avoidance_Action_pedestrian	Action from the pedestrian to avoid possible collision with e-scooter rider	Yes: 15% No: 85%
Awareness_from_escooter	Awareness from e-scooter riders for noticing pedestrians in time in order to avoid possible collision	Yes: 83% No: 17%
Awareness_from_pedestrian	Awareness from pedestrians for noticing pedestrians in time in order to avoid possible collision	Yes: 33% No: 67%
Category	Categories of incidents as identified from the verbal descriptions recorded in the field during the measurement period	Rear Side: 23% Very Close: 16% Stop and Walk: 11% Corner Meeting: 9% School-Student Incident: 6% Other: 35%
DV_category	Difference between the e-scooter speed before noticing the pedestrian and immediately after noticing the pedestrian	Acceleration ($DV < 0$): 19% No Reaction ($DV = 0$): 19% Mild Deceleration ($1 \leq DV \leq 4$): 14% Moderate Deceleration ($5 \leq DV \leq 9$): 26% Strong Deceleration ($DV > 9$): 22%
Cycle_Path	If the incident was captured inside or outside the cycle path.	Outside: 88% Inside:12%
Helmet	If the e-scooter rider wears a helmet	Yes: 12% No: 88%
Margin_of_Avoidance_escooter	Margin of avoidance (in terms of available space) for the e-scooter rider to perform an evasive action in order to avoid a potential incident with the pedestrians	Yes: 77% No: 23%

(*continued*)

Table 1. (*continued*)

Variable	Description	Levels
Margin_of_Avoidance_pedestrian	Margin of avoidance (in terms of available space) for the pedestrian to perform an evasive action in order to avoid a potential incident with the e-scooter rider	Yes: 64% No: 36%
Pedestrian_Density	The classification of the pedestrian Level of Service (LoS) based on the pedestrian density in the area where the incidents were recorded.	LoS A: 31% LoS B: 54% LoS C: 14% LoS D: 1%

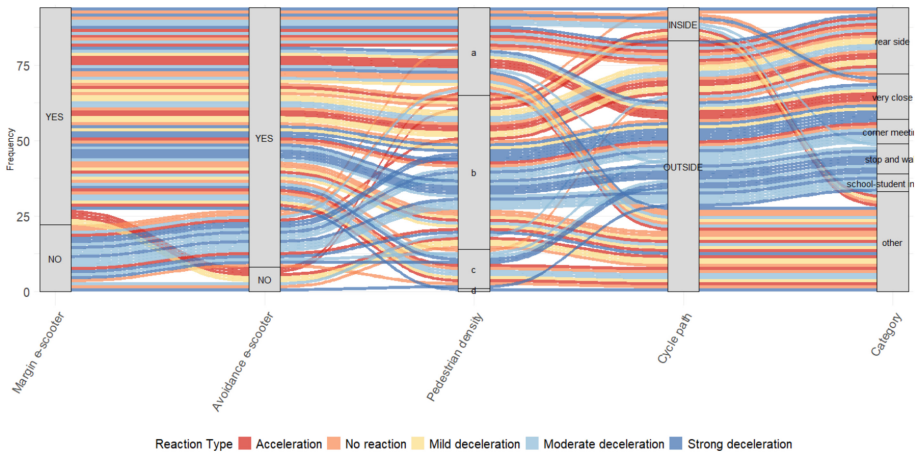

Fig. 1. Alluvial Representation of E-Scooter Rider Behavior, Environmental Conditions, and Near-Collision Characteristics

2.2 Ordinal Logistic Regression Model

Ordinal Logistic Regression is applied when the dependent variable consists of three or more ordered categories, where the intervals between categories are not necessarily equal. This modeling approach estimates the relationship between a set of explanatory variables and an ordinal outcome by assessing the likelihood of an observation falling into higher versus lower categories of the dependent variable. Specifically, the model assumes a cumulative logit structure, where the estimated coefficients represent the effect of the explanatory variables on the log-odds of being at or above a certain category threshold. A key assumption of the model is the proportional odds (parallel lines) assumption, which implies that the effect of each explanatory variable is constant

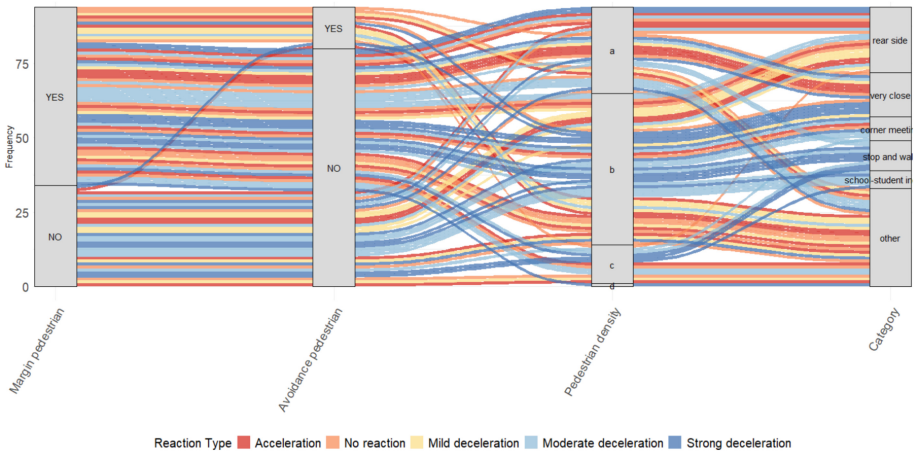

Fig. 2. Alluvial Representation of Pedestrian Behavior, Environmental Conditions, and Near-Collision Characteristics

across all category thresholds [14]. In this study, the ordinal model is used to examine how various behavioral and environmental factors influence the response of e-scooter riders in terms of speed change (i.e., acceleration, no reaction, and different levels of deceleration) when encountering pedestrians.

In this study, an Ordinal Logistic Regression model was employed to analyze the factors influencing changes in e-scooter speed in response to pedestrian presence. The dependent variable captures the rider's behavioral response and is categorized into three ordered outcomes: acceleration, indicating an increase in speed upon noticing a pedestrian; no reaction, indicating no change in speed; and deceleration, indicating a reduction in speed. This classification allows for the assessment of how various explanatory factors affect the likelihood of transitioning between different levels of speed adjustment.

2.3 Firth's Logistic Regression Model

To address issues related to small-sample bias and potential data separation, Firth's bias-reduced logistic regression method was employed. This approach is particularly suitable for binary outcome models where conventional maximum likelihood estimation may produce biased or unstable estimates, especially in the presence of rare events or complete/quasi-complete separation. Maximum likelihood estimates in standard logistic regression are known to be prone to bias in small samples. To mitigate this issue, Firth [15] proposed a penalized likelihood approach, which introduces a correction term to the likelihood function, resulting in more reliable and finite parameter estimates.

In this study, a binary logistic regression model based on Firth's method was developed, where the dependent variable represents the occurrence of high-risk conflicts. Specifically, the response variable takes the value of 1 for high-risk incidents and 0 for low- or moderate-risk incidents. High-risk incidents are defined as interactions in which the e-scooter rider accelerates upon detecting a pedestrian, while the pedestrian does not undertake any avoidance action, indicating a lack of behavioral adaptation from both

parties and an increased likelihood of conflict. This formulation enables the identification of behavioral personas, both for e-scooter riders and pedestrians, that are more prone to high-risk collision scenarios.

3 Application and Results

This chapter presents the results of the empirical analysis, focusing on the behavioral responses of e-scooter riders and their interactions with pedestrians in shared spaces. The analysis is structured in two main parts. First, the factors influencing changes in e-scooter speed are examined using an Ordinal Logistic Regression model. Second, behavioral personas for both e-scooter riders and pedestrians are identified, and their combined effects on the likelihood of high-risk conflicts are assessed using a Firth Logistic Regression model. The findings provide insights into the key behavioral and environmental determinants of near-collision events.

3.1 Factors Influencing E-Scooter Speed Adjustment in Pedestrian Interactions

An ordinal logistic regression model was estimated to examine how different factors influence the reaction behaviour of e-scooter riders and specifically the riders' reaction intensity with three ordered levels: acceleration, no reaction, and deceleration. The results are presented in Table 2, which indicate that the levels of only two variables (Category and Pedestrian Density) have, statistically, significant effect, which are the categories of incidents as identified from the qualitative descriptions recorded in the field during the observation period and the classification of the pedestrian Level of Service (LoS) based on the pedestrian density in the area where the incidents were recorded.

Due to the fact variable "Category" had many levels with small counts, which was the reason that the ordinal model was providing non-statistically significant variables, some of the levels were grouped. For the case of the category variable the levels "rear side" and "very close" were grouped as "passing", the levels "corner meeting" and "stop and walk" were grouped as "interaction" and the levels "school-student incident" and "other" were grouped as "other". As for the dependent variable the different levels of acceleration were grouped into one grouped, namely, "acceleration".

The analysis shows that the type of interaction between pedestrians and e-scooter riders (as denoted in the variable "Category") significantly influences rider behaviour. From the results both "passing" conflicts and "other" incidents present statistically significant coefficients compared with the reference category ("interaction" conflicts). The negative coefficients of both levels indicate that, compared with interaction conflicts, these incidents are less likely to lead to stronger deceleration actions. The odd ratios of the levels' estimates indicate that passing conflicts reduce the probability of stronger braking reactions by approximately 85%, while other types of incidents reduce the probability of stronger braking reactions by approximately 83%. These findings suggest that interaction conflicts, where pedestrians and e-scooter riders directly negotiate shared space, are more likely to trigger stronger deceleration behaviour from the rider.

The estimated coefficients for pedestrian density levels appear larger than the ones in "Category" and statistically significant. As can be seen from the results of this variable,

when there is enough space for movements e-scooter riders are less likely to decelerate but they instead are more likely to accelerate. Compared to Level of Service D (less space due to the increase of pedestrian density) LoS A is a factor that urges e-scooter riders to accelerate. LoS B acts the same but by less extent and LoS C lees than LoS A but higher than LoS B. From a safety perspective, pedestrian density can be interpreted as a proxy for congestion conditions in shared spaces. Higher levels of congestion increase the frequency of interactions between e-scooter riders and pedestrians, while simultaneously reducing available maneuvering space and reaction time. Under such conditions, even small behavioural differences may significantly influence the likelihood of near-collision events. The findings suggest that in less congested environments (LoS A and B), riders are more likely to accelerate, potentially increasing risk if sudden interactions occur. Conversely, higher density levels constrain movement but also create more complex and unpredictable interaction patterns, which may elevate safety risks when combined with inappropriate behavioural responses.

Additionally, the results from the Ordinal Logistic Regression indicate that situations involving direct interaction conflicts between pedestrians and e-scooter riders are more likely to trigger stronger deceleration actions compared with passing or other types of encounters. This suggests that when spatial interactions require active negotiation, such as in face-to-face or crossing movements, riders are more inclined to adjust their speed and adopt safer manoeuvres. In contrast, passing or less direct interactions tend to elicit weaker responses, with riders more likely to maintain their speed.

The substantial differences in coefficient magnitude between pedestrian density and interaction category indicate that congestion-related conditions exert a significantly stronger influence on rider behaviour than the type of interaction itself. While the interaction category captures the specific geometry and nature of encounters, pedestrian density reflects the broader environmental context in which these interactions occur. The much larger coefficients associated with density levels suggest that riders primarily adjust their behaviour in response to space availability and crowding conditions, which continuously constrain movement and decision-making. In contrast, interaction type appears to influence behaviour more locally, at the moment of the encounter, rather than shaping overall response intensity.

Significance codes: 0 ‘***’ 0.001 ‘**’ 0.01 ‘*’ 0.05 ‘.’ 0.1 ‘’ 1

3.2 Identification of Personas

While the perception of space remains unclear between e-scooter riders and pedestrians, it is important to identify which “personas” of users interact within a shared environment. These persona types emerge from the behavioral characteristics and actions of both groups. Based on the available data, personas were derived using a rule-based classification approach grounded on observed behavioral indicators (e.g., speed adjustment, awareness, avoidance actions, and helmet use), rather than purely qualitative judgment. Accordingly, five types of e-scooter riders and three types of pedestrians were identified.

Furthermore, e-scooter riders were classified into four behavior-based persona types:

- Aggressive: e-scooter riders that accelerate when noticing the pedestrian and do not conduct an evasive maneuver for avoiding the pedestrian.

Table 2. Estimation results of the ordinal logistic model for e-scooter speed adjustment

Variables	Estimates (Std. Error)	Thresholds	Estimates (Std. Error)
Category: Other	−1.79 * (0.82)	Acceleration | No reaction	−17.20 *** (0.59)
Category: Passing	−1.84 * (0.84)	No reaction | Deceleration	−16.17 *** (0.57)
Pedestrian Density: LoS A	−14.36 *** (0.40)		
Pedestrian Density: LoS B	−14,01 *** (0.34)		
Pedestrian Density: LoS C	−14.25 *** (0.48)		
Akaike Information Criterion (AIC): 179.27			

- Inattentive: e-scooter riders that decelerate when noticing the pedestrian and are unaware but are unaware are not aware of pedestrians and do not wear helmet.
- Cautious: e-scooter riders that are aware of pedestrians while riding and are proceeding with avoiding actions and deceleration once they notice a pedestrian and also wear a helmet while riding.
- Responsive: e-scooter riders that are aware for pedestrians and decelerate when noticing one but do not wear helmet.
- Risky: e-scooter riders that either accelerate or do not change there speed when noticing a pedestrian but are proceeding with an avoidance action.

Then, the segmentation of the pedestrian personas was followed concluding with the following persona types:

- Attentive: pedestrians that are aware of e-scooters and proceed to avoid action when noticing one.
- Unresponsive: pedestrians that are aware of e-scooters but do not proceed to avoid action when noticing one.
- Inattentive: pedestrians that are fully unaware and do not proceed to avoid action when noticing an e-scooter.

Like with the e-scooter riders this segmentation reduces multiple pedestrian variables into meaningful behavioral categories. Therefore, these behavioral segmentations create different e-scooter rider and pedestrian groups whose interactions will be analyzed in terms of risk of a near collision.

3.3 E-Scooter Riders and Pedestrians near Risk Collision

This application provides feedback on the near collision risk that exists when different behavioral types of e-scooter riders and pedestrians exist and commute in the same space. From a road safety perspective, risk can be conceptualized through three interrelated

components: occurrence, exposure, and vulnerability. Occurrence refers to the likelihood of a conflict taking place, exposure reflects the presence and interaction of users within a shared space, and vulnerability captures the severity of outcomes given a conflict. In this study, the proposed risk classification primarily reflects the vulnerability component, as it is based on the behavioral responses of e-scooter riders and pedestrians during near-collision events. While exposure and occurrence are implicitly present through the observed interactions, they are not explicitly modeled.

For instance, in Australia more of 50% of the participants in a survey had engaged in risky behaviors (i.e., speeding, doubling, not wearing a helmet and use of a smartphone) while riding [16]. Based on the recorded incidents in this study three levels of risk were identified:

- Low Risk: Occurs when the e-scooter rider decelerates upon detecting a pedestrian in their trajectory, and the pedestrian actively performs an avoidance maneuver. This reflects mutual awareness and cooperative conflict resolution.
- Moderate Risk: Occurs when the e-scooter rider maintains their speed despite detecting a pedestrian, while the pedestrian initiates an avoidance action. In this case, risk is partially mitigated by the pedestrian's response, but the rider does not contribute to conflict avoidance.
- High Risk: Occurs when the e-scooter rider accelerates upon detecting a pedestrian, and the pedestrian does not take any avoidance action. This represents a lack of adaptation from both parties, leading to a significantly increased likelihood of conflict.

Based on the recorded incidents every near-collision occasion was evaluated, and two risk values were given, one referring to the action taken from e-scooter riders and one for pedestrians. The mean value of both risk values was calculated and thus a risk index was provided for the combination of different e-scooter riders and pedestrian personas (Fig. 3).

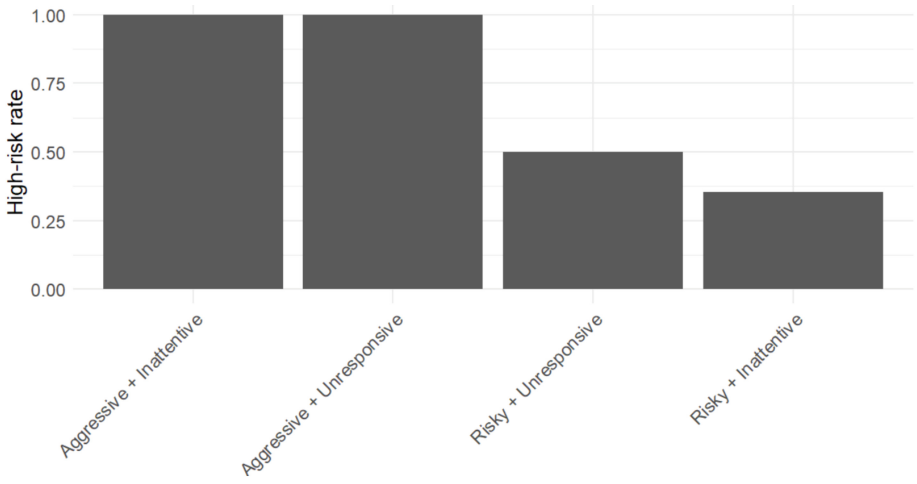

Fig. 3. High Risk by Meaningful Rider-Pedestrian Combinations

The rest of the possible combination produced zero risk and thus were not presented in the figure. Moreover, the findings indicate that aggressive and risk-prone e-scooter riders, in combination with inattentive and unresponsive pedestrians, represent the most hazardous interaction profiles. These results should be carefully considered by local authorities and policymakers when designing and implementing targeted enforcement measures in shared spaces, with the aim of reducing the likelihood of conflicts and preventing potential collisions between the two user groups.

Furthermore, for estimating which persona type of e-scooter riders and pedestrians are considered as risk-prone by there one a Firth Logistic Regression (FLR) model was developed using binary dependent variable, where the value 0 ("not high-risk conflict") concerned the low-risk incidents and the value 1 ("high-risk conflict") concerned the high-risk incidents and thus, this binary variable acts as a proxy for conflict severity. Table 3 presents the results from the analysis were the reference level for e-scooter personas was "Cautious" riders and for pedestrians was "Attentive". As can be seen from the table, the statistically significant Aggressive and Risky riders are both increasing the risk, compared to Cautious riders, of having a collision with pedestrians. Furthermore, compared to Attentive pedestrians, Inattentive and Unresponsive pedestrians also increase the risk of having a collision with e-scooter riders fact that validates the high-risk collision between the combinations as presented in Fig. 3.

Table 3. Estimation results of the Firth's Logistic Regression Model

Variables	Coefficients	Std. Error
Intercept	−7.36 ***	2.42
Aggressive Rider	5.44 ***	1.98
Risky Rider	2.30 *	1.47
Inattentive Pedestrian	4.50 **	1.97
Unresponsive Pedestrian	5.06 **	2.15
Akaike Information Criterion (AIC): 28.51		

Significance codes: 0 '***' 0.001 '**' 0.01 '*' 0.05 '.' 0.1 ' ' 1

These findings indicate the importance of understanding the different behavioral types of e-scooter riders and pedestrians that exist in a shared space and to be able to suggest possible solutions for avoiding collisions. Some suggestions might be the separation of e-scooter riders and pedestrians in urban mobility [17]. Another suggestion might be a stricter legislative framework that prevents e-scooter riders from disregarding regulations, combined with increased enforcement in shared public spaces.

4 Conclusions

This study investigated near-collision interactions between e-scooter riders and pedestrians in a shared pedestrian environment, emphasizing the role of behavioral dynamics in shaping safety outcomes. The findings indicate that although e-scooter riders predominantly adopt defensive strategies, such as deceleration, a non-negligible proportion of risky behaviors, namely acceleration and lack of reaction, persists across various conditions. The results further demonstrate that behavioral factors outweigh environmental conditions, as unsafe interactions occur even under low pedestrian density and sufficient spatial margins. In particular, pedestrian behavior plays a critical role, with inattentive and unresponsive pedestrians significantly increasing the likelihood of high-risk conflicts. Moreover, the combination of specific rider and pedestrian personas amplifies collision risk, highlighting that safety in shared spaces is inherently interaction-driven.

From a policy perspective, the findings suggest that infrastructure measures alone may be insufficient to ensure safety. Instead, targeted interventions focusing on behavioral awareness, enforcement, and regulation of both e-scooter riders and pedestrians are necessary. Strengthening legislative frameworks, improving compliance, and promoting mutual awareness among users can contribute to reducing conflicts in shared urban environments.

Despite the valuable insights provided, this study is subject to certain limitations. First, the analysis is based exclusively on near-miss incidents between e-scooter riders and pedestrians, and therefore does not account for actual collision events or interactions involving other mobility modes such as bicycles or motor vehicles. Second, although pedestrian density was considered as a proxy for congestion, the study does not explicitly model occurrence or exposure components of risk. Third, the dataset is based on observations from specific locations and may not fully capture the variability of behaviours across different urban contexts. These limitations should be considered when interpreting the results, and future research could expand the analysis by incorporating additional transport modes, broader datasets, and more comprehensive risk modelling approaches.

Future research should explore larger datasets and incorporate interaction effects more explicitly, as well as examine the impact of different urban designs and regulatory measures on user behavior and safety outcomes.

Disclosure of Interests. The authors have no competing interests to declare that are relevant to the content of this article.

References

1. Nalmpantidou, E., Sarafidis, D., Nikiforiadis, A., Stamatiadis, N., Fountas, G., Basbas, S.: Spatiotemporal analysis of e-scooter demand in Lexington, Kentucky. In: Computational Science and its Applications – ICCSA 2025 Workshops LNCS, pp. 35–47. Springer, Heidelberg (2025)
2. Burt, N., Ahmed, Z.: E-scooter attitudes and risk-taking behaviours: an international systematic literature review and survey responses in the west midlands, United Kingdom. Front. Public Health **11** (2023)

3. Naaseh, A., Tohmasi, S., Kranker, L.M., Schuerer, D.J.E.: Road traffic injury prevention: standing electric scooters. Curr. Trauma Rep. (2024)
4. Tuli, F.M., Mitra, S.: Dissecting shared e-scooters usage patterns and its impact on other transportation modes: a case study of Portland city. Travel Behav. Soc. **36**, 100812 (2024)
5. Nikiforiadis, A., Lioupi, C., Fountas, G., Stamatiadis, N., Basbas, S.: Determinants of the travel satisfaction of e-scooter users. Travel Behav. Soc. **37**, 100853 (2024)
6. Kazemzadeh, K.: Assessing e-scooter rider safety perceptions in shared spaces: evidence from a video experiment in Sweden. Accid. Anal. Prev. **211**, 107874 (2025)
7. Stigson, H., Malakuti, I., Klingegård, M.: Electric scooter accidents: analyses of two Swedish accident data sets. Accid. Anal. Prev. **163**, 106466 (2021)
8. Kazemzadeh, K., Haghani, M., Sprei, F.: Electric scooter safety: an integrative review of evidence from transport and medical research domains. Sustain. Cities Soc. **89**, 104313 (2023)
9. Campisi, T., Nikitas, A., Al-Rashid, M.A., Nikiforiadis, A., Tesoriere, G., Basbas, S.: The rise of e-scooters in Palermo: a SWOT analysis and travel time study. In: Gervasi, O., Murgante, B., Misra, S., Rocha, A.M.A.C., Garau, C. (eds.) ICCSA 2022 Workshops, LNCS, vol. 13380. Springer, Cham (2022)
10. Koop, P.: Country overview: e-scooter regulations in Europe. http://www.evz.de/en/travelling-motor-vehicles/e-mobility/two-wheelers/e-scooter-regulations.html. Accessed 24 Mar 2026
11. Delavary, M., Lyon, C., Vanlaar, W.G.M., Robertson, R.D., Nikolaou, D., Yannis, G.: E-scooter riders: a cross-cultural analysis of traffic safety attitudes and behaviors. IATSS Res. **49**(2), 247–258 (2025)
12. Bozovic, T., Flower, J., Parkin, J., Chatterjee, K.: Pedestrian experiences of rental e-scooter use and parking. Transp. Plan. Technol. (2025)
13. Son, Y.G., Kim, M.J., Lee, Y., Park, D.: Understanding risk perceptions of e-scooter use: e-scooter users and non-users. Heliyon **11**(3), e42312 (2025)
14. Washington, S., Karlaftis, M.G., Mannering, F., Anastasopoulos, P.: Statistical and Econometric Methods for Transportation Data Analysis. Chapman and Hall/CRC (2020)
15. Firth, D.: Bias reduction of maximum likelihood estimates. Biometrika **80**(1), 27–38 (1993)
16. George, A.M., Brown, P.M.: Risky e-scooter behaviours: the importance of descriptive norms and perceived behavioural control. Transport. Res. F: Traffic Psychol. Behav. **115**, 103350 (2025)
17. Šucha, M., et al.: E-scooter riders and pedestrians: attitudes and interactions in five countries. Heliyon **9**(4), e15449 (2023)

From Anxious Rushers to Attentive Observers: A Cluster Analysis of University Student Pedestrian Profiles

Efstathios Bouhouras(✉), Grigorios Fountas, Socrates Basbas, Panagiotis Giapitzoglou, Stefanos Tsouggaris, Georgios Zois, and Erlind Gishti

School of Rural and Surveying Engineering, Aristotle University of Thessaloniki, 54124 Thessaloniki, Greece
stbouch@hotmail.com

Abstract. This study presents a comparative analysis of pedestrian behavior and perceived safety among university students at two signalized intersections in Thessaloniki, Greece. While both locations serve high pedestrian volumes, one intersection permits vehicle left-turns during the pedestrian green phase (signified by flashing yellow arrows), whereas the other maintains a protected phase that restricts all conflicting vehicle movement. Utilizing data from two questionnaire-based surveys ($N_1 = 304$ and $N_2 = 301$), the research examines the interplay between infrastructure design, demographic factors, and behavioral traits. A K-Means clustering algorithm was applied to segment the target group into four distinct behavioral profiles based on levels of haste, distraction (e.g., mobile phone use, social interaction), and signal compliance. The results indicate that intersections permitting vehicle conflict are associated with significantly lower levels of perceived safety and a higher propensity for risk-taking behavior, such as crossing against the signal. The identified clusters, "The Distracted Law-Breaker," "The Anxious Rusher," "The 'Lost in Device' Waiter," and "The Attentive Observer", illustrate that individuals' behavioral tendencies significantly moderate the impact of intersection's operational phasing. The findings suggest that signal phasing that eliminates vehicle-pedestrian conflicts is the most effective intervention for increasing compliance and safety confidence. This research provides a methodological framework for urban planners to develop targeted safety interventions by understanding the diverse behavioral profiles within the student population.

Keywords: pedestrian safety · urban mobility · university students · signalized crosswalks

1 Introduction

A significant problem for high-density areas such as University campuses where heavy traffic intersects with pedestrians concerns their safety at signalized intersections. Based on the recent road safety data in Greece (year 2022), pedestrians represent approximately 17.1% of total traffic fatalities [72]. While elders often represent the majority of these fatalities, university students form a risk group presenting specific behavioral patterns, including haste and high usage of mobile devices while walking.

© The Author(s), under exclusive license to Springer Nature Switzerland AG 2027
O. Gervasi et al. (Eds.): ICCSA 2026 Workshops, LNCS 16761, pp. 256–271, 2027.
https://doi.org/10.1007/978-3-032-30527-5_17

The design and operation of road crossing is highly affected by the existence or not of traffic lights, arising a critical conflict at intersections where permitted phasing is used (vehicles are allowed to turn (often left) while pedestrians have a green walk signal). This problem is frequently managed by using flashing yellow arrows at traffic lights, forcing drivers to approach the intersection with caution giving priority to pedestrians. Protected or exclusive phasing restrict all vehicle movement during the pedestrian cycle, eliminating conflict points at least on a theoretical level. Although the so far research has concluded that protected phasing tends to reduce accidents rates, the way that these infrastructure types and the different types of pedestrians interact between hem (who may be distracted, rushing, or non-compliant) remains under-explored.

The majority of the existing literature concerning pedestrians' safety often addresses risk factors as separate, independently measurable variables. For example, studies have identified (statistically) correlations between pedestrian volumes and injury rates, or analyzed specific distractions (such as mobile phone use) which according to their findings lead a) to slower walking speeds and b) reduced situational awareness [62–64]. Other studies have modeled red-light running behavior based on waiting times or sequential traffic conflicts. However, these approaches usually analyze risk factors in isolation as they rarely identify patterns where distraction, haste, and signal compliance intersect. For example, a student who is highly distracted but strictly compliant with traffic lights, presents a different risk profile than one who is attentive but deliberately violates red lights due to haste. Understanding these different profiles is crucial for developing targeted safety interventions.

To address this gap, the current paper moves beyond descriptive statistics, applying K-Means Clustering to students of the Aristotle University of Thessaloniki (AUTh), in order to segment their behavioral on using road crosswalks into distinct behavioral profiles/ groups. The objectives of this research are first to identify University-related pedestrians profiles based on key behavioral attributes, including distraction frequency (phone, music, social interaction), haste, and signal compliance; second, to examine whether the distribution of these profiles/ groups differs between a Permitted and a Protected intersection, assessing thus how specific crosswalks' types may encourage or mitigate specific risk behaviors; and third to provide evidence-based recommendations for urban and transport planners in order to develop profile-specific behavioral interventions.

Based on the above, this research offers the perspective on the pedestrian-infrastructure relationship (often missed by aggregated analyses). The paper's structure is the following: Sect. 1 is the introductory section (Introduction), Sect. 2 presents the Literature Review, Sect. 3 describes the Methodology applied, Sect. 4 presents the Results and Sect. 5 the main findings and conclusions (Discussion and conclusions).

2 Literature Review

For the literature review evidence was extracted from the SCOPUS database, using the following query "TITLE-ABS-KEY (pedestrian and safety and signalized and crosswalks) AND PUBYEAR >2009 AND PUBYEAR <2026". In total, 319 articles were identified and extracted, presenting an increasing trend in the number of documents

that peaked in the year 2023 with 28 documents. A slight fluctuation is observed in the subsequent years, with a dip to 20 documents in 2024 followed by a resurgence to 27 documents in 2025. The highest activity period was recorded between 2020 and 2025. Out of the 319 articles, 305 of them contain the keyword "pedestrian" (95.6%), 287 contain the keyword "safety" (90.0%), 180 contain the keyword "signalized" (56.4%), 251 contain the keyword "crosswalk" (78.7%), 261 contain the keywords "pedestrian safety" (81.8%) combined, and 28 contain the keywords "signalized crosswalks" (8.8%) combined.

The majority of the identified documents/ papers comes from China, accounting 109 publications, the United States with 59 and India with 34, while Greece was in 13th place worldwide with 5 respective documents. This distribution highlights a strong research focus in regions facing rapid urban growth, dense pedestrian flows, and increasing safety challenges.

Jiang et al. (2011) [1] and Ren et al. (2011) [2] provided early cross-cultural evidence, highlighting that signal compliance is a social construct influenced by group size. Recently, the focus has shifted to cognitive drivers, as Costa et al. (2017) [3] linked attitudes directly to crossing speed. Virkler (1998) [4] and Guo et al. (2012) [5] identified that haste diminishes the reliability of a pedestrian's safety assessment. Wang et al. (2026) [6], Peche et al. (2026) [7], and Zhang et al. (2026) [8] based their analysis on machine learning to identify factors like waiting endurance. Additional studies on student and commuter behavior were conducted by Parvez et al. (2026) [9], Krizsik et al. (2026) [10], and Bouhouras et al. (2026) [11], highlight that crossing decisions are often probabilistic. Rafe et al. (2025) [12], Bouhouras et al. (2025) [13] and Zhang et al. (2025) [14], through their analyses identified behavioral shifts over the last decade.

Xie et al. (2012) [15] and Xie et al. (2013) [16] introduced cellular automaton models to simulate complex interactions at signalized crosswalks, while Fu et al. (2023) [17] and Arun et al. (2023) [18] developed advanced neural architectures for trajectory prediction. Sushmitha et al. (2023) [19] and Tahmasebi et al. (2025) [20] evaluate the Level-of-Service (LoS) at crosswalks. The optimization of mixed-traffic conditions based on the usage of Deep Learning was explored by Manthirikul et al. (2025) [21], Chun et al. (2025) [22], and Sulle et al. (2025) [23]. Furthermore, the integration of vision-based detection and AI-driven tracking was examined aiming on controlling the traffic lights in real time by Sun et al. (2025) [24], Anis et al. (2025) [25], Raha et al. (2025) [26], Arafat et al. (2025) [27], and Raoniar et al. (2025) [28].

Fu et al. (2018) [29] and Alhajyaseen et al. (2012) [30] developed frameworks for Surrogate Safety Measures (SSMs) like Time-to-Collision (TTC). Hashimoto et al. (2016) [31] introduced the estimation of crossing intention using probabilistic models, as a critical component for connected vehicle safety. Chen et al. (2024) [32] and Wang et al. (2024) [33] based their research on micro-level trajectory data to identify collision risks, while Sherif et al. (2025) [34], Oliva et al. (2025) [35], and Xie et al. (2025) [36], examined the red-light running phenomenon. Frej (2025) [37], Yokarasa et al. (2025) [38], Yan et al. (2025) [39], Subedi et al. (2025) [40], Peng et al. (2025) [41], and Wong et al. (2025) [42] focused their analyses on safety auditing and risk assessment methodologies.

Guidelines on how to install crosswalk were proposed by Smith et al. (1987) [43], while Steinman et al. (2004) [44] and Lee et al. (2005) [45] expanded the impact of bidirectional flows on pedestrian capacity. Recent research by Amarasingha et al. (2025) [46] and Saldivar-Carranza et al. (2024) [47] was based on LiDAR-derived data to prove that infrastructure improvements on crosswalks must be dynamic. Ištoka Otković et al. (2025) [48], Lin et al. (2025) [49], and Nasri et al. (2025) [50] investigated the role of different pavement designs on pedestrians' safety. Peche et al. (2025) [51], Li et al. (2025) [52], and Guo et al. (2024) [53] examined the operational performance and capacity impacts of right-turning vehicles. Finally, Kim et al. (2024) [54], Khademi et al. (2024) [55], and Sengupta et al. (2024) [56] through their research tried to optimize signal coordination and phase plan designs.

Barlow et al. (2005) [57] and Bentzen et al. (2004) [58] analysed the safety challenges that blind pedestrians face. Jiang et al. (2021) [59] and Ištoka Otković et al. (2021) [60] research on younger and older populations highlighted the necessity for age-specific crosswalks. Environmental factors like lighting were examined by Makó et al. (2026) [61]; Perra et al. (2022) [62] and Wei et al. (2017) [63] examined distraction caused by the usage of mobile phones as primary contributors to perceived safety risks. Ankunda et al. (2024) [64], Cheng et al. (2024) [65], and Taamneh et al. (2024) [66] examined the relation between public transport and pedestrians' safety. Lao et al. (2024) [67], Baldassa et al. (2024) [68], Xie et al. (2024) [69], and Shao et al. (2024) [70] analysed multi-stage crossings and drone-assisted interfaces.

Table 1 presents the identified and analysed literature review clustering.

Table 1. Literature review clustering

Category	Primary Research Focus	Authors (Year) [Reference]
Behavioral Psychology & Decision Making	Signal compliance, situational factors, red-light crossing, waiting time tolerance, and cognitive decision-making.	Jiang et al. (2011) [1]; Ren et al. (2011) [2]; Virkler (1998) [4]; Wang et al. (2026) [6]; Krizsik et al. (2026) [10]; Bouhouras et al. (2026) [11]; Rafe et al. (2025) [12]; Bouhouras et al. (2025) [13]; Wang et al. (2024) [33]; Frej (2025) [37]; Li et al. (2025) [52]; Taamneh et al. (2024) [66]; Baldassa et al. (2024) [68]; Xie et al. (2024) [69].
AI, Modeling & Simulations	YOLO, MCMC), social force models, cellular automata, trajectory prediction, and virtual reality simulations.	Parvez et al. (2026) [9]; Zhang et al. (2026) [8]; Zhang et al. (2025) [14]; Xie et al. (2012) [15]; Xie & Zhao (2013) [16]; Fu et al. (2023) [17]; Sun & Pei (2025) [24]; Hashimoto et al. (2016) [31]; Wong et al. (2025) [42]; Guo et al. (2024) [53]; Kim et al. (2024) [54]; Khademi et al. (2024) [55]; Makó et al. (2026) [61]; Shao et al. (2024) [70].

(*continued*)

Table 1. (*continued*)

Category	Primary Research Focus	Authors (Year) [Reference]
Safety & Conflict Analysis	Surrogate Safety Measures (SSM), TTC/PET analysis, crash causation models, and automated video-based conflict detection.	Costa et al. (2017) [3]; Guo et al. (2012) [5]; Peche & Saha (2026) [7]; Anis et al. (2025) [25]; Arafat et al. (2025) [27]; Raoniar et al. (2025) [28]; Fu et al. (2018) [29]; Alhajyaseen et al. (2012) [30]; Yan et al. (2025) [39]; Subedi et al. (2025) [40]; Peng & Liu (2025) [41]; Peche & Saha (2025) [51]; Sengupta et al. (2024) [56]; Ankunda et al. (2024) [64].
Signal Timing & Infrastructure Design	Signal phasing, Leading Pedestrian Intervals (LPI), Level of Service (LOS), crosswalk markings, and geometric optimization.	Sushmitha et al. (2023) [19]; Tahmasebi & Furth (2025) [20]; Manthirikul et al. (2025) [21]; Chun et al. (2025) [22]; Raha et al. (2025) [26]; Chen et al. (2024) [32]; Oliva et al. (2025) [35]; Smith & Knoblauch (1987) [43]; Steinman & Hines (2004) [44]; Lee et al. (2005) [45]; Amarasingha et al. (2025) [46]; Saldivar-Carranza et al. (2024) [47]; Lin et al. (2025) [49].
Vulnerable Groups & Distraction	Children's safety, visually impaired navigation, mobile phone distraction, and elderly pedestrian behavior.	Sulle et al. (2025) [23]; Sherif et al. (2025) [34]; Xie et al. (2025) [36]; Yokarasa & Sivakumar (2025) [38]; Ištoka Otković et al. (2025) [48]; Nasri et al. (2025) [50]; Barlow et al. (2005) [57]; Bentzen et al. (2004) [58]; Jiang et al. (2021) [59]; Ištoka Otković et al. (2021) [60]; Perra et al. (2022) [62]; Wei et al. (2017) [63]; Cheng et al. (2024) [65]; Lao & Furth (2024) [67].

3 Methodology

The paper analyses the data collected through an in situ, questionnaire-based survey implemented at two at-grade intersections in the Municipality of Thessaloniki, Greece on January 2025 and specifically at: a) Egnatia and third Septemvriou streets (intersection A), located near the AUTH Campus and b) Aggelaki and Alexandrou Svolou streets (intersection B), located near the AUTH Campus at the borders of the commercial center of the city (see Fig. 1).

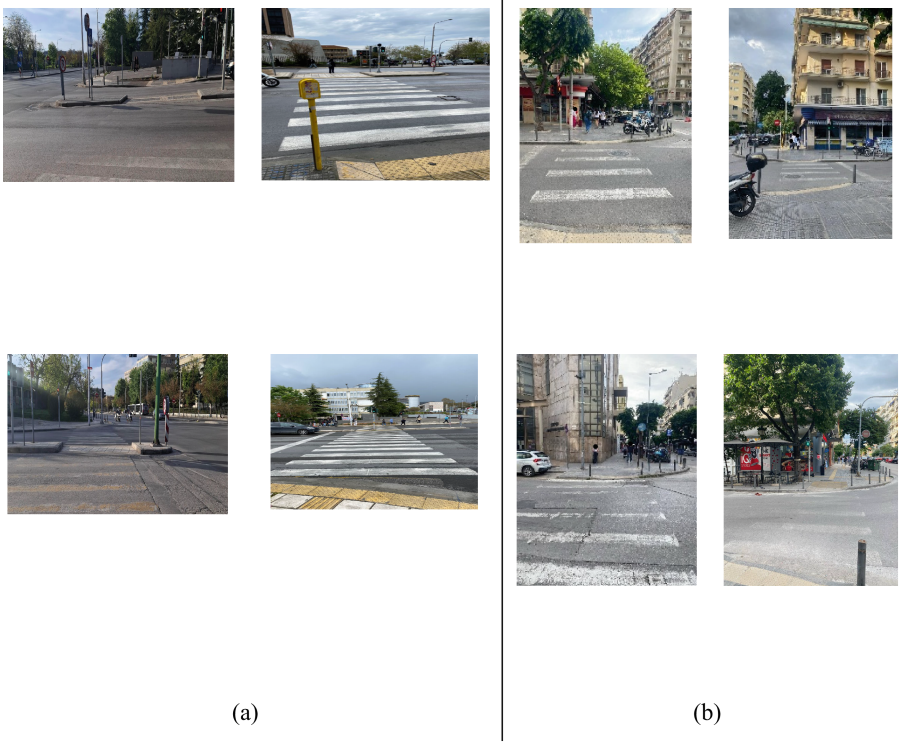

Fig. 1. At grade intersections of Egnatia and third Septemvriou streets (a) and of Aggelaki and Alexandrou Svolou (b)

Egnatia street serves as one of the main horizontal arterials in the city of Thessaloniki, running the urban landscape from one side of the city to the other in the direction of South East to North West. The street serves the traffic through two (2) lanes per direction as well as a bus lane located at the right side as vehicles move. The street is divided along its entire length with a median island (center island) of varying width per section. At each intersection with a major street, traffic is controlled by traffic signals installed at each crossing street for both the vehicles and the pedestrians. Right-turning movements are typically permitted while left-turning movements are allowed per case. Where permitted, the left turning movements are facilitated through a dedicated left turning lane and traffic lights. At Intersection A, vehicles can perform a left turning movement using a dedicated lane for this purpose.

At Intersection B, left-turn movements are controlled by flashing yellow arrows displayed alongside the green signal indication. In accordance with the Greek Road Traffic Code (Law 2696/1999, as amended), flashing arrows fall under the provisions governing vehicular lights (Article 6, paragraph 1, subparagraphs f–h). A yellow arrow (whether steady or flashing) forces the drivers to reduce speed and proceed with increased caution, giving the priority to pedestrians and other vehicles. It must be noted that pedestrian movements at this location are regulated by dedicated pedestrian traffic lights.

At each intersection research teams collected the necessary data through questionnaire-based survey addressed exclusively to students of the AUTh, collecting in total 607 questionnaires. After cleaning the data to remove incomplete or inconsistent entries, the final dataset consisted of 605 valid samples (N1 = 304 for intersection A, N2 = 301 for intersection B, N=N1 + N2)

It must be noted that the questionnaire used was structured to progressively record participants' attributes, habits, perceptions, related to pedestrian crossings. Therefore, the first section concerned socio-demographic information, including gender, age group, professional status, educational background, and household income. The second section, concerned questions on travel behavior, examining private vehicle ownership or regular use, as well as the frequency with which respondents use pedestrian crosswalks in their daily movements. The participants were asked whether they typically cross at designated locations and whether they comply with traffic lights indications, such as waiting for the green phase or choosing to cross during the red phase. Participants were also asked to rate how safe they feel when crossing at the under-study intersections, and whether specific modifications on them (such as upgrading the existing traffic lights) would make them feel mower confident or safe.

In order to better understand the decision-making processes, the survey examined a range of factors affecting the participants' choice to cross (including incoming vehicle speed, traffic volume, haste, presence of other pedestrians, and traffic lights indications). The participants were asked to rank these factors according to their perceived importance, allowing the research team to identify the most influential determinants of their crossing behavior. The questionnaire also addressed perceived risk sources, such as insufficient traffic lights indications' durations, driver non-compliance with traffic lights, and situations in which pedestrians and vehicles occupy the crossing simultaneously. Distraction related behavior was also addressed through phone use, music listening, and social conversation while using the crosswalks, along with how the participants felt their habits affected their safety awareness and their tendency to take risks.

The questionnaire had a final section on potential safety improvements (better lighting, clearer signage, lower speed limits, and enforcement cameras), asking the participants to rank these measures and to identify the dangers they regard as most serious. Overall, the questionnaire addressed six (6) questions related to socio-demographic characteristics and fourteen (14) questions on perceived risks, behaviors, and safety-related factors associated with pedestrian crossings.

4 Results

The application of the K-Means clustering algorithm (N = 605) identified four (4) behavioral clusters (k = 4). To ensure the robustness of these groupings, a one-way ANOVA was performed across all clustering variables (Haste, Distraction, Compliance). The results indicated that all variables contributed significantly to the cluster formation ($p < 0.001$), with Electronic Distraction and Signal Compliance showing the highest F-scores. The entire cluster analysis (including data preprocessing, K-Means implementation, Elbow Method, Silhouette Analysis, and ANOVA validation) was performed using Python (v3.11).

Specifically, the K-Means clustering was based on a multivariate set of parameters specifically selected to identify the three (3) core risk variables frequency of phone calls, texting or browsing, music listening, and conversation with other people. Time pressure was collected via a Haste Score reflecting each participant's delf-reported sense of urgency while crossing. Signal Compliance (that is the tendency to cross against a red signal or during an active flashing arrow phase) served as the primary behavioral outcome variable. Since these parameters were measured using a 5-point Likert scale while Signal Compliance was a binary one, Z-score standardization was applied to the full feature matric before the clustering process. Without this step, the wider numerical range of the Likert items would have exerted a disproportionate influence on the Euclidean distance calculations underlying the cluster assignments.

It must be noted that the K-Means unsupervised learning algorithm was used. Given a set of pedestrian observations (x1, x2, …, xn), where each observation is a d-dimensional vector of behavioral traits (Distraction, Haste, Compliance), the algorithm partitions the N observations into k($\leq$ N) sets S = {S1, S2, …, Sk} so as to minimize the within-cluster sum of squares (WCSS). The objective function is defined as:

$$\arg \frac{\min}{S} \sum_{i=1}^{k} \sum_{x \in Si} \|x - \mu i\|^2 \tag{1}$$

Where μi is the mean (centroid) of points in Si.

Because the survey used different measurement scales (e.g., Likert 1–5 for distraction and binary 0–1 for signal compliance), feature scaling was mandatory to prevent variables with larger ranges from dominating the Euclidean distance calculation, and thus standardization (Z-score normalization) was applied:

$$z = \frac{x - \mu}{\sigma} \tag{2}$$

The optimal number of clusters was determined using two primary heuristics:

1. The Elbow Method: The WCSS was plotted against a range of k values (1 to 10). The "elbow" point - where the rate of decrease in WCSS significantly levels off - was identified at k = 4.
2. Silhouette Analysis: To validate cluster separation, the Silhouette Coefficient (s) was calculated for each point:

$$s(i) = \frac{b(i) - a(i)}{\max\{a(i), b(i)\}} \tag{3}$$

where a(i) is the average distance to other points in the same cluster and b(i) is the average distance to points in the nearest neighboring cluster. Through this process an average silhouette score of 0.58 was achieved, indicating a strong structure in the data.

To visually assess the separation between the identified clusters, a Silhouette Plot was developed (see Fig. 2), presenting the silhouette coefficient for each sample, grouped by cluster. The majority of samples across all four clusters exceed the average score of 0.58, with very few negative values, confirming that the k = 4 solution provides minimal overlapping among groups.

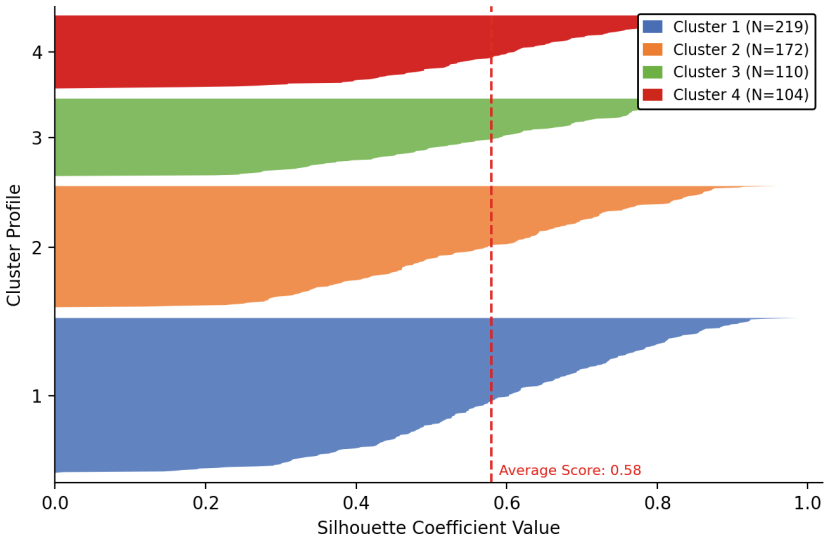

Fig. 2. Silhouette Plot for k = 4 Cluster Solution (N = 605).

Furthermore, a sensitivity analysis was performed to compare the $k = 4$ solution against alternative partitions ($k = 3$ and $k = 5$). As presented in Table 2, $k = 4$ provided the optimal balance between model complexity and group separation.

Table 2. Sensitivity analysis comparing different number of clusters Literature review clustering

Number Of Clusters (K)	*WCSS*	*Avg. Silhouette Score*	*Interpretability*
k = 3	*1240.5*	*0.49*	*Merges 'Anxious Rusher' And 'Law-Breaker'*
k = 4	***892.1***	***0.58***	***Distinct Behavioral Archetypes***
k = 5	*815.4*	*0.52*	*Splits 'Attentive Observer' Into Redundant Groups*

As a result, the K-Means clustering process identified the four following profiles/clusters:

- Cluster 1 - The Attentive Observer ($n = 219$): This is the largest and the least problematic cluster. The distraction levels are low across all modalities (mean 1.2/5.0). The Signal Compliance presents a 94% compliance rate even at Intersection A (Permitted), suggesting that infrastructure design does not affect their safety focus.
- Cluster 2 - The "Lost in Device" Waiter (n = 172): This group presented the highest "Digital Engagement" score (4.6/5.0). Interestingly, their "Haste" score was the lowest (1.8/5.0), implying they are willing to wait for the green light specifically because they use their mobile phones.
- Cluster 3 - The Distracted Law-Breaker (n = 110): This group presents a "Social Risk." Their social interaction score (4.2/5.0) was significantly higher than their

tendency on using their mobile phones. They are 3.5 times more likely to follow a lead pedestrian into the crosswalk against a red light than any other profile/ cluster.

- Cluster 4 - The Anxious Rusher (n = 104): They presented a very high Haste score (4.8/5.0). Their behavior is highly independent by the traffic lights indications as they choose to cross during small gaps in vehicles flow. At Intersection A (Permitted), this group accounted for 65% of all recorded near-miss interactions.

In order to evaluate the practical significance of the observed differences between clusters, Eta-squared (η^2) was calculated for each behavioral dimension. According to Cohen's criteria, values above 0.14 represent a large effect. As shown in Table 3, Signal Compliance ($\eta^2 = 0.64$) and Electronic Distraction ($\eta^2 = 0.59$) exerted the strongest influence on cluster membership, accounting for over 50% of the variance between groups.

Table 3. One-Way ANOVA of Behavioral Variables across Clusters (N = 605)

Behavioral Variable	*F-value (df = 3)*	*p-value*	*Eta-squared (η^2)*	*Effect Size Magnitude*
Signal Compliance	*214.52*	*< 0.001*	***0.64***	***Large***
Electronic Distraction	*186.10*	*< 0.001*	***0.59***	***Large***
Haste/Rushing	*92.34*	*< 0.001*	***0.38***	***Large***
Social Distraction	*45.12*	*< 0.001*	***0.22***	***Medium-Large***
Self-Reported Crossing Speed	*31.08*	*< 0.001*	***0.16***	***Medium***

5 Discussion and Conclusions

Through the analysis of the collected it was identified that Intersection B (Protected) successfully decreases the physical threat of vehicle-pedestrian conflict.

The significant 13% increase in the "Lost in Device" profile at the protected intersection highlights the fact that as the surrounding environment at crosswalks becomes objectively safer, pedestrians tend to increase their engagement with secondary tasks (using a mobile device). This tendency is dangerous during the transition from the sidewalk to the crosswalk, where pedestrians may step into the road based solely on the traffic light change without a primary visual scan of the environment/ road.

The difference between Anxious Rusher and Distracted Law-Breaker, affects sustainable mobility policy, because the two clusters/ profiles require different approaches. The Rusher as a cluster/ profile remains stable across both intersections (r = 0.91), suggesting that infrastructure changes alone cannot change their behavior. The Law-Breaker, is a different case. At Intersection A (Permitted), the presence of flashing yellow arrows

reduced the tendency of this group to cross the road by 4% compared to Intersection B (Protected). This indicates that a certain level of perceived complexity in the environment can discourage social distraction.

Based on the identified profiles/ clusters the following measures are proposed to be implemented at the crosswalks surrounding the AUTh campus:

- Dynamic Phasing for Peak Hours: To protect "Anxious Rushers" and "Law-Breakers", high-volume student crosswalks should use protected phasing during class-change intervals. However, during off-peak hours, a return to permitted phasing could be allowed.
- Multisensory Alerts for the "Lost in Device" profile: As nearly 30% of students are focused on their mobiles, standard visual lights tend to be insufficient. As a solution LED-embedded tactile paving at the curb are recommended - often referred to as "zombie lights" - to provide signal information within the downward peripheral vision of smartphone users.
- V2P (Vehicle-to-Pedestrian) Communication: For the "Anxious Rusher," smart city infrastructure could push real-time alerts to mobile devices when a student is approaching a curb at high walking speed during a red phase.

While the usage of K-Means clustering process and the applied statistical tests are considered successful on analysing the collected data, several limitations must be acknowledged. The sample is restricted to university students, a group that likely differs from the broader pedestrian population in terms of being familiar with the use of smartphones, risk attitudes, and walking pace. Furthermore, based on the fact that the data were collected through a questionnaire-based survey, the participants might have provided inaccurate of false answers. Finally, the collected data capture a snapshot of behavior as seasonal variations (e.g., weather-induced haste in winter) or long-term behavioral adaptation to the flashing yellow arrow were not captured.

Taking into consideration all the above, the pedestrians' safety at signalized intersection cannot be fully understood and explained through aggregate approaches only. The K-Means Clustering framework that was applied in the current research can be considered as feasible and useful on segmenting pedestrian target groups into behavioral profiles, presenting their risk configuration and respective measures to be applied.

For the City of Thessaloniki in general and the AUTh campus specifically, the findings suggest that even protected phasing may is not without complications. In order to create a sustainable and safe urban environment, urban planners and decision makers might move from one-size-fits-all infrastructure planning towards designs that take into consideration the different behavioral profiles of the users/ pedestrians.

Future research should focus on adapting these behavioral profiles to determine if the Lost in Device phenomenon is a permanent shift or a temporary response to infrastructure changes. Additionally, integrating the K-Means framework with real-time computer vision and analysis could allow for the automated identification of risky "Anxious Rusher" or "Distracted Law-Breaker" profiles/ clusters in smart city environments.

It should be also mentioned that Vehicle-to-Pedestrian (V2P) technologies could be explored, testing whether haptic alerts can effectively mitigate the risks and dangers identified at protected intersections. Finally, expanding this research to include elderly pedestrians and children, who are particularly vulnerable in urban intersections [71],

will be essential for developing an inclusive, age-aware sustainable mobility plan for Thessaloniki.

Acknowledgments. The authors acknowledge the use of AI-assisted tools (Claude, Anthropic) in conducting specific statistical analyses and in supporting the proofreading and linguistic revision of this manuscript. The AI tools were employed solely as technical aids to enhance the clarity and accuracy of the text and to assist with defined computational tasks. All conceptual development, interpretation of results, scientific conclusions, and intellectual contributions presented in this work are exclusively those of the authors. The authors take full responsibility for the integrity and originality of the knowledge produced herein.

Disclosure of Interests. The authors have no competing interests to declare that are relevant to the content of this article.

References

1. Jiang, X., Wang, W., Mao, Y., Bengler, K., Bubb, H.: Situational factors of influencing drivers to give precedence to jaywalking pedestrians at signalized crosswalk. Int. J. Comput. Intell. Syst. **4**(6), 1407–1414 (2011). https://doi.org/10.2991/ijcis.2011.4.6.35
2. Ren, G., Zhou, Z., Wang, W., Zhang, Y., Wang, W.: Crossing behaviors of pedestrians at signalized intersections: observational study and survey in China. Transp. Res. Rec. 65–73 (2011). https://doi.org/10.3141/2264-08
3. Costa, M., et al.: The influence of pedestrian crossings features on driving behavior and road safety. Transp. Infrastruct. Syst. 741–746 (2017). https://doi.org/10.1201/9781315281896-96
4. Virkler, M.R.: Pedestrian compliance effects on signal delay. Transp. Res. Rec. 88–91 (1998). https://doi.org/10.3141/1636-14
5. Guo, H., Wang, W., Guo, W., Jiang, X., Bubb, H.: Reliability analysis of pedestrian safety crossing in urban traffic environment. Saf. Sci. **50**(4), 968–973 (2012). https://doi.org/10.1016/j.ssci.2011.12.027
6. Wang, K., et al.: Identification of factors influencing pedestrians' red-light crossing behavior based on interpretable machine learning. Transport. Res. F: Traffic Psychol. Behav. 118 (2026). https://doi.org/10.1016/j.trf.2025.103487
7. Peche, G., Saha, A.: Investigating the safety of pedestrians at signalized intersection crosswalks in left-hand driving scenarios. J. Transp. Eng. Part A: Syst. **152**(2) (2026). https://doi.org/10.1061/JTEPBS.TEENG-9185
8. Zhang, C., Du, B., Shen, J., Xu, X., Wu, Z.: Modeling bidirectional mixed flow of pedestrians, bicycles and E-mopeds at signalized crosswalks. Reliab. Eng. Syst. Saf. 266 (2026). https://doi.org/10.1016/j.ress.2025.111654
9. Parvez, M., Moridpour, S., Tay, R., Shtayat, A.: Analysing pedestrian safety at intersections using video and AI-based tracking. Adv. Transdisciplinary Eng. **84**, 656–663 (2026). https://doi.org/10.3233/ATDE251540
10. Krizsik, N., Sipos, T., Berényi, J.: Factors affecting the yielding of the priority to pedestrians Lecture Notes in Mobility, Part F903, pp. 793–799 (2026). https://doi.org/10.1007/978-3-031-88974-5_114
11. Bouhouras, E., Tsouggaris, S., Zois, G., Fountas, G., Basbas, S.: Pedestrian Behavior and Safety Perceptions among University Students at Signalized Crosswalks Lecture Notes in Computer Science, 15892 LNCS, pp. 81–100 (2026). https://doi.org/10.1007/978-3-031-97638-4_6

12. Rafe, A., Singleton, P., Boyer, S., Mekker, M.: Pedestrian crossing behaviors at signalized intersections in Utah: factors affecting spatial and temporal violations. Int. J. Transp. Sci. Technol. **20**, 321–335 (2025). https://doi.org/10.1016/j.ijtst.2024.12.005
13. Bouhouras, E., Fountas, G., Basbas, S., Giapitzoglou, P., et al.: How signal phasing shapes university students' crossing decisions and confidence. Safety **11**(4) (2025). https://doi.org/10.3390/safety11040106
14. Zhang, G., Wang, Y., Hoggenmueller, M.: Designing drone interfaces to assist pedestrians crossing non-signalised roads. In: OZCHI 2025 Proceedings, pp. 111–121 (2025). https://doi.org/10.1145/3764687.3764700
15. Xie, D., Gao, Z., Zhao, X., Wang, D.: Cellular automaton modeling of the interaction between vehicles and pedestrians at signalized crosswalk. J. Transp. Eng. **138**(12), 1442–1452 (2012). https://doi.org/10.1061/(asce)te.1943-5436.0000462
16. Xie, D., Zhao, X.: Modeling mixed traffic flow at a crosswalk with push button. In: ICNM 2013 - 6th International Conference on Nonlinear Mechanics, pp. 601–605 (2013)
17. Fu, L., et al.: A modified social force model for studying nonlinear dynamics of pedestrian-e-bike mixed flow at a signalized crosswalk. Chaos, Solitons Fractals **174** (2023). https://doi.org/10.1016/j.chaos.2023.113813
18. Arun, A., Lyon, C., Sayed, T., et al.: Leading pedestrian intervals – yay or nay? Accid. Anal. Prev. **181** (2023). https://doi.org/10.1016/j.aap.2022.106929
19. Sushmitha, R., Srikanth, S., Reddy, S., Rayudu, A.: Level of service analysis of pedestrian crossing facilities at signalized intersections under heterogeneous traffic. Suranaree J. Sci. Technol. **30**(4), 010243 (2023). https://doi.org/10.55766/sujst-2023-04-e0143
20. Tahmasebi, M., Furth, P.: Reducing speeding by removing speeding opportunities: field test of safe waves traffic signal timing. Transp. Res. Rec. **2679**(11), 695–706 (2025). https://doi.org/10.1177/03611981251349432
21. Manthirikul, S., Jain, U., Kathuria, A.: Assessment of level of service at signalized midblock crosswalks under mixed traffic conditions. Innovative Infrastructure Solutions **10**(10) (2025). https://doi.org/10.1007/s41062-025-02283-5
22. Chun, G., Oh, S., Jang, K.: Effect of pedestrians on right-turn capacity under heterogeneous traffic conditions. Transp. Res. Rec. **2679**(10), 731–750 (2025). https://doi.org/10.1177/03611981251342767
23. Sulle, M., Mwakalonge, J., Comert, G., Siuhi, S., et al.: Digital healthcare applications in pedestrian safety: a VR-based predictive model for distracted crossing behavior. Digit. Eng. **6** (2025). https://doi.org/10.1016/j.dte.2025.100051
24. Sun, J., Pei, Y.: Behavior Spectrum-based pedestrian risk classification via YOLOv8–Byte-Track. Appl. Sci. (Switz.) **15**(18) (2025). https://doi.org/10.3390/app151810008
25. Anis, M., Geedipally, S., Lord, D.: Pedestrian crash causation analysis near bus stops: insights from random parameters models. Accid. Anal. Prev. **220** (2025). https://doi.org/10.1016/j.aap.2025.108137
26. Raha, F., Russo, B., Eschen, A., Elia, A., et al. (2025). How Do Leading Pedestrian Intervals (LPIs) Affect Turning Vehicle–Pedestrian Conflict Frequencies? Transp. Res. Rec. 2679(9), 518–532. https://doi.org/10.1177/03611981251338716
27. Arafat, M., Kaye, S., Schroeter, R., Haque, M.: A game theoretical model to examine pedestrian behaviour and safety using AI analytics. Accid. Anal. Prev. **217** (2025). https://doi.org/10.1016/j.aap.2025.108034
28. Raoniar, R., Singh, S., Pathak, A., & Maurya, A. (2025). Analysis of Pedestrian–Vehicle Interaction Dynamics: A Surrogate Safety Measure Approach. Transp. Res. Rec. 2679(4), 1042–1063. https://doi.org/10.1177/03611981241289412
29. Fu, T., Miranda-Moreno, L., Saunier, N.: A novel framework to evaluate pedestrian safety at non-signalized locations. Accid. Anal. Prev. **111**, 23–33 (2018). https://doi.org/10.1016/j.aap.2017.11.015

30. Alhajyaseen, W., Iryo-Asano, M., Nakamura, H.: Estimation of left-turning vehicle maneuvers for the assessment of pedestrian safety. IATSS Res. **36**(1), 66–74 (2012). https://doi.org/10.1016/j.iatssr.2012.03.002
31. Hashimoto, Y., Gu, Y., Hsu, L., Iryo-Asano, M., Kamijo, S.: A probabilistic model of pedestrian crossing behavior for connected vehicles. Transp. Res. Part C: Emerg. Technol. **71**, 164–181 (2016). https://doi.org/10.1016/j.trc.2016.07.011
32. Chen, W., Hu, L., Huang, K., et al.: Exploring optimal signal plans for isolated signalized intersections with central pedestrian refuges. J. Transp. Eng. Part A: Syst. **150**(5) (2024). https://doi.org/10.1061/JTEPBS.TEENG-8053
33. Wang, Y., Zhou, Z., Chen, W., Wang, T., Wang, L.: Modelling yielding dilemma zone for drivers at non-signalised crosswalks. Transp. Res. F. **102**, 213–232 (2024). https://doi.org/10.1016/j.trf.2024.02.018
34. Sherif, B., Abou-Senna, H., Radwan, E.: Exploring the impact of distracted pedestrians on traffic operations. J. Transp. Eng. Part A: Syst. **151**(2) (2025). https://doi.org/10.1061/JTEPBS.TEENG-7964
35. Oliva, F., Landolfi, E., et al.: Implementation and testing of V2I communication strategies for pedestrian safety. Sensors **25**(2) (2025). https://doi.org/10.3390/s25020485
36. Xie, S., Yang, Z., Xu, G.: Integrating acoustic-based risk quantification for modeling pedestrian-vehicle interactions. Int. J. Transp. Sci. Technol. (2025). https://doi.org/10.1016/j.ijtst.2025.01.003
37. Frej, D.: Observational study of pedestrian behavior at signalized crosswalks. Commun. – Sci. Lett. Univ. Zilina **27**(1), D54–D66 (2025). https://doi.org/10.26552/com.C.2025.013
38. Yokarasa, T., Sivakumar, T.: Evaluating pedestrian behaviors and safety risks at Colombo crosswalks. Moratuwa Eng. Res. Conf. MERCon, 705–710 (2025). https://doi.org/10.1109/MERCon67903.2025.11217106
39. Yan, X., Chen, P., Zhang, H.: Analysis of factors influencing the risk of pedestrian-vehicle conflict at signalized intersections. In: ICTIS 2025 Proceedings, pp. 1328–1337 (2025). https://doi.org/10.1109/ICTIS68762.2025.11214799
40. Subedi, P., Singleton, P., Gaither, A., Mekker, M.: Right-turn safety for pedestrians: insights from multilevel models of conflicts in Utah. Transp. Res. Rec. (2025). https://doi.org/10.1177/03611981251378144
41. Peng, T., Liu, J.: Analysis of conflict between right-turning vehicles and pedestrians using random parameter logit model. Traffic Inj. Prev. (2025). https://doi.org/10.1080/15389588.2025.2545001
42. Wong, S., Huang, P., Shih, C., Lin, G., Lin, W.: Traffic animation of pedestrian and vehicle interactions. IEEE Access. **13**, 141245–141262 (2025). https://doi.org/10.1109/ACCESS.2025.3597330
43. Smith, S.A., Knoblauch, R.L.: Guidelines for the installation of crosswalk markings. Transp. Res. Rec. 15–25 (1987)
44. Steinman, N., Hines, D.: Methodology to assess design features for pedestrian and bicyclist crossings at signalized intersections. Transp. Res. Rec. 42–50 (2004)
45. Lee, J., Goh, P., Lam, W.: New level-of-service standard for signalized crosswalks with bidirectional pedestrian flows. J. Transp. Eng. **131**(12), 957–960 (2005). https://doi.org/10.1061/(ASCE)0733-947X(2005)131:12(957
46. Amarasingha, N., Perera, J., Dissanayake, S.: Pedestrian level of Service at Signalized Intersections. ICTD 2025: Transp. Plann. Oper., 513–523 (2025). https://doi.org/10.1061/9780784486207.044
47. Saldivar-Carranza, E., Desai, J., Thompson, A., et al.: Vehicle and pedestrian traffic signal performance measures using LiDAR-derived trajectory data. Sensors **24**(19) (2024). https://doi.org/10.3390/s24196410

48. Ištoka Otković, I., Deluka-Tibljaš, A., et al.: Analysis of influencing parameters on children's crossing speeds at non-signalized crosswalks. Transp. Res. Procedia **90**, 543–550 (2025). https://doi.org/10.1016/j.trpro.2025.06.109
49. Lin, P., Keita, Y., Rangaswamy, R., et al.: Assessing the effectiveness and impact of LPIs on right-turning vehicle behaviors. In: ICTD 2025 Proceedings, pp. 349–359 (2025). https://doi.org/10.1061/9780784486207.030
50. Nasri, M., Yin, S., Wang, Y.: Comprehensive analysis of multi-modal road user behavior using big data. In: ICTD 2025 Proceedings, pp. 146–159 (2025). https://doi.org/10.1061/9780784486191.013
51. Peche, G., Saha, A.: A study on pedestrian-vehicle conflict at signalized crosswalks in an Indian traffic scenario Lecture Notes in Civil Engineering, vol. 622, pp. 101–118 (2025). https://doi.org/10.1007/978-981-96-1988-7_8
52. Li, T., Hu, C., Sze, N., et al.: Modelling Pedestrian-Vehicle Interaction Behaviours Incorporating Risk Perception. Transportmetrica A: Transp. Sci. (2025). https://doi.org/10.1080/23249935.2025.2479084
53. Guo, Y., Zou, H., Wei, F., et al.: Analysis of pedestrian second crossing behavior based on physics-informed neural networks. Sci. Rep. **14**(1) (2024). https://doi.org/10.1038/s41598-024-72155-y
54. Kim, H., Ko, J., Oh, C., Kim, S.: Evaluation of autonomous driving safety in mixed traffic. Sustain. (Switz.) **16**(22) (2024). https://doi.org/10.3390/su16229672
55. Khademi, N., Mazloum, S., Zabihpour, A., Chen, A.: Designing safer intersections: exploring the impact of warnings in VR. Saf. Sci. **178** (2024). https://doi.org/10.1016/j.ssci.2024.106604
56. Sengupta, A., Guler, S., Gayah, V., Warchol, S.: Evaluating the reliability of automatically generated crash surrogates. Accid. Anal. Prev. **203** (2024). https://doi.org/10.1016/j.aap.2024.107614
57. Barlow, J., Bentzen, B., Bond, T.: Blind pedestrians and the changing technology and geometry of signalized intersections. J. Vis. Impairment Blindness **99**(10), 587–598 (2005). https://doi.org/10.1177/0145482x0509901003
58. Bentzen, B., Barlow, J., Bond, T.: Challenges of unfamiliar signalized intersections for pedestrians who are blind. Transp. Res. Rec., 51–57 (2004). https://doi.org/10.3141/1878-07
59. Jiang, K., Wang, Y., Feng, Z., et al.: Research on intervention methods for children's street-crossing behaviour. Accid. Anal. Prev. **152** (2021). https://doi.org/10.1016/j.aap.2021.105979
60. Ištoka Otković, I., Deluka-Tibljaš, A., et al.: Development of models for children—pedestrian crossing speed. Sustain. (Switz.) **13**(2), 1–18 (2021). https://doi.org/10.3390/su13020777
61. Makó, E., Ittzés, M., Kálmán, V., et al.: Evaluating lighting and cognitive safety at pedestrian crossings Lecture Notes in Networks and Systems, 1768 LNNS, pp. 106–111 (2026). https://doi.org/10.1007/978-3-032-13898-9_13
62. Perra, V., Basbas, S., Nikiforiadis, A., Militsis, N.: Investigation of distracted Pedestrians' exposure duration. Period. Polytech. Transp. Eng. **50**(3), 235–244 (2022). https://doi.org/10.3311/PPTR.15963
63. Wei, Y., Zhang, C., Zhou, B., et al.: The mobile phone use behavior and its effect on pedestrian safety. In: ICTIS 2017 Proceedings, pp. 225–231 (2017). https://doi.org/10.1109/ICTIS.2017.8047769
64. Ankunda, D., Ali, Y., Mohanty, M.: Pedestrian crash risk analysis using extreme value models: new insights and evidence. Accid. Anal. Prev. **203** (2024). https://doi.org/10.1016/j.aap.2024.107633
65. Cheng, G., Sheng, L., Wang, H., Feng, T.: Safety evaluation method for pedestrians crossing street at signalized intersection. Jilin Daxue Xuebao (Gongxueban). **54**(7), 1903–1912 (2024). https://doi.org/10.13229/j.cnki.jdxbgxb.20221108

66. Taamneh, M., Alomari, A., Taamneh, S.: Using machine learning to predict pedestrian compliance at crosswalks in Jordan. Appl. Sci. (Switz.) **14**(11) (2024). https://doi.org/10.3390/app14114945
67. Lao, F. & Furth, P. (2024). Improving Pedestrian Progression at Multistage Crossings Using Pedestrian–Left Turn Overlaps. Transp. Res. Rec. 2678(6), 694–707. https://doi.org/10.1177/03611981231198848
68. Baldassa, A., Orsini, F., De Cet, G., et al. (2024). Which factors are related to young people's crossing behavior? European Transport - Trasporti Europei. https://doi.org/10.48295/ET.2024.97.7
69. Xie, S., Yang, Z., Qi, Y.: Identification of critical conditions for pedestrian-vehicle game modes. Proc. SPIE **13421** (2024). https://doi.org/10.1117/12.3054586
70. Shao, J., Zhao, R., Zhou, Q., et al.: Study on benefit analysis and setting condition of signal control right-turn vehicles. In: CICTP 2024 Proceedings, pp. 3879–3885 (2024). https://doi.org/10.1061/9780784485484.369
71. Fountas, G., Olowosegun, A., Basbas, S.: Assessing school travel safety in Scotland: an empirical analysis of injury severities for accidents in the school commute. Safety **8**(2), 29 (2022). https://doi.org/10.3390/safety8020029
72. Hellenic Statistical Authority: Road traffic accidents: Year 2022. ELSTAT (2024). https://www.statistics.gr/documents/20181/5e797464-9d74-f0f4-7f5a-53e2b937a006

A Logical Framework Approach to the Monitoring of an Emergency Evacuation Exercise for an Urban Transport System

Corrado Rindone[1](✉) and Antonio Russo[2]

[1] DIIES, Department of Information, Infrastructure and Sustainable Energy Engineering, Università degli Studi Mediterranea di Reggio Calabria, Reggio Calabria, Italy
corrado.rindone@unirc.it

[2] DIA, Department of Engineering and Environment, Università degli Studi di Enna "Kore", 94100 Enna, Italy
antonio.russo@unikore.it

Abstract. Disaster Risk Reduction (DRR) is one of the main challenges at the global level. The main goals and targets to be achieved are set out in Agenda 2030 and the Sendai Framework. According to the international risk management cycle, different actions can be implemented before (mitigation and preparedness) and after (response, recovery) a disaster event. This work focuses on preparedness actions. The main objective of this paper is to propose a Logical Framework Approach (LFA) to monitor an emergency evacuation exercise in a transport system. LFA allows the analysts to distinguish the involved resources (input), the exogenous activities to perform the exercise, and the products in terms of capacity (output). The paper investigates the issue related to increased capability (outcome) of emergency managers and people to perform evacuation planned activities in a real context, and then for achieving exposure reduction (goal). With respect to a classical LFA approach, the paper introduces two classes of endogenous activities to measure the transformation: 1) from capacity (output) to capability (outcome), by specifying specific statistical tests; 2) from capability (outcome) to exposure knowledge (goal), by adopting Transport System Models (TSM). The paper contributes to enhancing transparency in the evacuation exercise process by integrating LFA and TSM. The main results of the proposed method's application are presented in relation to an example of a discussion-based activity (workshop). LFA clarifies the existing gaps between capacities and capabilities in relation to DRR. The experimentation results show how it is possible to measure all components of a structure's training and exercises aimed at increasing the preparedness level of a community. The paper is of interest to researchers who study science-policy gaps and to public and private decision-makers involved in the emergency planning process.

Keywords: Emergency Evacuation · Preparedness · Emergency Training and Exercises · Transport System Models · Sustainable Development Goals

© The Author(s), under exclusive license to Springer Nature Switzerland AG 2027
O. Gervasi et al. (Eds.): ICCSA 2026 Workshops, LNCS 16761, pp. 272–283, 2027.
https://doi.org/10.1007/978-3-032-30527-5_18

1 Introduction

In recent decades, the frequency of natural and man-made disasters has increased. According to the EM-DAT international disaster database, the disasters' impacts on people and goods are relevant. In 2024 alone, EM-DAT recorded 393 disasters that caused 16,753 deaths, affected over 167 million people [1].

The 2030 Agenda for Sustainable Development acknowledges the necessity of taking action to reduce the risk of disasters. Some Sustainable Development Goals (SDGs) include direct or indirect references to disaster risk reduction. Some particularly relevant SDGs are SDG 1 – *No Poverty*, SDG 11 – *Sustainable Cities and Communities, SDG 12 – Responsible Consumption and Production* and SDG 13 – *Climate Action* [2]. The Sendai Framework for Disaster Risk Reduction 2015–2030 is closely related to the 2030 Agenda and is the United Nations' main global instrument for disaster risk management [3]. The Sendai Framework promotes the adoption of a structured Disaster Risk Management (DRM) cycle, integrating prevention and preparedness before a disaster event, as well as response and recovery afterwards.

This work regards the prevention and preparedness phases of the DRM cycle. In particular, the focus is on evacuation planning aimed at reducing exposure risk components. The objective of an evacuation plan is to reduce the number of people present in the area affected by the effects of the disaster by improving mobility in emergency conditions [4]. However, literature underlines the gaps between the planned actions and their implementation in a real context [5]. In order to reduce these gaps, it is possible to adopt Training and Exercise (T&E) actions. The final aim is to increase the level of capabilities and knowledge of people and managers about planned procedures and their implementation [6–11]. However, mere participation in a T&E action does not ensure the effectiveness of the prevention and preparedness phases. It is necessary to define a clear connection between the evacuation planned procedures and their implementation in real-world systems during a disaster.

To overcome the literature gaps, the paper proposes a Logical Framework Approach (LFA) to monitor an evacuation exercise or training action about transport system planning.

After this introduction, the paper has three sections. Section 2 proposes the LFA framework, illustrating its main components. Section 3 presents an example of the application of the proposed framework. Section 4 closes the paper with a discussion and some final remarks.

2 The LFA Framework for Controlling Training and Exercise Action

2.1 Training and Exercise Actions

During the preparedness phase, T&E activities help to raise awareness among people and managers of the planned procedures. The main aim is to trial these procedures in a stress-free environment. Different international agencies have provided guidelines to help emergency decision-makers design and implement T&E actions [12].

Literature underlines the main characteristics of each T&E action and the potential contribution to:

- *capability*, which assesses the ability to intervene in real conditions to reduce exposure, measured by indicators related to the objective of risk reduction;
- *complexity* of planning and training, measured in terms of the quantity and type of actors involved in the specific activity.

According to international guidelines, T&E actions can be classified into the two following main classes, in relation to an increasing level of complexity and capability:

- *discussion-based activities* conducted in virtual or simulated settings, including seminars, table-top and other activities aimed at illustrating planning contents with a desk approach;
- *operations-based* activities carried out in real-world environments, comprehending exercises involving different classes of actors to reproduce emergency planning settings.

One of the main consolidated international approaches is the Homeland Security Exercise and Evaluation Programme (HSEEP) developed in the US FEMA agency after the disastrous events occurred at the beginning of the third millennium [13]. In the FEMA guidelines, an exercise is "an event or activity, conducted through discussion or action, to develop, evaluate or validate plans, policies, procedures and capabilities that jurisdictions/organizations can use to achieve planned objectives". According to the HSEEP, the discussion-based class includes seminars, workshops, tabletops and games; the operation-based class includes drill, functional exercises and full-scale exercises. In both classes, each activity involves an increasing level of complexity and produces a higher level of capability in the participants (Fig. 1).

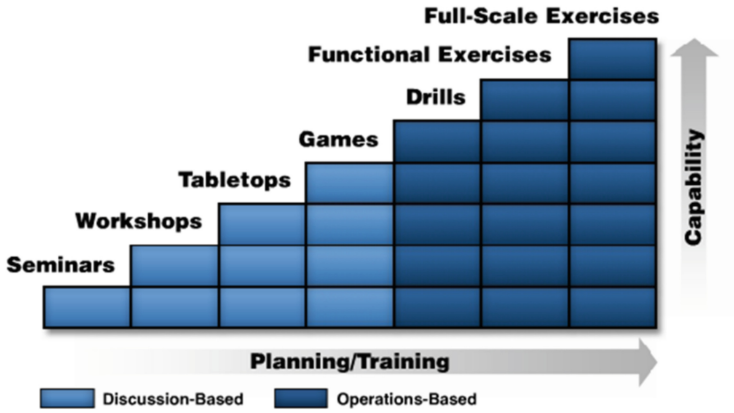

Fig. 1. Exercises classes (Source: [14])

Although the content and operations to be performed in each T&E action are well described and structured in international guidelines, the results of actions are often limited to certifying the ability of the actors involved to perform their assigned tasks. Unlike

material actions, where the product is tangible and measurable (e.g., the amount of temporary infrastructure to organize road signs), training and exercises produce intangible effects that are more complex to measure [15]. This involves the measurement of the awareness' level about evacuation procedures, the increase in skills and organizational capabilities of managers, as well as the changes in users' travel choices produced by a user information system.

2.2 Transport System Models and Transport Risk Analysis

Transport System Models (TSM) simulate the movement of people and goods to analyze, predict, and optimize the performance of transportation networks under ordinary and emergency conditions [16, 17]. This implies the study of transport, demand components and their interactions.

Transport Risk Analysis (TRA) involves evaluating potential hazards and operational uncertainties within transportation systems in order to assess their likelihood, vulnerability and exposure, thereby supporting decision-making processes in the event of an emergency [4, 18–20].

TSM and TRA can operate in an integrated digital platform to increase knowledge about potential effects produced by transport planning actions. The main actors involved should increase their knowledge of TSM and TRA to support their decision-making processes. This implies the necessity to define a framework for monitoring the acquisition of this knowledge.

2.3 The Proposed Framework

The Logical Framework Approach (LFA) was originally developed as a planning tool in a military context [21]. In recent decades, LFA has been adopted by the principal agencies for development as a "results-based" management approach [22]. In the context of the preparedness phase, LFA can be adopted to make the learning process more transparent, considering results connected to a T&E action [23–25].

LFA highlights the logic behind a generic activity in order to identify the components of an evacuation exercise and mutual relationships from the resources used to the specific and general objectives to be pursued.

The main components of LFA are here synthesised in the following subsections.

a. Input. Inputs include all the financial (e.g., amount of euros) and human (e.g., number of organisers) resources needed to conduct a T&E action. These resources must be sized according to the complexity of the specific **action**.

The *na* input indicators can be grouped into the following vector:

$$\mathbf{i^a} = \left(i^a{}_1, i^a{}_2, \ldots, i^a{}_{na}\right) \tag{1}$$

b. Exogenous activities. With the available resources, it is possible to organize and implement the T&E action [26, 27]. The sub-activities and the corresponding allocation of available resources must be defined. For example, the distribution of staff*hours required to complete each sub-activity is established. A preliminary assessment must first be carried out to measure the participants' initial knowledge of the plan procedures.

The *nb* exogenous activities can be represented with a function vector that collects the possible organizational variables:

$$\boldsymbol{\gamma}^{\mathbf{b}} = \left(\gamma^{\mathrm{b}}{}_1, \gamma^{\mathrm{b}}{}_2, \ldots, \gamma^{\mathrm{b}}{}_{\mathrm{nb}}\right) \tag{2}$$

c. Output. The implementation of the T&E action produces immediate, concrete effects that can be objectively measured. This is the quantity of plan procedure content transferred to participants. The main outcome is participant capacity, which can be measured through a set of indicators, such as the actual number of managers who have completed all the planned sub-activities.

The *nc* output indicators can be represented in the following vector**:**

$$\boldsymbol{i}^{\mathbf{c}} = \left(\mathrm{i}^{\mathrm{c}}{}_1, \mathrm{i}^{\mathrm{c}}{}_2, \ldots, \mathrm{i}^{\mathrm{c}}{}_{\mathrm{nc}}\right) \tag{3}$$

d. Endogenous Activities 1: from outputs to outcomes. Capacity is a necessary but not sufficient condition for the expected effects of the activities to be achieved. It is necessary to assess the current level of knowledge and skills acquired by participants following the training and/or exercise activities. To this end, a test can be administered to participants to measure the capability acquired by each participant. Capability measures the actual level of learning of the concepts taught during the generic activity. A questionnaire with closed-end questions on the topics illustrated can be used [28, 29].

The *nd* endogenous activities can be represented with a vector of functions that collects the possible tests that can be carried out to verify the acquisition of the capabilities:

$$\gamma^{\mathrm{d}} = \left(\gamma^{\mathrm{d}}{}_1, \gamma^{\mathrm{d}}{}_2, \ldots, \gamma^{\mathrm{d}}{}_{\mathrm{nd}}\right) \tag{4}$$

e. Outcomes. Endogenous activities produce outcomes in terms of the achievement of capability by participants. Outcomes can be measured through a set of indicators. For example, this involves measuring the number of participants who answered the questionnaire correctly. Achieving capability strengthens participants' ability to respond appropriately in a real-world situation where an evacuation procedure must be activated.

However, acquiring capability alone does not guarantee risk reduction. It is necessary to quantify the improvement in the performance of the transport system under evacuation conditions following the acquisition of knowledge and skills.

The *ne* outcome indicators can be grouped in the following vector**:**

$$\mathrm{i}^{\mathrm{e}} = \left(\mathrm{i}^{\mathrm{e}}{}_1, \mathrm{i}^{\mathrm{e}}{}_2, \ldots, \mathrm{i}^{\mathrm{e}}{}_{\mathrm{ne}}\right) \tag{5}$$

f. Endogenous Activities 2: from outcomes to goals. These activities reflect the effects of acquiring capabilities. Possible tools for evaluating ex ante the reduction of exposure are the Transport System Models and their components for representing the transport supply [30, 31], the transport demand [32–34] and their interaction [35, 36]. TSMs can be used, for example, to simulate the functioning of a transport network in an urban context, including estimated times for users to reach the safe areas established by the plan.

The *nf* endogenous activities can be represented with a vectorial function that collects the functions of the TSM models with which to estimate the performance of the transport network in evacuation conditions:

$$\boldsymbol{\gamma}^{\mathbf{f}} = \left(\gamma^{\mathrm{f}}{}_1, \gamma^{\mathrm{f}}{}_2, \ldots, \gamma^{\mathrm{f}}{}_{\mathrm{nf}}\right) \tag{6}$$

g. Goals. Goals represent the final results intended to be achieved through T&E actions. The final objective can be measured, for example, in terms of reducing evacuation times and thus increasing the probability of saving lives. The best performances have already been calculated during the planning (or mitigation) phase and represent target values to be achieved with a series of T&E actions [6]. It is therefore necessary to estimate the effects produced by each training/exercise activity in terms of contribution to improvement or deviation of performance from the targets to be achieved.

The *ng* goals indicators can be represented in the following vector:

$$\mathbf{i}^{\mathbf{g}} = \left(\mathrm{i}^{\mathrm{g}}{}_1, \mathrm{i}^{\mathrm{g}}{}_2, \ldots, \mathrm{i}^{\mathrm{g}}{}_{\mathrm{ng}}\right) \tag{7}$$

The synthetic representation of the components is obtained through a Logical Framework Matrix (LFM). This is a matrix consisting of

- Seven rows, one for each component of the LFA;
- Four columns which, for each component, report the description, the indicators, the means of verification and the external factors, i.e. those outside the control of the overall process.

A synthetic representation of a proposed LFM is reported in Fig. 2.

LFA component	Indicators	Means of verification	External factors
a. Inputs	i^{a}	monitoring	
b. Exogenous activities	γ^{b}	validation	elements out of control
c. Outputs	i^{c}	monitoring	
d. Endogenous activities 1	γ^{d}	validation	
e. Outcomes	i^{e}	monitoring	
f. Endogenous activities 2	γ^{f}	validation	
g. Goals	i^{g}	monitoring	

If

Then

Fig. 2. Generic LFM matrix

3 An Example of Training Action

The case study is a numerical example designed to illustrate the variables and functions introduced to specify the LFA process and the related LFM presented in Sect. 2. The specific problem to be addressed is the evacuation of a portion of a city in the event of a flood. For this problem, during the mitigation phase, an evacuation plan was developed that defined the procedures and estimated the quantitative effects measured through a set of indicators. Among these, the evacuation times for the entire area are considered ($t_{ev,\,tot}$).

3.1 Activities Description

The designed action concerns the training of managers in the evacuation procedures being analyzed. Specifically, reference is made to a discussion-based workshop activity. It is assumed that a generic organization invests a certain amount of financial resources to organize and conduct training for a defined number of managers.

The managers will be required to participate in the training course (capacity) and acquire the knowledge and skills (capability) to simulate an evacuation of an urban area. The goal is to ensure that the managers are able to use the acquired capabilities to reproduce the planned conditions through T&E action and thus reduce exposure.

3.2 LFA and LFM

The components of the LFA are explained below.

Input indicators are:

i^a_1 amount of financial resources to organize and implement the training course = 40.000€;

i^a_2:potential number of managers to be trained = 20 managers;

The vector of input indicators of Expression (1) therefore assumes the following values

$\mathbf{i^a}$ = (40.000 €, 20 managers)

The function which represents the exogenous activities is the distribution of total hours available (htot = 400 h) intended for the organization (h1 = 150 h) and realization of the course (h2 = 250 h). The vector function represented in Eq. (2) is:

$$\gamma^b = h_{tot} = h_1 + h_2$$

Output indicators are:

i^c_1 mandatory threshold of hours assigned to participants to acquire the capacity of manager = 200 h;

i^c_2:actual number of managers who attended the course for a number of hours exceeding the threshold = 18 managers;

i^c_3:percentage of managers actually trained = 90%.

The vector of output indicators of Eq. (3) therefore assumes the following values:

$\mathbf{i^c}$ = (200 h, 18 managers, 90%)

The endogenous activity 1 is represented by a function that corresponds to a test composed of a vector of k = 20 multiple-choice questions q.

$$\gamma_1^{\mathrm{d}} : \mathrm{R}(\mathrm{q}) = \mathrm{R}(\mathrm{q}_1, \mathrm{q}_2, \ldots, \mathrm{q}_\mathrm{k})$$

Therefore, the vector function represented in Eq. (4) is:

$$\gamma^{\mathrm{d}} = R(q)$$

Outcome indicators are:

$\mathrm{i}^{\mathrm{e}}{}_1$ minimum threshold in terms of percentage of correct answers to be provided to demonstrate having acquired the capability:

$\mathrm{i}^{\mathrm{e}}{}_1 = \eta_\mathrm{j} = (\mathrm{c_j} / \mathrm{k}) \geq 80\%$

for example, if a participant j answers 17 questions correctly

$\eta^{\mathrm{e}}{}_j = \mathrm{c_j} / \mathrm{k} = 17/20 = 85\%$

$\mathrm{i}^{\mathrm{e}}{}_2$ number of participants who exceeded the threshold $\mathrm{i}_2^{\mathrm{e}}$, and who have therefore acquired the capability, for example equal to 16 participants.

The vector of outcome indicators of Eq. (5), relating to the generic participant j, therefore assumes the following values:

$\mathbf{i^e} = (80\%, 16$ managers)

The function representing the endogenous activity 2 allows the 16 managers who have acquired the capability to estimate the evacuation times for the assigned study area. The function used by the generic participant, the only component of the vector introduced with the Eq. (6) is equal to:

γ_j^{f}: cost function for estimating evacuation times adopted by the generic participant

A possible cost function for estimating evacuation link travel time is the BPR.

These activities can be supported by emerging Information and Communication Technologies (e-ICT) that provide digital tools (e.g. web maps or simulations visualization tools) that enhance the representation of a virtual environment [37].

Goals indicators are:

$\mathrm{i}^{\mathrm{g}}{}_1$ minimum threshold in terms of percentage of evacuation time calculated by the generic participant j (tev,j) compared to that calculated by plan

$$\eta^{\mathrm{g}}{}_1 = \mathrm{tev/tev, tot} = 75\%$$

$\mathrm{i}^{\mathrm{g}}{}_2$:percentage of managers who correctly calculated evacuation times exceeding the threshold η^{g}; for example, if only 15 have calculated evacuation times which, compared to the times calculated by the plan, exceed the threshold η^{g}

$$\eta^{\mathrm{g}}{}_2 = 15/16 = 93.7\%$$

The vector of the goal indicators of the Eq. (7), relative to the generic participant j, therefore assumes the following values:

$\mathbf{i^g} = (75\%, 93.7\%)$

Figure *3* describes the LFM matrix sintetysing all the LFA components and logical connections. The matrix reports the obtained results obtained from the exercise.

LFA component	Indicators	Means of verification	External factors
a. Inputs	i_a = (40.000 €, 20 manager)	Budget	
b. Exogenous activities	$\gamma^b = h_{tot} = h_1 + h_2$	Project	elements out of control
c. Outputs	i^c = (200 hours,18 manager, 90%)	Course register	
d. Endogenous activities 1	$\gamma^d = R(\mathbf{q})$	Test register	
e. Outcomes	i^e = (80%, 16 manager)	Test register	
f. Endogenous activities 2	γ^f_j	TSM validation	
g. Goals	i^e = (75%, 93.7%)	TSM application	

If

Then

Fig. 3. Generic LFM matrix

4 Discussion and Conclusive Remarks

Disaster risk reduction is a global priority. Major international agencies are promoting various actions related to the DRM cycle. All stakeholders recognize the important role of T&E actions in increasing preparedness. Guidelines are available to guide the development of these actions. However, the focus is primarily on capacity building among stakeholders, especially managers. It is necessary to broaden the audience of participants in the actions by involving citizens. Furthermore, it is necessary to ensure that the trained personnel acquire capabilities in terms of knowledge and skills. In the case of evacuation plans aimed at reducing the exposure component of risk, it is necessary to ensure that those involved are aware of the best practices to implement to ensure high levels of efficiency and effectiveness of evacuation procedures. However, capacity and capability are necessary but not sufficient conditions for reducing exposure and therefore risk. It is necessary to evaluate how the acquired capabilities can contribute to reducing exposure by narrowing the gap between planned and actual conditions.

The LFA is a potential tool for increasing transparency in the evaluation and monitoring of training and evacuation activities. Explaining the individual components of the LFA and summarizing them through the LFM increases transparency and highlights any gaps between planning activities and their actual implementation in real-world situations.

The example presented, albeit in a simplified way, has shown how to apply the proposed framework and present the results obtained from the organization and implementation of a generic training action.

The paper has some limitations. The first limit regards the kind of evacuation exercise, restricted to a workshop. The second limitation concerns the definition of indicators and functions. The analytical formulations presented need further improvement. A further limitation concerns the contribution of ICT to improving the monitoring of exercises and training activities as well as the construction of TSMs.

Further research developments regard the extension of the experimentation, for instance a full-scale exercise. More in general, it is possible to develop methods and models to control more complex discussion-based and operation-based exercises.

The results of this paper and the further development of the research are of interest to public and private decision-makers involved in emergency planning processes. The proposed methodology can be adopted for measuring disaster risk reduction and the achievement of sustainability goals.

Acknowledgments. This study was carried out within the research project "RISK: Recovery Increasing by Social Knowledge" —2022B4TT2M (CUP 1-C53D23004800006), PIANO NAZIONALE DI RIPRESA E RESILIENZA (PNRR) Missione 4 "Istruzione e Ricerca"—Componente 1-C2, Investimento 1.1 "Fondo per il Programma Nazionale di Ricerca e Progetti di Rilevante Interesse Nazionale (PRIN)", D.D. n. 104 del 2 febbraio 2022, ERC SH7 "Human Mobility, Environment, and Space". This paper reflects only the authors' views and opinions, and neither the European Union, the European Commission, nor the Italian Ministry of the University and Research can be considered responsible for them.

Credit Author Statement. Conceptualization: C.R; Methodology: C.R. and A.R.; Software: A.R.; Validation: C.R. and A.R.; Formal analysis: A.R.; Investigation: C.R.; Resources: C.R.; Data curation: A.R.; Writing - Original Draft: C.R. and A.R.; Writing - Review & Editing: A.R.; Visualization: C.R.; Supervision: C.R.; Project administration: C.R.; Funding acquisition: C.R.

References

1. EM-DAT - The international disaster database.: https://www.emdat.be/. Accessed 11 Apr 2025
2. United Nations: Transforming our world: The 2030 Agenda for Sustainable Development (2015). https://sdgs.un.org/2030agenda
3. UNDRR: Sendai Framework for Disaster Risk Reduction 2015–2030. (2022)
4. Russo, F., Vitetta, A.: Risk evaluation in a transportation system. Int. J. SDP **1**, 170–191 (2006). https://doi.org/10.2495/SDP-V1-N2-170-191
5. Sakurai, A., Kumagai, M., Murayama, Y., Bisri, M.B.F., Sato, T.: Operationalizing updated tsunami Hazard assumptions in school evacuation planning: insights from teacher training and implementation challenges in Japan. JDR **21**, 138–150 (2026). https://doi.org/10.20965/jdr.2026.p0138
6. Russo, F., Rindone, C.: Methods for risk reduction: training and exercises to pursue the planned evacuation. Sustainability **16**, 1474 (2024). https://doi.org/10.3390/su16041474
7. Martino, G., Astarita, V., Guido, G., Haghshenas, S.S., Haghshenas, S.S.: Risk reduction in emergency evacuation through innovative Mobile applications: A study on user trust and behavior. In: Gervasi, O., Murgante, B., Garau, C., Karaca, Y., Faginas Lago, M.N., Scorza, F., Braga, A.C. (eds.) Computational Science and its Applications – ICCSA 2025 Workshops, pp. 226–238. Springer Nature, Switzerland, Cham (2026). https://doi.org/10.1007/978-3-031-97638-4_15
8. Li, H., Xie, Z., Liu, S.: The design and practice of an experimental teaching case for UAV-based field-data Acquisition in Outdoor Ecological Education. Sustainability **18**, 3340 (2026). https://doi.org/10.3390/su18073340
9. Xie, R., Zlatanova, S., Lee, J., Borrmann, A.: Evacuation Behavioural instructions with 3D motions: insights from three use cases. IJGI **14**, 197 (2025). https://doi.org/10.3390/ijgi14050197
10. Polydoropoulou, A., Bouhouras, E., Karakikes, I., Papaioannou, G.: Enhancing climate resilience in maritime ports: A decision support system approach. In: Gervasi, O., Murgante, B., Garau, C., Taniar, D., Rocha, C., A.M.A., and Faginas Lago, M.N. (eds.) Computational Science and its Applications – ICCSA 2024 Workshops, pp. 241–252. Springer Nature, Switzerland, Cham (2024). https://doi.org/10.1007/978-3-031-65329-2_16

11. Alakrawi, G.A., et al.: Evaluating the efficacy of full-scale and tabletop exercises in enhancing paramedic preparedness for external disasters: A quasi-experimental study. Medicine **103**, e40777 (2024). https://doi.org/10.1097/MD.0000000000040777
12. CEN: Evaluation of exercises - Implementation Guidelines. https://www.cencenelec.eu/media/CEN-CENELEC/CWAs/RI/cwa18009_2023.pdf. Accessed 30 Nov 2025
13. US FEMA: Homeland Security Exercise and Evaluation Program (HSEEP) (2020). https://preptoolkit.fema.gov/documents/1269813/1269861/HSEEP_Revision_Jan20_Final.pdf/65bc7843-1d10-47b7-bc0d-45118a4d21da?t=1580851559070
14. US FEMA: Homeland Security Exercise and Evaluation Program. Volume I: HSEEP Overview and Exercise Program Management. https://www.ojp.gov/pdffiles1/Archive/205244NCJRS.pdf. Accessed 03 Jan 2024
15. Twigg, J.: Disaster risk reduction: mitigation and preparedness in development and emergency programming | PreventionWeb (2009). https://www.preventionweb.net/publication/disaster-risk-reduction-mitigation-and-preparedness-development-and-emergency
16. Cascetta, E.: Transportation Systems Engineering Theory and Methods. Springer, US, S.l. (2013)
17. Ortúzar S., J. de D., Willumsen, L.G.: Modelling transport. Wiley, Hoboken, NJ (2024)
18. Zou, Z., Kang, S.: Route optimization for hazardous chemicals transportation under time-varying conditions. Sustainability **16**, 779 (2024). https://doi.org/10.3390/su16020779
19. Salvatore, W., et al.: A new methodology for the multi-risk assessment of existing road tunnels. Procedia Struct. Integrity **62**, 1112–1119 (2024). https://doi.org/10.1016/j.prostr.2024.09.147
20. Kovalenko, N., Malakhova, Y., Borets, I., Cherednichenko, K., Borets, O.: Assessment of risks during the transport process in integrated transport systems. In: Slavinska, O., Danchuk, V., Kunytska, O., Hulchak, O. (eds.) Intelligent Transport Systems: Ecology, Safety, Quality, Comfort, pp. 414–425. Springer Nature, Switzerland, Cham (2025). https://doi.org/10.1007/978-3-031-87379-9_38
21. Rodríguez-Rivero, R., Ortiz-Marcos, I.: The methodology of the logical framework with a risk management approach to improve the sustainability in the international development projects. Sustainability **14**, 756 (2022). https://doi.org/10.3390/su14020756
22. Sawadogo, J.-B., Dunlop, K.: Managing for results with a dynamic logical framework approach: from project design to impact measurement. Can. J. Dev. Stud./Revue canadienne d'études du développement. **18**, 597–612 (1997). https://doi.org/10.1080/02255189.1997.9669720
23. Di Gangi, M., Belcore, O.M.: Risk reduction in transport system in emergency conditions: a framework for decision support systems. Presented Safe. (2021). https://doi.org/10.2495/SAFE210251
24. Russo, F., Rindone, C.: Safety of users in road evacuation: the logical framework approach in evacuation planning. Presented Urban Transp. (2008). https://doi.org/10.2495/UT080721
25. Vitetta, A.: Risk reduction in transport system in emergency conditions: a framework for network design problems. Presented Safe (2021). https://doi.org/10.2495/SAFE210221
26. Russo, F., Rindone, C.: Planning in road evacuation: classification of exogenous activities. WIT Trans. Built Environ. **116**, 639–651 (2011). https://doi.org/10.2495/UT110541
27. Ranjan, S., Kim, Y.-C., Ranjan, N., Bhandari, S., Kim, H.: Large-scale road network traffic congestion prediction based on recurrent high-resolution network. Appl. Sci. **13**, 5512 (2023). https://doi.org/10.3390/app13095512
28. Rindone, C., Sgro, D., Vitetta, A.: Risk reduction by evacuation in transportation system: pilot survey with technology acceptance model. In: Gervasi, O., Murgante, B., Garau, C., Karaca, Y., Faginas Lago, M.N., Scorza, F., Braga, A.C. (eds.) Computational Science and its Applications – ICCSA 2025 Workshops, pp. 128–139. Springer Nature, Switzerland, Cham (2026). https://doi.org/10.1007/978-3-031-97638-4_9

29. Russo, F., Musolino, G., Moschella, M.: Risk reduction in urban areas by means of evacuation: survey design on use of emerging information and communication technologies. In: Gervasi, O., Murgante, B., Garau, C., Karaca, Y., Faginas Lago, M.N., Scorza, F., Braga, A.C. (eds.) Computational Science and its Applications – ICCSA 2025 Workshops, pp. 113–127. Springer Nature, Switzerland, Cham (2026). https://doi.org/10.1007/978-3-031-97638-4_8
30. Musolino, G.: Methods for risk reduction: modelling users' updating Utilities in Urban Transport Networks. Sustainability **16**, 2468 (2024). https://doi.org/10.3390/su16062468
31. Russo, F., Comi, A., Rindone, C.: The emerging ICT for exposure reduction in urban mobility: transport models for risk cycle. In: Intelligent Technology for Future Transportation. Springer Nature, Switzerland (2025). https://doi.org/10.1007/978-3-031-84148-4_14
32. Russo, F., Comi, A., Chilà, G.: Dynamic approach to update utility and choice by emerging technologies to reduce risk in urban road transportation systems. Future Transp. **4**, 1078–1099 (2024). https://doi.org/10.3390/futuretransp4030052
33. Astarita, V., Guido, G., Haghshenas, S.S., Haghshenas, S.S., Martino, G.: Risk reduction in transportation systems: A bibliometric-based literature review on artificial intelligence in disaster response. Transp. Res. Procedia **90**, 599–606 (2025). https://doi.org/10.1016/j.trpro.2025.06.102
34. Gerlici, J., Lovska, A.: Dynamic load of the tank container with Sandwich components. Appl. Sci. **15**, 11836 (2025). https://doi.org/10.3390/app152111836
35. Vitetta, A.: Network design problem for risk reduction in transport system: A models specification. Int. J. TDI **6**, 283–297 (2022). https://doi.org/10.2495/TDI-V6-N3-283-297
36. Vitetta, A.: A quantum utility model for route choice in transport systems. Travel Behav. Soc. **3**, 29–37 (2016). https://doi.org/10.1016/j.tbs.2015.07.003
37. Rindone, C., Russo, A.: Disaster risk reduction in a Manhattan-type road network: A framework for serious game activities for evacuation. Sustainability **17**, 6326 (2025). https://doi.org/10.3390/su17146326

Assessing the Potential of Demand Responsive Transit for Non-Emergency Healthcare Travel: An Accessibility-Based Approach

Antonio Russo(✉), Tiziana Campisi(✉), and Giovanni Tesoriere

Department of Engineering and Architecture, University of Enna Kore, 94100 Enna, Italy
{antonio.russo,tiziana.campisi}@unikore.it

Abstract. Demand Responsive Transit (DRT) is an important transport alternative that aims to promote greater sustainability in accordance with the goals of Agenda 2030. The possibility of implementing DRT must be considered in the presence of demand niches that are not covered by local public transport or other available transport modes. Among these demand niches, the demand for non-emergency healthcare travel is of particular interest due to its social implications.

This article proposes an aggregate methodology for the aggregate analysis of accessibility to hospital systems, to understand potentiality for implementation of DRT services. By combining the analysis of the accessibility of the hospital system and the study of the existing local public transport system, it is possible to identify suitable areas for further investigation of the applicability of a DRT system. Three attributes are analysed, based on available open-access data: distance to the nearest hospital, resident population and presence of a local public transport service. A pilot study is shown in which the proposed analysis is conducted considering the municipalities classified as "inland areas" of the Sicilian Region in Italy. The results show a poor condition of the mobility service system, highlighting how further analyses can be developed in the investigated area. The proposed model makes it possible to identify the areas in which DRT systems can help to support segments of demand for non-emergency healthcare travel.

The research is a prerequisite for a demand survey in areas characterised as critical, to assess the applicability of DRT services for healthcare trips. The research is of interest to public administrations, companies operating in the urban and suburban transport sector and researchers.

Keywords: Demand Responsive Transit · Healthcare accessibility · Non-emergency medical transport · Local public transport · Inland areas

1 Introduction

Health has assumed a significant role in humanity's sustainability goals. The United Nations 2030 Agenda for Sustainable Development outlines a global framework within which mobility policies and access to health services have a strategic and urgent place [1]. The 17 Sustainable Development Goals (SDGs) represent the global challenges to

© The Author(s), under exclusive license to Springer Nature Switzerland AG 2027
O. Gervasi et al. (Eds.): ICCSA 2026 Workshops, LNCS 16761, pp. 284–298, 2027.
https://doi.org/10.1007/978-3-032-30527-5_19

be addressed, further broken down into targets, specific results to be achieved; indicators are defined to measure progress in achieving the results [2, 3]. Among the 17 SDGs, Goal 3, "*Ensure healthy lives and promote well-being for all at all ages*" stands out. It establishes the principle of universal access to healthcare, defining equity in the provision of care as a prerequisite for community well-being. Target 3.8 states "*Achieve universal health coverage, including financial risk protection, access to quality essential healthcare services, and access to safe, effective, quality, and affordable essential medicines and vaccines for all*" explicitly defining health coverage for all. In this context, ensuring universal health coverage is not limited to providing adequate medical facilities and personnel; it also implies the concrete possibility for every individual to reach places of care.

In this sense, it is essential to emphasize the role of Goal 11 "*Make cities and human settlements inclusive, safe, resilient, and sustainable*". While target 11.1 identifies the need to provide access to basic services to all citizens, target 11.2 calls on Countries to ensure safe, affordable, accessible, and sustainable transport systems for all by 2030, with priority attention to the most vulnerable: older people, people with disabilities, women, and children. SDG 11 therefore highlights how mobility is not merely an infrastructural issue, but a social determinant of health.

Alongside these two objectives, with specific relevance to this paper, is Goal 9 "*Build resilient infrastructure, promote inclusive and sustainable industrialization and foster innovation*", which promotes the development of resilient and inclusive infrastructure and supports the adoption of innovative technological solutions at the service of the community.

Accessibility to hospital facilities is therefore an element at the intersection of different areas of sustainable development; specifically, elements related to health, community well-being, and the sustainability of cities converge. In this context, the study of healthcare mobility becomes relevant. A portion of healthcare-related travel is not related to emergency situations, but to scheduled visits or diagnostic tests. These non-emergency healthcare trips have specific characteristics: generally, they can be planned and often involve categories of users—the elderly, people with mobility disabilities, chronic patients—who do not have their own transportation or are unable to drive independently [4–7].

Due to its characteristics, scheduled public transport services may not be suitable to effectively respond to these needs, both due to the rigidity of the routes and to a structural difficulty in responding to door-to-door mobility [8]. In this context, DRT service emerges as a suitable response tool to various emerging problems. It is an on-demand, bookable service with intermediate rigidity characteristics between those of a classic, fully rigid PT service and a fully flexible taxi, for which it is defined as a semi-rigid service [9, 10]. Most of these services, in fact, have lines with fixed routes, but with the possibility of making detours based on booked stops. Services based on low-capacity vehicles are often more efficient in contexts characterized by limited or variable demand, as they allow for better adaptation of the offer to different time slots, avoiding the mismatch between vehicle capacity and number of users that frequently characterizes conventional public transport services [11].

This paper proposes a general framework for studying hospital accessibility, with the aim of identifying areas not served by public transportation, including hospital facilities and the affected population. In these areas, it is possible to consider implementing on-demand services. The proposed framework relies entirely on the use of open databases to ensure the study's replicability and scalability.

The remainder of the paper is organized as follows. Section 2 describes the state of the art, recalling the most significant contributions to the study of healthcare facility accessibility via public transportation. Section 3 outlines the main methodological components discussed in the paper. Section 4 presents the case study and the results of the application. Finally, Sects. 5 and 6, respectively, discuss the results and present the conclusions, limitations, and future developments of the research.

2 State of the Art

Demand Responsive Transit (DRT) can be framed as a flexible, user-oriented component of public transport systems, designed to adapt routes and schedules to actual demand rather than fixed timetables. It is typically deployed to complement conventional services in low-density or underserved areas, where fixed-route operations are inefficient or economically unsustainable [12]. Its effectiveness depends on the balance between service flexibility, operational costs, and user convenience, considering developing a network of DRT lines to serve an area already served by existing public transport, substitution of conventional bus lines or introduction of a service in an area not served by public transport due to low demand [13]. DRT are identified as a mode of transport who can improve hospital accessibility [14] [15]. identify hospital access as one of the market niches potentially interesting for the implementation DRT services. The authors define a separation between potential DRT users for hospital services, identifying staff, patients, and visitors as possible DRT users, staff trips more frequent and generally shorter, while patient and visitor trips longer and with highly variable frequencies. Furthermore, they underline how different services are operated by both car volunteers and equipped minibuses; services tend to be primarily door-to-door.

[16] highlight that published literature underlines how high costs is a major failure factor for DRT systems; on the other hand, specialist social-service-based DRT systems have been considered to warrant justifiable subsidies. From this perspective, therefore, it is necessary to emphasize the social component of a service to improve hospital accessibility. Temporal accessibility also plays a role in designing a DRT service for hospitals; a misalignment between a service's operating hours and the demand for hospital services could lead to a reduction in demand for these sectors [17].

The study of quantitative methodologies for analysing healthcare accessibility is a recently emerging topic in literature. Several studies have applied quantitative methodologies to assess how effectively public transportation networks enable the population to reach hospitals and healthcare services.

[18] analyse accessibility and equity in access to hospitals in six major cities in Ohio (USA), using indicators based on travel time by public transportation. The results highlight significant spatial disparities between central and peripheral areas, with lower accessibility in suburban areas. In a similar way, [19] conduct a comparative study of eight

Canadian metropolitan areas, showing how differences in the structure of transportation networks and the distribution of hospitals strongly influence accessibility levels.

Other works focus on specific European urban contexts [20]. analyse the case of Rome through a complex network analysis approach, highlighting how the structure of the public transport network influences connectivity between neighborhoods and healthcare facilities. Similarly, [21] propose a spatial analysis methodology applied to the city of Milan, using accessibility mapping techniques to identify urban areas with a potential lack of access to health services via public transport.

In North American context, [22] model multimodal access to primary care in an urban context, highlighting the importance of integrating different transport modes (public transport, active mobility and private vehicles) to improve overall accessibility [23]. proposes a comparative analysis of hospital accessibility in the city of Córdoba (Argentina) between 2019 and 2023, highlighting how changes to the public transport network can produce significant variations in access times to health services.

The studies show some methodological similarities, including the use of travel time-based indicators and the use of GIS tools for spatially assessing accessibility. However, significant differences also emerge in case studies, scales of analysis, and methodological approaches adopted, ranging from complex network models to multi-city comparative analyses. This heterogeneity reflects the need to adapt analysis tools to the specific territorial characteristics of transportation networks and the distribution of healthcare infrastructure.

The contributions focus primarily on large urban areas, with widespread public transport systems and a supply system with different modal alternatives and access to transportation. This paper investigates an urban-rural area, with the presence of small and medium-sized towns and large areas of low population density, with the aim of identifying, using open-source databases, areas where the use of DRT for access to healthcare facilities could be considered as an alternative.

3 Methodology

3.1 Modelling

The aim is to define an indicator that allows us to assess public transportation coverage for access to healthcare facilities in the study area. To formalize the problem, four subsets of information are defined based on the main components of the transportation system. For the modelling, reference is made to a transportation system modelling (TSM) approach [24–26].

The first subset is the set Z of N zones in the study area, defined as $Z = (z_1, z_2, \ldots, z_n, \ldots, z_N)$. Each zone in set Z can be characterised by different quantitative attributes, such as the population P_n and the surface area A_n. The population distributed across the territory allows us to model the demand side of the analyzed system.

The second subset is $H = (h_1, h_2, \ldots, h_w, \ldots., h_W)$, the set of healthcare facilities. The facilities are the points on the territory that indicate the potential destinations of healthcare trips and serve to represent the activity system. For simplicity, in the following we will refer to a case of a single hospital facility h in the study area. The third subset

$L = (l_1, l_2, \ldots, l_m, \ldots, l_M)$ represents the set of public transport lines; the fourth subset is $S = (s_1, s_2, \ldots, s_k, \ldots, s_K)$ the set of public transport stops. These two components represent the supply system.

Sequentially, it is necessary to define some conditions that allow to verify whether it is possible to reach h from the generic zone z_n via public transport.

The first is the condition of belonging of the generic stop s_k to the generic line l_m. The analytical definition of the first criterion specifically concerns the modeling of the timetable. It is defined as

$$A(s_k, l_m) = \begin{cases} 1, & \textit{if } s_k \textit{ is served from } l_m \\ 0, & \textit{otherwise} \end{cases} \tag{1}$$

The second condition concerns stop. It is necessary to define whether the generic stop s_k can is a stop serving the hospital. Having identified a generic distance *DIST*, the maximum threshold for walking between a public transport stop and a destination hospital and having evaluated the distance between s_k and h as $dist(s_k, h)$ it is possible to define $B(s_k, h)$ as

$$B(s_k, h) = \begin{cases} 1, & \textit{if } dist(s_k, h) < DIST \\ 0, & \textit{otherwise} \end{cases} \tag{2}$$

Starting from this condition, it is possible to define the set of lines that serve the hospitals L_h.

$$L_h = (l_m \in L | \exists s_k : A(s_k, l_m) = 1 \wedge B(s_k, h) = 1) \tag{3}$$

It is therefore possible to define the set S^* as the subset of S of stops belonging to at least one line of the set L_h.

$$S^* = \left\{ s_g \in S | \exists l_m : A\left(s_g, l_m\right) = 1, l_m \in L_h \right\} \tag{4}$$

The s_g stops are the set of stops that, belonging to a l_h line that makes a stop near the hospital, are eligible for accessibility to the facilities. Assuming a threshold Δ of maximum pedestrian distance for access to the public transport stops, we can evaluate the isodistance i_{Δ, s_g}, sg, the set of points distant Δ from the generic s_g, and the isodistance i_Δ as the overall isodistance.

Therefore, for each z_n, it is possible to describe an area $A_{n,\,\Delta}$, as the portion of the area A_n of the zone z_n contained within the isochrone i_Δ. Assuming the population is uniformly distributed across the surface of each zone z_n, it is possible to evaluate both the percentage of population and the total population living at a distance of Δ, or minor, in each zone z_n.

$$\%POP = A_{n,\Delta}/A_n = P_{n,\Delta}/P_n \tag{5}$$

$$P_{n,\Delta} = \%POP * P_n \tag{6}$$

3.2 Dataset

The study presented can be divided into two steps: data acquisition and data analysis. The first step concerns obtaining the data required for analysis. As previously defined, the data essentially concerns three different aspects of the transportation system:

- The demand system, expressed by the population living in the zones into which the study area is divided. The most common discretization, and generally available in open access format, is that of census zones, although the update time varies depending on national specificities. The extension of census zones allows working with the smallest aggregation available in a given country and having the most detailed information possible on population and age variables. An example is the Italian statistical agency Istat, which provides census parcels and sociodemographic variables in GIS format.
- The supply system, expressed by the lines and timetables of the operator managing public transport in the study area. The lines and timetables are always public. Open platforms such OpenStreetMap provide service routes and stop distribution in vector format.
- The activity system, expressed by the distribution of healthcare activities across the territory. The activities considered are easily reconstructed, even with the support of open platforms like OpenStreetMap, which specifically identify healthcare activity categories such as hospitals and clinics.

The general scheme is shown in Fig. 1.

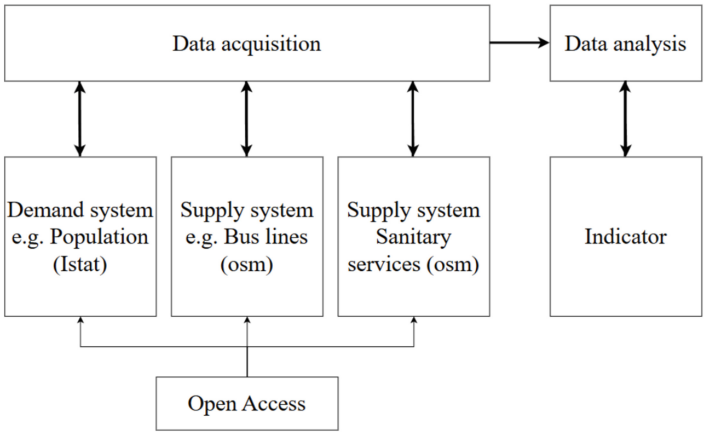

Fig. 1. General scheme of methodology.

4 Case Study

4.1 Case Study Description

The investigated area in this paper is the municipality of Enna, in Sicily, Southern Italy. It is a municipality of approximately 25,000 inhabitants located in the central part of the island (Fig. 2) [27].

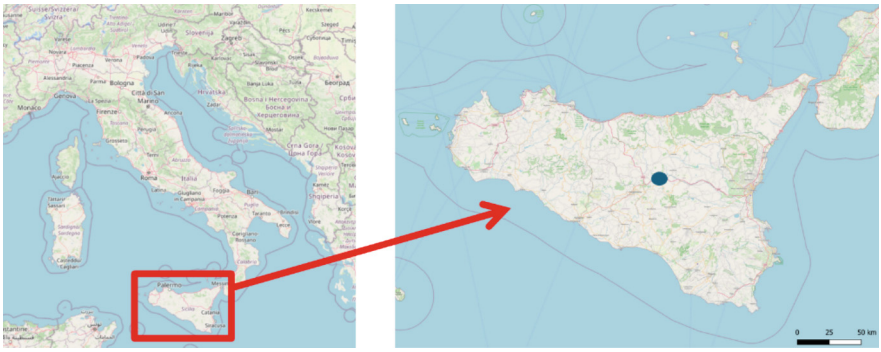

Fig. 2. Location of the study area in Italy. Source: [28].

There are three main areas where most of the population resides in the municipality of Enna: the main historic centre, the new part of the city, and a hamlet. The main town lies on a plateau approximately 900 m above sea level. The new part of the city, called "Enna Bassa," is located south of the mountain that hosts the historic centre; the new part hosts some more recently introduced services, such as the university and the hospital. To avoid confusion over names, and to reflect the different geographical location, the historic part of the city is often referred to as "Enna Alta". This area of the municipality is particularly affected by student mobility, due to the presence of the University. The municipality also includes a hamlet, Pergusa. It is located 10 km south of the main centre and has a tourism and hospitality-based economy due to the presence of a nature reserve. The remaining part of the municipality is predominantly agricultural, with large areas of extremely low population density. Figure 3 shows the study area, with the three main areas highlighted.

4.2 Results

To identify the areas, we refer to the division into census parcels established by Istat, the Italian national statistical agency. By referring to census parcels, it is possible to represent the population distribution in the most disaggregated manner publicly available. The georeferenced data on administrative borders and population are open access [29]. The population distribution on a municipal scale is shown in Fig. 4.

Figure 4 shows the highly uneven distribution of the population across the territory, with large agricultural areas and low population densities. Figure 5 focuses on the population distribution in the Enna Alta and Enna Bassa areas.

Further focus is placed on the hamlet of Pergusa. The population distribution in this area is shown in Fig. 6.

The city hospital is located in the south-eastern part of the city (Enna Bassa).

The local public transport service in Enna is managed by SAIS autolinee, through 8 lines that cover the territory of Enna Alta, Enna Bassa and Pergusa [30]. Lo schema generale delle linee è riportato in Table 1.

The eight lines cover the most densely populated areas. Line 1 connects the western and eastern sides of Enna Alta, where most of the resident population is concentrated.

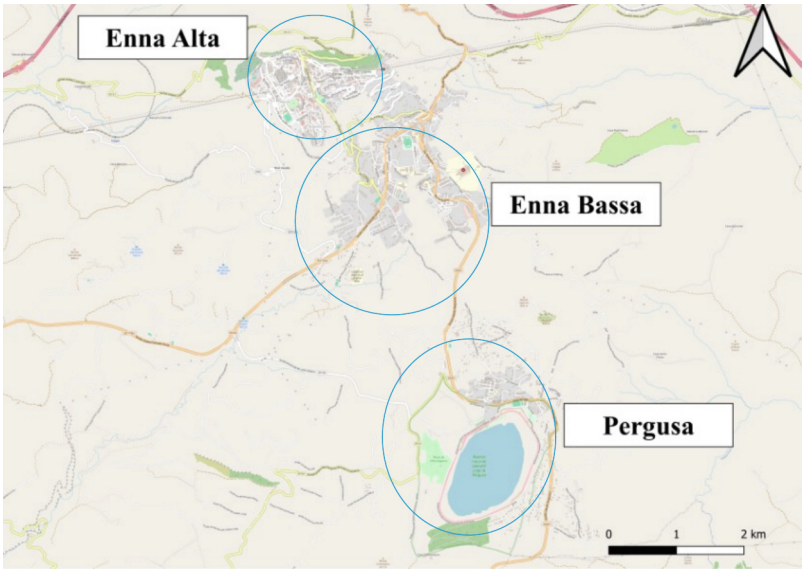

Fig. 3. Location of the three main inhabited areas. Source: [28]

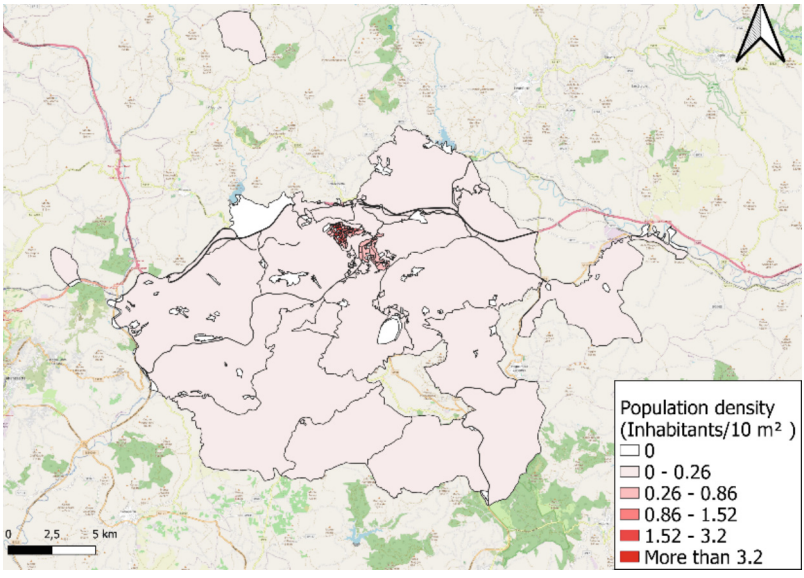

Fig. 4. Population distribution in the municipality of Enna. Source: [29]

Lines 2 and 3 connect the eastern and western sections of the old city, respectively, with the new area. Line 4 connects a large parking lot at the entrance to the old city to the city centre and serves to relieve congestion in the main residential area. Lines 5 and 6 connect the areas of Enna Alta and Enna Bassa with the southern hamlet of Pergusa.

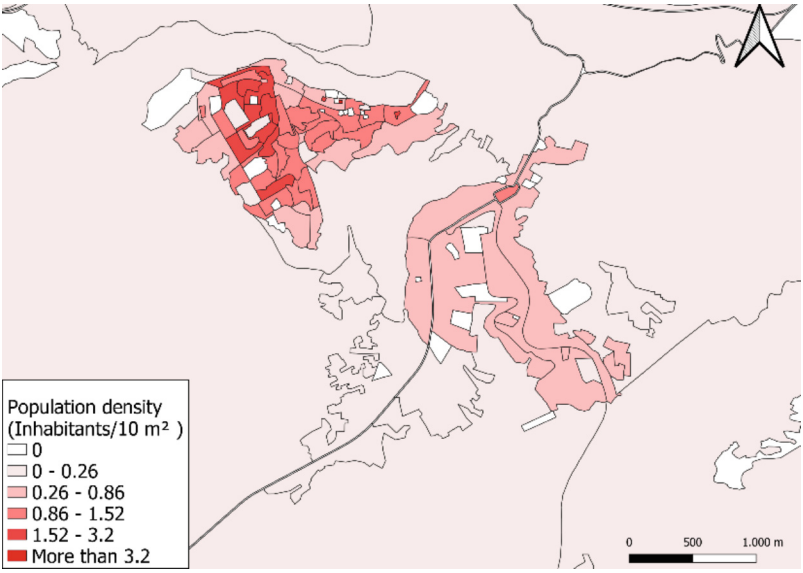

Fig. 5. Population distribution in the areas of Enna Alta and Enna Bassa. Source: [29]

Fig. 6. Population distribution in the area of Pergusa. Source: [29]

Lines 7 and 8 connect the historic centre with some school and university areas of Enna Bassa.

Table 1. Main characteristics of the lines

Line	Name
1	Spirito Santo – Valverde
2	Valverde – Ospedale
3	Spirito Santo – Università
4	Pisciotto – Piazza Garibaldi
5	T.bus Enna Alta – Pergusa
6	T.bus Enna Alta – Pergusa via Toscana
7	Piazza Europa – Enna Bassa
8	T. bus Enna Alta – Scuola Media Savarese

Of the 8 lines, 4 have a stop near the hospital: lines 2, 3, 5, 6. As an example, Fig. 7 shows the route of line 2 with respect to the towns of Enna Alta and Enna Bassa and the location of the hospital.

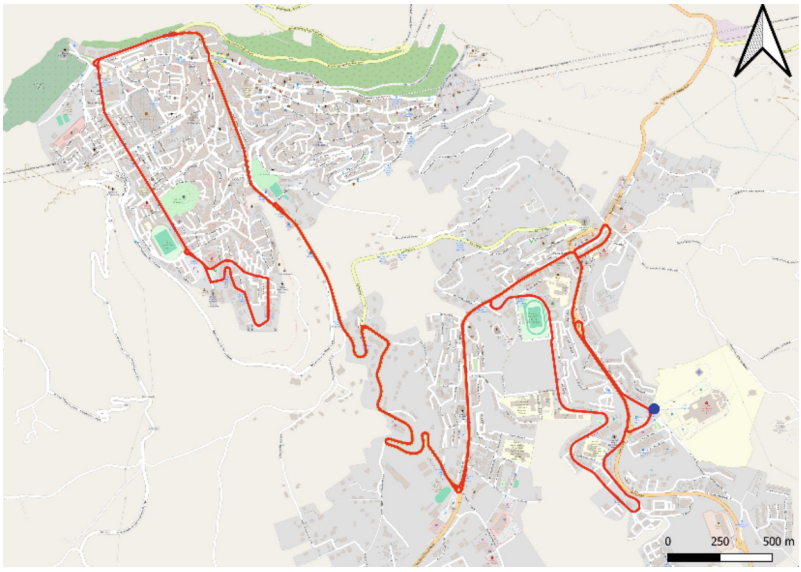

Fig. 7. Representation of the path of line 2 (red) and the positioning of the hospital (blue). Source: [28]

To study accessibility, an isodistance curve of $\Delta = 200$ m is considered. An isodistance of 200 m represents a short pedestrian distance, which can be covered in approximately 2–3 min, making it accessible to most users. This threshold reduces the effort and time required to reach a public transport stop. It also favors the use of public transport over private cars. In compact urban contexts, 200 m ensures good coverage of the area

with easily accessible stops. An isodistance of 200 m allows us to hypothesize coverage within the five-minute pedestrian period even for the older sections of the population, considering an average speed of 0.8 m/s [31]. Figure 8 shows the overall isochrone for the areas of Enna Alta, Bassa and Pergusa.

Fig. 8. 200 m Isodistance for the areas of Enna Alta and Enna Bassa (left) and Pergusa (right) [28]

The representation of the *%POP* for the census zones z_n identified in the study is shown in Fig. 9.

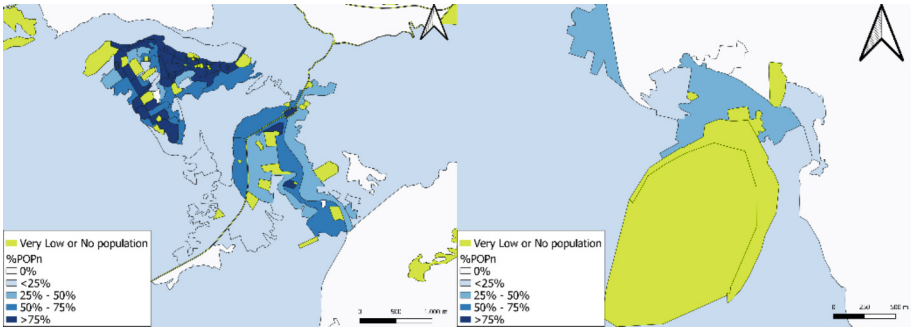

Fig. 9. POP% for Enna and Enna Bassa (left) and Pergusa (right). Source: [28]

Figure 9 highlights clear spatial patterns in accessibility, with higher coverage concentrated in the central and more densely populated areas, particularly in Enna Alta, while peripheral and low-density zones exhibit significantly lower values. The presence of public transport lines strongly influences the spatial distribution of accessibility, generating clusters of well-served areas around main corridors and leaving more fragmented coverage in recently developed or rural zones.

5 Discussion and Conclusion

The results show the distribution of the population covered by the 200 m walking distance from the transport supply system for accessing the hospital. The study area exhibits significant territorial differences, mainly related to the rural nature of the territory under consideration. The results in terms of POP% highlight how the lines offer good population coverage in the Enna Alta area, which is served by four lines connecting it to the hospital. Aside from a few zones in the central part of the city, Enna Alta have almost uniform coverage above 50%, exceeding 75% in some zones directly hosting one or more stops. In these zones, population coverage for hospital access can be improved not by the introduction of new services but by improving connections in uncovered areas. The potential adoption of potential on-demand services in these areas necessarily requires an assessment of time slot coverage. The adoption of new services must consider primarily temporal integration with existing public transport services that offer good territorial coverage.

The Enna Bassa area offers different results. The area is less densely populated, but there is a difference in coverage between the northern and eastern parts of the city, compared to the western part, particularly the southwest, where coverage remains below 25%. These more recently built residential areas represent the city's expansion area and could see future improvements in connectivity, especially due to the presence of university facilities. The introduction of DRT services, in this case too, must consider integration with pre-existing services.

Pergusa represents a different case compared to the two areas previously described. The main area achieves good coverage (40%) thanks to the two lines that pass along the main road. The resident population is low, while the area, due to the presence of numerous tourism-related activities like natural attractions and the Pergusa racetrack, sees significant seasonal flows. The distance from the main city, approximately 10 km, is relevant, especially for vulnerable population groups. These factors necessitate further demand analysis to evaluate the implementation of on-demand services.

An interesting topic remains the study of accessibility for all areas outside the three urban areas described. These areas, primarily agricultural, are very extensive, and a more disaggregated distribution of residential areas is not available; although sparsely populated, many areas of the municipality of Enna are home to a significant resident population, exceeding 500 people in some areas. The presence of residential buildings in such sparsely populated areas makes these areas potential locations for the presence of DRTs connecting to healthcare facilities in the central part of the city.

This paper presents a spatial approach for analyzing hospital accessibility via local public transportation. The methodology is based on entirely open-source data, is replicable, and scalable across a wide range of contexts. The results provide clear guidance for the implementation of DRT systems as a complementary layer to existing public transport. In areas with relatively high coverage, such as Enna Alta, DRT could be designed to improve first/last-mile connectivity and address residual gaps. In low-coverage areas such as the southwestern part of Enna Bassa and dispersed rural zones, DRT services could play a more structural role by ensuring direct access to healthcare facilities, especially for mobility-constrained users. In these areas, the spatial configuration of demand

suggests the adoption of flexible routing schemes, such as door-to-door services with variable itineraries, capable of adapting to scattered settlement patterns.

This study presents some limitations that should be acknowledged. Population is treated as uniformly distributed within census units derived from Istat data. Also, the adoption of a fixed walking threshold to access public transport does not account for heterogeneity in individual capabilities, trip purposes, or built environment characteristics. In addition, the analysis is based on aggregate indicators and does not explicitly consider service frequency, reliability, or temporal variations in accessibility. Future research could address these limitations by integrating more disaggregated population data, variable walking thresholds, and dynamic transport supply attributes, as well as validating results through user-based demand surveys.

The proposed study is a preliminary assessment, requiring further exploration with demand analyses aimed at identifying users most interested in a DRT service. The assessment conducted considered the resident population as the demand variable; further specifications can consider the percentage of the population by age group or according to criteria based on other socio-demographic variables. The paper highlights how zones with low population density, high land area, and a significant population are those in which more in-depth demand analyses are needed. Extensions of the model could include temporal variations and the frequency of hospital services, allowing for a more dynamic representation of accessibility conditions. Incorporating time-dependent factors, such as opening hours of healthcare facilities or public transport service frequency, would enable an assessment of actual service temporal availability. This approach could support the design of a services spatially and temporally optimized.

The applicability of the proposed methodology extends beyond the case study and can be explored through benchmarking with other territorial contexts in Italy and abroad. The framework can support comparative studies by analysing how gaps in healthcare accessibility vary based on different spatial structures and the extent to which existing public transport networks can be effectively integrated with Demand Responsive Transport services. This perspective is especially relevant in the Italian context, where many territories share structural characteristics similar to the case study, analyzed in this work, including small and dispersed settlements, low-density populations, and predominantly rural or inland configurations. Such conditions are widespread across inland areas, suggesting a high potential for replication of the proposed approach. By applying the same set of indicators to different regions, it is possible to identify recurring patterns and context-specific conditions that influence DRT feasibility, thereby enhancing the transferability of the results and supporting decision-makers in tailoring DRT strategies to diverse geographic and socio-demographic contexts.

The paper is of scientific interest for different categories, in particular for public authorities and territorial and transport planners, as it provides a replicable and scalable methodology for the analysis of accessibility to health facilities through public transport, entirely starting from open data.

Acknowledgments. Research is supported by the MUR (Italian Ministry of University and Research) through SMART3R-FLITS: SMART Transport for Travellers and Freight Logistics Integration Toward Sustainability (Project protocol: 2022J38SR9_03, CUP Code:

J53D23009330008), financed by the PRIN 2022 (Research Projects of National Relevance) programme. We authorise the MUR to reproduce and distribute reprints for Governmental purposes, notwithstanding any copyright notations thereon. Any opinions, findings, and conclusions, or recommendations expressed in this material are those of the authors and do not necessarily reflect the views of the MUR.

Credit Author Statement This paper is the result of the joint work of the authors. In particular, the "Abstract", "Introduction" and "Discussion and conclusion" were jointly written by the authors. AR and TC wrote "State of the art". AR wrote "Methodology" and "Results".

Disclosure of Interests. N.t.d.

References

1. United Nations: Transforming our World: The 2030 Agenda for Sustainable Development (2015). https://sustainabledevelopment.un.org/post2015/transformingourworld/publication. Accessed on 27 Mar 2026
2. United Nations: The sustainable development goals (2017a). https://unstats.un.org/sdgs/files/report/2017/thesustainabledevelopmentgoalsreport2017.pdf. Accessed on 27 Mar 2026
3. United Nations: Global Indicator Framework for the Sustainable Development Goals and Targets of the 2030 Agenda for Sustainable Development (2017b). https://unstats.un.org/sdgs/indicators/Global%20Indicator%20Framework%20after%202020%20review_Eng.pdf. Accessed on 27 Mar 2026
4. Satariano, W.A., Guralnik, J.M., Jackson, R.J., Marottoli, R.A., Phelan, E.A., Prohaska, T.R.: Mobility and aging: new directions for public health action. Am. J. Public Health **102**(8), 1508–1515 (2012)
5. Syed, S.T., Gerber, B.S., Sharp, L.K.: Traveling towards disease: transportation barriers to health care access. J. Community Health **38**(5), 976–993 (2013)
6. Smith, M.L., et al.: Non-emergency medical transportation needs of middle-aged and older adults: a rural-urban comparison in Delaware, USA. Int. J. Environ. Res. Public Health **14**(2), 174 (2017)
7. Du, F., Mao, L., Wang, J.: Determinants of travel mode choice for seeking healthcare: a comparison between elderly and non-elderly patients. J. Transp. Geogr. **92**, 103023 (2021)
8. Saxena, N., Rashidi, T., Rey, D.: Determining the market uptake of demand responsive transport enabled public transport service. Sustainability **12**(12), 4914 (2020)
9. Brake, J., Nelson, J.D., Wright, S.: Demand responsive transport: towards the emergence of a new market segment. J. Transp. Geogr. **12**(4), 323–337 (2004)
10. Campisi, T., Spadaro, C., Russo, A., Tesoriere, G., Torrao, G.: The development of integrated public transport and on demand services (PTs-DRTs) for greater flexibility and complementarity of transport mode choices. In: International Conference on Computational Science and its Applications, pp. 48–64. Springer Nature Switzerland, Cham (2025)
11. Vansteenwegen, P., Melis, L., Aktaş, D., Montenegro, B.D.G., Vieira, F.S., Sörensen, K.: A survey on demand-responsive public bus systems. Transp. Res. Part C: Emerg. Technol. **137**, 103573 (2022)
12. Campisi, T., Cocuzza, E., Ignaccolo, M., Inturri, G., Tesoriere, G., Canale, A.: Detailing DRT users in Europe over the last twenty years: a literature overview. Transp. Res. Procedia **69**, 727–734 (2023)
13. Papanikolaou, A., Basbas, S., Mintsis, G., Taxiltaris, C.: A methodological framework for assessing the success of demand responsive transport (DRT) services. Transp. Res. Procedia. **24**, 393–400 (2017)

14. Davison, L., Enoch, M., Ryley, T., Quddus, M., Wang, C.: Identifying potential market niches for demand responsive transport. Res. Transp. Bus. Manag. **3**, 50–61 (2012)
15. Ryley, T.J., Stanley, P.A., Enoch, M.P., Zanni, A.M., Quddus, M.A.: Investigating the contribution of demand responsive transport to a sustainable local public transport system. Res. Transp. Econ. **48**, 364–372 (2014)
16. Currie, G., Fournier, N.: Why most DRT/micro-transits fail–what the survivors tell us about progress. Res. Transp. Econ. **83**, 100895 (2020)
17. Russo, A., Campisi, T., Spadaro, C., Torrao, G., Tesoriere, G.: A logit approach to study the attractiveness of DRT stops location: the case study of Ragusa, Italy. Future Transp. **5**(4), 156 (2025)
18. Alam, M.S., Tabassum, N.J., Tokey, A.I.: Evaluation of accessibility and equity to hospitals by public transport: evidence from six largest cities of Ohio. BMC Health Serv. Res. **23**(1), 598 (2023)
19. Boisjoly, G., et al.: Measuring accessibility to hospitals by public transport: an assessment of eight Canadian metropolitan regions. J. Transp. Health **18**, 100916 (2020)
20. Bellantuono, L., et al.: Analyzing the accessibility of Rome's healthcare services via public transportation: a complex network approach. Sci. Rep. **15**(1), 22880 (2025)
21. Bruschi, M., Gelli, S.: Mapping public transport accessibility for urban health: a spatial method applied to Milan. Eur. J. Pub. Health **35**(Supplement_4), ckaf161-1348 (2025)
22. Del Conte, D.E., Locascio, A., Amoruso, J., McNamara, M.L.: Modeling multimodal access to primary care in an urban environment. Transp. Res. Interdisciplinary Perspect. **13**, 100550 (2022)
23. Martinazzo, L.: A comparative analysis of public transport accessibility to hospitals in Córdoba (2019–2023): where are we now? Data Policy **5**, e35 (2023)
24. Cascetta, E.: Transportation Systems Engineering: Theory and Methods, **49**. Springer Science & Business Media (2013)
25. Cantarella, G.E., Watling, D., De Luca, S., Di Pace, R.: Dynamics and Stochasticity in Transportation Systems: Tools for Transportation Network Modelling. Elsevier (2019)
26. de Dios Ortúzar, J., & Willumsen, L. G.: Modelling transport. John wiley & sons (2024)
27. ISTAT: Demografia in cifre (2026a). https://demo.istat.it/. Accessed on 20 Mar 2026
28. OpenStreetMap contributors: OpenStreetMap [Italy] (2026). https://www.openstreetmap.org. Accessed on 20 Mar 2026
29. Istat: Basi territoriali e variabili censuarie (2026b). https://www.istat.it/notizia/basi-territoriali-e-variabili-censuarie/. Accessed on 20 Mar 2026
30. SAIS Autolinee: Linee Urbane Enna: Autobus SAIS Autolinee in città (2026). https://www.saisautolinee.it/linee-urbane-sicilia/enna. Accessed on 23 Mar 2026
31. Busch, T.D.A., et al.: Factors associated with lower gait speed among the elderly living in a developing country: a cross-sectional population-based study. BMC Geriatr. **15**(1), 35 (2015)

Econometrics and Multidimensional Evaluation in Urban Environment (EMEUE 2026)

Pricing the Tide: The Effect of the Mo.S.E. System on the Venetian Residential Market

Pietro Bonifaci[1](✉), Sergio Copiello[1], and Aurora Peloso[2]

[1] Department of Architecture and Arts, University Iuav of Venice, Santa Croce 191, Venice, Italy
{pietro.bonifaci,sergio.copiello}@iuav.it
[2] Department of Information Engineering, University of Padova, Via Gradenigo 6/b, Padova, Italy
aurora.peloso@phd.unipd.it

Abstract. During the night between November 12 and 13, 2019, Venice was struck by an exceptional high tide, that caused the flooding of 90% of the city. On October 3, 2020, the Mo.S.E. was activated. It is a system of mobile barriers, whose purpose is to reduce the impact of high tides on the city of Venice by isolating the lagoon from the Adriatic Sea whenever a tide exceeding 110 cm is forecasted. The effects of this protection system have been extensively examined with regard to the safeguarding of Venice's historical, architectural, and artistic heritage, as well as to its ecological and environmental implications. However, only a limited number of studies have investigated its impact on real estate values. The present study contributes to this line of research by analyzing the increase in market values for ground-floor and raised-floor properties located in areas of the city most exposed to high-tide flooding following the activation of Mo.S.E. Using a hedonic price model, we analyze a sample of 240 listings published between 2018 and 2024 collected leveraging a public web archiving site. Advertisements published from 2021 onward exhibit a price premium of approximately 5%, while those posted after 2022 show an effect of about 10%. Additional variables related to suitability for tourist-rental use also display strong positive effects. On the one hand, the study provides evidence of the role of Mo.S.E. in increasing housing market values; on the other, it suggests that these effects may be capitalized primarily by the tourist-rental market.

Keywords: Housing Values · Hedonic Price Model · Environmental Protection

1 Introduction and Background Literature

During the night between November 12 and 13, 2019, Venice was struck by an exceptional high tide, the second highest since 1872 (the year when observations began). The tide reached 189 cm above the Mareographic Reference of Punta della Salute (MRPS), causing the flooding of 90% of the city [1].

The extraordinary phenomenon was caused by the combination of several factors during a month — November — already characterized by frequent high tides, to which

© The Author(s), under exclusive license to Springer Nature Switzerland AG 2027
O. Gervasi et al. (Eds.): ICCSA 2026 Workshops, LNCS 16761, pp. 301–315, 2027.
https://doi.org/10.1007/978-3-032-30527-5_20

were added the full moon that intensified the tidal effect, the difference in the atmospheric pressure between Venice and the central Adriatic Sea, and the alternation of Bora and Scirocco winds that pushed the water mass of the lagoon first toward Chioggia and then toward Venice.

High tides, which have always existed in Venice, have progressively worsened in recent years (Fig. 1) due to climate change [2], with consequent negative effects on the built environment of the city, whose pavement level is on average one meter above mean sea level [3]. The debate on safeguarding Venice from the phenomenon of high tides began to take on political significance after the 1966 flood, when the tide reached 194 cm above the MRPS. The issue of protecting Venice was declared to be of "overriding national interest" by the first special law for Venice (Law 171/1973). This marked the beginning of a long process aimed at creating a system to protect the city from exceptional tides, including the presentation of the first feasibility study in 1981, the Mo.S.E. (Experimental Electromechanical Module) tests in 1992, and the approval of the final project in 2002. The system consists of a series of mobile barriers located at the lagoon inlets, whose purpose is to reduce the impact of high tides on the city of Venice by isolating the lagoon from the Adriatic Sea whenever a tide exceeding 110 cm MRPS is expected.

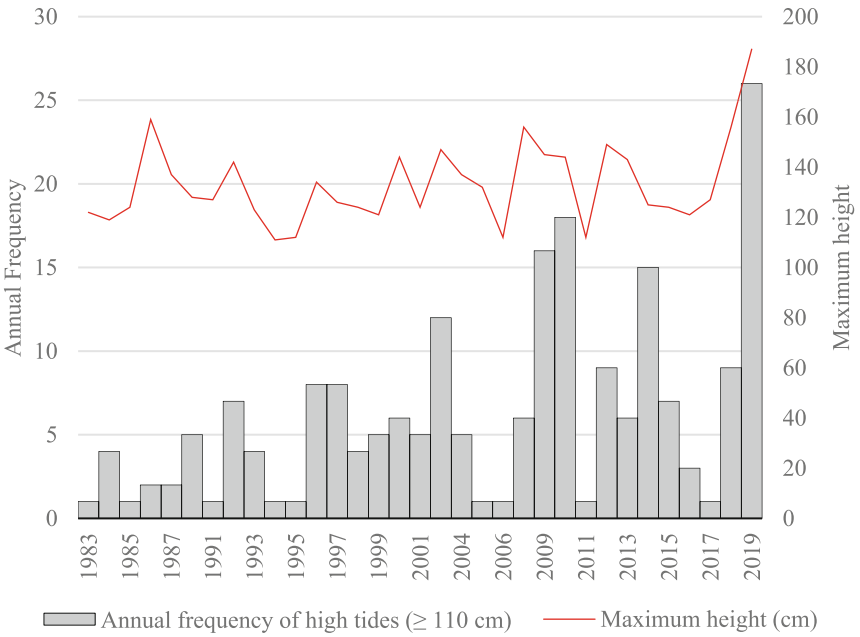

Fig. 1. High tides annual frequency and maximum height (1983–2019)

The laying of the cornerstone took place in May 2003. On October 3, 2020, the Mo.S.E. was activated for the first time. Since then, the barriers have been raised

more than 100 times, preventing damages estimated at over 2.6 billion euros.[1] Mo.S.E. has proven to be an effective system for safeguarding the historical and architectural heritage of Venice, but it has also had broader effects on the city, on residents and tourists, and on the delicate environmental system of the lagoon in which it is embedded. Mo.S.E. has attracted the attention of several scholars and has been studied from different perspectives.

Its effects have been examined with reference to the delicate environmental lagoon balance and the exchange of sediments and water between the lagoon and the Adriatic Sea [4–6], the formation of toxic substances [7], the mussels cultivation [8], the growth and adaptation strategies of algae [9], the microorganisms communities [10], and fish migration [11].

The impact of Mo.S.E. on the city has also been examined in relation to the vulnerability of architectural and cultural heritage, the assessment of restoration interventions [12], with particular focus on the rising damp in masonry buildings [13], the protection of St. Mark square [14], and the use of compensation, conservation and environmental requalification measures for the conservation of the military architectures that characterized the lagoon landscape [15].

Other studies have analyzed the economic consequences of raising the Mo.S.E. barriers on the operations of the Port of Venice, located within the lagoon [16–19], and the city itself [20].

In the scientific literature, however, only a limited number of studies examine the effect of the Mo.S.E. system on the real estate sector. The impact of high tides on hotel room fares is investigated in [21]. Using a regression discontinuity design, the authors find that hotel room prices listed on a well-known booking platform decrease when a tide exceeding 110 cm is forecasted. Although the data refer to the period preceding the activation of Mo.S.E., the study highlights the potential benefits of its operation in terms of reduced losses for the hotel industry.

A study by Rosato et al. [22], uses a GIS-integrated hybrid hedonic multi-attribute model to simulate the impact of Mo.S.E.'s activation on housing values in the historic center of Venice. The authors estimate a potential increase of 8.2% in the market value of ground-floor apartments and 3.8% for those located on upper floors. They also estimate a total increase of €1.4 billion of the city's property values (equal to approximately €320/m^2). Similarly, a research published by the Bank of Italy in November 2022 [23], based on a dataset of nearly 51,000 property listings published between 2016 and 2021, finds a 3% increase in the value of properties located above 110 cm MRPS (thus above the Mo.S.E. activation threshold), and an additional 7% increase for ground-floor apartments.

This study builds on this research strand and aims to estimate the effect of Mo.S.E. on the value of ground-floor residential properties located in the historic center of Venice five years after its first activation, through the application of a hedonic price model. The sample used for the analysis consists of listings posted on one of the main real estate advertising platforms between 2018 and 2025, collected automatically via a web-crawling program using a web-archiving platform.

[1] https://mit.gov.it/comunicazione/news/mit-con-il-centesimo-sollevamento-del-mose-altro-salvataggio-per-venezia

The remainder of the paper is structured as follows: Sect. 2 outlines the methodology, provides an overview of the data collection procedures, and describes the sample and variables employed. Section 3 discusses the empirical results, and Sect. 4 concludes by summarizing the main findings and offering suggestions for future research.

2 Analysis

2.1 The Hedonic Price Model

One of the most widely used and acknowledged methodologies for estimating property values as the sum of the implicit prices of their attributes, the hedonic price model, is based on the seminal work of Rosen [24], and can be expressed using the following equation:

$$y = \alpha + \beta_k X_k + \varepsilon \tag{1}$$

where y is the price of a property, α is the constant, β_k are the coefficients of a set of characteristics X_k (with $k = 1 \ldots l$) and ε is the error term.

In real estate valuation analyses, this model is often transformed into a semi-logarithmic specification. By using the natural logarithm of price as the dependent variable, the coefficients of the independent variables can be interpreted as percentage effects on property price [25]. The log-linear form is used in the present study and is expressed as follows:

$$\ln y = \alpha + \beta_k X_k + \varepsilon \tag{2}$$

As far as the model assumptions are concerned, homoscedasticity and normal distribution of residuals are verified by means of White Test and D'Agostino–Pearson Test respectively, while the absence of correlation among independent variables is tested using the Variance Inflation Factor (VIF).

2.2 Data Collection

To reconstruct historical data on real estate advertisements, the study leverages the public web archiving service known as Internet Archive – Wayback Machine.[2] This digital archive periodically crawls and stores complete HTML versions of publicly accessible web pages, generating time-stamped snapshots that reproduce the structure and content of the website at the moment of the capture. These snapshots are indexed chronologically and can be accessed to retrieve historical versions of a given domain. The procedure used in this study to collect the historical data is summarized in Fig. 2 and developed in the following steps:

1. **Retrieval of Archived Snapshots**. For the target real estate listing platform domain, all available snapshots for the considered year are queried and enumerated. Each snapshot represents the capture of the website at a precise date and time. For every retrieved snapshot, the procedure automatically accesses and downloads all pages reachable within the archived environment on that specific day.

[2] https://web.archive.org/

2. **HTML Parsing and Field Extraction**. The extraction of listing information is performed through structured parsing of the archived HTML documents using the Python library BeautifulSoup,[3] which facilitates the navigation and interpretation of each page's Document Object Model (DOM). Each property listing exhibits a recurring HTML structure that allows the systematic identification and retrieval of the target variables: price, surface area, location, listing description, and floor level. Asking price, surface area, and the description are retrieved by targeting specific HTML tags and class attributes in each advertisement. To determine the floor level, a different approach is followed. When explicitly provided within the structured metadata of the listing, the value is extracted directly through the same DOM-based approach described above. However, in cases where the field is not present in the listing, the extraction method performs a keyword search within the text of the description field to detect mentions of e.g. "piano terra" (ground floor). To mitigate the potential false positives (e.g., cases referencing ground-floor storage spaces rather than the property itself), a binary indicator is introduced. This "floor-source flag" distinguishes between values derived from structured metadata and those inferred from textual analysis. This flag allows manual verification and post-processing corrections where necessary.
3. **Location extraction**. The zone associated with each property is derived from the title of the listing, which follows a consistent syntactic structure. The title is organized as a comma-separated sequence in which the final element corresponds to the municipality ("Venezia"), while the immediately preceding element indicates the specific neighborhood or sub-area. For example: "Quadrilocale buono stato, primo piano, Sant'Elena, Venezia". Here, "Sant'Elena" represents the neighborhood, as it appears directly before "Venezia". The extraction procedure therefore isolates the segment preceding the municipal reference.
4. **Data Structuring and Output**. All the extracted information is consolidated into an output dataset saved in CSV format. Each record contains the following standardized fields: Title, Location, Price, Surface area, Floor level, Description, Floor source flag (structured field vs. inferred).
5. **Filtering and Cleaning**. A final post-processing step is conducted to improve dataset reliability by removing duplicate listings recurring across multiple snapshots and by selecting only those properties confirmed — either explicitly or through textual inference — to be ground or raised-ground floor units, which are required for the subsequent flood risk and housing market analyses.

The data collection process is subject to structural limitations inherent to web-archiving practices. First, the availability of archived snapshots is discontinuous. For the considered year, the Wayback Machine provides captures at an average frequency of approximately one snapshot per week. For this reason, the reconstructed dataset does not represent a continuous daily record of listings, but rather a series of periodic observations.

Second, archival completeness is partial. For each selected snapshot date, not all the pages that compose the real-estate platform were successfully preserved. On average, only 2–3 pages for a given date were retrievable. These two factors jointly constrain the final number of collected advertisements. Nevertheless, the number of listings that

[3] https://www.crummy.com/software/BeautifulSoup/bs4/

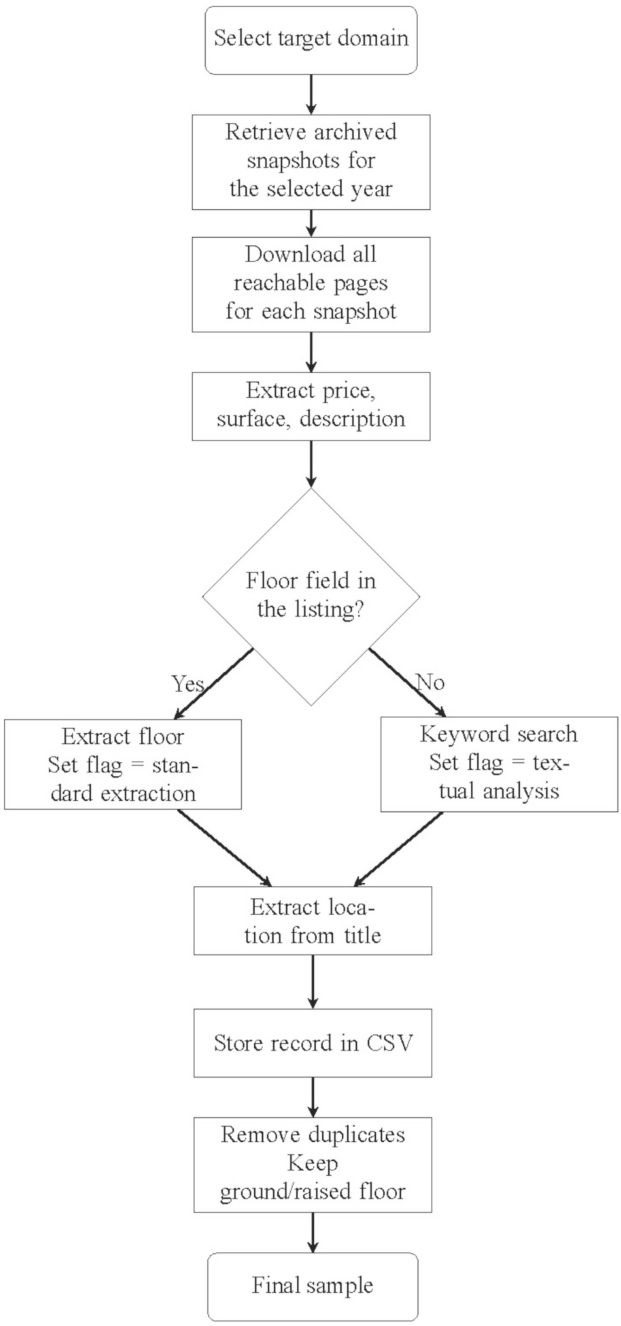

Fig. 2. Data collection workflow

could be collected for each year is comparable to the number of advertisements simultaneously published on the target real estate listing platform for the Municipality of Venice, amounting to approximately 3,000. Indeed, the procedure described above made it possible to gather a total of about 25,000 advertisements for the period 2018–2025 (no archived data were available before 2018). From this dataset, the procedure outlined in point 5 allowed the selection of a first sample of 370 non-duplicate listings referring to properties offered for sale and located on the ground or raised-ground floor levels. Listings located on the raised-ground floor level have been included due to the fact that typical residential buildings in the historic center of Venice do not feature true mezzanine or elevated floors (except for particular building typologies such as noble palaces). Rather, what is commonly referred to as a raised-ground floor level often corresponds to ground-floor units that, over the years, have undergone renovation works aimed at increasing the interior floor elevation. As a result, these units are frequently raised by only two or three steps above the external ground level.

2.3 Sample and Variables Description

Beyond the automatically collected data on property location, asking price, and floor area, a set of additional information was retrieved based on the descriptions provided in the listings. Each property's location was associated with one of the 11 OMI zones into which the historic center of Venice is divided (Fig. 3). OMI zones are defined by the Real Estate Market Monitor of the Italian Revenue Agency (Osservatorio del Mercato Immobiliare, in Italian, from which the acronym) and identify areas characterized by relatively homogeneous economic, social, and environmental conditions, within which property prices tend to be substantially uniform [26].

Asking prices were also standardized to 2018 values in order to remove the temporal component from the regression analysis, and, in particular, the effect generated by the pandemic, assuming that the impact of the Mo.S.E. on ground-floor properties can be isolated from the broader price dynamics affecting the residential sector as a whole. Using the semi-annual property value data provided by OMI, asking prices were adjusted using the average price variation relative to the first half of 2018 for each individual zone, considering properties in normal maintenance conditions. Subsequently, the 2018-homogenised unit price was calculated dividing the adjusted asking price by the floor area.

Information on the maintenance condition of each property was also extracted, distinguishing among "to be refurbished", "average", and "refurbished". For listings that provided no explicit information on maintenance condition, the average level was assumed.

The analysis of listing descriptions further revealed a set of recurrent characteristics that were explicitly coded and related to features that help position properties within the tourist rental market segment. Therefore the following dummy variables have been added to the sample: the presence of furniture; the presence of septic tanks, which — following a 2020 amendment to the municipal building code — are mandatory for Bed and Breakfasts and tourist rentals; and the compliance of the property with urban planning and cadastral regulations, whose absence, while not preventing the sale of the property, does preclude its lawful use within the tourist rental market. An additional

variable was included when the listing indicated that the property for sale was provided with a tourist rental license that is a mandatory permit for renting properties for short-term, leisure stays (in addition to the features mentioned above, starting a tourist rental business requires fulfilling several administrative procedures at both local, regional and national levels).

Fig. 3. The OMI zones of the historical center of Venice. B15 – Cannaregio Sud; B16 – San Polo; B17 – Castello Ovest; B19 – Cannaregio Nord; B20 – Dorsoduro Ovest; B21 – Castello Est; B22 – Sant'Elena; B23 – Dorsoduro Est; B24 – San Marco; B25 – Santa Croce; E5 – Giudecca;

Finally, two dummy variables identify whether a listing was published before or after the activation of the Mo.S.E. system. The first variable takes the value of 1 for all the advertisements published from 2021 onwards. The second reflects the hypothesis that the effects of Mo.S.E. on the property market may not be immediate but may become observable only after at least one year; it therefore takes the value of 1 for listings published since 2022. Table 1 summarizes the variables, their definitions, scales, and units of measurement or coding system.

Table 1. Summary of variables

Variable	Description	Scale of measures	Unit of Measure or Coding System
y	Property unit price adjusted to 2018	Ratio	€/m^2
MoSE_21	Advertisement published since 2021	Dummy	1 = yes
MoSE_22	Advertisement published since 2022	Dummy	1 = yes
Mc	Maintenance conditions	Nominal	-1 = To be refurbished 0 = Average 1 = Refurbished
Sa	Saleable area	Ratio	m^2
F	Forniture	Dummy	1 = yes
Upc	Urban planning compliance	Dummy	1 = yes
St	Septic tanks	Dummy	1 = yes
Trl	Tourist rental license	Dummy	1 = yes
MM	Area of the Real Estate Market Monitor	Nominal	B15, B16, B17 … E5

3 Results and Discussion

A preliminary analysis was carried out using the entire sample of 370 observations. The results were unsatisfactory in terms of statistical significance. The reason may lie in the fact that the listings are distributed across all Venice neighborhoods, which include areas that are more or less exposed to the phenomenon of high tides. It can therefore be assumed that the prices of ground-floor properties located in areas not affected by major tide events did not experience any change due to the activation of Mo.S.E. However, the available data do not allow for sufficiently precise geolocation of individual properties to match them with the city's altimetric profile.

For this reason, the analysis was restricted to a subset of neighborhoods that are more frequently exposed to high tides and are located between the northern side of the lagoon and the Canal Grande (Cannaregio, San Marco, Castello, and Sant'Elena). Figure 4 shows a map identifying the areas at risk of flooding at tide levels of 110 cm or higher, along with the zones included in the reduced analysis. The regression was thus conducted on a reduced sample of 240 observations.

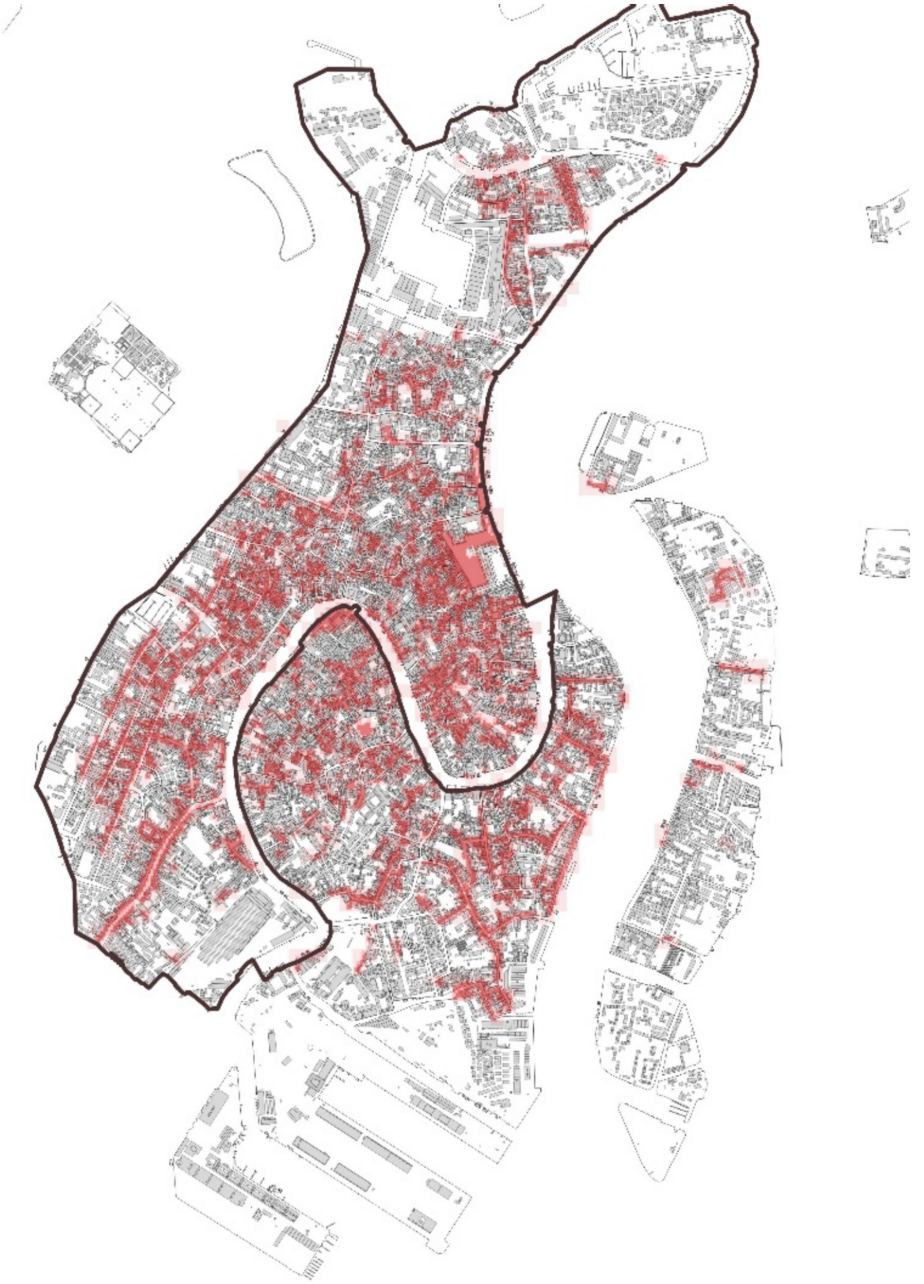

Fig. 4. Zones of the historic center at risk of flooding at tide levels of 110 cm or higher and selected area of analysis

The analysis was then performed using the natural logarithm of the 2018-homogenized unit price as the dependent variable and was carried out by progressively

excluding the independent variables that were found to be not statistically significant. The reduced specifications therefore include seven independent variables. In the first version of the model, the variable MoSE_21 is included among the regressors, whereas in the second version it is replaced by MoSE_22 in order to assess potential delayed effects of the Mo.S.E. activation on the Venetian real estate market.

Table 2. Results for the first model

	coeff	std err	t stat	p-value	vif	Sig.
Const.	9.2005	0.1320	69.7009	0.0000		***
MoSE_21	0.0492	0.0265	1.8560	0.0647	1.0217	*
Mc	0.1794	0.0218	8.2131	0.0000	1.0742	***
Upc	0.2978	0.0494	6.0301	0.0000	1.1631	***
St	0.1055	0.0312	3.3814	0.0008	1.0782	***
B21	−0.1443	0.0315	−4.5853	0.0000	1.0690	***
B17	−0.0991	0.0358	−2.7663	0.0061	1.0723	***
LN_Sa	−0.2860	0.0351	−8.1473	0.0000	1.1700	***
Adj. R^2 0.4862						
Significance level: *** $p < 0.01$; **$p < 0.05$; *$p < 0.1$.						

Table 3. Results for the second model

	coeff	std err	t stat	p-value	vif	Sig.
Const.	9.1678	0.1223	74.9796	0.0000		***
MoSE_22	0.0994	0.0259	3.8334	0.0002	1.0422	***
Mc	0.1772	0.0208	8.5226	0.0000	1.0721	***
Upc	0.2926	0.0482	6.0751	0.0000	1.1640	***
St	0.0901	0.0304	2.9633	0.0034	1.0931	**
B21	−0.1434	0.0307	−4.6645	0.0000	1.0680	***
B17	−0.1037	0.0342	−3.0289	0.0027	1.0738	***
LN_Sa	−0.2800	0.0328	−8.5400	0.0000	1.1740	***
Adj. R^2 0.5100						
Significance level: *** $p < 0.01$; **$p < 0.05$; *$p < 0.1$.						

Standard assumptions of regression are met by both models. The VIFs are always under the threshold of 2.5. In both models, the White Test does not detect heteroskedasticity at the 1% significance level (Model MoSE_2021: LM = 8.10, df = 2, p = 0.017; F = 4.14, df1 = 2, df2 = 237, p = 0.017; Model MoSE_2022: LM = 7,54, df = 2, p = 0,023; F = 3,84, df1 = 2, df2 = 237, p = 0,023). Furthermore, the D'Agostino–Pearson test does not indicate statistically significant departures from normality of residuals

(Model MoSE_2021: DA = 5.05, p = 0.080; Model MoSE_2022: DA = 4.21, p = 0.122).

Both models exhibit an adjusted R^2 of approximately 0.5. In the first specification, the variable MoSE_21 is significant at the 10% level and has a coefficient of 0.0492, whereas in the second specification the variable MoSE_22 is significant at the 1% level and displays a higher coefficient of 0.0994. All other variables in both models are statistically significant at least at the 5% level, and their signs are consistent with expectations (Table 2 and 3).

From an interpretative standpoint, the log-linear specification adopted here allows the coefficients of the independent variables to be read as percentage variations of the dependent variable. Accordingly, the results indicate that the activation of the Mo.S.E. system produced an immediate increase of approximately 5% in the unit values of ground and raised-ground floor properties in Venice, rising to nearly 10% one year after the system first became operational.

With regard to the remaining independent variables — and leaving aside variables whose effects are straightforward and consistent with basic real estate market dynamics — it is worth highlighting the influence on price of the two variables related to urban-planning compliance and the presence of septic tanks. Both have positive and economically meaningful effects on unit price: the presence of septic tanks is associated with an increase of roughly 10%, while full urban-planning compliance yields an estimated price premium of up to 30%.

4 Conclusions and Further Development

In order to assess the effect of the activation of the Mo.S.E. system on property values, using a hedonic price model, the study examined a sample of 240 real estate sale advertisements of housing units located on the ground or raised-ground floor level in selected areas of Venice's historic center that are at risk of flooding, published between 2018 and 2025.The results of the study reveal a positive influence of the Mo.S.E. system on the market value of ground and raised-ground floor housing units in Venice. This effect can be estimated as an increase of approximately 5% in property values starting from 2021, followed by a further rise of about 5% in the subsequent year. These findings are consistent with the estimates proposed by studies conducted both prior to or shortly after the activation of the flood-protection system. The delayed effect is consistent with the hypothesis that the real estate market requires operational and repeated evidence before capitalizing the value of such technological innovations. In other words, the reduction in perceived flood risk appears to have required a period of empirical confirmation before being fully capitalized into property values. Some limitations, however, concern the inability to geolocate the properties and therefore to verify their exact elevation with respect to flood risk, as well as the statistical significance, at the 10% level of the MOSE_21 variable.

It is nevertheless possible that the observed increase in value also incorporates other side effects, such as changes in the requirements for ground-floor units introduced into the municipal building code following the exceptional high tide of 2019. The Building Code of the Municipality of Venice contains a set of provisions specifically regulating ground-floor spaces and the conditions they must meet in order to be considered

suitable for residential use. The regulation stipulates that new constructions must have the ground-floor level set at 1.60 m above MRPS, whereas existing buildings — which constitute the vast majority of the housing stock in the Historic Centre of Venice — may have a ground-floor level as low as 1.00 m provided they are equipped with adequate flood-protection measures In 2019, in response to the extraordinary high tide, additional minimum standards were introduced for ground-floor units (e.g. positioning electrical outlets at least 1.10 m above the floor, installation of a bilge pump and an associated uninterruptible power supply with a minimum autonomy of six hours), which may have partly influenced the property values of ground and raised-ground floor houses after this year.

More broadly, the models highlight the strong positive influence of features such as the presence of septic tanks and full urban-planning compliance — both of which are requirements needed for properties to be used within the tourist-rental market. These aspects raise an important question regarding the true beneficiaries of the implementation of the Mo.S.E. system. While the benefits of Mo.S.E. in terms of safeguarding the city's architectural and artistic heritage are indisputable, the system may simultaneously exacerbate worrying urban dynamics, such as overtourism and depopulation. Indeed, the possibility of exploiting ground-floor spaces — made feasible by the activation of Mo.S.E. — appears to facilitate their conversion into tourist accommodations, thereby contributing to the growth of short-term tourism, a phenomenon associated with urban pressures and social tensions within the historic city.

Future research developments include extending the analysis to the full dataset by incorporating upper-floor properties. This will make it possible to assess whether these units also experienced price effects due, for example, to improved accessibility in areas of the city that were previously prone to rapid flooding. This type of analysis would make it possible to compare the cost of the public investment with the aggregate increase in property values for the city, thereby allowing verification of the results reported in the existing literature and providing useful information for the evaluation of public policies. Such analyses may also offer valuable insights for defining policy implications, particularly with regard to the risk that the entire value uplift could be captured by the short-term rental sector. This scenario would worsen the negative externalities imposed on the city by tourism characterized by very short stays, concentrated in specific periods of the year, which place additional strain on urban management (for example, public transport, waste disposal, and overall residential livability) without generating a commensurate economic return for the city itself.

References

1. ISPRA, CPSM, CNR-ISMAR: Dinamica e Anomalia dell'Evento del 12 Novembre 2019. (2019)
2. Mel, R.A., Viero, D.P., Carniello, L., Defina, A., D'Alpaos, L.: The first operations of Mo.S.E. System to prevent the flooding of Venice: insights on the hydrodynamics of a regulated lagoon. Estuar. Coast. Shelf Sci. **261** (2021). https://doi.org/10.1016/j.ecss.2021.107547
3. Mel, R.A., Carniello, L., D'Alpaos, L.: How long the Mo.S.E. Barriers will be effective in protecting all urban settlements within the Venice lagoon? The wind setup constraint. Coast. Eng. **168** (2021). https://doi.org/10.1016/j.coastaleng.2021.103923

4. Leoni, S., et al.: Sediment oxygen demand rate in a flow regulated lagoon (Venice, Italy). Front. Environ. Sci. **10** (2022). https://doi.org/10.3389/fenvs.2022.1000665
5. Scarpa, G.M., Davison, S., Manfè, G., Lorenzetti, G., Zaggia, L., Braga, F.: Suspended sediment dynamics at the inlets of Venice lagoon: unraveling the effects of storm surges and mobile barrier operations. J. Hydrol. (Amst) **651**, 132588 (2025). https://doi.org/10.1016/j.jhydrol.2024.132588
6. Zonta, R., Botter, M., Cassin, D., Bellucci, L.G., Pini, R., Dominik, J.: Sediment texture and metal contamination in the Venice lagoon (Italy): a snapshot before the installation of the MOSE system. Estuar. Coast. Shelf Sci. **205**, 131–151 (2018). https://doi.org/10.1016/j.ecss.2018.03.007
7. Pereira-Garcia, C., et al.: Potential impact of tide-regulation barriers on the formation of methylmercury in the Venice lagoon (Italy). J. Hazard. Mater. **485**, 136747 (2025). https://doi.org/10.1016/j.jhazmat.2024.136747
8. Bordignon, F., et al.: Spatio-temporal variations of growth, chemical composition, and gene expression in Mediterranean mussels (Mytilus galloprovincialis): a two-year study in the Venice lagoon under anthropogenic and climate changing scenarios. Aquaculture **578**, 740111 (2024). https://doi.org/10.1016/j.aquaculture.2023.740111
9. Sfriso, A., et al.: Biomass, production and growth strategies of the eelgrass Zostera marina, a relict cold-loving species: the Venice lagoon as a study case. Front. Mar. Sci. **11** (2024). https://doi.org/10.3389/fmars.2024.1424638
10. Baldassarre, L., et al.: The impact of MOSE (experimental electromechanical module) flood barriers on microphytobenthic Community of the Venice Lagoon. Microorganisms **11**, 936 (2023). https://doi.org/10.3390/microorganisms11040936
11. Cananzi, G., et al.: Environmental DNA metabarcoding reveals spatial and seasonal patterns in the fish community in the Venice lagoon. Front. Mar. Sci. **9** (2022). https://doi.org/10.3389/fmars.2022.1009490
12. Berto, L., et al.: A multidisciplinary approach for the vulnerability assessment of a venetian historic palace: high water phenomena and climate change effects. Buildings **12**, 431 (2022). https://doi.org/10.3390/buildings12040431
13. Falchi, L., Lucéro Gomez, P., Zendri, E.: On the contribution of tidal floods on damp walls of Venice. Int. J. Disaster Risk Reduction **110**, 104609 (2024). https://doi.org/10.1016/j.ijdrr.2024.104609
14. Simonini, P., Ceccato, F.: Geotechnical studies to optimize the protection measures against flooding of St. mark square (Venice, IT). In: Lancellotta, R., Viggiani, C., Flora, A., de Silva, F., Mele, L. (eds.) Geotechnical Engineering for the Preservation of Monuments and Historic Sites III - Proceedings of the 3rd International Issmge TC301 Symposium. CRC Press, London (2022). https://doi.org/10.1201/9781003308867
15. Grigoletto, A.: The recovery of the fortified system of the lagoon of Venice through the use of compensation, conservation and environmental requalification measures of the MOSE system [Il recupero del sistema fortificato della laguna di venezia mediante l'impiego delle misure di compensazione, conservazione e riqualificazione ambientale del sistema mose]. Sustain. Mediterranean Constr., 541–550 (2019)
16. Vergano, L., Umgiesser, G., Nunes, P.A.L.D.: An economic assessment of the impacts of the MOSE barriers on Venice port activities. Transp. Res. D Transp. Environ. **15**, 343–349 (2010). https://doi.org/10.1016/j.trd.2010.04.001
17. Cavallaro, L., Iuppa, C., Foti, E.: Effect of partial use of Venice flood barriers. J. Mar. Sci. Eng. **5**, 58 (2017). https://doi.org/10.3390/jmse5040058
18. Sheeran, P., Pilato, M.: The fall and rise of Venice as a sea port: marine management, sustainability, and the economics of heritage. Qual. Access Success **18**, 416–418 (2017)

19. Umgiesser, G., Matticchio, B.: Simulating the mobile barrier (MOSE) operation in the Venice lagoon, Italy: global sea level rise and its implication for navigation. Ocean Dyn. **56**, 320–332 (2006). https://doi.org/10.1007/s10236-006-0071-4
20. Giupponi, C., et al.: Boon and burden: economic performance and future perspectives of the Venice flood protection system. Reg. Environ. Chang. **24** (2024). https://doi.org/10.1007/s10113-024-02193-9
21. Angelini, F., Figini, P., Leoni, V.: High tide, low price? Flooding alerts and hotel prices in Venice. Tour. Econ. **30**, 876–899 (2024). https://doi.org/10.1177/13548166231174270
22. Rosato, P., Breil, M., Giupponi, C., Berto, R.: Assessing the impact of urban improvement on housing values: a hedonic pricing and multi-attribute analysis model for the historic Centre of Venice. Buildings. **7** (2017). https://doi.org/10.3390/buildings7040112
23. Benetton, M., Emiliozzi, S., Guglielminetti, E., Loberto, M., Mistretta, A.: Do House Prices Reflect Climate Change Adaptation? Evidence from the City on the Water (2022).
24. Rosen, S.: Hedonic prices and implicit markets: product differentiation in pure competition. J. Polit. Econ. **82**, 34–55 (1974)
25. Copiello, S., Donati, E.: Is investing in energy efficiency worth it? Evidence for substantial price premiums but limited profitability in the housing sector. Energ. Buildings **251** (2021). https://doi.org/10.1016/j.enbuild.2021.111371
26. Divisione Servizi Direzione Centrale Servizi Estimativi e Osservatorio Mercato Immobiliare ed: Manuale dell'Osservatorio del Mercato Immobiliare (2025)

When Prices Exceed Expectations: An Empirical Analysis of Overbidding in the Swedish Housing Market

Benedetto Manganelli[1(✉)], Francesco Paolo Del Giudice[1], Pierfrancesco De Paola[2], Francesco Tajani[3], and Beatrice Manganelli[4]

[1] Department of Engineering, University of Basilicata, Ateneo Lucano Avenue 10, 85100 Potenza, Italy
benedetto.manganelli@unibas.it
[2] Department of Industrial Engineering, University of Naples "Federico II", Vincenzo Tecchio Sq. 80, 80125 Naples, Italy
[3] Department of Architecture and Design, Sapienza University of Rome, Via Flaminia 359, 00196 Rome, Italy
[4] Department of Civil, Chemical, Environmental and Materials Engineering, Alma Mater Studiorum, University of Bologna, Via Zamboni 33, 40126 Bologna, Italy

Abstract. This study examines overbidding in the Swedish residential real estate market, defined as the difference between the asking price and the selling price when the latter is higher. The analysis is situated within the broader transition from traditional search-based markets to more auction-like settings, where prices are increasingly shaped by direct competition among buyers. Against this backdrop, the study investigates how property characteristics contribute to the observed price premium.

The empirical analysis focuses on the housing market of Falun, the capital of Dalarna County, over the period 2023–2025. The dataset includes 512 transactions, of which 306 are apartments and 206 are single-family houses. To account for structural differences between these segments, separate multiple linear regression models are estimated using Ordinary Least Squares (OLS).

The results indicate an average overbidding level of around 15%, with higher values for single-family houses (17,2%) than for apartments (13,8%). Property age emerges as a significant negative determinant in both segments. In addition, variables related to functional quality and spatial layout play an important role. Garden size is the most influential factor for single-family houses, whereas location and internal amenities are more relevant in the case of apartments.

The findings confirm that overbidding represents a structural feature of competitive real estate markets and provide empirical evidence on the role of property characteristics in the price formation process.

Keywords: Overbidding · Real estate market · Asking price · Hedonic models

© The Author(s), under exclusive license to Springer Nature Switzerland AG 2027
O. Gervasi et al. (Eds.): ICCSA 2026 Workshops, LNCS 16761, pp. 316–333, 2027.
https://doi.org/10.1007/978-3-032-30527-5_21

1 Introduction

The *asking price* is one of the critical factors in the formation of the final price on the housing market since it performs informational, selective, and strategic purposes. According to the theory of traditional search, the market was usually represented as a *search market* where, along with imperfect information and transaction costs, there were interactions of several participants in the market [1]. In such markets, trades are realized via bilateral negotiations, where the asking price becomes the starting point of negotiations.

This model, however, becomes less efficient in explaining the dynamics of modern real estate markets. There have been instances where the dynamics of such markets have become closer to an auction system, characterized by heightened competition between buyers. This means that real estate markets may be viewed as a blend of both search markets and *auction markets* [2]. In this situation, prices are formed not sequentially but rather simultaneously, where all the buyers change their estimates depending on the information they possess [3].

Therefore, the significance of the asking price is dramatically different. Instead of being a negotiating cap, the asking price may act as an entry price designed to draw attention and generate competition. Asking prices are empirically proven to affect the final outcome of the transactions, particularly in cases where demand exceeds supply [4]. Therefore, it is common for properties to be sold at higher prices than the ones indicated in the asking price [5].

This represents a departure from sequential bargaining to competition between buyers, and this is one reason why asking prices are frequently surpassed [6]. Overbidding, which refers to the situation where transaction prices are higher than asking prices, becomes an integral characteristic of real estate markets.

Research evidence reveals that the incidence of overbidding is especially prevalent in Scandinavia, which tends to conduct transactions like an auction process. In Sweden, for instance, over 80% of transactions tend to exceed the listed prices by about 20% on average [7], and the same trend is also evident in Norway [8]. The results imply that overbidding arises from competitive forces within a structured environment and not mere mispricing's or demand shocks [9].

In theory, there are a variety of economic and behavioral drivers that account for overbidding, such as information flow, changing expectations, *winner's curse* effect, and *auction fever*, among others [10, 11]. Competitive bidding offers yet another channel through which buyers update their valuation of products, thus resulting in higher bids.

Factors affecting overbidding have been identified in the literature; these include property features, bidding conduct, auction procedures, pricing practices, and market environment [7, 12, 13]. Overall, the issue arises due to the interplay of structure, institutions, and behavior.

In light of the above, this study examines oversupply behavior, with a particular focus on how property characteristics contribute to the supply premium. The empirical analysis involves applying OLS regressions to 512 sales cases in Falun, Sweden, for the years 2023–2025, covering 306 apartments and 206 single-family homes. This paper is structured as follows: the literature review is discussed in Sect. 2, the data description is presented in Sect. 3, the research methodology is outlined in Sect. 4, the results and

discussion are covered in Sect. 5, and the conclusions of the study are presented in Sect. 6.

2 Literature Review

Taking into consideration the theoretical background introduced above, overbidding could be interpreted as the result of the transformation of price formation methods, where the traditional method of sequential bargaining will be supplemented or even substituted by competition. In such a situation, overbidding is perceived as a fundamentally competitive process, where the price is formed through the interaction of various elements.

A first strand of the literature emphasizes the role of the sales mechanism, showing that the method through which properties are sold significantly affects both price levels and the gap between asking and selling prices. In particular, auction-based systems are associated with higher prices and stronger competitive dynamics than negotiated transactions. Quan [14] demonstrates that the choice between search and auction markets is endogenous, with higher-valuation buyers self-selecting into auctions, leading to systematically higher prices. Empirical evidence confirms that auction sales can generate premiums of around 30% compared to negotiated transactions.

Similar observations can be found in other empirical studies. According to Stevenson et al. [15], overbidding in auctions is significantly more prevalent than in bargaining situations, where differences are greater than 40% versus insignificant differences in negotiating transactions. Likewise, Lusht [16] demonstrates that auctions lead to a difference between the asking price and selling price equal to 8–9% as a result of competitive bidding.

The significance of information asymmetry is again highlighted by Chow et al. [17], whose findings reveal that auctions based on the principle of openness have better price premiums compared to sealed bid mechanisms with overbidding differences that range from 3–10%. This is explained by the information update phenomenon, which is typical of common value auctions [18].

A second strand of the literature focuses on competitive dynamics and bidder behavior. The number of participants plays a crucial role: empirical evidence shows that an increase in bidders significantly raises final prices and overbidding levels [19]. Similarly, strategic behaviors such as jump bidding intensify competition and contribute to price escalation [20], with empirical evidence showing additional overbidding effects of up to 14% in highly competitive contexts [12]. Time dynamics also matter, as faster bidding processes are associated with higher overbidding due to behavioral effects such as auction fever [8]. The temporary nature of these dynamics is highlighted by Ashenfelter et al. [21], who show that prices may decrease once competitive pressure dissipates.

Another key dimension concerns pricing strategies, particularly the role of the asking price as a strategic tool. In auction-like markets, the asking price influences participation and competition intensity. Hungria-Gunnelin et al. [22] show that overbidding is widespread in Sweden, with approximately 86% of transactions exceeding the asking price. However, the results suggest that excessive underpricing does not necessarily maximize final prices, although it reduces time on market. Behavioral effects also play

a role, Repetto et al. [23] document that psychological pricing strategies (e.g., left-digit bias) increase participation and lead to higher final prices.

The literature also highlights the importance of market conditions, showing that overbidding is strongly pro-cyclical. Haurin et al. [24] demonstrate that the ratio between sale and asking price increases significantly during market booms and declines during downturns, reflecting variations in demand pressure and competition intensity. In expansion phases, even non-auction markets tend to exhibit auction-like dynamics, with faster transactions and higher price premiums.

The institutional aspects also have a role to play in overbidding. Specifically, the difference between binding and non-binding bids can affect how many people participate and their bidding strategies. In non-binding mechanisms, like the Swedish market, the lower commitment issues make people bid aggressively and lead to overbidding, with studies showing that many deals happen at prices above the asking price [7, 25].

Thirdly, the attributes of the property will moderate the relationship. Although the attributes have a direct influence on the price of the property, they also have an indirect effect through competition. This is because very attractive properties attract more bidders, which results in over-bidding.

Generally, overbidding is described as a multifaceted concept emanating from the interplay of the factors mentioned above [26–28]. In this regard, overbidding is not a rare occurrence but is a predictable consequence of the competitive nature of real estate markets. The complexities associated with overbidding necessitate further research to establish the key determinants of overbidding.

3 Data

Empirical research is carried out with regard to the housing real estate market in the city of Falun, the capital of Dalarna County, situated in central Sweden. It could be said that the analyzed setting represents a middle-sized local market characterized by relatively high informational transparency and transactions which rely upon competitive mechanisms caused by the open ascending auction system. The studied area represents itself rather favorable in terms of studying price formation, especially overbidding.

The data set was created based on the data provided by *Hemnet*, which is one of the major Swedish property portals used to post offers and report deals made thereon. The data were collected in a systematic manner by capturing information about the properties which have been sold within the time span from 2023 to 2025.

The final sample size is made up of 512 cases of property transactions, which can be further split into two different market segments, namely 306 apartments (in the residential market), where the structures have several dwellings within each, and 206 single family homes, where there is more autonomy in the structure's functioning, along with more private exterior space. The difference between the two structures arises out of the necessity to account for differences in structure as well as behavior among the segments, which differ from one another not only physically but also in the characteristics of demand and supply.

Market prices for each observation were recorded, taking into account the ask price and the sell price. The percentage difference between the sell price and ask price was

used to generate a new variable called overbidding, and this is the foundation of the empirical analysis that follows.

Moreover, a full range of information concerning the physical, functional, and quality parameters of the properties and their spatial location are available in the data set. Specifically, information concerning such parameters as the size of the property, its interior configuration, additional attributes, and its location in the city are analyzed. Such an information system allows analyzing the problem of overbidding while taking into consideration structural factors that determine the value of real estate. The geographic location of the data sample is demonstrated in Fig. 1.

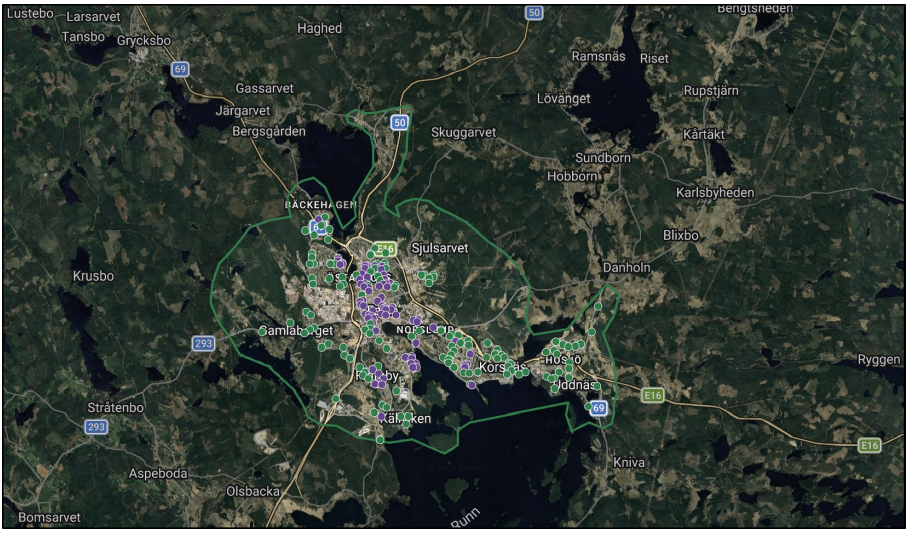

Fig. 1. The georeferenced location of the analyzed sample within the municipality of Falun. Apartment buildings (in purple) are mainly located in the city center, while single-family homes (in green) are widely distributed in the suburban area.

In terms of the distribution of both housing types studied, the maps reveal a distinct difference in their spatial distribution. The apartments are primarily clustered in the urban center where there is higher population density and a larger number of multi-story buildings, reflecting the denser nature of the urban area. The single-family houses, on the other hand, have a wider distribution compared to the apartments and extend beyond the urban center, reflecting the nature of the detached housing type [29].

It is clear that such a spatial pattern is not just an indicator but actually corresponds to the segmented nature of the real estate market in this locality. The fact is that the apartments tend to cluster around a central location while single-family houses are much more spread out. This means that there is more market activity with regard to the former type of property and greater buyer competition while the latter is concerned.

Such results are further proof that it is correct to study the two groups separately because imposing one model of parameters for analyzing buildings characterized by

many differences in physical properties as well as the mechanisms governing their markets seems inappropriate.

4 Methodology

The empirical investigation is carried out using an econometric technique designed to analyze the factors behind the existence of the overbidding problem within the residential real estate market, defined as the difference between the asking price and the selling price. Based on such consideration, overbidding may be seen as something more than just an anomaly; indeed, overbidding can be viewed as a synthesis of the competitive nature of price formation within a setting where information is imperfect and properties are heterogeneous.

The analysis is based on the estimation of multiple linear regression models using the Ordinary Least Squares (OLS) method, widely established in the economic and appraisal literature for identifying relationships between prices and property characteristics. The estimations are implemented using *IBM SPSS Statistics software*. The adoption of this methodology allows for the quantification of the marginal effect of individual explanatory variables on overbidding, holding other covariates constant, and thus enables the isolation of the specific contribution of the different dimensions that define the property.

In particular, the model makes it possible to distinguish between structural, functional, and locational components, providing a disaggregated interpretation of the phenomenon and allowing the observed price premium to be attributed to objective and measurable characteristics. In this sense, the adopted approach is consistent with the framework of hedonic models, in which price – and, in this case, its deviation from the expected level – is a function of the observable attributes of the asset [30].

The empirical strategy is based on the estimation of a baseline model that explains overbidding exclusively as a function of observable property characteristics.

This decision stems from the need to focus the study on easily measurable factors, excluding those related to pricing policies or consumer behavior, which are theoretical aspects and are not taken into account in this research. In this context, the analytical framework will therefore be geared toward examining how the intrinsic and extrinsic characteristics of the property determine competition among consumers [31].

To account for the differences in structure within the residential housing market, the analyses are carried out separately for two types of real estate, apartments and single-family units. While such differentiation is merely indicative, it does imply differences that exist not only in terms of the construction features of housing but also in the mechanisms of its pricing. Single-family units tend to be more heterogeneous in terms of area and quality as well as the importance of accessory factors (such as gardens), while apartments tend to be less diverse in nature. The use of different models, thus, allows for such differences to be captured.

In general, the analytical framework adopted provides a coherent picture of the phenomenon, identifying the role that property characteristics play in determining price premiums and offering a framework for interpreting the competitive dynamics that emerge in real estate markets characterized by negotiation processes and interactions between supply and demand that are not entirely transparent.

4.1 Baseline Model Specification and Definition of Variables

The objective of the empirical analysis is to identify the determinants of overbidding attributable to observable property characteristics. This approach makes it possible to construct a baseline model capable of measuring the marginal contribution of structural, distributive, qualitative, and locational characteristics in explaining the differential between asking price and selling price.

The dependent variable is represented by *overbidding* OB_i, defined as the percentage difference between the selling price and the asking price:

$$OB_i = \frac{SP_i - AP_i}{AP_i} \tag{1}$$

where SP_i denotes the *Selling Price* and AP_i the *Asking Price* of property *i.*

In order to improve the distributional properties of the variable and to mitigate the influence of extreme observations, the following logarithmic transformation is applied:

$$Y_i = \ln \cdot (1 + OB_i) \tag{2}$$

where Y_i represents the dependent variable used in the estimations.

For the *apartment segment*, the relationship between overbidding OB_i and property characteristics is modeled as follows:

$$\begin{aligned} Y_i = \alpha + \beta_1 \ln (IA_i) + \beta_2\, AGE_i + \beta_3\, RM_i + \beta_4\, BTH_i + \beta_5\, FLR_i \\ + \beta_6\, BAL_i + \beta_7\, GAR_i + \beta_8\, ELV_i + \beta_9\, LOC_i + \varepsilon_i. \end{aligned} \tag{3}$$

The variable *INTERNAL AREA* (IA) represents the net internal floor area of the property and is introduced in logarithmic form, in order to capture the possible presence of diminishing marginal effects. This transformation allows for a more realistic modeling of the relationship between property size and the observed price premium.

The variable *AGE* (AGE) is defined as the difference between the year of sale and the year of construction and serves as a proxy for the degree of obsolescence of the property. It is treated as a continuous quantitative variable.

The variables *ROOMS* (RM) and *BATHROOMS* (BTH) represent, respectively, the number of rooms and the number of bathrooms, and are included as discrete quantitative variables, treated in the model as metric covariates. They capture the internal layout configuration and the functional level of the housing unit.

The variable *FLOOR* (FLR) indicates the floor level and is included as a discrete numerical variable. It allows for the identification of potential effects related to the position of the property within the building.

The variables *BALCONY* (BAL), *GARAGE* (GAR), and *ELEVATOR* (ELV) are introduced as dichotomous variables, taking a value of 1 when the feature is present and 0 otherwise. These variables capture the presence of qualitative amenities that may influence the attractiveness of the property and, consequently, the intensity of competition among buyers.

The variable *LOCATION* (LOC) is constructed as an ordinal indicator of the property's position relative to the urban center. Specifically, it is measured on a numerical scale from 1 to 4, which depends on the location of the various geographic areas relative

to the city center. To be more precise, a value of 1 refers to the most central area, a value of 2 indicates the semi-central areas, a value of 3 reflects the peripheral areas, and a value of 4 indicates the outer peripheral areas. Consequently, lower numbers refer to the most central areas, while higher numbers correspond to geographic locations that are progressively farther from the city center.

For the *single-family housing segment*, the model is adjusted to fit the peculiarities of this structure type, which implies the importance of outdoor areas and another distribution of functions. The estimated model looks as follows:

$$Y_i = \alpha + \beta_1 \ln(IA_i) + \beta_2 \ln(GA_i) + \beta_3 AGE_i + \beta_4 RM_i + \beta_5 BTH_i + \beta_6 GAR_i + \beta_7 LOC_i + \varepsilon_i. \quad (4)$$

Alongside the variable INTERNAL AREA (IA), which represents the net internal area of the single-family home, the variable GARDEN AREA (GA) is included, which measures the size of the garden. Both variables are introduced in logarithmic form in order to capture the presence of diminishing marginal returns and to improve the distributional properties of the dimensional variables.

This choice reflects the hypothesis that increases in area influence overbidding in a non-proportional manner, with more significant effects at lower area levels compared to properties already characterized by large areas.

In particular, in the single-family housing segment, garden area represents a relevant component of the overall quality of the property, influencing its attractiveness and, consequently, the intensity of competition among buyers.

The variables *AGE* (AGE), *ROOMS* (RM), *BATHROOMS* (BTH), *GARAGE* (GAR), and *LOCATION* (LOC) retain the same definition and interpretation adopted for apartments.

A summary of the variables included in the model, together with their definitions and treatment, is reported in Table 1.

Table 1. Definition of variables and model specification.

Variable	Acronym	Description	Unit of measurement	Model treatment	Type	Segment
Overbidding	OB	Relative difference between selling price and asking price	%	ln(1 + OB)	Dependent	All
Internal Area	IA	Internal surface floor area	m^2	ln (IA)	Continuous	All
Garden Area	GA	Garden surface area	m^2	ln (GA)	Continuous	Single-family units

(*continued*)

Table 1. (*continued*)

Variable	Acronym	Description	Unit of measurement	Model treatment	Type	Segment
Age	AGE	Property age	years	Linear	Continuous	All
Rooms	RM	Number of rooms	n.	Linear	Discrete	All
Bathrooms	BTH	Number of bathrooms	n.	Linear	Discrete	All
Floor	FLR	Floor level	n.	Linear	Discrete	Apartments
Balcony	BAL	Presence of balcony	1 = yes; 0 = no	Dummy	Binary	Apartments
Garage	GAR	Presence of garage	1 = yes; 0 = no	Dummy	Binary	All
Elevator	ELV	Presence of elevator	1 = yes; 0 = no	Dummy	Binary	Apartments
Location	LOC	Ordinal distance from city center (higher values = more peripheral locations)	Scale (1–4),	Linear	Ordinal	All

5 Results

The empirical analysis for the *apartment segment* is based on a sample of 306 observations and involves the estimation of a multiple linear regression model in which the dependent variable Y is represented by the overbidding measure *(OB)*. The set of explanatory variables includes dimensional characteristics, functional quality elements, and locational factors, with the aim of capturing in an integrated manner the determinants of the phenomenon.

In terms of goodness of fit, the model exhibits a high explanatory power. The coefficient of determination is equal to $R^2 = 0{,}685$ (with adjusted $R^2 = 0{,}675$), indicating that approximately 68,5% of the variability in overbidding is explained by the independent variables included in the model.

The model is globally significant, as indicated by the value of the *F-test* for the joint significance of the regressors ($F = 71{,}362$; $p \leq 0{,}001$), confirming the overall explanatory capacity of the included variables in capturing the observed phenomenon.

The analysis of the coefficients reveals a well-defined structure of the determinants of overbidding. First, the age of the property *(AGE)* emerges as the variable with the

greatest explanatory weight in relative terms. The standardized coefficient is negative and very significant ($\beta = -0{,}575$; $p \leq 0{,}001$). This shows that older properties relate to lower levels of overbidding. This finding matches the greater uncertainty about building conditions, lower perceived quality, and higher expected maintenance costs, which together decrease competition among buyers. As a result, newer properties are linked to higher levels of overbidding. Lower obsolescence raises competitive pressure among buyers by indicating better building conditions, higher functional efficiency, and lower expected maintenance costs.

A second important factor is the number of bathrooms *(BTH)*, which has a positive and statistically significant effect ($\beta = 0{,}378$; $p \leq 0{,}001$). More bathrooms can be seen as a sign of the housing unit's quality and comfort. These aspects seem to directly affect the willingness to bid above the asking price.

Similarly, the locational variable *(LOC)* has a positive and highly significant impact ($\beta = 0{,}325$; $p \leq 0{,}001$). This confirms the key role of location in the competitive dynamics of the real estate market. Properties in more desirable areas tend to experience higher levels of overbidding. This shows how the spatial aspect increases demand pressure.

On the other hand, the interior area *(IA)* is not statistically significant ($p = 0{,}361$). This is very important from an interpretive standpoint, as it shows that the size of the property - a key factor in calculating its value - does not determine competitiveness among buyers.

The "rooms" variable *(RM)* is of minimal importance ($p = 0{,}083$), while factors such as "floor" *(FLR)*, "balcony" *(BAL)*, "garage" *(GAR)*, and "elevator" *(ELV)* are not statistically significant at all. This reveals a very important theoretical difference between the factors that influence the valuation of the property on the one hand and the competition that determines the property's price on the other. Not all factors that add value to the property can induce competition among buyers.

From an econometric perspective, the collinearity tests do not reveal any issues. The values of the variance inflation factors *(VIF)* are reasonably low, although there is some correlation among the variables, particularly between interior floor area and the number of rooms.

Table 2 presents the results of the regression analysis conducted on the apartment sub-segment. This table shows the estimated coefficients and key statistics for the model.

Table 2. OLS regression results for apartments: determinants of overbidding.

Variable	Coefficient	Std. error	β	T-value	P-value
Constant	0,128	0,019	–	6,866	0,00 1* * *
IA	-0,005	0,005	-0,063	-0,916	0,361
AGE	0,000	0,000	-0,575	−16,195	0,00 1* * *
RM	0,003	0,002	0,125	1,742	0,08 3*
BTH	0,026	0,003	0,378	9,548	0,00 1* * *
FLR	−0,001	0,001	−0,037	−1,017	0,310
BAL	0,000	0,002	−0,005	−0,139	0,890

(*continued*)

Table 2. (*continued*)

Variable	Coefficient	Std. error	β	T-value	P-value
GAR	−0,001	0,002	−0,017	−0,496	0,620
ELV	0,000	0,002	0,008	0,203	0,839
LOC	0,007	0,001	0,325	9,181	0,00 1* * *

The distribution of the standardized residuals is generally consistent with the assumption of normality, as shown by the histogram in Fig. 2, which exhibits no systematic biases or asymmetries that would compromise the validity of the inferences drawn from the model estimation process.

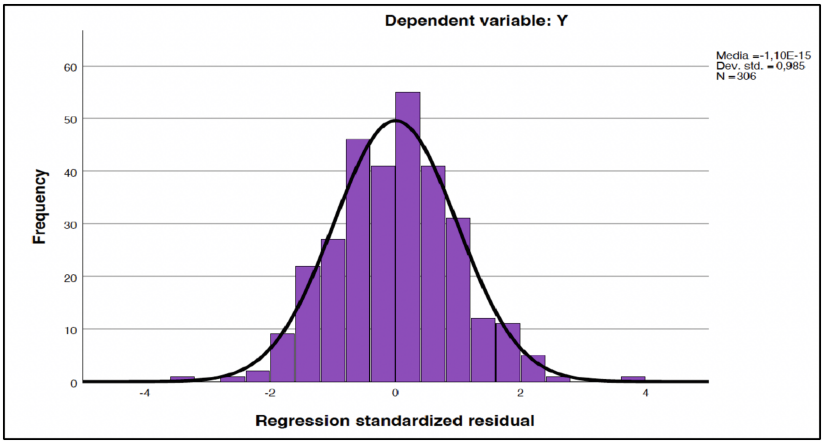

Fig. 2. Distribution of standardized residuals: histogram of the apartment regression model.

Subsequently, the normal probability plot of the standardized residuals shows a high degree of alignment between the empirical and theoretical distributions, confirming the overall compatibility of the residuals with the normality assumption. Graphically, this result is reflected in the arrangement of the observed points along the reference line: the closer the points lie to this line, the greater the consistency between the empirical distribution of the residuals and the theoretical one. Figure 3 provides visual evidence of the adequacy of the distributional fit and reinforces the reliability of the inferences based on the model.

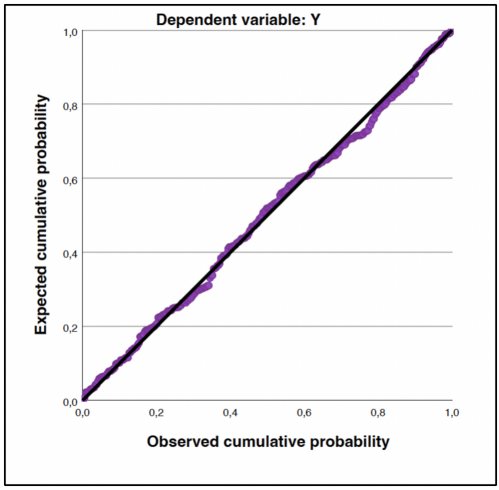

Fig. 3. Normal probability plot of standardized residuals, illustrating the agreement between empirical and theoretical distributions.

Similarly, the scatter plot of standardized residuals against predicted values does not reveal systematic patterns or signs of heteroskedasticity, indicating a substantially constant error variance. The random distribution of points around zero confirms the absence of residual structure in the data, as illustrated in Fig. 4.

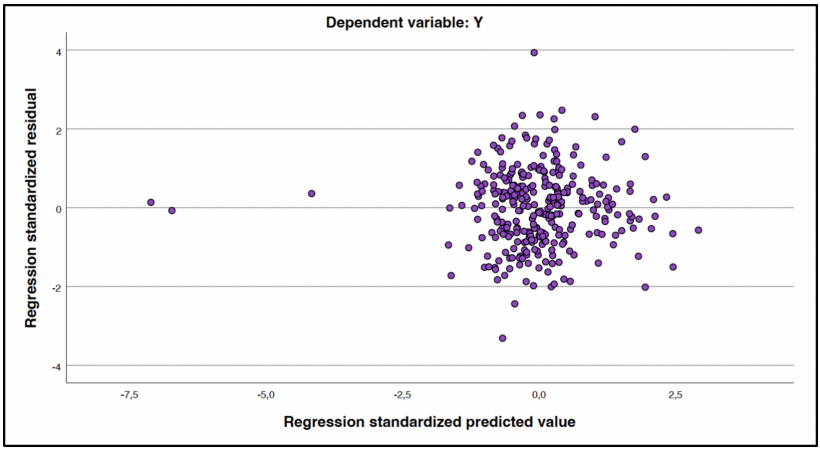

Fig. 4. Residuals versus fitted values plot (standardized), used to assess homoscedasticity and model specification

With regard to the empirical analysis conducted on the *single-family housing segment*, the model also exhibits a high explanatory power.

The coefficient of determination, R^2, is 0,711, and the adjusted value, Adjusted R^2, is 0,700. This means that the independent variables in the model explain about 70%

of the variation in overbidding. This result indicates a good quality of fit and a model performance that is slightly better than what was seen for the apartment segment.

The F-test value ($F = 69{,}445$; $p \leq 0{,}001$) shows that the model is important overall. This shows that the regressors work together to explain the overbidding phenomenon. This outcome enables the dismissal of the null hypothesis of overall insignificance and reinforces the robustness of the employed specification.

The examination of the coefficients uncovers a clearly delineated structure of the determinants of overbidding, which, in certain aspects, differs from that identified in the apartment segment.

The age of the property *(AGE)* is established as a primary explanatory variable, evidenced by a negative and highly significant standardized coefficient ($\beta = -0{,}602$; $p \leq 0{,}001$). This means that older properties are less likely to be overbid on, and on the other hand, that lower obsolescence tends to make competition among buyers stronger because it means better building conditions, higher functional efficiency, and lower expected maintenance costs.

In addition to this effect, the garden area *(GA)* variable stands out as the one that explains the most in relative terms ($\beta = 0{,}688$; $p \leq 0{,}001$). The positive sign and high significance show that adding more outdoor space is a big reason why people are bidding more, which shows that people really want better environmental quality, private outdoor spaces, and more exclusive housing conditions.

In contrast, the internal area *(IA)* exhibits a negative and statistically significant coefficient ($\beta = -0{,}132$; $p = 0{,}024$). This result indicates that, within the single-family housing market, an increase in internal size correlates with a diminished disparity between final price and asking price, presumably attributable to enhanced valuation transparency and reduced uncertainty in the establishment of price expectations for larger properties. To put it another way, when the internal area gets bigger, the chances for competitive bidding dynamics go down because those kinds of properties have less variability in their valuations and more predictability in their expected value.

Among the distributive variables, the number of rooms *(RM)* shows a positive and significant effect ($\beta = 0{,}242$; $p \leq 0{,}001$), indicating that a more articulated internal layout contributes to increasing the intensity of overbidding. The opposite signs of *IA* and *RM* reflect the distinction between size and spatial configuration. While a larger internal area tends to reduce overbidding, a more articulated spatial distribution increases its intensity, suggesting that, in the single-family segment, layout quality is more relevant than size per se in shaping competitive dynamics.

Similarly, the number of bathrooms *(BTH)* shows a positive and significant impact ($\beta = 0{,}128$; $p = 0{,}008$), although with lower intensity, confirming the role of functional amenities in supporting the competitiveness of bids.

Unlike what is observed for apartments, the variables related to the presence of a garage *(GAR)* and location *(LOC)* are not statistically significant. This result indicates that, in the single-family housing segment, these characteristics do not significantly affect overbidding dynamics. This may be explained by the fact that such features tend to represent widely available amenities already implicitly incorporated into the overall quality level of the property, making them less effective in generating competitive differentiation among units.

The results of the regression model estimation for the single-family housing segment are reported in Table 3, which summarizes the estimated coefficients and the main model statistics.

Table 3. OLS regression results for single-family units: determinants of overbidding.

Variable	Coefficient	Std. error	β	T-value	P-value
Constant	-0,040	0,036	-	-1,112	0,268
IA	-0,019	0,008	-0,132	-2,270	0,02 4**
GA	0,046	0,003	0,688	13,805	0,00 1* * *
AGE	-0,001	0,000	-0,602	-14,645	0,00 1* * *
RM	0,009	0,002	0,242	5,114	0,00 1* * *
BTH	0,011	0,004	0,128	2,694	0,00 8* * *
GAR	0,003	0,005	0,027	0,581	0,562
LOC	-0,001	0,002	-0,020	-0,491	0,624

Consistent with the previous discussion, the distribution of standardized residuals appears approximately normal, as evidenced by the histogram shown in Fig. 5.

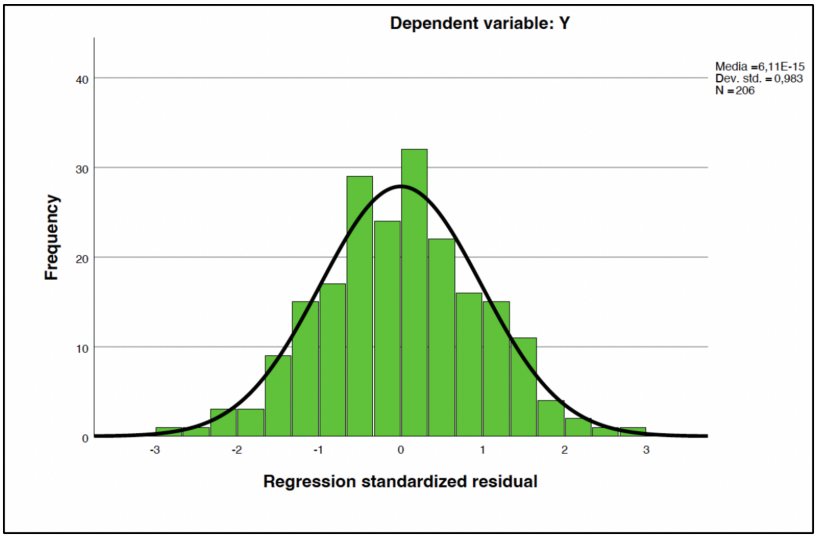

Fig. 5. Distribution of standardized residuals: histogram of standardized residuals from the regression model for single-family units.

Regarding the normal probability plot of standardized residuals shown in Fig. 6, a high degree of alignment between the empirical and theoretical distributions is observed. Graphically, this is reflected in the arrangement of points along the reference line, where

their proximity to the diagonal indicates a good approximation to the normal distribution and confirms the overall compatibility of the residuals with this assumption.

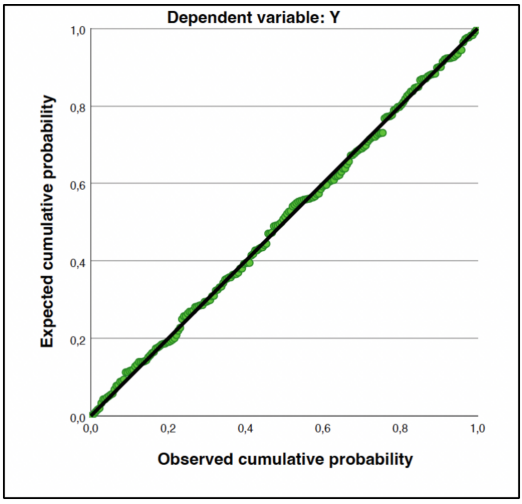

Fig. 6. Normal probability plot of standardized residuals, illustrating the agreement between empirical and theoretical distributions.

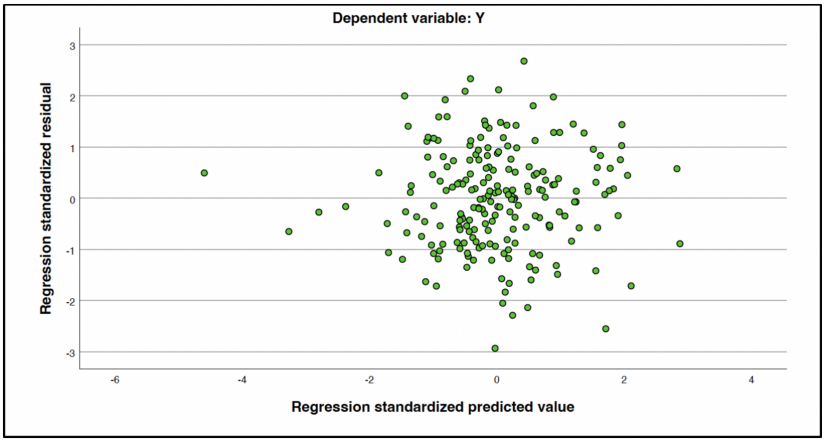

Fig. 7. Scatter plot of standardized residuals versus standardized predicted values, showing no evidence of systematic patterns or heteroskedasticity.

Similarly, the scatter plot of standardized residuals against predicted values (see Figure 7) does not reveal systematic patterns or signs of heteroskedasticity. The random distribution of points around zero suggests a substantially constant error variance across

the entire range of estimated values and the absence of residual relationships not captured by the model.

6 Conclusions

The present study has analyzed the phenomenon of overbidding in the residential real estate market of the city of Falun over the period 2023–2025, with the aim of identifying the role of property characteristics in determining the gap between asking price and selling price. The analysis was conducted through an econometric approach based on the estimation of multiple linear regression models (OLS), applied separately to the two main market segments − apartments and single-family units − in order to capture the structural and competitive specificities of each typology. The empirical results highlight a high explanatory power of the estimated models. In particular, the model for apartments shows a coefficient of determination equal to $R^2 = 0{,}685$, while for single-family units an even higher value is observed, equal to $R^2 = 0{,}711$.

These results show that a large part of the variation in overbidding can be explained by property characteristics that can be seen, which supports the strength of the chosen methodological framework.

In Falun, the average overbidding rate during the time period studied was 15%. This means that, on average, the selling price is 15% higher than the asking price. The phenomenon, on the other hand, shows different levels of intensity in the two groups: about 13,8% for apartments and 17,2% for single-family homes. This difference shows that the competitive dynamics are stronger in the single-family segment. This is because the real estate product is less standardized and the characteristics are more varied, which makes it harder to find a common equilibrium price. This gives buyers more room to bid competitively.

Looking at the factors that lead to overbidding can help explain why these differences exist. In the apartment market, the price premium is affected by a fairly wide range of characteristics that are more "standardized", such as the age of the property, its location, and its functional features (especially the number of bathrooms and the layout of the rooms). In this case, overbidding seems to happen because buyers are competing for properties based on features that are easy to compare with other properties. Buyers tend to compete more for newer, better-located units with better functional characteristics, which makes things less uncertain and easier to use.

In the case of single-family units, the phenomenon takes on a more selective shape, focusing on certain high-quality features. In particular, the garden area is the main reason why people bid more than they should. This shows how having outdoor space is a very appealing and hard-to-replicate feature that can lead to more competition.

This is accompanied by the role of property age which, as observed for apartments, negatively affects overbidding, indicating a greater propensity of buyers to compete for newer properties characterized by better building conditions and lower expected maintenance costs.

Overall, while in the apartment market the price premium results from the combination of multiple relatively standardized attributes, in the single-family segment it appears to be driven by specific high-quality characteristics and elements of uniqueness. This

helps explain the higher levels of overbidding observed in the latter segment and confirms the central role of product differentiation in shaping the intensity of competitive dynamics. The results therefore confirm the high level of competitiveness of the Swedish real estate market, in which the gap between asking price and selling price represents a structural component of the transaction process. The observed levels of overbidding, together with the significance of the explanatory variables, point to a context characterized by active demand and substantial competition among buyers, in line with the findings of the literature on Nordic housing markets.

Despite the robustness of the results, the study suggests possible directions for future research. The incorporation of variables associated with pricing strategies and demand-side behavior may facilitate the investigation of further dimensions of the over-bidding phenomenon. Additional extensions may encompass the examination of its temporal development and the application of the model to alternative territorial contexts, aimed at evaluating its robustness and generalizability.

Acknowledgments. The authors have no competing interests to declare that are relevant to the content of this article.

References

1. Ku, G., Malhotra, D., Murnighan, J.K.: Towards a competitive arousal model of decision-making: a study of auction fever in live and internet auctions. Organ. Behav. Hum. Decis. Process. **96**(2), 89–103 (2005)
2. Ettinger, D., Michelucci, F.: Hiding information in open auctions with jump bids. Econ. J. **126**(594), 1484–1502 (2016)
3. Easley, R.F., Tenorio, R.: Jump bidding strategies in internet auctions. Manag. Sci. **50**(10), 1407–1419 (2004)
4. Han, L., Strange, W.C.: Bidding wars for houses. Real Estate Econ. **42**(1), 1–32 (2014)
5. Björklund, K., Dadzie, J.A., Wilhelmsson, M.: Offer price, transaction price and time-on market. Prop. Manag. **24**(4), 415–426 (2006)
6. Kim, A., T.: Bidding in real estate: a game theoretic approach. J. Real Estate Financ. Econ. **2**(4), 239–251 (1989)
7. Hungria-Gunnelin, R.: An analysis of auction strategies in apartment sales. J. Eur. Real Estate Res. **11**(2), 202–223 (2018)
8. Dalland, S., Hammervold, R., Karlsen, H.T., Oust, A., Sønstebø, O.J.: Aggressive bidding strategies in real estate auctions – a structural equation modelling (SEM) approach. J. Eur. Real Estate Res. **14**(2), 229–245 (2021)
9. Ong, S.E.: Price discovery in real estate auctions: the story of unsuccessful attempts. J. Real Estate Res. **28**(1), 39–59 (2006)
10. Tse, M.K.S., Pretorius, F.I., Chau, K.W.: Market sentiments, winner's curse and bidding outcome in land auctions. J. Real Estate Financ. Econ. **42**(3), 247–274 (2011)
11. Chen, Y.F.: Auction fever: exploring informational social influences on bidder choices. Cyberpsychol. Behav. Soc. Netw. **14**(7/8), 411–416 (2011)
12. Khazal, A., Sønstebø, O.J., Olaussen, J.O., Oust, A.: The impact of strategic jump bidding in residential English auctions. J. Prop. Res. **37**(3), 195–218 (2020)
13. McAfee, R.P., McMillan, J.: Auctions and bidding. J. Econ. Lit. **25**(2), 699–738 (1987)

14. Quan, D.C.: Market mechanism choice and real estate disposition: search versus auction. Real Estate Econ. **30**, 365–384 (2002)
15. Stevenson, S., Gurdgiev, C.: A comparison of the appraisal process for auction and private treaty residential sales. J. Hous. Econ. **19**(2), 145–154 (2010)
16. Lusht, K.M.: A comparison of prices brought by English auctions and private negotiations. Real Estate Econ. **24**, 517–530 (1996)
17. Chow, Y.L., Ooi, J.T.L.: First-Price sealed-bid tender versus English open auction: evidence from land auctions. Real Estate Econ. **42**, 253–278 (2014)
18. Milgrom, P.R., Weber, R.J.: A theory of auctions and competitive bidding. Econometrica. **50**, 1089–1122 (1982)
19. Hungria-Gunnelin, R.: Impact of number of bidders on Sale Price of auctioned condominium apartments in Stockholm. Int. Real Estate Rev. Glob. Soc. Sci. Inst. **16**(3), 274–295 (2013)
20. Avery, C.: Strategic jump bidding in English auctions. Rev. Econ. Stud. **65**(2), 185–210 (1998)
21. Ashenfelter, O., Genesove, D.: Testing for Price anomalies in real-estate auctions. Am. Econ. Rev. **82**(2), 501–505 (1992)
22. Hungria-Gunnelin, R., Kopsch, F., Enegren, C.J.: Brokers' list price setting in an auction context. Int. J. Hous. Markets Anal. **14**(3), 481–497 (2021)
23. Repetto, L., Solís, A.: The Price of inattention: evidence from the Swedish housing market. J. Eur. Econ. Assoc. **18**(6), 3261–3304 (2020)
24. Haurin, D., McGreal, S., Adair, A., Brown, L., Webb, J.R.: List price and sales prices of residential properties during booms and busts. J. Hous. Econ. **22**(1), 1–10 (2013)
25. Amidu, A.R., Agboola, A.O.: Empirical evidence of the influences on first-Price bid auction premiums. Int. Real Estate Rev. **12**(2), 157–169 (2009)
26. Trifunovic, D.: Sequential auctions and Price anomalies. Econ. Ann. Fac. Econ. Bus. Univ. Belgrade. **59**(200), 7–42 (2014)
27. Manganelli, B., Del Giudice, F.P., Anelli, D.: Interpretation and measurement of the spread between asking and selling prices in the Italian residential market. Valori Valutazioni. **31**, 5–13 (2022)
28. Manganelli, B., Del Giudice, F.P., Anelli, D.: Analysis of the difference between asking Price and selling Price in the housing market. In: Gervasi, O., Murgante, B., Misra, S., Rocha, A.M.A.C., Garau, C. (eds.) Computational Science and its Applications – ICCSA 2022 Workshops. ICCSA 2022. Lecture Notes in Computer Science, vol. 13378. Springer, Cham (2022)
29. Molaei Qelichi, M., Murgante, B., Yousefi Feshki, M., et al.: Urbanization patterns in Iran visualized through spatial auto-correlation analysis. Spat. Inf. Res. **25**, 627–633 (2017)
30. De Paola, P., Previtera, S., Manganelli, B., Forte, F., Del Giudice, F.P.: Interpreting housing prices with a multidisciplinary approach based on nature-inspired algorithms and quantum computing. Buildings. **13**(7), 1603 (2023)
31. Manganelli, B., Murgante, B., Saganeiti, L.: The social cost of urban sprinkling. Sustainability. **12**(6), 2236 (2020)

The Fair Exchange: Public-Private Agreements for Zoning Variances in Local Town Planning

Sergio Copiello(✉), Alessandra Bacco, Ida Zelbi, and Pietro Bonifaci

Department of Architecture and Arts, University IUAV of Venice, Santa Croce, 191-30135 Venice, Italy
sergio.copiello@iuav.it

Abstract. This study investigates the fairness of public-private agreements for zoning variances within the Italian urban planning framework, which mandates that at least half of the additional property value generated by such agreements be returned to the community through a land value recapture mechanism. The research develops an analytical model grounded in property valuation theory, employing the residual method and discounted cash flow analysis to estimate development values before and after a zoning variance. The case study focuses on an agreement in Padua involving the transfer of development rights between two sites: the so-called Basso Isonzo area and the so-called former Rizzato area. Before the agreement, the combined development value of both sites was approximately €3.5 million. Following the zoning variance, which enabled changes in land use and the inclusion of student housing, the development value rose to €6.7 million, yielding an added value exceeding €3.1 million. According to national regulations, the statutory financial return to the community should amount to approximately €1.6 million; however, the analysis reveals the actual financial benefit secured by the municipality was only 18% of the legally required share, with the deficit offset by the inclusion of non-financial benefits. This discrepancy raises concerns regarding information asymmetries between public and private partners. Another source of concern is the reliance on non-financial benefits to justify the agreement. The findings highlight significant equity issues in land value recapture practices and suggest the need for improved valuation ability within planning authorities to ensure fair public-private exchanges in urban transformation processes.

Keywords: Public-private partnerships · Public-private agreements · Zoning variance · Property valuation · Residual method · Discounted cash flow analysis

1 Introduction and Background Literature

In Italy, since the introduction of Law 1150 in 1942, town planning has been characterized by a top-down approach, where lower-tier local plans are required to follow and strictly conform to the middle-tier provincial plans, which in turn are to follow and strictly conform to the top-tier regional plans [1–4]. Over time, organic, nationwide reform attempts essentially failed [5]. Although the above system remains in place – yet often disregarded, according to some observers [6, 7] – the town planning landscape has

© The Author(s), under exclusive license to Springer Nature Switzerland AG 2027
O. Gervasi et al. (Eds.): ICCSA 2026 Workshops, LNCS 16761, pp. 334–350, 2027.
https://doi.org/10.1007/978-3-032-30527-5_22

undergone remarkable changes over the last quarter-century or so [8]. The top-down approach has been heavily criticized, primarily due to its lack of flexibility, the excessive time required for implementation, and the lack of implementation on many occasions [9]. Since territorial planning is a primary responsibility of regional governments, several of them adopted a second wave of autonomous laws between the late 1990s and early 2000s, reforming part of the legal framework dealing with town planning rules and procedures [10–12]. Among others [13, 14], one of the most significant innovations introduced by the regional laws is the new active role for private entities, such as landowners and real estate investors, which can contribute to shaping the content of urban transformation projects through agreements with local public bodies that are empowered to exercise town planning functions [15].

When the aforementioned agreements entail a zone change request – meaning a zoning variance so that the involved private entity may obtain permission to build a structure different than the original intended use or larger than previously allowed – another recent legal innovation comes into play (Law 164 of 2014 art. 17 cl. 1 and Law 120 of 2020 art. 10 cl. 1, which modify the Presidential Decree 380 of 2001 art. 16 cl. 4). Indeed, introducing a kind of betterment levy or land value recapture mechanism [16, 17], it is now mandatory for the involved public bodies to assess the additional land and property value potentially originating from the zoning variance, and to obtain a payment equal to at least half of that extra value [18, 19]. The sums thus obtained should be used to finance public works, community services, and social housing.

This work aims to assess the allocation between a local public body and a private developer of the added land and property value originating from a specific agreement for a zoning variance, which also involves the transfer of development rights between two areas. The case study we focus on in this work is of significant interest, as it casts doubt on the actual equity and fairness of the agreement, suggesting that the municipality has been able to obtain properties and payments representing only a minority of the additional land and property value when closing the deal. If this is actually the case, further questions arise. Here are the most compelling ones. Is there evidence that the possibly low degree of fairness in the agreement somewhat depends on a regime of high information asymmetry and, ultimately, the impaired ability of the public body to assess the added value of the involved properties? Is the possibly low degree of fairness in the agreement balanced – in part, at least – by other non-monetary or even intangible community benefits, and, if so, how are they accounted for?

Aiming to address the research questions outlined above, the remainder of this paper is organized as follows. Section 2 defines the method within the framework of real estate appraisal and property valuation theory; it also describes the specific model used to assess land and property value appreciation generated by an urban transformation project, as well as its fair apportionment between the private entity promoting the project and the public body empowered to approve it. Section 3 introduces the case study used to test the model, namely an urban transformation project in the city of Padua, Northeastern Italy, which involves changes in the town planning regulations previously in force and the transfer of development rights between a suburban and a semi-downtown area. Section 4 presents the results and discusses them specifically as far as the land and property value appreciation and the fairness of the public-private agreement are concerned. Finally,

Sect. 5 draws the conclusions and paves the way to further development of the research strand focusing on the fair public-private exchange in urban planning.

2 Method and Model

Property valuation is characterized by a hierarchy of approaches, methods, and models [20–23]. The three approaches that shape the top layer of the hierarchy, along with the related economic principles, are as follows. The market approach stems directly from the economic principle of price equilibrium; accordingly, the value of a property – the so-called subject – can be identified by analyzing similar assets – the so-called comparables – that have been traded in the same market, provided their characteristics and prices are known [24, 25]. The cost approach has its roots in the economic principle of substitution; therefore, the value of a property can be identified based on the cost incurred to obtain a new asset of equal utility, thus suitable for replacing the subject, net of the appropriate depreciation [26, 27]. Finally, the income approach hinges on the economic principle of benefit anticipation, whereby the value of a real estate asset can be derived by converting its future cash flows into a current capital value [28]. Each approach is further characterized by a few methods, which form the second layer of the hierarchy. These methods, in turn, are applied through specific appraisal or assessment models, constituting the third layer of the hierarchy.

The research questions we address here encompass issues related to land and site valuation, which is usually carried out under the framework of the above-mentioned income approach [29], using the residual method [20, 30] or development method [31], primarily through applications of the discounted cash flow model [31–33].

The development method is specifically defined as "A method of estimating land value when […] development [is] the highest and best use of the parcel of land being appraised. All direct and indirect costs and entrepreneurial profit are deducted from an estimate of the anticipated gross sales price of the finished lots; the resultant net sales proceeds are then discounted to present value at a market-derived rate over the development and absorption period to indicate the value of the raw land." (p. 354) [34]. In the residual or development method, first, the gross development value or gross sales price of the finished buildings on a site is estimated according to the notion of its highest and best use; then, direct and indirect development costs are deducted.

The discounted cash flow (DCF) model identifies "the value of an asset" based on "the present value of the expected cashflows on the asset, discounted back at a rate that reflects the riskiness of these cashflows" (p. 696) [35]. The origins of the notion of discounting date to the first decades of the nineteenth century, with works on the topic of interest authored by a few economists [36–39]. Early applications in the realm of property valuation can be traced back to the late 1960s and early 1970s [40–44]. Therefore, in the DCF model [45–47], the timing of costs and revenue of a land development project is made explicit, so that the same expenses and inflows are discounted back to the present using an appropriate discount rate [48–50].

Let us denote the gross development value – or the gross sales price of the finished buildings on a site, if you will – as P, and the total direct and indirect costs that a developer is expected to incur as C, where C includes the developer's profit. Both P and

C are forecasts of values that are likely to be seen in the real estate and construction markets in the near future [51]. Let us also define T (with $t = 1..T$) the timespan required for development completion, including the specific time frame for obtaining building permits and drawing detailed designs, as well as the construction and absorption phases. Finally, let us assume that y is a discount rate representative of the developer's risk and expected return, estimated according to the cost of capital notion, and specifically to the expected return on equity. According to the residual method [52] and the DCF model, the land development value V can be identified as follows:

$$V = \sum_{t=1}^{T} (P_t - C_t)/(1 + y)^t \tag{1}$$

Since we are interested in identifying the additional land and property value A potentially originating from the zoning variance, let us denote with V' the land value before and with V'' 'the land value after the public-private agreement for the zoning variance is established, both calculated according to previous Eq. (1); therefore:

$$A = V'' - V' \tag{2}$$

The financial community benefit B stemming from the public-private agreement and the zoning variance, based on the legal framework presented in the introduction, is identified as at least half the value obtained with the previous Eq. (2), thus:

$$B \geq \left(V'' - V'\right)/2 \tag{3}$$

3 Case Study and Data

3.1 Public-Private Agreement Involving the Transfer of Development Rights

The public-private agreement for the regeneration of the so-called former Rizzato site and the enlargement of the so-called Basso Isonzo public park was negotiated in the time span of late 2020 and early 2022 between the municipality of Padua and the landowner of the involved areas, a major company operating in large-scale retail trade in Northeastern Italy, which manages nearly 600 supermarkets. Approved by the municipal council in April 2022, it is now part of the city's general town plan (Fig. 1), with the following specific regulations.

Before the agreement was reached, the two areas were completely independent in their planning regulations. The so-called Basso Isonzo area, located southwest of the historical center of the city, was intended to accommodate 30,020 cubic meters (equal to 10,000 square meters) of residential buildings, as outlined in a detailed plan approved in March 2009 and in effect until April 2025. The area was owned by a charitable institution – a Public Institution of Assistance and Charity, as defined by the Italian legal system – and was sold to the current owner in January 2021 for an undisclosed price.

The so-called former Rizzato area, located north-east of the historical center of the city, was intended to accommodate a business district of about 30,100 cubic meters (approximately between 9,000 and 10,000 square meters), with offices (80% of the

square footage) and commercial areas (the remainder 20% of the square footage) as specific functions. The municipal council approved the site's detailed plan in November 2001, and a building permit was issued in October 2019.

The public-private agreement aims to establish the following zoning variance (Figs. 2 and 3). The former Rizzato site retains its previous planning regulation as far as shop footage is concerned. In contrast, the footage for offices is partly cancelled, partly intended to enlarge the shopping area, and partly converted to other uses. In contrast, the Basso Isonzo site loses all of its previous development potential. Furthermore, for the purpose of transferring development rights, the Basso Isonzo area is identified as the sending site, and the former Rizzato area is recognized as the receiving site. Accordingly, the residential footage previously located in the Basso Isonzo area is transferred to the former Rizzato area, partly for dwellings and partly to accommodate a student housing facility (Fig. 4). Once the development rights are transferred, the Basso Isonzo site, totaling 30,056 square meters, will be transferred to the municipality free of charge to become a public park. The overall value of the transfer is estimated at Euros 270,504, based on a land unit value of 9 Euros per square meter, and it represents part of the additional land and property value potentially originating from the zoning variance, half of which the private entity is required to pay to the public body.

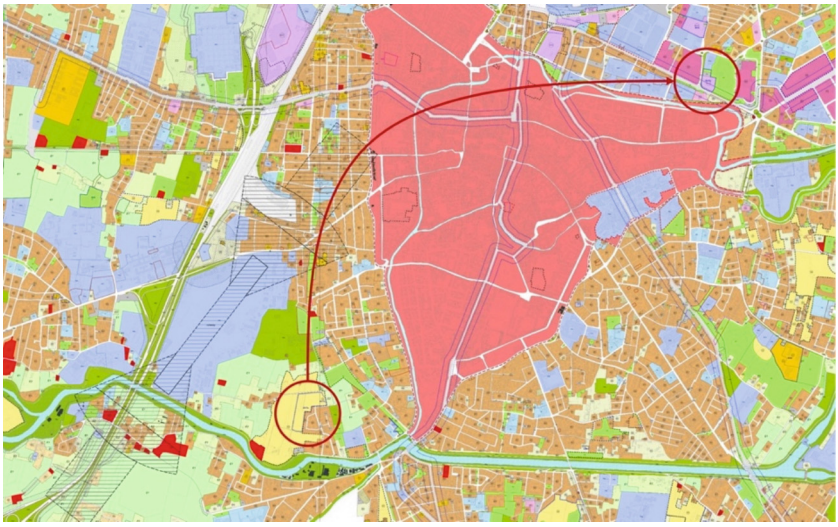

Fig. 1. Excerpt from the general town plan, lastly adopted by the Municipality of Padua, showing the two areas involved in the public-private agreement and the transfer of development rights.

3.2 The Public-Private Agreement in the Context of Padua's Current Urban Transformation Processes

The description in the previous subsection makes it clear that the two projects remained unrealized for many years. Therefore, the public-private agreement and the related zoning

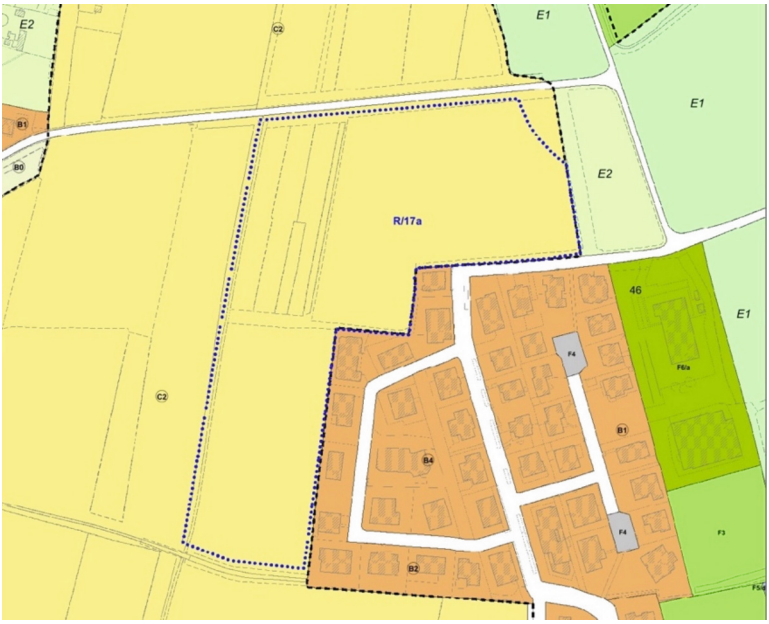

Fig. 2. Excerpt from the general town plan, lastly adopted by the Municipality of Padua, showing the sending site, namely the land parcels from which the development rights originate.

variance aim to define a new, more profitable project that is much more likely to be carried out.

It seems worth noting that, over the last two decades or so, this fate has been shared by several other urban renewal projects in Padua (a selection is shown in Fig. 5). Many of these cases also share other characteristics with the case study analyzed here (Fig. 6). Sometimes, such as in the well-known cases of the former Gasometer area (center-right panel) and the so-called former Ifip site (center-left panel), a detailed plan was approved over the years 2000s, but to no avail. Oftentimes, in more recent years, following one or more ownership changes, the new property owners have required a zoning variance, and a public-private agreement has been drafted. Not to mention that most of these cases now feature the planned construction of private purpose-built student accommodations [53–55] – sometimes subsidized under the auspices of the European Union (EU), especially the NGEU fund [56, 57], and specifically Italy's post-COVID recovery strategy, namely, the National Recovery and Resilience Plan [58, 59] – which are nowadays a trending topic in the urban renewal transactions across the city, much like elsewhere in Europe [60–62].

3.3 Data Sources

Below are the sources used to estimate costs and revenue – see earlier Eq. (1) – for the development projects before and after the establishment of the public-private agreement for the zoning variance.

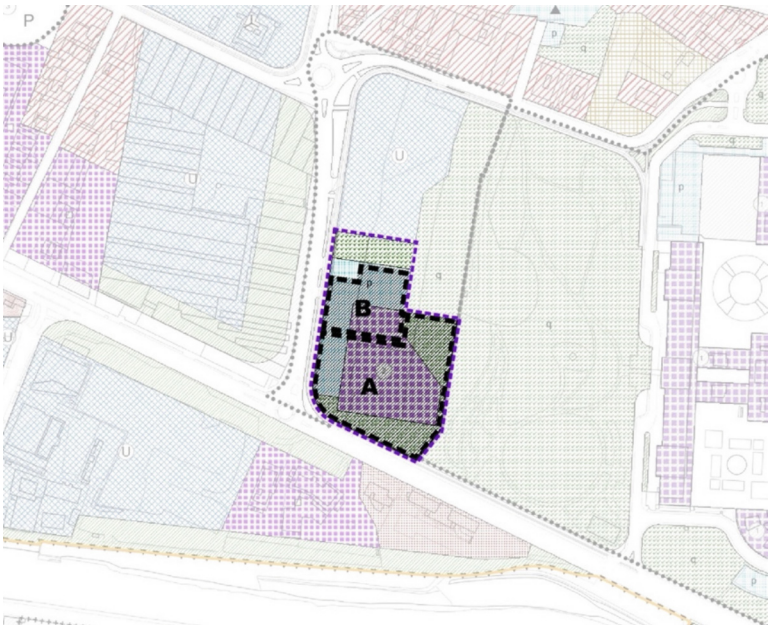

Fig. 3. Excerpt from the general town plan, lastly adopted by the Municipality of Padua, showing the receiving site, namely the land parcels to which the development rights are transferred.

	Development potential	
	Before the agreement (m2)	After the agreement (m2)
Basso Isonzo site		
Residential	10,000	0
former Rizzato site		
Shops	1,868	3,400
Offices	7,500	0
Residential	0	5,380
Student housing	0	7,250

Fig. 4. Transfer of development rights scheme.

As far as development costs are concerned, the appraisal of construction costs (*Cc*) relies on information from the main costbook on the Italian construction industry [63, 64]. Specific construction cost data are estimated based on the following case studies: a multifamily residential building, a shopping mall, an office building, and a hotel and accommodation. Planning fees (*Pf*) are estimated based on the latest reference values adopted by Padua's municipal council. Ancillary cost items are calculated as a percentage

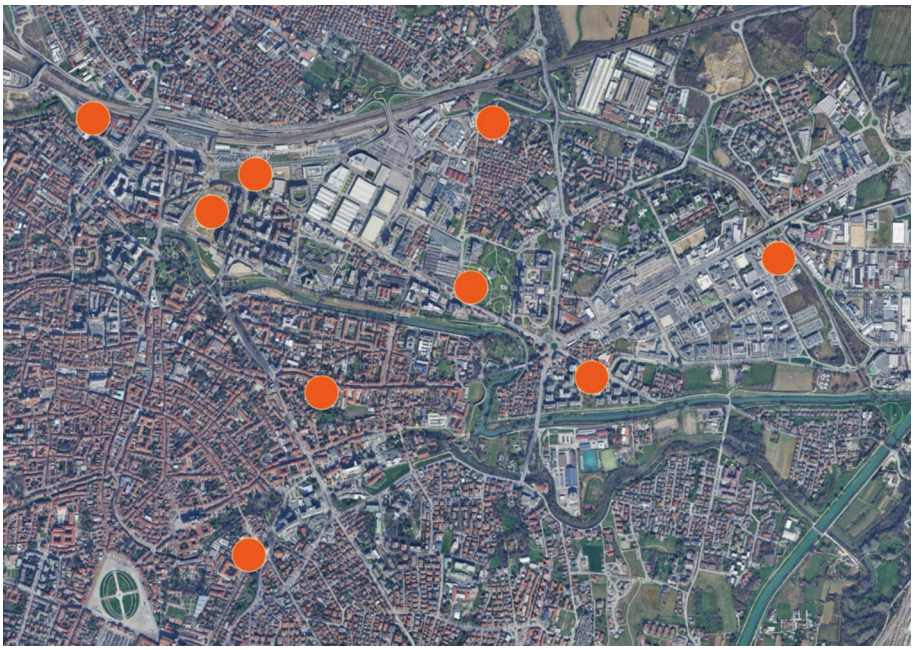

Fig. 5. Overview of urban renewal sites in Padua's central and semi-downtown areas.

of other costs, in accordance with local customs: design fees (Df) are set at 8% of Cc; borrowing costs (Bc) are 4% of the sum of Cc, Pf, and Df, also assuming a debt proportion of 50%; developer's profit (Dp) is 10% of Cc.

The revenue estimate is based on the figures provided by the real estate market monitor, managed by the Italian Revenue Agency [65–67], for both residential and commercial properties. The latest available data dates to the second half of 2024. According to the monitor, the so-called former Rizzato site lies within the boundaries of the C2 homogeneous area (Fig. 7, right panel). In contrast, the so-called Basso Isonzo site is part of the C6 homogeneous area (Fig. 7, left panel). The revenue from the student housing – namely, its market value – is estimated using a direct capitalization procedure. Thus, the ratio of its prospective rents to an all-risk yield is applied, and both values are derived from the data published in the aforementioned market monitor.

Fig. 6. Selection of urban renewal sites in Padua's central and semi-downtown areas.

Fig. 7. Overview of the homogeneous areas according to the real estate market monitor of the Italian Revenue Agency.

4 Results and Discussion

4.1 Development Value before the Public-Private Zoning Variance Agreement is Established

The assessment of the development value for the so-called Basso Isonzo and former Rizzato areas is affected not only by the estimated costs and revenue, as in the previous subsection, but also by different assumptions concerning timing and discounting, which depend on project sizes and risk profiles.

Table 1. Basso Isonzo area, before the agreement.

	Quantity	Unit value	Total value
	(m2, pct., y)	(Euro/m2)	(Euros)
Revenue			
Residential	10,000	2,850	28,500,000
Total revenue			**28,500,000**
Development costs			
Construction cost (*Cc*)	10,000	1,540	15,400,000
Planning fees (*Pf*)			1,472,000
Design fees (*Df*)	8.0%		1,232,000
Borrowing costs (*Bc*)	4.0%		1,086,240
Developer's profit (*Dp*)	10.0%		1,540,000
Total development costs			**20,730,240**
Time (revenue)	6.0		
Time (development costs)	3.0		
Discount rate	5.5%		
Development value			**3,015,351**

Timing depends on the project's size and also accounts for the time spans characteristic of similar work. Housing in the peripheral Basso Isonzo area is bound to be the last fully taken up by the players on the demand side of the local real estate market, along with the offices in the semi-downtown former Rizzato area. Instead, commercial and student housing are expected to deliver at a faster pace and experience shorter market absorption times. Discounting reflects the project's risk profile. The highest risk is associated with offices, followed by shops, while residential and student housing have a significantly lower risk.

In summary, the development values before the agreement – thus, according to the planning regulation without the zoning variance – amount to approximately 3 (Table 1) and 0.5 million Euros (Table 2), respectively.

Table 2. Former Rizzato area, before the agreement.

	Quantity	Unit value	Total value
	(m2, pct., y)	(Euro/m2)	(Euros)
Revenue			
Commercial	1,868	3,700	6,911,600
Offices	7,500	2,100	15,750,000
Total revenue			**22,661,600**
Development costs			
Construction cost (*Cc*)	9,368	1,395	13,068,360
Planning fees (*Pf*)			3,007,000
Design fees (*Df*)	8.0%		1,045,469
Borrowing costs (*Bc*)	4.0%		684,833
Developer's profit (*Dp*)	10.0%		1,306,836
Total development costs			**19,112,498**
Time (revenue)	4.0		
Time (development costs)	2.0		
Discount rate	7.3%		
Development value			**495,510**

4.2 Development Value after the Public-Private Zoning Variance Agreement is Established

Before the zoning variance agreement, the two areas were planned for separate, independent development. Once included in the agreement as sending and receiving sites, the sending site loses its development potential. However, the development value rises significantly - approximately 6.7 million Euros (Table 3). This is due to the transfer of development rights and changes in allowed uses. The commercial footage increases, the use shifts from offices to dwellings, and a student housing facility is included. These changes provide a significant boost to the project's economic viability.

Table 3. Former Rizzato area, after the agreement for the zoning variance.

	Quantity	Unit value	Total value
	(m2, pct., y)	(Euro/m2)	(Euros)
Revenue			
Commercial	3,400	3,700	12,580,000
Residential	5,380	2,600	13,988,000
Student housing	7,250	2,900	21,025,000

(*continued*)

Table 3. (*continued*)

	Quantity	Unit value	Total value
Total revenue			**47,593,000**
Development costs			
Construction cost (*Cc*)	16,030	1,595	25,567,850
Planning fees (*Pf*)			3,738,000
Design fees (*Df*)	8.0%		2,045,428
Borrowing costs (*Bc*)	4.0%		1,254,051
Developer's profit (*Dp*)	10.0%		2,556,785
Total development costs			**35,162,114**
Time (revenue)	4.0		
Time (development costs)	2.0		
Discount rate	5.7%		
Development value			**6,655,874**

4.3 A Few Remarks on the Fair Exchange Topic

The overall development value was approximately 3.5 million Euros before the agreement, then rising to nearly 6.7 million Euros once the agreement for the zoning variance is established. Accordingly, the added land and property value exceeds 3.1 million Euros, of which approximately 1.6 million Euros (Table 4) should be returned to the community to finance the construction of public infrastructure and facilities.

The zoning variance identifies the financial community benefit at 286,112 Euros – including 270,504 Euros, namely, the value of the Basso Isonzo area, and an additional 15,608 Euros – which is a figure far lower (barely 18%) than the one assessed here (Fig. 8). Nonetheless, the Municipality of Padua ultimately approved the zoning variance based on the acknowledgment of an occurring non-financial benefit, specifically that the landowner agreed not to exercise all the development rights previously granted.

Table 4. Summary of the results.

	Before		After
	Basso Isonzo	Former Rizzato	Former Rizzato
Development value (*V*)	3,015,351	495,510	6,655,874
Development value (*V*)	3,510,860		6,655,874
Added value (*A*)			3,145,014
Community benefit (*B*)			1,572,507

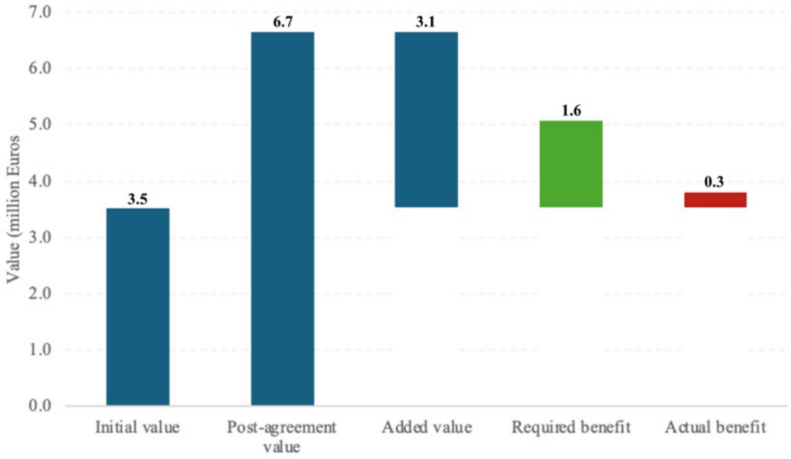

Fig. 8. Value flows.

This raises several issues. First, the national regulation concerning land value recapture explicitly states that half of the added land and property value must be provided as a financial benefit, meaning a direct payment. Secondly, the municipal government's belief that lower urban density stands as a community benefit is at odds with its goal to control and limit land take. In the third place, the corresponding value of the non-financial benefit – thus the renounced development rights – is assessed based on the market value of those same development rights, which is arguably a very loose estimate from the community's perspective. These issues cast doubt on the actual fairness of the public-private exchange, with advantages leaning toward the private entity.

5 Conclusions and Further Developments

In this paper, we focus on public-private partnership practices in town planning, specifically on public-private agreements meant to define the content of zoning variances. The Italian legal system includes a land value recapture mechanism, under which at least half of the added value resulting from the zoning variance must be returned to the community. Once the analytical model is developed within the framework of property valuation approaches and methodologies, we examine a case study, in the city of Padua, northeastern Italy, of a zoning variance deriving from a public-private agreement. We find evidence questioning the fairness of that agreement, as the financial community benefit paid by the private entity to the public body is far less than half the estimated increase in land and property value (Fig. 9).

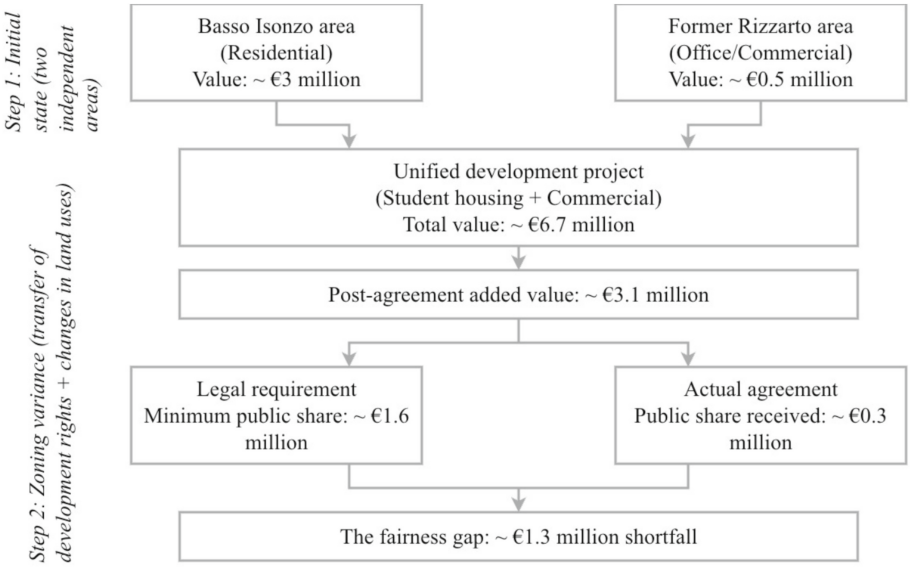

Fig. 9. Assessment of value flows and identification of the fairness gap.

Given the significant equity issues in land value recapture practices, further development of this research strand should focus on the potential role played by information asymmetry between private entities and public bodies, as well as on the valuation capacity within public bodies. The evidence here suggests the need for improved valuation methodologies and governance mechanisms to ensure fair public-private exchanges in urban transformation processes.

Acknowledgments. This paper is an outgrowth of the bachelor's degree thesis of AB, supervised by SC and PB and defended at the University IUAV of Venice in fall 2025.

Disclosure of Interests. The authors have no competing interests to declare that are relevant to the content of this article.

References

1. Treves, G.: Town and country planning law in Italy. In: Garner, J.F. (ed.) Planning Law in Western Europe, pp. 229–250. North-Holland, Amsterdam (1975)
2. Wynn, M.: Planning and Urban Growth in Southern Europe. Mansell, London (1984)
3. Ryser, J., Franchini, T.: International Manual of Planning Practice. ISOCARP (International Society of City and Regional Planners), The Hague (2015)
4. Astengo, G.: Town and regional planning in Italy. Town Plan. Rev. **23**, 166 (1952). https://doi.org/10.3828/tpr.23.2.627q22857683w784
5. Bernardini, G.: Italian Architects and the Reform of Urban Planning Legislation in the Early 1960s. A Long-Term Perspective on the Reasons for a Commitment. Annali dell'Istituto storico italo-germanico in Trento, Jahrbuch des italienisch-deutschen historischen Instituts in Trient. 2, 11–36 (2024)

6. Romano, B., Zullo, F., Marucci, A., Fiorini, L.: Vintage urban planning in Italy: land management with the tools of the mid-twentieth century. Sustainability. **10**, 4125 (2018). https://doi.org/10.3390/su10114125
7. Piccinato, G.: Urban landscapes and spatial planning in industrial districts: the case of Veneto. Eur. Plan. Stud. **1**, 181–198 (1993). https://doi.org/10.1080/09654319308720208
8. Colavitti, A.M., Usai, N., Bonfiglioli, S.: Urban planning in Italy: the future of urban general plan and governance. Eur. Plan. Stud. **21**, 167–186 (2013). https://doi.org/10.1080/09654313.2012.722913
9. Healey, P., Williams, R.: European urban planning systems: diversity and convergence. Urban Stud. **30**, 701–720 (1993). https://doi.org/10.1080/00420989320081881
10. Leonardi, R., Nanetti, R.Y., Putnam, R.D.: Italy - territorial politics in the post-war years: the case of regional reform. West Eur. Polit. **10**, 88–107 (1987). https://doi.org/10.1080/01402388708424653
11. Gabellini, P.: Profiles of Italian urban planning. Planum. **17**, 1–15 (2008)
12. Piccinato, G.: A brief history of Italian town planning after 1945. Town Plan. Rev. **81**, 237–259 (2010). https://doi.org/10.3828/tpr.2010.1
13. Micelli, E.: Development rights markets to manage urban plans in Italy. Urban Stud. **39**, 141–154 (2002). https://doi.org/10.1080/00420980220099122
14. Falco, E., Chiodelli, F.: The transfer of development rights in the midst of the economic crisis: potential, innovation and limits in Italy. Land Use Policy. **72**, 381–388 (2018). https://doi.org/10.1016/j.landusepol.2017.12.069
15. Stanghellini, S., Copiello, S.: Urban models in Italy: partnership forms, territorial contexts, tools, results. In: Dalla Longa, R. (ed.) Urban Models and Public-Private Partnership, pp. 47–130. Springer, Berlin, Heidelberg (2011). https://doi.org/10.1007/978-3-540-70508-6_3
16. Falco, E.: History of land value recapture in Italy. J. Plan. Hist. **15**, 230–245 (2016). https://doi.org/10.1177/1538513215615281
17. Colavitti, A.M., Serra, S.: Planning regulation and land value capture in Italy between traditional approaches and new perspectives. City Territ. Archit. **10**, 16 (2023). https://doi.org/10.1186/s40410-023-00202-8
18. Morano, P., Tajani, F., Anelli, D.: Urban planning variants: a model for the division of the activated "plusvalue" between public and private subjects. Valori Valutazioni. **28**, 31–47 (2021)
19. Micelli, E., Valier, A.: Capturing the public value in the public/private zoning agreements: evidence from Italian municipalities. In: Morano, P., Oppio, A., Rosato, P., Sdino, L., Tajani, F. (eds.) Appraisal and Valuation, pp. 19–28. Springer, Cham (2021). https://doi.org/10.1007/978-3-030-49579-4_2
20. French, N., Gabrielli, L.: Pricing to market: property valuation revisited – the hierarchy of valuation approaches, methods and models. J. Prop. Invest. Financ. **36**, 391–396 (2018). https://doi.org/10.1108/JPIF-05-2018-0033
21. Gabrielli, L., French, N.: Pricing to market: property valuation methods – a practical review. J. Prop. Invest. Financ. **39**, 464–480 (2021). https://doi.org/10.1108/JPIF-09-2020-0101
22. Pagourtzi, E., Assimakopoulos, V., Hatzichristos, T., French, N.: Real estate appraisal: a review of valuation methods. J. Prop. Invest. Financ. **21**, 383–401 (2003). https://doi.org/10.1108/14635780310483656
23. Copiello, S., Cecchinato, F., Salih, M.H.: The effect of hybrid attributes on property prices. Real Estate Manag. Valuation. **29** (2021). https://doi.org/10.2478/remav-2021-0028
24. Parker, D.: Int. Valuation Stan. Wiley (2016). https://doi.org/10.1002/9781118329795
25. Bonifaci, P., Grillenzoni, C., Copiello, S.: AHP and NLO-integrated SCA: improving the sales comparison technique through multicriteria optimization. J. Eur. Real Estate Res. 1–17 (2025). https://doi.org/10.1108/JERER-01-2025-0001

26. RICS: RICS Valuation - Global Standards 2017. Royal Institution of Chartered Surveyors, London (2017)
27. Copiello, S., Bonifaci, P.: Depreciated replacement cost: improving the method through a variant based on three cornerstones. Real Estate Manag. Valuation **26** (2018). https://doi.org/10.2478/remav-2018-0014
28. IVSC: International Valuation Standards. International Valuation Standards Council, London (2017)
29. Baum, A.E., Mackmin, D.: Nunnington, Nick.: the Income Approach to Property Valuation. Elsevier, Oxford (2014)
30. French, N., Byrne, P.: Concepts and models of value. In: Adair, A., Downie, M.L., McGreal, S., Vos, G. (eds.) European Valuation Practice. E & FN Spon, London (1996)
31. Appraisal Institute: The Appraisal of Real Estate. Appraisal Institute, Chicago (2013)
32. Wyatt, P.: Property Valuation. Wiley-Blackwell, Oxford (2013)
33. Isaac, D.: Property Investment. Macmillan, London (1998). https://doi.org/10.1007/978-1-349-14468-6
34. Appraisal Institute: The Dictionary of Real Estate Appraisal. Appraisal Institute, Chicago (1993)
35. Damodaran, A.: Valuation approaches and metrics: a survey of the theory and evidence. Found. Trends Financ. **1**, 693–784 (2006). https://doi.org/10.1561/0500000013
36. von Böhm-Bawerk, E.: Recent Literature on Interest. The Mac Millan Co., London (1903)
37. Marshall, A.: Principles of Economics. The MacMillan Co., London (1920)
38. Fisher, I.: The Rate of Interest. The MacMillan Co., New York (1907)
39. Fisher, I.: The Theory of Interest. The MacMillan Co., New York (1930)
40. Downs, A.: Characteristics of various economic studies. Apprais. J. **34**, 329–338 (1966)
41. Dilmore, G.: The New Approach to Real Estate Appraising. Prentice Hall, New Jersey (1971)
42. Ratcliff, R.U.: Valuation for Real Estate Decisions. Democrat Press, Santa Cruz (1972)
43. Greaves, M.J.: Discounted cash flow techniques and current methods of income valuation. Estates Gaz. **223**, 2147–2151 (1972)
44. Greaves, M.J.: Discounted cash flow techniques and current methods of income valuation. Estates Gaz. **233**, 2339–2345 (1972)
45. Kishore, R.: Discounted cash flow analysis in property investment valuations. J. Prop. Valuat. Invest. **14**, 63–70 (1996). https://doi.org/10.1108/14635789610118280
46. French, N., Gabrielli, L.: Discounted cash flow: accounting for uncertainty. J. Prop. Invest. Financ. **23**, 75–89 (2005). https://doi.org/10.1108/14635780510575102
47. Copiello, S.: A discounted cash flow variant to detect the optimal amount of additional burdens in public-private partnership transactions. Methods X. **3** (2016). https://doi.org/10.1016/j.mex.2016.03.003
48. Copiello, S.: Economic viability of building energy efficiency measures: a review on the discount rate. AIMS Energy. **9** (2021). https://doi.org/10.3934/ENERGY.2021014
49. Copiello, S., Gabrielli, L., Bonifaci, P.: Evaluation of energy retrofit in buildings under conditions of uncertainty: the prominence of the discount rate. Energy. **137** (2017). https://doi.org/10.1016/j.energy.2017.06.159
50. Copiello, S.: Economic Parameters in the Evaluation Studies Focusing on Building Energy Efficiency: a Review of the Underlying Rationale, Data Sources, and Assumptions (2019). https://doi.org/10.1016/j.egypro.2018.11.179
51. Sayce, S., Smith, J., Cooper, R., Venmore-Rowland, P.: Real Estate Appraisal: from Value to Worth. Blackwell, Orford (2006)
52. Isaac, D.: Property Valuation Principles. Palgrave, New York (2002)
53. Mulhearn, C., Franco, M.: If you build it will they come? The boom in purpose-built student accommodation in Central Liverpool: Destudentification, studentification and the future of

the city. Local Econ. J. Local Econ. Policy Unit. **33**, 477–495 (2018). https://doi.org/10.1177/0269094218792740
54. French, N., Bhat, G., Matharu, G., Guimarães, F.O., Solomon, D.: Investment opportunities for student housing in Europe. J. Prop. Invest. Financ. **36**, 578–584 (2018). https://doi.org/10.1108/JPIF-08-2018-0058
55. Anelli, D., Morano, P., Guarini, M.R., Tajani, F.: Student housing market: an evaluation model for the identification of the investment opportunities in the major European cities. In: Gervasi, O., Murgante, B., Garau, C., Karaca, Y., Faginas Lago, M.N., Scorza, F., Braga, A.C. (eds.) Computational Science and its Applications–ICCSA 2025 Workshops, pp. 393–409. Springer, Cham (2026). https://doi.org/10.1007/978-3-031-97603-2_25
56. Ladi, S., Tsarouhas, D.: EU economic governance and Covid-19: policy learning and windows of opportunity. J. Eur. Integr. **42**, 1041–1056 (2020). https://doi.org/10.1080/07036337.2020.1852231
57. Kempf, E., Linos, K.: NGEU: a new Marshall plan for Europe and a template for global finance. AJIL Unbound. **118**, 151–156 (2024). https://doi.org/10.1017/aju.2024.23
58. Tajani, F., Manganelli, B., Cerullo, G., Morano, P., Morente, M.A.: The student housing as a catalyst for virtuous processes of "win-win" revitalization of property assets in disuse. In: Gervasi, O., Murgante, B., Rocha, A.M.A.C., Garau, C., Scorza, F., Karaca, Y., Torre, C.M. (eds.) Computational Science and its Applications–ICCSA 2023 Workshops, pp. 387–400. Springer, Cham (2023). https://doi.org/10.1007/978-3-031-37120-2_25
59. Torrieri, F., Oppio, A., Rossitti, M.: Right to education and expectation of profit in the NRRP frame: a balance is possible? In: Oppio, A., Bottero, M., Stanghellini, S., Rossitti, M. (eds.) Local Economic Systems and Housing Real Estate Markets in University Towns, pp. 101–115. Springer, Cham (2025). https://doi.org/10.1007/978-3-031-91895-7_7
60. Franz, Y., Gruber, E.: The Changing Role of Student Housing as Social Infrastructure. Urban Plan 7 (2022). https://doi.org/10.17645/up.v7i4.5661.
61. Heslop, J., Chambers, J., Maloney, J., Spurgeon, G., Swainston, H., Woodall, H.: Re-contextualising purpose-built student accommodation in secondary cities: the role of planning policy, consultation and economic need during austerity. Urban Stud. **60**, 923–940 (2023). https://doi.org/10.1177/00420980221121569
62. Lee, C.: The market formation of private sector, purpose built student accommodation in Sheffield 2000–2019. Geogr. J. **191** (2025). https://doi.org/10.1111/geoj.12601
63. Milan Board of Engineers and Architects: Prezzi Tipologie Edilizie. DEI, Rome (2019)
64. Bonifaci, P., Copiello, S., Panarotto, F.: Construction Cost Estimate and Building Information Modeling in Renovation Projects Early Design Stages. Presented at the (2026). doi:https://doi.org/10.1007/978-3-031-97654-4_13.
65. Torre, C.M., Mariano, C.: Analysis of Fuzzyness in spatial variation of real estate market: some Italian case studies. In: Phillips-Wren, G., Jain, L.C., Nakamatsu, K., Howlett, R.J. (eds.) Advances in Intelligent Decision Technologies, pp. 269–277. Springer, Berlin (2010). https://doi.org/10.1007/978-3-642-14616-9_26
66. Copiello, S.: Spatial dependence of housing values in northeastern Italy. Cities. **96** (2020). https://doi.org/10.1016/j.cities.2019.102444
67. Bonifaci, P., Copiello, S.: Real estate market and building energy performance: data for a mass appraisal approach. Data Brief. **5** (2015). https://doi.org/10.1016/j.dib.2015.11.027

Unveiling Human-Flood Governance Interlinkages from Forensic Investigations

Edda Donati(✉) and Fernando Nardi

Department of Civil Engineering and Computer Science, University of Rome Tor Vergata, Via del Politecnico, 1, 00133 Rome, Italy
eddadonati@gmail.com

Abstract. In order to measure the relationship between governance structure and flood vulnerability, it is important to adopt an approach that can effectively analyze the multi-dimensional aspects of the institution as well as the heterogeneous profiles of the actors.

This paper makes use of Hierarchical Clustering on Principal Components (HCPC), where Multiple Correspondence Analysis (MCA) is combined with hierarchical agglomeration to classify respondents into groups of similar characteristics in a survey-based dataset about flood governance.

Firstly, the respondents are mapped to the principal components explaining most of the inertia, generally the first five, which explain the major sources of variability in flood governance systems. The clustering process continues with calculating Euclidean distances among projected coordinates using the Ward minimum-variance approach for reducing intra-cluster variance in each agglomerative stage. The obtained dendogram determines the optimal partition, whereas the silhouette score and bootstrap sampling are used to evaluate the robustness of the clusters. Symmetric dendrograms and cluster-specific bar plots highlight the main governance features distinguishing each group, enabling the identification of distinct vulnerability profiles.

The approach reveals how governance-related risk misjudgment, delayed decision-making, and preventive omissions systematically co-occur within specific clusters, pointing to structural bottlenecks in multi-level flood risk management.

By linking formal multivariate analysis to policy-relevant patterns, HCPC offers a robust framework to inform targeted disaster risk reduction strategies in flood-prone regions.

Keywords: flood governance · hierarchical clustering · vulnerability profiles

1 Introduction and Literature Background

Flood events are increasingly interpreted as socio-natural processes emerging from the interaction between extreme hydro-meteorological conditions and institutional arrangements [1, 2]. While the physical intensity of precipitation and hydrological dynamics defines the hazard, the severity of impacts often depends on governance structures, decision-making processes, and organizational coordination mechanisms [3–5].

© The Author(s), under exclusive license to Springer Nature Switzerland AG 2027
O. Gervasi et al. (Eds.): ICCSA 2026 Workshops, LNCS 16761, pp. 351–364, 2027.
https://doi.org/10.1007/978-3-032-30527-5_23

The literature on flood risk governance has extensively emphasized the importance of institutional capacity, inter-agency coordination, and preventive measures in mitigating disaster impacts [6, 7]. However, less attention has been devoted to the structural role of governance scale. In multi-level governance systems, responsibilities are distributed across local, regional, and national authorities, generating coordination challenges, overlaps, or scale mismatches [8–10]. Whether the administrative scale at which governance operates constitutes a primary determinant of flood severity remains an open empirical question [9, 11].

At the same time, research on disaster governance highlights the relevance of cognitive and organizational failures—such as risk misjudgment, delayed decision-making, and preventive omissions—in amplifying flood impacts [11, 12].

Yet it is unclear whether these failure configurations represent the dominant axis of structural variation across events, or whether governance scale exerts a stronger explanatory influence.

This study addresses this gap by investigating nine Italian flood events through judicial rulings of the Court of Cassation. Rather than treating governance scale and human failures as isolated explanatory factors, the analysis explores their relative structural positioning within a multidimensional categorical space. A Multiple Correspondence Analysis (MCA) is employed to uncover latent oppositions among variables, followed by Hierarchical Clustering on Principal Components (HCPC) to formalize case aggregation patterns.

The core of our study thus revolves around the following key question: "Is flood damage more structurally linked to scale of governance or to the pattern of cognitive and organizational failures?"

The rest of the paper is organized as follows. The second section describes the methodological approach, explaining both MCA and HCPC. The third section describes the data set used for the research, along with its variables. Section four provides the empirical findings, while section five discusses these findings and the shortcomings of this study. Finally, the conclusion is provided in section six.

2 Method

Considering the nature of the variables used in the study, which were categorical, and the sample size (N = 9), the exploratory technique of MCA was applied to investigate the possible latent structure that may be hidden behind the observed multidimensional phenomena of flooding.

In order to facilitate the classification of the cases into clusters based on the factorial structure, HCPC analysis using Ward's method was undertaken. This approach involves clustering cases by MCA axes as opposed to clustering them using categorical variables directly.

2.1 Multiple Correspondence Analysis (MCA)

In order to analyze the relationships among several categorical variables contained in a multidimensional contingency table, MCA was used. The procedure is based on the

principles of Correspondence Analysis (CA), a mathematical procedure developed for the study of mutual dependencies among rows and columns of a contingency table in terms of Cartesian projections [13, 14].

All entities in the dataset that have been processed have their location in a multidimensional Euclidean space, wherein the entity is situated based on its own weight, which determines its significance. The χ^2 distance between two sets of observations is one of the key metrics used in the method, calculated using the value of the χ^2 statistic and indicating the extent to which observed and expected frequencies diverge when assuming independence between variables [14–16].

The visualization of proximity and dissimilarity between categories is easy to understand because close profiles within the factorial space suggest high similarities, while far profiles imply high dissimilarities.

The formula for the chi-square distance is:

$$d^2_{\chi^2}(\mathbf{x}_i, \mathbf{y}_i) = \sum_{j=1}^{n} \frac{\left(x_j - y_j\right)^2}{c_j} \tag{1}$$

where:

- $\mathbf{x}_i = [x_1, x_2, \ldots, x_n]$: factorial coordinates of a profile in the multidimensional cloud;
- $\mathbf{y}_i = [y_1, y_2, \ldots, y_n]$: coordinates of a second profile;
- $\mathbf{c}_i = [c_1, c_2, \ldots, c_n]$: column mass weights (column total/table sum).

Total inertia, expressed by the ratio between $\chi^2_{\text{Pearson}}/n$, measures the proportion of explained variance and the degree of dispersion of the data, which means that higher total inertias correspond to more articulated structures and stronger connections among categories [17].

In situations where data is gathered through purposeful surveys containing sector-specific features and characteristics (such as levels of preparedness within flood-prone areas), factor maps generated through these profiles become differentiated into distinct groups of homogenous elements [14–16].

While symmetric visualizations focus on inter-categorical relationships on a global scale, asymmetric visualizations concentrate on intravariable particularities.

2.2 Hierarchical Clustering on Principal Components (HCPC)

In order to reveal homogeneous sets in the multidimensional space created by MCA or PCA, HCPC was utilized. HCPC is an amalgamation of PCA and hierarchical agglomerative clustering, which allows for the identification of partitions in multivariate datasets by aggregating the data points iteratively [18, 19].

In the processed dataset, individuals are first mapped into the principal components, keeping those that have high inertia (usually five principal components). The cluster formation process is done based on computing the Euclidean distances between the mapped data points using Ward's criteria of minimizing within-cluster variation [18, 20, 21].

Cluster hierarchy graphs are easily interpreted as follows: clusters with dense branches suggest compact groups with common traits, while far-off branches represent structural differences. Cluster partition stability is assessed using the silhouette score and bootstrap analysis methods [19, 20, 22].

The clustering process is formally defined as follows:

$$d\left(\mathbf{F}_i, \mathbf{F}_j\right) = \sqrt{\sum_{p=1}^{P} \left(F_{ip} - F_{jp}\right)^2} \tag{2}$$

where:

- $\mathbf{F}_i$: factorial coordinates of observation i on retained principal components;
- $d(\mathbf{F}_i, \mathbf{F}_j)$: Euclidean distance between observations i and j;

$\mathcal{L}(k)$: linkage criterion (Ward's minimum variance) for k clusters.

The objective at each step is to minimize the total inertia within clusters, computed as:

$$I_{total} = \sum_{c=1}^{k} \frac{1}{n_c} \sum_{i \in c} \|\mathbf{F}_i - \bar{\mathbf{F}}_c\|^2 \tag{3}$$

The total inertia is an indicator of partition quality; the lower the value of the total inertia, the greater cohesion among groups and the more distinct boundaries between groups will be.

Based on factorial coordinates obtained by MCA of surveys reflecting variables concerning flood management systems, HCPC gives well-calibrated dendrograms and clustered maps of the vulnerability profiles [18, 19]. he symmetrical dendrogram stresses hierarchical relations, while the bar charts related to each cluster reveal which variables contribute the most.

3 Data

The data set includes nine cases of floods, all collected from rulings made by the Italian Court of Cassation from 1998 to 2013 (as shown in Fig. 1 below). Cassation decisions were selected to ensure consistency in case reconstruction and responsibility attribution, as they represent the final level of judicial review within the Italian legal system. This guarantees a standardized and definitive account of events, suitable for systematic coding and comparative analysis.

All rulings were retrieved through the OneLegale platform (Wolters Kluwer), which provides access to Italian case law and legal documentation.

A set of descriptive variables was gathered for each case in order to help in its initial classification inside the dataset. The variables consist of the case number (CS), OneLegale reference (Ref. OL), location (city and region), year of the event, nature of the hydro-meteorological disaster, and scale of governance implicated.

These elements, summarized in Table 1, provide the contextual framework for subsequent multidimensional analysis.

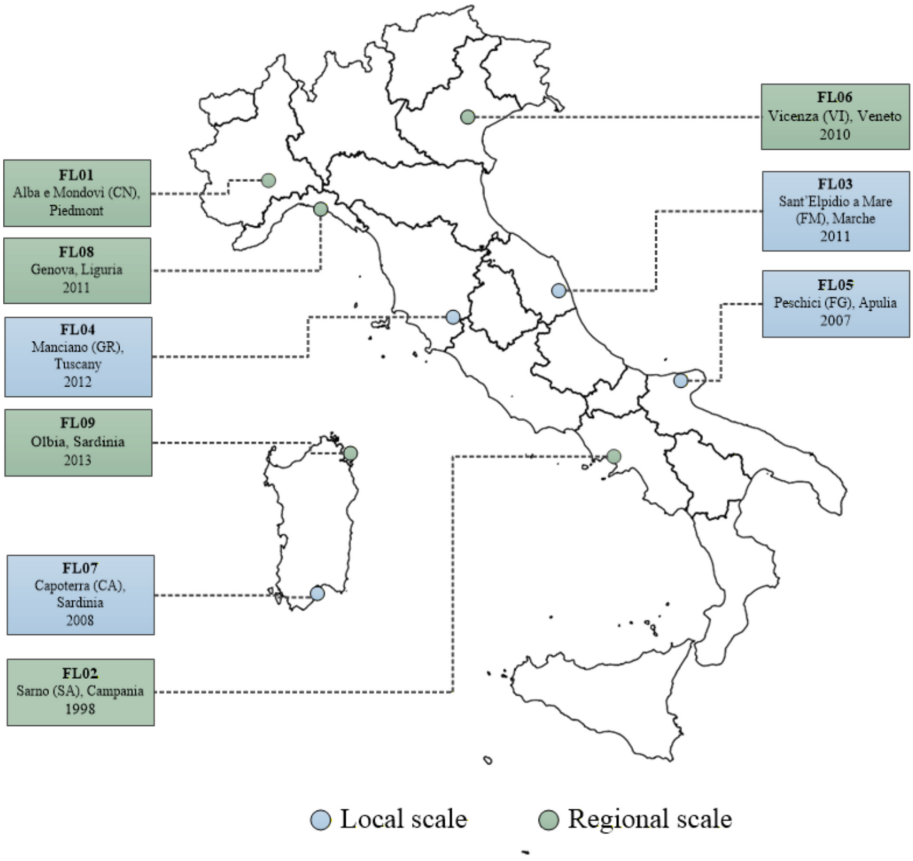

Fig. 1. Geographic distribution of the case studies by governance scale

Following this, the coding process involved identifying the variables needed to answer the following research question: "Does the level of governance matter as a primary determinant of the intensity of floods, or is the failure configuration a primary determinant of variation?" For this purpose, three main categories of variables have been identified: causative variables, effect variables, and the level of governance.

In the first category (causative variables), there are variables related to determinants that cause and escalate the hazard. They include psychological failures (PSY) and behavioral failures (ATT) of the persons involved in risk prevention and territory management, and residual causative factors (RES), which are natural elements and weather conditions that contributed to the occurrence and intensity of the disaster.

The second domain (effects) focuses on the gravest effect of flood occurrences, namely, human deaths (HUM_L), defined as a binary variable. Human casualties were selected as the primary outcome measure because they represent the most critical consequence of hydro-meteorological hazards and are consistently documented within judicial rulings. Other potential effects, such as economic or material damages, were not systematically included due to inconsistent reporting across cases.

Table 1. Case study's identification

Case study	Ref. OL	City and region	Year	Hydro-meteorological hazard typology	Governance scale
CS01	cass-pen-sez-iv-sent-data-ud-10-07-2001-13-09-2001.pdf	Alba e Mondovì (CN), Piedmont	1994	Riverine Flood	Regional
CS02	cass-pen-sez-iv-sent-data-ud-11-03-2010-03-05-2010.pdf	Sarno (SA), Campania	1998	Debris Flow / Landslide	Regional
CS03	cass-pen-sez-iv-sent-data-ud-13-11-2019-23-10-2020.pdf	Sant'Elpidio a Mare (FM), Marche	2011	Riverine Flood	Local
CS04	cass-pen-sez-iv-sent-data-ud-15-05-2025-03-06-2025.pdf	Manciano (GR), Tuscany	2012	Riverine Flood	Local
CS05	Peschici_cass-civ-sez-unite-sent-data-ud-05-12-2017-21-09-2.pdf	Peschici (FG), Apulia	2007	Multi-hazard / Cascading Disaster	Local
CS06	t-a-r-veneto-venezia-sez-iii-sent-data-ud-05-03-20.pdf	Vicenza (VI) Veneto	2010	Urban Flood	Regional
CS07	corte-d-appello-cagliari-sez-ii-sent-09-04-2020.pdf	Capoterra (CA), Sardinia	2008	Flash Flood	Local
CS08	Cass. pen., Sez. IV, Sent., (data ud. 12/04/2019) 22/05/2019, n. 22214.pdf	Genova, Liguria	2011	Flash Flood	Regional
CS09	Cassazione penale sez. IV - 20/12/2023, n. 15405.pdf	Olbia, Sardegna	2013	Flash Flood	Regional

The third domain concerns governance scale and represents the core variable of the study. It identifies whether the flood event primarily involved local or regional governance arrangements. The identified domains, corresponding variables, and their values are summarized in Table 2.

Table 2. Domain and variables coding

Domain	Code	Variable	Description	Values
Causes	PSY	Psychological causes	Cognitive and decision-making failures	0: Absent;
				1: Risk misjudgment;
				2: Flawed decision-making
	ATT	Attitude and behavioral causes	Managerial omissions and operational behaviors	0: Absent;
				1: Preventive failures;
				2: Implementation errors
	RES	Residual causes	External meteorological conditions and contributing factors	1: Exceptional rainfalls;
				2: Inclement weather
Effect	HUM_L	Human losses	External meteorological conditions and contributing factors	(Binary) 1: Yes
Governance scale	SCALE	Governance scale	Institutional level involved in flood management	1: Local
				2: Regional

4 Results

4.1 Multiple Correspondence Analysis (MCA)

The MCA results are reported in Fig. 2 and Table 3. The factorial map illustrates the relational structure among the modalities of the variables considered and allows the identification of the main axes of variation that organize the analyzed phenomenon.

Dimension 1, which explains 70.3% of the total inertia, clearly represents the dominant structural axis of the dataset, and the analysis of the column standard coordinates highlights a strong polarization along this first dimension.

Modalities with strongly positive coordinates include PSY = absent (1.86), ATT = absent (2.10), HUM_L = No (2.12), and RES = exceptional rainfall (1.38), whereas on

the negative side are PSY = risk misjudgment (–1.25), PSY = flawed decision-making (–0.87), ATT = preventive failures (–0.54), ATT = implementation errors (–0.96), and HUM_L = yes (–0.60). This configuration indicates that the first dimension contrasts coherent sets of modalities associated with different configurations of failure, in which psychological, attitudinal, response-related components, and human factors combine. The main axis is therefore not structured by an institutional variable but by systematic patterns of error and vulnerability.

By contrast, the variable SCALE shows limited coordinates along Dimension 1 (0.42 for SCALE = local and –0.34 for SCALE = regional), significantly lower than those observed for the variables defining the main polarization.

Table 3. Column Standard Coordinates of Categories (MCA Results)

Categories	Values	Dim1	Dim2
PSY	Absent	1.863	0.007
	Risk misjudgment	−1.252	−2.808
	Flawed decision-making	−0.868	0.557
ATT	Absent	2.101	−0.149
	Preventive failures	−0.540	−0.606
	Implementation errors	−0.961	3.934
RES	Exceptional rainfalls	1.383	−0.201
	Inclement weather	−0.395	0.058
HUM_L	No	2.117	−0.494
	Yes	−0.605	0.141
SCALE	Local	0.424	1.542
	Regional	−0.340	−1.233

This suggests that governance scale does not constitute the structuring factor of the dominant axis. Instead, SCALE shows greater differentiation along Dimension 2 (10.6% of the inertia), with values of 1.54 for SCALE = 1 and –1.23 for SCALE = 2.

However, since this dimension explains only a residual share of the variance, its role remains secondary in the overall structure of the factorial space. Dimension 2 appears rather to capture a differentiation among specific types of error, as also indicated by the high coordinates of ATT = 2 (3.93) and PSY = 1 (–2.81), rather than a genuine divide related to institutional scale.

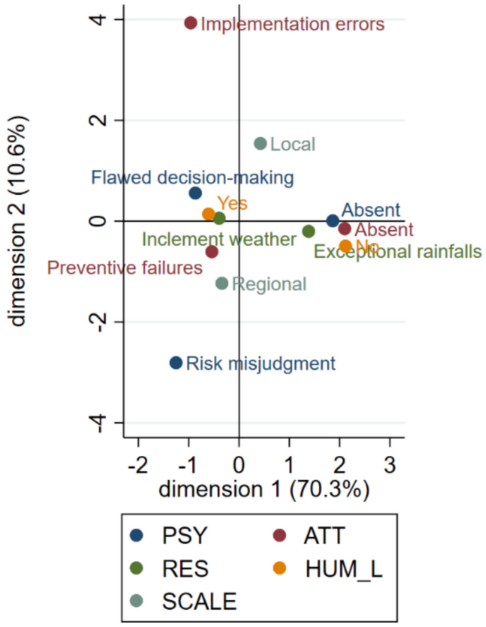

Fig. 2. MCA Factorial Map of Failure Configuration and Governance Scale

Overall, the MCA suggests that the configuration of failures constitutes the dominant axis of variation in the dataset, whereas governance scale does not emerge as a primary structural determinant of flood severity. Instead, event severity appears to be associated with systematic combinations of cognitive, decision-making, and operational errors, which occur across different levels of governance.

4.2 Hierarchical Clustering on Principal Components (HCPC)

To further examine the structural grouping of cases in the factorial space, a HCPC was performed using Ward's linkage method and the L2 squared dissimilarity measure on the first two MCA dimensions.

As shown in Fig. 3, the dendrogram reveals a marked increase in L2 squared dissimilarity in the final aggregation step, when the two main branches are merged into a single cluster. The substantial jump in fusion distance suggests that the two-cluster solution represents the most parsimonious and structurally coherent partition of the dataset.

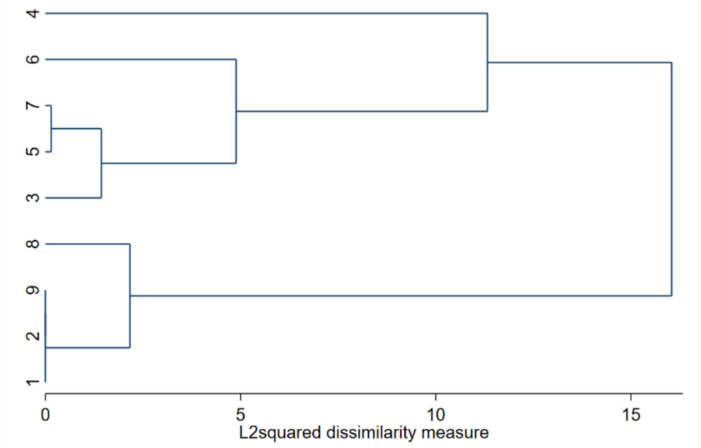

Fig. 3. Dendrogram for cluster analysis

The spatial distribution of the two clusters in the factorial plane is illustrated in Fig. 4. Cluster 1 groups four cases located predominantly on the negative side of Dimension 1, whereas Cluster 2 includes five cases mainly positioned on the positive side of the first dimension.

This separation reflects the dominant structural axis identified by the MCA and indicates that cluster allocation is strongly aligned with the principal latent contrast emerging from the data.

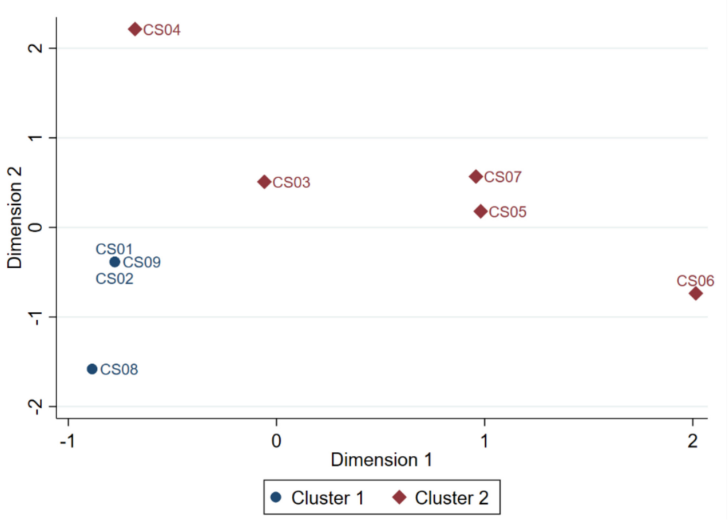

Fig. 4. Spatial distribution of the two clusters in the factorial plane

To evaluate whether cluster membership corresponds to governance scale, a cross-tabulation between clusters and SCALE was conducted (Table 4). The results reveal a marked association: all cases in Cluster 1 belong to scale category 2, while Cluster 2 is primarily composed of scale category 1 cases (4 out of 5). Fisher's exact test confirms that this association is statistically significant ($p = 0.048$).

Table 4. Distribution of case studies by cluster membership and governance scale

Case study	Place	Cluster 1	Cluster 2
CS01	Regional	1	0
CS02	Regional	1	0
CS03	Local	0	1
CS04	Local	0	1
CS05	Local	0	1
CS06	Regional	0	1
CS07	Local	0	1
CS08	Regional	1	0
CS09	Regional	1	0
Fisher's exact		0.048	
1-sided Fisher's exact		0.040	

Note: 1 = case belongs to the cluster; 0 = case does not belong to the cluster.

Although the limited sample size ($N = 9$) warrants cautious interpretation, the HCPC results indicate that governance scale is structurally embedded in the clustering pattern derived from the factorial coordinates. The observed partition suggests that institutional level contributes to the differentiation of case profiles within the multidimensional space identified by the MCA.

5 Discussion and Limitations

Although the analysis was conducted on a relatively small sample ($N = 9$), the results obtained through MCA and HCPC provide meaningful insights that deserve further discussion.

The MCA identifies Dimension 1 as the dominant axis of representation of the dataset, while Dimension 2 plays a secondary and comparatively weaker role. The first dimension clearly separates two opposing poles. The positive pole is characterized by events in which flood severity is primarily attributable to natural and physical causes, particularly exceptional rainfall (RES = 1). This configuration is associated with the absence of psychological and behavioral failures (PSY = 0; ATT = 0) and, notably, with the absence of human losses (HUM_L = 0).

This first structural result suggests that when preventive and decision-making mechanisms function effectively, even severe natural conditions do not necessarily translate

into fatal outcomes. In the cases analyzed, the absence of organizational and behavioral failures appears to mitigate the most critical consequences of the flood events.

The second pole, located on the opposite side of Dimension 1, presents a more complex configuration. Here, natural factors such as inclement weather (RES = 2) are combined with organizational and psychological failures that exacerbate the severity of the event and are associated with the presence of human losses (HUM_L = 1). Flawed decision-making (PSY = 2) and preventive failures (ATT = 1) appear strongly linked to this configuration. Conversely, risk misjudgment (PSY = 1) and implementation errors (ATT = 2) do not show a clear alignment with either pole.

While MCA provides an exploratory representation of latent structures, it does not formally define case groupings. The hierarchical clustering performed on the MCA coordinates through HCPC allows for the identification of structured aggregations within the same Euclidean space.

The HCPC results reveal that cluster membership is significantly associated with governance scale (Fisher's exact test, $p = 0.048$). One cluster is entirely composed of cases characterized by local governance, while the other is predominantly composed of regional cases. This indicates that even if governance scale is not the dominant factorial dimension, it is inherently structured within the case set up. Governance scale acts as the second-level factor influencing the expression of the failure structure. Decision-making and preventative failures do not occur independently of their institutional setting but could well depend on the structural attributes inherent to each level of governance.

The main limitation of the study lies in the small number of cases analyzed ($N = 9$), which constrains statistical generalization and limits the robustness of inferential claims. The findings should therefore be interpreted as exploratory rather than confirmatory. In addition, the use of MCA provides a structural representation of associations within the dataset but does not allow for causal inference. The coding of psychological and organizational variables, derived from judicial documents, may also involve interpretative margins, as court rulings reconstruct events through a legal lens rather than a purely managerial or governance perspective. Furthermore, cluster stability cannot be fully assessed given the limited sample size, and minor variations in the data could potentially affect case aggregation. Finally, governance scale is operationalized as a simplified binary variable, which may not fully capture the complexity and multi-level nature of institutional arrangements in flood risk governance.

6 Conclusions and Future Developments

The present contribution aimed to investigate whether governance scale plays a structural role in shaping flood events and their consequences within a dataset of nine flood cases that occurred in Italy between 1994 and 2013.

The results obtained through MCA and HCPC reveal a nuanced picture. On the one hand, the factorial structure highlights the dominant role of individual and organizational failures in differentiating flood severity. Behavioral and decision-making dimensions emerge as the primary axis structuring the dataset, suggesting that flawed decision-making and preventive failures represent critical factors in the escalation of flood impacts. On the other hand, the HCPC results indicate that governance scale, although not dominant along the main factorial dimension, is nonetheless significantly associated with case

aggregation patterns. This suggests that institutional level contributes to shaping how failure configurations manifest, even if it does not fully determine the severity outcomes. Overall, these results reveal that scale of governance is not adequate for explaining the magnitude of floods. Even though the institutional environment at the local and regional level affects organizational action, the behavioral aspects of failure continue to be structurally essential in the selected cases. Hence, scale of governance does not directly predict the magnitude of floods, but rather, it acts as a secondary but structurally significant variable that affects the manner in which behavioral and organizational aspects of failure are arranged within the local and regional institutional environment.

In contrast to other methods, including cluster analysis, for instance k-means method, the application of MCA and HCPC offers distinct advantages in this context. The k-means method is effective in terms of computation time but presupposes that the number of clusters be fixed in advance, as well as that there be no consideration of correlations between different variables. At the same time, the HCPC method makes it possible to determine clusters according to the MCA model and make the structure more interpretable.

Regression-based approaches (e.g., logistic models) could quantify predictive power but treat variables linearly, missing the multidimensional, non-linear associations revealed in this research. Therefore, MCA-HCPC offers a more sophisticated depiction of the structure that reflects the association—although not dominance—of the governance scale in the disaster governance context.

Further studies may consider widening the empirical basis through the inclusion of a larger number of cases, as well as cross-country analysis to test the resilience of the structural patterns established. Other innovations may enhance the measurement of governance scale through additional variables, including institutional coordination, resource distribution, and emergency planning capabilities.

Moreover, integrating quantitative structural analysis with qualitative process tracing could provide deeper insight into the mechanisms through which behavioral and institutional failures interact during extreme events. Such an approach would contribute to a more comprehensive understanding of how governance structures and human decision-making jointly shape disaster outcomes.

Disclosure of Interests.. The authors have no competing interests to declare that are relevant to the content of this article.

References

1. Quarantelli, E.L.: What Is a Disaster? A Dozen Perspectives on the Question. Taylor and Francis, Hoboken (2005)
2. Blake, K.S., Kellerson, R.L., Simic, A.: Measuring Overcrowding in Housing (2007)
3. Driessen, P.P.J., Hegger, D.L.T., Bakker, M.H.N., Van Rijswick, H.F.M.W., Kundzewicz, Z.W.: Toward more resilient flood risk governance. Ecol. Soc. **21**(4), 53 (2016)
4. Driessen, P.P.J., Hegger, D.L.T., Kundzewicz, Z.W.: Governance strategies for improving flood resilience in the face of climate change. Water. **10**(11), 1595 (2018)
5. Pahl-Wostl, C.: Water Governance in the Face of Global Change: from Understanding to Transformation. Springer International Publishing, Cham (2015)

6. Pahl-Wostl, C.: A conceptual framework for analysing adaptive capacity and multi-level learning processes in resource governance regimes. Glob. Environ. Chang. **19**(3), 354–365 (2009)
7. Alexander, M., Priest, S., Mees, H.: A framework for evaluating flood risk governance. Environ. Sci. Pol. **64**, 38–47 (2016)
8. Sayers, P.: Flood Risk Management: a Strategic Approach. Asian Development Bank, Mandaluyong City (2013)
9. Dieperink, C., et al.: Managing urban flood resilience as a multilevel governance challenge: an analysis of required multilevel coordination mechanisms. Ecol. Soc. **23**(1), art31 (2018)
10. Sayles, J.S., Baggio, J.A.: Social–ecological network analysis of scale mismatches in estuary watershed restoration. Proc. Natl. Acad. Sci. **114**(10), 2017
11. Raška, P., Warachowska, W., Slavíková, L., Aubrechtová, T.: Expectations, disappointments, and individual responses: imbalances in multilevel flood risk governance revealed by public survey. J. Flood Risk Manag. **13**(3), e12615 (2020)
12. Boin, A., 't Hart, P., Stern, E., Sundelius, B.: The Politics of Crisis Management: Public Leadership Under Pressure, 1st edn. Cambridge University Press, Cambridge (2005)
13. Abdi, H., Valentin, D.: Multiple correspondence analysis. In: Salkind, N.J. (ed.) Encyclopedia of Measurement and Statistics, pp. 651–657. Sage, Thousand Oaks (2007)
14. Greenacre, M.J.: Correspondence analysis. Wiley Interdiscip. Rev. Comput. Stat. **2**(5), 613–619 (2010)
15. Chen, Y., Shan, B., Yu, X., Zhang, Q., Ren, Q.: Comprehensive effect of the three-dimensional spatial distribution pattern of buildings on the urban thermal environment. Urban Clim. **46**, 101324 (2022)
16. Moschidis, O.E.: A different approach to multiple correspondence analysis (MCA) than that of specific MCA. Math. Sci. Hum. **186**, 77–88 (2009)
17. Greenacre, M.: The use of correspondence analysis in the exploration of health survey data. Working Paper 201017, Fundación BBVA, Madrid (2002)
18. Husson, F., Josse, J., Pagès, J.: Principal Component Methods–Hierarchical Clustering–Partitional Clustering: why Would we Need to Choose for Visualizing Data? Technical report, Agrocampus, Rennes (2010)
19. Maugeri, A., Barchitta, M., Basile, G., Agodi, A.: Applying a hierarchical clustering on principal components approach to identify different patterns of the SARS-CoV-2 epidemic across Italian regions. Sci. Rep. **11**(1), 7082 (2021)
20. Veri, F.: Mapping discourses through hierarchical clustering on principal components. Methodol. Innov. **18**(3), 180–192 (2025)
21. Husson, F., Le, S., Pagès, J.: Exploratory Multivariate Analysis by Example Using R. Chapman and Hall/CRC (2017)
22. Argüelles, M., Benavides, C., Fernández, I.: A new approach to the identification of regional clusters: hierarchical clustering on principal components. Appl. Econ. **46**(21), 2511–2519 (2014)

Economic Feasibility of Vacant Public Housing Reuse: A Financial Valuation Model for Socially Sustainable Regeneration in Historic Urban Contexts

Ida Zelbi(✉), Pietro Bonifaci, Carlo Grillenzoni, and Sergio Copiello

Department of Architecture and Arts, University IUAV of Venice, Santa Croce 191, 30135 Venice, Italy
izelbi@iuav.it

Abstract. Since the second half of the 20th century, Venice's historic center has faced a long-term population drop driven by industrial changes and, more recently, by the gentrification effects of overtourism. Beyond the impact of tourist rentals, the available building stock is largely obsolete and high-priced, making the historic center inaccessible to many potential residents. This study investigates the potential to reverse this trend by reusing vacant publicly owned housing, specifically that managed by the Local Public Housing Agency. By analyzing a sample of 49 properties, the paper proposes an economically sustainable model for recovery and management that facilitates low-priced rents. Renovation costs are estimated using a combination of direct site surveys and linear regression analysis, while the financial plan relies on a self-financing mechanism where rental income covers mortgage loan repayments. The project demonstrates strong financial feasibility, with indicators such as Net Present Value and the Annual Debt Service Cover Ratio ensuring viability. Furthermore, the model allows for a rent reduction of nearly 30% below market rates, bringing fees closer to social housing standards. Ultimately, the outcomes indicate that this self-sufficient system can be extended to the city's broader vacant building stock and replicated in different contexts, promoting favorable conditions for long-term repopulation.

Keywords: Public Housing Reuse · Social Housing · Economic Feasibility · Urban Repopulation

1 Introduction and Background Literature

The problem of population loss in the historic center of Venice began in the second half of the 20th century, due to changes in the city's economic landscape. Indeed, especially after WWII, important socio-cultural innovations began in the city [1]: the deindustrialization of the historic center and the industrial conversion of Porto Marghera transformed the historical work landscape. Due to these phenomena, the population had to move to the mainland, especially to Mestre and Marghera, just as it had done in many other historic centers of Italy. There, cars and newer, cheaper houses were able to better meet residents'

© The Author(s), under exclusive license to Springer Nature Switzerland AG 2027
O. Gervasi et al. (Eds.): ICCSA 2026 Workshops, LNCS 16761, pp. 365–379, 2027.
https://doi.org/10.1007/978-3-032-30527-5_24

needs. Throughout this period, between the 1950s and the 1970s, a significant drop in the population of the historic center is observed (up to -5.68% per year), while the mainland index rises (up to +6.4% per year) [2].

Alongside the socio-economic changes, building conditions also played a role. It should be pointed out that, according to 1985 data, 58% of the houses in downtown Venice were constructed before the Unification of Italy in 1861, and only 20% were constructed after 1945; between 43% and 48% needed drastic renovations; approximately 48% lacked an adequate heating system; 45% were exposed to significant humidity and approximately the same percentage received only three hours of sunlight a day in winter, due to the intricate labyrinth of small streets [3].

In the 1970s, the situation began to shift: the population was still leaving the historic center, but this time it was also due to the city's growing tourism. The uncontrolled expansion of this phenomenon was fueled by the workers and capital left in the historic center due to its deindustrialization, which could be used in other sectors, particularly tourism. Venice is currently experiencing the effects of gentrification due to overtourism. Throughout its history, the tourism industry has provided significant benefits, including the revaluation of real estate investments and new employment opportunities. However, it has also caused an excessive increase in the cost of living and real estate values, which has led more residents to leave [4]. The need for regulation is highlighted by municipal policies (such as the recently introduced entrance fee) and community voices. Visitors have a significant impact on the quality of life in the historic center, which is particularly problematic. The most significant problem, however, is the housing issue. The residential sector is negatively impacted by the lack of nearby services, as well as by the unavailability of prices and the shortage of homes in adequate condition. For this reason, we need to make improvements to the building stock to meet today's needs without making it economically unsustainable [5].

The purpose of this study is to assess the potential of reusing vacant publicly-owned dwellings to address the housing shortage and reverse depopulation in Venice's historic center. Finding suitable housing is a fundamental factor in choosing where to live and a significant challenge in the Venetian context. By increasing this supply, new residents and families could be attracted, also resulting in increased demand for the services they require.

To date, 17.3% of the city's buildings lack occupants [6], particularly in the historic center. Public entities hold 14.5% of this stock, with the Municipality and the Local Public Housing Agency (ATER) being the main owners. The latter oversees not only the properties constructed by the government specifically meant for low-income families as protected tenancies at social rents, but also additional properties available for regulated tenancies at fair rents, of which 169 are made available for this survey. Among them, a sample of 49 properties is chosen to investigate an economically sustainable model for recovery and management. A feasibility study is conducted by arranging to rent accommodation to teachers, technical staff and research fellows of one of Venice's universities. Better-maintained properties may be available immediately or in a short time. Therefore, the renovation of the remaining properties in the portfolio can be financed through a mortgage loan using the revenues from renting these properties. The project's economic strength is based on the auto-deduction of the rental sum from the university's salary,

which ensures stable and regular payment mechanisms. Over time, the financing of an increasing number of flats should be possible through the revenue from progressively renting the renovated properties.

The paper is organized as follows. Section 2 outlines the method used to calculate the costs of redeveloping the remaining units of the sample without conducting site inspections, and then presents data estimations for costs, revenues, interest rates, and the valuation model. The analyzed sample, the baseline data given by ATER for each of them, and the redevelopment costs derived for 21 of them based on actual site inspections are briefly described in Sect. 3. Ultimately, Sect. 4 presents the findings, while Sect. 5 draws conclusions and outlines further developments.

2 Methods and Data

2.1 Approaches, Methods and Models

To assess the economic feasibility of the entire project, the study is conducted as follows (Fig. 1). Rehabilitation costs are first estimated on a subsample of 20 dwellings based on a detailed survey of deterioration and work needed, before calculating the square meter cost of intervention. Then, statistical techniques are used to determine the costs for all other flats, utilizing information provided by ATER (e.g., last allocation date, last release date). Net revenues from housing leasing are then identified. Once a 10-year phased market entry schedule for all 49 units is established, the sources of project funding, interest rates, and debt service schedule are analyzed. The financial plan is reviewed and verified to ensure its overall feasibility, based on a cost-revenue analysis, viability for lenders, and project feasibility for promoters.

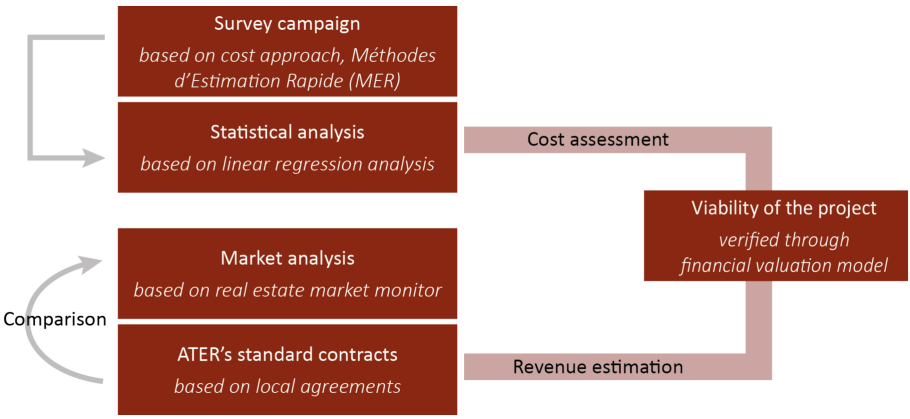

Fig. 1. Approaches used to assess the economic feasibility of the project

2.2 Cost Assessment

To estimate the redevelopment costs, the parametric and total costs for the redevelopment of the first core of 20 apartments are considered, calculated based on the survey conducted during the site inspections. The analysis of these data is done using economic statistical analysis software to compare them to the basic data available for all housing (last allocation date, last release date, floor level, gross and net floor area). Unit costs, total costs, and basic data are used as variables to fit linear regression curves (Fig. 2). The objective is to find a system that can recognize cause-and-effect relationships between them. These early models are examined, but no results of particular interest are found. Thus, a new criterion is assessed that turns out to be highly significant: a dichotomous variable associated with the illegal occupancy of the dwelling. Indeed, the maintenance status of a significant group of properties has been compromised because of that.

This first core of 20 dwellings is then divided into two subgroups based on the presence or absence of untitled occupations. The complementary criterion is the number of years since the last allocation, which is considered the most recent certain date of maintenance activities.

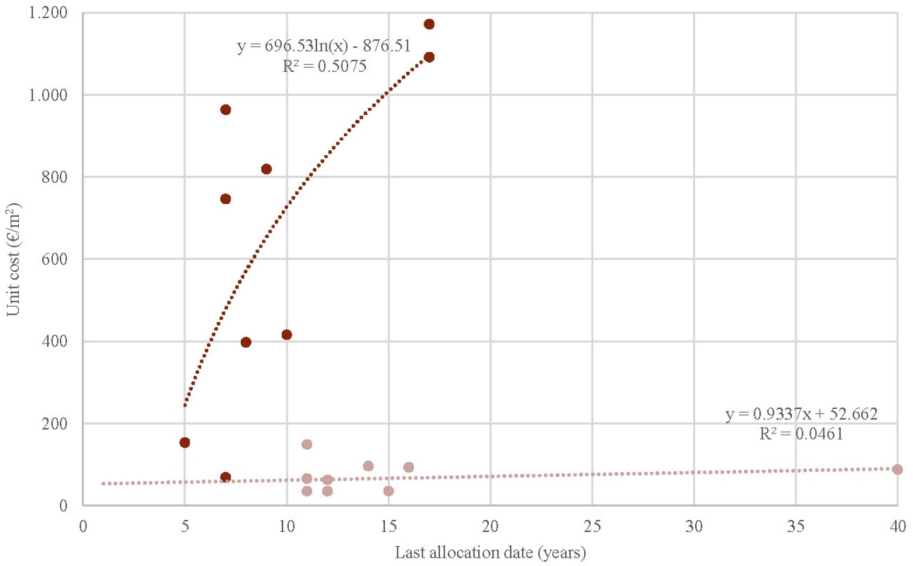

Fig. 2. Graphical linear regression analysis conducted to compare the unit costs of housing redevelopment to the last allocation date.

To determine the costs of renovation for the remaining 29 properties, two values are taken into account. For the first case of unoccupied properties, the median of their unit costs is considered, equal to €62.99. For the second case, the formula obtained from the statistical analysis is used:

$$Rc = 696.53 \ln (La)\text{-}876.51 \quad (1)$$

where *Rc* is the renovation's unit cost, while *La* stands for the number of years since the last allocation.

2.3 Revenue Estimation

Two sources are examined and compared to calculate housing rental fees and gross annual revenues once the first units are introduced to the market: the Real Estate Market Monitor (known in Italy as OMI) of the Italian Revenue Agency [7] and the so-called territorial agreements for the municipality of Venice, which ATER usually refers to sign social rent contracts [8].

OMI categorizes Venice's historic center into ten homogeneous areas based on uniform real estate values. OMI provides twice a year reports on the minimum and maximum market values and rental fees for various building typologies, intended uses, and conditions. The properties under examination will be rented in good condition, almost like new flats, but the same does not hold for the buildings they are in. Therefore, the average value of the rental fees is used in the analysis.

The territorial agreements for Venice's municipality are examined in relation to subsidized tenancies. Several oscillation bands are featured for different homogeneous areas. The fair rents vary within house ranges depending on the maintenance status of the flats and their equipment. Ultimately, the fair rent estimated according to the territorial agreements is approximately 20% lower than the OMI average rent.

The annual net revenues from leases are calculated by subtracting the following deductions, based on appraisal manuals and recent publications, from the gross sums [9–11]: administration costs (3.0%), vacancies and insolvencies (3.0%), maintenance (3.0%) and amortization (1.0%) costs, insurance costs (0.5%), and taxation, considering the tax concessions for these agreements (5.67%); resulting in a total deduction of 16.17%.

2.4 Timeline and Interest Rate

A timeline is established, featuring five groups of building units, distributed over time based on the scale and cost of maintenance (Fig. 3).

The time needed to complete work on the first group of apartments is estimated at roughly six months. The remaining groups are implemented gradually over a 10-year period, which is expected to be sufficient to complete the redevelopment of all 49 dwellings and repay the total debt.

It is assumed that ATER contributes 10.5% of the total funding. This amount can be used to cover the intervention costs for the first two groups of housing and as a guarantee for getting a loan from a lending institution. The latter will cover the remaining 89.5% of the expenses for redeveloping the three remaining groups.

The base interest rate is estimated as the average rate of 10-year fixed-rate mortgage loans, equal to 2.14% [12]. The spread is estimated based on the additional rate applied by the Italian Deposits and Loans Fund to public housing agencies, 1.25% for a 10-year maturity [13], leading to a total rate of 3.39%.

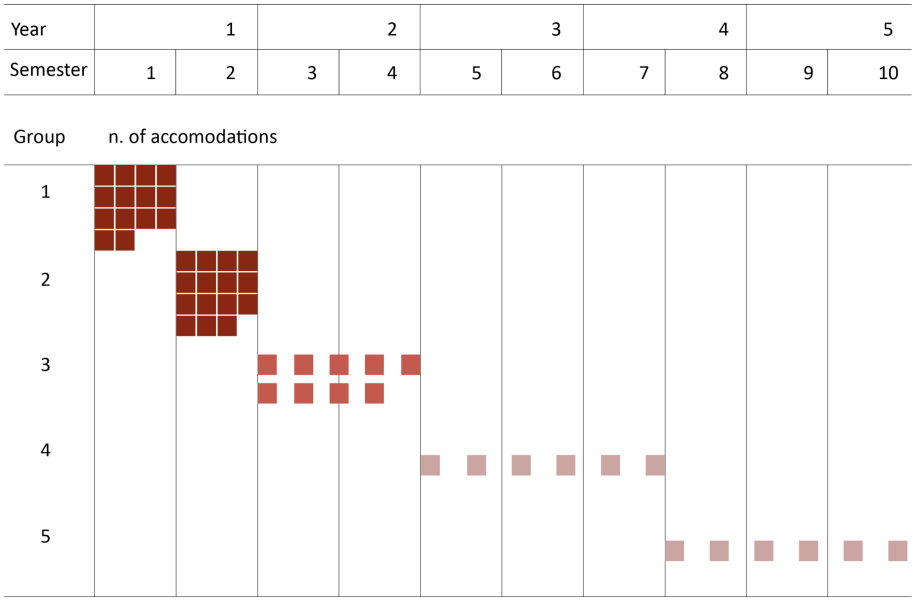

Fig. 3. Graphical diagram representative of the distribution over time of the works related to the groups.

2.5 Evaluation Model

A financial plan (FP) is developed for the analytical assessment of the economic viability of the project (Fig. 4). The initial analysis focused on the overall feasibility expressed by the Net Present Value (NPV). Then, the bankability for the lenders is considered, namely the ability of the project to repay the debt incurred and pay the interest accrued in each period. Lastly, the project's feasibility for the partners is analyzed, meaning the provision of social housing for its community from the University's perspective and asset value preservation from ATER's point of view.

Concerning the debt service, a ten-year amortization plan is created. Installments, paid in arrears and always of the same amount, are calculated according to the formula below:

$$I = D \cdot r / \left[1 - 1/(1+r)^n\right] \tag{2}$$

where: I is equal to the installment, D is the debt principal to be repaid, r is the interest on a half-yearly basis, and n is the number of installments.

Bankability is verified using the Annual Debt Service Cover Ratio (ADSCR), which measures the ratio between the year-by-year cash balance and the corresponding debt service. ADSCR should reach a minimum value of 1.35, as per the guidelines set by the national foundation of accountants association [14].

ATER's interest to ensure that its assets do not lose value over time is verified by setting a target yield (5.39%), which is slightly higher than the inflation rate estimated (2.1%) and includes an additional premium rate for capital immobilization over a ten-year time window (2%) [15, 16].

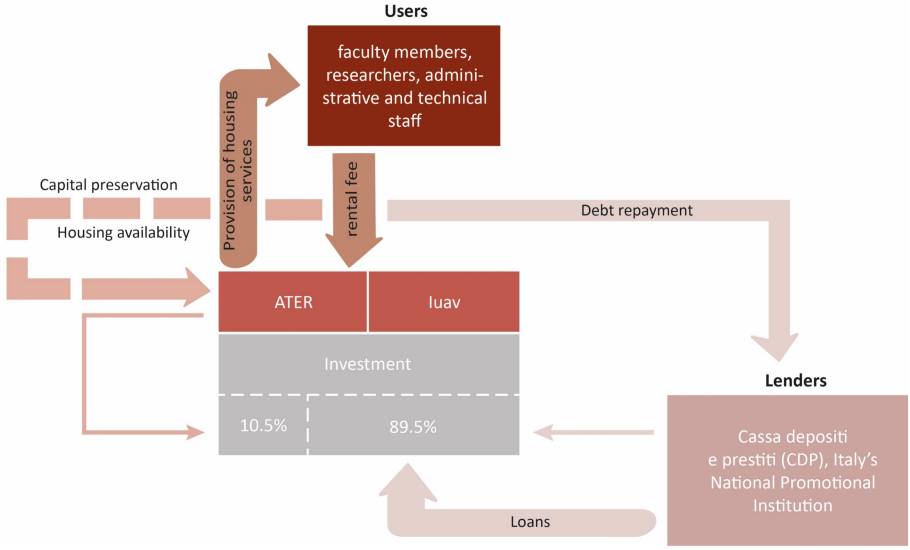

Fig. 4. Graphic representation of the financial plan that depicts the stakeholders involved.

3 Overview of the Property Sample

Following a first agreement signed in 2023 between ATER and the University Iuav of Venice, the public housing agency has provided a list of 169 accommodations spread throughout the historic center, except in the most central districts of San Polo and San Marco (Fig. 5). The 169 dwellings share the following characteristics: they are currently empty, they require renovation works that ATER can hardly afford to finance, and they are not intended for protected tenancies at social rents. Several of these building units are located in the same areas where major public housing construction initiatives took place in the 20th century [17]. Indeed, the buildings were constructed between 1901 and 1934 and have undergone various maintenance and building adaptations over time. However, there is no precise information on the date and type of the most recent maintenance work.

The accommodations differ in their maintenance status, classified as poor, mediocre, and excellent; surface area, ranging from 32 to 118 m2, with an average of 54 m2; and floor level, from ground to fourth, with an average between the first and second floors.

A sample of 49 units is chosen to assess the recovery intervention and its management. The extraction is conducted by increasingly ordering the homes according to three parameters: *La* (i.e., last allocation date) = number of years since the last housing allocation date, prioritizing the most recent ones as the last ones of intervention; *Lr* (i.e., last release date) = length of time since the last release date, which suggests the time since maintenance activities have ceased; *Oc* (i.e., period of occupation) = period of occupation (in months), which has proportionally affected the state of the place. Ordering houses in this manner will increase the likelihood of receiving housing in good condition, allowing the project to begin with lower costs and shorter renovation times. A

sample with better conditions than the overall average emerges, but it is still sufficient to represent the technical characteristics of the whole.

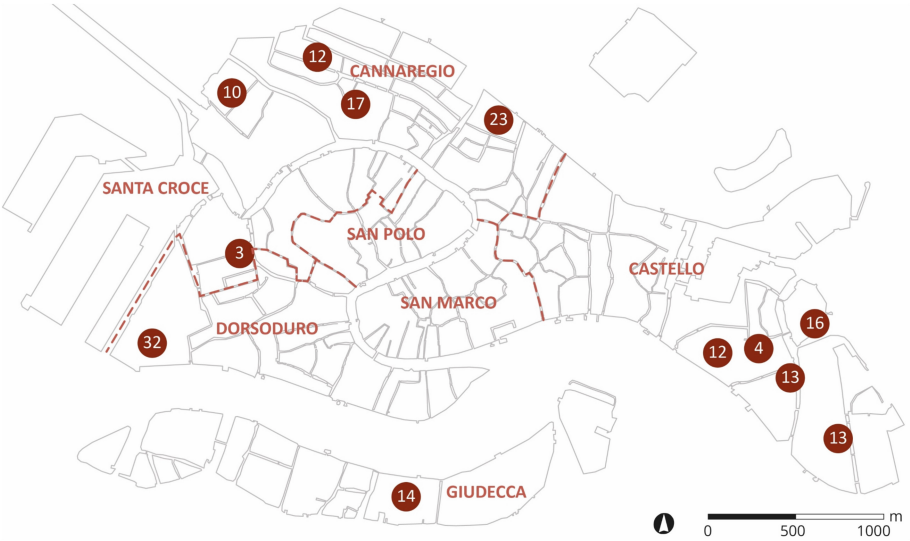

Fig. 5. Number of dwellings in Venice's historic center based on their location.

A survey campaign is carried out in 20 flats using a point survey sheet based on similar studies conducted in the 1970s and 1980s (Table 1, Table 2, Fig. 6). Depending on the extent of deterioration, the survey sheet assigns a score (from 1 to 4) to each building element and installation. The score is associated with the marginal restoration cost, expressed in €/m^2 for gross floor areas. By calculating the points assigned to each accommodation, we are able to determine the renovation cost per m^2, which in turn leads to the total maintenance costs. Related insights into cost estimation can be found in a recent dedicated publication [18].

Table 1. Excerpt of the survey sheet for the assessment of the deterioration: scores assigned during the survey (source: [18]).

Element	Score			
	Very good condition	Somewhat good condition	Somewhat poor condition	Very poor condition
	4	3	2	1
1. Internal wall cladding		X		
2. Independent heating system	X			

Table 2. Excerpt of the survey sheet for the assessment of the deterioration: the relationships between levels of deterioration and scores (source: [18]).

Element	Score	Description
Internal wall cladding	4	Excellent condition – no works needed
	3	Complete painting
	2	Partial renovation of plaster (up to 10%) and complete painting
	1	Complete renovation of plaster and painting
Independent heating system	4	Norm-compliant and excellent condition – no works needed works needed
	3	Boiler replacement
	2	Replacement of boiler and radiators
	1	Complete replacement of the heating system

Fig. 6. Images captured during the survey campaign. From left to right, the accommodations are classified as excellent, mediocre, and poor (source: authors' survey).

4 Results and Discussion

The model tested on the remaining 29 dwellings in the sample yields the following results. Table 3 displays the renovation costs obtained through statistical analysis and the rental fees. The renovation cost of the 49 apartments is expected to be close to one million euros, while their annual rent revenues will be approximately 0.3 million euros.

The cost estimation method used here lends itself to some additional remarks. The developed cost analysis model does not exhibit strong statistical significance, primarily due to the limited sample size of 20 apartments and the low R2 index associated with the curve fitted to the available data. Nevertheless, the results obtained are considered meaningful and provide relevant insights for the purposes of this study. The cost to restore a property that has never been unlawfully occupied since its last release is expected to be relatively low, ranging from 30 €/m^2 to 150 €/m^2, regardless of the last date of housing allocation. Indeed, this accommodation is considered to have remained closed and unused without undergoing any kind of significant degradation. Instead, the cost to refurbish a property that has been unlawfully occupied will be substantially higher, reaching up to 1,200 €/m^2, with an increase depending on the last allocation date.

According to the FP, the project has a high level of sustainability. From the beginning, the income generated by the rent payments is well beyond the repayment installment. This led to two thoughts. First, it is possible to maintain sustainability even in the event of delays. Even if the investment schedule drags out over time and subsequent housing groups delay in generating revenue, debt service can still be paid off due to the high degree of project feasibility. If this does not happen, then the project can be extended to the remaining 120 properties in the initial sample within a short period of time. Second, it is possible to decrease the rent. The project's economic viability is also confirmed by adopting a rent benchmark below average market rents, namely, agreed or fair rents.

The second observation is particularly important toward the goal of repopulating the historic center of the city, which is the main objective of this project. By accepting a small decrease in the bankability, which does not negatively impact the project's overall feasibility, rental fees can be decreased up to 28,5%. This change is significant because it reduces the average rental rate to nearly 8,50 €/m^2 monthly, which is closer to the social housing policies in Italy. The FP that comes from this choice can be seen in Table 4.

Table 3. Renovation costs obtained through statistical analysis and the annual revenues discovered. Data refers to 2024.

Ref	Unlawful occupation	UA	Unit cost (Eq. 1)	Gross floor area	Total cost	Area	Annual revenues
	(yes/no)	(years)	(€/m^2)	(m^2)	(€)		(€/y)
1	1	5	153.32	61	9,320	Castello east	5,436
2	0	6	62.99	46	2,918	Castello east	4,143
3	1	7	963.92	72	69,836	Dorsoduro	6,479
4	1	7	68.444	47	3,227	Cannaregio south	5,013
5	1	7	478.87	67	31,940	Castello east	5,964
6	1	8	397.33	83	32,899	Cannaregio north	7,404
7	1	7	746.29	84	62,650	Cannaregio north	7,507
8	1	7	478.87	56	26,692	Castello east	4,984
9	1	8	571.88	57	32,554	Cannaregio south	6,052
10	1	9	819.10	71	58,401	Cannaregio north	6,376
11	1	10	727.31	68	49,347	Castello east	6,067
12	1	10	415.68	79	32,983	Cannaregio north	7,096
13	0	11	35.46	68	2,405	Dorsoduro	6,067
14	0	11	35.46	63	2,242	Cannaregio north	5,656
15	0	11	35.46	61	2,161	Dorsoduro	5,450
16	0	11	62.99	43	2,680	Castello east	3,805
17	0	11	149.11	84	12,517	Castello east	7,507
18	0	11	66.02	63	4,175	Dorsoduro	5,656
19	0	11	62.99	53	3,324	Giudecca	4,719
20	0	11	62.99	68	4,273	Castello east	6,067
21	0	11	62.99	49	3,097	Giudecca	4,397
22	0	12	35.46	47	1,671	Cannaregio south	5,013
23	0	12	62.99	48	3,042	Cannaregio north	4,319

(*continued*)

Table 3. (*continued*)

Ref	Unlawful occupation	UA	Unit cost (Eq. 1)	Gross floor area	Total cost	Area	Annual revenues
	(yes/no)	(years)	(€/m^2)	(m^2)	(€)		(€/y)
24	0	12	62.99	60	3,766	Giudecca	5,347
25	0	14	95.98	72	6,953	Castello east	6,479
26	0	14	62.99	72	4,563	Castello east	6,479
27	1	14	961.67	37	35,389	Castello east	3,291
28	0	15	62.99	84	5,287	Castello east	7,507
29	0	16	62.99	46	2,897	Cannaregio south	4,891
30	0	16	62.99	47	2,951	Giudecca	4,191
31	0	15	62.99	74	4,636	Cannaregio north	6,581
32	0	15	62.99	52	3,259	Castello east	4,628
33	0	16	62.99	90	5,650	Cannaregio north	8,021
34	0	15	62.99	70	4,418	Cannaregio north	6,273
35	0	15	62.99	70	4,418	Cannaregio north	6,273
36	0	16	62.99	68	4,273	Cannaregio north	6,067
37	0	15	35.46	68	2,405	Castello east	6,067
38	0	16	62.99	53	3,332	Cannaregio south	5,624
39	0	16	93.26	71	6,649	Cannaregio north	6,376
40	1	17	1096.91	39	42,889	Castello east	3,496
41	1	17	1096.91	70	76,948	Castello east	6,273
42	1	17	1172.13	46	53,918	Dorsoduro	4,113
43	0	17	62.99	43	2,680	Castello east	3,805
44	0	16	62.99	72	4,563	Castello east	6,479
45	0	16	62.99	66	4,128	Cannaregio south	6,969
46	1	18	1136.72	54	61,439	Cannaregio north	4,833
47	1	17	1091.86	51	55,248	Castello east	4,525

(*continued*)

Table 3. (*continued*)

Ref	Unlawful occupation	UA	Unit cost (Eq. 1)	Gross floor area	Total cost	Area	Annual revenues
	(yes/no)	(years)	(€/m^2)	(m^2)	(€)		(€/y)
48	1	18	1136.72	63	71,897	Dorsoduro	5,656
49	0	40	87.77	47	4,138	Cannaregio south	5,013

Table 4. Financial plan developed for the analytical assessment of the economic viability of the project.

	Items	Units of measures	Values
	CAPITAL EXPENDITURE		
	Total redevelopment costs	€	979,260
	Total revenues	€	281,165
	TIMEFRAME		
ETC	Estimated Time of Completion	years	15
E	Equity	pct.	10.5%
D	Debt	pct.	89.5%
CoC	Cost of Capital		
ke	Cost of equity	pct.	5,39%
kd	Cost of debt	pct.	3,39%
wacc	Weighted cost of capital	pct.	3,60%
I	Instalment	€/semester	52,049
NPV	Net Present Value	€	1,570,231

5 Conclusion and Further Developments

The project is well-balanced, providing both economic and social benefits for all the involved stakeholders. By distributing the costs required for the redevelopment of the sample of 49 dwellings over time, the costs themselves can be covered by the revenue from housing entering the rental market. A system with economic self-sufficiency can be created. Therefore, the study presented demonstrates the project's economic sustainability and confirms its financial feasibility. Furthermore, it introduces the possibility of setting rent rates that are accessible to the majority of households, which addresses one of the primary causes of Venice's depopulation. This outcome aligns with the project's initial social objectives, which focus on promoting policy regeneration for the repopulation of the historic center.

The plan is capable of handling any adverse scenarios, such as lower-than-expected revenues, higher costs, and redevelopment times, as confirmed by the key indicators (ADSCR and NPV). This study suggests that the proposed plan can be applied positively to the entire property sample. It is feasible despite the advanced state of disrepair in some of them, which can lead to significant expenses when compared to the revenue generated.

Future developments are mainly focused on two strands. The research does not take into account measures aimed at improving the energy efficiency of the building units. Although higher costs may be introduced in the initial phase of work, they can still bring financial benefits to the property owner and tenants. Secondly, the accessibility issue is worthy of further investigation, as the dwellings require additional work to be made functional and suitable for various users, and especially for disabled people.

Acknowledgments. This paper is an outgrowth of IZ Master's degree thesis, defended at the University IUAV of Venice in spring 2025.

Disclosure of Interest. The authors have no competing interests to declare.

References

1. Zannini, A.: Il Turismo a Venezia Dal Secondo Dopoguerra Ad Oggi. Lab. Ital., 191–199 (2014). https://doi.org/10.4000/laboratoireitalien.848
2. Istat Popolazione Venezia 1871–2023 Available online: istat.it. Accessed on 1 Apr 2024
3. Pacione, M.: Venice, Cities 2, 290–296(1985) . https://doi.org/10.1016/0264-2751(85)90083-6.
4. Fregolent, L.: Cambiamenti Demografici e Socio-Economici Nella Venezia Contemporanea. In: La rivista di Engramma, vol. 155, pp. 163–174. Edizioniengramma (2018)
5. Basso, M., Di Croce, N.: Venezia: Casa, Spopolamento e Dinamiche Turistiche. In: Venezia città sostenibile, pp. 41–49. Anteferma Edizioni, Conegliano (2020)
6. Istat Censimento Della Popolazione e Delle Abitazioni Available online: istat.it. Accessed on 1 Sept. 2024
7. OMI Quotazioni Immobiliari Available online: agenziaentrate.gov.it. Accessed on 1 Nov 2024
8. Organizzazioni sindacali; Associazioni degli Inquilini e dei Proprietari Patti Territoriali 2018 Available online: comune.venezia.it. Accessed on 1 Nov 2024
9. Forte, C.; De' Rossi, B.: Principi Di Economia Ed Estimo, Milano, Etas (1979)
10. Orefice, M.: Estimo: UTET libreria: Torino, Vol. II, Estimo civile (1995)
11. Manuale Operativo Delle Stime Immobiliari. Agenzia del Territorio, Ed. Franco Angeli (2011)
12. Osservatorio Il Sole 24 Ore EURIRS. Available online: mutuionline.24oreborsaonline.ilsole24ore.com. Accessed on 5 Dec 2024
13. Cassa depositi e prestiti Condizioni Economiche Sintetiche Vigenti. Available online: cdp.it. Accessed on 5 Dec 2024
14. De Luca, R.; Lucido, N. Linee Guida per La Redazione Del Piano Economico-Finanziario Nelle Procedure Di Partenariato Pubblico-Privato: Aggiornamenti in Base al Nuovo Codice e Alla Prassi Recente Available online: fondazionenazionalecommercialisti.it. Accessed on 1 Dec 2024
15. Dipartimento del Tesoro Rendimenti All'emissione - 3° Trimestre (2024). Available online: dt.mef.gov.it. Accessed on 1 Dec 2024
16. Hoesli, M.; Morri, G. L'investimento Immobiliare. Mercato, Valutazioni, Rischio e Portafoglio, Milano, Hoepli (2010)

17. Ferrighi, A.lessandra:. Venezia e La Casa Salubre : Dai Piani per La Città Alle Abitazioni a Premio (1891–1925); Steinhaüser Verlag, Wuppertal (2020). ISBN 9783924774820
18. Bonifaci, P.; Donati, E.; Zelbi, I.; Copiello, S. Social Re-Housing in Venice. A Case Study on the Empty Dwellings of the Local Public Housing Agency. In: Oppio, A., Bottero, M., Stanghellini, S., Rossitti, M., (eds). Local Economic Systems and Housing Real Estate Markets in University Towns, pp. 17–32. Springer, Cham (2025)

Assessing the Liveability in the European Metropolitan Cities by Interpreting the Property Markets

Federico Stara(✉), Giuseppe Cerullo, Francesco Sica, and Francesco Tajani

Department of Architecture and Design, "Sapienza" University of Rome, 00196 Rome, Italy
federico.stara@uniroma1.it

Abstract. This study examines the functional relationship between urban liveability and residential property values in a sample of 53 European metropolitan cities. The underlying assumption is that housing prices incorporate not only the physical attributes of dwellings, but also the environmental, social, and economic factors of the urban context. To test this hypothesis, two hedonic models are estimated, using as dependent variables the average price per square metre of apartments located in the city centre and in the periphery. The explanatory variables include the Cost of Living, the Quality of Life, the Tree Cover, and the Population. The empirical results show high explanatory power for both models and confirm the statistical significance of all the variables considered. Among them, tree cover emerges as the most influential determinant of housing prices in both urban contexts, indicating the growing relevance of environmental quality in metropolitan housing markets. By contrast, the broader Quality of Life index appears less influential than variables associated with purchasing conditions and demographic pressure. These findings suggest that urban green infrastructure is more directly capitalised into the property values, whereas the social and service-related components of liveability exert a less immediate effect.

Keywords: Urban Liveability · Real Estate Prices · Tree Cover

1 Introduction

The contemporary urban landscape is undergoing a phase of profound transformation, in which the challenge of sustainability is inextricably intertwined with the need to ensure high standards of liveability for a population increasingly concentrated in large metropolitan hubs. In this scenario, European cities do not merely represent nodes of economic production and innovation but are configured as complex ecosystems where the quality of life of residents is constantly tested by conflicting pressures. On the one hand, the globalization and the international mobility have transformed historic centers into strategic assets for the global tourism market; on the other hand, the need to preserve the right to the city for local communities imposes an urgent reflection on the ways in which territory is managed and on the dynamics that regulate access to urban resources.

© The Author(s), under exclusive license to Springer Nature Switzerland AG 2027
O. Gervasi et al. (Eds.): ICCSA 2026 Workshops, LNCS 16761, pp. 380–393, 2027.
https://doi.org/10.1007/978-3-032-30527-5_25

Urban liveability, although a multidimensional concept and often difficult to define unambiguously, finds in many cases an effective synthetic indicator in the real estate market. As an expression of the preferences and the ordinary behaviors manifested during the negotiation phases by the actors operating in a given market, property prices can be interpreted as the economic materialization of the perception of social, environmental, and infrastructural well-being in a specific context. In economic terms, the housing prices reflect the capitalization of the so-called amenities: those locational advantages, tangible and intangible, that make one city more or less desirable than another. The subjects that purchase or rent a real estate unit are not simply paying for the physical property measured in square meters, but they are acquiring a "bundle of services" that includes proximity to green spaces, air quality, urban safety, the richness of the cultural heritage, and the social prestige associated with certain areas.

The delicate balance between attractiveness and liveability is now threatened by critical phenomena. The exponential growth of mass tourism (the so-called overtourism phenomenon) generates negative externalities that heavily affect the daily lives of residents [1]. Overcrowding, the rising cost of living, the saturation of public services, and the deterioration of environmental quality act as driving forces of displacement, transforming entire neighborhoods into areas with an exclusively tourist vocation and triggering gentrification processes that alter the original social structure. This friction between the tourism capital and the local social capital is directly reflected in the volatility of the real estate prices, creating increasingly marked spatial disparities between central cores, rich in amenities but congested, and peripheral areas, often characterized by fewer services but subject to different environmental pressures.

Within this framework, the present study aims to comparatively analyze 53 European cities, selected to represent the variety of the continent's development models, in order to interpret the preferences/needs in terms of liveability indirectly expressed in the property prices. The investigation seeks to answer crucial questions for urban planning and public governance: to what extent do environmental endowments, such as urban tree cover, contribute to the formation of real estate prices? Is there a measurable correlation between perceived quality of life and the market value of real estate? How do these dynamics change across different territorial areas within a city?

2 Aim

Through the development of hedonic models and the integration of accessible and open-source datasets, the research aims to make explicit the environmental and social variables that most affect operators' purchasing decisions and to highlight those that are most influential in the formation of property prices. The ultimate objective is not only to provide a statistical snapshot of the European real estate market, but also to offer policy makers and urban planners interpretative tools to promote resilient development models capable of fostering urban liveability and ensuring that economic growth does not occur at the expense of the quality of life of resident communities.

The present study arises from the need to decode the complexity of contemporary urban dynamics, placing emphasis on the dialectical tension between urban development and the safeguarding of urban liveability, while assuming the residential real estate market as the principal sensor and indicator of territorial imbalances.

The choice of the real estate market as an interpretative key is not accidental: it represents a "market of amenities" where prices do not merely reflect the physical value of the built environment, but also incorporate and externalize the benefits (or costs) deriving from the environmental, social, and tourist context. In particular, the research intends to verify and quantify the extent to which the different components of Quality of Life and environmental endowments affect the formation of real estate prices in metropolitan contexts subject to high international attractiveness.

The analysis is carried out on a heterogeneous sample of 53 cities with populations exceeding 500,000 inhabitants. The use of a harmonized dataset, integrating socio-economic indices extracted from crowdsourcing platforms with satellite environmental monitoring data, makes it possible to overcome the limits of purely local analyses, offering an overall view of the trends underway across the continent.

The structure of the contribution is articulated into five sections. Chap. 3 (Background) recalls the contributions of the international scientific literature on the themes of liveability, quality of life, and the relationship between amenities theory and real estate value. A specific focus is devoted to the phenomenon of overtourism, a current issue because of its influence on the quality of life of local communities, and to its evolution from an economic variable into a social and urban planning criticality. Chap. 4 (Method) illustrates the scientific basis of the hedonic pricing method, justifying the choice of the log-linear functional form and the use of logarithmic transformations for the dependent variables. Chap. 5 (Case study) presents in detail the constructed dataset: the criteria for selecting the sample of 53 European cities are presented, along with the analytical description of the variables (property prices in the city center, property prices in peripheral areas, cost of living, quality of life, tree cover, population), the data sources, and the normalization procedures applied to ensure the comparability of the estimated coefficients. Chap. 6 (Models) describes and comments on the two hedonic models obtained (one for the central area, the other for the peripheral area), attesting to the statistical and empirical reliability of the results. Finally, in Chap. 7 the conclusions are drawn, summarizing the main findings emerging from the research and outlining the practical implications in support of decisions for the development of public policies and city governance models, with a view to promoting resilient urban development oriented toward social and environmental sustainability.

3 Background

The starting point of the scientific debate on the contemporary city lies in the definition of liveability, a concept that Veenhoven (2011) [2] closely relates to "life satisfaction" and subjective well-being. According to the Author, livability represents the quality of the environmental context in which the individual operates, thus constituting a primary objective for policy makers who aim to guarantee high standards of happiness for the community.

However, the translation of this concept into concrete urban strategies presents significant interpretative challenges. As highlighted by Ruth and Franklin (2014) [3], liveability suffers from significant conceptual limitations due to its multidimensional nature; the Authors underline how the practical implications of planning must contend with the

difficulty of objectively measuring well-being in geographically diverse contexts, suggesting the need for models that go beyond abstract definitions in order to adhere to the real dynamics of the territory.

The economic analysis of liveability finds a solid foundation in amenities theory. According to Brueckner et al. (1999) [4], the spatial structure of cities and the distribution of different income groups depend closely on the relative advantage of the services and environmental endowments present in the urban fabric. In particular, the Authors point out that when the historic center has a strong advantage in terms of amenities compared to the periphery, dynamics of value polarization are triggered that attract the wealthier segments of the population, consolidating the prestige of the central core.

This approach was further developed by Glaeser et al. (2001) [5], who introduced the "Consumer City" paradigm. According to this theory, the success of contemporary metropolises is no longer linked exclusively to their productive function, but to their capacity to present themselves as centers of consumption of a high quality of life. A "livable" city must therefore offer a mix of public goods, architectural beauty, and environmental quality; in this context, the residential real estate market does not exchange only square meters, but reflects the economic value of the "right of use" of such urban amenities.

Environmental quality, however, does not represent a static value, since its perception and its economic impact can be eroded by external pressures and uncontrolled urban dynamics [6]. Jim and Chen (2006) [7] show how environmental elements significantly influence housing prices, but warn that such benefits are extremely sensitive to context: a deterioration of the urban environment or a saturation of public spaces can cancel out the economic "premium" generated by amenities.

With regard to the classification of environmental resources, Panduro and Veie (2013) [8] point out that urban green spaces do not constitute a uniform amenity, but rather a set of distinct goods whose impacts on housing prices vary significantly according to factors such as accessibility, maintenance levels, and the type of surrounding land use. In this context, the investigations conducted by Luttik (2000) [9] suggest that the presence of valuable landscape elements, such as trees, bodies of water, or views of open spaces, may determine an increase in the market value of residential properties, quantifiable on average between 8% and 10%.

The scientific literature, through the studies of Tyrväinen and Miettinen (2000) [10], further confirms that the benefits deriving from forest amenities and urban greenery are not only perceived qualitatively, but are translated into a direct increase in residential property prices as proximity to such areas increases. In this perspective, Gough (2014) [11] argues that the guarantee of sustainable well-being must be founded on the centrality of universal human needs, which represent the indispensable prerequisite for defining development policies capable of integrating environmental protection with the liveability of social contexts.

As highlighted by Biagi et al. (2020) [12], the well-being of the local population is closely influenced by urban tourism dynamics, which exert a significant impact on the quality of life of residents and make it necessary to carefully evaluate the trade-off between the economic benefits of the sector and the liveability of everyday life. In this context, Marans (2015) [13] considers it essential to deepen the links between studies on

urban quality of life and those on environmental sustainability, in order to identify new research opportunities that integrate citizens' well-being with the protection of urban ecosystems.

From a methodological point of view, Conway et al. (2010) [14] clarify that the analysis of the effects of green spaces on property values cannot disregard the use of spatial autocorrelation models, indispensable tools for accurately capturing how the geographical configuration of natural areas influences residential market prices.

Lazrak et al. (2014) [15] demonstrate how the application of spatial hedonic pricing models makes it possible to effectively quantify the market value of urban cultural heritage, highlighting how the conservation of historic assets generates an "ensemble effect" capable of significantly increasing the attractiveness and value of surrounding areas.

Within this scenario, the issue of the overtourism fits, which Dodds and Butler (2019) [16] define as the result of excessive tourism growth in areas where management is weak or lacking a long-term strategic vision. This phenomenon acts as a structural criticality that compromises local liveability, transforming residential neighborhoods into areas with an exclusively tourist vocation and generating negative externalities — such as noise, overcrowding, and the increase in the cost of living — that directly affect the quality of life of residents and the long-term stability of the real estate market [17].

In light of the evidence that has emerged, it appears clear that the protection of urban liveability cannot be entrusted to sectoral or emergency interventions. As argued by Capocchi et al. (2019) [18], overtourism and the consequent crisis of liveability are multidimensional phenomena that require a systemic vision. The Authors underline the importance of governance capable of integrating the economic, political, and environmental dimensions, shifting attention from the mere quantitative growth of flows toward the management of urban quality. Only through a profound understanding of the interconnections between the real estate market, environmental endowments, and external pressures is it possible to define resilient development models [19], capable of protecting the right to the city for resident communities and ensuring the sustainability of the urban system in the long term. Building on this literature, the present study contributes by addressing the still limited integration between overtourism assessment and residential market modelling, showing how tourism pressure interacts with socio-economic and settlement-related factors in shaping housing values at the intra-urban scale.

4 Method

Two hedonic price models (center and periphery) are obtained, by considering the market quotations for the two macro-areas as dependent variable. The methodological workflow of the study is summarized in Fig. 1.

Hedonic modelling seeks to explain the price of a complex good as a function of the characteristics that define it [20]. From a theoretical perspective, the observed price of the good can be decomposed into the implicit prices of its individual attributes. Such prices are not directly observable, because market transactions reveal only the overall price of the asset. According to the hedonic pricing principle, therefore, the set of characteristics incorporated into the asset determines its explicit market value [21].

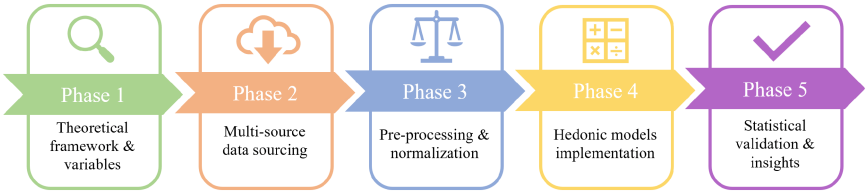

Fig. 1. Methodological workflow of the study. Source: authors' elaboration.

In real estate studies, hedonic price theory has been employed in several fields of application [22]. These include the prediction of property sale and rental prices [23], the measurement of the effects of social, environmental, and urban factors on property values [24, 25], the assessment of the implicit prices associated with specific property attributes [26, 27], and the examination of the role played by housing characteristics in shaping bargaining outcomes [28].

The empirical specification adopted in the present study is the log-linear one. The model is linear in the parameters and takes, as its dependent variable, the natural logarithm of the unit selling price, measured in euros per square meter of the property's floor area. Previous empirical findings indicate that the use of unit prices improves the goodness of fit of the specification [29]. The model can be expressed as follows in Eq. 1:

$$\ln Y = \alpha + \beta X + \varepsilon\# \tag{1}$$

where Y indicates the response variable, α corresponds to the intercept, β is the vector of coefficients to be estimated, $X = (X_1,\ldots, X_n)$ denotes the set of explanatory characteristics. The disturbance term ε accounts for random variation and unobserved stochastic effects, and is assumed to be normally distributed with mean equal to zero and variance σ^2. According to the literature, this functional specification is particularly well suited to the data [30].

5 Case Study

Using data extracted from "Numbeo" [31] for quality-of-life-related indicators [32, 33], from the "European Environment Agency's - Urban Tree Cover dataset" [34] for the environmental dimension, and from "Eurostat" [35] for the demographic variable, the study identified and analysed the main factors shaping the real estate market across 53 European metropolitan cities. The resulting integrated database enabled a comparative assessment of the determinants of housing market dynamics, with particular attention to the interplay between social, environmental, and demographic conditions. The variables included in the model, together with their acronyms, units of measurement, and data collection criteria, are described below.

1. Property prices *(Pc* and *Pp)*: measured in €/m^2, these represent the dependent variables of the study. In order to capture the dual structure of the urban housing market, the dataset distinguishes between the average price per square meter of apartments located in the city centre (Price City Center, Pc) and that of apartments located in peripheral areas (Price Periphery, Pp). This distinction is essential for testing whether environmental amenities exert differentiated effects according to urban location.

2. Cost of living (*C*): measured in euro, this variable is expressed through the indicator *"monthly costs for a single person, excluding rent"*. It is included as a control variable for purchasing power and the general price level in each city, thereby allowing the effects of the other independent variables to be isolated from the local inflationary context.
3. Quality of life (*Q*): this is a multidimensional index *"Quality of Life Index"* designed to estimate the overall quality of life in a city by considering several dimensions, including purchasing power, pollution, housing affordability, safety, healthcare quality, commuting time, and climate. Higher index values indicate better quality of life conditions. The inclusion of Q makes it possible to test the Consumer City hypothesis, assessing the extent to which overall urban well-being is reflected in real estate values.
4. Tree cover (*T*): measured as a percentage (%), this variable constitutes the key environmental indicator of the study. It serves as a proxy for the provision of urban green infrastructure and the ecosystem services delivered by the city, thereby enabling the quantification of the economic premium associated with natural amenities.
5. Population (*Pop*): the demographic dimension is introduced as a control variable for urban scale. It reflects both the pressure of potential demand and the agglomeration economies typically associated with large metropolitan areas.

Overall, the variables *Pc*, *Pp*, *C*, and *Q* were derived from Numbeo [31], *T* from the European Environment Agency [34], and *Pop* from Eurostat [35].

Table 1 reports the descriptive statistics of the variables considered in the analysis, calculated on the sample of 53 European cities. For each variable, the minimum value, maximum value, mean, and standard deviation (SD) are presented.

Table 1. Descriptive statistics of the variables

Variable	Min	Max	Mean	SD
Pc [€/m^2]	2,346.00	12,672.26	5,746.59	2,460.84
Pp [€/m^2]	1,077.32	8,599.05	3,536.09	1,566.55
C [€]	667.32	1,145.10	912.88	141.28
Q [no.]	115.90	213.10	170.93	27.30
T [%]	6.28	57.96	29.81	11.38
Pop [no.]	504,964.00	4,001,242.00	1,046,321.15	751,537.28

The data reported in Table 1 show that *Pc* has a mean value of 5,746.59 €/m^2 (SD = 2,460.84 €/m^2), with a minimum of 2,346.00 €/m^2 recorded in Palermo and a maximum of 12,672.26 €/m^2 observed in Paris. *Pp* exhibits a lower mean value of 3,536.09 €/m^2 (SD = 1,566.55 €/m^2), ranging from 1,077.32 €/m^2 in Genoa to 8,599.05 €/m^2 in Paris. *C* shows a mean of 912.88 € (SD = 141.28 €), with the lowest value registered in Sofia (667.32 €) and the highest in Amsterdam (1,145.10 €). *Q* has a mean value of 170.93 (SD = 27.30), with a minimum of 115.90 in Naples and a maximum of 213.10 in

Rotterdam. Regarding the environmental dimension, *T* records a mean value of 29.81% (SD = 11.38%), with values ranging from 6.28% in Zaragoza to 57.96% in Genoa. Finally, *Pop* presents a mean of 1,046,321.15 inhabitants (SD = 751,537.28), with a minimum of 504,964 in Lisbon and a maximum of 4,001,242 in Berlin.

Overall, the descriptive statistics suggest that the heterogeneity of the sample is most clearly reflected in the demographic and real estate dimensions. In the former case, the standard deviation of *Pop* is particularly high, reflecting the presence in the sample of cities that differ substantially in demographic size. In the latter case, greater variability emerges in *Pc*, which shows a higher standard deviation than that observed for *Pp* and, above all, for *C*. The latter variable instead displays a more contained distribution around its mean value, whereas *Q* and *T* occupy an intermediate position, indicating appreciable differences across cities, though less marked than those observed for *Pop* and for real estate prices.

The graphical analysis of the distributions, presented in Fig. 2, complements the synthetic information provided in Table 1 by offering a visual representation of data dispersion and the concentration of observations. These graphs are particularly useful for capturing the structure of the individual variables and for supporting a more in-depth interpretation of the differences across cities.

Figure 2 provides a graphical representation of the distribution of the variables included in the analysis. *Pc* is concentrated mainly between 4,000 €/m^2 and 8,000 €/m^2, with some observations above 10,000 €/m^2, whereas *Pp* is generally distributed between 2,000 €/m^2 and 4,000 €/m^2. *C* appears more compact, with most values lying between 700 € and 1,050 €, while *Q* is mostly clustered in the medium-high range of approximately 140–210. *T* is largely concentrated between 20% and 40%, whereas *Pop* shows the greatest asymmetry, with most cities below one million inhabitants and only a few observations reaching much higher values.

As required by the methodological protocol for multivariate regression models, the explanatory variables (*C, Q, T, Pop*) were subjected to a Min–Max normalization procedure. This transformation rescaled the original values to the [0, 1] interval, making the estimated β coefficients independent of their original units of measurement and allowing a direct comparison of the relative weight of each variable in shaping real estate prices. The normalization was performed according to Eq. 2:

$$X_{norm} = \frac{X - X_{min}}{X_{max} - X_{min}} \# \tag{2}$$

By contrast, the dependent variables (*Pc, Pp*) were log-transformed, as discussed in Chap. 4.

6 Models

The multiple regression analysis performed on the study dataset produced two model specifications, corresponding to the two dependent variables considered: *Pc* and *Pp*. The estimated coefficients and their levels of statistical significance are reported in Tables 2 and 3.

The coefficient of determination of the two models are respectively 0.904 and 0.903. For both models, the *Student's t* test on the significance of the individual explanatory

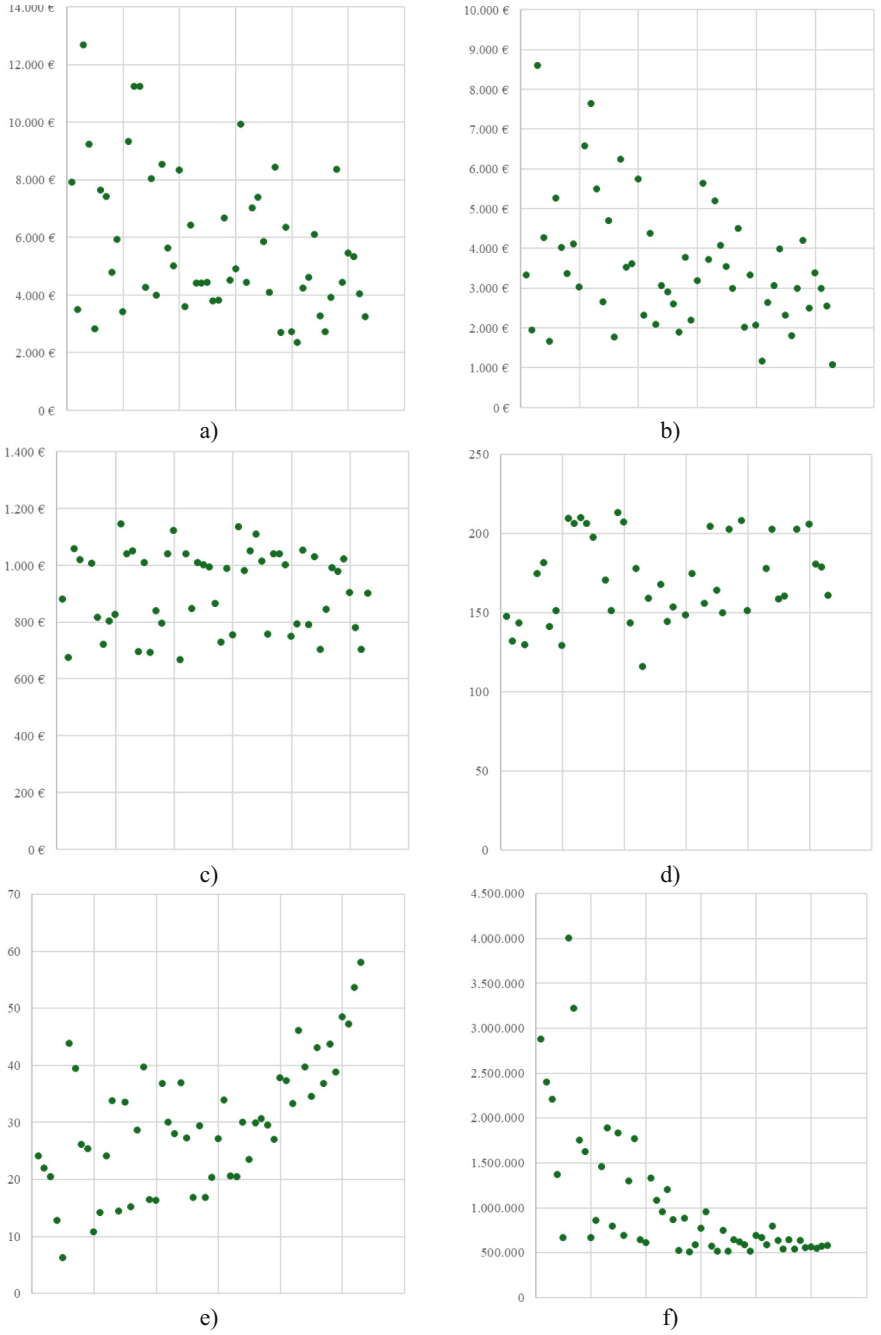

Fig. 2. Scatter plots of the variables included in the analysis: a) *Pc*, b) *Pp*, c) *C*, d) *Q*, e) *T*, and f) *Pop*. Source: authors' elaboration.

Table 2. Regression results on the sample for the center macro-area of the European metropolitan cities considered

Variable	Coefficient	Significance
Cost of living	4.606	***
Quality of life	4.023	**
Tree cover	5.945	***
Population	4.222	**

Notes: "***" is for <0.01, "**" is for <0.05, "*" is for <0.1.

Table 3. Regression results on the sample for the peripheral macro-area of the European metropolitan cities considered

Variable	Coefficient	Significance
Cost of living	4.300	***
Quality of life	3.961	**
Tree cover	5.416	***
Population	3.999	**

Notes: "***" is for <0.01, "**" is for <0.05, "*" is for <0.1.

variables indicates that all the variables offer a significant contribution to the explanation of the price. The F-Fisher test, performed at a confidence level of 95%, leads to the rejection of the hypothesis that the vector of the coefficients of the regression is zero. The standard error of the models is very good. The regression equation specification error tests, which reports any errors in the specification of the function adopted, the White test, relative to the absence of heteroskedasticity, and the Chow test, which verifies the existence of a structural break, have all p-values higher than 0.05, so that confirms the reliability of the two models. The values of the variance inflation factors (VIF) are all lower than 5, which endorse the absence of collinearity among the independent variables.

The estimated outputs give rise to several relevant considerations. In both models, tree cover emerges as the most influential variable in the formation of housing prices, followed by cost of living, population, and quality of life. These results suggest that, in large European cities, particular importance is attached to the environmental dimension, especially to the presence of urban greenery. At the same time, although quality of life is positively associated with property values, its influence appears slightly weaker than that of the variable linked to income and general purchasing conditions (cost of living) and that associated with potential housing demand (population).

Overall, the findings reveal a widespread and consolidated awareness of the strategic role played by urban green infrastructure in metropolitan contexts, particularly in relation to current environmental challenges such as the urban heat island effect [36]. By contrast,

factors contributing to the broader concept of quality of life appear to be less directly perceived in the housing market, despite their recognized importance. In this respect, the components underlying the Numbeo quality of life index — such as purchasing power, pollution levels, housing affordability, safety, healthcare quality, commuting time, and climate — seem to exert a more indirect effect on real estate values than the more immediately visible and spatially tangible contribution of urban tree cover.

7 Conclusions

The study conducted on a sample of 53 European metropolitan cities made it possible to outline a complex picture of the determinants of property values, offering relevant insights for urban governance and planning [37]. These results may also support property asset enhancement strategies based on the identification of suitable urban functions [38]. The research has investigated how liveability, interpreted through economic and environmental variables, is translated into market value, highlighting a hierarchy of parameters that reflects the priorities of residents and investors within the European context.

The overall analysis has shown that, in large cities, there is a clear sensitivity to the environmental quality. At the same time, it is noteworthy that the quality of life, considered in its broader multidimensional sense, appears to be slightly less influential than the variable associated with income conditions (Cost of Living) and that linked to demographic pressure (Population). The latter, in particular, continues to represent a major driver of housing demand, reflecting the persistent attractiveness of metropolitan centres despite the challenges affecting urban liveability. Overall, the results have revealed a widespread awareness of the importance of urban greenery — also in connection with the growing relevance of urban heat island issues — while the social and service-related factors embedded in the Quality of Life index appear to be less directly perceived in the housing market.

These findings also require further reflections on the composition of the indicators employed. The adopted Quality of Life index, based on Numbeo parameters, aggregates heterogeneous dimensions such as safety, healthcare, purchasing power, and pollution. Its comparatively lower statistical influence suggests that not all of its components weigh equally in housing decisions or in price formation [39]. This points to the need for future research to disaggregate this indicator in order to identify the individual components with stronger or weaker effects, which in turn requires an expansion of the database.

The study has also highlighted marked territorial disparities that urban planning cannot ignore [40]. Although tree cover emerges as a key factor in shaping property values, the data reveal critical contexts such as Rome, where tree cover remains particularly low compared with other European capitals. In such cases, housing demand may become disconnected from environmental quality, generating high-cost but low-liveability markets, with direct consequences for the long-term well-being of residents.

Within this framework, the issue of overtourism, already introduced in the opening sections, becomes especially relevant. The resilience of European cities depends on their capacity to protect the amenities that make them desirable. If green spaces and urban services become merely factors of valorisation for the tourism market or for elite

segments, there is a concrete risk of triggering displacement processes that progressively erode the residential function of cities.

In conclusion, the challenge for future urban policies lies in reconciling environmental enhancement with the social protection of quality of life. Only through a more granular monitoring of liveability factors and a management of tourism flows that does not undermine the residential market will it be possible to ensure that European metropolitan areas remain spaces of inclusion rather than mere arenas of speculation. A further line of research should therefore focus, on the one hand, on the construction of a broader dataset, and, on the other, on a more disaggregated examination of the variables underlying the Quality of Life index itself.

References

1. Gatto, R.V., Corrado, S., Scorza, F.: A taxonomy of specialized tourism ecosystems (STESY): toward new geographies for sustainable territorial planning. Int. J. E-Plann. Res. (IJEPR). **14**, 1–24 (2025)
2. Veenhoven, R.: Happiness: also known as "life satisfaction" and "subjective Well-being". In: Handbook of Social Indicators and Quality of Life Research, pp. 63–77. Springer (2011)
3. Ruth, M., Franklin, R.S.: Livability for all? Conceptual limits and practical implications. Appl. Geogr. **49**, 18–23 (2014)
4. Brueckner, J.K., Thisse, J.-F., Zenou, Y.: Why is Central Paris rich and downtown Detroit poor?: an amenity-based theory. Eur. Econ. Rev. **43**, 91–107 (1999)
5. Glaeser, E.L., Kolko, J., Saiz, A.: Consumer city. J. Econ. Geogr. **1**, 27–50 (2001)
6. Anelli, D., Morano, P., Tajani, F., Sabatelli, E.: Impacts of urban decay on the residential property market: an application to the city of Rome (Italy). Presented Int. Conf. Comput. Sci. Appl. (2024)
7. Jim, C.Y., Chen, W.Y.: Impacts of urban environmental elements on residential housing prices in Guangzhou (China). Landsc. Urban Plan. **78**, 422–434 (2006)
8. Panduro, T.E., Veie, K.L.: Classification and valuation of urban green spaces—a hedonic house price valuation. Landsc. Urban Plan. **120**, 119–128 (2013)
9. Luttik, J.: The value of trees, water and open space as reflected by house prices in the Netherlands. Landsc. Urban Plan. **48**, 161–167 (2000)
10. Tyrväinen, L., Miettinen, A.: Property prices and urban forest amenities. J. Environ. Econ. Manag. **39**, 205–223 (2000)
11. Gough, I.: Climate change and sustainable welfare: an argument for the centrality of human needs (2014).
12. Biagi, B., Ladu, M.G., Meleddu, M., Royuela, V.: Tourism and the city: the impact on residents' quality of life. Int. J. Tour. Res. **22**, 168–181 (2020)
13. Marans, R.W.: Quality of urban life & environmental sustainability studies: future linkage opportunities. Habitat Int. **45**, 47–52 (2015)
14. Conway, D., Li, C.Q., Wolch, J., Kahle, C., Jerrett, M.: A spatial autocorrelation approach for examining the effects of urban greenspace on residential property values. J. Real Estate Financ. Econ. **41**, 150–169 (2010)
15. Lazrak, F., Nijkamp, P., Rietveld, P., Rouwendal, J.: The market value of cultural heritage in urban areas: an application of spatial hedonic pricing. J. Geogr. Syst. **16**, 89–114 (2014)
16. Dodds, R., Butler, R.: Overtourism: Issues, Realities and Solutions. Walter de Gruyter GmbH & Co KG (2019)
17. Gatto, R.V., Scorza, F.: "Anti-gravity tourism planning": an analytical approach to manage tourism congestion, seasonality and overtourism. Urban Sci. **9**, 524 (2025)

18. Capocchi, A., Vallone, C., Pierotti, M., Amaduzzi, A.: Overtourism: a literature review to assess implications and future perspectives. Sustainability. **11**, 3303 (2019)
19. Anelli, D., Ranieri, R.: Resilience of complex urban systems: a multicriteria methodology for the construction of an assessment index. Presented at the International Symposium: New Metropolitan Perspectives (2022).
20. Rosen, S.: Hedonic prices and implicit markets: product differentiation in pure competition. J. Polit. Econ. **82**, 34–55 (1974)
21. Lind, R.C.: Spatial equilibrium, the theory of rents, and the measurement of benefits from public programs. Q. J. Econ. **87**, 188–207 (1973)
22. Morano, P., Tajani, F., Locurcio, M.: Land use, economic welfare and property values: an analysis of the interdependencies of the real-estate market with zonal and socio-economic variables in the municipalities of Apulia region (Italy). In: Sustainable Infrastructure: Breakthroughs in Research and Practice, pp. 414–437. IGI Global Scientific Publishing (2020)
23. Nguyen, N., Cripps, A.: Predicting housing value: a comparison of multiple regression analysis and artificial neural networks. J. Real Estate Res. **22**, 313–336 (2001)
24. Morancho, A.B.: A hedonic valuation of urban green areas. Landsc. Urban Plan. **66**, 35–41 (2003)
25. Brander, L.M., Koetse, M.J.: The value of urban open space: meta-analyses of contingent valuation and hedonic pricing results. J. Environ. Manag. **92**, 2763–2773 (2011)
26. Sheppard, S.: Hedonic analysis of housing markets. Handb. Reg. Urban Econ. **3**, 1595–1635 (1999)
27. Goodman, A.C., Thibodeau, T.G.: Housing market segmentation and hedonic prediction accuracy. J. Hous. Econ. **12**, 181–201 (2003)
28. Semeraro, P., Fregonara, E.: The impact of house characteristics on the bargaining outcome. J. Eur. Real Estate Res. **6**, 262–278 (2013)
29. Morri, M.H.G., Hoesli, M.: Investimento immobiliare. Mercato, valutazioni, rischio e portafoglio (2010).
30. Cassel, E., Mendelsohn, R.: The choice of functional forms for hedonic price equations: comment. J. Urban Econ. **18**, 135–142 (1985)
31. Numbeo - The biggest Internet Database about Cost of Living, Housing Indicators and many other informations about cities and countries!. https://www.numbeo.com/common/. Accessed 16 Mar 2026
32. Shu, Z., Carrasco, R.A., García-Miguel, J.P., Sánchez-Montañés, M.: Multiple scenarios of quality of life index using fuzzy linguistic quantifiers: the case of 85 countries in numbeo. Mathematics. **10**, 2091 (2022)
33. Salah, R., Elsappagh, H.: The NUBEO quality of life indicators methodology for analytical assessment of Urban Community public satisfaction and sustainable development. J. Eng. Adv. Technol. Sustain. Appl. **1**, 54–59 (2025)
34. Urban tree cover. https://www.eea.europa.eu/en/analysis/maps-and-charts/urban-tree-cover-dashboards. Accessed 16 Mar 2026
35. Database - Population and demography – Eurostat. https://ec.europa.eu/eurostat/web/population-demography/demography-population-stock-balance/database. Accessed 16 Mar 2026
36. Pilogallo, A., Scorza, F.: Mapping regulation ecosystem services specialization in Italy. J. Urban Plann. Dev. **148**, 04021072 (2022)
37. Morano, P., Anelli, D., Tajani, F., Roma, A.: The real estate risk assessment: an innovative methodology for supporting public and private subjects involved into sustainable urban interventions. Presented at the International Conference on Computational Science and Its Applications (2023).
38. Tajani, F., Morano, P., Di Liddo, F.: The optimal combinations of the eligible functions in multiple property assets enhancement. Land Use Policy. **99**, 105050 (2020)

39. Locurcio, M., Tajani, F., Anelli, D., Ranieri, R.: A multi-criteria composite indicator to support sustainable investment choices in the built environment. Valori E Valutazioni, 85–100 (2022)
40. Morano, P., Tajani, F., Di Liddo, F., La Spina, I.: The evaluation in the urban projects planning: a logical-deductive model for the definition of "warning areas" in the Esquilino District in the City of Rome (Italy). Smart Cities. **6**, 469–490 (2023)

Beyond Linear Impact: A Nonlinear Theory of Change and a Six-Level Indicator System for Evaluating Culture-Led Regeneration in Left-behind Territories

Giulia Candeloro(✉), Alessandro Crociata, and PierLuigi Sacco

Ud'A G. d'Annunzio University Chieti, Pescara, Italy
{giulia.candeloro,alessandro.crociata,pierluigi.sacco}@unich.it

Abstract. Left-behind territories have characteristics that are not easily identified using traditional impact assessment methods, in particular with regard to cultural-led initiatives. Evaluating cultural-led regeneration processes of such territories requires new assessment models capable of capturing processes of transformation that unfold across cognitive, relational, behavioural and socio-economic dimensions simultaneously. This paper presents a nonlinear, systemic Theory of Change (ToC) grounded in the capabilities approach and in the 4E cognition framework, implemented as part of the Metroborgo Observatory for the municipality of Montalto delle Marche (Marche region, Italy), selected as one of the beneficiary municipalities of the 'Bando Borghi' Line A under the Italian National Recovery and Resilience Plan (PNRR). The model conceptualises cultural investment as an activator of cognitive and relational processes, reconfiguring predictive models, expanding perceived agency and consolidating social cohesion, rather than as a direct generator of economic outcomes. The paper describes the resulting six-level indicator system comprising 36 indicators. It integrates composite indices derived from Likert-scale questionnaire items with direct indicators from secondary sources, including administrative records, business register data and mobile network-derived visitor flow estimates. The architecture is designed for longitudinal, independent-samples comparison and for disaggregated sub-group analysis, with explicit methodological provisions for addressing compositional confounds in low-density demographic contexts. The model contributes to the debate on multidimensional and evolutionary evaluation by proposing a socio-cognitive-behavioural framework that makes non-linear transformation processes observable and comparable over time.

Keywords: Theory of Change · Culture-led regeneration · Capabilities approach · 4E cognition · Indicator systems · Left-behind territories · Place-based development · Mixed-methods evaluation

© The Author(s), under exclusive license to Springer Nature Switzerland AG 2027
O. Gervasi et al. (Eds.): ICCSA 2026 Workshops, LNCS 16761, pp. 394–409, 2027.
https://doi.org/10.1007/978-3-032-30527-5_26

1 Introduction

The evaluation of cultural-led regeneration processes faces a persistent structural tension. On one side lies the need for measurable, accountable outcomes that satisfy the requirements of public funders and programme managers; on the other, the recognition that the most significant effects of cultural investment, for instance on individual agency, social cohesion, place identity and long-term behavioural change, are complex, distributed over time and not directly traceable to specific inputs.

Standard impact evaluation frameworks, including the logical framework approach (LFA) and its derivatives, address this tension by positing a linear causal chain from inputs to outputs, outcomes and impact. This scheme is both practically tractable and institutionally legible, but it systematically underestimates the role of intermediate cognitive and relational mechanisms through which cultural interventions generate effect.

In territories characterised by structural marginalisation, that is small municipality in mountain or inland areas with declining population, weak institutional capacity and limited economic alternatives, this underestimation risks to produce evidence that confirms the operational success of a programme while remaining blind to whether it has modified the conditions that generate territorial decline.

This paper presents the theoretical architecture and indicator system developed for the Metroborgo Observatory, a cultural impact monitoring initiative for Montalto delle Marche, a small municipality (2,300 inhabitants) in the inland Marche region of central Italy. The Observatory is designed to evaluate the medium- and long-term impact of a broad cultural regeneration programme, such as the "Bando Borghi" Line A of the Italian National Recovery and Resilience Plan (PNRR).

The contribution of the paper is twofold. First, it presents a nonlinear Theory of Change grounded in the capabilities approach and in the 4E cognition framework, which conceptualises cultural investment as an activator of cognitive and relational processes rather than as a direct generator of economic outcomes. Second, it describes the six-level indicator system that operationalises this ToC, integrating composite indices, derived from a purpose-built questionnaire, with direct indicators from secondary administrative and statistical sources.

The paper is structured as follows. Sect. 2 reviews the limitations of linear ToC models in cultural and territorial evaluation and introduces the systemic alternative. Sect. 3 presents the theoretical framework. Sect. 4 describes the questionnaire. Sect. 5 discusses the indicator system and its methodological architecture. Sect. 6 concludes.

2 Theorethical Framework

2.1 The Limitis of Linear Models in the Evaluation of Cultural-Led Processes

The standard Theory of Change approach [1] is based on an input-output-outcome logic inherited from programme theory [2, 3]. Resources invested generate activities; activities produce outputs; outputs, under the right conditions, generate intended outcomes; outcomes accumulate into long-term impact. This sequential structure is well-suited for the understanding of public funders or programme managers, or for any interventions where the causal mechanisms is recognizable because of clear competence targets. In cultural

regeneration processes, however, this linearity is structurally insufficient for at least three reasons. First, the mechanisms through which cultural interventions produce effects are not merely transactional but cognitive and relational. That means that they operate by modifying how people perceive and relate to their environment. The effect of opening a cultural space depends primarily on whether the experience reconfigures expectations, activates latent agency or consolidates community bonds. Second, the temporal structure of impact is non-linear. Some effects are rapid and easily observable (participation rates, visitor numbers), while others, namely changes in perceived self-efficacy, in the local sense of place, in the propensity to invest, are slow-forming, cumulative and only detectable over multiple observation cycles. Third, in structurally marginalised territories, the presence of an aesthetic trap [4] means that heritage valorisation and cultural activation do not automatically translate into expanded life chances for residents: without an effect on internal representations and perceived opportunity sets, even substantial investment may fail to generate systemic activation. The ToC adopted in the Metroborgo Observatory responds to these limitations by integrating three complementary theoretical bodies, described in the following paragraphs.

2.2 Capabilities Approach and Territorial Development

The capabilities approach, as originally formulated by Amartya Sen è [5] and further developed by Martha Nussbaum [6] and Ingrid Robeyns [7], distinguishes between resources (means), functionings (achieved states of being and doing) and capabilities (real opportunities to achieve those functionings). Applied to territorial development, and in particular to the place-based development paradigm [8], this framework redefines the objective of public investment as the expansion of the conditions under which local actors can effectively convert available opportunities into choices and actions.

Cultural regeneration, in this perspective, is about expanding territorial capabilities, namely the ensemble of conditions (cognitive, relational, material) that make it possible for residents to imagine, choose and construct their collective future rather than increasing cultural supply or tourist attractiveness. This reframing has direct evaluative implications: the relevant question whether the intervention has modified the perceived capacity of people to contribute to territorial life, strengthened the relational fabric that enables collective action, and generated new orientations toward the future.

2.3 4E Cognition, Embodied Simulation and the Aesthetic Trap

The 4E model of cognition [9] describes cognition as a process that is embodied, which means shaped by bodily states and sensorimotor capacities), enacted, namely constituted through action-environment interaction, extended, or distributed beyond the boundaries of the brain into tools and built environments, and embedded, i.e. shaped by social and material context. This framework dissolves the boundary between individual cognition and environmental affordances, making the built and cultural environment a cognitive resource that shapes how people perceive and act.

Embodied simulation theory [10] further specifies the mechanism. Cultural experiences are active simulations capable of mobilizing the motor, emotional and sensory resonance systems. Narrative devices, spatial configurations and participatory practices

act as predictive scaffolds that can modify the internal models with which individuals anticipate what the territory can offer them [11]

The predictive processing framework [11, 12] provides the formal architecture for understanding this process. Under this account, the brain continuously generates top-down predictions about sensory input and updates its generative model in response to prediction errors, namely discrepancies between what is expected and what is encountered. Action and perception are jointly optimised to minimise expected free energy, a quantity that bounds the long-run surprise an organism will encounter. Crucially, the system does not weight all prediction errors equally. Precision weighting determines which errors are treated as informative and which are suppressed. High precision assigned to a prediction error amplifies its influence on model updating; low precision attenuates it.

In structurally marginalised territories, this cognitive dimension is particularly critical. We have previously introduced the concept of the aesthetic trap [8], a condition in which the cultural and landscape heritage of a territory is valorised and recognised without this valorisation translating into transformed opportunity sets for residents. Residents who have experienced prolonged economic decline and institutional neglect develop generative models characterised by low expected precision on signals of opportunity: positive developments are discounted as noise rather than treated as evidence that the environment has changed. The trap can be understood in these terms as a condition in which the sensory richness of heritage and landscape generates positive valence without triggering the prediction errors necessary to update the generative model of territorial agency.

2.4 Integrating Capabilities and Predictive Processing

The capabilities approach and the predictive processing operate within different field (normative political philosophy and computational cognitive sciences respectively) but we can state that they converge on a shared structural insight. Capabilities, indeed, depend on conversion factors that determine whether a formally available resources becomes a substantive freedom. On the other hand, we can posit a conversion factor in predictive processing terms as a set of precision-weighted priors that determine whether an available opportunity generates a tractable action policy, one whose expected free energy is low enough to be selected over the default of inaction.

On this account, capabilities expansion is the reconfiguration of the generative model such that previously available but subjectively inaccessible options become actionable. A resident who has always had the formal possibility of starting a local enterprise but whose generative model assigns high expected free energy to that action (anticipating failure, bureaucratic obstruction, social disapproval) does not possess the corresponding capability in any substantive sense. The capability becomes real when the precision structure shifts. That is, when new evidence, for example a successful peer, a supportive institutional signal, an embodied experience of competence in a cultural workshop, updates the model sufficiently to lower the expected free energy of acting.

This integration has two consequences for evaluation design. First, it identifies the critical intermediate variable the transformation of the precision-weighted generative models that mediate between them (Levels 2-3, § 4.3). Second, it explains why the same intervention can succeed in one context and fail in another: the effect depends on the

prior state of the generative model and on the precision the intervention manages to assign to the prediction errors it generates.

3 A Non Linear Theory of Change: Six Interdependent Levels

3.1 The Model

From this theoretical architecture, our ToC takes the form of a dynamic, circular model represented as concentric rings, each corresponding to a level of analysis and measurement (Fig. 1).

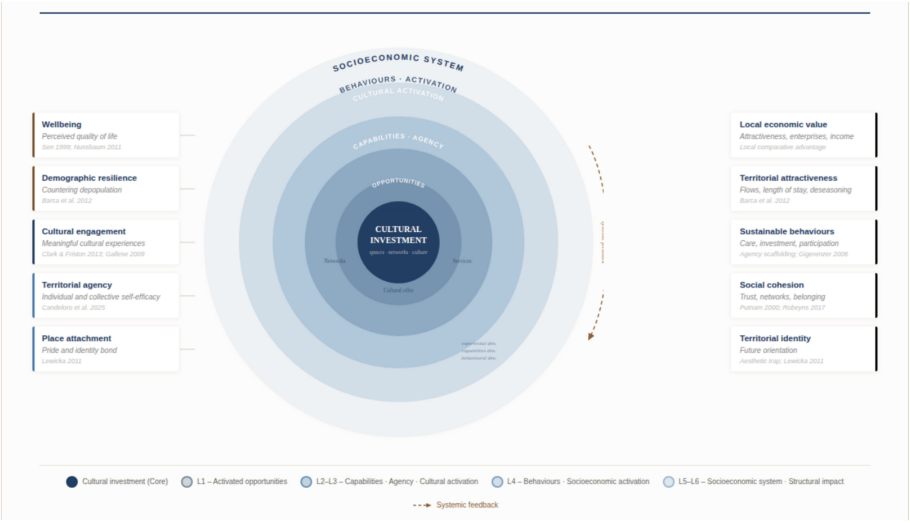

Fig. 1. The Non-Linear Theory of Change

Level 1 | Outputs and Activated Opportunities. The innermost ring represents the direct and immediately observable results of cultural investment: the recovery of architectural heritage, the activation of cultural spaces, cultural programming, the establishment of new businesses, the mobilisation of public and private resources, and the construction of collaborative networks among local actors. These elements constitute an expansion of the opportunity set available to the territory, but do not yet represent impact. They are the necessary precondition for the activation of subsequent levels, not its sufficient cause.

Level 2 | Capabilities and Agency. The second level concerns the transformation of the cognitive and relational conditions that determine whether the opportunities generated at Level 1 are effectively accessible and convertible into action. Four dimensions are operative here. Self-efficacy [13] captures the perceived capacity of individuals to contribute actively to territorial life and to initiate or participate in local initiatives. In predictive processing terms, self-efficacy corresponds to the precision assigned to action–outcome

contingencies: high self-efficacy reflects a generative model in which one's own actions are expected to produce meaningful effects. Social cohesion [14] encompasses the trust, collaboration and sense of community belonging that enable the conversion of individual capacity into collective action [15]. Place attachment [16] captures the emotional and identity bond with the territory, which the literature identifies as a predictor of behaviours of care, permanence and investment. For visitors, the quality of the visit experience constitutes the relational condition for deeper forms of engagement.

Level 3 | Cultural Activation. The third level captures the cognitive and emotional activation generated by cultural experiences, understood not as mere attendance at events but as an active process of sense-making and horizon-expansion. Cultural engagement describes the degree to which an experience reconfigures the predictive models through which individuals anticipate what the territory can offer them. In the terms developed in Sects. 2.4, this is where the precision structure shifts: effective cultural engagement generates the salient prediction errors that force model revision in the domain of agency and territorial possibility. This is the pivotal level of the model: it is the mechanism through which the opportunity expansion of Level 1 begins to modify the capabilities structures of Level 2, and through which the conditions for behavioural activation at Level 4 are generated.

Level 4 | Behaviours and Socioeconomic Activation. The fourth level captures the observable translation of expanded capabilities and cultural engagement into concrete practices. For residents, this means sustainable behaviours toward public spaces, attention to the future consequences of present choices, and civic participation. For visitors, it means responsible behaviours, local value creation, and intention to return. This level is the critical threshold at which change could become consolidable since behaviours, unlike attitudes, are observable by third parties, generate external effects and can be reinforced or disrupted by the social environment.

Level 5 | Socioeconomic System Outcomes. The fifth level captures the cumulative effects of the transformations at Levels 1-4 on the socioeconomic system of the territory. Subjective wellbeing, perceived income and property value changes, perceived environmental quality and business dynamics are tracked through both questionnaire and administrative sources. The outcomes at this level are not directly generated by investment. Rather, they emerge from the cumulative interaction of opportunity expansion, capability transformation, cultural activation and behavioural consolidation at the preceding levels.

Level 6 | Structural Cohesion and Demographic Dynamics. The outermost ring represents the long-term structural dimension of territorial transformation, detectable only over multiple years of observation. Population trends, age structure, new residents, voluntary participation, mutual-aid networks, perceived security, access to essential services, cultural inclusion and institutional capacity define the evaluative horizon of the model: the ultimate criterion of success is not increased visitor numbers or short-term investment, but whether the territory has become more capable, more cohesive and more demographically sustainable.

3.2 Cross-Level Dynamics and Evaluation Implication

The circular shape of the model is shown for clarity of exposition, but the six levels do not operate in a fixed sequence. Level 3 cultural engagement can precede and generate Level 2 capability changes rather than following them; Level 4 behavioural practices can reinforce Level 2 social cohesion; Level 5 economic outcomes feed back into the Level 1 opportunity set, modifying the context in which new investment is designed and implemented. A significant cultural experience can strengthen place attachment; stronger place attachment can stimulate behaviours of care; diffuse care behaviours can improve perceived environmental quality; improved environmental quality can attract new visitors or temporary residents; such attraction can generate economic effects that redefine the opportunity set for the next planning cycle.

This nonlinearity has specific consequences for evaluation design. Three are worth highlighting. First, the indicator system must support cross-level association analysis at the aggregate level: the capacity to test, for instance, whether population-level increases in Level 3 cultural engagement scores in wave t are associated with population-level increases in Level 2 self-efficacy scores in wave $t + 1$, or whether Level 4 behavioural activation co-varies with Level 2 social cohesion within the same wave. Because the design relies on independent samples rather than individual tracking (see Sect. 5.2), these associations are detectable as shifts in population distributions across waves, not as within-person trajectories; they provide indirect evidence for the feedback dynamics posited by the model, but do not support strict causal mediation inference. Second, the evaluation must accommodate differential temporal signatures across levels: rapid effects at Levels 1 and 3 (infrastructure delivery, event-driven engagement), medium-term consolidation at Levels 2 and 4 (capability and behavioural change), and slow structural shifts at Levels 5 and 6. A purely synchronic snapshot would collapse these temporal strata. Third, the distinction between shallow and deep interventions has measurable consequences: shallow interventions produce rapid, easily observable effects at Levels 3-4 that may not persist once the scaffolding is removed; deep interventions produce slower changes at Level 2 that, once consolidated, generate self-sustaining behavioural trajectories at Level 4. The indicator system is designed to detect both levels of effect and to track the processes of consolidation through which shallow activations may deepen over time.

4 Indicator System and Instrumentation

4.1 Architecture and Design Principles

The indicator system operationalises the nonlinear ToC through 36 indicators organised across six levels. The architecture is designed around three principles. First, multi-source triangulation: each level integrates at least one primary source (questionnaire) and, where available, secondary administrative or statistical sources, ensuring cross-validation and reducing the risk of source-specific bias. Second, methodological complementarity: composite indices and direct observational indicators are treated as analytically distinct but interpretively integrated capturing subjective and relational dimensions inaccessible to

administrative data and anchoring the evaluation in externally verifiable facts. Third, longitudinal comparability: all instruments maintain invariant structure across observation cycles, enabling independent-samples comparison over time.

The following subsections describe each level's indicators and their questionnaire operationalization in a single integrated presentation. The primary data collection instrument is a purpose-built questionnaire structured in four groups. Group 0 contains a routing question (G0Q00: «Do you live in or regularly visit Montalto delle Marche?») that directs respondents to either the residents' module (Group 1, annual administration) or the visitors' module (Group 2, seasonal administration). Groups 3 and 4 are common to both. The instrument is designed for mixed administration, online via link or QR code and assisted in-person, to reduce digital exclusion risk in a small, partially elderly population.

The residents' module opens with a profiling question on length of residence or regular frequentation (G1Q01: less than 1 year / 1-5 / 6-10 / over 10 / lifelong), used for sub-group disaggregation and for the compositional confound mitigation strategy described in Sect. 5.2. The visitors' module opens with six profiling questions covering first-visit status (G2Q01), type of visit, day trip, weekend or extended stay (G2Q02), main motivation, namely work, study or leisure (G2Q03), group composition (G2Q04), and event participation (G2Q05-G2Q06). These variables are not included in the indicator matrix but are essential for sub-group disaggregation, equity analysis and the detection of differential activation patterns across visitor types.

Both modules include closing items that fall outside the indicator system. The residents' module closes with a question on whether the respondent believes the project can foster new enterprises in the cultural, creative and tourism sectors (G1Q10) and an optional open-ended question on expected changes in territorial and personal life (G1Q11). The visitors' module closes with an optional open-ended question on the most significant aspect of the experience (G2Q13). Group 4 collects sociodemographic contextual variables: gender including non-binary option (G4Q01), age bracket (G4Q02), educational attainment (G4Q03) and occupation (G4Q04), which are indispensable for sub-group disaggregation but are not part of the indicator system.

4.2 Level 1:Outputs and Activated Opportunities

Seven indicators capture the direct results of cultural investment. Five are drawn from administrative and accounting sources: recovered architectural heritage (m^2), cultural spaces activated, cultural programming (events/year), new businesses established, and investments mobilized (€). Two perception-based indicators complete the level: satisfaction with investments (G3Q05) and perceived external visibility (G4Q05), both measured as single items on five-point ordinal and binary scales respectively. These indicators establish the factual baseline of what has been done and confirm that the intervention has generated an expanded opportunity set.

4.3 Level 2-3: Capabilities, Agency and Cultural Activation

Six composite indices capture the transformation of internal representations and relational conditions that the ToC posits as the critical intermediate mechanism.

At Level 2, the residents' module contributes three composite indices. Territorial agency / self-efficacy (G1Q02) comprises four Likert 1-7 items probing: the sense of being able to contribute actively to territorial life; the perception of being capable of acting in the face of local problems or opportunities; the sense of being heard when expressing ideas or proposals; and confidence in one's own capacity to initiate or participate in local initiatives. Social cohesion (G1Q03-Q05) comprises three Likert 1-7 items measuring perceived collaboration, sense of community belonging and mutual trust, complemented by two binary closure questions assessing the specific effect of the Metroborgo project: whether the respondent has perceived an improvement in social life (G1Q04) and whether they have engaged in dialogue with people from different cultural backgrounds (G1Q05). The binary items are analyzed as direct indicators (percentage distributions) and interpreted jointly with the Likert composite, enabling a degree of programme-attributional inference while preserving integrity. Place attachment (G1Q06) comprises four Likert 1-7 items: emotional bond with the place, pride in living there, identity connection, and anticipated regret of having to leave. The visitors' module contributes a quality-of-visit-experience index (G2Q07, four items: overall experience quality, sense of welcome, clarity and accessibility of spaces, perceived authenticity).

At Level 3, cultural engagement is measured via two five-item composite indices, one for residents (G1Q07) and one for visitors (G2Q08). The residents' items investigate participation in local cultural activities; stimulation toward new learning; reflection on the territory's present and future; sense of active involvement rather than passive spectatorship; and the role of culture in daily life. The visitors' items inquire understanding of the territory facilitated by activities; new learning; active involvement; emotional impact of places and stories; and capacity for reflection. Both indices are grounded in the predictive processing framework developed in Sect. 2.4: their items are designed to capture not mere attendance but experiences of novelty, disrupted expectations and expanded horizons that the theoretical model identifies as the mechanism of cognitive reconfiguration. An additional direct indicator, associative and civic participation, is drawn from municipal records and periodic surveys.

4.4 Level 4: Behaviours and Socioeconomic Activation

Five indicators capture the observable translation of expanded capabilities into practices. Sustainable behaviours among residents (G1Q08, four Likert 1-7 items) investigate attention to the care of public spaces; consideration of the future consequences of present choices; reduction of environmental impact in daily life; and adoption of respectful behaviours in public and cultural spaces. Responsible behaviours among visitors (G2Q09, four items) investigate respect for places and people; attention to the impact of one's own actions; awareness of the territory's value gained during the visit; and sense of responsibility toward future visits. Local value creation by visitors (G2Q10, five items) tracks interaction with local people; use of local services and products; perception of having contributed positively to the territory; propensity to recommend the experience; and intention to return or extend the stay. Two direct indicators complete the level: propensity to local investment (G3Q06–Q07, recording whether the respondent has made economic investments as a result of the project, and their approximate amount

by bracket) and visitor expenditure broken down by category (G2Q12: accommodation, food and drink, local products, transport, cultural activities).

4.5 Level 5: Socioeconomic System Outcomes

Eight indicators cover subjective wellbeing and system-level effects. Two composite indices measure wellbeing; for residents (G1Q09, five Likert 1-7 items: life satisfaction in the territory, perception of the place as wellbeing-promoting, contribution of social relationships to quality of life, positive perspectives on the community's future, mental and emotional wellbeing); for visitors (G2Q11, five items: general wellbeing during the visit, relaxation and stimulation, sense of connection with the place, enrichment of time, positive feeling at departure). Three direct ordinal indicators use five-point scales: perceived income change (G3Q01), perceived property value change (G3Q02) and perceived environmental quality (G3Q03). A further direct ordinal indicator tracks the influence of project investments on quality of life (G3Q04). These four items, though sharing the same response format, measure conceptually distinct constructs and are therefore treated as separate direct indicators. Two secondary-source indicators complete the level: local economy and businesses (business registers, INPS, ISTAT) and tourist attractiveness (ISTAT, accommodation records, mobile network-derived visitor flow estimates).

4.6 Level 6: Structural Cohesion and Demographic Dynamics

Ten indicators track the long-term structural dimension of territorial transformation: population trend, age structure / dependency ratio, new residents, participation and volunteering, proximity networks and mutual aid, social conflict and integration, perceived security, access to essential services, inclusion and accessibility, and institutional capacity. These indicators are derived primarily from administrative sources (ISTAT, municipal registry) and periodic surveys to be activated in subsequent phases of the Observatory, once a consolidated baseline has been established at Levels 1-5. This level is included in the matrix from the very beginning, before the data are available, because it specifies the evaluative horizon of the model (Table 1).

Table 1. Six.level indicator matrix for the Metrobrgo Observatory

Level	Dimension	Indicator	Source	Type
L1	Outputs	Recovered architectural heritage (m^2)	Municipal office / OpenCoesione	Direct
L1	Outputs	Cultural spaces activated	Municipality / managers	Direct
L1	Outputs	Cultural programming (events/year)	Cultural office / AMAT	Direct
L1	Outputs	New businesses established	Business register / INPS	Direct

(*continued*)

Table 1. (*continued*)

Level	Dimension	Indicator	Source	Type
L1	Outputs	Investments mobilised (€)	Accounting / OpenCoesione	Direct
L1	Outputs	Perceived quality of investments (G3Q05)	Questionnaire	Direct
L1	Outputs	External visibility (G4Q05)	Questionnaire	Direct
L2	Capabilities / Agency	Territorial agency - self-efficacy (G1Q02, 4 items)	Questionnaire Likert 1-7	Composite
L2	Capabilities / Agency	Social cohesion (G1Q03-Q05, 3 + 2 items)	Questionnaire Likert 1-7 + binary	Composite
L2	Capabilities / Agency	Place attachment (G1Q06, 4 items)	Questionnaire Likert 1-7	Composite
L2	Capabilities / Agency	Quality of visit experience (G2Q07, 4 items)	Questionnaire Likert 1-7	Composite
L3	Cultural Activation	Cultural engagement - residents (G1Q07, 5 items)	Questionnaire Likert 1-7	Composite
L3	Cultural Activation	Cultural engagement - visitors (G2Q08, 5 items)	Questionnaire Likert 1-7	Composite
L3	Cultural Activation	Associative and civic participation	Survey / Municipality	Direct
L4	Behaviours	Sustainable behaviours -residents (G1Q08, 4 items)	Questionnaire Likert 1-7	Composite
L4	Behaviours	Responsible behaviours - visitors (G2Q09, 4 items)	Questionnaire Likert 1-7	Composite
L4	Behaviours	Local value creation - visitors (G2Q10, 5 items)	Questionnaire Likert 1-7	Composite
L4	Behaviours	Propensity to local investment (G3Q06–Q07)	Questionnaire	Direct
L4	Behaviours	Visitor expenditure (G2Q12, by category)	Questionnaire	Direct

(*continued*)

Table 1. (*continued*)

Level	Dimension	Indicator	Source	Type
L5	Socioeconomic System	Subjective wellbeing - residents (G1Q09, 5 items)	Questionnaire Likert 1-7	Composite
L5	Socioeconomic System	Perceived wellbeing - visitors (G2Q11, 5 items)	Questionnaire Likert 1-7	Composite
L5	Socioeconomic System	Perceived income change (G3Q01)	Questionnaire ordinal	Direct
L5	Socioeconomic System	Perceived property value change (G3Q02)	Questionnaire ordinal	Direct
L5	Socioeconomic System	Perceived environmental quality (G3Q03)	Questionnaire ordinal	Direct
L5	Socioeconomic System	Influence on quality of life (G3Q04)	Questionnaire ordinal	Direct
L5	Socioeconomic System	Local economy and businesses	Business register / INPS / ISTAT	Direct
L5	Socioeconomic System	Tourist attractiveness	ISTAT / accommodation / mobile analytics	Direct
L6	Structural Cohesion	Population trend	ISTAT / Municipal registry	Direct
L6	Structural Cohesion	Age structure / dependency ratio	ISTAT / Municipal registry	Direct
L6	Structural Cohesion	New residents	Registry / periodic survey	Direct
L6	Structural Cohesion	Participation and volunteering	Periodic survey / Municipality	Direct
L6	Structural Cohesion	Proximity networks and mutual aid	Survey / Observation	Direct
L6	Structural Cohesion	Social conflict and integration	Survey / Interviews	Direct
L6	Structural Cohesion	Perceived security	Periodic survey	Direct
L6	Structural Cohesion	Access to essential services	Survey / Municipality	Direct
L6	Structural Cohesion	Inclusion and accessibility	Survey / Observation	Direct
L6	Structural Cohesion	Institutional capacity	Municipal budgets / Survey	Direct

5 Methods

5.1 Desk Data Collection

Secondary data analysis constitutes the structural layer of the Observatory's evaluation architecture. Desk data collection serves three evaluative functions: constructing a pre-intervention baseline, reconstructing the historical trajectory of the territory, and enabling comparative analysis with structurally similar territories.

The Italian National Institute of Statistics (ISTAT) provides the primary source for demographic monitoring (resident population, age structure, migratory balance) and for the socioeconomic framing of the municipality. In small municipalities, however, ISTAT data present significant interpretive constraints: publication lags, aggregation or suppression for privacy protection, high statistical volatility from small absolute numbers, and availability only at supra-municipal scale for some indicators. ISTAT data must therefore be read dynamically and accompanied by qualitative contextualisation.

The databases of Unioncamere and the local Chambers of Commerce provide the primary source for monitoring local economic dynamics: business birth and mortality rates, sectoral distribution, and the development of cultural and creative enterprises. The business register allows tracking of new enterprises across sectors, providing a direct desk-level signal for the Level 1 indicator 'new businesses established' and for the Level 5 indicator 'local economy and businesses', to be read in conjunction with INPS employment data. Records from the Revenue Agency and the Ministry of Economy enable analysis of income dynamics, the evolution of the local tax base, and real estate market trends via the Real Estate Market Observatory (OMI). OpenCoesione, the Italian government's open data platform for cohesion fund investments, enables tracking of public funds mobilised in the municipality across programmes and time periods. Complementary signals of economic activation are available from municipal administrative records on building permits, commercial licences and other administrative authorisations.

ISTAT's tourism statistics and data from local accommodation establishments provide the basis for monitoring tourist attractiveness. Accommodation-based statistics, however, systematically undercount visitor flows in small inland municipalities, where day-trippers and visitors staying with private contacts constitute a substantial share of total presence. To address this structural gap, the Observatory integrates official tourism data with aggregated and anonymised mobile network data (sourced from operators such as Vodafone Analytics or equivalent providers), which enable the estimation of total visitor numbers regardless of accommodation type, origin–destination pattern reconstruction, dwell time distributions and temporal presence curves at sub-municipal resolution. These sources are planned for activation in subsequent phases of the Observatory, once data access agreements have been established.

5.2 Index Construction, Validation and Longitudinal Comparison

All composite indices are constructed as arithmetic means of the constituent items, normalised to a 0- 100 scale using the transformation:

$$\text{Normalised index} = [(\text{mean score}--1)/6] \times 100.$$

This transformation preserves the metric properties of the Likert scale while producing a dimensionally interpretable score in which 0 corresponds to the minimum possible response (1 on all items) and 100 to the maximum (7 on all items), facilitating communication with non-specialist stakeholders and enabling cross-dimensional comparisons.

The use of arithmetic means as composite index scores rests on the assumption that the constituent items are unidimensional, that they load, in other words, on a single latent factor. This assumption will be tested empirically once a sufficient sample has been collected. At the baseline stage, the analytical plan includes internal consistency analysis via Cronbach's α for each composite index.

Longitudinal comparison across observation cycles is conducted as independent-samples analysis. Because the questionnaire does not include individual tracking identifiers, a deliberate design choice that reduces response bias and protects privacy in a small community, each wave constitutes a distinct sample. The comparison of index distributions across waves, using appropriate statistical tests for independent samples, effect size measures and confidence intervals, allows aggregate trend detection at the population level without requiring individual correspondence across editions. This choice is methodologically appropriate for low-density demographic contexts where panel construction is typically impracticable, but its implications warrant explicit acknowledgement. Independent-samples comparison measures changes in the distribution of a variable in the population, not changes in the same individuals over time. Observed shifts between waves may therefore reflect compositional effects, for instance, new residents with different socioeconomic profiles or stronger prior engagement entering the sample, rather than, or in addition to, genuine programme-induced change.

The primary mitigation strategy relies on the length-of-residence variable (G1Q01), which classifies respondents as recent arrivals (less than 1 year, 1–5 years) or long-established residents (6-10 years, over 10 years, lifelong). Disaggregated analysis by residential tenure allows the separation of two analytically distinct populations: those who were present before the intervention and may have experienced its effects directly, and those who arrived during or after its implementation, whose responses reflect a post-regeneration baseline rather than individual change. Comparing index distributions within each tenure subgroup across waves substantially reduces the compositional confound and enables more defensible causal attribution. This stratification is planned for activation from the second observation wave onward, once subsample sizes permit reliable inference.

The two binary closure questions on social cohesion (G1Q04-Q05), which ask whether the respondent has perceived a specific improvement in social life or has engaged in intercultural dialogue as a result of the Metroborgo project, provide a partial complement to the compositional limitation: a respondent who reports both increased social cohesion on the Likert scale and a programme-specific effect on the binary item supplies stronger attributional evidence than scale movement alone. Additional disaggregated analyses by age, gender and type of visit (G2Q02) are planned for successive waves, both for equity analysis and to detect differential patterns of activation across the capability and behavioural dimensions of the indicator system

6 Conclusion

This paper has presented a nonlinear Theory of Change and a six-level indicator system designed to evaluate cultural regeneration in left-behind territories. The framework departs from linear input-output-outcome models by grounding impact evaluation in a socio-cognitive-behavioural architecture that makes explicit the intermediate mechanisms (cognitive reconfiguration, relational activation, capability expansion) through which cultural investment generates territorial effects.

Three contributions stand out. First, the theoretical integration of the capabilities approach and predictive processing provides an empirically grounded and normatively rigorous account of why and how cultural interventions matter beyond their economic outputs. The identification of capability expansion as a shift in the precision-weighted generative models that mediate between formal opportunities and substantive freedoms connects the normative aspirations of the capabilities approach with a mechanistic account of how such expansion occurs at the cognitive level. Second, the six-level indicator system operationalises this account into a measurable, longitudinally comparable and decision-relevant framework, with explicit provisions for cross-level association analysis designed to detect the nonlinear dynamics the model posits. Third, the methodological architecture (composite indices with planned validation, direct indicators for specific observable facts, independent-samples longitudinal comparison, compositional confound mitigation through residential tenure stratification) provides a replicable template for impact evaluation in analogous territorial contexts.

The limitations of the present work are equally worth noting. The model is in its baseline phase: the first observation wave is underway and no longitudinal data are yet available. The causal claims embedded in the ToC, including the cross-level feedback dynamics that constitute its nonlinear character, remain partly hypothetical and will require empirical validation through successive waves. The psychometric properties of the composite indices await empirical confirmation. The independent-samples design, while appropriate for this context, limits the analysis to aggregate-level association rather than individual-level mediation; future phases may explore the feasibility of a voluntary panel subsample to complement the cross-sectional waves. The applicability of the framework to contexts beyond small Italian villages with a specific heritage-led regeneration profile will require adaptation and testing.

Future developments include the activation of Level 6 structural indicators through periodic surveys, the introduction of participatory indicators developed with community co-design methodologies, the elaboration of a simplified monitoring dashboard for non-specialist use by the local administration, and the empirical testing of cross-level association hypotheses once multi-wave data are available. The architecture of the Observatory is designed to support this evolutionary expansion: the ToC is not a fixed blueprint but a revisable hypothesis about how change happens, to be refined in light of what the evidence reveals.

References

1. Mayne, J.: Theory of change analysis: building robust theories of change. Can. J. Program Eval. **32**(2), 155–173 (2017)
2. Chen, H.T.: Theory-Driven Evaluations. Sage, Newbury Park (1990)
3. Weiss, C.H.: Nothing as practical as good theory: exploring theory-based evaluation for comprehensive community initiatives for children and families. In: Connell, J.P., et al. (eds.) New Approaches to Evaluating Community Initiatives, pp. 65–92 (1995)
4. Candeloro, G., Tartari, M., Bortolotti, A., Mastrolonardo, L., Uboldi, S., Sacco, P.L.: Cultural practices as emotional devices: Agency, inequalities and wellbeing in left-behind regions. Evidence from Aielli (under review). (2026).
5. Sen, A.: Development as Freedom. Oxford University Press, Oxford (1999)
6. Nussbaum, M.C.: Creating Capabilities: the Human Development Approach. Harvard University Press, Cambridge (2011)
7. Robeyns, I.: Wellbeing, Freedom and Social Justice: the Capability Approach re-Examined. Open Book Publishers, Cambridge (2017)
8. Barca, F., McCann, P., Rodríguez-Pose, A.: The case for regional development intervention: place-based versus place-neutral approaches. J. Reg. Sci. **52**(1), 134–152 (2012)
9. Varela, F.J., Thompson, E., Rosch, E.: The Embodied Mind: Cognitive Science and Human Experience. MIT Press, Cambridge (1991)
10. Gallese, V.: Mirror neurons, embodied simulation and the neural basis of social identification. Psychoanal. Dialogues. **19**(5), 519–536 (2009)
11. Clark, A.: Whatever next? Predictive brains, situated agents, and the future of cognitive science. Behav. Brain Sci. **36**(3), 181–204 (2013)
12. Friston, K.: The free-energy principle: a unified brain theory? Nat. Rev. Neurosci. **11**(2), 127–138 (2010)
13. Bandura, A.: On the functional properties of perceived self-efficacy revisited. J. Manag. **38**(1), 9–44 (2011)
14. Forrest, R., Kearns, A.: Social cohesion, social capital and the neighbourhood. Urban Stud. **38**(12), 2125–2143 (2001)
15. Putnam, R.D.: Bowling Alone: the Collapse and Revival of American Community. Simon & Schuster, New York (2000)
16. Altman, I., Low, S.M. (eds.): Place Attachment, vol. 12. Springer Science & Business Media (2012)

Ecosystem Services in Spatial Planning for Climate Neutral Urban and Rural Areas (ESSP 2026)

Urban Climate Adaptation in Naples: An Integrated Framework for Flood Risk, Urban Heat Island, and Nature-Based Intervention Planning

Carmela Gargiulo[1], Tonia Stiuso[1], Floriana Zucaro[1(✉)], Francesco Pugliese[1], Giuseppe Speranza[1], and Vincenzo Scarano[2]

[1] Department of Civil, Building and Environmental Engineering, University of Naples Federico II, P.le Tecchio 80, 80125 Naples, Italy
{gargiulo,tonia.stiuso,floriana.zucaro,francesco.pugliese,giuseppe.speranza}@unina.it

[2] A2A Ciclo Idrico S.p.A, Via Lamarmora 230, 25124 Brescia, Italy

Abstract. In densely built cities, the progressive replacement of permeable surfaces with impervious, heat-retaining materials simultaneously reduces infiltration capacity, amplifying urban flood risk and limits evapotranspiration, thus intensifying the Urban Heat Island (UHI) effect. These two climate-related hazards share a common structural driver and are particularly severe in compact, socially heterogeneous urban neighbourhoods where green infrastructures are scarce and drainage systems are ageing. This paper proposes an integrated methodology for urban climate adaptation applied to three Naples districts (Fuorigrotta, Ponticelli, Soccavo), combining: (i) flood risk mapping through coupled EPA SWMM+FLO-2D hydraulic modelling and CubiST machine learning vulnerability assessment; (ii) open space microclimate simulation via ENVI-met to quantify thermal co-benefits of greening scenarios; and (iii) spatially explicit Low-Impact Development-Best Management Practices (LID-BMP) and greening siting based on compound risk overlay. For flood risk (R), the formulation $R = H \times E \times V$ allows integrating the hydraulic hazard (H) with socio-economic vulnerability (V) and exposure (E) into a composite index suitable for spatial planning. For UHI, where no analogous probabilistic risk framework is established in the literature, thermal performance is assessed through ENVI-met simulations comparing the baseline scenario with design ones including post-greening open space configurations. Cooling co-benefits through PET and outdoor air temperature are also quantified. Results show that nature-based interventions in open spaces generate compound reductions in both flood risk and thermal stress, providing local decision-makers with a physically grounded, spatially explicit evidence base for urban renewal investment.

Keywords: Urban flood risk · Urban Heat Island · Low-Impact Development-Best Management Practices · ENVI-met · EPA SWMM · Nature-Based Solutions · Naples · Climate adaptation · Open spaces

© The Author(s), under exclusive license to Springer Nature Switzerland AG 2027
O. Gervasi et al. (Eds.): ICCSA 2026 Workshops, LNCS 16761, pp. 413–428, 2027.
https://doi.org/10.1007/978-3-032-30527-5_27

1 Introduction

Urban flooding and the Urban Heat Island (UHI) effect are two of the most pressing climate-related challenges for contemporary cities. According to the IPCC Sixth Assessment Report, coastal and inland cities deal with substantially higher exposure to extreme precipitation and rising mean temperatures [1], with UHI intensities in European cities typically ranging 2–6 °C and peaking above 8 °C during heat waves [2]. These two impacts share a structural driver: the progressive replacement of permeable, vegetated surfaces with impervious, heat-retaining fabrics that simultaneously reduces infiltration capacity and suppresses evapotranspiration – the primary cooling mechanism in urban environments [3].

The two phenomena nevertheless call for partially different assessment approaches. Flood risk is a composite, probabilistic quantity that can be formally expressed as $R = H \times E \times V$ [4], where hazard probability (H), exposed elements (E), and vulnerability (V) are independently quantifiable and can be spatially combined into a risk index that directly assists in emergency planning and building regulation. For UHI and thermal stress, no analogous consolidated probabilistic risk framework exists in the literature: thermal conditions vary continuously, are highly sensitive to local morphology, and their health and comfort consequences depend on individual physiological parameters. The proper assessment approach is thus scenario-based simulation, modelling how spatial interventions affect thermal comfort indices (PET, UTCI) under representative summer conditions – rather than probabilistic risk mapping. This methodological difference, embedded in Modules 1 and 2 of the proposed framework, reflects the current state of practice and the different nature of the two phenomena. Their integration in Module 3 thus allows both outputs to inform a unified spatial intervention strategy.

Nature-based interventions restoring permeability and vegetation in open spaces generate a distinctive double dividend: they reduce runoff and drainage stress while simultaneously lowering surface temperatures and improving thermal comfort [5, 6]. This paper proposes and tests an integrated framework applied to three morphologically contrasting Naples (Italy) districts of Fuorigrotta, Ponticelli, and Soccavo selected for their documented flood history, different urban morphologies, and distinct socio-economic features. The framework couples physically based hydraulic modelling (EPA SWMM+FLO-2D), CubiST machine learning vulnerability weighting, and ENVI-met microclimate simulation within a unified GIS workflow. Open spaces, squares, courtyards, parking areas, are the primary spatial units of analysis and intervention, as their surface characteristics jointly affect both hydrological performance and thermal regulation [7, 8].

The scientific contribution is threefold: (i) CubiST provides objective vulnerability weighting; (ii) EPA SWMM+FLO-2D coupled with ENVI-met enables simultaneous flood and UHI co-benefit quantification from the same interventions; (iii) the cross-neighbourhood comparison gives evidence on how urban structure and open space configuration shape compound climate vulnerability. The paper is structured as follows: Sect. 2 reviews the literature; Sect. 3 presents the methodology; Sect. 4 reports results; Sect. 5 draws conclusions.

2 Background and State of the Art

2.1 Shared Drivers and Integrated Approaches

In densely built urban environments, the gradual replacement of natural, permeable surfaces with impervious covers, roads, rooftops, paved squares, car parks, and the concurrent removal of trees and vegetation trigger two interconnected processes. On one hand, reduced infiltration and increased runoff speed overload urban drainage systems, thus intensifying flood hazard; on the other, the significant lowering of evapotranspiration and the thermal mass of built materials relies on the rising of surface temperatures compared to those of surrounding rural areas, then entailing the so-called UHI effect [3]. This shared physical driver is especially pronounced in compact, high-density districts where building coverage is high, open spaces are scarce, and the legacy of rapid, often unregulated post-war urbanisation has left behind ageing grey infrastructure with limited adaptive capacity [7, 9]. Open spaces, which surface features jointly determine hydrological capacity and thermal performance, are the natural focus for integrated adaptation strategies [7, 8].

2.2 Urban Flood Risk Assessment

Methodological approaches to flood risk assessment span three families: indicator-based (AHP, vulnerability indices) [10], physically based coupled 1D-2D hydrodynamic models (EPA SWMM+FLO-2D, HEC-RAS 2D) [11, 12], and machine learning ensemble methods (Random Forest, XGBoost, CatBoost) [1, 13]. Nevertheless, key gaps exist: vulnerability and hazard are typically assessed separately, ML-based vulnerability weighting is underused in Southern European contexts, and district-scale LID-BMP siting combining flood and UHI evidence remains largely unexplored.

2.3 UHI Simulation and Open Space Thermal Performance

ENVI-met is the most widely adopted tool for district-scale microclimate simulation, validated extensively in Mediterranean contexts [14]. Remote sensing-based Land Surface Temperature mapping provides the spatial thermal baseline, while ENVI-met assesses scenario-based cooling effectiveness through PET and UTCI [8, 9, 15, 16]. Research for the Naples metropolitan area has specifically confirmed ENVI-met's suitability for characterising Southern Italian urban fabrics and evaluating greening interventions [17, 18]. The complementarity between these two approaches is a key methodological asset of the present study.

2.4 Lid-BMPs and Nature-Based Solutions: Co-benefits

Nature-based Solutions (NbS) and Low Impact Development-Best Management Practices (LID-BMP) generate a distinctive double dividend: they address urban flooding by enhancing infiltration, retention, and evapotranspiration at source; and simultaneously mitigate the UHI effect by cooling the urban surface through evapotranspiration, shading, and increased albedo [6, 7, 19]. Among others, green roofs, bioretention cells, rain

gardens, detention ponds, permeable pavements, and trees were extensively investigated [8, 20]. Consistently, researchers proposed the combination of open space tree planting and permeable paving to reduce stormwater runoff while cooling the city in Mediterranean cities [15, 21]. In compact historic fabrics, researchers demonstrated that cooling and greening strategies significantly lower the energy needed for cooling by 31% and increase comfort hours by 27%, and a stormwater management model (EPA SWMM) based evaluation shows that LID measures can reduce stormwater runoff by 20–40% where the total LID area is 10–30% of the entire catchment [22, 23]. Recent works specifically addressing the Naples urban context further confirmed that greening transformations in small open spaces within dense historical fabrics can generate significant UHI mitigation effects at the district scale [9, 24, 25].

However, the systematic identification of open spaces where LID-BMP and greening interventions can generate maximum integrated benefits while remaining technically and economically feasible is a key methodological challenge. Space availability, structural loading capacity, competing land uses, and morphological variability across urban fabric types all impose context-specific constraints requiring site-by-site spatial analysis rather than generic prescriptions [8, 20].

2.5 Regulatory and Policy Context

Urban flood risk management and UHI mitigation are embedded within a multi-level governance architecture. At the global level, the Sendai Framework for Disaster Risk Reduction (2015–2030) calls for multi-hazard urban adaptation strategies, the Paris Agreement (2015) commits signatories to resilience-oriented planning, and the SDG Agenda 2030 contextualises urban climate adaptation within Goals 6, 11, and 13 [26], respectively. They train a contemporary triad of global alliances that convey a joint policy mandate for solutions to flooding and thermal risk [27]. Namely, the Floods Directive (2007/60/EC) refers to National Preliminary Flood Risk Assessments, Flood Hazard and Risk Maps, and Flood Risk Management Plans for three specified return periods [28]. The EU Climate Adaptation Strategy (2022–2024) directly promotes NbS and the use of integrated green and grey infrastructures as key strategies to deal with both flooding and thermal stress [29].

In Italy, Legislative Decree 49/2010 transposes the EU Floods Directive through eight, District Hydrographic Authorities, with hazard and risk classes categorized as H1– H3 and R1–R4; the national hazard maps are not yet high-resolution enough for a district-scale applications, and UHI is not considered in Flood Risk Management Plans yet. At the city-scale, China's Sponge City programme has promoted permeable pavements, bioretention, and green corridors in more than 30 pilot cities since 2015, with clear co-benefits for flood and urban cooling [23]. In Singapore, the ABC Waters Programme provides exemplary references for integrated management of water bodies using green infrastructures for flood and thermal benefits. Barcelona's urban greening plan, Rotterdam's Water Square concept, and Vienna's Cool Streets initiative all show examples of combined solutions for flood management and heat reduction. References are also found in the Flood Risk Management Policy (2014) of the Tokyo Metropolitan Government (TMG, 2014).

Against this background, this study contributes to the practice by testing the robustness of linked EPA SWMM+FLO-2D coupled with ENVI-met, and Machine Learning-based vulnerability analysis in an overall GIS workflow in addressing both flood risk and UHI mitigation. Applying the framework to a real-world Mediterranean city allows drawing out comparative results across three morphologically diverse districts of Naples municipality.

3 Methodology

The methodology is structured as an integrated three-module framework developed within a GIS environment (QGIS) on a 30 m × 30 m grid (Fig. 1). Module 1 returns flood risk maps through coupled hydraulic modelling and machine learning vulnerability assessment. Module 2 investigates open spaces thermally and simulates UHI mitigation through ENVI-met greening scenarios. Module 3 integrates both outputs to site and assess LID-BMPs and greening interventions. The two approaches differ by design: Module 1 adopts the probabilistic risk formulation $R = H \times E \times V$, which is well established in flood management regulation and allows composite spatial mapping of hazard and vulnerability. Module 2 does not produce a risk index, because no equivalent probabilistic framework for UHI is consolidated in the literature; instead, ENVI-met simulations compare current open space configurations (baseline scenario) with post-greening configurations (design scenarios) to assess the thermal improvement achievable by specific interventions – expressed through PET and outdoor air temperature – under representative summer conditions. Module 3 overlays flood risk maps with thermal priority zones to identify open spaces generating maximum compound benefit (Figs. 2, 3, 4, 5).

3.1 Module 1: Flood Vulnerability Assessment and Hazard Mapping

3.1.1 Vulnerability Parameters and Machine Learning Weighting

Flood vulnerability was assessed through a Vulnerability Index (IV) combining exposure and vulnerability on the 30 m grid. Following a review of 24 scientific case studies, 72 candidate parameters were filtered to 19 effective variables according to contextual coherence, data availability, and demonstrated explanatory power [10]. Data sources include ISTAT census data, Italian Ministry of Economy and Finance income data, Geofabrik road and transport network, and Urban Atlas land use layers. As a training dataset for machine learning, the output was used from the reference IV produced in the experimental task of the CO-FRAME_NA project on a total of 23,588 cells. Two learning algorithms were employed and compared, namely: (i) Random Forest (RF), (ii) CubiST (https://CRAN.R-project.org/package=CubiST accessed on 1 April 2023). The CubiST algorithm returns statistical trees based on a recursive partitioning approach commonly used in decision trees combined with linear regression models used at each terminal node of the tree. It is commonly applied to contexts when many observations but few predictor variables are available, notably a condition that often affects some phases of the vulnerability mapping process at the district scale [45,46].

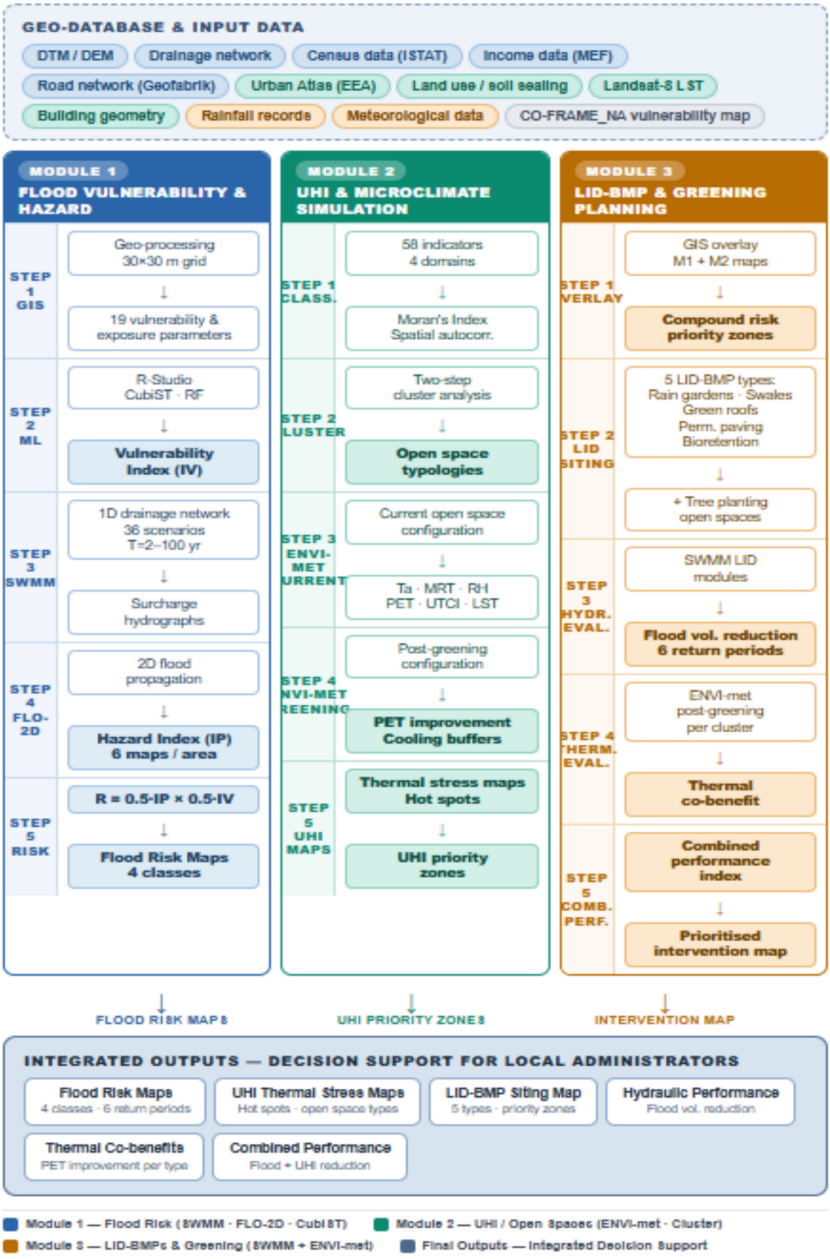

Fig. 1. Integrated Methodology Framework. All modules operate within a GIS environment, 30 m × 30 m grid.

A comparative assessment of the results of the two learning algorithms using R^2 and Mean Squared Error (MSE) indicators enabled the selection of the best-fitting model,

CubiST, which reports the accuracy of approximately 60% for this kind of application, which is an acceptable value considering the approximated nature of the reference output variable. The resulting parameter weights were applied to compute IV for each cell as the weighted sum of normalised parameter values.

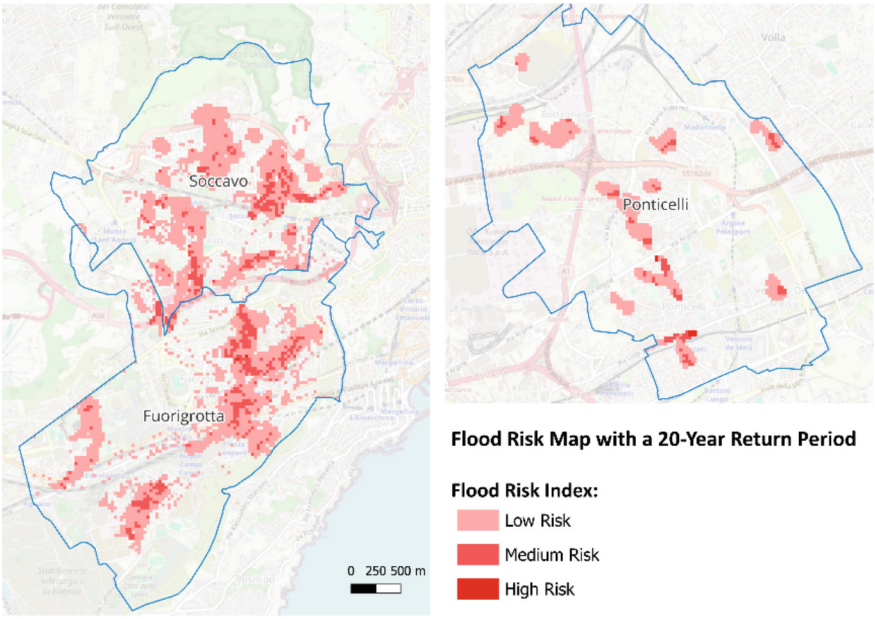

Fig. 2 Flood Risk Map for T = 20-year (Fuorigrotta, Ponticelli, Soccavo).

3.1.2 Hydraulic Hazard Modelling: EPA SWMM and FLO-2D

Following the modelling in EPA SWMM environment available in [30, 31], the drainage systems of the investigated districts were implemented and tested, by simulating different design rainfall events according to the regional frequency curve $h(t,T) = K^t \cdot a \cdot t^n$ (Naples Capodimonte station, 2000–2020) for six return periods (T = 2, 5, 10, 20, 50, 100 years) and five durations ($t \in [0.2, 6]$ hours). Dynamic Wave routing was set for simulations to account for both unsteady flows and pressurized occurrences of the system. Overall, 36 scenarios were yielded per district, then deriving the flooding hydrographs at critical nodes which allowed implementing the FLO-2D two-dimensional flood propagation and thus generating maps of the normalised Hydraulic Hazard Index (IP), given the maximum flood depth and velocity.

3.1.3 Flood Risk Mapping

Risk maps were computed as $R = 0.5 \cdot IP \times 0.5 \cdot IV$ (equal weighting, MATTM 2014 and IPCC framework [4]), classified into four levels (null, low, medium, high) for each of the

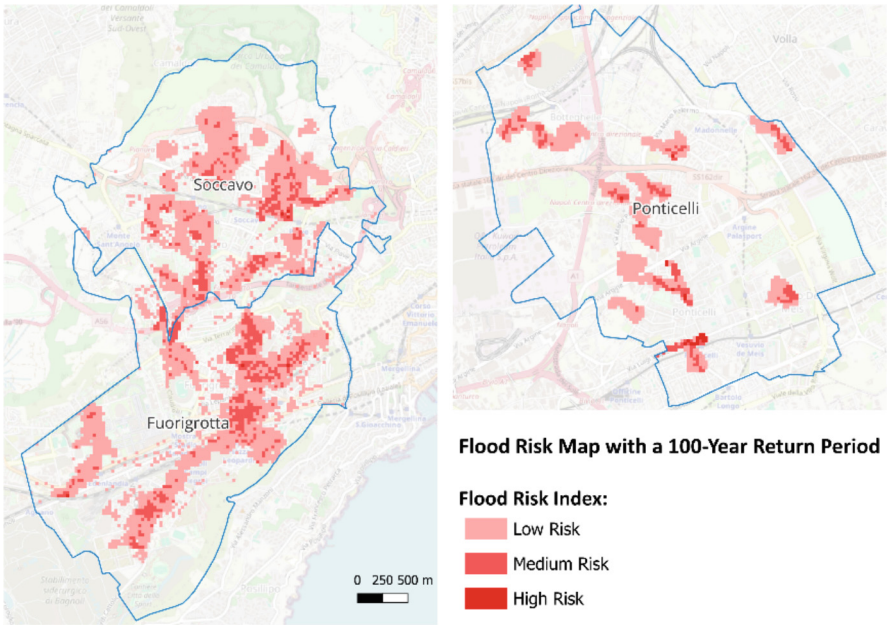

Fig. 3 Flood Risk Map for T = 100-year (Fuorigrotta, Ponticelli, Soccavo).

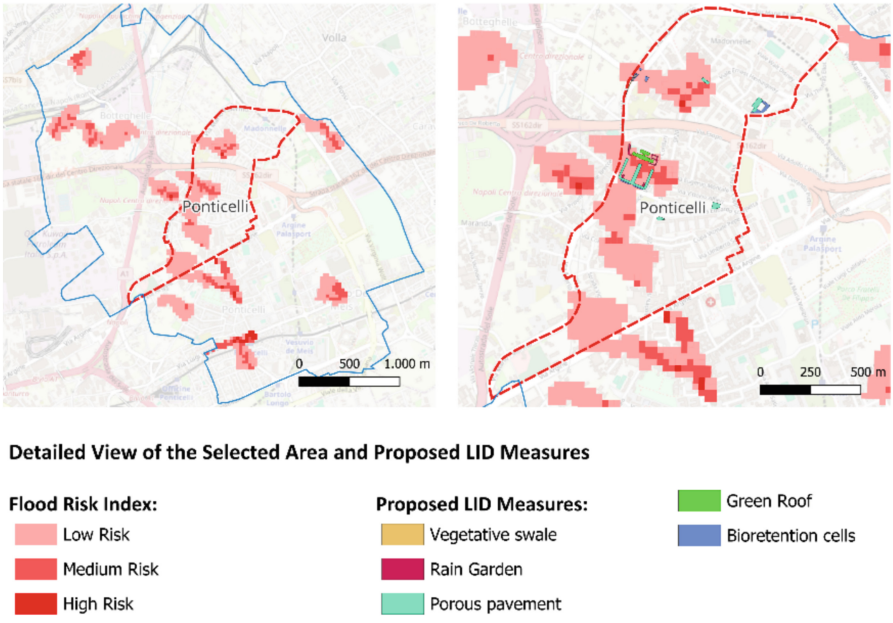

Fig. 4. Detailed View of the Selected Area and Proposed LID Measures in Ponticelli district.

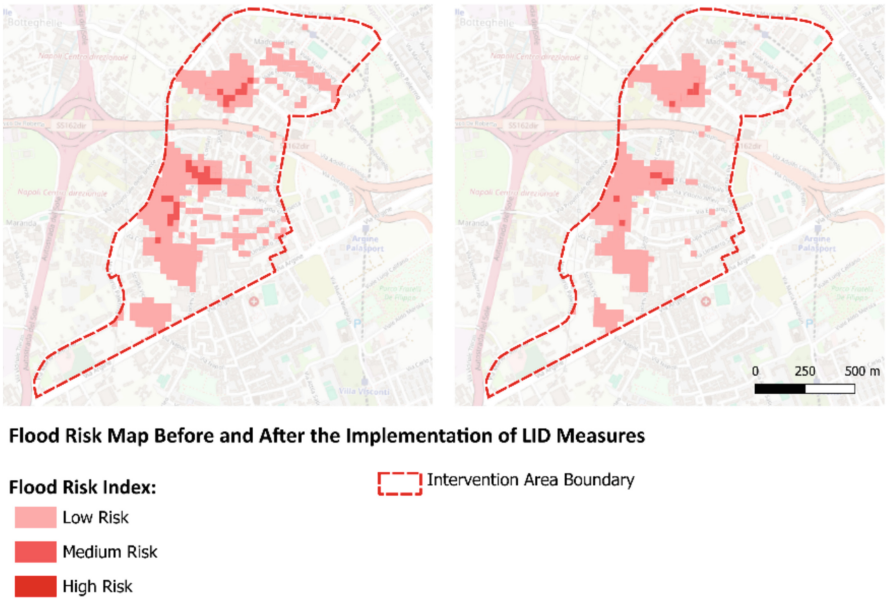

Fig. 5 Pre- and Post-Intervention Flood Risk Map Based on LID Measures.

six simulated return periods. The mapping entailed the spatial foundation for LID-BMP siting in Module 3.

3.2 Module 2: Open Space Classification and ENVI-Met Simulation

Open spaces were classified using a 58-indicator framework across four domains: open space features (permeability, vegetation cover), urban context (soil sealing, building materials), microclimatic and geomorphological characteristics (LST from Landsat-8, solar access, MRT), and socio-economic indicators [17, 18].

ENVI-met (v. 5.x) simulations were performed by comparing current open space conditions (baseline scenario) with post-greening configurations (design scenarios). The post-greening configuration relies on tree planting and permeable surface replacement, maintaining identical meteorological boundary conditions (clear-sky July design day). Among the possible outputs, the PET ones are provided as they can be considered representative of the potential benefits of reforestation solutions [8, 15].

3.3 Module 3: Integrated LID-BMP and Greening Siting

GIS overlay of flood risk maps (Module 1) with UHI thermal priority zones (Module 2) identifies open spaces where both stresses simultaneously exceed threshold values. Five LID-BMP were mapped against eligible surfaces: rain gardens and bioretention cells (green areas), vegetated swales (road shoulders), green roofs (flat rooftops), permeable pavements (parking areas), and bioretention cells with drainage layer. Urban tree planting was additionally allocated to all eligible hard-surface open spaces [8, 15]. Hydraulic

performance was re-simulated in EPA SWMM with modified subcatchment parameters; thermal performance was then evaluated through ENVI-met post-greening simulations.

4 Results

The integrated framework was applied to the three study districts, producing spatially differentiated outputs across all three modules. Results are discussed by linking quantitative values to the specific morphological and socio-economic features of each district.

4.1 Flood Vulnerability and Risk Mapping

The CubiST vulnerability weights reveal a structure closely tied to each neighbourhood's urban history. The income index (12.98%) carries the highest weight, followed by commercial buildings (10.22%), non-national residents (9.53%), young population (8.98%), structurally vulnerable buildings pre-1970 stock (8.56%), and residential density (8.43%). Road network parameters account for approximately 12% collectively, reflecting functional exposure of mobility infrastructure.

Fuorigrotta's planned twentieth-century development shows a heterogeneous vulnerability pattern, with high values concentrated in the commercial central strip and lower values around the university campus and Mostra d'Oltremare complex. Ponticelli – with the highest residential density in the Campania region, the largest share of pre-1970 building stock, and the lowest income levels among the three study areas – exhibits the most extensive high-vulnerability surface. Soccavo, morphologically characterised by hillside terrain, concentrates high vulnerability along the valley floor and in the oldest residential blocks, while medium vulnerability extends widely across the hillside fabric.

EPA SWMM simulations ($n = 0.1995$; $a = 25.97$–26.13 mm/h per district) reveal strongly differentiated drainage behaviour. Fuorigrotta's 1950 network (catchment 1.89 km^2) mainly fails at only two nodes, responding worse to short high-intensity events. Ponticelli's complex multi-municipality system (Sbauzone and Cuozzo-Reale channels; basin 20 km^2) shows more diversified crisis patterns across scenarios. Soccavo's 26 ha northern subcatchment, subdivided into four subcatchments (1.97–15.55 ha), has a structurally deficient drainage system – downstream pipes are smaller than upstream ones – producing failure at 3–4 nodes even at low return periods. FLO-2D propagation maps confirm that in Fuorigrotta flooding conveys toward the Agnano plain; in Ponticelli the flat Sebeto plain morphology produces extensive shallow inundation already at $T =$ 20-year; in Soccavo flooding is concentrated in hillside depressions.

Combining IP and IV yields six risk maps per district. In Fuorigrotta, high-risk cells at $T = 100$-year align with the commercial strip and the two EPA SWMM critical nodes. In Ponticelli, high-risk zones at $T = 100$-year overlay much of the densely urbanised central area – a compounding of flat drainage, old building stock, and social deprivation. In Soccavo, high-risk areas are more spatially contained but medium-risk cells extend broadly, thus defining a diffuse medium-priority intervention landscape.

4.2 LID-BMP Siting and Hydrological Performance

The spatial overlay of risk maps with land use identified eligible LID-BMP surfaces across all three districts, distributed as high-priority (high/medium-high risk) and low-priority (low risk) sites.

The hydraulic performance evaluation, conducted on a Ponticelli sub-area offering receptivity to all five LID types simultaneously, shows that LID-BMP are most effective at low return periods ($T \leq 5$ years), producing measurable reductions in peak runoff at critical nodes. At $T = 5$–100-year, relative flooded volume reduction decreases, confirming that LID-BMPs primarily act as source-control complements for frequent events, while structural measures are more effective for extreme ones. The urban planning implication is direct: LID strategies are the appropriate primary tool for managing the high-frequency, moderate-intensity events responsible for the majority of cumulative annual flood disruption in dense Southern Italian neighbourhoods.

4.3 Open Space Typologies and Greening Intervention Map

Three open space clusters were identified across the three districts: (i) large structured green spaces (parks, sports fields), with high vegetation cover and good baseline thermal performance; (ii) hard-surface open spaces (squares, parking areas, courtyards), with high imperviousness and elevated thermal stress; and (iii) residual interstitial open spaces (road shoulders, degraded courtyard edges), with intermediate permeability. Clusters (ii) and (iii) dominate in Ponticelli and Soccavo districts, reflecting decades of speculative densification that progressively expunged vegetated areas. Fuorigrotta's planned fabric concentrates cluster-(i) spaces around the Mostra d'Oltremare and University campus.

Greening interventions were allocated to clusters (ii) and (iii) in high and medium flood-risk zones, producing the combined siting map shown in Fig. 6. The spatial distribution reveals concentration in the historical central cores of Fuorigrotta and Ponticelli, where hard-surface inner courtyards and tree-free squares create co-located hydrological and thermal hotspots. In Ponticelli, the number and accessibility of hard-surface courtyards within the dense residential fabric represents a significant and spatially precise intervention potential that is invisible at the city scale [8, 15].

4.4 UHI Mitigation: ENVI-Met Simulation Results

ENVI-met simulations confirm that greening interventions generate measurable and spatially differentiated thermal co-benefits. Tree planting reduces outdoor air temperature by 1–3 °C near canopy during peak summer afternoon hours in the post-greening configuration, with magnitude modulated by canopy geometry, street aspect ratio, and pre-existing surface albedo [8, 9, 15].

As shown in Fig. 7, the PET improvement following greening is strongly differentiated by open space morphology. Inner courtyards in Ponticelli and Fuorigrotta show the highest thermal gains (PET reductions of 11–18 °C), because enclosed geometries amplify mean radiant temperature under current conditions and canopy shading intervenes precisely on this mechanism. Public squares and parking areas show intermediate

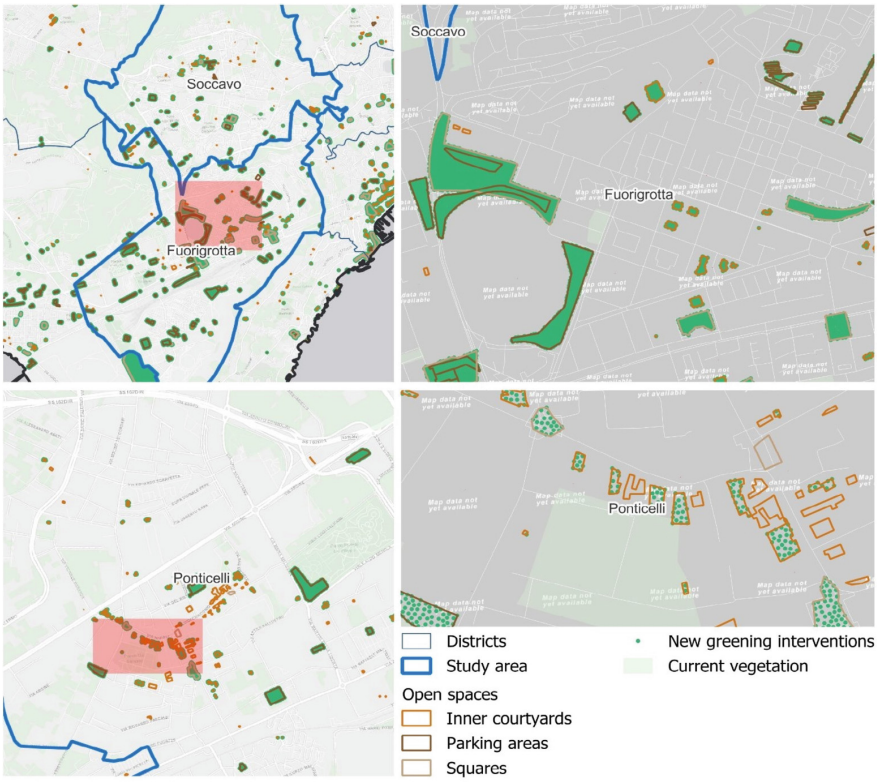

Fig. 6. Spatial distribution of greening intervention sites (Fuorigrotta, Ponticelli, Soccavo).

thermal improvement (PET reductions of 2–10 °C), concentrated within tree shadow zones and diminishing rapidly beyond the cooling buffer [8, 15].

The urbanistic reading is direct: the compact, poorly planned morphology of Ponticelli and Soccavo – narrow canyons, enclosed courtyards, minimal existing greenery – simultaneously produces the highest current thermal stress and the greatest thermal improvement potential from targeted greening. Fuorigrotta's planned layout shows lower current PET values but also lower marginal gain from additional tree planting. This confirms the planning principle that UHI mitigation investments should prioritise the most morphologically compact and thermally stressed portions of the urban fabric [16–18].

Critically, the highest-priority LID-BMP sites in Ponticelli and Soccavo – high flood-risk cells – are simultaneously the spaces with the greatest thermal improvement potential. This spatial convergence validates the integrated framework's core hypothesis: compound climate risk and compound nature-based response can be identified and prioritised within a single consistent GIS workflow, without separate planning processes for flooding and thermal stress [15, 33].

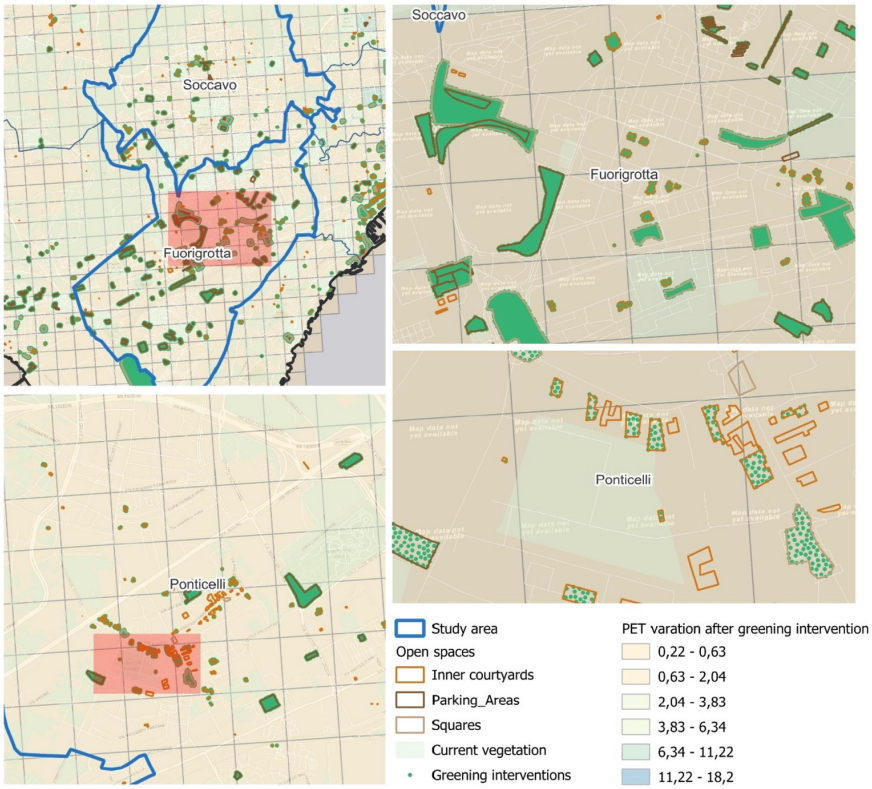

Fig. 7. PET improvement (°C) in open spaces of Fuorigrotta and Ponticelli, following greening interventions. Classes range from 0.22–0.63 °C (large open squares) to 11.22–18.2 °C (enclosed inner courtyards).

5 Conclusions

Urban flooding and the UHI effect are not two independent challenges: they are two displays of the same urban transformation process, and thus they should be addressed through integrated approaches, aimed at enhancing the resilience improvement. This study demonstrates that such integration is operationally feasible at the district scale through the coupling of established hydraulic and microclimate simulation tools within a GIS-based framework.

The application to Fuorigrotta, Ponticelli, and Soccavo (Naples, Italy) shows that compound vulnerability to flooding and thermal stress concentrates in the densest, most socio-economically fragile, and most morphologically unplanned portions of the urban fabric: the post-war spontaneous settlements where sealing is most extensive and green infrastructure most lacking. In these areas, LID-BMPs and urban greening in open spaces can simultaneously limit flooded volumes at low-to-moderate return periods and produce thermal comfort improvements of 2–18 °C PET. Both effects are delimited in the same

priority locations such as hard-surface inner courtyards, treeless squares, parking areas within high flood-risk perimeters.

The methodological contributions are threefold. First, CubiST ML weighting provides objective, reproducible vulnerability assessment overcoming the subjectivity of indicator weighting methods. Second, the 58-indicator open space classification with cluster analysis enables identification of thermally critical urban space typologies at a spatial resolution essential for effective intervention design. Third, the explicit coupling of EPA SWMM+FLO-2D with ENVI-met, demonstrated here in the Naples metropolitan context, transforms two disciplinary traditions into a jointly interpretable planning evidence base. The key asymmetry between the two modules – probabilistic risk mapping for flooding versus scenario-based comfort assessment for UHI – reflects the different state of practice and the fundamentally different nature of the two phenomena and is explicitly preserved in Module 3's spatial overlay logic.

The urgency of integrated approaches is reinforced by climate projections for Mediterranean cities: both extreme rainfall frequency and summer heat stress are projected to increase substantially under RCP4.5 and RCP8.5 scenarios. Cities that continue addressing these risks through separate sectoral processes, flood risk management plans blind to thermal consequences, and greening strategies oblivious to hydrological performance, will increasingly implement redundant or counterproductive investments. The framework proposed here, anchored in open space transformation as the shared spatial logic, offers a decision-support architecture through which local authorities can consistently identify and prioritise the nature-based interventions most likely to generate compound resilience gains [8, 9, 15, 16, 20].

Future work will extend ENVI-met simulation to full neighbourhood coverage, integrate building energy performance data, develop IPCC-scenario risk projections for Naples, and embed the framework within participatory planning processes. The methodology relies exclusively on open-source data and tools and is directly transferable to comparable Southern European urban contexts.

Acknowledgments. The research leading to the results related to the micro-climate simulations has received funding from the project "Definition of a guidelines handbook to implement climate neutrality by improving ecosystem service effectiveness in rural and urban areas" CUP E53D23018970001 funded by EU in the NextGenerationEU Plan through the Italian "Bando Prin 2022-D.D. 1409 del 14-09-2022".

Disclosure of Interests. The authors have no competing interests to declare.

References

1. Wei, Q., Zhang, H., Chen, Y., Xie, Y., Yin, H., Xu, Z.: City scale urban flooding risk assessment using multi-source data and machine learning approach. J. Hydrol. **651**, 132626 (2025)
2. Santamouris, M., Cartalis, C., Synnefa, A., Kolokotsa, D.: On the impact of urban heat island and global warming on the power demand and electricity consumption of buildings. Energ. Buildings. **98**, 119–124 (2015)
3. Oke, T.R.: The energetic basis of the urban heat island. Q. J. R. Meteorol. Soc. **108**(455), 1–24 (1982)

4. Varnes, D.J.: Landslide Hazard Zonation: a Review of Principles and Practice. UNESCO Press (1984)
5. Fang, X., Li, J., Ma, Q., Zhou, R., Du, S.: A quantitative review of nature-based solutions for urban sustainability (2016–2022). Sci. Total Environ. **927**, 172219 (2024)
6. Bowler, D.E., Buyung-Ali, L., Knight, T.M., Pullin, A.S.: Urban greening to cool towns and cities: a systematic review. Landsc. Urban Plan. **97**(3), 147–155 (2010)
7. Chen, Y., et al.: Integrating NbS in compact city renewal: preferences, constraints, and opportunities. Ecol. Indic. **178**, 114003 (2025)
8. Gargiulo, C., Stiuso, T., Zucaro, F.: Reducing UHI in historical centres: the greening transformation of open small spaces in San Lorenzo district in the city of Naples (Italy). TeMA J. Land Use Mob. Environ. **2**, 67–87 (2025). https://doi.org/10.6093/1970-9870/12416
9. Longato, D., Romanato, N., Maragno, D.: Assessing heat stress risk to inform urban heat adaptation. A method applied in the Friuli Venezia Giulia region, Italy. TeMA J. Land Use Mob. Environ. **18**(3), 381–397 (2025). https://doi.org/10.6093/1970-9870/11738
10. Aydin, H.E., Iban, M.C.: Predicting and analyzing flood susceptibility using boosting-based ensemble machine learning algorithms with SHapley additive ex Planations. Nat. Hazards. **116**(3), 2957–2991 (2023)
11. Sañudo, E., Cea, L., Puertas, J.: IberSWMM+: a high-performance computing solver for 2D-1D pluvial flood modelling in urban environments. J. Hydrol. **645** (2024)
12. Cea, L., Costabile, P.: Recent advances and future challenges in urban pluvial flood modelling. Urban Water J. **22**(2), 149–173 (2025)
13. Yan, M., et al.: Urban waterlogging susceptibility assessment based on hybrid ensemble machine learning models: Beijing. J. Hydrol. **630**, 130695 (2024)
14. Bruse, M., Fleer, H.: Simulating surface-plant-air interactions inside urban environments with a three-dimensional numerical model. Environ. Model. Softw. **13**(3–4), 373–384 (1998)
15. Gargiulo, C., Zucaro, F.: A method proposal to adapt urban open-built and green spaces to climate change. Sustainability. **15**(10), 8111 (2023). https://doi.org/10.3390/su15108111
16. Darbani, E.S., Aghaabbasi, M., Ashouri, A., Razzaghi, A.: Outdoor thermal comfort in Mediterranean cities: a systematic review. Sustain. Cities Soc. **92**, 104478 (2023)
17. Carpentieri, G., Gargiulo, C., Guida, C., Zucaro, F.: Beyond City average: spatial analysis to support energy-saving interventions in urban planning. In: Gervasi, O., et al. (eds.) ICCSA 2024 Workshops. LNCS, vol. 14818. Springer, Cham (2024). https://doi.org/10.1007/978-3-031-65273-8_26
18. Carpentieri, G., Gargiulo, C., Stiuso, T., Zucaro, F.: Climate change and urban open spaces: a spatial-statistical analysis of adaptive capacity in Naples. In: Gervasi, O., et al. (eds.) ICCSA 2025 Workshops. LNCS, vol. 15890. Springer, Cham (2026). https://doi.org/10.1007/978-3-031-97606-3_12
19. Ro, S., et al.: Integrated urban flood risk management: influences of the Sendai framework, Paris climate agreement, and SDGs. Sustain. Dev. (2025). https://doi.org/10.1002/sd.70533
20. Wang, M., Gou, Z.: Urban open space surrounded by low-rise buildings and low-built density fabrics exhibits highest thermal comfort. Landsc. Urban Plan. **243**, 104968 (2024)
21. Bouketta, S.: Outdoor thermal comfort and urban cooling strategies in Mediterranean cities. Urban Clim. **47**, 101354 (2023)
22. Diz-Mellado, E., et al.: Shading and comfort in urban courtyards of a Mediterranean historical Centre. Energ. Buildings. **292**, 113150 (2023)
23. Li, C., et al.: Review on urban flood risk assessment. Sustainability. **15**(1), 765 (2023)
24. Liu, Z., et al.: Integrated flood modelling and risk assessment in urban areas: a review. J. Flood Risk Manag. (2025) in press
25. Zhu, X., Guo, H., Huang, J.J.: Urban flood susceptibility mapping using remote sensing, social sensing and an ensemble machine learning model. Sustain. Cities Soc. **108**, 105508 (2024)

26. UN: Transforming our World: the 2030 Agenda for Sustainable Development. United Nations (2015)
27. UNDRR: Sendai Framework for Disaster Risk Reduction 2015–2030. United Nations Office for Disaster Risk Reduction (2015)
28. European Parliament & Council: Directive 2007/60/EC on the assessment and management of flood risks. OJ EU L. **288**, 27–34 (2007)
29. European Environment Agency: European Climate Adaptation Strategy 2022–2024. EEA Report (2022)
30. De Paola, F., Giugni, M., Pugliese, F., Romano, P.: Optimal design of LIDs in urban Stormwater systems using a harmony-search decision support system. Water Res. Manag. **32**, 4933–4951 (2018)
31. Pugliese, F., Gerundo, C., De Paola, F., Caroppi, G., Giugni, M.: Enhancing the urban resilience to flood risk through a decision support tool for the LID-BMPs optimal design. Water Res. Manag. **36**, 5633–5654 (2022)
32. TMG: Basic Policy for Flood Management in the Tokyo Metropolitan Area (Updated). Bureau of Environment, TMG (2014)
33. Wang, D., Fu, X., Luan, Q., Liu, J., Wang, H., Zhang, S.: Effectiveness assessment of LID for urban waterlogging mitigation. Hydrol. Res. **52**(1), 284–304 (2021)

Mapping Gaps: Evidence-Based Analysis of Urban Emissions Trends and Climate Commitment in Major Italian Cities

Laura Ascione, Carmela Gargiulo, and Carmen Guida(✉)

Department of Civil, Building and Environmental Engineering, University of Naples Federico II, Naples, Italy
carmen.guida@unina.it

Abstract. Cities are pivotal to the European decarbonization path, yet the efficacy of their institutional responses remains poorly mapped. This paper assesses the "state of the art" of climate commitment across major Italian cities, exploring the nexus between strategic pledges, financial allocation, and actual emission outcomes. The research adopts a multidimensional methodology by triangulating three key datasets: (i) sectoral CO_2 equivalent emissions (2000–2023); (ii) per capita public investments from Open Coesione (2017–present) directed toward climate-sensitive sectors such as energy efficiency and sustainable mobility; and (iii) institutional progress within the Covenant of Mayors framework (distinguishing between commitment, planning, and monitoring phases).

By correlating these indicators through spatial analysis and bivariate mapping, the study identifies significant misalignments. Preliminary findings suggest that high financial effort and formal strategic adherence do not linearly translate into immediate carbon mitigation. The analysis reveals structural mismatches between dominant local emission sources and targeted funding. From an urban planning perspective, these results challenge the assumption that climate and sustainable transition are a mere financial or bureaucratic exercise. The paper argues that effective mitigation requires strict policy-sectoral alignment, ensuring investments address a city's specific fingerprint, while acknowledging how urban form and institutional inertia may resist rapid decarbonization. This study provides a critical evidence-based framework for evaluating the actual impact of urban climate governance in Italy.

Keywords: Urban Climate Planning · Mitigation · Climate Commitment

1 Introduction

Climate action in urban planning is structured around two distinct yet complementary strategies: adaptation and mitigation [1, 2]. While adaptation focuses on increasing the territorial resilience to unavoidable climatic impacts, such as urban heat islands or extreme flooding, mitigation targets the root causes of the crisis by reducing greenhouse gas emissions [3–5]. For urban planners, managing this duality is a major challenge. For

© The Author(s), under exclusive license to Springer Nature Switzerland AG 2027
O. Gervasi et al. (Eds.): ICCSA 2026 Workshops, LNCS 16761, pp. 429–444, 2027.
https://doi.org/10.1007/978-3-032-30527-5_28

example, the measures proposed for each objective often suggest conflicting land-use options [6, 7]. However, given the pursuit of carbon neutrality, mitigation has become a structural objective in European urban planning, driven by the ambitious targets of the Green Deal and the specific "100 Climate-Neutral and Smart Cities" mission [8–10].

In Italy, the institutional response to this challenge is centred on major cities, the capitals of Italian provinces. Such cities serve as primary laboratories for environmental transition but also exhibit deep historical and structural resistance to change [11–13]. For urban planners, decarbonization is not merely a climatological target; it represents a radical reshuffling of territorial assets, from the retrofitting of the historical building stock to the total reorganisation of metropolitan mobility. However, the current state-of-the-art suggests that, despite increases in planning activities and available capital, the correlation between institutional intent and actual emission reductions remains poorly documented [14–16].

The Covenant of Mayors (CoM) framework is a big part of this change because it makes local climate goals official. Italy has adopted this framework widely, making it the European country with the most signing mayors. However, the adoption is still not uniform. The level of municipal commitment is a sign of how mature the administration is. It goes through a clear hierarchy, starting with the first political signal, then the creation of integrated strategies (Sustainable Energy and Climate Action Plans - SECAPs), and finally the strict monitoring of results. From the point of view of territorial and urban governance, the change from planning to monitoring is very important; it represents the juncture at which strategic decisions must undergo empirical evaluation. However, in numerous Italian contexts, the disparity between these phases persists, prompting inquiries regarding whether such commitments serve as authentic catalysts for change or merely as superficial bureaucratic adherence.

Despite the formal commitments made by cities to these initiatives, resources have been extensively directed toward solutions and interventions addressing climate change. Since 2017, the OpenCoesione portal has continuously documented investments explicitly designated as "Climate Change Strategies Focus". Economic resourses have gone to important areas like building infrastructure for sustainable transportation, using renewable energy, and making public assets more efficient. These expenditures embody the tangible implementation of urban policies; however, their efficacy necessitates validation through longitudinal physical data. By cross-referencing these financial flows with CO2 emissions trends from 2000 to 2023, we can go from a story-based state of the art to an evidence-based audit. This longitudinal data encompasses various socio-economic cycles, enabling us to evaluate whether the recent surge of "green" capital has effectively dissociated urban growth from carbon emissions.

The research presented here focuses on major Italian cities as the main characters of the national climate strategy. By examining the mismatch between what cities have committed to, what they have spent, and how they have performed in terms of mitigation, this study seeks to identify empirical inconsistencies. Specifically, the paper investigates if current climate funding is correctly aligned with the metabolic profile of the city, addressing the actual dominant sources of emissions, such as residential heating or private transport, or if there is a sectoral misalignment that undermines the path to neutrality. Ultimately, the work questions whether the planning efforts of the last two decades

have been sufficient to transform the carbon trajectory of Italian urban environments, or whether a more radical, spatially driven approach to investment is required.

2 Materials and Method

To address the research questions identified in the previous section, this study employs a multi-dimensional methodological framework grounded in the triangulation of three distinct datasets.

The goal is to look at how climate commitments, financial flows, and emission trends affect each other in Italy's provincial capitals (namely, *capoluogo di provincia*). This method goes beyond merely assessing the quality of urban climate governance; it seeks an empirical framework that spans the entire policy cycle, from formal strategic intent and actual capital investment to verified performance assessment. The next three sections give a detailed look at the datasets that were used and the steps that were taken to make the data consistent and standardise it, to ensure that Italy's major urban centres can be compared in a strong way. The final subsection focuses on a subset of synthetic indicators developed to provide further insights into the empirical framework.

2.1 CO_2 Emissions: Enel YoUrban

The data used to assess trends in CO_2 emissions were drawn from a dataset provided by Enel X, which has developed the new CO_2 City Index 2023 [17]. The tool, designed for policymakers, allows users to navigate, simply and intuitively, via a map, estimates of anthropogenic CO_2 emissions across the whole of Italy from 2000 to 2023, expressed as total CO_2 per square kilometres and CO_2 per inhabitant, both in tons per year. From 2020 to 2023, it also provides a detailed overview of the top 10 emitting sectors. The sectors range from industrial activities, agricultural activities, residential buildings, commercial and public buildings, and extra-urban, logistics, private and local public transport, ports, to airports. The stated aim of this tool is to raise awareness among public administrations regarding emissions in their respective territories and to provide them with an initial assessment that serves as a basis for more detailed territorial analyses.

The CO_2 City Index 2023 uses multi-scalar triangulation of national institutional data and spatial proxies to transform top-down national reporting into evidence-based territorial measurement. The methodology uses national inventory reports from ISPRA [18] and the UNFCCC [19] as a base, so that emission levels are in line with international "Scope 1" direct emissions. The national figures are then downscaled to the municipality using socio-demographic and economic variables from ISTAT [20], including census data and ATECO [21] industrial classes to weigh emissions from houses and businesses.

OpenStreetMap roads and hierarchy and flow data from the Automobile Club d'Italia (ACI) [22, 23] are incorporated. Specific traffic volumes from Assaeroporti and Assoporti [24] will identify the impacts of port-based transport and airports on the ground. For agriculture, the model uses Copernicus Corine Land Cover [25] data and Ministry of Energy and Trade and Industry records from Mase and Mimit [26] about provincial gas and fuel sales. The model is compared against the EDGAR inventory and ODIAC models to produce a high-resolution spatial grid of 1x1km [27, 28]. This integration of

open data sources allows a precise assessment of the urban carbon footprint over the past 23 years.

In order to operationalise the dataset, CO_2 emission records have been normalised to allow comparison across the different case studies among the sample.

2.2 Urban Investments on Climate Change Strategies: OpenCoesione

To define the financial flows, the cohesion policy funds freely available on the OpenCoesione.gov.it website were taken into account [29]. Specifically, the data available in the section entitled 'Focus on Climate Change Strategies' was considered [30]. This section is dedicated to EU cohesion policy interventions which, according to the criteria set out in European Commission Implementing Regulation No 215/2014 for the 2014–2020 programming cycle, contribute to preventing climate change [31]. Based on the common provisions in the regulation, which outline methodologies for calculating contributions to climate change mitigation and the types of interventions funded, the dataset identifies two broad categories of projects. The first category comprises projects that are directly and entirely focused on combating climate change (contributing 100%). Funding is allocated to initiatives that substantially reduce emissions or increase resilience. The second category includes projects that have a positive impact on the climate, although indirectly or partially, or that represent preparatory actions towards environmental sustainability (contributing 40%) [31, 32]. The methodology used aims to provide an initial estimate of the investments made using European funds to achieve the target of reducing CO2 emissions [30]. Although the analysis focuses on climate change strategies, the initiatives have been grouped under 13 broad themes identified by OpenCoesione. The themes of cohesion are "Research and Innovation", "Digital Networks and Services", "Business Competitiveness", "Energy", "Environment", "Culture and Tourism", "Transport and Mobility", "Employment and Work", "Social Inclusion and Health", "Education and Training" and "Administrative Capacity". In particular, the initiatives included in the database focusing on climate change strategies belong to only some of these categories ("Environment", "Competitiveness and Enterprise", "Culture and Tourism", "Energy", "Digital Networks and Services", "Research and Innovation" and "Transport and Mobility"). This classification allows us to see how the climate objective intersects with sectors, providing an overview of investment priorities. All projects in the dataset were taken into account, covering all stages of progress, from those not yet started to those already completed, thereby considering not only what has already been achieved but also the total financial commitment. Consequently, the financial dimension considered is the sum of total public funding, excluding public funding, foreign resources, and other similar items. In order to ensure the greatest possible comparability between the cities in the sample, the thematic categories 'Culture and Tourism', 'Digital Networks and Services' and 'Research and Innovation' were excluded from the analysis. Their exclusion is justified by the highly asymmetrical distribution of funds across these categories. As these are expenditure items present only in a very limited number of cities, their inclusion would have introduced a bias into the IM index, penalising cities lacking such investments and inflating the apparent diversity of those that benefited from them. The analysis is therefore conducted on the four thematic categories with sufficiently widespread coverage in the sample: Energy, Environment, Competitiveness of companies and Mobility and

Transport. The Energy theme covers the construction of facilities for generating energy from renewable sources and the promotion of energy saving among citizens, businesses and the public sector, including schools. It also includes measures to promote district heating and cooling, and the development of cogeneration (electricity and heat) and trigeneration (electricity, heat and cooling). As far as the Environment theme is concerned, it covers measures relating to waste and wastewater management. It also includes actions to prevent environmental risks, coastal erosion and hydrogeological instability, including measures to adapt to climate change, promote biodiversity and protect nature. The Business Competitiveness theme includes incentives and practical support for the creation of new businesses and new production facilities, or for the expansion and modernisation of existing plants and production areas. It also includes support for financial engineering instruments for businesses (guarantee funds, loan funds and access to credit, and venture capital funds). In the end, the Mobility and Transport theme covers the upgrading of railway lines, the road network, port connections and intramodality. It also includes measures to encourage sustainable mobility and those promoting public transport in congested urban areas [29].

2.3 Commitment Level: Covenant of Mayors

The third dataset is based on an open database relating to the Covenant of Mayors (CoM) [31]. This database tracks the Italian cities participating in the CoM and monitors their progress through the various stages [33]. The CoM represents one of the largest voluntary institutional movements for local authorities on climate governance [34]. The initiative initially united mayors who pledged to exceed the EU's target of reducing CO_2 emissions by at least 20% in their territories by 2020. The rapid growth of the EU Covenant underscored the determination and leadership of local authorities in confronting the climate crisis from the ground up. It was launched in 2008 and currently has around 10,800 signatories representing 220 million citizens [34]. By signing up, mayors formally commit to implementing European climate and energy objectives at the local level [34]. By joining the EU Covenant of Mayors, cities and towns pledge to develop, implement and monitor Sustainable Energy and Climate Action Plans (SECAPs) [35]. The first step is to sign the Pact and formalise the commitment before the local council. This is a necessary declaratory step and has no operational content whatsoever. The second step involves planning the presentation of the SECAP, which must take place within two years of signing [35]. The SECAP is a plan in which local authorities outline the measures and policies the administration intends to implement to achieve its climate governance objectives [35]. Both the commitments and the drafting of the SECAP are envisaged across three different timeframes: 2020, 2030 and 2050. Signatory municipalities commit to reducing CO_2 emissions by at least 20% by 2020, with an obligation to submit a Sustainable Energy Action Plan (SEAP) focused exclusively on mitigation [34]. With the second update, launched in 2015, the target was raised to a 40% reduction in climate-changing emissions by 2030 and the framework was extended to include adaptation, with the SEAP replaced by the more comprehensive SECAP [35]. With the third update, however, the scheme aligns with the European Green Deal and the European Climate Law, guiding signatories towards carbon neutrality by 2050, with an indicative interim target of a 55% reduction by 2030 compared to 1990 levels [34]. A key analytical

feature is the flexibility introduced with respect to the 2030 horizon: municipalities that commit to 2050 are not obliged to set a binding interim target for 2030, allowing them to structure their own milestones toward climate neutrality autonomously [34]. This option creates structural heterogeneity within the sample between municipalities with dual 2030/2050 targets and those with exclusively long-term commitments. The final step for the signatories of the pact is to commit to submitting monitoring reports [35]. The local authorities undertake to monitor the extent to which the actions and measures contained in the SECAP are being implemented [35]. This step represents the most demanding operational challenge for the local authorities, who will have to prepare up-to-date inventories of emissions and implement climate policies.

2.4 Data Integration and Synthesis

Having three heterogeneous databases poses an analytical challenge in terms of how to compare the data analytically in order to identify patterns between cities, investments and CO_2 emissions. To this end, data integration was achieved through various methodological operations: (i) the normalisation and standardisation of data relating to changes in CO2 emissions and total public investment extracted from OpenCoesione; (ii) the construction of two composite indicators that simplify the complexity of the information; (iii) the use of bivariate graphs as the primary tool for interpreting the relationships between the three dimensions

CO_2eq emissions had already been calculated in tCO_2eq per capita, while the following percentage formula was used to assess the change in emissions over the period 2000–2023:

$$\Delta CO_{2,i} = \frac{CO_{2,i,2023} - CO_{2,i,2000}}{CO_{2,\ i,\ 2000}} \times 100$$

Where ΔCO_2,i,t represents the total emissions of municipality i in year t. A negative value indicates a trajectory towards decarbonisation, whereas a positive value indicates an increase in emissions over this period. OpenCoesione Public investment has also been expressed in per capita terms (€ per inhabitant), calculated based on the ISTAT population at 31 December 2024.

The first composite indicator is the Investment Mix Index (IMI), which measures the degree of sectoral diversification of investments, based on the 13 composite themes of OpenCoesione. The index was constructed on the basis of the entropy index, which has been used in numerous studies to represent the land use mix [36, 37]. The land use mix measures the distribution of heterogeneous categories within a spatial unit. Entropy scores range from 0 to 1, where 0 indicates a homogeneous land use and 1 indicates a balanced mix of the categories present. This same approach was applied to the thematic investment categories extracted from OpenCoesione, whilst maintaining the logic of the entropy index. The formula used is as follows:

$$IMI_i = -\frac{\sum_{s=1}^{n} \left(p_{i,s} \bullet \ln\left(p_{i,s}\right)\right)}{\ln(n)}$$

Where $p_{i,s} = I_{i,s}/I_{i,tot}$ is the share of thematic category s in the total OpenCoesione investment of municipality i, and n is the total number of thematic categories considered. The denominator $\ln(n)$ normalises the index within the interval [0,1], making it possible to compare cities with investments spread across a different number of active sectors. An IMI value close to 1 indicates an even distribution of expenditure across all available categories; a value close to 0 indicates that almost all investments are concentrated in a single sector.

The second composite indicator is the Level of Commitment (LoC), which measures institutional governance by distinguishing between cities that are only formal members of the CoM and those that are actively committed to achieving the objectives. The LoC summarise the ability to complete the institutional cycle of three phases described above in a scalar index ranging from 0 to 1, divided into four thresholds, as summarised in the following Table 1.

It is important to emphasise that the LoC does not measure the quality of the plan or the ambition of the stated targets, but solely the degree to which the institutional cycle set out in the CoM framework has been completed. In this sense, the index serves as a proxy for the municipal administration's administrative capacity and procedural consistency, rather than as a direct indicator of climate performance. The association between the LoC and changes in emissions is therefore one of the central interpretative axes of the analysis, allowing us to test empirically whether more structured climate governance translates, and to what extent, into actual decarbonisation outcomes.

Table 1 Structure of the LoC Index_ values assigned to the institutional phases of the CoM

Level of commitment	LoC value
Municipality not signed the CoM	0
Commitment to the CoM (2020, 2030, 2050)	0.33
Submission of Action Plan (SEAP or SECAP)	0.66
Monitoring latest Action Plan	1

Once the indicators had been developed, the three datasets were integrated using a series of bivariate graphs. The aim is to identify possible relationships between the commitment of cities and local authorities, the economic resources at their disposal, and actual changes in emissions.

3 Results

This section presents the results of the analysis, structured on different levels of interpretation. Firstly, it describes the emissions trajectories of Italy's provincial capitals over the period 2000–2023.

It then analyses the structure of the cities' institutional commitment within the CoM framework. Finally, the two analyses are integrated with the dimension of public investment in climate strategies through bivariate graphs constructed using the synthetic LoC index.

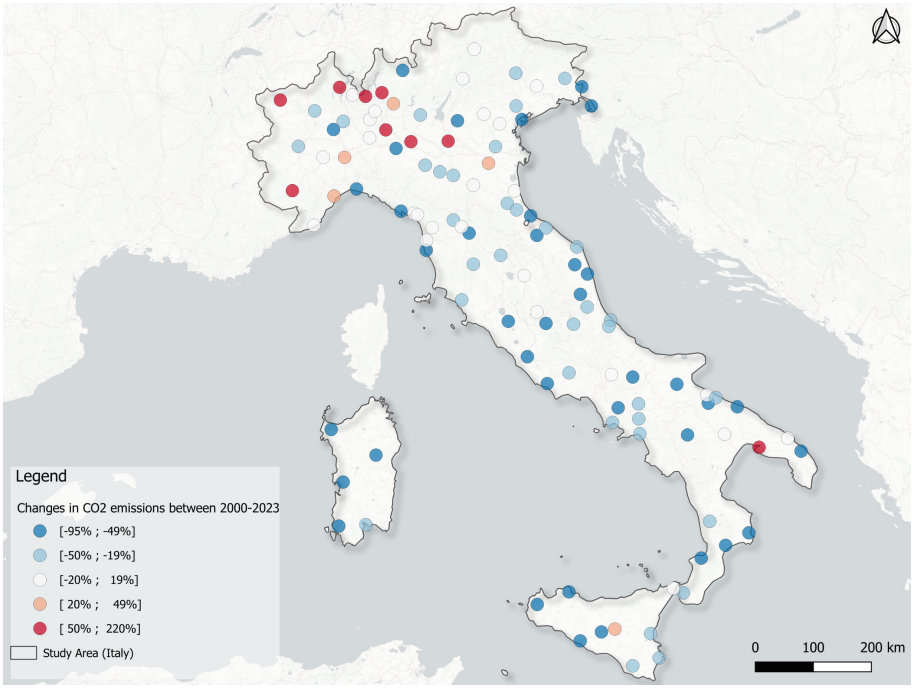

Fig. 1 Spatial analysis of CO_2 emissions trend in Italian provincial capitals, from 2000 to 2023. Authors' elaboration from Enel YoUrban database.

The study aims to identify recurring patterns or misalignments between the three analytical dimensions.

The analysis of the percentage changes in CO2 emissions over the period 2000–2023 (Fig. 1) shows an overall positive trend, with an average decrease of 23%. The most significant reductions, ranging from 50% to 95%, were observed mainly in cities in northern Italy and in some in central Italy. Cases of increased emissions are in the minority, but are not to be overlooked, given that the increases reach up to 220% (in Lecco). The moderate variation range (−20% to +19%), which includes provincial capitals with essentially stable trends, is distributed across the entire country, representing a widespread condition independent of regional location.

The Sankey diagram (Fig. 2) provides an immediate overview of the structure of institutional commitment among the 112 provincial capitals in relation to the CoM framework, revealing a gradual decline in the number of cities as the operational demands of each phase increase. The rate of formal participation is very high, with around 94% of cities having signed the Covenant. However, the distribution by level of commitment shows that most cities have committed only to 2020, with just a small number also committing to 2030. By 2050, only 19 cities have committed to producing a SECAP, suggesting that most cities have not yet renewed their commitment to more ambitious timeframes. The transition to the planning phase reveals a significant initial decline: whilst 80 cities submitted an Action Plan under the CoM 2020, only 43 did so for 2030

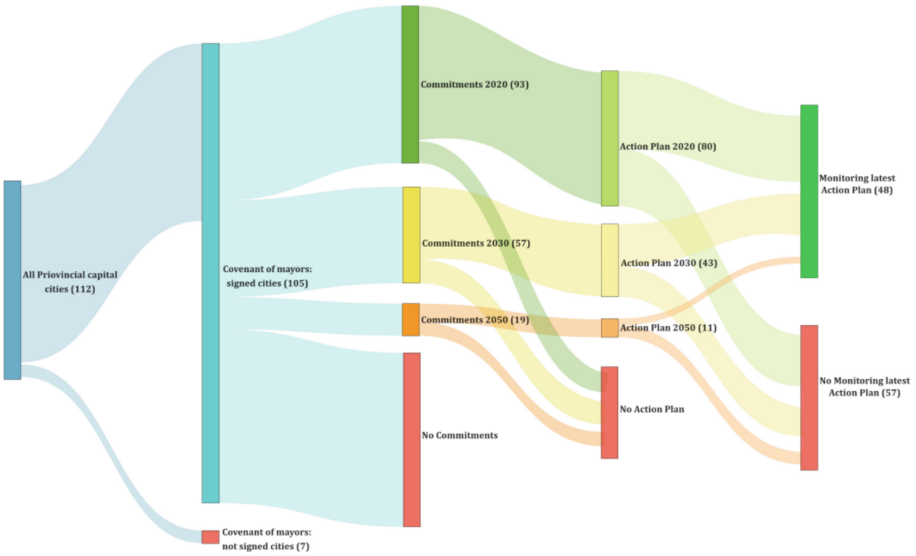

Fig. 2 Institutional funnel of Covenant of Mayors participation among Italian provincial capitals (n = 112).

and just 11 for 2050. Overall, therefore, a not insignificant proportion of signatories have not yet translated their political commitment into an operational planning tool. As regards the monitoring phase, less than half of the signatories have drawn up a monitoring report on the latest actions implemented.

The scatter plot in Fig. 3 plots the 112 cities on a bivariate graph defined by per capita investment (X-axis) and the percentage change in CO_2 emissions (Y-axis), grouping the cities by LoC class. The linear regression lines for all four LoC classes show a negative slope, indicating that, regardless of the level of institutional commitment, higher per capita investment tends to be associated with greater reductions in emissions. However, the slopes are similar to one another, and the 'No commitment' class (LoC = 0) exhibits the regression with the steepest slope, an apparently counterintuitive result suggesting that the effect of investment on emissions reduction is not associated with the commitment generated by the CoM. Most cities fall within a range of an average per capita investment of €0–200 per inhabitant and a reduction in emissions, regardless of the LoC group to which they belong.

Figure 4 completes the analysis of these data, grouping the cities by LoC and simultaneously showing, in a combined graph, the average CO_2 emissions (in gold, left-hand axis) and the average per capita investment (in green, right-hand axis). The most striking finding is that, in both cases, the differences between the groups do not follow the expected gradient. It is the LoC = 0.33 group, which corresponds to cities that have signed the Covenant of Mayors but have not produced either an action plan or a monitoring report, that shows the most pronounced average reduction in emissions across the entire sample. Cities with the most comprehensive institutional cycle (LoC = 1, active monitoring) show a more modest average reduction. In terms of investment, it is the LoC

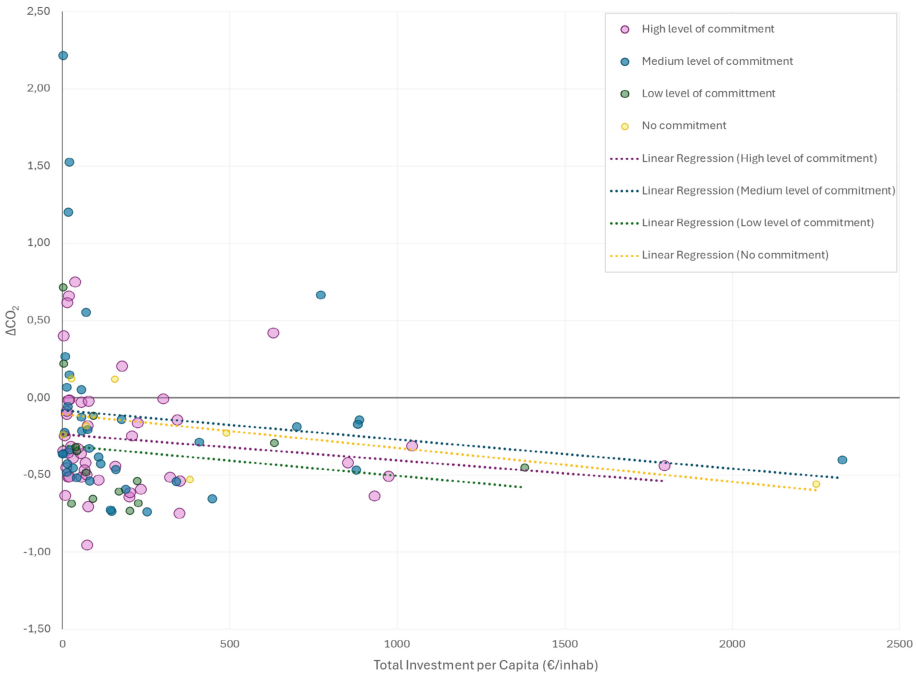

Fig. 3. Bivariate scatter plot of total public investment per capita (€/inhabitant, x-axis) and percentage change in CO_2 emissions 2000–2023 (ΔCO_2, y-axis), stratified by Level of Commitment (LoC).

= 0 group: cities with no commitment to the CoM show the highest average per capita investment in the sample, with a particularly pronounced upward dispersion

To explore the unexpected patterns revealed by the bivariate analysis, the internal sectoral composition of investment for the cities in these two groups was examined by visualising the investment by thematic category (Environment, Energy, Mobility and Transport, Competitiveness of companies) in the Fig. 5. For the group of cities with Loc = 0.33 (Fig. 5a), the average IM index is 0.39. This is also evident when examining the investment sectors, which are heterogeneous. Some cities show a clear dominance of the Energy category (Avellino, Gorizia, Sondrio, Terni, Crotone), others are almost entirely focused on Mobility and Transport (Carbonia, Caserta, Rovigo), whilst

Como concentrates almost all of its expenditure in the Environment category. Ferrara has a significant share in the Competitiveness of companies category, even though this is not directly linked to a sectoral decarbonisation strategy, accounting for over 65% of total investment. The graph for cities with LoC = 0 (Fig. 5b) shows an even more pronounced pattern of mono- or bi-sectoral concentration. Indeed, from the perspective of the IM index, most cities have low values. Almost all cities in this group have investments spread across no more than two categories, with a clear alternation between Energy and Mobility and Transport. Imperia and Padua concentrate almost all their expenditure on Energy; Carrara, Catanzaro, Reggio Calabria and Vibo Valentia are dominated by Mobility and Transport, with varying shares of Energy; Reggio Emilia has the most varied

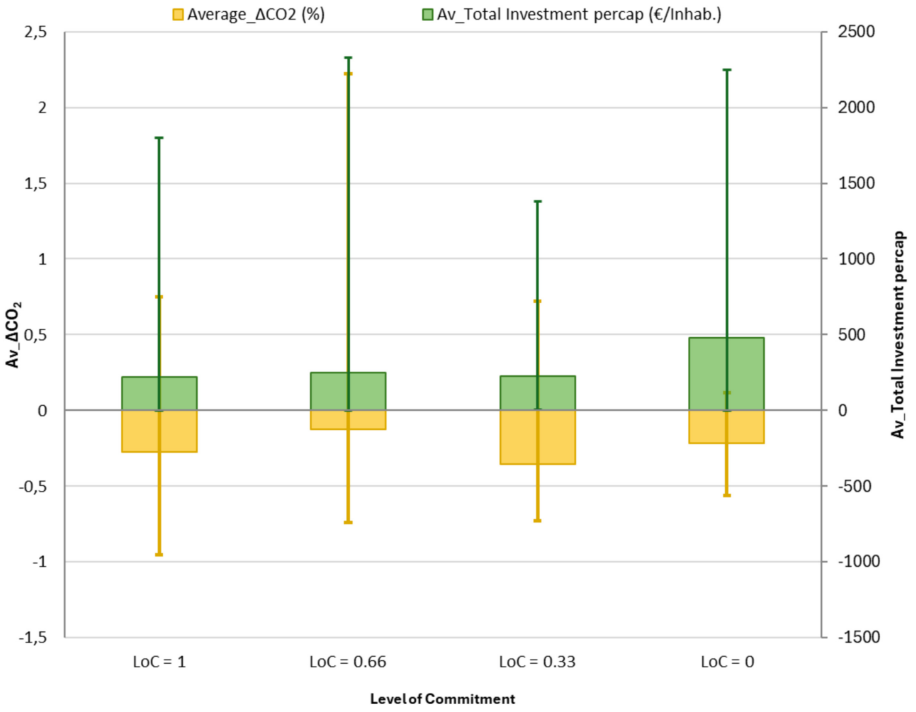

Fig. 4. Grouped bar chart comparing average ΔCO_2 (%, left axis, gold) and average total investment per capita (€, right axis, green) across Level of Commitment tiers (LoC = 1, 0.66, 0.33, 0).

distribution in the group, with a significant Environment component alongside Energy and a residual share of Mobility. The most significant finding for interpretative purposes is that no city in this group exhibits a diversified portfolio, and the 'Competitiveness of companies' category is virtually absent, unlike what was observed in the LoC = 0.33 group. This suggests that the high levels of investment recorded in the LoC = 0 group are concentrated in infrastructure sectors with a more direct climate relevance, namely energy and mobility

Fig. 5. Sectoral composition of climate-sensitive investments as used in the construction of the Investment Mixité Index (IMI), for the two groups showing the most anomalous patterns relative to the expected LoC–performance gradient: cities with LoC = 0.33 (a) and cities with LoC = 0 (b). Bars represent the proportional share of expenditure by thematic category (Environment, Energy, Mobility and Transport, Competitiveness of companies) over total per capita investment. Authors' elaboration on Open Coesione data.

4 Discussions and Conclusions

The results driven by this contribution aim to empirically delineate the status of urban climate governance in Italy by triangulating three distinct yet complementary dimensions: the actual trajectory of CO_2 emissions in Italian provincial capitals from 2000 to 2023, the volume and sectoral composition of public investments facilitated by EU

cohesion policy funds, and the institutional maturity of cities within the Covenant of Mayors framework. The evidence obtained contradicts numerous established beliefs about the relationship among climate commitment, financial investment, and decarbonisation outcomes.

The spatial analysis of emission trends shows that most of Italy's provincial capitals have been able to lower their per capita CO_2 emissions over the study period. There is a clear concentration of deep reductions (over 49%) in mid-sized and smaller cities, especially in the Centre-South. Nonetheless, a substantial cluster of cities, particularly in the North-West, has experienced considerable increases in emissions, highlighting the spatial heterogeneity of Italy's decarbonisation trajectory and the dangers of using national or regional aggregates as a substitute for urban climate performance.

The institutional landscape, as highlighted in Fig. 2, reveals a system with broad but uneven formal participation. The CoM has been signed by 105 of the 112 provincial capitals, but as governance improves, the number of cities that have reached the monitoring phase, which is the stage that requires real accountability, drops to only 48. The fact that many cities were arrested during the commitment or planning phases suggests that institutional participation is more common than institutional performance. This supports the idea that signing the CoM is often more of a statement than an action.

The bivariate analysis of investment intensity and emission change, categorised by LoC, leads to a result that is simultaneously promising and warning. The regression trends indicate a negative relationship between investment per capita and ΔCO_2 across all commitment groups. This means that more investment is linked to less emissions. But the link is weak, especially when investments are low, and the wide range of outcomes within each group shows that the amount invested does not determine climate outcomes. Cities with the highest Level of Commitment (LoC = 1) show the widest range of emission trajectories, with some of the biggest drops and some of the biggest rises. This finding carries a potentially important interpretive implication: in cities where climate commitment is most seriously institutionalised, mitigation may not be the only objective shaping urban policy. The integration of adaptation, resilience, and quality-of-life targets within mature governance frameworks may partially explain why emission reduction alone does not emerge as a linear outcome of high institutional commitment, pointing to the inherent multi-objective complexity of advanced urban climate governance.

On the other hand, the grouped bar chart comparing average ΔCO_2 and average investment per capita across LoC tiers shows a surprising pattern: cities that do not have a CoM commitment (LoC = 0) invest more money per person on average than cities that do, but they also cut emissions by about the same amount or a little less. This finding does not absolve institutional disengagement; however, it reveals the structural disconnection between the channels for fund allocation and the governance frameworks that formalise climate objectives. These two systems seem to operate simultaneously rather than together, which limits their potential for synergistic impact.

A wider look at the results of this empirical research shows a major problem with how Italy manages its urban climate: there is a gap between investments, what cities have officially committed to, and what emissions trajectories really look like on the ground. The implication for urban planning is clear. Decarbonization is not a straightforward

result of financial volume or bureaucratic compliance. It depends on how well investments are tailored to each city's unique metabolic profile, focusing on the main sources of emissions in that area rather than using general sectoral templates. It also depends on whether institutional frameworks create real operational accountability instead of just following procedures [38].

Future research should deepen the sectoral decomposition of both investments and emissions, moving beyond aggregate indicators to map whether cohesion funds are actually directed toward the emission sources that most characterise each city's carbon fingerprint. The integration of urban features to capture the unique urban footprint (e.g. as building stock age, land use mix, and transport network density) would further enrich the analytical framework and begin to account for the structural inertia that this study has identified as a persistent mediating factor between policy intent and territorial outcomes [39]. As the European climate mission accelerates toward Net-Zero targets, the evidence produced here suggests that Italy's major cities need not more commitments, but better-aligned ones. In this sense, the empirical framework developed here is intended as a first step toward a broader research agenda: one that treats major Italian cities not merely as objects of analysis, but as the primary drivers of national climate transition. The heterogeneity of urban profiles documented in this study, ranging from emission trajectories, investment intensities, and governance maturity, ultimately motivates the need for decision-support tools capable of translating this complexity into actionable, city-specific guidance for policymakers, moving from the diagnosis of misalignment to the design of tailored climate solutions.

Acknowledgment. The authors wish to thank Enel X for providing access to the data and analyses available via the Enel X YoUrban platform, which were essential to this work's development.

References

1. Ye, X., et al.: Urban planning and IPCC-like city assessments integration for climate-resilient cities. Environ. Plann. B Urban Anal. City Sci. **52**(7), 1549–1556 (2025)
2. Herziger, A., Guerriero, J.G., Levontin, L., Swim, J.K.: Adaptation versus mitigation: does goal-framing influence the appeal of climate-relevant behaviors? J. Environ. Psychol. **110**, 102934 (2026)
3. Grafakos, S., Trigg, K., Landauer, M., et al.: Analytical framework to evaluate the level of integration of climate adaptation and mitigation in cities. Clim. Chang. **154**, 87–106 (2019)
4. Lee, T., Yang, H., Blok, A.: Does mitigation shape adaptation? The urban climate mitigation-adaptation nexus. Clim. Pol. **20**(3), 341–353 (2020)
5. Ramavat, A., Chatterjee, A., Hossain, I.: Climate change mitigation, adaptation, and resilience policies. In: Hossain, I., Ghosal, I., Haque, A.K.M.M. (eds.) Green Policies for a Sustainable World. Springer, Cham (2026)
6. Andauer, M., Juhola, S., Klein, J.: The role of scale in integrating climate change adaptation and mitigation in cities. J. Environ. Plan. Manag. (2018). https://doi.org/10.1080/09640568.2018.1430022
7. Sharifi, A.: Urban sustainability assessment: an overview and bibliometric analysis. J. Clean. Prod. **276**, 124187 (2020). https://doi.org/10.1016/j.jclepro.2020.122813
8. Wolf, S., Teitge, J., Mielke, J., et al.: The European green Deal — more than climate neutrality. Intereconomics. **56**, 99–107 (2021)

9. Salvia, M., Pietrapertosa, F., D'Alonzo, V., Maestosi, P.C., Simoes, S.G., Reckien, D.: Key dimensions of cities' engagement in the transition to climate neutrality. J. Environ. Manag. **344**, 118519 (2023)
10. Shtjefni, D., Ulpiani, G., Vetters, N., Koukoufikis, G., Bertoldi, P.: Governing climate neutrality transitions at the urban level: a European perspective. Cities. **148**, 104883 (2024)
11. Pietrapertosa, F., et al.: Urban climate change mitigation and adaptation planning: are Italian cities ready? Cities. **91**, 93–105 (2019)
12. Ascione, L., Gargiulo, C., Guida, C.: Adaptation and energy saving through urban green spaces in climate action plans: the experiences of 20 global cities. TeMA - J. Land Use Mobility Environ. (2), 31–46 (2025)
13. Berti, K., Bienvenido-Huertas, D., Rubio-Bellido, C., Romero-Recuero, I.: Changing climate in Italian cities and Italian building regulations: analysis focused on future climate change scenarios. Urban Clim. **61**, 102408 (2025)
14. Loftus, P.J., Cohen, A.M., Long, J.C.S., Jenkins, J.D.: A critical review of global decarbonization scenarios: what do they tell us about feasibility? WIREs Clim. Change. **6**, 93–112 (2015)
15. Haarstad, H.: Do climate targets matter? The accountability of target-setting in urban climate and energy policy. In: Sareen, S. (ed.) Enabling Sustainable Energy Transitions. Palgrave Pivot, Cham (2020)
16. Brand, U., Hausknost, D., Brad, A., et al.: Structural limitations of the decarbonization state. Nat. Clim. Chang. **15**, 927–934 (2025)
17. Enel X: https://yourban. enelx.com
18. Istituto Superiore per la Protezione e la Ricerca Ambientale (ISPRA): Fattori emissivi settore trasporti e combustioni. ISPRA, Rome (2019)
19. United Nations Climate Change: Reporting requirements. https://unfccc.int/process-and-meetings/transparency-and-reporting/ (2023); Common Reporting Format: Tabelle nazionali italiane (2022). https://unfccc.int/documents/461710
20. Istituto Nazionale di Statistica (ISTAT): Portale I.Stat (2023). http://dati.istat.it/
21. Istituto Nazionale di Statistica (ISTAT): Portale I.Stat (2023). https://www.istat.it/classificazione/classificazione-delle-attivita-economiche-ateco/
22. Automobile Club d'Italia (ACI): Classificazione e portata stradale (2023). https://www.aci.it
23. OpenStreetMap contributors: Planet dump (2023). https://www.openstreetmap.org
24. Assaeroporti: Dati traffico aeroportuale (2023). https://www.assaeroporti.com (2023); Assoporti: Dati infrastrutture portuali. https://www.assoporti.it
25. Copernicus Land Monitoring Service: CORINE land cover (2023). https://land.copernicus.eu/pan-european/corine-land-cover
26. Ministero dell'Ambiente e della Sicurezza Energetica (MASE): Energia e clima 2030 (2023). https://www.mase.gov.it/energia/energia-e-clima-2030
27. Monforti Ferrario, Fabio; Crippa, Monica; Guizzardi, Diego; Muntean, Marilena; Schaaf, Edwin; Lo Vullo, Eleonora; Solazzo, Efisio; Olivier, Jos; Vignati, Elisabetta) EDGAR v6.0 Greenhouse Gas Emissions. European Commission, Joint Research Centre (JRC) (2021)
28. Oda, T., Maksyutov, S.: A very high-resolution (1 km × 1 km) global fossil fuel CO_2 emission inventory derived using a point source database and satellite observations of nighttime lights. Atmos. Chem. Phys. **11**, 543–556 (2011). https://doi.org/10.5194/acp-11-543-2011
29. OpenCoesione. OpenCoesione – Open data sulla coesione in Italia. Dipartimento per le Politiche di Coesione e per il Sud, Presidenza del Consiglio dei Ministri. https://opencoesione.gov.it/it/. Accessed March 2026
30. OpenCoesione. Focus Strategie – Cambiamento climatico. Interventi della politica di coesione comunitaria 2014–2020 che contribuiscono a contrastare il cambiamento climatico. Dipartimento per le Politiche di Coesione e per il Sud, Presidenza del Consiglio dei Ministri. https://opencoesione.gov.it/it/dati/focus/clima/. Accessed March 2026

31. European Commission: Commission implementing regulation (EU) no 215/2014 of 7 march 2014 laying down rules for implementing regulation (EU) no 1303/2013. Official J. Eur. Union L. **69**, 8 (2014) https://eur-lex.europa.eu/legal-content/EN/TXT/?uri=CELEX:32014R0215
32. European Commission: NextGenerationEU Green Bond Framework – Annex: EU Climate Coefficients. European Commission (2021) https://commission.europa.eu/document/download/e92e0cf1-28e8-46ee-a821-609992356756_en
33. EU Covenant of Mayors: Covenant of Mayors Open Data. European Commission. https://www.covenantofmayors.eu/en/resources/data.html
34. EU Covenant of Mayors: Why the Covenant of Mayors? European Commission. https://eu-mayors.ec.europa.eu/en/Why-the-Covenant-of-Mayors
35. EU Covenant of Mayors: Planning. European Commission. https://eu-mayors.ec.europa.eu/en/Support/Planning
36. Bordoloi, R., Mote, A., Sarkar, P.P., Mallikarjuna, C.: Quantification of land use diversity in the context of mixed land use. Procedia. Soc. Behav. Sci. **104**, 563–572 (2013). https://doi.org/10.1016/j.sbspro.2013.11.151
37. Hofer, E., Musakwa, W., van Lanen, S., Gumbo, T., Netsch, S., Gugerell, K.: Inclusivity insights: two urban development projects in Johannesburg. J. Housing Built Environ. **37**(4), 1835–1858 (2022). https://doi.org/10.1007/s10901-021-09916-y
38. Gargiulo, C., Murgante, B., Zoppi, C.: Climate crisis and spatial planning. Green infrastructure and supply of ecosystem services. TeMA J. Land Use Mobility Environ. **2**, 3–11 (2025). https://doi.org/10.6093/1970-9870/12807
39. Gargiulo, C., Guida, C.: Climate-proofing cities: a focus on vulnerability indices. Int. Plan. Stud., 1–19 (2026)

Mapping Spatial Synergies and Trade-Offs: A Geographically Weighted Analysis of Ecosystem Services and Carbon Sequestration in Southern Italy

Federica Isola[1], Bilge Kobak[1,2(✉)], Sabrina Lai[1], Francesca Leccis[1], Federica Leone[1], and Corrado Zoppi[1]

[1] Department of Civil and Environmental Engineering, and Architecture, University of Cagliari, Cagliari, Italy
bilge.kobak@unica.it

[2] University School for Advanced Studies IUSS Pavia, Pavia, Italy

Abstract. Moving toward climate neutrality calls for spatially explicit planning frameworks that reflect territorial diversity and land-use change processes. Within this conceptual framework, this study has the objective of identifying and discussing spatially explicit planning approaches that can support the transition to climate neutrality in different regional spatial contexts. Therefore, a methodological framework is introduced and applied, designed to support climate neutrality through spatial planning strategies. Carbon sequestration (CS) serves as a key metric to evaluate both the current state and the temporal evolution of this process, examined in connection with the provision of specific ecosystem services (ESs) within the relevant spatial setting. The work is structured as follows. An approach is developed to define the provision of ESs. Drawing on previous research and assessments of environmental, landscape, and socio-cultural features, the study considers the following ESs: quality of habitat to sustain the life cycles of species valuable to humans; regulating climate by mitigating land sur-face temperature; agricultural and forestry production; and nature-based recreational opportunities. Moreover, spatial relationships between CS capacity and ES provision are examined through geographically weighted regressions, allowing comparisons across Basilicata, Campania, and Sardinia, regions in Italy forming the Italian Mezzogiorno. The multifunctional characteristics of ES supply contribute to optimizing CS capacity and advancing climate neutrality goals. In all regional contexts, high values of CS capacity elasticity are recognized in relation to habitat quality and ground temperature mitigation, and very low elasticity conditions as regards the supply of recreational ESs and agricultural and forestry production.

Keywords: Carbon sequestration · Climate neutrality · Ecosystem services · Geographically weighted regression (GWR) · InVEST model · Spatial planning

© The Author(s), under exclusive license to Springer Nature Switzerland AG 2027
O. Gervasi et al. (Eds.): ICCSA 2026 Workshops, LNCS 16761, pp. 445–462, 2027.
https://doi.org/10.1007/978-3-032-30527-5_29

1 Introduction

One of the biggest threats to global stability today is climate change (CC), which is having a rising impact on both rural and urban areas by affecting people's health, physical well-being, and general quality of life [1]. The evident consequences of global warming necessitate urgent action to meet the Paris Agreement target of limiting warming to 1.5 °C above pre-industrial levels. Achieving this objective requires a long-term balance between greenhouse gas emissions and removals, a pursuit often referred to as climate neutrality. Consequently, the European Union has committed to a 55% reduction in emissions by 2030 and full climate neutrality by 2050.

A third of the potential biological productivity of the global carbon cycle has been utilized by human activities, especially the use of fossil fuels and land clearing, which have fundamentally disturbed the cycle. In the Italian context, this pressure is manifested in increasing land consumption and urban sprawl, leading to biodiversity loss and heightened environmental risks such as floods and heat islands [2, 3]. Within this framework, regulating ecosystem services (ESs), specifically Carbon Capture and Storage (CCAS), are vital for mitigation and adaptation. CCAS is a natural phenomenon, primarily driven by photosynthesis, through which terrestrial ecosystems remove CO_2 from the atmosphere and store it in biomass and soil [4]. Natural ecosystems provide a multifunctional supply of services that interact in complex ways. While the principle of multifunctionality suggests that a single area can provide multiple benefits, certain functions may be mutually conflicting, leading to trade-offs where the enhancement of one service (e.g., carbon storage) may negatively affect another (e.g., biodiversity or agricultural production). Conversely, synergies occur when multiple services improve simultaneously.

Multiple studies such as Früh-Müller et al. [5] and Bateman et al. [6] document trade-offs and synergies between CCAS and other services. Viglizzo et al. [7] provide a comprehensive regression-based analysis, to examine how carbon sequestration partitions with water-flow, soil and climate regulation. Although regression analysis is commonly used to analyze relationships among multiple ESs [7, 8], these relationships are analyzed in a stationary way. This study seeks to go beyond the limitations of stationary regression analysis by studying non-stationary relationships in Mediterranean landscapes using a geographically weighted regression (GWR).

From this perspective, this work aims to analyze the relationship between CCAS and multiple ESs, such as quality of habitat (QOHA), land surface temperature mitigation (LOHM), agricultural and forestry production (AFPL), and nature-based outdoor activity potential (NOAP) using a GWR model, in order to determine and critically examine geographically delineated planning methodologies capable of facilitating the progression toward climate neutrality across heterogeneous regional territorial configurations. A GWR-based approach is preferred over ordinary regression models in ES studies for its ability to handle spatial non-stationarity, where relationships vary across locations.

The study employs a methodological framework aimed at promoting climate neutrality through spatially oriented planning policies. CCAS is employed as a central indicator to assess both the existing conditions and the dynamic progression of sequestration processes, analyzed in relation to the supply of selected ESs, with two main steps. First

step is the assessment of four ESs and the second is the investigation of the spatial interdependencies between CS potential and ES distribution using a GWR model, enabling comparative analyses among the selected Italian regions.

The paper is structured as follows. Section two outlines the case studies and methods. Section three presents the results obtained, which are then discussed in section four. Finally, section five concludes with final remarks and future research directions.

2 Materials and Methods

2.1 Study Area

The study area comprises three regions of the Italian "Mezzogiorno": Basilicata, Campania, and Sardinia (Fig. 1). Basilicata covers an area of approximately 10,000 km^2 [9] which is predominantly hilly, with 10% constituting plains and mainly concentrated along the Ionian coastline, and its landscape is predominantly agricultural, with extensive farming practices and high biodiversity [10]. Concerning land covers, according to the latest CORINE data [11], around 57% of the region is agricultural, 41% is forests and semi-natural vegetation, and only 1.6% is artificial. Campania extends over 13,700 km^2 [9] with mainly hilly and mountainous territory, while alluvial plains account for about 14% of the surface. The main mountain systems include the Matese Mountains and the Cilento Massif. Volcanic landforms are a distinctive feature of the region. Around 55% of the region is agricultural, around 37% is covered by forests and semi-natural vegetation, and 7.5% is artificial. Sardinia is the second-largest island in the Mediterranean Sea and has a landmass of approximately 24,000 km^2. The regional territory is predominantly hilly and characterized by numerous isolated mountain groups, including Gennargentu, Sette Fratelli, and Limbara [13], and coastal wetlands constitute a distinctive landscape feature. Around 46% of the region is agricultural, around 50% is covered by forests and semi-natural vegetation, and only 3% is classed as artificial. As of 1 January 2025, the population is 530,005 in Basilicata, 5,582,337 in Campania, and 1,562,381 people in Sardinia [12].

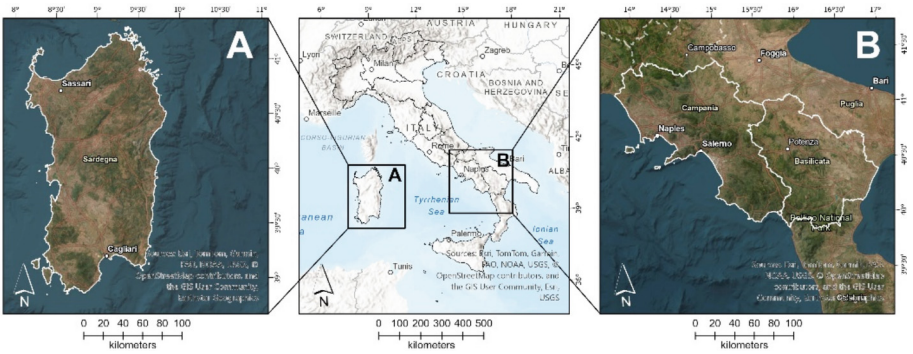

Fig. 1. Study areas: Sardinia (panel A), Basilicata, and Campania (panel B).

2.2 ESs Assessments

The methodology employed for assessing CCAS, QOHA, LOHM and NOAP is explained in Table 1 below.

Table 1. Data sources used for ESs assessments

ES	Method	Input/Parameter	Source
CCAS	InVEST Suite carbon storage and sequestration model	Land cover map	Corine Land Cover 2018
		CSV table showing carbon density values	NASA'S ORNL DAAC National Inventory of Forests and Carbon Pools in Italy ISPRA AGRIS Sardegna
QOHA	InVEST Habitat Quality model	Land cover map	Corine Land Cover
		Threat maps	Geofabrik Download Server
		Sensitivity table	Habitat classification and related parameters defined by Sallustio et al. [14] were adopted in this study.
LOHM	Land Surface Temperature (LST)	Satellite images	USGS Earth Explorer
NOAP	ESTIMAP Recreation model [15]	Degree of naturalness (Hemeroby index)	ISTAT 2019 for Sardinia, ISTAT 2023 for Basilicata and Campania livestock density Forested areas
		Protected and natural sites	National and regional parks Ramsar sites Natura 2000 sites
		Attractiveness of coastal zones	(i) distance from the coastline, modeled via an inverse logistic function; (ii) coastal geomorphology, using the Eurosion dataset; and, (iii) bathing water quality, based on European Bathing Water Directive data

(*continued*)

Table 1. (*continued*)

ES	Method	Input/Parameter	Source
AFPL	overlay of the land cover map with the agro-forestry value map	Average monetary values per unit area for agricultural lands	(i) the national agricultural land value database produced by the Council for Agricultural Research and Economics (CREA)
		mean land values for forestry areas	(ii) the dataset issued by the National Revenue Agency (NRA)

2.3 Geographically-Weighted Regressions

The relationship between CCAS capacity and the supply of the four ESs selected for the study proposed here was investigated using a GWR model, according to the formalization proposed by [16]. The model assesses the non-stationary relationship between CCAS (dependent) and ES supply (explanatory) variables, building upon a spatially stationary multiple linear regression that assumes constant coefficients across Basilicata, Campania, and Sardinia formulized as:

$$\mathrm{CCAS} = \alpha 0 + \alpha\ 1\ \mathrm{LOHM} + \alpha 2\ \mathrm{QOHA} + \alpha 3\ \mathrm{AFPL} + \alpha 4\ \mathrm{NOAP} \quad (1)$$

where CCAS is the density of carbon capture and storage capacity (Mg/m^2); LOHM is the heat mitigation reference, i.e., the land surface temperature (LST) with values in °C.; QOHA measures the level of habitat quality, and takes values ranging from 0 and 1; AFPL is the value of agricultural and timber production (€/ha); NOAP measures the potential for nature-based outdoor activities, and takes values ranging from 0 to 1.

The estimated coefficients of the explanatory variables show the marginal impacts of these covariates on the CCAS. The regression model is typically used when no prior assumptions can be made about the functional relationships between the variables [17–20]. Significance tests for the estimated coefficients are usually assessed using p-values, and the adjusted R-squared is the reference for evaluating the goodness of fit.

The GWRs model replaces the linear regression model when relationships vary spatially across large, non-homogeneous datasets—like the tens of thousands of records in Basilicata, Campania, and Sardinia—where coefficients are location-specific and not stationary. For each of the points in three spatial contexts, the regression estimate was implemented by assuming that the influence of the explanatory variables on the dependent variable decreases when distance increases, by introducing a Gaussian weighting scheme. According to the detailed and analytical discussion of the model [16], the value of *b*, called bandwidth, must be chosen in such a way as to account for the trade-off in terms of unbiasedness and reliability of the GWR estimate. It is therefore very important, for the GWRs model, to identify the bandwidth that balances minimizing the variance and the bias of the estimate of the dependent variable CCAS (x_i, y_i). The search for the

value of the bandwidth *b* that solves the minimization problem can be carried out, as suggested by [16], by applying the golden section share algorithm.

With regard to the goodness-of-fit of the GWRs estimate, the following statistics are important: (i) the adjusted R-squared which measures the variance of CCAS, explained by the GWRs estimate, purifying this measurement from the increase in the coefficient linked to the number of explanatory variables; (ii) the adjusted critical value of pseudo-t statistics, used to verify the statistical significance of the estimated coefficients using a two-tailed t-test, at a significance level of 5%; while checking in the family-wise error rate (FWER). The resulting vector, $\hat{a}(x_i,y_i)$, locally characterizes the correlations between CCAS (x_i,y_i) and the four ES availability variables.

3 Results

3.1 Carbon Capture and Storage

The CCAS taxonomy is intrinsically linked to the biophysical characteristics of the territory, with particular reference to land cover, especially with forest types. The spatial distribution of this ES supply is highest in forest-covered soils, varying by type, while lower values are found in sparse vegetation, and, in built-up areas.

The CCAS assessment yields that in all three regions highest capacity is observed in forests (Fig. 2). Campania exhibits the highest density at 23.82 kg/m^2, followed by Basilicata at 21.21 kg/m^2, both observed in broad-leaved forests, whilst Sardinia's maximum value is 17.75 kg/m^2, noted in the coniferous category. In all three regions, forests represent the primary carbon pool. However, average forest productivity varies significantly. Campania's forests range from 15.07 to 17.40 kg/m^2, followed by Basilicata (12.88–14.76 kg/m^2) and Sardinia (10.99–12.65 kg/m^2). Spatially, high-density clusters are correlated with mountainous and protected areas, and the eastern/southwestern massifs in Sardinia. Intermediate storage levels (7.77–10.54 kg/m^2) are found in shrublands and marshes, while artificial areas and water bodies consistently yield the lowest results. Moreover, these regions act as natural reservoirs: Campania as high-capacity tank, Basilicata as a well-distributed network of medium basins, and Sardinia as a specialized reservoir where coniferous forests are more efficient than others.

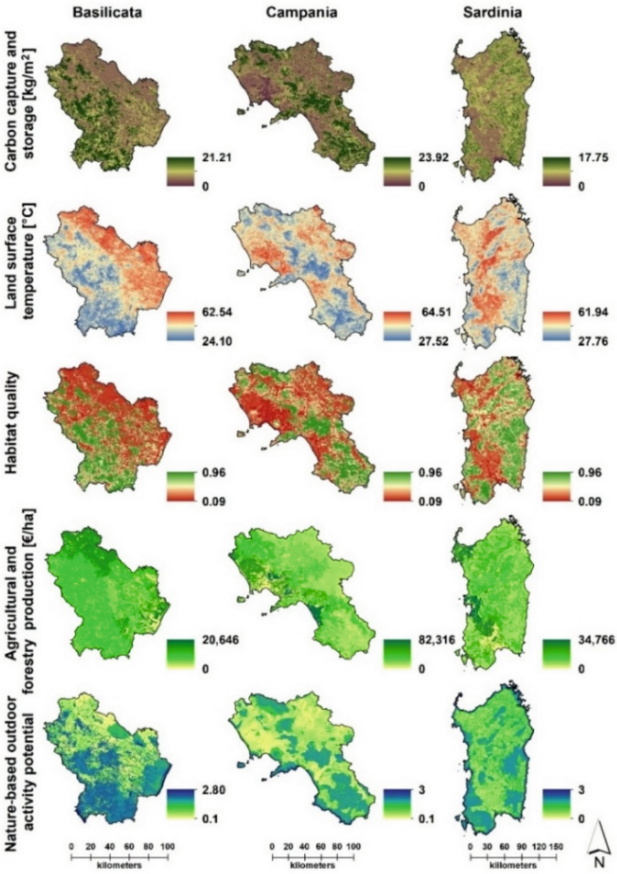

Fig. 2. Spatial distribution of the five ecosystem services in the three study areas.

3.2 Quality of Habitat Analysis

The analysis of QOHA, represented as HQ scores, shows consistent contrasts between high values characterizing natural areas and low values found in urban and intensive agricultural areas. Human infrastructures are recognized as major sources of degradation, reducing HQ scores according to their proximity and their threat level.

Sardinia records the highest average HQ (0.54) and the greatest proportion of high-quality habitats (40.86%). Basilicata follows with an average score of 0.51, but with the highest percentage of low-quality habitats (44.45%). Campania reports the lowest average HQ (0.49) and the smallest share of high-quality habitats (31.43%). In all regions, the best habitats are forested areas; broadleaved forests exhibit the highest mean scores (ranging from 0.85 to 0.86), followed by grasslands and wetlands. Conversely, artificial surfaces and impervious areas score near zero (0.09) across all regions, with open urban fabric and intensive arable land also exhibiting very low values (0.21–0.25).

The biophysical characteristics across three regions - are decisive in identifying the HQ level. First, through their influence on threat classification linked to agricultural use and soil permeability, which are influenced by human activities and infrastructure, highlighting radical differences between threats related to green and gray infrastructure.

3.3 Regulating Local Climate: Land Surface Temperature Mitigation

In Campania, LST ranges from about 27.5 to 64.5 °C (Fig. 2), with the highest values concentrated in densely urbanized and artificial areas. Lower temperatures occur where mountainous and hilly landscapes dominate. Overall, thermal patterns align with land-use intensity, with cooler conditions in vegetated and high-elevation zones. In Sardinia, LST ranges from around 27.8 to 61.9 °C (Fig. 2). The highest temperatures occur mainly in agricultural zones, while cooler values characterize mountainous, forested, and protected. The highest temperatures are observed in agricultural fields and discontinuous urban fabric (both 61.9 °C), whereas the highest mean values are observed in artificial areas. Water bodies and forests remain the coolest (32–40 °C). Basilicata's LST ranges from 24.1 to 62.5 °C (Fig. 2). Higher values occur in industrial, commercial, and agricultural areas of the northeast, including the Bradano basin, Vulture Hills, and the urban zone of Matera etc. Cooler temperatures characterize the Lucanian Apennines. CLC data indicates the highest means of LSTs in irrigated and mixed agriculture and artificial surfaces, and the lowest in water bodies, forests, and rocky areas.

In the three regions, the highest temperatures are consistently found in intensive agricultural areas, in urbanized areas with high building density, and in peri-urban areas characterized by scattered settlements with marked fragmentation of the spatial continuity of permeable soils and habitats. The relationship between the territorial distribution of LST and spatial biophysical characteristics is evident from the above results since across all regions lowest temperatures in the mountainous areas or areas in proximity to or inclusion of wetlands, waterways, lakes, woods, and forests.

3.4 Agricultural and Forestry Production

The 2023 AFPL map for Campania reveals a highly uneven spatial configuration, with values ranging from zero, where no agricultural or forestry classification is present, to a maximum of EUR 82,316/ha (Fig. 2). About 22.08% of the region records a null value, while the mean reaches EUR 12,552/ha. Over half of the territory (52.11%) shows values below EUR 10,000/ha, mainly in the eastern Campanian Apennines and the Cilento area, while the highest AFPL values occur in the coastal hills of Naples and the Sorrento Peninsula, characterized by high-value arable and horticultural production.

A similar distribution emerges in Sardinia, where the 2023 AFPL values range from zero to EUR 34,766/ha (Fig. 2). Around 17.41% of the region falls below EUR 1,000/ha, with an overall mean of EUR 5,091/ha. Values above EUR 10,000/ha are concentrated in fertile plains such as Campidano di Cagliari, Oristano, and Nurra, areas typically dedicated to vineyards, orchards, citrus groves, and horticultural crops. Peaks exceeding EUR 30,000/ha occur in the coastal hills of Sarrabus, in the Lower Tirso plain, and in the Campidano of Serrenti.

In Basilicata, AFPL values range from zero to EUR 20,646/ha (Fig. 2). Approximately 9.86% of the Region shows a null value, while 11.44% falls below EUR 1,000/ha. The average value is EUR 5689/ha. Higher AFPL values, above EUR 20,000/ha, are found in the Metapontino Plain near the river mouths of the Sinni, Agri, Cavone, Basento, and Bradano, where agricultural production is dominated by orchards and vineyards. Even in the case of AFPL it is clear that supply is closely linked to the biophysical characteristics of the territory in all three regions considered in which the highest values are found where there are flat or hilly, arable soils characterized by vegetable crops, olive groves, vineyards, and citrus groves.

3.5 Nature-Based Outdoor Activity Potential

The assessment of NOAP in all regions reveals significant spatial heterogeneity driven by naturalness and coastal proximity. Values range from 0.1 to 2.8 in Basilicata and 0.1 to 3.0 in Campania, while Sardinia covers the full 0 to 3 scale with a mean of 1.21 (Fig. 2). A common geographical trend emerges, represented by high-value clusters predominantly located along coastal strips, such as the Tyrrhenian and Ionian coasts in Basilicata and the Campania coastline, and within mountainous protected areas in Sardinia. Statistical analysis of CLC classes confirms that natural and semi-natural areas provide the highest service levels such as salt marshes, beaches, and water bodies. Conversely, the lowest values are systematically associated with anthropized environments, including industrial units, urban fabrics, and intensive agricultural plains. These results emphasize that NOAP is intrinsically linked to environmental conservation and the presence of significant landscape features. Moreover, the biophysical characteristics of the territory align in a clear and homogenous way with the spatial taxonomy of the ES.

3.6 Geographically Weighted Regressions

To run the GWR, a vector layer composed of one-kilometer square polygons arranged in a regular grid was created. For each polygon, the average values of CCAS, LOHM, QOHA, AFPL, and NOAP were calculated from the ES maps described in Sects. 3.1–3.6 and shown in Fig. 2, using zonal statistics.

Prior to the GWR, an ordinary least squares regression was performed to check for global multicollinearity. All variables had a Variance Inflation Factor lower than four, and therefore below ten, a commonly used threshold for multicollinearity [21]. Subsequently, the GWR model in which the dependent variable CCAS is locally regressed against the four explanatory variables was implemented by using the tool "Geographically Weighted Regression (GWR) (Spatial Statistics)" in ESRI ArcGIS Pro 3.6.0 separately for each of the three study areas [22]. Table 2 provides the mean statistics of the coefficients α_1, α_2, α_3, α_4, as well as of the local coefficient R^2, for Basilicata, Campania, and Sardinia, respectively.

Table 2. GWR: mean statistics of the coefficients of the models presented in Eq. (3) for Campania, Basilicata, and Sardinia.

Region	Explanatory Variable	Coefficient Mean Value	% Significant Records at 0.95 Level
Basilicata	LOHM	−0.1541	87.35
	QOHA	10.0357	99.88
	AFPL	0.0003	79.83
	NOAP	0.928	62.43
Campania	LOHM	−0.2787	96.78
	QOHA	12.3032	100.00
	AFPL	0.00004	62.01
	NOAP	−0.0876	38.14
Sardinia	LOHM	−0.0377	70.84
	QOHA	7.9304	100.00
	AFPL	0.0001	38.75
	NOAP	−0.3321	45.54

Table 2 shows QOHA as the most significant variable, nearly always at the 0.95 level. LOHM ranks second, with 0.95 ranging from 71% to 97% of the records in Sardinia and Campania, respectively. Regarding AFPL and NOAP, significant estimates are high in Basilicata (AFPL $\simeq$ 80% and NOAP $\simeq$ 62%) and low in Sardinia (AFPL $\simeq$ 39% and NOAP $\simeq$ 46%), intermediate in Campania (AFPL $\simeq$ 62% and NOAP $\simeq$ 38%). Figs. 3, 4, 5 show the spatial distribution of the coefficients of the GWR model for the three case studies, with red indicating negative values and blue indicating positive.

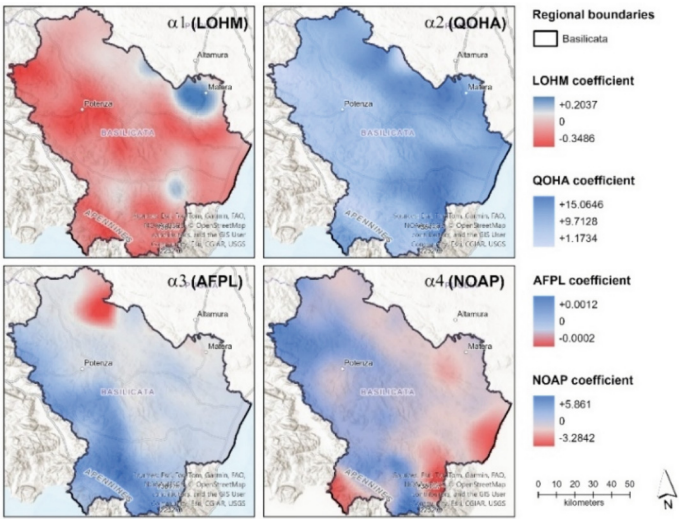

Fig. 3. GWR coefficients in Basilicata.

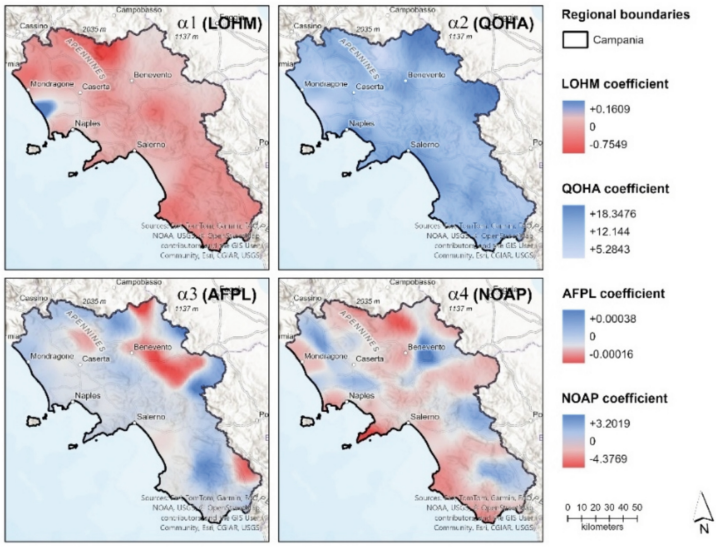

Fig. 4. GWR coefficients in Campania.

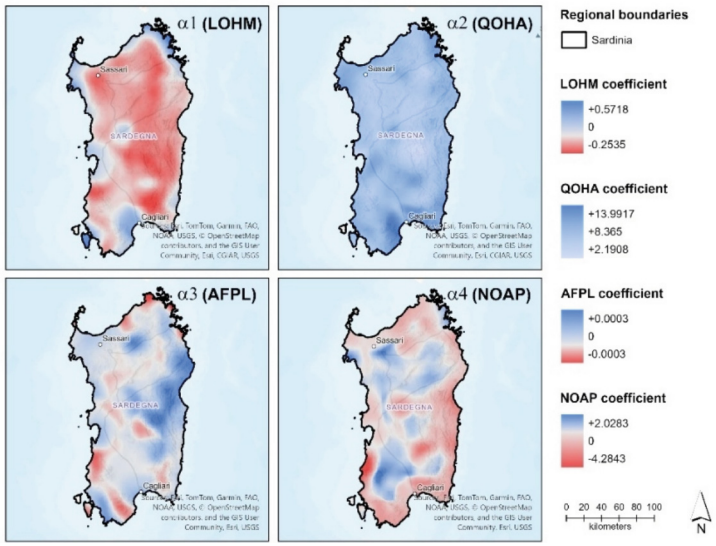

Fig. 5. GWR coefficients in Sardinia.

For LOHM, the mean values in Table 2 are negative, as seen as red shades in Figs. 3, 4, 5, indicating that higher LOHM generally decreases CCAS and vice versa; a 1 °C LST increase decreases CCAS by 0.17 kg/m^2 in Basilicata, 0.30 in Campania, and 0.05 in Sardinia. This association is more pronounced in Basilicata and Campania, whereas

in Sardinia positive (blue) values are mainly distributed along the coastline and in some inland clusters, with very low absolute magnitudes. Most settlements show negative coefficients (red), except for Matera (Fig. 3) where the significance of correlation is low and Cagliari, where positive coefficients (blue) likely reflect its location within coast and wetlands.

QOHA is the only explanatory variable whose coefficients in Table 2, in addition to being relatively high, are always positive across the three regions. This pattern is clearly illustrated in Figs. 3, 4, 5, which display only varying shades of blue and no red tones, signaling that an increase in QOHA is consistently associated with an increase in CCAS. A 10% increase in QOHA raises CCAS by 1.12 kg/m^2 in Basilicata, 1.37 in Campania, and 0.88 in Sardinia, roughly a 10% change in all cases. Although the coefficient is always positive, lower values tend to correspond to main settlements and transport infrastructures. While in Basilicata and Campania, the darker shades are generally associated with hilly landscapes, in Sardinia (Fig. 5) the darker shades are found in a flat, low-elevation area in the southeastern part of the island.

AFPL takes an average positive, but very small value in the three regions, The dominance of blue shades in Figs. 3, 4, 5 indicates that the coefficients are mostly positive, with negative (red) values clustering in a distinct area in northeast Basilicata and in a few isolated clusters in Campania, whereas in Sardinia several negative clusters are spread across the island. An increase in AFPL of one euro, on average, does not produce any changes in CCAS in Campania, and an increase of only 0.1 g/m^2 in Sardinia and 0.3 in Basilicata.

Finally, as for NOAP, the coefficients are the highest after those of QOHA, and their spatial distribution varies considerably across the three regions. An increase in NOAP of one unit, on average, is associated with an increase of CCAS by 1.03 kg/m^2 in Basilicata and a decrease by 0.1 kg/m^2 in Campania, and 0.37 in Sardinia. In Basilicata, the mean value reported in Table 2 is positive; accordingly, the prevalence of blue shades in Fig. 3. Conversely, in Campania the mean value is negative, shown in red shades in Fig. 4, with four notable positive (blue) agglomerations in inland areas, largely coinciding with natural protected areas. In Sardinia the mean value is also negative. Moreover, values are less clustered than in the other two regions and are predominantly negative (red) (Fig. 5), observed in natural lands covers such as the Gennargentu-Supramonte massifs, while positive (blue) clusters appear inland, similar to the patterns in Campania.

4 Discussion

Regarding habitat quality, as seen in the figures and Table 2, the GWR results for all three regions consistently show that increases in QOHA correspond to increases in CCAS at its mean level. The positive correlation between CCAS and the habitat quality level is consistent with several studies available in the current literature concerning this issue such as the findings of Spohn et al. [23], which suggest that plant species richness can enhance soil organic carbon sequestration by improving the quality of organic inputs rather than their overall quantity, indicating that t management practices aimed at recovering plant diversity can promote greater soil organic carbon (SOC) sequestration. Schittko et al. [24] show that the quality of habitats has a consistently positive impact on both soil multifunctionality and soil organic carbon stocks. Structural equation modeling indicates

that these effects are largely mediated by an increase in the diversity of soil-dwelling organisms.

Furthermore, a comparison of the spatial distribution of the GWR coefficients of QOHA and LOHM shows a significant association between growth in carbon capture and storage capacity, improvement in habitat quality, and a decrease in LST, and therefore a positive correlation between the latter two variables. In other words, in all three regional cases examined, where carbon storage capacity is higher, habitat quality is also comparatively higher and LST is lower. This result is supported by the study by Hu et al. [25], in the context of China, showing that higher levels of LST are associated with lower habitat quality values, thus with opposite spatial patterns. Furtjermore, a study by Müllerová and Šiffel [26], conducted in Czech Republic, shows that areas with better vegetation conditions and greater water availability tend to have lower LSTs, while areas with more or less pronounced vegetation cover degradation show higher LSTs, thus revealing a negative correlation.

Regarding the local climate mitigation, in all three regions, GWR estimates show that decreasing LOHM increases average CCAS. This relationship is roughly proportional in Basilicata (89% elasticity) and Campania (150%), but significantly lower in Sardinia (2%). This different pattern can be explained by the significant presence of wetlands in the Sardinian coastal areas, which are much more widespread than in Basilicata and Campania and distributed over much longer stretches of coastline: the coastline of Sardinia is almost 1900 km long, that of Campania about 500 km, and that of Basilicata about 70 km. As Zhang et al. [27] point out with regard to Bohai Bay, China, the spatial distribution of SOC is associated with environmental variables that include various climatic factors, with areas of higher SOC corresponding to areas with higher temperatures, which favor carbon input into wetland soils. The inland areas of Sardinia, on the other hand, offer a spatial pattern very similar to those of Basilicata and Campania, characterized by a generalized positive correlation between CCAS and decrease in LOHM. This result finds numerous and consistent confirmations in the current literature such as the results proposed by Hartley et al. [28], where they analyze over 9000 soil profiles located in the five continents, yielding the result that stored organic carbon decreases sharply with an increase in average annual temperature, thus finding that lower soil temperatures are associated with higher amounts of organic carbon.

In terms of agricultural and forestry production, the consistently positive but very small AFPL coefficients in Table 2 show that increases in AFPL are associated with only modest increases in CCAS at mean values. Overall, the impact of AFPL on CCAS is quite weak, and less significant than that of QOHA and LOHM, particularly in Sardinia, where significance occurs for only about 38% of observations. This limited effect may reflect the heterogeneous and sometimes contradictory evidence from the literature. Aryal et al. [29] identify the trade-off between crop production and carbon or climate services as the most frequently studied relationship between 2005 and 2020. Such trade-offs have been observed in Quebec, Canada [30], and the Beijing area, China [31], Conversely, some studies report synergistic relationships between food production and carbon sequestration or storage [32]. For forested areas, most studies report a positive association with carbon sequestration; however, as with agriculture, effective management is essential [33] to ensure the synergistic effect: timber harvesting can either increase or decrease

carbon storage depending on management strategies [34]. Moreover, the inner hilly and mountain landscapes in all three regions are characterized by traditional Mediterranean grazing practices, with livestock living on natural pastures and wooded grassland [35] and, in the case of sheep and goats, even on mediterranean maquis and garrigue or forest undergrowth [36]. While these practices are not only culturally and socially rooted but also generally sustainable due to their low intensity, long-term grazing is associated with reductions in carbon stocks, as shown in other studies such as [37].

As for nature-based recreation, Table 2 indicates that GWR results differ across the three regions. An increase in NOAP is associated with higher CCAS values at the mean level in Basilicata, whereas it corresponds to modest decreases in Campania and Sardinia. The estimated supply elasticity of CCAS at the mean level is approximately 13% in Basilicata, −1% in Campania, and − 5% in Sardinia; in the latter two regions, fewer than 50% of the records are statistically significant. A clear pattern emerges from the spatial distribution of the negative coefficients along coastal areas across all regions, indicating that increased recreation is associated with reduced CS. The recreation potential in coastal areas is high due to the combined presence of natural ecosystems such as sandy beaches, proximity to water, and protected areas [38]. This pattern is intuitive and consistent with empirical evidence worldwide, which confirms the popularity of coastal areas for daily recreation due to the abundance of recreational opportunities and high environmental quality [39, 40]. On the other hand, CS tends to be lower in arid regions such as Mediterranean coastlines, driven by the relatively limited forest cover and by calcareous and acidic soils [41], and in spite of the presence of coastal wetlands acting as carbon sinks [42]. This suggests a trade-off in these regions, where enhancing recreation may reduce carbon storage, requiring a balance. This balance could be supported through the adoption of sustainable tourism and land-use policies, which have been shown to mitigate environmental impacts while maintaining economic and recreational benefits in Mediterranean contexts [43]. By contrast, positive coefficients are observed in Basilicata and large inland areas of Campania and Sardinia, likely due to the forests and other vegetated areas that simultaneously support carbon storage and outdoor recreation. Proximity to urban settlements is a key determinant of daily recreation. Hence, from a policy perspective, increasing recreational opportunities through afforestation in inland areas near human settlements could also lead to enhanced CCAS.

5 Conclusions

This study establishes a comprehensive methodological framework for analyzing the functional relationships between CCAS, assumed as the reference ES for evaluating the role of regional spatial contexts in achieving global climate neutrality, and the provision of four additional ESs: QOHA and LOHM (regulating ESs); AFPL (provisioning ES); and NOAP (cultural ES) in the contexts of Basilicata, Campania, and Sardinia. The core of the analysis involves correlating the spatial distribution of each of these four ESs with the taxonomy of CCAS in urban, peri-urban, rural, and natural areas.

Since these relationships are not stationary in the spatial contexts of reference, they are analyzed by employing a GWR, run on 1-km grid cells, adopting a Gaussian-based weighting approach, and choosing bandwidths that are optimized through the golden

search selection method. QOHA consistently showed a strong positive relationship with CCAS, indicating that areas with higher ecological integrity tend to support greater carbon stocks. Conversely, LOHM shows negative associations, confirming that cooler microclimatic conditions are associated with higher carbon stocks. AFPL shows a negligible association with CCAS, which can be positive or negative, depending on management strategies. Similarly, NOAP displays spatially variable results, negative correlations in coastal areas, and synergistic relationships in forested inland regions.

GWR maps reveal spatially varying ES correlations, enabling identification of leverage areas, where local coefficients are higher and targeted interventions (e.g., habitat restoration) would yield the greatest synergistic co-benefits (e.g., CCAS), as well as the delineation of zones of inevitable trade-offs, where conflicting ES priorities, such as tensions between coastal tourism and CCAS, must be negotiated. By making these spatial asymmetries explicit, GWR provides a direct, evidence-based foundation for differentiated regional planning, supporting targeted measures that maximize synergies and balance competing demands, priority-setting, and context-sensitive policy design that cannot be derived from non-spatial models.

Despite its innovative contribution, the proposed methodology has some limitations. First, it relies on proxy-based estimations from secondary sources, which may affect accuracy. Second, ES assessments based on expert judgment (e.g., HQ) may introduce subjectivity. Third, it does not explicitly account for the influence of human infrastructure on ES trade-offs. Future research could expand the range of ESs considered and extend the framework to include climate change mitigation scenarios, dynamic land-use modeling, and applications in other geographical contexts to explore long-term synergies and trade-offs.

Author Contributions. Conceptualization, Methodology, Investigation, Data Curation, Writing – Original Draft Preparation, and Writing – Review & Editing: F.I., B.K., S.L., Fr.L., F.L., and C.Z. Specific task-level contributions were distributed as follows: F.L. contributed to Sects. 1, 2.6, and 3.5; S.L. to Sects. 2.1, 3.6, 4.3, and 4.4; B.K. and F.L. to Sects. 2.2 and 3.1; B.K. and Fr.L. to Sects. 2.3 and 3.2; B.K. and F.I. to Sects. 2.4 and 3.3; F.I. to Sects. 2.5 and 3.4; C.Z. to Sects. 2.7, 4.1, and 4.2; and Fr.L. to Sect. 5. All authors have read and agreed to the published version of the manuscript.

Acknowledgments. This study was carried out as follows: i. within the RETURN Extended Partnership and received funding from the European Union Next-GenerationEU (National Recovery and Resilience Plan—NRRP, Mission 4, Component 2, Investment 1.3—D.D. 1243 2/8/2022, PE0000005); ii. with the financial support under the National Recovery and Resilience Plan (NRRP), Mission 4, Component 2, In-estment 1.1, Call for tender No. 1409 published on 14.9.2022 by the Italian Ministry of Universi-ty and Research (MUR), funded by the European Union—NextGenerationEU—Project Title "Definition of a guidelines handbook to implement climate neutrality by improving ecosystem service effectiveness in rural and urban areas"—CUP F53D23010760001- Grant Assignment Decree No. 1378 adopted on 1 September 2023, by the Italian Ministry of University and Research (MUR); iii. the research grant CUP F73C23001680007 for the project "Geodesign for climate change mitigation and adaptation in the Mediterranean region" funded in 2022 by Fondazione di Sardegna. This article is a condensed and adapted version of the paper: Isola, F., Kobak, B., Lai, S., Leccis, F., Leone, F., & Zoppi, C. (2026). Mapping Spatial Synergies and Trade-Offs: A Geographically Weighted Analysis of Ecosystem Services

and Carbon Sequestration in Southern Italy. Sustainability, 18(4), 2146. https://doi.org/10.3390/su18042146**.**

References

1. Driga, A.M., Drigas, A.S.: Climate change 101: how everyday activities contribute to the ever-growing issue. iJES. **7**(1), 22–31 (2019). https://doi.org/10.3991/ijes.v7i1.10031
2. Mussinelli, E., Tartaglia, A., Castaldo, G., Riva, R., Cerati, D., Sereni, A.: The mitigation potential of environmental compensations: a challenge for the carbon neutrality transition. IOP Conf. Ser. Earth. Environ. Sci. **1402**(012064) (2024). https://doi.org/10.1088/1755-1315/1402/1/012064
3. Munafò, M.: Consumo di Suolo, Dinamiche Territoriali e Servizi Ecosistemici Edizione 2023 [Land Consumption, Territorial Dynamics and Ecosystem Services 2023 Edition]; Report Sistema Nazionale per la Protezione dell'Ambiente (SNPA) 37/23. Sistema Nazionale per la Protezione dell'Ambiente, Rome, Italy (2023)
4. Lal, R.: Carbon sequestration. Philos. T. Roy. Soc. B. **363**, 815–830 (2008). https://doi.org/10.1098/rstb.2007.2185
5. Früh-Müller, A., Hotes, S., Breuer, L., Wolters, V., Koellner, T.: Regional patterns of ecosystem services in cultural landscapes. Land. **5**(2), 17 (2016). https://doi.org/10.3390/land5020017
6. Bateman, I.J., et al.: Bringing ecosystem services into economic decision-making: land use in the United Kingdom. Science. **341**, 45–50 (2013). https://doi.org/10.1126/science.1234379
7. Viglizzo, E.F., Jobbágy, E.G., Ricard, M.F., Paruelo, J.M.: Partition of some key regulating services in terrestrial ecosystems: meta-analysis and review. Sci. Total Environ. **562**, 47–60 (2016). https://doi.org/10.1016/j.scitotenv.2016.03.201
8. Tian, S., Wu, W., Chen, S., Li, Z., Li, K.: Global mismatch between ecosystem service supply and demand driven by climate change and human activity. Environ. Sci. Ecotechnol. **26**(100573) (2025). https://doi.org/10.1016/j.ese.2025.100573
9. ISTAT (Istituto Nazionale di Statistica) [National Institute of Statistics]: Superficie di Comuni, Province e Regioni Italiane al 9 Ottobre 2011 [Area of Italian Local Municipalities, Provinces and Regions as of 9 October 2011]. https://www.istat.it/classificazione/principali-statistiche-geografiche-sui-comuni/. Accessed 02 Feb 2026
10. Fiorentino, C., D'Antonio, P., Toscano, F., Donvito, A., Modugno, F.: New technique for monitoring high nature value farmland (HNVF) in Basilicata. Sustainability. **15**(8377) (2023). https://doi.org/10.3390/su15108377
11. Copernicus Land Monitoring Service: CORINE Land Cover. https://land.copernicus.eu/en/products/corine-land-cover. Accessed 02 Feb 2026
12. ISTAT (Istituto Nazionale di Statistica) [National Institute of Statistics]: Popolazione Residente al 1° Gennaio [Resident Population as of 1st January]. https://esploradati.istat.it/databrowser/#/it/dw/categories/IT1,POP,1.0/POP_POPULATION/DCIS_POPRES1/IT1,22_289_DF_DCIS_POPRES1_1,1.0. Accessed 02 Feb 2026
13. Pungetti, G., Marini, A., Vogiatzakis, I.: Sardinia. In: Vogiatzakis, I., Pungetti, G., Mannion, A.M. (eds.) Mediterranean Island Landscapes, Landscape Series, vol. 9, pp. 143–169. Springer, Dordrecht, The Netherlands (2008). https://doi.org/10.1007/978-1-4020-5064-0_8
14. Sallustio, L., et al.: Assessing habitat quality in relation to the spatial distribution of protected areas in Italy. J. Environ. Manag. **201**, 129–137 (2017). https://doi.org/10.1016/j.jenvman.2017.06.031

15. Zulian, G., Paracchini, M.L., Maes, J., Liquete, C.: ESTIMAP: Ecosystem Services Mapping at European Scale. JRC (European Commission—Joint Research Centre—Institute for Environment and Sustainability). Technical Report EUR 26474. ENG; Publications Office of the European Union, Luxembourg (2013). https://doi.org/10.2788/64369
16. Fotheringham, A.S., Charlton, M.E., Brunsdon, C.: Geographically weighted regression: a natural evolution of the expansion method for spatial data analysis. Environ. Plann. A. **30**, 1905–1927 (1998). https://doi.org/10.1068/a301905
17. Cheshire, P., Sheppard, S.: On the price of land and the value of amenities. Econ. New Ser. **62**, 247–267 (1995). https://doi.org/10.2307/2554906
18. Sklenicka, P., Molnarova, K., Pixova, K.C., Salek, M.E.: Factors affecting farmlands in the Czech Republic. Land Use Policy. **30**, 130–136 (2013). https://doi.org/10.1016/j.landusepol.2012.03.005
19. Stewart, P.A., Libby, L.W.: Determinants of farmland value: the case of DeKalb County. Illinois. Rev. Agric. Econ. **20**, 80–95 (1998) https://www.jstor.org/stable/1349535
20. Zoppi, C., Argiolas, M., Lai, S.: Factors influencing the value of houses: estimates for the City of Cagliari Italy. Land Use Policy. **42**, 367–380 (2015). https://doi.org/10.1016/j.landusepol.2014.08.012
21. O'Brien, R.M.: A caution regarding rules of thumb for variance inflation factors. Qual. Quant. **41**, 673–690 (2007). https://doi.org/10.1007/s11135-006-9018-6
22. Geographically Weighted Regression (GWR) (Spatial Statistics).: https://pro.arcgis.com/en/pro-app/latest/tool-reference/spatial-statistics/geographically-weighted-regression.htm. Accessed 02 Feb 2026
23. Spohn, M., et al.: The positive effect of plant diversity on soil carbon depends on climate. Nat. Commun. **14**(6624) (2023). https://doi.org/10.1038/s41467-023-42340-0
24. Schittko, C., et al.: Biodiversity maintains soil multifunctionality and soil organic carbon in novel urban ecosystems. J. Ecol. **110**, 916–934 (2022). https://doi.org/10.1111/1365-2745.13852
25. Hu, Y., Xu, E., Kim, G., Liu, C., Tian, G.: Response of spatio-temporal differentiation characteristics of habitat quality to land surface temperature in a fast urbanized city. Forests. **12**(1668) (2021). https://doi.org/10.3390/f12121668
26. Müllerová, J., Šiffel, E.: Cooling the land surface: ecosystem health and water availability drive the landscape capacity to mitigate climate change. Ecol. Indic. **172**(113265) (2025). https://doi.org/10.1016/j.ecolind.2025.113265
27. Zhang, Y., et al.: Estimation of coastal wetland soil organic carbon content in Western Bohai Bay using remote sensing, climate, and topographic data. Remote Sens. **15**(4241) (2023). https://doi.org/10.3390/rs15174241
28. Hartley, I.P., Hill, T.C., Chadburn, S.E., Hugelius, G.: Temperature effects on carbon storage are controlled by soil stabilisation capacities. Nat. Commun. **12**(6713) (2021). https://doi.org/10.1038/s41467-021-27101-1
29. Aryal, K., Maraseni, T., Apan, A.: How much do we know about trade-offs in ecosystem services? A systematic review of empirical research observations. Sci. Total Environ. **806**(151229) (2022). https://doi.org/10.1016/j.scitotenv.2021.151229
30. Raudsepp-Hearne, C., Peterson, G.D., Bennett, E.M.: Ecosystem service bundles for analyzing tradeoffs in diverse landscapes. Proc. Natl. Acad. Sci. USA. **107**, 5242–5247 (2010). https://doi.org/10.1073/pnas.0907284107
31. Chen, T., Feng, Z., Zhao, H., Wu, K.: Identification of ecosystem service bundles and driving factors in Beijing and its surrounding areas. Sci. Total Environ. **711**(134687) (2020). https://doi.org/10.1016/j.scitotenv.2019.134687
32. Lyu, R., Clarke, K.C., Zhang, J., Feng, J., Jia, X., Li, J.: Spatial correlations among ecosystem services and their socio-ecological driving factors: a case study in the City Belt along the

Yellow River in Ningxia China. Appl. Geogr. **108**, 64–73 (2019). https://doi.org/10.1016/j.apgeog.2019.05.003
33. Schwaiger, F., Poschenrieder, W., Biber, P., Pretzsch, H.: Ecosystem service trade-offs for adaptive forest management. Ecosyst. Serv. **39**(100993) (2019). https://doi.org/10.1016/j.ecoser.2019.100993
34. Ciesielski, M., Gołos, P., Wysocka-Fijorek, E., Kaliszewski, A.: Relationships between forest ecosystem services—current state of knowledge. Folia For. Pol. **66**, 228–248 (2024). https://doi.org/10.2478/ffp-2024-0017
35. Seddaiu, G., et al.: Mediterranean cork oak wooded grasslands: synergies and trade-offs between plant diversity, pasture production and soil carbon. Agrofor. Syst. **92**, 893–908 (2018). https://doi.org/10.1007/s10457-018-0225-7
36. Scotti, R., Cadoni, M.: A historical analysis of traditional common forest planning and management in Seneghe, Sardinia—lessons for sustainable development. For. Ecol. Manag. **249**, 116–124 (2007)
37. Zhou, G., et al.: Effects of livestock grazing on grassland carbon storage and release override impacts associated with global climate change. Glob. Change Biol. **25**, 1119–1132 (2019). https://doi.org/10.1111/gcb.14533
38. Paracchini, M.L., et al.: Mapping cultural ecosystem services: a framework to assess the potential for outdoor recreation across the EU. Ecol. Indic. **45**, 371–385 (2014). https://doi.org/10.1016/j.ecolind.2014.04.018
39. Kline, J.D., Swallow, S.K.: The demand for local access to coastal recreation in southern New England. Coast. Manag. **26**, 177–190 (1998). https://doi.org/10.1080/08920759809362351
40. Paudel, K.P., Caffey, R.H., Devkota, N.: An evaluation of factors affecting the choice of coastal recreational activities. J. Agric. Appl. Econ. **43**, 167–179 (2011). https://doi.org/10.1017/S1074070800004144
41. Romanyà, J., Rovira, P.: An appraisal of soil organic C content in Mediterranean agricultural soils. Soil use and management. Soil Use Manag. **27**, 321–332 (2011). https://doi.org/10.1111/j.1475-2743.2011.00346.x
42. Romo, S., et al.: Nutrients and carbon in some Mediterranean dune ponds. Hydrobiologia. **782**, 97–109 (2016). https://doi.org/10.1007/s10750-016-2692-z
43. Yıldırım, S., Yıldırım, D.Ç., Aydın, K., et al.: Regime-dependent effect of tourism on carbon emissions in the Mediterranean countries. Environ. Sci. Pollut. Res. **28**, 54766–54780 (2021). https://doi.org/10.1007/s11356-021-14391-7

The 16th International Workshop on Future Information System Technologies and Applications (FiSTA 2026)

VM-Based Power Management for Embedded Multicore Systems

Kazuaki Tanaka[1(✉)], Hayato Tsuru[1], Ko-ichiro Sugiyama[2], and R. Krishnamoorthy[3]

[1] Kyushu Institute of Technology, Fukuoka, Japan
kazuaki@ics.kyutech.ac.jp
[2] National Institute of Technology, Matsue College, Matsue, Japan
[3] Chennai Institute of Technology, Chennai, India

Abstract. Multi-core systems in embedded systems improve performance and enable power reduction through core-level power management. However, conventional implementations require complex low-level programming.

This paper presents a VM-based program execution model for a multi-core microcontroller. This approach simplifies multi-core and multi-task execution through a script programming environment that manages memory contention and synchronisation issues, thereby reducing application-level complexity. A prototype implementation using mruby/c on a dual-core microcontroller platform evaluates the supporting overhead for multi-core and multi-task execution.

Keywords: mruby/c · Embedded Multicore Systems · Virtual Machine (VM) · Power Management · Memory Management

1 Introduction

The Internet of Things (IoT) and edge computing applications have increased the demand for greater performance and flexibility in embedded systems. To achieve these requirements, recent microcontrollers have adopted multi-core architectures, even in resource-constrained environments. Multi-core embedded systems not only enable the parallel execution of tasks and improved throughput, but also reduce power consumption through task management, synchronisation and power-aware operation.

Traditionally, embedded multi-core systems have been programmed using low-level languages such as C, which requires developers to manage task scheduling, memory access and synchronisation between cores explicitly. Maintaining correctness in shared-memory environments is particularly challenging due to race conditions and execution state management. Consequently, developing applications for embedded multicore systems remains complex and can sometimes result in serious errors.

© The Author(s), under exclusive license to Springer Nature Switzerland AG 2027
O. Gervasi et al. (Eds.): ICCSA 2026 Workshops, LNCS 16761, pp. 465–478, 2027.
https://doi.org/10.1007/978-3-032-30527-5_30

This paper explores the use of a VM-based approach to managing task execution in embedded multicore systems. Integrating multi-core task management into the VM itself centralises execution control and synchronisation.

Multi-core task management is performed at runtime rather than being handled by mruby/c , a lightweight scripting language runtime for embedded systems. The mrubyc VM handles concurrent task execution across multiple cores.

The key idea behind this work is to assign task ownership on a per-core basis, while also enabling the safe migration of tasks between cores. To achieve this, we introduce a FIFO-based mechanism for passing tasks between cores and transferring TCBs. This is combined with a two-level synchronisation strategy consisting of lightweight, intra-core mutual exclusion and inter-core synchronisation using a global lock. This design allows tasks to be executed in parallel while avoiding excessive memory contention and the need for complex fine-grained locking.

The remainder of this paper is organized as follows. Section 2 reviews related work on embedded multicore systems and virtual machines. Section 3 describes the system model and assumptions. Section 4 presents the design of the proposed VM-based task management approach. Section 5 discusses implementation details. Section 6 evaluates the performance of the system. Finally, Sect. 7 discuss the results and conclude the paper.

2 Related Work

2.1 Power Management in Embedded Multicore Systems

Power management is a widely studied technique for reducing energy consumption in embedded multicore systems with limited power budgets. Many existing approaches focus on hardware-supported mechanisms, such as dynamic voltage and frequency scaling (DVFS), clock gating and core-level power gating. These techniques can effectively lower power consumption during periods of low workload by selectively deactivating idle cores or reducing operating frequency [1,2].

In addition to these hardware-level mechanisms, software-based power management techniques have also been proposed. Operating system-centric approaches, including those implemented in real-time operating systems (RTOS), manage task scheduling and idle states to control power consumption. These approaches typically require the operating system to monitor system load and dynamically decide when to transition cores into low-power states. While effective, such solutions assume the presence of an OS and impose a relatively complex software stack, which may be unsuitable for resource-constrained or bare-metal embedded systems. In bare-metal environments, power management is often implemented directly in C code, with application developers controlling core activation, synchronization and low-power transitions explicitly. While this approach provides fine-grained control, it also tightly couples application logic with hardware-specific power management code, increasing development complexity and the risk of programming errors, particularly in multicore environments with shared memory [3].

2.2 Virtual Machines in Embedded Systems

VMs and scripting language runtimes have been explored as a means of improving productivity and portability in embedded systems. Lightweight VMs such as Lua-based runtimes, MicroPython, and mruby/c are designed to operate under tight memory and performance constraints while providing high-level programming abstractions. These systems execute application code on a VM that manages memory allocation, execution flow, and object lifetime [4–6].

Prior research has demonstrated that VMs can improve software maintainability and development efficiency by abstracting hardware-specific details from application code. In particular, memory allocation and garbage collection in VMs reduce the risk of memory-related errors that are common in low-level programming. However, many existing embedded VMs are designed for single-core execution only and do not address multi-core execution or inter-core task migration.

Some related studies have explored ways of extending VM-supported concurrency through threads or message-passing models. These efforts mainly focus on functional correctness and performance isolation rather than developer performance.

Consequently, little attention has been paid to the interactions between VM-level concurrency and multi-core microcontrollers, or even power management.

2.3 Comparison with Existing Approaches

Compared with existing VMs that support multi-core microcontrollers, the proposed approach is different. Unlike OS-based solutions, it does not rely on a full operating system and can be used in bare-metal environments. Unlike conventional C-based implementations, core control and memory management are not exposed directly to application developers, but are instead abstracted by the VM.

While previous VM-based approaches have simplified application development, they have typically treated power control as an underlying platform feature. This work, however, integrates the power control mechanism directly into the VM design, enabling execution control and memory management to be coordinated within a single abstraction layer.

Furthermore, existing multi-tasking in a multi-core environment often requires explicit synchronisation and careful handling of shared memory at the application level. By managing memory via the VM and restricting unsafe object sharing, the proposed approach absorbs memory contention and synchronisation complexity within the VM. This integration is key to the proposed method compared to previous work, enabling a simpler, safer and more efficient power management model for embedded multicore systems.

3 System Model and Assumptions

This section describes the system model assumed in this work and clarifies the hardware and software assumptions underlying the proposed VM-based power

management approach. The design goals derived from these assumptions are also presented.

3.1 Target System Model

We consider an embedded multicore system consisting of a small number of homogeneous processor cores integrated on a single microcontroller. The target platform is assumed to provide shared on-chip memory accessible by all cores, as well as hardware support for independent core activation and deactivation. Each core can be individually started, stopped, or transitioned into a low-power state by software (Fig. 1).

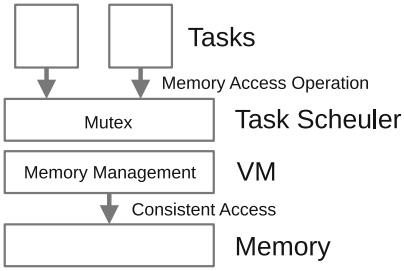

Fig. 1. Single mruby/c Task Model.

The cores execute application code without a memory management unit (MMU), and all memory accesses are performed through a shared address space. As a result, concurrent execution on multiple cores may lead to memory contention and consistency issues if not properly coordinated.

The system is assumed to operate under tight resource constraints in terms of memory size and processing power, which is typical for IoT and deeply embedded applications.

3.2 Software Stack

The software environment assumed in this work consists of a lightweight runtime executing on a bare-metal or minimal system configuration. A scripting language VM runs directly on top of the hardware abstraction layer (HAL) without relying on a full-featured operating system. The HAL provides basic services such as core control, interrupt handling, and access to low-power modes.

The VM executes application logic written in a high-level scripting language and is responsible for managing execution state, memory allocation, and object lifetime. Power management primitives, such as core activation and deactivation, are exposed to applications through VM-provided interfaces rather than direct hardware access.

This design allows hardware-specific details to be encapsulated within the runtime layer.

3.3 Design Goals

Based on the target system model and software assumptions, the following design goals are established:

Safety Ensure memory consistency and correct execution during concurrent operation and power state transitions, without requiring application-level synchronization.

Simplicity Reduce the complexity of application development by abstracting multicore control and power management within the VM.

Efficiency Minimize runtime and memory overhead introduced by the VM-based abstraction to remain suitable for resource-constrained embedded systems.

Generality Design the approach so that it can be applied to different embedded multicore platforms and scripting language VMs with minimal modification.

These goals guide the design of the proposed VM-based power management architecture described in the following section.

4 VM-Based Power Management Design

This section describes the design of the proposed VM-based power management approach for embedded multicore systems. The design integrates task execution control, memory management, and power state transitions within a VM, enabling safe and efficient power-aware operation. Particular attention is given to task management using TCBs and safe task migration across cores [7].

4.1 Design Overview

The proposed approach places the VM at the center of power management in embedded multicore systems. Instead of allowing applications to directly control processor cores and power states, the VM abstracts these operations and exposes them through high-level interfaces. This design enables power management decisions to be tightly coupled with execution flow and memory state, while reducing application-level complexity. By integrating power management into the VM, execution control, memory allocation, and power state transitions can be coordinated at well-defined points. This unified control model is particularly beneficial in multicore environments, where power state transitions must be synchronized with concurrent execution and shared memory access.

4.2 Task Management Using TCBs in mruby/c

To support multiprogramming in resource-constrained embedded systems, mruby/c manages program execution using a TCB-based model(Fig. 2 Left). Each task executed by the VM is represented by a TCB, which encapsulates the execution context of a script program, including the program counter, stack state, and references to task-specific memory.

The VM scheduler operates by selecting a TCB for execution and switching between TCBs at well-defined points, such as instruction boundaries or explicit yielding operations. This cooperative execution model allows mruby/c to precisely control task execution without relying on preemptive scheduling mechanisms, which are often costly or unavailable in small embedded systems. In the proposed design, the TCB abstraction provides a natural unit for coordinating execution and power management. Power-aware decisions, such as suspending execution or stopping a core, are performed only when the execution state of the active TCB is consistent and safely preserved.

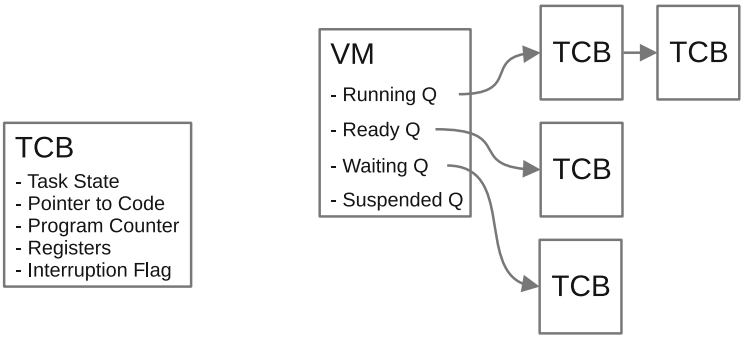

Fig. 2. TCB (Left) and Task State Model (Right).

4.3 Single-Core and Multicore TCB Management

In a single-core system, task management can be handled using a single active TCB, as only one execution context exists at any given time. All tasks are serialized, and memory access contention does not arise. This model simplifies execution control and is sufficient for single-core embedded environments.

Figure 2 Right illustrates the task state model in a single-core system, where only one TCB, which is the first TCB in Running Q, is active and all tasks are executed sequentially.

In contrast, multicore systems require a different strategy. A common approach is to maintain separate TCBs for each core, allowing multiple tasks to execute concurrently. This per-core TCB model improves parallelism and scalability by localizing execution state and minimizing synchronization during normal execution. Using a single shared TCB across multiple cores is impractical, as concurrent accesses to the same execution state lead to frequent memory contention and significantly degrade performance. Therefore, isolating TCBs per core is essential for efficient multicore execution.

4.4 TCB Contention During Task Migration

While per-core TCBs reduce contention during normal execution, additional challenges arise when tasks must be migrated between cores (Fig. 3). Task migration is necessary to support dynamic load balancing and power-aware core control, such as consolidating tasks onto fewer cores before deactivating unused cores. During task migration, ownership of a TCB must be transferred from one core to another. If multiple cores directly access or modify the same TCB during this transition, contention may occur, potentially resulting in inconsistent execution state or excessive synchronization overhead. Therefore, a safe and efficient mechanism for inter-core TCB transfer is required.

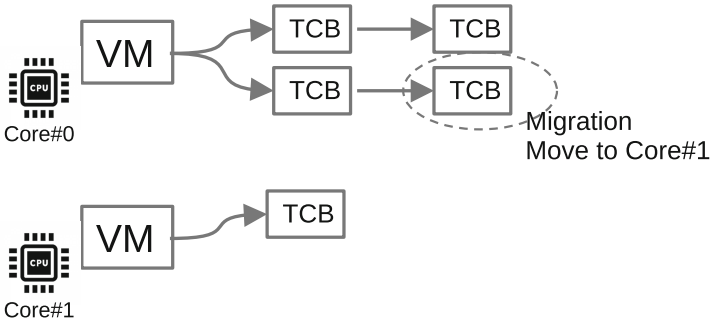

Fig. 3. Task Migration among Cores.

4.5 Task FIFO-Based Inter-core Migration

To address TCB contention during task migration, the proposed design introduces a task FIFO mechanism dedicated to inter-core task transfer. Each core exclusively manages its local TCBs during normal execution. When a task needs to be migrated to another core, the source core enqueues the corresponding TCB into a FIFO structure shared between the cores. The destination core dequeues the TCB from the FIFO and assumes exclusive ownership of the task.

This mechanism ensures that no TCBs are accessible at the same time across multiple cores. To separate task migration from direct TCB sharing, the migrating queue interface can use fine-grained locking or complex synchronisation. This design enables safe task migration while preserving high execution performance (Fig. 4). It also allows task redistribution and power management decisions to be implemented within the VM, ensuring that cores can be activated or deactivated dynamically without application developers being exposed to low-level concurrency concerns.

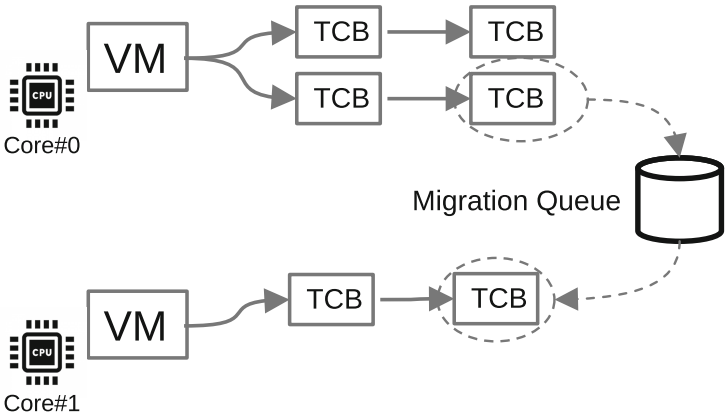

Fig. 4. Task Migration Queue.

5 Implementation

This section describes the implementation of the proposed VM-based multitasking system on a multicore microprocessor. The prototype system uses mruby /c and is implemented on a dual-core embedded microcontroller (RP2350) in a bare-metal environment. Our focus is on task management based on TCBs, inter-core task migration using a task migration queue and the synchronization mechanisms required to ensure the system operates correctly.

5.1 Prototype System Overview

The prototype system is designed for a dual-core embedded microcontroller and runs on bare metal rather than an operating system. One core is primarily responsible for system control, including VM initialisation, interruptions and power management coordination, while the other core executes tasks assigned by the VM.

The mruby/c VM runs on both cores and each core independently maintains its own execution context and local task set. A lightweight hardware abstraction layer (HAL) provides access to the low-level hardware functions, such as core activation, deactivation, mutual exclusion and power state control.

5.2 TCB Management and Scheduling

In the proposed implementation, each script task executed by the VM is represented by a TCB. A TCB data structure contains a task's execution state, including the program counter, stack information and references to VM-managed memory. During normal execution, each core maintains a local list of TCBs that it exclusively owns, in a manner similar to a single-core environment.

Context switches only occur at VM-defined safe points, ensuring that the state of the TCBs remains consistent and avoiding unexpected preemption. By restricting direct access to TCBs to the owning core, the system minimises memory contention during multicore execution and avoids the need for fine-grained locking within the VM.

5.3 Task FIFO for Inter-core Task Migration

To support dynamic task redistribution across cores, a task FIFO is introduced for inter-core task migration. The task FIFO is implemented as a bounded queue shared between cores and stores references to TCBs that are pending migration. When the VM determines that a task should be moved to another core—for example, to consolidate tasks before deactivating a core—the source core enqueues the corresponding TCB into the task FIFO and releases ownership. The destination core periodically checks the FIFO and dequeues TCBs when available, after which it assumes exclusive ownership of the tasks. This FIFO-based approach ensures that a TCB is accessed by at most one core at any time, preventing concurrent modification and eliminating direct TCB sharing between cores. As a result, task migration is performed safely without introducing complex synchronization mechanisms.

5.4 Integration with Power Management

Power management operations are integrated into the VM's task management flow. Before a core is transitioned into a low-power state, the VM migrates all remaining tasks on that core to another core using the task FIFO. Once the local TCB list becomes empty, the VM invokes the HAL to deactivate or suspend the core.

Similarly, when workload increases, a previously deactivated core can be reactivated and assigned tasks via the same FIFO mechanism. By performing power state transitions only at VM-defined safe points, the system ensures that no task execution state is lost and that memory consistency is preserved.

5.5 Mutual Exclusion and Synchronization

To ensure correct behavior in a multicore environment, the implementation employs two levels of mutual exclusion mechanisms: intra-core mutual exclusion and inter-core mutual exclusion using a giant lock.

Intra-core Mutual Exclusion. Within a single core, the VM uses lightweight mutual exclusion when manipulating internal data structures such as local TCB lists and scheduler state. Because mruby/c relies on cooperative multitasking, concurrent execution within a single core does not occur. Therefore, intra-core mutual exclusion is only required to protect critical sections during task scheduling or TCB state updates.

This intra-core synchronization is implemented using short critical sections, such as temporarily disabling interrupts. The limited scope of these critical sections ensures low overhead and deterministic behavior.

Inter-core Mutual Exclusion Using a Giant Lock. In contrast, inter-core mutual exclusion is required for operations that involve shared resources across cores. The implementation employs a giant lock shared by all cores to serialize access to the following resources:

- Hardware registers related to power control and core management
- Global variables shared between cores
- Shared data structures such as the task FIFO

Before accessing any of these shared resources, a core must acquire the giant lock. This approach ensures that hardware state and global data remain consistent and prevents race conditions between cores.

Although the giant lock introduces serialization, it is used only for infrequent operations such as task migration and power state transitions. Normal task execution and local TCB management are performed without acquiring the giant lock, keeping contention low.

Coordinated Use of Both Lock Levels. When the VM performs operations that involve both task management and power control, the two levels of mutual exclusion are used in a coordinated manner. First, intra-core mutual exclusion is applied to ensure the consistency of local TCB state. Then, the inter-core giant lock is acquired before accessing shared resources or hardware registers.

This hierarchical locking strategy ensures that:

- TCBs are never concurrently modified by multiple cores
- Power state transitions are performed atomically
- Global system state remains consistent across cores

As demonstrated in the evaluation section, the overhead introduced by this synchronization strategy remains acceptable for resource-constrained embedded systems.

6 Evaluation

This section evaluates the proposed VM-based multicore execution and task management mechanisms on a real embedded platform. The evaluation focuses on execution performance and synchronization overhead to assess the practicality of the proposed design.

6.1 Experimental Setup

All experiments were conducted on a dual-core embedded microcontroller operating at a fixed clock frequency. The system was configured in a bare-metal environment without a full-featured operating system. The proposed implementation using mruby/c was compared with a conventional C-based implementation that executes tasks directly on multiple cores without a VM. Execution time was measured using on-chip timers. Each experiment was repeated multiple times, and average values were reported to reduce measurement noise.

6.2 Workloads

To evaluate the system under representative operating conditions, the following workloads were prepared:

Single-core workload: All tasks are executed on a single core while the other core remains inactive. Parallel workload: Tasks are distributed across both cores to evaluate parallel execution performance. Dynamic workload: Tasks are dynamically redistributed between cores, triggering task migration via the task FIFO.

These workloads represent typical embedded use cases in which task parallelism and runtime task redistribution are required.

6.3 Performance Evaluation

Execution performance was evaluated by measuring task completion time under each workload. Figure 5 shows the relationship between the number of tasks and execution time for both single-core and dual-core configurations. Every task is categorised as a heavy load. In this evaluation, each task involves calculating a Fibonacci number using a recursive call. Compared with single-core execution, parallel execution using two cores achieved a performance improvement of up to 180%, single core execution time was 5.8×10^8 [μs], while dual-core execution reduced it to 3.2×10^8 [μs].

The VM-based implementation introduced a moderate runtime overhead relative to the C-based implementation due to instruction interpretation and VM-level task management. However, this overhead remained within 1%, indicating that the VM abstraction is feasible even in resource-constrained embedded environments.

The performance impact of task migration was also evaluated. Migrating a task between cores via the task FIFO incurred an overhead of 1.1–20.0 [ms] per migration. It was observed that the migration overhead varies depending on the runtime load of the destination core. When the destination core operates under low or moderate load, the migrated task is quickly incorporated into the local scheduling queue, and the associated TCB is updated with minimal delay.

In contrast, when the destination core is under heavy load, the migration overhead increases. This behavior is caused by the VM's cooperative execution model: when the VM load is high, the entire allocated time slice is consumed

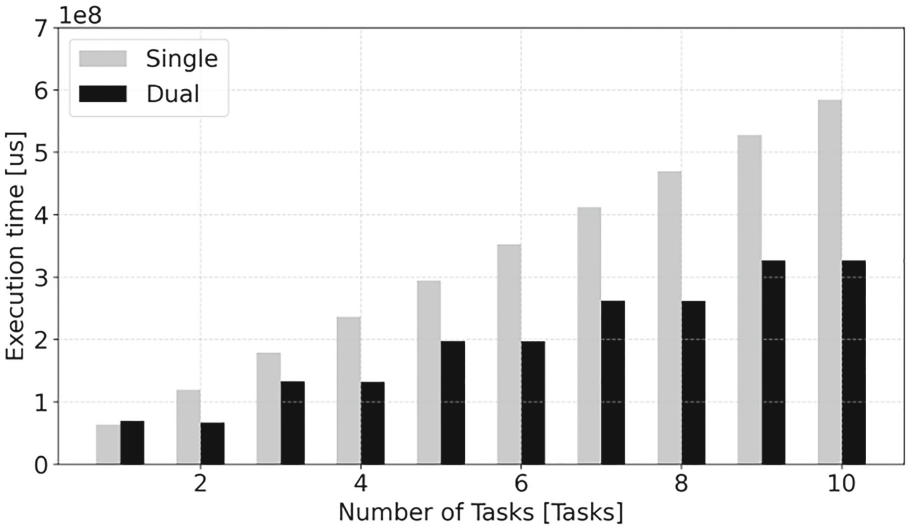

Fig. 5. Execution Performance Evaluation.

by task execution, and TCB update operations related to task migration are deferred until a scheduling safe point is reached. As a result, the completion of TCB state updates required for task migration may be delayed, leading to increased migration latency under high VM load.

Despite this variability, the observed migration overhead remains small relative to typical task execution times. Therefore, dynamic task redistribution using FIFO-based migration does not significantly degrade overall system performance in practical embedded workloads.

6.4 Synchronization Overhead

Synchronization overhead was analyzed by measuring the frequency and duration of mutual exclusion operations. The proposed implementation employs two levels of synchronization: intra-core mutual exclusion and inter-core mutual exclusion using a giant lock. Intra-core mutual exclusion incurs minimal overhead because task execution within a core is cooperative and serialized. Inter-core synchronization using the giant lock occurs primarily during task migration and hardware access. Measurements show that giant lock acquisition events are rare, and that the time spent holding the lock accounts for only a small proportion (a maximum of 20 ms) of the execution time. The holding time depends on the load on each core; especially when executing a heavy load, the holding time increases. However, since the giant lock is only held during infrequent operations such as task migration and power state transitions, the overall impact on performance is minimal. These results demonstrate that the use of a simple giant lock is sufficient for ensuring correctness while keeping synchronization overhead low.

6.5 Summary of Evaluation Results

The evaluation results show that the proposed VM-based design enables efficient multicore execution with acceptable overhead. Task management using per-core TCBs and FIFO-based inter-core migration provides good parallel performance while avoiding excessive synchronization costs. Overall, the proposed implementation demonstrates that VM-level task management and synchronization can be practically applied to embedded multicore systems without sacrificing performance.

6.6 Discussion

The proposed VM-based approach demonstrates that multicore task management can be effectively centralized within a lightweight virtual machine in embedded systems. By leveraging the TCB-based execution model of mruby /c , the VM provides a clear abstraction for task execution, synchronization, and core coordination, significantly reducing application-level complexity. A key advantage of the design is the combination of per-core TCB ownership and FIFO-based inter-core task migration, which enables parallel execution while avoiding frequent memory contention. In addition, the two-level synchronization strategy—lightweight intra-core mutual exclusion and inter-core synchronization using a giant lock—offers a practical balance between correctness and implementation simplicity. The evaluation results indicate that the resulting synchronization overhead remains low in a dual-core environment. Nonetheless, several limitations remain. The use of a giant lock may limit scalability as the number of cores increases, and VM-based execution inevitably introduces runtime overhead compared with native implementations. Furthermore, this study focuses primarily on execution performance and synchronization behavior; quantitative power consumption evaluation is left for future work. Despite these limitations, the proposed design principles are not specific to mruby/c or a particular hardware platform. The presented approach provides a general framework for VM-based multicore task management that can be adapted to other lightweight runtimes and embedded multicore systems.

7 Conclusion

This paper presents a VM-based approach to task management and synchronization for embedded multicore systems. By integrating multicore execution control into the virtual machine, the proposed design abstracts complex concurrency and synchronization issues away from application developers. The proposed method leverages the TCB-based execution model of mruby/c , introduces per-core task ownership, and employs a FIFO-based mechanism for safe inter-core task migration. A two-level mutual exclusion strategy combining intra-core synchronization and an inter-core giant lock ensures correctness while keeping overhead low. Experimental evaluation on a real dual-core embedded platform

demonstrated that the proposed approach achieves efficient multicore execution with acceptable performance and synchronization overhead. These results indicate that VM-based task management is a practical and effective solution for embedded multicore systems. Future work includes extending the approach to systems with higher core counts, conducting detailed power consumption evaluations, and exploring integration with real-time operating systems and adaptive scheduling policies.

References

1. Qualcomm Technologies, Inc.: Dynamic voltage and frequency scaling. Qualcomm Documentation. https://docs.qualcomm.com/bundle/publicresource/topics/80-70018-30/dcvs.html, updated 10 Apr 2025, Accessed 30 Mar 2026
2. Massari, G., Terraneo, F., Zanella, M., Zoni, D.: Towards Fine-Grained DVFS in Embedded Multi-core CPUs. In: Berekovic, M., Buchty, R., Hamann, H., Koch, D., Pionteck, T. (eds.) ARCS 2018. LNCS, vol. 10793, pp. 239–251. Springer, Cham (2018). https://doi.org/10.1007/978-3-319-77610-1_18
3. Kim, S.H., et al.: C-LockâĂŕ: energy efficient synchronization for embedded multicore systems. IEEE Trans. Comput. **63**(8), 1962–1974 (2014). https://doi.org/10.1109/TC.2013.84
4. Silangern, H., Tanaka, K.: Internet of things implemented with Mruby. In: Gervasi, O., Murgante, B., Garau, C., Taniar, D.C., Rocha, A.M.A., Faginas Lago, M.N. (eds.) Computational Science and Its Applications(ICCSA) 2024 Workshops. ICCSA 2024. Lecture Notes in Computer Science, vol. 14819. Springer, Cham (2024). https://doi.org/10.1007/978-3-031-65282-0_11
5. Tanaka, K., Higashi, H.: Mruby—rapid IoT software development language. In: 2017 12th IEEE Conference on Industrial Electronics and Applications (ICIEA), Siem Reap, Cambodia, pp. 415–418 (2017). https://doi.org/10.1109/ICIEA.2017.8282880
6. Go, S., Takuo, W., Sosuke, M.: Mruby on Resource-Constrained Low-Power Coprocessors of Embedded Devices. In: MPLR 24: 21st ACM SIGPLAN International Conference on Managed Programming Languages and Runtimes, pp. 41–47 (2024). https://doi.org/10.1145/3679007.3685064.
7. Yao, J., Mo, L., Han, J., Niu, D.: Task scheduling and temperature optimization codesign for multi-core embedded systems. In: International Symposium of Electronics Design Automation (ISEDA), vol. 2025, pp. 683–688. Hong Kong, China (2025). https://doi.org/10.1109/ISEDA65950.2025.11100782

Two-Stage Pavement Distress Detection and Classification Using UAV Imagery in Unstructured Road Environments

Earl Ryan Aleluya[1,2(✉)], Melody Mae Maluya[2], Francis Jann Alagon[1,2], Edward Rowe Aleluya[3], and Carl John Salaan[2,4]

[1] Department of Computer Engineering and Mechatronics, Mindanao State University - Iligan Institute of Technology, Iligan 9200, Philippines
{earlryan.aleluya,francisjann.alagon}@g.msuiit.edu.ph
[2] Center for Mechatronics and Robotics, Mindanao State University - Iligan Institute of Technology, Iligan 9200, Philippines
{melodymae.maluya0101,carljohn.salaan}@g.msuiit.edu.ph
[3] Department of Physical Sciences and Mathematics, Mindanao State University at Naawan, Naawan 9023, Philippines
edwardrowe.aleluya@msunaawan.edu.ph
[4] Department of Mechanical Engineering and Technology, Mindanao State University - Iligan Institute of Technology, Iligan 9200, Philippines

Abstract. Although tracking road degradation for timely maintenance extends infrastructure lifespan, UAV-based automation struggles on developing regions' unstructured roads due to missing lane markings, irregular surfaces, inconsistent signage, and frequent visual occlusions. This study introduces a two-stage predictive system in which the first stage concurrently detects road lanes and pavement panels, and the second stage uses these outputs to classify each pavement panel into one of four categories: non-distressed, sealed patch, sealed crack, or thin crack. Experimental evaluation on the pavement distress classification task shows that the proposed method achieves a mean Average Precision (mAP) of 0.9775±0.0015 across all classes. Future work will extend the classification framework to incorporate additional distress types observed in concrete, asphalt, and composite road surfaces.

Keywords: Aerial vehicles · Computer vision · Deep learning · Pavement management system · Road transportation · Vision transformers

1 Introduction

Routine road inspection helps modern pavement management systems (PMS) to identify structural degradation early, mitigate severe accident risks, and facilitate proactive maintenance planning for long-term infrastructure sustainability [11,26]. The primary objective of these assessments is the detection of pavement distress, which is defined as any observable surface damage or structural

© The Author(s), under exclusive license to Springer Nature Switzerland AG 2027
O. Gervasi et al. (Eds.): ICCSA 2026 Workshops, LNCS 16761, pp. 479–490, 2027.
https://doi.org/10.1007/978-3-032-30527-5_31

deterioration—such as cracking and rutting—that negatively impacts a roadway's functional performance and overall safety [9]. To localize this degradation, condition evaluations are spatially organized along a road lane, defined as the continuous longitudinal surface corridor designated to guide directional vehicular transit. For high-resolution, localized assessment, these lanes are frequently partitioned into a pavement panel, which refers to a specific, bounded structural slab or segmented physical unit of the road surface utilized by automated systems and surveyors to precisely isolate damage [12]. Identifying distress features at the granular level of individual panels and lanes is imperative for tailoring material-specific repair strategies. As a result, it can reduce the hazards associated with manual field labor, and improve the transportation infrastructure management [6,14].

Replacing conventional manual surveys, unmanned aerial vehicles (UAVs) recently serve as a transformative technology for the automated identification of pavement degradation. To optimize the precision and speed of these inspections, numerous investigations have merged drone technology with advanced deep learning frameworks. The literature covers various applications of diverse neural network architectures, including Vision Transformers (ViT) [24], Faster R-CNN [26], and multiple YOLO iterations—ranging from YOLOv3 and YOLOv4 [17,26] to YOLOv8 [12,13,16] and YOLOv5 enhanced with an Efficient Channel Attention module [23]. By training on aerial image datasets, these models map distresses such as potholes [16,17,21], patching [21], delamination [16], structural repairs [16], and specific crack morphologies (longitudinal, transverse, alligator, and oblique) [16,21,23].

Vision-based pavement distress analysis is typically addressed by single-stage architectures to integrate detection and classification for real-time applications. While earlier approaches often treated classification using standalone Convolutional Neural Networks (like ResNet and VGG) or Vision Transformers as distinct from spatial detection, modern systems demand rapid, unified processing. Consequently, single-stage detectors—particularly YOLO-based models—emerge as off-the-shelf solution to simultaneously localizing and categorizing distresses like cracks and potholes across vehicle-mounted and UAV platforms [5,16]. Coupling these streamlined single-stage models with advanced UAV sensors, such as multispectral and binocular imaging, broadens distress monitoring frameworks [15,23].

In pavement distress monitoring, the multi-stage architectures divide the complex inspection tasks of localization and pixel-level extraction into distinct, manageable phases. A dominant two-stage implementation utilizes bounding-box object detection models to first isolate distress regions like cracks and potholes, followed immediately by semantic segmentation networks to extract the exact damage pixels [8,10,20]. Other two-stage predictors prioritize broad identification first, employing convolutional neural networks to select crack-containing images before applying transformers for detailed pixel detection [7], using Mask R-CNN for initial detection prior to severity classification via image processing [19], or extracting potential anomalies from smartphone geospatial series before

categorizing them [25]. Expanding into three-stage architectures introduces dedicated preprocessing or refinement steps, such as the sequence of image enhancement, YOLO-SAMT detection, and K-means clustering in [22], or the pipeline of saliency-based localization, CNN-based pixel recognition, and region growing in [18].

While existing multi-stage frameworks isolate distress localization from pixel-level segmentation [8,10,20] or severity classification [19], they predominantly target the damage features directly rather than establishing the broader structural context of the road. These conventional methods typically depend on unified distress datasets and are largely optimized for standard, well-defined driving conditions [7,25], which may become vulnerable to the high variability and noise of unstructured roads. To address these limitations, our work's main contributions are as follows.

1. We introduce a two-stage framework that first performs concurrent binary detection of road lanes and pavement panels to anchor the subsequent distress classification.
2. We design the first stage to suppress false positives by constraining panels to detected lanes and recover false negatives via lane boundary estimation.
3. We implement disjoint multi-task learning approach across three specific datasets—single-class road lane data, single-class pavement panel data, and 4-class labeled pavement panel data.
4. We design our two-stage framework for the unstructured road environments.

The rest of the paper are organized as follows. Section 2 presents the two-stage framework, while the experimental validations are discussed in Sect. 3. Lastly, Sect. 4 concludes the paper.

2 Materials and Methods

2.1 Problem Formulation

The pavement distress identification task is formulated as a supervised object detection and segmentation problem, where a given input image $I \in \mathbb{R}^{(H \times W \times 3)}$ represents an RGB scene of road surface conditions. The objective is to learn a mapping function f_θ parameterized by network weights θ, such that $f_\theta(I) = \{(B_i, M_i, c)\}_{i=1}^{N}$, where $B_i \in \mathbb{R}^4$ denotes the bounding box coordinates, $M_i \in \{0,1\}^{H \times W}$ is the binary segmentation mask, and $c_i \in \mathcal{C}$ is the class label for the i-th detected distress instance among N objects. The learning objective is to minimize a composite loss function $\mathcal{L}(\theta)$, which jointly optimizes classification accuracy, localization precision, and mask quality.

This study introduces a two-stage framework that extends the base detection formulation. As shown in Fig. 1, parallel segmentation predictors in the first stage are defined as $f_{\theta_1}^{\text{lane}}(I) \rightarrow \mathcal{B}_{\text{lane}} = \left\{ b_i^{(l)} \right\}_{i=1}^{m}$ and $f_{\theta_2}^{\text{panel}}(I) \rightarrow \mathcal{B}_{\text{panel}} = \left\{ b_j^{(p)} \right\}_{j=1}^{n}$, where each $b^{(\cdot)} \in \{0,1\}^{H \times W}$ represents a binary mask for road lanes and pavement panels, respectively. A post-processing operator $\mathcal{R}(\cdot)$ is then applied to

enforce spatial consistency, which yields refined panel masks $\tilde{\mathcal{B}}_{\text{panel}} = \left\{\tilde{b}_j^{(p)}\right\}$ such that $\tilde{b}_j^{(p)} = b_j^{(p)} \odot \left(\bigvee_{i=1}^{m} b_i^{(l)}\right)$, where $\odot$ denotes element-wise multiplication and $\bigvee$ is the pixel-wise logical OR to merge lane masks. In the second stage, a classification network g_{θ_3} maps each refined mask region to a class label, i.e., $g_{\theta_3}(\tilde{b}_j^{(p)}) = c_j$, where c_j is either non-distressed, sealed patch, sealed crack, or thin crack. This decomposition adopts structured learning by decoupling geometric segmentation from semantic distress classification.

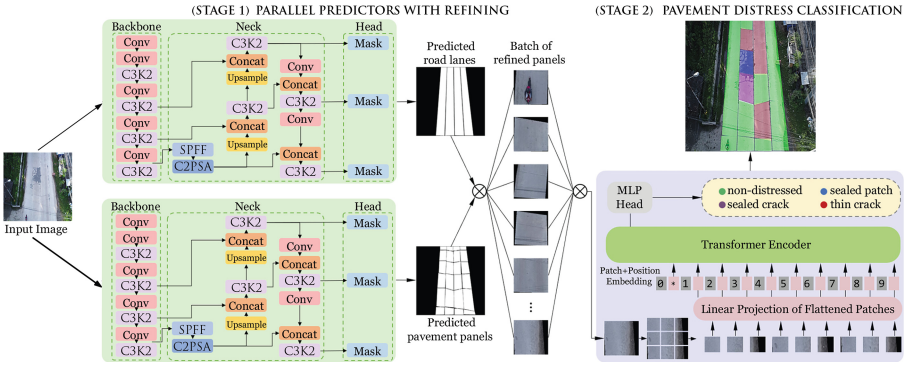

Fig. 1. The overview of the two-stage prediction pipeline, which contains parallel predictors for road lanes and pavement panels, and pavement distress classification using Vision Transformer.

2.2 Parallel Predictors with Refining

The first stage has two disjoint segmentation models that adopt the YOLO11-*seg* architecture. The architecture builds upon its predecessors by integrating advanced feature extraction and segmentation mechanisms, which resulted in better accuracy and computational efficiency. One of its core innovations is the C3K2 block, which employs smaller kernel sizes to refine feature extraction while reducing computational cost. The architecture also incorporates the Spatial Pyramid Pooling Fast (SPPF) module, which facilitates multi-scale feature aggregation. Given an F-sized input sequence of aerial images $I = \{I_i\}_{i=1}^{F}$ such that each input image $I_i \in \mathbb{R}^{H \times W \times C}$, the YOLO11-*seg* models for road lanes and pavement panels produce the corresponding lane segmentation masks $\mathcal{S}_{\text{lane}} = \{S_1^{(l)}, \cdots, S_m^{(l)}\}$ and pavement panel segmentation masks $\mathcal{S}_{\text{panel}} = \{S_1^{(p)}, \cdots, S_n^{(p)}\}$.

To train the lane and pavement panel models, we use a loss function combines four components: bounding box regression loss $\mathcal{L}_{box}$, segmentation loss $\mathcal{L}_{seg}$, classification loss $\mathcal{L}_{cls}$, and distribution focal loss $\mathcal{L}_{dfl}$.

The overall loss function can be elaborated as,

$$\mathcal{L} = \lambda_{box} \sum_{i \in F_G} \mathbb{1}_{\{i \in F_G\}} \mathcal{L}_{\text{CIoU}} \left(B_i, \hat{B}_i \right) + \frac{\lambda_{dfl}}{N} \sum_{i=1}^{N} \sum_{j=1}^{4} \left(-w_{ij} \log \hat{w}_{ij} \right) + \frac{\lambda_{seg}}{N} \sum_{i=1}^{N} \left[\mathcal{L}_{BCE}(M_i, \hat{M}_i) + \mathcal{L}_{Dice}(M_i, \hat{M}_i) \right] + \frac{\lambda_{cls}}{N} \mathcal{L}_{BCE}(y_i, \hat{y}_i) \quad (1)$$

where,

- B_i is the ground truth bounding box,
- $\hat{B}_i$ is the predicted bounding box,
- $\mathbb{1}_{\{i \in F_G\}}$ is an indicator function that is 1 if object i is a foreground sample and 0 otherwise,
- F_G refers to the foreground matched objects,
- N is the number of cells containing an object,
- M_i corresponds to the ground truth segmentation mask for an instance i,
- $\hat{M}_i$ is the predicted segmentation mask,
- y_i is the ground truth class probability,
- $\hat{y}_i$ is the predicted class probability,
- w_{ij} represents the ground truth distribution of bounding box coordinates, and
- $\hat{w}_{ij}$ is the predicted probability distribution.

In this work, the values for the four weight component hyperparameters were set to $\lambda_{box} = 7.5$, $\lambda_{seg} = 7.5$, $\lambda_{cls} = 0.5$, and $\lambda_{dfl} = 1.5$, respectively. Additionally, the training process is influenced by several optimization hyperparameters. The initial learning rate was set to $\eta_0 = 0.01$, with a final learning rate of $\eta_f = 0.01\eta_0$. The momentum coefficient was $\beta = 0.937$, while the weight decay was applied with a factor of $\phi = 5 \times 10^{-4}$.

After 100 epochs, the validation losses for the five YOLO11 variants in the road lane segmentation task using the NoMURLane dataset [2] were $\mathcal{L}_{box} = 0.139 \pm 0.002$, $\mathcal{L}_{seg} = 0.589 \pm 0.017$, $\mathcal{L}_{cls} = 0.075 \pm 0.001$, and $\mathcal{L}_{dfl} = 0.72 \pm 0.02$. In comparison, the training losses using NoMURPanel dataset [3] were $\mathcal{L}_{box} = 0.317 \pm 0.003$, $\mathcal{L}_{seg} = 0.744 \pm 0.06$, $\mathcal{L}_{cls} = 0.191 \pm 0.011$, and $\mathcal{L}_{dfl} = 0.805 \pm 0.014$.

Given an input image I_i, lane segmentation masks $\mathcal{S}_{\text{lane}}$, and pavement segmentation masks $\mathcal{S}_{\text{panel}}$, the post-processing involves bitwise operation between two masks to construct refined pavement panel polygons and extract corresponding image patches for classification.

As presented in Algorithm 1, the process first converts segmentation masks into quadrilateral polygons using extremal coordinates. Each pavement panel is assigned to a lane by minimizing the perpendicular distance to lane boundary curves. The resulting panel groups are vertically ordered to form a structured grid. Missing panels are reconstructed iteratively using neighboring polygon vertices until no further updates are possible. Each polygon is then refined by intersecting its edges with the corresponding lane boundaries, which obtains geometrically consistent panel regions. Finally, the refined polygons are rasterized to extract cropped image patches $\{x_k\}$ for downstream classification.

Algorithm 1 Refine Pavement Panel Masks (Filter Non-Lane Panels and Find Missing Panels)

Require: I_i, $\mathcal{S}_{\text{lane}}$, $\mathcal{S}_{\text{panel}}$
Ensure: Cropped panel images $\{x_k\}$

$\mathcal{B}_{\text{lane}} \leftarrow$ polygons from points $(x_{tl}, y_{tl}), (x_{bl}, y_{bl}), (x_{br}, y_{br}), (x_{tr}, y_{tr})$ of each mask in $\mathcal{S}_{\text{lane}}$
$\mathcal{B}_{\text{panel}} \leftarrow$ polygons formed analogously from $\mathcal{S}_{\text{panel}}$
$\mathcal{C}_{\text{lane}} \leftarrow \{(a, b, c) \mid a = y_{bl} - y_{tl},\ b = x_{tl} - x_{bl},\ c = x_{bl}y_{tl} - x_{tl}y_{bl},\ b_i \in \mathcal{B}_{\text{lane}}\}$
Assign each $b_i \in \mathcal{B}_{\text{panel}}$ to lane index

$$j = \arg\min_{\ell} \frac{|a_\ell x_{tl} + b_\ell y_{tl} + c_\ell|}{\sqrt{a_\ell^2 + b_\ell^2}}$$

$\mathcal{P}_{\text{panel}} \leftarrow \{\text{sort}_y(\{b_i \mid \text{lane}(b_i) = j\})\}$
Iteratively fill missing panels:
while $\exists\, \mathcal{P}_{i,j} = \mathbf{0}$ **do**
    Collect neighboring vertices T_L, B_L, B_R, T_R from valid adjacent panels
    if $|T_L| = |B_L| = |B_R| = |T_R| = 1$ **then**
        $\mathcal{P}_{i,j} \leftarrow [T_L, B_L, B_R, T_R]$
    end if
end while
Refine polygons using lane boundaries:
for each $p \in \mathcal{P}_{\text{panel}}$ **do**
    Form line sets $\mathcal{C}_L^{(l)}, \mathcal{C}_R^{(l)}$ (lane boundaries) and $\mathcal{C}_T^{(p)}, \mathcal{C}_B^{(p)}$ (panel edges)
    Compute vertices via pairwise intersections:

$$\begin{bmatrix} x \\ y \end{bmatrix} = \begin{bmatrix} a_1 & b_1 \\ a_2 & b_2 \end{bmatrix}^{-1} \begin{bmatrix} -c_1 \\ -c_2 \end{bmatrix}$$

    Construct refined polygon p^*
end for
Rasterize polygons and extract patches:
for each $p_k^* \in \mathcal{P}_{panel}^*$ **do**
    Initialize mask $M \leftarrow \mathbf{0}$ with size of I_i
    for each scanline y between $\min_y(p_k^*)$ and $\max_y(p_k^*)$ **do**
        Compute intersection points $\{x_m\}$ of scanline y with polygon edges
        Sort $\{x_m\}$ in ascending order
        for $m = 1$ to $|\{x_m\}|$ step 2 **do**
            Fill pixels $M(x, y) = 1$ for $x \in [x_m, x_{m+1}]$
        end for
    end for
    $x_k \leftarrow I_i \odot M$
end for
return $\{x_k\}$

2.3 Pavement Distress Classification

In our study on pavement distress classification, we modified the Vision Transformer (ViT-Base) model in [4] to categorize pavement conditions into four

classes: *non-distressed*, *sealed patch*, *sealed crack*, and *thin crack*. The ViT-Base model consists of 12 Transformer layers, each with 12 self-attention heads, a hidden size D of 768, and an MLP size of 3072. The input image x_k obtained from the refined pavement panel polygons is resized into a 224×224 RGB image. It is then divided into 16×16 patches, forming a sequence of $N = \frac{HW}{P^2} = \frac{224 \cdot 224}{16^2} = 196$ patches. Each patch is flattened into a vector of size $P^2 \cdot C$ and projected into a 768-dimensional latent space through a trainable linear projection $\mathbf{E} \in \mathbb{R}^{(P^2 \cdot C) \times D}$. We added a single linear layer to the MLP in the transformer's head during fine-tuning to learn our four pavement distress types.

We used the cross-entropy loss for multiclass classification to quantify the discrepancy between the predicted logits and the true class label. The formulation combines softmax and negative log-likelihood. Given logits $\mathbf{x} = [x_1, x_2, \cdots, x_C]$ and the correct class index y, the loss is defined as,

$$\mathcal{L}(\mathbf{x}, y) = -x_y + \log \sum_{c=1}^{C} e^{x_c} \tag{2}$$

Network training on the NoMURDistress dataset [1] terminated after 50 epochs, as the patience-based stopping criterion was met. As a result, our trained ViT model achieved a best validation loss of 0.0575.

3 Results and Discussion

3.1 Precision of Parallel Predictors

Stage 1 of the proposed two-stage network consists of two parallel segmentation predictors. The performance of these trained models affects the overall robustness of the pipeline. To assess their capability in generating segmentation masks for road lanes and pavement panels, the first ablation study focused on evaluating model performance using mean Average Precision (mAP). This was computed by averaging the Intersection over Union (IoU) thresholds ranging from 0.50 to 0.95 in increments of 0.05. Its goal is to provide a comprehensive measure of detection and localization consistency under varying levels of strictness.

As shown in Fig. 2, the road lane segmentation model achieved an mAP of approximately 0.95 among five YOLO11 variants (YOLO11n, YOLO11s, YOLO11m, YOLO11l, and YOLO11x), while the pavement panel segmentation model attained a slightly lower mAP of around 0.88. Model performance remained consistent across different export formats—ONNX and OpenVINO—indicating minimal impact from model conversion. The latency of originally trained PyTorch models and the exported ONNX models were evaluated using CUDA on an NVIDIA GeForce GTX 1050 Ti GPU, whereas the OpenVINO model was tested on an Intel Core i7-7700HQ CPU.

The pavement panel segmentation predictor yielded a noticeably lower mAP than the road lane predictor. It indicates the performance limitations that warrant further analysis. To explore this, the second experiment analyzed missed detections. As shown in the left plot of Fig. 3, the road lane segmentation model

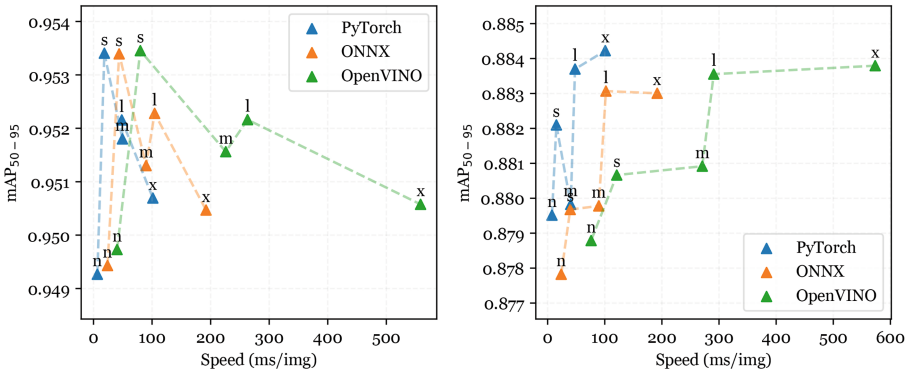

Fig. 2. Mean Average Precisions (@50-95 IoUs) of various Model Exports for (*left*) road lane segmentation and (*right*) pavement panel segmentation.

maintained consistently low false negative rates across various IoU thresholds. It demonstrates its strong ability to identify road lanes in the test images. In contrast, the pavement panel segmentation model exhibited significantly higher false negative rates, particularly at IoU thresholds above 0.7.

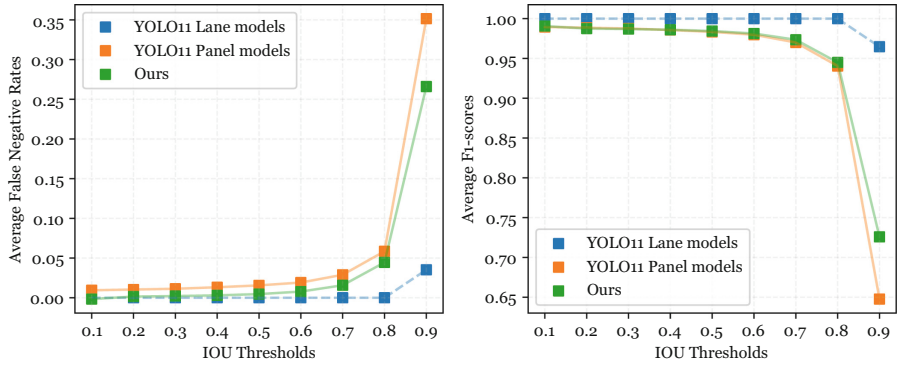

Fig. 3. Recall-sensitive metrics for pavement panel detection—(*left*) average false negative rates and (*right*) F1 scores.

To mitigate this deficiency, the proposed refining technique was introduced. The results show that it substantially reduced the false negative rate compared to the baseline pavement panel model. Additionally, the right plot in Fig. 3 presents the corresponding F1 scores—the harmonic mean of precision and recall—which further confirm the module's effectiveness. The improvement in F1 scores indicates that the refining technique improved both precision and recall.

3.2 Pavement Distress Classification Report

The final ablation study investigates whether the two-stage architecture performs better than directly using the trained YOLO11 pavement panel segmentation models. It also assesses the consistency of classification results between unrefined and refined cropped pavement panel images in the set $\{x_k\}$. In the conventional method, the YOLO11 model segments the panels, and a Vision Transformer classifies the resulting patches, forming the `YOLO11Panel+ViT approach`. We use the `YOLO11n` pre-trained variant for pavement panel segmentation in both methods and for road lane segmentation in the two-stage framework.

The one-vs-rest precision-recall curve analysis compares the performance of the `YOLO11Panel+ViT` approach with the proposed pipeline. As shown in Fig. 4, the pipeline achieves higher average precision (AP) scores for both the *sealed-crack* and *thincrack* classes. The mean Average Precision among the four classes is 0.9775±0.0015. This signifies that the proposed two-stage pipeline improved the classification performance.

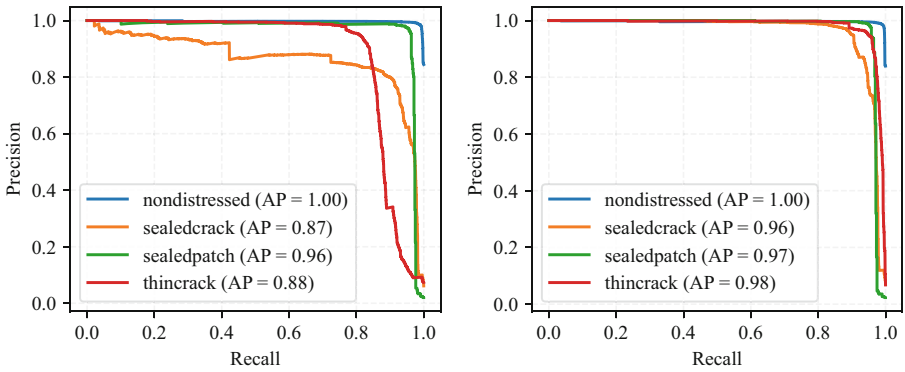

Fig. 4. One-vs.-rest precisionâĂŞrecall curve comparison between (*left*) the `YOLO11Panel+ViT` approach and (*right*) our two-stage architecture.

Figure 5 presents a qualitative demonstration of correct classification results obtained from the proposed pipeline. It can be observed that the extracted pavement panels exhibit irregular geometries, where several instances deviate from ideal rectangular structures with balanced sides. Despite these unstructured shapes, the proposed architecture can delineate pavement panels and can classify the corresponding distress types.

However, the presence of occlusions, particularly from vehicles obstructing the pavement panels, introduces noticeable degradation in classification performance, as evidenced by several prediction samples. This suggests the need for an additional annotation category to explicitly model such cases; specifically, panels occluded by vehicles should be labeled as a distinct vehicle presence class. A further limitation is its inability to adopt to curved road segments. This is

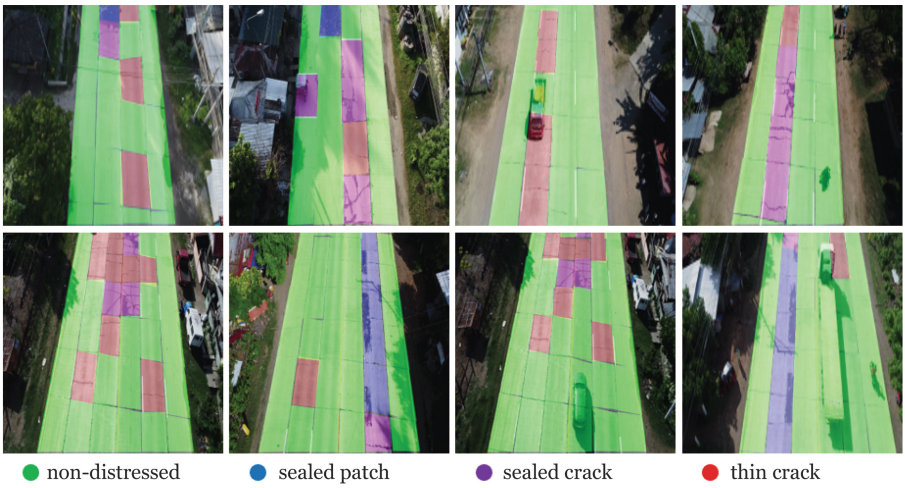

Fig. 5. Qualitative demonstration of correct classification results from our two-stage architecture.

primarily due to the constraints of the refinement procedure, which relies on linear interpolation.

4 Conclusion

This study presents a two-stage architecture designed to detect pavement distresses in aerial images: parallel YOLO-based predictors with refining technique, and a pavement distress classifier. Experimental results show that producing refined pavement panel mask reduces false positive/negatives and improves overall classification performance. The future direction will involve exploring additional distress types found in concrete, asphalt, or hybrid road surfaces. Conducting extensive experiments on these new distress categories will be necessary in the next phase of research.

References

1. Aleluya, E.R., et al.: NoMURDistress (2025). https://doi.org/10.7910/DVN/HUEFOS
2. Aleluya, E.R., et al.: NoMURLane (2025). https://doi.org/10.7910/DVN/BAMYR1
3. Aleluya, E.R., et al.: NoMURPanel (2025). https://doi.org/10.7910/DVN/PSFTEH
4. Dosovitskiy, A., et al.: An Image is Worth 16x16 Words: Transformers for Image Recognition at Scale (2021). https://doi.org/10.48550/arXiv.2010.11929
5. Du, Y., Pan, N., Xu, Z., Deng, F., Shen, Y., Kang, H.: Pavement distress detection and classification based on YOLO network. Int. J. Pavement Eng. **22**, 1–14 (2020). https://doi.org/10.1080/10298436.2020.1714047

6. Guan, S., Liu, H., Pourreza, H.R., Mahyar, H.: Deep learning approaches in pavement distress identification: A review. arXiv preprint arXiv:2308.00828 (2023). https://doi.org/10.48550/arXiv.2308.00828
7. Guo, F., Liu, J., Xie, Q., Yu, H.: A two-stage framework for pixel-level pavement surface crack detection. Eng. Appl. Artif. Intell. **133**, 108312 (2024). https://doi.org/10.1016/j.engappai.2024.108312
8. Jiang, Y., Pang, D., Li, C., Yu, Y., Cao, Y.: Two-step deep learning approach for pavement crack damage detection and segmentation. Int. J. Pavement Eng. **24**(2), 2065488 (2023). https://doi.org/10.1080/10298436.2022.2065488
9. Kothai, R., Prabakaran, N., Srinivasa Murthy, Y.V., Reddy Cenkeramaddi, L., Kakani, V.: Pavement distress detection, classification, and analysis using machine learning algorithms: a survey. IEEE Access **12**, 126943–126960 (2024). https://doi.org/10.1109/ACCESS.2024.3455093
10. Liu, J., et al.: Automated pavement crack detection and segmentation based on two-step convolutional neural network. Comput.-Aided Civil Infrastruct. Eng. **35**(11), 1291–1305 (2020). https://doi.org/10.1111/mice.12622
11. Lv, Z., Hao, Z., Zhu, Y., Lu, C.: A review on automated detection and identification algorithms for highway pavement distress. Appl. Sci. **15**(11) (2025). https://doi.org/10.3390/app15116112
12. Maluya, M.M.O., et al.: Rural Road Pavement Panel Detection with Unmanned Aerial Vehicles. In: 2023 IEEE 15th International Conference on Humanoid, Nanotechnology, Information Technology, Communication and Control, Environment, and Management (HNICEM), pp. 1–6 (2023). https://doi.org/10.1109/HNICEM60674.2023.10589124
13. Maluya, M.M.O., Aleluya, E.R.M., Opon, J.G., Salaan, C.J.O.: Lane tracking for autonomous road pavement inspection with unmanned aerial vehicles. In: 2023 6th International Conference on Applied Computational Intelligence in Information Systems (ACIIS), pp. 1–6 (2023). https://doi.org/10.1109/ACIIS59385.2023.10367228
14. Maluya, M.M.O., Aleluya, E.R.M., Salaan, C.J.O.: Flexible and rigid pavement binary classifier using vision transformer. In: 2024 IEEE 16th International Conference on Humanoid, Nanotechnology, Information Technology, Communication and Control, Environment, and Management (HNICEM), pp. 1–6 (2024). https://doi.org/10.1109/HNICEM64917.2024.11258762
15. Pan, Y., Zhang, X., Cervone, G., Yang, L.: Detection of asphalt pavement potholes and cracks based on the unmanned aerial vehicle multispectral imagery. IEEE J. Selected Top. Appl. Earth Observations Rem. Sens. **11**(10), 3701–3712 (2018). https://doi.org/10.1109/JSTARS.2018.2865528
16. Samadzadegan, F., Dadrass Javan, F., Ashtari Mahini, F., Gholamshahi, M., Nex, F.: Automatic road pavement distress recognition using deep learning networks from unmanned aerial imagery. Drones **8**(6) (2024). https://doi.org/10.3390/drones8060244
17. Silva, L.A., Sanchez San Blas, H., Peral García, D., Sales Mendes, A., Villarubia González, G.: An architectural multi-agent system for a pavement monitoring system with pothole recognition in UAV images. Sensors **20**(21) (2020). https://doi.org/10.3390/s20216205
18. Song, Q., Liu, L., Lu, N., Zhang, Y., Muniyandi, R.C., An, Y.: A three-stage pavement image crack detection framework with positive sample augmentation. Eng. Appl. Artif. Intell. **129**, 107624 (2024). https://doi.org/10.1016/j.engappai.2023.107624

19. Tran, T.S., Tran, V.P., Lee, H.J., Flores, J.M., Le, V.P.: A two-step sequential automated crack detection and severity classification process for asphalt pavements. Int. J. Pavement Eng. **23**(6), 2019–2033 (2022). https://doi.org/10.1080/10298436.2020.1836561
20. Wang, A., Lang, H., Chen, Z., Peng, Y., Ding, S., Lu, J.J.: The two-step method of pavement pothole and raveling detection and segmentation based on deep learning. IEEE Trans. Intell. Transp. Syst. **25**(6), 5402–5417 (2024). https://doi.org/10.1109/TITS.2023.3340340
21. Yan, H., Zhang, J.: UAV-PDD2023: a benchmark dataset for pavement distress detection based on UAV images. Data Brief **51**, 109692 (2023). https://doi.org/10.1016/j.dib.2023.109692
22. Yang, Z., Ni, C., Li, L., Luo, W., Qin, Y.: Three-stage pavement crack localization and segmentation algorithm based on digital image processing and deep learning techniques. Sensors **22**(21) (2022). https://doi.org/10.3390/s22218459
23. Zhang, J., Xia, H., Li, P., Zhang, K., Hong, W., Guo, R.: A pavement crack detection method via deep learning and a binocular-vision-based unmanned aerial vehicle. Appl. Sci. **14**(5) (2024). https://doi.org/10.3390/app14051778
24. Zhang, Y., Chen, J., Wu, Z., Guo, X., Jia, S.: Optimizing pavement distress detection with UAV: a comparative study of vision transformer and convolutional neural networks. KSCE J. Civil Eng. 100095 (2024). https://doi.org/10.1016/j.kscej.2024.100095
25. Zhao, K., Xu, S., Loney, J., Visentin, A., Li, Z.: Road pavement health monitoring system using smartphone sensing with a two-stage machine learning model. Autom. Constr. **167**, 105664 (2024). https://doi.org/10.1016/j.autcon.2024.105664
26. Zhu, J., Zhong, J., Ma, T., Huang, X., Zhang, W., Zhou, Y.: Pavement distress detection using convolutional neural networks with images captured via UAV. Autom. Constr. **133**, 103991 (2022). https://doi.org/10.1016/j.autcon.2021.103991

Geographical Analysis, Urban Modeling, Spatial Statistics (Geog-And-Mod 2026)

Mitigating Weight Explosion in Rare-Feature Co-location Pattern Mining: A Cauchy Distribution-Based Approach

Vanhiep Duong, Vanthuc Nguyen, Xuankhang Pham, Thanhduy Pham, and Vanha Tran(✉)

FPT University, 155514 Hanoi, Vietnam
{hiepdvhe181185,thucnvhe181431,khangpxhe180735,duypthe181990}@fpt.edu.vn, hatv14@fe.edu.vn

Abstract. Spatial co-location pattern (SCP) mining aims to identify groups of spatial features whose instances tend to appear near one another. A key difficulty is evaluating patterns that include rare features, particularly when feature frequencies are highly imbalanced. In such cases, the traditional participation index (PI) can be too strict and may overlook rare but meaningful spatial associations. While the proposed rarity-aware measures, they frequently utilize exponential weighting functions that provide insufficient compensation under moderate imbalance and suffer from numerical instability or excessive amplification under extreme disparity. To address these limitations, we propose a novel Cauchy distribution-based weighting framework for prevalence evaluation of SCPs. By defining a Cauchy Rare Intensity, we develop the Cauchy Weighted Participation Index (WPI_C), which offers more stable and proportionate rarity compensation across different imbalance regimes. To enhance mining efficiency, this measure is integrated into a clique-based framework that employs an optimized maximal clique enumeration and hash table-base query strategy. Extensive experiments on multiple real-world datasets demonstrate that our proposed method significantly improves the discovery of rare-feature co-locations while maintaining robust and efficient mining performance.

Keywords: Spatial data mining · Co-location pattern · Rare features · Cauchy Distribution · Maximal clique

1 Introduction

Today, with the rapid development of positioning technologies, massive amounts of data with coordinate information are generated and stored every day. Discovering valuable knowledge from such massive spatial data is extremely important in many fields, such as urban facility analysis, environmental monitoring, and geographic relationship mining [7,9,11]. Many data mining techniques have been

© The Author(s), under exclusive license to Springer Nature Switzerland AG 2027
O. Gervasi et al. (Eds.): ICCSA 2026 Workshops, LNCS 16761, pp. 493–508, 2027.
https://doi.org/10.1007/978-3-032-30527-5_32

proposed, and among them, spatial co-location pattern (SCP) mining refers to finding a set of spatial features from a dataset whose instances frequently appear together in close geographic proximity, typically forming cliques. Traditionally, SCP mining relies on the participation index (PI) [7] to measure pattern prevalence, which is determined by the minimum participation ratio (PR) among all constituent features. However, this strictly minimum-based metric struggles significantly when spatial datasets contain rare features. A feature is rare if the number of its instances is obviously less than that of other features [13].

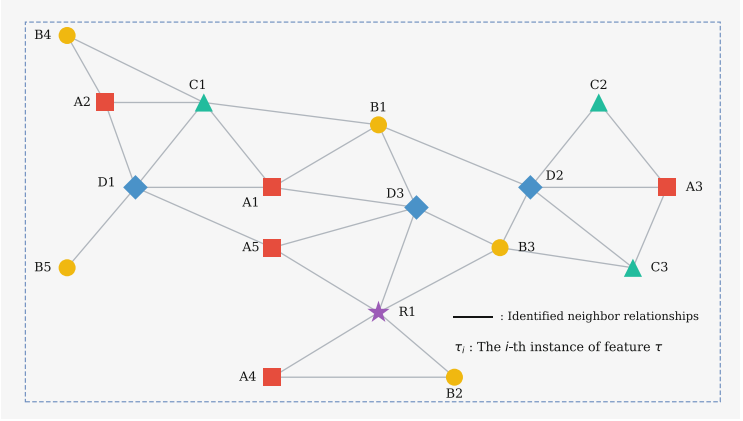

Fig. 1. An illustrative spatial dataset for SCP mining with varying feature frequencies and identified neighbor relationships.

Figure 1 depicts an illustrative spatial dataset containing five features with varying instance counts: $|\mathrm{A}| = 5$, $|\mathrm{B}| = 5$, $|\mathrm{C}| = 3$, $|\mathrm{D}| = 3$, and a strictly rare feature $|\mathrm{R}| = 1$. A user sets a distance threshold ε to determine the neighbor relationships between instances, connected by solid lines. When applying the traditional SCP mining technique to evaluate the candidate combination $p = \{\mathrm{A}, \mathrm{D}, \mathrm{R}\}$, the identified neighbor relationships show that the sole instance R_1 is perfectly co-located with A_5 and D_3. Thus, the participation ratio of the rare feature R is $PR(\mathrm{R}|p) = 1/1 = 1.0$, while the ratios for the other features are $PR(\mathrm{D}|p) = 1/3 \approx 0.33$, and $PR(\mathrm{A}|p) = 1/5 = 0.20$. Consequently, the overall prevalence degree of this pattern is $PI(p) = \min\{0.20, 0.33, 1.0\} = 0.20$. If a user sets a minimum prevalence threshold *min_prev* (e.g., *min_prev* $= 0.30$), this highly meaningful rare-feature pattern would be prematurely pruned, even though the rare feature R relies entirely on this spatial association.

The example in Fig. 1 is merely a miniature representation of real-world datasets. The actual data contains a massive amount of instances, and the number of instances belonging to each feature varies drastically. To capture such valuable rare-feature co-locations, recent studies introduced the Weighted Participation Index (WPI) [13], which compensates for feature-frequency disparity

by utilizing a Gaussian kernel function to assign relative weights. While conceptually innovative, the exponential nature of the Gaussian weight ($w \propto \exp(v^2)$, where v is the frequency disparity ratio) introduces critical mathematical flaws when applied to massive spatial data [13]. For example, when the illustrative case is scaled to a more realistic setting with $|A| = 1000$ and $|R| = 10$, the frequency disparity becomes $v = 100$. When this value is used in the Gaussian weighting function, the resulting weight can become extremely large, even exceeding 10^{18}. Such a value may lead to numerical instability and can over-amplify very small participation ratios. Another limitation appears under moderate imbalance. For a pattern such as $p' = \{D, R\}$, where $|D| = 30$ and $|R| = 10$ ($v = 3$), the Gaussian weight remains close to 1.0. As a result, the method provides little adjustment and may still miss moderately rare but meaningful co-location patterns. Consequently, the algorithm offers virtually no compensation, easily leading to the loss of interesting moderately rare patterns.

This bipolar behavior makes the Gaussian-based WPI highly unreliable for datasets with skewed distributions. Therefore, this paper designs a novel weighting framework based on the Cauchy distribution to overcome these limitations. By featuring a smoother, heavy-tailed response curve, the Cauchy distribution-based approach accelerates earlier to adequately rescue moderately imbalanced features while growing polynomially rather than exponentially at the tail to definitively prevent weight explosion. To further ensure high mining efficiency, we integrate this robust prevalence measure into a clique-based mining framework. The specific contributions of this paper are as follows:

- We propose a Cauchy distribution-based rare-feature weighting framework, define a Cauchy Rare Intensity factor, and develop the Cauchy Weighted Participation Index (WPI_C) for robust prevalence evaluation in SCP mining. This design addresses two main limitations of exponential weighting: weight explosion under severe imbalance and weak compensation under moderate imbalance.
- We incorporate the proposed prevalence measure into a clique–hash-table-based SCP mining pipeline. The pipeline uses a hybrid Bron–Kerbosch-style maximal clique enumeration strategy, following prior graph mining studies [2,8], to support efficient pattern discovery.
- We evaluate the proposed method on several real-world datasets and compare it with existing baselines in terms of discovery effectiveness, numerical stability, and performance under highly imbalanced feature-frequency distributions.

2 Related Work

SCP mining is related to traditional frequent itemset mining, but it is more difficult because spatial instances are linked through neighborhood relationships rather than transaction records. Shekhar and Huang first introduced the SCP

mining problem and proposed the participation index (PI) to evaluate the prevalence of a co-location pattern [7,9]. Since then, several algorithmic frameworks have been developed to improve mining efficiency. Among them, clique-based methods have been widely used because they model neighborhood relations as graph structures [1,12]. By applying maximal clique enumeration, these methods can reduce redundant candidate generation. Bron–Kerbosch-type algorithms and their improved variants are commonly used for this task in graph mining [2,5,8]. Hybrid strategies that adapt to the structure of real-world graphs have also been shown to improve performance in dense neighborhoods [8].

The PI metric is commonly used for prevalence evaluation because it satisfies the anti-monotone property, which helps prune the search space. However, PI takes the minimum participation ratio among all features in a pattern. This makes it conservative when feature frequencies are highly imbalanced, since a low participation ratio from a frequent feature can cause a rare-feature pattern to be discarded. To address this problem, several alternative measures have been proposed. For example, MaxPR relaxes the strict bottleneck effect of PI to better support rare-feature discovery [6]. More recently, the Weighted Participation Index (WPI) introduced a rarity-aware weighting mechanism based on a Gaussian kernel function.

Although these methods improve SCP mining from different perspectives, they do not fully consider how the weighting function behaves under different imbalance levels. As discussed in Sect. 1, exponential weighting may provide limited compensation under moderate imbalance but can produce excessively large weights under extreme imbalance. This motivates the use of a more stable weighting function for rare-feature co-location mining. The literature still lacks a prevalence function explicitly designed to balance sensitivity and control. Therefore, in the following sections, we introduce a Cauchy distribution-based weighting framework and integrate it into an efficient clique-based SCP mining framework to overcome these shortcomings.

3 The Proposed Algorithms

3.1 Basic Concepts and Problem Formulation

A spatial dataset, denoted as $\mathcal{O}$, comprises a finite collection of spatial objects. Each object $x \in \mathcal{O}$ is characterized by a specific feature type $\tau \in \mathcal{T}$ and a geographical coordinate $\mathbf{s}(x)$, where $\mathcal{T} = \{\tau_1, \tau_2, \ldots, \tau_m\}$ represents the universal set of distinct features. The subset of objects belonging to a specific feature τ is denoted by $\mathcal{O}_\tau$, with its cardinality given by $cnt(\tau) = |\mathcal{O}_\tau|$.

Definition 1 (Neighborhood and Co-location Instance). *A spatial neighborhood relationship, denoted as $x \sim_\varepsilon y$, exists between two objects x and y if their spatial distance satisfies a given threshold ε under a specific metric (e.g., Euclidean distance) [7]. Given a candidate SCP, $p \subseteq \mathcal{T}$, ($|p| \geq 2$), a strict type-unique instance of p is defined as a subset of objects $S \subseteq \mathcal{O}$ satisfying two structural constraints: (1) $|S| = |p|$, ensuring a bijective mapping between the*

objects in S and the feature types in p, and (2) all objects in S form a spatial clique (i.e., they are pairwise neighbors) [9]. The set of all such instances for pattern p is denoted as $\mathcal{T}(p)$.

Definition 2 (Participation Ratio and Participation Index). *To evaluate the significance of a pattern, we quantify the contribution of each individual feature. The Participation Ratio (PR) of a feature $\tau \in p$ is the fraction of its objects that appear in at least one valid instance of p:*

$$PR(\tau \mid p) = \frac{|\mathcal{O}_\tau^p|}{cnt(\tau)} \tag{1}$$

where $\mathcal{O}_\tau^p = \{x \in \mathcal{O}_\tau \mid \exists S \in \mathcal{I}(p), x \in S\}$. Consequently, the Participation Index (PI) of the entire pattern p is bounded by its least participating feature:

$$PI(p) = \min_{\tau \in p}\{PR(\tau \mid p)\} \tag{2}$$

A pattern p is deemed a Prevalent Co-location Pattern (PCP) if $PI(p) \geq min_prev$, where min_prev is a user-specified threshold.

3.2 Robust Cauchy Distribution-Based Interest Measure

To alleviate the strict bottleneck of PI under heavy-tailed feature distributions, recent works apply exponential weights. However, as frequency discrepancies grow infinitely large, exponential kernels succumb to "weight explosion," generating excessive false positives. To overcome this mathematical bottleneck, we propose shifting the weighting mechanism to the Lorentzian form of the Cauchy distribution kernel [3].

Definition 3 (Original Weighted Participation Index [13]). *To compensate for the rare-feature dilemma, the traditional Weighted Participation Index (WPI) evaluates the prevalence of a co-location pattern p by incorporating a rarity-aware weighting mechanism. The metric is defined as:*

$$WPI(p) = \min_{\tau \in p}\{PR(\tau \mid p) \cdot weight(\tau, p)\} \tag{3}$$

where $weight(\tau, p)$ is the dynamic weight assigned to feature τ, traditionally formulated using a Gaussian kernel function to exponentially amplify the participation ratio of rare features:

$$weight(\tau, p) = \exp\left(\frac{(r(\tau, p) - 1)^2}{2\kappa^2}\right) \tag{4}$$

with $r(\tau, p)$ representing the relative frequency disparity of the feature within the pattern, and κ serving as the global dispersion parameter of the dataset.

Definition 4 (Global Pairwise Dispersion). *Assuming the feature types in $\mathcal{T}$ are indexed in ascending order of their frequencies such that $cnt(\tau_1) \leq cnt(\tau_2) \leq \ldots \leq cnt(\tau_m)$, the global dispersion parameter κ is formulated as the arithmetic mean of all pairwise frequency ratios:*

$$\kappa = \frac{2}{m(m-1)} \sum_{i=1}^{m-1} \sum_{j=i+1}^{m} \frac{cnt(\tau_j)}{cnt(\tau_i)} \tag{5}$$

Functionally, κ serves as a global bandwidth parameter that encapsulates the intrinsic frequency skewness across the entire spatial domain.

Definition 5 (Cauchy Rare Intensity). *For any candidate pattern p, let $\tau_{\min} = \arg\min_{\tau \in p} cnt(\tau)$ be its limiting (rarest) feature. We quantify the relative abundance of any feature $\tau \in p$ using the within-pattern ratio $r(\tau, p) = cnt(\tau)/cnt(\tau_{\min})$. To model the statistical rarity of a feature without aggressive penalization, we define its Rare Intensity (RI_C) using the Cauchy distribution:*

$$RI_C(\tau, p) = \frac{1}{1 + \left(\frac{r(\tau,p)-1}{\kappa}\right)^2} \tag{6}$$

Definition 6 (Cauchy Distribution-based Weighting). *Unlike the exponential function used in the original WPI (Eq. 2), our framework calculates the feature weight $\omega(\tau, p)$ simply as the reciprocal of the Cauchy Rare Intensity:*

$$\omega(\tau, p) = \frac{1}{RI_C(\tau, p)} = 1 + \left(\frac{r(\tau, p) - 1}{\kappa}\right)^2 \tag{7}$$

Weight Analysis and Mathematical Properties: The polynomial formulation (Eq. 5) resolves two main drawbacks of the Gaussian kernel (Eq. 2):

- **Asymptotic Stability (Preventing Weight Explosion):** Extreme frequency imbalances (large r) cause exponential functions to output unmanageable values. Given a global dispersion $\kappa = 8$ and a ratio $r(\tau, p) = 81$, the Gaussian kernel yields $\exp(10^2) \approx 2.68 \times 10^{43}$. This inflation pushes random noise above the prevalence threshold. The Cauchy distribution avoids this via its heavy-tailed polynomial decay [4]. Under the same parameters, our Cauchy weight is strictly bounded at $\omega = 1 + 10^2 = 101$. This naturally limits the maximum influence of rare features and prevents false positives.
- **Early Sensitivity (Recovering Missed Patterns):** Exponential curves offer minimal compensation for moderate discrepancies (small r). Consequently, meaningful spatial patterns with slight imbalances are often pruned. The Cauchy function grows more steadily early on. In our evaluation of a moderately rare pair, the Gaussian model produced a weight of 1.08, leaving the pattern below the threshold. Our framework assigned a weight of 1.16. This adjustment is sufficient to retain valid spatial relationships.

Definition 7 (Cauchy Weighted Participation Index). *Replacing the exponential weight with our robust Cauchy weight, we define the Cauchy Weighted Participation Ratio (WPR_C) by multiplying a feature's raw PR with its dynamically calculated Cauchy weight:*

$$WPR_C(\tau \mid p) = PR(\tau \mid p) \cdot \omega(\tau, p) \tag{8}$$

A spatial co-location pattern is considered prevalent when its Cauchy Weighted Participation Index (WPI_C) reaches or exceeds the threshold min_prev. We define $WPI_C(p)$ as the bottleneck WPR_C across all features present in p:

$$WPI_C(p) = \min_{\tau \in P} WPR_C(\tau \mid p) \tag{9}$$

We formulate the Cauchy Weighted Participation Ratio (WPR_C) by scaling the raw PR with the proposed Cauchy weight:

Impact of Cauchy Weight on Feature Selection. Equation (6) avoids the instability of exponential scaling. The Cauchy kernel preserves the statistical validity of the prevalence score. In traditional models, inflated weights often eclipse the actual PR. Even negligible, coincidental co-occurrences (e.g., $PR = 10^{-5}$) are artificially pushed above the *min_prev* threshold by weights like 10^{43}, generating severe noise. By replacing the Gaussian kernel with $\omega(\tau, p)$ to ensure a predictable polynomial growth curve while providing early sensitivity, WPI_C guarantees that rare-feature compensation is proportionate across all levels of imbalance. The raw PR thus retains its discriminative power: a pattern achieves prevalence only if it exhibits genuine spatial proximity coupled with a mathematically sound weight boost. This optimally filters out frequency-induced noise while recovering moderately rare patterns that the traditional WPI discards.

3.3 The Designed Mining Algorithm

After establishing neighbor relationships, data points are represented as an undirected graph $G(V, E)$ with vertices $V \equiv \Psi$ and edges E. Each edge is formed between any two vertices whose instances meet the neighborhood condition.

Definition 8 (Maximal Clique, MC). *A subset of instances $cl = \{o_1, \ldots, o_l\}$ is called a clique if all instances have a neighboring relationship. Furthermore, a clique cl is defined as a maximal clique if it cannot be included by any larger clique cl' ($cl \subset cl'$).*

This study focuses on using MCs to optimize the SCP mining process rather than creating a new MC enumeration. Although enumerating MCs is an NP-hard problem, it still is an appeal domain with numerous established solutions have been proposed. In particular, hybrid strategies that adapt clique enumeration to the structural properties of real-world graphs have been shown to improve efficiency in dense neighborhoods. For the purposes of this work, we employ the MCEHybrid algorithm, which is the hybrid approach of BK_{rcd} and BK_{pivot}, to

identify maximal cliques. Detailed mechanics of this algorithm are omitted due to space constraints. However, comprehensive explanations can be found in [8].

To demonstrate Definition 8, we utilize the toy spatial dataset depicted in Fig. 1. Once the neighborhood relationships among the instances are materialized, the underlying structure is captured as a neighbor graph. By executing the MCEHybrid algorithm on this graph, we can extract all maximal cliques as shown in Fig. 2(a).

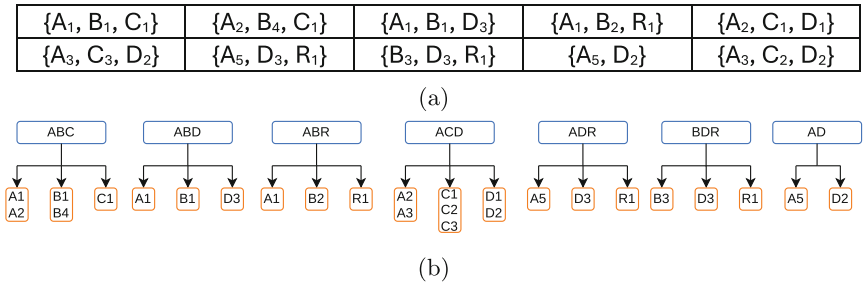

Fig. 2. The constructed participating instance hash table.

Definition 9 (Participating Instance Hash Table). *A participating instance hash table is defined as a hash-map structure which the keys represent feature sets extracted from instances within maximal cliques, and the corresponding values hold the actual instances of those cliques.*

Figure 2(b) illustrates the generated participating instance hash table from all the MCs extracted in Fig. 1. Suppose we are evaluating a candidate pattern $p = \{A, B\}$. To calculate the participating instances for the features in p, we identify all keys in the hash table that are supersets of {A, B}. By accessing the pattern {A, B, C}, {A, B, D} and {A, B, R} associated with these matching keys, we can extract the valid co-location instances $\{A_1, B_1\}$, $\{A_2, B_4\}$ and $\{A_1, B_2\}$. Aggregating these instances return the complete set of participating instances for candidate p.

Algorithm 1 is the pseudo-code of the designed mining SCP algorithm, named MCR. The detail of MCR is described as below.

Initialization (Steps 1–7). Initially, the features within the dataset are counted and sorted to compute their dispersion (Step 1–2). Following this, the neighbor graph among instances are constructed based on a user-specified threshold ϵ (Step 3). Subsequently, the MCEHybrid algorithm, is applied to enumerate the MCs (Step 4). Finally, a PriorityQueue extracts all keys from the hash table to form the initial candidate set for the mining process (Step 5).

Candidate Pattern Evaluation and Generation (Step 8–17). The algorithm iteratively processes the Pattern Queue until it is empty. In each iteration,

it extracts the highest-priority candidate pattern p (Step 9). To prevent redundant computations, the algorithm checks if p is already in the processed set or not. If so, it skips to the next iteration (Step 10–12). Otherwise, p is added to the processed set. After that, the participating instances of p is retrieved by querying the hashmap (Step 14). Following this, it calculates the rare intensity (RI_c) and uses it to compute the weighted participating instances (WPI_c) for the candidate (Step 15–16). Finally, the algorithm derives a new set of sub-patterns from p to be evaluated in subsequent steps (Step 17).

Algorithm 1: MCR Colocation Mining

Input: Spatial instance set $\mathcal{O}$, Feature set $\mathcal{T}$, Distance threshold ϵ, Prevalence threshold min_prev

Output: Set of spatial co-location patterns with rare features($SCPs$)

1 $feat_freq \leftarrow$ `CountAndSortFeatures`$(\mathcal{O}, \mathcal{T})$;
2 $\kappa \leftarrow$ `CalculateDispersion`$(feat_freq)$;
3 $G(V, E) \leftarrow$ `BuildNeighborGraph`$(\mathcal{O}, \epsilon)$;
4 $clique_map \leftarrow$ `ExecuteMCEHybrid`$(G(V, E))$;
5 $PatternQueue \leftarrow$ `PriorityQueue`(`ExtractCandidates`$(clique_map)$);
6 $PCPs \leftarrow \emptyset$;
7 $SCPs \leftarrow \emptyset$;
8 $processed \leftarrow \emptyset$;
9 **while** *PatternQueue is not empty* **do**
10 $p \leftarrow PatternQueue$.`pop_max()`;
11 **if** $p \in processed$ **then**
12 **continue**
13 **end**
14 $processed \leftarrow processed \cup \{p\}$;
15 $PartI \leftarrow$ `QueryInstances`$(p, clique_map)$;
16 $RI_c \leftarrow$ `CalcRareIntensity`$(p, feat_freq, \kappa)$;
17 $WPI_c \leftarrow$ `ComputeWeightedPI`$(PartI, P, RI_c, feat_freq)$;
18 $newCs \leftarrow$ `DeriveSubPatterns`(p);
19 **if** $WPI_c \geq min_prev$ **then**
20 $PCPs \leftarrow PCPs \cup \{p\}$;
21 $InferredPCPs \leftarrow$ `InferPrevalentSubsets`$(newCs, p, feat_freq)$;
22 $SCPs \leftarrow SCPs \cup \{p\} \cup InferredPCPs$;
23 $newCs \leftarrow newCs \setminus InferredPCPs$;
24 **end**
25 **foreach** $subset \in newCs$ **do**
26 **if** $subset \notin processed$ **then**
27 $PatternQueue$.`push`$(subset)$;
28 **end**
29 **end**
30 **end**
31 **return** $SCPs$;

Select Prevalent Co-locations (Lines 18–30). The algorithm evaluates whether the WPI_c of candidate meets the minimum prevalence threshold (Step 18). If the condition is satisfied, the candidate p is added to PCPs. The algorithm then infers prevalent subsets via InferPrevalentSubsets, and accumulates all confirmed patterns—both directly evaluated and inferred—into SCPs (Steps 20–23). The final output SCPs thus contains the complete set of discovered rare-feature co-location patterns. Finally, the algorithm iterates through these remaining subsets. Any subset that has not yet been processed is pushed into the candidate queue for subsequent processing (Step 24–30).

4 Experiments and Analysis

This section presents a comprehensive evaluation of the proposed algorithm. The evaluation is conducted between three baseline methods: PI [14], MaxPR [6], and the original WPI method with the ordered NR-tree structure [13].

The PI-based baseline used the prevalence-driven approach which evaluated the pattern significance through the participation index and leverages its anti-monotone property for candidate pruning. MaxPR focused on co-location patterns with rare features but has limited effectiveness due to the weak constraints of anti-monotonic property. The original WPI method improved rare-feature discovery by using a Gaussian weighting method and utilizes ordered NR-tree approach for retrieving instances faster. Generally, these three methods highlighted varying strategies for mining spatial co-location, particularly rare features, and established robust frameworks for comparison.

All algorithms are implemented and executed on a computer with the configuration of an Intel(R) Core i7-12700H CPU, 16 GB of main memory, and running in Windows 11 operating system.

4.1 Datasets

Our approach is evaluated on four real world datasets namely Las Vegas, Toronto, Beijing, and Shanghai. The Las Vegas dataset is extracted from the Yelp Open Dataset[1], including varying venue categories in the United States. The remaining three datasets are constructed from public Point-of-Interest (POI) sources [1,10,11] and undergo preprocessing processes to eliminate invalid records.

Table 1 illustrates the key features of each dataset. Beyond basic statistics which are number of feature types, total instances, and spatial coverage, we have the global dispersion κ as defined in Definition 5. This feature captures the difference in instance counts across all feature pairs in the dataset. A higher κ value indicates the larger imbalance in feature frequencies, reflecting more pronounced rare-feature characteristics in the dataset. In contrast, a lower κ implies a relatively uniform distribution. The four datasets provide a wide range

[1] https://business.yelp.com/data/resources/open-dataset.

Table 1. Datasets characteristics

Name	# Features	# Instances	Spatial Coverage	κ
Las Vegas	17	22,725	$38{,}649 \times 62{,}985$ km^2	2.90
Toronto	20	17,129	$23{,}417 \times 56{,}036$ km^2	7.86
Shanghai	14	41,454	$65{,}557 \times 113{,}690$ km^2	13.22
Beijing	19	104,909	138.7×227 km^2	16.74

of κ values (from 2.90 to 16.74), which providing a comprehensive element for assessing the behavior of rare-feature discovery strategies under varying degrees of skewness.

4.2 Effectiveness in Pattern Discovery

To evaluate the effectiveness of the proposed method in practical scenarios, we analyze a subset of representative patterns extracted from the Toronto dataset (represented in Table 1) under the distance threshold $\epsilon = 120$ m and minimum prevalence threshold $min_prev = 0.2$. Table 2 shows a detailed comparison of these patterns to illustrate the advantages of our Cauchy-based approach over WPI approach. We analyze the patterns in two different categories; those new patterns (*Added*) and those correctly pruned (*Removed*) by our algorithm.

Table 2. The differences between patterns discovered by WPI and the proposed method.

Group	Pattern	WPI		Ours	
		WPRs	Weights	WPRs	Weights
Added	{R, E}	[0.4661, 0.1894]	[1.0, 2.08]	[0.4661, **0.2245**]	[1.0, **2.46**]
	{S, F}	[0.6000, 0.1902]	[1.0, 1.46]	[0.6000, **0.2289**]	[1.0, **1.76**]
Removed	{T, G, C}	[0.2857, 0.5986, 4.60×10^{10}]	[1.0, 27.35, $\mathbf{7.19}\times10^{12}$]	[0.2857, 0.1667, 0.3848]	[1.0, 7.62, **60.21**]
	{T, G, D}	[0.2500, 0.6447, 2.10×10^{6}]	[1.0, 27.35, $\mathbf{1.82}\times\mathbf{10^8}$]	[0.2500, 0.1795, 0.4510]	[1.0, 7.62, **39.04**]

The *Added* group highlights the additional rare-feature co-location pattern that are not captured by the traditional WPI under the frequency imbalance. For example, in pattern {S, F}, the traditional WPI assigns a smaller weight of 1.46 to the rare feature, leading to a minimum WPR of 0.1902. Because this prevalence score falls below the minimum threshold ($min_prev = 0.2$), this co-location is missed. By contrast, our proposed method illustrates early sensitivity by assigning a significantly higher weight of 1.76. This decisive boost the pattern's final prevalence score to 0.2289, which is higher than the required minimum threshold, resulting in the recovered of the pattern {S, F}.

In contrast, the *Removed* group exposes the numerical instability of the exponential Gaussian kernel under extreme disparity. With the patterns like {T, G, C} and {T, G, D}, the traditional WPI generates an extremely large weights

for rare features C and D with 7.19×10^{12} and 1.82×10^{8}, respectively. These massive numbers completely hide the true spatial participation of the instances. When the raw PR is multiplied by such extreme weights, the true spatial proximity becomes completely irrelevant. The mathematical artifact makes the WPR extremely high (for example 4.60×10^{10}). As a result, random noise patterns go well above the 0.2 threshold although they have very little spatial importance. By proposing a heavy-tailed polynomial curve, our Cauchy based framework completely resolve this explosion. The extreme weight for feature C is reduced to 60.21 while the weight for feature D is reduced to 39.04. Consequently, the true prevalence of the pattern {T, G, C} is correctly evaluated with 0.1667, allowing our algorithm to identify and prune the patterns that the traditional WPI promotes falsely.

4.3 Computational Efficiency: Time and Memory

Efficient in the Execution Time. Figures 3 and 4 illustrates the execution time under varying distance thresholds ϵ and prevalence thresholds min_{prev}. As shown in Fig. 3, a large ϵ causes the runtime of all methods to rise significantly. The reason for this is that the more neighboring relationships are established, the larger number of co-location instances and an expanded candidate search space. PI and MaxPR, which are built based on the joinless approach, are heavily affected. Specifically, their candidate sets and row instances grow rapidly as the neighborhood expands, leading to considerably increases in runtime. Besides, WPI mitigates some redundant join operations through its ordered NR-tree structure. However, constructing and querying this index still introduces considerable time overhead. Under different min_{prev} (Fig. 4), a stricter the prevalence condition prunes the search space more effectively, decreasing the runtime for all algorithms. PI and MaxPR still generate a substantial number of intermediate candidates due to their exhaustive level-wise traversal, while WPI incurs additional computational cost from maintaining ordered neighborhood structures. In contrast, our method, which stores maximal cliques in a hash map, remains stable across both parameter settings. This structure avoids redundant instance enumeration and enables efficient candidate evaluation.

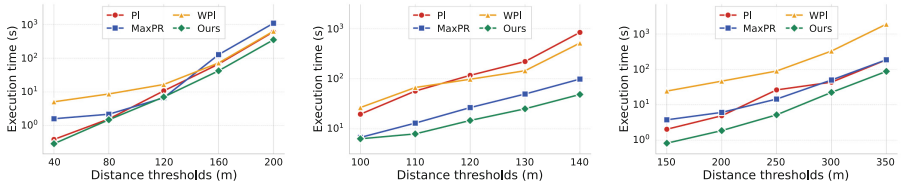

(a) Las Vegas (min_{prev} = 0.15) (b) Toronto (min_{prev} = 0.2) (c) Shanghai (min_{prev} = 0.2)

Fig. 3. Comparison of execution time under varying distance thresholds (ϵ).

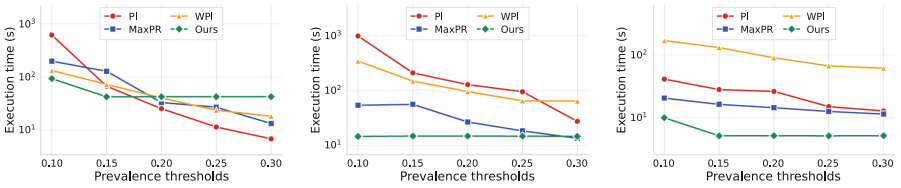

(a) Las Vegas ($\epsilon = 160$m) (b) Toronto ($\epsilon = 120$m) (c) Shanghai ($\epsilon = 250$m)

Fig. 4. Comparison of execution time under varying prevalence thresholds (min_{prev}).

Efficient in the Memory Consumption. Figures 5 and 6 report the memory consumption under varying distance thresholds (ϵ) and prevalence thresholds (min_{prev}), respectively. Overall, a similar trend is observed between memory consumption and runtime. When ϵ increases (Fig. 5), PI and MaxPR must retain large rowsets to support their join operations, resulting in rapid memory growth and making them the most memory consumption methods. WPI generally uses less memory than PI and MaxPR but still incurs significant overhead. Under varying min_{prev} (Fig. 6), the memory footprint of all baselines decreases because fewer patterns survive under the stricter prevalence conditions. In contrast, our approach demands significantly less memory than the baselines across all parameter settings and datasets. This is because our method stores maximal cliques in a hash map and retrieves participating instances directly based on key lookup. This method avoids the materialization of large intermediate tables. This advantage allows our method to operate with an small and stable memory footprint, even when the search space expands significantly.

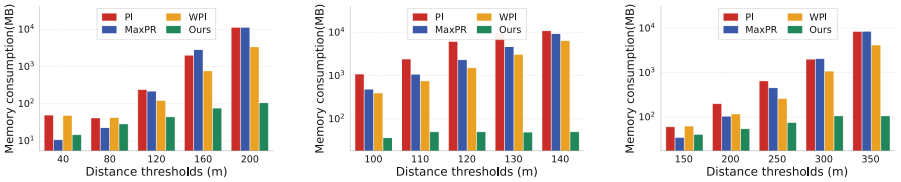

(a) Las Vegas (min_{prev}=0.15) (b) Toronto (min_{prev} = 0.2) (c) Shanghai (min_{prev} = 0.2)

Fig. 5. Memory consumption comparison under varying distance thresholds (ϵ).

4.4 Scalability Analysis

Figures 7 and 8 report how execution time and memory scale as the dataset proportion grows from 20% to 100%. Across all algorithms, both metrics increase with data size, driven by the rapid expansion of neighboring relationships and

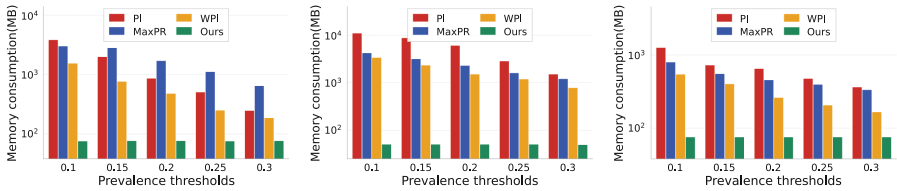

(a) Las Vegas ($\epsilon = 160$m) (b) Toronto ($\epsilon = 120$m) (c) Shanghai ($\epsilon = 250$m)

Fig. 6. Memory consumption comparison under varying prevalence thresholds (min_{prev}).

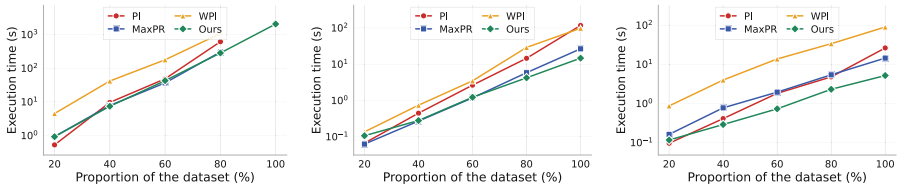

(a) Beijing ($\epsilon = 250$m) (b) Toronto ($\epsilon = 120$m) (c) Shanghai ($\epsilon = 250$m)

Fig. 7. Scalability of execution time across three datasets with varying proportions of instances (from 20% to 100%, all cases $min_{prev} = 0.2$).

the resulting growth in candidate patterns. PI and MaxPR are most adversely affected, as their joinless level-wise paradigm requires maintaining and extending large rowsets proportional to the number of instances. WPI reduces some of this overhead through its ordered NR-tree, but tree traversal and maintenance become increasingly costly at larger scales. Our method exhibits the most gradual growth in both time and memory, attributable to the hash-map-based maximal clique storage, which enables direct instance retrieval and avoids repeated traversal of neighborhood structures as data volume increases. Overall, these results confirm that the proposed approach achieves superior scalability relative to both joinless-based and tree-based competitors.

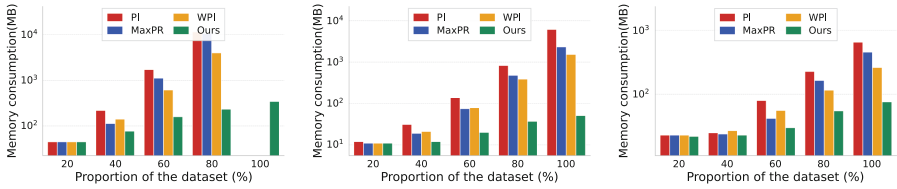

(a) Beijing ($\epsilon = 250$m) (b) Toronto ($\epsilon = 120$m) (c) Shanghai ($\epsilon = 250$m)

Fig. 8. Scalability of memory consumption across three datasets with varying proportions of instances (from 20% to 100%, all cases $min_{prev} = 0.2$).

5 Conclusion

This paper addressed spatial co-location pattern mining under severe feature-frequency imbalance. To overcome the weight explosion and insufficient compensation flaws of traditional exponential weighting (WPI), we proposed a robust Cauchy Distribution-based prevalence measure (WPI_C). By leveraging a heavy-tailed polynomial formulation, WPI_C prevents numerical instability under extreme disparity while preserving early sensitivity to moderately rare features. Furthermore, we integrated this measure into an efficient maximal-clique enumeration framework to improve scalability. Extensive experiments demonstrated that our method successfully discovers more informative rare-feature patterns than existing approaches while maintaining superior computational efficiency.

However, relying on a global dispersion measure limits the framework's adaptability to highly variable local skewness and dynamic environments. In future work, we will study locally adaptive parameterization, extend the framework to find spatio-temporal co-location patterns, and explore mining in streaming data where feature distributions change over time.

References

1. Bao, X., Wang, L.: A clique-based approach for co-location pattern mining. Inf. Sci. **490**, 244–264 (2019)
2. Bron, C., Kerbosch, J.: Algorithm 457: finding all cliques of an undirected graph. Commun. ACM **16**(9), 575–577 (1973)
3. Carrillo, R.E., Aysal, T.C., Barner, K.E.: A generalized Cauchy distribution framework for problems requiring robust behavior. EURASIP J. Adv. Sig. Process. **2010**(1), 312989 (2010)
4. Foss, S., Korshunov, D., Zachary, S.: An Introduction to Heavy-Tailed and Subexponential Distributions, vol. 6. Springer, Cham (2011). https://doi.org/10.1007/978-1-4614-7101-1
5. Hou, B., et al.: Efficient maximal clique enumeration over graph data. Data Sci. Eng. **1**(4), 219–230 (2016)
6. Huang, Y., Pei, J., Xiong, H.: Mining co-location patterns with rare events from spatial data sets. GeoInformatica **10**(3), 239–260 (2006)
7. Huang, Y., Shekhar, S., Xiong, H.: Discovering colocation patterns from spatial data sets: a general approach. IEEE Trans. Knowl. Data Eng. **16**(12), 1472–1485 (2004)
8. Li, Y., Shao, Z., Yu, D., Liao, X., Jin, H.: Fast maximal clique enumeration for real-world graphs. In: Li, G., Yang, J., Gama, J., Natwichai, J., Tong, Y. (eds.) DASFAA 2019. LNCS, vol. 11446, pp. 641–658. Springer, Cham (2019). https://doi.org/10.1007/978-3-030-18576-3_38
9. Shekhar, S., Huang, Y.: Discovering spatial co-location patterns: a summary of results. In: Jensen, C.S., Schneider, M., Seeger, B., Tsotras, V.J. (eds.) SSTD 2001. LNCS, vol. 2121, pp. 236–256. Springer, Heidelberg (2001). https://doi.org/10.1007/3-540-47724-1_13

10. Tran, V., Wang, L., Chen, H., Xiao, Q.: MCHT: a maximal clique and hash table-based maximal prevalent co-location pattern mining algorithm. Expert Syst. Appl. **175**, 114830 (2021)
11. Tran, V., Wang, L., Zhang, J., Do, T.: Efficient mining of high utility co-location patterns based on a query strategy. In: Yang, X., et al. (eds.) ADMA 2023. LNCS, vol. 14176, pp. 401–416. Springer, Cham (2023). https://doi.org/10.1007/978-3-031-46661-8_27
12. Tran, V., Wang, L., Zhou, L.: A spatial co-location pattern mining framework insensitive to prevalence thresholds based on overlapping cliques. Distrib. Parallel Databases **41**(4), 511–548 (2023)
13. Yang, P., Wang, L., Wang, X., Zhou, L.: Efficient discovery of co-location patterns from massive spatial datasets with or without rare features. Knowl. Inf. Syst. **63**(6), 1365–1395 (2021)
14. Yoo, J.S., Shekhar, S.: A joinless approach for mining spatial colocation patterns. IEEE Trans. Knowl. Data Eng. **18**(10), 1323–1337 (2006)

Multi-model Data Warehouse for Multidimensional Analysis of Flavescence Dorée: Application to the Bordeaux Region

Sandro Bimonte[1(✉)], Fagniné Alassane Coulibaly[1], Frederic Fabre[2], Sylvie Malembic-Maher[3], and Stefano Rizzi[4]

[1] TSCF, INRAE, University Clermont Auvergne, Clermont-Ferrand, France
{sandro.bimonte,fagnine.coulibaly}@inrae.fr
[2] UMR SAVE, INRAE, Bordeaux Sciences Agro, Villenave d'Ornon, France
frederic.fabre@inrae.fr
[3] UMR BFP, INRAE, Université Bordeaux, Villenave d'Ornon, France
sylvie.malembic-maher@inrae.fr
[4] DISI, University of Bologna, Bologna, Italy
stefano.rizzi@unibo.it

Abstract. Flavescence Dorée is a highly contagious grapevine disease that poses a significant economic threat to European viticulture. Its current management relies on symptom monitoring, uprooting infected plants, insecticide treatments, and reservoir management. However, effective disease control is hindered by the disease's asymptomatic period and symptom similarities with Bois Noir, necessitating complex data-driven monitoring. Currently, the reliance on traditional spreadsheet software limits the scalability and spatio-temporal analysis of the massive datasets collected. To address these issues, this paper proposes a Business Intelligence architecture based on Spatial OLAP (OnLine Analytical Processing). By integrating Data Warehousing with Geographic Information Systems, the proposed system enables intuitive, multi-dimensional analysis of diverse data types——including graphs for dispersal modeling and JSON for scientific flexibility. Relying on a Multi-Model Data Warehouse with schema-on-read extensibility, this architecture provides an agile, "drag-and-drop" platform for extension services, farmers and researchers in epidemiology. This approach could facilitate rapid detection, predictive modeling, and optimized resource allocation, ultimately shifting pest control towards a more ecological and economically sustainable model.

Keywords: Flavescence dorée · Multi-model data · Spatial OLAP

1 Introduction

Flavescence Dorée (FD) is a grapevine disease caused by a wall-less bacterium (phytoplasma) that circulates in the plant's phloem. It is transmitted by the

© The Author(s), under exclusive license to Springer Nature Switzerland AG 2027
O. Gervasi et al. (Eds.): ICCSA 2026 Workshops, LNCS 16761, pp. 509–525, 2027.
https://doi.org/10.1007/978-3-032-30527-5_33

leafhopper *Scaphoideus titanus* or through grafting [13]. First identified in Armagnac in the 1950s, FD has since spread across France and much of Southern Europe. FD phytoplasma is classified as a quarantine organism in European Union. Symptoms include leaf rolling and discoloration (yellow or red), drying of clusters, and a failure of new shoots to lignify. However, visual diagnosis is difficult because the non-epidemic phytoplasma associated to Bois Noir (BN) disease induces identical symptoms; only molecular testing can distinguish them. Furthermore, symptoms in plants only appear at least one year after infection. This means plants infected in year n act as asymptomatic sources of spread throughout the spring of year $n+1$ before they are even detected. The strategy to control FD relies on four pillars: (i) monitoring symptomatic plants and insect vector populations, (ii) uprooting infected plants to eliminate the inoculum source; (iii) using insecticide treatments to reduce vector populations; (iv) managing uncultivated grapevines to remove potential disease reservoirs. The *Groupement de Défense contre les Organismes Nuisibles* (GDON) of Bordeaux monitors 74,000 hectares in the French department Gironde to control FD. They conduct leafhopper counts and symptom inspections from May to October of each year. If symptoms are detected in new areas, laboratory samples confirm if the cause is FD or BN. The monitoring protocol of GDON of Bordeaux is described in [4]. This targeted monitoring allows for a more ecological and economic approach by adjusting treatment levels based on real-time insect vector and disease pressure. Although GDON collect huge volume of data, data management and analysis is conducted by means of classical spreadsheet software (like Excel), which present several limitations in terms of scalability, management of complex data, and visual spatio-temporal analysis capabilities.

Data Warehouses (DWs) and OLAP systems are first-class citizens of Business Intelligence systems and have been used for several years in the agricultural context [6]. A DW acts as a centralized repository that consolidates large volumes of diverse, historical data from multiple sources. OLAP is the visual metaphor used to interact with this data, allowing non-technical users to perform multidimensional analysis through intuitive drag-and-drop operations. Together, they enable the creation of interactive dashboards by structuring data into cubes that can be easily aggregated, sliced, and diced. This combination transforms raw data into actionable business intelligence, facilitating rapid decision-making without requiring complex programming or data science expertise. The integration of OLAP and Geographic Information Systems (GIS) leads to the concept of Spatial OLAP (SOLAP), which enables spatial and OLAP queries as well as the visualization of query results by means of interactive maps [6].

Data variety characterizes agricultural pest monitoring applications since they need to analyze diverse formats of data like spatio-temporal files, satellite rasters, and connectivity graphs [18]. Data is obtained from field surveys, crowdsourcing, IoT, and remote sensing to capture complex ecological dynamics. To maintain data expressivity and avoid complex Extraction-Transformation-Loading processes, it is crucial to store information in its native model rather than forcing a relational transformation. In particular, graphs have been proved

to be effective for modeling epidemiological dispersal and social knowledge-sharing networks [14], while JSON offers the schemaless flexibility needed for hierarchical and evolving scientific data. Ultimately, centralizing these multi-model data in their original formats within a DW ensures better integrity and higher-quality analysis for plant disease surveillance. Moreover, DW extensibility is mandatory for agricultural epidemiology, meaning that new schema elements can be incrementally added without redesigning the entire system [5]. While traditional schema-on-write approaches are rigid and time-consuming, a *Multi-Model Data Warehouse* (MMDW) that relies on a schema-on-read approach allows for agile, near-instant OLAP queries on new data [11,12]. This agility is vital for epidemiological surveillance under the *One Health* framework, where scientific knowledge and pathogen life cycles evolve rapidly [18,27]. For example, recent findings on FD regarding landscape geometry, heavy-tailed dispersal kernels, and phytoplasma genotypes necessitate flexible systems to refine control strategies [3,16].

Finally, analytical tools must be inherently extensible to integrate these diverse, emerging data types and multidisciplinary insights without technical bottlenecks. To support diverse actors like epidemiologists, policy makers and farmers who may lack data science expertise, OLAP tools provide intuitive drag-and-drop interfaces for multidimensional analysis. However, standard OLAP lacks the cartographic visualization and spatial analysis methods essential for tracking disease outbreaks [6]. SOLAP bridges this gap by integrating GIS capabilities, allowing for sophisticated spatio-temporal queries and interactive mapping of massive datasets [18]. This integration is crucial for identifying infection hotspots, understanding dispersal dynamics, and optimizing resource allocation for pest control. Ultimately, combining OLAP and GIS creates a powerful analytical platform for epidemic detection, predictive modeling, and the overall protection of crops.

Motivated by the lack of proposals of DW and OLAP systems for agricultural epidemiology, we propose in this paper a Business Intelligence architecture that supports the SOLAP analysis of FD observations according to a multi-model and extensible approach. The paper is organized in the following way: Sect. 2 presents the related work in OLAP and plant health management, Sect. 3 outlines our solution dedicated to the analysis of FD observations, and Sect. 4 details the implementation of each layer of our architecture to the FD monitoring data of GDON of Bordeaux between 2017 and 2020. Some examples of SOLAP analyses offered to the decision-makers are shown in Sect. 5.

2 Related Work

The role of OLAP tools for managing plant pests and diseases is emphasized in [10,17,22,25]. Although these works are conceptual, they highlight urgent needs: for example, [22] proposed a web solution for Florida citrus diseases using algorithms to merge agricultural data for real-time mapping and OLAP reporting. Similarly, [10] identified the multidimensional and spatio-temporal nature

of pest data, leading them to evolve their database schema towards an OLAP approach to analyze pest pressure by farm, crop, and region. [25] also advocates for OLAP to enrich the analysis of environmental variables and crop growth. At the implementation level, [26] developed an OLAP system for olive crop Integrated Pest Management, integrating the Growing Season Index [15] to farming data in order to compare farm performance under similar climatic conditions; this system uses a relational storage model with a Mondrian server but lacks GIS integration.

In the context of cotton management, [2] established the *Pest-Pesticide-Metereology Data Warehouse* (PPM-DWH) in Pakistan. Using a constellation schema, it correlates major facts (production and pest quantity) with dimensions like weather and pesticide use. This work was expanded by [1] into the ADSS-OLAP system, a MOLAP (Multidimensional OLAP) implementation using Microsoft Analysis Services. Similarly, [19] utilized Microsoft Business Intelligence to provide multidimensional exploration of rice pest data in Vietnam for farmers and researchers.

Addressing Big Data challenges, [20] introduced an architecture to manage the "four Vs" (volume, variety, velocity, veracity). Critiquing the rigidity of star schemata [21], they adopted a flexible constellation schema featuring 3 fact tables and 19 dimensions. They argue that traditional relational approaches [23,24] and RDF triplestores suffer from performance issues during complex analytical queries. The polyglot architecture they propose utilizes Hive, MongoDB, and Cassandra for better scalability, though it relies on predefined HQL/SQL queries rather than on a dedicated OLAP server. While handling diverse data like JSON, this approach faces typical polyglot limitations regarding extensibility.

Overall, these works highlight the potential of OLAP systems in the agricultural field in general, and specifically for plant disease surveillance. The integration of these technologies in agriculture marks a significant advance in how agricultural data is analyzed and used for decision-making. OLAP systems allow for the exploration and analysis of large volumes of agricultural data across multiple dimensions, thereby facilitating decision-making. The studies described in this section demonstrate a diversity of applications in agriculture, ranging from the monitoring of plant diseases and pests to water resource optimization and crop management. These systems utilize data from various sources, notably those provided by weather stations and sensors, as well as data related to different crops or soil characteristics.

Table 1 lists some case studies regarding the use of OLAP tools for plant disease surveillance. To evaluate the case studies listed in Table 1, we have identified the following criteria: the type of pest/bio-aggressor, the type of data stored in the DW, the OLAP server used (either MOLAP or ROLAP, i.e., Relational OLAP), and the integration of a GIS.

The nature of the pest and the associated crop are important for assessing the specificity of each study as well as its socio-economic impact. In particular, [1,2, 19,22,26] respectively study pests affecting olive trees, rice, cotton, and citrus. These studies cover a fairly wide range of pests, from insects (mealybugs, flies,

Table 1. Existing works on OLAP and pest analysis

Paper	Pest	Data type	OLAP Server	GIS
[1]	Mealybug (cotton)	Relational	MOLAP	No
[2]	Cotton pests	Relational	MOLAP	No
[10]	Not specified	Relational	Pre-built queries	No
[17]	Not specified	Relational	Pre-built queries	No
[19]	Rice pests	Relational	MOLAP	No
[20]	Not specified	Rel./Document	Pre-built queries	No
[22]	Citrus insects and pests	Relational	Pre-built queries	No
[25]	Not specified	Relational	Pre-built queries	No
[26]	Olive fruit fly and moth	Relational	ROLAP	No

and moths) to pathogens (microorganisms associated with cankers and bacteria responsible for citrus "greening"). These works present many similarities with our case study, which focuses on the design of a SOLAP tool for the surveillance of FD, a phytoplasma disease of the grapevine spread by a leafhopper.

The second criterion chosen for evaluating these works is the type of data stored within the DW. This criterion is essential for assessing the proposed solution's ability to adapt to the evolution toward big data, thus, toward data that is voluminous and varied. The majority of the mentioned studies are limited to the storage of relational data, except for [20], which stores and analyzes JSON documents in addition to relational data. Thus, in most cases, the issue of agricultural data variety is addressed during the transformation phase of the Extraction-Transform-Load (ETL) process. [20] provides an innovative response to this problem by proposing a polyglot system; however, it is not accompanied by an OLAP server implementation capable of performing multidimensional analysis operations.

The type of OLAP server constitutes the third evaluation criterion, as it represents the central core of an OLAP system. MOLAP servers, such as those used in [1,2,19], generally offer better performance than ROLAP servers for multidimensional analysis operations. However, it is important to emphasize that ROLAP servers are better suited for integration with GIS [8], as well as for managing data variety [9] and extensibility [7,12]. Nevertheless, the consideration of variety and extensibility in these works remains limited, as they use either MOLAP servers or ROLAP servers with exclusively relational data storage.

Although not integrated into any of the works mentioned above, the inclusion of a GIS could significantly enrich OLAP analyses in the field of epidemiological surveillance, because it would allow for the integration of a spatial dimension into the analyses. This is crucial for understanding the dispersal of pests and the impact of numerous spatially structured factors on their development. This spatial dimension is particularly relevant for the implementation of targeted surveillance or control strategies and for the optimization of field interventions.

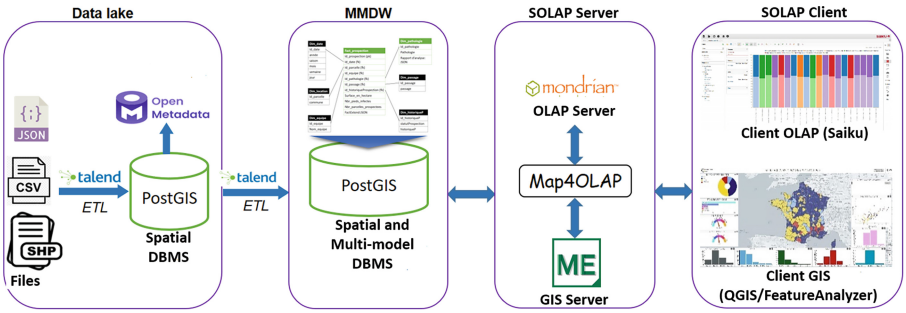

Fig. 1. Overall architecture.

In conclusion, it should be noted that despite the advantages offered by SOLAP tools, their adoption in agriculture faces several challenges. The complexity of agricultural data, the need to integrate GIS for spatial analysis, and the limitations of existing architectures are significant obstacles [6]. Furthermore, the design and development of these systems require close collaboration between agronomists, computer scientists, and decision-makers to ensure that the solutions developed effectively meet their needs.

3 Architecture

This section presents the architecture of our SOLAP solution dedicated to epidemiological surveillance. Inspired by previous works [7,8,12], this architecture is centered on an MMDW.

3.1 Overview

The architecture is an extension of the architecture proposed in [7,12]. It integrates the Map4OLAP tool [8], aimed at taking into account the geographic component of the spatial dimension, which is particularly important in the context of epidemiological surveillance. As illustrated in Fig. 1, it relies on four main layers: (i) Data Lake, (ii) MMDW, (iii) SOLAP server, and (iv) SOLAP client. It is a multi-model spatial data processing and analysis architecture, combining spatial data management technologies (PostGIS), ETL tools (Talend), as well as an OLAP front-end (Saiku) and GIS (QGIS or Feature Analyser) for decision-making analysis.

3.2 Data Lake Layer

In the Data Lake layer, raw data from different sources are stored in various formats, such as SHP files (Shapefile) for geospatial data, JSON files for semi-structured data, and CSV for structured data. This data is then integrated into

PostGIS, a spatial and multi-model database management system, via a simple ETL process performed with Talend Open Studio.

An important element of this layer is the management of metadata via the OpenMetadata tool. OpenMetadata is an open-source metadata management and cataloguing solution that centralizes descriptive information of the data in the data lake. It also stores the schemata of this data and a sample of the data itself. It thus allows for the cataloguing of data and searching via tags to facilitate identification and reuse. Data cataloguing facilitates the discovery of additional data that could be integrated into the MMDW layer to implement extensibility in case of evolving analytical needs for end-users.

Certain data present in the Data Lake layer are integrated into the next layer, MMDW, through a more complex ETL process that ensures not only data transfer but also its transformation and organization according to a multi-model star schema. This ETL process also ensures the high quality of data imported into the MMDW layer to guarantee the reliability of OLAP analyses; among other things, it includes managing missing and erroneous values, harmonizing municipality names, and replacing special characters.

3.3 MMDW Layer

The primary goal of the MMDW layer is to prepare data for decision-making exploitation through the SOLAP client layer. Here, data is stored in PostGIS and organized according to a multi-model star schema designed to meet specific analytical needs. This star schema will be described in more detail in Subsect. 4.1; it combines relational data and JSON documents, making it more flexible and enabling extensibility [9].

The MMDW layer communicates directly with the SOLAP server layer using *XML for Analysis* (XMLA), a computing standard designed to allow access to data in analytical systems, particularly in OLAP systems. This standard relies on other pre-existing standardized web technologies such as XML, SOAP, and HTTP.

The MMDW layer executes queries coming from the OLAP Server. These multi-model OLAP queries are implemented through a mix of languages like SQL for relational data, Cypher for graphs, and the appropriate language for querying JSON documents (see Sect. 4.3). After the execution of these queries by PostGIS, the MMDW layer returns the corresponding results to the OLAP server, which writes them into a well-structured file in the form of dynamic cross-tabulations.

3.4 SOLAP Server Layer

The SOLAP Server layer consists of an OLAP server (Mondrian), the Map4OLAP tool, and a GIS server (M.App Enterprise). These components ensure the exploitation of data from the MMDW layer for spatial and multi-dimensional analyses.

- Mondrian allows the exploration and analysis of multidimensional data via OLAP cubes; it is responsible for translating MDX (Multidimensional Expressions) queries from the OLAP client into queries adapted to the MMDW layer where the data is stored. Mondrian also reads the XMLA file resulting from the OLAP queries and sends it to the OLAP client.
- Map4OLAP is a Java program that links the OLAP server (Mondrian) and the GIS server (M.App Enterprise). It retrieves the OLAP server results written in XMLA and transforms them into GeoJSON files compatible with the GIS server. This process also includes decision rules on how the GIS client should visualize interactive maps. For example, it allows defining specific graphical representations (such as pie charts or histograms) for polygons (such as municipalities), while specifying how to handle missing or null values.
- M.App Enterprise is used to manage cartographic aspects. It is responsible for making the cartographic data (created by *Map4OLAP*) available to the GIS client. Furthermore, it implements features associated with interactive maps.

3.5 SOLAP Client Layer

The SOLAP Client layer consists of two main elements:

- The OLAP Client we adopt is Saiku. It works in a traditional manner, allowing end-users to interact with OLAP cubes and perform multidimensional analyses via an intuitive user interface. It translates dynamic cross-tabulations into MDX queries sent to the OLAP server.
- The GIS Client is used to visualize the maps created by Map4OLAP. We currently rely on QGIS, but we plan to replace it with Feature Analyser to implement all the functionalities of Map4OLAP.

The integration of OLAP and GIS clients in this layer ensures that the analysis of multidimensional data and its cartographic visualization are carried out in an efficient and fluid manner.

4 Implementation

This section describes in more detail the implementation of the MMDW layer (Sect. 4.1) and of the OLAP server component of the SOLAP layer (Sect. 4.2). The extension of the DW with additional complex data is described in Sect. 4.3. Data used are collected by GDON from 2017 and 2020.

4.1 MMDW Layer

Usually, a DW schema is composed by the fact table, which contains measures, and a set of dimension tables that represent the dimensions levels. The logical schema of our MMDW is shown in Fig. 2.

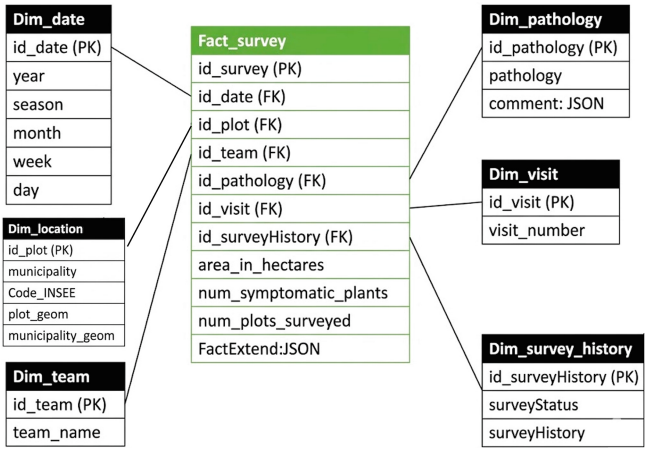

Fig. 2. Logical schema of the MMDW for FD Monitoring.

It hinges on a fact table, Fact_survey, defined at the finest possible granularity, i.e., at the plot and day level (differently from the dashboards defined by the GDON, which show data by year and across the intervention zone of the GDON Bordeaux in Gironde). Our approach allows for analyzing data with full detail for each survey and explains aggregated data. This fact table includes a primary key, the set of foreign keys from the dimensions, the measures, and a JSON-type column to ensure extensibility. Its columns are:

- id_survey is the primary key.
- id_date is a foreign key referencing the Dim_date dimension table.
- id_plot is the identifier of the plot where the survey took place. It is assigned by the GDON to each plot and is a foreign key referencing the Dim_location dimension table.
- id_team identifies the team that performed the survey (foreign key referencing Dim_team).
- id_pathology identifies the disease detected during the survey and subsequent analyses (foreign key referencing Dim_pathology).
- id_visit identifies the visit/pass (foreign key referencing Dim_visit).
- id_survey_history, area_in_hectares, num_symptomatic_plants, and num_plots_surveyed are measures; their explanation will be given in Sect. 4.2.
- FactExtend is a JSON field that facilitates the integration of additional information specific to each survey.

As to the dimension tables:

- The time dimension table, Dim_date, provides different aggregations of the date when the survey was conducted.

- The spatial dimension table, Dim_location, provides geographical information about the plot. Besides the INSEE code and name of the municipality, it includes a spatial representation of the geometry of the plot and of the municipality.
- The Dim_team dimension table provides details about the GDON team performing the survey.
- The Dim_pathology dimension table represents information related to the detected pathologies.
- The Dim_visit dimension table provides information regarding the visits (passes) conducted during the survey (visit_number is a Boolean value that represents if it is the first or the second visit).
- The Dim_surveyHistory dimension table represents the survey history, specifying whether a plot has been surveyed or not. If the plot has already been surveyed, it specifies whether it is a first survey or not; it also indicates if the plot has been surveyed in both the current and the previous year.

4.2 OLAP Server

The OLAP server uses an XML file to generate queries to be sent to the MMDW layer. This file defines multidimensional elements such as measures, dimensions, and hierarchical levels; it also specifies the mappings between these multidimensional elements and the data stored in the MMDW layer. For example, it indicates to the OLAP server that Fact_survey is the fact table and that Dim_location contains data related to the location dimension. The OLAP server also specifies the measures and their aggregation functions. In our implementation we have defined the following measures:

- Number of symptomatic plants (corresponding to num_symptomatic_plants in the fact table) is an additive measure (i.e., it can be aggregated using the sum on all the dimensions) referring to the number of symptomatic plants observed by agents during survey visits.
- Number of surveyed plots (num_plots_surveyed in the fact table) represents the number of plots surveyed. It is calculated using the `distinct count` operator on the result of concatenating the plot id and the survey year. This ensures that, when a plot is surveyed in two different years, it is counted twice, whereas if it is surveyed twice in the same year (in the case of a second pass), it is counted only once.
- Area in hectares (area_in_hectares in the fact table) is a semi-additive measure (i.e., it cannot be aggregated using the sum along all the dimensions) because, although the area surveyed at a municipality level is obtained by adding the areas of the plots in that municipality, and the area surveyed during a year corresponds to the sum of the areas of plots surveyed that same year, this does not apply to second passes. Indeed, if a plot is surveyed twice in the same year, its area should not be counted twice. Thus, this measure is additive across spatio-temporal dimensions but not across the visit dimension.

- Number of symptomatic plants per hectare is derived by dividing the number of symptomatic plants by the surveyed area in hectares to measure the density of symptomatic plants.
- Multiplication rate of symptomatic plants measures the year-over-year change in the number of symptomatic plants.

All these measures are implemented using the `Measure` and `Calculated Member` statements of Mondrian.

4.3 Extensibility

To give our MMDW the extensibility required by the application, we adopted the *xCube* approach, proposed in [7] to provide on-demand, supply-driven extensibility of multidimensional cubes. *xCube* allows users to select a specific element within the schema of the DW and expand it using supplementary data, often sourced from a data lake. The system then extends the multidimensional schema by incorporating the functional dependencies found within this new data, providing users with an updated schema ready for immediate OLAP analysis. *xCube* follows these steps:

1. Selection of the target element: the user identifies the specific component within the schema of the DW to be expanded——either the fact table (to add new measures or dimensions) or a specific level (to introduce new hierarchies). The columns used for extension must be defined as a JSON type.
2. Data sourcing: the user selects supplementary data from the data lake, which may include relational tables, document collections, or graphs. These datasets are then automatically imported into the MMDW layer.
3. Schema extension: the system extends the schema of the DW by identifying functional dependencies between the selected schema element and the newly imported data.

The additional data we used for the extension of our MMDW are taken from the Casier Viticole Informatisé (CVI), a digital tool established in 1998 by the viticulture services of the French directorate general of customs. It lists all vineyard cadastral plots in France along with their characteristics, such as owner, area, grape variety, planting year, planting density, and spacing, among others. We used an anonymized version of the 2016 CVI for the Bordeaux territory. Figure 3 shows an excerpt of the JSON CVI data, where the French terms "refCadastrale", "cepage", "typeCepage" and "densite" represent the plot identifier, the grape variety, the type of variety, and the number of plants, respectively. The protocol for attributing CVI variables to fields sampled by GDON is described in [4]. This data is stored in the Data Lake layer, and it was not integrated at the time the MMDW of Fig. 2 was created.

Following the *xCube* approach, it was decided to extend the MMDW with a new measure quantifying the density of plants, which corresponds to the densite attributes in the CVI JSON data. Therefore, the MMDW was extended by designers with a new measure number_of_plants, fed via an SQL query in the

```
{
    "refCadastrale": "refCadastrale1",
    "cepage": "semillon B",
    "typeCepage": "cepage blanc",
    "densite": 5000
},
{
    "refCadastrale": "refCadastrale2",
    "cepage": "CABERNET FRANC N",
    "typeCepage": "cepage noir",
    "densite": 4000
},
```

Fig. 3. Additional CVI data.

XML Mondrian file as shown in Fig. 4. It is important to note that, since this measure is computed from the JSON document stored in the FactExtend column of the fact table, it is defined as a query over a JSON document. This is technically possible since the PostGIS extension of the PostgreSQL DBMS used for the implementation of the MMDW layer supports multi-model data storage and querying.

```
<Measure name="Number_of_plants" column="nb_plants" aggregator="avg">
  <SQL>
    SELECT
      COALESCE((Fact_survey.FactExtend->>'densite')::INTEGER, 4000) AS nb_plants
    FROM Fact_survey
  </SQL>
</Measure>
```

Fig. 4. Fact extended with a new measure.

5 SOLAP Analysis

In this section, we show the results of some analyses that could be conducted by decision-makers for the monitoring of FD. Due to confidentiality requirements, the data presented here has been modified and does not represent real values.

Figure 5 shows the number of symptomatic plants identified per plot and per day. Note that plot "0002" was surveyed on 7th September 2018, 3rd September 2019, and 7th August 2020, with 14, 8, and 70 symptomatic plants identified, respectively. Thus, Saiku allows for a precise analysis of a plot's surveying history. Figure 6 shows the distribution of the number of symptomatic plants per plot for three years (only five plots are shown for better readability), plot "0005" recording the highest number of symptomatic plants. Thus, these pie charts help identify the most affected plots.

Figure 7 shows a choropleth map of the vineyard plots in a specific municipality. In this map, the color of the plots varies according to the total number of symptomatic plants observed between 2017 and 2020. The data presented in this

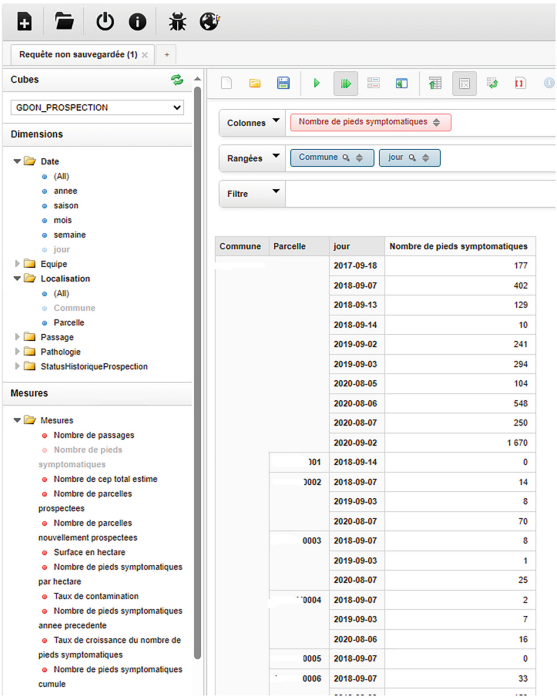

Fig. 5. Number of symptomatic plants per plot and per day.

map were obtained by aggregating the data illustrated in Fig. 5 across all years. This corresponds to a *Roll-Up* operation applied to the Date dimension. The value categories are defined using the quantiles method, so as to distribute the number of plots equally across each of the 10 categories. This approach prevents the majority of plots from falling into the first class, given that they generally have a very low number of symptomatic plants.

Thanks to this representation, it is easy to identify the plots requiring special attention, particularly those belonging to the bottom classes (in red), characterized by more than 75 symptomatic plants. Furthermore, unlike visualization techniques such as pie charts or evolution curves, which lose readability as the number of plots increases, the choropleth map remains legible. Finally, this map allows for the identification of potential contamination hotspots (clusters of geographically close plots with many symptomatic plants). For example, it appears that several plots located in the northeast of the municipality (top and right part of Fig. 7) stand out due to a high presence of symptomatic plants.

Finally, Fig. 8 shows a map of the vineyard plots in the same municipality, where each plot is associated with a bar chart consisting of four bars, each representing the number of symptomatic plants observed between 2017 and 2020. The data presented in this map were obtained by aggregating the data in Fig. 5 by year rather than by day. This corresponds to a *Roll-Up* operation applied

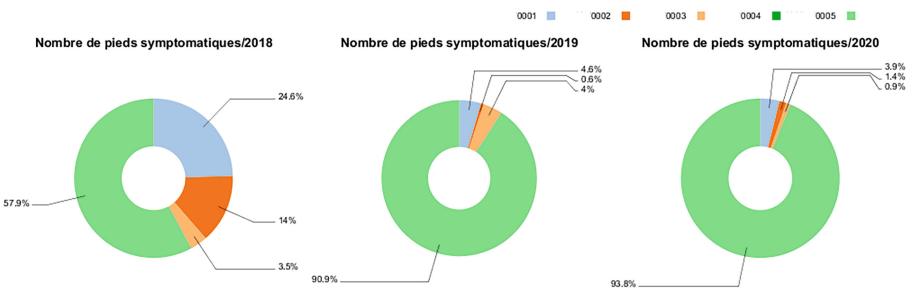

Fig. 6. Evolution of the distribution of symptomatic plants per plot.

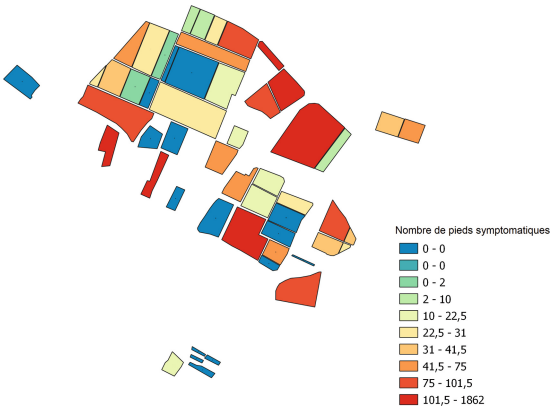

Fig. 7. Choropleth map of the total number of symptomatic plants (observed between 2017 and 2020) per plot in a specific municipality. (Color figure online)

to the Date dimension. This figure complements Fig. 7 by showing, for example, that the plots in the northeast of the municipality identified previously record a relatively low number of symptomatic plants compared to plot "0005" to the west, where more than 1,700 symptomatic plants were identified in 2020. Indeed, the northeast plots have symptomatic vine counts closer to 100 than to 1,800.

6 Conclusion

In this work, we described the design and implementation of a MMDW dedicated to the monitoring of FD in the Bordeaux wine region. The proposed SOLAP architecture integrates the key components necessary for the analysis of spatial and multidimensional data. In particular, the use of the Map4OLAP tool enriched the DW functionalities by providing cartographic visualization capabilities and interaction with spatial data. The results obtained show that the designed MMDW could meet the GDON's needs for managing and analyzing survey data. It facilitates the production of detailed reports, the spatio-temporal

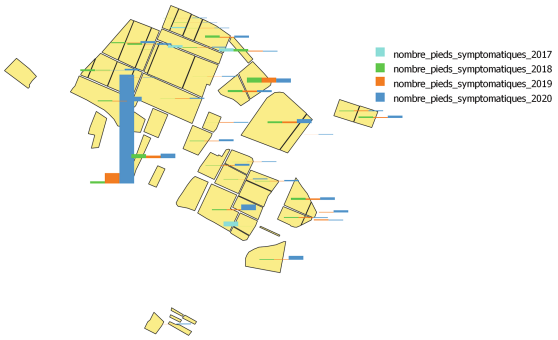

Fig. 8. Evolution map of the number of symptomatic plants (observed between 2017 and 2020) per plot in a specific municipality.

tracking of FD, and can adapt to the evolving analytical needs of users. Furthermore, the established architecture provides a foundation for integrating new data sources and extending the tool's analytical capabilities, thus reinforcing its relevance in the context of epidemiological surveillance.

In conclusion, beyond offering a dashboard of FD distribution, the MMDW has the potential to drive the development of predictive risk maps. By cross-referencing domain expertise with model outputs, operational stakeholders could use these maps to significantly improve FD monitoring strategies. For instance, risk mapping could leverage graph-based methods to explicitly model infectious "contacts" between plots, offering a robust framework for simulating epidemic spread over real-world vineyard landscapes. The probability of FD propagation would be dynamically updated year-over-year at the local level through a model incorporating: (i) the structural graph of the vineyards (derived from CVI data); (ii) empirical knowledge of FD dispersal (e.g., [3]; (iii) historical data from prior field surveys; and (iv) key risk factors (e.g., cultivar type, landscape composition and configuration, proximity to abandoned vines; [4]).

Acknowledgements. This work is partially funded by the BEYOND ANR-20-PCPA-0002 project and the 101226371-HORIZON MSCA DN-JD grant "IoRT Data Management and Analysis for Sustainable Agriculture (GreenFieldData)". We sincerely thank Sophie Bentejac and Charlotte Labit from the GDON of Bordeaux who sampled and provided data and for their help for formatting data.

References

1. Abdullah, A.: Analysis of mealybug incidence on the cotton crop using ADSS-OLAP (Online Analytical Processing) tool. Comput. Electron. Agric. **69**(1), 59–72 (2009)
2. Abdullah, A., Brobst, S., Umer, M., Khan, M.F.: The case for an agri data warehouse: enabling analytical exploration of integrated agricultural data. In: Proceedings of Databases and Applications, pp. 139–144 (2004)

3. Adrakey, H.K., Gibson, G.J., Eveillard, S., Malembic-Maher, S., Fabre, F.: Bayesian inference for spatio-temporal stochastic transmission of plant disease in the presence of roguing: a case study to characterise the dispersal of flavescence dorée. PLoS Comput. Biol. **19**(9), e1011399 (2023)
4. Adrakey, H.K., et al.: Field and landscape risk factors impacting flavescence dorée infection: insights from spatial Bayesian modeling in the Bordeaux vineyards. Phytopathology® **112**(8), 1686–1697 (2022)
5. Bazza, H., Bimonte, S., Rizzi, S., Laneurit, J., Badir, H.: A UML profile for variety and variability awareness in multidimensional design: an application to agricultural robots. In: Proceedings of DOLAP, pp. 1–10 (2022)
6. Bimonte, S.: Current approaches, challenges, and perspectives on spatial OLAP for agri-environmental analysis. Int. J. Agric. Environ. Inf. Syst. **7**(4), 32–49 (2016)
7. Bimonte, S., Coulibaly, F.A., Rizzi, S.: An approach to on-demand extension of multidimensional cubes in multi-model settings: application to IoT-based agro-ecology. Data Knowl. Eng. **150**, 102267 (2024)
8. Bimonte, S., Edoh-Alove, E., Coulibaly, F.A.: Map4OLAP: a web-based tool for interactive map visualization of OLAP queries. In: Proceedings of Big Data, pp. 3747–3750 (2021)
9. Bimonte, S., Gallinucci, E., Marcel, P., Rizzi, S.: Data variety, come as you are in multi-model data warehouses. Inf. Syst. **104**, 101734 (2022)
10. Boll, R., Bout, A., Doise, S., Bernardet, X., Poncet, C.: "Data_market" as a realistic tool for decision-making in the integrated pest management challenge. In: Proceedings of IHC2010, pp. 163–170 (2010)
11. Cohen, J., Dolan, B., Dunlap, M., Hellerstein, J.M., Welton, C.: Mad skills: new analysis practices for big data. Proc. VLDB Endow. **2**(2), 1481–1492 (2009)
12. Coulibaly, F.A., Sandro, B., Rizzi, S.: Towards a multi-model approach to support user-driven extensibility in data warehouses: agro-ecology case study. In: Proceedings of DataPlat, vol. 3379, pp. 1–5 (2023)
13. (EFSA), E.F.S.A., Tramontini, S., Delbianco, A., Vos, S.: Pest survey card on flavescence dorée phytoplasma and its vector scaphoideus titanus. EFSA Support. Public. **17**(8), 1909E (2020)
14. Gent, D.H., Mahaffee, W.F., McRoberts, N., Pfender, W.F.: The use and role of predictive systems in disease management. Annu. Rev. Phytopathol. **51**, 267–289 (2013)
15. Jolly, W.M., Nemani, R., Running, S.W.: A generalized, bioclimatic index to predict foliar phenology in response to climate. Glob. Change Biol. **11**(4), 619–632 (2005)
16. Malembic-Maher, S., et al.: When a palearctic bacterium meets a nearctic insect vector: genetic and ecological insights into the emergence of the grapevine flavescence dorée epidemics in Europe. PLoS Pathog. **16**(3), e1007967 (2020)
17. Mir, S., et al.: Decision support systems in a global agricultural perspective - a comprehensive review. Int. J. Agric. Sci. **7**(1), 403–415 (2015)
18. Morris, C.E., Géniaux, G., Nédellec, C., Sauvion, N., Soubeyrand, S.: One health concepts and challenges for surveillance, forecasting, and mitigation of plant disease beyond the traditional scope of crop production. Plant. Pathol. **71**(1), 86–97 (2022)
19. Nghia, P.Q.: Building OLAP application to exploit database of rice pests. Int. J. Emerg. Technol. Adv. Eng. **3**(11), 130–137 (2013)
20. Ngo, V.M., Le-Khac, N.A., Kechadi, M.T.: Designing and implementing data warehouse for agricultural big data. In: Proceedings of Big Data, pp. 1–17 (2019)
21. Nilakanta, S., Scheibe, K., Rai, A.: Dimensional issues in agricultural data warehouse designs. Comput. Electron. Agric. **60**(2), 263–278 (2008)

22. Rogers, S.: Real-time internet-PDA-based survey and modeling systems for agricultural insects and diseases: integrated fruit fly, citrus canker and greening surveys. In: Proceedings of Florida State Horticultural Society, vol. 119, pp. 107–119 (2006)
23. Schuetz, C.G., Schausberger, S., Schrefl, M.: Building an active semantic data warehouse for precision dairy farming. J. Organ. Comput. Electron. Commer. **28**(2), 122–141 (2018)
24. Schulze, C., Spilke, J., Lehner, W.: Data modeling for precision dairy farming within the competitive field of operational and analytical tasks. Comput. Electron. Agric. **59**(1–2), 39–55 (2007)
25. Wang, C., Wang, L., Dong, P., Qiao, X.: Research of decision support system (DSS) for greenhouse based on data mining. In: Proceedings of CCTA, pp. 1071–1076 (2008)
26. Zaza, C., Bimonte, S., Faccilongo, N., La Sala, P., Contò, F., Gallo, C.: A new decision-support system for the historical analysis of integrated pest management activities on olive crops based on climatic data. Comput. Electron. Agric. **148**, 237–249 (2018)
27. Zinsstag, J., Schelling, E., Crump, L., Whittaker, M., Tanner, M., Stephen, C.: One Health: The Theory and Practice of Integrated Health Approaches. CABI (2020)

Spatial Assessment of PM10 Concentrations and Population Exposure in the Emilia-Romagna Region (Italy): A Geostatistical Approach

Beatrice Manganelli[1], Rachele Vanessa Gatto[2(✉)], Simone Corrado[2], and Benedetto Manganelli[2]

[1] Department of Civil, Chemical, Environmental and Materials Engineering (DICAM), University of Bologna, Via Terracini 28, 40121 Bologna, Italy
[2] Department of Engineering (DIING), University of Basilicata, Viale Dell'Ateneo Lucano, Potenza, Italy
{rachelevanessa.gatto,simone.corrado, benedetto.manganelli}@unibas.it

Abstract. Airborne particulate matter remains one of the most critical environmental pollutants affecting urban and regional air quality, with significant implications for public health and territorial sustainability. This study investigates the spatial distribution of annual mean PM10 concentrations and associated population exposure patterns across the provinces of Parma, Reggio Emilia, Modena, and Bologna, located in a representative portion of the Emilia-Romagna region (Northern Italy), within the broader environmental context of the Po Valley, one of Europe's most critical air-pollution hotspots. The analysis is based on official monitoring data from the regional air-quality network and applies a geostatistical interpolation approach to reconstruct the spatial continuity of PM10 concentrations beyond fixed observation points. An experimental semivariogram and ordinary kriging was used to generate a continuous concentration surface at 1 km spatial resolution, together with the corresponding uncertainty map. The interpolated PM10 surface was then spatially integrated with high-resolution ISTAT population data in order to estimate the resident population exposed to different concentration classes. The findings highlight a well-defined spatial structure, with elevated PM10 concentrations in the central lowland urban system and lower levels in mountainous areas, reflecting significant variability among the main urban centers within the study area. The study highlights the relevance of geographically informed exposure assessment as a support tool for air-quality governance, spatial planning, and targeted environmental policies.

Keywords: environmental pollutants · exposure assessment · spatial planning

© The Author(s), under exclusive license to Springer Nature Switzerland AG 2027
O. Gervasi et al. (Eds.): ICCSA 2026 Workshops, LNCS 16761, pp. 526–541, 2027.
https://doi.org/10.1007/978-3-032-30527-5_34

1 Introduction

Airborne particulate matter (PM) represents one of the most critical components of air pollution and remains a major concern for both environmental monitoring and public health protection [1]. The increasing attention to PM dynamics is strongly related to the well-established link between pollutant exposure and adverse health effects, particularly respiratory and cardiovascular diseases [2]. PM is widely acknowledged as a key risk factor, especially in densely populated and highly urbanized areas.

In recent years, growing emphasis has been placed on the spatial dimension of exposure, highlighting two key implications. First, there is a need to complement traditional emission-reduction policies with place-based strategies aimed at limiting pollutant accumulation and reducing exposure in vulnerable urban contexts. Second, it becomes essential to identify the role of spatial characteristics, such as settlement morphology, industrial location patterns, and environmental assets, in influencing the distribution and concentration of PM [3].

Within this framework, green infrastructure (GI) has emerged as a relevant element in urban air-quality regulation. In addition to its ecological and climatic functions, GI contributes to pollutant mitigation through both deposition and aerodynamic processes [4]. Vegetation can enhance the capture of airborne particles due to its high surface-to-volume ratio, while deposition efficiency varies according to species-specific characteristics such as leaf morphology, size, porosity, and canopy structure. Moreover, GI can influence local airflow dynamics, thereby affecting the dispersion and redistribution of atmospheric pollutants [5].

These dynamics are particularly significant in urbanized and infrastructurally complex territories, where high population density [2], intense traffic flows, industrial activities, and land-use transformations generate persistent air-quality pressures. At the global scale, urbanization is expected to continue rapidly, with approximately 68% of the world's population projected to live in urban areas by 2050 (https://www.un.org/uk/desa/68-world-population-projected-live-urban-areas-2050-says-un). Simultaneously, the expansion of urbanized surfaces and the reduction of green spaces are exacerbating environmental stressors, including urban heat island effects and declining air quality [2].

Current international estimates indicate that a substantial share of the global urban population is exposed to air pollution levels exceeding the health-based thresholds recommended by the World Health Organization (WHO), including the annual PM10 guideline value of 15 $\mu g/m^3$ (https://www.un.org/sustainabledevelopment/blog/2016/05/).

Although particulate matter may originate from natural processes such as soil resuspension, marine aerosols, and volcanic emissions, anthropogenic sources dominate in urban and peri-urban contexts. These include vehicular traffic, industrial activities, and biomass combustion [6].

In Italy, according to the National Emissions Inventory developed by ISPRA (Italian Institute for Environmental Protection and Research) (http://www.sinanet.isprambiente.it/it/sia-ispra/serie-storiche-emissioni), the residential sector accounted for approximately 40% of primary PM10 emissions in 2011, followed by transport activities, which contributed about 24%, with more than two-thirds attributable to road traffic. Industrial

processes represented approximately 19% of emissions, while farming accounted for around 11%. Notably, nearly 90% of PM10 emissions from residential heating were associated with biomass combustion.

Within this broader context, the Po Valley in Northern Italy is recognized as one of the most critical air pollution hotspots in Europe (EEA, 2020). Its geomorphological configuration, characterized by a closed basin, limited atmospheric ventilation, and frequent stagnation episodes, favors the accumulation and persistence of particulate matter. Numerous studies have highlighted the significant implications of these conditions for public health and life expectancy [2, 5–11].

The Emilia-Romagna region, located in the central-eastern sector of the Po Basin, constitutes a particularly relevant case study within this context. The region is characterized by high population density, extensive urbanization, major industrial and logistics systems, and widespread agricultural and manufacturing activities, all of which contribute to a strong anthropogenic pressure on air quality [7].

In addition, approximately 24% of PM10 emissions in Emilia-Romagna have been attributed to road transport (ARPAE, 2022), confirming the relevance of mobility-related emissions within the regional emission structure.

For these reasons, this study focuses on the Emilia-Romagna region as representative and policy-relevant territorial context for investigating the spatial distribution of PM10 concentrations and associated population exposure patterns. In particular, the analysis addresses the regional-scale annual PM10 concentrations in relation to the settlement structure and spatial distribution of the resident population, with the aim of supporting Decision Makers with geographically informed exposure assessment[12].

The analysis focuses on the provinces of Parma, Reggio Emilia, Modena, and Bologna, which represent the central urban-industrial corridor of the Emilia plain. The year 2021 was selected because it represents the most recent year with complete validated PM10 and ISTAT population datasets available at comparable spatial resolution.

A detailed reconstruction of PM10 spatial distribution, combined with a fine-scale estimation of the exposed population and contextualized through emission-source contributions, provides a robust basis for orienting targeted mitigation policies toward areas where local air-quality improvements may generate the greatest public-health benefits. In this regard, the results show a clear concentration of pollutants within the lowland basin downstream of the Apennine system, confirming the role of geomorphological and atmospheric conditions in shaping pollutant accumulation. However, the analysis also reveals a non-linear relationship between population concentration and exposure intensity. In particular, although Bologna represents the most populated urban centre in the study area, it does not fall within the highest PM10 exposure class, unlike Modena and Reggio Emilia. This finding suggests that local exposure patterns are not determined solely by demographic concentration, but also by the interaction of settlement structure, mobility-related emissions, urban form, and territorial context. Such evidence supports the need for geographically differentiated and place-based policies aimed at improving air quality through locally adapted mitigation strategies. In this sense, Bologna constitutes a particularly relevant case, as it has recently promoted policy actions aligned with the Sustainable Development Goals and progressively integrated these objectives into its territorial governance and planning instruments.

2 Study Area, Data and Methodology

2.1 Case Study

The Po Valley is widely recognized as a major air-pollution hotspot in Europe (Fig. 1) and sustained exposure to ambient pollutants in this region has been linked to adverse public-health outcomes, including reduced life expectancy [13].

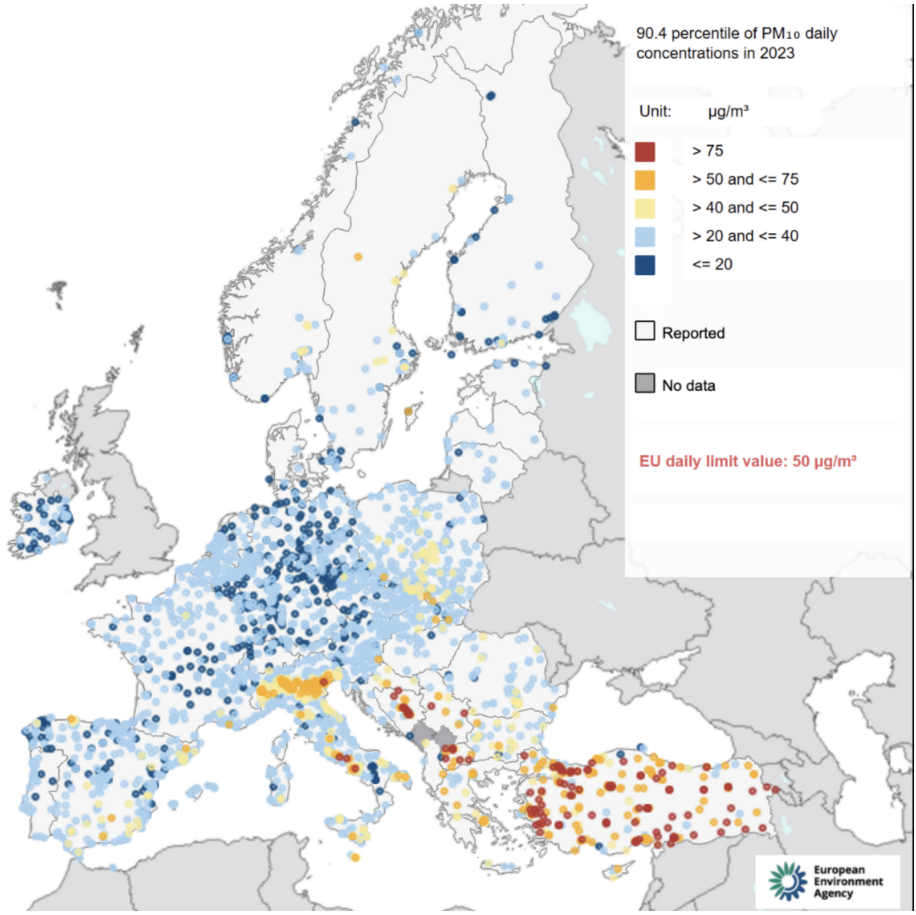

Fig. 1. The map shows the 90.4th percentile of daily PM_{10} concentrations recorded in 2023 at monitoring stations across Europe, expressed in $\mu g/m^3$. Source: European Environment Agency (EEA).

This study concentrates on the Emilia-Romagna region in Italy, which constitutes a salient case within the Po Basin, given the joint influence of relatively high population density, substantial industrial activity, pronounced urban concentration, and intensive agricultural and manufacturing production (eea.europa.eusnpambiente.it, 08/01/2026).

These pressures are further shaped by the area's geomorphological context; in particular, the enclosed basin topography and relatively weak atmospheric ventilation can facilitate pollutant build-up and prolong their residence in the local environment.

Recent monitoring data underscore both progress and ongoing issues in the region's cities concerning population exposed to PM10 (Fig. 2). PM10 annual average concentrations have generally declined or stabilized in the last 15–20 years, now usually staying below the EU annual limit of 40 $\mu g/m^3$ [10]. The 2022 annual mean PM10 was about 29–30 $\mu g/m^3$ at urban background sites in Parma and Reggio Emilia, 30–36 $\mu g/m^3$ in Modena, and around 23–27 $\mu g/m^3$ in Bologna, all within legal limits and indicative of a long-term downward trend compared to the early 2000s (when many sites averaged well above 40 $\mu g/m^3$). These improvements reflect better vehicle emissions standards, shifts from heavy fuel use, and regional policies.

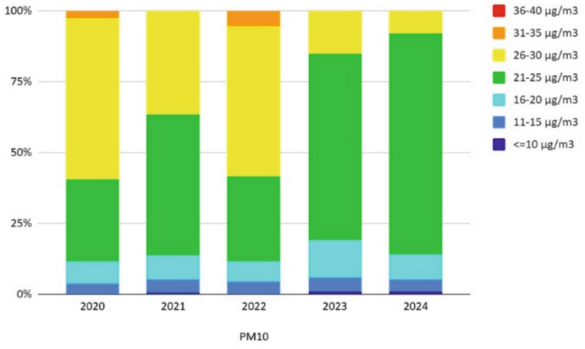

Fig. 2. Regional population exposed to annual mean concentrations of PM10. Source: ARPAE

However, daily PM10 pollution peaks continue to be problematic. Under EU standards, the 24-h average PM10 concentration should not exceed 50 $\mu g/m^3$ on more than 35 days in a year. This daily limit was frequently violated in the 2000s across the Po Valley, and while the frequency of exceedances has declined, it remains a critical issue in the cited cities. In 2022, 12 out of 43 monitoring stations in Emilia-Romagna recorded more than 35 high-PM10 days [13]. Urban centers in the central Po Valley zone saw the highest exceedances: for instance, *Modena*'s Giardini station endured 75 exceedance days (the worst in the region), *Reggio Emilia*'s Timavo station had 64**,** and *Parma*'s Montebello station 46 days beyond the 50 $\mu g/m^3$ threshold.

By contrast, in 2022, none of Bologna's PM monitoring stations surpassed the 35-day limit. Legislative standards currently lag behind health guidelines: the World Health Organization's latest recommendations (PM10 24-h guideline of 45 $\mu g/m^3$, and annual 15 $\mu g/m^3$) are far more stringent than the EU's limits (eea.europa.eu, 08/01/2026).

If these tighter limits are adopted (as proposed for 2030 in the new EU air quality directive), most Po Valley cities would be out of compliance, indicating the need for further pollution reduction acts.

To manage exceedances, regional authorities adopt short-term mitigation measures (traffic restrictions, biomass burning limits) during forecasted high-pollution episodes,

especially under the Pan-European air quality plan for the Po Basin (https://www.arpae.it/it/notizie/prosegue-lallerta-smog-in-4-province-della-regione). This includes coordinated efforts among Po Valley regions (acknowledging that "air has no boundaries" and a basin-wide approach is needed), covering sectors from transport and residential heating to agriculture (e.g. ammonia emission reductions to curb secondary PM). The regional Air Quality Plan (PAIR 2030) under development reflects these priorities, aiming to ensure sustained compliance and prepare for stricter future standards.

2.2 Data

PM10

This analysis uses an official air-quality monitoring dataset that reports PM10 levels across the Emilia-Romagna region, and it focuses on the provinces of Parma, Reggio Emilia, Modena, and Bologna (Fig. 3).

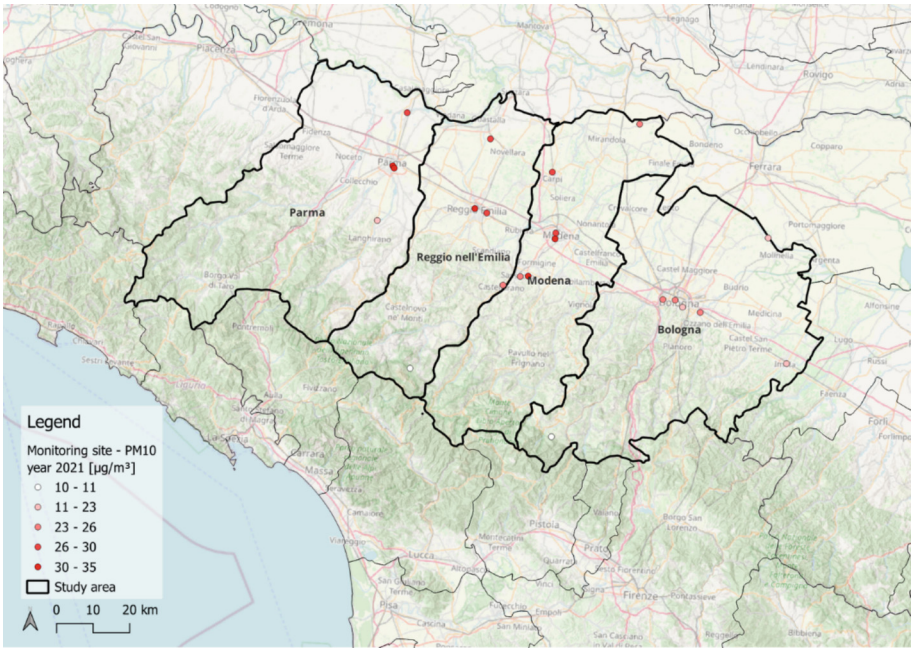

Fig. 3. Map of the study area: the provinces of Parma, Reggio Emilia, Modena and Bologna (Emilia-Romagna, Northern Italy). Black boundaries delineate the study area, while colored points represent PM_{10} monitoring stations. Symbols are classified according to annual mean PM10 concentrations recorded in 2021 ($\mu g/m^3$).

The data came from the regional air-quality monitoring network run by ARPAE (the Regional Agency for Prevention, Environment and Energy of Emilia-Romagna) and were provided in a table (Fig. 4).

The dataset is made up of on-site observations gathered from fixed monitoring stations, and the measurements are generally reliable and have been formally validated by

station_eu_code	id_regione	id_provinc	id_comune	station_co	Regione	Provincia	Comune	nome_staz	tipo_zona	tipo_stazio	TIPO	Lon	Lat	yy	n	sup50	sup45	media_yy
IT1910A	8	34	8034010	803409	Emilia-Rom	Parma	Colorno	SARAGAT	SUBURBAN	FONDO	SF	1E+07	4,5E+07	2008	277	27	34	28
IT1910A	8	34	8034010	803409	Emilia-Rom	Parma	Colorno	SARAGAT	SUBURBAN	FONDO	SF	1E+07	4,5E+07	2009	317	37	45	31
IT1910A	8	34	8034010	803409	Emilia-Rom	Parma	Colorno	SARAGAT	SUBURBAN	FONDO	SF	1E+07	4,5E+07	2010	352	28	36	27
IT1910A	8	34	8034010	803409	Emilia-Rom	Parma	Colorno	SARAGAT	SUBURBAN	FONDO	SF	1E+07	4,5E+07	2011	334	52	75	34
IT1910A	8	34	8034010	803409	Emilia-Rom	Parma	Colorno	SARAGAT	SUBURBAN	FONDO	SF	1E+07	4,5E+07	2012	338	42	63	31
IT1910A	8	34	8034010	803409	Emilia-Rom	Parma	Colorno	SARAGAT	SUBURBAN	FONDO	SF	1E+07	4,5E+07	2013	333	31	43	28
IT1910A	8	34	8034010	803409	Emilia-Rom	Parma	Colorno	SARAGAT	SUBURBAN	FONDO	SF	1E+07	4,5E+07	2014	345	29	41	27
IT1910A	8	34	8034010	803409	Emilia-Rom	Parma	Colorno	SARAGAT	SUBURBAN	FONDO	SF	1E+07	4,5E+07	2015	357	47	63	30
IT1910A	8	34	8034010	803409	Emilia-Rom	Parma	Colorno	SARAGAT	SUBURBAN	FONDO	SF	1E+07	4,5E+07	2016	355	27	30	27
IT1910A	8	34	8034010	803409	Emilia-Rom	Parma	Colorno	SARAGAT	SUBURBAN	FONDO	SF	1E+07	4,5E+07	2017	360	69	81	33
IT1910A	8	34	8034010	803409	Emilia-Rom	Parma	Colorno	SARAGAT	SUBURBAN	FONDO	SF	1E+07	4,5E+07	2018	359	24	35	28
IT1910A	8	34	8034010	803409	Emilia-Rom	Parma	Colorno	SARAGAT	SUBURBAN	FONDO	SF	1E+07	4,5E+07	2019	360	32	43	28
IT1910A	8	34	8034010	803409	Emilia-Rom	Parma	Colorno	SARAGAT	SUBURBAN	FONDO	SF	1E+07	4,5E+07	2020	360	49	54	28
IT1910A	8	34	8034010	803409	Emilia-Rom	Parma	Colorno	SARAGAT	SUBURBAN	FONDO	SF	1E+07	4,5E+07	2021	361	36	50	28
IT1910A	8	34	8034010	803409	Emilia-Rom	Parma	Colorno	SARAGAT	SUBURBAN	FONDO	SF	1E+07	4,5E+07	2022	360	33	55	30
IT1912A	8	34	8034014	803411	Emilia-Rom	Parma	Fidenza	LEOPARDI	Urbana	Fondo	UF	1E+14	4,5E+14	2008	238	21	33	28
IT1912A	8	34	8034014	803411	Emilia-Rom	Parma	Fidenza	LEOPARDI	Urbana	Fondo	UF	1E+14	4,5E+14	2009	318	38	45	29
IT1912A	8	34	8034014	803411	Emilia-Rom	Parma	Fidenza	LEOPARDI	Urbana	Fondo	UF	1E+14	4,5E+14	2010	339	34	43	26
IT1911A	8	34	8034018	803410	Emilia-Rom	Parma	Langhiranc	BADIA	RURALE	FONDO	RF	1E+07	446575	2009	266	5	7	19
IT1911A	8	34	8034018	803410	Emilia-Rom	Parma	Langhiranc	BADIA	RURALE	FONDO	RF	1E+07	446575	2010	346	14	23	20
IT1911A	8	34	8034018	803410	Emilia-Rom	Parma	Langhiranc	BADIA	RURALE	FONDO	RF	1E+07	446575	2011	359	16	23	22
IT1911A	8	34	8034018	803410	Emilia-Rom	Parma	Langhiranc	BADIA	RURALE	FONDO	RF	1E+07	446575	2012	360	11	13	21
IT1911A	8	34	8034018	803410	Emilia-Rom	Parma	Langhiranc	BADIA	RURALE	FONDO	RF	1E+07	446575	2013	348	5	6	17
IT1911A	8	34	8034018	803410	Emilia-Rom	Parma	Langhiranc	BADIA	RURALE	FONDO	RF	1E+07	446575	2014	329	5	8	16
IT1911A	8	34	8034018	803410	Emilia-Rom	Parma	Langhiranc	BADIA	RURALE	FONDO	RF	1E+07	446575	2015	354	6	10	21
IT1911A	8	34	8034018	803410	Emilia-Rom	Parma	Langhiranc	BADIA	RURALE	FONDO	RF	1E+07	446575	2016	356	8	14	20
IT1911A	8	34	8034018	803410	Emilia-Rom	Parma	Langhiranc	BADIA	RURALE	FONDO	RF	1E+07	446575	2017	361	29	37	25

Fig. 4. The main characteristics of the PM10 monitoring stations included in the analysis.

the institution. PM10 levels are given in $\mu g\ m^{-3}$, in line with the units used in European air-quality regulations.

Population

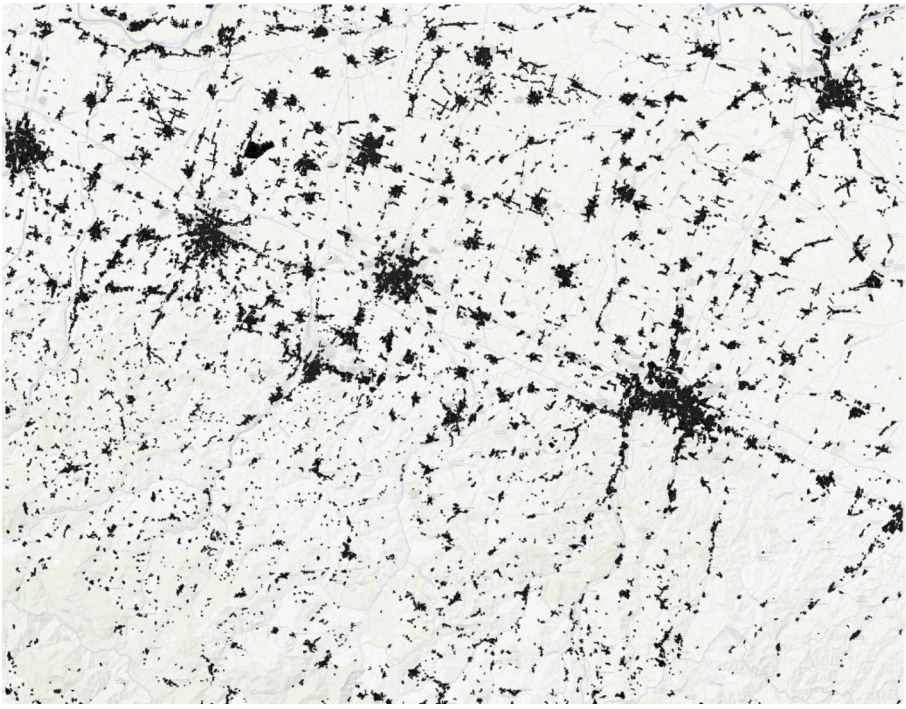

Fig. 5. Spatial Population data from ISTAT.

Population data of 2021 were obtained from the ISTAT Population and Housing Census database (Fig. 5). At the sub-municipal scale, this provides a highly detailed spatial representation of the resident population and enables the dissemination of statistical indicators at finest territorial scales.

2.3 Methodology

Traditional air quality monitoring networks provide accurate measurements at fixed locations but are inherently limited in their ability to resolve spatial continuity or to characterize pollutant levels in areas lacking direct observations. To overcome these limitations, data-driven methods have been widely adopted to reconstruct and analyze the spatial distribution of PM10 concentrations.

The interpolation was implemented using SGeMS (Stanford Geostatistical Modeling Software) [14]**.** Monitoring station data were imported as a point dataset, and a regular grid covering the study area was generated to support spatial estimation.

Ordinary kriging was selected due to the absence of a known global mean and the assumption of second-order stationarity. The final kriging outputs consist of continuous PM10 concentration surfaces and associated estimation variance maps, enabling the identification of pollution gradients and uncertainty patterns.

Once the map of the annual mean PM10 distribution for 2021 had been generated at a spatial resolution of 1km × 1km, it was spatially intersected with ISTAT population data referring to residential settlement clusters. To facilitate the interpretation of exposure patterns, the annual mean PM10 concentration map was reclassified into four concentration classes (<15 $\mu g/m^3$, 15–20 $\mu g/m^3$**,** 20–25 $\mu g/m^3$, and 25–30 $\mu g/m^3$). These classes were then used to estimate the exposure in terms of resident population related to different levels of air pollution exposure. This procedure is based on the association of PM10 concentration values with the spatial distribution of resident population across the study area.

3 Results

3.1 Spatial Structure of PM10 Concentrations

The experimental semivariogram computed from the 22 monitoring stations in the study area reveals a clear spatial dependence of annual PM10 concentrations across the whole territorial system. As expected in a lowland basin such as the Po Valley, nearby stations tend to show similar concentration values, while differences progressively increase with distance.

Directional semivariograms calculated along the four principal orientations (0°, 45°, 90°, and 135°) exhibit some variability in both shape and range (Fig. 6). In particular, a slightly more structured behaviour can be observed along the East–West direction, suggesting a potential directional influence on spatial continuity. However, these differences are not sufficiently consistent to support a robust anisotropic model. The directional curves appear irregular and affected by noise, likely due to the limited number of station pairs available in each direction and the uneven spatial distribution of the monitoring network, which is denser in urban areas and sparser in peripheral zones.

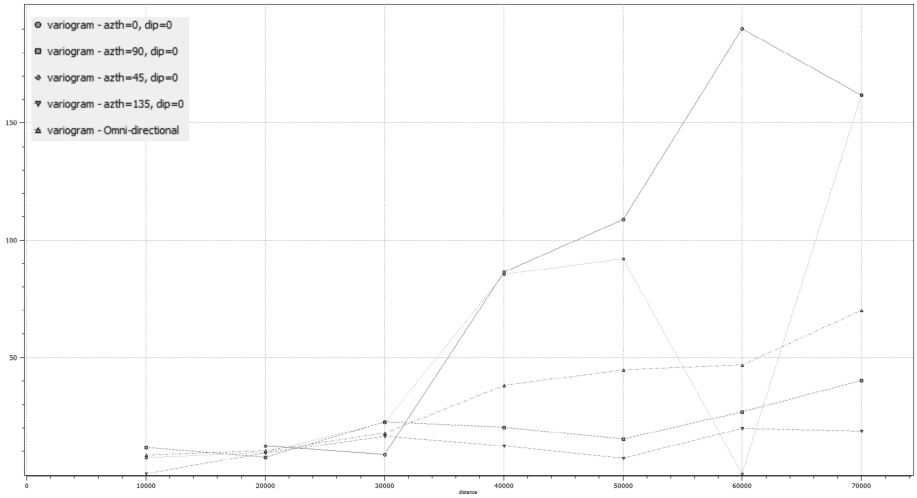

Fig. 6. The experimental variograms of 2021 PM10 concentrations computed for four principal directions (azimuths 0°, 45°, 90°, and 135°).

Given these limitations, the omnidirectional experimental variogram was considered more reliable, as it incorporates all available point pairs and provides a statistically more stable representation of spatial dependence. The omnidirectional variogram shows a rapid increase at short distances, followed by a gradual transition towards a plateau, indicating the presence of spatial correlation over several tens of kilometres.

Among the tested theoretical models (exponential, spherical, and Gaussian), the Gaussian model provided the best overall fit, effectively capturing both the smooth increase at short lag distances and the transition towards the sill. The fitted model is characterised by a nugget effect of approximately 8 ($\mu g/m^3$)2, corresponding to local residual differences of about 2.8 $\mu g/m^3$, indicating limited but non-negligible small-scale variability and/or measurement uncertainty. The sill is approximately 36 ($\mu g/m^3$)2, representing the structured component of spatial variance. This implies that PM10 concentrations may differ by approximately 6 $\mu g/m^3$ between distant locations beyond the spatial correlation range. The estimated range is about 55 km, suggesting that PM10 concentrations remain spatially correlated over relatively large distances. This result is consistent with the atmospheric behaviour of the Po Valley, were limited ventilation and basin morphology favour pollutant persistence and regional coherence.

3.2 Interpolated PM10 Surface and Uncertainty

Based on the fitted Gaussian variogram model, ordinary kriging was applied to generate a continuous surface of annual PM10 concentrations at a spatial resolution of 1 km × 1 km. This resolution allows the reconstruction of spatial gradients at the sub-provincial scale while maintaining consistency with the available monitoring data.

The interpolated PM10 map (Fig. 7) reveals a spatial pattern consistent with both the distribution of monitoring stations and known emission hotspots.

Higher concentration values, generally exceeding 25 $\mu g/m^3$, are observed in correspondence with the main urban and industrial areas, where traffic density and anthropogenic activities are more intense. These high-value clusters are primarily located along the central lowland belt of the region.

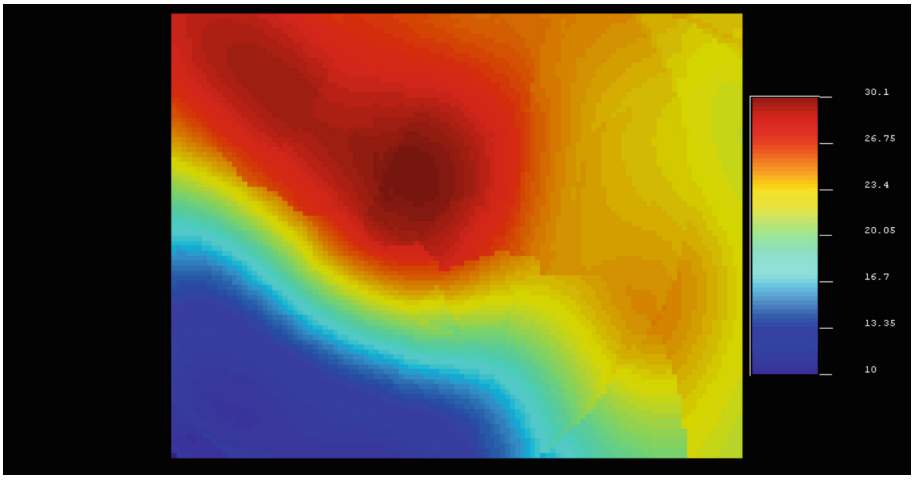

Fig. 7. Ordinary kriging interpolation of 2021 PM_{10} concentrations.

In areas characterised by a higher density of monitoring stations, the interpolated surface displays more pronounced local variability, closely reflecting observed measurements. Conversely, in peripheral and mountainous areas, where monitoring stations are sparse, the kriging surface appears smoother. This is a typical outcome of geostatistical interpolation under limited data conditions, where estimates tend to be more influenced by the overall spatial structure rather than local observations.

The kriging variance map (Fig. 8) provides a spatially explicit representation of estimation uncertainty. Lower variance values are observed in areas with a dense monitoring network, indicating higher confidence in the interpolated estimates. In contrast, variance increases significantly in areas located far from monitoring stations. This spatial pattern reflects both the geometry of the monitoring network and the estimated variogram range. Peripheral areas, particularly in the southern mountainous sectors and in the north-eastern part of the study area, show the highest uncertainty, highlighting the limitations of the current monitoring configuration and the need for caution when interpreting interpolated values in these zones.

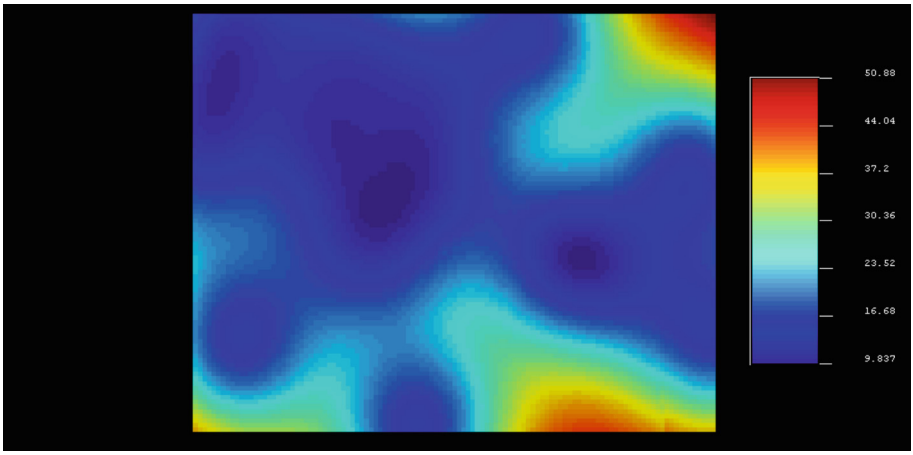

Fig. 8. Spatial distribution of kriging variance for annual PM_{10} concentrations

3.3 Spatial Distribution of Population Exposure

The integration of the interpolated PM10 surface with ISTAT population data enables the assessment of population exposure across different concentration classes. The results highlight a strong territorial polarization, with the majority of the resident population concentrated within the 20–25 $\mu g/m^3$ and 25–30 $\mu g/m^3$ classes (Fig. 9).

	<15	15 > x > 20	20>x>25	25>30	tot
Bologna	0	0	382.935,94	0	382.935,94
Modena	0	0	0	173.324,97	173.324,97
Reggio nell'Emilia	0	0	0	158.323,19	158.323,19
Parma	0	0	2.851,99	140.332,5	143.184,49
Ferrara	0	0	114.944,18	0	114.944,18
Carpi	0	0	0	66.410,19	66.410,19
Sassuolo	0	0	69	40.148,23	40.217,23
Casalecchio di Reno	0	0	37.267,1	0	37.267,1
Formigine	0	0	0	33.333,75	33.333,75
Cento	0	0	30.862,39	240,33	31.102,72
San Lazzaro di Savena	0	0	30.413	0	30.413
Imola	0	0	29.034,64	0	29.034,64
Castelfranco Emilia	0	0	0	28.708,47	28.708,47
Valsamoggia	0	440,21	9.202,56	16.688,94	26.331,71
Scandiano	0	0	362,61	23.352,06	23.714,67
San Giovanni in Persiceto	0	0	68,04	23.188,08	23.256,12
Vignola	0	0	0	22.985,39	22.985,39
Mirandola	0	0	0	22.222,71	22.222,71
Correggio	0	0	0	21.950,52	21.950,52
Zola Predosa	0	0	18.369,11	83,76	18.452,87
Casalgrande	0	0	0	17.626,79	17.626,79
Fiorano Modenese	0	0	0	17.230,56	17.230,56
Castel Maggiore	0	0	17.011,03	0	17.011,03
Castel San Pietro Terme	0	0	16.795,63	0	16.795,63
Viadana	0	0	0	16.198,05	16.198,05
Maranello	0	0	0	15.856,6	15.856,6
Finale Emilia	0	0	11.262,95	4.396,16	15.659,11
Pianoro	0	0	15.005,25	0	15.005,25
Nonantola	0	0	0	14.777,93	14.777,93
Budrio	0	0	14.457,39	0	14.457,39
Castelnuovo Rangone	0	0	0	14.379,24	14.379,24
Castellarano	0	0	4.948,34	9.281,93	14.230,27
Molinella	0	0	14.120,43	0	14.120,43

Fig. 9. Population exposure across different concentration classes annual PM_{10} concentrations.

The main urban centres of the region are almost entirely associated with medium-to-high PM10 levels (Fig. 10). Bologna, the most populated municipality, falls entirely within the 20–25 $\mu g/m^3$ class, with approximately 382,936 inhabitants exposed within this range. Similarly, Ferrara, Casalecchio di Reno, San Lazzaro di Savena, and Imola are predominantly included in the same class, indicating a widespread exposure to intermediate concentration levels across the metropolitan and peri-urban system.

A more critical situation emerges in the 25–30 $\mu g/m^3$ class, which includes several major urban and productive centres of the Emilia plain. Modena, Reggio nell'Emilia, and Parma show a large share of their population within this range, together with numerous medium-sized municipalities such as Carpi, Formigine, Castelfranco Emilia, Mirandola, Correggio, and Vignola. This confirms that the highest PM10 levels are not limited to isolated hotspots but characterize a broad and densely populated territorial system. In contrast, the lowest exposure classes (<15 $\mu g/m^3$ and 15–20 $\mu g/m^3$) are mainly associated with mountain and foothill municipalities along the Apennine belt. In these areas, lower settlement density and more favourable dispersion conditions result in significantly reduced PM10 concentrations. Municipalities such as Alto Reno Terme, Castelnovo ne' Monti, Fanano, Ventasso, and Frassinoro show a substantial proportion of their population within these lower concentration ranges.

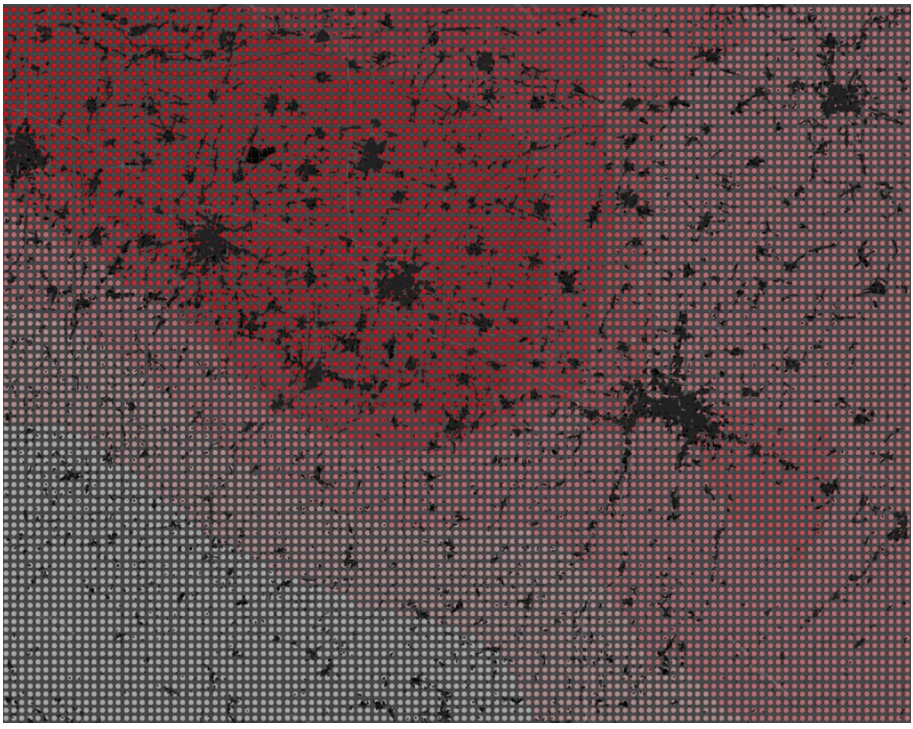

Fig. 10. Spatial distribution of kriging variance for annual PM_{10} concentrations and urban residential distributions.

3.4 Synthesis of Spatial Patterns

Overall, the results demonstrate that PM10 concentrations in the study area exhibit a well-defined spatial structure at the regional scale. The use of an omnidirectional Gaussian variogram model proved to be a robust and physically consistent choice, given the limited and uneven distribution of monitoring stations. The kriging-based maps successfully capture both the spatial distribution of concentrations and the associated uncertainty, providing a coherent framework for interpreting PM10 dynamics. When combined with population data, these results highlight spatial relations between air pollution levels, settlement patterns, and territorial structure.

In particular, the analysis shows that population exposure is strongly concentrated in the central lowland urban system, where both pollutant levels and demographic density are highest (i.e. Parma, Modena, Sassuolo, Reggio Emilia), while lower exposure levels are mainly confined to mountainous south-west municipalities (Fig. 11).

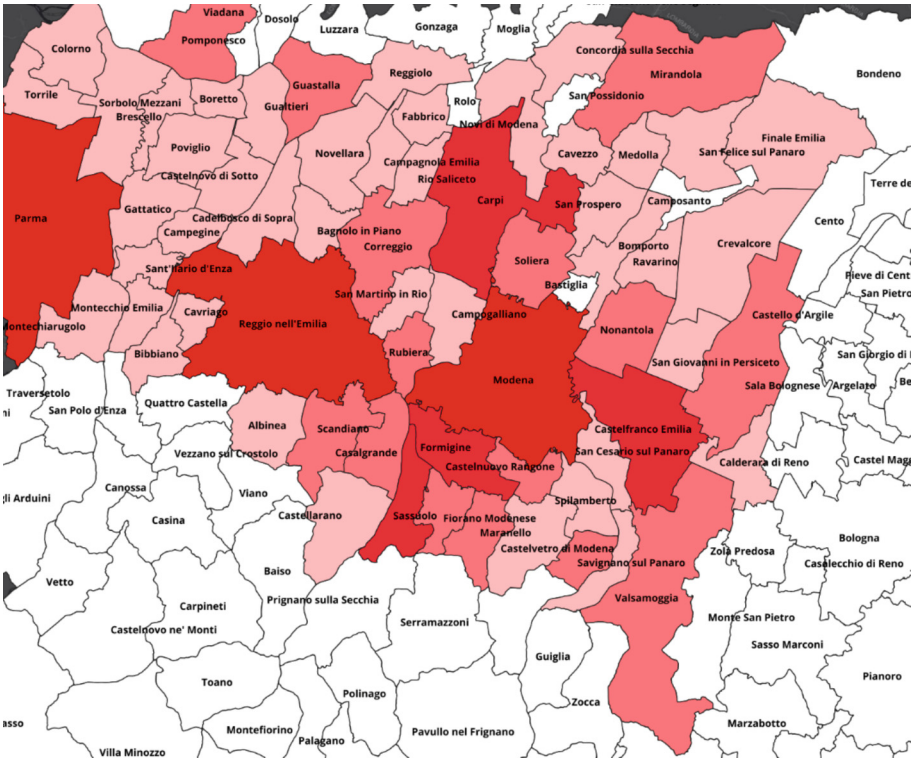

Fig. 11. Municipalities entirely included in the 25–30 $\mu g/m^3$ PM10 concentration class are highlighted in red, whereas municipalities with the largest exposed population are represented in dark red.

This confirms that PM10 exposure in the region is not randomly distributed, but structurally embedded within the geography of urbanization in the region.

4 Discussion

The results provide a spatially explicit interpretation of annual PM10 concentrations and population exposure across the study area, highlighting a clear territorial organization of air-pollution patterns within the Emilia-Romagna sector of the Po Valley. Overall, the analysis confirms the presence of a marked concentration of pollutants within the lowland basin, where geomorphological conditions, atmospheric stability, and the structure of urbanized and productive systems contribute to the persistence of PM10 accumulation.

At the same time, the findings suggest that the relationship between pollutant concentration and exposed population is not merely linear, nor can it be explained exclusively by the demographic size of urban centres. In this regard, the case of Bologna is particularly significant. Although Bologna represents the most populated urban nucleus within the study area, it does not fall within the highest PM10 concentration class identified in the analysis. However, a very large share of its resident population remains exposed to intermediate concentration levels, particularly within the 20–25 $\mu g/m^3$ range. This result is highly relevant from a public-health and planning perspective, as it shows that even concentration levels below the highest observed class may still involve a very large number of exposed inhabitants when they affect major metropolitan systems.

5 Conclusions

This study explored the spatial distribution of annual PM10 concentrations and associated population exposure patterns within a representative portion of the Emilia-Romagna region, using a geostatistical interpolation framework integrated with high-resolution population data. The results show that PM10 concentrations exhibit a well-defined spatial structure, with higher values concentrated in the central lowland urban system and lower levels in mountainous and peripheral areas.

The integration of concentration map with population data makes it possible to move beyond a purely descriptive reading of pollution patterns and to identify those territorial contexts where air-quality conditions may generate the greatest exposure burden for residents. In this sense, the analysis demonstrates that the most densely populated urban centres are not necessarily those falling within the highest PM10 concentration class. Bologna represents the clearest example of this pattern: despite not belonging to the most critical concentration class, it concentrates a very high number of exposed inhabitants due to its demographic weight and urban structure.

This finding is particularly relevant for environmental governance, as it underlines the importance of considering both pollutant intensity and exposed population in the design of local mitigation strategies.

A detailed reconstruction of PM10 spatial distribution, combined with a fine-scale estimation of the resident population exposed and interpreted in light of emission-source contributions, can provide a robust basis for orienting targeted environmental policies toward the areas where mitigation actions may produce the greatest collective benefit. In this perspective, the results support the relevance of place-based and geographically differentiated interventions, capable of addressing local pollution dynamics more effectively [4].

Consequently, the findings emphasize the importance of targeted policy actions, such as the expansion of urban green spaces, the adoption of cleaner technologies, and the strengthening of public transportation system[4]. Integrating tree-planting strategies with sustainable urban planning initiatives may contribute to reducing pollutant levels while also improving accessibility to green areas. To maximize effectiveness, afforestation efforts should prioritize high-efficiency PM-absorbing tree species, particularly in high-traffic and environmentally critical urban sectors [6].

Moreover, considering that a substantial share of PM10 emissions is likely associated with the civil sector, especially residential heating, mitigation strategies [15] should also address the improvement of heating systems and the progressive transition toward more efficient and less emissive energy solutions, including district heating where applicable [16]. In this sense, integrated environmental and urban policies may represent a key lever for improving local air quality and reducing population exposure in the most sensitive urban contexts [17].

Declaration of Generative AI and AI-Assisted Technologies in the Writing Process. During the preparation of this work the authors used ChatGPT 3.5 in order to improve the readability of parts of the text. After using this tool/service, the authors reviewed and edited the content as needed and take full responsibility for the content of the publication.

Data Availability. Data will be made available on request.

References

1. Slini, T., Kaprara, A., Karatzas, K., Moussiopoulos, N.: PM10 forecasting for Thessaloniki. Greece. Environ. Modell. Softw. **21**, 559–565 (2006). https://doi.org/10.1016/j.envsoft.2004.06.011
2. Cocchi, D., Greco, F., Trivisano, C.: Hierarchical space-time modelling of PM10 pollution. Atmos. Environ. **41**, 532–542 (2007). https://doi.org/10.1016/j.atmosenv.2006.08.032
3. Sloss, L.L., Smith, I.M.: PM10 and PM2.5: an international perspective. Fuel Process. Technol. **65–66**, 127–141 (2000). https://doi.org/10.1016/S0378-3820(99)00081-8
4. Islam, A., Pattnaik, N., Moula, Md.M., Rötzer, T., Pauleit, S., Rahman, M.A.: Impact of urban green spaces on air quality: a study of PM10 reduction across diverse climates. Sci. Total Environ. **955**, 176770 (2024). https://doi.org/10.1016/j.scitotenv.2024.176770
5. Baek, S., Kim, J., Kang, J.: Impact of green infrastructure on PM10 in port-adjacent residential complexes: a finite volume method-based computational fluid dynamics study. Sustain. Cities Soc. **115** (2024). https://doi.org/10.1016/j.scs.2024.105815
6. Queiroz Diniz Oliveira, M.C., Maura de Miranda, R., de Fátima Andrade, M., Kumar, P.: Impact of urban green areas on air quality: an integrated analysis in the metropolitan area of São Paulo. Environ. Pollut. **372** (2025). https://doi.org/10.1016/j.envpol.2025.126082
7. Ragosta, M., D'emilio, M., Casaletto, L., Telesca, V.: A statistical procedure for analyzing the behavior of air pollutants during temperature extreme events: the case study of Emilia-Romagna region (northern Italy). Appl. Sci. (Switz.) **11** (2021). https://doi.org/10.3390/app11178266
8. Shtein, A., et al.: Estimating daily PM2.5 and PM10 over Italy using an ensemble model. Environ. Sci. Technol. **54**, 120–128 (2020). https://doi.org/10.1021/acs.est.9b04279

9. Bonaventura, L., Castruccio, S., Crippa, P., Lonati, G.: Geostatistical estimate of PM10 concentrations in Northern Italy: validation of kriging reconstructions with classical and flexible variogram models (2008)
10. Bartzis, J.G., Kalimeri, K.K., Sakellaris, I.A.: Environmental data treatment to support exposure studies: the statistical behavior for NO2, O3, PM10 and PM2.5 air concentrations in Europe. Environ. Res. **181** (2020). https://doi.org/10.1016/j.envres.2019.108864
11. Beloconi, A., Chrysoulakis, N., Lyapustin, A., Utzinger, J., Vounatsou, P.: Bayesian geostatistical modelling of PM10 and PM2.5 surface level concentrations in Europe using high-resolution satellite-derived products. Environ. Int. **121**, 57–70 (2018). https://doi.org/10.1016/j.envint.2018.08.041
12. Perez, P., Reyes, J.: An integrated neural network model for PM10 forecasting. Atmos. Environ. **40**, 2845–2851 (2006). https://doi.org/10.1016/j.atmosenv.2006.01.010
13. Fabbi, S., Veratti, G., Bigi, A., Ghermandi, G.: Air quality (PM 10) scenarios resulting from the expansion of hydrogen fuel cell electric vehicle in Emilia-Romagna (Northern Italy). In: 21st International Conference on Harmonisation within Atmospheric Dispersion Modelling for Regulatory Purposes (2022)
14. Remy, N.: S-GeMS: the stanford geostatistical modeling software: a tool for new algorithms development. In: Leuangthong, O., Deutsch, C.V (eds.) Geostatistics Banff 2004, pp. 865–871. Springer, Dordrecht (2005). https://doi.org/10.1007/978-1-4020-3610-1_89
15. Murgante, B., Borruso, G., Balletto, G., Castiglia, P., Dettori, M.: Why Italy first? Health, geographical and planning aspects of the COVID-19 outbreak. Sustain. (Switz.). **12** (2020). https://doi.org/10.3390/su12125064
16. Stadlober, E., Hörmann, S., Pfeiler, B.: Quality and performance of a PM10 daily forecasting model. Atmos. Environ. **42**, 1098–1109 (2008). https://doi.org/10.1016/j.atmosenv.2007.10.073
17. Zhu, L., Huang, X., Shi, H., Cai, X., Song, Y.: Transport pathways and potential sources of PM10 in Beijing. Atmos. Environ. **45**, 594–604 (2011). https://doi.org/10.1016/j.atmosenv.2010.10.040

Water Quality Predictors for Harmful Algal Blooms Occurrence in the Mississippi Sound, USA

Vladimir J. Alarcon[1(✉)], Paul F. Mickle[1], and Ruben A. Alvarado[2]

[1] Northern Gulf Institute, 1021 Balch Blvd., Stennis Space Center, Mississippi 39529, USA
{valarcon,pmickle}@ngi.msstate.edu
[2] Universidad Católica de Salta, Salta, CP 4400, República Argentina

Abstract. From July 2019 to September 2019, harmful algal blooms (HABs) were observed in the State of Mississippi coast at the Northern Gulf of America (Mississippi Sound). In this paper, several multiple linear regression models (MLR models) based on observed water quality data and simulated water quality data are presented. Fourteen environmental and water quality observed variables and four model-simulated water quality variables were included in the study. Several combinations of those variables were used to generate MLR models which could help identify the main water quality and/or environmental predictors for HAB occurrence in the Mississippi Sound, during 2019.

Keywords: Mississippi Sound · Harmful Algal Blooms · Water Quality · Multiple Linear Regression · Microcystis

1 Introduction

The Mississippi Sound (MS Sound) is an estuarial water body located between the Mississippi Gulf Coast and the barrier islands extending from Lake Borgne (Louisiana) to Mobile Bay (Alabama) (Fig. 1). It is connected to Lake Pontchartrain (Louisiana) through a narrow natural channel [1]. The Bonnet Carré Spillway (BCS) is a flood control structure that diverts Mississippi River water to Lake Pontchartrain (in Louisiana) allowing floodwaters from the Mississippi River to flow into Lake Pontchartrain (Louisiana). The opening of the Bonne Carre Spillway has a strong effect on the water quality of the MS Sound.

Nutrient loadings from urban areas [2] affect water quality and biological species in the MS Sound, both of which support the economy of the State of Mississippi coastal area [3]. Nitrogen and phosphorus loading and their effects to the MS coastal waters should be studied to support sound management strategies [4].

In addition to contaminant inputs from urban areas, the MS Sound receives pollutant loads from Lake Pontchartrain, especially when the Bonnet Carré Spillway (BCS) is open. The BCS is a flood control structure which diverts waters from the Mississippi River to Lake Pontchartrain (Louisiana) when water stage at the river increases flood risk

© The Author(s), under exclusive license to Springer Nature Switzerland AG 2027
O. Gervasi et al. (Eds.): ICCSA 2026 Workshops, LNCS 16761, pp. 542–556, 2027.
https://doi.org/10.1007/978-3-032-30527-5_35

in the city of New Orleans. Since the Lake is a shallow water body connected to the Gulf of America through the Rigolets strait (which allows bidirectional flow depending on the tidal regime) flushing of lake waters to the MS Sound can occur relatively fast depending on the magnitude of the inflow rate through the BCS. Alarcon et al. [1] report flushing times between 25 to 40 days. This means that pollutants present in Lake Pontchartrain before BCS openings may also be flushed out during BCS openings and could reach the MS Sound in 30 to 50 days. Over the past few decades, the impacts of BCS openings to adjacent estuaries have been scientifically investigated [5]. Nevertheless, observed water quality conditions in the MS Sound during HAB events may also be a factor for HAB presence.

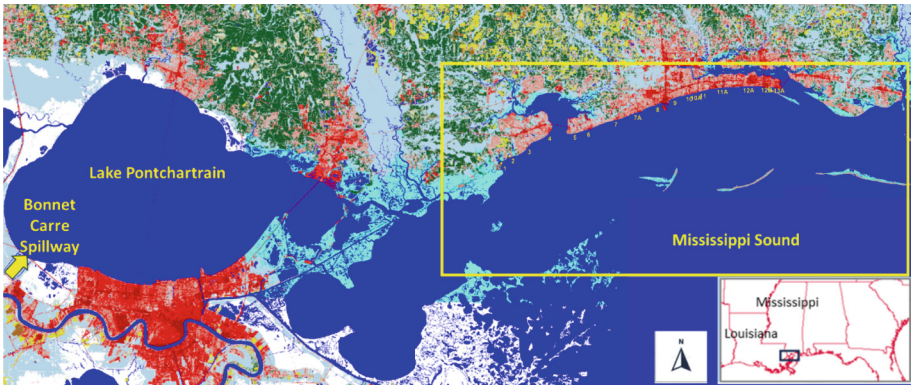

Fig. 1. Mississippi Sound (MS Sound). The MS Sound is located at the coast of the State of Mississippi (USA) (Northern Gulf of America).

In this research, a multiple linear regression model (MLR model) is developed based on observed and simulated water quality data. Fourteen environmental and water quality observed variables and five model-simulated water quality variables were included in the study. Several combinations of those variables were explored to identify the main water quality and/or environmental predictors for HAB occurrence in the Mississippi Sound.

2 Methods

2.1 Study Area

Figure 2 shows the study area including Mississippi Department of Environmental Quality sampling locations along the State of Mississippi coast. The figure also shows the predominant land use and land cover in the inland urban or undeveloped watersheds that drain to the MS Sound. As shown, dense urban areas located along the coast are potential sources of pollution. Rivers and minor streams in the inland area may also collect non-point source pollutants from agricultural areas (cultivated crops, pasture/hay) located outside in undeveloped areas, while stormwater outfalls from urban areas transport sediment loads and other contaminants to the MS Sound.

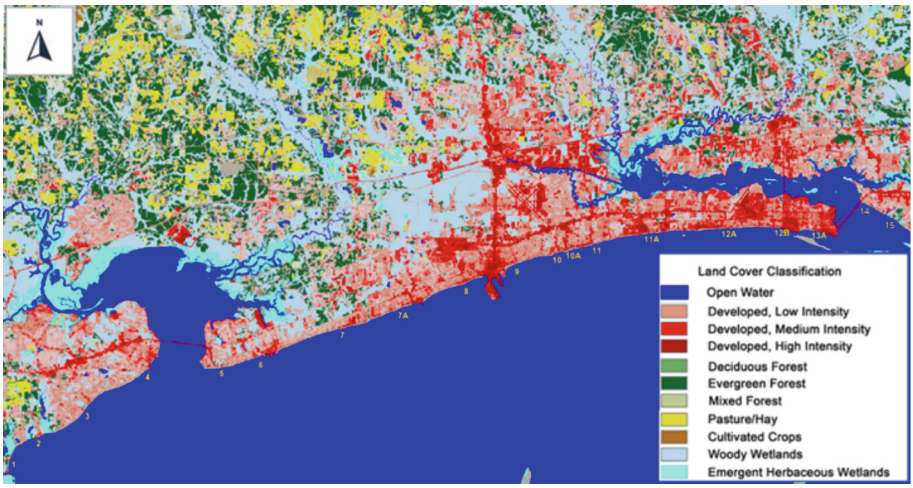

Fig. 2. Study Area. Land use and land cover in the Mississippi Sound. Land use/land cover in urban areas draining to the MS Sound are shown. MDEQ water quality sampling locations along the Mississippi coast are shown.

2.2 Observed and Simulated Water Quality Data

The Mississippi Department of Environmental Quality (MDEQ) performs routine water quality analyses in the Mississippi Sound. Under the MDEQ Mississippi Beach Monitoring Program, coastal water (at locations shown in Fig. 2) is monthly tested for the presence of nutrients, totals suspended solids (TSS), chlorophyl-a, fecal bacteria, and other water quality constituents. During the months of July, August, and September of 2019, MDEQ additionally analyzed for HAB. The species for which presence was mostly observed were: Microcystis spp. and Chattonella spp. Since Microcystis blooms were significantly more present than Chattonella during 2019, in this research Microcystis blooms were chosen as harmful algal blooms (HABs) indicator.

Observed Water Quality Data Used in the Study
Monthly observed Total Kjeldahl Nitrogen (TKN), Total Phosphorus (TP), Total Suspended Solids (TSS), salinity, Total Suspended Solids (TSS), Total Organic Carbon (TOC), chlorophyll-a, turbidity, TKN/TP ratio, and Temperature are used in the model development. The number of Microcystis bloom (BLOOM) sightings were monthly summed. Data from stations 1 through 11 (Fig. 2) were used for the development of the MLR models. Data from stations 12B, 14, and 15, located at the eastern-most border of the study area (Fig. 2) were used for assessing the predictive ability of the MLR models.

Simulated Water Quality Data used in the Study
A water quality model (described in [6]) was used to simulate Total Kjeldahl Nitrogen (TKNsim), Total Phosphorus (TPsim), and Total Nitrogen (TNsim). The ratios TKNsim/TPsim and TNsim/TPsim were also computed. Since the water quality model outputs are at hourly temporal resolution, the simulated data correspond exactly to the time of day in which HAB blooms were reported by MDEQ.

In addition to water quality data, tidal data at three locations along the MS sound were also used as input data: Biloxi, Gulfport, and Saint Joseph Island. Also, since the opening of the Bonnet Carre Spillway is a key factor in MS Sound HAB events, the inflow rate (Q in m3/s) was also input as predictor variable.

2.3 Multiple Linear Regression Model (MLR Model)

A multiple linear regression model can be represented by the following equation [7].

$$y_i = \beta_0 + \beta_1 x_{i,1} + \beta_2 x_{i,2} + \ldots + \beta_k x_{i,k} + \varepsilon_i.$$

In this research, y_i represents predicted number of HAB sightings per month, x_i are the predictor water quality variables included in the model, k is the number of predictor water quality variables, and the β_k coefficients are the values that minimize the sum of squared errors for the sample. ε_i are the residuals which are assumed to have a normal distribution with mean 0 and constant variance σ^2. In this research, several combinations of variables were performed to achieve the best statistical fit when comparing observed HAB sightings versus predicted HAB sightings. The statistical fit was measured calculating the r^2 coefficient of determination for each combination of variables included in the analysis.

Potential predictor water quality variables (observed and simulated) were organized in 3 batches: a) observed and simulated water quality data, b) only observed water quality data, c) only simulated water quality data. Each of these batches were used for generating MLR models with 2, 3, 4, and 5, minimum number of predictor variables. Therefore, 12 linear models were developed and assessed for statistical fit.

3 Results

3.1 Microsystis sp. and Chattonella sp. in the MS Sound

Figure 3 shows observed monthly blooms sightings for Microcystis sp. and Chattonella sp. The figure includes number of monthly bloom sightings for July, August, and September 2019. For brevity, the most representative locations are shown: Lakeshore (station 1), Bay Saint Louis (station 4), Jourdan River (station 4A), Long Beach (station 8), and Edgewater (station 11A). Microcistys sp. is shown to have a more pervasive presence than Chattonella sp. during all months, therefore this research focuses primarily on Microcystis blooms. Figure 3 shows that Bay Saint Louis (station 4) was the location where the largest number of blooms were recorded during July and August, 2019. The second 2019-opening of the Bonnet Carre Spillway took place from May 10 to July 27th, 2019. Nevertheless, peak inflow (4559 m^3/s) took place on May 22. According to Alarcon et al. [1], for an inflow of this magnitude Lake Pontchartrain flushing time is 33 days. Therefore, HAB present in Lake Pontchartrain may have reached the Northern Gulf of America by late-June 2019. Since Lakeshore and Bay Saint Louis are the locations closest to the Rigolets (Lake Pontchartrain's outfall to the gulf), if HAB would have been transported from the lake, HAB should have been observed in July 2019. This is clearly illustrated in Fig. 3: 13 bloom sightings in Lakeshore, and 15 sightings

in Bay Saint Louis were recorded during July 2019. Since Bay Saint Louis has more urban areas than Lakeshore, nutrients from those areas may have enhanced blooms in the area. This is consistent with the number of blooms observed in Edgewater and Long beach during July 2019; those locations also have large coastal urban areas. In station 4A (Jourdan River outfall) 10 bloom sightings during July were also reported. Nutrients from agricultural areas in the river's watershed together with hydrodynamically transported Microcystis may explain those sightings. Interestingly, during August 2019, Bay Saint Louis and Jourdan River are the locations with the greatest number of bloom sightings. The rest of the stations still recorded at least 7 HAB sightings in August. During September, the closest location to Lake Pontchartrain (Lakeshore) showed the greatest number of HAB sightings, which indicates potential HAB migration or remanent HAB present in the lake.

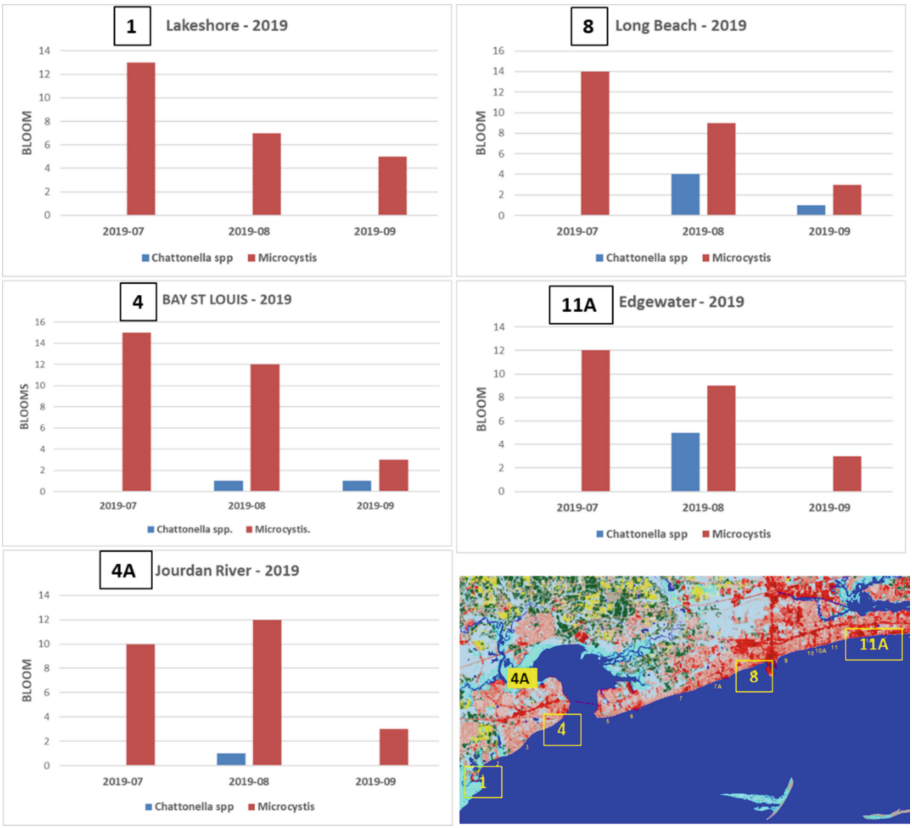

Fig. 3. Harmful algal bloom sightings during July, August, and September 2019.

Usually, HAB presence is related to nutrient enrichment and chlorophyll-a is a standard HAB indicator. To explore the relationship between nutrient-related observed water quality constituents, total nitrogen (TN), total phosphorus (TP), chlorophyll-a (Chl-a),

and total organic carbon (TOC) were scatter-plotted. As shown in Fig. 4, Chl-a strongly correlates with TN, TP, and TOC.

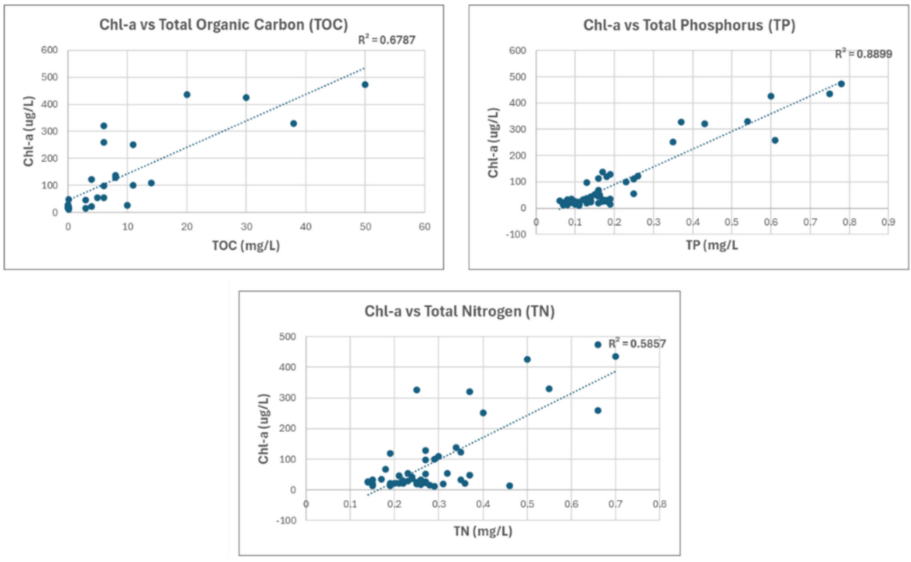

Fig. 4. Relationship between total nitrogen (TN), total phosphorus (TP), and chlorophyll-a (Chl-a) in the MS Sound.

Nevertheless, none of the nutrient constituents (TN or TP) and Total Organic Carbon (TOC) showed a strong correlation with HAB presence (Fig. 5).

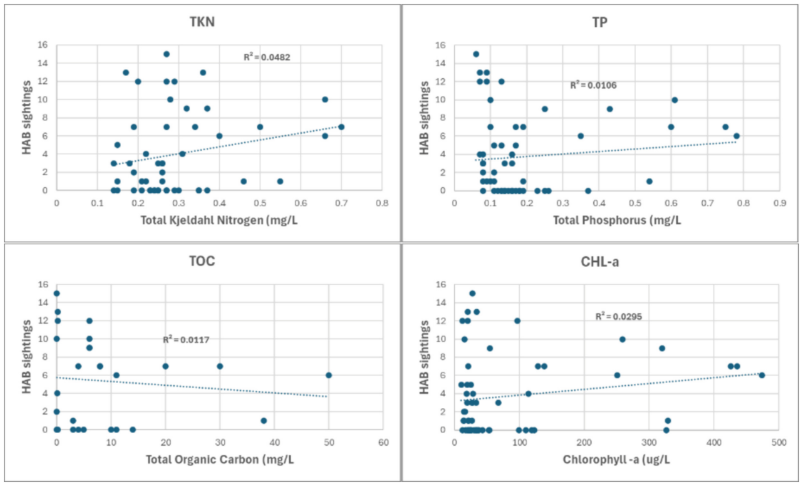

Fig. 5. HAB sightings versus nutrients (TN, TP), and Chlorophyll-a (CHL-a) concentrations.

As shown in Fig. 6, salinity was the only water quality variable that showed moderate correlation ($R^2 = 0.51$). While nutrients or chlorophyll-a correlated poorly with HAB presence, the ratio TKN/TP was shown to have a moderate correlation ($R^2 = 0.55$).

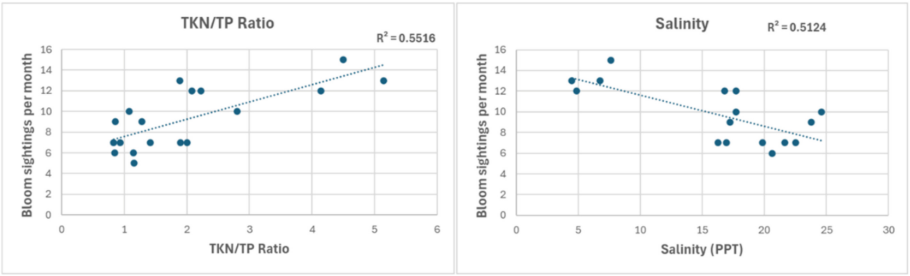

Fig. 6. Relationship between salinity and TKN/TP ratio with HAB presence.in the MS Sound.

Since one-to-one relationships are shown to be not evident, combining water quality variables to predict HAB seems to be necessary. These results reinforce the objective of this research.

3.2 Multiple Linear Regression Models' Results

As described earlier, for the development of MLR models the data was organized in three groups, each of which was tested for 2, 3, 4, and 5 predictor variables: a) observed and simulated water quality data, b) only observed water quality data, c) only simulated water quality data. Nevertheless, the MLR models for which the R^2 value was smaller than 0.5 were considered unsatisfactory, and the results are not reported below. The results for acceptable MLR models are as follows.

MLR Models with Observed and Simulated Predictor Variables
Figure 7 shows that MLR models that mix input data (observed and simulated) as predictor variables to estimate HAB presence have good statistical fit between observed HAB data and predicted HAB data. All R^2 indicators are above 0.57 and the Root Mean Square errors (RMS) range from 2.21. to 2.75 (Table 1).

MLR Models with only Observed Predictor Variables
Figure 8 shows that using only observed data to predict HAB presence slightly decreases the quality of the statistical fit between predicted HAB and observed HAB. Nevertheless, all R^2 values range between 0.53 and 0.66, and RMS values ranged from 2.59 to 2.94.

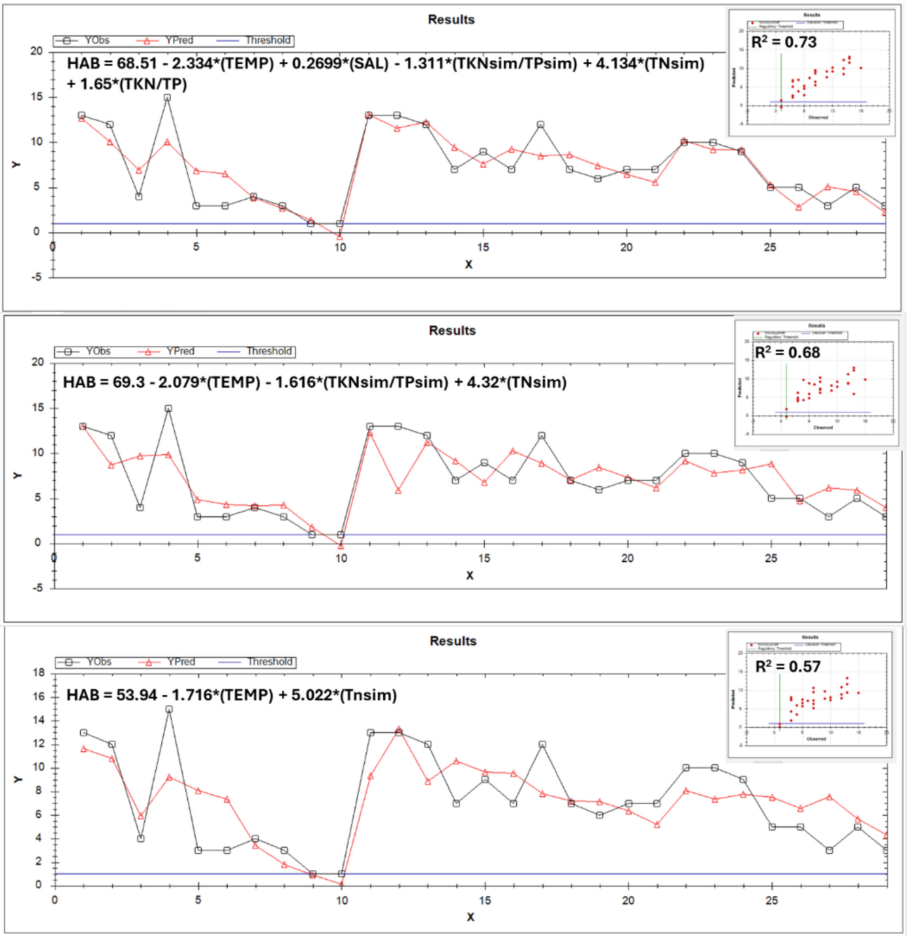

Fig. 7. MLR models generated with observed and simulated water quality data. The resulting models include 5, 4, and 3 predictor variables. Resulting linear model equations are shown in each chart, including the response variable (HAB) and the predictor variables.

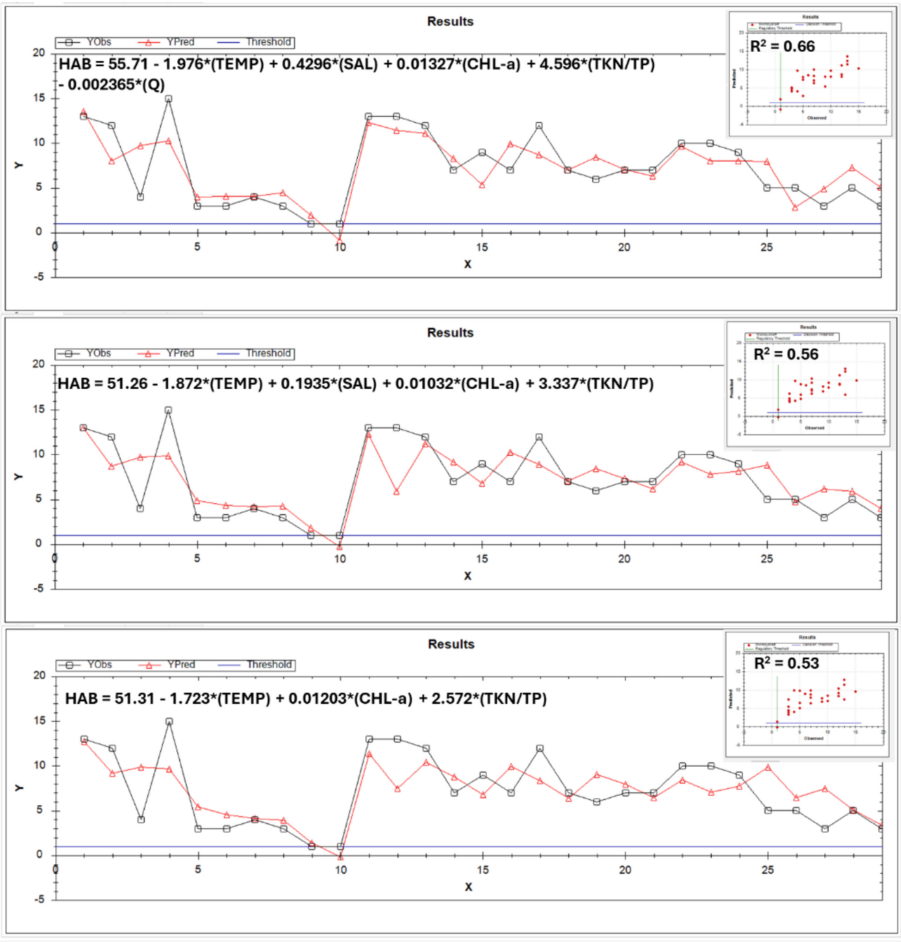

Fig. 8. MLR models generated with only observed water quality data. The resulting models include 5, 4, and 3 predictor variables. Resulting linear model equations are shown in each chart, including the response variable (HAB) and the predictor variables.

Adjusted R^2 values (Table 1) suggest that models 1 through 4 provide better quality fit between observed and simulated response variable (Adj. $R^2 > 0.63$). The adjusted Akaike criterion indicates that models 1, 2, and 4 seem to be better candidates for HAB prediction. The Bayesian criterion suggests that among the models that used simulated and observed variables, models 1 and 2 are more parsimonious than model 3. Among the models that used only observed variables, model 4 is shown to be the most parsimonious.

Table 1. Summary of indicators or fit for MLR models.

Model	Number of predictor variables	R^2	Adj. R^2	RMS	Adj. Akaike	Bayes. C.
1	2 simulated, 3 observed	0.73	0.73	2.21	80.33	56.16
2	2 simulated, 1 observed	0.68	0.65	2.42	84.05	57.16
3	1 simulated, 1 observed	0.57	0.54	2.75	90.49	62.22
4	5 observed	0.66	0.63	2.59	89.65	65.49
5	4 observed	0.56	0.52	2.89	95.11	69.59
6	3 observed	0.53	0.49	2.94	95.21	68.31

Table 1 shows that mixing simulated and observed predictor variables may provide MLR models which generate better quality HAB predictions than using only observed predictor variables. Nevertheless, recent research on HAB prediction shows similar statistical fit values as those shown in Table 1. Wen et al. [8] used machine learning to predict Alexandrium sp. algal blooms in the Gulf of Maine (USA). In their study, the following predictor variables were selected: PO4, NH4, Si(OH)4, NO2 + NO3, and Chl-a. The R^2 values reported in [8] range between 0.53 to 0.83. Yu et al. [9] proposed a method based on machine learning to predict the occurrence of Lingulodinium polyedrum algal blooms in the Southern California coastal ocean, and Sishili bay (Shandong province, China). Yu et al. [9] found that for California coastal ocean the main predictor variables were ammonia, chlorophyll-a and temperature. For Sishili bay (China) Yu et al. [9] selected DO, Ammonia, chlorophyll-a, and nitrite. The resulting R^2 in the study values range between 0.501 and 0.956 [9]. Therefore, the statistical fit results achieved in this research and shown in Table 1 are within ranges reported in the literature.

Table 2 shows additional statistics for the resulting MLR models. All models include water temperature (TEM)P as primary predictor variable as shown by the corresponding t-statistic and P-value. Salinity (SAL) is a predictor variable in models 1, 4 and 5. Nevertheless, Although Model 5 is shown to have a decent R2 value (see Table1), salinity's t-statistic is smaller than 2.0, and its P-value is 0.18 (the highest for all models). Also, in Model 5, predictor variable chlorophyll-a (CHL-a) has P-value = 0.0379 and t-statistic = 2.1976, which makes Model 5 the weakest of all MLR models. On the other hand, all the other models have |t-statistic| > 2.47 and P-value < 0.022, which, together with the R2 and RMS values shown in Table 1, makes them valid representation of the observed data.

Multiple Linear Regression (MLR) models have been used for HAB prediction in lakes and coastal waters, as well as water quality and/or biological species prediction. MLR models (as opposed to other prediction methods), aim at predicting continuous outcomes, based on independent variables which may include various water quality parameters, hydrological parameters, and meteorological parameters [10].

Table 2. Resulting MLR models.

	Predictor variables	Coeff.	Std. Err.	t-Stat.	P-Value	Std.Coeff.
Model 1	Intercept	68.509	9.081	7.5443	1.16E-07	
	TEMP	−2.3337	0.3019	−7.7288	7.71E−08	−1.0039
	SAL	0.2699	0.1091	2.4727	0.0212	0.4342
	TKNsim/TPsim	−1.3111	0.517	−2.5362	0.0185	−0.3194
	TNsim	4.1341	1.1285	3.6634	0.0013	0.5546
	TKN/TP	1.6496	0.6599	2.4998	0.02	0.5011
Model 2	Intercept	69.299	9.7248	7.1261	1.81E−07	
	TEMP	−2.0788	0.3126	−6.6509	5.72E−07	−0.8942
	TKNsim/TPsim	−1.6158	0.5457	−2.9608	0.0066	−0.3936
	TNsim	4.3199	0.952	4.5378	0.0001	0.5795
Model 3	Intercept	53.936	9.3331	5.779	4.36E−06	
	TEMP	−1.7159	0.3263	−5.2592	1.70E−05	−0.7382
	TNsim	5.0223	1.0462	4.8006	5.69E−05	0.6738
Model 4	Intercept	55.709	8.9929	6.1948	2.55E−06	
	TEMP	−1.9759	0.3325	−5.9425	4.66E−06	−0.85
	SAL	0.4296	0.155	2.7716	0.0109	0.6912
	CHL-a	0.0133	0.0044	3.0456	0.0057	0.4805
	Q	−0.0024	0.0009	−2.654	0.0142	−0.4177
	TKN/TP	4.5964	0.8755	5.2499	2.52E−05	1.3963
Model 5	Intercept	51.263	9.8458	5.2067	2.46E−05	
	TEMP	−1.8717	0.3679	−5.0871	3.33E−05	−0.8052
	SAL	0.1935	0.1414	1.3679	0.184	0.3113
	CHL-a	0.0103	0.0047	2.1976	0.0379	0.3735
	TKN/TP	3.337	0.8199	4.0699	0.0004	1.0137
Model 6	Intercept	51.306	10.0093	5.1258	2.69E−05	
	TEMP	−1.723	0.3574	−4.8216	5.92E−05	−0.7412
	CHL-a	0.012	0.0046	2.616	0.0149	0.4356
	TKN/TP	2.5717	0.6093	4.2204	0.0003	0.7812

Table 3 summarizes the MRL models equations generated in this research. From a water quality management perspective, MLR models are a straight-forward and simple method which could be used by managers. Nevertheless, a model with many predictor variables may be costly to operate, especially if those predictor variables depend on field campaigns and laboratory analysis. An MLR model could also be computationally and/or financially expensive if the model relies on simulated data from other models (e.g.,

[11–13]. For example, MLR models 1 and 2 seem to be the best models because of their statistical performance (see Tables 1, 2 and 3). However, Model 1, besides depending on observed TEMP and SAL (which are relatively inexpensive to measure), also depends on observed TKN and TP, as well as simulated TKN, TP and TN (TKNsim, TPsim, TNsim), which makes Model 1 a costly alternative. Models 2 and 3, on the other hand, seem to be more implementable, although their dependance on simulated data might is a drawback.

Table 3. Summarized MLR models' equations

Model	MLR models using observed and simulated predictor variables
1	HAB = 68.51 – 2.334*(TEMP) + 0.2699*(SAL) - 1.311*(TKNsim/TPsim) + 4.134*(TNsim) + 1.65*(TKN/TP)
2	HAB = 69.3 – 2.079*(TEMP) – 1.616*(TKNsim/TPsim) + 4.32*(TNsim)
3	HAB = 53.94 – 1.716*(TEMP) + 5.022*(TNsim)
	MLR models using observed and simulated predictor variables
4	HAB = 55.71 – 1.976*(TEMP) + 0.4296*(SAL) + 0.01327*(CHL-a) + 4.596*(TKN/TP) – 0.002365*(Q)
5	HAB = 51.26 – 1.872*(TEMP) + 0.1935*(SAL) + 0.01032*(CHL-a) + 3.337*(TKN/TP)
6	HAB = 51.31 – 1.723*(TEMP) + 0.01203*(CHL-a) + 2.572*(TKN/TP)

From the MLR models based on observed data, Model 4 has the greatest R^2 (Table 1) and the t-statistic and P-value for the predictor variables are optimal. Variables TEMP, SAL, TKN and TP, are routinely measured by MDEQ and USGS. CHL-a could be acquired from public-domain NASA imagery [14]. Bonnet Carre inflow rate (Q) can be provided by USACE during spillway openings. Nevertheless, its actual predictive ability must be assessed.

3.3 Using the Developed MLR Models to Predict HAB Sightings

As described earlier, water quality data from stations 1 through 11 were used to generate the MLR models. To assess the predictive ability of the models, water quality data from stations 12B (Biloxi East Central), 14 (Frontbeach), and 15 (Shearwater) were used. Figure 9 shows HAB sighting predictions corresponding to models 4, 5, and 6.

Model 4 is shown to provide limited HAB prediction capability. Although the decreasing trend shown by observed data is replicated, Model 4 overestimates HAB sightings for August and July 2019. Nevertheless, HAB sightings equal or below 10 are predicted acceptably. Models 5 and 6 successfully capture the trend and magnitude of HAB sightings throughout the observation period. The R^2 for these models is also better than the R^2 corresponding to Model 4. Model 6 captures better the magnitude of the HAB sightings which is reflected on its R^2 (0.54). The three models underpredict one HAB sightings for September 2019, being one of those predictions negative. Nevertheless, the occurrence of this false negative can be avoided in future research using

shrinkage methods that apply a penalty term to the loss function embedded in the linear regression to avoid over- and underfitting [15, 16].

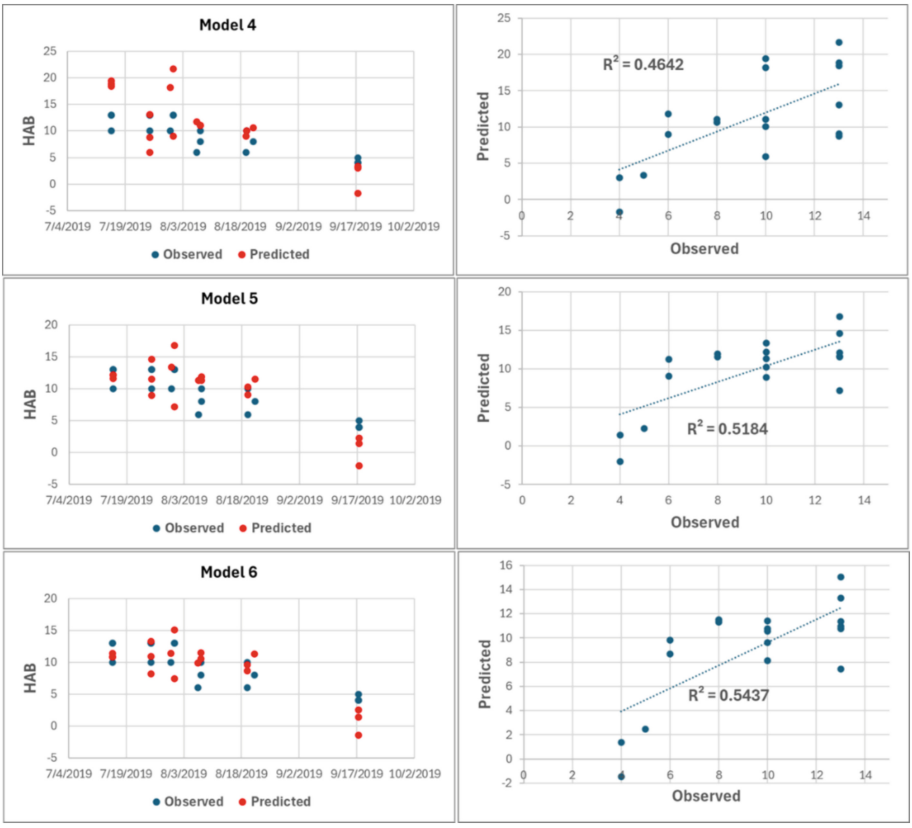

Fig. 9. Prediction of HAB sightings. Model 6 is shown to be the best predictor of HAB sightings.

Between the models that were developed using only observed data, Model 4 showed the best statistical fit (Fig. 8). However, its predictive ability is shown to be limited when compared to models 5 and 6 (Fig. 9). This seems to be a typical case of overfitting. Overfitting may lead to poor generalization of new data [17] because increasing input dimensionality does not necessarily guarantee improved predicting performance [18][19], as shown in Fig. 9.

There have been several modeling approaches to predict HAB which have relied on conventional water quality indicators, such as temperature, and nutrient concentrations but they use chlorophyll-a as the primary response variable [15, 20, 21]. The models presented in this paper predict HAB sightings, which are a closer surrogate to actual HAB concentrations. All the equations shown in Table 3 identify temperature, chlorophyl-a, and nutrients as predictor variables which coincides with previous research on this topic [22–26].

4 Conclusions

Six multiple linear regression (MRL) models based on observed water quality data and simulated water quality data are presented. Fourteen environmental and water quality observed variables (salinity, temperature, chl-a, turbidity, TP, TN, TKN, TOC, TSS, TKN/TP, Biloxi tides, Gulfport tides, St. Joseph tides, Q at Bonnet Carre) and four model-simulated water quality variables (TPsim, TNsim, TKNsim, TKNsim/TPsim) were included in the study. Several combinations of those variables were used to develop the MLR models presented in this paper. The models using only observed data were assessed in their predictive ability of HAB sightings since models dependent on simulated data are costly to be used for water quality management. Model 6, which predictor variables are water temperature, chlorophyll-a, and TKN/TP ratio, is shown to have the best predictive ability.

Acknowledgements. This research was funded by grant: MS GOMESA 2022 MS-363507.

References

1. Alarcon, V.J., Mickle, P.F., Alvarado, R.A.: A Hydrodynamic model of the Mississippi sound. In: Gervasi, O., et al. (eds.) ICCSA 2025. LNCS, vol. 15890, pp. 281–294. Springer, Cham. Springer, Cham (2025). https://doi.org/10.1007/978-3-031-97606-3_19
2. Fennel, K., Laurent, A.: N and P as ultimate and proximate limiting nutrients in the northern Gulf of Mexico: implications for hypoxia reduction strategies. Biogeosciences **15**(10), 3121–3131 (2018). https://doi.org/10.5194/bg-15-3121-2018
3. Sankar, M.S., et al.: Seasonal changes of trace elements, nutrients, dissolved organic matter, and coastal acidification over the largest oyster reef in the western Mississippi sound, USA. Environ. Monitor. Assess. **195**(1) (2023). https://doi.org/10.1007/s10661-022-10719-z
4. Camacho, R.A., Martin, J.L., Watson, B., Paul, M.J., Zheng, L., J.B.: Stribling, modeling the factors controlling phytoplankton in the St. Louis Bay estuary, Mississippi and evaluating estuarine responses to nutrient load modifications. J. Environ. Eng. **141**(3) (2015). https://doi.org/10.1061/(ASCE)EE.1943-7870.0000892
5. Beck, R., Xu, M., Zhan, S., et al.: Comparison of satellite reflectance algorithms for estimating turbidity and cyanobacterial concentrations in productive freshwaters using hyperspectral aircraft imagery and dense coincident surface observations. J. Great Lakes Res. **45**(3), 413–433 (2019). https://doi.org/10.1016/j.jglr.2018.09.001
6. Alarcon and Mickle 2025: A Conceptual Model for Water Quality Simulation in the Mississippi Sound, USA. State of the Coast Conference, New Orleans (2025). https://www.stateofthecoast.org/wp-content/uploads/2025/05/2025_-Session-24_-Vladimir-Alarcon.pdf
7. Pardoe, I.: Applied Regression Modeling. Wiley, New York (2012). https://doi.org/10.1002/9781118345054
8. Wen, J., Yang, J., Li, Y., Gao, L.: Harmful algal bloom warning based on machine learning in maritime site monitoring. Knowl.-Based Syst. **245**, 108569 (2022). https://doi.org/10.1016/j.scitotenv.2024.173546
9. Yu, P., Gao, R., Zhang, D., Liu, Z.-P.: Predicting coastal algal blooms with environmental factors by machine learning methods. Ecol. Indic. **123**, 107334 (2021). https://doi.org/10.1016/j.ecolind.2020.107334

10. Park, J., Patel, K., Hyong Lee, W.: Recent advances in algal bloom detection and prediction technology using machine learning. Sci. Tot. Environ. **938**, 173546 (2024). https://doi.org/10.1016/j.scitotenv.2024.173546
11. Alarcon, V.J., Johnson, D., McAnally, W.H., et al.: Nested hydrodynamic modeling of a coastal river applying dynamic-coupling. Water Resour. Manag. **28**, 3227–3240 (2014). https://doi.org/10.1007/s11269-014-0671-6
12. Alarcon, V.J., et al.: Coastal inundation under concurrent mean and extreme sea-level rise in Coral Gables. Nat. Hazards **2022**, 1 (2022). https://doi.org/10.1007/s11069-021-05163-0
13. Alarcon, V.J., Linhoss, A., Kelble, C., Mickle, P.: Potential challenges for the restoration of Biscayne Bay (Florida, USA) in the face of climate change effects revealed with predictive models. In: Elsevier (ed.) Ocean & Coastal Management, vol. 247, pp. 25–33. Elsevier, Amsterdam (2024). https://doi.org/10.1016/j.ocecoaman.2023.106929
14. Alarcon, V.J., van der Zwaag, J., Moorhead, R.: Estimation of estuary phytoplankton using a web-based tool for visualization of hyper-spectral images. In: 35th IEEE Applied Imagery and Pattern Recognition Workshop (AIPR'06), Washington, DC, USA, pp. 25–25 (2006). https://doi.org/10.1109/AIPR.2006.22
15. Izadi, M., Sultan, M., Kadiri, R.E., Ghannadi, A., Abdelmohsen, K.: A remote sensing and machine learning-based approach to forecast the onset of harmful algal bloom. Remote Sens. **13**(19), 3863 (2021). https://doi.org/10.3390/rs13193863
16. James, G., Witten, D., Hastie, T., Tibshirani, R.: An Introduction to Statistical Learning. Springer, New York (2000). ISBN 978-1-4614-7137-0
17. Yan, Z., Kamanmalek, S., Alamdari, N.: Predicting coastal harmful algal blooms using integrated data-driven analysis of environmental factors. Sci. Total Environ. **912**(2024), 169253 (2023). https://doi.org/10.1016/j.scitotenv.2023.169253
18. Lee, Y.K., Oh, H., Leeb, B.-M., Hur, J.: Deciphering and predicting algal bloom variability using size-fractionated organic matter and machine learning in a complex watershed. Ecol. Indicat. **178**, 114067 (2025). https://doi.org/10.1016/j.ecolind.2025.114067
19. Acuña-Alonso, C., Barba-Barragáns, D., Martínez-Sánchez, J., Álvarez, X.: Predictive mapping of harmful algal blooms with Sentinel-2 imagery and random forest modelling. Water Secur. **27**(2026), 100194 (2026). https://doi.org/10.1016/j.wasec.2025.100194
20. Lee, D., Kim, M., Lee, B., Chae, S., Kwon, S., Kang, S.: Integrated explainable deep learning prediction of harmful algal blooms Technol. Forecast. Soc. Chang. **185**, 122046 (2022)
21. Mermer, O., Zhang, E., Demir, I.: A comparative study of ensemble machine learning and explainable AI for predicting harmful algal blooms. Big Data Cogn. Comput. **9**(2025), 138 (2025)
22. Goldman, J.C., Carpenter, E.J.: A kinetic approach to the effect of temperature on algal growth. Limnol. Oceanogr. **19**, 756–766 (1974)
23. Hallegraeff, G.M.: Ocean climate change, phytoplankton community responses, and harmful algal blooms: a formidable predictive challenge. J. Phycol. **46**, 220–235 (2010)
24. Bricaud, A., Bosc, E., Antoine, D.: Algal biomass and sea surface temperature in the Mediterranean Basin: intercomparison of data from various satellite sensors, and implications for primary production estimates. Remote Sens. Environ. **81**, 163–178 (2002)
25. Errera, R.M., Yvon-Lewis, S., Kessler, J.D., Campbell, L.: Reponses of the dinoflagellate Karenia brevis to climate change: PCO2 and sea surface temperatures. Harmful Algae **37**, 110–116 (2014)
26. Sarma, Y.V.B., Al-Hashmi, K., Smith, S.L.: Sea surface warming and its implications for harmful algal blooms off Oman. Int. J. Mar. Sci. **3**, 65–71 (2013)

Machine Learning Algorithms for Statistical Spatial Analysis of Waste Collection in an Italian Region

Gabriella Schoier(✉) and Giuseppe Borruso

DEAMS – Department of Economic, Business, Mathematic and Statistical Sciences "Bruno de Finetti", University of Trieste, Valerio, 4/1 – 34127, Trieste, Italy
{gabriella.schoier,giuseppe.borruso}@deams.units.it

Abstract. The aim of this paper is to consider machine learning algorithms to analyze the problem of the waste collection of an Italian region. This paper aims to thoroughly analyze data relating to separate waste collection in the Veneto region (Italy) at municipality level for the year 2023. Different variables have been considered.

After solving the problem of cleaning data a descriptive analysis has been done both with a graphical analysis using QGIS software and a statistical analysis using SAS software.

At this point some different machine learning methods has been applied using SAS in particular we used a principal component analysis to reduce the complexity of the phenomenon and then a non hierarchical cluster analysis to use a descriptive method.

The result indicates a constant improvement in the differentiated waste collection in the Veneto region.

Keywords: Machine Learning · Spatial Data Mining · Multivariate Methods · Waste Collection

1 Introduction

In the last decades one of the main problem has been how to extract information from data in our case we consider spatial data [10][1].

Big data analytics could provide opportunities to develop new knowledge to reshape our understanding of different fields and to support decision-making [7].

A huge amount of data i.e. big data have been collected by private and public organizations (see eg. [11]).

Moreover AI is becoming a part of our life and is conditioning our job, private life and social relationships and nowadays is strictly in conjunction with decisions in almost all our life [11].

[1] We are grateful to doctor Jacopo Vergine for the elaborations and the comments.

© The Author(s), under exclusive license to Springer Nature Switzerland AG 2027
O. Gervasi et al. (Eds.): ICCSA 2026 Workshops, LNCS 16761, pp. 557–567, 2027.
https://doi.org/10.1007/978-3-032-30527-5_36

This analysis is connected with the problem of sustainability at urban level that is a crucial economical social and political objective. To analyze the notion of sustainable urban life and to choose appropriate indicators it is necessary to choose appropriate indicators enabling its measurement, this is what the region Veneto try to do [5, 8].

The aim of this paper is to try to explain the development of the waste collection in an Italian region i.e. Veneto region which is in the North-East of Italy, its most known city is Venezia.

Based on the most recent data available, Veneto remains one of Italy's leading waste management regions, with high rates of separate waste collection and a strong focus on the circular economy [1, 4, 5].

The data are collected in the year 2023 by Arpa Veneto (see [1]) and regards different type of waste.

After a cleaning of the data a spatial descriptive statistical analysis as been performed to individuate the main characteristics of the waste different collection.

At this point we consider the possibility of obtain a piece of information by reducing the number of variables using principal component analysis (PCA) (see e.g. [2, 3]).

The results are encouraging as it is possible to give a label to the new variables.

On the base of these new variables a non hierarchical cluster analysis has been performed. The results can be useful to improve different policies.

1.1 The Data and the Variables

The dataset regards the waste collection in the Veneto region in the year 2023.

It contains detailed data relating to the production of municipal waste considering different aspects of waste collection. This dataset contains geographical, graphic and demographic information such as the name of the basin, the name of the municipality and the population, furthermore, for each municipality there are the different types of waste in kilograms. From these data, it is possible to obtain a comparative measure of the waste produced per person in each municipality, allowing for the analysis of waste management efficiency and differences between different locations.

The variables present in the dataset are:

- ISTAT: ISTAT numerical code that uniquely identifies the municipality;
- Territorial basin of the region Veneto for instance Padova Sud, Padova Centro etc.
- Municipality: name of the municipality to which the data refers;
- Population (Popolazione): number of inhabitants residing in the municipality FORSU (organic fraction of urban solid waste) collected
- Green (Verde): kg per capita of plant waste (pruning, grass, mowing) collected
- Glass (Vetro): kg per capita of glass collected in differentiated mode
- Paper and Cardboard: (Carta e Cartone) kg per capita of paper collected
- Plastic (Plastica): kg per capita of plastic collected
- Metal (Metallo): kg per capita of metal waste collected
- Wood (Legno): kg per capita of wooden material collected
- Multimaterial (Multimateriale): kg per capita of wooden material collected

- WEEE (Waste from Electrical and Electronic Equipment): kg per capita of waste from electrical and electronic equipment collected
- Textiles (Tessili) kg per capita collected
- Other Recoverable (Altro Recuperabile) kg per capita collected
- Special wastes (Rifiuti Particolari) kg per capita collected
- Bulky wastes (Ingombrante) kg per capita collected
- Sweeping (Spazzamento) kg per capita collected
- Residue (Residuo) kg per capita collected
- RU (Urban Waste) (Rifiuto Totale): kg per capita of municipal waste generated which includes both the differentiated fraction (RD) and the non-differentiated fraction;
- RD (Differentiated Collection) (Rifiuti Differenziati): kg per capita of waste collected differently, calculated as the sum of the individual fractions, in the municipality
- RUND (Non-Differentiated Urban Waste) (Rifiuti non Differenziati): quantity of indierenziated waste (dry residue) collected in the municipality, i.e. the part of RU excluding the RD.
- Percentage of separate waste collection (% Raccolta Differenziata) kg per capita collected
- Domestic users (Utenze Domestiche) represents the housing units registered in the waste collection service (TARI) as a residential use.

After importing the Excel file into the QGIS software, the data set variables were merged into the spatial layer using the Spatial Joins function.

These modifications allowed us to obtain a dataset ready for the subsequent analysis phases and a shapefile suitable for an exploratory spatial analysis. From this point on, it is also possible to generate geographic visualizations of the distributions of the common seventeen variables using the QGIS Symbology function. The following graphs collected in Fig. 1 illustrate the positive trend in the percentage of separate waste collection in recent years, obtained by downloading and displaying shapefiles for previous years.

The trend reflects effective environmental policies, integrated waste management and a growing awareness of the population, which allowed the Veneto Region, with a total percentage of 77.6%, to exceed both the national average (65.2%) and that of Northern Italy (71.2%) in 2023 [1].

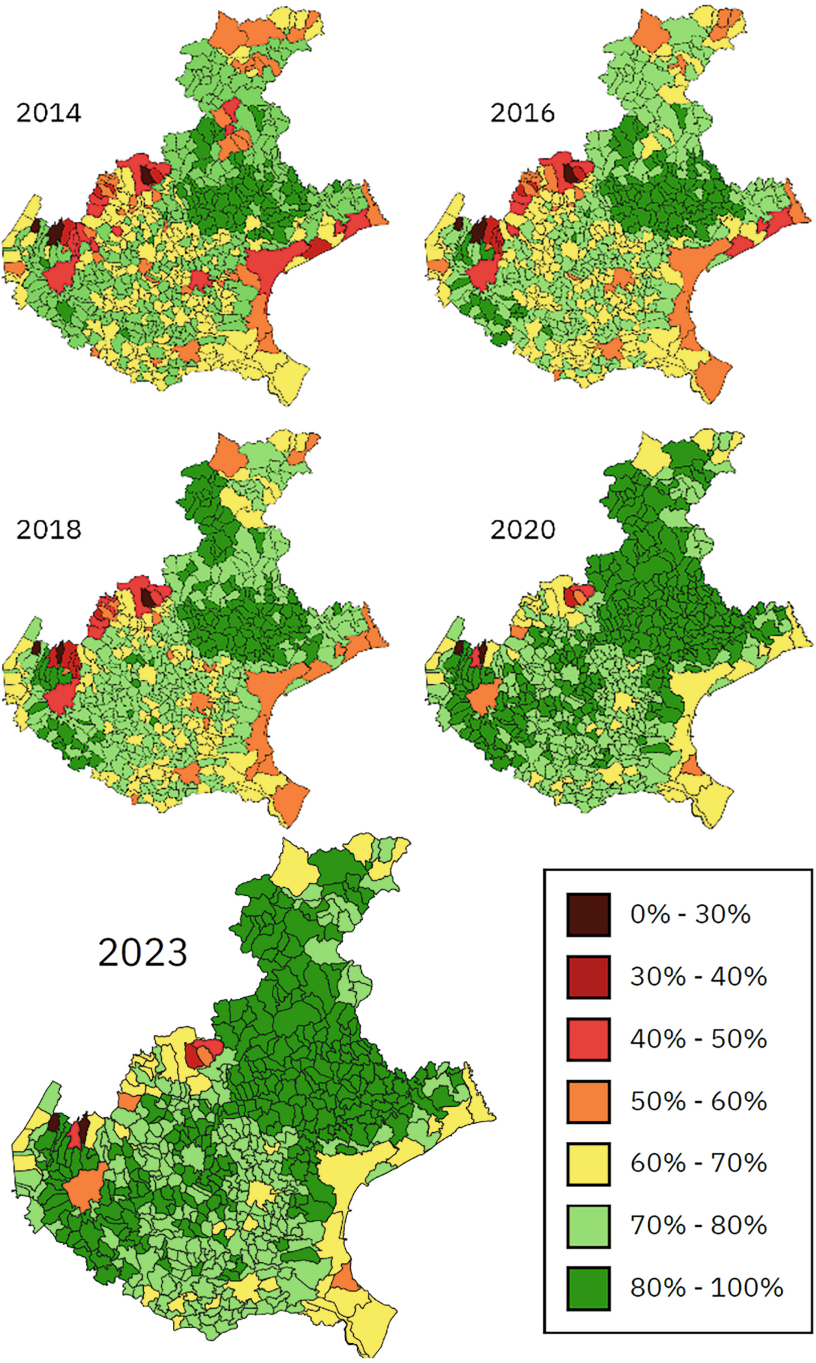

Fig. 1. Maps representation in different years of percentage of differentiated waste

1.2 A Descriptive Spatial Statistical Analysis

In the following we present some descriptive statistical analysis regarding the collected variables (Table 1).

Table 1. Descriptive Statistics

Variable	N	Mean	Median	Std Dev	Minimum	Maximum	1st Pctl	99th Pctl	IQR	Skewness	Kurtosis
Popolazione	563	8647.57	4852	19270.37	126	257213	320	49985	7010	9.95	116.2
FORSU	559	80.16	76.72	25.91	25.52	236.71	32.38	184.76	23.11	1.84	6.34
Verde	552	62.72	55.36	47.18	0.33	514.38	3.63	226.01	50	3.28	22.36
Vetro	531	35.64	36.82	23.88	0.02	207.06	0.27	129.45	11.77	2.33	13.85
Carta e Cartone	562	54.27	50.61	16.77	18.36	160.87	32.39	138.89	14.41	2.79	12.41
Plastica	344	8.63	4.45	12.52	0.01	66.23	0.1	60.09	5.98	2.59	6.28
Metalli	504	6.8	5.22	5.42	0	28.58	0.27	22.78	5.91	1.49	1.75
Multimateriale	553	51.01	40.02	29.24	0.04	205.4	0.36	148.66	26.15	1.71	3.93
RAEE	555	5.88	5.48	2.46	0.02	18.76	1.72	12.17	2.62	1.4	3.73
Tessili	510	3.51	3.25	2.77	0	41	0.12	10.35	2.83	5.42	65.9
Altro Recuperabile	506	21.93	20.39	11.14	0.04	101.84	0.43	52.29	10.65	1.52	6.06
Rifiuti Particolari	559	1.74	1.69	0.83	0.08	5.01	0.31	4.37	0.97	0.97	1.71
Ingombrante	562	18.85	16.92	9.68	1.23	95.9	4.84	54.53	9.78	2.59	12.81
Spazzamento	479	11.47	7.74	12.7	0.28	144.84	0.61	66.5	6.91	4.39	30.87
Residuo	563	89.55	76.87	68.65	23.47	636.95	26.37	434.28	45.39	3.9	20.55
Rifiuto Totale	563	438.89	411.42	155.02	227.75	1685.4	276.42	1305.66	109.22	4.34	25.73
Rifiuti Differenziati	563	353.58	335.38	104.9	161.67	1181.46	188.32	887.85	77.52	3.76	21.91
Rifiuti Indifferenziati	563	85.3	71.57	68.09	19.56	626.74	23.54	417.87	44.81	3.89	20.61
% Raccolta Differenziata	563	0.82	0.82	0.08	0.28	0.95	0.56	0.93	0.1	-1.75	7.73
Utenze Domestiche	522	0.11	0.08	0.12	0	2.1	0	0.44	0.1	8.47	125.72

Although some variations between municipalities fall within the physiological variability expected for this type of indicators, the analysis found marked variability in the distributions of observed values, with standard deviations suggesting, in most cases, strong territorial heterogeneity. This phenomenon is also reflected in the production of total waste, which is characterized by great variability, extreme values that are very far from each other and high values of asymmetry and kurtosis. These elements suggest a notable diversification in local waste gestion behaviors and strategies, with some municipalities deviating significantly from the average. For many variables, moreover, interquartile range (IQR) is high, indicating that within the central 50% of the data there is considerable variability.

The skewness of the distribution is positive for almost all variables, suggesting longer tails to the right due to the presence of a few municipalities with values much higher than the average. The only exception is the percentage of separate waste collection, with negative asymmetry, which indicates that most municipalities are concentrated towards high values. Variables such as Textiles, Sweeping, and Total Waste also exhibit very high kurtosis, suggesting heavy tails.

Other variables, such as WEEE, Metals and Particular Waste present a more "moderate" kurtosis, indicating a distribution closer to a normal one.

We proceeded with a univariate analysis of the distribution of all numeric variables, using the univariate procedure of SAS and the Symbology function of QGIS. Below are the most relevant visualizations and only a few particularly significant variables are analyzed (Fig. 2).

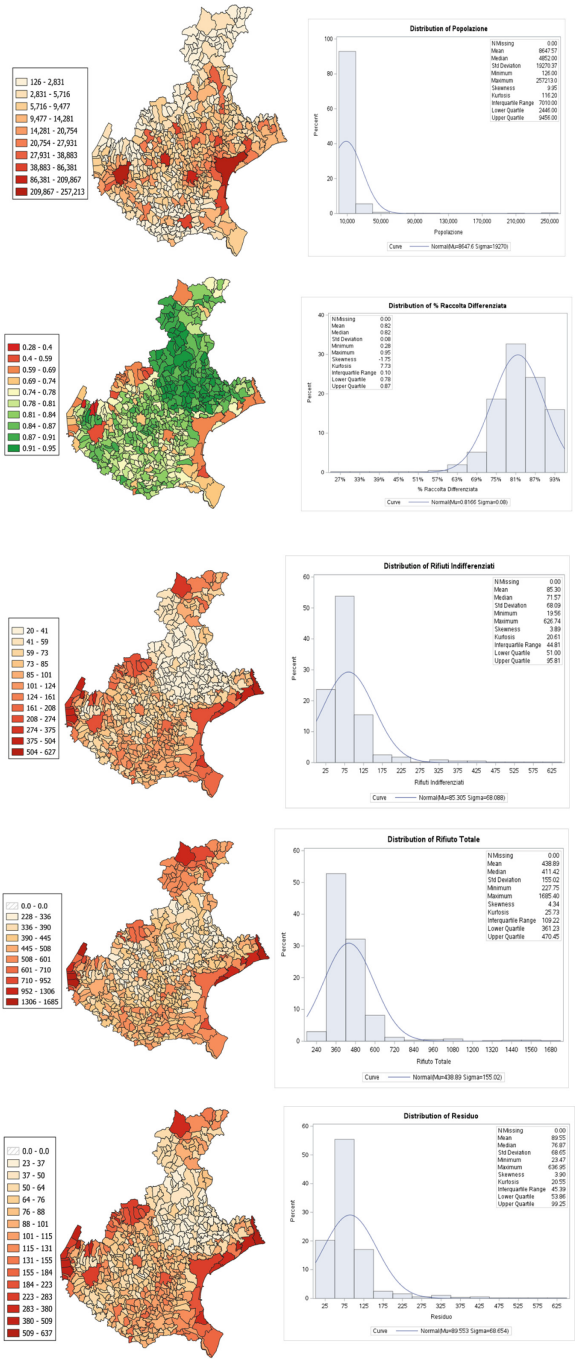

Fig. 2. Maps representation of different types of waste

As already highlighted, the dataset shows considerable heterogeneity between municipalities.

The main variables show highly skewed distributions, with mean values often unrepresentative due to the presence of outliers. Although these are relationships that should be formally analyzed, it is immediately evident, from the visualization of geographical distributions, that the variability in values is often explained by the presence of tourists, morphological factors of the territory, population density and the position of industrial zones.

The distribution of Total Waste Per Capita, for example, reflects population density and tourism. The strong rightward skewness and the heavy tails of the distribution indicate the presence of municipalities with a much higher per capita waste production than the regional average i.e. large cities and tourist resort in which the presence of hotel, restaurants and commercial activities produces waste flows that cannot be assigned to the resident population. For instance the municipalities around Lake Garda, Venice and the coastal areas show very high values of waste.

The percentage of Differentiated Collection has a negative skewness, with most values concentrated at the top of the distribution. The few negative exceptions are related to large cities, which probably present critical issues related to population density, or organization and tourist resorts (in which external influx generates large quantities of waste. Finally, lagoon areas and small mountain and isolated municipalities show difficulties related to logistics which complicates waste management.

The areas with the highest values of residual Waste and undifferentiated waste per capita correspond to tourist cities and, to a lesser extent, to industrial areas and areas where collection services are probably less efficient. Low values, however, correspond to the central Veneto region and part of the Belluno area, where municipalities show good performance thanks to efficient door-to-door collection systems and extensive service coverage.

2 Principal Component Analysis

2.1 Some Results

Principal component analysis (PCA) is a widely used unsupervised dimensionality reduction technique that simplifies complex, high-dimensional datasets into a smaller set of uncorrelated variables the so called principal components trying to retain the maximum variance explained by the original variables.

This methods allows to reduce the dimensionality of the dataset and identify underlying patterns or structures in order to understand which variables explain most of the variability.

In our analysis, all variables relating to the product categories of differentiated and undifferentiated waste were selected. It was decided to exclude the overall totals, since, being sums of the components already present, they are linearly dependent or highly colli-near with the variables used. The variable “Population” has been also excluded, as it is just comprehensive in per capita calculation of the indicators.

The output of the PCA includes several fundamental elements for interpretation. The covariance or correlation if we consider standardized variables matrix describe how the variables in the dataset depend on each other. This is essential in PCA, because

principal components are constructed as linear combinations of variables that explain the maximum possible variance in the dataset and are uncorrelated. In the matrix generated by SAS Studio, strong covariances are noted between some variables, such as Paper.

Conversely, variables such as Green and Textiles show very low or negative covariances, indicating different dynamics (Table 2).

Table 2. Eigenvalues

Eigenvalue	Eigenvalue value	Proportion	Cumulative
1	4.61	0.38	0.38
2	2.74	0.23	0.61
3	1.05	0.09	0.70
4	0.84	0.07	0.77
5	0.66	0.05	0.82

The table shows the eigenvalues of the covariance matrix, each representing the amount of variance explained by each principal component. A high eigenvalue indicates that the corresponding component can explain a significant share of the overall variability of the data set. The eigenvalues indicate that the first component (Prin1) alone explains 38.4% of the variance, the first two components together explain 61.3%, and the first three components reach 70.1%, thus reaching an already considerable threshold. The first five components finally explain l'82.6%, a high share that indicates a good explanation of the initial phenomenon.

Eigenvectors indicate the contribution of each original variable to each component. The values therefore show how the components are built as linear combinations of the original variables moreover these new variables are uncorrelated.

The higher the absolute value of the coefficient, the greater the weight that variable has on the component.

The important thing is if we can understand the meaning of the new variables otherwise these new variables can not be used in subsequent analysis.

In this case:

- Prin1 is characterized by high and positive coefficients for most of the variables, in particular Multimaterial (0.378), WEEE (0.370), Paper and Cardboard (0.354), Recoverable Other (0.349), Metals (0.330), Sweeping, FORSU and Particular Waste. This component effectively synthesizes the overall intensity of separate collection. It could be labelled as *Component of the Complex Differentiated Collection.*
- Prin2 shows the highest coefficients on Green (0.446) and Residue (0.456), while Particular Waste and WEEE show negative values. This dimension seems to reflect a dichotomy between organic or plant-based waste and more technological waste. It can be defined as *Environmental-Organic Component*.
- Prin3 is dominated by the Textiles variable (0.766), the only one to have a high loading, while all the others show values close to zero or negative. This component appears to identify a specific variability related to a rare and inhomogeneous fraction. It can be interpreted as a *Component of Textile Specificity.*

- Prin4 shows high values on Textiles (0.566) and Bulky (0.507), which can be repaired and could indicate occasional or non-systematic waste. It could be seen as a *Component of Special Waste.*
- Prin5 has the highest loads on Sweeping (0.459), Bulky (0.537), Residue (0.252), with opposite directions for other variables. It could represent an *Urban Structural Component*, linked to waste management in urban areas. These labels summarize the structural and territorial significance of the components, and could also be used in subsequent analyses (e.g. regression, clustering, or classification), as well as in spatial mapping for the identification of regional patterns.

The choice to keep up to 5 components is supported by the cumulative curve that consider the explained variance, but for a synthetic and visual analysis, the first 2 or 3 are the most interpretable (Figs. 3 and 4).

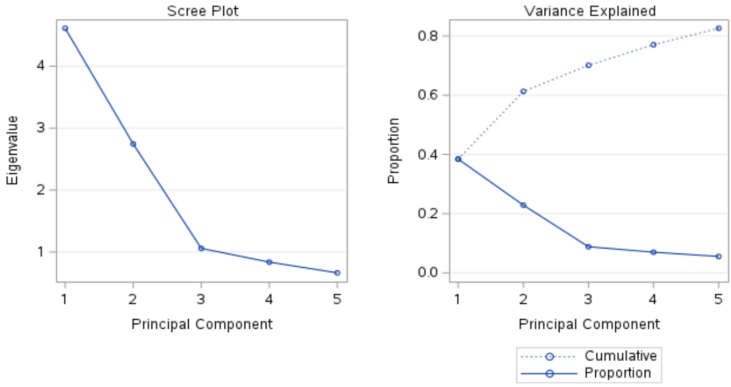

Fig. 3. Scree Plot and Variance Explained

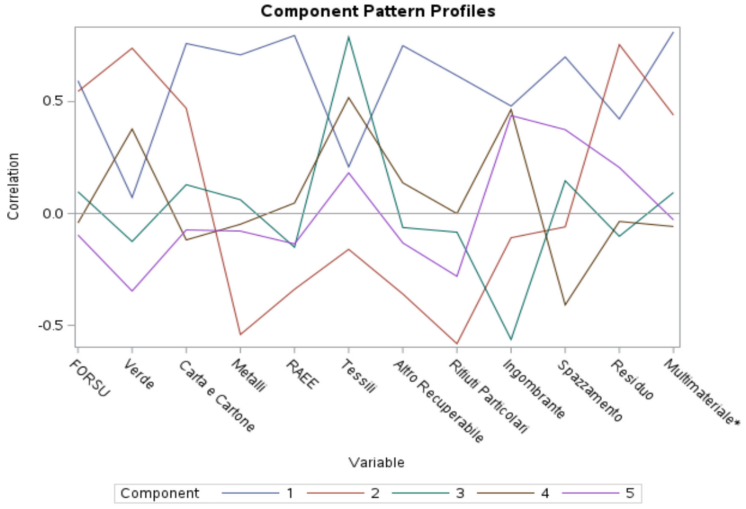

Fig. 4. Component Pattern Profiles

The Component Pattern Profiles graph shows the correlation between each original variable and the first five main components, supporting the interpretation of the new variables.

The colored lines represent the trend of the eigenvectors for each component, highlighting which wastes contribute most to each latent dimension.

The PCA results are overall good and indicate that the analysis is useful, especially considering the socio-ambiental context of the study. The analysis effectively reduced the complexity of the dataset by synthesizing twelve original variables into components components that explain over'82% of the variance.

In particular, the first two components explain over 61% of the total variance, the first three reach 70%, and the first five exceed'82%, allowing for a compact and faithful representation of the data.

The presence of a sharp "elbow" within the scree plot between the second and third components suggests that the first components capture the dominant information in the dataset. The eigenvectors of the principal components finally show a coherent structure: some variables contribute strongly to the first components, suggesting non-random structured patterns, which makes it possible to attribute meaning to the new components as seen.

3 Cluster Analysis

On the base of the results of the PCA a non-hierarchical cluster analysis has been performed [6]. In more details we used a k-means method implemented on SAS platform [9].

The first cluster contains 5 observations among which Cortina d'Ampezzo, its standard deviation is equal to 1,533 and is the highest, so it could be said that this cluster is the least compact. The maximum distance between a point and the center of the cluster is 3.65.

The second cluster contains 23 observations.

The third cluster contains 202 observations it contains 35.88%of the observations.

The fourth cluster contains more than half of the observations, has a frequency of 326 or a percentage of 57.90%. This cluster has a standard deviation less than 1 and is therefore more compact than the other clusters. There is a satisfactory separation since the sum of the r-squares is slightly high.

The fifth cluster contains 7 observations,

As there are a lot of municipalities we just have a look to the observations of the provinces of Belluno and Vicenza.

The province of Belluno has 61 municipalities in particular the municipality of "Cortina d'Ampezzo" is assigned to the first cluster and the remaining 60 municipalities are assigned to the third cluster, the municipality of "Auronzo di Cadore" is the furthest from the center of the cluster since it has the maximum distance between the centroids which is equal to 3.942, the municipality of "Vigo di Cadore" is the closest from the center of the cluster since it has the minimum distance between the centroids which is equal to 0.472, the municipality of "Colle Santa Lucia" is the municipality with the

highest metallurgical index, it is equal to 4.408, the municipality of "Borca di Cadore" is the municipality with the highest organic degradability index, it is equal to 1,962.

The province of Vicenza has 90 municipalities, 8 municipalities are assigned to the second cluster, 20 municipalities to the third cluster and 62 municipalities to the fourth cluster. The municipality of "Calvene" is the furthest from the center of the cluster since it has the maximum distance between the centroids which is equal to 2,733. The municipality of "Orgiano" is the closest from the center of the fourth cluster since it has the minimum distance between the centroids which is equal to 0.552.

4 Conclusions

In this paper we have analyzed data from waste collection in an Italian region i.e. Veneto region, we have also illustrated processes of extraction of information from this kind of data.

The analysis can be extended in various ways, such as applying clustering algorithms on PCA scores, or using the first components as input to predictive models, including classification decision trees. In our case after an application of a principal component analysis we have consider a non hierarchical cluster analysis.

The results show that in the year the citizens' awareness regarding separate collection has increased over time. This has led to an improvement in waste storage conditions.

Moreover the subsequent non hyerachical cluster analysis has show the differences in the municipalities. This is due to the diversity of the territory from coast to mountain and to the presence of art cities.

References

1. Arpa Veneto (2026). https://www.arpa.veneto.it/temi-ambientali/rifiuti/rifiuti-urbani/rifiuti-urbani-2023
2. Bolasco S.: Analisi Multidimensionale dei Dati. Metodi, strategie e criteri d'interpretazione, Carrocci editore, Roma (2005)
3. Gareth J., Witten D., Hastie T., Tibshirani R.: Introduzione all'apprendimento statistico. In: Salini, S., Gaito, S., Boracchi, P., Ambrogi, F., Manzi, G., Biganzoli, E. (eds.) Piccin Editore (2021)
4. ISTAT: Il Censimento permanente della popolazione in Veneto Anno 2023 (2025)
5. ISTAT: Il Benessere Equo e Sostenibile dei Territori: Veneto 2025 (2025). https://www.istat.it/wp-content/uploads/2025/12/BesT2025_Veneto.pdf
6. Jan, A.K.: Data Clustering. 50 years beyond K-means. Pattern Recogn. Lett. 651–666 (2010)
7. Mayer-Schonberger, V., Cukier, K.: Big Data: A Revolution That Will Transform How We Live, Work, and Think. Mariner Books, Boston (2013)
8. Monte, A., Schoier, G.: A Multivariate statistical analysis of equitable and sustainable well-being over time. Soc. Indicat. Res. **161**(2–3), 735–750 (2020)
9. SAS on Demand. https://welcome.oda.sas.com/. Accessed 30 Mar 2026
10. Schoier, G., Borruso, G.: A methodology for dealing with spatial big data. Int. J. Bus. Intell. Data Min. **12**(1), 1–13 (2017)
11. Software Testing Help: Data Mining Vs Machine Learning Vs Artificial Intelligence Vs Deep Learning. http://www.intelligenzaartificiale.it/data-mining/. Accessed 30 Mar 2026

Spatially Targeting the Expansion of Agricultural Land in a Mountainous Catchment for Maximal Sediment Export Avoidance: Heuristic Optimization Considering Spatial Interaction

Pablo Vanegas-Peralta[1,2], René Estrella[3(✉)], Geovanny García[1], Marcelo Peñafiel[1], Patricia Cazorla[1], Elina Ávila-Ordóñez[1], Grethell Castillo-Reyes[4], Gerdys Jiménez-Moya[5], Dirk Roose[6], and Jos Van Orshoven[7]

[1] Research Group Models, Analysis and Simulations, Department of Computer Science, University of Cuenca, Cuenca, Ecuador
[2] Vicerrectorado de Investigación y Posgrado, Escuela Superior Politécnica de Chimborazo (ESPOCH), Riobamba, Ecuador
[3] Department of Computer Science, University of Cuenca, Cuenca, Ecuador
rene.estrella@ucuenca.edu.ec
[4] Center for Computational Mathematics Studies, University of Informatics Sciences, Havana, Cuba
[5] Vice-Rectorate for Academic Affairs, University of Informatics Sciences, Havana, Cuba
[6] Department of Computer Science, KU Leuven, Leuven, Belgium
[7] Division of Forest, Nature and Landscape, Department of Earth and Environmental Sciences, KU Leuven, Leuven, Belgium

Abstract. Vegetation cover has a large impact on the soil loss dynamics of non-sealed, natural surfaces. Forests have meaningful effects on avoiding the production and transport of sediment. In this study, a combination of methods was applied to locate areas within a river catchment in the southern Andes of Ecuador that would produce a maximal or minimal impact on the sediment yield when deforested. RUSLE was applied to compute the amount of local sediment production within the study region. Then CAMF-MFD was used to simulate sediment flow throughout the catchment and to select cells with maximal/minimal impact on sediment yield at the catchment outlet and/or the urban border of the populated area within the catchment. Six scenarios were devised taking all possible combinations of two factors: reference areas (outlet, urban border, or the combination of both), and type of optimization (maximal- or minimal-impact afforested areas that would be converted to agriculture). The outcomes showed the results of CAMF-MFD are in the same order of magnitude as the sediment values obtained by related studies. Additionally, this work provides a means, based on scientifically sound methods, to discriminate between afforested areas that may be converted, in case it is required, to agriculture with a minimum impact on sediment

© The Author(s), under exclusive license to Springer Nature Switzerland AG 2027
O. Gervasi et al. (Eds.): ICCSA 2026 Workshops, LNCS 16761, pp. 568–585, 2027.
https://doi.org/10.1007/978-3-032-30527-5_37

yield, and afforested areas that must not, under any circumstances, be converted to land use types that are less protective to the soil.

Keywords: sediment production · flow and yield · deforestation · heuristic optimization · spatial interaction · CAMF · RUSLE

1 Introduction

Comprehensive land use planning requires the capability to integrate and analyze geospatial data from various sources and to tradeoff between different planning criteria complying with constraints. A specific planning task for which geospatial decision support systems are indispensable is the determination of the optimal sites in a landscape to perform a certain intervention [19,24,36].

Sediment delivery to rivers reduces channel and reservoir capacity and leads to water quality degradation and biodiversity decline because of suspended mineral and organic substances [9]. These issues are particularly undesirable in regions where the river is used as a source of drinking or irrigation water or for electricity production. Moreover, extreme discharge of water and/or sediment in populated places can cause catastrophic floods and mudflows. Forests have proven to be effective to reduce local runoff, sediment production and their downstream discharge and to alleviate the associated water quality decline [6,15,18,31]. Forests protect the soil surface against the ability of raindrops and runoff to detach and transport soil particles [20,33]. Agriculture, on the other hand, favors the detachment of soil particles through erosion and makes the detached materials more susceptible to being transported, especially in sloping landscapes. Therefore, expanding agricultural land use after deforestation will most certainly lead to an increase in local sediment production, transport and delivery to the downstream sedimentation sites and water bodies.

An important planning question for any afforestation or deforestation project is to identify the most suitable sites to plant or remove the trees, i.e. sites on which the objectives are achieved while complying with the constraints with maximal effectiveness. The discrimination between suitable and unsuitable sites for afforestation or deforestation typically depends on criteria adopted by forest managers, which range from maximizing societal and financial profits and minimizing on-site and off-site environmental consequences. In this study we address the selection of initially forested sites within a hydrological catchment with the objective to expand agricultural land while keeping the increase in sediment delivery to the river system and/or to urbanized zones to the minimum. In this way we intended to co-address the abatement of urban mudflows resulting from uncontrolled deforestation and agricultural expansion in peri-urban areas, especially within hilly or mountainous catchments.

As an alternative for exact optimization, [27,29,30] proposed the Cellular Automata for Minimizing Flow (CAMF) heuristic to locate the cells within a rasterized river catchment that should be forested to minimize the amount of sediment that reaches the outlet while accounting for the transport of sediment

between the cells. In this paper, we make use of the multiple flow direction variant of CAMF (CAMF-MFD, [3]). Whereas [3] applied CAMF-MFD in the context of afforestation, we deal for the first time with deforestation which is a pressing issue in Latin America and elsewhere across the globe.

2 Materials and Methods

2.1 The Cellular Automata for Minimizing Flow (CAMF) Heuristic

The original version of CAMF was introduced by [27] and further elaborated and evaluated in a number of case studies by [11,28–30]. CAMF finds the maximum- or minimum-impact cells in a raster dataset through iterative simulation of the local sediment production and flow considering spatial interaction (SI), followed by ranking the cells according to their impact, hence combining simulation and optimization. SI refers to the fact that changes in the state of a location can have an impact on the state of neighboring or even distant locations [13,14,34] so that the effect of an intervention at a particular location cannot be determined independently of the interventions in other locations [13,34]. In the case of CAMF, SI refers to the phenomenon that a land use change in a cell leads to changes of the local sediment production and local sediment transport capacity, which in turn affect the amount of sediment flowing from that cell into its downstream neighbor cells and, eventually, the sediment yield of the whole catchment. Accordingly, due to SI, changing the original land use type of a cell into agriculture will, in most cases, increase the sediment production and sediment transport capacity of that individual cell and, therefore, the sediment that flows into its neighbors and the river system. The original version of CAMF made use of a Single Flow Direction model. CAMF was later elaborated to include a Multiple Flow Direction (MFD) model in [3,10]. Moreover, [4] implemented and evaluated several elaborations of CAMF-MFD to reduce its computational requirements. Figure 1 shows the interaction of the modules for simulation and optimization incorporated in CAMF.

In this study, CAMF-MFD is applied as described and implemented by [3] for modeling sediment flow. In contrast to what was done by [3], where CAMF-MFD was applied to locate a predefined number of cells within a river catchment that should be changed from agriculture or pasture to forest in order to maximize the reduction of the amount of sediment that reaches the catchment outlet, we apply CAMF-MFD to determine the predefined number of cells that must or must not be changed into agriculture so that the increase in sediment delivery is minimized. Besides taking the outlet of the catchment as the reference cell for which sediment yield is to be minimized, we also consider the amount of sediment that is delivered to the cells that are part of the border of the major urban area in the study region.

In Fig. 1, in the preceding paragraph, and throughout the rest of this paper, the term 'local sediment production' refers to the amount of detached soil particles in each cell in each time step (year), while the term 'sediment accumulation' is used to designate locally-produced sediment plus sediment that leaves other

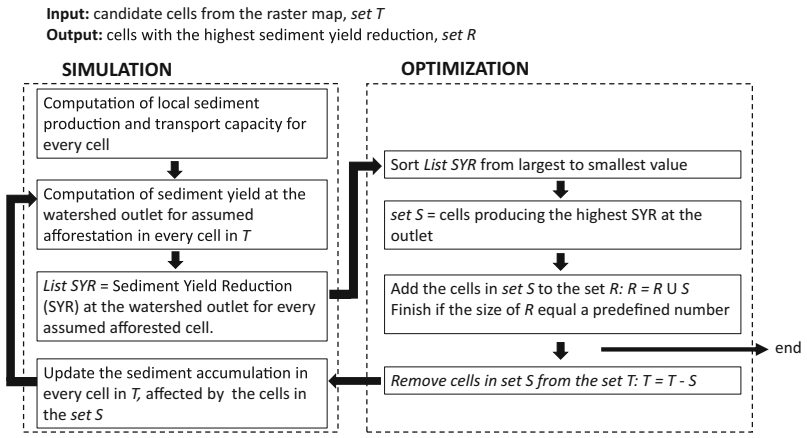

Fig. 1. Modules of CAMF to identify an optimal set of cells in a raster dataset while accounting for spatial interaction.

cells and that is delivered to the current cell. The term 'sediment yield' refers to the amount of sediment accumulation in the outlet cell(s) or in the cells that are part of the urban border. Hence, the only difference between sediment yield and sediment accumulation is that the former refers specifically to sediment accumulated in the outlet or urban border, while the latter refers to sediment accumulated in any cell of the catchment. The concept of 'sediment yield' is equal to what other authors call 'sediment export' or 'sediment loss'. In some cases, the term 'initial' is added as a prefix to indicate that sediment values correspond to the catchment under its initial land use distribution. This is in contrast with a 'final' situation, in which the selected cells are assumed to be converted to agriculture.

2.2 Study Region

The study region was the hydrological catchment of the Cumbe river, located in the province of Azuay, in the southern Andes of Ecuador, South America. The area of the catchment is around 45 km^2 and its altitude ranges from 2600 to 3500 masl. The Cumbe river is a tributary of the Paute river draining a basin, which has an area of 6442 km^2. The Paute river is important for hydropower generation, given that it is used as the source for the main hydroelectric production plants of the country, that generate around 38% of the hydroelectricity in Ecuador.

For the purpose of this study, the Cumbe catchment was represented by means of raster datasets with a resolution of 30×30 m. Figure 2a shows the Digital Elevation Model (DEM) and the river network of the Cumbe catchment while Fig. 2b shows the land use map compiled using data for 2009–2015 and published by the SIGTierras project of the Ecuadorian government (www.sigtierras.gob.ec). Figure 2c shows the location of the Cumbe catchment in the Paute basin and Fig. 2d the location of the Paute basin in Ecuador. The economy of Cumbe

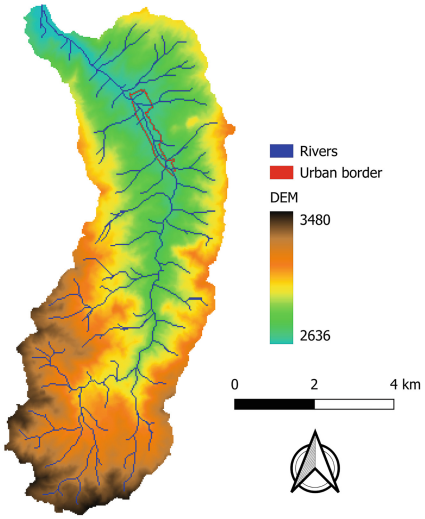

(a) Digital Elevation Model (altitude values in masl), river network and the border of the urban center inf the Cumbe catchment

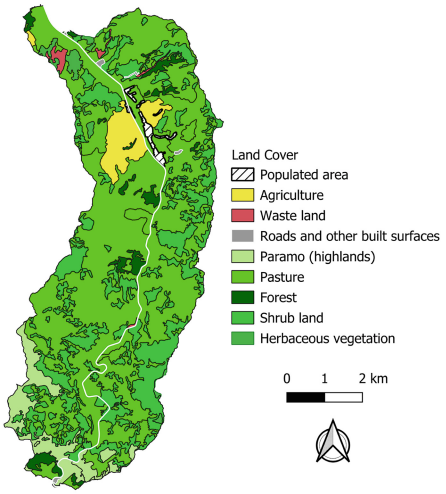

(b) Initial land use distribution in the Cumbe catchment (Source: SIGTierras project of the Ecuadorian government, www.sigtierras.gob.ec)

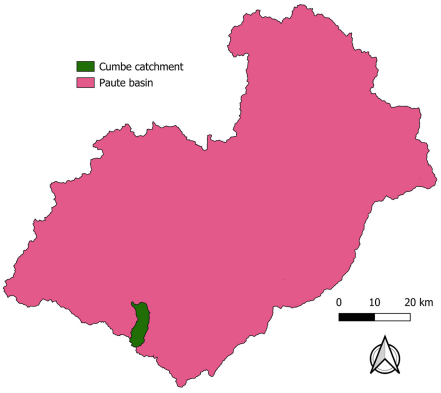

(c) Location of the Cumbe catchment in the Paute river basin

(d) Location of the Paute basin in Ecuador

Fig. 2. The Cumbe geodataset shown in this figure was downloaded from the SIGTierras project of the Ecuadorian government (www.sigtierras.gob.ec), and the geodatasets for the Paute basin and Ecuador were downloaded from the IDE system of Universidad del Azuay (Ecuador) (gis.uazuay.edu.ec).

depends mainly on agriculture and local commerce and is characterized by small markets and businesses.

2.3 Computation of Local Sediment Production

A fundamental input dataset required by CAMF is the local sediment production raster. To compute the local sediment production, the Revised Universal Soil Loss Equation (RUSLE), as proposed by [21], was applied. The RUSLE is shown in Eq. 1.

$$A = R \times K \times LS \times C \times P \tag{1}$$

where:

- R: Rainfall Erosivity factor [MJ mm ha^{-1} h^{-1} yr^{-1}]
- K: Soil Erodibility factor [T ha h MJ^{-1} ha^{-1} mm^{-1}]
- LS: Slope Length and Slope Steepness factor [unitless]
- C: Land Cover and Land Use factor [unitless]
- P: Support Practice factor [unitless]

The resulting soil loss value A (amount of detached soil particles) is expressed in T ha^{-1} yr^{-1}.

Rainfall Erosivity (R Factor). To compute the R factor, Eq. 2 [16,35] was chosen because only monthly precipitation data were available, rather than daily precipitation over a specific period of time as required by other models.

$$R = \sum_{i=1}^{12} 1.735 \times 10^{\left(1.5 \log_{10}\left(\frac{P_i^2}{P}\right) - 0.08188\right)} \tag{2}$$

where:

- R: Rainfall Erosivity factor [MJ mm ha^{-1} h^{-1} yr^{-1}]
- P_i: Precipitation in ith month of considered year [mm]
- P: Annual precipitation [mm]

The monthly precipitation data originate from a hydro-meteorological station located at [LON -79 03' 00", LAT -3 03' 00"] in the Cumbe catchment. Using this dataset as a basis, the R-factor was computed for each year between 1964 and 2016. Following this procedure, an average annual R-value of 413 [MJ mm ha^{-1} h^{-1} yr^{-1}] was found. As a reference, the peak R value of approximately 824 [MJ mm ha^{-1} h^{-1} yr^{-1}] corresponds to 1993, and the lowest value of 124 [MJ mm ha^{-1} h^{-1} yr^{-1}] was occurred in 1980. The calculated R factor for the Cumbe meteorological station is significantly lower when compared to many other rainfall stations in the Andes (cf., for example, [5]), which is due to relatively low monthly precipitation values.

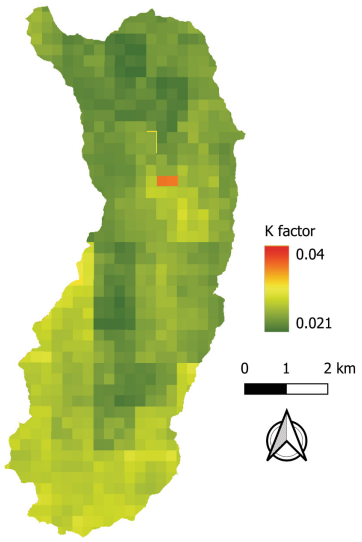

(a) K factor (resolution 250x250m) computed using Eq. 3 and the SoilGrids 2.0 database

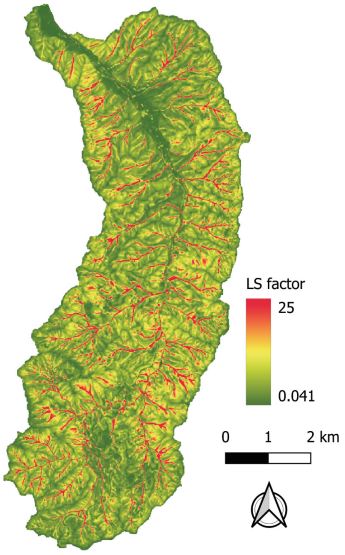

(b) LS factor (resolution 30x30m) computed using Eq. 6 and the Digital Elevation Model

Fig. 3. K and LS factors for the Cumbe catchment.

Soil Erodibility (K Factor). To compute the K factor for the RUSLE, Williams' equation (Eq. 3) was applied. Details of this formulation can be found in [22].

$$K = 0.1317 \times f_{csand} \times f_{cl-si} \times f_{orgc} \times f_{hisand} \tag{3}$$

where:

- K: Soild erodibility factor [T ha h MJ^{-1} ha^{-1} mm^{-1}]
- f_{csand}: Sand and silt content in the topsoil [%]
- f_{cl-si}: Silt and clay content in the topsoil [%]
- f_{orgc}: Organic carbon content in the topsoil [%]
- f_{hisand}: Sand content in the topsoil [%]

The required data to apply Williams' equation were retrieved from the Soil Grids database version 2.0 (http://soilgrids.org). This database with global coverage offers soil characteristics at a 250×250 m resolution as derived from a machine learning approach. The considered depth of the topsoil was between 0 and 5 cm. The result is one K factor value for every cell, as shown in Fig. 3a.

Slope Length and Steepness (LS Factor). The Digital Elevation Model (DEM, 30×30 m) was the main input to compute the LS factor. The slope

length factor (L) was computed by means of the Desmet and Govers equation (Eq. 4).

$$L_{(i,j)} = \frac{\left[A_{(i,j)} + D^2\right]^{m+1} - A_{(i,j)}^{m+1}}{x^m D^{m+2} (22.13)^m} \tag{4}$$

where:

- $L_{(i,j)}$: Slope length factor in cell (i, j)
- $A_{(i,j)}$: Flow accumulation in cell (i, j)
- D: Pixel size
- x: Size coefficient (x = 1)
- m: Slope length exponent

The slope steepness factor (S) was computed using the piecewise function in Eq. 5.

$$S_{(i,j)} = \begin{cases} 10.8 \sin\theta + 0.03 & \text{if slope} < 9\% \\ 16.8 \sin\theta - 0.5 & \text{if slope} \geq 9\% \end{cases} \tag{5}$$

The final unitless LS factor was then computed by Eq. 6.

$$LS_{(i,j)} = L_{(i,j)} \times S_{(i,j)} \tag{6}$$

The resulting LS raster is shown in Fig. 3b. Its resolution is 30×30 m.

Cover Management (C Factor). Table 1 presents the values that were assigned to the C factor corresponding to each of the land use types found in the Cumbe catchment (see Fig. 2b).

Table 1. C factor value assigned to each land use type in the Cumbe catchment before (Initial C factor) and after (Final C factor) converting it to agriculture [10].

Land use type	Initial C factor	Final C factor
Populated area	0	0
Agriculture	0.2	0.2
Waste land	0.01	0.01
Páramo	0.0005	0.2
Pasture	0.003	0.003
Forest	0.001	0.2
Shrub land	0.003	0.2
Herbaceous vegetation	0.003	0.2

The lower C factor values in Table 1 express the presence of a protective artificial ('urban') or semi-natural cover ('vegetation') that reduces the production and transport of sediment (e.g., páramo, and forest). High C factor values correspond to land use types on which larger amounts of detached soil particles are available to be transported (e.g., agriculture). The column "Initial C factor" indicates the C factor values corresponding to the original land cover of the Cumbe catchment. The column "Final C factor" indicates the C factor values after deforestation/remove of vegetation (change into agriculture), for the land use types that can be deforested, that is, páramo, forest, shrub land and herbaceous vegetation. Cells in urban zones, waste land and grassland are not considered as candidates for removal of vegetation/deforestation; hence the final C factor value is the same as the initial value.

Conservation Support Practice (P Factor). The P factor represents the impact of local practices implemented to mitigate soil erosion. These practices can include terraces, contour farming, vegetative strips, or any other soil management techniques designed to reduce erosion. Such practices are not found in the Cumbe catchment. Therefore, in our application of the RUSLE equation, the P factor was set to 1. This value indicates that soil erosion is computed without any modification or benefit from conservation measures.

Average Annual Local Sediment Production (A). Once all RUSLE-factor datasets were computed, their resolution was uniformized by means of an upsampling procedure based on interpolation. Specifically, the datasets obtained from the Soil Grids database, whose original resolution was 250×250 m were upsampled to 30×30 m in order to make their resolution coincide with the other datasets. Next the RUSLE equation was applied to obtain the initial local sediment production for each cell in the rasterized representation of the Cumbe catchment (Fig. 4a). As expected, the agricultural zones and flanks of the river valleys stand out as the major sediment producing areas.

2.4 Computation of Transport Capacity (TC)

After computing the amount of detached soil particles available in each cell (Fig. 4a), the fraction of those particles that would effectively leave the cell as well as the fraction retained were computed. To this end, it was required to model the amount of sediment that flowing water can transport under specific hydrodynamic conditions, i.e. the sediment load. The Transport Capacity (TC) is defined as the maximum sediment load that can be transported from one cell to another in a given time step, i.e. one year. The TC acts as a threshold: the fraction of the total amount of local sediment in a cell that is below the TC will be transported and delivered to its neighbors, while the local sediment amount exceeding the TC value will be retained. The equation employing three of the factors used in the RUSLE (i.e., the R-, K- and LS-factors) proposed by [25,26]

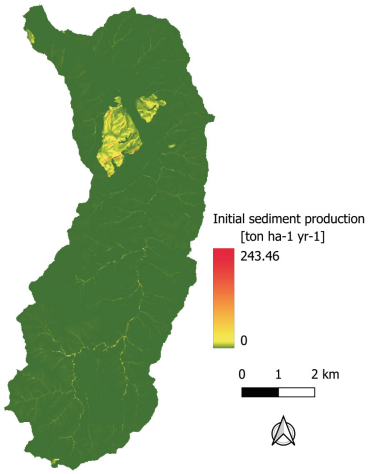

(a) Initial local sediment production computed using RUSLE

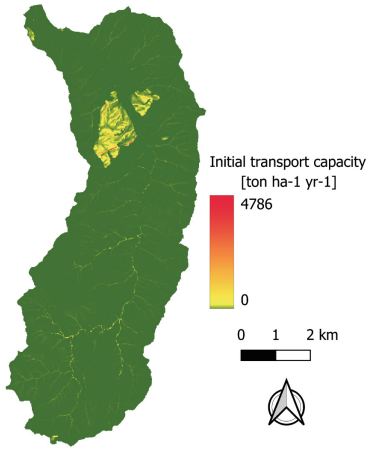

(b) Transport capacity dataset computed using Eq. 7

Fig. 4. Local sediment production and transport capacity before deforestation for the Cumbe catchment.

was applied to compute the transport capacity in conditions with limited data available (Eq. 7).

$$TC = kTC \times K \times R \times T \tag{7}$$

where:

- TC: Transport Capacity [T ha^{-1} yr^{-1}]
- kTC: Transport capacity coefficient [m]
- R: Erosivity factor [MJ mm ha^{-1} h^{-1} yr^{-1}]
- K: Erodibility factor [T h MJ^{-1} mm^{-1}]
- T: Topographic factor [unitless]

The topographic factor was calculated using Eq. 8 [3].

$$T = LS - 4.12S_g^{0.8} \tag{8}$$

where LS is the slope length and steepness factor (unitless) and S_g is the normalized slope (unitless).

The kTC coefficient is a piecewise function of the C factor value (Eq. 9). To this purpose, a threshold value, kTC_{limit}, needs to be defined.

$$kTC_i^k = \begin{cases} kTC_{Low}, & \text{if } \zeta_i^k \leq kTC_{limit} \\ kTC_{High}, & \text{if } \zeta_i^k > kTC_{limit} \end{cases} \tag{9}$$

where ζ_i^k is the C factor for cell i before (k = 1) and after (k = 2) changing its land use type.

Based on the reasoning described in [2], the value for kTC_{limit} was set to 0.01 in line with [8], while the value for kTC_{Low} was set to 0.04 and kTC_{High} was set to 4, following [32].

The TC value for each cell was computed by means of Eq. 7, 8 and 9 at a resolution of 30×30 m. The resulting TC dataset is shown in Fig. 4b.

2.5 Scenarios

The CAMF-MFD-heuristic was applied to select the cells in the Cumbe catchment for which the replacement of the natural vegetative cover by agricultural fields would lead to minimal and maximal increase of the sediment yield at the outlet of the catchment as well as through the cells representing the perimeter of an urbanized settlement. Sediment export is a process subject to spatial interaction since it is the result of local production and displacement of soil particles along topographical flow paths governed by each cell's transport capacity.

The term 'candidate cells' stands for a subset of the cells representing the Cumbe catchment of which the land use type can potentially be changed to agriculture. In this study, cells under forest, pàramo, shrublands and herbaceous vegetation were considered as the candidates.

All input datasets of the CAMF-MFD heuristic are rasterized representations of the Cumbe catchment. Datasets are in a resolution of 30×30 m, and each raster comprises 429 (width) × 194 (height) cells. These settings result in a total of 83226 cells of which 16412 (19.7%) are considered as candidates for agricultural expansion. The problem to be solved is a combinatorial optimization problem whereby the cells to be selected are an optimal subset taken from the candidate cells.

Six different scenarios were studied:

1. Select a subset of candidate cells (total number of candidate cells: 16412), that is, 5% (821 cells), 10% (1641 cells), 15% (2462 cells) and 20% (3282 cells), that would produce a **maximum** increase in sediment reaching the **outlet** when converted to agriculture.
2. Select a subset of candidate cells, that is, 5%, 10%, 15% and 20%, cells that would produce a **minimum** increase in sediment reaching the **outlet** when converted to agriculture.
3. Select a subset of candidate cells, that is, 5%, 10%, 15% and 20%, that would produce a **maximum** increase in sediment reaching the **urban boundary** when converted to agriculture.
4. Select a subset of candidate cells, that is, 5%, 10%, 15% and 20%, cells that would produce a **minimum** increase in sediment reaching the **urban boundary** when converted to agriculture.
5. Select a subset of candidate cells, that is, 5%, 10%, 15% and 20%, cells that would produce a **maximum** increase in the total sediment reaching both the outlet and the **urban boundary** when converted to agriculture.

6. Select a subset of candidate cells, that is, 5%, 10%, 15% and 20%, cells that would produce a **minimum** increase in the total sediment reaching both the outlet and the **urban boundary** when converted to agriculture.

3 Results

3.1 Sediment Yield Before Deforestation

In the first stage, CAMF-MFD was executed to determine the amount of sediment delivered to the outlet of the catchment and/or the urban border under the original land use distribution (before deforestation). The computed sediment yield at the outlet was 2678.2 T yr^{-1}, at the urban border was 2596.31 T yr^{-1}, and the amount of sediment yield at both the outlet and the urban border combined was 2790.75 T yr^{-1}. The combined value of sediment yield shows that part of the sediment that is delivered to the urban border leaves those cells and eventually end up at the outlet cells. This is the reason why the combined sediment yield is not equal to the sum of sediment yield at the outlet and at the urban border. We can, therefore, infer that most of the sediment that reaches the outlet passes through the urban border. This behavior was expected, considering that the urban area in the Cumbe catchment is located in the valley along a segment of the river that is relatively close to the outlet. Additionally, the urban area is surrounded by agricultural parcels, which are among the main producers of sediment (see Fig. 2b and 4a).

[17] reports values of sediment yield for watersheds around the world that are between 0.01 and 64 T ha^{-1} yr^{-1}. [17] reports sediment yield levels of 6.74 and 5.97 T ha^{-1} yr^{-1} for the Tomebamba and Yanuncay watersheds respectively, which like the Cumbe watershed are located in the Paute river basin. It is evident that the diversity of sediment yield levels is a consequence of the characteristics of a watershed, e.g., land use, topography, rainfall depth, among others. The computed sediment yield values are in the order of magnitude of the data reported by [17]. The initial combined sediment yield in the Cumbe catchment (4500 Ha) reaches 2790.75 T yr^{-1}, that is, 0.62 T ha^{-1} yr^{-1}. This rather low sediment yield is explained by the fact that Cumbe is a well-preserved small watershed with most of its area covered by moorland, grassland, herbaceous vegetation, and shrub land. Another aspect that greatly influences these relatively low sediment yield values is the low rainfall erosivity (R factor) that was estimated for the Cumbe catchment using the precipitation dataset of the only meteorological station available in this region.

3.2 Scenarios 1, 3 and 5: Cells that Would Produce a Maximum Increase in Sediment When Converted to Agriculture

Table 2 shows the amount of sediment that would be delivered to the i) catchment outlet, ii) urban border, and iii) both the outlet and urban border combined when the land use type of 5, 10, 15, and 20% of the candidate cells is converted to agriculture (i.e., after deforestation). The values in the columns labeled as

'Sediment Increase' correspond to the number of extra tons per year with respect to the values obtained under the original land use distribution (Sect. 3.1). The values in the columns labeled as 'Sediment Yield' correspond to the sum of the amount of sediment under the original land use distribution in Sect. 3.1 plus the sediment increase values of Table 2.

Table 2. Results for Scenarios 1, 3 and 5 expressed in T yr^{-1}. For sediment increases, both absolute and relative (percentages between brackets with regard to values under initial land distribution) are reported

	Sediment Yield				Sediment Increase			
% selected	5%	10%	15%	20%	5%	10%	15%	20%
Outlet	5534.37	6582.82	7295.06	7769.51	2856.17 [107%]	3904.32 [146%]	4616.86 [172%]	5091.30 [190%]
Urb. border	5322.05	6294.51	6930.84	7318.67	2725.74 [105%]	3698.20 [142%]	4334.53 [167%]	4722.37 [182%]
Combined	5648.13	6696.60	7409.40	7884.48	2857.38 [102%]	3905.85 [140%]	4618.64 [165%]	5093.72 [183%]

Table 2 shows that there is an increase of more than 100% in the sediment yield in all scenarios. The sediment yield increase percentage decreasingly increases with increasing number of deforested candidate cells, and it approaches 200% when the percentage of deforested candidates is 20%. In all these scenarios, the closer a cell is to a riverbed, the more likely it is to be selected. Additionally, the C factor assigned to each land use type for the RUSLE equation (Table 1) has a fundamental effect regarding which cells are selected, for instance many maximum-impact cells correspond to páramo (land use type with minimum C factor and hence largest difference in C factor value compared to agriculture).

In Fig. 5 (results for Scenarios 1, 3 and 5), a lot of similarities can be observed between the outcomes for the river outlet and the urban border. This is mainly due to the intersection of the urban border and the river plus the fact that most of the cells around the urban border are already under agriculture.

Cells with maximum impact must not be converted to agriculture. Doing so would produce a large increase in the amount of sediment that is delivered to the river, with the corresponding negative consequences for drinking water provision, hydroelectricity production and biodiversity. Furthermore, converting these cells to agriculture would result in large amounts of sediment reaching the urban border, which considerably increases the risks of mudflows which is a recurring problem in Ecuador (e.g. [23]).

3.3 Scenarios 2, 4 and 6: Cells that Would Produce a Minimum Increase in Sediment When Converted to Agriculture

These scenarios were explored with CAMF-MFD in order to determine the areas (cells) that would produce a minimum impact on sediment yield increase at the outlet, the urban border, and in the combination of both if converted into agriculture. The results show that the selected cells would produce a negligible

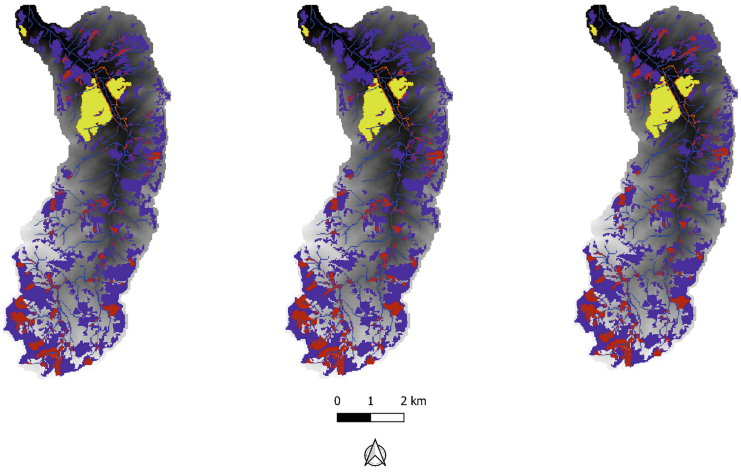

Fig. 5. Cells (20% of the candidates) with maximum impact (brown-red) regarding the increase in sediment delivered to the i) river outlet (left), ii) to the urban border (center), and ii) both outlet and urban border (right). Increasing elevation of each cell is indicated by a lighter gray shade. Purple cells indicate non-selected candidates. Yellow cells indicate the areas that were originally under agriculture. The river network is shown in blue, and the urban border is indicated in orange. (Color figure online)

increase in sediment delivery compared to the values in under the original land use distribution (Sect. 3.1). Therefore, in practice, at least 20% of the candidate cells can be converted from their original land use type to agriculture resulting in a negligible sediment delivery increase both at the outlet and at the urban border. These minimum-impact candidate cells may be converted to agriculture in case it is required.

Figure 6 (results for Scenarios 2, 4 and 6) shows that most cells with almost-zero-impact in sediment delivery to the catchment outlet (left) are located away from the river, which indicates the importance of the role of the river when considering the outlet as the target for our analysis. Specifically, the further away a cell is located from the river, the more likely is that the sediment leaving this cell will find "barriers" in its path to the river, where sediment will be retained. Additionally, most cells under páramo (see Fig. 2b) do not belong to the set of cells with minimum impact, which confirms that it is preferable to avoid human intervention on cells with large differences between the initial and the final C factor value, also when they are located far away from the rivers. This finding comes on top of the inherent value and importance of páramo for several other ecosystem services like water provision and biodiversity conservation as mentioned in [1,12]. In Fig. 6 (center) (cells with minimum impact to the urban border), most selected cells are located down-slope from the urban area, which is in agreement with intuition: changes in the land use type of such cells will not have any impact on cells up-slope, including the urban boundary. The map

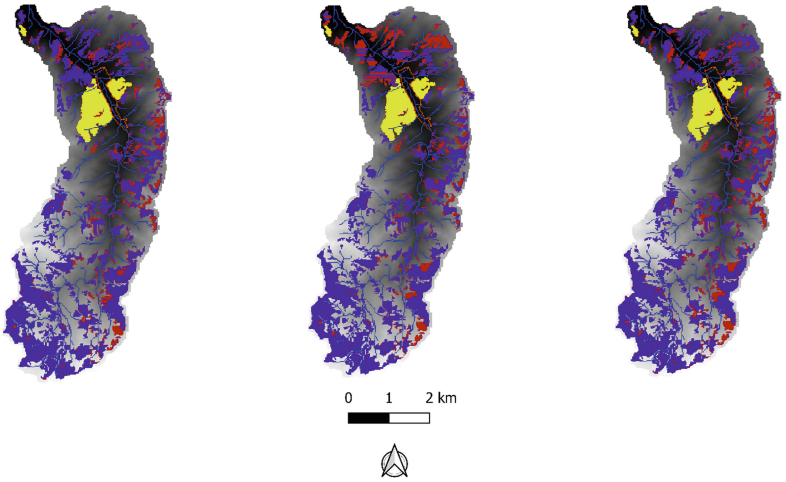

Fig. 6. Cells (20% of the candidates) with minimum impact (brown-red) regarding the increase in sediment delivered to the i) river outlet (left), ii) to the urban border (center), and iii) both outlet plus urban border (right). Increasing elevation is indicated by a lighter gray shade. Purple cells indicate non-selected candidates. Yellow cells indicate the areas that were originally under agriculture. The river network is shown in blue, and the urban border is indicated in orange. (Color figure online)

in Fig. 6 (right) (combined effects on both outlet and urban border) is quite similar to the map in Fig. 6 (left) (only outlet), which indicates that most cells with impact on the sediment delivery at the outlet clearly also impact the urban border.

4 Discussion and Conclusions

To increase the accuracy on the computation of the amount of sediment delivered, CAMF-MFD should include information about the contribution from unpaved roads and footpaths and from any other important sediment sources and channels (cf. [7]). Regarding the simulation process, the input data used to compute the R factor for the RUSLE were based on annual average rainfall in one station while a year-to-year and spatial variability of this factor would be more realistic. In case of afforestation the effects produced by this land use change will evolve through time. This holds but to a lesser extent also for deforestation, due to regrowth of vegetation after removal of the trees. This behavior is not currently implemented in CAMF-MFD.

In this study, the increase or decrease of sediment yield was the only criterion considered for the selection of optimal cells. Clearly, other environmental and socio-economic aspects would be of interest for simulation and optimization, such as maximization of water retention in forests and minimization of water

reaching riverbeds for land use planning. Likewise, CAMF can also consider a limited monetary budget for afforestation as a constraint.

This paper showed that CAMF-MFD is not only applicable to 'Where to afforest?' planning problems but also to questions like 'Where to deforest?' or 'Where to expand agriculture?' with minimization of sediment export from the catchment and/or minimization of sediment influx in urbanized areas as the objective function. The power of the iterative simulation followed by ranking approach implemented in CAMF-MFD is reflected in the speed of execution, the ranking of the selected cells aiding in priority setting and the possibility to extend it with region growing, financial and ecological budget constraints, and additional criteria beyond sediment delivery, both off-site and on-site.

The located cells that would produce a maximum sediment increase when its land use is converted to agriculture show that when the distance from a cell to the riverbed is short, the probability of that cell being selected is high. Therefore, changing the land use of those cells to agriculture would result in big amounts of sediment reaching the river outlet or the urban border, which considerably increases the risk of mudflows. Additionally, in these scenarios, land cover plays a fundamental role in the cells being selected. This is inferred from the fact that many maximum impact cells correspond to moorland (páramo).

In scenarios where minimum impact cells are to be selected, many of these cells produce no increase whatsoever in sediment yield when deforested. These cells should be considered first when an expansion of the agricultural land is deemed necessary. Additionally, the further away a cell is located from the riverbed, the more likely the sediment leaving this cell is to find "barriers" in the cell-to-river path.

Given that CAMF-MFD is a heuristic to identify sets of optimal cells in the presence of spatial interaction, it requires the integration of simulation processes for local sediment production and transport. The results show that both the optimization and simulation capabilities of CAMF-MFD and its computational performance are sufficiently promising to warrant further testing and elaboration to achieve a robust capability to identify regions in which an intervention (e.g., afforestation/deforestation) is to be applied without neglecting the spatially interactive nature of the impacts of the intervention.

References

1. Buytaert, W., Iñiguez, V., Celleri, R., De Biévre, B., Wyseure, G., Deckers, J.: Analysis of the water balance of small Páramo catchments in South Ecuador. In: Krecek, J., Haigh, M. (eds.) Environmental Role of Wetlands in Headwaters – NATO Science Series: IV: Earth and Environmental Sciences, vol. 63, pp. 271–281. Springer, Dordrecht (2006). https://doi.org/10.1007/1-4020-4228-0_24
2. Castillo-Reyes, G.: Extension and acceleration of the CAMF approach to select optimal intervention sites in the presence of spatial interaction. Ph.D. thesis, Belgium (2024)
3. Castillo-Reyes, G., Estrella, R., Gabriels, K., Van Orshoven, J., Abrams, F., Roose, D.: Selecting sites for afforestation to minimize sediment loss from a river basin: computational complexity of single and multiple flow direction methods in raster databases. Comput. Geosci. **171**, 105269 (2023)

4. Castillo-Reyes, G., Estrella, R., Roose, D., Abrams, F., Jimenez-Moya, G., Van Orshoven, J.: Spatially targeted afforestation to minimize sediment loss from a catchment: an efficient hill climbing method considering spatial interaction. Environ. Model. Softw. **176**, 106000 (2024)
5. Cisneros, P.: Mapping of soil erosion risk zones in a part of the watershed of Rio Paute (Ecuador). Master's thesis, Belgium (1999)
6. Costin, A.: Runoff and soil and nutrient losses from an improved pasture at Ginninderra, Southern Tablelands, New South Wales. Aust. J. Agric. Res. **31**(3), 533–546 (1980)
7. De Meyer, A., Poesen, J., Isabirye, M., Deckers, J., Raes, D.: Soil erosion rates in tropical villages: a case study from lake Victoria Basin, Uganda. CATENA **84**(3), 89–98 (2011)
8. Deproost, P., Renders, D., Van de Wauw, J., Van Ransbeeck, N., Verstraeten, G.: Herkalibratie van watem/sedem met het dhmv-ii als hoogtemodel. eind-rapport, Departement Omgeving, Brussel (2019)
9. Drzewiecki, W., Mularz, S.: Simulation of water soil erosion effects on sediment delivery to Dobczyce Reservoir. Int. Arch. Photogramm. Remote. Sens. Spat. Inf. Sci. **37**, 787–794 (2008)
10. Estrella, R.: Where to afforest? Single and multiple criteria evaluation methods for spatio-temporal decision support, with application to afforestation. Ph.D. thesis, Belgium (2015)
11. Estrella, R., Vanegas, P., Cattrysse, D., Van Orshoven, J., RÃžckemann, C.P., Doytsher, Y.: Trading off accuracy and computational efficiency of an afforestation site location method for minimizing sediment yield in a river catchment. In: Proceedings of GEOProcessing 2014: The Sixth International Conference on Advanced Geographic Information Systems, Applications, and Services, pp. 94–100. International Academy, Research, and Industry Association (IARIA) (2014)
12. García, V.J., Márquez, C.O., Rodríguez, M.V., Orozco, J.J., Aguilar, C.D., Ríos, A.C.: Páramo ecosystems in Ecuador's southern region: conservation state and restoration. Agronomy **10**(12), 1922 (2020)
13. Gersmehl, P.: Spatial interaction. J. Geogr. **69**(9), 522–530 (1970)
14. Hayes, M.C., Wilson, A.G.: Spatial interaction. Socioecon. Plann. Sci. **5**(1), 73–95 (1971)
15. Heil, G.W., Muys, B., Hansen, K.: Environmental Effects of Afforestation in North-Western Europe: From Field Observations to Decision Support, vol. 1. Springer, Cham (2007). https://doi.org/10.1007/1-4020-4568-9
16. Maurya, N.K., Tanwar, P.S.: Estimation of temporal r-factor based on monthly precipitation data. J. Phys: Conf. Ser. **1** (2021). IOP Publishing
17. Mora, D.: Actualización del conocimiento sobre la producción de sedimentos a diversas escalas en la cuenca hidrográfica del Río Paute. Master's thesis, Ecuador (2005)
18. Nearing, M., et al.: Modeling response of soil erosion and runoff to changes in precipitation and cover. CATENA **61**(2–3), 131–154 (2005)
19. Nguyen, L., Chou, T.Y., Fang, Y.M., Lin, F.C., Van Hoang, T., Huang, Y.M.: Optimal site selection for land use planning: a comparison between two approaches of fuzzy analytic hierarchy process and fuzzy analytic network process. In: Proceedings of International Conference on Engineering and Natural Science (2017)
20. Piégay, H., Walling, D.E., Landon, N., He, Q., Liébault, F., Petiot, R.: Contemporary changes in sediment yield in an alpine mountain basin due to afforestation (the upper Drôme in France). CATENA **55**(2), 183–212 (2004)

21. Renard, K.G., Foster, G.R., Weesies, G.A., Porter, J.P.: Rusle: revised universal soil loss equation. J. Soil Water Conserv. **46**(1), 30–33 (1991). https://doi.org/10.1080/00224561.1991.12456571
22. Rodríguez-Pinargote, L.F., Pico-Quijije, J.H., Delgado, D.: Análisis de la distribución espacial de la erodabilidad del suelo en la cuenca del río portoviejo-ecuador. Dominio de las Ciencias **10**(1), 1313–1327 (2024). https://doi.org/10.23857/dc.v10i1.3777, https://dominiodelasciencias.com/ojs/index.php/es/article/view/3777
23. SNGR: Informe de situación aluvión quito - la gasca (31/01/2022). Technical report, Secretaría Nacional de Gestión de Riesgos, Gobierno del Ecuador (2022). https://www.gestionderiesgos.gob.ec/wp-content/uploads/2022/02/Informe-de-Situacion-011-Aluvion-Quito-08022022.pdf
24. Strauch, M., et al.: Constraints in multi-objective optimization of land use allocation-repair or penalize? Environ. Model. Softw. **118**, 241–251 (2019)
25. Van Oost, K., Govers, G., Desmet, P.: Evaluating the effects of changes in landscape structure on soil erosion by water and tillage. Landscape Ecol. **15**(6), 577–589 (2000)
26. Van Rompaey, A.J., Verstraeten, G., Van Oost, K., Govers, G., Poesen, J.: Modelling mean annual sediment yield using a distributed approach. Earth Surf. Proc. Land. **26**(11), 1221–1236 (2001)
27. Vanegas, P.: A Spatially explicit approach to the site location problem in raster maps with application to afforestation. Ph.D. thesis, Belgium (2010)
28. Vanegas, P., Cattrysse, D., Van Orshoven, J.: A multiple criteria heuristic solution method for locating near to optimal contiguous and compact sites in raster maps. In: Murgante, B., Borruso, G., Lapucci, A. (eds.) Geocomputation, Sustainability and Environmental Planning. SCI, vol. 348, pp. 35–56. Springer, Heidelberg (2011). https://doi.org/10.1007/978-3-642-19733-8_3
29. Vanegas, P., Cattrysse, D., Van Orshoven, J.: Allocating reforestation areas for sediment flow minimization: an integer programming formulation and a heuristic solution method. Optim. Eng. **13**(2), 247–269 (2012)
30. Vanegas, P., Cattrysse, D., Wijffels, A., Van Orshoven, J.: Compactness and flow minimization requirements in reforestation initiatives: a heuristic solution method. Ann. Oper. Res. **219**(1), 433–456 (2014)
31. Vanwalleghem, T.: Soil erosion and conservation. In: International Encyclopedia of Geography: People, The Earth, Environment and Technology: People, the Earth, Environment and Technology, pp. 1–10 (2016)
32. Verstraeten, G., Prosser, I.P., Fogarty, P.: Predicting the spatial patterns of hillslope sediment delivery to river channels in the murrumbidgee catchment, Australia. J. Hydrol. **334**(3–4), 440–454 (2007)
33. Vought, L.B.M., Pinay, G., Fuglsang, A., Ruffinoni, C.: Structure and function of buffer strips from a water quality perspective in agricultural landscapes. Landsc. Urban Plan. **31**(1–3), 323–331 (1995)
34. Wang, J.: Economic geography: spatial interaction. In: International Encyclopedia of Geography: People, the Earth, Environment and Technology: People, the Earth. Environment and Technology, pp. 1–4 (2016)
35. Wischmeier, W.H., Smith, D.D.: Predicting rainfall-erosion losses from cropland east of the Rocky Mountains: guide for selection of practices for soil and water conservation. Agricultural Research Service, US Department of Agriculture (1965)
36. Witlox, F.: Expert systems in land-use planning: an overview. Expert Syst. Appl. **29**(2), 437–445 (2005)

Possible Relationships Between the Spread of Tourism and Urban Zoning

Francesco Rotondo[1(✉)], Paola Perchinunno[2], and Samuela L'Abbate[2]

[1] DICEA, Polytechnic University of Marche, Ancona, Italy
f.rotondo@univpm.it
[2] DEMDI, University of Bari, A. Moro, Italy

Abstract. The spread of tourism in Italy, beyond the already well-known art cities, is a phenomenon that is also growing in the south. The well-known phenomena of the spread of short-term tourism and operators such as Airbnb, Booking and many others, raise significant questions of coexistence between resident populations and temporary users brought by the spread of mass tourism. This paper in the first part analyzes hospitality models in their territorial dimension.

Organizational strategies, forms of intermediation, and guest experiences are rooted in specific spatial contexts, characterized by varying levels of supply density, functional specialization, and coordination capacity between operators.

So, it becomes important to understand where and how the hospitality offering is organized across the territory.

In the second part it investigates the possible relationships between the spread of tourism in some cities in the Puglia region in Southern Italy and the urban zoning of the planning tools that govern the land use regime in those territories according to the classical rational model of modern architecture. We want to understand whether the spread of hospitality facilities is related to the different types of homogeneous territorial zones in the municipal urban plan that define the permissible functions in the urban territory. The possible presence of these relationships can provide important insights into urban planning tools for attempting to manage these mass phenomena, which are so fragmented that they often prove unmanageable for the municipal administrations charged with managing them. We will use cluster analysis applying DBSCAN algorithm, aimed at identifying territorial hospitality systems in two Apulian cities, to verify the relationships with the zoning of the urban plan: Bari and Monopoli.

Keywords: urban zoning · fuzzy clustering · tourism planning

1 Introduction

Over the past two decades, the hospitality sector has undergone reconfiguration processes that have progressively challenged established models of supply and intermediation.

The contribution is the result of joint reflections by the authors, with the following contributions attributed to P. Perchinunno (chapter 1), to S. L'Abbate (chapter 2) and to F. Rotondo (chapters 3). Chapter 4 is a joint work done by all the authors.

© The Author(s), under exclusive license to Springer Nature Switzerland AG 2027
O. Gervasi et al. (Eds.): ICCSA 2026 Workshops, LNCS 16761, pp. 586–597, 2027.
https://doi.org/10.1007/978-3-032-30527-5_38

The traditional distinction between hotel and non-hotel hospitality, historically based on organizational and regulatory differences, appears increasingly inadequate to describe a landscape characterized by hybrid solutions, networks of independent operators, and digital platforms capable of coordinating supply and demand on a global scale.

At the same time, tourism demand has undergone significant evolution, shifting toward experiential forms of consumption that prioritize authenticity, personalization, and quality of the relationship over the mere consumption of a service.

In this context, the guest experience tends to be configured as a process articulated throughout the entire customer journey, in which material, symbolic, and relational dimensions interact. This evolution has significant implications for operators, who are being forced to reconsider their competitive strategies in a context marked by high uncertainty, seasonality of flows, and growing competitive pressure.

An additional element of complexity is the role of technology and digitalization. Online platforms, data management systems, and artificial intelligence tools are progressively changing the ways in which businesses access markets, interact with customers, and organize internal processes.

However, recent literature suggests that technological innovation does not act as an independent driver of growth, but rather as an enabling factor, whose impact depends on its ability to integrate with strategies geared toward experience and perceived value.

Consequently, understanding the industry's evolutionary trajectories requires an analysis that considers the combination and interdependence of various strategic levers.

In this scenario, analyzing operators' perceptions plays a central role. The expectations and assessments expressed by industry players are not simply individual opinions but reflect collective learning processes and strategic adaptation to structural constraints and emerging opportunities.

Examining these perceptions therefore allows us to detect early signs of change and identify the levers deemed most relevant for future growth. Considering these transformations, the analysis of hospitality models cannot ignore a territorial dimension. Organizational strategies, forms of intermediation, and guest experiences are rooted in specific spatial contexts, characterized by varying levels of supply density, functional specialization, and coordination capacity between operators.

From this perspective, understanding where and how the hospitality supply is organized across the region represents a preliminary step in interpreting the competitive dynamics and development trajectories of the sector. For this reason, the following section adopts a spatial analysis approach based on the DBSCAN algorithm, aimed at identifying territorial hospitality systems that go beyond the simple concentration of accommodations, returning a functional geography of regional tourist territories.

The second part of the paper compares the distribution of tourist facilities analyzed using the cluster analysis techniques illustrated in the first part with the distribution of zoning in the master plans of the cities of Bari and Monopoli, attempting to highlight possible relationships.

2 The Cluster Analysis

2.1 The DBSCAN Method

The territorial cluster map was constructed using the DBSCAN algorithm [1], a spatial clustering technique that does not impose a priori the number of groups but rather makes them emerge directly from the geographical distribution of accommodation facilities.

The DBSCAN method is based on two fundamental parameters:

– *Eps*, proximity radius, is the maximum distance within which two facilities are considered "close." In our case, eps was chosen to be around 3 km, a value that allows us to connect facilities belonging to the same territorial context and avoid merging distinct but geographically close tourist areas into a single group. In practice, two facilities within 3 km of each other tend to be considered part of the same local system.
– *MinPts,* minimum density, is the minimum number of facilities that must be within the eps radius for an area to be recognized as a cluster. Setting values around 5–6 facilities ensures that an area is classified as a "tourist area" only if there is a continuous, non-episodic concentration. Isolated or very scattered facilities are therefore excluded from the main clusters and classified as "noise".

2.2 Cluster and Geographical Distribution of Accommodations

Unlike density maps, such as the "classic" Airbnb-style (Fig. 1), which simply shows where accommodations are most concentrated, the DBSCAN map (Fig. 2) identifies actual tourist territories, that is, continuous areas where the accommodation offering is sufficiently dense and spatially connected to function as a single system (cluster).

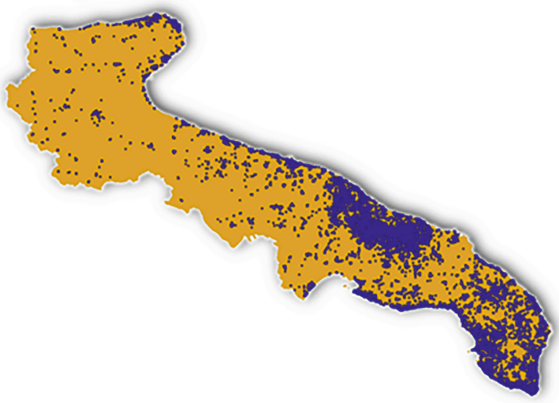

Fig. 1. Geographic distribution of Airbnb accommodations in Puglia (Source: Inside Airbnb March 2025).

Identifying territorial clusters allows us to interpret the accommodation offering as a spatially organized system, divided into functional areas characterized by different configurations of density and type of accommodation. Within this framework, analyzing the concentration of short-term rentals in Puglia allows us to identify the five municipalities with the highest absolute number of listings, based on data from Inside Airbnb.

Bari emerges as the municipality with the most listings, followed by Ostuni, Lecce, Gallipoli, and Porto Cesareo. This initial comparison allows us to immediately identify the main supply hubs in absolute terms, highlighting the central role of large urban centers and more established tourist destinations.

However, an interpretation based solely on raw values risks underestimating the intensity of the phenomenon in smaller municipalities, where even a smaller number of listings can translate into significant pressure on the local housing market.

This configuration reflects the structure of the Apulian tourism system, characterized by a strong bias toward coastal resorts and more accessible urban centers, and suggests that the spread of short-term rentals responds to territorial attractiveness rather than uniform distribution.

In particular, the analysis highlights how the phenomenon is strongly polarized in a few municipalities, corresponding to the region's main tourist and urban hubs. Among these, Bari, Ostuni, Lecce, Gallipoli, Porto Cesareo, Otranto and Monopoli stand out, representing the municipalities with the highest number of Airbnb listings.

The recurrence of the same municipalities already identified by the analysis of absolute values confirms the existence of areas where the short-term rental market is structurally more developed and consolidated, establishing itself as a significant component of the local housing system.

In these contexts, the pressure of the short-term rental market appears particularly significant, suggesting that the critical issues related to housing availability and competition with the residential market are concentrated primarily in these areas rather than uniformly across the entire region.

Analyzing the map resulting from the DBSCAN application (Fig. 2), it emerges that the clusters represent homogeneous macro-tourism areas and not individual municipalities. Each cluster corresponds to an area where the offerings are dense and spatially connected, meaning they follow similar patterns within a few kilometers.

The largest clusters coincide with the region's main tourist hubs:

- coastal Salento (Gallipoli–Otranto–Leuca area),
- the urban area of Bari,
- the Lecce system and hinterland,
- the Itria Valley and the central Adriatic coast (Monopoli–Polignano–Ostuni),
- the Gargano.

Among these we will focus, in our work, on the two following areas:

1. the urban area of Bari,
2. the central Adriatic coast (Monopoli).

The areas in gray or classified as "noise" do not indicate a lack of offerings, but rather a presence too dispersed to be interpreted as a true tourist district: these are areas where facilities exist, but do not form a continuous territorial system.

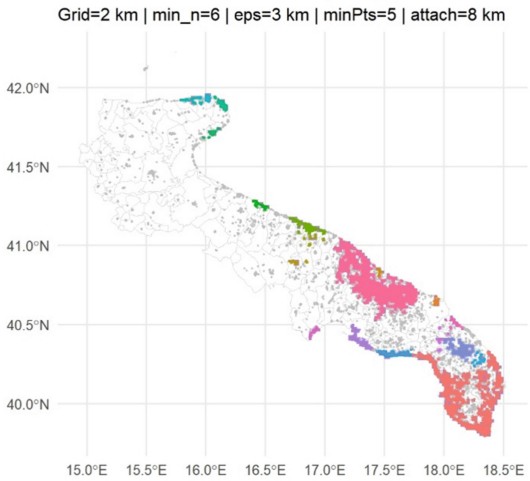

Fig. 2. Territorial clusters of accommodation offerings in Puglia (DBSCAN).

Unlike other methods, DBSCAN does not require to predetermine how many clusters we want. The final number emerges automatically based on how broadly we scope (eps) and how strict we are in requiring density (minPts).

This way, the clusters are not an arbitrary choice, but the result of a balance between geographic proximity, territorial continuity, and the intensity of the accommodation offering.

The result is not just a concentration map, but a true functional geography of tourism in Puglia, made up of recognizable and comparable tourist areas.

2.3 Breakdown of Clusters by Type of Accommodation

The breakdown of clusters by accommodation type (Fig. 3) shows an interesting distribution.

The *"Entire home/apt"* category dominates in all major tourist areas, particularly along the coastal Salento, the Itria Valley, and the Lecce area. This confirms that the prevailing model of non-hotel accommodation in Puglia is that of the complete housing unit.

However, the other types are not simply marginal but follow specific territorial logics.

"Hotel rooms" are concentrated primarily in the main urban centers, along some more structured coastal stretches, and in areas with a more consolidated tourism tradition.

"Private rooms" show a more widespread but less continuous distribution, often linked to medium-sized urban centers, inland areas with more mixed tourism, and contexts where hospitality is more integrated into the residence.

"Shared rooms" while representing a lower overall share than entire apartments, are not distributed randomly and are concentrated in a few specific clusters, especially in areas with high tourism intensity and in contexts with a strong presence of Young or international tourism.

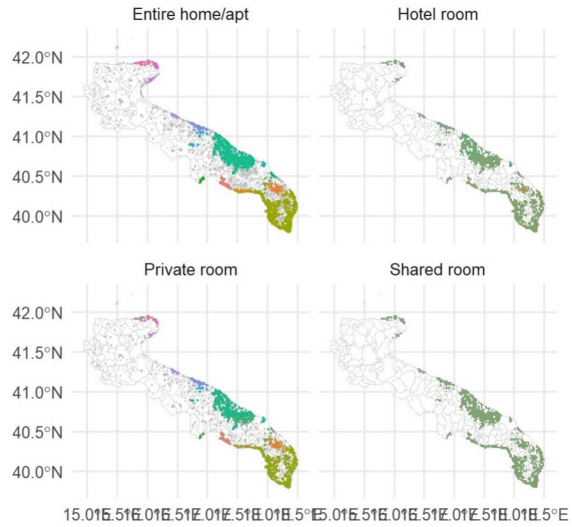

Fig. 3. DBSCAN Cluster by Type of Accommodation in Puglia.

Overall, the clusters not only describe where the facilities are concentrated but also show that each tourist area tends to have its own "offer profile".

In this sense, the map illustrates not only the geography of tourism, but also the geography of hospitality models in Puglia region.

The identification of territorial clusters allows us to understand the accommodation offering as a spatially organized system, characterized by differentiated configurations in terms of density and type of accommodation.

3 The Spread of Tourism in Some Cities in the Puglia Region and the Urban Zoning of the Planning Tools

3.1 Introduction

After attempting to understand, through analysis of data provided by the Airbnb platform, where tourist flows are concentrated in the cities of the Puglia region, we seek to understand whether these densities have any possible relationship with the urban destinations of the municipal plans of these cities, observing two of the cities with the highest tourist density: Bari and Monopoli.

The history of urban planning and its first tool, zoning, is essentially the story of how cities tried to control growth, land use and raising the level of health and safety, as they became more crowded and complex.

Urban planning and zoning have evolved significantly over time in response to changing social, economic, and environmental conditions. As we know, the Industrial Revolution in the 19th century marked a turning point in urban development. Rapid industrialization led to overcrowded cities, pollution, and poor living conditions. Polluting

factories were often located near residential areas, without any particular restrictions, exposing people to harmful environments.

In response, governments introduced public health laws and basic land-use controls to separate industrial and residential functions. These early efforts laid the groundwork for modern zoning. Modern zoning began in the late 19th and early 20th centuries. Germany was among the first countries to implement systematic zoning regulations, dividing cities into districts based on land use [2].

In the United States, New York City adopted the first comprehensive zoning resolution in 1916. This law regulated building heights, land use, and density, largely in response to concerns about skyscrapers blocking light and air [3].

Several urban planning movements shaped zoning practices. Later, modernist planners like Le Corbusier advocated for strict functional zoning, separating cities into areas for living, working, recreation, and transportation. These ideas influenced urban development throughout the 20th century. After World War II, zoning became widespread, particularly in suburban development.

While this improved organization, it also led to urban sprawl, increased car dependency, and social segregation. By the late 20th century, critics argued that rigid zoning reduced urban vitality and contributed to inequality. Large residential zones lacked diversity, and cities became less walkable [4].

In recent decades, urban planning has shifted toward more flexible and sustainable approaches. Movements such as New Urbanism promoted mixed-use development, walkability, and human-centered design. Cities are increasingly adopting form-based codes, which focus on the physical form of buildings rather than strictly separating land uses [5, 6].

Modern zoning also addresses global challenges such as climate change and housing shortages. Strategies like transit-oriented development encourage dense, mixed-use areas around public transportation, while inclusionary zoning policies aim to increase affordable housing [7].

Public space returns to the center of urban policies with the 15-min city proposal implemented during Mayor Hidalgo's two terms in Paris [8, 9]. The history of zoning in Italy reflects the country's broader urban development, shaped by centuries of cultural, political, and social change. The late 19th century saw the introduction of early planning tools aimed at improving infrastructure, sanitation, and urban growth [10, 11].

A major turning point came in the early 20th century with the introduction of Law No. 1150 in 1942. This law laid the foundation for modern urban planning in Italy by establishing the *Piano Regolatore Generale* (PRG), or General Master Plan. For the first time, Italian cities adopted formal zoning practices, dividing land into functional categories such as residential, industrial, and agricultural areas. This approach was influenced by modernist planning principles, promoted by figures such as Le Corbusier [12].

In the post-World War II period, Italy experienced rapid urbanization and reconstruction. Cities expanded quickly to accommodate population growth and rural-to-urban migration. Zoning became a central tool for managing this growth, with the PRG guiding development [13].

Further reforms in the 1960s and 1970s strengthened the zoning system. The Ministerial Decree No. 1444 of 1968 introduced a standardized classification of land-use zones, which remains fundamental today. These included:

- Zone A for historic centers;
- Zone B for existing built-up areas;
- Zone C for expansion zones;
- Zone D for industrial areas;
- Zone E for agricultural land;
- Zone F for general urban public services (different from neighborhood services).

The decree also established minimum standards for urban services, such as green spaces, schools, and public facilities, helping to improve living conditions. From the 1970s onward, planning responsibilities were increasingly decentralized, with greater authority given to regional and local governments. This shift allowed for more context-specific planning but also introduced complexity and variation across different parts of the country [14].

In recent decades, Italian urban planning has evolved to address new challenges such as sustainability, heritage conservation, and urban regeneration. Modern approaches tend to move beyond rigid zoning, incorporating more flexible and integrated planning tools [13].

Despite these advancements, Italy continues to face challenges, including bureaucratic delays, illegal construction, and the need to balance development with preservation. Issues such as climate change and tourism pressures, especially in historic and coastal cities, have made urban planning even more complex.

3.2 Relationships Between Zoning and Geographic Distribution of Airbnb Accommodations

This is the context in which we superimposed the distribution of Airbnb listings at the municipal level with the urban zoning of the two cities chosen as case studies: Bari and Monopoli.

Bari is a major city in southern Italy and the capital of the Puglia region. Located on the Adriatic Sea, it is an important economic, cultural, and transportation hub, with strong connections to the Balkans and the wider Mediterranean. The city has a population of approximately 315,000 inhabitants (2021 Census), while its metropolitan area exceeds 1 million people, and it covers a territorial surface of about 117 km^2.

In The case of the city of Bari, its General Master Plan is yet a *Piano Regolatore Generale* (PRG, approved in 1976), despite the fact that the Puglia Region has amended its regional law (R.L. 20/2001), replacing this instrument with a new generation one called the *Piano Urbanistico Generale* (PUG), which is more flexible and attentive to landscape and environmental issues.

In the Fig. 3, we can see that short-term rentals offered on Airbnb platform is mainly located in Zone A (historic centers) and Zone B (existing built-up areas, nearest to the historic centers) and just in some Zone C (expansion zones established by the PRG approved in 1976) located on the most attractive coast for mass tourism.

Very few, if any, tourist facilities in agricultural areas or other homogeneous areas of the PRG. Given the landscape, economic, and social characteristics of the city of Bari, it evidently attracts a type of tourism more closely tied to its historical, architectural, business characteristics.

This may offer potential keys to understanding these initial findings. In the following image (Fig. 4) we show the overlap between the distribution of AirBnB tourist facilities and the urban zoning of the Bari PRG.

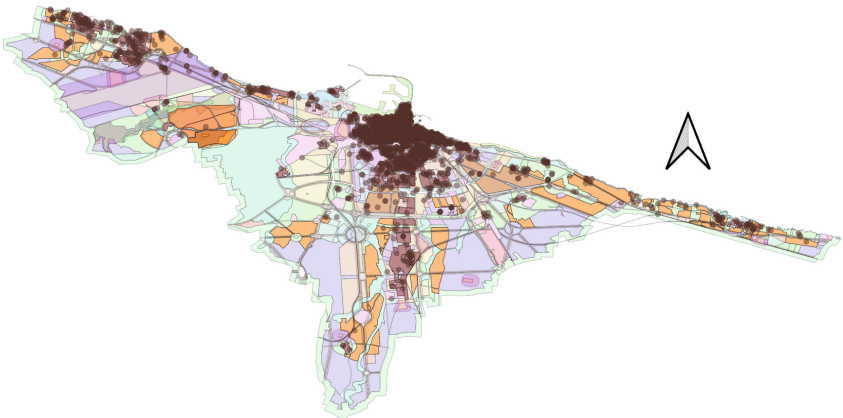

Fig. 4. Spatial distribution of short-term rentals offered on Airbnb in September 2025 in the city of Bari superimposed on the urban zoning of the Bari PRG (Source: authors' elaboration on Municipality of Bari's data).

Monopoli is a coastal city in southern Italy, located in the Apulia (Puglia) region along the Adriatic Sea, not far from Bari. It is known for its picturesque historic center, and strong connection to the sea. The city has a population of approximately 49,000 inhabitants and covers a territorial area of about 157 km^2. Monopoli's economy is based on fishing, agriculture—particularly olive oil production—tourism, and small-scale industry.

In recent years, it has become an increasingly popular tourist destination due to its beaches, cultural heritage, and relaxed Mediterranean atmosphere. From an urban planning perspective, the Municipality of Monopoli approved a new-generation municipal planning tool (compliant with Regional Law 20/2001, unlike the older one in Bari) in 2010.

The Plan developed new forms of economic and social development (with a significant focus on tourism), significantly increasing the protection and enhancement of the environment and landscape.

Also in this case, like Bari, in the Fig. 5, we can see that short-term rentals offered on Airbnb platform is mainly located in Zone A (historic centers) and Zone B (existing built-up areas, nearest to the historic centers) and just in some Zone C (expansion zones established by the PRG approved in 1976) located on the most attractive coast for mass tourism.

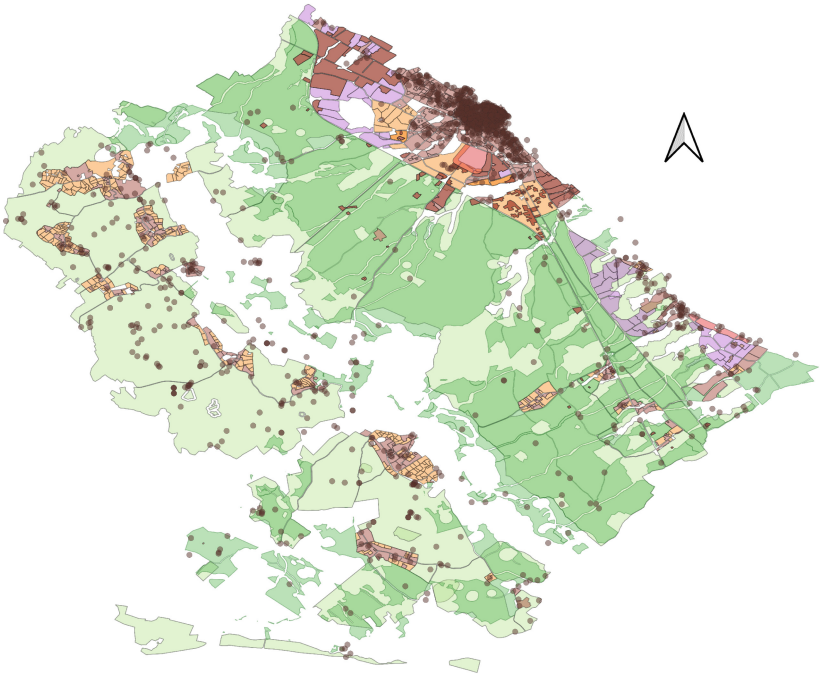

Fig. 5. Spatial distribution of short-term rentals offered on Airbnb in September 2025 in the city of Monopoli superimposed on the urban zoning of the Monopoli PUG (Source: authors' elaboration on Municipality of Monopoli's data).

However, unlike the city of Bari, the agricultural areas of Monopoli are significantly affected by the presence of tourist activities, particularly in the western part of the municipal territory, where a hilly area of notable landscape value develops, traditionally inhabited during the hot summers by the resident population.

4 Conclusions

This study first analyzed hospitality industry operators' perceptions regarding future growth prospects, with the aim of understanding which choices and factors are considered most relevant for long-term growth.

The results clearly show that there is no one-size-fits-all strategy, but that growth expectations depend heavily on the business model already adopted by operators' decisions. This means that development trajectories are differentiated and that the most effective strategies must be consistent with the organization's identity and the context in which it operates.

The analysis also highlights structural limitations that characterize the sector. The fragmentation of the offering and the difficulty of coordinating between operators are perceived as persistent problems, difficult to resolve in the short term. This suggests that many of the identified potentials may remain untapped unless accompanied by more stable forms of collaboration and shared governance tools.

The second part of the paper shows how the short-term rentals offered on Airbnb platform are more diffused areas classified by the urban city plan as Zone A (historic centers), Zone B (existing built-up areas, nearest to the historic centers) and only in the C areas present on the coast.

As we know, the growth in tourism demand and the spread of short-term rentals have prompted several European cities, including Barcelona, Venice, Florence, Lisbon and Amsterdam, to adopt new regulatory measures.

These include authorisation systems, licence limits or specific restrictions to curb the impact on the local property market, opening a debate between local administrations, tourism operators and digital platforms on the delicate balance between economic development and the protection of the right to housing.

The issue has also gradually entered the agenda of the European Commission working on the first Affordable Housing Action Plan [15] in cooperation with several mayors of European capitals.

The results suggest that the future development of hospitality will depend also on possible rules to regulate this type of tourism in areas where they are most prevalent, including through urban zoning, as the city of Florence has already done in 2025, prohibiting the opening of new Short-Term Tourist Rentals within the area or homogeneous zone identified as the Historic Core (Zone A), as defined in Article 65 of the NTA of the city's Urban Planning Regulations [16].

Zoning, therefore, despite the limitations that international literature has now identified in this traditional model of urban planning regulation, still appears to be able to play an effective role as a tool for limiting or regulating phenomena distributed across the territory, also in this relevant phenomenon for housing market and the quality of life of residents.

References

1. Ester, M., Kriegel, H.P., Sander, J., Xiaowei, X.: A density-based algorithm for discovering clusters in large spatial databases with noise. In: Proceeding of the 2nd International Conference on Knowledge Discovery and Data Mining, pp. 94–99 (1996)
2. Schröteler-von Brandt, Hildegard: The history of urban planning. https://nbn-resolving.org/urn:nbn:de:0156-55997441. Accessed 12 Mar 2026
3. Hall, P.: Cities of Tomorrow. Blackwell Publishers, Oxford (UK) (2014)
4. Airey, J., Doughty, Ch.: Rethinking the Planning System for the 21st Century. Policy Exchange, London. https://policyexchange.org.uk/publication/rethinking-the-planning-system-for-the-21st-century/. Accessed 12 Mar 2026
5. Carmona, M., Marshall, S., Stevens, Q.: Design codes: their use and potential. Progr. Plan. **65**(4), 209–289 (2006). https://doi.org/10.1016/j.progress.2006.03.008. Accessed 12 Mar 2026
6. Form-Based Codes Institute (n.d.). Form-based Codes Defined. https://formbasedcodes.org/definition/. Accessed 12 Mar 2026
7. Schulze Bäing, A., Webb, B.: Planning Through Zoning. https://www.rtpi.org.uk/new-from-the-rtpi/planning-through-zoning/. Accessed 12 Mar 2026
8. Murgante, B., Patimisco, L., Annunziata, A.: Developing a 15-minute city: a comparative study of four Italian Cities-Cagliari, Perugia, Pisa, and Trieste. Cities **146**, 1–22 (2024)

9. Moreno, C.: The 15-Minute City: A Solution to Saving Our Time and Our Planet. Wiley, Oxford (UK)
10. Benevolo, L.: The European City. Blackwell Publishers, Oxford (UK) (1993)
11. Secchi, B.: La città del ventesimo secolo. Laterza, Bari-Roma (2005)
12. Gabellini, P.: Tecniche urbanistiche. Carocci, Roma (2010)
13. Rotondo, F., Selicato, F.: Progettazione urbanistica. McGraw-Hill Companies, Milano – New York (2010)
14. Secchi, B.: La città dei ricchi e la città dei poveri. Laterza, Bari-Roma (2013)
15. EC: Affordable Housing Action Plan. https://housing.ec.europa.eu/european-affordable-housing-plan%5Fen. Accessed 12 Mar 2026
16. City of Florence, Regulation for short-term tourist rentals. https://www.comune.firenze.it/turismo/locazioni-turistiche-brevi. Accessed 12 Mar 2026

Generative and Neuro-Symbolic Artificial Intelligence for Real-World Systems (GNS-AI 2026)

Extracting Models of Dynamic Human Health Behaviour from Real-Life Personal Health Data

Afonso Sarmento(✉) and José Machado

LASI/ALGORITMI, University of Minho, Braga, Portugal
pg55831@uminho.pt

Abstract. The rise of lifestyle-related chronic diseases has increased the need for data-driven methods that capture how health behaviours unfold in daily life. Mobile and wearable technologies now enable continuous, multimodal health data collection, but most behavioural models use static or aggregated representations that overlook temporal dependencies and context.

In this work, we adopt a process-oriented perspective, modelling health behaviour as a dynamic process and present a novel methodological contribution: a pipeline that transforms multimodal streams (meals, physical activity, continuous glucose monitoring (CGM), self-reports) into event logs suitable for both traditional and object-centric process discovery. We apply and compare several process discovery algorithms to a longitudinal multimodal dataset from individuals with diabetes, deriving models that capture interactions among activities, physiological measures, and daily routines. Our results indicate that Object-Centric Process Mining (OCPM) can extract interpretable, clinically meaningful insights from heterogeneous sensor and self-report data, supporting its use as a methodological foundation for modelling dynamic health behaviour in real-world care.

Keywords: Process Mining · Human Health Behaviour · mHealth

1 Introduction

According to the World Health Organization (WHO), the global prevalence of diseases aggravated by unhealthy lifestyle, habits and behaviours, such as cardiovascular diseases, cancer or diabetes, is increasing. This highlights the necessity of developing strategies of facilitating the practice of health-promoting behaviours in individuals [1]. This includes engagement in self-monitoring behaviours and the adoption of self-care practices that may improve long-term health outcomes and overall well-being. These advances have been supported by technologies such as wearables or mobile apps (especially mHealth apps) with the purpose of helping this self-control [2,3].

© The Author(s), under exclusive license to Springer Nature Switzerland AG 2027
O. Gervasi et al. (Eds.): ICCSA 2026 Workshops, LNCS 16761, pp. 601–618, 2027.
https://doi.org/10.1007/978-3-032-30527-5_39

Recent work has shown that human health behaviour follows a process-like structure [4]. A process-oriented perspective is particularly relevant because it preserves the temporal ordering, timing, and interaction of behaviours, enabling the identification of behavioural sequences that precede health outcomes and can be targeted by personalised and temporally optimised interventions [5]. A dynamic perspective analyses behaviour not as a fixed attribute but as a time-dependent process shaped by variability that emerges across multiple levels of human activity [6].

Process mining differs from traditional data mining by explicitly reconstructing how behaviours unfold in time rather than extracting aggregated patterns from static features. By reconstructing event order and revealing branching points and deviations, process mining produces an interpretable, process-centred view that is directly useful for identifying actionable behavioural sequences and designing timely, personalized interventions [7].

There is a lack of approaches capable of accurately interpreting the human health behaviour dynamics from these data. This represents a clear gap between the availability of data and the tools needed to model health behaviour as a dynamic process. As a result, it remains unclear how different process discovery techniques model health behaviour, what behavioural characteristics they capture or miss, and which modelling choices lead to interpretable and clinically plausible representations.

This study addresses the following research question: How can we model health behaviour processes from real-life health data?

To address this gap, we propose a process-oriented approach based on process mining techniques, guided by three sub-questions: Which process-discovery and object-centric techniques exist for modelling health behaviour, and how do they compare?; How can multimodal sensor and self-report data be transformed into event logs for process discovery?; Which discovery algorithms and modelling choices produce the most interpretable and robust models on real-world diabetes data?

We aim to transform heterogeneous sensor and self-report records into event logs suitable for process discovery, compare discovery algorithms in terms of interpretability and robustness, and validate the discovered models using process-mining quality metrics and comparison with established reference patterns. The central contribution of this work is the development and evaluation of an end-to-end methodological pipeline that operationalizes OCPM for multimodal, real-life personal health data. While the paper includes a comparative benchmark of algorithms, its primary novelty lies in the transformation of continuous sensor streams into object-centric event logs, enabling the capture of complex interactions between physiological responses and daily behaviours that traditional case-centric approaches overlook.

2 State of the Art

2.1 Foundations of Human Health Behaviour

Health behaviour refers to the set of patterns, activities, and habits undertaken with the purpose of prevention and health maintenance, improvement and to promote well-being [8].

Human behaviour is central to health and illness. Behaviours, activities, and self-regulation shape the biopsychosocial state, including motivations, actions, and processes that support well-being, such as the practice of regular physical activity and a balanced diet [8]. Health-promoting behaviours are associated with lower morbidity and mortality and better quality of life [9].

Because individuals vary in capability, context, and motivation, personalised behavioural models can tailor interventions to their specific needs, increasing effectiveness and improving health outcomes [10,11].

In this context, numerous conceptual theories and models (e.g. COM-B, Theory of Planned behaviour, HAPA, Social Cognitive Theory) have been developed to explain the behaviours. While these models provide valuable frameworks for understanding health behaviour and behaviour change, they have key limitations for digital health personalisation [10]. Although some models allow for change across stages or motivational states, they still lack formal mechanisms for stochasticity, multidimensional interactions, partial structure, and fine-grained context adaptation.

To address this gap, this study specifies explicit characteristics of human behaviour, detailed in the next section. We operationalize each characteristic for digital health data by representing observations as time-stamped events and objects, encoding context as event attributes and temporal windows, and allowing probabilistic transition models and optional paths in discovered processes.

Health Behaviour Characteristics The characteristics that guide this study are the following:

- **Partially structured or unstructured** - Behavioural sciences describe human behaviour as a combination of habitual routines and adaptive responses to changing contexts, aligning with the assumption that human behaviour does not always follow rigid, linear, or formally defined rules [12]. It is important to consider that human behaviour can also be structured. Daily and weekly patterns, habitual activities or the circadian cycle exhibit structured and predictable patterns. This supports the use of discovery techniques that allow for flexible and non-linear process representations instead of rigid or fully structured models [13].
- **Stochastic** - The individual responses vary due to internal states, environmental influences and unobserved factors [14]. As a result, behaviour cannot be assumed to be fully predictable, even under similar circumstances. This assumption motivates the use of probabilistic and entropy-aware process discovery techniques, which can capture behavioural variability rather than enforcing deterministic models [12].

- **Multidimensional** - Human behaviour emerges from interactions across multiple domains, being consistent with behavioural theories that emphasize cognitive, emotional, and social determinants [15]. This supports the adoption of modelling approaches capable of integrating and jointly analysing multiple behavioural dimensions, enabling the discovery of interdependencies across heterogeneous data sources. [12].
- **Context-dependent** - The behaviour varies according to situational, cultural, social, and environmental conditions and, in different contexts, the same individual may behave differently. Probabilities, context-specific entropy, and interaction measures can quantify the extent to which behaviours shift in response to context changes. This motivates the use of approaches that can incorporate this information into behavioural modelling, enabling the analysis of how behavioural patterns adapt across varying situational and environmental conditions. [12].

Collectively, these characteristics establish a robust foundation for the selection and evaluation of process mining techniques that can adequately capture the dynamic, variable, and context-sensitive characteristics of human health behaviour.

2.2 Data-Driven Approaches

Data-driven methodologies are being developed as means to enable personalisation and variability within digital health interventions and tools. These methods rely on event-based data that capture user behaviours and contexts, providing the empirical traces needed to operationalize personalised interventions. These approaches aim to identify patterns and relationships in data, enabling the construction of models that capture how individuals behave in practice rather than how behaviour is theoretically described [7].

Although these techniques can uncover associations between variables, most data mining techniques are not process-oriented. Without this temporal structure, these patterns remain invisible, the sequences cannot be reconstructed, and process-oriented patterns are overlooked. [7].

In the context of mHealth, personalisation depends not only on which behaviours occur, but also on when and in what order they occur, as interventions must respond to individuals' evolving behavioural trajectories [16]. For clarity, in a control-flow perspective, a process is modelled as ordered sequences of events (traces) governed by control-flow constructs such as sequence, choice, concurrency and loops. By aggregating and transforming these behavioural data into static features, these temporal dynamics are ignored, limiting the ability to reconstruct behavioural processes and constraining the design of personalised and adaptive digital interventions.

This deeper understanding motivates the use of process-oriented, data-driven techniques to model and analyse real-world human health behaviour, which is essential to develop real-time and personalised digital health interventions.

Process Perspective: Process Mining According to Wil van der Aalst, process mining is between machine learning and data mining on the one hand, and process modelling and analysis on the other [14]. The idea of process mining is to discover, monitor and improve real processes by extracting knowledge from event logs readily available in today's systems [14].

Process mining offers approaches explicitly designed to improve process analysis. One of its main advantages is its objectivity, as it relies on real data event logs [17]. Each event is associated with an event type, which specifies the lifecycle transition or state change it represented by the event within a process execution. In other words, it provides semantic information about how an event relates to the progression of an activity or process instance [17].

Process mining techniques reconstruct process models, enabling identification of temporal structures such as routines, transitions, deviations, and behavioural cycles [18]. By preserving the order and timing of events, process mining captures aspects of human behaviour that are lost in traditional data mining—such as the sequence in which actions occur, the repetition of behavioural loops, or the conditions under which decisions are made [18]. Consequently, process mining provides dynamic representations and has the potential to support more precise and adaptive personalisation in digital interventions. A key challenge of process mining lies not only in appropriate data use, but also in selecting modelling formalisms capable of representing essential properties of human behaviour. Although good data use can return powerful conclusions, poor data preprocessing and use can lead to unexpected results. Even with high-quality data, models that fail to capture behavioural concurrency, stochasticity, or cross-object relations will limit the validity and usefulness of the resulting insights [7].

Object-Centric Process Mining Traditional process mining was created with the capability of dealing with a single type of objects at a time, where each event corresponds to exactly one object and the process models created through them describe their patterns and lifecycle. While this assumption is suitable for well-structured organizational processes, it becomes restrictive when modelling complex, multidimensional phenomena such as human health behaviour, where multiple interacting entities evolve simultaneously, such as physiological measurements, activities or context factors.

Object-centric appears with the goal of working without the classical constraints, with multidimensionality in the type of objects [19]. An object is an identifiable entity in the system that participates in events and around which processes are observed, analysed, and modelled [20]. Object-centric has the advantages of providing a multidimensional representation of the processes, by explicitly modelling objects and their relationships, which in traditional process mining is abstracted away.

This capability is essential for capturing the complexity of health behaviour and enables process-oriented analyses from multiple perspectives without requiring data re-extraction or the definition of a case notion [19].

The next step is to examine the process discovery techniques that are suitable for this case study.

3 Process Discovery Techniques

Process mining aims to improve operational processes through the use of event data during the discovery of process models from event logs [14,21].

Its importance lies in its potential to identify processes, standardize clinical practices, support evidence-based decisions and improve the quality of healthcare and health habits [22]. These processes consist of sequences of daily activities and health-related events, such as meals, physical activity, and physiological responses, with the goals of improving patient outcomes and monitoring patient trajectories. They involve clinical and non-clinical activities performed by diverse resources and can vary widely. Personal health management processes are highly dynamic and individual-centred, which makes their analysis and optimisation particularly challenging [22].

Over the past years, numerous process mining techniques have been developed, as summarized in Table 1.

Table 1. Comparison of explored process mining techniques and their supported characteristics.

			Behavioural				Technical							
Name	Reference	Year	Multidimensional	Stochastic	Partially structured	Context-dependent	Control-flow	Loops	Duplicate tasks	Hidden tasks	Noise	Missing data	Clustering-based	Algorithmic approach
Markov	[23]	1998	x	x	x		x	x		x	x	x		x
Alpha/Alpha+	[23]	2004					x							x
Heuristics Miner	[23,24]	2006	x				x	x		x	x	x		x
Decision Miner	[25]	2006				x								x
Genetic Miner	[23]	2007					x	x		x	x	x		
DT Genetic Miner	[23]	2007					x	x	x	x	x	x	x	
Fuzzy Miner	[23]	2007	x		x		x	x			x	x	x	x
Alpha++	[23]	2007	x				x							x
ILP Miner	[23]	2009					x			x		x		x
FSM Miner/Petrify	[25]	2010					x	x	x	x				x
FSM Miner/Genet	[23]	2010					x	x						x
Inductive Miner	[25]	2013					x	x			x		x	x
Inductive Miner (infrequent)	[25]	2014					x	x		x	x			x
Fodina	[12]	2017	x		x		x	x	x	x	x	x		x
Split Miner	[12]	2017					x	x			x			x
Hybrid ILP Miner	[25]	2018					x	x		x	x			x

While control-flow models provide an effective representation of the structural ordering of activities, standard process discovery algorithms generally fail to capture the stochastic variability that is intrinsic to health behaviour data, including probabilistic transition choices, temporal variability, and the influence of unobserved events. In typical applications, sequence discovery often begins by extracting transitions as ordered pairs of consecutive events from the event log. The aggregation of these pairs produces a transition matrix and an associated directed graph that summarises the most frequent paths and branching patterns. However, they do not encode explicit temporal information or probabilistic dynamics. Consequently, we adopt control-flow models as an interpretable

structural core and explicitly augment them with temporal and pattern-based analyses to characterise inter-event intervals, transition probabilities, and the impact of missing or latent events [5].

4 Methods

4.1 Dataset

To analyse process mining techniques in health data, this study is guided by dataset-related selection criteria that define the data's scope and selection criteria, ensuring it serves as a good use case and satisfies the following conditions:

- **Be an open-source dataset**, allowing transparency, reproducibility of results and facilitating comparative and follow-up studies.
- **Include sensor data**, preferably from two different types of sensors or modalities.
- **Reflect real-world conditions**, meaning data were collected without instructing participants to change their usual routines or behaviours.
- **Contain manual logs**, corresponding to self-reported activity log data.
- **Meet a minimum continuous recording period**, sufficient to capture longitudinal patterns.

With all these requirements in mind, the *Longitudinal Multimodal Dataset of Type 1 Diabetes* was identified as a suitable choice.

This dataset was created by collecting health data from 17 individuals, with ages between 23 and 70 years [15]. Data registers were collected during a continuous 90-day period [15].

Health-related information was captured through dedicated platforms using standardized protocols. CGM data were derived from multiple commercially available systems (LibreView, Dexcom, Medtronic), whereas insulin administration data were obtained from insulin pump platforms or electronic logs documenting multiple daily injection regimens. Dietary intake was recorded using Nutritics software, and physical activity and sleep were quantified with Garmin Forerunner 45 smartwatches, providing high-resolution, sensor-based measurements [15].

4.2 Framework

Traditionally, process mining is designed and studied following specific guidelines for its execution: the Process Mining Project Methodology (PM^2). These guides are created with the aim of improving process performance and compliance to rules and regulations, as represented in Fig. 1 [26].

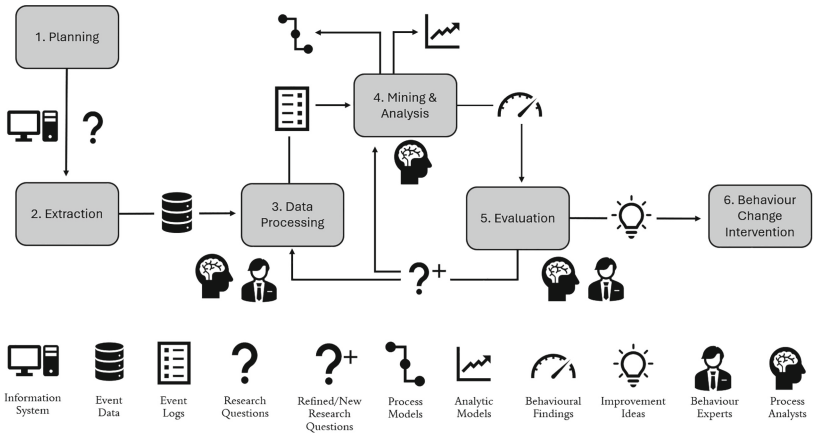

Fig. 1. Overview of the PM^2 methodology.

Event Log Creation The creation of the event logs is the first part in the processing and study of process mining techniques. It is through event logs that processes are analysed and the information, patterns and inferences are executed [7].

For these experiments, we test the case IDs of *meals* and *days*, with and without filters for events of hyperglycaemia and hypoglycaemia. The study of different case notions provides a more accurate representation of real-world processes. The four slicing strategies we used were the Day strategy, which groups all events for a patient within the same calendar day, Day_HH which subdivides each day into shorter time blocks to capture finer temporal granularity, the Meal strategy which defines cases around recorded meal timestamps, and Meal_HH which extends meal-based cases by applying a fixed temporal window to include surrounding events. Specifically, Day_HH subdivides each day into four fixed 6-h blocks (00 h–06 h, 06 h–12 h, 12 h–18 h, 18 h–00h). Meal_HH extends the case duration to a window starting 30 min before the meal and ending 4 h after, to capture the full postprandial glucose curve and late insulin effects.

We implement a compact, rule-based inference pipeline to map continuous sensor data into discrete event types. First, signals are preprocessed (time alignment across sensors, smoothing using a 15-min moving average to reduce high-frequency sensor noise, and outlier removal defined as the exclusion of glucose rate-of-change values exceeding 5 mg/dL/min, which are physiologically implausible). Then the following behavioural events are inferred programmatically:

- **Meal start**, derived from recorded meal timestamps.
- **Bolus insulin**, detected from timestamped insulin-administration records and associated to the nearest meal within a predefined window.
- **Postprandial peak**, identified as the local maximum within a three-hour post-meal window that exceeds the preprandial baseline (the preprandial

baseline is computed as the median glucose level during the 30 min preceding the meal timestamp).
- **Recovery (return to baseline)**, defined as the first timestamp after the peak at which glucose returns to or falls below the preprandial baseline.

To illustrate the practical application of the proposed pipeline, a representative behavioural vignette is defined as follows: a 'Meal' event (e.g., breakfast) is recorded alongside a synchronous 'Insulin Bolus' administration. These events trigger a temporal window that monitors the CGM stream, identifying a 'Post-Prandial Blood Glucose (PPBG)' episode. This episode is characterized by a transition from a 'Baseline' state to 'Hyperglycemia', followed by a 'Recovery' event once the glucose levels return to the target range.

Pipeline For this pipeline, a set of process discovery algorithms was selected to be tested: Heuristics Miner, Inductive Miner, Integer Linear Programming (ILP) Miner, Alpha Plus and Fodina, because together they align with the behavioural characteristics outlined above.

The object-centric Heuristics Miner extends frequency-based dependency analysis to object-centric event logs by computing directly following relations conditioned on object types and instances. The object-centric Inductive Miner adapts recursive block-structured process discovery to object-centric event logs by identifying control-flow constructs while respecting objectâĂŞevent associations. It produces sound, structured process models that support conformance checking and reproducible behavioural analysis, making it suitable for hypothesis-driven evaluation and clinical validation.

Following the PM^2 methodology, the pipeline executes the data extraction, transformation, discovery, and evaluation phases. The event data is loaded and preprocessed by renaming the case identifier, activity label, and timestamp columns, normalizing timestamps, and ordering events chronologically. During the transformation phase, two event log representations are constructed: a case-centric event log exported in eXtensible Event Stream (XES) format, and an Object-Centric Event Log (OCEL), where relevant object types and their associations with events are explicitly defined. This object-centric transformation enables events to be linked to multiple object instances and supports the application of object-centric discovery techniques.

The object-centric event log is structured around PPBG episodes, which serve as the primary object type for the analysis. The OCEL was constructed by mapping events to objects using a 'many-to-many' relationship: a single physical activity event could be linked to two different 'PPBG Episode' objects if it occurred within their respective 4-hour post-meal windows. Quality measures for OCPM were computed using the OC-Discovery framework, where fitness and precision are calculated relative to object-event associations rather than linear traces. In this representation, each event can reference multiple object instances, allowing behavioural and physiological entities to coexist within the same event context. Each episode represents a temporally delimited physiological response following a meal and links behavioural and physiological events such as meals,

insulin administrations, glucose peaks, and recovery phases. Using PPBG as the central object enables the representation of interactions between behavioural actions and physiological responses within the same episode while preserving temporal ordering and relationships between entities.

From standardized data event log, we perform process discovery by applying the data to the different established algorithms described in Sect. 3. Then, we conduct a quantitative evaluation across multiple dimensions, as referred in Sect. 4.3. Conformance checking via token-based replay (TBR) is then executed by simulating each trace against the discovered Petri Net. This allows us to identify fitting and non-fitting cases and to assess how well the observed behaviour is captured by the model and, consequently, by its Petri Net representation. All discovery experiments were executed using the same preprocessing pipeline and identical parameter settings to ensure comparability between techniques. Figure 2 provides an overview of the proposed pipeline.

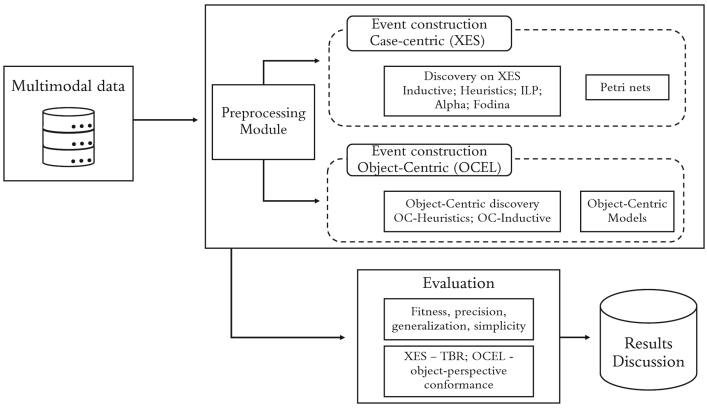

Fig. 2. Overview of the PM^2-aligned pipeline, illustrating the parallel case-centric (XES) and object-centric (OCEL) discovery paths and their evaluation.

4.3 Evaluation Parameters

To analyse the tested models, we consider a set of evaluation dimensions that are used as indicators to evaluate the quality of the executed models. These dimensions, shown on Fig. 3, tell us how well a technique can create a reliable process model, capable of capturing process behaviour with the greatest resemblance to what reality is. These evaluation dimensions also indicate how well the techniques can capture behavioural variability inherent in human-driven processes, including optional, repeated, or noisy activities.

To evaluate a discovery model, two main dimensions are considered: fitness and comprehensibility.

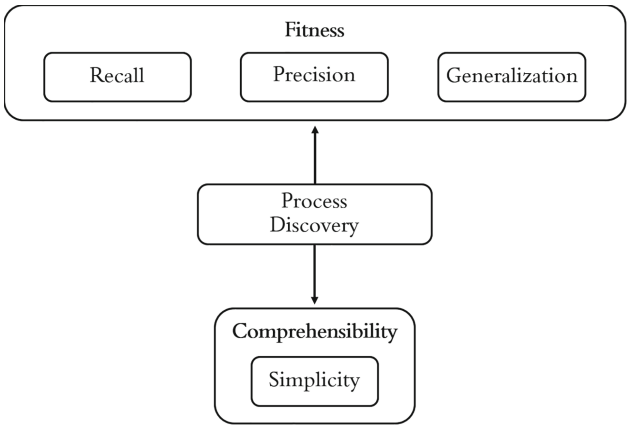

Fig. 3. Framework of evaluation metrics for assessing process discovery techniques.

Four dimensions are evaluated: fitness, precision, generalisation, and simplicity. Fitness, operationalised as trace fitness, measures the extent to which the behaviour recorded in the event log can be replayed by the discovered model, and thus captures the recall of observed traces. Precision checks that the model neither overfits the data nor becomes too general by allowing behaviour not supported by the log. Generalisation assesses whether the model correctly represents not only observed behaviour but also unseen yet plausible behaviour that may occur in the real process [23].

Comprehensibility includes simplicity and evaluates how easily humans can understand and interpret a discovered process model, considering its complexity and ease of interpretation. It is largely determined by structural complexity, including size, structure, and concurrency [23].

Together, these metrics provide a comprehensive evaluation of model quality by considering behavioural fidelity, precision over unobserved behaviour, generalisation capacity, and structural interpretability.

5 Results

This section reports the obtained results and evaluation about all the tested models, following the evaluation criteria defined in Sect. 4.3. Highlight to fitness, precision, generalisation and simplicity. The results are explicit in Table 2.

Inductive Miner and ILP Miner achieved the highest fitness values (1.00 and 0.9985), indicating a strong ability to reproduce the event-log behaviour. Inductive Miner's perfect fitness suggests an exact replay of the observed traces, while ILP Miner combines similarly high fitness with very low precision and low simplicity.

Regarding precision, Fodina and Alpha Plus reached the highest values (1.000 and 0.9183), suggesting better control over unobserved behaviour. Despite this,

Table 2. Evaluation of process discovery techniques across fitness, precision, generalisation and simplicity.

Technique	Precision	Fitness	Generalisation	Simplicity	CS
Heuristics Miner	0.5064	0.9608	0.9290	0.4959	0.7230
Inductive Miner	0.4388	1.0000	0.9455	0.6570	0.7603
ILP Miner	0.3679	0.9985	0.9774	0.1648	0.6272
Alpha Plus	0.9183	0.8063	0.9797	0.8036	0.8770
Fodina	1.0000	0.4297	0.9823	0.3861	0.6995

Fodina's precision coincides with lower fitness (0.4297), indicating that it may fail to reproduce a substantial portion of the observed traces, effectively capturing a limited subset with high exactness.

For generalisation, Fodina (0.9823) and Alpha Plus (0.9797) scored highest. Alpha Plus combines high generalisation with high precision and moderate fitness, indicating a balanced ability to go beyond the observed traces while maintaining behavioural control. In contrast, ILP Miner shows very high fitness and generalisation but lower precision and simplicity, typical of models that fully reproduce the log.

The combined quality metric (CS), computed as an equally weighted average of fitness, precision, generalisation and simplicity (0.25 each), ranks Alpha Plus highest overall, as it offers the most balanced trade-off, followed by Inductive Miner and Heuristics Miner. Alpha Plus does not achieve the best fitness individually, showing that the combined metric rewards balanced performance and better captures heterogeneous behavioural patterns than extreme values on a single dimension.

In OCPM, Table 3 shows that both Heuristics Miner and Inductive Miner achieve perfect fitness, which means they fully replay the recorded object-centric traces. However, Inductive Miner has higher precision and generalisation than Heuristics Miner, as well as greater simplicity, resulting in a better combined quality score.

Table 3. Object-centric process discovery techniques across the four evaluation metrics.

Technique	Precision	Generalisation	Simplicity	Fitness	CS
Heuristics Miner	0.6103	0.9657	0.6577	1.0000	0.8084
Inductive Miner	0.9972	0.9774	0.7333	1.0000	0.9270

Together, these results suggest that, using the object-centric interpretation of the dataset, Inductive Miner produces models that are both truthful to the log and more constrained with respect to unobserved behaviour, while still permitting good generalisation over the observed traces. By contrast, Heuristics Miner

is more open to behaviour not present in the log, permitted by lower precision, which may reflect either loose control in the object-centric models or sensitivity to concurrency/noise introduced by multiple object types.

To assess the robustness of the techniques and the possible effect of different case definitions, an experimental matrix was constructed using multiple case IDs derived from the same dataset (daily and meal-based event logs, with and without filters for hypoglycaemia and hyperglycaemia), as seen in Table 4.

Table 4. Experimental matrix with combined score values across different case attribute definitions.

	Day	Meal	Meal_HH	Day_HH
Heuristics Miner	0.6596	0.8067	0.8132	0.6125
Inductive Miner	0.6892	0.8989	0.7905	0.6657
ILP Miner	0.5822	0.7085	0.6506	0.5709
Alpha Plus	0.9800	0.8744	0.5587	0.5322
Fodina	0.7616	0.7035	0.4270	0.6810

Results show that Heuristics and Inductive Miner remain relatively stable across the different case definitions, although some variability is observed, particularly for Inductive Miner. In contrast, Alpha Plus and Fodina exhibit higher sensitivity to case-definition granularity, with substantial performance degradation under more granular and dense case notions. ILP Miner consistently produces lower combined scores and shows little variation between case definitions, indicating uniformly weaker performance rather than strong sensitivity to changes in case granularity.

These results suggest that case definition plays a critical role in process discovery from health data, and that not all algorithms are equally resilient to changes in temporal or semantic aggregation.

The two discovered Petri Nets exhibit different structural characteristics that reflect the underlying modelling choices.

The object-centric Petri Net (Fig. 4) is substantially more compact and more clearly organised. By representing post-prandial episodes and related entities as distinct object types, the object-centric miner separates concerns that would, otherwise, be blended in a single case stream. This separation creates a net in which relations between events are more explicit and semantically coherent. Recurring episode patterns (for example, the sequence meal → peak → recovery cycles) are represented as compact looping structures that are easy to follow visually and to interpret analytically.

By contrast, the traditional Petri Net produced using meal-based case identification (Fig. 5) is considerably more complex. Aggregating heterogeneous attributes and concurrent behaviours into a single case identifier forces the discovery algorithm to encode a large number of distinct behaviours and contextual

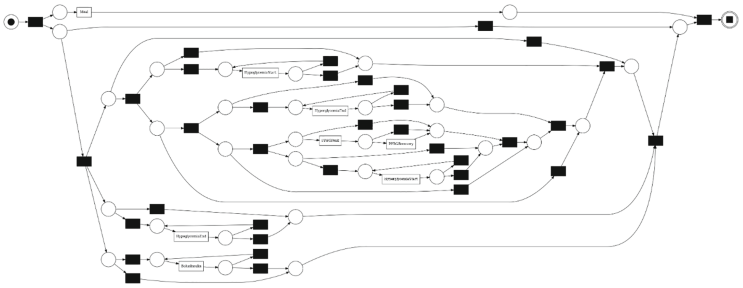

Fig. 4. Petri Net obtained using the Object-Centric Heuristics Miner.

arrangements within one net, resulting in many places, transitions, and alternative paths. This structural complexity difficult human interpretability and, as observed in the literature, tends to reduce model generalisation: highly complex networks can reproduce the observed traces closely (high fitness)but often exhibit behaviour that overfits the sample and performs worse on plausible unseen traces.

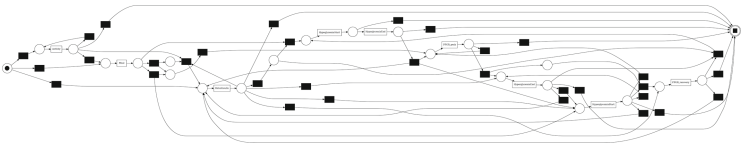

Fig. 5. Petri Net discovered using the traditional Heuristics Miner with meal-based case identification, filtered for hypoglycaemia and hyperglycaemia events.

Taken together, these observations suggest a pragmatic trade-off for multimodal health data: the object-centric representation improves interpretability by making inter-entity relations explicit and by exposing looping and concurrent patterns in a semantically meaningful way, while case-centric flattening into a single case stream can generate more complex nets that attempt to accommodate many attributes simultaneously.

6 Discussion

The results address the three sub-questions defined in the introduction. Regarding the first sub-question, Table 1 provides a structured comparison of available process discovery and object-centric techniques, and Tables 2, 3 and 4 quantify their performance across four quality dimensions on real health data. Regarding the second sub-question, the event log construction pipeline described in Sect. 4.2 demonstrates that multimodal sensor and self-report streams can be systematically transformed into both XES and OCEL formats through rule-based inference and temporal windowing. Regarding the third sub-question, Heuristics

Miner and Inductive Miner consistently achieve the best balance of fitness, interpretability, and robustness across case definitions, with object-centric variants further improving precision and generalisation.

The main goal of this study is to investigate how human health behaviour can be modelled from real-world, multimodal data and to evaluate whether process mining can produce meaningful, personalized representations of such behaviours.

The results show that Heuristics Miner presents a profile characterized by high fitness and generalisation, but with moderate precision. This behaviour suggests that the discovered models reproduce a large portion of observed traces while still allowing some additional variability beyond the log.

In the context of human health data, which are usually affected by noise and large variability, this kind of behaviour can be beneficial. The technique reliably represents recurring patterns without over-constraining the model so much that slightly atypical traces are excluded. For clinical use, however, moderate precision means that the models may include false behaviour.

Inductive Miner exhibits a performance profile of achieving perfect fitness, high simplicity and high generalisation, while maintaining stability across different case definitions. The lower precision observed is consistent with the algorithm's abstraction mechanism, which compresses observed behaviour into a smaller structural model, improving interpretability but sometimes omitting fine-grained differences between traces.

In this domain, model interpretability and structural clarity are essential for clinical validation, analysis, and communication with non-technical stakeholders. Although Inductive Miner exhibits lower precision on this dataset, this behaviour can be attributed to its structural assumptions and abstraction mechanisms, which compress observed behaviour into compact representations. Consequently, some fine-grained behavioural aspects may be lost.

Alpha Plus, despite achieving the highest combined score, exemplifies the limitations of trusting only on aggregate metrics. This observation reinforces the importance of aligning the evaluation criteria with domain-specific objectives rather than optimizing generic quality scores.

The object-centric analysis reinforces these conclusions by revealing structural and behavioural properties that are difficult to capture under traditional case-centric. In contrast to single-case modelling, OCPM enable a more truthful representation of multimodal and context-dependent human health behaviour, where actions emerge from the interaction of behavioural and context objects rather than from a single linear case. Variability across days, meals, and context conditions are not treated as deviation from a single trace, but as a natural consequence of interacting behavioural dimensions.

Additionally, the object-centric representation tends to reduce overgeneralisation and over-fitting effects observed in the case-centric setting. By preserving object relations, concurrency, and shared events, object-centric models provide a more grounded behavioural space, offering greater expressive power while remaining suitable for abstraction, comparison, and conformance analysis.

This study has some limitations. The analysis is based on a single, diabetes-focused dataset, which limits the generalisability of the findings. Given the small sample size ($n = 17$) and the specific nature of Type 1 Diabetes management, the behavioral patterns discovered should be viewed as a methodological validation of the OCPM pipeline rather than universal claims about human health behavior. Second, the discovered models and their quality assessments are sensitive to methodological choices, particularly case-ID definitions, temporal segmentation strategies, and preprocessing decisions. Additionally, the modelling approach adopted in this study is predominantly deterministic, relying on control-flow representations that encode observed behavioural sequences as fixed structural relations. Human health behaviour, however, is stochastic, context-dependent, and probabilistic in nature. As a consequence, deterministic process models cannot fully capture the intrinsic variability, uncertainty, and adaptive dynamics that characterise real-world behaviour. While the discovered models approximate dominant behavioural patterns, they cannot represent human behaviour with total exactness.

Together, the findings suggest that no single technique universally captures all relevant aspects of human health behaviour. Instead, Heuristics Miner and Inductive Miner emerge as suitable for this domain due to their complementary strengths: the capacity to capture frequent patterns with high fidelity, while Inductive Miner provides structurally sound and interpretable models that support formal analysis and clinical validation. Their relative robustness to case definitions further supports their applicability in real-world health datasets, where temporal aggregation and semantic boundaries are not clearly defined.

6.1 Future Work

Future work can focus on extending both the methodological and application-oriented aspects of this work. From a methodological perspective, research can explore how the development or adaptation of algorithms that more closely align with specific behavioural patterns of interest, particularly in scenarios where existing approaches fail to adequately capture such behaviours' dynamics. An important direction consists in designing an interface capable of assisting users by providing contextually relevant and actionable feedback, while simultaneously promoting greater user autonomy. Such an interface would support personalised monitoring, behaviour recommendations and adaptive guidance, providing informed decision-making and progressive behavioural adjustment over time.

7 Conclusions

The findings provide insights about how such methods can support a deeper understanding of behavioural dynamics while informing the design of more personalised and adaptive digital health solutions.

Overall, the results demonstrate that no single process discovery technique can be assumed as ideal for modelling human health behaviour.

OCPM emerges not as a technical alternative, but as a more appropriate modelling interpretation for health-related data, as it enables the representation of interacting behavioural and context entities. Techniques such as Heuristics Miner and Inductive Miner, particularly under object-centric interpretations, demonstrate characteristics that align more closely with the requirements of human behaviour modelling, offering a balanced trade-off between behavioural fidelity, interpretability, and generalisation.

References

1. World Health Organization. Noncommunicable diseases (2021). https://www.who.int/news-room/fact-sheets/detail/noncommunicable-diseases
2. Topol, E.: The Creative Destruction of Medicine: How the Digital Revolution Will Create Better Health Care. Basic Books (2019)
3. Almeida, M., Machado, J., Sousa, R., Peixoto, H.: AI-powered automation in healthcare: a multi-agent approach with LLM. Commun. Comput. Info. Sci. **2644**, pp. 132–143. Springer, Deutschland, Journal Abbreviation: Commun. Comput. Inf. Sci (2025)
4. Brzychczy, E., Aleknonytė-Resch, M., Janssen, D., Koschmider, A.: Process mining on sensor data: a review of related works. Knowl. Inf. Syst. **67**(6), 4915–4948 (2025)
5. Ferreira, D.R.: Control-flow perspective. In: Ferreira, D.R. (ed.) A Primer on Process Mining: Practical Skills with Python and Graphviz, pp. 15–29. Springer, Cham (2020)
6. White, D.R.: Dynamics of human behavior. World Futures **65**(1), 25–35 (2009)
7. Saylam, R., Sahingoz, O.K.: Process mining in business process management: concepts and challenges. In: 2013 International Conference on Electronics, Computer and Computation (ICECCO), pp. 131–134 (2013)
8. Conner, M.: Health behaviors. In: International Encyclopedia of the Social & Behavioral Sciences (2015)
9. Sztyler, T., Völker, J., Carmona, J., Meier, O., Stuckenschmidt, H.: Discovery of personal processes from labeled sensor data: an application of process mining to personalized health care. In: Business Process Management Workshops. LNBIP, vol. 256, pp. 164–175. Springer, Cham (2015)
10. Cancela, J., Charlafti, I., Colloud, S., Wu, C.: Digital health in the era of personalized healthcare: opportunities and challenges for bringing research and patient care to a new level. In: Digit. Health, 7–31. Elsevier (2021)
11. GCruz, ., Guimarães, T., Santos, M.F., Machado, J.: Decentralize healthcare marketplace. Procedia Comput. Sci. **231**, 439–444. Elsevier B.V. (2024)
12. Rehse, J.-R., Leemans, S.J.J., Fettke, P., van der Werf, J.M.E.M.: On process discovery experimentation: addressing the need for research methodology in process discovery. ACM Trans. Softw. Eng. Methodol. **34**(1), 3:1–3:29 (2024)
13. Zee, P.C., Attarian, H., Videnovic, A.: Circadian rhythm abnormalities. Continuum: Lifelong Learn. Neurol. **19**(1 Sleep Disorders), 132–147 (2013)
14. van der Aalst, W.: Process Mining. Springer, Heidelberg (2016). https://doi.org/10.1007/978-3-662-49851-4
15. Alsuhaymi, A., et al.: A Longitudinal multimodal dataset of type 1 diabetes. Sci. Data **12**(1), 1379 (2025)

16. Fallon, M., Rehse, J.-R., Heinzl, A.: Human behavior mining: a framework for theorizing about mHealth behavior using digital trace data. J. Assoc. Inf. Syst. **26**(3), 633–667 (2025)
17. Leemans, M.: Hierarchical Process Mining for Scalable Software Analysis. Technical report, Eindhoven University of Technology (2018)
18. Conradi, R., Jaccheri, M.L.: Process modelling languages. In: Derniame, J.-C., Kaba, B.A., Wastell, D. (eds.) Software Process: Principles, Methodology, and Technology. LNCS, vol. 1500, pp. 27–52. Springer, Heidelberg (1999). https://doi.org/10.1007/3-540-49205-4_3
19. van der Aalst, W.M.P.: Object-centric process mining: an introduction. In: Cerone, A. (ed.) ICTAC 2021. LNCS, pp. 73–105. Springer, Cham (2023)
20. Celonis. Getting started with object-centric process mining. Accessed 12 Mar 2026
21. van der Aalst, W.M.P., Carmona, J. (eds.): Process Mining Handbook. LNBIP, vol. 448. Springer, Cham (2022). https://doi.org/10.1007/978-3-031-08848-3
22. Aversano, L., Iammarino, M., Madau, A., Pirlo, G., Semeraro, G.: Process mining applications in healthcare: a systematic literature review. PeerJ Comput. Sci. **11**, e2613 (2025). Publisher: PeerJ Inc
23. De Weerdt, J., De Backer, M., Vanthienen, J., Baesens, B.: A multi-dimensional quality assessment of state-of-the-art process discovery algorithms using real-life event logs. Inf. Syst. **37**(7), 654–676 (2012)
24. Kurniati, A.P., Kusuma, G.P., Wisudiawan, G.A.A.: Implementing heuristic miner for different types of event logs. ARPN J. Eng. Appl. Sci. **11**(8), 5114–5120 (2016)
25. Folz-Weinstein, S., Bergenthum, R., Desel, J., Kovář, J.: ILP2 miner - process discovery for partially ordered event logs using integer linear programming. In: Gomes, L., Lorenz, R. (eds.) PETRI NETS 2023. LNCS, vol. 13929, pp. 59–76. Springer, Cham (2023). https://doi.org/10.1007/978-3-031-33620-1_4
26. van Eck, M.L., Lu, X., Leemans, S.J.J., van der Aalst, W.M.P.: PM^2: a process mining project methodology. In: Zdravkovic, J., Kirikova, M., Johannesson, P. (eds.) CAiSE 2015. LNCS, vol. 9097, pp. 297–313. Springer, Cham (2015). https://doi.org/10.1007/978-3-319-19069-3_19

Data-Driven Hospital Scheduling: A Multi-criteria Evaluation of Algorithmic Approaches

Rafael Amorim, Afonso Lobo, João Lopes(✉), Tiago Guimarães, Júlio Duarte, and Manuel Filipe Santos

ALGORITMI/LASI Research Centre, University of Minho, Braga, Portugal
jlopes@dsi.uminho.pt

Abstract. It is critical in a health care institution to efficiently schedule medical assessments considering resources, clinical priorities and operational limits, and create a delicate balance to deliver efficient, timely and quality care. This work studies the medical exam scheduling problem using real data from Unidade Local de Saúde de Santo António (ULSSA), which has to allocate exams into operational time slots, with multiple competing constraints. An assessment of three optimization methods, namely Mixed-Integer Linear Programming (MILP), Particle Swarm Optimization (PSO) and Genetic Algorithms (GA) is presented. The proposed solutions are evaluated through a multi-criteria objective function that includes penalties for patient waiting time, deadline violations, priority non-compliance and idle time in scheduling blocks. This formulation allows for a realistic expression of operational-clinical trade-offs of the hospital. The results indicate that GA achieves the best overall performance among the evaluated methods, obtaining the lowest total penalty value and demonstrating superior ability to balance solution quality with scheduling flexibility under the defined multi-criteria objective function. In addition to optimizing the best-found solution, clustering analysis is performed on it to understand any hidden patterns in examination sequencing, specifically in the occurrence of consecutive examinations possessing the same attributes. Overall, the results highlight the usefulness of coupling optimization methods with data-driven pattern assessment to improve hospital scheduling systems. It will help in making decision-support systems in healthcare operations more adaptive, effective and clinically optimized.

Keywords: Medical Examination Scheduling · Healthcare Optimization

1 Introduction

Efficient scheduling of clinical services represents a critical challenge in modern healthcare systems. Hospital scheduling systems are essential for managing

© The Author(s), under exclusive license to Springer Nature Switzerland AG 2027
O. Gervasi et al. (Eds.): ICCSA 2026 Workshops, LNCS 16761, pp. 619–630, 2027.
https://doi.org/10.1007/978-3-032-30527-5_40

patient access to medical professionals and diagnostic resources, playing a central role in ensuring timely care delivery and the efficient utilization of available capacity [1]. However, the inherent variability in service durations, uncertainty associated with patient behavior, and the limited availability of healthcare resources significantly increase the complexity of scheduling decisions [1,2]. As a result, healthcare scheduling has been extensively studied within the field of operations research [3,4].

Hospital scheduling problems typically involve multiple and often conflicting operational constraints, including patient prioritization, heterogeneous service times, resource availability, and shift-related limitations. These characteristics render the problem highly complex, frequently leading to formulations based on combinatorial optimization [5]. To address this complexity, a wide range of solution approaches has been proposed, including exact mathematical programming methods and metaheuristic techniques tailored to healthcare service planning [3,6]. Despite the significant body of research in this domain, several challenges remain. In particular, there is a lack of systematic comparative analyses of exact and metaheuristic approaches under realistic multi-criteria formulations that simultaneously capture operational efficiency and clinical priorities. Furthermore, limited attention has been given to the integration of optimization outputs with data-driven analytical techniques capable of extracting actionable patterns from scheduling solutions.

In this context, this study addresses the medical examination scheduling problem in a real hospital setting by developing and evaluating three optimization approaches: Mixed-Integer Linear Programming (MILP), Particle Swarm Optimization (PSO), and Genetic Algorithms (GA) [8,11,12]. The proposed solutions are assessed using a multi-criteria objective function that incorporates key operational constraints, including waiting times, deadline adherence, priority compliance, and resource utilization. Additionally, this work extends beyond optimization by incorporating a post-optimization clustering analysis on the best-performing solution, aiming to identify latent patterns in exam sequencing and scheduling structures. This combined approach contributes to the development of more informed and data-driven decision-support mechanisms for healthcare operations, bridging optimization techniques with knowledge discovery processes.

This paper is organized as follows. Section 2 provides the background, covering the scheduling process, a review of related work, and the identification of operational gaps in the literature. Section 3 describes the three optimization approaches proposed in this study. Section 4 outlines the Design Science Research methodology followed. Section 5 formally defines the problem and the multi-criteria objective function. Section 6 presents and discusses the results, including the multi-criteria evaluation, the comparison with the hospital's current scheduling process, the clustering analysis, and the main contributions of the proposed approach. Finally, Sect. 7 draws the conclusions and outlines directions for future research.

2 Background

2.1 Scheduling Process

The problem involves assigning exam requests to available time slots. Each exam is characterized by attributes relevant to the decision-making process, such as the request creation date, the estimated duration, the priority level, the exam description, and the deadline for completion. The time structure consists of a single time slot per day, within a fixed daily operating window. The problem was thus modeled as a process of allocating exams to daily shifts with limited time capacity. Solutions are constructed from an ordered sequence of exams, which determines the order in which they are considered for allocation, always ensuring that the total duration of the exams does not exceed the capacity of the shift in which they are scheduled. To evaluate the quality of the generated solutions, operational criteria are considered, such as patient wait times, delays relative to the deadline, clinical priorities, efficient use of shifts, and operational continuity between exams with similar descriptions.

2.2 Related Work

The operations research literature has seen substantial studies on healthcare scheduling problems because of their impact on service efficiencies, resource utilization, and patient waiting time [1]. These problems exist in almost every hospital environment such as outpatient scheduling, surgical planning and diagnostic examination allocation. Each of them exhibits a different level of complexity thanks to the clinical and operational constraints involved [5,7].

As various type of optimization approaches have been devised for these challenges. Methods based on mathematical programming, particularly Mixed-Integer Linear Programming (MILP), facilitate the explicit formulation of operational constraints and optimization goal, which are well suited for structured problems [3]. Nevertheless, these strategies exhibit important computational restrictions that restrict their scalability and usability when the difficulty and dimensions of the problem rise [6].

Heuristic and metaheuristic methods have become an extensively researched alternative to address large and complex scheduling problems. These techniques allow for an efficient search within large solution spaces and an ability to achieve good quality solutions within acceptable computational times. In particular multi-constraint and multi-objective environments [3,4]. Nature-inspired algorithms and population-based techniques, like Particle Swarm Optimization and Genetic Algorithms, have made remarkable strides in healthcare scheduling [8].

Also, in the scheduling literature, the definition of job sets containing a certain similarity in characteristics is partly used for batching, sequence-dependent scheduling where the order of execution affects the systems' performance [6]. Hospital environments are especially affected by this since tests that are similar may be grouped together to make operations easier and to cut down on set-up or gap times.

2.3 Operational Gaps

Despite the significant number of existing studies, some relevant limitations persist in the literature on healthcare scheduling. Many studies focus on the application of a single optimization method, making it difficult to directly compare different approaches when applied to the same problem [3]. Similarly, a considerable portion of the studies relies on simplified scenarios or simulated data, which do not always adequately capture the complexity and operational constraints present in real hospital settings [5,6]. There is also limited exploration of the structural patterns present in the generated schedules. In particular, the relationship between the criteria defined in the objective function and the organization of exams over time remains largely unexplored. It is therefore important not only to compare different optimization approaches to the same problem using real data, but also to analyze, in a complementary manner, the patterns emerging in the generated solutions, allowing for a more detailed interpretation of each model's behavior in scheduling problems.

3 Proposed Algorithms

This study aimed to evaluate three different optimization approaches: Mixed-Integer Linear Programming (MILP), Genetic Algorithm (GA), and Particle Swarm Optimization (PSO). The MILP method relate to an exact method that is based on mathematical programming. While GA and PSO are population-based metaheuristics that are widely used to solve complex combinatorial optimization problems [8,11,12].

All methodologies share a common representation for solutions. A candidate solution is constructed as an ordered sequence of exam requests defining the order in which exams are considered for allocation. Next, a decoding procedure is implemented to convert the obtained sequence into a feasible schedule by assigning examinations to daily time slots sequentially within capacity constraints. In particular, each exam is assigned to the first available time slot that has enough available capacity, and where the total bookable duration does not exceed the shift limit. Different optimization algorithms can try out other permutations of exam sequences in the same search space. Thus using the same representation makes it consistent.

All methods optimize the same multi-criteria objective functions capturing key operational and clinical aspects, such as patient waiting times, deadline adherence, priority compliance and resource utilization. This objective function allows for a fair comparison between exact and meta-heuristic methods, which have entirely distinct characteristics.

The MILP model provides a mathematical description of the scheduling problem and its respective decision variable and constraints that characterizes their allocation. The HiGHS solver is used to solve the model with a time limit of 60 s and a tolerance for relative optimality gap of 10% for a balance between solution quality and computational tractability.

The GA has a population of 80 individuals for 12 generations, with a crossover probability of 0.9 and a mutation probability of 0.2. Tournament selection with size 3 is used, as well as elitism that maintains the best two individuals per generation. The Particle Swarm Optimization algorithm involved a population size of 100 particles, while performing in 40 iterations, utilizing inertia weight of 0.65, cognitive coefficient and social coefficient are set as 1.4. To ensure a proper balance between exploring the search space and identifying the optimal solution, these parameters were adjusted as the models were tested and implemented.

4 Methodologies

This study follows a Design Science Research (DSR) approach [9,10], which provides the overarching methodological framework guiding the research process. DSR is particularly well suited for this work as it focuses on the design and evaluation of artefacts (in this case, computational models) intended to solve real-world problems in organizational contexts such as healthcare operations.

The research process is structured around three DSR stages that map directly onto the contributions of this paper. In the problem identification stage, the scheduling problem is defined using real hospital data from ULSSA, and operational constraints are elicited with the support of medical professionals. This grounds the artefact design in authentic clinical and organizational requirements rather than simplified assumptions.

In the artefact design stage, three optimization approaches are developed under a unified problem formulation and shared objective function. This design choice ensures that differences in performance are attributable to the algorithms themselves, rather than to inconsistencies in problem representation.

Finally, in the evaluation stage, the artefacts are assessed through computational experiments, compared against each other and against the hospital's current scheduling practice. Each algorithm is executed 30 times to account for the stochastic nature of metaheuristic methods, with results reported as mean and standard deviation. This evaluation closes the DSR cycle by producing actionable knowledge about which algorithmic approaches best address the identified problem.

5 Problem Definition

Each test is defined by attributes relevant to decision-making, which were identified with the help of medical professionals who supported the strategic approach to this problem, identifying the expected duration, clinical priority level, request creation date, and completion deadline as the most important parameters. Following an initial analysis of the data, a time structure was defined consisting of a single daily shift, corresponding to the operating period between 8:00 a.m. and 11:00 p.m., during which a higher volume of exams was historically recorded. In addition to capacity constraints, it was determined that the scheduling process must take into account multiple operational factors, including patient wait times,

delays relative to deadlines, adherence to clinical priorities, and efficient use of available capacity. Furthermore, operational continuity is considered between consecutively scheduled exams with similar characteristics.

The problem can therefore be formulated as a combinatorial optimization problem, where different permutations of examination sequences lead to distinct scheduling solutions. The quality of each solution is evaluated through a multi-criteria objective function:

$$\begin{aligned} Z = {} & w_1 \textstyle\sum_{i \in A} \max(0, W_i) + \\ & w_2 \textstyle\sum_{i \in A} \max(0, D_i) + \\ & \textstyle\sum_{i \in A} \left(w_3 N_i^{(1)} + w_4 N_i^{(\geq 2)} \right) + \\ & w_5 \textstyle\sum_{p \in P} C_p - w_6 \sum_{p \in P} B_p + \\ & w_7 \textstyle\sum_{p \in P} I_p + w_8 \sum_{p \in P} I_p \, \delta \end{aligned}$$

where A denotes the set of scheduled examinations and P the set of available time slots (shifts).

- W_i: waiting time of examination i;
- D_i: delay of examination i relative to its deadline;
- $N_i^{(1)}$: number of pending examinations with a higher priority level by one level;
- $N_i^{(\geq 2)}$: number of pending examinations with a higher priority level by two or more levels;
- C_p: number of type changes between consecutive examinations in shift p;
- B_p: number of consecutive pairs of examinations of the same type in shift p;
- I_p: idle time in shift p;
- δ: binary indicator equal to 1 if there exist unscheduled examinations, and 0 otherwise.

The objective is to minimize Z, reducing waiting times, delays, priority violations, and idle time, while promoting the grouping of examinations with similar characteristics within each shift.

6 Results

6.1 Multi-criteria Evaluation

The optimization approaches were compared using the formulating multi-criteria objective function which takes into consideration important operational aspects of the scheduling process, including patient waiting time, delayed deadline, prioritized patient compliance, and shift capacity utilization.

The findings demonstrate that the methods exhibit a significant difference in performance, which leads to different quality solutions. The objective function values indicate the capability of the models to minimize operational inefficiencies without being in contradiction to clinical priorities.

Figure 1 presents the total penalty values obtained by the three evaluated models: Genetic Algorithms (GA), Mixed-Integer Linear Programming (MILP,

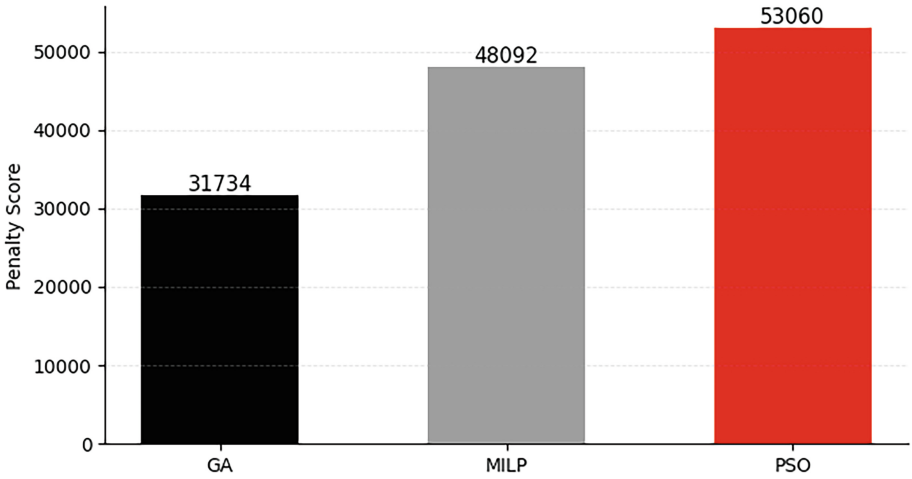

Fig. 1. Comparison of total penalty values achieved by the different optimization models under the defined multi-criteria objective function.

and Particle Swarm Optimization (PSO). As the objective function aggregates multiple operational criteria, lower penalty values indicate more effective scheduling solutions according to the defined objectives.

The results show that GA achieves the best performance, with the lowest total penalty of all the approaches we analyzed, due to its ability to explore all possible solutions and adjust the order of tests to fit the specific constraints of the problem. This flexibility is fundamental and is what allowed it to achieve optimal performance across all the different criteria we considered. Compared to the other methods, the advantage of GA in handling the problem's complexities and finding the best solution is evident. The MILP and PSO models exhibited higher penalty values, meaning they were not as effective at satisfying all conditions of the objective function simultaneously, leading to the conclusion that, for this specific scheduling problem and given the size of the dataset and the identified constraints, GA is more effective at striking a balance between solution quality and scheduling flexibility.

Based on these results, the GA model was selected for further comparison with the scheduling process currently used in the hospital.

6.2 Hospital Solution Comparison

A practical comparison between the GA-based schedule and the hospital's existing scheduling practice was carried out to examine the real-world implications of the proposed approach. Both were evaluated on the same dataset, covering the three-month period from October to December 2021.

Restricting the analysis to examinations performed within the model's operational window—08:00 to 23:00—was a necessary condition for the comparison

to hold methodological ground. Without this constraint, differences in temporal scope would confound any direct assessment of the two approaches' relative performance.

Table 1. Performance comparison between the optimization model (GA) and the hospital scheduling process

Metric	GA Model	Hospital Scheduling
Penalty score	31734	787635.5
Consecutive identical exam descriptions (%)	13.07	12.60
Scheduled examinations	3382	7488
Unscheduled examinations	6648	1781
Scheduled priority 0 (%)	0	33.48
Scheduled priority 1 (%)	0	32.20
Scheduled priority 2 (%)	100	34.32
Scheduled after deadline (%)	0	0
Scheduled before or on deadline (%)	100	100

Table 1 summarises the global comparison between the two approaches. The GA model achieves a substantially lower total penalty—a gap that reflects, above all, a closer alignment with the criteria encoded in the multi-criteria objective function.

One result that warrants attention is the higher absolute number of examinations scheduled by the hospital. This is, in fact, expected: the hospital operates through multiple concurrent teams and resources, whereas the proposed model assumes sequential allocation within a single daily shift, which inherently caps overall throughput. The difference in scheduling volume is therefore a structural consequence of these distinct operating assumptions, not an indicator of inferior optimisation performance.

It is identified that the two approaches differ in how they handle priorities. The hospital distributes exams across the different priority levels in a relatively balanced manner, while the GA model schedules exclusively high-priority cases. This behavior results directly from the penalty structure of the objective function, in which delaying or failing to assign urgent exams incurs disproportionately high costs, which guides the model toward a systematic prioritization of the most critical requests. Regarding the sequence of exams, the GA model produces a slightly higher proportion of consecutive exams with identical descriptions. An efficiency gain is observed, modest in absolute terms but consistent with the model's optimization goal of grouping similar exams within a shift, reducing costs associated with switching between exam types.

Figure2 shows the weekly trend of this metric throughout the entire analysis period. Expressing the values as percentages distinguishes the comparison from variations in the absolute number of exams, providing a clearer picture of how

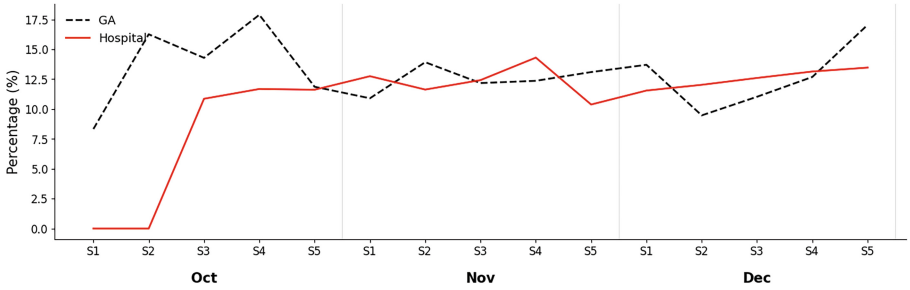

Fig. 2. Comparison of the weekly percentage of consecutively scheduled exams by description.

the metric has changed over time. Across most weeks, the GA model achieves values comparable to those recorded in the hospital scheduling process. Taken together, these results suggest that the proposed approach not only improves quantitative outcomes but also produces schedules with greater structural regularity, exploiting patterns in examination sequencing in a way the hospital's current process does not systematically attempt.

6.3 Clustering Analysis

Using K-Means clustering technique with k = 8 (determined using elbow method), k-means clustering was applied on unscheduled and scheduled examination data separately for the period OctoberâĂŞDecember 2021 using four normalized features: examination duration, priority, request creation time, and time window up to deadline. Table 2 summarizes the distinguishing profile of each group.

Table 2. Summary of K-Means clustering results for scheduled and unscheduled examinations ($k = 8$).

Group	Modality	Duration (min)	Priority	Temporal Window
Scheduled examinations				
S1–S4	CT	15–20	High (P2)	Favorable
S5–S8	MRI	40–45	High (P2)	Favorable
Unscheduled examinations				
U1–U4	Mixed	40–45	Low (P0–P1)	Tight or expired
U5–U8	Mixed	40–45	Low (P0–P1)	Less favorable

Scheduled clusters exhibit the same compositions of modality (basically CT and MRI), and shorter duration of examinations. The objective function

supports this behaviour by giving higher incentive to bunch similar examination types and also lower operational transitions. Unscheduled clusters have longer duration, lesser priority and worse time windows which makes them non-competitive for just those reasons as per the criteria. These results illustrate that the objective function governs scheduling behavior, and the output of clustering provides a clear and data-driven explanation of allocation.

6.4 Scheduling Approach and Main Contribution

The scheduling model which is proposed is based on sequential representation of the requests of examination and every solution corresponds to ordering of processing. A constructive procedure assigns examinations to free shifts subject to temporal capacity constraints to transform this sequence into a feasible schedule.

The quality of solution is assessed against a multi-criteria objective function inclusive of some of the main operational characteristics in a hospital environment, such as patient waiting time, deadline compliance, priority compliance, and capacity utilization. Through this framework, we can evaluate scheduling performance through multiple lenses. With real hospital data and experimental conditions, the proposed method is a distinctive approach to compare various optimization paradigms. In particular, both exact and metaheuristic methods are evaluated in the same decision framework. Additionally, this study goes beyond the conventional quantitative evaluation as clustering techniques were harnessed to assess structural patterns in the schedules generated. This further analysis then allows for a connection between the objective function design and observed scheduling behaviour.

This work offers three major contributions. First, it systematically evaluates different optimization approaches according to the case of a real-world hospital scheduling problem. Second, it formulates a multi-criteria objective function consistent with operational and clinical constraints. Lastly, it performs clustering-based analysis for insights into scheduling and model behaviour. As a whole, these contributions allow for performance evaluation and the explainability of healthcare scheduling systems.

7 Conclusion

Three algorithmic approaches were developed under a unified problem formulation and assessed through a shared multi-criteria objective function, enabling a systematic comparison between exact and metaheuristic methods. The results show that the GA achieves the best overall performance under the defined objective function, recording the lowest total penalty value and demonstrating a stronger capacity to simultaneously balance multiple operational and clinical criteria. This outcome suggests that population-based metaheuristic approaches are well suited to complex scheduling problems shaped by competing constraints, settings where exact methods tend to face computational limitations and metaheuristics such as PSO may struggle to consistently exploit the structure of the

solution space. The comparison with the hospital's current scheduling practice further supports the value of the proposed approach. Although the GA model operates under more restrictive assumptions (most notably, sequential allocation within a single daily shift), it achieves substantially lower penalty scores and yields schedules with greater structural regularity, particularly in the grouping of consecutive exams sharing similar characteristics. Taken together, these findings point to the practical potential of optimization-based tools to strengthen both operational efficiency and clinical priority compliance in real hospital settings.

The complementary clustering analysis offered further insight into how the objective function shapes scheduling behaviour. Examinations that were successfully scheduled consistently exhibited high priority levels, shorter durations, and favorable time windows, whereas unscheduled ones clustered around lower priorities, longer durations, and tighter or expired deadlines. This perspective confirms that the objective function effectively steers allocation decisions and provides a transparent account of the model's behaviour, adding to the overall interpretability of the scheduling system. Despite these contributions, the model rests on assumptions that constrain its direct applicability to real hospital operations. Most notably, the single-shift sequential allocation structure does not capture the concurrent use of multiple clinical teams and resources that is typical of real hospital environments. Addressing this limitation is the most pressing direction for future work.

In the short term, several extensions could increase the model's realism and robustness. The framework should be adapted to accommodate multiple concurrent shifts and parallel resource allocation, better reflecting the operational structure of hospital departments. A sensitivity analysis of the objective function weights would also be valuable, helping to clarify how different prioritization schemes influence scheduling outcomes and to support more balanced decisions across clinical priority levels. Beyond this, testing the proposed models on larger datasets and across different hospital services or exam types would help establish how broadly the findings generalize. Looking further ahead, more substantial developments become possible. The incorporation of dynamic and real-time scheduling capabilities would allow the model to handle the kinds of disruptions (cancellations, urgent requests, unexpected resource unavailability) that are routine in clinical practice but absent from the current static formulation. Introducing uncertainty in exam durations and patient arrival patterns, through stochastic or robust optimization, would bring the model closer to the variability that characterizes real healthcare operations. These extensions, taken together, would move the proposed framework toward a more adaptive and operationally grounded decision-support tool for hospital scheduling.

Acknowledgments. This work has been supported by FCT âĂŞ Fundação para a Ciência e Tecnologia within the R&D Unit Project Scopes UID/00319/2025 - Centro ALGORITMI (ALGORITMI/UM) and 2024.07481.IACDC.

References

1. Gupta, D., Denton, B.: Appointment scheduling in health care: challenges and opportunities. IIE Trans. **40**(9), 800–819 (2008). https://doi.org/10.1080/07408170802165880
2. Hall, R.: Handbook of Healthcare System Scheduling. Springer, Cham (2012). https://doi.org/10.1007/978-1-4614-1734-7
3. Abdalkareem, Z.A., Amir, A., Al-Betar, M.A., Ekhan, P., Hammouri, A.I.: Healthcare scheduling in optimization context: a review. Heal. Technol. **11**(3), 445–469 (2021). https://doi.org/10.1007/s12553-021-00547-5
4. Ala, A.L., Al-Fuqaha, A.A., Abu-Alhaj, M.M.: Outpatient appointment scheduling: a systematic review. Healthcare **10**(9), 1732 (2022). https://doi.org/10.3390/healthcare10091732
5. Hulshof, P.J.H., Kortbeek, N., Boucherie, R.J., Hans, E.W., Bakker, P.J.M.: Taxonomic classification of planning decisions in health care: a structured review of the state of the art in OR/MS. Health Syst. **1**(2), 129–175 (2012). https://doi.org/10.1057/hs.2012.18
6. Cardoen, B., Demeulemeester, E., Beliën, J.: Operating room planning and scheduling: a literature review. Eur. J. Oper. Res. **201**(3), 921–932 (2010). https://doi.org/10.1016/j.ejor.2009.04.011
7. Ahmadi-Javid, A., Jalali, Z., Klassen, K.: Outpatient appointment systems in healthcare: a review of optimization studies. Eur. J. Oper. Res. **258**(1), 3–34 (2017). https://doi.org/10.1016/j.ejor.2016.06.064
8. Squires, M., Tao, X., Elangovan, S., Gururajan, R., Zhou, X., Acharya, U.: A novel genetic algorithm-based system for the scheduling of medical treatments. Expert Syst. Appl. **195**, 116464 (2022). https://doi.org/10.1016/j.eswa.2021.116464
9. Hevner, A.R., March, S.T., Park, J., Ram, S.: Design science in information systems research. MIS Q. **28**(1), 75–105 (2004)
10. Peffers, K., Tuunanen, T., Rothenberger, M.A., Chatterjee, S.: A design science research methodology for information systems research. J. Manag. Inf. Syst. **24**(3), 45–77 (2007)
11. Huangfu, Q., Hall, J.A.J.: Parallelizing the dual revised simplex method. Math. Program. Comput. **10**(1), 119–142 (2018). https://doi.org/10.1007/s12532-017-0130-5
12. Kennedy, J., Eberhart, R.: Particle swarm optimization. In: Proceedings of ICNN'95 - International Conference on Neural Networks, vol. 4, pp. 1942–1948. (1995). https://doi.org/10.1109/ICNN.1995.488968

Supporting Hospital Operational Decision-Making Through Early Prediction of Length of Stay

Matilde Sousa[1], João Lopes[1(✉)], Tiago Guimarães[1], Agostinho Barbosa[2], and Manuel Filipe Santos[1]

[1] ALGORITMI/LASI Research Centre, University of Minho, Braga, Portugal
jlopes@dsi.uminho.pt
[2] Unidade Local de Saúde Tâmega e Sousa (ULSTS), Penafiel, Portugal

Abstract. Early prediction of hospital Length of Stay (LOS) is essential for effective bed management, discharge planning, and hospital operational coordination. While Machine Learning (ML) has been widely applied to LOS prediction, limited evidence exists on how model performance varies across different hospital operational contexts when predictions rely only on information available at admission or transfer. This study compares classical ensemble models and neural network approaches for early LOS prediction in two operational scenarios: emergency admissions and internal hospital transfers. A retrospective analysis was conducted using anonymized administrative and temporal data from Unidade Local de Saúde Tâmega e Sousa (ULSTS). Results show that gradient boosting models achieved strong ordinal performance in large emergency datasets, whereas neural networks provided more balanced predictions in smaller, highly imbalanced transfer data. These findings highlight the importance of context-aware model selection when developing predictive decision-support tools for hospital operations.

Keywords: Healthcare · Machine Learning · Length of Stay

1 Introduction

Efficient inpatient management represents a major operational challenge for modern healthcare systems worldwide. The growing demand for hospital care, driven by ageing populations, increasing prevalence of chronic diseases, and rising patient complexity, combined with inherently limited physical and human resources, contributes to persistent hospital overcrowding and negatively affects key performance indicators such as waiting times, bed availability, staff workload, and overall operational efficiency [1–5]. These pressures place considerable strain on healthcare institutions, undermining their capacity to deliver timely, high-quality care and highlighting the urgent need for more effective approaches to inpatient resource planning and management [1,3].

© The Author(s), under exclusive license to Springer Nature Switzerland AG 2027
O. Gervasi et al. (Eds.): ICCSA 2026 Workshops, LNCS 16761, pp. 631–643, 2027.
https://doi.org/10.1007/978-3-032-30527-5_41

Length of Stay (LOS) is widely recognised as a central indicator for hospital resource management, directly influencing bed allocation, discharge planning, patient flow coordination, and overall capacity management. Prolonged or unpredictable hospitalizations generate cascading inefficiencies throughout the hospital system, from delayed admissions in emergency departments to suboptimal utilisation of surgical and intensive care capacity [6,7]. Accurate LOS prediction at the time of admission allows hospital managers and clinicians to anticipate bed requirements, optimise patient pathways and workflows, support earlier discharge planning, and reduce costs associated with unnecessarily prolonged hospitalizations, all while maintaining the quality and safety of care delivered to patients [6–8]. Beyond its administrative relevance, reliable LOS estimation also carries direct clinical implications, enabling more proactive and personalised care coordination throughout the inpatient episode [8].

In this context, data-driven approaches have gained substantial traction as a means of improving predictive accuracy and supporting clinical decision-making. Recent studies have increasingly applied Machine Learning (ML) techniques to LOS prediction, demonstrating that predictive models are capable of capturing complex, non-linear interactions among demographic, clinical, and operational variables that traditional statistical methods often fail to adequately represent [6–11,17]. Algorithms such as gradient boosting, random forests, and deep learning architectures have shown promising results across a range of clinical settings, suggesting the potential for ML-based tools to become integrated components of hospital management systems [9–11]. Nevertheless, several methodological challenges persist and limit the broader adoption of these approaches in routine clinical practice. These include the appropriate selection and engineering of predictive features, the inherent heterogeneity and incompleteness of clinical data collected in real-world settings, the risk of overfitting to specific institutional contexts, and the limited generalisability of trained models across different patient populations, care pathways, or clinical environments [6,7,18]. Addressing these challenges is essential to developing LOS prediction systems that are not only statistically robust but also practically deployable and equitable across diverse healthcare contexts.

1.1 Operational Pressure and the Strategic Role of Length of Stay

LOS is a key operational indicator in hospital management, as it directly affects bed occupancy, discharge planning, staffing needs, and overall healthcare costs [6,7]. Variations in LOS can lead to capacity constraints that extend across multiple medical specialties, disrupting patient flow and limiting the system's ability to accommodate new admissions [1,19]. For this reason, a reliable estimate plays a key role in hospital capacity planning and day-to-day operational decisions [2,3,19]. Its relevance becomes even more critical in high-uncertainty settings, such as Emergency Departments. In these environments, demand variability and limited information at the time of admission make timely decision-making particularly challenging. Overcrowding in emergency departments is consistently associated with longer wait times and reduced operational efficiency [4,11,20].

This metric also has a direct relationship with the hospital's internal dynamics, particularly in the context of interdepartmental transfers, where it influences both workload distribution and bed turnover. However, despite its clear operational importance, the application of predictive models in transfer scenarios remains relatively limited in the existing literature.

1.2 Predictive Modeling of LOS: From Statistical Approaches to Deep Learning

Predictive modelling has become an important research direction for estimating hospital LOS, driven by the increasing availability of electronic health records and administrative Healthcare datasets. Early studies relied mainly on traditional statistical methods, such as linear regression, logistic regression, and survival analysis, which provided interpretable insights into hospitalization duration but often assumed linear relationships between variables [9,18].

With the growth of Healthcare data, ML techniques have increasingly been adopted to capture nonlinear relationships and complex interactions among demographic, clinical, and operational variables. Tree-based ensemble models, including Random Forest and Gradient Boosting, have shown strong predictive performance in structured datasets and are widely used in LOS prediction tasks [7,12,21].

More recently, deep learning approaches have been explored for modeling high-dimensional clinical data, demonstrating promising results in predicting outcomes such as LOS, mortality, and readmission [10,13,14]. Neural architectures designed for tabular Healthcare data have further expanded the applicability of deep learning methods in structured datasets [11,15].

Despite these advances, systematic reviews indicate that no single modelling approach consistently outperforms others across all Healthcare contexts, as performance often depends on dataset size, eature availability, class imbalance, and the clinical environment in which predictions are applied [6,7,22].

1.3 Study Objective and Contributions

Despite the growing use of ML techniques for predicting hospital LOS, several methodological and operational limitations remain. Many models rely on clinical variables that become available only during hospitalization, such as laboratory tests or treatment information. Although these variables may improve predictive performance, they limit the practical applicability of models intended to support early operational decision-making at the time of admission or transfer [6,7,18].

Additionally, there is no consensus on the most appropriate formulation of the LOS prediction problem. Some studies treat LOS as a regression task, while others adopt binary classification to identify prolonged hospitalizations, approaches that may not reflect the operational need to interpret LOS through clinically meaningful time intervals for capacity planning [9,21].

Unlike many previous approaches that rely on variables collected during hospitalization, the proposed models use information realistically available for operational planning [6,7]. The study evaluates LOS prediction across two distinct hospital contexts: emergency admissions and internal patient transfers. These scenarios differ in dataset scale, feature availability, and class imbalance, allowing analysis of model behaviour under heterogeneous operational conditions. Classical ensemble ML models and neural network architectures are compared using consistent validation procedures and imbalance-aware evaluation metrics. The main contributions are:

1. Context-aware formulation of the LOS prediction problem aligned with hospital operational workflows, using only information available at the time of admission or transfer;
2. Systematic comparison between classical ensemble and deep learning models across two operationally distinct hospital contexts with different data regimes;
3. Analysis of how dataset scale, class imbalance, and structural heterogeneity influence predictive performance and model generalisation;
4. Discussion of the trade-off between predictive optimality and operational maintainability as an explicit criterion for model selection in hospital decision-support contexts.

This paper is organised as follows. Chapter 2 describes the research methodology, including the study design, ethical considerations, problem formulation, data understanding and preprocessing procedures, and the Machine Learning models developed for each operational context. Chapter 3 presents the comparative results across the emergency admission and internal hospital transfer scenarios. Chapter 4 discusses the findings in relation to the existing literature and reflects on the practical implications for hospital decision support. Finally, a conclusion for the paper, emphasizing directions for future research.

2 Methods

2.1 Ethical Considerations

This study used exclusively anonymous data provided by ULSTS and did not involve any sensitive personal information. As a result, review by an ethics committee was not required, in accordance with the General Data Protection Regulation (GDPR).

2.2 Study Design

The study followed a Design Science Research (DSR) methodology [24], operationalized through the Cross-Industry Standard Process for Data Mining (CRISP-DM) framework [25].

DSR provided the framework for the research, guiding the development and evaluation of artifacts designed to address a specific organizational problem [24].

Within this paradigm, the research problem was identified, and the resulting predictive models were treated as artifacts whose value is ultimately assessed by their practical utility.

CRISP-DM supplemented this methodological framework by providing a structured process model for data mining activities [25]. The framework organized the analytical workflow into six sequential phases:

1. Business Understanding, in which the organisational objectives and predictive requirements were translated into concrete data mining goals;
2. Data Understanding, encompassing the initial collection, exploration, and quality assessment of the available clinical and operational data;
3. Data Preparation, involving the transformation, cleaning, and feature engineering steps necessary to construct analysis-ready datasets;
4. Modelling, in which a range of Machine Learning algorithms were selected, configured, and trained;
5. Evaluation, where model performance was assessed against both technical metrics and the broader research objectives;
6. and Deployment, addressing the practical considerations for integrating the resulting models into hospital decision-support workflows.;

The iterative nature of CRISP-DM allowed the findings from later phases to serve as a foundation and refine the decisions made in earlier phases, ensuring that the final results were methodologically sound and aligned with the operational realities of the clinical setting.

2.3 Problem Statement

Efficient management of hospital resources requires forecasting patient flow and length of stay. LOS is a critical operational indicator that influences bed occupancy, discharge planning, staffing, and the overall performance of the system. An inaccurate estimate of LOS can lead to overcrowding, delays in admissions, and inefficient allocation of resources.

Although hospital information systems collect large volumes of administrative and operational data, planning decisions are often based on historical averages or subjective clinical judgments. Furthermore, many predictive studies use variables that are not available at the time of operational decision-making, limiting their real-world applicability. This study addresses two operational challenges:

1. **Early LOS prediction in emergency admissions (Problem A):** Emergency departments operate under high demand variability and limited downstream capacity. Admission decisions must often be made with limited information, yet accurate LOS estimates are essential for proactive bed management and atient flow coordination.
2. **LOS prediction in internal hospital transfers (Problem B):** Transfers between hospital units affect workload distribution and bed turnover. Unanticipated prolonged stays may generate congestion across departments, yet

predictive tools supporting LOS estimation at the time of transfer remain scarce.

2.4 Data Understanding and Preprocessing

Data for both use cases were extracted from the hospital information systems of ULSTS, covering emergency admission episodes and internal hospital transfer events. In both contexts, only administrative, demographic, and temporal variables available at the time of admission or transfer decision were included, ensuring real-world operational applicability and preventing information leakage from variables that arise only during hospitalization.

The emergency admissions dataset comprised historical inpatient episodes with predictors including patient demographic attributes (e.g., age, sex), admission timestamps, day-of-week and seasonal indicators, and operational descriptors such as the care location within the emergency department. LOS was defined as the elapsed time between admission and discharge and transformed into five ordinal categories ($\leq$3 days, 4–7 days, 8–14 days, 15–30 days, and >30 days), framing the prediction task as an ordinal multiclass classification problem aligned with clinically and operationally meaningful duration thresholds. Episodes were further segmented by care location, as each unit reflects a distinct clinical workflow and patient case-mix that may differentially influence LOS dynamics.

The internal transfer dataset comprised intra-hospital movement episodes between clinical specialties and physical units. Available predictors included demographic attributes, origin and destination units, transfer timestamps, and calendar-derived temporal features. LOS in this context was discretized into operationally relevant multiclass intervals, with short stays (1–3 days) aggregated into a single category to reduce class sparsity, while longer duration intervals were preserved as distinct classes to support meaningful operational differentiation.

Data preprocessing involved systematic cleaning, treatment of missing values, categorical variable encoding, and feature engineering of temporal variables to derive calendar-based indicators (e.g., day of week, month, admission period). To prevent post hoc bias, only predictors available at the time of the operational decision were retained in the modelling pipeline. Both datasets exhibited asymmetric LOS distributions characterised by a predominance of short hospitalizations and a smaller proportion of prolonged stays, a structural imbalance that informed the selection of evaluation metrics and the design of training strategies. During the exploratory phase, multiple LOS interval aggregation schemes were assessed; the final class definitions were selected based on predictive performance, class distribution stability, and alignment with operational planning requirements.

2.5 Proposed Machine Learning Models

ML Approach for Problem A (Emergency Admissions). In this context, LOS prediction was formulated as an ordinal multiclass classification task. Given

the relatively large dataset, both classical ensemble models and deep learning architectures were evaluated. Classical approaches included tree-based ensemble methods, which are well suited for structured Healthcare datasets due to their ability to capture nonlinear relationships and handle mixed feature types. In parallel, neural networks were implemented to assess whether learned embeddings and nonlinear feature representations could improve predictive performance.

ML Approach for Problem B (Internal Hospital Transfers). For internal transfers, LOS prediction was formulated as a multiclass classification task. The smaller dataset and stronger class imbalance required careful attention to model stability and generalization. Baseline classical models included Random Forest and Histogram-based Gradient Boosting, selected for their robustness in structured datasets. To mitigate class imbalance, class weighting and sampling strategies were applied during training.

Hyperparameters were optimized through cross-validation. Neural models incorporated embedding layers for categorical variables and fully connected layers to capture nonlinear feature interactions. Regularization techniques and early stopping were used to reduce overfitting.

3 Results

3.1 Comparative Results Across Operational Contexts

Although both problems involve predicting LOS, they differ substantially in class distribution and operational constraints. These differences directly influence the model's behavior, generalization ability, sensitivity to class imbalance, and the criteria used for final model selection. In the context of the emergency department, episodes were grouped by care location, representing distinct operational units within the emergency department. Each location corresponds to a specific clinical workflow, a set of patients, and a configuration of factors that can influence the dynamics of LOS. The ML models were trained independently for each location to capture specific patterns and relationships within the data. The performance of the Random Forest (RF) model across the different locations is summarized in Table 1.

Table 1. Random Forest Performance by Emergency Context

Location	Accuracy	F1-macro	AUC	QWK
1	0.832	0.830	0.971	0.875
3	0.915	0.867	0.987	0.919
4	0.651	0.658	0.891	0.758
9	0.838	0.820	0.969	0.853

The model performed well in locations 1, 3, and 9, with QWK values above 0.85, indicating agreement between the predicted and actual LOS classes. However, performance was notably lower at location 4, where both Precision and QWK decreased significantly. This decline is consistent with the reduced number of available training observations at that location. HistGradientBoosting (HGB), shown in Table 2, demonstrated consistent improvements over Random Forest at most locations.

Table 2. HGB Performance by Location in Emergency Context

Location	Accuracy	F1-macro	AUC	QWK
1	0.863	0.863	0.981	0.906
3	0.937	0.896	0.987	0.933
4	0.651	0.658	0.891	0.758
9	0.877	0.862	0.976	0.882

HGB achieved strong predictive performance at locations 1 and 3, with QWK values exceeding 0.90, indicating high agreement among the LOS categories. This confirms the effectiveness of the methods for structured data in high-volume contexts. At location 4, results stabilized due to data scarcity and a more pronounced class imbalance, which limited the model's ability to learn robust decision boundaries.

Error analysis revealed that most misclassifications occurred between adjacent LOS categories. Performance was also stronger for extreme LOS categories compared to intermediate ranges, reflecting the difficulty of distinguishing hospitalizations of average duration.

Although site-specific models achieved high performance in some units, maintaining multiple models introduced scalability and maintenance challenges. To address this limitation, a global ordinal neural network was trained using all emergency episodes collectively. The validation results for this model are presented in Table 3.

Table 3. Global Neural Network

Metric	Value
F1-macro	0.365
QWK	0.453
Within ± 1 class	$\sim$0.65

Although the macro-F1 and QWK scores were lower than those achieved by the best classical models per location, approximately 65% of the predictions fell

within ±1 LOS of the true class. The neural model preserved the ordinal structure and incorporated an auxiliary regression task to improve training stability. It is important to note that it provided several structural advantages, including a single global model applicable across all locations, embedding-based categorical representations, and improved scalability. For these reasons, the neural model was selected as the final solution for the emergency context.

The transfer setting presented a different scenario, with a smaller dataset and severe class imbalance. The classic ensemble baselines exhibited severe overfitting, and to improve generalization, a robust pipeline incorporating temporal validation, correlation filtering, and ensemble techniques was introduced. The best-performing classic model (Bagging) is presented in Table 4.

Table 4. Advanced Temporal Pipeline (Bagging)

Model	Holdout Accuracy	Macro F1	Weighted F1	Holdout Kappa
Bagging	0.888	0.220	0.870	0.711

The holdout Kappa result indicates a significant predictive structure, beyond random agreement. The F1-macro performance is below the desired threshold, reflecting a persistent difficulty in recognizing minority LOS categories due to class imbalance. To improve performance, a neural network was trained using early stopping and weighted sampling. The final validation results are presented in Table 5.

Table 5. Neural Network

Metric	Value
Accuracy	0.855
Balanced Accuracy	0.855
Macro F1	0.849
Macro Precision	0.862
Macro Recall	0.855
Kappa	0.850

The global ordinal neural network achieved balanced and stable predictive performance, with Macro F1 $\approx$ 0.85 and QWK $\approx$ 0.85. Low variability across validation folds indicated strong robustness and generalization. The neural approach provided consistent performance across LOS categories and mitigated class imbalance by improving discrimination in minority and intermediate classes while preserving ordinal consistency. This resulted in more homogeneous predictions across operational units, supporting a scalable and unified deployment.

In the emergency setting, the larger dataset enabled strong performance of classical per-location models, with QWK values above 0.90 in some units. However, maintaining multiple models introduced fragmentation and scalability challenges. In contrast, the transfer context was characterised by a smaller dataset and severe class imbalance. Classical models showed poor generalisation, whereas the neural model achieved balanced macro-level performance and stronger inter-class agreement.

4 Discussion

The results align with the broader literature on ML-based LOS prediction [6,17]. The strong performance of gradient boosting in the emergency context is consistent with evidence that tree-based ensembles effectively capture nonlinear interactions in structured administrative data [9]. The superiority of the neural model in the transfer context corroborates findings that deep architectures offer advantages under class imbalance and limited sample sizes [11]. A notable divergence, however, is that the global neural model did not surpass the best per-location classical models in the emergency setting, suggesting that gradient boosting remains highly competitive when sufficient structured data are available. The near-zero Cohen's Kappa of classical baselines in the transfer context, despite moderate accuracy, further highlights that accuracy is a misleading metric in severely imbalanced multiclass settings. Macro F1 and Kappa proved essential for detecting model collapse in minority classes.

From a practical standpoint, these results reinforce the idea that model selection in healthcare data analysis must balance predictive performance with operational feasibility. The global neural model in the emergency department setting, despite exhibiting slightly lower peak metrics, reduces implementation complexity by providing a single artifact for all care settings (a consideration that is often just as important as marginal gains in metrics in real-world hospital settings).

These findings are specific to ULSTS and should not be generalised without further validation. Differences in patient case-mix, specialty configurations, coding conventions, and data quality across institutions may substantially affect model performance. External validation and context-specific recalibration would be required before deployment in other settings.

5 Conclusion

This study evaluated ML approaches for early LOS prediction across two operationally distinct contexts at ULSTS demonstrating that no single modelling approach dominates across settings. The effectiveness of each approach depends on the type of data: Gradient Boosting performed well on large, structured datasets, while neural networks proved to be more robust with small sample sizes and severe class imbalances. Model selection was therefore guided not only by predictive metrics but also by operational considerations related to scalability and implementation feasibility.

The results are limited to the scope of a single institution. Implementing these models as operational decision-support tools would require several steps that were not addressed in this study. From an integration perspective, the predictive results should be incorporated into existing hospital workflows, with bed managers, clinical coordinators, and admissions staff as the primary stakeholders. Explanation mechanisms, such as summaries of the contribution of features or risk alerts for predicted prolonged stays, would be essential to bolster clinicians' confidence and feasibility. From an operational perspective, implementation would require automated data flows linked to the hospital information system, mechanisms for detecting data anomalies, and periodic retraining of the models to account for changes in the composition of the patient population or in care pathways. Finally, evaluation studies (e.g., bed turnover rates, unplanned prolonged stays, and discharge preparation times) would be needed to determine whether predictive accuracy translates into measurable operational benefits. Additionally, validation across multiple sites would be necessary to assess the model's transferability between institutions with different organizational structures and patient populations.

Acknowledgments. This work has been supported by FCT–Fundação para a Ciência e Tecnologia within the R&D Unit Project Scope UID/00319/2025 - Centro ALGORITMI (ALGORITMI/UM).

References

1. Bagust A, Place M, Posnett, J.W.: Dynamics of bed use in accommodating emergency admissions: stochastic simulation model. BMJ. **319**, 155 (1999). https://doi.org/10.1136/bmj.319.7203.155
2. Hulshof, P., Kortbeek, N., Boucherie, R., et al.: Taxonomic classification of planning decisions in health care: a structured review of the state of the art in OR/MS. Health Syst. **1**, 129–175 (2012). https://doi.org/10.1057/hs.2012.18
3. Litvak, E., Bisognano, M.: More patients, less payment: increasing hospital efficiency in the aftermath of health reform. Health Affairs. **30**(1), 76–80 (2011). https://doi.org/10.1377/hlthaff.2010.1114
4. Hoot, N.R., Aronsky, D.: Systematic review of emergency department crowding: causes, effects, and solutions. Ann Emerg Med. **52**(2), 126–136 (2008). https://doi.org/10.1016/j.annemergmed.2008.03.014
5. Morley, C., Unwin, M., Peterson, G.M., Stankovich, J., Kinsman, L.: Emergency department crowding: a systematic review of causes, consequences and solutions. PLoS One. **13**(8), e0203316 (2018). https://doi.org/10.1371/journal.pone.0203316
6. Gokhale, S., Taylor, D., Gill, J., et al.: Hospital length of stay prediction tools for all hospital admissions and general medicine populations: systematic review and meta-analysis. Front Med (Lausanne). **10**, 1192969 (2023). https://doi.org/10.3389/fmed.2023.1192969
7. Lequertier, V., Wang, T., Fondrevelle, J., Augusto, V., Duclos, A.: Hospital length of stay prediction methods: a systematic review. Med Care. **59**(10), 929–938 (2021). https://doi.org/10.1097/MLR.0000000000001596

8. Beam, A.L., Kohane, I.S.: Big data and machine learning in health care. JAMA. **319**(13), 1317–1318 (2018). https://doi.org/10.1001/jama.2017.18391
9. Baek, H., Cho, M., Kim, S., Hwang, H., Song, M., Yoo, S.: Analysis of length of hospital stay using electronic health records: a statistical and data mining approach. PLoS One. **13**(4), e0195901 (2018). https://doi.org/10.1371/journal.pone.0195901
10. Rajkomar, A., Oren, E., Chen, K., et al.: Scalable and accurate deep learning with electronic health records. NPJ Digit. Med. **1**, 18 (2018). https://doi.org/10.1038/s41746-018-0029-1
11. Chen, J., Qi, T.D., Vu, J., Wen, Y.: A deep learning approach for inpatient length of stay and mortality prediction. J. Biomed. Inform. **147**, 104526 (2023). https://doi.org/10.1016/j.jbi.2023.104526
12. Breiman, L.: Random Forests. Machine Learning. **45**, 5–32 (2001). https://doi.org/10.1023/A:1010933404324
13. Shickel, B., Tighe, P.J., Bihorac, A., Rashidi, P.: Deep EHR: A Survey of Recent Advances in Deep Learning Techniques for Electronic Health Record Analysis. IEEE J. Biomed. Health Inform. **22**(5), 1589–1604 (2018). https://doi.org/10.1109/JBHI.2017.2767063
14. Harutyunyan, H., Khachatrian, H., Kale, D.C., Ver Steeg, G., Galstyan, A.: Multitask learning and benchmarking with clinical time series data. Sci. Data. **6**(1), 96 (2019). https://doi.org/10.1038/s41597-019-0103-9
15. Borisov, V., Leemann, T., Seßler, K., Haug, J., Pawelczyk, M., Kasneci, G.: Deep Neural Networks and Tabular Data: A Survey. IEEE Trans. Neural Netw. Learn. Syst. **35**(6), 7499–7519 (2024). https://doi.org/10.1109/TNNLS.2022.3229161
16. Goldstein, B.A., Navar, A.M., Pencina, M.J., Ioannidis, J.P.: Opportunities and challenges in developing risk prediction models with electronic health records data: a systematic review. J Am Med Inform Assoc. **24**(1), 198–208 (2017). https://doi.org/10.1093/jamia/ocw042
17. Farimani, R.M., Karim, H., Atashi, A., et al.: Models to predict length of stay in the emergency department: a systematic literature review and appraisal. BMC Emergency Med. **24**(1), 54 (2024). https://doi.org/10.1186/s12873-024-00965-4
18. Futoma, J., Simons, M., Panch, T., Doshi-Velez, F., Celi, L.A.: The myth of generalisability in clinical research and machine learning in health care. Lancet Digit. Health. **2**(9), e489–e492 (2020). https://doi.org/10.1016/S2589-7500(20)30186-2
19. Gualandi, R., Masella, C., Tartaglini, D.: Improving hospital patient flow: a systematic review. Bus. Process Manage. J. **26**(6), 1541–1575 (2020). https://doi.org/10.1108/BPMJ-10-2017-0265
20. Obermeyer, Z., Emanuel, E.J.: Predicting the future — Big Data, Machine Learning, and Clinical Medicine. New England J. Med. **375**, 1216–1219 (2016). https://doi.org/10.1056/NEJMp1606181
21. Esteva, A., Robicquet, A., Ramsundar, B., et al.: A guide to deep learning in healthcare. Nat. Med. **25**, 24–29 (2019). https://doi.org/10.1038/s41591-018-0316-z
22. Sendak, M.P., D'Arcy, J., Kashyap, S., et al.: A path for translation of machine learning products into healthcare delivery. EMJ Innov. (2020). https://doi.org/10.33590/emjinnov/19-00172
23. Peffers, K., Tuunanen, T., Rothenberger, M.A., Chatterjee, S.: A design science research methodology for information systems research. J. Manage. Inf. Syst. **24**(3), 45–77 (2007). https://doi.org/10.2753/MIS0742-1222240302

24. Design Science Methodology for Information Systems and Software Engineering. Springer, Heidelberg (2014). https://doi.org/10.1007/978-3-662-43839-8_20
25. Chapman, P., Clinton, J., Kerber, R., et al.: CRISP-DM 1.0: Step-by-step data mining guide. CRISP-DM Consortium (2000)

Lightweight Multi-sensor Modeling for Virtual Braking-Force Sensing

Mariana Fernandes[1], Mariana Almeida[1], Hugo Baptista[1], Suelma Pina[2], Ricardo Teixeira[2], Tiago Vale[2], Cristiana Neto[1], Diana Ferreira[1], Tiago Aston[3], Carlos Ferreira[3], Nuno M. C. da Costa[2], José Machado[1], Susana Bulas Cruz[2], and Hugo Peixoto[1(✉)]

[1] LASI, Algoritmi Center, University of Minho, 4710-057 Braga, Portugal
hpeixoto@di.uminho.pt
[2] DTx–Digital Transformation CoLab, University of Minho, Azurém Campus, 4800-058 Guimarães, Portugal
[3] Electronics and Connectivity (EC) Team, CEiiA, 4450-017 Matosinhos, Portugal

Abstract. We present a lightweight virtual sensing framework for braking force estimation focused on micro electric mobility, where direct pedal force sensing is unavailable due to cost and hardware constraints. It uses a load cell on the braking pedal as ground truth and applies machine learning to low-cost multi-sensor telemetry, combining fixed temporal window aggregation, sparse feature selection through L1 regularisation, and a computationally efficient LightGBM regressor, suitable for real-time embedded deployment. The method is developed and evaluated on the Q-Brake dataset, collected on a micro electric vehicle under diverse but controlled driving conditions. A systematic study examines the influence of window size, sensor modalities, feature selection strategies, and sampling rates. Our analysis shows that inertial measurements dominate braking force related information, with motor telemetry offering complementary benefits. The final 36 feature LightGBM model achieves robust performance on an independent naturalistic trip (RMSE 8.37 N; MAE 4.38 N), demonstrating good generalisation. Due to its bounded per cycle computational cost and hardware friendly design, the proposed virtual sensor is suitable for real time embedded deployment in resource constrained micro EV platforms, enabling scalable and cost-effective solutions for vehicle dynamics monitoring.

Keywords: Braking Force Estimation · Virtual Sensing · Automotive Sensor Fusion · Embedded Machine Learning · Micro Electric Vehicles · Vehicle Dynamics Monitoring

1 Introduction

Braking force is key for understanding vehicle dynamics, ensuring safe operation, and supporting functions such as wear assessment and predictive maintenance. Defined here as the force applied to the brake pedal and measured via a load

© The Author(s), under exclusive license to Springer Nature Switzerland AG 2027
O. Gervasi et al. (Eds.): ICCSA 2026 Workshops, LNCS 16761, pp. 644–661, 2027.
https://doi.org/10.1007/978-3-032-30527-5_42

cell sensor, it is typically not available in production vehicles, where dedicated sensing hardware is uncommon due to cost and integration complexity.

This is particularly relevant in micro electric vehicles (EVs) and urban mobility platforms, where compact architectures, limited energy budgets, and cost sensitive designs restrict the integration of additional hardware. Their sensor suites are usually limited to basic powertrain telemetry. Low-cost inertial and GPS data may be integrated or available through external devices (e.g. driver's smartphone).

Virtual sensing provides an attractive alternative by estimating otherwise unmeasured physical quantities from existing onboard telemetry, thus enabling cost efficient monitoring. While it has been applied to tyre forces and brake torque, pedal force estimation in micro EVs remains largely underexplored, despite its relevance.

Traditional braking-related estimation approaches have several limitations. Physics-based friction or slip models are sensitive to road conditions, tyre wear, and calibration drift. Observer-based methods demand detailed vehicle dynamics models. Deep learning (DL) imposes computational and memory overhead unsuitable for resource constrained embedded electronic control units (ECUs).

To address these challenges, this work proposes a lightweight virtual sensor for braking force estimation based on supervised learning over multi-sensor temporal windows. Our design focuses on bounded computation per cycle, achieved through fixed-size window aggregation, sparse feature selection, and an efficient tree-based regression model, a structure well suited for embedded deployment while retaining strong predictive power.

The main contributions of this work are:

- A computational virtual sensor for braking force using only low-cost signals.
- A window-based multi sensor modelling strategy with constant per-window computational cost, supporting real time oriented deployment.
- Sparse and interpretable feature selection preserving predictive performance.
- A systematic design space analysis covering algorithm, window size, feature selection strategies, sampling rates and sensor subsets.
- A reproducible and modular machine learning (ML) pipeline tailored to vehicle dynamics virtual sensing.
- Q-Brake dataset, a multi-sensor braking dataset for micro-EVs, enabling reproducible research in lightweight virtual sensing.

The remainder of this paper is organised as follows: Sect. 2 reviews related work; Sects. 3 and 4 describe data collection and processing, respectively; Sect. 5 presents computational methodology; Sect. 6 reports results; Sect. 7 discusses implications and limitations; and Sect. 8 provides conclusions and future work.

2 Related Work

Over the past decades, the automotive industry has extensively focused on improving vehicle control and safety. Virtual sensing techniques have emerged as

a viable solution, estimating unmeasurable variables through software observers implemented in ECUs, reducing system cost and complexity [14]. This paradigm has been applied to a wide range of vehicle dynamic quantities, from longitudinal and lateral tyre force estimation using both model-based and model-less techniques [1], to the simultaneous estimation of tyre forces and braking torques via an LPV Unknown Input Observer validated on a real vehicle prototype [10]. Similarly, brake clamping force estimation in electromechanical brake systems has been addressed using a Kalman Filter Unknown Input Observer combined with nonlinear model predictive control [12]. Although effective, such model based approaches depend on accurate system representations, making them sensitive to parameter uncertainty and limiting robustness across operating conditions.

Several data-driven methods have also been explored for vehicle dynamics estimation. Manghai et al. [2] applied tree-based models such as Random Forest (RF) and Logistic Model Trees for brake-fault diagnosis from vibration signals, achieving high classification accuracy in controlled setups, but relying on small datasets and simplified experimental conditions. Pan et al. [9] proposed a hybrid approach combining a thermal model with a Neural Network (NN) to estimate braking torque, though with limited real-time feasibility. For tyre force estimation, Xu et al. [13] compared NN, RF, and Recurrent Neural Networks using intelligent tyre accelerometers, finding that NN achieved the best accuracy, although performance degrades under extreme conditions, requires specialised in-tyre sensors and controlled testing environments. Barbosa et al. [4] demonstrated accurate lateral force prediction using Gaussian Process Regression, at the expense of high computational cost and limited scalability. More recently, Lu et al. [7] showed that Long Short-Term Memory models outperform traditional observers for tyre force estimation in electric vehicles, although with inherent limitations such as high computational cost, limited scalability, reduced generalisation to unseen driving conditions, and lack of real-world validation.

Since vehicle sensor data typically consists of high-frequency time-series signals, appropriate preprocessing is essential. Window segmentation can be used to transform continuous sensor streams into fixed-length segments suitable for data-driven models [6,8]. Within each window, statistical features such as mean, standard deviation, minimum, and maximum values are extracted to summarise the temporal behaviour of the signals [5,8].

In practical automotive applications, estimation algorithms must operate within ECUs, where strict latency and resource constraints require computationally efficient solutions [11]. While recent ML approaches achieve notable accuracy, many rely on DL architectures with memory and execution requirements incompatible with embedded platforms. To bridge the gap between accuracy and efficiency for ECU deployment, this work adopts a lightweight virtual sensing approach, combining window-based feature extraction with sparse feature selection and an efficient tree-based regressor. This design aims to capture relevant braking dynamics while meeting the computational demands of real time embedded execution.

3 Experimental Setup and Data Collection

This study, focused on micro electric mobility, uses data from Q-Brake dataset [3], collected from a single acquisition session on an L6e electric quadricycle prototype in Matosinhos, Portugal, illustrated on the data collection stage of our methodological pipeline (Fig. 1).

It encompasses 14 trips (total of 23.9 km) under diverse conditions, such as varying number of occupants, their weight ranges, road surface, road inclination, and braking duration and intensity.

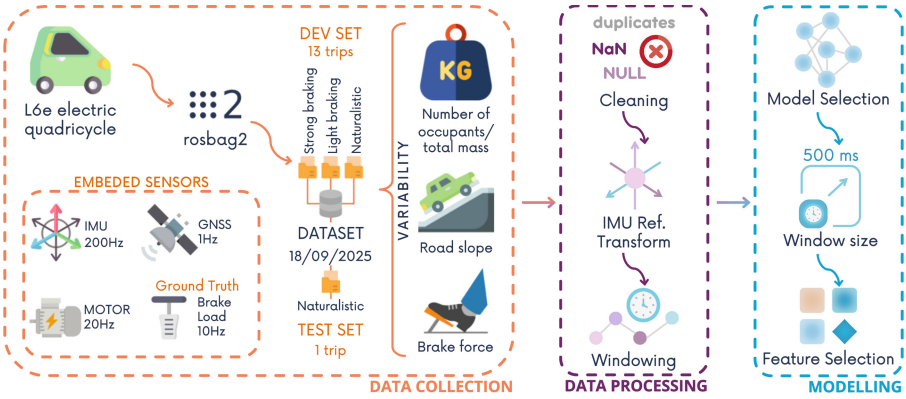

Fig. 1. Overview of the methodological pipeline used in the study. This figure has been designed using resources from Flaticon.com.

3.1 Sensor Instrumentation

We performed data acquisition using ROS 2 (Robot Operating System 2, Humble version) nodes for real time publication and logging of each sensor stream. All sensors were rigidly mounted to minimise vibration artefacts. The collected signals and sampling rates were:

- **IMU**: inertial measurement unit with 3-axes accelerometer and gyroscope data measured in the local X-Y-Z coordinate system of the device [180 Hz];
- **MOTOR**: motor telemetry data from the vehicle CAN (Controller Area Network) bus, including motor performance and EV battery metrics [32 Hz];
- **GNSS**: Global Navigation Satellite System location and velocity data [1 Hz];
- **Brake pedal force (ground truth)**: acquired through a load cell that measures the force that the driver exerts on the brake pedal [10 Hz].

Data streams were stored as rosbag2 files to enable reproducible playback and also converted to CSV for ML workflows.

3.2 Q-Brake Dataset and Data Acquisition Protocol

Because the prototype vehicle cannot operate on public roads, all trips were executed on a 500 m private circuit, shown in Fig. 2 (M). An extended version with an extra loop (E) was also used to introduce additional gradients. Both routes were driven counter clockwise.

This environment allowed consistent yet diverse conditions, including road surfaces (asphalt, cobblestone, and polished concrete), as well as level, uphill, and downhill segments.

Fig. 2. Main Circuit (M) and Extended Circuit with the added detour (E).

The vehicle has three seats, two in the front, and a third in the back, behind the front passenger. To introduce variability in the vehicle's total mass during braking events, passenger configurations and weight ranges were varied, while the driver was fixed, producing masses between 876 kg to 1030 kg. The dataset includes:

- 10 controlled trips (19.1 km) with frequent instructed braking events, ranging from light to strong and also varying in duration (extended circuit);
- 4 naturalistic trips (4.9 km), where braking was performed freely by the driver where appropriate (main circuit), one for each possible number of occupants (1–3), and an additional one with two occupants for final independent testing.

Figure 3 shows how braking force distributions differ across trip types: strong braking trips reach approximately 900 N, while light braking sessions peak near 300 N, and naturalistic trips near 200 N. Light braking trips show more frequent low force inputs (0–50 N), whereas naturalistic trips contain proportionally more moderate forces (50–100 N), reflecting unconstrained driving behaviour.

4 Data Processing

The raw sensor streams were processed through a pipeline to ensure data quality for machine learning experiments. The steps included:

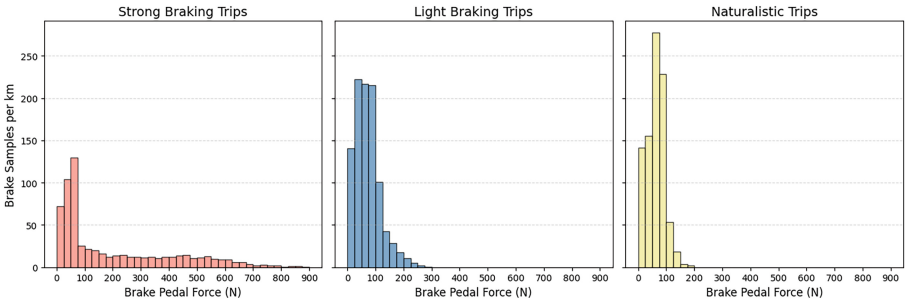

Fig. 3. Brake Pedal Force Distribution Histograms by Trip Type.

1. **Cleaning**: removal of null and duplicate values.
2. **IMU frame transformation**: conversion of IMU measurements from the device's local coordinate system to the vehicle's Front–Left–Up frame, using GNSS speed and heading, and accelerometer data to determine orientation.

After preprocessing, the following variables were available:

- **IMU**: *acc front*, *acc left*, *acc up*, *gyr front*, *gyr left*, *gyr up*;
- **MOTOR**: *current*, *voltage*, *rpm*, *throttle position*, *torque request* and *applied*.
- **GNSS**: *speed* (heading used only for coordinate calibration).

To capture short term temporal behaviour, ensure a fixed computational load during inference without redundancy, and accommodate variable sampling rates, the signals were segmented into fixed size, non overlapping windows. Four statistical features were extracted within a window for each signal: *mean*, *median*, *standard deviation*, and *slope* (defined as the difference between last and first samples), producing 48 aggregated features from the 12 variables (IMU and Motor). GNSS speed was only used in sensor ablation studies due to its sampling rate lower than considered window sizes (producing only mean). The target value for each window was defined as the corresponding average brake pedal force.

Because the analysis focuses on dynamic behaviour, static windows were removed. These were defined as consecutive windows (≥ 3) with GNSS speed below 0.5 m/s, ensuring the retained samples represent active vehicle motion.

5 Computational Method

5.1 Data Partitioning

The dataset was split into a development set of 13 trips and an independent test trip recorded under naturalistic driving with two occupants. The development set included the ten controlled trips with frequent braking events and three naturalistic trips with varying occupancy. These 13 trips were randomly divided into 80% for training and 20% for validation. The independent trip was withheld entirely during model development to provide an unbiased evaluation of the final model.

5.2 Model Training

Data processing and model training were implemented in Python using standard machine-learning libraries. Model selection was performed via 3-fold cross-validation on the training portion of the development set. Validation metrics guided all remaining design choices, and the final selected configuration was retrained on the full development set before evaluation on the independent test trip.

Twelve regression models were evaluated as candidates: CatBoost, XGBoost, LightGBM, Gradient Boosting Regressor (GBR), Random Forest (RF), Extra Trees, Decision Tree, K-Nearest Neighbors (KNN), Stochastic Gradient Regressor (SGR), Support Vector Machine (SVM) with linear kernel, Linear Regression (LR) and Multi-Layer Perceptron (MLP). Tree based ensembles were prioritised due to their favourable balance of prediction accuracy and computational efficiency, making them suitable for embedded deployment.

Hyperparameter tuning explored typical configurations for each model family, including number of estimators, maximum depth, learning rate, and regularisation parameters for tree based regressors; number of layers and units for MLP; and number of neighbours for KNN.

5.3 Experimental Design

A series of controlled experiments was conducted to evaluate the impact of key design choices on braking force estimation. Each experiment varied a single component while keeping all others fixed, enabling an isolated assessment of its contribution to overall performance.

Window Size: The temporal window defines the interval over which sensor data streams are synchronised and aggregated to form each training sample. Window durations from 100 ms to 1000 ms in 100 ms increments were compared. Smaller windows provide higher temporal resolution and lower latency but contain noisier, less stable features, and may capture only partial braking phases. Larger windows offer richer temporal context and improved noise averaging but risk masking brief events and increasing latency. The goal is to identify a window size that balances model performance and system responsiveness.

Feature Selection: To reduce model complexity and improve computational efficiency for embedded deployment, several feature selection techniques were evaluated to identify informative variables and remove redundant ones: L1 regularisation (Lasso), variance-based selection, recursive feature elimination with cross-validation (RFECV), variance inflation factor (VIF), Random Forest Regressor feature importance, and R-regression correlation methods. Each method was assessed using the same model configuration to quantify its effect on dimensionality and predictive performance.

Sampling Rate Variation: Since sensors operate at different native frequencies, an additional experiment assessed the effect of resampling the signals to alternative uniform rates prior to window aggregation. This evaluation examines if lower sampling rates, common in constrained embedded platforms, degrade the quality of the extracted statistical features. Multiple rates were tested while keeping all other components of the pipeline fixed, without feature selection to facilitate interpretation. Comparing performance across these configurations enables understanding the extent to which braking force estimation depends on high frequency dynamics versus aggregated temporal descriptors, and indicates whether the framework remains robust under reduced sensor bandwidth.

Sensor Ablation Study: To evaluate the contribution of each sensor modality, we conducted a systematic ablation study in which sensor subsets were removed or added. Using the final model configuration from previous optimisation stages, without feature selection, different combinations of IMU, motor, and GNSS signals were tested. This analysis identifies the most influential sensor sources, highlights opportunities for reducing hardware requirements, and helps understand expected performance on limited hardware scenarios.

Training Scope Comparison: In embedded deployments, braking instants can be detected from the binary brake light signal available on the CAN bus. Since the Q-Brake dataset does not include this signal, we trained on all dynamic windows, avoiding obtaining a binary indicator directly from the ground truth pedal force to prevent data leakage. To assess the influence of the training-data composition on predictive performance, an additional experiment compared models trained on all windows against models trained exclusively on braking instances. The former reflects scenarios where an external device (e.g. a smartphone) has no access to brake pedal status, while the latter isolates the estimator on braking events.

5.4 Evaluation Metrics

To assess predictive performance of the braking force estimation models, we calculate a set of standard regression metrics. Model selection during cross-validation was based on Mean Squared Error (MSE), since being more sensitive to outliers (due to its quadratic weighting) is critical for identifying potential failures in safety-critical braking estimation. We report the following evaluation metrics to provide a more comprehensive evaluation, as each metric captures different aspects of prediction error:

- **Mean Absolute Error (MAE)**: provides a direct and interpretable measure of prediction error in the original units (N).
- **Root Mean Squared Error (RMSE)**: penalises larger errors while maintaining the same units as the target variable (N).

- **Coefficient of Determination ($\mathbf{R^2}$)**: represents the proportion of variance in the observed target variable (braking force measurements) explained by the model, serving as a standardised measure of goodness-of-fit.
- **Adjusted $\mathbf{R^2}$ ($\mathbf{R^2_{adj}}$)**: modified version of R^2, penalises the inclusion of non-informative predictors, ensuring that performance improvements are due to actual information gain rather than simply increasing the number of features.

To maintain clarity and avoid redundancy, we report a subset of these metrics depending on the experimental context. Particularly, we use R^2 for comparing different ML architectures with a fixed feature set, and R^2_{adj} during feature selection and sensor ablation studies to evaluate the efficiency of the input signals.

6 Results and Evaluation

6.1 Comparative Model Performance

The initial stage of the evaluation consisted of comparing the predictive performance of twelve models. To ensure a consistent comparison across algorithms, all were trained using standard feature normalisation, no feature selection and an intermediate window size of 500 ms. The results are summarised in Table 1.

Hyperparameter tuning explored different configurations for each model. The main search ranges were:

Table 1. Cross-validation performance (mean ± standard deviation).

Model	RMSE	MAE	R^2
LightGBM	**15.32 ± 0.27**	6.48 ± 0.25	**0.957 ± 0.002**
CatBoost	15.57 ± 1.31	6.81 ± 0.73	0.955 ± 0.008
GBR	15.76 ± 0.37	**6.28 ± 0.15**	0.954 ± 0.002
XGBoost	16.59 ± 0.84	6.60 ± 0.13	0.949 ± 0.005
Decision Tree	20.66 ± 0.51	7.87 ± 0.15	0.921 ± 0.004
LR	20.95 ± 0.00	11.77 ± 0.00	0.919 ± 0.000
SVM	22.16 ± 0.34	11.20 ± 0.17	0.910 ± 0.003
RF	22.61 ± 4.19	8.67 ± 1.52	0.903 ± 0.036
KNN	23.97 ± 2.37	10.72 ± 0.68	0.894 ± 0.022
SGR	28.82 ± 9.68	13.84 ± 3.65	0.834 ± 0.113
MLP	30.47 ± 12.07	15.22 ± 5.35	0.808 ± 0.129
ExtraTrees	42.65 ± 6.98	18.65 ± 2.81	0.657 ± 0.111

- Tree-based models: number of estimators/iterations (50–500), maximum depth (3–10), learning rate (0.01–0.2), and regularisation terms ([0, 1]; [1, 10] for CatBoost).

- MLP: number of hidden layers (1–3) and units per layer (10–20).
- KNN: number of neighbours (1–10).
- SVM: regularisation parameter C (0–1).

Among the evaluated models, LightGBM achieved the best overall performance, obtaining the lowest RMSE and highest R^2, and GBR achieved the lowest MAE. CatBoost also demonstrated competitive performance, with results close to LightGBM across all metrics.

Based on these results, LightGBM was selected for the subsequent experiments. Since tree-based models are inherently insensitive to feature scaling, feature normalisation was not applied in the subsequent steps.

6.2 Influence of Window Size

Using the best-performing model from the selection phase, different window sizes were compared, considering their impact on the regression performance.

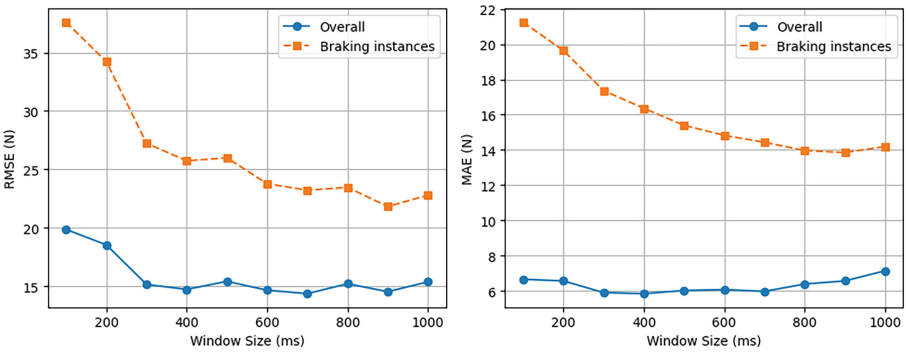

Fig. 4. Effect of temporal window size on model performance (validation set).

The results presented in Fig. 4 show that increasing the window size improves model performance (both RMSE and MAE decrease) when moving from very small windows (100–200 ms) to larger temporal contexts. Beyond approximately 500 ms, the improvements become less pronounced and the performance metrics remain relatively stable. This behaviour suggests that sufficient temporal context has already been captured for reliable feature extraction.

Considering these observations, a window size of 500 ms was selected for the final model and used in the following experiments. This value lies within the region of consistent performance improvement and provides an effective balance between estimation quality and temporal responsiveness.

6.3 Influence of Feature Selection Strategies

The impact of six feature selection strategies on LightGBM regressor performance was evaluated. Table 2 summarises the results, showing only the best performing experiment for each strategy with the respective parameter.

The Variance method achieved the strongest overall performance, yielding the lowest RMSE of 14.48 and the highest R^2_{adj} of 0.966, better than using no feature selection, while selecting 45 features (3 less features). However, since one of the objectives of this work is to reduce model complexity by limiting the number of input features, the Lasso method ($\alpha = 0.2$) was selected for subsequent experiments. Despite presenting slightly lower RMSE and MAE, Lasso achieves a comparable performance while reducing the feature set 25% to 36 variables, offering a better trade-off between accuracy and complexity.

Table 2. Impact of different feature selection strategies on performance (validation set). "Brk" stands for braking instances, "# feat." is the number of selected features.

FS Method	Param.	RMSE	MAE	R^2_{adj}	RMSE (Brk)	MAE (Brk)	R^2_{adj} (Brk)	# feat.
Variance	0.1	**14.48**	5.90	**0.966**	**24.38**	15.37	**0.949**	45
RFECV	2	14.57	5.79	0.965	24.58	15.20	0.948	48
None	–	14.58	**5.76**	0.965	24.58	**15.06**	0.948	48
Lasso	0.2	14.63	6.05	0.965	24.66	15.75	**0.949**	36
VIF	10	15.45	6.38	0.962	25.77	16.34	0.945	23
RF	25	21.21	8.39	0.928	35.31	20.43	0.900	2
R-Regr.	10	30.88	15.58	0.848	48.75	33.17	0.807	10

Regarding the remaining methods, RFECV did not remove any features relative to the no-selection baseline, offering no dimensionality reduction. The VIF, Random Forest Regressor, and R-Regression methods removed the largest number of features, which is reflected in a degradation of predictive performance.

The top 10 feature importance distributions resulting from Lasso ($\alpha = 0.2$) and Variance (threshold = 0.1) are illustrated in Fig. 5. We observe that *acc_front* is the most influential parameter, having the top two features with its mean and median, respectively, and its standard deviation and slope among top 7, in both cases. This is consistent with the underlying physical relationship between longitudinal deceleration and braking force. Motor RPM (mean and slope) and lateral standard deviation of gyroscope are also amongst the most important features for braking estimation.

6.4 Influence of Sampling Rates

Sensor signals may be acquired at different sampling rates, which can affect both the quality of the extracted features and the robustness of the model.

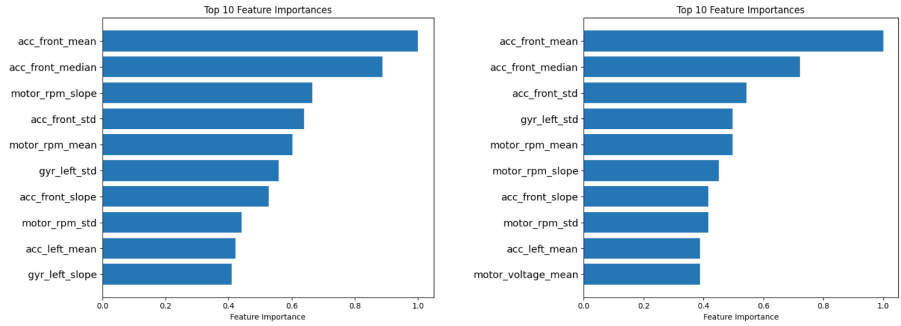

Fig. 5. Feature importance for the LightGBM model using Lasso ($\alpha = 0.2$) (left) and Variance (threshold = 0.1) (right).

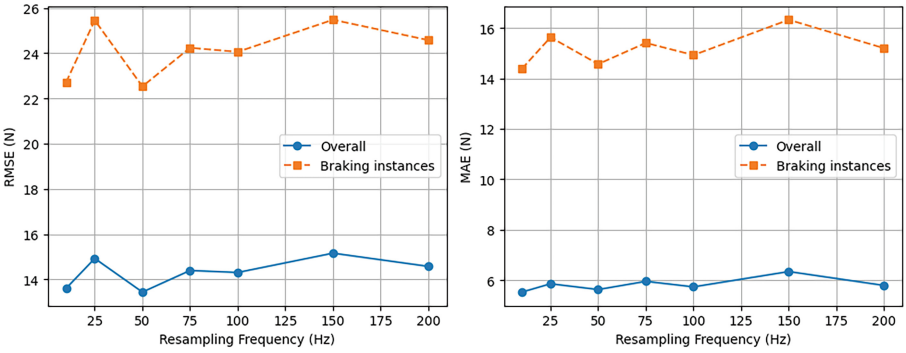

Fig. 6. Effect of sampling rate (after resampling) on model performance.

The reference frequency in this study is 10 Hz, corresponding to the sampling rate of the brake pedal sensor, which provides the target variable used in brake force estimation. As illustrated in Fig. 6, performance remained stable across the tested frequency range, with no meaningful degradation at frequencies as low as 10 Hz. Values of RMSE and MAE on both the full dataset and braking instances show similar insensitivity to resampling rate.

From a practical perspective, this suggests that the framework can operate effectively with moderate sampling rates (≤ 50 Hz), which are commonly supported by low-cost sensors and embedded systems. Consequently, this makes the method compatible with low-cost embedded platforms, where sensor bandwidth is typically limited.

6.5 Sensor Contributions

To analyse the contribution of each sensor modality to the braking force estimation task, several sensor configurations were evaluated with no feature selection

strategy applied. The evaluated configurations include combinations of IMU, motor and GNSS signals, as well as single-sensor variants.

The results in Table 3 show that the combined use of IMU and motor (I+M) achieves the best overall performance, with the lowest RMSE and MAE and the highest adjusted R^2. As we suspected due to its lower sampling frequency than the size of the windows, the inclusion of GNSS (I+M+G) does not improve results when added to any configuration, often leading to slightly worse performance.

Among single-sensor configurations, IMU (I) clearly outperforms motor-based setups (M), indicating that inertial signals capture most of the relevant braking dynamics, while motor signals alone are insufficient. This is consistent with longitudinal acceleration being the most important parameter, and its mean as the most important feature.

Table 3. Comparison of braking-force estimation performance across different sensor configurations, where G=GNSS, I=IMU, M=Motor.

Sensors	RMSE	MAE	R^2_{adj}	RMSE (Brk)	MAE (Brk)	R^2_{adj} (Brk)	# feat.
I+M	**14.58**	**5.76**	**0.965**	24.58	**15.06**	**0.948**	48
I+M+G	15.39	6.47	0.961	**25.04**	15.62	0.948	49
I	17.65	6.96	0.950	29.39	17.30	0.929	24
I+G	20.20	8.48	0.933	32.34	19.00	0.909	25
M+G	26.14	12.64	0.885	40.63	27.47	0.852	25
M	26.51	12.36	0.877	42.11	28.17	0.838	24

The configuration with both sensors was kept for subsequent experiments, providing the best balance between estimation accuracy and sensor complexity.

6.6 Effect of Training Scope

To analyse the impact of training strategy on braking force estimation, a comparative study was conducted considering different model configurations: using all dynamic windows ("Dynamic") and using only braking instances ("Brk").

The results show that the LightGBM model trained on all dynamic windows outperforms the braking-only variant on braking instances by a small margin, suggesting that exposure to the complete range of driving dynamics provides a beneficial regularisation effect.

While training solely on braking windows, we decided to apply a simplified Linear Regression (LR) model as a low-complexity alternative and benchmark to the proposed model. It was applied using the mean longitudinal acceleration (*acc_front_mean*) as the sole predictor, based on our previous feature importance analysis and reflecting the underlying linear physical relationship between vehicle deceleration and braking force. The results are summarised in Table 4.

Table 4. Comparison of training strategies for braking force estimation on all active vehicle motion windows (Dyn: dynamic) and windows containing braking events (Brk).

Model	RMSE	MAE	R^2_{adj}	RMSE (Brk)	MAE (Brk)	R^2_{adj} (Brk)	# feat.
LightGBM Dyn	14.63	6.05	0.965	24.66	15.75	0.949	36
LightGBM Brk	–	–	–	25.05	16.06	0.948	37
LR Brk	–	–	–	35.69	22.07	0.894	1

The linear regression model, despite its simplicity, achieves an adjusted R^2 of 0.894, confirming that longitudinal acceleration is a meaningful predictor. As a single-feature model, it captures the dominant physical trend but exhibits substantially larger errors, with RMSE and MAE higher by about 11 N and 6 N, respectively, compared with the more complete LightGBM model. This indicates that a single-feature linear formulation is insufficient to capture the complexity of braking force dynamics. Figure 7 illustrates the behaviour of both models on active braking instances.

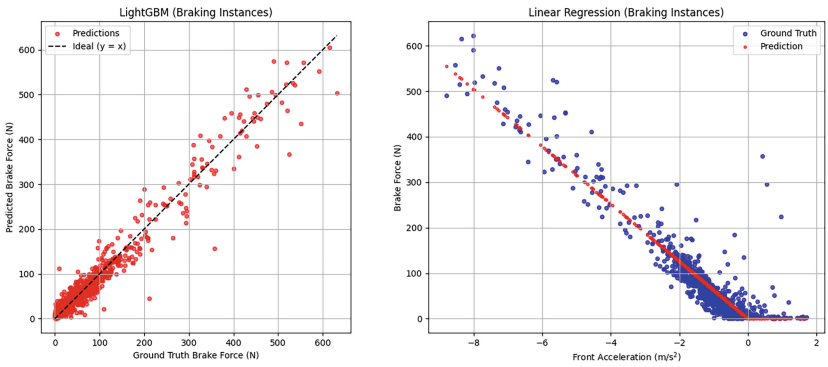

Fig. 7. LightGBM (left) prediction vs ground truth comparison; Linear Regression (right) relationship between front acceleration and braking force for active braking instances.

On the left, the LightGBM shows strong agreement with ground truth values, as evidenced by the alignment along the identity line, despite increased variance at higher forces. Conversely, the Linear Regression (right) exhibits a clear correlation between braking force and front acceleration. However, its univariate nature prevents the model from capturing the non-linear complexities present in the dataset.

6.7 Independent Test Set Results

This section assesses the performance of the final model on previously unseen data in order to evaluate its generalisation capability beyond the training data. The final model corresponds to a LightGBM trained on the full development set with a temporal window of 500 ms, and Lasso feature selection ($\alpha = 0.2$). Model training resulted on the following hyperparameter configuration: Gradient Boosting Decision Tree as the boosting algorithm, 20 leaves, maximum depth of 10, learning rate of 0.168, and no regularization (reg_alpha = 0, reg_lambda = 0).

Table 5. Comparison between cross-validation (best validation fold) and independent test set performance on the final LightGBM model with 500 ms windows and 36 features.

Set	RMSE	MAE	R^2	RMSE (Brk)	MAE (Brk)	R^2 (Brk)
Validation	15.8	6.30	0.958	–	–	–
Test	8.37	4.38	0.912	13.94	10.98	0.803

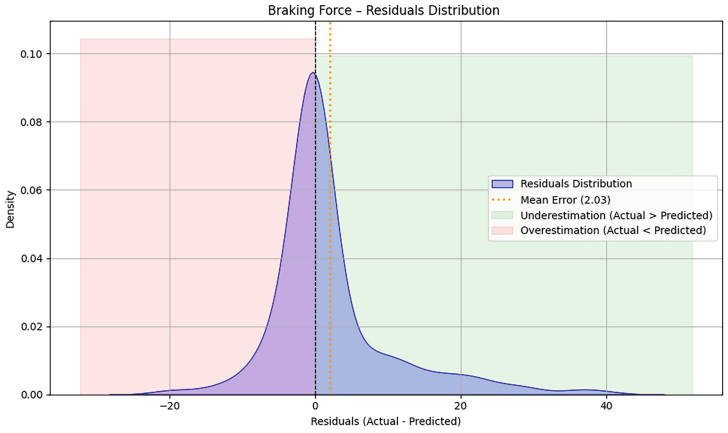

Fig. 8. Distribution of prediction residuals of the LightGBM braking force estimation model on the independent test set.

As shown in Table 5, the model achieves significantly lower RMSE and MAE on the independent test set than on the best fold of CV (with the same hyperparameters), while also presenting lower values on R^2. This happens because the independent test trip contains only light naturalistic braking, leading to substantially lower variance in the braking force target compared with the controlled braking sessions used for training and validation (see Fig. 3), which include very

strong braking events. Although the model achieves lower absolute errors on this easier regime (MAE and RMSE decrease), the reduced variance of the ground truth lowers the achievable R^2, explaining the slightly lower R^2 value despite improved error metrics.

Results indicate good generalisation and adequate errors on unseen data both on all dynamic windows and on braking instances only, although the latter show higher errors as expected. To further analyse the model behaviour, the distribution of prediction residuals is illustrated in Fig. 8.

The residuals are centred close to zero, although a slight positive bias can be observed, suggesting a tendency of the model to underestimate higher braking forces. This behaviour is consistent with the inherent difficulty of modelling sharp braking transitions using aggregated sensor features.

7 Discussion

The results demonstrate that the proposed virtual sensing framework provides a reliable braking force estimation using only existing vehicle telemetry and lightweight architectures. The superior performance of LightGBM over other ensemble methods and NN validates the use of tree-based architectures for automotive virtual sensing. From an embedded systems perspective, the inference complexity of a decision tree is $O(d)$, where d denotes the maximum tree depth, ensuring deterministic latency and a low memory footprint. Furthermore, the model uses 36 statistical features and since LightGBM is invariant to feature scaling, the normalisation step can be omitted in production, simplifying the software pipeline and reducing the computational cost per window.

The simplified linear model captures a large portion of the variance in braking force, indicating that the target signal is strongly influenced by fundamental vehicle kinematics. Longitudinal acceleration exhibits a direct physical relationship with braking force, which explains why a single-variable model can approximate it reasonably well. However, the considerably lower prediction errors reveal that our LightGBM model effectively better captures the nonlinear and multi-sensor dependencies present in real braking dynamics.

Nevertheless, several limitations must be acknowledged to contextualise the scope of these findings. First, our dataset was collected using a single micro-EV on a private circuit, which, despite controlled variation in load, slope, and braking behaviour, does not encompass the diversity of real urban traffic, multiple drivers, or adverse weather conditions. Further validation across additional vehicles, routes, and environments is needed to establish broader generalisability. These controlled acquisition conditions represent the primary limitation of this work. Second, although the framework is explicitly designed for resource-constrained systems, we have not yet conducted runtime benchmarking on embedded hardware. Evaluating latency, memory usage, and energy consumption on representative automotive edge devices will be essential to fully confirm real-time feasibility. Finally, the absence of a CAN-based brake-light signal limited our ability to isolate braking-only intervals without deriving indicators from

the target itself. While we implemented a braking-window variant for comparison, future studies could incorporate such signals to strengthen training-data selection and further reduce noise associated with non-braking intervals.

8 Conclusion and Future Work

This work presents a lightweight virtual sensing framework for braking force estimation using multi-sensor vehicle telemetry and ML. It uses data from Q-Brake dataset, collected on a L6e quadricycle, representative of micro electric mobility, a context where this is particularly relevant given the stringent hardware constraints typical of this vehicle category. The proposed approach combines window statistics, sparse feature selection through L1 regularisation, and a LightGBM model to provide accurate braking force estimation while maintaining computational efficiency suitable for real-time embedded systems.

The analysis of sensor modalities showed that inertial measurements provide most of the relevant information for braking force estimation, while the combination of IMU and motor telemetry yielded the lowest prediction errors. The evaluation of a minimal linear baseline also showed that longitudinal acceleration alone explains a significant portion of braking force variability, although the nonlinear LightGBM model substantially reduces prediction errors by capturing additional dynamics, including effects associated with regenerative braking.

The results further indicate that the proposed framework remains robust across moderate sampling rates, confirming its compatibility with resource-constrained embedded platforms. Evaluation on an independent test trip demonstrates good generalisation capability, achieving an RMSE of 8.37 N, a MAE of 4.38 N and an R^2 of 0.912, although prediction errors increase on braking events due to the higher variability of these dynamics. However, the test trip covers mainly light braking, so these results reflect a less demanding regime than training.

Although the proposed design is computationally efficient by construction, real-time latency has not yet been experimentally benchmarked on target embedded hardware. Future work will focus on expanding the dataset to include multiple micro-EV platforms, a wider range of driving environments, such as urban traffic conditions, different drivers and driving behaviour, and adverse weather scenarios. Furthermore, the proposed virtual sensor will be deployed within a ROS-based pipeline on an edge device to assess real-time performance, including latency and resource usage under embedded constraints.

Acknowledgments. This work has been supported by the European Union under the NextGenerationEU, through a grant of the Portuguese Republic's Recovery and Resilience Plan (PRR) Partnership Agreement, within the scope of the project BE.NEUTRAL – "Agenda da Mobilidade para a neutralidade carbónica das cidades", aiming at the development, industrialization and operation of new carbon-zero mobility cyber-physical products that will accelerate the transition to carbon-neutral cities by 2030 (Project ref. nr. 35 - C644874240-00000016; Total project investment: 221.376.867,63 Euros; Total Grant: 128.619.400,50 Euros).

References

1. Acosta, M., Kanarachos, S., Blundell, M.: Virtual Tyre force sensors: an overview of Tyre model-based and Tyre model-less state estimation techniques. Proc. Inst. Mech. Eng. Part D: J. Automob. Eng. **232**(14), 1883–1930 (2018). https://doi.org/10.1177/0954407017728198
2. Alamelu Manghai, T.M., Jegadeeshwaran, R.: Vibration based real-time brake health monitoring system: a machine learning approach. In: IOP Conference Series: Materials Science and Engineering. vol. 624, no. 1, p. 012027 (2019). https://doi.org/10.1088/1757-899X/624/1/012027
3. Baptista, H., et al.: Q-brake: L6e quadricycle multi-sensor braking-dynamics dataset (2026). https://doi.org/10.17632/4m5h6bv5s4.1
4. Barbosa, B.H.G., Xu, N., Askari, H., Khajepour, A.: Lateral force prediction using gaussian process regression for intelligent tire systems. IEEE Trans. Syst. Man Cybern. Syst. **52**(8), 5332–5343 (2022). https://doi.org/10.1109/TSMC.2021.3123310
5. Hirawat, A., Taterh, S., Sharma, T.K.: A dynamic window-size based segmentation technique to detect driver entry and exit from a car. J. King Saud Univ. – Comput. Inf. Sci. (2022). https://doi.org/10.1016/j.jksuci.2021.11.006
6. Lesti, G., Spiegel, S.: A sliding window filter for time series streams. In: Proceedings of the ECML/PKDD Workshop on IoT Streaming. CEUR Workshop Proceedings, vol. 1958 (2017)
7. Lu, L., Xu, G., Chen, X.: Tire force estimation using model-based and machine learning approaches for distributed drive electric vehicles. In: Proceedings of the 8th CAA International Conference on Vehicular Control and Intelligence (CVCI). IEEE (2024). https://doi.org/10.1109/CVCI63518.2024.10830206
8. Mozaffari, L., Mozaffari, A., Azad, N.L.: Window-based feature extraction framework for multi-sensor data: a posture recognition case study. In: IEEE International Conference on Systems, Man, and Cybernetics. IEEE (2015). https://doi.org/10.1109/SMC.2015.7321471
9. Pan, Y., Sun, Y., Li, Z., Gardoni, P.: Braking torque estimation through machine learning algorithms. Mater. Res. Proc. **26**, 213–218 (2023). https://doi.org/10.21741/9781644902431-35
10. Sentouh, C., Fouka, M., Popieul, J.C.: Virtual sensor: simultaneous state and input estimation for nonlinear interconnected ground vehicle system dynamics. Sensors **23**(9), 4236 (2023). https://doi.org/10.3390/s23094236
11. Wang, J.: Real-Time Embedded Systems. John Wiley & Sons, Hoboken, NJ, USA (2017)
12. Wei, W., He, T., Men, Y., Wang, J., Xiong, L.: Nonlinear model predictive clamping force control for electromechanical brake system. IEEE Int. Conf. Adv. Robo. (2024)
13. Xu, N., Askari, H., Huang, Y., Zhou, J., Khajepour, A.: Tire force estimation in intelligent tires using machine learning. IEEE Trans. Intell. Transp. Syst. **23**(4), 3565–3574 (2022). https://doi.org/10.1109/TITS.2020.3038155
14. Zaharia, C., Clenci, A.: Study on virtual sensors and their automotive applications. Sci. Bull. Automotive Series (2013)

Author Index

A
Alagon, Francis Jann 479
Alarcon, Vladimir J. 542
Aleluya, Earl Ryan 479
Aleluya, Edward Rowe 479
Almeida, Mariana 644
Alvarado, Ruben A. 542
Amorim, Rafael 619
Ávila-Ordóñez, Elina 568
Ascione, Laura 429
Aston, Tiago 644
Aulisio, Asja 148, 206
Azimi, Sarah 162

B
Bacco, Alessandra 334
Baptista, Hugo 644
Barbero, Silvia 206
Barbosa, Agostinho 631
Barreca, Alice 177, 206
Basbas, Socrates 227, 256
Bimonte, Sandro 509
Bonifaci, Pietro 301, 334, 365
Borruso, Giuseppe 557
Bouhouras, Efstathios 256
Buccellato, Federico 162
Butticè, Roberta 148

C
Calabrò, Francesco 113
Campisi, Tiziana 284
Candeloro, Giulia 394
Castillo-Reyes, Grethell 568
Catabriga, Lucia 39
Cazorla, Patricia 568
Cerullo, Giuseppe 380
Copiello, Sergio 301, 334, 365
Corrado, Simone 526
Coulibaly, Fagniné Alassane 509
Crisopulli, Alessia 194
Crociata, Alessandro 394
Cruz, Susana Bulas 644

D
da Costa, Nuno M. C. 644
de Macedo Mourelle, Luiza 3
De Menech, Sara 206
De Paola, Pierfrancesco 316
De Sio, Corrado 162
de Souza e Silva Junior, Luneque Del Rio 3
Del Giudice, Francesco Paolo 316
Demiris, Athanasios 227
Donati, Edda 351
Duarte, Júlio 619
Dubrovina, Valeria 58
Duong, Vanhiep 493

E
Estrella, René 568

F
Fabre, Frederic 509
Fernandes, Mariana 644
Ferreira, Carlos 644
Ferreira, Diana 644
Fountas, Grigorios 227, 256

G
García, Geovanny 568
Gargiulo, Carmela 413, 429
Gatto, Rachele Vanessa 526
Giapitzoglou, Panagiotis 256
Gishti, Erlind 256
Gondyul, Elena 58, 70
Grigorios, Fountas 242
Grillenzoni, Carlo 365
Guida, Carmen 429
Guimarães, Tiago 619, 631

I
Isola, Federica 445

J
Jiménez-Moya, Gerdys 568

© The Editor(s) (if applicable) and The Author(s), under exclusive license to Springer Nature Switzerland AG 2027
O. Gervasi et al. (Eds.): ICCSA 2026 Workshops, LNCS 16761, pp. 663–665, 2027.
https://doi.org/10.1007/978-3-032-30527-5

K
Kalisperatos, Argyrios 242
Khachkova, Tatyana 98
Kobak, Bilge 445
Kontorinis, Stavros 227
Krishnamoorthy, R. 465

L
L'Abbate, Samuela 586
Lai, Sabrina 445
Leccis, Francesca 445
Leone, Federica 445
Lisitsa, Vadim 58, 70, 98
Lobo, Afonso 619
Lopes, João 619, 631

M
Macedo Mourelle, Luiza de 22
Machado, José 601, 644
Malavasi, Giorgia 148, 177
Malembic-Maher, Sylvie 509
Maluya, Melody Mae 479
Manganelli, Beatrice 316, 526
Manganelli, Benedetto 316, 526
Mickle, Paul F. 542
Minniti, Giovanna Emanuela 113
Moura, Rafael C. 39

N
Nardi, Fernando 351
Nasca, Ludovica 129
Nedjah, Nadia 3, 22
Neto, Cristiana 644
Nguyen, Vanthuc 493
Nikiforiadis, Andreas 242
Nikolaou, Paraskevas 242

P
Peixoto, Hugo 644
Peloso, Aurora 301
Peñafiel, Marcelo 568
Perchinunno, Paola 586
Pham, Thanhduy 493
Pham, Xuankhang 493
Pina, Suelma 644
Pugliese, Francesco 413

R
Rebaudengo, Manuela 177
Reshetova, Galina 84
Rindone, Corrado 272
Rizzi, Stefano 509
Rolando, Diana 148, 177
Romenski, Evgeniy 84
Roose, Dirk 568
Rossitti, Marco 194
Rotondo, Francesco 586
Russo, Antonio 272, 284

S
Sacco, PierLuigi 394
Salaan, Carl John 479
Santos, Isaac P. 39
Santos, Manuel Filipe 619, 631
Sarmento, Afonso 601
Scarano, Vincenzo 413
Schoier, Gabriella 557
Sica, Francesco 380
Socrates, Basbas 242
Sousa, Matilde 631
Speranza, Giuseppe 413
Stara, Federico 380
Staropoli, Rosa Maria 113
Sterpone, Luca 162
Stiuso, Tonia 413
Sugiyama, Ko-ichiro 465

T
Tajani, Francesco 316, 380
Tanaka, Kazuaki 465
Teixeira, Ricardo 644
Telles, Flávia 22
Tesoriere, Giovanni 284
Tiziana, Campisi 242
Torrieri, Francesca 194
Tran, Vanha 493
Trovato, Maria Rosa 129
Tsouggaris, Stefanos 256
Tsuru, Hayato 465

V
Vale, Tiago 644
Van Orshoven, Jos 568
Vanegas-Peralta, Pablo 568
Vishnevsky, Dmitry 58, 70

Z
Zelbi, Ida 334, 365
Zois, Georgios 256
Zoppi, Corrado 445
Zucaro, Floriana 413